

CIP - Каталогизација у публикацији
Народна и универзитетска библиотека
Републике Српске, Бања Лука

621.3(082)(086.76)
621(082)(086.76)

МЕЂУНАРОДНА конференција о достигнућима у машинству и
индустријском инжењерству (16 ; 2023 ; Бања Лука)

Proceedings [Електронски извор] : DEMI 2023 / [16th
international conference on accomplishments in mechanical and
industrial engineering, Banja Luka, Jun 2023 ; editor in chief Petar
Gvero]. - El. zbornik. - Banja Luka : Faculty of Mechanical
Engineering, 2023. - 1 електронски оптички диск (CD-ROM) :
слика ; 12 cm

Систематски захтјеви: нису наведени. - Насл. са насл. екрана. -
Ел. публикација у ПДФ формату опсега 533 стр. - Опис извора
дана 7. 06. 2023. - Библиографија уз сваки рад.

ISBN 978-99976-11-04-8

COBISS.RS-ID 138545409

University of Banja Luka
Faculty of Mechanical Engineering

PROCEEDINGS
DEMI 2023

Banja Luka, Jun 2023

**16TH INTERNATIONAL CONFERENCE ON ACCOMPLISHMENTS IN
MECHANICAL AND INDUSTRIAL ENGINEERING**

DEMI 2023

Supported by:

MINISTRY FOR SCIENTIFIC AND TECHNOLOGICAL DEVELOPMENT, HIGHER
EDUCATION AND INFORMATION SOCIETY
OF THE REPUBLIC OF SRPSKA

Organizer and publisher:

FACULTY OF MECHANICAL ENGINEERING UNIVERSITY OF BANJA
LUKA

Co-organizer:

FACULTY OF MECHANICAL ENGINEERING UNIVERSITY OF NIŠ,
SERBIA

FACULTY OF MECHANICAL ENGINEERING UNIVERSITY OF
PODGORICA, MONTENEGRO

FACULTY OF ENGINEERING HUNEDOARA
UNIVERSITY POLITEHNICA TIMIȘOARA, ROMANIA REYKJAVIK

UNIVERSITY, ICELAND

For publisher:

Full Prof. Aleksandar Milašinović, PhD

Editor of chief:

Full Prof. Petar Gvero, PhD

Executive editor:

Biljana Prochaska, PhD
Milivoj Stipanović, BsC

ORGANIZING COMMITTEE

Prof. Petar Gvero, PhD
Chairman of Organizing and Scientific Committee
Faculty of Mechanical Engineering, University of Banja Luka

Prof. Aleksandar Milašinović,
PhD Prof. Zorana Tanasić, PhD
Assoc. Prof. Stevo Borojević, PhD
Assoc. Prof. Goran Janjić, PhD
Assist. Prof. Dejan Branković, PhD
Prof. Uroš Karadžić, PhD
(Faculty of Mechanical Engineering, Podgorica)
Assoc. Prof. Dejan Mitrović, PhD
(Faculty of Mechanical Engineering, Niš)
Assoc. Prof. Sorin Ioan Deaconu, PhD
(Faculty of Engineering Hunedoara, Romania)
Assist. Prof. David C. Finger, PhD
School of Science and Engineering University of Reykjavik, Iceland
Goran Jotić, Senior Assistant, MSc
Saša Tešić, Assistant, MSc
Gordana Tošić, Assistant, MSc
Ivana Savković, Assistant, MSc
Dijana Đeordić, Assistant, MSc
Biljana Prochaska, PhD
Sanja Maglov, MA+
Boro Marić, BA Law
Nedeljka Sladojević Putnik, BA Economics
Milivoj Stipanović, BSc
Zoran Grahovac, Assistant, MSc
Milisav Marković, Senior Assistant, MSc

SCIENTIFIC COMMITTEE

Prof. Darko Knežević, PhD
Faculty of Mechanical Engineering
University of Banja Luka

Prof. Radivoje Mitrović, PhD Faculty of
Mechanical Engineering University of
Belgrade

Prof. Vlastimir Nikolić, PhD Faculty of
Mechanical Engineering University of Niš

Prof. Nenad T. Pavlović, PhD Faculty of
Mechanical Engineering University of Niš

Prof. Igor Vušanović, PhD
Faculty of Mechanical Engineering
Podgorica, University of Montenegro

Prof. Gelu Ovidiu Tirian, PhD University
Politehnica Timisoara Romania

Prof. Dejan Lukić, PhD Faculty of Technical
Sciences University of Novi Sad

Prof. Saša Živanović, PhD
Faculty of Mechanical Engineering
University of Belgrade

Prof. Mijodrag Milošević, PhD Faculty of
Technical Sciences University of Novi Sad

Prof. Aleksandar Milašinović, PhD Faculty of
Mechanical Engineering University of Banja
Luka

Prof. Milan Tica, PhD
Faculty of Mechanical Engineering
University of Banja Luka

Prof. Izet Bjelonja, PhD
Faculty of Mechanical Engineering
University of Sarajevo

Prof. Milan Zeljković, PhD Faculty of
Technical Sciences University of Novi Sad

Prof. Slobodan Tabaković, PhD Faculty of
Technical Sciences University of Novi Sad

Prof. Franci Pušavec, PhD
Faculty of Mechanical Engineering
University of Ljubljana

Prof. Miodrag Manić, PhD
Faculty of Mechanical Engineering
University of Niš

Prof. Milenko Sekulić, PhD Faculty of

Technical Sciences University of Novi Sad

Prof. Mileta Janjić, PhD
Faculty of Mechanical Engineering
Podgorica, University of Montenegro

Assist. Prof. Davorin Kramar, PhD University
of Ljubljana, Slovenia

Prof. Simo Jakanović, PhD
Faculty of Mechanical Engineering
University of Banja Luka

Prof. Gordana Globočki-Lakić, PhD Faculty of
Mechanical Engineering University of Banja
Luka

Prof. Ardelean Erika, PhD University
Politehnica Timisoara Romania

Prof. Petar Gvero, PhD
Faculty of Mechanical Engineering
University of Banja Luka

Prof. Slobodan Lubura, PhD
Faculty of Electrical Engineering University
of East Sarajevo

Prof. Sanda Midžić – Kurtagić, PhD Faculty of
Mechanical Engineering University of
Sarajevo

Assoc. Prof. Srđan Vasković, PhD Faculty of
Mechanical Engineering University of East
Sarajevo

Prof. Bratislav Blagojević, PhD Faculty of
Mechanical Engineering University of Niš

Prof. Milan Radovanović, PhD Faculty of
Mechanical Engineering University of
Belgrade

Prof. Dragoslava Stojiljković, PhD Faculty of
Mechanical Engineering University of
Belgrade

Prof. Nebojša Manić, PhD
Faculty of Mechanical Engineering
University of Belgrade

Prof. Milan Lečić, PhD
Faculty of Mechanical Engineering
University of Belgrade

Prof. Neven Duić, PhD
Faculty of Mechanical Engineering and Naval
Architecture
University of Zagreb

Prof. Vojislav Novaković, PhD NTNU, Norway

Prof. Milan Rackov, PhD Faculty of Technical
Sciences University of Novi Sad

Prof. Mirko Blagojević, PhD Faculty of
Engineering Sciences University of
Kragujevac

Prof. Sanjin Troha, PhD
Faculty of Engineering University of Rijeka,
Croatia

Prof. Nebojša Rašović, PhD
Faculty of Mechanical Engineering,
Computing and Electrical Engineering,
University of Mostar

Prof. Miroslav Milutinović, PhD Faculty of
Mechanical Engineering University of
University of East Sarajevo

Prof. Nataša Trišović, PhD
Faculty of Mechanical Engineering
University of Belgrade

Prof. Mladimir Milutinović, PhD Faculty of
Technical Science University of Novi Sad

Prof. Dražan Kozak, PhD
University of Josip Juraj Strossmayer in
Osijek, Croatia

Prof. Dragan Milčić, PhD
Faculty of Mechanical Engineering
University of Niš

Prof. Radoslav Tomović, PhD
Faculty of Mechanical Engineering
Podgorica, University of Montenegro

Prof. Janko Jovanović, PhD
Faculty of Mechanical Engineering
Podgorica, University of Montenegro

Prof. Nebojša Radić, PhD
Faculty of Mechanical Engineering
University of East Sarajevo

Prof. Tomaž Berlec, PhD
Faculty of Mechanical Engineering
University of Ljubljana

Prof. Janez Kušar, PhD
Faculty of Mechanical Engineering

University of Ljubljana

Prof. Platon Sovilj, PhD Faculty of Technical
Sciences University of Novi Sad

Prof. Gordana Stefanović, PhD Faculty of
Mechanical Engineering University of Niš

Prof. Miladin Stefanović, PhD Faculty of
Engineering Sciences University of
Kragujevac

Prof. Vlado Medaković, PhD Faculty of
Mechanical Engineering University of East
Sarajevo

Prof. Valentina Golubović-Bugarski, PhD,
Faculty of Mechanical Engineering, University
of Banja Luka

Prof. Strain Posavljak, PhD
Faculty of Mechanical Engineering
University of Banja Luka

Prof. Vid Jovišević, PhD
Faculty of Mechanical Engineering
University of Banja Luka

Prof. Živko Babić, PhD
Faculty of Mechanical Engineering
University of Banja Luka

Prof. Atul Bhaskar, PhD University of
Southampton United Kingdom

Prof. Socalici Ana, PhD University
Politehnica Timisoara Romania

Prof. Milan Banić, PhD
Faculty of Mechanical Engineering
University of Niš

Prof. Aleksandar Sedmak, PhD Faculty of
Mechanical Engineering University of
Belgrade

Prof. Branko Blanuša, PhD Faculty of
Electrical Engineering University of Banja
Luka

Assist. Prof. Srđan Savić, PhD Faculty of
Technical Sciences University of Novi Sad

Prof. Dejan Mitrović, PhD
Faculty of Mechanical Engineering
University of Niš

Prof. Goran Janevski, PhD
Faculty of Mechanical Engineering
University of Niš

Prof. Uroš Karadžić, PhD
Faculty of Mechanical Engineering
Podgorica, University of Montenegro

Prof. Deaconu Sorin, PhD University
Politehnica Timisoara Romania

Prof. Bordeasu Ilare, PhD University
Politehnica Timisoara Romania

Assist. Prof. Dejan Branković, PhD Faculty of
Mechanical Engineering University of Banja
Luka

Prof. Vinko Babić, PhD
Faculty of Mechanical Engineering
University of Banja Luka

Prof. Jovanka Lukić, PhD Faculty of
Engineering Sciences University of
Kragujevac

Prof. Goran Petrović, PhD
Faculty of Mechanical Engineering
University of Niš

Prof. Radoje Vujadinović, PhD Faculty of
Mechanical Engineering Podgorica,
University of Montenegro

Prof. Snežana Petković, PhD Faculty of
Mechanical Engineering University of Banja
Luka

Prof. Miodrag Hadžistević, PhD Faculty of
Technical Sciences University of Novi Sad

Prof. Branko Štrbac, PhD, PhD Faculty of
Technical Sciences University of Novi Sad

Prof. Bratislav Blagojević, PhD Faculty of
Mechanical Engineering University of Niš

Prof. Peđa Milosavljević, PhD Faculty of
Mechanical Engineering University of Niš

Prof. Jelena Šaković Jovanović, PhD Faculty
of Mechanical Engineering Podgorica,
University of Montenegro

Prof. Mladen Todić, PhD
Faculty of Mechanical Engineering
University of Banja Luka

Prof. Milija Krajišnik, PhD
Faculty of Mechanical Engineering
University of East Sarajevo

Prof. Ilija Ćosić, Emeritus Faculty of
Technical Sciences University of Novi Sad

Prof. Zorana Tanasić, PhD
Faculty of Mechanical Engineering
University of Banja Luka

Prof. Mirko Soković, PhD
University of Ljubljana, Slovenia

Prof. Miroslav Bobrek, PhD Faculty of
Mechanical Engineering University of Banja
Luka

Prof. Goran Janjić, PhD
Faculty of Mechanical Engineering
University of Banja Luka

Prof. Igor Budak, PhD Faculty of Technical
Sciences University of Novi Sad

Prof. Tihomir Latinović, PhD Faculty of
Mechanical Engineering University of Banja
Luka

Assist. Prof. Bojan Knežević, PhD Faculty of
Mechanical Engineering University of Banja
Luka

Prof. Sead Pašić, PhD
Faculty of Mechanical Engineering, "Džemal
Bijedić", University in Mostar

Prof. Borut Kosec, PhD
Faculty of Natural Sciences and Engineering,
University of Ljubljana

Prof. Darko Bajić, PhD
Faculty of Mechanical Engineering
Podgorica, University of Montenegro

Prof. Dragoslav Dobraš, PhD Faculty of
Mechanical Engineering University of Banja
Luka

Senior Scient. Eng. Milica Grahovac, PhD,
Lawrence Berkeley National Laboratory,
USA

Prof. Doina Frunzaverde, PhD Faculty of
Engineering Resita Babeş-Bolyai University

Prof. Mihajlo Stojčić, PhD
Faculty of Mechanical Engineering
University of Banja Luka

Assist. Prof. Esad Tombarević, PhD Faculty
of Mechanical Engineering Podgorica,
University of Montenegro

Assist. Prof. Boško Matović, PhD Faculty of
Mechanical Engineering Podgorica,
University of Montenegro

Assist. Prof. Milovan Kotur, PhD Faculty of
Mechanical Engineering University of Banja
Luka

Prof. Hasan Smajić, PhD
University of Applied Sciences Keln Germany

Assist. Prof. David C. Finger, PhD School of
Science and Engineering University of
Reykjavik, Iceland

Assoc. Prof. Edin Berberović, PhD
Polytechnical Faculty University of Zenica

Assoc. Prof. Siniša Bikić, PhD Faculty of
Technical Sciences University of Novi Sad

Prof. Živojin Stamenković, PhD Faculty of
Mechanical Engineering University of Niš

Prof. Miloš Simonović, PhD Faculty of
Mechanical Engineering University of Niš

Prof. Jasna Glišović, PhD Faculty of
Engineering Sciences University of
Kragujevac

Research Associate Vencislav
Grabulov, PhD, IMS Institute,
Belgrade, Serbia

Prof. Nenad Djordjevic, PhD Senior
Lecturer in Mechanical Engineering
CASMEC Research Centre Director,
United Kingdom

Prof. Radovan Bulatović, PhD Faculty of
Mechanical and Civil Engineering Kraljevo,
Serbia

Prof. Predrag Živković, PhD Faculty of
Mechanical Engineering University of
Niš

CONTENT

KEYNOTE LECTURE	1
1. BOSNIA AND HERZEGOVINA – ICELAND ENERGY COOPERATION: A PARTNERSHIP TOWARDS CLIMATE NEUTRALITY AND ENERGY INDEPENDENCE David Christian Finger	3
2. CONTEMPORARY PLANETARY GEARBOXES AND THEIR CALCULATION Ž. Vrcan, M. Tica, S. Troha, K. Marković, M. Milutinović	8
PRODUCTION AND COMPUTER-AIDED TECHNOLOGIES	26
1. A POST-PROCESSOR FOR THE FIVE-AXIS MACHINE MULTIPRODESK BASED ON INVERSE KINEMATIC TRANSFORMATION J. Maletić, S. Živanović	28
2. CONCEPTUAL DESIGN OF A NOVEL MECHANISM WITH PARALLEL KINEMATICS BASED ON CHEBYSHEV'S LINKAGE Lj. Nešovanović, S. Živanović	35
3. ENERGY CONSUMPTION ANALYSIS AND PARAMETER OPTIMIZATION IN HIGH-FEED MILLING OPERATION B. Sredanović, S. Borojević, Đ. Čiča, S. Tešić, D. Jokić, D. Kramar	41
4. EXAMINATION OF THE POSITIONING ACCURACY OF THE MACHINE TOOL WITH HYBRID KINEMATICS S. Tabaković, S. Živanović, M. Zeljković, A. Budimir, Z. Dimić	47
6. EXPERIMENTAL INVESTIGATION OF MACHINING PARAMETERS IN TURNING OF ALUMINIUM ALLOY 7075-T6 A. Aleksić, M. Sekulić, B. Savković, A. Košarac, S. Moljević, J. Anić	54
5. FINITE ELEMENT AND EXPERIMENTAL MODAL ANALYSIS OF HIGH SPEED SPINDLE M. Knežev, A. Živković, C. Mladenović, D. Marinković, V. Ilić, M. Moravec	60
6. INDUSTRY 4.0 TECHNOLOGIES AND SYSTEMS FOR THE TRANSFORMATION OF COMPANIES INTO LOW-CARBON COMPANIES L. Črpić, J. Butara, M. Mavko, K. Kofalt, N. Sovec, E. Hozdić	64
7. INFLUENCE OF EXPERIMENTAL METHOD ON PLASTIC STRAIN RATIO DETERMINATION S. Aleksandrović, Đ. Ivković, D. Arsić, M. Delić	76
8. INFLUENCE OF PROCESS PARAMETERS IN THE PROCESS OF DEEP DRAWING WITH PLASTIC TOOL J. Ilić, T. Grbić, M. Hadžistević, M. Milutinović, M. Krašnik, D. Movrin	84
9. MATHEMATICAL MODELING OF THE ROUGHNESS OF THE ALUMINIUM ELEMENT SURFACE PROCESSED ON A CNC MACHINE Sanela Hrnjica, Sanel Gredelj	90
10. OPTIMIZATION OF CUTTING PARAMETERS FOR MINIMIZING UNIT PRODUCTION TIME IN MULTI-PASS ROUGH TURNING OF S355JR STRUCTURAL STEEL M. Trifunović, M. Madić, N. Vitković	99
11. OPTIMIZATION OF HIGH-SPEED MACHINING PARAMETERS OF THIN- WALLED ALUMINIUM STRUCTURES IN THE FUNCTION OF SURFACE ROUGHNESS J. Vukman, M. Milošević, A. Antić, D. Božić, V. Todić, D. Lukić	104
12. OPTIMIZATION OF SURFACE ROUGHNESS AND ITS VARIANCE IN CO ₂ LASER CUTTING USING DESIRABILITY FUNCTION APPROACH V. Marinković, M. Madić, P. Janković	110

13. OPTIMIZATION PROBLEM WITH THE GOAL OF MINIMIZING THE MASS OF GEARS	117
Anja Velemir, Ljubica Spasojević, Nenad Petrović, Nenad Kostić, Nenad Marjanović	
14. OPTIMIZATION SURFACE ROUGHNESS IN POWDER MIXED ELECTRICAL DISCHARGE MACHINING OF TITANIUM ALLOY	121
D. Rodic, M. Gostimirovic, M. Sekulic, B. Savkovic, A. Aleksic	
15. PARAMETRIC OPTIMIZATION IN END-MILLING OPERATION OF ALMGSI1 ALLOY USING A HYBRID WASPAS-TAGUCHI TECHNIQUE	126
Adnan Mustafić, Ragib Spahić	
16. PROGRAMMING METHODS AND PROGRAM VERIFICATION FOR 3-AXIS RECONFIGURABLE HYBRID KINEMATICS MACHINE	136
S. Zivanovic, G. Vasilic, Z. Dimic, N. Vorkapic, B. Kokotovic, N. Slavkovic	
17. STRUCTURE AND MECHANICAL PROPERTIES OF MIG WELDED BUTT-JOINTS OF ALUMINUM ALLOY 2024 T351	144
D. Milčića, M. Milčića, D. Klobčarb, A. Đurić, N. Zdravkovića	
18. TOWARDS OPTIMISED END-OF-LIFE PRODUCT DISASSEMBLY SYSTEM SELECTION	151
D. Mlivić, Z. Kunica, J. Topolnjak	
19. DECISION SUPPORT SYSTEM FOR MATERIAL SELECTION	159
D. Petković, M. Madić, P. Živković	
20. DEPENDENCE OF THE TEMPERATURE FIELD ON THE NUMBER OF SIMULTANEOUSLY FDM-PRINTED PLA SAMPLES	165
R.-R. Turiac, V. Cojocar, N. Bacescu, D. Frunzaverde, C.-O. Miclosina, G. Marginean	
21. DETERMINATION OF THE MACHINABILITY OF LEADED BRONZE BY MEASURING CUTTING FORCES AT TURNING WITH WC – CO COATED CARBIDE INSERTS	173
N. Šibalić, M. Mumović, O. Mijanović	
22. INFLUENCE OF THE LAYER THICKNESS AND THE FILAMENT COLOR ON THE SURFACE FINISH OF PLA SAMPLES PRINTED BY FDM	178
N. Bacescu, D. Frunzaverde, R.-R. Turiac, V. Cojocar, C.-R. Ciubotariu, G. Marginean	
ENERGETICS AND THERMAL ENGINEERING	185
1. OCCURRENCE OF CRACKS DUE TO INADEQUATE TURBINE SHAFT CONSTRUCTION	187
Srđan Bulatović, Vujadin Aleksić, Bojana Zečević, Biljana Prochaska	
2. EXPERIMENTAL RESEARCH OF THERMAL DRYING CONDITIONS IN FOOD DRYER	193
F. Mojsovski, V. Mijakovski	
3. FLUE GAS ANALYSIS, NECESSITY OR OBLIGATION	198
Vladimir V. Jovanović, Dragoslava D. Stojiljković, Nebojša G. Manić	
4. INCREASING THE ENERGY EFFICIENCY OF EDUCATIONAL BUILDINGS AS A FUNCTION OF ADAPTATION TO CLIMATE CHANGES	204
M. Radujković, G. Janjić	
5. INFLUENCE OF SOLAR FRACTION ON PHOTOVOLTAIC GENERATED ENERGY AT SERBIAN RESIDENTIAL BUILDING	210
Danijela Nikolić, Saša Jovanović, Vanja Šušteršić, Natalija Aleksić, Zorica Đorđević	
6. LONG TERM SIMULATION OF VERTICAL GCHP SYSTEM FOR A BUILDING WITH ASYMMETRIC COOLING AND HEATING LOADS	216

M. Đekić, E. Tombarević	
7. PERFORMANCE ANALYSIS OF A BIOMASS-FIRED STEAM BOILER WITH FGR USING AGRICULTURAL RESIDUE STRAW AS FUEL M. Tomić, P. Živković, J. Škundrić, M. Kljajić, B. Stepanov, Ž. Vlaović	221
8. THE CONCEPT OF ESTIMATING THE HYDROPOWER POTENTIAL OF AN UNGAUGED WATERSHED IN MONTENEGRO Milena Ostojic, Goran Sekulic, David C. Finger, Ivana Cipranic	227
9. AIR TIGHTNESS OF RESIDENTIAL BUILDINGS AND ITS IMPACT ON ENERGY CONSUMPTION E. Tombarević, V. Ivanović	235
10. THE IMPACT OF CIRCULATING FLUIDIZED BED BOILERS ON THE ENVIRONMENT – ON THE EXAMPLE OF STANARI TPP M. Nježić, V. Babić	244
11. THERMODYNAMIC ANALYSIS OF THE THEORETICAL COOLING SYSTEM BASED ON MEASURED CLIMATE DATA Danijela Kardaš Ančić, Petar Gvero, Mirko Komatina	256
12. WASTEWATER AS A NEW SOURCE OF ENERGY V. Sustersic, N. Aleksic, N. Rakic, M. Josijevic	259
13. AIR FLUIDIZED BED THERMAL DIFFUSIVITY COEFFICIENTS J. Janevski, P. Živković, M. Vukić, G. Cvetanović, M. Tomić	265
14. CASCADE SYSTEM FOR OPTIMAL USE OF DEEP GEOTHERMAL ENERGY S. I. Deaconu, M. Topor, F. Bu, A. M. Blaj	272
15. COMPREHENSIVE STUDY OF RAYLEIGH–BÉNARD CONVECTION IN A RECTANGULAR TANK WITH MOTOR OIL P. Živković, M. Tomić, J. Janevski, G. Cvetanović, C. Barz	278
16. ASSESSMENT OF THE TECHNICAL JUSTIFICATION AND PROFITABILITY OF THE NEWLY BUILT SHPP-S IN MONTENEGRO V. Vilotijević, V. Nikolić, U. Karadžić, V. Kovijanić, I. Božić	282
17. PARAFFIN IN LATENT HEAT STORAGE SYSTEMS P. Živković, G. Cvetanović, P. Rašković, J. Janevski, D. Petković	288
MECHANICS AND DESIGN	294
1. ANALYTICAL FUNCTIONS FOR GRADED COMPOSITE MATERIALS MODELLING D. Čukanović, G. Bogdanović, A. Radaković, D. Milosavljević, N. Velimirović	296
2. COLD ROLLED VS. HOT ROLLED STEEL SECTIONS IN THE DESIGN OF CANTILEVER RACKING R. Vujanac, N. Miloradovic, S. Vulovic, A. Pavlovic	301
3. CONTROL CALCULATION OF CLEARANCES IN HIGH-BAY WAREHOUSE OPERATED BY STORAGE AND RETRIEVAL MACHINES N. Miloradović, R. Vujanac	305
4. DELAYED ACCELERATION FEEDBACK FRACTIONAL ORDER CONTROL OF CART PENDULUM SYSTEM – SOME STABILITY ISSUES M. P. Lazarević, D. Radojević, Lj. Bučanović, S. Pišl	311
5. DIFFERENT APPROACHES TO THE PHASES OF INDUSTRY 4.0 PRODUCT DEVELOPMENT L. Šarović, B. Marković, A. Đurić	316
6. METHODOLOGY REVIEW FOR GETTING FUNCTIONALLY GRADED LATTICE STRUCTURE FOR SIMULATION AND EXPERIMENTAL TESTING M. Soldo, D. Šaravanja, N. Rašović	322

7.	SELECTION OF ZIPLINE CABLE T. Jojić, J. Vladić, R. Đokić	327
MECHATRONICS AND ROBOTICS		332
1.	ASSESSMENT OF FRACTIONAL ORDER IMPACT ON PERFORMANCE OF FRACTIONAL ILC CONTROLLER FOR UPPER LIMB EXOSKELETON N. Živković, M. Lazarević, J. Vidaković	333
2.	CONTRIBUTION OF RESEARCH ON THE APPLICATION OF ACTIVE MAGNETIC BEARINGS IN ORDER TO REDUCE THE INFLUENCE OF UNBALANCE ON THE VIBRATIONS INTENSITY OF A RIGID ROTOR A. Tomović, M. Damjanović, R. Tomović, J. Jovanović	339
3.	INTERNAL MODEL CONTROL OF TWO-TANK SYSTEM USING NEURAL NETWORKS P. Stepanić, S. Marinković, J. Vidaković, N. Dučić, N. Živković	345
4.	SYNCHRONIZATION OF TWO NON-SYNCHRONIZABLE INDUSTRIAL ROBOTS R. Jalić, B. Z. Knežević, D. Erceg	351
5.	SYNTHESIS OF THE CONTROL UNIT OF THE DESKTOP ROBOT ARM ACTUATED BY STEPPER MOTORS A. Dević, J. Vidaković, N. Živković, M. Lazarević	361
AUTOMOTIVE AND TRANSPORTATION ENGINEERING		366
1.	DESIGN OF EXPERIMENTAL RESEARCH ON INFLUENCING FACTORS ON THE PARTICLE EMISSION CAUSED BY BRAKE WEAR S. Vasiljević, D. Taranović, J. Lukić, D. Miloradović, J. Glišović	368
2.	IMPACT OF NON-EXHAUST PARTICLE EMISSIONS FROM MOTOR VEHICLES ON HUMAN HEALTH O. Bobičić, M. Damjanović, D. C. Finger, R. Vujadinović, B. Matović	376
3.	RECYCLING OF USED ENGINE OIL FILTERS IN THE CONTEXT OF SUSTAINABLE DEVELOPMENT Diana Miruna Armioni, Sorin Aurel Rațiu, Ioana Ionel	386
4.	THE INFLUENCE OF THE CROSSWIND ON THE LIFT COEFFICIENT, VEHICLE STABILITY AND SAFETY N. Stojanovic, I. Grujic, B. Boskovic	391
5.	THE INFLUENCE OF THE HYDROGEN INJECTION PARAMETERS ON THE COMBUSTION PROCESS OF IC ENGINE I. Grujic, N. Stojanovic, M. Petrovic	396
6.	REALIZING PRIORITIES FOR OCCUPATIONAL SAFETY AT AGRICULTURE M. Lutovska, V. Mijakovski, S. Kjosevski	402
QUALITY AND ECOLOGY		407
1.	IC ENGINE, HYDROGEN, COMBUSTION PROCESS, INJECTION PARAMETERS M. Rajić, B. Šumaković, P. Milosavljević, Z. Kostić	409
2.	CALORIFIC VALUE OF WOOD PELLETS B. Karpe, T. Udir, L. Lavrenčić, Z. Tanasić, A. Benčina, B. Kosec	419
3.	EFFECTIVE MONITORING AND ANALYSIS OF ERRORS THROUGH THE APPLICATION OF QUALITY TOOLS Maja Vuković, Goran Janjić, Zorana Tanasić, Borut Kosec, Miroslav Bobrek	423

4.	ENERGY MANAGEMENT MATURITY MODEL FOR SERBIA: LINKING ISO 50001 AND EXISTING PRACTICES M. Rajić, P. Milosavljević, R. Maksimović	427
5.	GLOBAL ELECTRONIC WASTE B. Dudić, P. Kovač, B. Savković, E. Beňová, D. Ješić	435
6.	INVESTIGATION OF THE INFLUENCE OF CHARACTERISTIC PARAMETERS ON THE ACCURACY OF CT MEASUREMENT G. Jotić, B. Štrbac, T. Toth, M. Ranisavljev, M. Hadžistević, M. Dovica, B. Runje	439
7.	LIFE-CYCLE COMPARISON OF THE HALL-HEROULT PROCESS, INERT ELECTRODES, AND ENERGY SUPPLY IN ALUMINUM PRODUCTION B. Bronkema, G. Sævarsdóttir, D. C. Finger	445
8.	METHODOLOGY OF EVALUATION OF ECOLOGICAL CHARACTERISTICS OF RESIDENTIAL BUILDINGS IN BOSNIA AND HERZEGOVINA Dragica Arnautović-Aksić	452
9.	QUALITY MANAGEMENT OF THE PRODUCTION OF PLASTIC INJECTION MOLDING TOOLS G. Janjić, J. Marić, Z. Tanasić, M. Vuković, T. Berlec	458
10.	THE EVALUATION OF PROCESS PERFORMANCE BY APPLYING THE DEA METHOD FOR EVALUATING 3D PRINTERS A. Tomović, J. Šaković Jovanović, A. Vujović	464
11.	A SURVEY ON LEAN METHODOLOGY IMPLEMENTATION IN A SMALL AND MEDIUM ENTERPRISES IN THE REPUBLIC OF SERBIA D. Pavlović, P. Milosavljević, S. Mladenović	470
	MAINTENANCE OF ENGINEERING SYSTEMS AND OCCUPATIONAL SAFETY ENGINEERING	475
1.	IMPORTANCE OF EXAMINATION OF COLLECTOR FOR IMPURITIES AFTER OIL PURIFICATION FOR HUMAN AND ENVIRONMENTAL SAFETY M. Jaric, S. Petronic, N. Budimir, B. Rajcic, Z. Stevic	477
2.	TECHNICAL DIAGNOSTICS – THE BASIS OF PREVENTIVE OR CORRECTIVE MAINTENANCE? D. Branković, Z. Milovanović	483
	MATERIALS AND WELDING	488
1.	LIFE ASSESSMENT USING THE FINITE ELEMENT METHOD OF HIGH- STRENGTH LOW- ALLOY STEEL SAMPLES EXPOSED TO LOW-CYCLE FATIGUE V. Aleksić, S. Bulatović, B Zečević, A. Maksimović, Lj. Milović	490
2.	CHARACTERIZATION AND HEAT TREATMENT OF ARMOUR STEEL OF NEW GENERATION D. P. Kosec, J. Bernetič, A. Nagode, G. Kosec, M. Soković, B. Kosec	500
3.	EFFECT OF SOLUTION ANNEALING PARAMETERS ON MICROSTRUCTURE AND MECHANICAL PROPERTIES OF NICKEL FREE AUSTENITIC STEELS I. Halilović, D. Sprečić, E. Nasić, Dž. Kovačević	505
4.	FINITE ELEMENT CALCULATION OF REDESIGNED WELDED JOINT AT SUPPORT FOR FRAME STAGE-LIKE STRUCTURE Aleksandra Arsić, Željko Flajs, Vlada Gašić, Nenad Zrnić	511
5.	INFLUENCE OF INJECTION MOLDING PARAMETERS AND GATE POSITION ON THE TENSILE STRENGTH OF POLYMER PART Edis Nasić, Denijal Sprečić, Jasmin Halilović, Džemal Kovačević	517

6. EDUCATION 4.0: APPLYING KNOWLEDGE TO PRACTICE IN A HYBRID LABORATORY FOR AUTOMATION AND MECHATRONIC: A SOLUTION WITH DIGITAL TWINS AND VIRTUAL REALITY 521
H. Smajic, F. Tiriyaki, D. Janjic, T. Duspara
7. DEEP LEARNING APPROACH FOR MONITORING AND MANAGEMENT OF ENERGY EFFICIENCY DATA IN PRODUCTION 528
H. Smajic, C. Faller, F. Tiriyaki

PREFACE

Dear colleagues,

Welcome to the 16th DEMI Conference and to our beautiful city of Banja Luka. The first DEMI Conference was established 25 years ago, as a scientific and professional conference at the Faculty of Mechanical Engineering Banja Luka. After a quarter of a century, DEMI has grown to become a relevant international scientific and professional conference in the field of mechanical engineering. Having started as a local conference, DEMI has grown to become the international scientific conference of the first category. Back then, organizers had difficulty bringing plenary speakers who are internationally notable scientists in their field of expertise. However, a great number of research papers from a variety of countries, as well as interesting social events have placed DEMI on the list of the most significant conferences in the field of mechanical engineering. We have succeeded to achieve these results thanks to the people employed at the Faculty of Mechanical Engineering Banjaluka and their commitment, but also thanks to the involvement of our co-organizers and all participants, authors, and co-authors of scientific and professional papers. It is very important that the evolution of this conference went hand in hand with the involvement of co-organizers. Bearing that in mind, we can proudly say that for this 16th DEMI Conference our co-organizers are Faculty of Mechanical Engineering, University of Podgorica, Montenegro, Faculty of Mechanical Engineering, University of Nis, Serbia, Engineering Faculty Hunedoara University Polytechnic Timișoara România, and Reykjavik University, Iceland. At this 16th conference, we have decided to go one step forward, making arrangements with some journals and motivating people to increase the quality of their papers, by recommending excellent ones for the publication in these journals.

There are a lot of challenges that we are faced with in the engineering society, due to the post-covid process of economic recovery, energy and economy crisis caused by the war in Ukraine, climate change, etc. Also, Artificial Intelligence has started to change our worldview and how we approach engineering. Mechanical engineering is a field that specifically focuses on finding solutions to the problems, but also adapting to new trends and technologies.

This is also the first DEMI conference, which will be organized live, after the Covid-19 pandemic, because we think that live communication, shared experiences and knowledge among the engineers and professionals, does not have an alternative. The following 16th DEMI Conference will be held from 1 to 2 June in Banja Luka. We hope that all participants will have a chance

to present their results and exchange their experiences with the colleagues, and enjoy spending time together in Banja Luka. We would also like to thank those who supported the organization of our conference.

We wish you a very warm welcome to the 16th DEMI Conference, on behalf of the Organizing Committee, Faculty of Mechanical Engineering, and University of Banja Luka.

Banja Luka, 24 May 2023

Chair of the Organizing Committee
of the 16th DEMI Conference

Prof. Petar Gvero, PhD

Keynote Lectures



Banja Luka
1-2 Jun 2023.

DEMI 2023

16th International Conference on Accomplishments in Mechanical and Industrial Engineering

www.demi.mf.unibl.org



Bosnia and Herzegovina - Iceland Energy Cooperation: a partnership towards climate neutrality and energy independence

David Christian Finger ^a

^a Department of Engineering, Háskólinn í Reykjavík | Reykjavik University, Menntavegur 1, Nauthólsvík | 101 Reykjavík | Iceland

Abstract *Iceland and Bosnia Herzegovina are two countries with contrasting energy profiles and approaches to sustainability. Iceland, known for its abundant renewable energy resources, has successfully transitioned to a low-carbon economy, primarily powered by geothermal and hydropower sources. On the other hand, Bosnia Herzegovina heavily relies on fossil fuels, resulting in high greenhouse gas emissions and energy dependence. Iceland's energy transition journey began in the 1970s when the country faced an oil crisis and decided to harness its geothermal and hydropower potential. Today, these renewable sources provide nearly 100% of Iceland's electricity and heating needs. This transition has not only reduced Iceland's reliance on imported fossil fuels but has also positioned the country as a global leader in geothermal energy utilization. Iceland's commitment to sustainability extends beyond its borders as it actively participates in international collaborations and shares its expertise in geothermal technology. In contrast, Bosnia Herzegovina faces significant challenges in its energy transition. The country's energy sector heavily relies on coal, which not only contributes to high carbon emissions but also poses environmental and health risks. Efforts to diversify the energy mix and promote renewables have been hampered by various factors, including political and institutional obstacles, lack of investments, and an outdated energy infrastructure. However, recent initiatives have aimed to promote clean energy, such as wind and solar power, with the goal of reducing Bosnia Herzegovina's carbon footprint and enhancing energy security. The strong contrasts between the two countries provides excellent opportunities for joint research collaboration.*

Keywords *Climate neutrality, energy independence*

1. Energy Transition in Iceland

Iceland and Bosnia Herzegovina are two countries with contrasting energy profiles and approaches to sustainability.

Iceland has undergone a remarkable energy transition, becoming a global leader in renewable energy utilization [1,2]. The country's journey began in the 1970s when it faced an oil crisis and decided to tap into its abundant geothermal and hydropower resources. Today, these indigenous renewable

sources provide nearly 100% of Iceland's electricity and heating needs.

By harnessing geothermal energy, which involves extracting heat from beneath the Earth's surface, Iceland has achieved a remarkable feat in reducing its reliance on imported fossil fuels. Geothermal power plants now supply a significant portion of the country's electricity, while also providing heating to homes, businesses, and even greenhouses, allowing for year-round agricultural production.

In addition to geothermal energy, Iceland has maximized its hydropower potential by utilizing its numerous rivers and waterfalls [3]. Large-scale hydropower plants have been developed, contributing to the country's clean energy mix and further reducing dependence on fossil fuels. The electricity generated from these renewable sources powers industries, supports transportation infrastructure, and even provides charging stations for electric vehicles.

Iceland's energy transition has not only provided environmental benefits but has also had positive economic and social impacts. The abundance of renewable energy has attracted energy-intensive industries, such as aluminum smelting, which benefit from the low-cost and sustainable electricity supply. This has contributed to job creation and economic growth in the country. Furthermore, Iceland's commitment to renewable energy has positioned it as a global leader in geothermal technology, fostering innovation and attracting international collaborations.

The success of Iceland's energy transition can be attributed to several factors. The country's unique geological features, characterized by volcanic activity and geothermal reservoirs, provide a natural advantage for geothermal energy production. Moreover, Iceland has implemented favorable policies and incentives to encourage the development and adoption of renewable energy technologies. The government's long-term vision, commitment to sustainability, and collaboration with industry stakeholders have played pivotal roles in achieving the transition.

Iceland serves as an inspiring example of how a country can leverage its natural resources and embrace renewable energy to achieve energy independence, reduce greenhouse gas emissions, and foster economic growth. The lessons learned from Iceland's energy transition can serve as a valuable blueprint for other nations seeking to decarbonize their energy systems and transition towards a more sustainable future.

2. Energy Transition in Bosnia Herzegovina

The energy transition in Bosnia Herzegovina presents several challenges that need to be addressed to facilitate a sustainable and low-carbon energy system. Here are some key aspects which could potentially lead to

prosperous collaborations between Bosnia Herzegovina and Iceland:

Bosnia Herzegovina heavily relies on coal for electricity generation. To transition to a more sustainable energy system, there is a need to diversify the energy mix by increasing the share of renewable energy sources such as hydropower, wind, solar, and biomass. This requires investments in renewable energy projects and the development of supportive policies and regulations.

The country's energy infrastructure requires significant upgrades to facilitate the integration of renewable energy sources. Modernizing the grid and transmission systems is crucial to accommodate the fluctuating nature of renewable energy generation and ensure efficient and reliable energy supply.

Developing a clear and supportive policy and regulatory framework is essential for driving the energy transition. This includes establishing renewable energy targets, implementing feed-in tariffs or other incentives to attract investments, and streamlining permitting and licensing processes for renewable energy projects.

Limited access to financing and investment capital is a major challenge for the energy transition in Bosnia Herzegovina. Overcoming financial barriers and attracting domestic and foreign investments require creating favorable conditions, such as offering financial incentives, improving credit access, and reducing investment risks.

Stakeholder engagement and capacity building: Engaging all relevant stakeholders, including government agencies, energy companies, local communities, and civil society organizations, is crucial for a successful energy transition. Promoting dialogue, collaboration, and capacity building efforts can help foster a shared understanding of the benefits and challenges of renewable energy and facilitate the transition process.

Improving energy efficiency across sectors, including buildings, industry, and transportation, can significantly contribute to the energy transition. Implementing energy-efficient technologies and practices can reduce energy consumption, lower greenhouse gas emissions, and enhance energy security.

Addressing these challenges requires a coordinated and multi-faceted approach. A cooperation between Bosnia Herzegovina and

Iceland can also play a vital role in supporting the energy transition in Bosnia Herzegovina, helping the country achieve its sustainable energy goals while addressing socio-economic considerations and ensuring a just transition for affected communities.

3. Geothermal district heating

Geothermal district heating has the potential to play a significant role in the energy transition of Banja Luka, the second-largest city in Bosnia Herzegovina. The Icelandic company Mannvit hf. has initiated a comprehensive pilot project in Bosnia and Herzegovina and has established a subsidiary in the country to support the initiative [4].

Here are some key points related to the implementation of geothermal district heating in Banja Luka:

Banja Luka is located in a region with known geothermal potential. Geological surveys and assessments can help identify suitable geothermal resources for district heating purposes (Fig. 1). Utilizing these resources can provide a reliable and sustainable heat source for the city.

Geothermal energy is a clean and renewable energy source, emitting minimal toxic air pollutants and greenhouse gases compared to fossil fuel-based heating systems. Shifting to geothermal district heating can contribute to reducing the city's carbon footprint, improving air quality, and mitigating climate change.

Developing a local geothermal district heating system can enhance energy independence and reduce reliance on imported fossil fuels. By utilizing indigenous geothermal resources, Banja Luka can ensure a more secure and resilient heat supply for residential, commercial, and public buildings.

Geothermal energy has the potential to offer cost-effective heating solutions in the long term. Although the initial investment for geothermal infrastructure can be significant, the operational costs are generally lower compared to conventional heating systems. This can result in lower energy bills for consumers and reduce the overall energy expenses for the city.

Implementing geothermal district heating in Banja Luka can stimulate local economic development. The construction, operation, and maintenance of geothermal infrastructure can create job opportunities and support the

growth of a local geothermal industry, including specialized services and equipment providers.

While geothermal district heating offers significant potential, there are challenges to be addressed. These include conducting comprehensive feasibility studies and resource assessments, securing financing for infrastructure development, and addressing potential technical and geological challenges specific to the region. Additionally, public awareness and support are essential for successful implementation.

To fully leverage the benefits of geothermal district heating in Banja Luka, it is crucial to involve relevant stakeholders, including local authorities, energy companies, investors, and the community. Collaboration, strategic planning, and a supportive policy and regulatory framework are essential for the successful integration of geothermal energy into the city's heating infrastructure, contributing to a sustainable and resilient energy future for Banja Luka. Banja Luka University and Reykjavik University intend to work on these issues during the next three years in the frame of a university research exchange.



Fig. 1. The district heating plant of Banja Luka is powered by heavy oil and biomass and was constructed on top of a geothermal reservoir.

4. Hydropower

While hydropower offers various benefits [5], there are also environmental concerns associated with its development and operation in Bosnia Herzegovina. Here are some key environmental considerations [6]:

The construction of hydropower dams and reservoirs can lead to the alteration and fragmentation of river ecosystems. Dams can

disrupt natural river flows, affecting fish migration, sediment transport, and the overall ecological balance. Reservoirs can flood large areas, resulting in the loss of habitats and displacement of flora and fauna.

Hydropower projects can impact the biodiversity of rivers and surrounding areas. The alteration of river flows and habitat destruction can harm fish populations, including migratory species, and other aquatic organisms. The loss of biodiversity can have cascading effects on the ecosystem, including impacts on other wildlife and plant species that depend on rivers and streams.

Hydropower operations require the management of water resources. This can lead to changes in downstream water availability, affecting ecosystems, agriculture, and water supply for communities. Balancing the needs of hydropower generation with other water users and maintaining ecological flow regimes is crucial for sustainable water resource management.

Hydropower dams can trap sediment upstream, leading to reduced sediment transport downstream. This can impact downstream ecosystems, river morphology, and the availability of sediment for agricultural and coastal areas. Furthermore, altered flow patterns caused by dams can contribute to erosion downstream, potentially affecting riverbanks and adjacent land.

While hydropower is a renewable energy source, climate change can pose challenges to its sustainability. Changes in precipitation patterns and water availability due to climate change can affect the reliability of hydropower generation and exacerbate water-related issues. Long-term planning and adaptation strategies are necessary to ensure the resilience of hydropower infrastructure in the face of changing climatic conditions.

Addressing these environmental concerns requires careful project planning, environmental impact assessments, and the implementation of mitigation and conservation measures. Balancing the benefits of hydropower with the protection and restoration of river ecosystems is crucial for achieving sustainable hydropower development in Bosnia Herzegovina. Banja Luka University and Reykjavik University will collaborate on these issues during the next three years.



Fig. 1. Small scale hydropower in Bosnia Herzegovina: the last wild forest of Europa can be severely damaged by new construction.

5. Conclusions and Outlook

Geothermal energy and hydropower are just the two main topics that Banja Luka University and Reykjavik University intent to collaborate on. The collaborations will include systems analysis, environmental impact assessments and stakeholder analysis, to name just the most relevant methods. Furthermore, the collaboration intends to be inclusive, with an open spirit for innovation and progress towards a clean, prosperous and energy independent Bosnia Herzegovina.

6. Conclusions and Outlook

Bosnia Herzegovina and Iceland have a tremendous joint potential for energy cooperation. In the private sector Icelandic companies might start cooperation with companies of Bosnia Herzegovina. Banja Luka and Reykjavik University are committed to initiate, facilitate, support and provide scientific insight to any developing project aiming at a energy transition towards renewable energies in Bosnia Herzegovina.

REFERENCES

- [1] Finger, D.C., Saevarsdottir, G., Svavarsson, H., Björnsdóttir, B., Arason, S., L. Böhme (2022). Improved value generation from residual resources in Iceland: the first step towards a circular economy. *Circular Economy and Sustainability*, vol. 1, pages 525-543. DOI: <https://doi.org/10.1007/s43615-021-00010-7>

- [2] The National Energy Authority of Iceland, From: <https://nea.is/>
- [3] Finger D. (2018) The value of satellite retrieved snow cover images to assess water resources and the theoretical hydropower potential in ungauged mountain catchments, *Jökull*, 68, 47-66. doi.org/10.33799/jokull.2018.68.047
- [4] Nopef, managed by Nefco since 2014 and financed by the Nordic Council of Ministers From: (<https://nopef.com/cases/geothermal-energy-bosnia-herzegovina/>)
- [5] Kelag, Carinthian Energy provider, From: <https://www.kelag.at/international-activity.htm>
- [6] RiverWatch, a society for the protection of rivers, From: <https://riverwatch.eu/en/balkanrivers/news/devastating-business-kelag-balkans>



Banja Luka
1–2 Jun 2023.

DEMI 2023

16th International Conference on Accomplishments in Mechanical and Industrial Engineering

www.demi.mf.unibl.org



Contemporary planetary gearboxes and their calculation

Ž. Vrcan^a, M. Tica^b, S. Troha^a, K. Marković^a, M. Milutinović^c

^aFaculty of Engineering, University of Rijeka, Vukovarska 58, HR-51000 Rijeka, Croatia

^bUniversity of Banja Luka, Faculty of Mechanical Engineering, Vojvode Stepe Stepanovića 71, BA-78000 Banja Luka, Bosnia and Herzegovina

^cFaculty of Mechanical Engineering, University of East Sarajevo, Vuka Karadžića 30, BA-71123 Istočno Sarajevo, Bosnia and Herzegovina

Abstract The increased demands for driver comfort and stringent pollution control measures have resulted in a revival of planetary gearboxes for road applications, due to their possibility to change the transmission ratio under load in synchronism with engine operation. Modern boxes provide as many transmission ratios as possible from the least possible number of simple component planetary gear trains (PGTs) by providing links between elements of multiple component PGTs. The application conditions decide to prioritize either the maximum number of transmission ratios, or ruggedness and reliability. Power circulation, hollow shafts, or complex planet carrier arrangements are avoided if possible. This paper deals with multispeed complex PGTs composed of at least two interconnected simple component PGTs controlled by brakes and clutches. Several variants of complex PGTs and the placement of brakes and clutches on external shafts of the gear trains are examined, and the transmission ratio functions derived. The kinematics of multi speed gear trains are obtained as combinations of two or more two-speed gear trains. An analysis of several contemporary gearbox layouts is provided together with the transmission ratio functions, together with an overview of the procedure for the calculation of creation of multi-speed gear trains is given.

Keywords Planetary gear trains, multi speed transmission, gearbox design

1. INTRODUCTION

Internal combustion engines (ICEs), regardless of their operating cycle, have been used in road and off-road vehicle applications since the late 19th century as a replacement for horse and steam drawn vehicles. Unlike a steam engine, the ICE is unable to self-start from standstill, and therefore it requires a transmission to match the speed and torque of the engine to the revolutions of the wheels [1]. The transmission must also

allow for the ICE to idle while the vehicle is stationary.

As the ICE is a constant power machine, the transmission must amplify the output torque in the range of almost 60:1 to about 4:1, appropriately split between the final drive and the gearbox. Depending on the application, the gearbox must have an adequate number of transmission ratios to enable the whole power range of the engine to be used. The transmission must also be built with a high internal efficiency to meet environmental demands and reduce operating costs. It must also be robust, reliable, and low maintenance, and should not have adverse reactions to extreme climatic conditions.

Until the early 2000s, mechanical transmissions were used almost exclusively in motor vehicles. They are robust, simple to manufacture and

Corresponding author

Associate Professor Željko Vrcan, D. Sc. M. E.
zeljko.vrcan@riteh.hr

Faculty of Engineering, University of Rijeka
Vukovarska 58
HR-51000 Rijeka, Croatia

maintain, and can be built with as many gear ratios as required. Their main downside is the relatively high skill required to operate a manual transmission, and the requirement of a clutch used to disconnect the engine from the gearbox while changing gears and to “slip” on starting from standstill. This results in wear, and it essentially mandates a very large transmission ratio for the bottom gear and the reverse gear as they must both be able to move the vehicle from standstill with the clutch slipping, resulting in only a quarter of the normally available engine available for rolling off.

Vehicle manufacturers have been aware of this since the introduction of the Ford Model T, which used a planetary gear train (PGT) very similar to the modern Ravigneaux to obtain two forward and one reverse gear selected by depressing a pedal. The transmission used a wet plate clutch. Several designs of manual planetary-based boxes followed, however the first true automatic gearboxes, able to change gears without reducing or interrupting engine power output, appeared just before World War II. These boxes are either torque converter based with a simple planetary stage for reverse and low gear or use a fluid coupling with three or four forward gears derived by a planetary gear train. All those boxes exhibit low fuel efficiency due to the lack of a lock-up clutch in the hydrodynamic elements, and efforts were made to combat this by providing “split power”, i.e., connecting some transmission elements directly to the engine flywheel. On the other hand, having a fluid stage means that the first gear can have a smaller transmission ratio, especially when combined with a torque converter.

Automatics following modern design principles will appear only in the 1960s with the widespread adoption of the Simpson gear train combined with the three-element torque converter equipped with a lock-up clutch. Further development was in the form of adding overdrive and/or low gear trains to existing gearsets and the addition of electronic shifting controls.

From this point, gear trains have evolved in two directions. The first direction is to extract the greatest possible number of gear ratios from a gearset by adding brakes and clutches and is most common for passenger car transmissions. The other design direction prioritizes ruggedness and reliability and prefers to add component geartrains to achieve extra gear

ratios. In this case, power circulation is avoided whenever possible, and the use of hollow shafts, especially for sun gears, is reduced to a minimum.

It should also be mentioned that manual transmissions have evolved into automated manuals, however they still have clutch wear issues and require very large low gear ratios.

Current designs of PGT based gearboxes use a torque converter stage and can withstand power inputs of about 600 kW, the actual limit being the centrifugal loads inside the gearbox.

Modern planetary gearboxes essentially use combinations of two and three-carrier gear trains controlled by clutches, with a single-carrier stage usually used either as a low gear or overdrive stage [2-10].

It is well known that gearboxes using application of PGTs have considerable advantages in comparison to conventional boxes, with expanded possibilities for application [11-14].

Two-carrier PGTs with four external shafts composed of two PGTs of the basic type were primarily considered for the purposes of the research presented in this article, extended to more component PGTs where appropriate. An overview of the internal structure of the researched gear trains is given, and all schemes and layout variants systematized. Due to the large number of permutations involved, a software program for numerical simulation and calculation of PGT parameters was developed to determine the internal workings and most important basic parameters of the component gear trains and the whole gear train. The acceptable transmission solutions analysed in this paper were generated using this specially developed computer program. The rule of torques will be used on some gear train examples to demonstrate the calculation procedure and to point out specific design solutions.

2. THE PLANETARY GEARBOX

Planetary gear trains with shifting capabilities are created by connecting several component trains and by adding conveniently placed brakes and clutches. For example, it is possible to extract 6-12 transmission ratios from two simple PGTs just by using clutches and brakes [15-19], and such layouts may be even interconnected in various ways. Therefore, it is very important to explore the shifting capabilities of each layout

and to have tools for the selection for the most appropriate layout. The basic simple gear train for all PGTs researched in this paper is the 2k-h, type A according to Kudryavtsev, or \overline{AI} according to Arnaudov and Karaivanov. This simple PGT can be very easily represented by a Wolf-Arnaudov symbol. These symbols mark each shaft in a different way, i.e., the sun shaft 1 is marked by a thin line, the ring gear shaft 3 with a thick line, and the planet carrier shaft S by two parallel lines (Fig. 1). The relationships between the torques acting on the simple PGT shafts are laid out in Eqs. 1-3. The shaft torques are given as functions of the ideal torque ratios which are the basic value when calculating the transmission ratios of complex planetary gearboxes. It should be noted that the equations in Fig. 1 do not take efficiencies into consideration (1):

$$\eta_0 = \eta_{13(S)} = \eta_{31(S)} = 1 \quad (1)$$

The torque ratio is defined by (2):

$$t = \frac{T_3}{T_1} = \frac{T_{D\max}}{T_{D\min}} = \left| \frac{z_3}{z_1} \right| > +1 \quad (2)$$

The relations between the torques present in the simple PGT are defined by the equations (3):

$$\begin{aligned} T_1 : T_3 : T_S &= T_{D\min} : T_{D\max} : T_\Sigma = \\ T_1 : t \cdot T_1 : -(1+t) \cdot T_1 &= +1 : +t : -(1+t) \end{aligned} \quad (3)$$

The following conditions (4) also apply:

$$T_1 \equiv T_{D\min} < T_3 \equiv T_{D\max} < |T_S| \equiv |T_\Sigma| \quad (4)$$

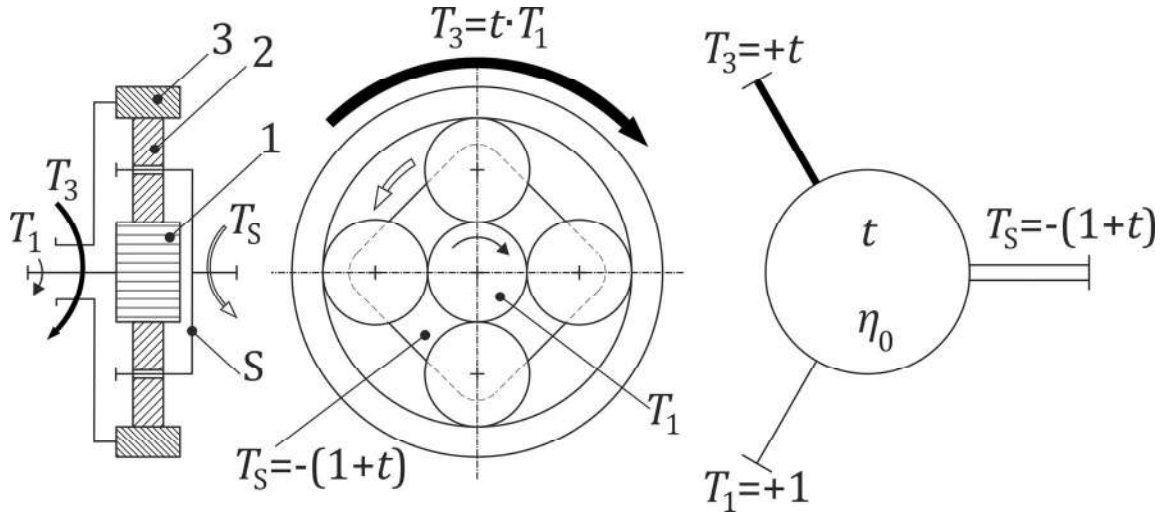


Fig. 1. The most used simple planetary gear train, 2k-h or 1A1)

3. TWO-CARRIER PGTs WITH TWO CONNECTING AND FOUR EXTERNAL SHAFTS

The characteristics of two-carrier PGTs with two connecting and four external shafts have been extensively analysed in [6], with brakes placed on two external shafts, while the remaining two shafts are used to connect the power source and the load. The reactive member is determined by activation of the respective brake, thus changing the both the direction of the power flow through the gear train, and the transmission ratio. As previously mentioned, these PGTs are composed of two interconnected simple

component gear trains of the 1A1 (or 2k-h) type, as those types offer most advantages in actual use.

Analysis has shown that these PGTs can be used for a broad spectrum of combinations of transmission ratios and can be used in a wide range of applications, ranging from lifting devices and machine tools main drives to main propulsion gearboxes for fishing boats and pleasure craft and railway vehicle main gearboxes or reversing drives.

A basic layout of a two-carrier PGT with two connecting and four external shafts may be seen in Fig. 2.

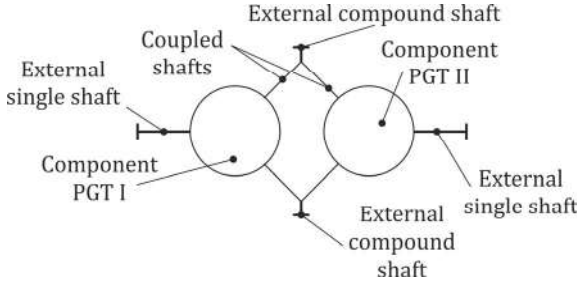


Fig. 2. Basic layout of two-carrier PGT

Figure 3 shows the possible layouts for two-carrier PGTs with two connecting and four external shafts, while Figure 4 shows the layout variants according to the convention in [13,20]. Furthermore, the letters A and B in Fig. 4. are used to display the energy flow and denote the layout variant. Besides that, the locations of brakes Br1 and Br2 are marked, and any variant can be applied to any layout.

The layout variant nomenclature using the cardinal points must be explained at this point.

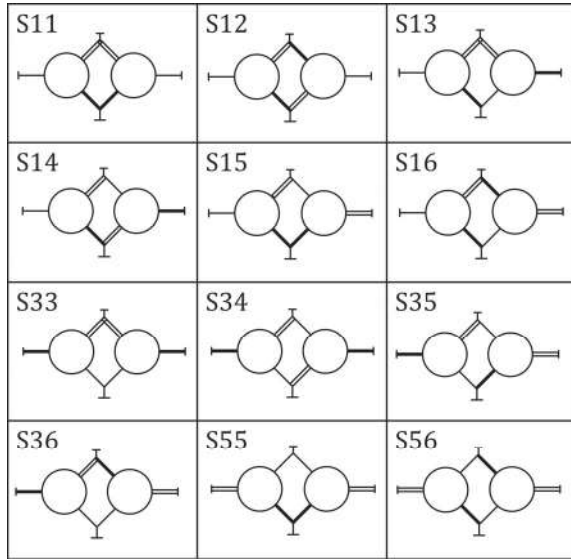


Fig. 3. Possible layouts of two-carrier PGTs with four external shafts

For example, S36WN(S/E) used for a PGT with two brakes means layout S36, power input on the western external shaft, power output on the northern external shaft, and (S/E) means that the southern and eastern external shafts have brakes mounted on them.

Depending on the brake, which is activated, the layout variant is denoted as S36WN(S) or

S36WN(E). The remaining unnamed shaft rotates freely and transmits no torque.

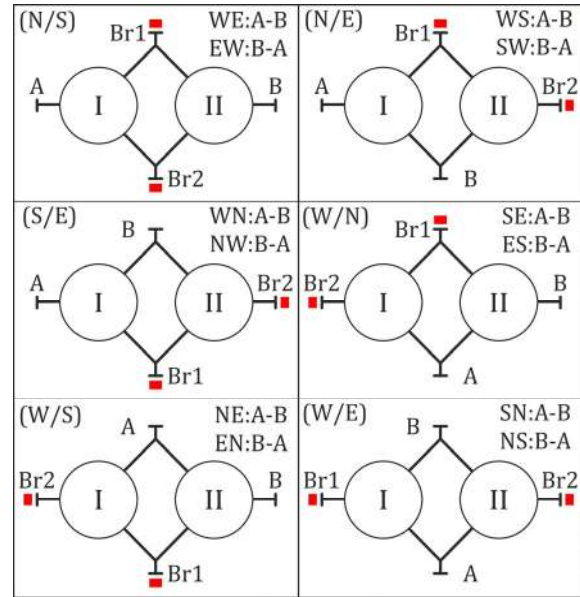


Fig. 4. Possible layout variants of two-carrier PGTs

Figure 5 displays the kinematic scheme of the S12WS(N/E) planetary gearset.

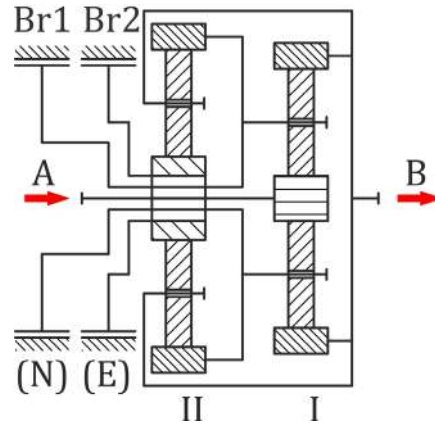


Fig. 5. Kinematic scheme of the S12WS(N/E) PGT

This gearset will be subject to structural analysis, the results of which will be displayed in Figure 6. The image on the left shows the operation of the gearset with brake Br 1 (N) on as S12WS(N), while the right image shows the operation of the gearset with brake Br2 (E) on as S12WS(E). The ideal torques have been determined for all shafts, and transmission ratios i_{Br1} and i_{Br2} have been calculated as a function of the ideal torque ratios of the component PGTs t_I and t_{II} . The ideal torque ratio is numerically equal to the ratio of

the number of teeth of the ring gear and the sun gear for each component PGT (5,6):

$$t_I = \left| \frac{z_{3I}}{z_{1I}} \right| \quad (5)$$

$$t_{II} = \left| \frac{z_{3II}}{z_{1II}} \right| \quad (6)$$

The analysis of the transmission ratio functions shows that the PGT with brake Br1 on works like a multiplier with the output shaft running in the opposite direction to the input shaft, while with brake Br2 on the PGT operates like a reducer with the output shaft rotating in the same direction as the input shaft.

It should be also noted that with brake Br1 on only geartrain I operates, while true two-carrier operation is achieved with brake Br2 on, unfortunately with power circulation present

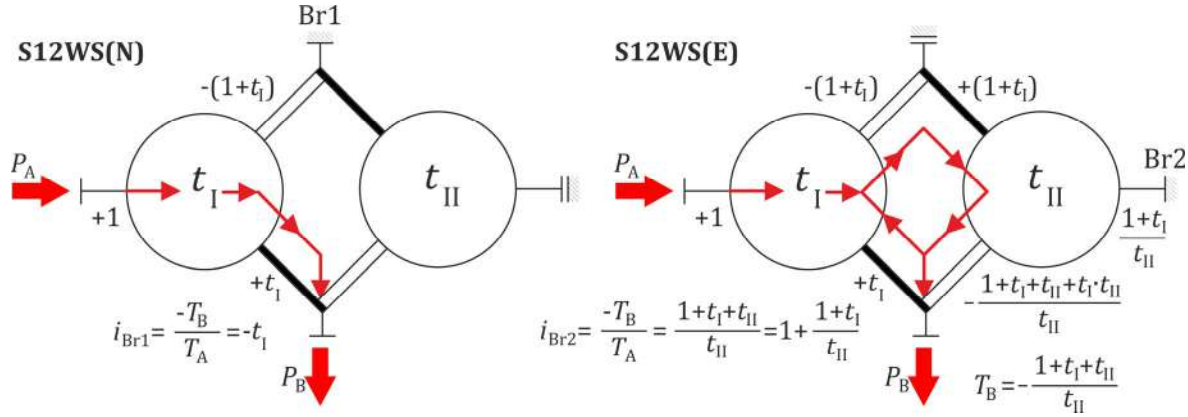


Fig. 6. Determining the transmission ratio functions for the S12WS(N/E) gear train with brake Br1 (N) on and with brake Br2 (E) on

The kinematic scheme of complex planetary gear train S12NS(W/E) is displayed in Figure 7.

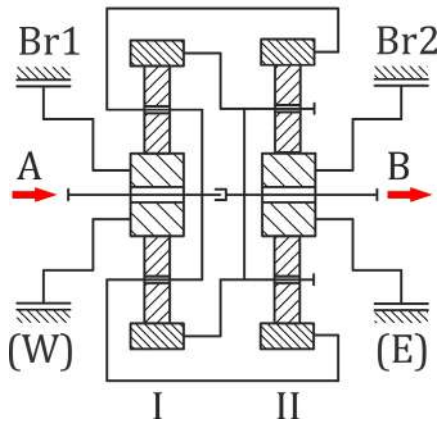


Fig. 7. Kinematic scheme of the S12NS(W/E) PGT

This gear train retains the same structure of S12WS, however in this case external shafts N and S are the respective power input and output,

while the brakes are placed on external shafts W and E. The results of the structural analysis of this PGT are displayed in Figure 8.

The image on the left shows the operation of the gearset with brake Br 1 (W) on as S12NS(W), while the right image shows the operation of the gearset with brake Br2 (E) on as S12NS(E).

It is possible to deduct from the transmission ratio functions that with brake Br1 on the gear train works like a multiplier, with both the input and output shafts turning in the same direction, while with brake Br2 on the gear train works like a reduction gear with both shafts also turning in the same direction. The difference from the case of the S12WS(N/E) train is that with either brake on only one component PGT transmits power, and there is no case of true two-carrier operation or power circulation.

It should be noted that this kind of analysis can be performed for any layout variant discussed in this paper.

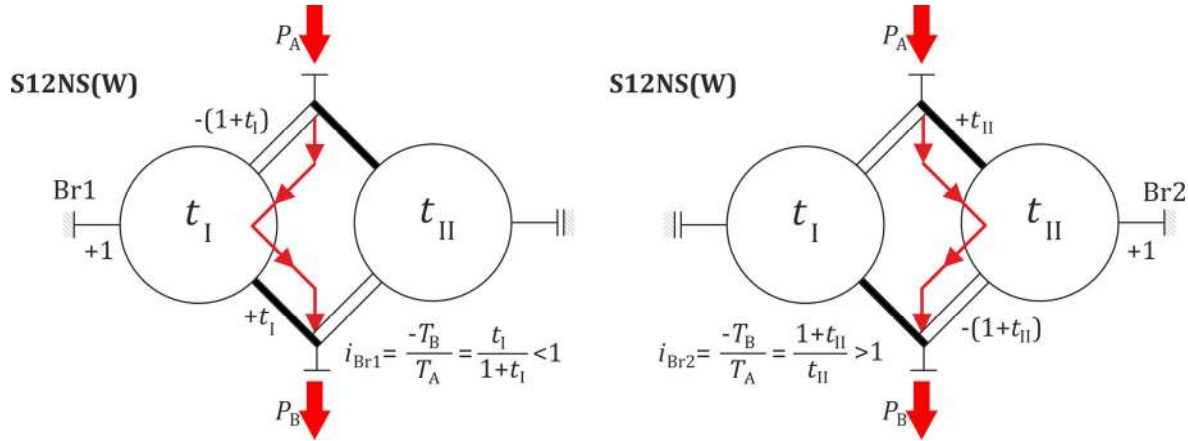


Fig. 8. Determining the transmission ratio functions for the S12NS(W/E) gear train with brake Br1 (W) on and with brake Br2 (E) on

4. MULTIVARIANT PLANETARY GEAR TRAIN

It is possible to increase the number of possible transmission ratios of a planetary gear train composed of two or more component trains by adding a control system able to change the input and/or output shaft of the gearbox, as the change of shaft essentially means that the PGT has changed into a different layout variant. Assuming that only two-carrier PGTs are taken into consideration, as each layout variant can

provide two transmission ratios, each compound PGT could provide up to six different transmission ratios. For example, just by enabling the power source and driven machine to be connected to two different shafts (two-variant compound PGT) it is possible to create four transmission ratios, and by expanding this to three (three-variant) it is possible to create up to six transmission ratios. The kinematic layout and structural scheme of such a PGT, S12NS(W/E)-WS(N/E) is shown in Figure 9.

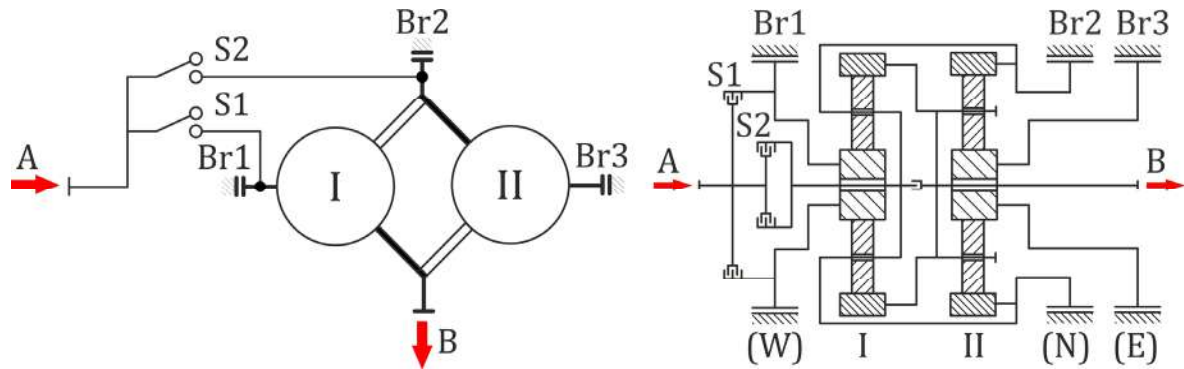


Fig. 9. Structural scheme (left) and kinematic scheme (right) of the two-shaft, four-layout gear train S12NS(W/E)-WS(N/E) gear train

This PGT combines the PGTs from Fig. 5 and 7 in one single package. It should be noted that for multivariant PGTs a naming convention has been accepted that the main layout variant with the input shaft closest to the north external shaft is named first, followed by the next external input shaft in the anti-clockwise direction. The four transmission ratios that this gear train is capable of are achieved with the clutch – brake combinations S1-Br2, S1-Br3, S2-Br1 and S2-

Br3. Therefore, it is obvious that multivariant PGTs can be successfully used in practical applications, so their possibilities must be thoroughly investigated. Kinematic analysis of the layout variants has pointed out that it is not possible to combine all variants within one scheme, but only those having a common input or output shaft, and that shaft must remain permanently coupled to the power source or powered machine.

Table 1 lists all the possible combinations of two layout variants, giving a total of 12 gear train pairs and their kinematic inversions (driving and driven machine shaft swaps).

Table 1. Theoretical combinations of two different layout variants within the same scheme for multivariant PGTs

No.	Combination	Kinematic inverse
1	WE(N/S), WS(N/E)	EW(N/S), SW(N/E)
2	WE(N/S), WN(S/E)	EW(N/S), NW(S/E)
3	EW(N/S), ES(N/W)	WE(N/S), SE(N/W)
4	EW(N/S), EN(W/S)	WE(N/S), NE(W/S)
5	WS(N/E), WN(S/E)	SW(N/E), NW(S/E)
6	SW(N/E), ES(N/W)	WS(N/E), SE(N/W)
7	SW(N/E), NS(W/E)	WS(N/E), SN(W/E)
8	NW(S/E), EN(W/S)	WN(S/E), NE(W/S)
9	NW(S/E), NS(W/E)	WN(S/E), SN(W/E)
10	ES(N/W), EN(W/S)	SE(N/W), NE(W/S)
11	SE(N/W), SN(W/E)	ES(N/W), NS(W/E)
12	NE(W/S), NS(W/E)	EN(W/S), SN(W/E)

The analysis of symbolic representations (Fig. 4) has shown that only four pairs of three layout variants make sense from a design standpoint, and those are listed in Table 2. The other combinations cannot be built as their layout variants do not share a common input or output shaft. The sets in table 2 are marked **blue** for shared input and **red** for shared output.

Table 2. Feasible combinations of three different layout variants within the same scheme for multivariant PGTs

No.	Combination	Kinematic inverse
1	WE(N/S), WS(N/E), WN(S/E)	EW(N/S), SW(N/E), NW(S/E)
2	EW(N/S), ES(N/E), EN(W/S)	WE(N/S), SE(S/E), NE(W/S)
3	SE(N/W), SN(W/E), SW(N/E)	ES(N/W), NS(W/E), WS(N/E)
4	NE(W/S), NW(S/E), NS(W/E)	EN(W/S), WN(S/E), SN(W/E)

5. KINEMATIC CHARACTERISTICS OF MULTIVARIANT PLANETARY GEAR TRAINS

The operating conditions of all variants of two-carrier compound PGTs with four external shafts have been determined using the transmission ratio functions derived according to the procedure used in Figs. 6 and 8 [6]. This procedure involves determining whether the PGT is operating as a reducer or a multiplier, and whether the input and output shaft rotate in the same direction or not.

This data was used to synthetise the vectorized data on the operating conditions of all theoretically possible two-variant and three-variant PGTs.

The data is vectorized using vectors codified in the norm of AB CD EF GH, where each position has its assigned meaning (Table 3), and each vector position can assume a value increasing from 0 to 9. The data for theoretically possible two-variant PGTs is given in (Table 4), while the data for three-variant PGTs is given in (Table 5). A designer can use these tables to obtain information about the theoretical capabilities of each layout variant quickly and restrict their choices to those variants that can match the required operating conditions.

Table 3. Characterization vector breakdown for multivariant PGTs

Pos.	Combination Kinematic inverse
A	Largest confirmed number of positive transmission ratios
B	Largest confirmed number of negative transmission ratios
C	Largest confirmed number of reduction transmission ratios
D	Largest confirmed number of multiplication transmission ratios
E	Largest confirmed number of positive reduction transmission ratios
F	Largest confirmed number of negative reduction transmission ratios
G	Largest confirmed number of positive multiplication transmission ratios
H	Largest confirmed number of negative multiplication transmission ratios

Table 4. Vectorized operating condition kinematic data for two-variant PGTs

Layout	Variants			
	WE(N/S), WS(N/E)	WE(N/S), WN(S/E)	WE(N/S), SE(N/W)	WE(N/S), NE(W/S)
S11	21 11 01 00	30 11 10 00	21 11 00 01	30 11 00 10
S12	13 20 11 00	22 20 20 00	22 02 00 20	13 02 00 11
S13	22 40 22 00	31 40 31 00	31 40 31 00	40 31 30 10
S14	13 40 13 00	22 40 22 00	22 22 02 20	13 31 03 10
S15	13 40 13 00	31 40 31 00	31 40 31 00	31 31 21 10
S16	13 40 13 00	31 40 31 00	31 40 31 00	31 31 21 10
S33	21 02 00 01	30 02 00 10	30 20 10 00	30 20 10 00
S34	13 22 11 02	22 31 21 01	22 13 01 21	13 22 02 11
S35	13 22 11 02	31 31 30 01	31 31 30 01	31 22 20 11
S36	13 11 10 01	31 30 30 00	31 30 30 00	31 21 20 10
S55	30 02 00 10	30 02 00 10	30 20 10 00	30 20 10 00
S56	40 13 10 30	31 22 11 20	31 22 20 11	40 31 30 10
	WS(N/E), WN(S/E)	WS(N/E), SE(N/W)	WS(N/E), SN(W/E)	WN(S/E), NE(W/S)
S11	11 22 11 00	02 22 01 01	21 31 21 00	20 22 10 10
S12	31 40 31 00	31 22 11 20	31 31 21 10	31 22 20 11
S13	13 40 13 00	13 40 13 00	22 40 22 00	31 31 21 10
S14	31 40 31 00	31 22 11 20	31 31 21 10	31 31 21 10
S15	22 40 22 00	22 40 22 00	13 31 12 01	40 31 30 10
S16	22 40 22 00	22 40 22 00	13 40 13 00	40 31 30 10
S33	11 04 00 11	11 11 10 01	21 22 20 01	20 22 10 10
S34	31 31 30 01	31 13 10 21	31 22 20 11	31 31 21 10
S35	22 31 21 01	22 31 21 01	13 22 11 02	40 31 30 10
S36	22 21 20 01	22 21 20 01	13 21 11 01	40 31 30 10
S55	20 04 00 20	20 22 10 10	12 04 00 12	20 22 10 10
S56	31 13 01 30	31 13 10 21	22 13 01 21	31 31 21 10
	WN(S/E), SN(W/E)	SE(N/W), NE(W/S)	SE(N/W), SN(W/E)	NE(W/S), SN(W/E)
S11	30 31 30 00	11 22 00 11	21 31 20 01	30 31 20 10
S12	40 31 30 10	31 04 00 31	40 13 10 30	31 13 10 21
S13	31 40 31 00	31 31 21 10	31 40 31 00	40 31 30 10
S14	40 31 30 10	31 13 01 30	40 13 10 30	31 22 11 20
S15	31 31 30 01	40 31 30 10	31 31 30 01	31 22 20 11
S16	31 40 31 00	40 31 30 10	31 40 31 00	31 31 21 10
S33	30 22 20 10	20 40 20 00	30 40 30 00	30 40 30 00
S34	40 31 30 10	31 13 01 30	40 13 10 30	31 22 11 20
S35	31 31 30 01	40 31 30 10	31 31 30 01	31 22 20 11
S36	31 40 31 00	40 31 30 10	31 40 31 00	31 31 21 10
S55	12 04 00 12	20 40 20 00	12 22 10 02	12 22 10 02
S56	13 22 02 11	31 31 30 01	13 22 11 02	22 31 21 01

The concepts of “confirmed numbers” will be explained here. In most layout variants, the direction of rotation of the output shaft in relation to the input shaft and whether the PGT

will operate as a reducer or a multiplier does not depend on the ideal torque ratios of the component PGTs but exclusively on the linkages between the PGT elements. In such cases, the

vectorization provides complete data on the operating regime. However, some variants exist on which the operating regime also depends on

the component PGT torque ratios, and such variants are excluded from Tables 4 and 5.

Table 5. Vectorized operating condition kinematic data for three-variant PGTs

Layout	Variants			
	WE(N/S), WS(N/E), WN(S/E)	WE(N/S), SE(S/E), NE(W/S)	WS(N/E), SE(N/W), SN(W/E)	WN(S/E), NE(W/S), SN(W/E)
S11	31 22 11 00	31 22 00 11	22 42 21 01	40 42 30 10
S12	33 40 31 00	33 04 00 31	51 33 21 30	51 33 30 21
S13	33 60 33 00	51 51 41 10	33 60 33 00	51 51 41 10
S14	33 60 33 00	33 33 03 30	51 33 21 30	51 42 31 20
S15	33 60 33 00	51 51 41 10	33 51 32 01	51 42 40 11
S16	33 60 33 00	51 51 41 10	33 60 33 00	51 51 41 10
S33	31 04 00 11	40 40 20 00	31 42 30 01	40 42 30 10
S34	33 42 31 02	33 24 02 31	51 24 20 31	51 42 31 20
S35	33 42 31 02	51 42 40 11	33 42 31 02	51 42 40 11
S36	33 31 30 01	51 41 40 10	33 41 31 01	51 51 41 10
S55	40 04 00 20	40 40 20 00	22 24 10 12	22 24 10 12
S56	51 24 11 40	51 42 40 11	33 24 11 22	33 42 22 11

6. METHODICS FOR THE SYNTHESIS OF MULTIVARIANT PLANETARY GEAR TRAINS

The transmission ratio functions of the obtainable two-speed variants are the basis for the kinematic synthesis of multivariant PGTs, since the PGTs are essentially combinations of two or three layout variants. The relations of the transmission ratios i to the ideal torque ratios t_I and t_{II} for each transmission ratio of every variant are given in [6]. A graphical representation of the transmission ratio functions of a two-variant PGT will provide four stacked surfaces that share a common domain with the independent variables t_I and t_{II} . The graphical representation of the transmission ratios that can be obtained from a two-variant PGT that can provide four transmission ratios is provided in Figure 10 (left). The intervals of the required transmission ratios I_1, I_2, I_3 and I_4 which satisfy the condition (7) are shown on the z-axis in Figure 10 (right).

$$i_1 \in I_1, i_2 \in I_2, i_3 \in I_3, i_4 \in I_4 \quad (7)$$

A software program was developed that determines the values of the transmission ratio functions for every possible combination of ideal

torque ratios and verifies whether the value falls within the demanded ranges of ratios I_1, I_2, I_3 and I_4 . If such pairs of ideal torque ratios exist, the software lists them as solutions. The solutions are then evaluated according to additional relevant criteria, i.e., diameter of component PGTs, equivalent efficiency ratio etc. [26-28].

A three-speed multivariant PGT will be synthesised to demonstrate operation of the program. The test data is presented in Table 6.

Table 6. Test data for the synthesis of a three-speed multivariant PGT

Data	Value
Transmission ratio 1	$2,4 \leq i_{k1} \leq 2,6$
Transmission ratio 2	$1,35 \leq i_{k2} \leq 1,45$
Transmission ratio 3	$-2,7 \leq i_{k3} \leq -2,6$
Sun gear tooth number	$z_{1I} = z_{1II} = 18$
Input torque	$T_A = 50 \text{ Nm}$

The software program has found six combinations (Table 7) that provide two solutions each in the required intervals. In addition to the data on ideal torque ratios, transmission ratios and ring gear pitch circle diameters, the program has determined the exact variant and brake to be used. If the criteria

of the minimal outside diameter of the component PGTs is applied, the S36WN(S/E)-

SN(W/E) gear train with $t_I = 2,5$ and $t_{II} = 2,6667$ presents an optimal solution.

Table 7. Valid solution combinations for three-speed PGT synthesis. The optimal solution is in light blue.

Scheme LV	t_I	t_{II}	i_{k1}	i_{k2}	i_{k3}	z_{3I}	z_{3II}	d_{3I} [mm]	d_{3II} [mm]
S12 EN(W/S)- SN(W/E)	2,3333	2,6667	2,571 EN(W)	1,428 SN(E)	-2,666 EN(S)	42	48	94,5	96
S12 EN(W/S)- SN(W/E)	2,5	2,6667	2,466 EN(W)	1,4 SN(E)	-2,666 EN(S)	45	48	101,25	96
S12 WS(N/E)- NS(W/E)	2,6667	2,3333	2,571 WS(E)	1,428 NS(E)	-2,666 WS(N)	48	42	96	94,5
S12 WS(N/E)- NS(W/E)	2,6667	2,5	2,466 WS(E)	1,4 NS(E)	-2,666 WS(N)	48	45	96	101,25
S36 WN(S/E)- SN(W/E)	2,3333	2,6667	2,571 WN(E)	1,428 WN(S)	-2,666 SN(E)	42	48	63	96
S36 WN(S/E)- SN(W/E)	2,5	2,6667	2,466 WN(E)	1,4 WN(S)	-2,666 SN(E)	45	48	61,87	96

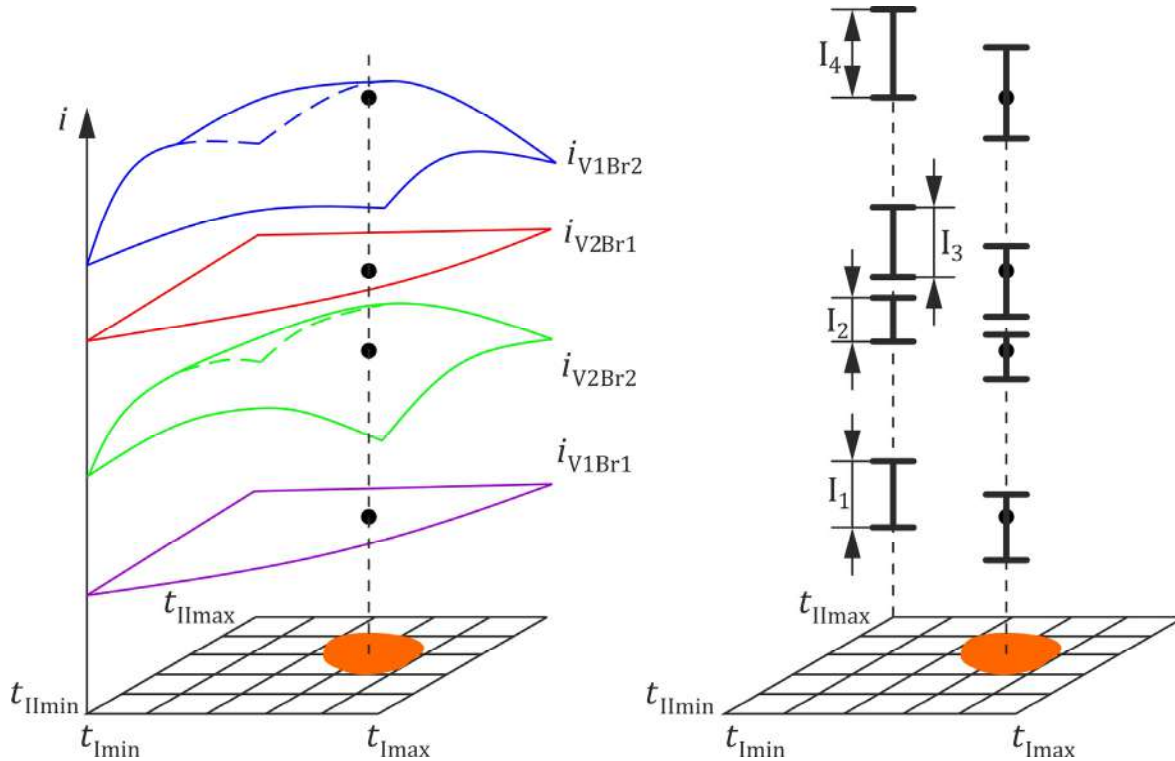


Fig. 10. Domain search procedure for detecting the combination of variants that fulfils the required transmission ratio intervals. Left: obtainable intervals. Right: overlap of the required transmission ratio intervals and layout variant capabilities

The scheme and layout variant data supplied by the program was used to create the structural and kinematic scheme in Figure 11. It must be

said that the most convenient procedure is to create the structural scheme first, and then proceed to create the kinematic scheme [21-25].

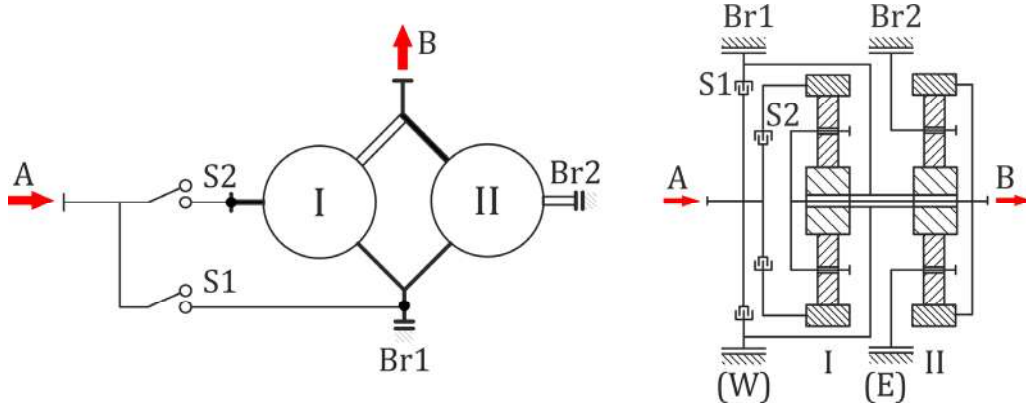


Fig. 11. Structural (left) and kinematic scheme (right) of the two-variant PGT S36WN(S/E)-SN(W/E)

7. CALCULATION OF THE LOAD FUNCTIONS OF THE PLANETARY GEAR TRAIN ELEMENTS

The torques acting on the basic elements of the PGT can be determined by separately analysing each component PGT. The procedure begins by selecting a convenient sun gear and assigning it the torque of +1. The torques acting on the other elements are then easily calculated by means of equations (2) and (3).

After the analysis of a component PGT is complete, the values are transferred to connecting shafts while taking care that the torque receives an opposite sign when entering the next planetary gearset. For example, if two planetary sets are joined by their sun gears, the torque on the second sun gear will be equal to that on the first gear, but of opposite sign.

In case there are several shafts linked at one point, it becomes a nodal point, and it is important that the sum of torques at each point equals zero. Furthermore, the torques on the input and output members are equal to the sum of all torques related to the respective gear train member.

After the calculation is complete, the overall transmission ratio is then calculated using the input torque T_A and output torque T_B (8):

$$i = \frac{-T_B}{T_A} \quad (8)$$

When dealing with complex, multi-carrier gear trains the complexity of the calculation depends on the starting point. Sometimes several starts might be needed to avoid situations with two unknowns at nodal points.

For all torques to be expressed as a function of the input torque, every calculated torque must be multiplied with the reciprocal value of the input torque, which is then reduced to one. All further torques are then calculated by multiplying with the input torque.

The torque on any locked element is an external torque, and it can be used as a sanity check for the calculations as the sum of torques across the shafts of any component PGTs must be equal to zero.

7.1 The Simpson gearset

The calculation procedure will be now demonstrated on the example of a three-speed, two-variant PGT commonly called the "Simpson gearset".

The gearset is well known in automatic transmission design since the 1950s and the abandonment of split-torque transmissions with the introduction of torque converter lockup clutches.

Essentially it is a S36WN(S/E)-S36SN(W/E) gear train, however the S36SN(W) variant is not possible due to kinematics limiting brake placement.

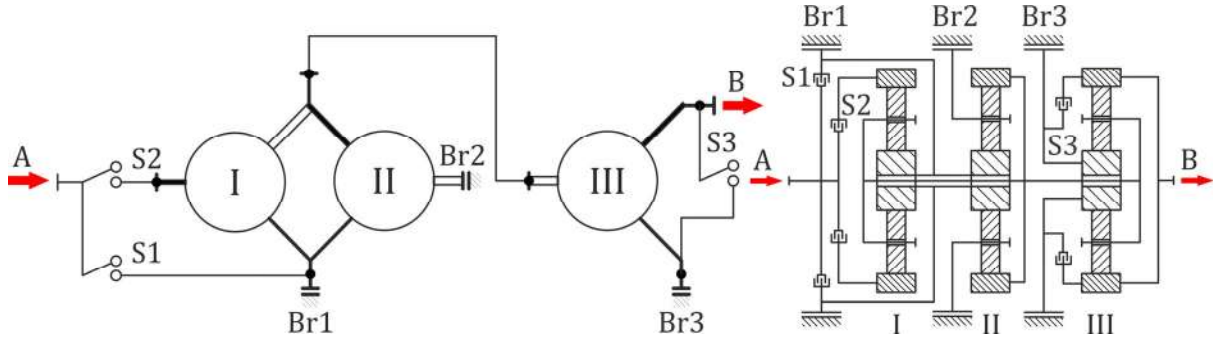


Fig. 12. Structural (left) and kinematic scheme (right) of the Simpson gearset, expanded to 4 “forward” and one “reverse” gear

The transmission in this form provides two gears in which the input and output shafts rotate in the same direction, and one gear in which the output shaft rotates in the opposite direction.

In automotive applications, a direct drive gear is obtained by connecting the W and S shafts together, while an extra multiplication gear was achieved by adding a simple output gearset (Fig. 12), which can be easily calculated separate from the main gear train. It should be also mentioned that there are two valid placements for gearset 3, either before gearset I or after gearset II. The position behind gearset II is most common, however more recent designs place the gearset before gearset I. This option has the potential to be used as a pre-gearbox to extract six forward and two reverse gears, however the authors are unaware of such a solution being deployed.

The highest transmission ratio is achieved in layout variant S36WN(E). This is achieved by closing clutch S1 and applying brake Br2 (Fig. 13):

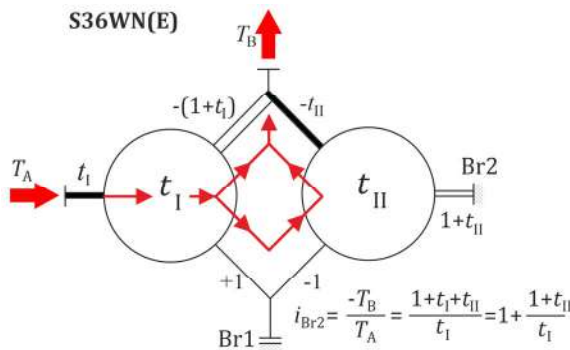


Fig. 13. Kinematic scheme of the gearset shifted into S36WN(E) mode

In this case, the power enters through the ring gear of PGT I and then splits over to PGT II before

re-joining at shaft N through planet carrier I and ring gear II.

The transmission ratio is given by equation (9):

$$i_{Br2} = -\frac{T_B}{T_A} = \frac{1+t_I+t_{II}}{t_I} = 1 + \frac{1+t_{II}}{t_I} \quad (9)$$

The second highest transmission ratio is achieved by layout variant S36WN(S), which is achieved by closing clutch S2 and applying brake Br1 (Fig. 14):

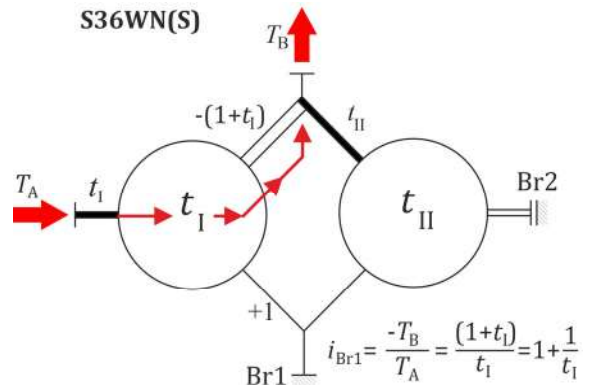


Fig. 14. Kinematic scheme of the gearset shifted into S36WN(S) mode

In this case, power is transmitted through ring gear I to the planet carrier I with sun gear I locked. The gearset effectively operates in single-PGT mode.

The transmission ratio is given by equation (10):

$$i_{Br1} = -\frac{T_B}{T_A} = \frac{1+t_I}{t_I} = 1 + \frac{1}{t_I} \quad (10)$$

The gear train has a transmission ratio in which the output shaft rotates in the opposite direction

to the input shaft. This is achieved with layout variant S36SN(W) (Fig. 15):

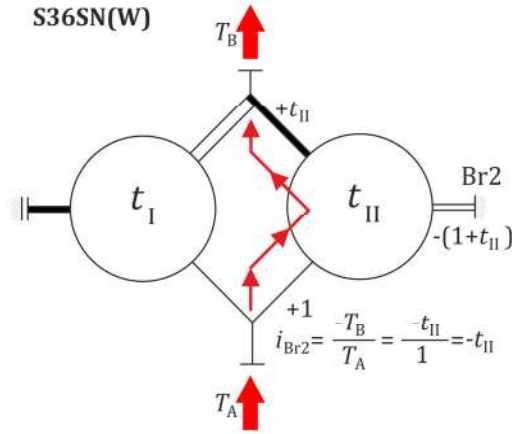


Fig. 15. Kinematic scheme of the gearset shifted into S36SN(W) mode

For this variant, clutch S1 is engaged and brake Br2 is on. Power is transmitted from sun gear II to ring gear II with carrier II held stationary. This causes the output element to rotate in the direction opposite to the input shaft.

The transmission ratio is given by equation (11):

$$i_{Br2} = -\frac{T_B}{T_A} = \frac{-t_{II}}{1} = -t_{II} \quad (11)$$

The gearset is capable of another transmission ratio as layout S36SN(E) (Fig 16.):

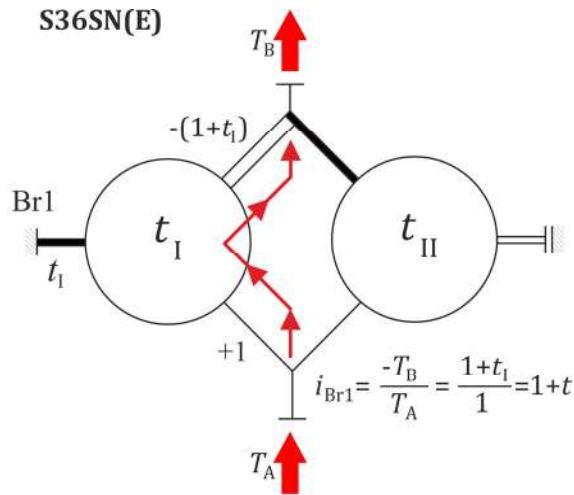


Fig. 16. Kinematic scheme of the gearset shifted into S36SN(E) mode

In this mode, the power enters the gearset through external shaft S, enters PGT I via the sun

gear, and exits PGT I to external shaft N via planet carrier I.

The transmission ratio for this case given by equation (12):

$$i_{Br1} = -\frac{T_B}{T_A} = \frac{1+t_{II}}{1} = 1+t_{II} \quad (12)$$

However, this transmission ratio is not kinematically practicable as it renders impossible the installation of clutch S1 (Fig. 12). The gear train has a direct drive mode that is achieved by closing simultaneously the clutches S2 and S1 with both brakes released. In this mode the ring and sun gears of PGT I are locked together and cause the whole gear train to rotate in unison.

PGT III is present only in newer iterations of the gearbox. It was added to provide a transmission ratio in which the output shaft would rotate faster than the input shaft.

The transmission ratio for this stage is given by equation (13):

$$i_3 = -\frac{T_B}{T_A} = \frac{t_{III}}{1+t_{III}} \quad (13)$$

The gear train is normally held locked by clutch S3, connecting the sun and ring gears, however when engaging fourth gear this clutch is released together with brake Br3 engaging to lock the sun gear III, increasing the speed of the output shaft. To conclude, even if the original concept is somewhat dated, the transmission is robust and proven to a point that a variant of the Simpson gearset combined with the 4th gear PGT was developed for Porsche as a the ZF4HP22HL automatic with manual control (Tiptronic) gearbox [29-30].

7.2 The ZF HP500 gearbox family

The ZF HP500 family of gearboxes is interesting for study as it is a family of gearboxes built for mid to high power applications in city and highway buses.

The gear train is clearly designed for high loads, as most of the shifting is done by three or four brakes depending on the model, and two or three clutches. The base model extracts six forward gears and one reverse gear from a three-PGT gearset (Fig 17).

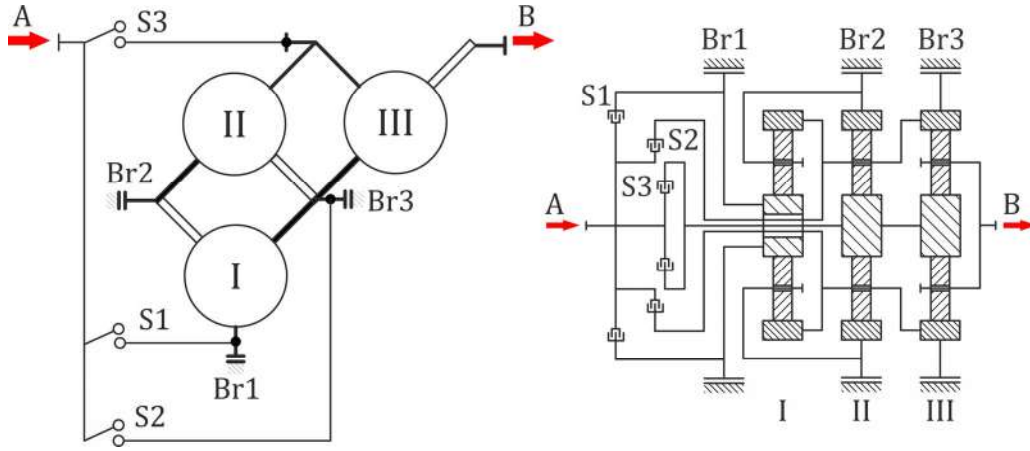


Fig. 17. Structural (left) and kinematic scheme (right) of the three-carrier, six-speed ZF 6HP500 gearbox

The gearbox is obviously built for reliability as most interconnections are made through planet carriers and ring gears, with sun gears II and III sharing a common shaft.

The same gearbox exists with four and five gears. For five gears, sixth gear is disabled in the control system, while the clutch connecting the input shaft to rings I and III and carrier 2 is deleted in the four-gear version (Fig. 18):

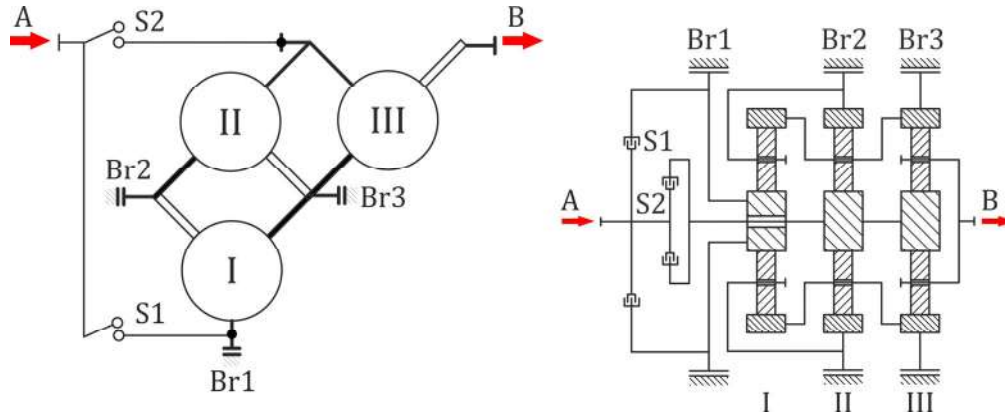


Fig. 18. Structural (left) and kinematic scheme (right) of the three-carrier, six-speed ZF 4HP500 gearbox

First gear is achieved by engaging clutch S3 and brake Br3, effectively engaging the gearbox in single carrier mode over PGT III, and obtaining a transmission ratio of (14):

$$i_1 = 1 + t_{III} \quad (14)$$

Second gear engages clutch S3 and brake Br2 to send PGTs II and III into two-carrier mode as S36SE(W). The gear ratio equals (15):

$$i_2 = \frac{1 + t_{II} + t_{II}t_{III} + t_{III}}{1 + t_{II} + t_{III}} \quad (15)$$

For third gear, clutch S3 is engaged with brake Br1 and PGTs I, II and III operate in three-carrier mode. The gear ratio equals (16):

$$i_3 = \frac{1 + t_I + t_{II} + t_{III} + t_I t_{III} + t_{II} t_{III}}{1 + t_I + t_{II} + t_{III}} \quad (16)$$

Fourth gear activates clutches S3 and S2 at the same time, resulting in PGT III being locked in unison, providing direct drive with $i_4 = 1$. Fifth gear returns to three-carrier mode, with brake Br1 and clutch S2 engaged (17):

$$i_5 = \frac{t_{II} + t_{III} + t_I t_{III}}{t_I t_{II} - t_{II} - 1 - t_I + t_{III} + t_I t_{III}} \quad (17)$$

Sixth gear is achieved by activating brake Br2 with clutch S2 at the same time, sending PGTs II and III into two-carrier mode as S36NE(W). The gear ratio equals (18):

$$i_6 = \frac{1 + t_{III}}{1 + t_{II} + t_{III}} \quad (18)$$

Reverse is obtained by activating brake Br3 and clutch S1. This causes PGT I, II and III to operate as three serially connected simple PGTs. Carrier

I outputs to ring II, carrier II is locked, which causes sun II to turn sun III opposite to sun I. The gear ratio equals (19):

$$i_R = -\frac{1 + t_I + t_{III} + t_I t_{III}}{t_{II}} \quad (19)$$

The gearbox is also manufactured in a high-capacity variant with four gearsets and six forward gears. This variant has an extra gearset IV with its carrier mated to carrier III and an extra brake. This gearset IV is used as first gear, and the gears from 1 to 5 of a standard gearbox become gears 2 to 6 in the four gearset model (Fig. 19):

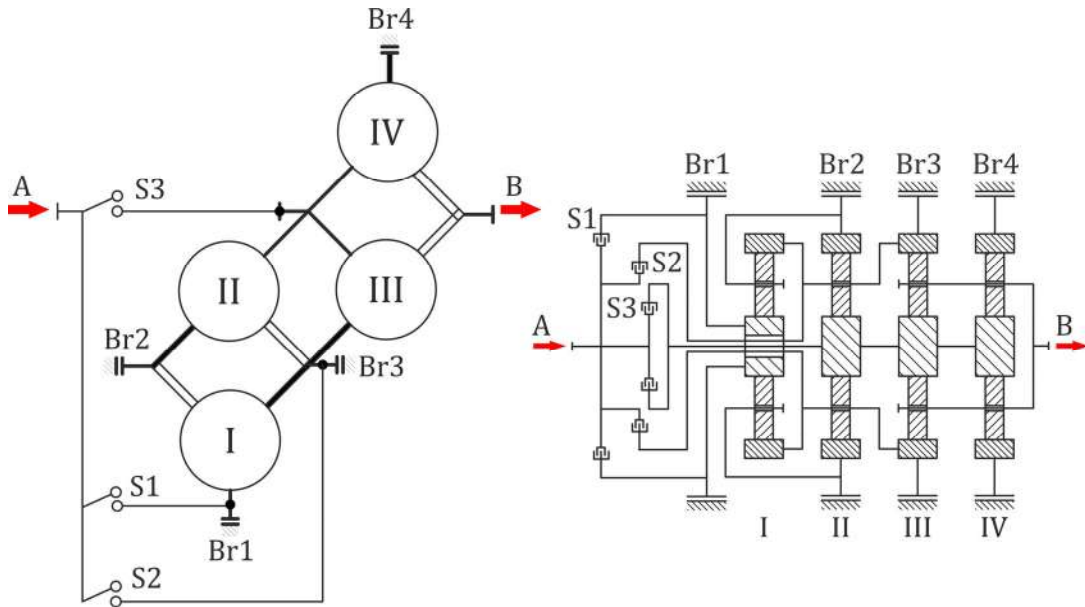


Fig. 19. Structural (left) and kinematic scheme (right) of the three-carrier, six-speed ZF 6HP500 gearbox

The first gear calculation in this case is numerically equal to calculation for the three-gearset variant (20):

$$i_1 = 1 + t_{IV} \quad (20)$$

It is interesting that this gearset is capable of seven gears, but the seventh gear remains disabled in the control unit.

7.3 The ZF 8HP gearbox family

The ZF 8HP family of gearboxes is interesting as a contemporary gearbox family for mid to high powered road applications and has recently been updated for mild hybrid applications using

a “pancake” motor generator bolted to the engine flywheel.

The 8HP family of gearboxes represents a common trend in planetary gearbox design that is characterized by the abandonment of Lepelettier and Ravigneaux sets due to the high torque outputs of electrically assisted internal combustion engines.

The 8HP family of gearboxes is characterized by four component gearsets, of which I and II have interconnected suns, ring II is permanently connected to sun II, sun III is permanently connected to sun IV, and carrier I is permanently connected to ring IV. There are two brakes, Br1 acting on sun I and II, and brake Br2 acting on ring I. Carrier II is permanently connected to the input shaft, while clutch S3 connects the input

shaft to the link between ring III and sun IV. This link is connected to sun III and ring II by clutch S1. Finally, clutch S2 connects planet carrier III to planet carrier IV. It should be said that most of

the shifting is done by clutches, unlike commercial vehicle transmissions where most of the shifting is done by brakes. The structural and kinematic schemes may be seen in Figure 20.

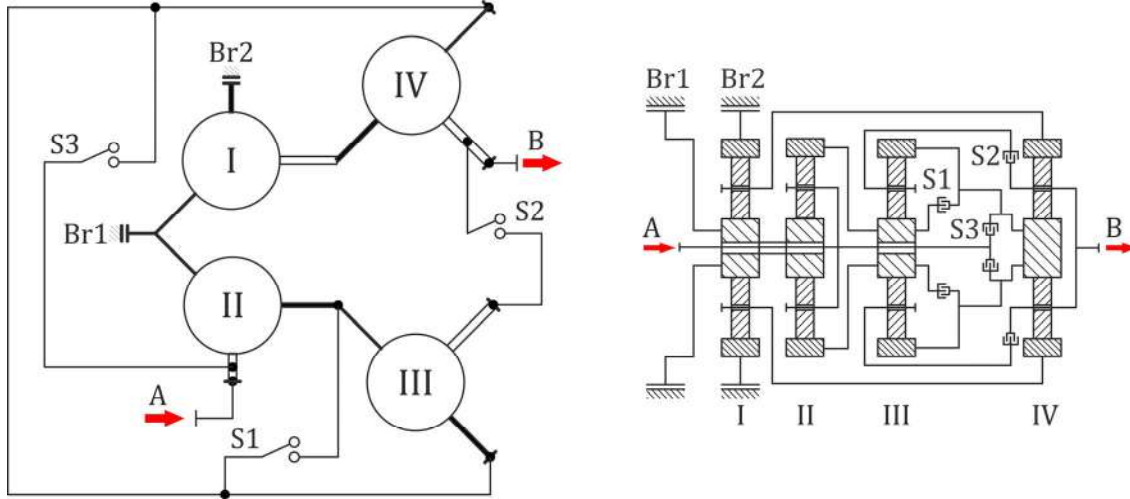


Fig. 20. Structural (left) and kinematic scheme (right) of the four-carrier, eight-speed ZF 8HP70 gearbox

First gear is achieved by engaging brakes Br 1 and Br2, to lock ring IV, while clutch S3 connects sun gear IV to the input shaft, effectively engaging the gearbox in single carrier mode over PGT IV, and obtaining a transmission ratio of (21):

$$i_1 = 1 + t_{IV} \quad (21)$$

Second gear engages brakes Br1 and Br 2 to lock sun II and ring gear IV. Input is via carrier II to ring II, and clutch S1 completes the connection to the sun gear IV. The PGT is effectively a combination of two linearly joined PGTs, and the gear ratio equals (22):

$$i_2 = \frac{t_{II}(1 + t_{IV})}{1 + t_{II}} \quad (22)$$

In third gear, brake Br2 is engaged stopping ring gear I. Clutch S3 connects sun gear IV to the input shaft, while clutches S1 connects ring gear II to the input shaft, causing PGT 2 to turn like a block. This in turn causes PGTs I and IV to operate in two-carrier mode as S36SE(W). The gear ratio equals (23):

$$i_2 = \frac{1 + t_I + t_I t_{IV} + t_{IV}}{1 + t_I + t_{IV}} \quad (23)$$

In fourth gear, brake Br2 holds ring gear I, while the application of clutches S1 and S2 causes gearsets III and IV to rotate like a block, while also connecting carrier I to ring gear II. Input is through carrier II, and there is a constant connection between suns I and II. This in turn causes PGTs I and II to operate in two-carrier mode as S36EN(W). The gear ratio equals (23):

$$i_4 = \frac{1 + t_I + t_{II}}{1 + t_{II}} \quad (23)$$

When fifth gear is engaged, brake Br2 locks ring gear I. Clutch S3 connects sun gear IV and ring gear III to the input shaft, and clutch S2 connects carrier III to carrier IV. Carrier II then drives the sun gears II and I which in turn drive carrier I, operating the gear train in true four-carrier mode. The gear ratio equals (24):

$$i_5 = \frac{1 + t_{IV} + t_{II} t_{IV} (1 + t_{III})}{1 + t_I + t_{IV} (1 + t_{III} (1 + t_{II}))} \quad (24)$$

In sixth gear, clutches S1, S2 and S3 engage to connect PGTs III and IV as a block to the input shaft. This results in the PGT being locked in direct drive with $i_6 = 1$.

For seventh gear, brake Br1 locks sun gears I and II, while clutch S3 connects ring gear III to the

input shaft. Input is through carrier II which drives ring gear II and in turn sun gear III. Output is through gearset IV which rotates as a block with carrier III. This results in gearsets II and III operating as a two-carrier train S16NE(W). The gear ratio equals (25):

$$i_7 = \frac{t_{II}(1+t_{III})}{t_{II}(1+t_{III})+1} \quad (25)$$

Eighth gear is achieved with Br1 holding sun gears I and II, with power flow from carrier II to ring II. Clutches S1 and S2 engage to cause PGTs III and IV to rotate in unison with ring gear II. The transmission ratio equals (26):

$$i_8 = \frac{t_{II}}{1+t_{II}} \quad (26)$$

Reverse is obtained by activating brakes Br1 and Br2. to hold down sun gears I and II. Clutch S2 engages to connect ring gear III to the output shaft, causing a reversal of rotation. Ring gear III is connected to sun IV, driving PGT IV in the opposite direction of the input shaft. Analysis shows that in this configuration, the gear train is PGT II operating as a carrier to ring multiplier connected to trains III and IV operating as two-carrier train S13WN(E). The gear ratio equals (27):

$$i_R = \frac{-t_I t_{III}(1+t_{IV})+t_{II}(1+t_{III})}{1+t_{II}} \quad (27)$$

8. CONCLUSION

This paper deals with the calculation procedures for the calculation of two-carrier, two-variant switching PGTs. These PGTs enable the creation of gearboxes with not more than four transmission ratios plus direct drive by means of a two-carrier gear train. Extended analysis of the properties of two and three variant trains has been performed, enabling this procedure to be extended to three-variant PGTs providing a maximum of six transmission ratios plus direct drive.

As there is a lot of PGTs fulfilling these general characteristics, the design of PGTs requires methodical approach or software support to avoid selecting a suboptimal solution.

The kinematic characteristics of multivariant planetary gear trains are thoroughly analysed, and a procedure for their classification is proposed, together with the methods for planetary gear synthesis. As this procedure covers the operating regimes of every gear drive, this enables the designer to select only the variants that fulfil the application demands.

Experience has shown that it is best practice to create kinematic schemes from structural symbols instead of attempting to assemble the gear train from zero.

The torque method is an important tool in these calculations. It has been presented in this paper and thoroughly explained on a Simpson gearset. Furthermore, another two contemporary gearsets have been analysed to illustrate the procedure, the first a heavy-duty commercial gearbox, and the other a somewhat light duty box for hybrid motor vehicles. Both PGTs have been analysed to demonstrate the difference in the design approach and reduced to their actual operating units for every transmission ratio, effectively proving that most gearsets operate in two-carrier mode at maximum in most cases, and that operation with more than three PGTs is generally avoided by designers, most probably due to the complexity of the calculation. pass to multiple shafts only on few occasions. Four-carrier mode is usually restricted to few occasions for gearsets that must extract many transmission ratios from a small number of gearsets.

It can be concluded that the methods presented in this paper are applicable to various gear trains, including those with two and more than two carriers, and the methods for selecting the optimal gear train configurations presented in this paper may be successfully applied in future computer programs.

REFERENCES

- [1] Syzrantsev, V., Syzrantseva, K.: The Arc Teeth Semi-rolled Cylindrical Gear Meshing Geometry, *Acta Polytechnica Hungarica*, Vol. 19, No. 2, 2022, p. 173-192.
- [2] Müller, H. W. (1998). *Die Umlaufgetriebe. 2. Auflage.* (in German) Springer Verlag, Berlin.
- [3] Kudriavtsev, V. N., Kirdyashev, I. N. (1977). *Planetary Gears Handbook.* Mashinostroenie, Leningrad.
- [4] Tkachenko, V. (2003). *Planetary Mechanisms Optimal Design*, (in Russian) HAI, Kharkiv.

- [5] Arnaudov, K., Karaivanov, D.: The torque method used for studying coupled two-carrier planetary gear trains, *Transactions of FAMENA*, Vol. 37, No. 1, 2013, p. 49-61.
- [6] Troha, S.: *Analysis of a planetary change gear train's variants*. (in Croatian). PhD Thesis. Rijeka: Faculty of Engineering – University of Rijeka, 2011.
- [7] Jelaska, D. T. (2012). *Gears and Gear Drives*. Wiley & Sons, Chichester.
- [8] Looman, J. (1996). *Zahnradgetriebe. 3. Auflage*. Springer Verlag, Berlin.
- [9] Troha, S., Vrcan, Ž., Karaivanov, D., Isametova, M. (2020). The Selection of Optimal Reversible Two-speed Planetary Gear Trains for Machine Tool Gearboxes. *Facta Universitatis-Series Mechanical Engineering*, Vol. 18, No. 1, 2020, p. 121 – 134.
- [10] Arnaudov, K., Karaivanov, D. (2019). *Planetary Gear Trains, 1st edition*. CRC Press, Boca Raton.
- [11] Stefanović-Marinović, J., Vrcan, Ž., Troha, S., Milovančević, M.: Optimization of two-speed planetary gearbox with brakes on single shafts, *Reports in Mechanical Engineering*, Vol. 3, No. 1, 2022, p. 94–107.
- [12] Pavlovic, A., Fragassa C.: Geometry optimization by FEM simulation of the automatic changing gear, *Reports in Mechanical Engineering*, Vol. 1, No. 1, 2020, p. 195–205.
- [13] Vrcan, Ž., Stefanović-Marinović, J., Tica, M. & Troha, S. (2022) Research into the Properties of Selected Single Speed Two-Carrier Planetary Gear Trains. *Journal of Applied and Computational Mechanics*, vol, 8 no. 2, p.699-709 DOI:10.22055/JACM.2021.39143.3358.
- [14] Karaivanov, D., Troha, S. (2021). Optimal Selection of the Structural Scheme of Compound Two-Carrier Planetary Gear Trains and their Parameters. Radzevich, S. P. (editor), *Recent Advances in Gearing: Scientific Theory and Applications*, Springer International Publishing, Basel, 2021, p. 339-403.
- [15] Simpson, H. W. (1956). *US Patent 2749775, Planetary transmission for self-propelled vehicle*, Dearborn, Michigan.
- [16] Simpson, H. W. (1959). *US Patent 2873623, Six Speed Transmission*, Dearborn, Michigan.
- [17] Simpson, H. W. (1959). *US Patent 2914967, Planetary transmission*, Dearborn, Michigan.
- [18] Simpson, H. W. (1962). *US Patent 3031901, Twelve speed power shift planetary transmission*, Dearborn, Michigan.
- [19] Kim, W. Y. (2010). *US Patent 7846058 B2, Power train of automatic transmission*, Seoul, Republic of Korea.
- [20] Vrcan, Ž., Troha, S., Stefanović-Marinović, J., Marković, K. Opportunities for the Application of Reversing Planetary Transmissions. *Latin American International Conference on Natural and Applied Sciences-II Proceedings Book* . 2022, Bogota, Colombia. p.462-469.
- [21] Leistner, F., Lörsch, G., Wilhelm, O. (1987). *Umlaufrädergetriebe. 3. Auflage*. (in German), VEB Verlag Technik, Berlin.
- [22] Müller, H. W. (1998). *Die Umlaufgetriebe – Auslegung und vielseitige Anwendungen. 2. Auflage*. Springer-Verlag, Berlin.
- [23] Troha, S., Vrcan, Ž., Stefanović-Marinović, J., Sedak, M. (2023). Comparison of the size and efficiency of a two– carrier planetary gear train and kinematically equivalent planetary gear train. *Acta Technica Corviniensis*, Vol. 17, No. 2, p.13-20.
- [24] Vrcan, Ž., Ivanov, V., Alexandrov, A., Isametova, M. (2023). Size and efficiency-based comparison of kinematically equivalent two-carrier planetary gear trains. *Engineering review* Vol. 42, No. 3, p.17-31. DOI:10.30765/er.1989.
- [25] Tica, M., Vrcan, Ž., Troha, S., Marinković, D. (2023). Reversible Planetary Gearsets Controlled by Two Brakes, for Internal Combustion Railway Vehicle Transmission Applications. *Acta Polytechnica Hungarica*, Vol. 20, No. 1, p. 95-108. DOI:10.12700/APH.20.1.2023.20.7.
- [26] Troha, S., Karaivanov, D., Vrcan, Ž. Analysis of nine-speed planetary change-gears through the torque method. *MATEC Web of Conferences Volume 366 (2022), 8th International BAPT Conference "Power Transmissions 2022"* DOI:10.1051/mateconf/202236601008.
- [27] Troha, S. Vrcan, Ž., Stefanović-Marinović, J., Sedak, M. Comparison of the Size and Efficiency of a Two-carrier Planetary Gear Train and Kinematically Equivalent Planetary Gear Trains. *10th International Scientific Conference - IRMES 2022 Research and Development of Mechanical Elements and Systems PROCEEDINGS* Belgrade, 2022. p. 117-124.
- [28] Stefanović-Marinović, J., Vrcan, Ž., Troha, S., Milovančević, M. (2022) Optimization of two-speed planetary gearbox with brakes on single shafts. *Reports in Mechanical Engineering*, Vol. 3 No. 1, p. 94-107 DOI:10.31181/rme2001280122m.
- [29] Sclater, N. (2011). *Mechanisms and Mechanical Devices Sourcebook, 5th Edition*. McGraw Hill, New York.
- [30] Garrett, T. K., Newton, K., Steeds. (2001). *W. The Motor Vehicle, Thirteenth Edition*. Butterworth-Heinemann, Boston.

*Production and
Computer-Aided Technologies*



Banja Luka
1–2 Jun 2023.

DEMI 2023
**16th International Conference on
Accomplishments in Mechanical and
Industrial Engineering**
www.demi.mf.unibl.org



A post-processor for the five-axis machine MultiProDesk based on inverse kinematic transformation

J. Maletić^a, S. Živanović^b

^a*LOLA Institute, Belgrade, Serbia*

^b*University of Belgrade, Faculty of Mechanical Engineering, Belgrade, Serbia*

Abstract *This paper shows the development of a post-processor for a five-axis table tilting machine. Post-processing software transforms a machining toolpath in CL file into G-code, which is necessary for the machining process in most CNC. The subject of this analysis is the MultiProDesk machine with two rotary axes on the machine table. The kinematic structure of the proposed machine is C'A'Y'OXZ. The machine can be modeled with two kinematic chains, one carrying the workpiece and the other carrying the tool. Equations needed to transform the CL data into the displacement of the machine's axis were derived using the inverse kinematic model. Currently, the machine has a three-axis configuration, and the model was extended using simplified versions of the two rotary axes. The inverse kinematic equations were implemented in a post-processing algorithm in the Matlab software. The calculated data was tested in the form of a G-code on a virtual model of the machine in the Vericut software. The simulated workpiece machined in the virtual surrounding matched the original workpiece used to calculate the toolpath, verifying the developed post-processor for the considered machine.*

Keywords *Post-processor, inverse kinematics, verification, simulation, virtual machine tools*

1. INTRODUCTION

Five-axis machining is widely used today for machining parts with complex surfaces. What differentiates five-axis machining from standard three-axis machining is the addition of two rotational axes, which enables two more degrees of freedom for the machine. The additional rotational axes reduce the set-up time needed for complex parts, as most complex parts can be manufactured using one fixture. Using only one

fixture per manufacturing process eliminates the misalignment of the workpiece during a single operation. Therefore, using five-axis machines in manufacturing complex parts increases accuracy. Multi-axis machining utilizes shorter tools, as it is easier to reach all the workpiece parts. Shorter tools minimize vibrations, which results in a better surface finish of the machined part. Last, the most important advantage of five-axis machines is their ability to machine highly complex surfaces that would not be possible to produce on a three-axis mill. Conventional three-axis machines have three translational axes that are normal to each other. During the machining process, the orientation of the tool does not change, and it is always fixed in the direction of the machine's Z axis. With the addition of two rotational axes, five-axis machines enable the

Corresponding author

Julija Maletić
julija.maletic@li.rs

LOLA Institute
Kneza Višeslava 70a
Belgrade, Serbia

change of the tool's orientation. Consequently, the programming of five-axis machining must be done using CAD/CAM software, as it is more complex than programming a three-axis machine. When creating a machining program using CAM software, the toolpath is first generated as a CL file that needs to be post-processed to obtain a machining program that can be implemented in a machining process.

A CL file is a general machining program containing the tool's position and orientation regarding the workpiece coordinate system, as shown in Fig. 1. The data contained in a CL file cannot be used in a machining process directly, as it has no information about the layout of the axes of the machine. A post-processor is a program designed specifically for a certain machine that translates the CL file into a G-code suited for running on said machine.

Multiple solutions in developing the mathematical model of multi-axis machine kinematics were developed. Lee and She proposed an inverse kinematic model for three typical types of five-axis machines [1]. Later, the kinematics of five-axis machine types were developed based on a similar principle for five-axis machines with nutating head and table configurations [2-4]. The analysis of structural configuration and geometry of possible solutions for multi-axis machine tools was done by Chen in [5]. This paper proposes a method for deriving the kinematic equations for all feasible configurations of multi-axis machine tools based on inverse kinematic transformations using six elementary transformational matrices for translation and rotation. The method of using inverse kinematic transformation for developing post-processing kinematic equations was implemented and verified with experiments on multiple multi-axis machines [6-7].

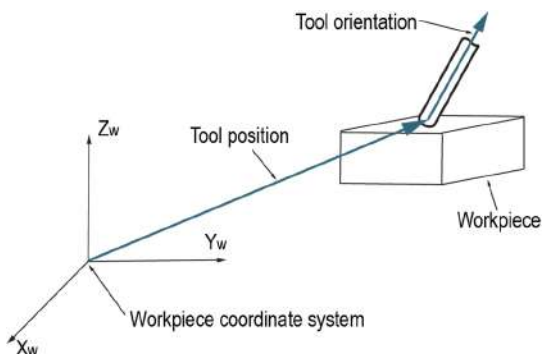


Fig. 1. CL data representation

This paper describes a post-processing method based on inverse kinematic transformation for the machine MultiProDesk [9]. Currently, MultiProDesk is a 3-axis mill with two additional rotary axes in preparation. This paper proposes post-processing software for the five-axis version of the machine. This version of the machine has two rotary axes, A and C, on the table of the machine. A post-processor software, based on the algorithm developed in [8], was developed using the derived kinematic equations. The kinematic model of the MultiProDesk was tested using the Vericut software. The three-axis machine model was augmented with a planned fourth rotary axes A and a simplified version of rotary axes C to test the five-axis kinematic equations.

This paper shows developing the inverse kinematic equations for a five-axis table-tilting machine MultiProDesk. The equations are derived using the inverse kinematic method by modeling the machine as two open kinematic chains. The inverse kinematic equations were implemented into a post-processing algorithm using MatLab software. The post-processing software was tested for a concave surface machining CL file. In order to verify the kinematic model of the machine, a five-axis machining simulation was configured and tested in the Vericut software.

2. KINEMATIC MODELLING OF THE MULTIPRODESK MACHINE

Machine tools can be defined as open kinematic chains of serially connected links with rotational or translational joints. In compliance with this definition, the kinematic equations of a machine tool can be acquired by defining the relative positions of these links in respect of one another. The main objective in deriving these equations is to determine the displacements of the machine's axes to get the desired position and orientation of the tool regarding the workpiece's coordinate system. This kinematic model is obtained by assigning each joint of the machine a coordinate system and using them to define the relative motions between the adjacent joints. By representing each axis of the machine with its coordinate system, the relative motions of the axes can be defined with an elementary transformation matrix, in which a simple translation or rotational transformation is defined. The machine's configuration is

C'A'Y'OXZ, which determines that the Z and X axes drive the tool motions, and the workpiece is moved using the Y, A, and C axes. An illustration of the machine's axes and the necessary transformation matrices is shown in Fig. 2. First, a base coordinate system is defined. This coordinate system will be used as a starting point for the kinematic chains of the workpiece and tool. The position of the base coordinate system is chosen to be at the intersection of the axes of the machine's rotary components with axes matching the direction of the machine tools' axes, shown in Fig. 3. The workpiece kinematic chain is comprised of one translation and two rotational axes.

Each moving element of the machine is assigned a coordinate system. The coordinate systems of the workpiece kinematic chain are $O_{w1}x_{w1}y_{w1}z_{w1}$, $O_{w2}x_{w2}y_{w2}z_{w2}$, and $O_{w3}x_{w3}y_{w3}z_{w3}$, shown in Fig. 4. A transformation matrix is defined between the workpiece coordinates system $O_w x_w y_w z_w$ and the C axes' coordinate system to close the kinematic chain. The first elementary transformation matrix, T_{w1}^0 , is defined between the base coordinate system and the coordinate system attached to the Y axes of the machine.

$$T_{w1}^0 = \begin{bmatrix} 1 & 0 & 0 & x_{w1} \\ 0 & 1 & 0 & Y \\ 0 & 0 & 1 & z_{w1} \\ 0 & 0 & 0 & 1 \end{bmatrix} \quad (1)$$

The transformation matrix displayed in Eq. 1. defines the elementary translation transformation along the Y axes of the machine. Values x_{w1} and z_{w1} represent the constant distances along the X and Z axes of the machine between the base and the first coordinate system in the workpiece kinematic chain.

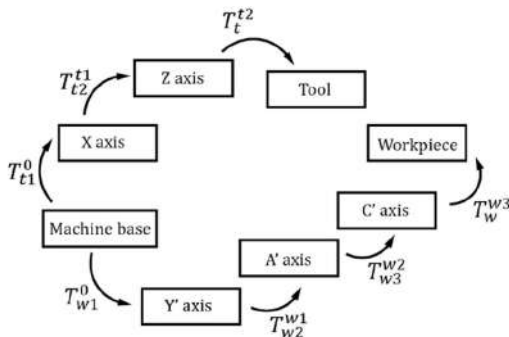


Fig. 2. Schematic diagram of machine tool kinematic chains

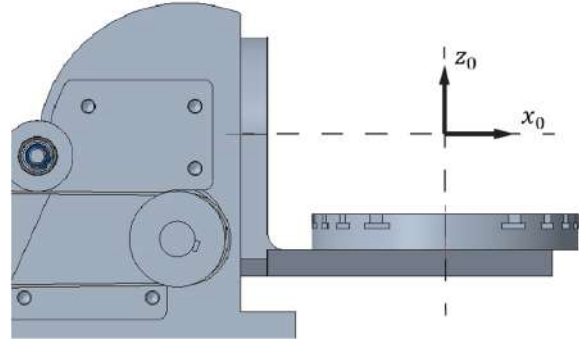


Fig. 3. The position of the base coordinate system

The value Y is the only variable in the first matrix, defining the machine table's movement along the machine's Y axes. The next two axes of the machine are the A and C rotary axes. Their transformation matrices are defined as follows:

$$T_{w2}^1 = \begin{bmatrix} 1 & 0 & 0 & x_{w2} \\ 0 & \cos(A) & -\sin(A) & 0 \\ 0 & \sin(A) & \cos(A) & z_{w2} \\ 0 & 0 & 0 & 1 \end{bmatrix} \quad (2)$$

$$T_{w3}^2 = \begin{bmatrix} \cos(C) & -\sin(C) & 0 & 0 \\ \sin(C) & \cos(C) & 0 & 0 \\ 0 & 0 & 1 & 0 \\ 0 & 0 & 0 & 1 \end{bmatrix} \quad (3)$$

In Eq. 2. and Eq. 3, the variables A and C represent the angles of the machine's rotary axes. Values x_{w2} and z_{w2} represent the constant distance between the coordinate systems $O_{w1}x_{w1}y_{w1}z_{w1}$ and $O_{w2}x_{w2}y_{w2}z_{w2}$ along the X and Z axes of the machine.

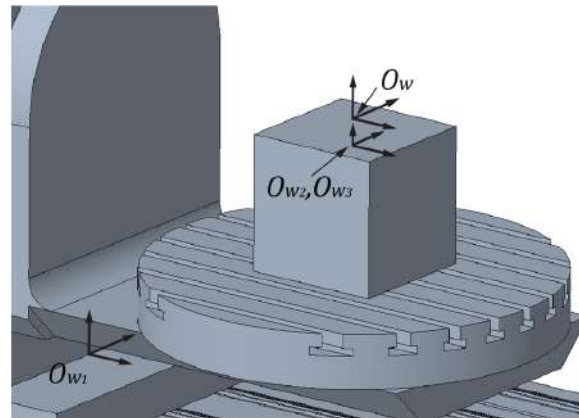


Fig. 4. The position of the coordinate systems of the workpiece kinematic chain

In order to simplify the resulting kinematic equations, coordinate systems $O_{w2}x_{w2}y_{w2}z_{w2}$ and $O_{w3}x_{w3}y_{w3}z_{w3}$ were placed at the intersection of the machine's rotary axes. Last, a transformation matrix defining the workpiece coordinate system regarding the C-axis coordinate system is defined. This matrix has no variable values, as the workpiece is fixed to the machining table.

$$T_w^{w3} = \begin{bmatrix} 1 & 0 & 0 & x_w \\ 0 & 1 & 0 & y_w \\ 0 & 0 & 1 & z_w \\ 0 & 0 & 0 & 1 \end{bmatrix} \quad (4)$$

The second kinematic chain contained in this machine is the tool kinematic chain. The coordinate systems of the tool kinematic chain are shown in Fig. 5. The tool kinematic chain comprises the X and Z axes, so modeling the tool kinematic chain begins with defining the transformation matrix (T_{t1}^0) between the machine's X axis and the base coordinate system.

$$T_{t1}^0 = \begin{bmatrix} 1 & 0 & 0 & X \\ 0 & 1 & 0 & y_{t1} \\ 0 & 0 & 1 & z_{t1} \\ 0 & 0 & 0 & 1 \end{bmatrix} \quad (5)$$

In Eq. 4. the variable X represents the necessary motions of the machine's X axes. Next, the Z-axis coordinate system is defined regarding the X-axis coordinate system. The defined transformation matrix in Eq. 5 contains the constant distance values between the coordinate systems along the machine's X and Y axes.

$$T_{t2}^{t1} = \begin{bmatrix} 1 & 0 & 0 & x_{t2} \\ 0 & 1 & 0 & y_{t2} \\ 0 & 0 & 1 & Z - z_{t1} - H_t \\ 0 & 0 & 0 & 1 \end{bmatrix} \quad (6)$$

The last coordinate system that is defined for the kinematic model of the 5-axis MultiProDesk machine is the tool coordinate system $O_t x_t y_t z_t$. The last transformation matrix is an elementary translation matrix containing the tool length correction.

$$T_t^{t2} = \begin{bmatrix} 1 & 0 & 0 & 0 \\ 0 & 1 & 0 & 0 \\ 0 & 0 & 1 & H_t \\ 0 & 0 & 0 & 1 \end{bmatrix} \quad (7)$$

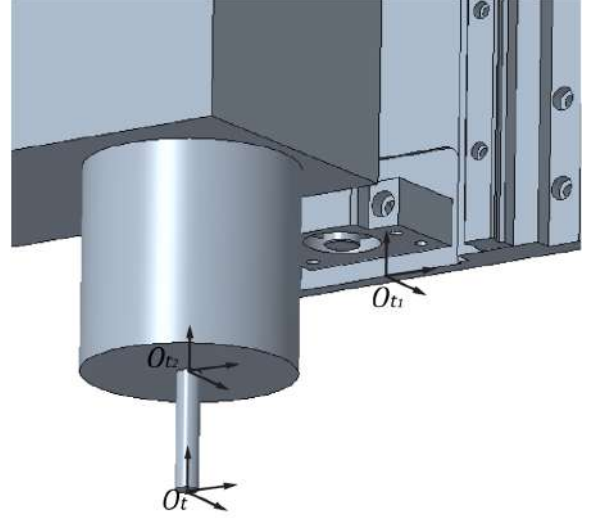


Fig. 5. The position of the coordinate systems of the tool kinematic chain

As previously stated, the CL file contains information about the position and orientation of the tool coordinate system regarding the workpiece coordinate system. This dependence can also be defined as a transformation matrix containing the CL data - T_t^w . The position and orientation of the tool tip vector regarding the base coordinate system can be obtained in two ways, either using the workpiece kinematic chain or the tool kinematic chain, presented in the following equations:

$$r_t^0 = T_{w1}^0 \cdot T_{w2}^{w1} \cdot T_{w3}^{w2} \cdot T_w^{w3} \cdot T_t^w \quad (8)$$

$$r_t^0 = T_{t1}^0 \cdot T_{t2}^{t1} \cdot T_t^{t2} \quad (9)$$

These equations are equivalent and can be presented in the following way:

$$T_{w1}^0 \cdot T_{w2}^{w1} \cdot T_{w3}^{w2} \cdot T_w^{w3} \cdot T_t^w = T_{t1}^0 \cdot T_{t2}^{t1} \cdot T_t^{t2} \quad (10)$$

Eq. 9. can be transformed to get the T_t^w matrix as a function of the elementary transformation matrices previously defined, shown in Eq. 10.

$$T_t^w = (T_w^{w3})^{-1} \cdot (T_{w3}^{w2})^{-1} \cdot (T_{w2}^{w1})^{-1} \cdot (T_{w1}^0)^{-1} \cdot T_{t1}^0 \cdot T_{t2}^{t1} \cdot T_t^{t2} \quad (11)$$

The T_t^w matrix contains the CL data, and the elementary transformation matrices contain the length and angles of the machine's axis motions. Using Eq. 10, the machine axis variables X, Y, Z, A, and C can be defined as the functions of the CL

data. The resulting matrix transformation T_t^w has the following form:

$$T_t^w = \begin{bmatrix} u_x & v_x & w_x & p_x \\ u_y & v_y & w_y & p_y \\ u_z & v_z & w_z & p_z \\ 0 & 0 & 0 & 1 \end{bmatrix} \quad (12)$$

The resulting matrix describes the tool coordinate system position and orientation regarding the workpiece coordinate system. The third column represents the cosines of the tool coordinate systems, deriving the equations for calculating the necessary angles of the rotational axes.

$$w_x = K_x = \sin(A) \cdot \sin(C) \quad (13)$$

$$w_y = K_y = \sin(A) \cdot \cos(C) \quad (14)$$

$$w_z = K_z = \cos(A) \quad (15)$$

The tool coordinate system position, corrected to compensate for the movements of rotational axes, is defined in the fourth column of the resulting matrix and defines the following equations:

$$p_x = Q_x = a_1 \cos(C) + X \cos(C) + a_2 \sin(A) \sin(C) + (Z - a_3) \sin(A) \sin(C) - Y \cos(A) \sin(C) \quad (16)$$

$$p_y = Q_y = b_1 \sin(C) - X \sin(C) + b_2 \cos(C) \sin(A) + (Z - b_3) \cos(C) \sin(A) - Y \cos(A) \cos(C) \quad (17)$$

$$p_z = Q_z = c_1 \cos(A) + Y \sin(A) + (Z - c_2) - c_3 \quad (18)$$

In the previous equations, a_i, b_i , and c_i ($i = 1..3$) are constant values resulting from the constant distances between the coordinate systems. Solving the system of trigonometric equations, Eq. 13-15 yields the functions of the machine's rotational axes angles in the form:

$$A = \arccos(K_z) \quad (19)$$

$$C = \text{atan2}(K_x, K_y) \quad (20)$$

The necessary lengths of the machine's translation axes movements are derived by solving the system of linear equations 16-18. This process yields the following equations:

$$X = \cos(C) (Q_x - a_1 \cos(C)) - \sin(C) (Q_y - b_1 \sin(C)) - \sin(A) \sin(C) \cos(C) (a_2 - a_3 - b_2 + b_3) + a_1 \cos^2(C) + b_1 \sin^2(C) \quad (21)$$

$$Y = c_3 \sin(A) - \cos(A) (Q_x \sin(C) + Q_y \cos(C)) + \cos(A) \sin(A) (\cos^2(C) (b_2 - b_3 - c_1 + c_2) + \sin^2(C) (a_2 - a_3 + c_1 + c_2)) + \cos(A) \cos(C) \sin(C) (b_1 + a_1) \quad (22)$$

$$Z = \sin(A) (Q_y \cos(C) + Q_x \sin(C)) + c_3 \cos(A) - \cos^2(A) (c_1 - c_2) + \sin^2(A) (\cos^2(C) (b_3 - b_2) + \sin^2(C) (a_3 - a_2)) - \cos(C) \sin(A) \sin(C) (a_1 + b_1) \quad (23)$$

3. POSTPROCESSOR IMPLEMENTATION AND VERIFICATION

Derived functions for calculating the necessary angles and displacements of the machine's axes were implemented into a postprocessing program developed in the MatLab software. The algorithm used for this program is based on the postprocessing program developed in [8]. The CL file and G-code, besides the statements for tool motions, consist of other data needed for a manufacturing process. Since this test aims to verify the inverse kinematic equations, only the necessary data outside the motion statements in the CL file were translated into a G-code. The main algorithm implemented into the postprocessing software consists of an iterative process, where one by one, the sets of data that include to tool's position and orientation from the CL file are read and calculated using Eq. 19-23. First, the current data set is read, then, using Eq. 19 and 20, the necessary angles of the machine's rotary axes are calculated. The lengths of the translation axis movements are computed by implementing the calculated angles into Eq. 21-23 calculated angles of the rotary axes. The transformed data set is written in the G-code syntax into a separate file. Given the tool motions that occur with multi-axis machining, only the linear interpolation G1 is used while constructing the G code.

The G-code generated using the beforementioned equations was tested using the Vercut software, where it is possible to simulate a material removal process based on a G-code program. For the experiment, a workpiece with a concave surface was formed to verify the correct engagement of both rotary axes. The design of the workpiece and writing of the manufacturing program was done in the PTC Creo software. The simulation of the manufacturing based on CL file is shown in Fig. 6.

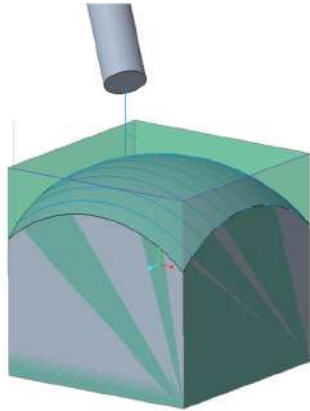


Fig. 6. Toolpath generated using PTC Creo

This experiment can be defined as virtual machining, as the finished virtual workpiece can be saved in a standard CAD format and then compared to the original CAD model of the workpiece. The resulting shape of the workpiece matches the desired starting part, so it can be concluded that the experiment was a success. The simulation of the G-code in the Vericut software is shown in Fig. 7.

4. CONCLUSION

This paper presented a method for developing kinematic equations for a multi-axis post-processor. Software for transforming CL data into G-code was developed for the multi-axis version of the machine MultiProDesk. The proposed machine's mathematical model was developed using the inverse kinematic methodology. Elementary transformational matrices described the motions between the machine's moving segments. The post-processing software was then implemented to transform the CL file for concave workpiece machining. The formed G-code was tested on a virtual model of the machine MultiPro Desk in the Vericut software. The process was determined to be a success, as the workpiece machined during the simulation reflected the geometry of the desired workpiece. The proposed method can be utilized for various types of multi-axis machines. Further research can be extended by developing post-processing software for the four-axis version of the proposed machine or different configurations of the machine's rotary axis.

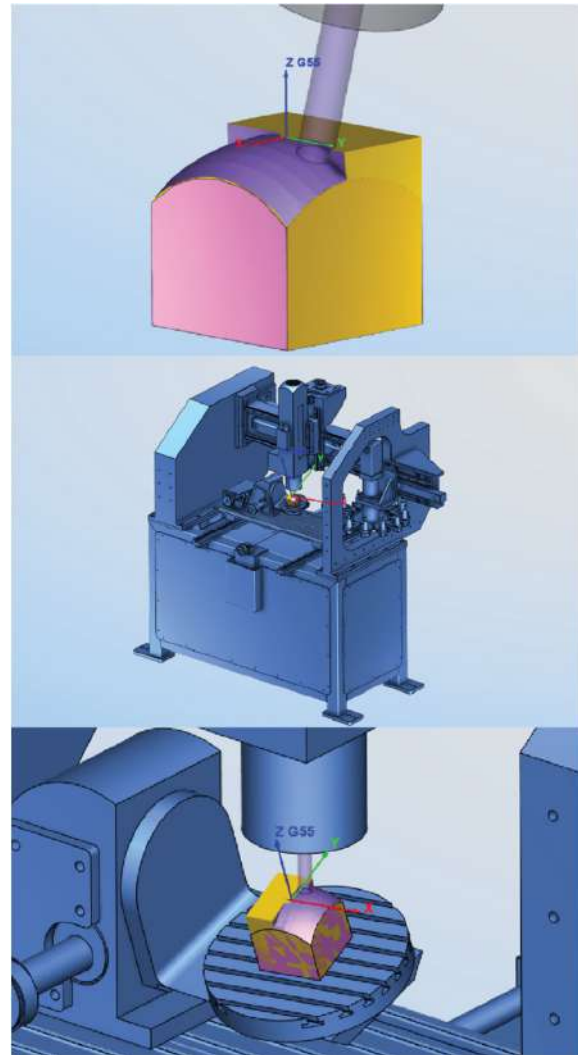


Fig. 7. Testing the G-code in Vericut

Acknowledgement

The presented research was supported by the Ministry of Education, Science and Technological Development of the Republic of Serbia by contract no. 451-03-47/2023-01/200105 dated 3 February 2023 and by contract 451-03-47/2023-01/ 200066 dated 2023.

REFERENCES

- [1] Lee, R.S. and C.H. She, (1997). Developing a postprocessor for three types of five-axis machine tools, *International Journal of Advanced Manufacturing Technology*, vol.13, p. 658–665.
- [2] Jung, Y.H., Lee, D.W., Kim, J.S., Mok, H.S. (2002). NC Post-processor for 5-axis milling machine of table-rotatin/tilting type, *Journal of Material Pocessing*

- technology vol.130-131, p.641-646. DOI: 10.1016/S0924-0136(02)00725-2.
- [3] She, C.H., Chang, C.C (2007). Development of a five-axis post-processor system with a nutating head. *Journal of Materials Processing Technology* vol.187-188(2), p.60-64 DOI: 10.1016/j.jmatprotec.2006.11.101.
- [4] She, C.H, Huan, Z.T, (2008) Postprocessor development of a five-axis machine tool with nutating head and table configurations. *The International Journal of Advanced Manufacturing Technology*, vol. 38(7), p.728-740 DOI: 10.1007/s00170-007-1126-5.
- [5] Chen, F.C. (2001). On the structural configuration synthesis and geometry of machining centres. *Proceedings of the Institution of Mechanical Engineers, Part C: Journal of Mechanical Engineering Science*. 2001, vol. 215(6), p.641-652. DOI: 10.1243/0954406011524018.
- [6] Tran, T.D., (2013) A five-axis CNC machine postprocessor based on inverse kinematic transformation. *Advanced Materials Research* vol. 622-623, pp. 525-530 DOI: 10.4028/www.scientific.net/AMR.622-623.525.
- [7] Chu, M.,A., Nguyen C. V., Nguyen H.M., Bohez, E. LJ., (2020) Transformation of CAM data for 5-axis CNC machine Spinner U5-620. *International Journal of Mechanical Engineering and Robotics Research*, vol.9, no.2, DOI: 10.18178/ijmerr.9.2.233-237.
- [8] Maletić J., Živanović S., (2021) Verification of inverse kinematic equations for a five-axis machine tool with a spindle tilting configuration. *Advanced Technologies & Materials*, vol. 47, no. 1, DOI: 10.24867/ATM-2022-1-006.
- [9] Project Multifunctional rapid prototyping desktop machine – MULTIPRODESK, Project ID 1129, Technology Transfer Program, Innovation Fund, Republic of Serbia, 2023.



Banja Luka
1-2 Jun 2023.

DEMI 2023

16th International Conference on Accomplishments in Mechanical and Industrial Engineering

www.demi.mf.unibl.org



Conceptual design of a novel mechanism with parallel kinematics based on Chebyshev's linkage

Lj. Nešovanović^a, S. Živanović^b

^aLOLA Institute, Belgrade, Serbia

^bUniversity of Belgrade, Faculty of Mechanical Engineering, Belgrade, Serbia

Abstract *The mechanisms with parallel kinematics are applied to a significant extent in today's industry because of the advantage over the mechanisms with serial kinematics. But the size and shape of workspace as the main problem of parallel kinematic machine stands. The proposed mechanism has parallel kinematics and can achieve three degrees of freedom (DOF) with a moving platform. The considered mechanism is actuated with translation actuated joints and has three kinematic chains, which are the connection between the stationary base and the moving platform. The kinematic chains arrangement is set to allow the extension of one of the mechanism's horizontal axis. This means the proposed mechanism has one extended horizontal axis, meaning physical length is the only limitation. This characteristic is very important because of the shape and size of the workspace. The main characteristic of the proposed mechanism is the third kinematic chain, which is based on Chebyshev's mechanism and presents the passive translational rotary joint. Because of the mechanism complexity, it is necessary to simplify the kinematic model for further mathematical analysis.*

Keywords *parallel kinematics, extended axis, Chebyshev's mechanism, simplification*

1. INTRODUCTION

This paper presents the new conceptual design of a parallel kinematics mechanism with one extended axis. The mechanism presented in this paper represents the specific approach to designing a mechanism that can transform the rotary motion of linkages into the rectilinear motion of the desired point. The main idea of this paper is to propose a new concept of a parallel kinematic mechanism that can achieve all advantages of parallel kinematic mechanisms over serial ones and overcome some usual

disadvantages of parallel kinematic mechanisms. The idea of using one extended axis has already been introduced. One of the examples is presented in [1], where are shown advantages of mechanisms with one extended axis. The mechanism proposed in this paper as well as the mechanism presented in [1], have 3DOF. It is important to note that the extended axis presented in the paper [1] is horizontal with actuated translation joints as well as in mechanisms like UraneSX [2]. However, many more mechanisms have extended the vertical axis or have a physical possibility for the vertical axis extension [3, 4]. Straight-Line Generators are the mechanisms that can transform the rotary motion of linkages into the rectilinear motion of the desired point.

Corresponding author

M.Sc., Ljubomir Nešovanović
ljubomir.nesovanovic@li.rs

LOLA Institute
Kneza Višeslava 70a
Belgrade, Serbia

Many mechanisms are created for this purpose, some of which are Watt's linkage, Robert's linkage, Chebyshev's linkage, and Peaucillier invensor, shown in Fig. 1. [5]. Characteristic for mechanisms like Watt's, Robert's, and Chebyshev's linkage is the possibility of forming an approximately straight line [5].

These mechanisms make mistakes in straight-line forming, and only the Peaucillier invensor can form the perfect straight line [5].

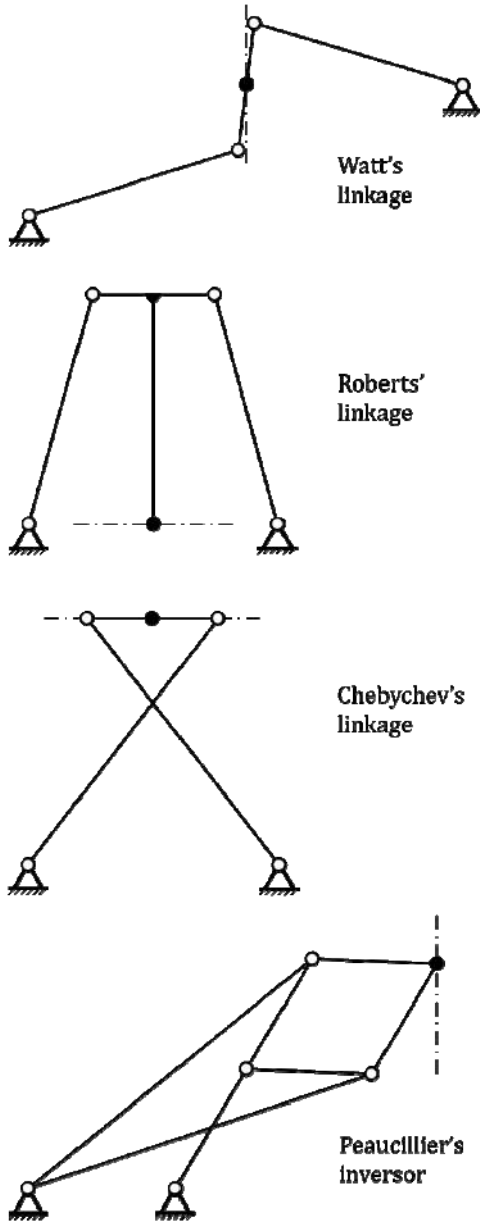


Fig. 1. Straight-line Generators [5]

Because of Peaucillier's invensor complexity and numerous required parts, this mechanism is complex for machining, but it is possible to use it, as shown in [1]. Chebyshev's linkage, the work of Pafnutii Lvovich Chebyshev, presents the best option for usage as part of the mechanism because of its simplicity, rigidity, and potential to form a straight line on one part of the moving trajectory.

Because of its simple design, Chebyshev's mechanism is often used as a part of some complex construction to generate a straight line. Applications of Chebyshev's mechanisms are often connected with vehicle construction as a suspension and wheel mechanism for special vehicles and robots [6, 7]. This paper presents the proposed mechanism's kinematic and simplified model acceptable for further analysis.

2. KINEMATIC STRUCTURE OF THE PROPOSED MECHANISM

The kinematic model of the proposed mechanism is shown in Fig. 2. Considered mechanism has 3DOF, and the moving platform (MP) is connected to a stationary base (SB) with three kinematic chains. The proposed mechanism has three independently actuated translation joints, and each translation joint allows 1 DOF. The motion of the MP results from the independent motion of each kinematic chain.

The proposed mechanism has two similar kinematic chains used for planar movements. The third kinematic chain is based on Chebyshev's mechanism, and it is used to create the tridimensional motion of the MP.

The similar kinematic chains present the four-bar linked mechanisms connected in a shape of a parallelogram. Both four-bar linked mechanisms are connected to the translation joint on the SB on one mechanism side and to the moving platform from another. Every link of the four-bar mechanism is connected with another using the spherical joints, and every spherical joint allows 3 DOF. The four-bar linked mechanisms are arranged to cross each other without collision, and this arrangement is possible by rotating one of the mechanisms for 90°. The proposed arrangement of the four-bar linked mechanisms demands the complex MP shape but makes the proposed mechanism more stable and rigid.

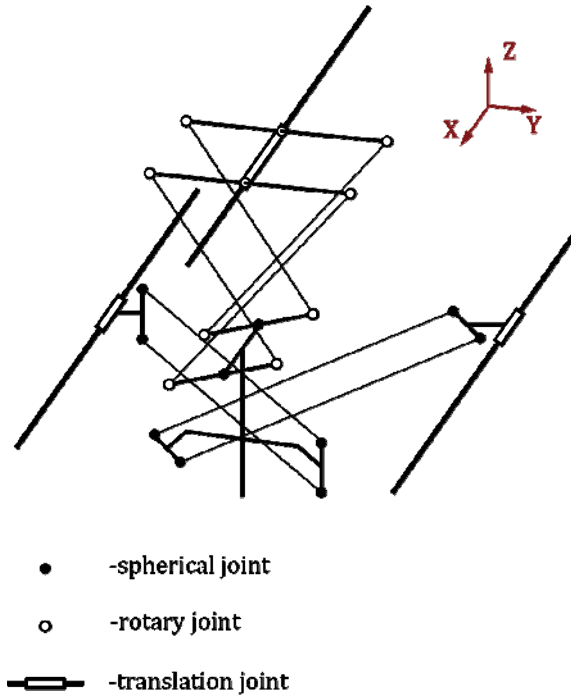


Fig. 2. The kinematic model of the proposed mechanism

As already said, the third kinematic chain is based on Chebishev's mechanism. The third kinematic chain is in the form of four connected elements. The first element is the translation joint on SB, and the second is part of the platform. The remaining two elements consist of Chebishev's mechanisms. Chebishev's mechanisms connect the translation joint on SB and the platform of the considered kinematic chain. Chebishev's mechanisms are connected to the translation joint on SB with one rotary joint, which allows 1 DOF. The connection between MP and Chebishev's mechanism is accomplished by using the spherical joints.

As previously mentioned, Chebishev's mechanism is the straight-line generator. This characteristic allows this mechanism to generate a straight line with the spherical joint connected to the platform. With this considered, Chebishev's mechanism presents the passive translational rotary joint, which allows the motion of the P point in the direction perpendicular to the motion of actuated translation joints.

Chebishev's mechanism consists of four connected links. The first link of Chebishev's mechanism is the smallest link of Chebishev's

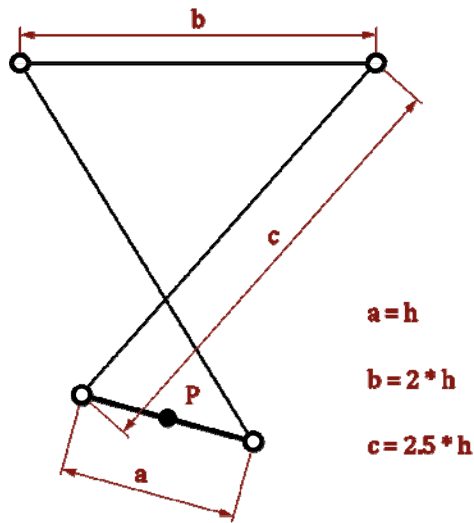
mechanism, which is connected to the MP with a spherical joint placed in the P point. The second link of Chebishev's mechanism is connected to the active translation joint with a rotary joint. The connection between the first and the second link of Chebishev's mechanism is accomplished with two crossed links. Links that connect the first and the second links of Chebishev's mechanism are the same length. The connection between every link of Chebishev's mechanism is accomplished using rotary joints. It is important to say that crossed links of Chebishev's mechanism are not in the collision.

For Chebishev's mechanism to generate a straight line, it is crucial to use the optimized lengths of every link used in Chebishev's mechanism. The mathematician Pafnuty Lvovich Chebyshev has established the proper proportion between links for the mechanism to work [1]. The dimension of the first, smallest link (a) is parametrized and has the value $a = h$. The second link (b) of Chebishev's mechanism has a dimension twice as big as the first one, $b = 2 * h$. The crossed links of Chebishev's mechanism have dimension: $c = 2.5 * h$. The Chebishev's mechanism with desired proportion between links is shown in Fig. 3.

3. SIMPLIFICATION OF THE PROPOSED MECHANISM

The proposed mechanism has a complex structure, and the complexity of the proposed mechanism is based on parallel kinematics. Mechanisms with parallel kinematics relative to the mechanism with serial kinematics have much more links used in construction.

The difference in link number is because the links of the serial kinematic machine are much heavier than those of the parallel kinematic machine. Because of the previously explained reason, parallel kinematic mechanisms have many links to establish stability and the rigidity of the construction.



- -spherical joint (P point)
- -rotary joint

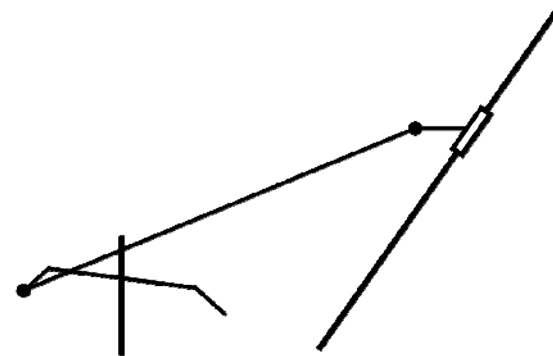
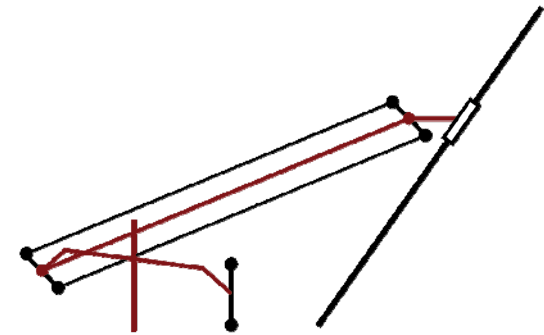
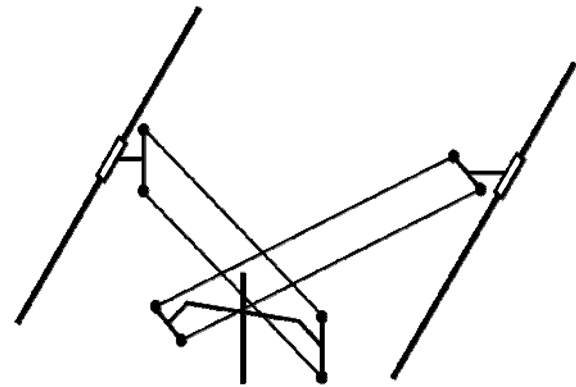
Fig. 3. The Chebishev's mechanism

To design the physical model of the proposed mechanism, it is important to analyze the workspace of the mechanism. Kinematic equations are needed for workspace analysis. The kinematic equations present the mathematical model of the mechanism and are established using the wireframe representation of the mechanism.

The representation of the mechanism structure shown in Fig. 1 needs to be simplified for analysis. The simplification process needs to be done in a way to keep the simplified mechanism possible to move the same way as the original mechanism. This process enables the creation of the mathematical model of the machine, which is crucial for future mechanism research.

As previously said, the proposed mechanism contains three kinematic chains. The first and the second kinematic chains are similar, which means that the connection between those two kinematic chains and MP, as well as between those two kinematic chains and SB is the same. The only difference between the first and second kinematic chain is their arrangement. The second one is rotated for 90° relative to the first kinematic chain.

The simplification of one of the similar kinematic chains is shown in Fig. 4.



- -spherical joint
- ▭ -translation joint

Fig. 4. The simplification process of one of the similar kinematic chains

The idea is to reduce the number of links from four to one. With this, the considered kinematic chain becomes more suitable for kinematic analysis.

As well as simplifying the similar kinematic chains of the proposed mechanism, it is important to perform simplification in the third kinematic chain. The third kinematic chain, as already said, is based on Chebyshev's mechanism. The third kinematic chain consists of four elements, two of which are Chebyshev's mechanisms. The simplification process is similar to the process performed on similar kinematic chains. The idea is to replace four elements with only one as a representation for kinematic analysis purposes. The simplification process of the third kinematic chain is shown in Fig. 6. and the simplified model of the proposed mechanism is shown in Fig. 5.

The one element which replaces the four elements presented in the original version is Chebyshev's mechanism.

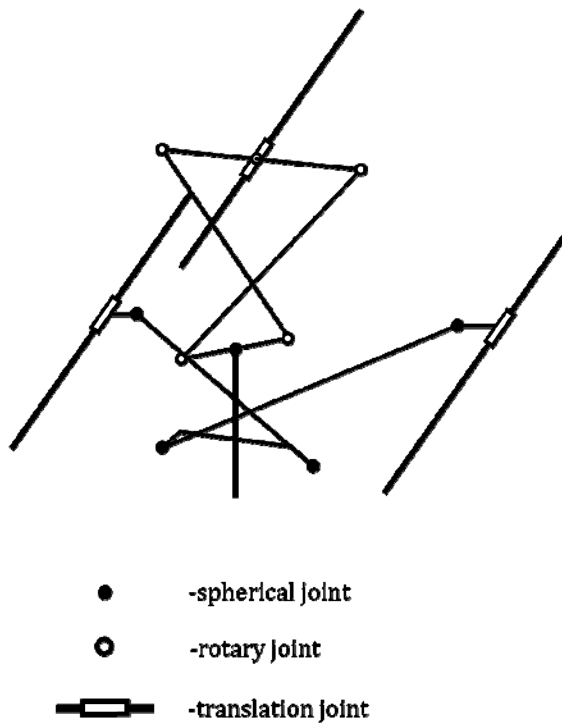


Fig. 5. The simplified model of the proposed mechanism

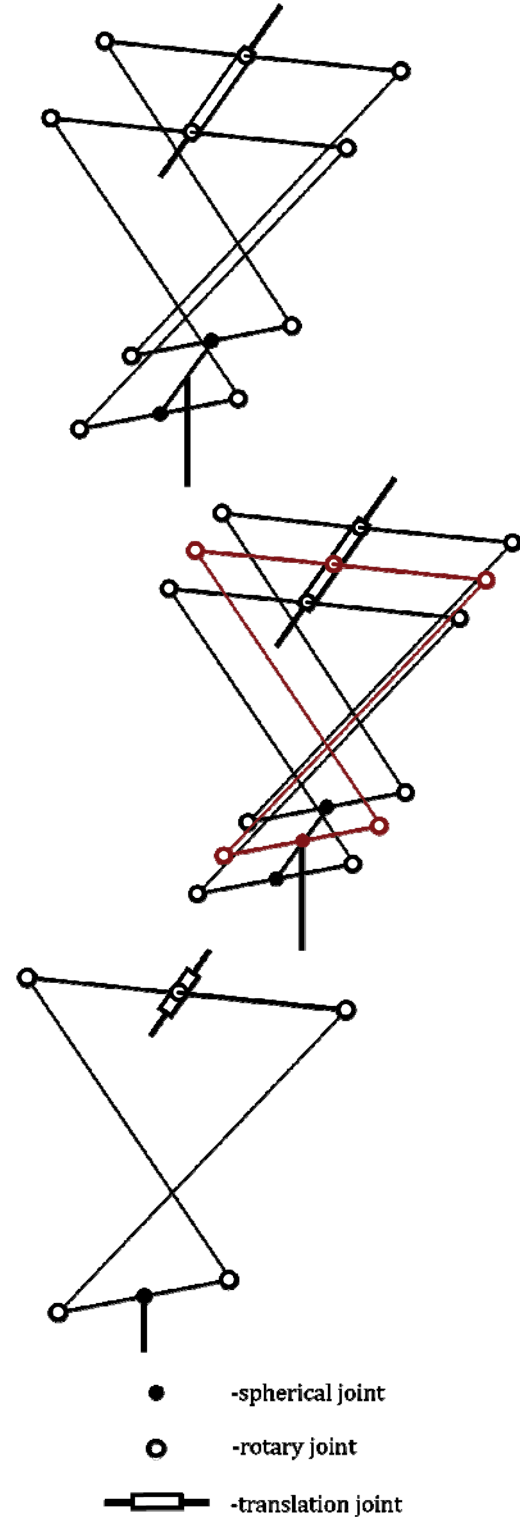


Fig. 6. The simplification process of the third kinematic chain

Whit simplification of all three kinematic chains of the proposed mechanism is possible to generate a model of the mechanism more suitable for kinematic analysis. With proposed simplification the foundation for future research is formed.

4. CONCLUSION

The mechanism presented in this paper offers a new conceptual design. The extended horizontal axis of the mechanism provides numerous possible usages in different industries. The proposed mechanism can be used as a machine tool for the milling process with the horizontal or vertical orientation of the main spindle. The usage of the proposed mechanism can be found in the wood industry with an extended horizontal axis as the advantage over serial machines. The proposed mechanism usage is also possible in additive manufacturing, laser engraving, and other engineering areas. The rigidity and stability of the proposed mechanism have the potential to be very high, and yet the mechanism construction is not robust and heavy. The proposed mechanism has numerous links specifically arranged, which are not large and heavy, further confirming the previous statements.

Geometric model analysis and simplification of the mechanism structure presented in this paper are the base for further research. This means that the presented structural design is not final, and some structural changes might be provided by details gained from future research. Future research will be focused on the kinematic model of the mechanism. The main idea will be to optimize the parameters of the machine to get the most acceptable size and shape of the workspace, as the weakest characteristic of parallel kinematic machines.

Acknowledgement

The presented research was supported by the Ministry of Education, Science and Technological Development of the Republic of Serbia by contract no. 451-03-47/2023-01/200105 dated 3 February 2023 and by contract 451-03-47/2023-01/ 200066 dated 2023.

REFERENCES

- [1] Glavonjić, M., Milutinović, D., Živanović, S., Troosni paralelni mehanizmi sa specifičnim rešenjima pasivnog translatorsnog zgloba. (In Serbian) *Proceeding of 32th Jupiter Conference*, 2006, Zlatibor, ppt. 3.1-3.4.
- [2] Briot, S., Pashkevich, A., Chablat, D., Technology-oriented optimization of the secondary design parameters of robots for high-speed machining applications, *Institut de recherches en Communications et Cybernétique de Nantes (IRCCyN)*, UMR CNRS 6597, 44321 Nantes Cedex 3 France.
- [3] Nešovanović, Lj., Živanović, S., (2022). Workspace and Kinematic Structure Analysis of a 6-DOF Lambda Parallel Kinematic Machine, *International Journal of Electrical Engineering and Computing*, Vol. 6, No. 1, pp.1-8, UDC 004.45:004.388]:621.9, DOI 10.7251/IJEEC2206001N.
- [4] Weiyao, Bi., Fugui, Xie., Xin-Jun, Liu., Xuan, Luo., (2017). Optimal design of a novel 4-degree-offreedom parallel mechanism with flexible orientation capability, *Jurnal of Engineering manufacture*, IMechE, DOI: 10.1177/0954405417731469.
- [5] Shigley, J.E., Uicker J. J., (1980). *Theory of Machines and Mechanisms*, McGraw-Hill.
- [6] Manickavelan, K., Balkeshwar, S., Sellappan, N., (October 2014). Design, Fabrication and Analysis of Four Bar Walking Machine Based on Chebyshev's Parallel Motion Mechanism, *European International Journal of Science and Technology*, Vol. 3 No. 8.
- [7] Nayak, A., Gupte, V., Singru, P., (October 2022). Studying the Effects of Varying Link Lengths in Double Lambda Mechanism and Its Application to Rover Suspension Design, *Recent Advances in Machines and Mechanisms* (pp.43-50), DOI:10.1007/978-981-19-3716-3_4.



Banja Luka
1–2 June 2023.

DEMI 2023

16th International Conference on Accomplishments in Mechanical and Industrial Engineering

www.demi.mf.unibl.org



Energy consumption analysis and parameter optimization in high-feed milling operation

B. Sredanović^a, S. Borojević^a, Đ. Čiča^a, S. Tešić^a, D. Jokić^b, D. Kramar^c

^aUniversity of Banja Luka, Faculty of Mechanical Engineering, Banja Luka, Bosnia and Herzegovina

^bVENDOM d.o.o. company, Laktaši, Bosnia and Herzegovina

^cUniversity of Ljubljana, Faculty of Mechanical Engineering, Ljubljana, Slovenia

Abstract

Improving the performance, efficiency and productivity of the machining, reducing energy consumption and establishing control over the machining process are the main goals of the production technologies development. This paper provides the basis for establishing of a process management and determining of optimal conditions for performing high-feed milling, as a special machining method. An experimental study of the analysis of the influence of process parameters, namely depth of cut and feed rate, on the output parameters of high-feed milling were carried out. As output indicators of the performance of the high-feed milling, namely the energy efficiency of the machine tool and the productivity of the machining process were analysed. Based on experimental data, analysis and modelling of the material removal rate per unit of time and electrical energy consumption were carried out. A workpiece made from aluminium was machined on a three-axis machining centre. By using the boundaries of the domain of process parameters and the optimization objective function, the optimization of the values of the process parameters was carried out. As an optimal solution, the following process parameters were obtained: cutting depth $a_p = 2$ mm and feed rate $v_f = 1500$ mm/min.

Keywords high-feed milling, energy consumption, modelling, optimisation

1. INTRODUCTION

The modern market constantly demands better quality of the product, its improved functionality, low cost of the product and delivery in the shortest possible time interval. Consequently, manufacturers are forced to shorten the time from order to delivery, and reduced costs related to production, by reducing the number of engaged production means and process operations [1].

Corresponding author

PhD Branislav Sredanović, assistant professor
branislav.sredanovic@mf.unibl.org

University of Banja Luka, Faculty of Mechanical Engineering
Stepe Stepanovica 75, 78000 Banja Luka
Republic of Srpska, Bosnia and Herzegovina

The manufacturer's responds, which was based on the use of advanced machining processes, is impossible to imagine without the use of special, unconventional and hybrid processes. Continuous improvement of the performance of the processes is a basic task in production technologies, which requires an ever wider application of advanced machining processes, as well as concepts of sustainable production [2]. Great attention is paid to special machining methods, and especially to highly efficient methods whose performance enables efficiently fulfillment of quality and accuracy requirements, as well as significant time and cost savings during machining process. Special machining methods are developed in order to increase productivity, quality and accuracy of

machining, as also cost and time reduction. High-efficiency and high-performance machining methods are based on a significant change in some of the geometric or process parameters. These changes refer to their significant increasing or decreasing; and the most common are: increasing of cutting speed, increasing of cutting depth, increasing of feed rate, decreasing the contact on the cutting tool edge, etc.

2. HIGH-FEED MILLING

High-feed milling (HFM) is used in roughing and semi-finishing processes, where the main goal is to remove as much material from the workpiece as possible in the shortest possible time, with maximum preservation of the cutting tool edge. HFM can be considered as type of highly efficient machining, where large values of feed rate per tooth f_z or feed rate v_f are used, which results in a high degree of removal of material from workpiece. This leads to a reduction in processing time and a maximization of the degree of material removal rate per time unit (MRR).

The mechanism of high-feed milling is based on the so-called "chip ticking" effect - the effect of chip thinning or its retention at the recommended value. If the effect of reducing the entering angle is observed, while keeping the chip thickness constant, a significant increase in the value of the feed rate per tooth can be achieved (Fig. 1).

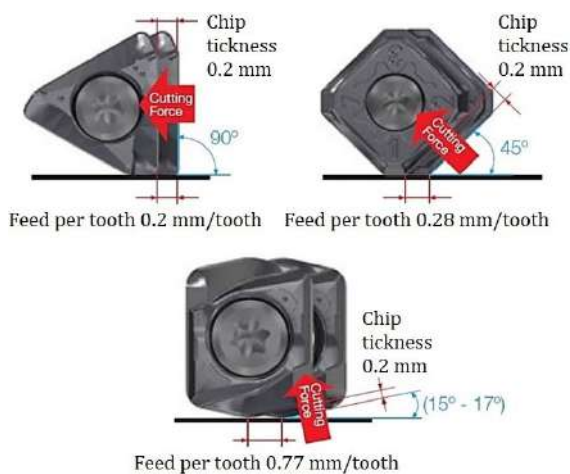


Fig. 1. Influence of the entering angle on feed rate per tooth

Small values of the entering angle of the cutting tool lead to the directing of the resultant cutting force in the direction of the tool axis (Fig. 2). This results in stable machining because the cutting tool has much greater rigidity in the axial direction than in the radial direction. Orientation in the radial direction leads to a greater deformation of the tool and thus to a higher machining error. Smaller cutting depth and the directing of the resultant cutting force in the direction of the tool axis, enables increasing of the cutting width. This results also in increasing of material removal rate and enables more efficient cooling and lubrication.

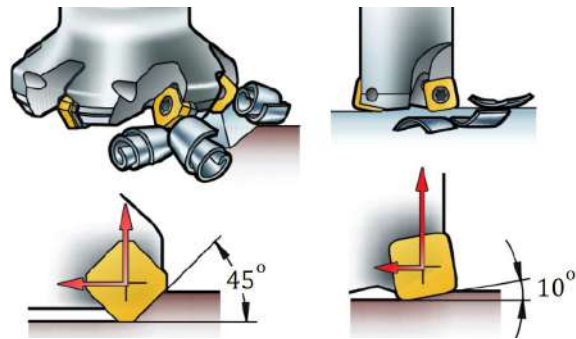


Fig. 2. Influence of entering angle on the cutting force direction

High-efficiency milling processes primarily include high-feed milling, which is accompanied by the appearance of negative effects such as tool deflection, intense tool wear, high cutting forces, vibrations, and similar [3]. Zhu et al. [4] investigated the influence of cutting parameters and tool geometry on cutting forces and tool wear during high-feed milling with ceramic inserts. Araujo et al. [5] analysed the possibilities of high-feed milling during machining titanium super-alloy Ti6Al4V with PCD tools. Jiang et al. [6] developed a model for identification and analyses of tool wear and tool vibration during high-feed milling. In order to enable the maintenance of a constant cutting force, Saikumar and Shunmugam [7] developed feed rate adaptation control systems for high-speed milling of hardened EN24 steel. From the point of view of energy consumption, high-feed milling is an energy-efficient machining process. Zhang et al. [8] investigated the energy efficiency in high-feed milling and concluded that with an increase in the feed rate, there is an improvement in the energy efficiency of the milling process.

3. EXPERIMENTAL SETUP

The experiment was performed on a three-axis machining center EMCO Concept Mill 450, which was equipped with a control unit Sinumerik 810D/840D (Fig. 3). The available power of the machine is 11 [kW], while the maximum spindle speed is 12000 [rpm]. As a cutting tool, a face mill with circular inserts by Sandvik R300-1240M was used; the material designation of the inserts is GC4230. The designation of the face mill is R300-050Q22-12M. The nominal diameter of the face mill is $D_c = 50$ (mm), and the effective diameter of the face mill is $D_e = 38$ (mm). The face mill has $Z_n = 4$ circular inserts, mechanically fixed with a screw to the body of the face mill.



Fig. 3. Experimental set-up

A face mill with circular inserts was chosen for application in high-feed milling in order to analyze its possibilities during exploitation. Due to the characteristic geometry of the workpiece, there is a variable value of the entering angle, which depends on the insert diameter D_t (mm) and the cutting depth a_p (mm). The feed rate per tooth depends on the thickness of the chip, i.e. the maximum thickness of the cutting layer, as well as on the cutting depth and the diameter of the insert. The material of the workpiece, which was used to perform the experimental research, was aluminum. Due to its low density, it is often used in cases where it is necessary to reduce the weight, especially for parts of the aviation and automotive industry, but also for other functional parts of mechanisms in machines. A full orthogonal design of the engineering experiment was used, whereby all variations of

variable parameters were combined with each other, which gave an experiment plan of nine combinations (Table 1). Cooling and lubricating fluids were not used during the high-feed milling. During the entire experiment, the spindle speed n was constant with value of $n=3000$ (rpm), so the cutting speed was constant. The milling width was also constant with value of $a_e=30$ (mm).

Table 1. Experiment plan

Exp no.	Cutting depth a_p [mm]	Feed rate v_f [mm/min]
1	2.0	1500
2	2.0	1000
3	2.0	500
4	1.5	1500
5	1.5	1000
6	1.5	500
7	1.0	1500
8	1.0	1000
9	1.0	500

A 3-phase MAVOWATT 30 analyzer was used to measure power and energy consumption during the experiment. This device meets standards EN50160, EN61000-4-7 and EN61000-4-15, which are relevant for measuring power supply quality, and EN61000-4-30, which specifies measuring voltage quality procedures. The software used to analyze the experimental results was *DesignExpert 7.1.5* through which a mathematical model of the behavior of the output machining parameters were generated. The software was intended for experiment planning, modeling, analysis of model accuracy, determination of the significance of individual parameters, as well as optimization of results, and graphical presentation.

4. RESULTS AND DISSCUSIONS

Data processing and analysis of the results obtained by practical measurements was performed based on experimental measurements. The data analysis, statistical processing and modeling of energy consumption during high-feed milling were presented below. The analysis of the measured results was carried out using the statistical

method of analysis of variance (ANOVA). In addition to measuring of the electrical energy consumption, for the purpose of analysing the observed process, the components of the cutting force were also measured. At higher values of the cutting depth, the cutting force F_x has a higher value than the cutting force in the direction of the axis of the cutting tool F_z . As the value of the cutting depth decreases, the opposite happens, and the cutting force F_z becomes greater than the cutting force F_x (Fig. 4). Using smaller values of the cutting depth, a smaller entering angle was obtained, so that the resultant of the cutting force was closer to the axis of the tool, which coincides with the previous theoretical settings. Smaller cutting depth and approaching the resulting cutting force to the direction of the tool axis, allows increasing of the cutting width in terms of keeping the resulting cutting force within certain limits.

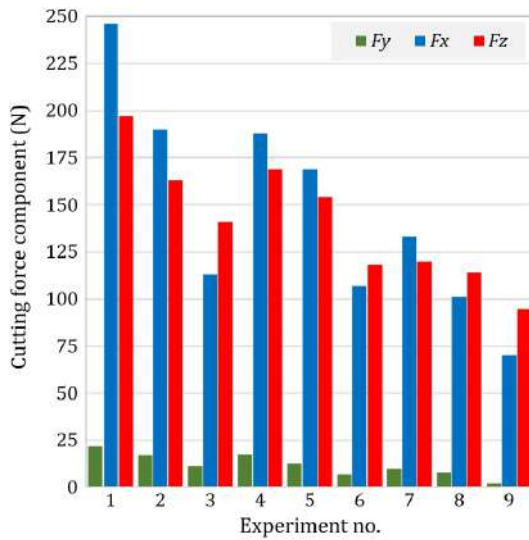


Fig. 4. Measured cutting forces per directions

The basic indicator of the energy efficiency of the machining process or the machining system during this experiment, the electrical energy consumption E (kWh) during high-feed milling was measured and analysed. With a change of the milling parameters, there is also a change in the energy efficiency of the machine tool, i.e. parameters such as the required power and the total consumed electrical energy. In the down-mentioned table, calculated data of the productivity of the milling operation, which was represented by the degree of material removal

rate per time unit, was obtain as a multiplication of the feed rate, the cutting depth and the cutting width, was added (Table 2).

Table 2. Experimental results

Exp no.	a_p [mm]	v_f [mm/min]	MRR (mm ³ /min)	E (kWh)
1	2.0	1500	90000	0.00512
2	2.0	1000	60000	0.00525
3	2.0	500	30000	0.01105
4	1.5	1500	67500	0.00434
5	1.5	1000	45000	0.00529
6	1.5	500	22500	0.00854
7	1.0	1500	45000	0.00402
8	1.0	1000	30000	0.00457
9	1.0	500	15000	0.00905

From the Table 2 can be concluded that the highest value of total consumed electrical energy $E = 0.01105$ kWh was obtained by applying the following parameters $a_p = 2.0$ mm and $v_f = 500$ mm/min, while the smallest value of consumed electrical energy $E = 0.00402$ kWh was obtained by using the process parameters $a_p = 1.0$ mm and $v_f = 1500$ mm/min. The lowest value of total consumed electrical energy during observed milling process occurs at the lowest cutting depth and at the highest feed-rate, and vice versa (Fig. 5).

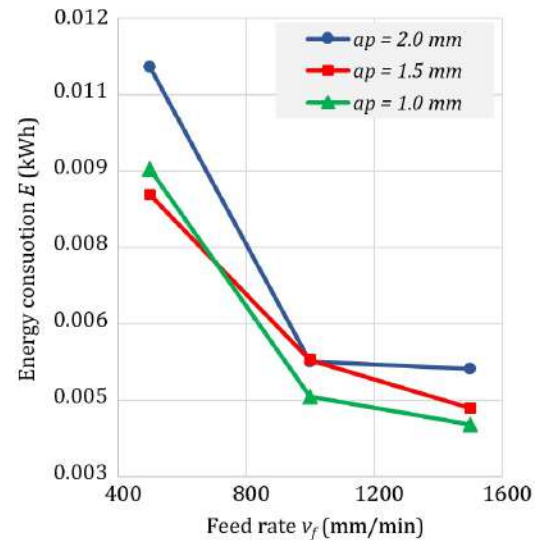


Fig. 5. Influence of feed rate and cutting depth on the total energy consumption

In order to form a mathematical description of the changing of the total electrical energy consumption during the milling process based on the least squares method, a linear model was proposed and selected as opposed to a model with parameter interaction (Quadratic vs 2FI). After the variance analysis, the results shown in Table 3 were obtained. Based on the values of the F and P parameters, it can be concluded that the model was significant.

Table 3. Results of the ANOVA

Source	Adj SS	Adj MS	F values	p values
Model	4.9·10 ⁻⁵	1.22·10 ⁻⁵	28.88083	0.0033
A - a_p	2.38·10 ⁻⁶	2.38·10 ⁻⁶	5.618571	0.0768
B - v_f	3.83·10 ⁻⁵	3.83·10 ⁻⁵	90.37341	0.0007
A ²	4.11·10 ⁻⁷	4.11·10 ⁻⁷	0.969748	0.3805
B ²	7.87·10 ⁻⁶	7.87·10 ⁻⁶	18.56158	0.0126
Residue	1.7·10 ⁻⁶	4.24·10 ⁻⁷		
Total	5.07·10 ⁻⁵			

Statistically, the mean value of the consumed electrical energy $\bar{x}=0.0064$ was obtained, with a standard deviation of the $SD = 0.00065$, with the value of the signal-to-noise ratio $S/N = 13.1$. The regression coefficient was $R^2 = 0.97$, which proves the alignment of the measured and modeled data. Based on the above mentioned data, it can be concluded that the model is adequate. The mathematical dependence between the consumed electrical energy and the process parameters, the cutting depth a_p and the feed rate v_f , was given on the basis of the following formula:

$$E = 0.02 - 0.0042 \cdot a_p - 2.1 \cdot 10^{-5} \cdot v_f + 0.008 \cdot a_p^2 + 7.93 \cdot 10^{-9} \cdot v_f^2$$

By using the previously mentioned formula in the software, the response of the model of the consumed electrical energy during the milling process, obtained on the basis of various parameters, was formed. Observing the diagram from Fig. 6, it can be concluded that with increasing of the feed rate and decreasing the cutting depth, the total consumption of electrical energy decreases, and while with a decreasing of the feed rate and increasing of the cutting depth, the opposite situation occurs, i.e. the total consumption electrical energy during

milling process increase. This is a consequence of the shorter processing time, which was obtained during use a high value of the feed rate and relatively higher power of the machine tool.

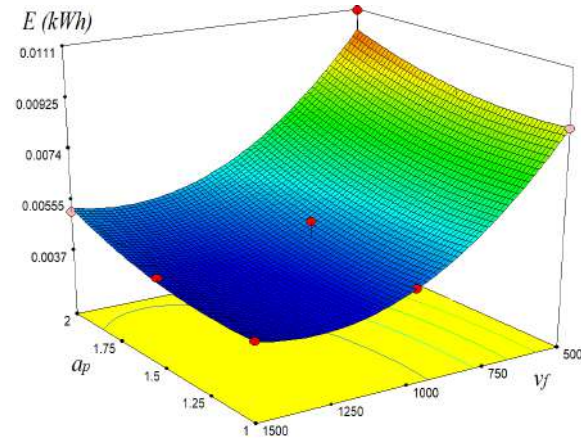


Fig. 6. Response surface plot – effect of the feed rate and cutting depth on the total energy consumption

4.1 Process parameter optimisation

In the case of rough milling, the main goal is to remove as much material as possible from the workpiece in the shortest possible time, and all this with the less amount of total consumed electrical energy. The final goal, which refers to the greatest possible material removal in the shortest possible time, can be represented by maximizing productivity, i.e. the degree of material removal rate per time unit. The goal of consuming as less energy as possible can be represented by minimizing the electrical energy consumption. For all parameters, the same importance and degree of priority in terms of impact on the optimization process and procedure was defined (Table 4).

Table 4. Mathematical frame of optimization

Parameter	Goal	Lower	Upper
		Limit	Limit
a_p (mm)	Stay in a domen	1	2
v_f (mm/min)	Stay in a domen	500	1500
MRR (mm ³ /min)	Maximise	15000	90000
E (kWh)	Minimise	0.00402	0.01105

Based on the set mathematical formulation of the optimization, several suitable solutions were obtained, ordered according to the

desirability of the solution, which represents the percentage of satisfaction of the optimization goals. As an optimal solution, the following process parameters were obtained: cutting depth $a_p = 2$ mm and feed rate $v_f = 1500$ mm/min. The amount of material removed rate per time unit, for optimal parameters, is $MRR = 90000$ mm³/min, and the amount of total consumed energy is $E = 0.005274$ kWh. The diagram of the optimization results which is in function of cutting depth and the feed rate is shown in the Fig. 7. According to the diagram and the previously set of optimization goals, it can be concluded that it is preferable to use higher values of the process parameters, which is in accordance with the theoretical settings. The percentage of the optimization goals satisfaction, with the optimal solution, is 91%.

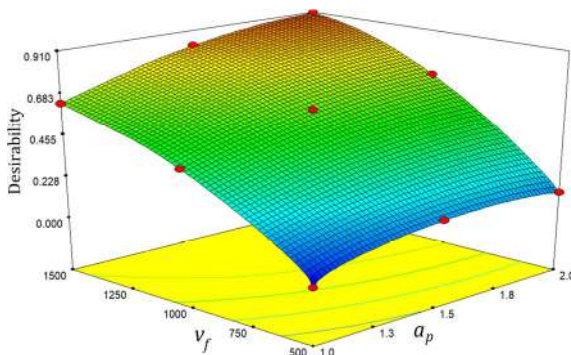


Fig. 7. Diagram of the optimization desirability results

5. CONCLUSIONS

The analysis of the results showed that using lower values of the cutting depth and higher values of the feed rate results in less total consumption of electrical energy during milling, while in the opposite case, during using higher values of the cutting depth and lower feed rate, relatively higher consumption of electricity was obtained. By using the developed model, the optimization of the high-feed milling process on the machining centre was carried out. As a criterion, it was chosen that the cutting depth and the feed rate were in the domain between the smallest and the largest value, and their optimal values were obtained. By summarizing the research and defining the mathematical bases for static analysis, model development and the mathematical framework for the optimization process, resulted in a successfully

developed methodology for planning of the high-feed milling operations. Future research should be based on the analysis of high-feed milling of other materials, i.e. hard-to-machine materials, such as: titanium, hardened steel, gray cast iron and similar.

Acknowledgement

This research is results of activities on interstate bilateral project, FME Ljubljana and FME Banja Luka. The project is supported by governments of Republic of Slovenia and Republic of Srpska.

REFERENCES

- [1] Gresik, W. (2008). *Advanced Machining Processes of Metallic Materials: Theory, Modelling and Application*. Elsevier, Amsterdam.
- [2] Davim, J. P. (2017). *Sustainable Machining*, Springer - Verlag, Berlin.
- [3] Zhao, P., Zhang, L., Jiang, B., Wang, Y. (2022). Instantaneous friction energy consumption and its evolution of high energy efficiency milling cutter. *Advances in Mechanical Engineering*, vol. 14, no. 5, DOI: 10.1177/16878132221095917
- [4] Zhao, P., Cheng, K., Jiang, K., Jiang, B., Zuo, L. (2021). Development of the innovative differential tool wear modelling for high-feed milling and its experimental verification. vol. 235, no. 1-2, DOI: 10.1177/0954405420949226
- [5] Araujo, A.C., Fromentin, G., Blandent, P. (2020). Investigation on PCD cutting edge geometry for Ti6Al4V high-feed milling, vol. 111, p. 1785 – 1796, DOI: 10.1007/s00170-020-06086-z
- [6] Jiang, B., Nie, Q., Zhao, P., Ma, Q., Sun, S. (2023). Identification method for Instantaneous Friction and Wear Energy Density Variation of High-Feed Milling Tool Flank, vol. 13, no. 8, DOI: 10.3390/app13084807
- [7] Saikumar, S., Shunmugam, M.S. (2012). The International Journal of Advanced Manufacturing Technology, vol. 59, p. 869 – 884, DOI: 10.1007/s00170-011-3561-6
- [8] Zhang, T., Liu, Z., Sun, X., Xu, J., Dong, L., Zhu, G. (2020). Investigation on specific milling energy and energy efficiency in high-speed milling based on energy flow theory., vol. 192, DOI: 10.1016/j.energy.2019.116596



Banja Luka
1–2 Jun 2023.

DEMI 2023

16th International Conference on Accomplishments in Mechanical and Industrial Engineering

www.demi.mf.unibl.org



Examination of the positioning accuracy of the machine tool with hybrid kinematics

S. Tabaković^a, S. Živanović^b, M. Zeljković^a, A. Budimir^a, Z. Dimić^c

^aUniversity of Novi Sad, Faculty of Technical Sciences, Republic of Serbia

^bUniversity of Belgrade, Faculty of Mechanical Engineering, Republic of Serbia

^cLOLA Institute, Belgrade, Republic of Serbia

Abstract

The intensive development of machine production in recent years has enabled the emergence of machine tools with parallel and hybrid kinematic structure and their integration into industrial production. Therefore, extensive research has been conducted in recent years to examine the exploitation possibilities of such machines and the justification of their application in certain areas of mechanical engineering. An important part of that research is the examination of accuracy and the possibility of calibrating machine tools with non-trivial kinematics.

The paper presents a part of the research carried out to determine the influence of the characteristics of individual machine components on the overall positioning accuracy of the machine tool prototype based on the O-X glide hybrid mechanism.

Keywords machine tool, hybrid kinematics, accuracy positioning

1. INTRODUCTION

Machine tools have been the basis of production systems in the industry for more than two hundred years. In that period, there were significant changes in the driving and building elements of the machines, which enabled the intensive development of the industry. However, in that period, changes in the kinematic conception of machine tools were minimal. In modern conditions, most machine tools are based on a serial kinematic structure, as in the first industrial revolution.

The idea of using closed kinematic structures contained in parallel mechanisms as a supporting structure of machine tools arose in

the middle of the 20th century (Stewart's platform from 1965) [1].

The main obstacle to making such machines was the impossibility of realizing a control system with non-linear kinematics. Commercial application, due to the specifics of management, began only in the last thirty years (at the IMTS fair in Chicago in 1984) [2]. During that period, a significant number of conceptual solutions for machine tools with parallel and hybrid (serial/parallel) kinematic structures were developed.

The paper discusses the problem of positioning accuracy of machine tools with hybrid kinematics according to the ISO 230-2 [3] standard, conducted on the example of a machine tool based on the original O-X glide mechanism [4].

The basic problem of testing the positioning accuracy of machine tools based on non-trivial kinematics is the fact that testing determines the state of the programmed (external) axes of the machine, which are formed by the

Corresponding author

Prof. dr Slobodan Tabaković
tabak@uns.ac.rs

University of Novi Sad, Faculty of Technical Sciences
Trg D. Obradovića 6
Novi Sad, Republic of Serbia

combination of movements performed by two or more machine axes (internal coordinates) [5].

Therefore, the machine test defined by the standard does not give an image of the condition of the machine components, but of the movement that is the result of their movement following the laws of inverse kinematics of the mechanism [6], [7].

The research presented in the paper represents a step in the definition of a general methodology for calibrating machine tools regardless of their kinematic structure.

2. KINEMATIC STRUCTURE OF THE O-X GLIDE MECHANISM

The prototype of machine tool based on the O-X glide mechanism contains a planar parallel mechanism that moves on a gantry structure using a serial linear axis (Fig. 1). At the same time, the parallel mechanism contains a movable platform connected to rods of constant length by means of corresponding joints. The other end of the rods is connected to the rotary joints for the sliders, which move linearly along their own guide [4].

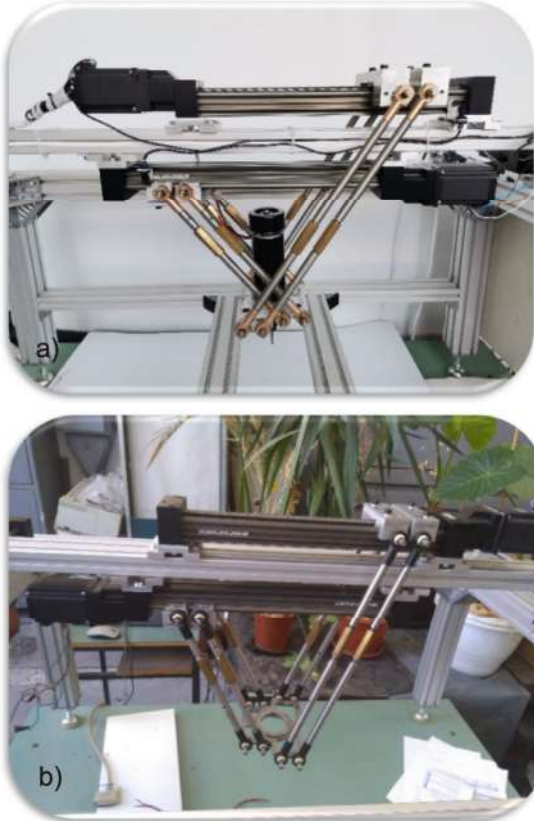


Fig. 1. O-X glide hybrid kinematic machine tool

In order to increase the movement possibilities of the slider, they are arranged in height at different distances, enabling passing in the plane of movement. This gives the original ability to reconfigure the mechanism from an extended (O) to a crossed (X) shape and vice versa. The parallel mechanism enables the movement of the moving platform in the (XZ) plane, and the translational movement of the parallel mechanism is realized by linear movement along the Y axis [2]. Figure 1 (a) shows the X configuration and Figure 1 (b) shows the O configuration of the machine tool.

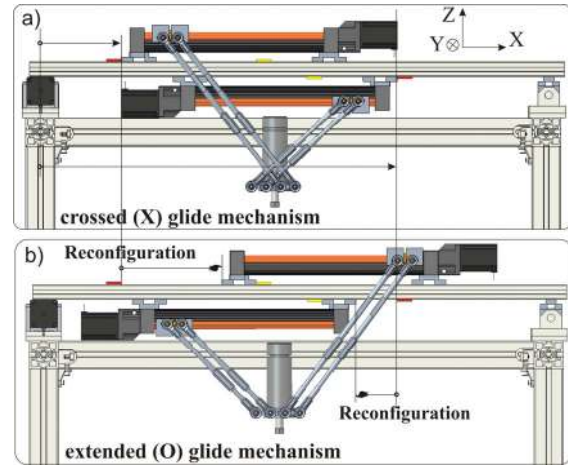


Fig. 2. Configurations of hybrid machine tools [4].

The analysis of positioning accuracy realized for work purposes was carried out on the X configuration of the mechanism whose kinematic model is shown in Fig.3.

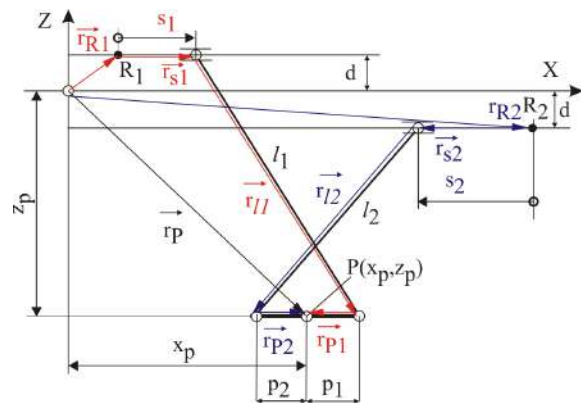


Fig. 3. Kinematic model of the parallel mechanism [4]

The parallel mechanism of Figure 3 is shown in an arbitrary position for the crossed (X) variant

of the mechanism. Solving kinematic problems is performed in the plane (X, Z). The internal coordinates of the parallel mechanism are the positions of the sliders s_1 and s_2 , while the external coordinates are the position of the platform P (X_p , Y_p). The solution of kinematic problems is given in detail in [4], while here only the final solutions of IKP are given as:

$$s_1 = x_p - x_{R1} + p_1 - \sqrt{l_1^2 - (z_p - d)^2} \quad (1)$$

$$s_2 = -(x_p - x_{R2} - p_2 + \sqrt{l_2^2 - (z_p + d)^2}) \quad (2)$$

$$s_3 = y_p \quad (3)$$

The same expressions and equations of the direct kinematic chain were used when configuring the control system based on the LinuxCNC platform, which is shown in detail in [4].

3. PROCEDURE FOR TESTING THE ACCURACY OF POSITIONING

Testing the positioning accuracy of linear axes of numerically controlled machine tools is one of the most important indicators of the current state of machine tools. The procedure for testing and calculating the results is covered by the ISO 230-2 [3] standard. Basically, this standard is intended for the testing of medium-heavy and light machine tools, where certain test details such as the method of movement, the number of measuring points, and the number of repetitions can be adapted to the specific machine. That is why it was chosen for the evaluation of a specific machine tool whose

prototype belongs to the category of midi or mini machine tools.

ISO 230-2 is the most frequently mentioned standard in professional literature for determining the accuracy of machine tool positioning. It defines the methods of testing and evaluating the accuracy and repeatability of the positioning of individual numerically controlled axes of machine tools. The standard provides for two methods of movement of machine elements during measurement, a minimum number of 8 measurement points and 5 repetitions of measurement when moving in the + and - direction of a particular axis.

The results obtained by testing machines according to this standard are used to assess the state of the machine, calibrate the control system, categorize the machine according to applicability for certain types of processing, etc.

Testing the positioning accuracy of the O-X glide machine tools was realized by using laser measuring instrumentation, the content and characteristics of which are prescribed by the standard. Instrumentation consists of:

- Measuring head that contains a laser beam source and two receiving channels (detail 1 in Figure 4),
- Electronic display,
- Interferometer and retroreflector (details 2 and 3 in Figure 4),
- External conditions compensator



Fig. 4. Measurement procedure

Memorization of the obtained results and their processing were realized using the original acquisition system and software solution [8].

4. RESULTS

Testing the positioning accuracy of the machine tool based on the O-X glide hybrid mechanism includes testing the state of the external coordinates of the machine tool movement (coordinates with which the tool moves) in all three orthogonal axes (X, Y, and Z). Analysis of machine characteristics includes defining errors in internal coordinates. The movement of the slider according to the internal coordinates in the X configuration of the mechanism takes place by the movement of the slider in the same (when moving in the direction of the X axis) or opposite (when moving in the direction of the Z axis) directions. Analysis of the inverse kinematics equations (1-3) for both axes of the XZ plane provides the values of S1 and S2. Tables 1, 2, and 3 show the results of positioning accuracy measurements for S1, S2, and serial Y axis. The test was carried out using the following parameters:

- • Movement cycle of machine elements - linear
- • Number of measurement points –
 - X and Y axis - 11
 - Z axis - 21
- Speed of auxiliary movement of the machine - $v=200\text{mm/min}$
- Dwell time at the measuring point - $t=3\text{s}$

The results shown in the tables and graphs include the display of the less favorable measurement variant.

Table 1 and Figure 5a show the results for the internal S1 axis.

Table 1. Values obtained for the S1 axis

Test parameter	Value [mm]
Maximum deviation range of mean values – B	0.0312
One-way repeatability of position by axis – R↑ and R↓	0.0167
Maximum two-way repeatability of position per axis – R	0.0521

Test parameter	Value [mm]
One-way systematic error of positioning along the axis - E↑ and E↓	0.1001
Two-way systematic error of axis positioning – E	0.1293
Maximum two-way positioning error by axis – M	0.1012
One-way positioning error along the axis – A↑ and A↓	0.1181
Two-way axis positioning error – A	0.1340

The results of the second internal axis of the planar parallel mechanism, the S2 axis, which is structurally parallel to the S1 axis but with a different direction of movement, are shown in Table 2 and Figure 5b:

Table 2. Values obtained for the S2 axis

Test parameter	Value [mm]
Maximum deviation range of mean values – B	0.0447
One-way repeatability of position by axis – R↑ and R↓	0.0216
Maximum two-way repeatability of position per axis – R	0.0615
One-way systematic error of positioning along the axis - E↑ and E↓	0.1101
Two-way systematic error of axis positioning – E	0.1193
Maximum two-way positioning error by axis – M	0.0912
One-way positioning error along the axis – A↑ and A↓	0.1176
Two-way axis positioning error – A	0.1240

The results of the third axis of the O-X glide mechanism, the Y axis that provides the translation of the parallel mechanism Y are given in Table 3 and shown in Figure 5c:

Table 3. Values obtained for the Y axis

Test parameter	Value [mm]
Maximum deviation range of mean values – B	0.0537

Test parameter	Value [mm]
One-way repeatability of position by axis – R↑ and R↓	0.0718
Maximum two-way repeatability of position per axis – R	0.1038
One-way systematic error of positioning along the axis - E↑ and E↓	0.1106
Two-way systematic error of axis positioning – E	0.1616
Maximum two-way positioning error by axis – M	0.1757
One-way positioning error along the axis – A↑ and A↓	0.1873
Two-way axis positioning error – A	0.2044

Figures 5a, 5b, and 5c. shows diagrams of positioning accuracy for the S1 and S2 axes obtained by calculating the X and Z-axis tests, respectively, and the Y axes.

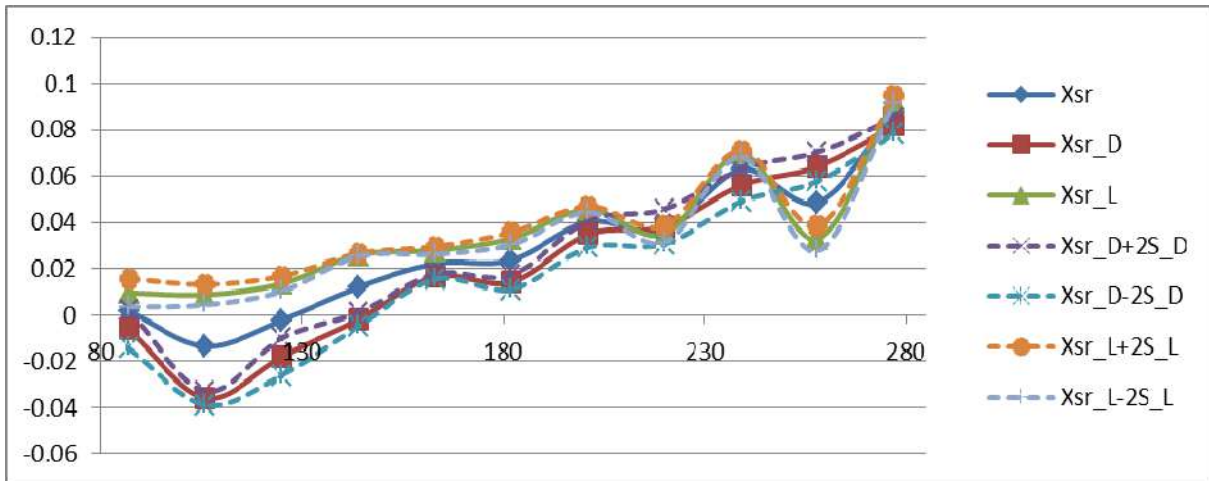


Fig. 5a. S1 axis positioning accuracy

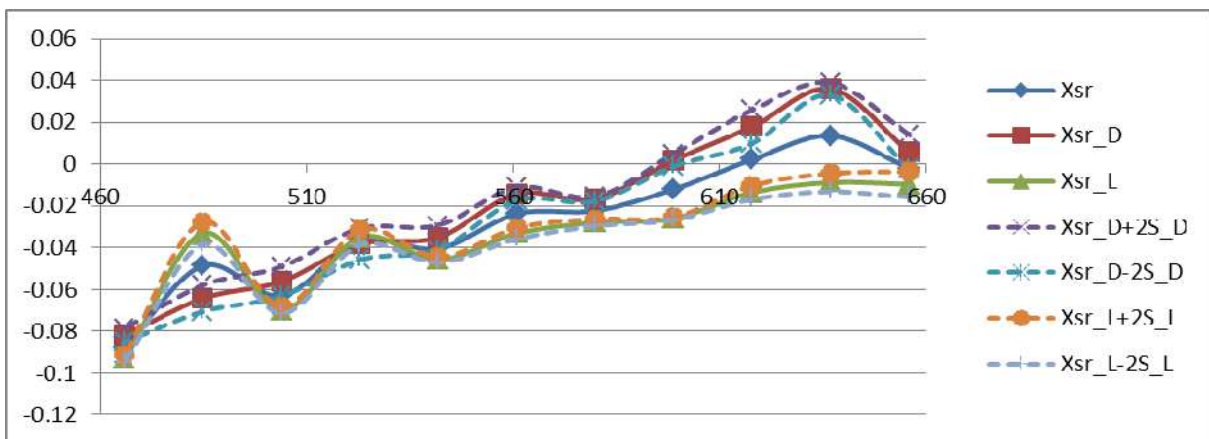


Fig. 5b. S2 axis positioning accuracy

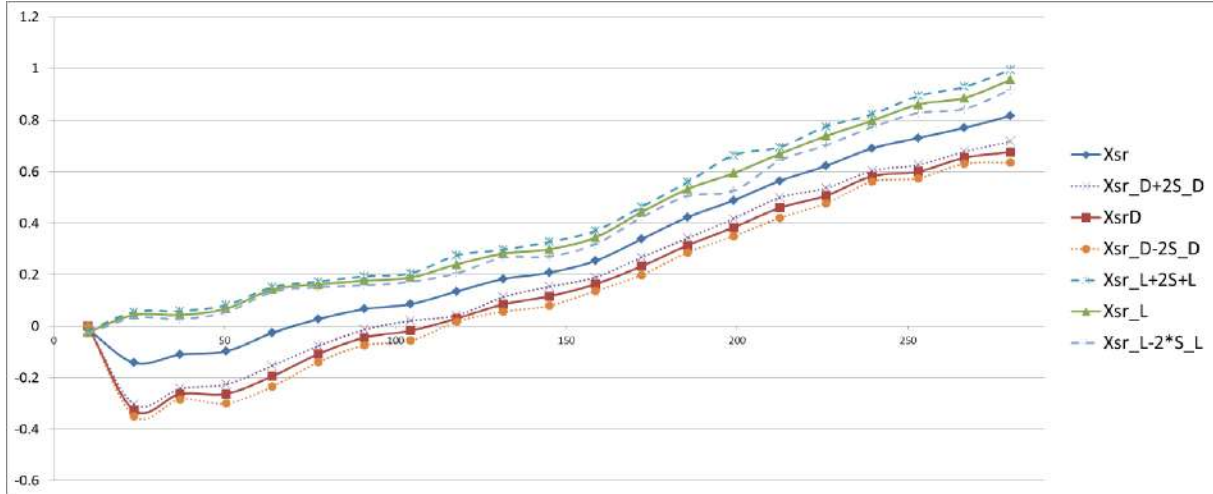


Fig. 5c. Y axis positioning accuracy

All analyzes were carried out with the monitoring of the measurement conditions (air pressure, relative humidity as well as the temperature of the environment and the machine) and automatically compensating the measurement results accordingly.

5. DISCUSSION

Based on the analysis of the test results of the machine tool based on the O-X glide mechanism, conclusions can be formed about the construction of the machine tool, the condition of its elements, as well as potential adjustments to the testing methodology. It should be noted that the presented prototype was developed for the purpose of proving the concept of usability of the proposed mechanism, as well as for determining the methodology for its evaluation in relation to machine tools with serial kinematics. Therefore, linear axes with a helical spindle have been used for its production, it has a frictional connection between the spindle and the nut, as well as an open loop control system. This resulted in results that are not comparable to commercial machine tool solutions.

The conversion of the test results of the external axes of the machine tool enables the analysis of the construction solution of the tested prototype. This primarily refers to the state of linear axes based on an open loop control where the definition of the position is based on the calculation of the position based on the set control values without an additional measurement of the realized movements. The

obtained results per axis are several times higher than the results expected for linear axes of machine tools with modern closed loop control. This is most pronounced with the Y axis, which is the longest and where the movement of the plane parallel mechanism is constructed by a linear axis located on one side of the mechanism and the movement is transmitted to the other by a rigid connection. Since the length of the portal on which the planar parallel mechanism is placed is about 600mm (due to the possibility of testing the reconfiguration feature), this greatly affected the systematic error of measurement, but also the occurrence of pronounced random errors in certain movement zones.

In addition, it can be observed that the building elements of the machine tool provide relatively good results, which are applicable for the construction of prototypes. The entire machine tool is suitable for compensating systematic errors by applying the process of calibrating the control system of the machine tool.

Finally, the conducted research indicates the possibility of applying a standardized methodology for determining the state of machine tools and machines based on hybrid and parallel kinematics.

6. FINAL CONSIDERATIONS

The conducted research made it possible to confirm the initial hypothesis that by applying the procedure defined by the ISO230-2 standard, it is possible to test the positioning

accuracy of machine tools with a kinematic structure that is not based on serial kinematics. In addition, the research indicates that the mentioned methodology enables obtaining several different results for the internal axes of the mechanism, based on which conclusions can be drawn about random and systematic errors that, when combined with another internal axis, affect the creation of a smaller or larger resultant error of the entire mechanism.

The obtained results are of great importance for defining the process of calibration of machine tools with hybrid kinematics and the formation of solutions that, with relatively simple components, ensure the development of machine tools competitive with higher quality commercial solutions based on a serial kinematic structure. In addition, the obtained results represent the basis for research of improving machine tools and defining the optimal area on application of machine tools with non-trivial kinematics in modern mechanical engineering.

Acknowledgement

The paper presents part of the research carried out on the project: "Innovative scientific and artistic research in the field of FTN activities", supported by the Ministry of Science, Technological Development and Innovation of the Government of the Republic of Serbia and the project "Integrated research in the field of macro, micro and nano mechanical engineering" and subproject TR35022 "Development of a new generation of domestic manufacturing systems", which is financially supported by the Ministry of Science, Technological Development and Innovation of the Government of the Republic of Serbia (contract no. 451-03-47/2023-01/200105 dated 3 February 2023).

REFERENCES

- [1] Tabaković, S. (2008). Razvoj programskog sistema za automatizovano projektovanje mašina alatki na bazi paralelnih mehanizama i optimalni izbor njihovih komponenti. Phd. thesis, University of Novi Sad, Faculty of Technical Sciences
- [2] Živanović, S. Konfigurisanje novih mašina alatki. Phd. thesis. University of Belgrade, Faculty of Mechanical Engineering, 2010.
- [3] International Standard Organisation. (2011). ISO, DIN. 230-2. 2011-11: Test code for machine tools-Part 2: Determination of accuracy and repeatability of positioning numerically controlled axes
- [4] Zivanovic, S., Tabakovic, S., Zeljkovic, M. and Dimic, Z. (2021). Modelling and analysis of machine tool with parallel-serial kinematics based on OX glide mechanism. Journal of the Brazilian Society of Mechanical Sciences and Engineering 43.10: 1-15. <https://doi.org/10.1007/s40430-021-03171-6>
- [5] Mekid, S, Ogedengbe, T. (2010). A review of machine tool accuracy enhancement through error compensation in serial and parallel kinematic machines. Vol 1 No. 3. pp.:251-283. International Journal of Precision Technology. DOI: 10.1504/IJPTECH.2010.031657
- [6] Elmelegy, A., Zahwi, S. (2023). Comparative study of error determination of machine tools. Int J Adv Manuf Technol 124, 4575–4602 <https://doi.org/10.1007/s00170-022-10358-1>
- [7] Zhen, G. Zhang, D. (2014). Performance analysis, mapping, and multiobjective optimization of a hybrid robotic machine tool. IEEE Transactions on industrial electronics Vol.62. No.1 pp. 423-433. DOI: 10.1109/TIE.2014.2327008
- [8] Tabaković, S. Zeljković, M. (2019). Prediction of positioning accuracy parameters. 14th International Conference on Accomplishments in Mechanical and Industrial Engineering DEMI. Banja Luka. Vol. 1. pp.57-64



Banja Luka
1–2 Jun 2023.

DEMI 2023
**16th International Conference on
Accomplishments in Mechanical and
Industrial Engineering**
www.demi.mf.unibl.org



Experimental investigation of machining parameters in turning of aluminium alloy 7075-T6

A. Aleksić^a, M. Sekulić^a, B. Savković^a, A. Košarac^b, S. Moljević^b, J. Anić^b

^aUniversity of Novi Sad, Faculty of Technical Sciences, Trg D. Obradovica 6, 21000 Novi Sad, Serbia

^bUniversity of East Sarajevo, Faculty of Mechanical Engineering, V. Karadzica 30, 71126 Lukavica, East Sarajevo, Republic of Srpska, Bosnia and Herzegovina

Abstract Aluminum alloy 7075-T6 is a widely used material in the aerospace, marine and automotive industries. Its wide application shows the importance of researching this material in the field of manufacturing. This study focuses on investigating the influence of the input parameters of the turning process when machining aluminum 7075-T6 with a cemented carbide inserts. The input parameters for machining are the depth of cut, feed rate and cutting speed, while the output parameter is the surface roughness of the workpiece. A Central composite experimental design was used for the experiments. The statistical method of analysis of variance (ANOVA) was applied to study the effects of cutting speed, feed rate and depth of cut on surface roughness. The results of this study show that feed rate is the most important factor, followed by cutting speed. The depth of cut is the least significant factor. In addition, the process of Built-Up Edge (BUE) formation on the tool was observed. It was found that as the cutting speed increases, the Built-Up Edge forms more slowly on the tool.

Keywords Aluminium alloys, machining parameters, surface roughness, dry turning

1. INTRODUCTION

Aluminum is the third most abundant metal in the Earth's crust. Aluminum contains extremely stable oxygen compounds, which is why it took scientists a long time to figure out how to turn it into a pure metal. The process was first carried out in 1824 in the laboratory of H.C. Ørsted in Denmark. It took half a century for scientists to discover a process to mass production of aluminum. P.L.T. Héroult invented the electrolytic reduction process for aluminum production in 1886. In the early years, aluminum production amounted to 45,000 tons per year,

while in 1999 it was 25 million tons [1]. Today, the consumption of aluminum is an incredible 67 million tons per year, and it is predicted to increase year by year up to 78.4 million tons per year in 2029 [2].

The largest application is in transportation (32%), followed by containers and packaging (21%) and construction (13%). The amount of aluminum in a car has increased from 36 kg in 1973 to 161 kg in 2010 [3].

Aluminum alloys are of particular interest to both the aerospace and automotive industries. Therefore, improved surface quality of machined parts is required for such applications [4]. To expand the use of aluminum alloys, their strength must be increased. This is achieved with alloying elements such as manganese, magnesium, silicon, zinc and copper.

Ab Aziz N.S.D. and others investigated the cutting material performance of an uncoated cemented carbide tool in dry turning of Al 7075-T651,

Corresponding author

MSc, Anđelko Aleksić
andjelkoa94@uns.ac.rs

University of Novi Sad, Faculty of Technical Sciences,
Department for Production Engineering
Trg Dositeja Obradovića 6
Novi Sad, Serbia.

studying the tool wear rate, material removal rate, wear mechanism and surface roughness. Two different cutting speeds (250 and 450 m/min) were used for the experiment, while the other two parameters of the machining process, feed rate ($s=0.05$ mm/o) and depth of cut ($a=1.0$ mm), were constant. The experiment was conducted for 40 minutes and the results showed that tool wear was 33% lower at lower cutting speeds than at a cutting speed of 450 m/min. With the same flank wear $VB=0.6$ mm, productivity at a cutting speed of 250 m/min is 71 % higher than at a speed of 450 m/min. As for the wear mechanism, in both cases the adhesive wear of the tool is dominant. When turning at a higher than at a lower cutting speed, a lower roughness value of the machined surface was obtained [5].

Martin-Bejar S. and others studied tool wear during turning of Al 7075-T6 aluminium alloy on a CNC lathe with carbide inserts with TiN coating in dry condition. The parameters of the process were as follows: Cutting speed $40\div 200$ m/min, feed rate $0.05\div 0.30$ mm/o and depth of cut $0.5\div 2$ mm. Adhesive wear is the main wear mechanism that occurs during dry turning of this aluminium alloy, in two different ways: Built-Up Layer (BUL) and Built-Up Edge (BUE). The results of the tests show that the values of Built-Up Layer (BUL) and Built-Up Edge (BUE) increase at higher values of feed rate and depth of cut. On the other hand, at constant depth of cut and minimum feed rate, the values of Built-Up Layer (BUL) and Built-Up Edge (BUE) on the tool decrease with increasing cutting speed. At maximum feed rate, the occurrence of Built-Up Layer (BUL) and Built-Up Edge (BUE) on the tool can be seen at all cutting speeds [6].

Beatriz de Agustina, in machining Al 7050-T7 aluminum alloy, has demonstrated that the feed rate has the greatest influence on the roughness of the machined surface, followed by the cutting speed with a smaller percentage, while the depth of cut has the least influence on the roughness of the machined surface. In addition, the chip was also observed, concluding that at lower feed rate values (0,05 mm/rev), a long continuous chip in the form of a "nest" occurs, while at higher feed values (0,25 mm/rev) a short broken chip occurs [4].

2. MATERIAL AND METHODS

2.1 Experimental setup

The experimental work was carried out at the Faculty of Technical Sciences in the Conventional Machining Laboratory. The conditions for the experimental tests are given in this chapter.

The conditions apply to:

- The workpiece material,
- the machine tool,
- the cutting tool and
- the machining conditions,
- the measuring technique.

The workpiece material: The experimental tests were carried out with the aluminum alloy 7075-T6. This material is used in almost all fields, especially in aerospace, marine and automotive industries. The chemical structure is shown in Table 1. The workpiece had a length of 450 mm (cut length) and a diameter of 55 mm.

Table 1. Chemical structure of AL 7075-T6

Si	Cu	Fe	Zn	Mg	Mn
0,14	1,57	0,24	5,58	2,38	0,15
Ni	Pb	Sn	Ti	Cr	Ti+Zr
0,03	0,03	0,03	0,03	0,22	0,22

Machine tool: Machining was performed on an Index GU -600 CNC lathe in dry condition.

Cutting tool: A turning cutter SDJCR2020K11, with cemented carbide inserts ("SECO" type DCGT11T308F- AL KX). Table 2 illustrates the geometrical characteristics of the cutting tool on the tool holder [7].

Table 2. Geometrical specifications of DCGT11T308F-AL KX insert

Geometrical Characteristics of DCGT11T308F-AL KX insert	Value
Clearance angle major	7°
Insert included angle	55°
Theoretical cutting edge length	11,60 mm
Corner radius	0,80 mm
Insert thickness	3,97 mm

Machining conditions: Depth of cut, feed rate, and cutting speed were used as cutting conditions. In Table 3 lists the cutting parameters and their values depending on the

workpiece material of the workpiece and the tool manufacturer's recommendations.

Table 3. Machining parameters and their levels

Levels	Depth of cut a [mm]	Feed rate f [mm/rev]	Cutting speed v [m/min]
Max. +1	0,5	0,05	200
Medium 0	0,75	0,11	315
Min. -1	1	0,18	430

Measuring technique: A Mitutoyo SurfTest SJ-210 was used for the surface roughness measurements. Measurements were taken three times for each experiment, and the mean value was selected for data processing. To monitor the formation of BUE and BUL on the tool, a "NEXIUS zoom trinto EVO 6.5-55x" microscope with a "CMEX - 5 Pro" camera was used.

3. RESULTS AND DESCUSSION

In Table 4 shows the experimental setup and the measured results of surface roughness R_a . A central composite experimental design was used. All experiments were performed with an insert without coolant.

Table 4. The setup of experiments and results of surface roughness

Exp no.	Machining parameters			R_a [μm]
	a [mm]	f [mm/rev]	v [m/min]	
1	0,5	0,05	200	0,360
2	1	0,05	200	0,375
3	0,5	0,18	200	1,082
4	1	0,18	200	1,581
5	0,5	0,05	430	0,730
6	1	0,05	430	0,617
7	0,5	0,18	430	1,696
8	1	0,18	430	0,977
9	0,5	0,11	315	0,587
10	1	0,11	315	0,519
11	0,75	0,05	315	0,242
12	0,75	0,18	315	1,254
13	0,75	0,11	200	0,747
14	0,75	0,11	430	0,752
15	0,75	0,11	315	0,563
16	0,75	0,11	315	0,506
17	0,75	0,11	315	0,542
18	0,75	0,11	315	0,581
19	0,75	0,11	315	0,575
20	0,75	0,11	315	0,496

3.1 Response surface regression: R_a

The statistical software "Design Expert 7.1.5" was used to analyse the experimentally obtained results and to determine the mathematical model for the arithmetic mean roughness of the machined surface. Analysis of variance was used to determine the significance of the input parameters of the machining process as well as the mathematical model itself [8], [9].

Analysis of variance was performed based on Table 4. The results of the analysis are shown in Fig. 1.

ANOVA for Response Surface Quadratic Model

Analysis of variance table (Partial sum of squares - Type III)

Source	Sum of Squares	df	Mean Square	F Value	p-value Prob > F	
Model	2.73	9	0.30	16.81	< 0.0001	significant
A-a	0.015	1	0.015	0.83	0.3848	
B-f	1.82	1	1.82	100.89	< 0.0001	
C-v	0.039	1	0.039	2.18	0.1706	
AB	1.860E-003	1	1.860E-003	0.10	0.7547	
AC	0.23	1	0.23	12.55	0.0053	
BC	0.045	1	0.045	2.51	0.1441	
A ²	3.914E-005	1	3.914E-005	2.170E-003	0.9636	
B ²	0.10	1	0.10	5.57	0.0399	
C ²	0.10	1	0.10	5.66	0.0386	
Residual	0.18	10	0.018			
Lack of Fit	0.17	5	0.035	27.00	0.0013	significant
Pure Error	6.443E-003	5	1.289E-003			
Cor Total	2.91	19				

Fig. 1. Response surface regression: R_a versus a, f, v.

Based on the value of P, a decision is made about the significance of the parameters. If the value of $P < 0,05$, the parameter is significant [8]. From the observation of Fig. 1, it can be concluded that the feed rate parameter is significant, while the other parameters, depth of cut and cutting speed, are not significant.

After analyzing the mathematical model ($R_{sq}=0,94$ and $R_{sq(adj)}=0,88$), it is concluded that the model is appropriate. Since the value of the reduced model is about 90 %, it is adopted (Equation 1).

$$R_a = -0,079258 + 0,027988 * s - 5,85217E - 0,03 * a * v + 45,26089 * s^2 + 1,45730E - 0,05 * v^2 \quad (1)$$

Figure 2 shows the data distribution, which indicates that the results of the experiment are normally distributed, i.e., none of the results deviates from true normality, from which it can be concluded that the experimental design is set up correctly.

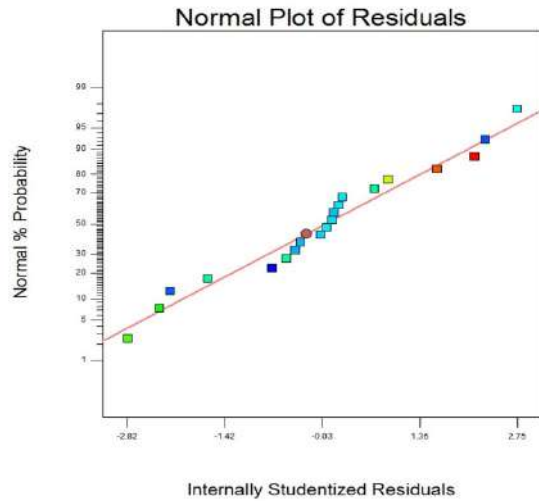


Fig. 2. Normal probability plot of the residuals

3D reaction surfaces can be created to better illustrate the dependence of the studied reaction on the selected factors. Figure 3 shows the influence of depth of cut and feed rate at constant cutting speed is constant, on the arithmetic mean roughness of the machined surface.

From the diagram (Fig. 3), it can be seen that changing the depth of cut has almost no effect on the performance characteristic, while increasing the feed rate linearly increases the value of the performance characteristic. It can be concluded that the feed rate has a great influence on the output characteristic, while the depth of cut has no influence.

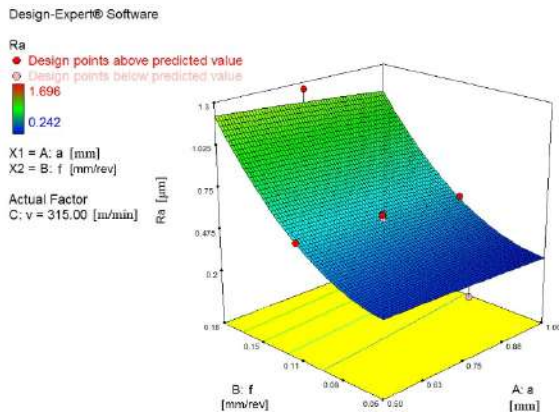


Fig. 3. 3D response surface for Ra: the depth of cut and feed

Figure 4 shows the influence of depth of cut and cutting speed at constant feed on the performance characteristic Ra. It can be seen from the diagram that these two input values are

interdependent. At minimum values of the depth of cut, there is a linear increase in the output characteristic when the cutting speed is increased above 300 m/min, while the opposite effect occurs when the depth of cut is increased to the maximum value. The reason for this behaviour is that at low depth of cut and high cutting speeds, the machining process is not stable, which is directly reflected in the mean arithmetic roughness of the machined surface.

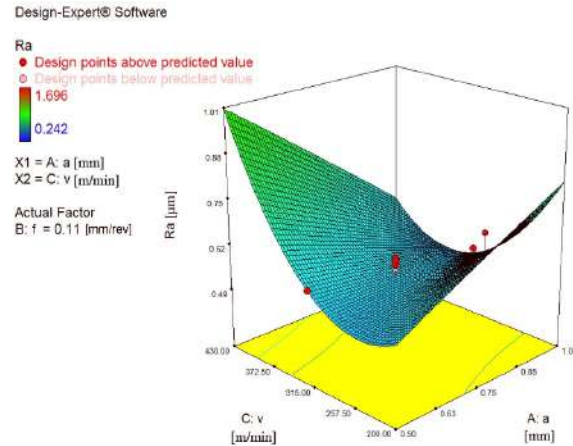


Fig. 4. 3D response surface for Ra: the depth of cut and cutting speed

Figure 5 shows the influence of the feed rate and the cutting speed on the performance characteristic Ra, while the depth of cut is constant. From the diagram, it can be concluded that when feed rate and cutting speed are combined, the feed has a dominant influence on the output characteristic.

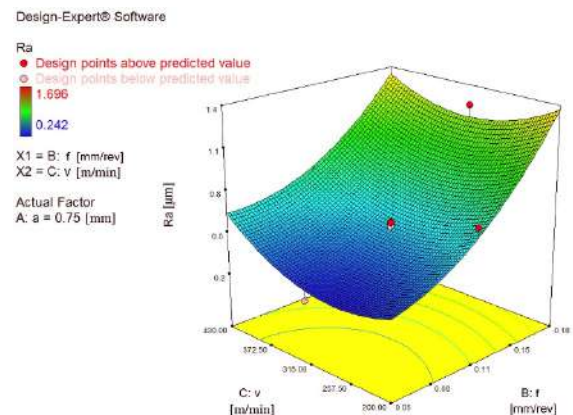


Fig. 5. 3D response surface for Ra: feed and cutting speed

3.1 Tool wear

The second part of the experiment was based on monitoring the formation of BUE and BUL on the cutting tool. During the experiment, their formation was monitored at three different cutting speeds ($v=200$, 315 and 430 m/min), while the values of depth of cut and feed rate were constant ($a=0,75$ mm and $f=0,11$ mm/rev). The result shows that BUE and BUL on the cutting tool increase over time at all three cutting

speeds, but at higher cutting speeds the process of formation of BUE and BUL on the cutting tool is much slower than at lower cutting speeds (Fig. 6).

The reason for this phenomenon is that at higher cutting speeds, the BUE and BUL are led off from the cutting edge, thus getting started their re-formation and so on in a circular pattern.

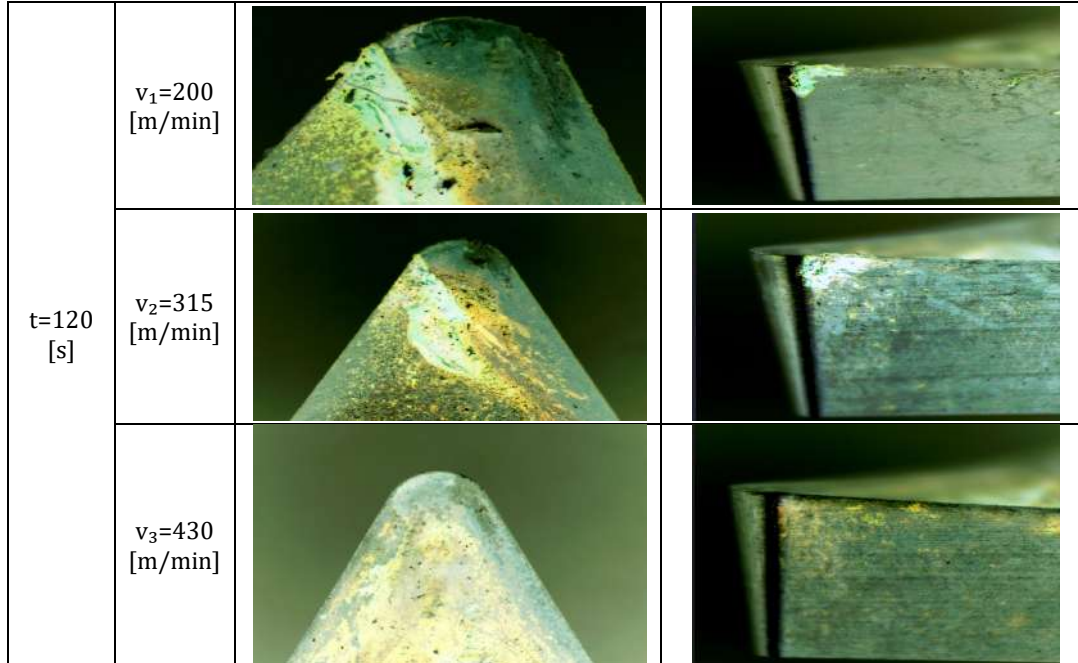


Fig. 6. Deposits on the cutting edge after 120 seconds of cutting

4. CONCLUSION

This paper presents the results of an experimental investigation carried out with the aim of determining the influence of the input parameters (a , f , v) on the output characteristics of R_a . In addition, the formation of BUE and BUL on the cutting edge was monitored. Based on the theoretical and experimental studies carried out and the analyses performed, the following conclusions can be drawn:

- Regression analysis and ANOVA contribute the most to accurately represent the adequacy and significance of models and cutting parameters, thus facilitating the work of researchers.
- For surface roughness, feed rate is the most significant factor, followed by

cutting speed. The depth of cut is the least significant factor.

- The accuracy of the mathematical model is high, but it could be better. One way to improve the mathematical model is to change the parameter values or reduce the differences between the maximum and minimum values.
- As the cutting speed increases, the BUE and BUL on the tool decrease. It was also observed that at a cutting speed of 430 m/min, the BUE and BUL on the tool formed more slowly and broke off from the tool over time.

Further research in the field of machining aluminium alloys with carbide inserts can go in the direction of expanding the factors that affect surface roughness during turning, such as the effects of coolants and lubricants and nose

radius. Optimization of the process should also be the focus of further research.

Acknowledgement

This research (paper) has been supported by the Provincial Secretariat for Higher Education and Scientific Research AP of Vojvodina through project No. 142-451-334/2023-01/2: "Advanced processing technologies of modern engineering materials".

REFERENCES

- [1] T. Cock, "Aluminium - A Light Metal," *TALAT - Train. Alum. Appl. Technol.*, pp. 1–10, 1999.
- [2] Statista, "Global aluminum consumption projections from 2021 to 2029," *Statista Research Department*, 2022. <https://www.statista.com/statistics/863681/global-aluminum-consumption/> (accessed Jan. 19, 2023).
- [3] B. Stempel, "The Road Ahead Looks Brighter and Lighter," in *American Metal Market's North American Aluminum Conference*, Jun. 2007.
- [4] B. De Agustina, E. M. Rubio, M. Villeta, and M. A. Sebastian, "Experimental investigation of dry turning of UNS A97050-T7 aluminium alloy bars based on surface roughness," *Int. J. Mechatronics Manuf. Syst.*, vol. 3, no. 5/6, p. 437, 2010, doi: 10.1504/IJMMS.2010.036068.
- [5] N. A. Raof, N. S. Daud @Ab Aziz, A. R. A. Ghani, A. N. Dahnel, S. Mokhtar, and N. K. Muhamad Khairussaleh, "CUTTING TOOL PERFORMANCE IN TURNING OF AL 7075-T651 ALUMINIUM ALLOY," *IJUM Eng. J.*, vol. 21, no. 2, pp. 177–185, Jul. 2020, doi: 10.31436/iiumej.v21i2.1227.
- [6] S. Martín-Béjar, F. J. Trujillo, L. Sevilla, and M. Marcos, "Indirect adhesion wear parametric analysis in the dry turning of UNS A97075 Alloys," *Procedia Manuf.*, vol. 13, pp. 418–425, 2017, doi: 10.1016/j.promfg.2017.09.036.
- [7] "Secotools.com," "Elektronski katalog reznih alata za obradu struganjem," Feb. 21, 2021. https://www.secotools.com/article/p_0040400 (accessed Feb. 21, 2023).
- [8] A. Aleksic, D. Rodic, M. Sekulic, M. Gostimirovic, and B. Savkovic, "Effect of cutting parameters on surface roughness in turning of CPM 10V steel," in *2022 21st International Symposium INFOTEH-JAHORINA (INFOTEH)*, Mar. 2022, pp. 1–4. doi: 10.1109/INFOTEH53737.2022.9751329.
- [9] A. Aleksić, M. Sekulić, M. Gostimirović, D. Rodić, B. Savković, and A. Antić, "EFFECT OF CUTTING PARAMETERS ON CUTTING FORCES IN TURNING OF CPM 10V STEEL," *J. Prod. Eng.*, vol. 24, no. 2, pp. 5–8, Dec. 2021, doi: 10.24867/JPE-2021-02-005.



Banja Luka
1–2 Jun 2023.

DEMI 2023
**16th International Conference on
Accomplishments in Mechanical and
Industrial Engineering**
www.demi.mf.unibl.org



Finite element and experimental modal analysis of high speed spindle

M. Knežev^a, A. Živković^a, C. Mladenović^a, D. Marinković^a, V. Ilić^a, M. Moravec^b

^a University of Novi Sad, Faculty of Technical Sciences, Trg Dositeja Obradovića 6, 21000 Novi Sad

^b Technical University of Košice, Faculty of Mechanical Engineering, Park Komenského 5, 04200 Košice

Abstract Prediction of the dynamic behavior of machine tools in the design phase is an important step in their development. Earlier research related to the main spindles was primarily based on static and quasi-static analyses, while lately they have been extended to optimal design using dynamic analysis. Mathematical description of dynamic behavior can be obtained only for simple and idealized cases. Consequently, the finite element method (FEM) is the most commonly used method for analyzing the dynamic behavior of the main spindle. When defining the FEM model of the spindle, the type of finite element must first be chosen correctly. The most commonly used types of finite elements are based on three theories: Euler-Bernoulli, Rayleigh's and Timoshenko's beam theory. In this work, a model was developed based on computer modeling using a general-purpose programming system based on the finite element method. Using this system, an analysis of the dynamic behavior of the motor-spindle was performed, in order to compare the results of computer modeling and the results obtained by experimental testing.

Keywords Modal analysis, FEM, High speed spindle

1. INTRODUCTION

The machine tools behavior in exploitation is conditioned by the behavior of certain vital assemblies [1]. One of the most influential machine tool components, affecting the accuracy and productivity of machining is the spindle unit. According to Li [2], the magnitude of the natural frequency also depends on the installation method of the angular contact ball bearings. It was noticed that for the "X" bearing layout, the values of the natural frequencies increase as the number of revolutions increases, while for the

"O" bearing layout with the same preload, the value of the natural frequency decreases with the increase in the number of revolutions [3] [4]. Prediction of the dynamic behaviour of machine tools in the design phase is an important step in their development.

A particularly important place is the identification of the dynamic behaviour of the main spindles, which is conditioned by the behaviour of individual elements (bearings, tool holder, tool,), as well as the influence of connections (joints) between elements. The dynamic behaviour of the main spindle assembly directly affects the stability of the cutting process. Its properties also affect the reliability of the entire system. The problem of looking at the dynamic properties of the system mainly spindle bearings, lies in the fact that with every change in the number of revolutions, tool, tool

Miloš Knežev

PhD, Miloš Knežev
knezev@uns.ac.rs

University of Novi Sad, Faculty of Technical Sciences
Trg Dositeja obradovića 6
Novi Sad, Serbia

holder, the conditions and properties of the system change.

Finding the natural frequencies affects the RPM ranges in which the machine will operate, i.e. vice versa, the spindle will be modified so that the natural oscillation frequencies are outside the standard RPM ranges at which the machine tool operates. Bearing positions, type of bearing method and type of tools and tool holders, etc. it will affect the shape of the main spindle oscillation and the reliability of the system. The movement of the spindle tip during oscillation affects the stability of the cutting process, contributes to a lower quality of the processed surface and lower accuracy of the work piece.

2. EXPERIMENTAL AND FEM ANALYSIS OF MOTORIZED SPINDLE

An analysis of the dynamic behaviour of the motorized spindle was carried out for a freely supported main spindle with bearing. This analysis included the development and determination of natural frequencies and main modes of shaft oscillation without damping, and without taking into account damping in the material. After the evaluation of the results obtained by the FEM method, a comparison will be made with the results obtained by the experimental test.

2.1 Motorized spindle

Tested motorized spindle the GMN TSSV 90000, whose cross-section is shown in figure 1.

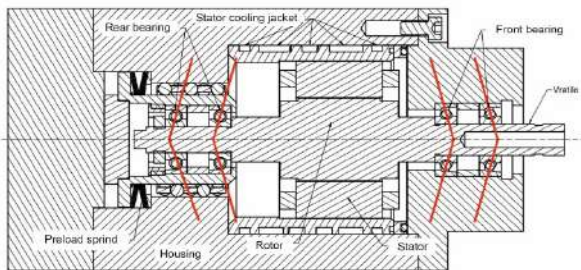


Fig. 1. Cross section of GMN TSSV 90000 motorized spindle assembly

The shaft is fitted with two pairs of high precision ball bearings with angular contact, the front bearing is EX 12 7C1 DUL SNFA while the rear is EX 10 7C1 DUL SNFA, mounted in a "tandem" arrangement in pairs, so that the entire

bearing forms an "O" arrangement. The high-speed motorized spindle assembly is designed as an asynchronous electric motor, so the stator is mounted in the housing, and the rotor is integrated with the shaft. One of the sources of generated heat is the asynchronous motor, while the other source is the bearings. For this reason, the stator is mounted in a sleeve with a channel around it, through which the cooling fluid flows, while the cooling of the bearing is done by pressurized air and oil, i.e. oil mist flowing through the bearings and in the gap between the rotor and the stator.

2.2 FEM modal analysis

In general, the assembly of the motorized spindle is complex for simulation, due to the nonlinearity of the system itself, as well as the complexity of mechanical and thermal phenomena. In order to examine the influence of certain parameters on the dynamic behaviour of the main spindle, a dynamic numerical model of the spindle was developed in the paper (figure 2). An isoparametric hexahedron (SOLID 187) was used for the discretization of FEM spindle model 27606 of them.

The analysis of dynamic behavior was performed without the effect of the excitation force (modal) and with the effect of the excitation force on the top of the spindle (harmonic), in order to define the amplitude-frequency characteristics of the considered main spindle for certain natural frequencies and given excitation. The force (220 N) is given at the top of the spindle, while the spindle responses are observed at points 1, 2, 3, 4 and 5 (Figure 2)



Fig. 2. Discretized model of shaft

2.2 Experimental model analysis

Through experimental tests (Figure 3), it is possible to generate the frequency response function (FRF) or the system transfer function (TF). The basic idea is to excite the machine structure with a force of a certain frequency at a certain place, and to monitor the dynamic

response of the system at the same or some other place.

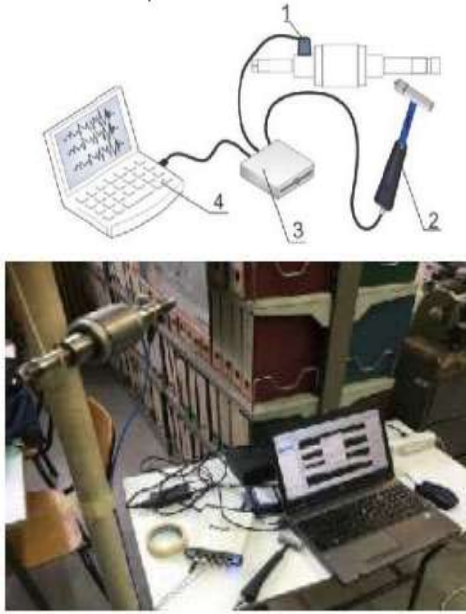


Fig. 3. Discretized model of a) main spindle, b) bearing

During the experimental modal analysis using impulse excitation, the system is excited by a wide range of different frequencies in just one test, while the system's response.

When the recorded data are transformed into the frequency domain, using the fast Fourier transform, the frequency response function between the point where the system response was measured (i) and the point where the excitation force (j) was applied is obtained, which can be displayed as follows [5]:

$$FRF_{ij}(\omega) = \frac{X_i(\omega)}{F_j(\omega)} \quad (1)$$

Also, it should be noted that in most cases, as a response of the system, it is necessary to obtain displacement X . However, if the measurement is performed by acceleration sensors, the previous equation has the form [5]:

$$FRF(\omega) = \frac{\ddot{X}}{F(\omega)} = \frac{A(\omega)}{F(\omega)} \quad (2)$$

The modal parameters of the system that are calculated based on the real and imaginary part of the FRF are: dimensionless damping coefficient " ζ ", modal stiffness k , modal mass m :

$$2\zeta_1 = \frac{\left(\frac{f_2}{f_1}\right)^2 - 1}{\left(\frac{f_2}{f_1}\right)^2 + 1} \quad (3)$$

$$k = \frac{-1}{2\zeta H} \quad (4)$$

$$m = \frac{k}{f_n^2} \quad (5)$$

Also, if the modal parameters of the system are known, the real and imaginary parts of its frequency response function are calculated using the expressions:

$$Re\left(\frac{X}{F}\right) = \frac{1}{k} \left[\frac{1-r^2}{(1-r^2)^2 + (2\zeta r)^2} \right] \quad (6)$$

$$Im\left(\frac{X}{F}\right) = \frac{1}{k} \left[\frac{-2\zeta r}{(1-r^2)^2 + (2\zeta r)^2} \right] \quad (7)$$

$$r = \frac{f}{f_n} \quad (8)$$

3. RESULTS AND DISCUSION

The defined frequency response function obtained by the numerical model (Figure 4), i.e. its real and imaginary part, is used to calculate the modal parameters of the modal stiffness (k) and modal mass (m) system in the form:

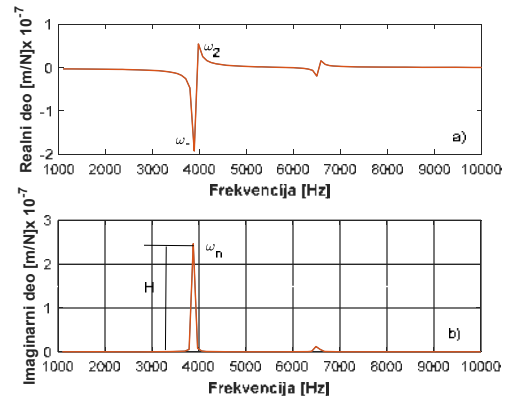


Fig. 4. a) Real; b) imaginary part of the frequency response function at point 1 for a freely supported main spindle

$$k = \frac{-1}{2\zeta H} \quad (9)$$

$$m = \frac{k}{\omega_n^2} \quad (10)$$

Figure 5 shows the first form of oscillation of a freely supported shaft.

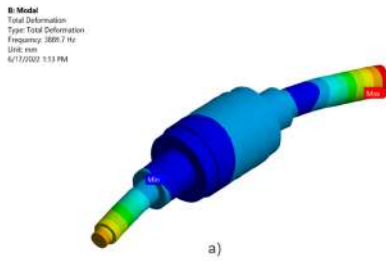


Fig. 5 First natural frequency and form of oscillation for freely supported shaft

During the mathematical modeling of the dynamic behaviour of the coefficient value, the damping was varied in a very wide range from 0.003 to 0.3 for the case of the action of the excitation force on the top of the spindle. During experimental testing, the damping coefficient values were accurately calculated using the frequency response function.

Figure 6 shows the first three forms of oscillation, i.e. the first three natural oscillation frequencies of the freely supported main spindle without consideration of damping.

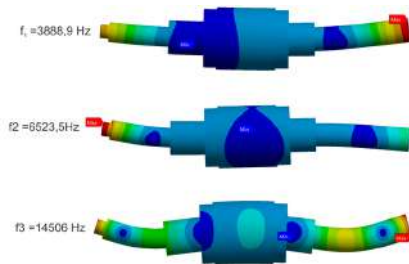


Fig. 6 The first two forms of oscillation and natural frequencies

In the analysis with the excitation force at the top of the spindle, the frequency ranges up to 10 [kHz] was observed because the first natural frequency is twice as high as the rotation frequency of the motor-spindle, so frequencies above 10 [kHz] are not critical. For different values of the relative damping coefficient (ξ). Comparisons of natural frequencies for the first two oscillation modes determined by FEM modeling and experimental testing are shown in table 1. It should be noted here that the first two natural frequencies are the same in all considered points, only the amplitudes at these frequencies differ.

Table 1. Comparison of the first two natural frequencies (f_1 and f_2) obtained by FEM modeling and experimental testing

Exp no.	Natural frequencies	FEM model [Hz]	Experiment [Hz]
1	f_1	3887.2	3838
2	f_2	6580.3	6525

4. CONCLUSION

By comparing the values of the characteristic natural frequencies (Table 1), it can be seen that the deviation between the frequencies determined by FEM modeling and experimental testing, on the first mode is 1.2 [%], which is also the most dominant. Based on this, it can be concluded that FEM modeling gives satisfactory results, especially considering that the difference between FEM modeling and experimental testing at the second natural frequency is only 0.8 [%].

Acknowledgement

This research (paper) has been supported by the Ministry of Science, Technological Development and Innovation through project no. 451-03-47/2023-01/200156 "Innovative scientific and artistic research from the FTS (activity) domain".

VEGA nr.1/0485/22

REFERENCES

- [1] A. Živković, M. Zeljković, and M. Knežev, "Thermal model of high speed main spindle," in *3th International Scientific conference, Conference on Mechanical Engineering Technologies and Applications - COMETA 2016*, 2016, pp. 215–220.
- [2] H. Li and Y. C. Shin, "Analysis of bearing configuration effects on high speed spindles using an integrated dynamic thermo-mechanical spindle model," *Int. J. Mach. Tools Manuf.*, vol. 44, no. 4, pp. 347–364, Mar. 2004, doi: 10.1016/j.ijmachtools.2003.10.011.
- [3] M. Knežev, A. Živković, M. Zeljković, and C. Mladenović, "Numerical and experimental modal analysis of high speed spindle," in *13th International Conference on Accomplishments in Mechanical and Industrial Engineering-DEMI*, 2017, pp. 101–108.
- [4] M. Knežev, "Modelovanje toplotno-mehaničkog ponašanja visokobrzinskog Motor-vretena mašina alatki," University of Novi Sad, Faculty of Technical Sciences, 2022.
- [5] C. Mladenović, "Dinamičko ponašanje obradnih sistema za mikroobradu," University of Novi Sad, Faculty of Technical Sciences, 2020.



Banja Luka
1-2 Jun 2023.

DEMI 2023

16th International Conference on Accomplishments in Mechanical and Industrial Engineering

www.demi.mf.unibl.org



Industry 4.0 technologies and systems for the transformation of companies into low-carbon companies

L. Črpič, J. Butara, M. Mavko, K. Kofalt, N. Sovec, E. Hozdić

*University of Novo mesto, Faculty of Mechanical Engineering, Department of Production Engineering and Design,
Na Loko 2, SI-8000 Novo mesto, Slovenia*

Abstract *Modern manufacturing companies are in the phase of digital transformation according to the principles of the concept of the fourth industrial revolution - Industry 4.0. Industry 4.0 technologies and systems enable the transformation of companies and the restructuring of their production structures with the aim of achieving global goals and concepts of the circular economy. Achieving global goals is made possible by the use of modern information and communication technologies (ICT), the Internet of Things, the Internet of Services, social networks, and so on. The concepts of the circular economy require modern manufacturing systems that will enable monitoring the impact of products and their manufacture on the environment throughout their life cycle. Over the past ten years, various concepts for modern production systems have been developed as part of the Industry 4.0 concept. Such systems are cyber-physical production systems (CPPS), which are the basic building blocks for smart factories.*

The paper presents technologies that enable digital transformations and systemic restructuring of manufacturing systems, such as ICT, Internet of Things, Internet of Services, social networks, 3D technologies, cyber-physical systems and cyber-physical production systems. The implementation of the presented Industry 4.0 technologies and systems opens the way to low-carbon operations for modern manufacturing companies.

Keywords *Information-communication technology (ICT), 3D technology, cyber-physical systems, Industry 4.0*

1. INTRODUCTION

The EU Industrial Strategy, presented by the European Commission in 2020 and updated in 2021, is putting forth the strengthening of the single market, which is the basis for the EU's competitiveness in the global market. The objective of the updated industrial strategy is to strengthen Europe's leading role as a global

industrial force to ensure competitive advantage in digital and green technologies [1]. Today's modern manufacturing companies are in the phase of digital transition, following the principles of the concept of the Fourth Industrial Revolution, the so-called Industry 4.0. This transition enables the transformation of manufacturing companies and their production structures with the aim of achieving global goals [2] and concepts of the circular economy [1]. Based on a review of domestic and foreign scientific literature, we conclude that the digital transition to a circular economy encourages manufacturing companies to transform their production structures, reuse, repair, and recycle

Corresponding author

Asst. Prof. Elvis Hozdić, PhD
elvis.hozdic@fs-unm.si

*University of Novo mesto, Faculty of Mechanical Engineering
Na Loko 2
8000 Novo mesto, Slovenia*

existing materials and products, use energy from renewable sources, eliminate the use of hazardous chemicals, reduce the use of environmentally unfriendly raw materials, and carefully design products that have the least impact on the environment.

The introduction of Industry 4.0 technologies and systems is a low-carbon reality for modern companies. By reducing all gasses, not just carbon, which causes emissions to the environment and consequently destroys ozone and nature, companies are trying to run processes with fewer emissions and environmental impacts. Even from an energy loss perspective, modern companies say they are already having an impact on reducing energy loss and carbon dioxide (CO₂) when developing new products with Industry 4.0 technologies and systems.

The following article presents industry 4.0 technologies and systems, and an industrial example of the implementation of such technologies and systems in the real environment in the development of modern products.

2. INDUSTRY 4.0 TECHNOLOGIES

Industry 4.0 [3,4] is a term that use to describe the next stage of the industrial revolution, where advanced technologies connect physical and virtual, digital or cyber systems, processes and people. It is a holistic approach to the design of a manufacturing process that includes a comprehensive digital transformation of the enterprise. This technological change is leading to a revolution in production processes as the focus shifts from mass production to individualized production, tailored to the needs of each customer. This enables a faster and more flexible response to market needs and the provision of high quality and more individualized products.

Industry 4.0 is a concept that has been much discussed at various levels of society over the last fifteen years. According to academics, the concept of Industry 4.0 was first mentioned by a working group that presented proposals and a strategy for it to the German government. A similar initiative was launched in the USA.

Industry 4.0 aims to increase the level of automation in all areas of industry and to take the next step towards a new industrial revolution, called Industry 5.0, based on

artificial intelligence and cognitive technologies [5-7]. In this way, manufacturing companies will increase their productivity and efficiency and make the manufacturing industry more employable and profitable.

The fourth industrial revolution attaches great importance to the concept of connecting existing physical, digital or cyber environments in so-called cyber-physical environments. Many scientific discussions and articles assume that new business models, production and work systems, digitized and cybernated work processes in modern manufacturing companies will emerge in the context of cyber-physical integration and networking. These changes will also have a profound impact on society and people, especially with regard to the transition to a circular economy.

2.1 Information-communication technologies

Advanced information and communication technologies (ICT) represent one of the fundamental features of the 21st century [8]. The use of ICT in manufacturing is one of the biggest changes in the business of manufacturing companies in the last 30 years [9].

Today there are many definitions of ICT. In [10], Bakopoulos defined ICT as a variety of means for collecting, transmitting and processing data and information with the aim of supporting the implementation of business processes in companies.

In [11], Weill and Broadbendt point out that ICT includes all means and devices used to collect, process, analyse and store data.

ICT enables the use of information and communication via digital devices and networks and is important for everyday work as well as for companies, as it enables business that is more efficient and improves process management.

ICT is structured into various information systems in manufacturing companies to implement supporting business and production processes.

In [12], the author defines the information systems as: "... it can be any organized combination of people, communications networks, data sources, hardware and software that collect, process, transform, and disseminate information within your organization."

Key tasks of information systems and comprehensive system solutions in advanced production systems are data acquisition, data processing, organization of data and information in a useful form (creation of a data model), data storage and filing, and data transfer.

ICT is also key to the implementation of Industry 4.0 concepts by enabling the integration of machines and the analysis of big data to improve production and services [13].

Advanced ICT, from the perspective of industrial production, is a technology for the development of information systems of manufacturing enterprises and networked manufacturing systems, see Figure 1.

ICT systems consist of various components that work together to ensure efficient transmission of information. These components include: 1) computer hardware and software with computers, servers, routers, and other devices used for processing, storing, and transmitting information; 2) network communication technologies that include the Internet (Internet of Things and Internet of Services), local area networks (LAN), broadband access networks (WAN), and other technologies for transmitting information over various channels such as wired and wireless connections; 3) applications and services include various applications such as e-mail, video conferencing, social networks, etc., that enable communication, collaboration, and information management; 4) information or security services, data protection, cloud storage services, data management, and other services that enable efficient information management; 5) cloud related services, such as cloud data storage services or cloud data management and analysis services, enable organizations and businesses to effectively manage data and provide them with fast and reliable ways to share and process information over the Internet.

The Internet is a new, rapidly evolving paradigm [14] that has emerged in the field of modern communication technologies. The Internet refers to a global information system that: 1) is logically connected to a globally unique Internet Protocol (IP) address space or its extensions/upgrades; 2) supports communication with the use of Internet Protocol stack (TCP/IP) or its extensions; and 3) provides, uses or enables public or private

access to high-level services at the communication level [15].

Thanks to the Internet, today we have developed smart environments in the form of smart things or the Internet of Things (IoT) and smart services or Internet of Service (IoS) that can communicate with each other.

The IoT is a technology that allows you to connect to different devices over the Internet.

In [14], the authors define IoT as a computing concept that describes a future in which everyday physical objects are connected to the Internet and can communicate and collaborate with other devices.

In the industrial context, the IoT is used to connect various devices and sensors in the production process.

These devices can connect to each other and to the cloud, enabling real-time data collection, data analysis, and process adaptation. For example, IoT sensors can detect problems in the manufacturing process, such as machine breakdowns, and send immediate notifications for quick action.

The IoT concept and vision are presented in part [16], see Fig. 1.

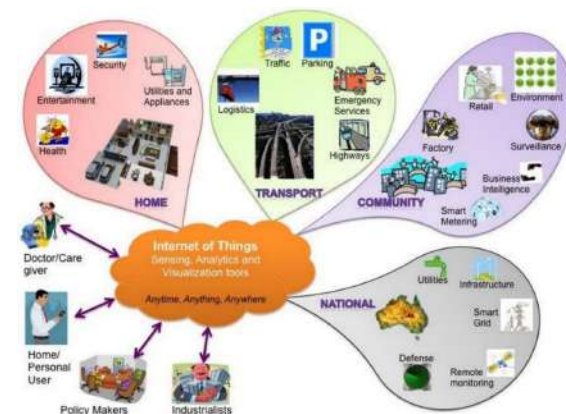


Fig. 1. The Internet of Things concept [16]

The IoT is a revolutionary advance in the field of the Internet, where things (objects) become self-recognizing and communicative, resulting in the creation of a special intelligence through the ability to make decisions. With such characteristics, things become “smart”.

Analysing the literature dealing with IoT, it can be observed that many authors [16], [17], [18] propose different definitions, but roughly speaking or summarizing the goal of IoT is to integrate physical objects into a global network

where they have their own identification and communicate with other objects to obtain information and generate new knowledge. Fundamental technologies for the implementation of the IoT are Radio-Frequency Identification (RFID) [19], Sensor Networks – SNet, wireless technologies [20], Quick Response Codes – QR, Machine-to-Machine communication – M2M communication [21], Internet Protocol – IP, semantic data integration, agent technologies, etc., see Fig. 2.

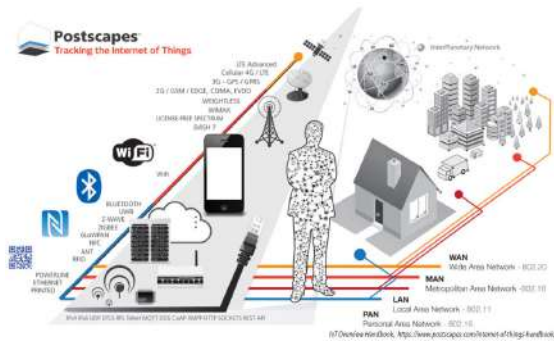


Fig. 2. IoT enabling technologies [22]

Internet of Service (IoS) are software applications that enable interaction and communication between different computer systems over the Internet. These services provide access to data and functions available on remote servers through standard protocols such as HTTP, FTP, SMTP, etc. IoS have become important to many organisations and businesses, because they provide access too many functions and services without having to maintain their infrastructure. This, in turn, allows companies to focus on their core activities.

IoS can be understood as a form of infrastructure and business model that radically changes the way services are developed, and used. IoS uses the Internet as a medium to create new value through services.

IoS provides, from an ICT perspective, a global description of standards, tools, applications and architectures to support business activities and the development of various forms of online services.

In [23], Xu identified the three most common types of models for service delivery, i.e., Software as a Service – SaaS, Platform as a Service – PaaS and Infrastructure as a Service – IaaS. These service models are usually

implemented using industry standard interfaces such as Service Oriented Architecture (SOA) and Web Services – WS.

SOA is an application architecture [24] that connects heterogeneous, distributed, complex and inflexible business entities and divides them into individual business functions – services. SOA is capable of developing, implementing, discovering, integrating, and reusing services independently of the applications and computing platforms on which they are implemented, making business processes simpler, more consistent, and more flexible.

The fundamental meaning of SOA is that services can be searched over a network that is accessible at the time of implementation [25]. This allows the same services to run in different processes without the need to know their exact location. In order for the service to be used, information about each specific service must be stored in one or more central registers.

The WS represents any software application that is accessible through a network and those benefits from a standardized Extensible Markup Language – XML message exchange standard. The WS architecture is described in article [26].

2.1 Cloud computing

Computer clouds (CC) are a new technology that has been conceptually conceivable for a long time, but has only come into wider use in recent years [27], see Fig. 3.

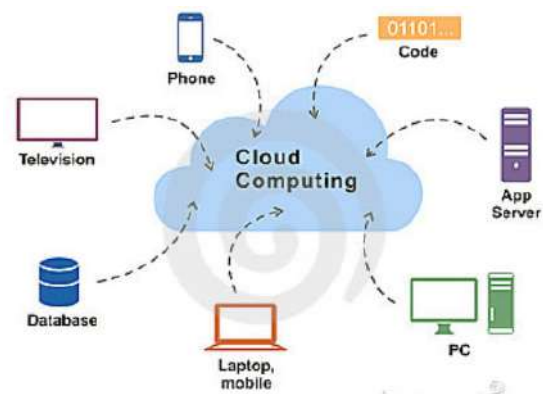


Fig. 3. Cloud computing [28]

Collaboration, IoT and CC are identified in [29] as key links that will enable the development of new forms of business around the world.

In [30], the authors define CC as follows: A computer cloud is a set of network services used to provide various computer services (a type of digital data storage or software solution implementation).

Cloud production is defined as a subscriber-centric model that takes advantage of shared access to a different of production resources on demand. In this way, it is possible to implement production lines with the possibility of modification, which higher efficiency and lower costs for the existence of the product, and allow optimal disposal of the equipment in the light of the changing requirements of the clients [31]. The cloud-based production system is implemented by three key actors: service providers, cloud operators and service users [31].

The fundamental characteristic of cloud production is that it enables dynamic production structuring based on virtual production facilities. A virtual production facility represents a real object in a network environment and provides insight into its functional and business characteristics. Based on the information obtained from the virtual objects, the process of production structuring can be performed [32].

The reference architecture of the cloud-based computer cloud and production system is presented in [23], the cloud-based decentralised network architecture is presented in [33], while the possible uses are discussed in parts [34,35].

2.3 3D technologies

The 3D scanning and measurement technologies, mentioned by Mortensen, Shortis, and Yang [36] are used to capture and analyse three-dimensional information about objects or surfaces.

Non-contact scanning technologies [37] include laser scanning, optical scanning, stereoscopic scanning, structural light scanning, magnetic resonance imaging, and others.

Laser scanning is a technology that uses lasers to record information about the surface of an object or space, which is then processed into a three-dimensional model.

Optical scanning is a technology that uses cameras and light sources to capture information about an object or space.

Stereoscopic scanning uses two cameras pointed at the object to obtain depth information and calculate a three-dimensional model.

Structural light scanning is used to collect data on the depth of an object by resisting light samples.

Magnetic resonance imaging (MRI) uses magnetic fields and radio waves to capture the internal structure of an object.

Contact scanning technologies include coordinate measuring machines (CMM), hand-made measuring devices and tactile probes. CMM is a computerized device that uses tactile probes to collect point data over the surface of an object. Handheld measuring devices are mobile and allow the user to touch the surface of the object and capture form data. Tactile probes are devices used in combination with handheld devices or CMMs that allow data to be collected over the surface of the object.

Scanning software [38] can improve the accuracy and reliability of the data obtained by the scanner. This can help increase the precision and speed of the production process, as users can more efficiently plan and implement production processes with precise information about the shape and dimensions of products. It can also help correct errors and improve product quality.

In line with the growing demand for more accurate and efficient processes, 3D technologies are rapidly becoming key elements in industry. These technologies enable the production of accurate three-dimensional models that can be used to design and implementation of production processes. 3D scanning technologies facilitate product quality control, leading to quality improvements and defect reduction. All this contributes to make manufacturing companies more efficient and competitive [38,39].

3. CYBER-PHYSICAL SYSTEMS

Cyber-physical systems (CPS) are essentially a new generation of systems that integrate computing and physical capabilities [40], [41], Fig. 4.

CPS rely on sensors, actuators and other physical components to collect data and take action in the physical world, while promoting computer algorithms for software for information interpretation and analysis,

decision-making and action based on that information [43].

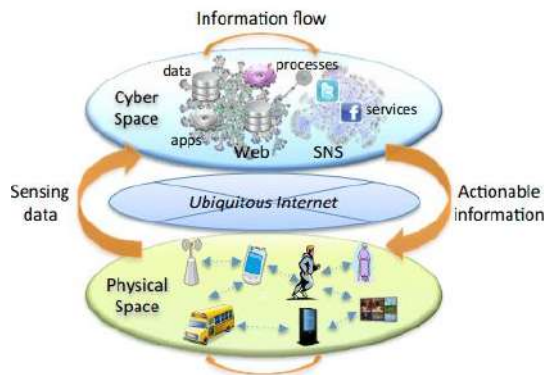


Fig. 4. Cyber-physical systems [42]

The complex definition of CPS was given by the authors in [44]: » *Cyber-physical systems combine computer and communication capabilities to monitor and control entities in the physical world. These systems usually consist of a set of networked agents, including sensors, actuators, control units and communication devices.* «

The CPS provides a number of possibilities in different domains of human life [45-47] such as: Power supply in distribution networks; in the field of medical devices and systems, traffic control, advanced automotive systems, aerospace control systems, distributed robotic systems, defence systems and smart manufacturing structures.

These systems can be used in many industries, including industrial manufacturing, automotive and aerospace control, environmental protection, and healthcare.

CPS have become essential for advanced applications that require high levels of automation and accuracy. In the future, the use of CPS will increase as advanced technologies and automation become key to the development of industry and society as a whole [48].

3.1 Cyber-physical production systems

CPS creates a basis for structuring new production systems [49] that can respond to any change in the market in real time, as well as with high flexibility within and outside the boundaries of the company itself. This not only makes production faster and more consistent with individual customer requirements, but also

allows production processes within the company to be optimized and production systems to be innovative, evolutionary and self-organizing.

The first areas of application for CPS in industrial production are certainly robotics, mechatronics and adaptive distributed production systems.

Cyber-physical production systems (CPPS) play an important role in the development of industrial production in the developed countries of Europe and North America [50-52] and represent a fundamental way to realize a new production philosophy, or rather, the strategy of Industry 4.0 [3].

In the paper [49], Monostori defines CPPS as: »...*based on cyber-physical systems and consisting of autonomous and cooperative elements and subsystems that connect at all levels of production through communications and interactions in a wide range of positions: from machinery and processes to production and logistics networks. Operational modelling and control of cyber-physical production systems enables the realization of a range of basic applied tasks and, above all, the control of the system at any level in real time.*»

In the paper [53] the authors highlight three key CPPS characteristics, namely:

- Intelligence – elements are able to collect data from their surroundings themselves.
- Connectivity – elements connect over the Internet in terms of cooperation, including connecting changes.
- Responsiveness to internal and external changes.

The realisation of the CPPS according to the principles of integration of holons, agent structures and function blocks are the theme of the paper [54]. The prototype implementation of industrial automation based on CPS technologies such as SOAs, agents and cloud is described by Leitão et al. in the paper [55].

According to [56], the transition to new production structures based on CPS concepts requires the development of new models of production systems at all levels. These should enable: 1) the appropriate placement of humans in a system whose role is significantly changing in CPS; 2) the digitisation and cybernetization of existing work processes; 3) the development and realization of new functionalities enabled by the digitisation and cybernetization of work;

4) integration into “smart environments”; 5) vertical integration into integrated work structures; 6) horizontal networking at different levels of manufacturing systems, see Fig. 5.

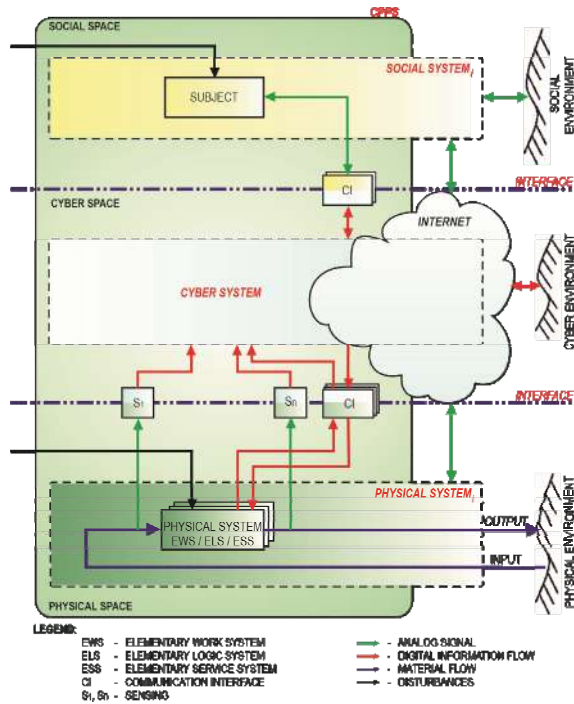


Fig. 5. The conceptual model of social, cyber and physical integration [56,57]

CPPS [57-59] station systems with a certain level of intelligence, or a station of so-called smart systems, which will allow for significantly greater agility and adaptivity of elements of production companies for the needs of modern markets and society. In this way, the CPPS represents systems based on the principles of the fourth industrial revolution and enabling them to operate on a global market under competitive conditions [56].

3.1 Potential of the CPS and CPPS

CPS and CPPS have become indispensable for increasing the efficiency, safety, and sustainability of industrial and transportation systems and enabling new applications and services that were previously impossible. They also make it easier for people to interact with these systems by providing more intuitive interfaces and feedback mechanisms, leading to a more user-centered approach to design and development [60].

CPS are used to improve production efficiency by increasing the speed and accuracy of production, reducing costs and making production more flexible.

Examples of CPS include autonomous vehicles and robotic systems for storing and transferring materials, as well as smart sensors and actuators used in the manufacturing process, smart grids, medical monitoring, autopilot aircraft and industrial control systems. CPS components can be found in areas as diverse as aerospace, automotive and chemical processes, energy, healthcare, manufacturing, transportation, entertainment, consumer products and civil infrastructure [61].

In robotic systems, CPS plays a role in improving efficiency and reliability. It enables precise design and management of robot motions, which increases accuracy and speed. In addition, CPS are key to control and safety of the robot and avoid dangerous situations for the user. They can also be used for inventory management and production processes optimisation. Connecting sensor data with software tools can improve product quality and reduce errors [62].

CPPS enable manufacturers to monitor and control their production processes in real time. The sensors used in CPPS allow monitoring of temperature, pressure, speed and other parameters in the production process to generate accurate production data. This data can be analysed using machine learning algorithms to discover a more efficient method for producing products. They also enable manufacturers to reduce production lines and adapt to real-time changes, enabling the production of high-quality products with fewer losses. Therefore, CPPS is considered one of the most promising areas of Industry 4.0 [39].

4. EXAMPLE OF THE APPLICATION OF INDUSTRY 4.0 TECHNOLOGIES AND SYSTEMS IN A REAL INDUSTRIAL ENVIRONMENT

In order to become and remain competitive in the global and highly turbulent market, modern companies are intensively exploring the possibilities and opportunities of implementing Industry 4.0 technologies and systems in their production environments.

The following chapter briefly presents an example of the use of Industry 4.0 technologies

and systems in a manufacturing company engaged in the development and production of brake discs for passenger and freight trains and other large goods vehicles. This company is strongly oriented towards the implementation of technologies and systems brought about by the industry 4.0 concept with the aim of improving the quality and efficiency of its production processes. An example of the use of Industry 4.0 technologies and systems, is the measuring station for measuring the air resistance of brake discs, see Fig. 6.



Fig. 6. Measurement of the air resistance of brake discs at rotation [63]

The use of modern technologies and systems of Industry 4.0 enabled the development and optimization of products in the production program of the company under consideration (CFD calculations, structural calculations, temperature analyses, etc.) with the aim of developing new products that are more environmentally friendly and enable the company to move towards green transition, see Fig. 7.

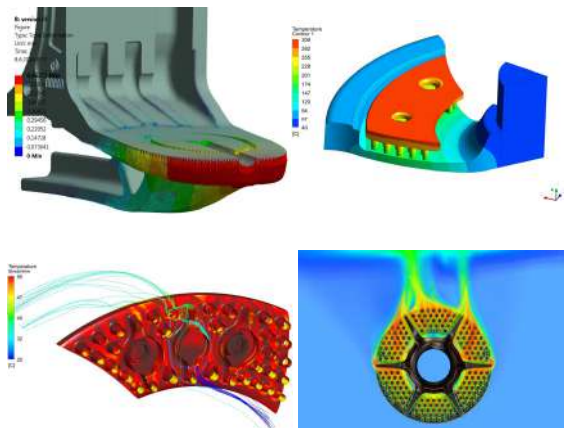


Fig. 7. Examples of the use of modern technologies and systems in the development of products in the company under the case [63]

As part of the FUTURA project, the company under consideration developed a new type of brake discs DRFB (see Fig. 8) using modern technologies and Industry 4.0 systems with the aim of achieving better safety, thermal efficiency (which in turn has an impact on reducing the energy impact on the environment), a reduction in mass, and an increase in the service life of the product.

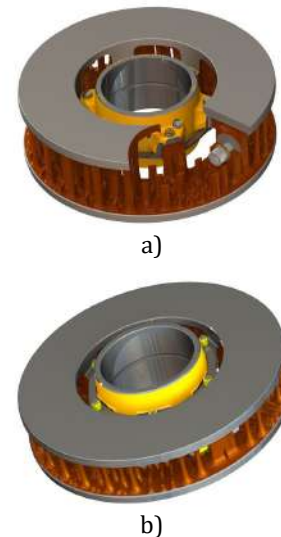


Fig. 8. a) Existing type of brake disc DRFB 170mm and b) newly developed DRFB brake disc type 110mm [63]

In the design of the DRFB brake disc (170mm) (Fig. 8a), the mass was reduced by 22.7% compared to the original DRFB disc, air resistance by 21%, and the thermal power dissipation efficiency increased by 17.3%. The main characteristics of the 170 mm DRFB brake disc are presented in Table 1.

Table 1. Main characteristics of the brake disc DRFB 170mm [63]

Characteristics	Description
Outer diameter	590mm
Internal diameter	325mm
Width	170mm
Mass	112kg
Ventilation losses	372 W at 165 km/h
Material	Cast iron

In the final prototype of the DRFB disc of 110mm width (Fig. 8b), the emphasis was further reducing the DRFB brake disc mass while maintaining the same level of safety and thermal efficiency. With this prototype, the mass was reduced by 34.5% compared to the original DRFB disc, air resistance by 34% and thermal dissipation efficiency increased by 32.7%. The main features of the newly developed 110mm DRFB brake disc are presented in Table 2.

Table 2. Main characteristics of the brake disc DRFB 110mm [63]

Characteristics	Description
Outer diameter	590mm
Internal diameter	325mm
Width	110mm
Mass	95kg
Ventilation losses	311W at 165 km/h
Material	Cast iron

As can be seen from the comparison of the data shown in Table 1 and Table 2, the development of a new type of brake discs has had an impact on reducing the use of materials and reducing ventilation losses, which consequently has a lower impact on environmental pollution in the use of the product.

In the company in the case, they strive to provide the customer with only high-quality products. To this end, with the help of modern technologies and systems of Industry 4.0, they perform various types of quality control from dimensional control using 3D scans and measurements to specific quality control such as hardness testing, paint thickness control, paint gloss control, UT ultrasonic testing, MT magnetic particle inspection, VT visual control, penetrant control, etc.

By using modern ICT, the company in question has ensured the traceability of products and services through the barcode system. Examples of the use of modern technologies and systems of Industry 4.0 for quality control in considered manufacturing enterprise are shown in Fig. 9.

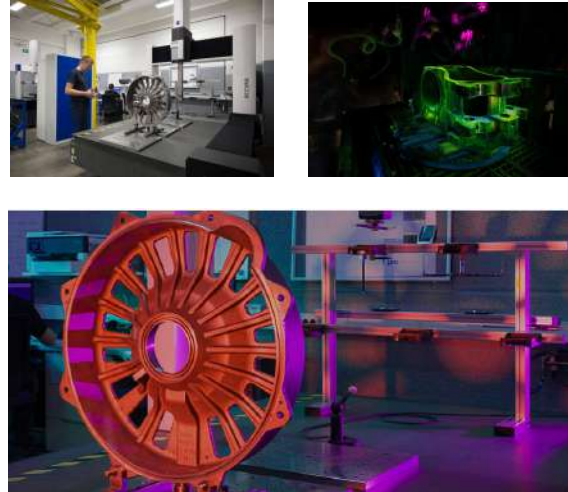


Fig. 9. Examples of use of Industry 4.0 technologies and systems for quality control in the considered company [63]

5. CONCLUSION

The article presents technologies and systems of Industry 4.0 that enable the restructuring of manufacturing systems and the digitization of their production processes towards a low-carbon enterprise.

Modern manufacturing companies are striving to maintain their competitiveness in the modern market by implementing Industry 4.0 technologies and systems as much as possible in their production environment. This implementation enables the transformation of existing production systems into new forms of production systems based on CPS and CPPS concepts.

The introduction of CPP and CPPS in companies can bring great benefits from the point of view of digital and green transition. With the introduction of new systems, the company achieves better control and management of production processes, which can lead to a reduction in waste and energy consumption, contributing to the reduction of the carbon footprint.

The use of advanced work and measurement systems helps to improve production efficiency, which in turn reduces the consumption of energy and raw materials and contributes to lower resource consumption.

The implementation of CPP and CPPS in the production domain improves the sustainability of products and contributes to an efficient recycling process. Industry 4.0 technologies and

systems such as IoT, IoS, etc., enable monitoring of products throughout their life cycle and tracking of materials through production systems.

In the applied case of implementation of technologies and systems of Industry 4.0, the production company and its processes in the field of product development and optimization of products of this quality domain, based on the processes of digitization of functions are presented.

This article is part of a research project (Using the Concepts of Industry 4.0 to transition to a low-carbon company) conducted by a research group at the Faculty of Mechanical Engineering of the University of Novo mesto in collaboration with a company that manufactures brake discs for trains.

The following research will focus on the processes of further digitisation and the implementation of Industry 4.0 technologies and systems in the manufacturing domain.

Acknowledgement

This work was partially supported by the University of Novo mesto.

REFERENCES

- [1] Ministry of Economic Development and Technology, *Slovenian Industrial Strategy 2021-2023*. 2021.
- [2] Hozdić, E., Kendić, S., Jurković, Z. Complex Adaptive Manufacturing System Concept as a Cyber-Physical Production System: Solutions to the Covid-19 Pandemic Challenges. Tushar, S., Faiz, I. (editors). *Cyber-Physical Systems*, Boca Raton: CRC Press, 2022, pp. 129–156.
- [3] Kegermann, H., Wahlster, W., Johannes, H. Recommendations for implementing the strategic initiative INDUSTRIE 4.0, Final report of the Industrie 4.0 Working Group. Frankfurt am Main, 2013.
- [4] Spath, D., Ganschar, O., Gerlach, S. *Produktionsarbeit der Zukunft-Industrie 4.0*. 2013.
- [5] Zizic Crnjac, C., Mladineo, M., Gjeldum, N., Celent, L. (2022). From Industry 4.0 towards Industry 5.0: A Review and Analysis of Paradigm Shift for the People, Organization and Technology. *Energies*, vol. 15, no. 14, p. 5221.
- [6] Özdemir, V., Hekim, N. (2018). Birth of Industry 5.0: Making Sense of Big Data with Artificial Intelligence, The Internet of Things and Next-Generation Technology Policy. *Omi. A J. Integr. Biol.*, vol. 22, no. 1, pp. 65–76.
- [7] Hozdić, E., Jurković, Z. Cyber-physical cognitive production systems: New concept of manufacturing systems on the way to Industry 5.0. Karabegović, I., Kovačević, A., Pašić, S., Mandžuka, S. (editors). *New Technologies, Development and Application - NT-2023*, 2023.
- [8] Luftman, J. N. (2003). *Competing in the Information Age: Align in the Sand*. Oxford University Press.
- [9] Schermerhorn, J. R., Hunt, J. G., Osborn, R. N. (2002). *Organizational Behavior*. New York, SAD: John Wiley and Sons.
- [10] Bakopoulos, J. A. Y. (1985). Toward a More Precise Concept of Information Technology. Center for Information Systems research Sloan School of Management, Massachusetts Institute of Technology.
- [11] Weill, P., Broadbent, M. (1998). *Leveraging the New Infrastructure: How Market Leaders Capitalize on Information Technology*. Harvard Business Review Press.
- [12] O'Brien, J. A. (2003). *Introduction to Information Systems: Essentials for the E-business Enterprise*. McGraw-Hill Education.
- [13] Parthiban, P. V. P. (2021). Industry 4.0 technologies: A review of the concepts, enablers, and opportunities. *J. Manuf. Syst.*
- [14] Giusto, D., Iera, A., Morabito, G., Atzori, L. (2010). *The Internet of Things*. Springer.
- [15] Leiner, R. M. et al. (2009). A brief history of the Internet. *ACM SIGCOMM Comput. Commun. Rev.*, vol. 39, no. 5, pp. 22–31.
- [16] Gubbi, J., Buyya, R., Marusic, S., Palaniswami, M. (2013). Internet of Things (IoT): A vision, architectural elements, and future directions. *Futur. Gener. Comput. Syst.*, vol. 29, no. 7, pp. 1645–1660.
- [17] Haller, S. Internet of Things. (2009). [Online]. Available: <http://services.future-internet.eu/images/1/16/A4 Things Haller.pdf>.
- [18] Miorandi, D., Sicari, S., De Pellegrini, F., Chlamtac, I. Internet of things: Vision, applications and research challenges. *Ad Hoc Networks*, vol. 10, no. 7, pp. 1497–1516, 2012.
- [19] Want, R. (2006). An Introduction to RFID Technology. *IEEE Pervasive Comput.*, vol. 5, no. 1, pp. 25–33.
- [20] Lee, J. Su, Y. Shen, C. (2007). A Comparative Study of Wireless Protocols: Bluetooth, UWB, ZigBee, and Wi-Fi. *IECON 2007 - 33rd Annual Conference of the IEEE Industrial Electronics Society*, 2007, pp. 46–51.
- [21] Verma, P. K., et al. (2016). Machine-to-Machine

- (M2M) communications: A survey. *J. Netw. Comput. Appl.*, vol. 66, pp. 83–105.
- [22] Baird, M. Ng, B. Seah, W. (2017). WiFi Network Access Control for IoT Connectivity with Software Defined Networking. *Proceedings of the 8th ACM on Multimedia Systems Conference*, Jun. 2017, pp. 343–348.
- [23] Xu, X. (2012). From cloud computing to cloud manufacturing. *Robot. Comput. Integr. Manuf.*, vol. 28, no. 1, pp. 75–86.
- [24] Kulkarni, N., Dwivedi, V. (2008). The Role of Service Granularity in a Successful SOA Realization: A Case Study. *2008 IEEE Congress on Services - Part I*, 2008, pp. 423–430.
- [25] Will, T., Blecker, T. (2012). RFID-driven process modifications in container logistics: SOA as a solution approach. *Int. J. Logist. Res. Appl.*, vol. 15, no. 2, pp. 71–86.
- [26] Curbera, F., Duftler, M., Khalaf, R., Nagy, W., Mukhi, N., Weerawarana, S. (2002). Unraveling the Web services web: an introduction to SOAP, WSDL, and UDDI. *IEEE Internet Comput.*, vol. 6, no. 2, pp. 86–93.
- [27] Caseres, J., Vaquero, L., Rodero-Merino, L., Polo, A., Hierro, J. (2010). Service Scalability Over the Cloud. *Handbook of Cloud Computing*. Furht, B. Escalante, A. (editors). New York, NY, USA: Springer, pp. 357–377.
- [28] Suthar, A. A. (2013). An Overview of Using Cloud Computing in Libraries. *INDIAN J. Appl. Res.*, vol. 3, no. 6, pp. 303–305.
- [29] Bughin, J., Chui, M., Clouds Manyika, J. (2010). *Big data, and smart assets: teh tech-enabled business trends to wath*. McKinsey Quarterly. McKinsey Global Institute.
- [30] Wang, L., von Laszewski, G. (2008). *Cloud Computing – A Perspective Study*. Rochester, New York: Rochester Institute of Technology.
- [31] Wu, D., Greer, M. J., Rosen, D. W., Schaefer, D. (2013). Cloud manufacturing: Strategic vision and state-of-the-art. *J. Manuf. Syst.*, vol. 32, no. 4, pp. 564–579.
- [32] Škulj, G. (2016). *Self-organisation of autonomous work systems in a decentralised production system (Slovenian language: Samoorganizacija avtonomnih delovnih sistemov v decentraliziranem proizvodnem sistemu)*. Dissertation. University of Ljubljana, Faculty of Mechanical Engineering.
- [33] Škulj, G., Vrabič, R., Butala, P., Sluga, A. (2015). Decentralised network architecture for cloud manufacturing. *Int. J. Comput. Integr. Manuf.*, pp. 1–14.
- [34] Wei, X., Liu, H. A. (2015). A cloud manufacturing resource allocation model based on ant colony optimization algorithm. *Int. J. Grid Distrib. Comput.*, vol. 8, no. 1, pp. 55–66.
- [35] Lin, Y.-K., Chong, C. S. (2015). Fast GA-based project scheduling for computing resources allocation in a cloud manufacturing system. *J. Intell. Manuf.*, pp. 1–13.
- [36] Theiler, P. W., Schindler, K. (2012). Automated Registration of Terrestrial Laser Scanner Data Using Natural Features. *ISPRS Annals of the Photogrammetry, Remote Sensing and Spatial Information Sciences*, 173–178.
- [37] Remondino, F., El-Hakim, S. (2006). A review of 3D scanning technologies for digitizing heritage artefacts. *J. Cult. Herit.*, vol. 7(3), pp. 177–196.
- [38] Cignoni, G. R. P., Callieri, M., Corsini, M., Dellepiane, M., Ganovelli, F. (2008). MeshLab: An Open-Source 3D Mesh Processing System. *Eurographics Ital. Chapter Conf.*, pp. 129–136.
- [39] Monostori, L. (2014). Cyber-physical Production Systems: Roots, Expectations and R&D Challenges. *Procedia CIRP*, vol. 17, pp. 9–13.
- [40] Lee, E. A. (2008). Cyber Physical Systems: Design Challenges. In *International Symposium on Object/Component/Service-Oriented Real-Time Distributed Computing (ISORC)*, pp. 363–369.
- [41] Lee, E. A., Seshia, S. A. (2011). *Introduction to Embedded Systems A Cyber - Physical Systems Approach*. California, USA: Berkeley University of California.
- [42] Eric, D. S., et al. (2013). *A Vision of Cyber - Physical Cloud Computing for Smart Networked Systems*. National Institute of Information and Communications Technology, Department of Commerce.
- [43] Baheti, R., Gill, H. (2011). Cyber-physical systems, in *The Impact of Control Technology. J. Eng. Power*.
- [44] Cardenas, A. A., Amin, S., Sastry, S. (2008). Secure Control: Towards Survivable Cyber-Physical Systems. *The 28th International Conference on Distributed Computing Systems Workshops*, pp. 495–500.
- [45] Kumar, P. R. (2012). Cyber-Physical Systems: A Perspective at the Centennial. *Proc. IEEE*, vol. 100, no. Special Centennial Issue, pp. 1287–1308.
- [46] Geisberger, E., Broy, M. (2012). *Agenda CPS: integrierte Forschungsagenda Cyber-Physical Systems*. Springer.
- [47] Hu, F. (2013). *Cyber-Physical Systems: Integrated Computing and Engineering Design*. CRC Press.
- [48] Reinhart, G., Krug S. (2009). Robotersysteme in der Kleinserie – Effizienz von der Planung bis zum Einsatz. *Munchen Utz*.

- [49] Hozdić, E. (2020). Integrating Cyber and Physical Environments for Adaptive Process Control in Work Systems. *Handbook of Research on Integrating Industry 4.0 in Business and Manufacturing*. IGI Global Publisher of Timely Knowledge.
- [50] Broy, M. (2010). *Cyber-Physical Systems*. Berlin: Springer.
- [51] Detlef, Z., Lisa, O. (2011). Agile Automation Systems Based on Cyber - Physical Systems and Service - Oriented Architectures. *Advances in Automation and Robotics, Vol. 1*. Lee, G. (editor). Springer - Verlag Berlin Heidelberg, pp. 567–574.
- [52] Spath, D., Gerlach, S., Schlund, S. (2013). Cyber-physical system for self-organised and flexible labour utilisation. *22nd International Conference on Production Research, ICPR 2013*, p. 6.
- [53] Monostori, L. *et al.* (2016). Cyber-physical systems in manufacturing. *CIRP Ann. - Manuf. Technol.*, vol. 65, no. 2, pp. 621–641.
- [54] Wang, L. Haghighi, A. (2016). Combined strength of holons, agents and function blocks in cyber-physical systems. *J. Manuf. Syst.*
- [55] Leitão, P., Colombo, A. W., Karnouskos, S. (2016). Industrial automation based on cyber-physical systems technologies: Prototype implementations and challenges. *Comput. Ind.*, vol. 81, pp. 11–25.
- [56] Hozdić, E. (2020). *Model of Cyber-Physical Manufacturing Systems*. Dissertation. (Slovenian language: *Model kibernetско-fizičnih proizvodnih sistemov*). University of Ljubljana, Faculty of Mechanical Engineering.
- [57] Hozdić, E., Kozjek, D., Butala, P. (2020). A cyber-physical approach to the management and control of manufacturing systems. *Strojniški Vestnik – J. Mech. Eng.*, vol. 66, no. 1, pp. 61–70.
- [58] Hozdić, E., Butala, P. (2020). Concept of Socio-Cyber-Physical Work Systems for Industry 4.0. *Tech. Gaz.*, vol. 27, no. 2.
- [59] Hozdić, E. (2019). Socio-Cyber-Physical Systems Alternative for Traditional Manufacturing Structures. *New Technologies, Development and Application II. NT 2019. Lecture Notes in Networks and Systems*, vol. 76. Karabegović, I. (editor). Cham: Springer.
- [60] Gill, H., Koehler, M., Rajkumar, R., Lee, J. K. M. (2016). Cyber-physical systems: A new frontier. *Proc. IEEE*, vol. 104(5), pp. 834–840.
- [61] Rajkumar, J., Lee, R., Sha, I., Stankovic, L. (2010). Cyber-physical systems: Past, present, and future. *Proc. IEEE*, vol. 100, pp. 153–165.
- [62] Gordon, S. S. G. F., Wright, C. R. B. (2015). Cyber-physical systems in robotics: A review of CPS technologies for robotics applications. *Annu. Rev. Control*, vol. 40, pp. 44–53.
- [63] Kovis d.o.o. Brežice, <https://www.kovis-group.com/kovis/>.



Banja Luka
1-2 Jun 2023.

DEMI 2023

16th International Conference on Accomplishments in Mechanical and Industrial Engineering

www.demi.mf.unibl.org



Influence of experimental method on plastic strain ratio determination

S. Aleksandrović^a, Đ. Ivković^a, D. Arsić^a, M. Delić^a

^a Faculty of Engineering, University of Kragujevac, Sestre Janjića 6, 34000 Kragujevac, Serbia

Abstract

This paper is relating to anisotropy of thin sheet metals phenomena, especially to, so called, normal (orthogonal) anisotropy which expresses by plastic strain ratio, or "r" value. The paper presents the results of experimental investigation which main goal was to evaluate influence of two elements of plastic strain ratio experimental method of determination. The first element is value of plastic strain, and second is specimen geometry. Extensive experiment was conducted according to appropriate tensile test procedure with 3 materials and 5 different specimen geometries. Materials used are: steel sheet S235JR, austenitic stainless steel sheet X5CrNi18-10 and Al alloy sheet AlSi0,9MgMn (i.e. ENAW 6081). Nominal thickness of all of three sheets are 1 mm. Three specimens are with 20 mm width and gage length of 60, 120 and 160 mm. Two specimens are with 15 mm width and gage length of 50, 100 mm. All the specimens were laser cutted in rolling direction. In preparatory part of experiment, behind material characterization (obtaining base mechanical properties) performed was identification of homogenous deformation field, i.e. plastic strain at the beginning of localization, for each specimen. Related to that strain value realized were 6 deformation degrees: 75%, 80%, 85%, 90%, 95% i 100%. Results are shown known significant difference in "r" value for used materials, perceptible influence of specimen geometry and very low influence of realized plastic strains.

Keywords sheet metal, anisotropy, plastic strain ratio

1. INTRODUCTION

Thin sheet metals usually are anisotropic materials. This property is expressed most often by two ways: plane anisotropy and normal (orthogonal) anisotropy. Normal anisotropy is related to the difference in sheet metal strains in plane and along its thickness. Main characteristic which completely explained normal anisotropy is plastic strain ratio or "r" value. Significance of "r" value outgoing from its application in anisotropic plasticity theory,

numerical simulation of metal forming processes and from its direct practical using as formability parameter in deep drawing sheet metal forming processes.

"r" value usage lasts for decades and there are extensive literature about theory and process of experimental determination (e.g. [1] - [12]). In modern research activities "r" value is important parameter for consideration of anisotropy influence in different forming processes or theory investigations (e.g. [13] - [19]).

Determination of "r" value is experimentally only ([1], [5], [7], [8], [10]) and that is matter of standards ([7], [8]). However, standards recommendation in many cases are not precise and obligate. In standard procedures such a situation is with influence of specimen

Corresponding author

Dr Srbslav Aleksandrovic, full professor
srb.alexand@gmail.com

Faculty of Engineering, University of Kragujevac
Sestre Janjića 6
34000 Kragujevac, Serbia

geometry and degree of plastic strain. Thereabout is main goal of this research and report.

Process in experimental determination of "r" value is uniaxial tension. Form of specimen is known, but dimensions can be different and that make geometry insufficiently defined in some way. So, because of that, there is a space for investigation. Similar matter is also about amount of plastic strain.

According ([1], [5], [7], [8], [12]) definition of "r" value is given as following expressions:

$$r = \frac{\varphi_b}{\varphi_s} = \frac{\ln \frac{b}{b_0}}{\ln \frac{s}{s_0}}$$

$$l_0 \cdot b_0 \cdot s_0 = l \cdot b \cdot s = \text{const.}$$

$$\frac{s}{s_0} = \frac{l_0 b_0}{l b} \quad \text{and finally}$$

$$r = \frac{\ln \frac{b}{b_0}}{\ln \frac{l_0 b_0}{l b}} = \frac{\ln \frac{b}{b_0}}{\ln \frac{l_0 b_0}{l b}}$$

φ_b is logarithmic (true) plastic strain of specimen width; φ_s is logarithmic (true) plastic strain of specimen thickness, l_0 , b_0 , s_0 are initial specimen dimensions, length, width and thickness; l , b , s are in process, or final, specimen dimensions, length, width and thickness. Fig. 1 shows specimen standard form.

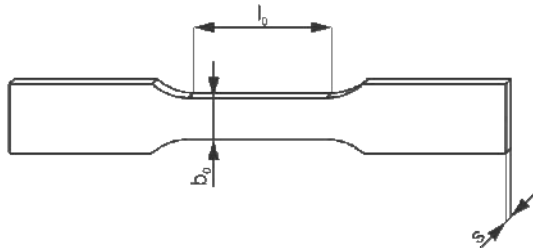


Fig. 1. Uniaxial tension test specimen

2. EXPERIMENT

Extensive experiment was planned according to appropriate uniaxial tensile test procedure with 3 materials and 5 different specimen geometries. Materials used are: steel sheet S235JR (here signed S), austenitic stainless steel sheet X5CrNi18-10 (here signed X) and Al alloy sheet AlSi0,9MgMn (i.e. ENAW 6081) (here

signed A). Nominal thickness of all of three sheets are 1 mm.

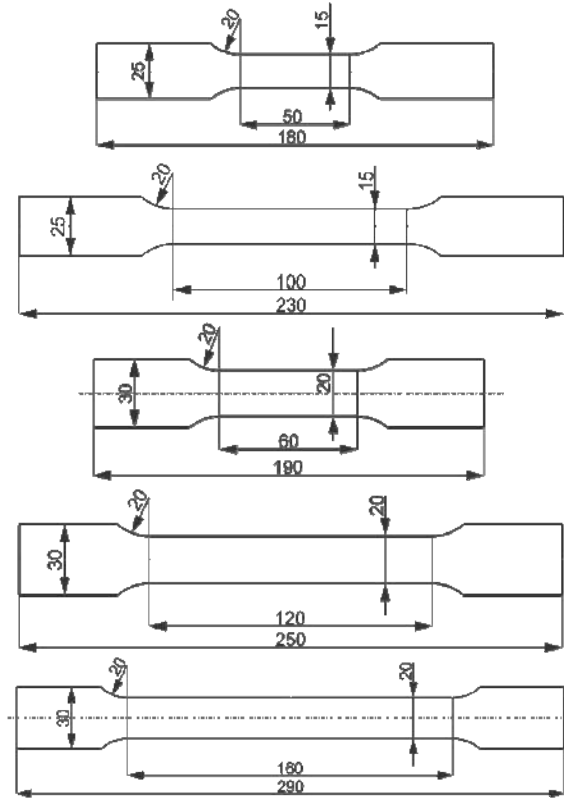


Fig. 2. Test specimens geometry

Test specimen geometry was defined in following way: three specimens are with 20 mm width and gage length of 60, 120 and 160 mm; two specimens are with 15 mm width and gage length of 50, 100 mm (Fig.2). According Fig. 2 specimens signs up to down are: a, b, c, d and e. All the specimens were laser cutted in rolling direction. In preparatory part of experiment, behind material characterization (obtaining base mechanical properties) performed was identification of homogenous deformation field, i.e. plastic strain at the beginning of localization A_g , for each specimen. Related to that strain value realized were 6 deformation degrees: 75%, 80%, 85%, 90%, 95% and 100%, and signed 2, 3, 4, 5, 6, and 7. Sign 1 relate to specimen for fracture test. This plan gives need of 105 successfully tested specimens in total. Prepared were about 120 specimens. Examples are shown in Fig. 3.

Uniaxial tests were performed on computerized test machine Zwick/Roell Z 100 ([9]). Deformations were measured manually,

without extensometers. Reasons are following: first, very difficult measuring width change on minimum 5 places; second, problems with elimination of elastic deformation, i.e. precise measuring of plastic strain; third, problems of using extensometers with sharp edges ([10]).



Fig. 3. Examples of test specimens

Longitudinal strains were measured with digital calliper (accuracy 0,01 mm), and lateral strains with micrometer (accuracy 0,005 mm).

In width locations for measuring lateral deformations were carefully marked (Fig. 3). First and last mark were used for measuring longitudinal deformation, at the same time.

In literature and standards ([1], [2], [5], [7], [8] etc.) can find noted general recommendations about necessary previous plastic deformation. It is convenient that elongation would be larger, but in field of homogenous forming, i.e. before maximum force point on the force-elongation (or stress-strain) diagram. Larger strain is need for error decrease. For low carbon steels recommended elongation is about 20%, but for any other material must be check end of homogenous and start of localized forming. In particular case fracture tests were performed and exactly defined maximal plastic strain at the end of homogenous forming. Adopted were 6 amounts of deformation for evaluation of strain degree influence on "r" value determination, as previously mentioned.

Similar is in case of specimen geometry influence. Recommendations are general. In this experimental study goal is evaluate influence of specimen geometry with different length-width ratio.

3. RESULTS OF EXPERIMENT AND DISCUSSIONS

Performed extensive experiment resulted with large quantity of data: diagrams, tables, histograms and all of that can't be presented here because of limited space. Shown will be selected significant results like illustrations of completeness.

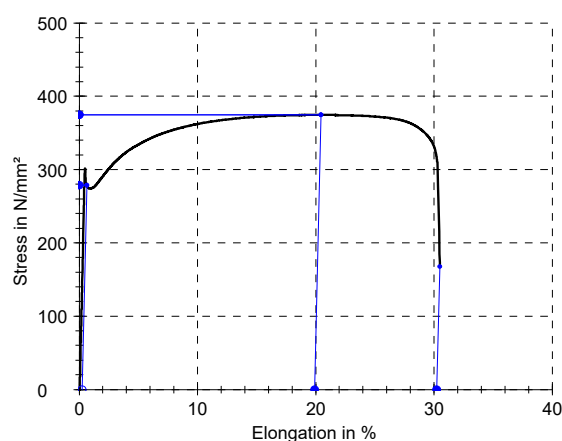


Fig. 4. Tensile diagram for specimen Sd1

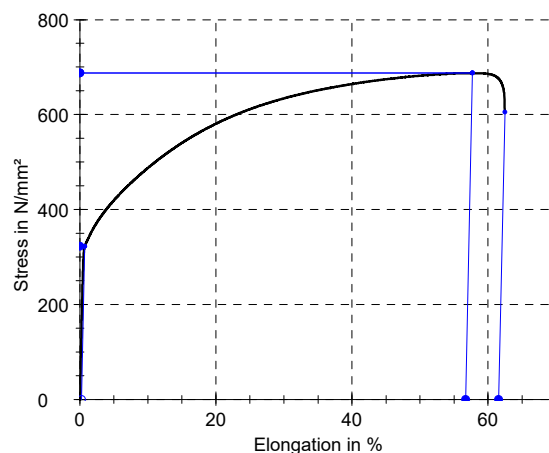


Fig. 5. Tensile diagram for specimen Xd1

In the figures 4, 5 and 6 shown are stress-strain tensile diagrams which main purpose is determination of strain at the end of homogenous forming. On this strain depends

other used strains. Signs (Sd1, Xd1, Ad1) were explained in previous chapter.

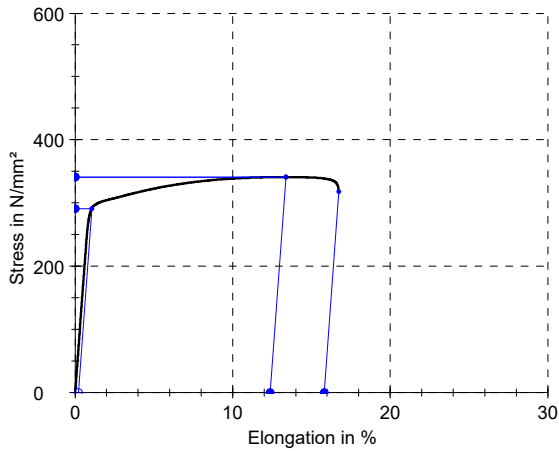


Fig. 6. Tensile diagram for specimen Ad1

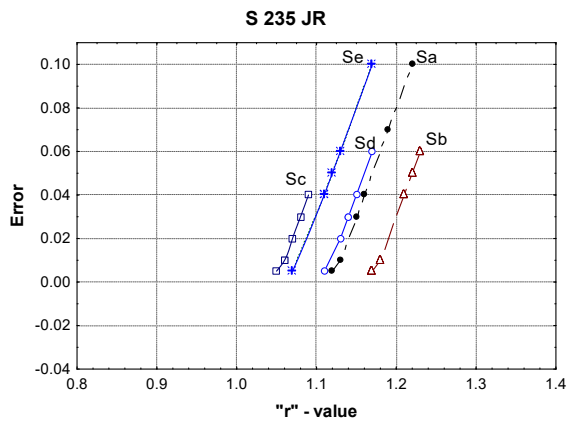


Fig. 7. "Error" relation to "r"-value

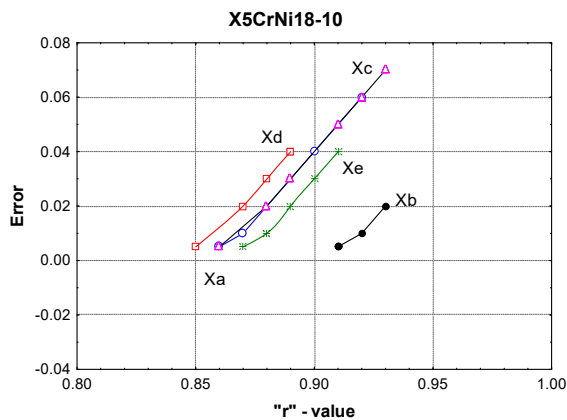


Fig. 8. "Error" relation to "r"-value

Figures 7, 8 and 9 shows relations of, so called, error on "r" value. True meaning of "error" is how change "r" value depending on kind of material and type of geometry. For calculating "error" need is exactly true "r" value which is unknown. There was adopted minimal "r" value as that true and referent value.

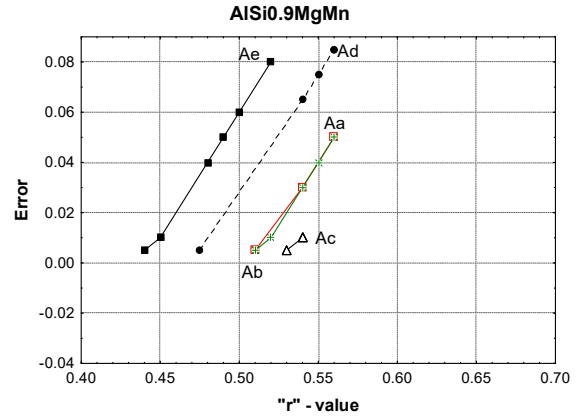


Fig. 9. "Error" relation to "r"-value

In Fig. 7 can be see, first of all, influence of specimen type on "r" value and at same time change of "error" for structural steel sheet S 235. Engineering logic require to accept lower values, so according to that specimens **c** and **e** are more convenient. For austenitic stainless steel (Fig. 8) slightly better is specimen **d** and for aluminium alloy (Fig. 9) specimen **e**.

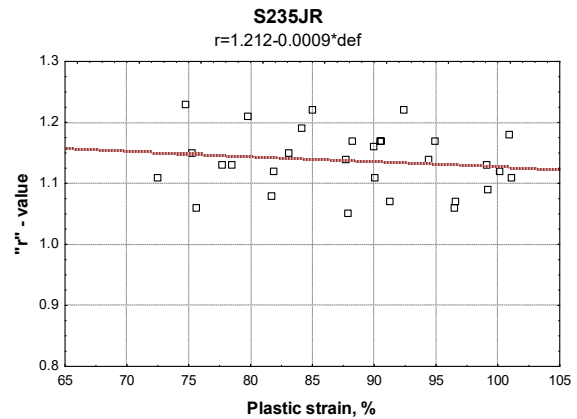


Fig. 10. "r"-value dependence on plastic strain

Fig. 10 shows that cloud of points and fitted line indicate very slightly influence of plastic strain on "r" value. With increasing strain "r" value decreasing but almost negligible. Similar

annotation is valid for stainless steel and Al alloy both (Fig. 11 and Fig. 12).

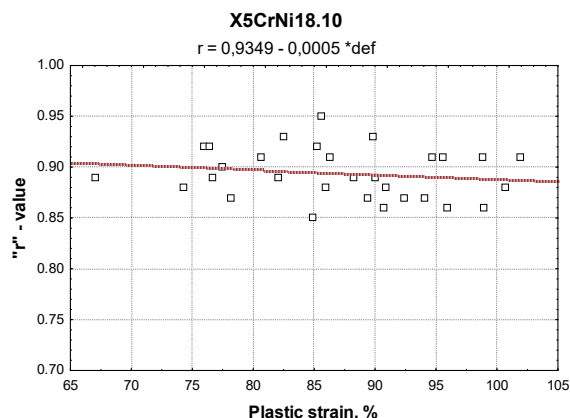


Fig. 11. "r"-value dependence on plastic strain

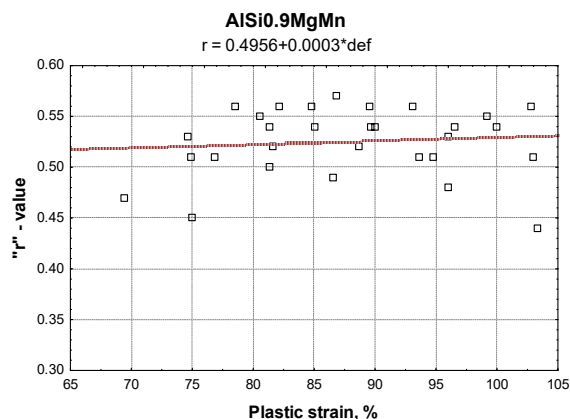


Fig. 12. "r"-value dependence on plastic strain

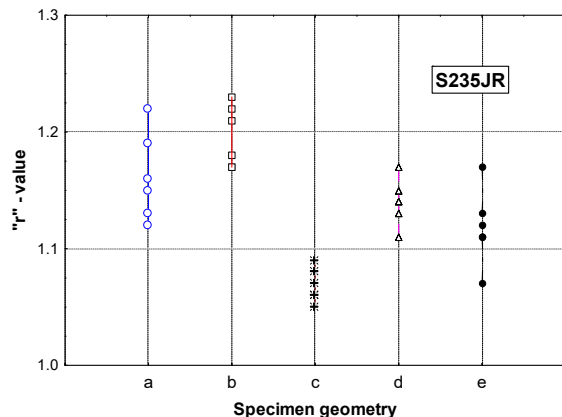


Fig. 13. "r"-value dependence on specimen geometry

Figures 13, 14 and 15 more clearly shows influence of specimen type on "r" value than

Figures 7, 8 and 9. Annotations are the same. For structural steel lower "r" values (here adopted as better, more precise) are with specimens **c** and **e**.

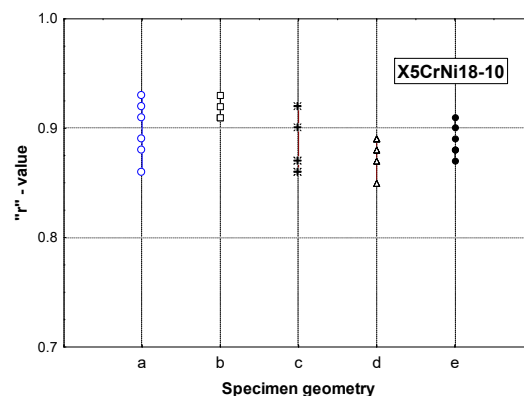


Fig. 14. "r"-value dependence on specimen geometry

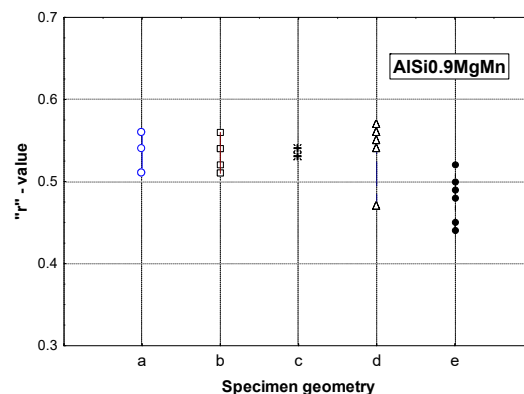


Fig. 15. "r"-value dependence on specimen geometry

For stainless steel sheet slightly more convenient specimen is **d** (Fig. 14). Specimen **e** is better for Al alloy (Fig. 15).

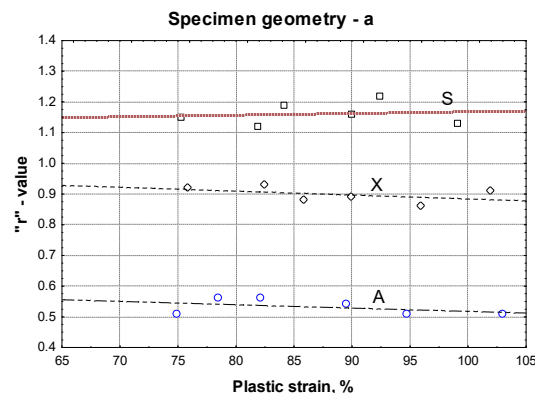


Fig. 16. "r"-value dependence on plastic strain

Influence of plastic strain on "r" value can be expressed in different way than in Figures 10, 11 and 12. Fig. 16 illustrate this approach. Made were diagrams for all the specimens and all materials. Here is shown only Fig. 16 as example. Reason is almost negligible influence of plastic strain.

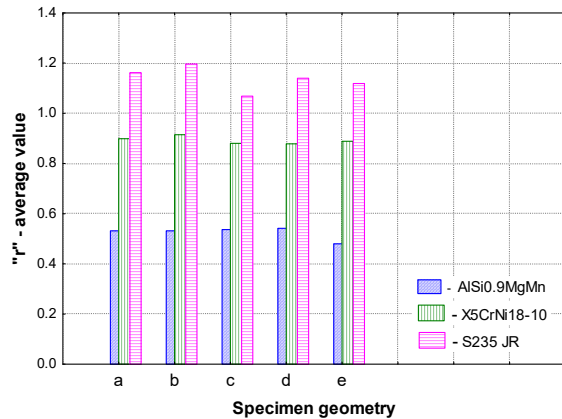


Fig. 17. "r"-average value dependence on specimen geometry

Presentation on Fig. 17 is summary histogram which shows specimen geometry influence on average "r" value. Once again can be confirms previous annotations. For structural steel more convenient are specimen **c**, for stainless steel specimen **d** and for Al alloy specimen **e**.

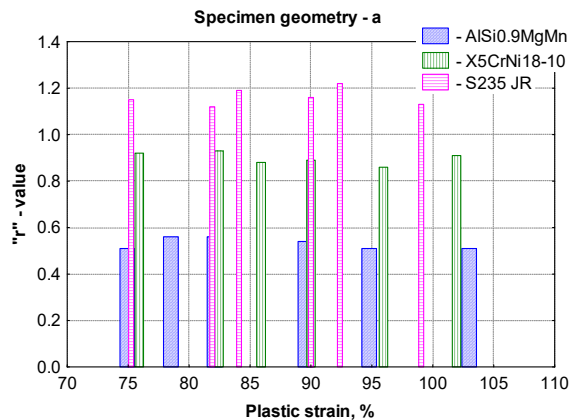


Fig. 18. "r"-value dependence on real plastic strain

In Fig. 18 presented are histogramic dependence of "r" value on real plastic strain. Nominal plastic strain as set up value can't be reach exactly in every measurement. This small differences are visible in Fig. 18. However, more

clear is Fig. 19 which shows "r" value dependence on nominal plastic strain.

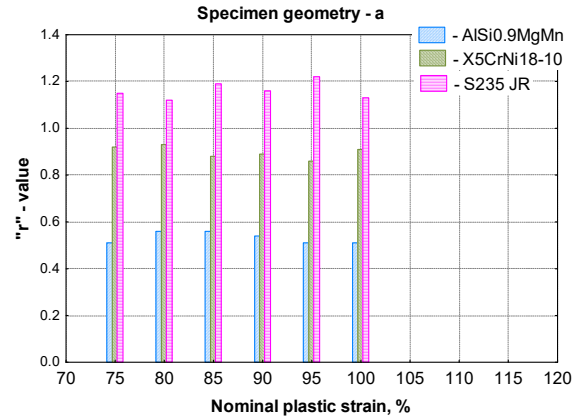


Fig. 19. "r"-value dependence on nominal plastic strain

Because of relatively small plastic strain influence on "r" value, once again given are only histogram for specimen **a**, as example.

4. CONCLUSIONS

Based on the results of performed extensive experiment the following observations and conclusions can be drawn:

- Influence of specimen geometry is visible. Increasing specimen width cause increasing width measurement accuracy, and smaller "r" value intensity.
- Influence of specimen length changing can't be isolated in this approach.
- Realised plastic strain in tensile process have relatively small affect, almost negligible. Possible cause may be quite large strain intensity. Minimal strain value was 75% of maximum allowed strain. In further experiment it is needed to use more smaller plastic strain intensities.
- Precise reaching of plastic strain goal value was difficult in experiment because of relatively large elastic deformation. So, there is a need previously evaluate intensity of elastic strain in preparatory part of experiment.
- In working without extensometers in uniaxial tensile process, like in this case, must be aware about volume that really deformed. Best results were obtained if jaws of tensile machine clamping test

specimen very close to the beginning and last mark line.

- In further experiments in attempts to evaluate influence of different test specimen geometries and plastic strain intensities on "r" value there are needs to extend fields of strains intensities and types of geometries both.
- In working without extensometers based on experience in this experiment seems suitable to use series of simple test specimens in form of strip with different width.

Acknowledgement

The experimental research with results reported in this paper was partially supported by the Ministry of Education, Science and Technological Development, Republic of Serbia through contract TR34002 and authors appreciate for that.

REFERENCES

- [1] Devedžić, B. (1972). Obradivost materijala dubokim izvlačenjem (Formability of materials in deep drawing process), Mašinski fakultet u Kragujevcu, Kragujevac. (p. 151-156) (In Serbian)
- [2] Devedžić, B. (1975). Osnovi teorije plastičnog deformisanja metala (Fundamentals of theory of metal plastic forming), Mašinski fakultet u Kragujevcu, (p. 305-324). (In Serbian)
- [3] Devedžić, B. (1992). Plastičnost i obrada metala deformisanjem (Plasticity and metal forming), Naučna knjiga, Beograd, (p. 64-65, 250-254). (In Serbian)
- [4] Aleksandrović, S., Stefanović, M. (2010). Tehnologija plastičnog oblikovanja metala (Technology of metal plastic forming), Mašinski fakultet Univerziteta u Kragujevcu. (In Serbian)
- [5] Aleksandrović, S. (2014). Deformabilnost – Anizotropija (Deformability - Anisotropy), lecture for FIAT Automobili Srbija, Fakultet inženjerskih nauka Univerziteta u Kragujevcu. (In Serbian)
- [6] Aleksandrović, S. (2018). Savremeni postupci plastičnog oblikovanja (Advanced processes of plastic forming), script, Fakultet inženjerskih nauka Univerziteta u Kragujevcu. (In Serbian)
- [7] Standard ISO 10113:2020(E). (2020). Metallic materials — Sheet and strip— Determination of plastic strain ratio, International Organization for Standardization, Geneva, Switzerland, p. 1-7.
- [8] ASTM Standard E 517-00. (2002). Standard test method for Plastic Strain Ratio r for Sheet Metal, Annual Book of ASTM Standards, ASTM, West Conshohocken, PA, USA.
- [9] Instruction manual for materials testing machines XC – FR100TLA80 – 003. (2003). Zwick GMBH&CO; Ulm, FR Germany.
- [10] Gedney, R., (2005). Measuring the Plastic strain Ratio of Sheet Metals, ADAMET Inc., Norwood, MA, USA.
- [11] Danckert, J., Nielsen, K.B., (1998). Determination of the plastic anisotropy r in sheet metal using automatic tensile test equipment, Journal of Mat. Proc. Technology, ISSN 0924-0136, vol. 73, p. 276-208., [https://doi.org/10.1016/s0924-0136\(97\)00238-0](https://doi.org/10.1016/s0924-0136(97)00238-0).
- [12] Aleksandrović, S., Stefanović, M., Adamović, D., Lazić, V., (2009). Variation of Normal Anisotropy Ratio „ r ” During the Plastic Forming, Journal of Mechanical Engineering, ISSN 0039-2480, vol. 55, p. 392-399.,
- [13] Banabic, D., (2016). Advances in Plastic Anisotropy and Forming Limits in Sheet Metal Forming, Journal of Manufacturing Science and Engineering, ISSN 1087-1357, vol. 138, p. (090801-1)-090801-9)., <https://doi.org/10.1115/1.4033879>.
- [14] Rahmaan, T., Bardelcik, A., Imbert, J., Butcher, C., Worswick, M.J., (2016). Effect of strain rate on flow stress and anisotropy of DP600, TRIP780, and AA5182-O sheet metal alloys, International Journal of Impact Engineering ISSN 0734-743X, vol. 88, p. 72-90, <http://dx.doi.org/10.1016/j.ijimpeng.2015.09.006>
- [15] Yoshida, K., Yamazaki, Y., Nakanishi, H., (2021). Experiments and Crystal Plasticity Simulations on Plastic Anisotropy of Naturally Aged and Annealed Al-Mg-Si Alloy Sheets, Metals, vol. 11, 1979, p. 1-17. <https://doi.org/10.3390/met11121979>
- [16] Ailinei, I.I, Galatanu, S.V., Marsavina, L., (2022). Influence of anisotropy on the cold bending of S600MC sheet metal, Engineering Failure Analysis, ISSN 1350-6307, vol. 137, no. 106206, <https://doi.org/10.1016/j.engfailanal.2022.106206>
- [17] Tardif, N., Kyriakides, S., (2012). Determination of anisotropy and material hardening for aluminum sheet metal, International Journal of Solids and Structures, ISSN 0020-7683, vol. 49, p. 3496-3506., <https://doi.org/10.1016/j.ijsolstr.2012.01.011>.
- [18] An, Y.G., Vegter, H., Melzer, S., Romano Triguero, P., (2013). Evolution of the plastic anisotropy

- with straining and its implication on formability for sheet metals, *Journal of Mat. Proc. Technology*, ISSN 0924-0136, vol. 213, p. 1419-1425., <http://dx.doi.org/10.1016/j.jmatprotec.2013.02.008>.
- [19] Wuyang L., Takashi I., (2019). Fundamental apparent plastic anisotropy of duplex embossed aluminum sheet, *International Journal of Mechanical Sciences*, ISSN 0020-7403, vol. 163, no. 105125, <https://doi.org/10.1016/j.ijmecsci.2019.105125>.
- [20] Steel number, From: <https://www.steelnumber.com> (accessed on: March 25, 2023.)



Banja Luka
1–2 Jun 2023.

DEMI 2023

16th International Conference on Accomplishments in Mechanical and Industrial Engineering

www.demi.mf.unibl.org



Influence of process parameters in the process of deep drawing with plastic tool

J. Ilić^a, T. Grbić^b, M. Hadžistević^b, M. Milutinović^b, M. Krašnik^c, D. Movrin^b

^aUniversity of Banja Luka, Faculty of Mechanical Engineering, Banja Luka, Republic of Srpska, B&H

^bUniversity of Novi Sad, Faculty of Technical Sciences, Novi Sad, Serbia

^cUniversity of East Sarajevo, Faculty of Mechanical Engineering, East Sarajevo, Republic of Srpska, B&H

Abstract *The analysis of influential parameters and the discovery of their influence on the deep drawing process itself is very important for the production of quality and cheap workpieces. The application of plastic for the production of basic tool elements, which are in contact with sheet metal, has significant advantages compared to classic metal tool elements. This paper analyzes the influence of deep drawing process parameters such as die radius, blank holder force and lubrication conditions on the change in wall thickness on radius on axisymmetric workpieces. The Taguchi method, used as a statistical method for planning the experiment, allows us to determine the influence of process parameters with minimal variability.*

Keywords *Deep Drawing, Rapid Tooling, Sheet Metal Forming*

1. INTRODUCTION

Deep drawing is a sheet metal forming process with extensive practical application and is used for the large batch production of parts for the needs of various branches of industry [1]. This is a sheet metal forming process that allows us to obtain a drawn part of a specific geometry and dimensions from a simple sheet metal blank with a minimal number of operations (Fig. 1.). What is essential in the process of deep drawing is that the drawn part has the appropriate dimensions and wall thickness of the part, without cracks and creases on the drawn part. This can be achieved by analyzing the influencing parameters on the deep drawing process and choosing the optimal process parameters. As part of this research, the

possibility of making axisymmetric pieces from sheet DC01 with a thickness of 0.8 mm was considered. At the same time, we analyzed the influence of the deep drawing process parameters on the variation of radius thickness on deep drawn part. A deep drawing tool with basic plastic elements was used [3]. The process parameters observed in the research and whose influence was analyzed are the die radius, blank holder force, and lubrication conditions [6]. For this research, Taguchi's method of experiment planning was used. Nine experiments were performed according to Taguchi's L9 plan of experiments. Taguchi's method is a statistical method that allows us to get a lot of information about the observed process or system, with a minimized number of experiments that need to be conducted [7].

Corresponding author

MSc Jovica Ilić, Senior Teaching Assistant
jovica.ilic@mf.unibl.org
University of Banja Luka, Faculty of Mechanical Engineering
Vojvode Stepe Stepanovića 71, 78000 Banja Luka
Republic of Srpska, Bosnia and Herzegovina

2. EXPERIMENTAL RESEARCH WORK

The tests were performed on a deep drawing tool, which was modified in such a way that the basic elements of the tool, which are in contact

with the sheet metal, were made by vacuum casting technology, according to Fig. 1.

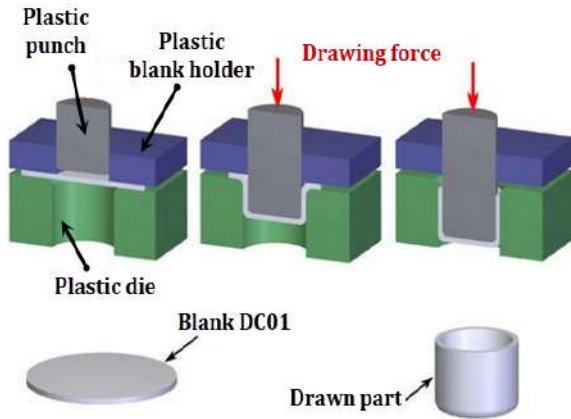


Fig. 1. Schematic view of deep drawing process with plastic tool elements [2]

For the vacuum casting process and the fabrication of plastic tool elements, it is necessary to produce negatives of the tool elements, based on which the casting molds will be made. This is where additive manufacturing technology is of great use, allowing us to quickly and easily create master models for the preparation of a silicone mold, which must be a faithful copy of the elements of the deep drawing tool which we want to create using vacuum casting technology. This is especially important when we need to make parts of complex geometry when the making of tools using conventional methods becomes problematic. The process of vacuum casting and making molds and tool parts consists of the following steps, according to Fig.2. [4]:

1. Preparation of tool parts for the casting process. Setting the parting tape on the tool parts negatives that will facilitate the separation of silicone mold.
2. Bonding plastic gates on the tool parts negatives which has a role to form an inlet channel in the silicone mold and to facilitate the positioning and fixation of the negative in the silicone casting frame.
3. Calculation of the necessary quantity of silicone mixture to form a silicone mold to be used for molding the deep drawing tool parts. The silicone mixture is poured into the frame with fixed tool parts negatives and then the frame with the negative submerged in silicone is

placed in a vacuum chamber in order to remove the residual air bubbles from silicon.

4. Positioning of the silicone mold in a vacuum chamber. After solidification of silicone, silicone mold is cut to parting line, during which we relieve the negative and get a silicone mold for casting a replica of a given negative
5. The molding halves are then combined and the next step is to calculate necessary quantities of resin for molding of the deep drawing tool parts. The amount of resin is commonly determined by weighing the individual master model which is increased by 20-30%, taking into account the loss of material in vessels and inlet channels. In this case, to cast the deep drawing tool parts, components made by Axson Technologies were used, thus by mixing them in the casting process the parts with physical characteristics according to Table 2 are obtained.
6. After a certain quantity of the material needed for molding and the proportion of the individual components of the material in a total amount are determined, then vacuum casting process follows. The casting process takes place in a vacuum chamber under conditions that are recommended for corresponding elements and components of the material.
7. After solidification of the molded material in a vacuum chamber, mold halves are separated and, if necessary, post-processing of the molded item follows.

The two-component resin PX 223/HT from Axson Technologies was used to produce the blank holder, die and punch. Combining these two components, we obtained tool parts with mechanical and physical characteristics according to Table 1 and 2.

Table 1. Mechanical properties of vacuum casting resin PX 223/HT [5]

<i>Mechanical properties at 23°C for PX 223/HT</i>		
Flexural modulus of elasticity	Mpa	2300
Flexural strength	Mpa	80
Tensile strength	MPa	60
Elongation at break in tension	%	11
Charpy impact resistance	kJ/m ²	>60
Hardnes at 23°C	Shore D1	80
Hardnes at 23°C	Shore D1	> 65

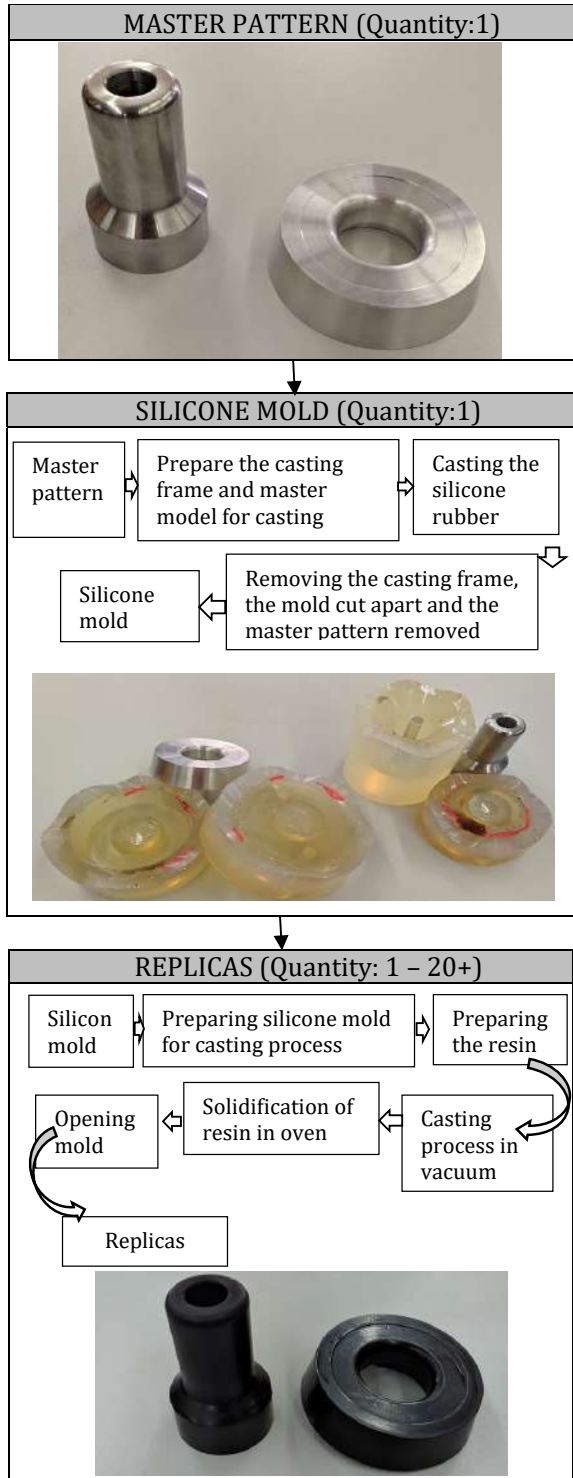


Fig. 2. Rapid tooling using vacuum casting process

As mentioned in the previous chapter, the experiment was planned according to Taguchi's experimental plan [7]. Taguchi's L9 orthogonal sequence was applied, during which we observed three influential parameters.

Table 2. Physical properties of vacuum casting resin PX 223/HT [5]

Physical properties for PX 223/HT			
	Part A	Part B	Mixing
Composition	ISOCYANATE	POLYOL	
Mixing ratio by wight at 25°C	100	80	
Aspect	liquid	liquid	liquid
Color	colorless	black	black
Viscosity at 25°C [BROOKFIELD LVT]	1.100	300	850

The influencing factors observed were the lubrication conditions during which the deep drawing process was carried out with three different lubrication conditions. A dedicated deep drawing lubricant Martol EP 180 was used, followed by cold-pressed pumpkin seed oil, and the deep drawing process was carried out without lubrication. Three die with different radius sizes of 4.5, 6, and 7.5 mm were also used. The blank holder force was also changed during the experiment, and its values were 15, 20 and 25 kN. The process parameters and their variations are shown in Table 3.

Table 3. Process parameters and variation levels

Process parameters:	Levels		
	1	2	3
Die radius (R [mm])	4.5	6	7.5
Blank Holder Force (BHF [kN])	15	20	25
Lubricants (Lub)	Without Lubricant- WL	Martol EP180 - L1	Pum-pkin Seed Oil - L2

In the deep drawing process, sheet metal DC01 with a thickness of 0.8 mm was used. A complete view of the orthogonal L9 Taguchi sequence is shown in the Table 4.

Table 4. Taguchi's L9 experiment plan [7]

Exp. no.	Parameters:		
	R	BHF	Lub
1	1	1	1
2	1	2	2
3	1	3	3
4	2	1	2
5	2	2	3
6	2	3	1
7	3	1	3
8	3	2	1
9	3	3	2

The parts made according to the conditions and the set plan of the experiment were then cut on a grinder for sample preparation and polished in order to be able to measure the part wall thickness on a microscope. The thickness variation in radius area of parts was measured using a Mitutoyo TM-505 instrument microscope equipped with a high resolution MOTICAM 5 camera and connected to a PC using Motic Images Plus 2.0 software.

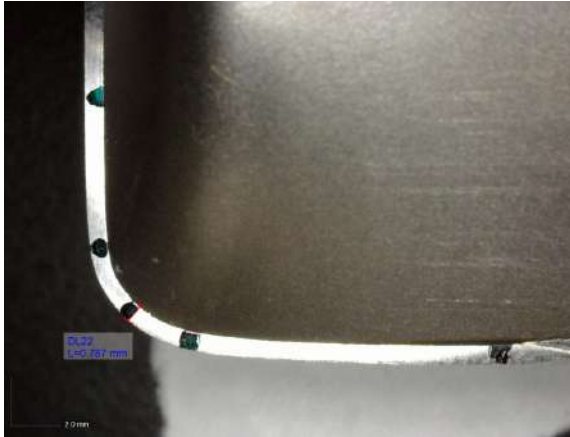


Fig. 3. Radius thickness shown on microscope

The results of the measurements and wall thickness variations in the radius zone, according to the set experiment plan, are shown in Table 5.

Table 5. Experimental design using L9 orthogonal array and experimental results

Exp. No.	Parameters:			Radius thickness variation	Thickness deviation
	R	BHF	Lub		
1	4.5	15	WL	0,793	0,007
2	4.5	20	L1	0,787	0,013
3	4.5	25	L2	0,763	0,037
4	6	15	L1	0,784	0,016
5	6	20	L2	0,75	0,05
6	6	25	WL	0,742	0,058
7	7.5	15	L2	0,76	0,04
8	7.5	20	WL	0,741	0,059
9	7.5	25	L1	0,737	0,063

3. ANALYSIS OF EXPERIMENTAL RESULTS

In the deep drawing process, considerations are often made under the assumption that the thickness of the material is the same in all sections of the drawn workpiece. However, measurements show that this is often not true. For these reasons, the primary goal of this

research is to determine the wall thickness distribution on the workpiece radius. The influence of the observed parameters on the wall thickness distribution on the radius of drawn part was analyzed using the Taguchi method. Since our goal is to achieve a nominal radius wall thickness of 0.8 mm for the DC01 sheet used, we will consider the radius wall thickness deviation from the nominal measurement. From this, it is obviously concluded that in this study, the objective function must be set as: Smaller-the-Better.

$$S/N = -10 \log \left(\frac{1}{n} \sum_{i=1}^n y_i^2 \right)$$

The S / N values for each experiment are shown in Table 6.

Table 6. S/N values for each experiment

Exp. No.	Parameters:			Thickness deviation	S/N ratio [dB]
	R	BHF	Lub		
1	4.5	15	WL	0.007	43.098
2	4.5	20	L1	0.013	37.721
3	4.5	25	L2	0.037	28.636
4	6	15	L1	0.016	35.917
5	6	20	L2	0.05	26.020
6	6	25	WL	0.058	24.731
7	7.5	15	L2	0.04	27.959
8	7.5	20	WL	0.059	24.583
9	7.5	25	L1	0.063	24.013

The S / N response for each input parameter is shown in Table 7.

Table 7. S/N response table for thickness deviation on radius

Level	R	BHF	Lub
1	36.49	35.66	30.80
2	28.89	29.44	32.55
3	25.52	25.79	27.54
Delta	10.97	9.86	5.01
Rank	1	2	3

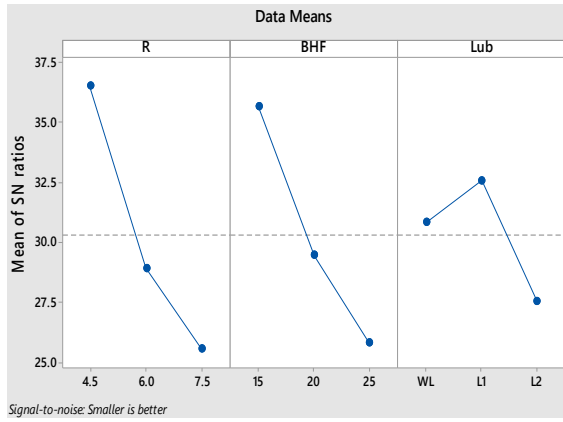


Fig. 4 S/N response for thickness deviation on radius

From the analysis of S / N ratio, it is easy to determine which of the three compared parameters have the greatest influence on the thickness variation on part radius. From Table 8, based on the rank of impact, and Figure 4, it was obtained that the most significant impact on thickness in the radius zone has die radius. On the other hand, the lubricant has the least impact. From Table 7 and the graph from Figure 4, the optimal deep drawing parameters within the offered levels can also be seen, considering the goal function "smaller-the-better" criterion. The optimal combination of selected parameters is the die radius at level 1, BHF at level 1 and the lubricant condition at level 2.

Table 8. Results of the analysis of variance

Source	DF	Adj SS	Adj MS	F-Value	P-Value	Involvement %
R	2	0.001884	0.000942	116.15	0.009	51.13
BHF	2	0.001534	0.000767	94.53	0.010	41.63
Lub	2	0.000251	0.000125	15.47	0.061	6.81
Error	2	0.000016	0.000008			0.43
Total	8	0.003685				100

Analysis of variance was performed to determine the statistical significance of die radius, blank holder force and lubrication condition on the variation of radius thickness on a deep drawn part. The results of the analysis of variance are shown in Table 9. The analysis was performed with a confidence level of 95%.

Table 9 revealed that two parameters i.e., die radius and blank holder force have a significant effect on the variation of radius thickness on deep drawn part. The P-values of these factors indicate that the confidence level is more than 95.00%, which shows their strong influence. Lubrication conditions do not have a significant influence, although they are on the border of significance. The influence of die radius, blank holder force and lubrication conditions was again calculated by percentage contribution. It has been observed that the percentage contribution of die radius (factor R) on the variation of radius thickness on deep drawn part was the largest (51.13%), followed by blank holder force (factor BHF) and lubrication

condition (factor Lub) with contributions of 41.63% and 6.81%, respectively. The remaining 0.43% is due to the error of the experiment, i.e., the influence of other factors. As the error of the experiment is minimal, it follows from this that the experiment is very well set up and that, in the observed case, there are no significant influences of other factors on radius thickness on deep drawn part.

4. CONCLUSIONS

This paper analyzed the influence of die radius, blank holder force and lubrication condition on the variation of radius thickness on deep drawn part. The experiment was performed according to Taguchi's L9 orthogonal array. Taguchi techniques and ANOVA analysis was used to determine the level of influence of deep drawing parameters on the variation of radius thickness on a deep drawn part. According to the results of the research and the conducted S/N analysis we can single out the parameters that have the most favorable influence on the

variation of radius thickness on a deep drawn part. Optimal combination levels of deep drawing parameters is die with radius 4.5 mm, a blank holder force 15 kN and lubrication conditions with Total Martol EP 180 lubricant. The ANOVA reveals that the most significant factor in affecting the variation of radius thickness on a deep drawn part was the die radius having a percentage contribution of 51.13%, followed by blank holder force and lubrication condition with contributions of 41.63% and 6.81%, respectively. With an experimental error of 0.43%, it was proven that significant process parameters were observed and that the influence of other process parameters is minimal. It was shown that the lubrication condition has no significant influence on the thickness at the radius of the deep drawn part. This confirms the assumption that it makes sense to go with a deep drawing process without lubricants while using the main tool elements made of plastic. This is particularly important from the point of view of environmental protection, and at the same time, the costs of deep drawing process and subsequent degreasing of parts are reduced.

- [6] Padmanabhan, R., Oliveira, C. M., Alves, C.M., Menezes, F.L. (2003). Influence of process parameters on the deep drawing of stainless steel, *Finite Elements in Analysis and Design* 43, p.p. 1062 – 1067.
- [7] Lin, BT., Yang, CY. , (2017) Applying the Taguchi method to determine the influences of a microridge punch design on the deep drawing. *Int J Adv Manuf Technol* **88**, 2109–2119.

REFERENCES

- [1] Schuh, G., Bergweiler, G., Bickendorf, P., Fiedler, F., Colag, C. (2020). Sheet Metal Forming Using Additively Manufactured Polymer Tools, *Procedia CIRP* 93, p.p. 20–25.
- [2] IXmetal, Sheet Metal Fabrication, Deep drawing&Expanding
<https://www.ixmetal.com/processing-service/sheet-metal-fabrication/deep-drawing-expanding/>, accessed 14. 4.2023.
- [3] Durgun, I. (2015). Sheet metal forming using FDM rapid prototype tool, *Rapid Prototyping Journal*, vol. 21 iss 4, p.p. 412-422.
- [4] Šljivić, M., Krašnik, M., Ilić, J., Anić, J. (2018) Development of small batches of functional parts using integration of 3D printing and vacuum casting technology, *A CTA TECHNICA CORVINIENSIS – Bulletin of Engineering*, Tome XI, Fascicule 2, pp. 35-38
- [5] RapidPrototyping.NL, Downloads, Datasheets material,VAC,
https://www.rapidprototyping.nl/fileadmin/_migrated/content_uploads/VAC_PX_223HT_ABSlike_HighTemp_120_.pdf, accessed 21. 4.2023.



Banja Luka
1-2 Jun 2023.

DEMI 2023

16th International Conference on Accomplishments in Mechanical and Industrial Engineering

www.demi.mf.unibl.org



Mathematical Modeling of the Roughness of the Aluminium Element Surface Processed on a CNC Machine

Sanela Hrnjica^a, Sanel Gredelj^b

^a PSM Protech GmbH & Co. KG Alpenstrasse 70, Marktschellenberg, Bavarska, Deutschland

^b University of Bihać, Faculty of Technical Engineering, dr I. Ljubijankića, Bihać, Bosnia and Herzegovina

Abstract

Aluminium elements are exposed to the different types of loads. Surface roughness affects the element strength which are used during the cyclic and alternating loads. In addition to functionality, roughness also has an aesthetic role in construction. Therefore, it is necessary to ensure that the surface roughness of aluminium elements is as small as possible. During the production of elements on CNC machines there are many factors which affect the surface roughness. In this paper input model parameters are: spindle speed, feedrate, tool diameter and depth cut. The output parameter is mean arithmetic profile deviation. After factor determination the experiment was conducted according to the experimental plan. In the experiment, variation of the input parameters is done on five levels, in order to obtain non-linear mathematical model. Then the coefficients and adequacy of the mathematical model were determined in coded form. Mathematical model in physical form is derived based on the coded mathematical model. Suitable model for analysis and optimization is a non-linear and adequate mathematical model. In this case that means determination of input parameters that give the minimum roughness and the influence of individual parameters.

Keywords

aluminium, CNC milling machine, mathematical modelling, nonlinear model, surface roughness

1. INTRODUCTION

Aluminum machine elements are produced to get a quality surface and reduce the roughness of the surface. The first reason is that these machine parts are often exposed to different types of dynamic load. The quality of the treated surface affects the element's dynamic endurance. If the element's surface is rough, endurance is also lower, because unevenness becomes a source of voltage concentration.

Corresponding author

doc. dr sc. Sanel Gredelj
sanel.gredelj@unbi.ba

University of Bihać, Faculty of Technical Engineering
dr I. Ljubijankića, Bihać
Bosnia and Herzegovina

Aluminum has a sensitivity rate of 60-80%, which is a high value for [1], and that is one of the reasons it reduces roughness. Aesthetics, which is essential to marketing and advertising, is another reason.

Optimization is required to obtain as minimal surface roughness as possible. For this, the mathematical model (target function) is determined according to the experimental-stochastic method, based on the planning and execution of the experiment. [2, 3, 4]

During the milling operations on CNC machines there are lot of parameters that affects surface quality. When planning an experiment, it is necessary to select those input parameters that can be varied and that have an essential impact on roughness.

In this paper, the input parameters of the model are: tool diameter d , spindle speed n , feedrate s , and cutting depth a . The output factor is the mean arithmetic deviation of the profile.

2. RESEARCH EQUIPMENT

The machine „VM6“ from manufacturer „HAAS“ (fig. 1.) whose characteristics are given in table 1. was selected for the experiment.



Fig. 1. CNC milling machine VM6

Table 1. Machine characteristics

Karakteristika	Value
Max movement along X-axis	1626 mm
Max movement along Y-axis	813 mm
Max movement along Z-axis	762 mm
Table length	1626 mm
Table width	711mm
Max weight on the table	1814 kg
Spindle speed	12000 o/min
Speed strength	22.4 kW
Tool number in the machine	30+1
Max tool diameter	64 mm
Max tool length	406 mm
Max tool weight	5,4 kg
Time to change a tool	2,8 s
Machine weight	10887 kg
Manufacturer	„HAAS“



Fig. 2. „Dohre“ milling tools

The milling tools are from „Dohre“ manufacturer (fig. 2.), whose characteristics are given in table 2.

Table 2. Characteristics of milling tools

Characteristic	Value
Tool material	HM- Hard metal
Diameter	6 mm
	8 mm
	10 mm
	12 mm
	16 mm
Cutting length	17 mm
	22 mm
	27 mm
	32 mm
	42 mm
Manufacturer	„Dohre“

According to the experiment plan, the aluminum workpiece was modeled in the CAD program "SolidWorks", and then programmed in the CAM program "Esprit", fig. 3.

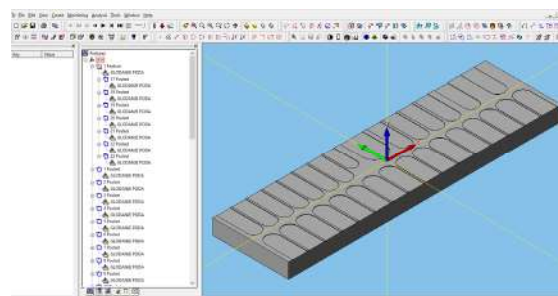


Fig. 3. CAD/CAM production preparation

Aluminum material is prismatic, whose characteristics are given in table 3. Material is set up in the clamp on the machine, fig. 4.

Table 3. Part characteristics

Characteristic	Value
Material	Al Mg 4.5Mn
Length	360 mm
Width	100 mm
Hight	20 mm
Mass	1,966 kg

The NC code is post-processed and transferred to the control part of the CNC machine so that the element creation can be started, fig. 4. After cleaning the part, the roughness measurement is carried out. During the roughness test, the "Mahr" measuring device was used, as shown in fig 5.

The Mahr measuring device is a modulated computer device for testing and analyzing roughness, shape, and topography. It consists of a computer that connects the unit of measurement to the needle as well as a printer to print the test results.



Fig. 4. CNC milling machine processing

Depending on the type of test, the modulated computer device can be equipped with several components, including a needle (sensor), measuring unit, measuring stand, and positioning table, as illustrated in fig. 5.



Fig. 5. Measuring device "Mahr"

Fig. 6. shows the "Mahr" device is a contact device, where the needle moves along the normal path to the desired surface. Mechanical vibrations relative to the head occur at places of microroughness (indentations and protrusions). These vibrations are transmitted to a sensor, which converts mechanical energy into electrical energy. The converter's signal is amplified and measured. Its parameters are used to determine the surface irregularities of

the part or product. Unevenness is studied in several phases. The profile is "dipped" a certain number of times, and only after a series of measurements is the final or average value of the parameter calculated.



Fig. 6. Examination of roughness with the Mahr device

Upon completion of the element, the roughness was measured three times on each separate piece of the finished item so called Pocket, and the average value of Ra was the output parameter of the experiment.

3. EXPERIMENT PLAN AND RESULTS

The goal of this experiment is to develop a nonlinear output mathematical model so that a rotatable plan is used as a special form of a central compositional plan. Rotatable plans have applicability and optimality properties, so they are suitable for modeling machining processes that need optimization. The rotatable plan contains the base part of plan 2^k , where k is the number of independent variable factors. It also contains symmetrically placed points n_α around the center of the plan and the repetition point n_0 in the center of the plan. In this experiment, four independent variables are considered, which means $k = 4$. The total number of measurements and repetitions at the central point depends on the number of variables k , size α , and size $p = 0$. The listed and other relevant sizes for the experiment are shown in table 4. The total number of measurements was [3]:

$$N = 2^k + 2k + n_0 = 2^4 + 2 \cdot 4 + 7 = 31. \quad (1)$$

The input parameters of the experiment are tool diameter d mm, spindle speed n o/min, feedrate s mm/min, and cutting depth a mm. The output parameter is the mean arithmetic deviation of the Ra μm .

Table 4. Second-order rotatable plan parameters for $k = 4$, $n_0 = 7$ and $N = 31$ [3]

Parameter	Value
α	2
λ_4	0,8611
$a_1 = a_{11}$	0,1428
$a_2 = a_7 = a_{17}$	- 0,0357
$a_3 = a_{12}$	0,0416
$a_4 = a_{13}$	0,0625
a_5	0,0312
$a_6 = a_{18}$	0,0037
a_{14}	0,0349

To make the experiment matrix plan, it is necessary to code the basic factors, which means to translate them into the space of coded coordinates, table 5. Coding is performed according to the formula [4]:

$$X_i = \frac{x_i - x_{0i}}{\Delta x_i}, \quad i = 1, 2, 3, 4, \quad (2)$$

where the mean level is the value of the i -th factor:

$$x_{0i} = \frac{x_{i\max} + x_{i\min}}{2}, \quad (3)$$

and variation interval:

$$\Delta x_i = \frac{x_{i\max} - x_{i\min}}{2}. \quad (4)$$

Table 5. Physical and coded values

Impact factors	Encoded and physical values of input parameters				
$x_1 = d$	6	8	10	12	16
$x_2 = n$	7000	7500	8000	8500	9000
$x_3 = s$	2000	2500	3000	3500	4000
$x_4 = a$	0,4	0,5	0,6	0,7	0,8
X_i	-2	-1	0	+1	+2

After encoding the independent variable (baseline factors), the plan-result experiment matrix has the form shown in table 6.

Table 6. Plan matrix with the experiment results

N_j	Encoded values				Results
	X_1	X_2	X_3	X_4	Ra μm
1	-1	-1	-1	-1	1,986
2	+1	-1	-1	-1	1,135
3	-1	+1	-1	-1	1,714
4	+1	+1	-1	-1	0,931
5	-1	-1	+1	-1	2,929
6	+1	-1	+1	-1	1,668
7	-1	+1	+1	-1	2,333
8	+1	+1	+1	-1	1,527
9	-1	-1	-1	+1	2,223
10	+1	-1	-1	+1	1,203
11	-1	+1	-1	+1	1,950
12	+1	+1	-1	+1	0,971
13	-1	-1	+1	+1	3,111
14	+1	-1	+1	+1	1,666
15	-1	+1	+1	+1	2,606
16	+1	+1	+1	+1	1,428
17	0	0	0	0	0,191
18	0	0	0	0	0,196
19	0	0	0	0	0,189
20	0	0	0	0	0,207
21	0	0	0	0	0,198
22	0	0	0	0	0,210
23	0	0	0	0	0,209
24	-2	0	0	0	1,909
25	+2	0	0	0	0,694
26	0	-2	0	0	0,224
27	0	+2	0	0	0,186
28	0	0	-2	0	0,188
29	0	0	+2	0	0,196
30	0	0	0	-2	0,214
31	0	0	0	+2	0,234

4. HOMOGENITY OF EXPERIMENT RESULTS

After the experiment is performed, the uniformity of dispersions or homogeneity of experiments is checked.

Repeating the experiment with constant values of input parameters can determine the difference in the numerical output results.. Checking the homogeneity of variances at a certain level of confidence ($P = 0.95$) can be performed by Cochran's criterion or Fisher's criterion for approximately normal distributions. The homogeneity of dispersions will be checked according to the Cochran criterion for confidence level $P = 0.95$ [5]:

$$K_h = \frac{\max S_j^2}{\sum_{j=1}^N S_j^2} \leq K_t(f_j, N_u), \quad (5)$$

where are:

K_t – tabular value according to Cochran's

criteria for degrees of freedom f_j and $N = n_0$;

f_j – degree of freedom ($f_j = n_0 - 1$);

n_0 – the number of repetitions in the sample;

S_j^2 – sample variance:

$$S_j^2 = \frac{1}{n_0 - 1} \sum_{i=1}^n (y_{ji} - \bar{y}_j)^2. \quad (6)$$

Mean sample value:

$$\bar{y}_j = \frac{1}{n_0} \sum_{i=1}^n y_{ji}, \quad j = 1, 2, \dots, N_u; \quad i = 1, 2, \dots, n. \quad (7)$$

As can be seen from table 6, repetition was carried out in measurements 17 - 23 in the mean values of the varied parameters, which means at the zero point of the plan. The degree of freedom is calculated according to the pattern:

$$f_j = n_0 - 1 = 7 - 1 = 6. \quad (8)$$

Cochran's criteria:

$$K_h = \frac{\max S_j^2}{\sum_{j=1}^N S_j^2} = \frac{2,01 \cdot 10^{-5}}{7,35 \cdot 10^{-5}} = 0,274. \quad (9)$$

In table I [3] – Cochran's criteria there are $K_t(f_j, N_u)$, where are:

$f_j = 6$ – degree of freedom,

$n_0 = 7$ – sample number,

so it is at the risk level $\alpha = 0,05$:

$$K_t(f_j, n_0) = K_t(6, 7) = 0,3974. \quad (10)$$

Table 7. Calculation of experiment homogeneity

Ordinal number of experiments N_i	Measurement result	Mean value	Sum of squares	Variance	Degree of freedom
	$y_j = Ra$	\bar{y}_j	$(y_{ji} - \bar{y}_j)^2$	S_j^2	f_j
17	0,191	0,2	$7,51 \cdot 10^{-05}$	$1,25 \cdot 10^{-05}$	6
18	0,196	0,2	$1,60 \cdot 10^{-05}$	$2,68 \cdot 10^{-06}$	6
19	0,189	0,2	$1,21 \cdot 10^{-04}$	$2,01 \cdot 10^{-05}$	6
20	0,207	0,2	$4,44 \cdot 10^{-05}$	$7,41 \cdot 10^{-06}$	6
21	0,198	0,2	$4,00 \cdot 10^{-06}$	$6,68 \cdot 10^{-07}$	6
22	0,210	0,2	$9,34 \cdot 10^{-05}$	$1,56 \cdot 10^{-05}$	6
23	0,209	0,2	$8,71 \cdot 10^{-05}$	$1,45 \cdot 10^{-05}$	6
$\sum_{i=1}^n S_j^2 =$				$7,35 \cdot 10^{-05}$	

Since it is valid

$$K_h = \frac{\max S_j^2}{\sum_{j=1}^N S_j^2} = \frac{2,01 \cdot 10^{-5}}{7,35 \cdot 10^{-5}} = 0,274 < 0,3974 = K_t(6, 7) = K_t(f_i, N_u). \quad (11)$$

the experiment is controlled (can be continued if the first measurements were made at central point of the plan), because the dispersion is homogeneous with a reliability of 95 %.

5. MATHEMATICAL MODELS AND COEFFICIENT CALCULATION

The roughness is modeled by a non-linear model, i.e. a second-order polynomial for $k=4$:

$$\begin{aligned}
 Ra = & b_0 + b_1X_1 + b_2X_2 + b_3X_3 + b_4X_4 + \\
 & + b_{11}X_1^2 + b_{22}X_2^2 + b_{33}X_3^2 + b_{44}X_4^2 + \\
 & + b_{12}X_1X_2 + b_{13}X_1X_3 + b_{14}X_1X_4 + \\
 & + b_{23}X_2X_3 + b_{24}X_2X_4 + b_{34}X_3X_4.
 \end{aligned} \quad (12)$$

The coefficients of the mathematical model (12) are calculated according to the following equations [3]:

$$\left. \begin{aligned}
 b_0 &= a_1 \sum_{j=1}^N Y_j + a_2 \sum_{i=1}^k \sum_{j=1}^N X_{ij}^2 Y_j, \\
 b_i &= a_3 \sum_{j=1}^N X_{ij} Y_j, i = 1, 2, \dots, k, \\
 b_{im} &= a_4 \sum_{j=1}^N X_{ij} X_{mj} Y_j, 1 \leq i < m \leq k, \\
 b_{ii} &= a_5 \sum_{j=1}^N X_{ij}^2 Y_j + a_6 \sum_{i=1}^k \sum_{j=1}^N X_{ij}^2 Y_j + a_7 \sum_{j=1}^N Y_j.
 \end{aligned} \right\} \quad (13)$$

where are:

X_{ij}, X_{mj} – coded values (table 5.);

a_i ($i = 1, 2, \dots, 7$) – parameters determined from the table 4.

According to (12) and (13) a concrete non-linear mathematical model is:

$$\begin{aligned}
 Ra = & 0,1999 - 0,4473 \cdot X_1 - 0,1056 \cdot X_2 + \\
 & + 0,2151 \cdot X_3 + 0,0406 \cdot X_4 + 0,4972 \cdot X_1^2 + \\
 & + 0,2234 \cdot X_2^2 + 0,2141 \cdot X_3^2 + 0,2221 \cdot X_4^2 + \\
 & + 0,0519 \cdot X_1X_2 - 0,066 \cdot X_1X_3 - \\
 & - 0,0576 \cdot X_1X_4 - 0,0313 \cdot X_2X_3 - \\
 & - 0,0021 \cdot X_2X_4 - 0,0141 \cdot X_3X_4
 \end{aligned} \quad (14)$$

By inserting the values X_1, X_2, X_3 and X_4 into the mathematical model (14) for each of the 31. measurements, the calculated values of y_R are obtained as shown in table 8.

By including the expressions:

$$\left. \begin{aligned}
 X_1 &= 2 \frac{d-d_0}{d_{+1}-d_{-1}} = 2 \frac{d-10}{12-8} = \frac{d-10}{2} \\
 X_2 &= 2 \frac{n-n_0}{n_{+1}-n_{-1}} = 2 \frac{n-8000}{8500-7500} = \frac{n-8000}{500} \\
 X_3 &= 2 \frac{s-s_0}{s_{+1}-s_{-1}} = 2 \frac{s-3000}{3500-2500} = \frac{s-3000}{500} \\
 X_4 &= 2 \frac{a-a_0}{a_{+1}-a_{-1}} = 2 \frac{a-0,6}{0,7-0,5} = \frac{a-0,6}{0,1}.
 \end{aligned} \right\} \quad (15)$$

in the coded mathematical model (14) the mathematical model is obtained in physical form:

$$\begin{aligned}
 Ra = & 106,6597 + 0,1243d^2 + 8,936 \cdot 10^{-7}n^2 + \\
 & + 8,564 \cdot 10^{-7}s^2 + 88,84a^2 + 0,0000519dn - \\
 & - 0,000066ds - 0,576da - 1,252 \cdot 10^{-7}ns - \\
 & - 0,00042an + 0,000282as - 2,58125d - \\
 & - 0,014627n - 0,0028774s - 98,854a.
 \end{aligned} \quad (16)$$

Then the significance of the coefficients was evaluated, which shows how much confidence the obtained results should be observed. The significance check of the coefficients was performed in the "Design Expert" program, a software package intended for experiment planning. The program calculates p-values for each coefficient. The coefficient is significant if $p < 0.05$ (table 8). P-values less than 0.05 indicate model terms are significant. In this case b_1 and b_1^2 are significant model terms. Values greater than 0.100 indicate the model terms are not significant. If there are many insignificant model terms, model reduction may improve model.

Table 8. Evaluation of the significance of the coefficients

Coefficient	p-value	Evaluation
b_0	-	excluded
b_1	$0,0165 < 0,05$	significant
b_2	$0,5366 > 0,05$	insignificant
b_3	$0,2163 > 0,05$	insignificant
b_4	$0,8113 > 0,05$	insignificant
b_{12}	$0,8032 > 0,05$	insignificant
b_{13}	$0,7514 > 0,05$	insignificant
b_{14}	$0,7824 > 0,05$	insignificant
b_{23}	$0,8810 > 0,05$	insignificant
b_{24}	$0,9961 > 0,05$	insignificant
b_{34}	$0,9457 > 0,05$	insignificant
b_1^2	$0,0048 < 0,05$	significant
b_2^2	$0,1578 > 0,05$	insignificant
b_3^2	$0,1635 > 0,05$	insignificant
b_4^2	$0,1498 > 0,05$	insignificant

Since only two coefficients are significant, it is necessary to repeat the experiment or adjust the mathematical model. In this case, the roughness is modeled by a linear model, according to an orthogonal plane that contains only the base part of the rotatable plane $2k$, i.e. by a second-order polynomial for $k = 4$:

$$Ra = b_0 + b_1X_1 + b_2X_2 + b_3X_3 + b_4X_4 + b_{12}X_1X_2 + b_{13}X_1X_3 + b_{14}X_1X_4 + b_{23}X_2X_3 + b_{24}X_2X_4 + b_{34}X_3X_4. \quad (16)$$

$$\left. \begin{aligned} b_0 &= \frac{1}{N-n_0} \sum_{j=1}^N y_j, \\ b_i &= \frac{1}{N-n_0} \sum_{j=1}^N X_{ij}y_j, \text{ za } i = 1, \dots, k, \\ b_{im} &= \frac{1}{N-n_0} \sum_{j=1}^N X_{ij}X_{mj}y_j, \text{ za } i \leq m \leq k. \end{aligned} \right\} \quad (17)$$

According to (16) and (17), the concrete linear mathematical model after eliminating insignificant coefficients is:

$$Ra = 1,84 - 0,5202 \cdot X_1 - 0,1538 \cdot X_2 + 0,322 \cdot X_3 + 0,0584 \cdot X_4 + 0,0519 \cdot X_1X_2 - 0,066 \cdot X_1X_3 - 0,0576 \cdot X_1X_4. \quad (17)$$

By inserting the expression (15) into coded mathematical model (17) a linear mathematical model is obtained in physical form:

$$Ra = 2,948 - 0,1324d - 0,00082n + 0,0013s + 6,92a + 0,000052dn - 0,000066ds - 0,576ad. \quad (18)$$

The mathematical model (17) is simpler than (14), but it is not suitable for optimization.

6. ADEQUACY OF THE MATHEMATICAL MODEL

In order for a coded model (14) to be fully analyzed, it is necessary to examine the adequacy of the mathematical model itself, that is, whether the output parameters y_R calculated from the model correspond to the output y_E of the experiment, fig. 7..

The adequacy of the coded mathematical model is checked by comparing the experimentally obtained value y_E with the values calculated from y_R model.

The most significant criterion for selecting a mathematical model is the multiple regression coefficient R (coefficient of determination). When two or more models describe the process well, the decision on the most appropriate

model is made based on the multiple regression coefficients.

Table 9. Experimental and calculated results

N_j	Rezultati		$(y_R - \bar{y}_E)^2$	$(y_E - \bar{y}_E)^2$
	y_E	y_R		
1	1,986	1,548	0,191	0,755
2	1,135	0,783	0,124	0,0003
3	1,714	1,286	0,183	0,357
4	0,931	0,743	0,035	0,034
5	2,929	2,187	0,550	3,284
6	1,668	1,172	0,245	0,303
7	2,333	1,814	0,269	1,478
8	1,527	1,006	0,270	0,168
9	2,223	1,763	0,211	1,223
10	1,203	0,782	0,177	0,007
11	1,950	1,506	0,197	0,695
12	0,971	0,732	0,057	0,021
13	3,111	2,360	0,564	3,978
14	1,666	1,114	0,304	0,302
15	2,606	1,978	0,394	2,216
16	1,428	0,940	0,238	0,097
17	0,191	0,199	0,00007	0,857
18	0,196	0,199	0,00002	0,848
19	0,189	0,199	0,00012	0,861
20	0,207	0,199	0,00005	0,829
21	0,198	0,199	0,00000	0,844
22	0,210	0,199	0,00009	0,823
23	0,209	0,199	0,00009	0,824
24	1,909	3,083	1,379	0,627
25	0,694	1,293	0,360	0,179
26	0,224	1,304	1,168	0,797
27	0,186	0,882	0,486	0,867
28	0,188	0,626	0,192	0,864
29	0,196	1,486	1,665	0,848
30	0,214	1,007	0,629	0,816
31	0,234	1,169	0,875	0,779

The regression coefficient is also used to test the relationship (fit) between y_R and y_E (table

8.) and is calculated according to the formula [5]:

$$R = \sqrt{1 - \frac{\sum_{j=1}^N (y_{Rj} - y_{Ej})^2}{\sum_{j=1}^N (y_{Ej} - \bar{y}_E)^2}}, \quad (19)$$

where is:

$$\bar{y}_E = \frac{\sum_{j=1}^N y_{Ej}}{N}, \quad (20)$$

arithmetic mean of all experimental results.

According to the values of the experimental and calculation results (table 9.) the following result can be obtained:

$$R = \sqrt{1 - \frac{10,7687}{26,5812}} = 0,7714. \quad (21)$$

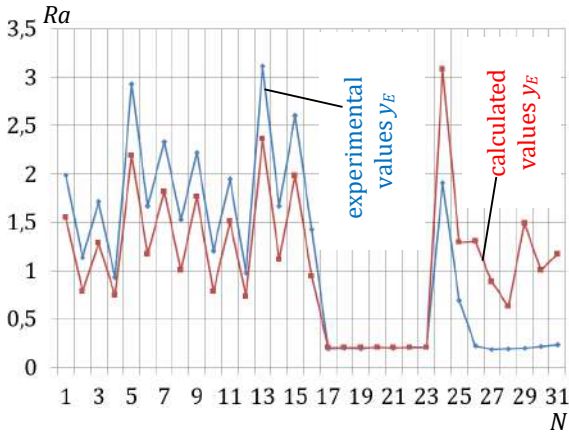


Fig. 7. Experimental and calculated values of Ra

The value of $R = 0.7714$ means that mathematical models (14) and (16) with a reliability of 77.14% describe the experiment results, which is satisfactory. That is, mathematical models fit experimental data in 77.14% of cases. Consequently, nonlinear mathematical models (14) and (16) can be used for optimization if insignificant coefficients are not excluded.

Multiple regression coefficients $R = 0.996321$ are obtained for linear mathematical models (17) and (18), which indicate excellent adequacy.

7. CONCLUSION

The roughness of the treated surface must be reduced to the lowest acceptable value in relation to the customer's functionality and wishes. This is achieved through fine processing. Fine processing can ensure the required quality, but such processing makes production more expensive, so it is necessary to find an optimal value between functionality and economy, which would mean that the surface will be rougher so that production is cheaper but functional.

One of the ways is the methodology shown in this paper. This is based on the experimental stochastic method, which is experiment planning. A rotatable plan for four input and one output parameter was used as the basic model. Input parameters: spindle speed, feedrate, tool diameter, and depth of cut, are varied at five levels. The output parameter is the mean arithmetic deviation of the Ra profile, which depends on the input parameters variation. After the experiment, using the plan-matrix, the coefficients of the nonlinear mathematical model were determined. The adequacy of this model is satisfactory. However, considering the poor significance of the coefficients, a linear mathematical model was also determined, according to the orthogonal plan, which has excellent adequacy. Given the satisfactory multiple regression coefficient value, nonlinear mathematical models can be used for optimization. By optimizing the nonlinear mathematical model, the minimum value of the mean arithmetic deviation $Ra_{opt} = 0.05066 \mu\text{m}$ is obtained. This is an extremely low roughness value, i.e. high quality of the processed surface. This minimum value is calculated from realistic values of input parameters: tool diameter $d_{opt} = 11 \text{ mm}$, spindle speed $n_{opt} = 7000 \text{ rpm}$, feedrate $s_{opt} = 2000 \text{ mm/min}$, and cutting depth $a_{opt} = 0.6 \text{ mm}$. The obtained values can be used in real production when milling aluminum elements.

The linear mathematical model is not suitable for optimization and gives unrealistic results at the limits of inbound data variation. This can be concluded without any optimization procedure being implemented.

Advantage is that this methodology is simple and has realistic results for a specific production.

The disadvantage is that the procedure must be repeated for the production of elements from

different materials with different tools. For example, steel reacts differently to tool passes than light alloys and other materials. This directly affects the quality of the finished surface. Also, each tool, depending on its geometry and machining process, leaves a unique mark on the machined surface. This also affects the machined surface quality. This means the methodology is efficient and cost-effective in serial and mass production, unlike individual production.

REFERENCES

- [1] Manjgo M., Islamović. F., Gačo, Dž. (2014). *Mašinski elementi I*. Univerzitet Džemal Bijedić, Mašinski fakultet, Mostar, BiH.
- [2] Belegundu, D. A., Chandrupatla, R. T. (2011). *Optimization Concepts and Applications in Engineering*, Second Edition. New York: Cambridge University Press, USA.
- [3] Jurković, M. (1999). *Matematičko modeliranje inženjerskih procesa i sistema*, Mašinski fakultet, Bihać, BiH.
- [4] Montgomery, C., D. (2015). *Design and Analysis of Experiment*, Arizona State University, John Wiley and Sons, USA.
- [5] Hodžić, D., Džanić, A. (2020). *Planiranje eksperimenta*, Univerzitet u Bihaću, BiH.



Banja Luka
1–2 Jun 2023.

DEMI 2023
**16th International Conference on
Accomplishments in Mechanical and
Industrial Engineering**
www.demi.mf.unibl.org



Optimization of Cutting Parameters for Minimizing Unit Production Time in Multi-Pass Rough Turning of S355JR Structural Steel

M. Trifunović^a, M. Madić^a, N. Vitković^a

^aUniversity of Niš, Faculty of Mechanical Engineering in Niš, Aleksandra Medvedeva 14, 18104 Niš, Serbia

Abstract Prediction of tool life is one of the key factors that the day-to-day metal cutting practitioner finds valuable. In this paper, a model for prediction of tool life for rough turning of S355JR structural steel with DNMG 15 04 12-PR GC4425 cutting insert was developed. Data for model development were obtained using cutting tool manufacturer online software for tool and cutting data recommendations. An analysis of the constants of prediction model for tool life showed that the cutting speed has the greatest effect on tool life, followed by the feed rate. The effect of the depth of cut was negligible. Developed prediction model was used in the formulation of the single-objective optimization problem with practical constraints for longitudinal multi-pass rough turning. The unit production time was used as an objective function. The optimization problem was solved using a deterministic approach, i.e., a brute force optimization algorithm which guarantees the optimality of the optimization solutions. Predicted tool life for optimal combination of cutting parameter values was validated in the cutting tool manufacturer online software.

Keywords tool life, multi-pass turning, optimization, unit production time

1. INTRODUCTION

Surface roughness and dimensional accuracy of the machined part deteriorate with the progress of tool wear [1]. This leads to changing the worn tool. Tool life (T) defines the time, expressed in minutes, from the first cut, up to the moment when the measured wear level exceeds an established limit (critical value) [2]. Tool life is needed for the definition of the unit production time, which is directly related to other machining process performances, such as part production costs and consumed energy [3]. A number of factors related to the cutting tool, the workpiece material, the cutting parameters, the cutting mode, and the machine tool affect the tool life [1]. In practice, most often, only the effects of cutting parameters are analysed. Prediction of tool life is one of the key factors that the day-to-day metal

cutting practitioner finds valuable [1]. Development of empirical tool life prediction model for a given combination of the cutting tool and the workpiece material from physical experimental trials is time consuming and expensive.

Economic considerations are obviously important in planning a machining process. The economics of machining considers three factors: the production cost per component, the production time per component (unit production time) and the profit rate [4]. Cutting parameters are directly related to unit production time in multi-pass rough turning operations. Therefore, selection of optimal cutting parameters is the best way to minimize unit production time (or equivalently maximize production rate). There are only two recent single-pass turning optimization studies based

on analytical modelling and formulation of a mathematical optimization problem, that consider unit production time as objective function [5, 6]. There is also one recent multi-pass turning optimization study that considers production rate as objective function [7]. All these studies considered already developed mathematical optimization models. Optimization problems in these studies were solved using meta-heuristic algorithms: Monte Carlo [5], particle swarm optimization [6], and probabilistic version of the non-dominated sorting genetic algorithm [7].

In this paper, a model for prediction of tool life for rough turning of S355JR structural steel with DNMG 15 04 12-PR GC4425 cutting insert was developed. Full factorial design was applied to define experimental hyper-space wherein depth of cut, feed rate and cutting speed were varied at three levels. Data for the model development were obtained using a tool and cutting data recommendation system of the cutting tool manufacturer [8] and were modelled using power law in the form of extended Taylor's tool life model. The present study also considers newly developed optimization model for multi-pass rough turning [3]. Since meta-heuristic optimization algorithms cannot guarantee optimal solutions [9], single-objective optimization problem for multi-pass rough turning developed in this study was solved using a deterministic approach, i.e., a brute force optimization algorithm, which guarantees the optimality of the optimization solutions.

2. TOOL LIFE PREDICTION MODEL

The workpiece material was S355JR unalloyed medium-carbon structural steel (hardness 161 HB). It is used for medium to high strength non-vital machine parts, with good toughness and easy formability. The machine tool was the CNC lathe with the motor power of $P_m = 37$ kW, the maximum spindle speed of $n_{max} = 2000$ rpm, and the maximum torque of $M_{cmax} = 4200$ Nm. Sandvik Coromant was selected as cutting tool manufacturer. The cutting tool was a toolholder

DDJNR 3225P 1504 (cutting edge angle of $\kappa = 93^\circ$, rake angle of $\gamma_{oh} = -6^\circ$) with a DNMG 15 04 12-PR GC4425 insert for roughing, rake angle of $\gamma_{oi} = 22^\circ$, nose radius $r_\epsilon = 1.2$ mm, and grade of GC4425 (coated carbide). Recommended cutting conditions were the depth of cut of $a_p = 1.0 - 6.0$ mm, the feed rate of $f = 0.25 - 0.70$ mm/rev, and the cutting speed of $v_c = 245 - 350$ m/min.

Ranges and levels for the depth of cut and feed rate were selected considering recommended cutting conditions for the insert. The cutting speed values were selected considering availability and capabilities of the tool and cutting data recommendation system of the cutting tool manufacturer. It allows selection of values for the cutting speed from ranges that are different for different feed rate values, due to power limitation. The minimal and maximal selected cutting speed values were 164 m/min and 514 m/min, respectively. Data for the model development were obtained using a tool and cutting data recommendation system of the cutting tool manufacturer [8]. The total number of different cutting conditions that were attempted in the virtual experiment was 27.

The resulting tool life prediction model was obtained in the following form:

$$T = \frac{e^{21.6}}{a_p^{0.0092} \cdot f^{2.26} \cdot v^{3.59}} \quad (1)$$

An analysis of the constants of tool life prediction model showed that the cutting speed has the greatest effect on tool life, followed by the feed rate, while the effect of the depth of cut is negligible.

Validity of the developed tool life prediction model was checked for several combinations of cutting parameter values. On average, the deviation was between 6 and 7 %.

3. CASE STUDY

The longitudinal turning operation (multi-pass rough turning) of S355JR structural steel using a coated carbide tool was considered in the present study (Fig. 1).

Stock was a bar with the diameter of 90 mm and the length of 170 mm, made of S355JR structural steel with a specific cutting force for the unit cutting cross-section $k_{c1.1} = 1500$ N/mm² and $m_c = 0.25$. The multi-pass rough turning starts at the diameter of $D_0 = 90$ mm, and finishes at the diameter of $D_1 = 40$ mm. The mean cutting diameter for multi-pass rough turning is $D_m = 65$

Corresponding author

Ph.D., Milan Trifunović
milan.trifunovic@masfak.ni.ac.rs

University of Niš, Faculty of Mechanical Engineering in Niš
 Aleksandra Medvedeva 14
 18104 Niš, Serbia

mm. The cutting length is $L = l + l_1 = 50 + 2 = 52$ mm, where l is the length and l_1 is the cutting tool approach distance.

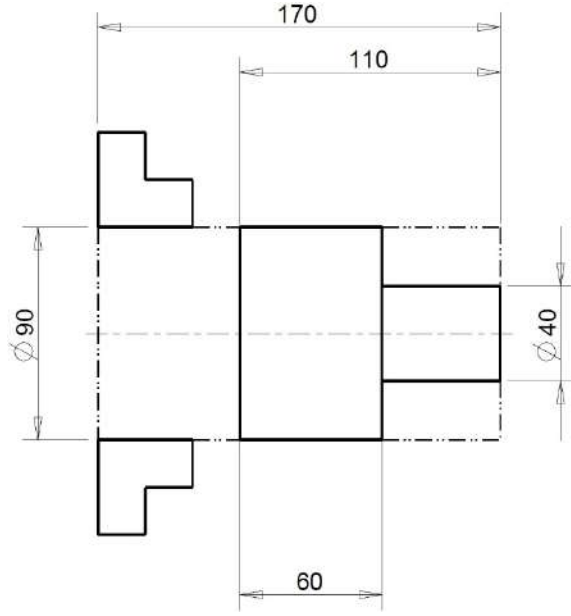


Fig. 1. Technical drawing of the finished part and stock

The machine tool was the CNC lathe Gildemeister NEF 520 with the motor power of $P_m = 12$ kW and the efficiency of $\eta = 0.8$. The spindle speed range is $n = 10 - 3000$ rpm and the maximal feed velocity is $v_{fmax} = 5000$ mm/min. The maximum allowed force is $F_{max} = 5000$ N.

4. FORMULATION OF THE OPTIMIZATION PROBLEM

The unit production time for multi-pass rough turning is defined as [10]:

$$t_1 = t_{mp} + t_c + t_r + t_p + t_{rm} + t_m + t_{tc} \quad (2)$$

where:

$$t_{rm} = \frac{L}{v_{fmax}} \cdot i \quad (3)$$

$$t_m = \frac{L}{n \cdot f} \cdot i = \frac{\pi \cdot D_m \cdot L}{1000 \cdot v_c \cdot f} \cdot i \quad (4)$$

$$t_{tc} = t_m \cdot \frac{t_{tc1}}{T} \quad (5)$$

The unit production time for multi-pass rough turning in the final form is:

$$t_1 = t_{mp} + t_c + t_r + t_p + \frac{L}{v_{fmax}} \cdot i + \frac{\pi \cdot D_m \cdot L}{1000 \cdot v_c \cdot f} \cdot i \cdot \left(1 + \frac{t_{tc1}}{T}\right) \quad (6)$$

where t_1 (min) is the unit production time, t_{mp} (min) is the total machine tool preparation time ($t_{mp} = 3$ min), t_c (min) is the stock clamping time ($t_c = 0.25$ min), t_r (min) is the workpiece release time ($t_r = 0.25$ min), t_p (min) is the positioning time ($t_p = 0.047$ min), t_{rm} (min) is the return motion time, t_m (min) is the machining time, t_{tc} (min) is the tool changing time reduced to one workpiece, L (mm) is the cutting length, v_{fmax} (mm/min) is the maximal feed velocity, i is the number of passes, n (rpm) is the spindle speed, f (mm/rev) is the feed rate, D_m (mm) is the mean cutting diameter, v_c (m/min) is the cutting speed, t_{tc1} (min) is the tool changing time ($t_{tc1} = 1$ min), T (min) is the tool life.

A realistic optimization of machining process should consider the numerous technological and practical constraints, which limit the feasible domain for the selection of optimal cutting parameters.

The goal in rough turning is to remove large volumes of workpiece material as fast as possible, considering that required machine tool power (P_c/η) does not exceed machine tool motor power (P_m):

$$\frac{P_c}{\eta} = \frac{F_c \cdot v_c}{60000 \cdot \eta} = \frac{k_{c1.1} \cdot a_p \cdot f \cdot v_c \cdot \left(\frac{1}{f \cdot \sin \kappa}\right)^{m_c} \cdot \left(1 - \frac{\gamma_o}{100}\right)}{60000 \cdot \eta} \leq P_m \quad (7)$$

where: η is the efficiency, F_c (N) is the cutting force, $k_{c1.1}$ (N/mm²) is the specific cutting force for the unit cutting cross-section of 1 mm², κ (°) is the cutting edge angle, m_c is the material dependent constant and γ_o (°) is the cutting tool rake angle.

Unfavourable chip forms can inhibit the machining process, damage the cutting tool, the machine tool, and the surface of the finished part, or even represent an increased hazard to machine tool operator [11]. The ratio of the depth of cut to the feed rate, which is termed as chip slenderness ratio, influences the chip morphology in turning [12]. To avoid unfavourable chip forms (ribbon, snarled, flat helical), this ratio must be kept at a certain range. With respect to favourable chip slenderness the following constraint may be added:

$$4 \leq \frac{a_p}{f} \leq \xi_{max} \quad (8)$$

where ξ_{max} is the maximal chip slenderness ratio which depends on the workpiece material ($\xi_{max} = 16$ for unalloyed structural steel) [13].

The following set of constraints can be formulated based on the recommended cutting conditions provided by the cutting insert manufacturer (Sandvik Coromant):

$$\begin{aligned} v_{cmin} &\leq v_c \leq v_{cmax} \\ a_{pmin} &\leq a_p \leq a_{pmax} \\ f_{min} &\leq f \leq f_{max} \end{aligned} \quad (9)$$

Considering the available machine tool spindle speed range, as well as the change in the workpiece diameter during machining, the following cutting speed constraint can be formulated:

$$\frac{\pi \cdot D \cdot n_{min}}{1000} \leq v_c \leq \frac{\pi \cdot D \cdot n_{max}}{1000} \quad (10)$$

To avoid unmachined areas on the workpiece surface [11], the following inequality constraint was also considered:

$$f \leq r_\epsilon \quad (11)$$

where r_ϵ (mm) is the cutting tool nose radius.

The constraint of equality type for the determination of the number of passes can be formulated as follows:

$$i = \frac{D_0 - D_1}{2 \cdot a_p} \quad (12)$$

The proposed mathematical model of the multi-pass rough turning optimization problem aims at determining the set of cutting parameter values to minimize unit production time, while considering several constraints. It considers one objective function, four parameters (feed rate, depth of cut, cutting speed and number of passes), five machining constraints and three machining parameter bounds, and can be defined as follows:

$$\begin{aligned} \text{Minimize: } t_1 &= t_{mp} + t_c + t_r + t_p + \frac{L}{v_{fmax}} \cdot i + \\ &\frac{\pi \cdot D_m \cdot L}{1000 \cdot v_c \cdot f} \cdot i \cdot \left(1 + \frac{t_{tc1}}{T}\right) \end{aligned}$$

Subject to:

$$\frac{k_{c1.1} \cdot a_p \cdot f \cdot v_c \cdot \left(\frac{1}{f \cdot \sin \kappa}\right)^{m_c} \cdot \left(1 - \frac{\gamma_o}{100}\right)}{60000 \cdot \eta} \leq P_m$$

$$4 \leq \frac{a_p}{f} \leq \xi_{max}$$

$$v_{cmin} \leq v_c \leq v_{cmax}$$

$$a_{pmin} \leq a_p \leq a_{pmax}$$

$$f_{min} \leq f \leq f_{max}$$

$$\frac{\pi \cdot D \cdot n_{min}}{1000} \leq v_c \leq \frac{\pi \cdot D \cdot n_{max}}{1000}$$

$$f \leq r_\epsilon$$

$$i = \frac{D_0 - D_1}{2 \cdot a_p}$$

5. RESULTS AND DISCUSSION

The optimization problem for multi-pass rough turning was coded and solved in the Brutomizer software tool [14], using the brute force algorithm. Values of all cutting parameters are discretized by defining appropriate step sizes, in order to obtain practically feasible solutions that could be easily set on machine tool. In this way all possible candidates for the solution are enumerated. By checking whether each candidate satisfies the problem's statement, brute-force algorithm guarantees the optimality of the solution for the given discrete search space.

The optimization solution was determined in 13.3 s, which represents a reasonable optimization time.

The cutting regime which was realised in nine passes ($i = 9$), with the depth of cut of 2.78 mm, feed rate of 0.58 mm/rev, and cutting speed of 247 m/min, ensured minimal unit production time of 4.34 min. The values of constraints for this cutting regime are required machine tool power (P_c/η) of 11.97 kW and chip slenderness ratio of 4.79. The resulting (predicted) tool life is 20.97 min. The tool life for the optimal cutting parameter values obtained using a tool and cutting data recommendation system of the cutting tool manufacturer was 22 min.

Recommended cutting regime for the cutting insert is: depth of cut $a_p = 4.0$ mm (seven passes), feed rate $f = 0.40$ mm/rev, and cutting speed $v_c = 305$ m/min. Resulting chip slenderness in this case is 10, which is within the favourable chip slenderness range for unalloyed structural steel. However, the recommended cutting regime violates the required machine tool power constraint ($P_c/\eta = 16.78$ kW), which means that it cannot be realised on the machine tool.

6. CONCLUSIONS

The analysis of the obtained results leads to the following conclusions:

- Tool life prediction model developed on the basis of data from the tool and cutting data recommendation system of the cutting tool manufacturer can be successfully used in

formulation of single-objective turning optimization problems.

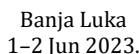
- Analysis of the constants of prediction model for tool life showed that the cutting speed has the greatest effect on tool life, followed by the feed rate, while the effect of the depth of cut is negligible.
- The applied deterministic approach may be justified for solving turning optimization problems due to its effectiveness and ability to deal with a number of nonlinear constraints of the inequality and equality type and high-dimensional domains.
- In situations when the cutting parameter values recommended by the cutting insert manufacturer violate one or more constraints, and therefore cannot be realised on the machine tool, the approach proposed in this paper can be used for determining optimal cutting parameter values resulting in minimal unit production time.

Acknowledgement

This research was financially supported by the Ministry of Science, Technological Development and Innovation of the Republic of Serbia (Contract No. 451-03-47/2023-01/ 200109).

REFERENCES

- [1] Grzesik, W. (2017). *Advanced Machining Processes of Metallic Materials: Theory, Modelling, and Applications (second edition)*. Elsevier, Amsterdam. DOI: [10.1016/B978-0-444-63711-6.00001-6](https://doi.org/10.1016/B978-0-444-63711-6.00001-6)
- [2] Toenshoff, H.K., Denkena, B. (2013). *Basics of Cutting and Abrasive Processes*. Springer-Verlag, Berlin Heidelberg. DOI: [10.1007/978-3-642-33257-9](https://doi.org/10.1007/978-3-642-33257-9)
- [3] Trifunović, M., Madić, M., Radovanović, M. (2020). Pareto optimization of multi-pass turning of grey cast iron with practical constraints using a deterministic approach. *The International Journal of Advanced Manufacturing Technology*, vol. 110, no. 7-8, p. 1893-1909. DOI: [10.1007/s00170-020-05994-4](https://doi.org/10.1007/s00170-020-05994-4)
- [4] Stephenson, D.A., Agapiou, J.S. (2016). *Metal Cutting Theory and Practice (third edition)*. Taylor & Francis Group, Boca Raton. DOI: [10.1201/9781315373119](https://doi.org/10.1201/9781315373119)
- [5] Sahali, M.A., Belaidi, I., Serra, R. (2015). Efficient genetic algorithm for multi-objective robust optimization of machining parameters with taking into account uncertainties. *The International Journal of Advanced Manufacturing Technology*, vol. 77, no. 1-4, p. 677-688. DOI: [10.1007/s00170-014-6441-z](https://doi.org/10.1007/s00170-014-6441-z)
- [6] Hassine, H., Barkallah, M., Bellacicco, A., Louati, J., Riviere, A., Haddar, M. (2015). Multi Objective Optimization for Sustainable Manufacturing, Application in Turning. *International Journal of Simulation Modelling*, vol. 14, no. 1, p. 98-109. DOI: [10.2507/IJSIMM14\(1\)9.292](https://doi.org/10.2507/IJSIMM14(1)9.292)
- [7] Sahali, M.A., Belaidi, I., Serra, R. (2016). New approach for robust multi-objective optimization of turning parameters using probabilistic genetic algorithm. *The International Journal of Advanced Manufacturing Technology*, vol. 83, no. 5-8, p. 1265-1279. DOI: [10.1007/s00170-015-7526-z](https://doi.org/10.1007/s00170-015-7526-z)
- [8] Sandvik Coromant. CoroPlus ToolGuide. From: <https://www.sandvik.coromant.com/en-gb/tools/coroplus-toolguide>, accessed on: February 15, 2023.
- [9] Diyaley, S., Chakraborty, S. (2019). Optimization of multi-pass face milling parameters using metaheuristic algorithms. *Facta Universitatis, Series Mechanical Engineering*, vol. 17, no. 3, p. 365-383. DOI: [10.22190/FUME190605043D](https://doi.org/10.22190/FUME190605043D)
- [10] Cukor, G. (2006). *Proračuni u obradi skidanjem strugotine*. Sveučilište u Rijeci, Tehnički fakultet: Rijeka.
- [11] Klocke, F. (2011). *Manufacturing Processes 1 – Cutting*. Springer-Verlag, Berlin Heidelberg. DOI: [10.1007/978-3-642-11979-8](https://doi.org/10.1007/978-3-642-11979-8)
- [12] Demir, Z., Adiyaman, O. (2019). Investigation of influence of approach angle and chip slenderness ratio on vibration, chip formation and surface quality in turning of AISI 1050 steel. *Journal of the Brazilian Society of Mechanical Sciences and Engineering*, vol. 41, article number: 467, 15 pages. DOI: [10.1007/s40430-019-1977-3](https://doi.org/10.1007/s40430-019-1977-3)
- [13] Kopač, J. (1991). *Odrezavanje*. Fakulteta za strojništvo: Ljubljana.
- [14] Virtuode. Brutomizer. From: <https://www.virtuode.com/index.php/products/brutomizer20/>, accessed on: February 15, 2023.



16th International Conference on Accomplishments in Mechanical and Industrial Engineering

www.demi.mf.unibl.org



Vukman, J.^a, Milošević, M.^a, Antić, A.^a, Božić, D.^a, Todić, V.^a, Lukić, D.^a

Abstract *Due to their homogeneity and excellent ratio between load capacity and weight, thin-walled aluminum structures are used as structural parts in the aerospace, automotive and military industries. The manufacture of these thin-walled structures is mainly done by removing a large amount of material from full raw pieces, sometimes up to 95% of their initial mass. Because of a large volume of material removing, it is necessary to achieve high productivity, which is limited by the lack of rigidity of the thin walls of these structures. As a result, errors occur, while reducing accuracy and machining quality.*

The main subject and objective of this paper is related to the optimization of high-speed machining parameters of linear thin-walled structures made of aluminum alloy Al7075 from the aspect of surface quality of processed superficial as a goal function. For this purpose, experiments were carried out based on which conclusions were made of the influence of input parameters on the surface roughness.

Keywords Optimization of machining parameters, thin-walled parts, Al 7075, surface roughness

Theory of optimization as a scientific discipline has a great application in solving engineering problems, where based on the set criteria of optimization/goal function, using optimization methods, the best solution is found on the selected object of optimization for certain conditions [1].

Due to their homogeneity, corrosion resistance and excellent ratio between the load capacity and mass of thin-walled aluminum parts are increasingly used as structural parts in the

Corresponding author

PhD, Dejan Lukic,
lukicd@uns.ac.rs

University of Novi Sad, Faculty of Technical Sciences,
Department of Production Engineering, Novi Sad, Serbia
www.ftn.uns.ac.rs, www.dpm.ftn.uns.ac.rs

aerospace, automotive, military, and other branches of the electro-mechanical industry.

The production of thin-walled parts is mainly carried out by removing materials from full raw pieces. Due to such a large volume of material removal, it is necessary to achieve high productivity while ensuring the required accuracy and quality [2-5].

The object of research in this paper are linear type of thin-walled parts of aluminium alloy Al7075, thin-wall thickness 0.5-1.5 mm, moderate and large height in relation to wall thickness (20:1, 30:1 and 60:1).

Machining process of these parts is very complex, because it requires the fulfillment of numerous structural and technological characteristics, for the realization of which it is necessary to use high-quality machining systems (machines, tools, fixtures, measuring instruments, workers), machining parameters, cooling and lubrication agent, etc. [6, 7].

The main subject and objective of the research in this paper refers to the optimization of parameters of high-speed machining of thin-walled linear parts made of aluminum alloy from the aspect of the quality of the surface roughness as a goal function.

2. REVIEW OF THE PROBLEM AND RESEARCH METHODOLOGY

By increasing the market demands for the machining of thin-walled parts, at the same time, research is being realized that is oriented towards optimizing the construction and technological processes of manufacturing these components. Optimization of the structure is carried out in order to reduce mass, deformation, vibration, or increase the loading capacity and strength, while the optimization of technological processes is carried out in order to reduce machining time and cost, increase the accuracy and surface roughness, etc. [1, 6-10]. To analyze the influence of the parameters of thin-walled parts on the surface roughness, it was necessary to set up and realize experimental research, and then to analyze the results and make certain conclusions.

Taguchi's method of experiment planning is a unique and very powerful technique for experimental analysis and optimization of products, processes, etc. In order to eliminate the disadvantages of the classical planning of experiments, which are reflected in the too complex and time-consuming execution of a large number of experiments, an alternative was found in the Taguchi method based on the application of special, partial factorial plans obtained from orthogonal plans that cover the entire experimental space of interest, and with a minimum number of experiments [11-14]. Taguchi proposed an aggregate statistical evaluation that combines information about mean and variance into a single measure of performance, known as the *signal-to-noise* ratio (*S/N ratio*). For a more detailed examination of the importance of the influence of the main factors and their interactions on the response, analysis of variance (*Analysis Of Variance - ANOVA*) can be used. Taguchi recommended analysis of mean values and *S/N* ratios using 2D response graphs instead of ANOVA analysis. Analysis of Means (*ANOM*) is a statistical approach that serves to determine the mean

S/N ratios for each factor and each of its levels. There are three categories of *S/N* ratios, *the smaller the better*, *the bigger the better* and *nominally the best* [13, 15, 16].

The procedure for planning experiments is based on a statistical approach and involves several activities: (a) identifying and formulating problems, (b) selecting dependent (output) variables (c) selecting independent (input) variables as well as levels and ranges of intervals, (d) choosing an experiment plan, (e) conducting experiments, (f) statistical processing and analysis of experimental data, (h) conclusions and recommendations.

3. EXPERIMENTAL RESEARCH

The main optimization task is to define the influence of input parameters: wall thickness (*a*), number of revolutions (*n*), feed ratio (*f*), depth of cut (*δ*) and tool path - TPS (*Tool Path Strategy*), on the surface roughness (*Ra*), Figure 1. Material of thin-walled parts is aluminum alloy Al7075 (AlZnMgCu 1.5). For the machining process, a tool manufactured by YG, No. E5909080 [17] was chosen. Diameter of end mill is 8 mm and consist of two cutting edges. The machine is a high-speed five-axis CNC machining center for milling - DIGMA HSC 850. For purpose of generated numerical control programs is used software Cimatron 11, where they were used machining strategies *climb*, *convencional* and *mixed*.

Assuming that the mathematical relations between input parameters and process performance are complex and nonlinear, three levels of variation were selected for each of the five input parameters, Table 1. Based on selected variable process factors and corresponding levels of variation, an experimental matrix plan was created in accordance with the standard Taguchi orthogonal sequence L27. As stated in the research plan, the surface roughness was measured in 4 places, directed to the direction of tool movement, Table 2. Since it is a linear part, it is divided into left and right sides, so that the roughness of the left side of the horizontal and vertical surfaces of Ra_{LH} and Ra_{LV} , as well as the right sides of Ra_{RH} and Ra_{RV} , is measured. Roughness measurement was carried out using the Mitutoyo SJ-301 device.

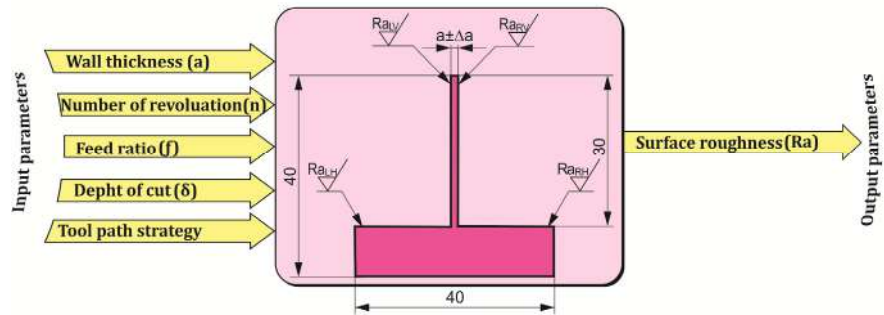


Fig 1 Model of experimental research [1, 6]

Table 1. Input parameters and levels of variations


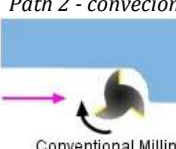

Parameter and label	Units	Level		
Wall tickness (<i>a</i>)	mm	0,5	1,0	1,5
Number of revolutions (<i>n</i>)	o/min	6000	12000	24000
Feed ratio (<i>f</i>)	mm/min	600	1200	2400
Depth of cut (<i>δ</i>)	mm	1	2	3
Tool Path Strategy (TPS) - Cimatron	-	<div style="display: flex; justify-content: space-around; align-items: center;"> <div style="text-align: center;">  <p>Path 1 - climb Climb Milling</p> </div> <div style="text-align: center;">  <p>Path 2 - convecional Conventional Milling</p> </div> <div style="text-align: center;">  <p>Path 3 - mixed Mixed Milling</p> </div> </div>		

Table 2. Meassuring results of surface roughness - Ra

Exp. no	A	B	C	D	E	Ra _{vl}	Ra _{vd}	Ra _{hl}	Ra _{hd}	Ravsr= (Rav _l +Rav _d)/2	Rahsr= (Rah _l +Rah _d)/2	Rasr= (Ravsr+Rahsr)/2
1	0,5	6000	600	1	1	0,28	0,23	0,26	0,23	0,255	0,245	0,250
2	0,5	6000	1200	2	2	1,73	2,97	0,23	0,31	2,350	0,270	1,310
3	0,5	6000	2400	3	3	0,67	1,4	0,69	0,56	1,035	0,625	0,830
4	0,5	12000	600	2	3	0,57	1,45	0,81	0,54	1,010	0,675	0,843
5	0,5	12000	1200	3	1	0,52	0,54	0,15	0,14	0,530	0,145	0,338
6	0,5	12000	2400	1	2	1,35	1,41	0,36	0,32	1,380	0,340	0,860
7	0,5	24000	600	3	2	0,88	0,42	0,22	0,12	0,650	0,170	0,410
8	0,5	24000	1200	1	3	0,84	0,27	0,21	0,26	0,555	0,235	0,395
9	0,5	24000	2400	2	1	0,32	0,23	0,36	0,26	0,275	0,310	0,293
10	1,0	6000	600	2	2	2,56	2,94	0,36	0,27	2,750	0,315	1,533
11	1,0	6000	1200	3	3	0,2	0,21	1,68	0,23	0,205	0,955	0,580
12	1,0	6000	2400	1	1	0,56	0,29	0,54	0,65	0,425	0,595	0,510
13	1,0	12000	600	3	1	0,13	0,16	0,11	0,15	0,145	0,130	0,138
14	1,0	12000	1200	1	2	0,89	1,2	0,28	0,16	1,045	0,220	0,633
15	1,0	12000	2400	2	3	0,38	0,3	0,61	2,73	0,340	1,670	1,005
16	1,0	24000	600	1	3	0,34	0,15	0,11	0,14	0,245	0,125	0,185
17	1,0	24000	1200	2	1	0,3	0,15	0,15	0,17	0,225	0,160	0,193
18	1,0	24000	2400	3	2	0,6	0,25	0,17	0,2	0,425	0,185	0,305
19	1,5	6000	600	3	3	0,61	0,16	0,13	0,13	0,385	0,130	0,258
20	1,5	6000	1200	1	1	0,66	0,22	0,36	0,29	0,440	0,325	0,383
21	1,5	6000	2400	2	2	3,27	2,22	1,35	1,08	2,745	1,215	1,980
22	1,5	12000	600	1	2	2,05	1,92	0,3	0,37	1,985	0,335	1,160
23	1,5	12000	1200	2	3	2,93	1,39	0,45	0,54	2,160	0,495	1,328
24	1,5	12000	2400	3	1	0,39	0,7	0,28	0,26	0,545	0,270	0,408
25	1,5	24000	600	2	1	0,16	0,11	0,21	0,12	0,135	0,165	0,150
26	1,5	24000	1200	3	2	0,45	0,3	0,13	0,21	0,375	0,170	0,273
27	1,5	24000	2400	1	3	1,36	0,22	0,27	0,17	0,790	0,220	0,505

4. OPTIMIZATION OF MACHINING PARAMETERS IN THE FUNCTION OF SURFACE ROUGHNESS

In the analysis of the obtained surface roughness following factors are observed wall tickness (A), number of revulation (B), feed ratio(C), depth of cut (D) and tool path strategy (E). Since the goal is to make the surface roughness as low as possible, *Smaller is better*) was chosen.

The S/N values for each factor are shown in Table 3. The mean S/N response for each influential factor is shown in Table 4.

Figure 2 shows the S/N response for the surface roughness by influence factors, while Figure 3 shows the response of the medium arithmetic surface roughness of influence factors.

Table 3. S/N response for surface roughness

Level	A	B	C	D	E
1	5,560	3,598	8,492	6,544	11,352
2	7,480	4,161	6,151	3,163	2,374
3	5,772	11,053	4,169	9,106	5,086
Difference	1,921	7,455	4,323	5,943	8,978
Rank	5	2	4	3	1

Table 4. Response of surface roughness by influencing factors

Level	A	B	C	D	E
1	0,6142	0,8481	0,5472	0,5422	0,2956
2	0,5644	0,7456	0,6033	0,9592	0,9403
3	0,7158	0,3008	0,7439	0,3931	0,6586
Difference	0,1514	0,5472	0,1967	0,5661	0,6447
Rank	5	3	4	2	1

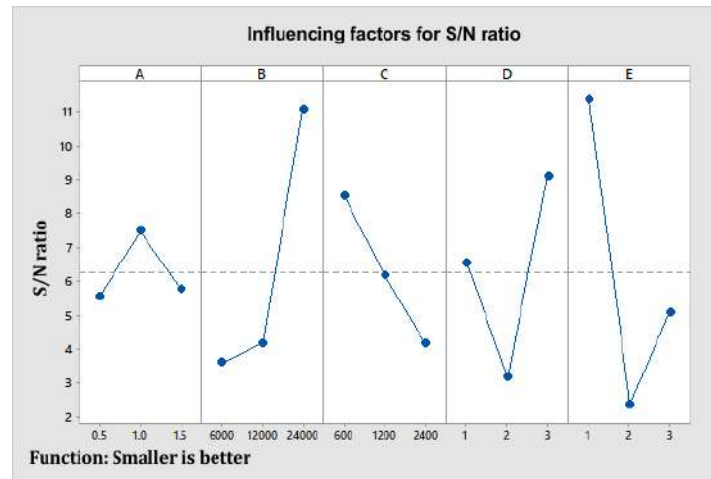


Fig. 2. S/N response for surface roughness

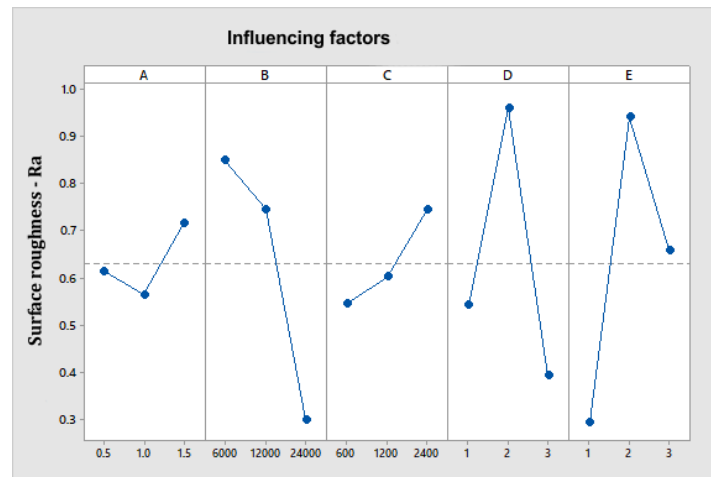


Fig. 3. Response of surface roughness by influencing factors

By analyzing the results, which are presented in Table 3 and Figure 2, it can be concluded that the greatest impact on the surface roughness has the tool path strategy, the number of revolutions and the depth of cut.

Based on Table 4 and Figure 3, the optimal input parameters within the offered factor levels can be determined, based on the goal function "the lower the value the better".

The results of the ANOVA analysis show that of the five inputs, *f*-values of factors related to number of revolutions, depth of cut and tool path strategies are greater than the critical value of *F*_{cr} (*F*_{cr} = 3.35, for a confidence level of 95%), implying that these factors are significant compared to the error factor and have a significant impact on the responsive surfaces. While on the other hand wall thickness and feed ratio do not have a significant impact because their *F*-values are less than the critical *F*_{cr} value. The use of percentage share (%*P*) in ANOVA analysis is an auxiliary solution for quantitative evaluation of impact factors on responsive surfaces. Wall thickness affects with 1.80%, the number of revolutions affects with 25.51%, feed ratio affects with 3.09%, the depth of cut affects with 25.95%, and the greatest impact on the surface roughness a tool path strategy with 31.49%. The error of the experiment is 12.51%, that is, the influence of other factors that were not considered in this experiment.

After defining optimal input parameters, optimal responses are predicted using Taguchi and ANOVA methods. The prediction of optimum input parameters in order to obtain the least surface roughness applied by Taguchi's method was found at the following level: A2-B3-C1-D3-E1.

Figure 4 shows Taguchi's predictive results for optimal input parameters using MiniTab software. After finding the optimal input parameters of the obtained S/N response, the dependence of the input factors on the surface roughness *Ra* was obtained.

Using regression analysis, a regression equation (1) was obtained for a linear model of input factor.

$$Ra = 0,6315 - 0,0173 A_{0,5} - 0,0670 A_{1,0} + 0,0844 A_{1,5} + 0,2166 B_{6000} + 0,1141 B_{12000} - 0,3306 B_{24000} - 0,0843 C_{600} - 0,0281 C_{1200} + 0,1124 C_{2400} - 0,0893 D_1 + 0,3277 D_2 - 0,2384 D_3 - 0,3359 E_1 + 0,3088 E_2 + 0,0271 E_3 \quad (1)$$

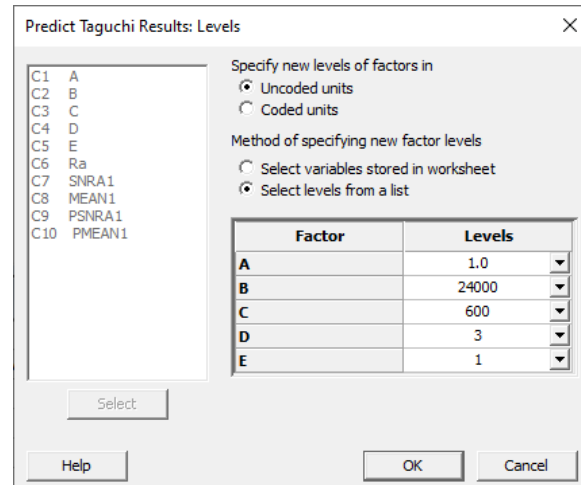


Fig. 4. Taguchi predictive results for optimal input parameters

Table 5 shows the optimal input parameters, significant parameters as well as the prediction of the optimal response of the target function.

Table 5. Output results of analysis and optimization

Response	Optimal Input parameters	Significant parameters	Prediction of optimal response	
			S/N Response	Value
<i>Ra</i>	A2-B3-C1-D3-E1	B-D-E	22,4003	0,0183

5. CONCLUSION

Based on the obtained results of the experiments, ANOVA analysis, regression analysis and finally optimization of the parameters of high-speed machining process of thin-walled linear parts made of alloy AL 7075 was performed. The paper implemented a one-criterion optimization of the criterion of surface roughness depending on the input factors, wall thickness, number of revolutions, feed ratio, depth of cut tool path strategies.

The analysis of the results concluded that the greatest impact on the surface roughness has the tool path strategy, depth of cut and the number of revolutions, and the smallest impact has wall thickness.

The tool path strategy has the greatest impact on the surface roughness, because the tool, depending on the path or the tool-contour movement, leaves a trace, while the wall thickness at lower machining cutting conditions does not affect because the vibration smaller.

Acknowledgement

This paper is part of a study in the project "Collaborative systems in the digital industrial environment" No. 142-451- 3178/2022-01/01, supported by the Provincial Secretariat for Higher Education and Scientific Research of the Autonomous Province of Vojvodina and project "Innovative scientific and artistic research from the FTS domain", No. 451-03-47/2023-01/200156, supported by the Ministry of Science, Technological Development and Innovation of the Republic of Serbia.

REFERENCES

- [1] Lukic, D.; Cep, R.; Vukman, J.; Antic, A.; Djurdjev, M.; Milosevic, M. (2020). Multi-Criteria Selection of the Optimal Parameters for High-Speed Machining of Aluminum Alloy Al7075 Thin-Walled Parts. *Metals*, Vol. 10, No. 12, 1570. <https://doi.org/10.3390/met10121570>
- [2] Hirsch, J., Al-Samman, T. (2013). Superior light metals by texture engineering: Optimized aluminum and magnesium alloys for automotive applications. *Acta Materialia*, Vol. 61, No. 3, p. 818-843. <https://doi.org/10.1016/j.actamat.2012.10.044>
- [3] Scippa, A., Grossi, N., Campatelli, G. (2014). FEM based cutting velocity selection for thin walled part machining. *Procedia CIRP*, Vol. 14, p. 287–292. [DOI:10.1016/j.procir.2014.03.023](https://doi.org/10.1016/j.procir.2014.03.023)
- [4] Huang, X., Sun, J., Li, J. (2015). Effect of initial residual stress and machining-induced residual stress on the deformation of aluminium alloy plate. *Strojniški vestnik - Journal of Mechanical Engineering*, Vol. 61, No. 2, p. 131-137. [DOI:10.5545/sv-jme.2014.1897](https://doi.org/10.5545/sv-jme.2014.1897)
- [5] Izamshah, R., Mo, J.P.T., Ding, S. (2011). Hybrid deflection prediction on machining thin-wall monolithic aerospace components. *Proceedings of the Institution of Mechanical Engineers, Part B: Journal of Engineering Manufacture*, vol. 226, no. 4, p. 592-605. [DOI:10.1177/0954405411425443](https://doi.org/10.1177/0954405411425443).
- [6] Vukman, J. (2022) *Optimization technological process of machining thin-walled aluminium structures* (In Serbian). PhD thesis. Faculty of Technical Sciences, University of Novi Sad.
- [7] Borojevic, S.; Lukic, D.; Milošević, M.; Vukman, J.; Kramar, D. (2018). Optimization of Process Parameters for Machining of Al 7075 Thin—Walled Structures. *Adv. Prod. Manag.*, Vol.13, p. 125–135. [DOI.org/10.14743/apem2018.2.278](https://doi.org/10.14743/apem2018.2.278)
- [8] Popma, M. (2010). *Computer aided process planning for high-speed milling of thin walled parts*, PhD. Thesis. University of Twente, Netherlands.
- [9] Zhang, D., Gao, K., Zhou, T. (2015) Discussion on NC machining process of thin walled parts technical measures, *Applied Mechanics and Materials*, Trans Tech Publications, Switzerland, Vol. 701-702, p. 864-868. <https://doi.org/10.4028/www.scientific.net/AMM.701-702.864>
- [10] Bolar, G.: *Numerical and Experimental Studies on Thin-Wall Machining of Aerospace Grade Aluminum Alloy*. PhD thesis. Indian Institute of Technology Guwahati, 2017.
- [11] Dean, A., Voss, D., Draguljić, D.: *Design and analysis of experiments* (Vol. 2). New York: Springer, 2017.
- [12] Deresse, N. C., Deshpande, V., Taifa, I. W. (2020). Experimental investigation of the effects of process parameters on material removal rate using Taguchi method in external cylindrical grinding operation. *Engineering Science and Technology, an International Journal*, Vol. 23, No.2, p. 405-420. <https://doi.org/10.1016/j.jestch.2019.06.001>
- [13] Taguchi, G., Chowdhury, S., Wu, Y. (2005). *Taguchi's Quality Engineering Handbook*, John Wiley & Sons, Inc.
- [14] Athreya, S., Venkatesh, Y.D. (2012). Application Of Taguchi Method For Optimization Of Process Parameters In Improving The Surface Roughness Of Lathe Facing Operation, *International Refereed Journal of Engineering and Science (IRJES)*, Vol. 1, No. 3, p. 13-19.
- [15] Montgomery, D.C. (2001). *Design and Analysis of Experiments*, John Wiley & Sons, Inc., 2001.
- [16] Dean, A., Voss, D., Draguljić, D. (2017). Response surface methodology. In *Design and analysis of experiments*, p. 565-614, 2017. https://doi.org/10.1007/978-3-319-52250-0_16
- [17] [ALU-pow \(140513 \) \(yg-1.pl\)](#) available at 18.04.2023.



Banja Luka
1–2 Jun 2023.

DEMI 2023

16th International Conference on Accomplishments in Mechanical and Industrial Engineering

www.demi.mf.unibl.org



Optimization of surface roughness and its variance in CO₂ laser cutting using desirability function approach

V. Marinković, M. Madić, P. Janković

Faculty of Mechanical Engineering in Niš, University of Niš, Aleksandra Medvedeva 14, 18000 Niš, Serbia

Abstract *In practice, there is often a need for multi-response optimization of laser cutting process with respect to different performance characteristics. The present research is focused on optimization of cutting conditions, in terms of severance energy and assist gas flow, in CO₂ laser cutting of stainless steel AISI 316L for simultaneous optimization of resulting surface roughness and its variance. For this aim 3² factorial experimental design was realized. The obtained experimental data were used for the development of nonlinear mathematical models which were used as responses in the formulation of multi-response laser cutting optimization model. For multi-response optimization a desirability function approach (DFA) was applied to obtain a robust solution for considered performance characteristics. The optimization results meet the required conditions and are quite acceptable for practical needs.*

Keywords *CO₂ laser cutting, multi-response optimization, DFA, stainless steel 316L*

1. INTRODUCTION

Laser cutting technology is one of the first industrial applications of lasers and is currently one of the most widely used non-conventional technologies in the manufacturing industry [1]. Currently, CO₂, fiber, disk and Nd:YAG lasers are predominantly used for metal cutting, ranging from 0.5–30 mm in thickness, as these laser cutting machines provide the most cost effective solution.

Compared to other technologies, there are a number of advantages including ability to cut complex geometries with tight tolerances, high material removal rate, low operational costs, localized heat affected zone, good verticality of the cut, high surface quality, ease of automation and programming, etc.

As many other manufacturing technologies, the laser cutting itself is a very complex technology, influenced by a number of parameters. By altering just some of the most important parameters, such as laser power, cutting speed,

type, pressure and purity of the assist gas, focus position, stand-off distance, etc., multiple and interdependent physical processes, such as beam absorption, the fluid dynamics of the assist gas and cut front characteristics are affected, which ultimately define a number of output process performances [2].

Commonly, efficacy and suitability of laser cutting technology for cutting certain sheet materials is assessed with respect to a number of cut quality characteristics, such as kerf width [3], kerf taper angle [4], surface roughness [5], burr formation [6], heat affected zone [7], productivity [2], costs [8], processing efficiency [9] or environmental issues [10].

Considering a number of output performances of the laser cutting process, as well as customer needs in terms of satisfying multiple requirements, there is often a need for multi-response optimization of laser cutting process. Formulation and solving of such multi-response problems (models) is especially justified when

it comes to serial production and when quality non-conformances can be expensive.

In the open literature and manufacturing practice one can identify three main approaches for determining the laser cutting conditions with respect to several goals, i.e., conflicting responses, including: (1) modelless approach based on integration of Taguchi method with grey relational analysis, principal component analysis, grey-fuzzy methodology, (2) application of multiple-criteria decision-making (MCDM) methods, and (3) desirability function approach (DFA) for formulation and solving multi-response optimization models.

DFA represents, unlike the other two approaches, higher level approach enabling continuous optimization of process parameters with possibility to handle a number of objective functions and functional constraints. Previously DFA was applied for optimization of CO₂ laser cutting of aluminium metal matrix composites with respect to kerf deviation and surface roughness [11], CO₂ laser cutting of aluminium alloy sheet with respect to kerf taper and surface roughness [12], Nd: YAG laser cutting of titanium superalloy sheet with respect to kerf deviation and material removal rate [13], CO₂ laser cutting of plywood materials with respect to different kerf geometry characteristics and operational costs [14] and fiber laser cutting of aluminium alloy sheet with respect to cut quality and operational costs [15].

The goal of the present study is the optimization of surface roughness and its variance in CO₂ laser cutting of AISI 316 stainless steel using DFA.

2. DESIRABILITY FUNCTION APPROACH

The desirability function approach (DFA) is one of the most widely used methodologies in industry for solving the multi-response optimization problems.

That is an attractive, well-established, flexible, easy to implement approach, and, as such, quite acceptable to many researchers and practitioners.

The application of the DFA is not limited to any specific optimization problem.

In the first stage in applying the DFA, it is necessary to define the individual desirability function. Several DFs have been proposed over time with the aim of improving the performance of DFA [16-19].

Among them, a continuous, non-linear, and differentiable on entire domain DF was defined as [19]:

$$d_j(\psi_j) = \begin{cases} (1 - \psi_j^2)^{r_j} & \text{for } -1 \leq \psi_j \leq 1 \\ 0 & \text{otherwise} \end{cases} \quad (1)$$

where $\psi_j = f(\hat{y}_j(\mathbf{x}))$ is the dimensionless converting function ($j=1, 2, \dots, m$), $\hat{y}_j(\mathbf{x})$ is the j -th estimated response function, \mathbf{x} is the vector of the input variables (process parameters), r_j is the user-specified shape parameter ($r_j > 0$).

Each individual DF is defined according to the particular response. For instance, for the smaller-the-better (STB) type response (used in this paper) the individual DF is expressed as follows:

$$d_j = (1 - \psi_j^2)^{r_j} = \left\{ 1 - \left[\frac{\hat{y}_j(\mathbf{x}) - y_j^{\min}}{y_j^{\max} - y_j^{\min}} \right]^2 \right\}^{r_j} \quad (2)$$

where y_j^{\min} and y_j^{\max} are the lower and upper bound on the j -th response, respectively.

For more details about the aforementioned DF, the readers are referred to the papers [19, 20].

The composite or overall desirability is most often defined as the geometric mean of the individual DFs:

$$D(\mathbf{y}) = \left[\prod_{j=1}^m d_j(\hat{y}_j) \right]^{\frac{1}{m}} ; \quad (0 < D < 1) \quad (3)$$

where m is the number of responses.

3. EXPERIMENTAL WORK

3.1. Experimental details

The laser cutting experiment was realized using a Prima Industry 3D CO₂ laser cutting machine with maximum power output of 4 kW. The experimental units were cut from sheet with thickness of 2 mm made of AISI 316L stainless steel.

Necessary empirical models for prediction of surface roughness and its variance were developed upon realization of 3² factorial design. Two process parameters were varied at three levels (Table 1). In the experiment,

experimental trials were replicated twice. Other technical parameters were kept constant throughout the entire experiment.

Table 1. Process parameters used in the experiment

Parameters	Level 1	Level 2	Level 3
Severance energy E_s (J/mm ²)	16	32	48
Assist gas flow Q_a (m ³ /h)	10.17	12.02	13.87

The experimental space was selected according to pilot experiments and industrial recommendations with respect to type and thickness of sheet metal.

The levels of variation of severance energy were defined by using constant laser power of 3.2 kW and three levels of cutting speed (2, 3 and 6 m/min). Similarly, the levels of variation of assist gas flow were defined by using constant nozzle diameter of 1.5 mm and three levels of assist gas pressure (10, 12 and 14 bar).

Application of this design allows for systematical analysis of the effects of selected process variables and development of non-linear prediction models of considered process performances by performing nine experimental trials with unique combinations of process variable values.

The lens with a focal length of 190.5 mm was used to focus the laser beam to the lower part of the sheet. The stand-off distance was kept constant at 0.7 mm. Nitrogen 5.0 (Istrabenz Plini) was coaxially supplied using the conical shape nozzle. The laser system generated the fundamental-mode Gaussian beam (TEM₀₀) and was operated in continuous wave mode.

After physical realization of the experiment the cut specimens were measured in order to assess surface roughness in terms of arithmetic mean deviation of the profile (R_a) and its variation. To this aim Marsurf XR 1 surface roughness tester was used to measure the R_a values in three equally spaced places along the middle of the cut for each specimen.

3.2. Pre-processing of experimental data

Due to the replication in each trial, the mathematical model, i.e., regression equation not only for the sample mean but also for the sample standard deviation of the quality characteristic (surface roughness) can be fitted.

The third-order (cubic) mathematical model was utilized to find an appropriate approximation for the functional relationship between process parameters and the response for both responses independently, as follows:

$$\begin{aligned} \hat{y}_\mu = & 1.1731 - 0.3180x_1 + 0.0177x_2 + 0.4970x_1^2 \\ & - 0.1272x_2^2 + 0.1537x_1x_2 - 0.2282x_1^2x_2 + \\ & 0.0595x_2^2x_1 \quad (R=0.976) \end{aligned} \quad (4)$$

$$\begin{aligned} \hat{y}_\sigma = & 0.0599 + 0.0014x_1 - 0.0004x_2 + 0.00638x_1^2 \\ & - 0.0426x_2^2 + 0.0180x_1x_2 - 0.0354x_1^2x_2 - \\ & 0.0396x_2^2x_1 \quad (R=0.878) \end{aligned} \quad (5)$$

Note that the subscripts μ and σ in Eqs. (4) and (5) represent the sample mean and sample standard deviation, respectively. As usually, in these equations the process parameters (design factors) are marked with the symbol "x".

The R values are relatively high, indicating a good correlation between the predicted and the actual data.

The higher-order polynomial models were chosen because the models should be fitted reasonably well. Namely, some researchers have been shown that these models may be more effective in finding the better solutions than the commonly-used second-order model or other existing lower-order models [21, 22]. In general, the response modeling can have strong impact on the optimization results [23].

According to the manufacturing industry practice, it is reasonable to prescribe allowable bounds on the mean and standard deviation. In the absence of *a priori* preference from decision maker (DM), the experimental results may be applied for these purposes.

In this work, the experimental data indicate that the observed responses lie in the intervals: $y_\mu \in [1.0355, 2.1190]$ (μm); $y_\sigma \in [0.0092, 0.1570]$ (μm). The adopted bounds (specification limits) for both responses are listed in Table 2.

It is worthwhile to note that y_σ^{\min} is typically set equal to zero. However, if DM does not care about the process variability up to a certain level, y_σ^{\min} may be prescribed some acceptable positive value.

Table 2. Type of responses and their specifications

Response	Type	$y_j^{\min} = T_j$	y_j^{\max}
1. y_{μ}	STB	1.0	2.0
2. y_{σ}	STB	0	0.15

Note: T_j ($j=1, 2$) are the target values

4. OPTIMIZATION METHODS

There are different deterministic or stochastic (meta-heuristic) optimization methods with distinct characteristics and algorithms which are used to solve non-linear single- and multi-response optimization problems.

The direct search (DS) methods, known as so-called derivate-free search techniques, are popular, because they are simple, flexible, and easy to understand and implement.

Nowadays, the non-traditional meta-heuristic search methods for global optimization, such as genetic algorithm, simulated annealing, particle swarm algorithm, teaching-learning-based optimization method, gray wolf optimizer, and many others are also very popular among the researchers and practitioners.

However, it is commonly known that there is no single universal optimization method suitable for each particular real-life problem.

4.1. Single-response optimization

In the single-response optimization approach, the basic idea is to minimize (or maximize) the mean value (location) of the quality characteristic (response) being investigated. In this work, Eq. (4) is used for predicting the surface roughness, as the only target for the optimization procedure.

In this work, the Pattern search (PS) from the family of DS methods was chosen and implemented in the final stage of the optimization procedure. It has been found that the PS algorithm has good competitive potential in solving many machining optimization problems in comparison with some other search approaches such as meta-heuristic algorithms [24].

In this case, the optimal solution is obtained by minimizing the surface roughness function. Table 3 shows the outcome of applying the PS algorithm.

Table 3. Optimal solution by ignoring variance

Method	x_1	x_2	y_{μ}	y_{σ}
Single-optim. (PS)	0.2919	-0.8784	1.0000	0.0223

A subsequent check revealed that the Nelder-Mead simplex algorithm yielded the same solution.

It should be noted that some efficient gradient-based optimization methods can be used instead of the direct search techniques, because the surface roughness function in the example under consideration is continuous and differentiable function.

4.2. Dual-response optimization

Unlike the traditional engineering practice, which is mostly focused on the mean of a given quality characteristic (response), the dual-response approach also considers its variability. In other words, the dual-response approach builds two mathematical models, namely, one for the mean and one for the standard deviation.

The process variance (or standard deviation) $y_{\sigma}(\mathbf{x})$ was not considered in the single-response optimization procedure, but was estimated *a posteriori* by including the optimal input variables (process parameters) \mathbf{x}^* into the standard deviation function.

If the DM is concerned only with the mean of the response $y_{\mu}(\mathbf{x})$, ignoring its variability, generally, there is no guarantee that the yielding $\hat{y}_{\mu}(\mathbf{x}^*)$ would be an acceptable solution. Namely, the assumption of homogeneous variance is not, as a rule, valid in real application. Such a problem arises in many examples in industrial practice, which requires simultaneously achieving the target response value and keeping its variance small.

The dual-response optimization approach, as a specific case of the multi-response optimization method, explicitly considers both the location and dispersion effect of the target response within the continuous feasible experimental region and optimizes them simultaneously.

From the point of view of optimization, the optimal values of both functions must lie within the prespecified limits. In this case, because the response y_{μ} and y_{σ} are STB -type responses, the DM does not accept an optimal solution \mathbf{x}^*

for which $\hat{y}_\mu < y_\mu^{\min}$ nor $\hat{y}_\mu > y_\mu^{\max}$, also for which $\hat{y}_\sigma < y_\sigma^{\min}$ nor $\hat{y}_\sigma > y_\sigma^{\max}$.

Strictly speaking, the first condition for STB-type responses does not have to be taken as a lower specification limit in the optimization procedure, but this issue is out of the scope of this investigation.

By using Eq. (2), with data from Table 2, the following individual DFs were obtained:

$$d_\mu = \left\{ 1 - \left[\frac{\hat{y}_\mu(\mathbf{x}) - 1.0}{1.0} \right]^2 \right\}^{2.5} \quad (6)$$

$$d_\sigma = \left\{ 1 - \left[\frac{\hat{y}_\sigma(\mathbf{x}) - 0}{0.15} \right]^2 \right\}^{2.5} \quad (7)$$

In Eqs. (6) and (7), the adjustable shape parameter is chosen to be equal to 2.5, which is its "default" value [20].

The overall desirability for two responses is calculated using a simple formula:

$$D(\mathbf{y}) = (d_\mu d_\sigma)^{0.5} = \sqrt{d_\mu d_\sigma} \quad (8)$$

In this example, by using the dual-response optimization procedure and DF the optimization problem can be stated as:

$$\begin{aligned} & \text{Maximize } D[d(\mathbf{y})] \\ & \text{subject to } 1.0 \leq y_\mu \leq 2.0 \\ & \quad 0 \leq y_\sigma \leq 0.15 \\ & \quad -1.0 \leq x_i \leq 1.0, \quad i=1,2 \end{aligned} \quad (9)$$

Table 4 shows the outcome of applying the dual-response optimization method.

Table 4. Optimal solution by considering variance

Method	x ₁	x ₂	y _μ	y _σ
Dual-optim. (DFA)	0.0796	-1.0000	1.0000	0.0139

Apparently, the predicted response values lie within the bounds given in Table 2. Figure 2 shows a response surface and contour plot of the overall desirability function D . The graphic presentation may be helpful for a better understanding of the problem at hand. In this case, the experimenter can visually verify the resulting solution.

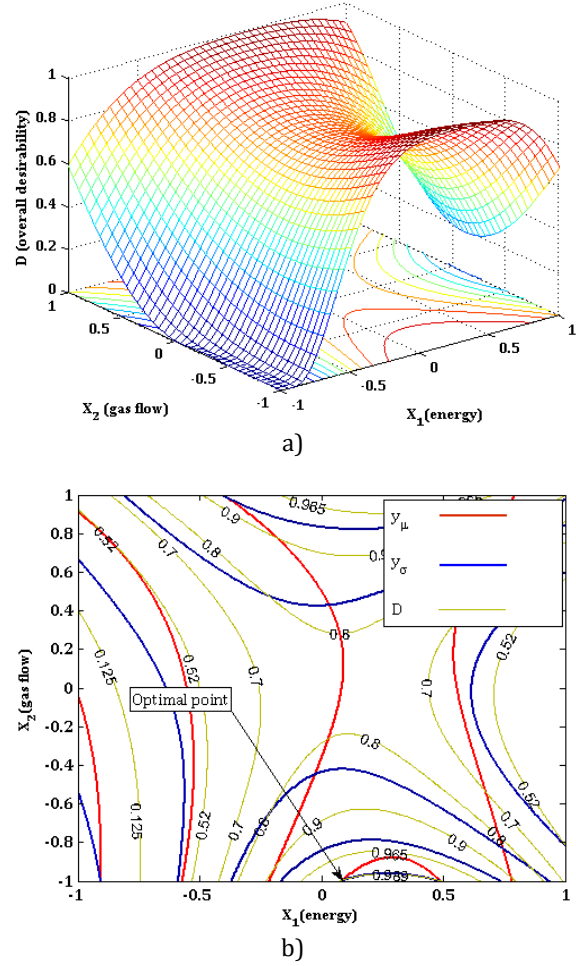


Fig. 2. Presentation of overall desirability $D=f(x_1, x_2)$: a) response surface plot; b) overlaid contour plot

5. RESULTS AND DISCUSSION

As can be seen from Tables 3 and 4 the predicted surface roughness value is identical to the target value.

Albeit in single-response optimization procedure the target value was reached, the standard deviation was relatively high. On the contrary, the obtained standard deviation, after optimizing by means of the dual-response optimization procedure, it was considerably improved. This result once more highlights the importance of including the variability of the available data set in the optimization procedure. It is worth mentioning that, in general, a potentially better optimal solution may be achieved by altering the shape parameters in Eqs. (6) and (7) [25], because DF has the inherent flexibility that allows the researchers to find an improved solution.

However, due to the high value of overall desirability in this example ($D^* = 0.989$), it is very likely that no improved result would be found.

It may be expected that laser cutting using lower severance energies will result in reduced heat input in terms of HAZ and recast layer given that severance energy determines the energy input per unit length. In addition, since processing cost is the function of assist gas flow, the use of lower assist gas flow is economically justified, particularly in the case of high-pressure nitrogen fusion laser cutting.

6. CONCLUSION

In this study, the single-response and dual-response optimization approaches in CO₂ laser cutting of AISI 316 stainless steel are presented and compared. The research was focused on determining the optimal laser cutting parameters in order to obtain the desired quality of processing surface.

The obtained results showed the effectiveness of using the dual-response optimization approach in considering the real-world engineering problems. This procedure provides noticeably better estimation of process variability than the single-optimization method. By solving this case study it was shown that it is possible to obtain the same target value of surface roughness and reduce its variance by about 60% by a combination of laser cutting parameter values that are more justified from the aspect of ensuring cut quality and cutting costs.

The only disadvantage of the dual-response optimization approach is higher experimental costs, because this approach requires the repetition of trials through the entire experiment in order to define the standard deviation model. It is hoped that this deficiency can be compensated by a gain on the other side, because this approach provides a valid, reliable and robust solution with a good balance among the responses, i. e. among the location effect and the dispersion effect.

Acknowledgement

This research was financially supported by the Ministry of Science, Technological Development and Innovation of the Republic of Serbia (Contract No. 451-03-47/2023-01/200109)

REFERENCES

- [1] Riveiro, A., Quintero, F., Boutinguiza, M., Del Val, J., Comesaña, R., Lusquiños, F., Pou, J. (2019). Laser cutting: A review on the influence of assist gas. *Materials*, vol. 12, no. 1, 157. DOI: [10.3390/ma12010157](https://doi.org/10.3390/ma12010157)
- [2] Madić, M., Mladenović, S., Gostimirović, M., Radovanović, M., Janković, P. (2020). Laser cutting optimization model with constraints: Maximization of material removal rate in CO₂ laser cutting of mild steel. *Proceedings of the Institution of Mechanical Engineers, Part B: Journal of Engineering Manufacture*, vol. 234, no. 10, p. 1323-1332. DOI: [10.1177/0954405420911529](https://doi.org/10.1177/0954405420911529)
- [3] Olaru, S.C., Coteață, M., Nagîț, G., Hrițuc, A., Dodun, O., Slătineanu, L. Analysis of laser cut slots on different thickness steel plates. *24th International Conference on Material Forming ESAFORM 2021*. 14th -16th April 2021, Liège, Belgique, p. 2681/1 - 2681/8. DOI: [10.25518/esaform21.2681](https://doi.org/10.25518/esaform21.2681)
- [4] Fountas, N.A., Ninikas, K., Chaidas, D., Kechagias, J., Vaxevanidis, N.M. (2022). Neural networks for predicting kerf characteristics of CO₂ laser-machined FFF PLA/WF plates. *MATEC Web of Conferences* (Vol. 368, p. 01010). EDP Sciences. DOI: [10.1051/mateconf/202236801010](https://doi.org/10.1051/mateconf/202236801010)
- [5] Turkkan, Y. A., Aslan, M., Tarkan, A., Aslan, Ö., Yuce, C., Yavuz, N. (2023). Multi-objective optimization of fiber laser cutting of stainless-steel plates using Taguchi-based grey relational analysis. *Metals*, vol. 13, no. 1, 132. DOI: [10.3390/met13010132](https://doi.org/10.3390/met13010132)
- [6] Duspara, M., Matysiak, W., Vidaković, I., Sedmak, S. (2022). Optimization of nitrogen use efficiency in cutting of austenitic stainless steel by a fiber laser. *FME Transactions*, vol. 50, no. 4, p. 745-751. DOI: [10.5937/fme2204745D](https://doi.org/10.5937/fme2204745D)
- [7] Tahir, A.F.M., Aqida, S.N. (2017). An investigation of laser cutting quality of 22MnB5 ultra high strength steel using response surface methodology. *Optics and Laser Technology*, vol. 92, p. 142-149. DOI: [10.1016/j.optlastec.2017.01.005](https://doi.org/10.1016/j.optlastec.2017.01.005)
- [8] Guarino, S., Ponticelli, G.S., Venettacci, S. (2020). Environmental assessment of selective laser melting compared with laser cutting of 316L stainless steel: a case study for flat washers' production. *CIRP Journal of Manufacturing Science and Technology*, vol. 31, p. 525-538. DOI: [10.1016/j.cirpj.2020.08.004](https://doi.org/10.1016/j.cirpj.2020.08.004)
- [9] Girdu, C.C., Gheorghe, C. (2022). Simulation of Melting Efficiency in Laser Cutting of Hardox

- 400 Steel. *Materials*, vol. 15, no. 20, 7192. DOI: [10.3390/ma15207192](https://doi.org/10.3390/ma15207192)
- [10] Yilbas, B.S., Shaukat, M.M., Ashraf, F. (2017). Laser cutting of various materials: kerf width size analysis and life cycle assessment of cutting process. *Optics and Laser Technology*, vol. 93, p. 67-73. DOI: [10.1016/j.optlastec.2017.02.014](https://doi.org/10.1016/j.optlastec.2017.02.014)
- [11] Sharma, V., Kumar, V. (2016). Multi-objective optimization of laser curve cutting of aluminium metal matrix composites using desirability function approach. *Journal of the Brazilian Society of Mechanical Sciences and Engineering*, vol. 38, p. 1221-1238. DOI: [10.1007/s40430-016-0487-9](https://doi.org/10.1007/s40430-016-0487-9)
- [12] Yaka, H. (2022). Multiple optimization of cutting parameters affecting kerf formation and surface roughness in laser cutting of Al 5052 alloy. *El-Cezeri Journal of Science and Engineering*, vol. 9, no. 1, p. 220-231. DOI: [10.31202/ecjse.958728](https://doi.org/10.31202/ecjse.958728)
- [13] Tamilarasan, A., Rajamani, D. (2017). Multi-response optimization of Nd: YAG laser cutting parameters of Ti-6Al-4V superalloy sheet. *Journal of Mechanical Science and Technology*, vol. 31, p. 813-821. DOI: [10.1007/s12206-017-0133-1](https://doi.org/10.1007/s12206-017-0133-1)
- [14] Eltawahni, H.A., Rossini, N.S., Dassisti, M., Alrashed, K., Aldaham, T.A., Benyounis, K.Y., Olabi, A.G. (2013). Evaluation and optimization of laser cutting parameters for plywood materials. *Optics and Lasers in Engineering*, vol. 51, no. 9, p. 1029-1043. DOI: [10.1016/j.optlaseng.2013.02.019](https://doi.org/10.1016/j.optlaseng.2013.02.019)
- [15] Scintilla, L.D. (2014). Continuous-wave fiber laser cutting of aluminum thin sheets: effect of process parameters and optimization. *Optical Engineering*, vol. 53, no. 6, 066113. DOI: [10.1117/1.OE.53.6.066113](https://doi.org/10.1117/1.OE.53.6.066113)
- [16] Derringer, G., Suich, R. (1980). Simultaneous optimization of several response variables. *Journal of Quality Technology* vol. 12, p. 214-219. DOI: [10.1080/00224065.1980.11980968](https://doi.org/10.1080/00224065.1980.11980968)
- [17] Kim, K.J., Lin, D.K.J. (2000). Simultaneous optimization of mechanical properties of steel by maximizing exponential desirability functions. *Applied Statistics-Series C*, vol. 49, no 3, p. 311-325. DOI: [10.1111/1467-9876.00194](https://doi.org/10.1111/1467-9876.00194)
- [18] Ch'ng, C.K., Quah, S.H., Low, H.C. (2005). A new approach for multiple-response optimization. *Quality Engineering*, vol. 17, no 4, p. 621-626. DOI: [10.1080/08982110500225505](https://doi.org/10.1080/08982110500225505)
- [19] Marinković, V. (2020). A novel desirability function for multi-response optimization and its application in chemical engineering. *Chemical Industry and Chemical Engineering Quarterly*, vol. 26, no 3, p. 309-319, DOI: [10.2298/CICEQ190715007M](https://doi.org/10.2298/CICEQ190715007M)
- [20] Marinković, V. (2021). Some applications of a novel desirability function in simultaneous optimization of multiple responses. *FME Transactions*, vol. 49, no .3, p. 534-548. DOI: [10.5937/fme2103534M](https://doi.org/10.5937/fme2103534M)
- [21] Shaibu, A.B., Cho, A.B. (2009). Another view of dual response surface modeling and optimization in robust parameter design. *International Journal of Advanced Manufacturing Technology*, vol. 41, p. 631-641. DOI: [10.1007/s00170-008-1509-2](https://doi.org/10.1007/s00170-008-1509-2)
- [22] Goethals, P., Cho, B. (2011). Using higher precision-based response surface design to determine the optimal process target. *International Journal of Advanced Manufacturing Technology*, vol. 56, p. 13-30. DOI: [10.1007/s00170-011-3161-5](https://doi.org/10.1007/s00170-011-3161-5)
- [23] Das, R.N. (2014). On estimating the optimal process parameters in quality engineering using generalized linear models approach. *Model Assisted Statistics and Applications*, vol. 9, no 3, p. 201-211, DOI: [10.3233/MAS-140293](https://doi.org/10.3233/MAS-140293)
- [24] Madić, M., Radovanović M. (2014). Optimization of machining processes using pattern search algorithm. *International Journal of Industrial Engineering Computations*, vol. 5, p. 223-234. DOI: [10.5267/j.ijiec.2014.1.002](https://doi.org/10.5267/j.ijiec.2014.1.002)
- [25] Jeong, I., Kim, K. (2009). An interactive desirability function method to multiresponse optimization. *European Journal of Operational Research*, vol. 195, no 2, p. 412-426, DOI: [10.1016/j.ejor.2008.02.018](https://doi.org/10.1016/j.ejor.2008.02.018)



Banja Luka
1-2 Jun 2023.

DEMI 2023
**16th International Conference on
Accomplishments in Mechanical and
Industrial Engineering**
www.demi.mf.unibl.org



Optimization problem with the goal of minimizing the mass of gears

Anja Velemir, Ljubica Spasojević, Nenad Petrović, Nenad Kostić, Nenad Marjanović

University of Kragujevac, Faculty of Engineering, Kragujevac, Serbia

Abstract *One of the existing problems with mechanical structures occurs in the form of oversizing components which lead to unnecessary, increased costs. This paper presents an application of the optimization problem with the goal of minimizing the mass of gears in a single stage geared speed reducer. Aside from cost savings through the use of less material, a reduction in mass also results in improvement of efficiency during operation. In this paper, this was achieved to a large extent and demonstrated using standardized examples from literature in order to have comparable result. With the help of the existing parameters, various combinations of possible solutions were developed and the corresponding optimal solution was selected. The solution was compared with the existing solutions from literature and appropriate conclusions were drawn. The Excel Solver tool was used for the purposes of this the research in order to show that practically applicable optimal results can be achieved without the use of additional specialized software*

Keywords *Optimization, gears, mathematical model, Excel Solver, minimal mass*

1. INTRODUCTION

To ensure successful market placement of a new design, it is necessary for it to have the best characteristics. Some parameters that fall under this category are product dimensions, weight, manufacturing process and technology, materials, manufacturing duration, and so on. Product optimization is often employed to choose the best possible values for these parameters, especially in the case of weight and dimensions.

For the purpose of this study, gears were selected as one of the main mechanical components with a wide range of applications in

mechanical engineering. Gears can be found everywhere and their main feature is power transmission, so it is necessary to manufacture them with great precision. Due to their complex geometry and shape, analytical calculations during gear design can often result in errors. While results obtained by computer analysis are only sometimes optimally calculated. Therefore, for this study, parameter analysis was chosen to minimize the weight of the gear to optimize it.

The increasing use of gears and higher demand requires the use of optimization in gear design. The main goal of this study is to highlight the advantages of parameter optimization that contribute to reducing the weight of gears. The obtained results are compared to the previously published results from the literature [1].

In order to perform parameter optimization in this study, Excel Solver tool was used.

In addition to the mentioned literature, several other papers were considered during the

Corresponding author

Anja Velemir
anja.velemir@fink.rs
University of Kragujevac, Faculty of Engineering
Sestre Janjic 6
34000 Kragujevac, Serbia

research process in order to have referent results. These papers dealt with similar or identical optimization problems, such as the paper by Golabi S. and Jafari J., which deals with weight optimization of gears based on the minimum required weight in design [2], and the paper that deals with practical optimization of cylindrical gears [3].

2. OPTIMIZATION WITH EXCEL SOLVER

Optimization problems are real-world problems that we encounter on a daily basis. These problems are often related to areas such as mathematics, engineering, science, business, economics, and accounting. The goal is to find the optimal or most efficient solution for use in a specific sphere for which optimization is being performed. Optimization achieves various benefits such as increasing profits, reducing costs, extending the lifespan of certain products, minimizing the overall time to complete a particular project, and so on. A mathematical model must be created to observe the situation for a given problem best and perform optimization in the most efficient way possible [4]. The model consists of the following:

1. Objective function, [5]

$$\max \{f(x)\} = -\min\{-f(x)\}$$

2. Constraints, [5]

$$g_i(x) = 1; \quad i=1,2,m_i$$

3. Decision variables, [5]

$$x = (x_1, x_2, \dots, x_n)$$

For the purpose of this study and optimization application for reducing the weight of gears, a tool called Excel Solver was used, which is a part of the Microsoft Excel program. It is often used for optimization purposes and is widely used because it is the most accessible tool of its kind. Creating and defining a mathematical model is done very simply, as shown in Fig 1.

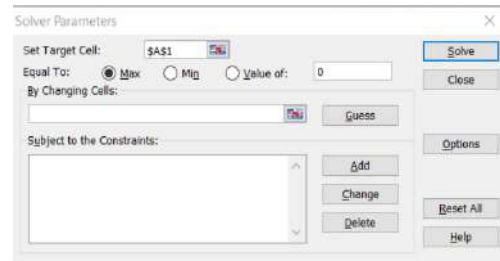


Fig. 1. The environment of the Excel Solver tool

The most important role in the overall optimization process is satisfying the objective function, primarily in a way that the obtained results are within the appropriate range of constraints. The optimization process is not a simple one-way process [5] because, in most cases, many conditions that are set can be unclear, ambiguous, or inaccessible. Due to a lack of information, this can significantly hinder the designer's ability to arrive at optimal solutions. Optimization requires precise definition in any sense to be calculated as accurately as possible for specific parameters. The purpose of optimization in technology is to reduce the time required to find a satisfactory solution. In this regard, the idea is to solve optimization problems that are already available, as well as those similar to them, but with minor differences, and to set new optimization problems using already developed models. In other words, everything that is available should be considered and used individually or collectively for new mathematical models [3].

3. EXAMPLE

This paper analyzes parameters influencing the minimization of mass, aiming to improve the solution by applying Excel Solver on the same optimization model as in the previously published paper by V. Savsani [1]. Figure 2 shows the models based on the obtained results in the paper to be analyzed, where the larger gear has 25 teeth.



Fig. 2. Gear with 25 teeth

The influential parameters for this study are

$x(b, d_1, d_2, m, z_1)$, where since this is about minimizing mass, it is obtained as:

$$\text{Weight} = F(x) = (\pi\rho/4000) * [bm^2Z_1^2(1 + a^2) - (D_1^2 - d_0^2) * (1 - b_w) - nd_p^2b_w - (d_1^2 - d_2^2)b] \text{ [kg]} \quad [1]$$

The parameters must be within the range:

$$20 \leq b \leq 32$$

$$10 \leq d_1 \leq 30$$

$$30 \leq d_2 \leq 40$$

$$18 \leq z_1 \leq 25$$

$$m = \{2.5, 2.75, 3, 3.5, 4\}$$

While the constraints must range between [1]:

$$g_1(x) = F_s \geq b_1$$

$$g_2(x) = (F_s/F_p) \geq b_2$$

$$g_3(x) = d_1^3 \geq b_3$$

$$g_4(x) = d_2^3 \geq b_4$$

Given the calculated values shown in Table 1, where:

$$a = 4, \rho = 8, P = 7.5, n = 6, \sigma = 294.3, y = 0.102, b_2 = 0.193, \tau = 19.62, K_w = 0.8, K_v = 0.389, H = 7.5 \text{ [6]}$$

Table 1. Calculated parameter for optimization [1] [4]

exp No.	Needed dimensions	Calculated dimensions
1	$D_r = m(aZ_1 - 2.5)$	191,125
2	$l_w = 2.5m$	6,875
3	$D_i = D_r - 2l_w$	177,375
4	$b_w = 3.5m$	9,625
5	$d_0 = d_2 + 25$	55
6	$d_p = 0.25(D_i - d_0)$	30,593
7	$D_1 = mZ_1$	49,5
8	$D_2 = amZ_1$	198
9	$N_2 = N_1/a$	375
10	$Z_2 = Z_1D_2/D_1$	72
11	$\vartheta = \pi D_1 N_1 / 60.000$	3,887
12	$b_1 = 1000P/\vartheta$	1929,150
13	$b_3 = (48.68e6P)/(N_1\tau)$	0,202
14	$b_4 = (48.68e6P)/(N_2\tau)$	0,809
15	$F_s = \pi K_v K_w \sigma b m y$	1936,97
16	$F_p = (\pi K_v K_w D_1 b Z_2) / (Z_1 + Z_2)$	591,528

The Fig 3 shows some important parameters that affect the optimization of the gear.

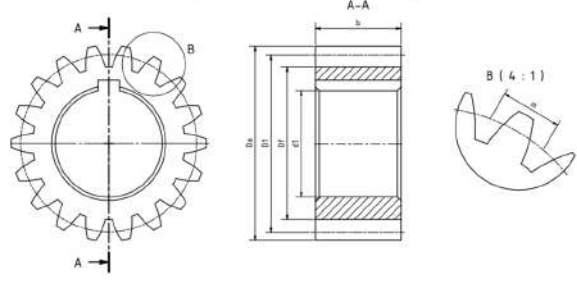


Fig. 3. Parameters of gears

According to the obtained values in Table 1, which are necessary for calculating the mass from the main form and the set constraints, the results shown in Table 2 are obtained.

Table 2. Results calculated in this paper

Exp no.	Range of values	Calculated values	Constraints
m	2-2.5	2.5	0.145313
b	20-32	28.92455	3.081529
D ₁	10 do 30	30	14594.29
D ₂	30 do 40	36.75119	15.1762
Z ₁	18 - 25	18	/

When the results obtained in this paper are compared to the best results obtained in the paper by V. Savsani (table 3), it can be observed that the proposed method achieved a significant reduction in the weight of the gear while satisfying all constraints.

Table 3. Results calculated in paper V.Savsani [1]

Exp no.	Range of values	Calculated values	Constraints
m	2-2.5	2	1193,652926
b	20-32	32	2,164660844
D ₁	10 do 30	30	14594,29154
D ₂	30 do 40	36.75119	8,7799E-08
Z ₁	18 - 25	25	/

Based on the presented tables, it can be concluded that the minimization of the gear was carried out with greater success, under the same constraints and parameter ranges in this study, as the obtained mass was 2830.96 kg, as shown in Fig. 4.

Fig 4 show a graphical representation of the obtained parameters and their comparison,

as well as the representation of the obtained results

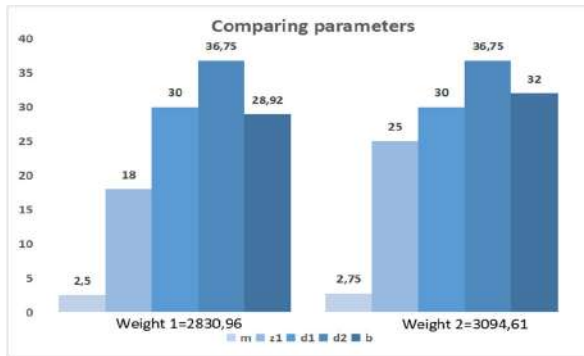


Fig. 4. Diagram of parameters from this research (left), from research [1] (right)

The gear model based on the obtained results of minimization is shown in Fig 5.



Fig. 5. Model of gears with 18 and 25 teeth

Figure 4 allows for a comparison of the appearance of the gear with 18 teeth (smaller gear) compared to the gear with a larger number of teeth.

4. CONCLUSIONS

Considering the wide range of applications of gears, there is often a desire to improve them in various aspects. One of these aspects is the gear mass, which is examined in this paper, with the goal of minimizing it. The constraints that are set depend on strength, durability, bending, surface, etc., while the parameters being examined have the greatest impact on mass, such as module, width, number of teeth, and diameters. According to the optimization performed, the solutions obtained are better compared to the modified gear design carried out by V. Savsani, R. V. Rao, and D. P. Vakharia in their work [1]. Their analysis was conducted using two algorithms,

PSO and SA, but the results obtained and presented in this paper are significantly better.

Their obtained weight solutions are, in the best case, 3094.61[kg]. However, better solutions were obtained in this paper, with a mass of 2830.82[kg] at parameters: $m=2.5$, $b=28.9$, $d_1=30$, $d_2=36.756$, $z_1=18$, which is about 9.009% better. This shows that better results can be achieved using simpler optimization software such as Excel Solver. It can be concluded that, regardless of the optimization tool we use, the only important thing for successful optimization is to set appropriate constraints and examine all parameters to obtain the correct solution. This is just one optimization problem that could contribute to improvement in this field. However, there are still open problems that leave room for further exploration in the future.

REFERENCES

- [1] Savsani, V., Rao R.V, Vakharia D.P. (2009). Optimal weight design of a gear train using particle swarm optimization and simulated annealing algorithms. Mechanism and Machine Theory, Vol 45, No 3, p. 531-541, ISSN 0094-114X.
DOI: [10.1016/j.mechmachtheory.2009.10.010](https://doi.org/10.1016/j.mechmachtheory.2009.10.010)
- [2] Golabi S., Fesharaki J., Yazdipoor M (2013). Gear train optimization based on minimum volume/weight design. Mechanism and Machine Theory, Vol 73, p. 197-217, ISSN 0094-114X
DOI: [10.1016/j.mechmachtheory.2013.11.002](https://doi.org/10.1016/j.mechmachtheory.2013.11.002)
- [3] Marjanovic N., Isailovic B., Marjanovic V., Milojevic Z., Blagojevic M., Bojic M. (2012). A practical approach to the optimization of gear trains with spur gears. Mechanism and Machine Theory, Vol 53, p. 1-6, ISSN 0094-114X
DOI: [10.1016/j.mechmachtheory.2012.02.004](https://doi.org/10.1016/j.mechmachtheory.2012.02.004)
- [4] Leslie Chandrakantha. Mathematics and Computer Science Department.
From: <https://people.computing.clemson.edu/~jmar ty/courses/commonCourseContent/common/OR-Intro/courses/OptimizationWithExcel/ExampleExcelUsingInvestments.pdf>
Accessed on: April 14, 2023.
- [5] Vučina D., Metode inženjerske numeričke optimizacije – s primjerima primjene u programsku jezik C i Matlab, Fakultet elektrotehnike, strojarstva i brodogradnje, Split, 2005.
- [6] YOKOTA T., TAGUCHI T., GEN M. (1998) . A Solution Method for Optimal Weight Design Problem of the Gear Using Genetic Algorithms. Computers ind. Engng Vol. 35, Nos 3--4, pp. 523-526,



Banja Luka
1–2 Jun 2023.

DEMI 2023

16th International Conference on Accomplishments in Mechanical and Industrial Engineering

www.demi.mf.unibl.org



Optimization surface roughness in powder mixed electrical discharge machining of titanium alloy

D. Rodic, M. Gostimirovic, M. Sekulic, B. Savkovic, A. Aleksic

Department of Production Engineering, Faculty of Technical Sciences, University of Novi Sad, 21000 Novi Sad, Republic of Serbia

Abstract To further improve the efficiency of electrical discharge machining of advanced materials, the possible technological improvement of the process is achieved by adding graphite powder to the dielectric. In this study, the Taguchi approach was applied to determine the effects of input parameters such as discharge current, pulse duration, duty cycle, and graphite powder concentration on surface roughness in machining titanium alloys. L9 orthogonal array, signal-to-noise ratio (S/N), and ANOVA were used to design and analyze the experiment. Discharge current was determined to be the factor that had the strongest influence on surface roughness. Based on ANOVA, pulse duration was the second influential parameter, followed by graphite powder and duty cycle. In addition, an optimum condition was found to improve surface roughness. A discharge current of 1.5 A, a pulse duration of 32 μ s, a duty cycle of 30% and a powder concentration of 12 g/l resulted in minimum surface roughness.

Keywords Taguchi, surface quality, graphite powder, ANOVA, PMEDM

1. INTRODUCTION

Due to the combination of excellent mechanical properties and outstanding biocompatibility, titanium alloys are often used as a material for the manufacture of complex components. This is precisely why titanium alloys are difficult to process using classical methods, especially from the point of view of tool wear. When it comes to the production of complex parts, it is necessary to analyze the use of electrical discharge machining. In EDM, no mechanical stresses are introduced into the workpiece during machining because there is no direct contact between the electrode and the workpiece.

However, when machining titanium alloys with aluminium impurities, the EDM process becomes unstable and inefficient. In order to establish process stability and improve EDM performance, various researchers have proposed adding powder to the dielectric. In this way, one of the innovative processes called powder-mixed electrical discharge machining (PMEDM) was created.

Electrically conductive powder added to the dielectric reduces the insulating properties and causes an increase in the gap distance between the tool and the workpiece. This increase means a more efficient circulation of the dielectric, i.e. a washout of the working space between the tool and the workpiece. In this way, EDM becomes more stable, which improves the machining performances such as higher machining productivity and lower surface roughness, and also leads to a lower wear rate

Corresponding author

PhD, Dragan Rodić
rodicdr@uns.ac.rs

*Department of Production Engineering, Faculty of Technical Sciences, University of Novi Sad
Novi Sad, Serbia*

of the tools. The powder particles change the properties of the discharge channel, which equalises the distribution of sparks among the powder particles and thus reduces the current density [1]. Due to this uniform distribution of the discharges, there is uniform erosion, i.e. flat craters on the workpiece, which leads to a reduction in surface roughness and thus to an increase in machining accuracy.

Various types of electrically conductive powder can be mixed with liquid dielectric, including: aluminum, graphite, silicon, copper, silicon carbide and others. For example, Wong used powders of different electrical conductivity, such as graphite, silicon, aluminum, crushed glass, silicon carbide, and molybdenum sulfate, and studied their influence on the roughness of the treated surface [2]. He concluded that the powders: graphite (grain size 40 μm) and silicon (grain size 45 μm) gave the best results of surface roughness. A significant reduction in the surface roughness was obtained, i.e. $R_a = 0.62 \mu\text{m}$ with silicon powder, while $R_a = 0.75 \mu\text{m}$ was obtained with graphite powder, i.e. a surface with high gloss (mirror effect), which is the opposite of classical EDM, where mostly dull surfaces are obtained. What types of powders can be used with liquid dielectric, what particle size, at what concentration, and what effect they have on the performance of the PMEDM process have been studied by a small number of researchers.

Therefore, the introduction of an additional parameter, for example, the concentration of powder in the dielectric in PMEDM, is a challenge for many researchers. The analysis of the change of the surface roughness depending on the input parameters in PMEDM with chromium powder was processed in the work [3]. The obtained results show that the discharge current and the concentration of the powder in the dielectric have the greatest influence on the surface roughness in machining carbon steel. By applying the response surface method, a model was created that allows the determination of optimal machining regimes, where the objective function was the minimum surface roughness. Interesting results of the research work on single-objective optimization of the PMEDM procedure are presented in the paper [4]. The aim of the research was to determine the optimal input parameters in PMEDM. Three types of tool steels were machined using three types of tools, first in a dielectric with aluminum mixture and then in a

dielectric with graphite powder. In order to optimize the process, Taguchi method was applied according to the experimental plan L27. Based on the Taguchi method, different optimal machining input parameters were determined for the different steels, representing the complexity of the PMEDM system.

Determining the optimal processing parameters for PMEDM remains a topical problem, as evidenced by the numerous research papers on the subject. There is still no concrete answer to the question of which powder concentration gives the best processing performance. Therefore, the main objective of this research is to determine the optimal machining parameters using the Taguchi approach. A single-objective optimization was performed by adjusting input parameters such as discharge current, pulse duration, duty cycle, and graphite powder concentration to achieve minimum surface roughness when machining titanium alloys.

2. MATERIAL AND METHODS

In the present study, a titanium alloy (TiAl_4V_6) was chosen as the workpiece material. The experiments are carried out on an Agie Charmie SP1-U die-sinking EDM machine. A commercial graphite electrode TTK50 with a cross section of 10x10 mm was used as the tool. The pure graphite powder with a particle size of 19 μm (Asbury PM19) was chosen as an additive for the dielectric fluid. In addition, the surfactant Tween 20 $\text{C}_{58}\text{H}_{114}\text{O}_{26}$ is added. The role of the surfactant is to ensure a homogeneous mixture of powder and dielectric during PMEDM. In order to conduct the experiments, a tank with supporting elements for PMEDM was designed, figure 1.

Finally, four input parameters were selected for this study from the preliminary experiments and the available literature on PMEDM [5, 6]. The input parameters were discharge current (I_e), pulse duration (t_i), duty cycle (τ), and graphite powder concentration (GR). The conditions for processing titanium alloy are shown in table 1.

The Taguchi plan is a method that allows reducing the number of experimental points by orthogonal arrangements and minimizing the effects outside the influential parameters. It was applied in this study with the aim of more accurately optimizing and analyzing the influence of the input parameters on the tool

wear rate. The processing parameters and their values are listed in Table 2. An experimental design according to the Taguchi orthogonal array L9 (3⁴) was established.



Fig. 1. Setup of PMEDM.

Table 1. Machining conditions

Parameters of EDM	Label	Value	Units
Discharge current	I_e	1.5 ÷ 7.5	A
Pulse on time	t_i	24 ÷ 240	μs
Pulse off time	t_o	24 ÷ 240	μs
Open circuit voltage	U_o	100	V
Polarity	Pol	(-)	/
Duty factor	τ	30 ÷ 70	%

Table 2. Taguchi orthogonal array L9 (3⁴) at PMEDM TiAl₆V₄

No.	Factor				Surface roughness	
	I_e (A)	t_i (μs)	τ (%)	GR g/l	Ra (μm)	S/N
1.	1.5	32	30	0	1.78	-5.01
2.	1.5	75	50	6	2.01	-6.06
3.	1.5	180	70	12	2.61	-8.33
4.	3.2	32	50	12	3.47	-10.81
5.	3.2	75	70	0	4.11	-12.27
6.	3.2	180	30	6	4.47	-13.01
7.	6.0	32	70	6	8.12	-18.19
8.	6.0	75	30	12	7.16	-17.09
9.	6.0	180	50	0	9.84	-19.86

3. RESULTS AND DISCUSSION

For single objective parameter optimization, the Taguchi method was used, where the output Ra was optimized based on the Taguchi orthogonal array L9 (3⁴) for PMEDM titanium alloy. This method does not require the creation of a mathematical model and is an alternative approach to identifying optimal input parameters. The MiniTab 17 software tool was used for statistical data processing. Based on the measured Ra values, the S/N ratio was calculated for all 9 experiments. The values of the S/N ratio for Ra are calculated based on the Taguchi quality feature "Smaller is better", Table 2.

Table 3 shows the S/N ratios with each factor and the corresponding level for surface roughness. The factors with the largest difference in mean values (max-min) have the greatest influence on the output size. The table shows that discharge current has the greatest influence on Ra, followed by pulse duration, duty cycle and graphite powder concentration.

Table 3. Response table of S/N ratio for surface roughness

Factors	Levels			min-max	Rang
	1	2	3		
(A) I_e	-6.46	-12.03	-18.38	11.91	1
(B) t_i	-11.33	-11.81	-13.73	2.39	2
(C) τ	-11.71	-12.24	-12.93	1.22	3
(D) GR	-12.38	-12.42	-12.07	0.34	4

The influence of individual input parameters on the output power of the processing process can be illustrated with the help of a reaction diagram showing the change of the S/N ratio at the moment of changing the level of the control parameter from 1 to 3. Accordingly, the influence of individual parameters on the output characteristics of the processing process is graphically expressed by an angle of the slope of the line connecting different levels of the parameters.

Looking at the slope of the lines, we can see that the steepest line applies to factor A, then B, then C, and finally D. This order corresponds to the calculated rank (Table 7-2). According to Figure 2, the highest S/N ratio indicates the optimal level of each factor. Therefore, based on the

"smaller is better" criterion, the optimum combination of the PMEDM titanium alloy input parameters as a function of surface roughness is A=1, B=1, C=1 and D=3.

The prediction of the output power value ($R_a = 1.72 \mu\text{m}$) and the calculation of the corresponding S/N ratio ($S/N = -19.42$) based on the optimal combination of input parameters can be found in Table 4.

Based on the ANOVA analysis performed using the F-test, the influence, i.e., the percentage involvement of each factor in PMEDM titanium alloy on surface roughness can be seen. Factors with an F-value of less than 1 were excluded from the analysis, which was the case for the

impulse action coefficient (factor C) and the concentration of graphite powder (factor D). After excluding insignificant factors, the analysis ANOVA for the remaining members is shown in the reduced Table 5, where the percentage participation for factors A and B is given. Discharge current has the greatest influence on the mean arithmetic roughness of the treated surface, with a percentage of 93.08%. The percentage of 4.35% is taken by the pulse length for the set processing conditions. The presented ANOVA analysis confirms the results obtained with the Taguchi method.

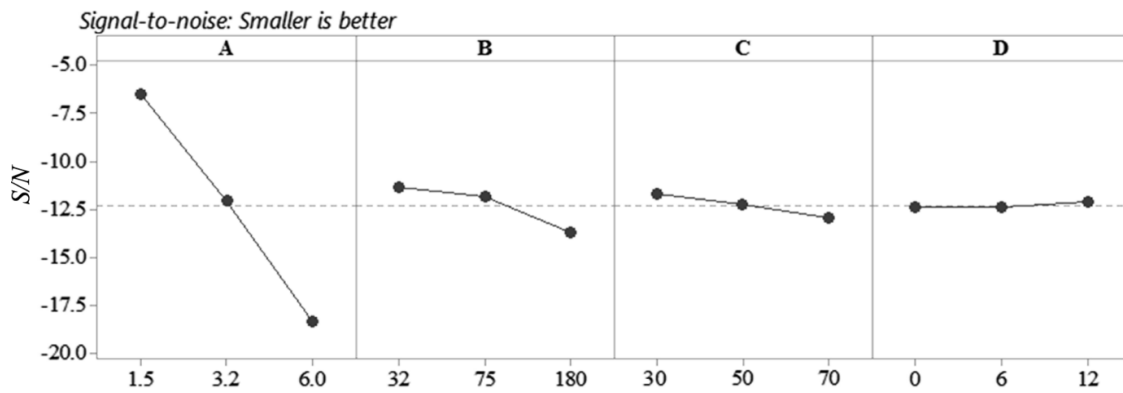


Fig. 1. Graphic representation of the S/N ratio for Ra

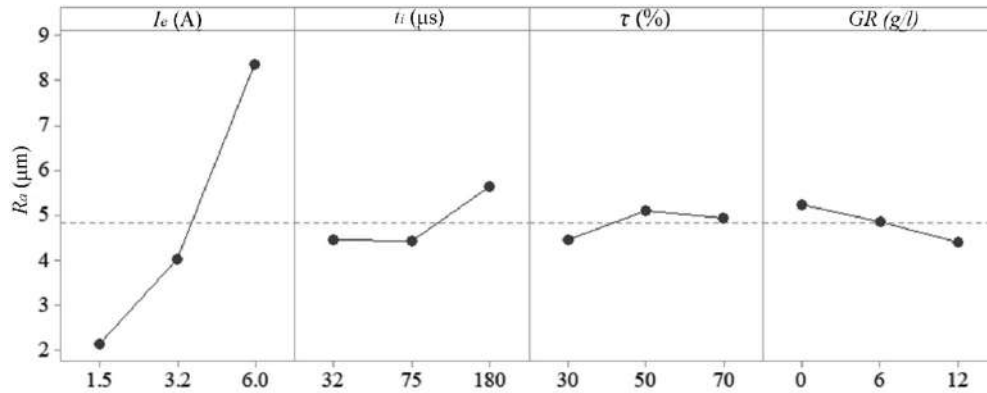


Fig. 2. Response ANOVA graph for the Ra

Table 4. Optimal setting of input parameters with confirmation experiment

Input	Level	Value	Ra	Confirmation experiment
I_e (A)	1	1.5	$S/N = -4.71$ $R_a = 1.72 \mu\text{m}$	$R_a = 1.62 \mu\text{m}$
t_i (μs)	1	32		
τ (%)	1	30		
GR (g/l)	3	12		

The average error between the EDM output values obtained by prediction based on Taguchi analysis and the values obtained after the verification experiments (with optimal input parameter values) was only 5.8%. Therefore, the single-objective optimization of the input parameters of the PMEDM can be considered successful. This analysis confirmed the order of influence of input parameters during processing

compared to published research on PMEDM titanium alloys.

Table 5. Reduced ANOVA table for Ra

Source	DF	Sum sq	Mean sq	F-value	Percent %
A - I_e	2	61.465	30.7325	72.55	93.08
B - t_i	2	2.873	1.4367	3.39	4.35
D - GR	4	1.694	0.4236		2.57
Error	8	66.033			
Total	2	61.465	30.7325	72.55	93.08

In addition to discharge current, which had the greatest influence on Ra as expected, pulse duration, duty cycle, and graphite powder concentration had less influence than expected. This can be explained by the results of the preliminary tests. The explanation for excluding duty cycle from the analysis of ANOVA is justified by the fact that this parameter does not have a significant effect on surface roughness at relatively short pulse durations, up to 180 μ s in this study. A significant effect of the pulse action coefficient is expected for values of pulse length greater than 200 μ s, since a higher discharge energy occurs. A higher discharge energy has a detrimental effect on the surface roughness of titanium alloy if the pause duration is too short (calculated in $\tau > 90\%$), which has been confirmed in research [7].

4. CONCLUSION

The aim of this study is to optimize Ra using the Taguchi approach and to determine the influence of the main input factors. Based on the experimental and statistical results, the discharge current (I_e), pulse duration (t_i), duty cycle (τ) and graphite powder concentration (GR) were the main factors that affected the Ra. According to the Taguchi method, the discharge current has the greatest influence on Ra, followed by the pulse duration, duty cycle, and graphite powder concentration. This statement was confirmed by the ANOVA analysis using the F-test. The influence, i.e. percentage participation of each factor in PMEDM titanium alloy on surface roughness for discharge current is 93.08%. The percentage of 4.35% is taken by the pulse duration for the specified machining conditions. Based on the "smaller is better" criterion, the optimal combination of PMEDM input parameters for the titanium alloy

as a function of surface roughness is A=1, B=1, C=1, and D=3. The prediction of the output power gave a value of Ra = 1.72 μ m, while the confirming experiment gave a value of 1.66 μ m. Therefore the single-objective optimization of the input parameters of the PMEDM can be considered successful. Although the analysis of ANOVA showed that graphite powder has no influence, the minimum Ra value is achieved with a concentration of 12 g/l. Future research should focus on wider intervals of input factors as well as on different powder types.

Acknowledgement

This paper has been supported by the Provincial Secretariat for Higher Education and Scientific Research through the project no. 142-451-1772/2022-01/01: "Research on the innovative process of electrical discharge machining of titanium alloy".

REFERENCES

- [1] Ramana, P., Kharub M., Singh J., Singh J. (2021). *On material removal and tool wear rate in powder contained electric discharge machining of die steels*. Materials Today: Proceedings, Vol. 38, pp. 2411-2416.
- [2] Wong, Y.S., Lim L.C., Rahuman I., Tee W.M. (1998). *Near-mirror-finish phenomenon in EDM using powder-mixed dielectric*. Journal of Materials Processing Technology, Vol. 79, pp. 30-40.
- [3] Ojha, K., Garg R.K., Singh K.K. (2013). *Effect of chromium powder suspended dielectric on surface roughness in PMEDM process*. Tribology - Materials, Surfaces & Interfaces, Vol. 5, pp. 165-171.
- [4] Bhattacharya, A., Batish A., Singh G., Singla V.K. (2011). *Optimal parameter settings for rough and finish machining of die steels in powder-mixed EDM*. The International Journal of Advanced Manufacturing Technology, Vol. 61, pp. 537-548.
- [5] Hasçalık, A., Çaydaş U. (2007). *Electrical discharge machining of titanium alloy (Ti-6Al-4V)*. Applied surface science, Vol. 253, pp. 9007-9016.
- [6] Huu-Phan, N., Tien-Long B., Quang-Dung L., Duc-Toan N., Muthuramalingam T. (2019). *Multi-criteria decision making using preferential selection index in titanium based die-sinking PMEDM*. Journal of the Korean Society for Precision Engineering, Vol. 36, pp. 793-802.
- [7] Kumar, M., Datta S., Kumar R. (2018). *Electro-discharge Machining Performance of Ti-6Al-4V Alloy: Studies on Parametric Effect and Phenomenon of Electrode Wear*. Arabian Journal for Science and Engineering, pp. 1-16.



Banja Luka
1-2 Jun 2023.

DEMI 2023

16th International Conference on Accomplishments in Mechanical and Industrial Engineering

www.demi.mf.unibl.org



Parametric Optimization in End-Milling Operation of AlMgSi1 Alloy Using a Hybrid WASPAS-Taguchi Technique

Adnan Mustafić^a, Ragib Spahić^b

^aUniversity of Tuzla, Faculty of Mechanical Engineering, Bosnia and Herzegovina

^bAS Holding d.o.o., Bosnia and Herzegovina

Abstract The milling process is one of the fundamental machining techniques and process parameter optimization is very important in manufacturing as it leads to better machining performances without compromising the product quality. In this work, a parametric optimization of milling process parameters was carried out using a hybrid WASPAS-Taguchi method while milling AlMgSi1 alloy. Initially, a Taguchi L18 orthogonal array was developed with five factors, i.e. spindle speed, feed rate, depth of cut, nozzle stand-off distance, and the nozzle position relative to the cutting direction in different cooling environments (dry, Minimum Quantity Lubrication - MQL and conventional). Surface roughness parameters (R_a , R_z , R_{max}) and the material removal rate (MRR) were measured as the output variables. According to the optimization results it was observed that the cutting speed, depth of cut and the cooling environment (MQL) were the most dominant factors on the performance score. Analysis of variance (ANOVA) results show that the cutting speed and depth of cut significantly affects the weighted performance score given through the WASPAS method. Further, the results were compared with other existing multi-criteria decision-making methods and induced overall good results.

Keywords Milling, MQL, Multi-Criteria Decision-Making method, WASPAS, Taguchi method, AlMgSi1

1. INTRODUCTION

Efficient, cost-effective, and productive machining operations are essential in the machining industry, making it crucial to carefully choose appropriate machining parameters [1]. For instance, a good quality of surface finish, higher tool life values and higher material removal rates are favored in every machining process. In most cases, the goal of these responses is conflicting because of less combinations of process parameters which simultaneously improve the above-mentioned

response variables.

It is well known that for higher material removal rates (MRR) high cutting speed, feed rate, and depth of cut are required, but on the other hand such combination of parameters produces high heat at the cutting zone and therefore affect the overall surface integrity.

Proper selection of metalworking fluids in the machining processes can manage these phenomena. But on the other hand, conventional mineral oil-based metalworking fluids are detrimental to the environment and human health, and they bring significant additional costs to production. As a result, they are recognized as a major unsustainable element, and therefore alternative cooling and/or lubrication techniques are increasingly being developed.

Corresponding author

PhD, Adnan Mustafić, Assistant Professor
adnan.mustafic@unitz.ba

University of Tuzla, Faculty of Mechanical Engineering
Urfeta Vejzagića 4., 75000 Tuzla
Tuzla, Bosnia and Herzegovina

One of the promising solutions besides the complete dry machining is the minimum quantity lubrication (MQL) technique, also known as near-dry machining. In MQL technique, extremely small amounts of biodegradable metalworking fluid, measured in milliliters per hour (mL/h) is delivered into the cutting zone instead of using conventional circulation emulsion flood systems [2]. There are numerous studies available which describe the successful application of MQL technique in machining of various ferrous and non-ferrous materials.

The application of aluminum and its alloys in automotive and aerospace industries is widely growing. Because aluminum alloys have highly adhesive characteristics compared to steels, more effective lubrication is often necessary in cutting, though they are not hard in nature [3]. Since traditional coolant-based methods are typically used in aluminum processing, MQL technique would have massive benefits in the machining process of its alloys.

Milling process is classified as one of those processes that have the most frequent application in the metalworking industry. Considering the large number of influential parameters as well as response variables, modeling and optimization of milling process parameters is extremely difficult, which indicates the needs for multi-criteria decision-making (MCDM) methods.

To the best knowledge of the authors, limited literature has been found applying these techniques with the Taguchi based DOE approach in the comparative analysis of various cooling environment techniques in the machining processes. Therefore, in this research paper the Taguchi methodology is combined with the WASPAS method with the purpose of estimating the optimal parameters in one single process performance characteristic in the end milling process of a frequently used aluminum alloy.

2. EXPERIMENTAL SETUP

The experimental studies were performed on a vertical machining center FAMUP MCL 120.E as shown in Fig. 1.

The cutting fluid in case of MQL cooling environment was atomized by means of a spray gun and an air compressor at 5 bars, and was delivered through one nozzle to the tool-

workpiece interface. A vegetable based MQL oil (Castrol Hyspray V1066) was used because of its biodegradability and good lubrication properties with a kinematic viscosity of 39 mm²/s at 40°C.



Fig. 1. Experimental setup for milling test

For all cooling and lubrication techniques the nozzle elevation angle was kept constant and set at approximately 45° to the tool-workpiece interface as shown in Fig. 2a. The different nozzle positions (at 0°, 90°, and 180°) relative to the feed direction (Fig. 2b) were observed as an input parameter and were varied during the experimental runs.

It is important to emphasize that in the dry milling tests only compressed air was supplied to the cutting zone in order to remove the generated chips, and thus prevent the possibility of re-cutting of chips.

The milling experiments were performed using an HSS 4-flute end mill with a diameter of 16mm. AlMgSi1 (EN AW-6082 T6) aluminum alloy (0,2%Fe, 0,53%Mn, 0,64%Mg, 0,01%Ti, and 1,02%Si, balance %Al) of 20mm thickness as the workpiece material was used in all experiments. AlMgSi1 aluminum alloy has a hardness of 99 HB, yield strength of 265 MPa and tensile strength of 312 MPa.

Mohr M1 perthometer was used for the measurement of surface roughness parameters (Ra, Rz, Rmax) according to the DIN EN 10049 standard. All measurements were made parallel to the cutting direction of the tool, and are given as the average value of three readings taken from the same surface, shown in Fig. 3.

All tests were conducted with different settings of spindle speed, feed per tooth, axial depth of cut, cooling environment and nozzle parameters as given in Table 1.

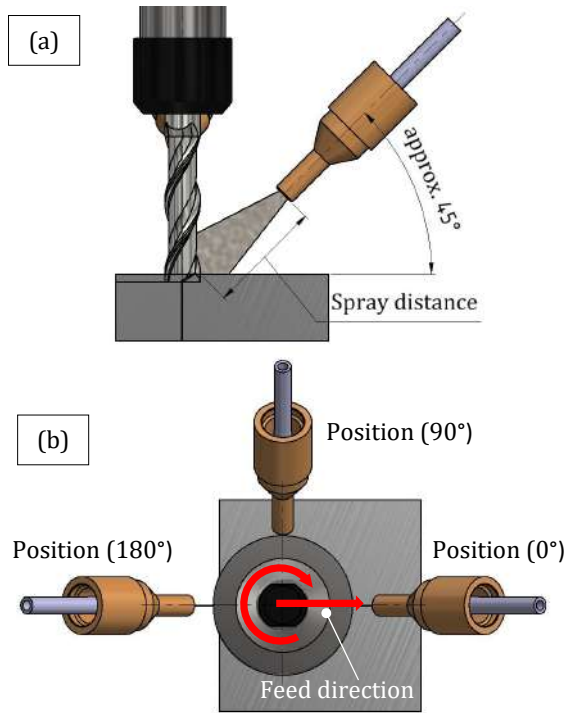


Fig. 2. (a) Schematic view of nozzle position for slot milling, (b) nozzle position in relation to the feed direction



Fig. 3. Setup for surface roughness measurement

The cutting parameters for spindle speed, feed per tooth and depth of cut were selected according to the recommendations of the tool manufacturer.

2.1 Design of Experiments

Taking into account the limitations of the experimental setup, as well as the number, level and nature (categorical and numerical values) of the input parameters, the Taguchi method

was chosen for the experimental plan. In this regard, according to the Taguchi quality concept a L18 ($2^1 \times 3^5$) orthogonal array was used for the experimental design. For instance, there are 486 experimental runs needed using the multilevel full factorial design (FFD), or 92 experimental runs by using Box-Behnken design, which confirms the justification of the Taguchi design application.

Table 1. Experimental design settings

Sym.	Parameters	Level Values		
		1	2	3
A	Spray distance (mm)	20	70	-
B	Cooling environment	MQL	Dry	Wet
C	Spindle speed (rpm)	1500	2500	3200
D	Feed rate (mm/t)	0,01	0,025	0,033
E	Depth of cut (mm)	1	2	3,5
F	Nozzle position (°)	0	90	180

As mentioned earlier, the average values of surface roughness parameters were considered for the optimization analysis. The material removal rate (MRR) was calculated for each experimental run according to the following equation.

$$MRR = \frac{a_e \cdot a_p \cdot n \cdot f_z \cdot z}{1000} \left[\frac{cm^3}{min} \right] \quad (1)$$

where a_e and a_p are the width (tool diameter) and axial depth of cut, respectively. Variables n, f_z, z are the spindle speed, feed per tooth, and number of teeth, respectively. The experimental design and response values are presented in Table 2.

3. OPTIMIZATION METHODOLOGY

Multi-criteria decision-making methods (MCDM) have been used to solve issues when there is a large number of conflicting criteria. There are different methods that have been used to treat decision-making problems in diverse research fields such as material selection, service quality, construction site locations, industrial robot selection problems, and manufacturing processes [4-8].

Table 2. Experimental run based on the L18 orthogonal array and measured responses

Exp. no.	A	B	C	D	E	F	R _a (μm)	R _z (μm)	R _{max} (μm)	MRR (cm ³ /min)
1	1	1	1	1	1	1	0,761	4,390	5,243	0,96
2	1	1	2	2	2	2	0,714	4,223	5,708	8
3	1	1	3	3	3	3	0,662	3,448	4,433	23,65
4	1	2	1	1	2	2	0,708	4,093	5,203	1,92
5	1	2	2	2	3	3	0,607	3,643	4,208	14
6	1	2	3	3	1	1	0,661	3,738	4,965	6,75
7	1	3	1	2	1	3	1,328	6,335	7,683	2,4
8	1	3	2	3	2	1	1,098	4,963	6,048	10,56
9	1	3	3	1	3	2	0,363	2,315	3,050	7,16
10	2	1	1	3	3	2	1,135	5,560	6,808	11,08
11	2	1	2	1	1	3	0,486	3,063	4,785	1,6
12	2	1	3	2	2	1	0,510	2,718	3,108	10,24
13	2	2	1	2	3	1	0,988	5,288	6,145	8,4
14	2	2	2	3	1	2	0,936	5,848	9,138	5,28
15	2	2	3	1	2	3	0,382	2,508	2,883	4,09
16	2	3	1	3	2	3	1,370	5,983	6,940	6,33
17	2	3	2	1	3	1	1,846	8,423	11,078	5,6
18	2	3	3	2	1	2	0,666	3,543	4,150	5,12

One of the frequently used MCDM methods is the Weighted Aggregated Sum Product Assessment (WASPAS). WASPAS is a multi-objective optimization-making method, which is one category of MCDM, and is used to determine the weight of output characteristics, and to rank process parameters to choose the best alternative among several. This method is introduced by Zavadskas et al. [9,10] in 2012, and is considered as one of the new powerful MCDM techniques, since it combines two different well-established methodologies, namely the weighted sum model (WSM) and the weighted product mode (WPM). WASPAS allows determination of weights according to the importance of each attribute, which helps in rational decision-making [11].

A brief description of the WASPAS method is presented in the following steps [12].

Step 1. Development of the decision matrix showing the performance of different alternatives with respect to various criteria.

$$X = \begin{bmatrix} x_{11} & x_{12} & \cdots & x_{1n} \\ x_{21} & x_{22} & \cdots & x_{2n} \\ \vdots & \vdots & \ddots & \vdots \\ x_{m1} & x_{m2} & \cdots & x_{mn} \end{bmatrix} \quad (2)$$

where m corresponds to the number of experimental trials (alternatives) and n is the number of criteria.

Step 2. Normalization of the decision matrix. In the WASPAS technique, all experimental data of the measured or calculated responses are first normalized in the range of 0 to 1. This procedure is required since the range units may differ between the responses. In other words, it is necessary to convert the original sequence of data in a compatible sequence of data [13]. Depending on whether data corresponds to non-beneficial (smaller-is-better) or beneficial (larger-is-better) criteria, the following equations are employed.

For larger-is-better criteria:

$$\bar{x}_{ij} = \frac{x_{ij}}{\max x_{ij}} \quad (3)$$

For smaller-is-better criteria:

$$\bar{x}_{ij} = \frac{\min x_{ij}}{x_{ij}} \quad (4)$$

where \bar{x}_{ij} is a dimensionless number between 0 and 1 corresponds to the normalized value of x_{ij} .

Step 3. Calculation of the first criterion of optimality (WSM) using the following equation:

$$WSM = Q_i^{(1)} = \sum_{j=1}^n \overline{x_{ij}} \cdot w_j \quad (5)$$

where w_j is the weight of each criterion. The alternative with the highest $Q_i^{(1)}$ score becomes the preferential choice according to WSM. Weights of responses were determined according to the entropy method.

Step 4. Calculation of the second criterion of optimality (WPM) using the following equation:

$$WPM = Q_i^{(2)} = \prod_{j=1}^n (\overline{x_{ij}})^{w_j} \quad (6)$$

In this case, $Q_i^{(2)}$ denotes the relative importance of the i^{th} alternative based on WPM. Unlike the WSM approach, which strives toward additive aggregation properties, WPM is based on multiplicative aggregation properties. Additionally, the alternative with the highest $Q_i^{(2)}$ value is considered as the most suitable option.

Step 5. In this step the final performance score according to the WASPAS method is calculated. In order to unify the relative importance of WSM and WPM, the relative importance score proposed by Zavadskas et al. [9,10] is applied as shown in the following equation:

$$Q_i = \lambda \cdot Q_i^{(1)} + (1 - \lambda) \cdot Q_i^{(2)} \quad (7)$$

where λ is a coefficient that linearly combines both methodologies. The preferred value is 0.5 since it gives equal relative importance to each methodology and, therefore, this value is employed in this study. When λ takes the value of 0, the alternatives are ranked according to the WPM, and when λ takes the value of 1, the preference ranking is selected according to the WSM.

Step 6. Finally, the optimal parameter settings are obtained according to the Taguchi larger-the-better S/N ratio (Equation 8) of the final performance score for each process parameter at each level. Higher values of the preference score represent better response performances.

$$S / N = -10 \cdot \log \left[\frac{1}{m} \left(\sum_{i=1}^m \frac{1}{y_i^2} \right) \right] \quad (8)$$

3.1 Entropy Method for Weight Criteria Calculation

A very important step in the MCDM methodology is the determination of criteria weights. When using the entropy method to calculate the weight of criteria, the following procedure was adopted to evaluate the criteria weights:

Step 1. Calculate the indicator of normalized values by using Equation (9).

$$p_{ij} = \frac{x_{ij}}{\sum_{i=1}^m x_{ij}} \quad (9)$$

Step 2. Calculate the indicator entropy values by using Equation (10).

$$e_j = -\frac{1}{\ln(m)} \times \sum_{i=1}^m [p_{ij} \times \ln(p_{ij})] \quad (10)$$

Step 3. In the last step the criterion weight is determined according to Equation (11).

$$w_j = \frac{1 - e_j}{\sum_{j=1}^n (1 - e_j)} \quad (11)$$

4. RESULTS AND DISCUSSION

As mentioned in the previous sections, in order to minimize the surface roughness parameters (Ra, Rz, Rmax) and maximize the material removal rate (MRR), the multi-response optimization was performed based on the hybrid WASPAS-Taguchi technique. The following step is to find the performance ranking of all milling experiments according to the WASPAS technique. The performance score for each experiment is determined from the response variables by using Equation (3) through Equation (7). First, the normalized decision matrix for beneficial (larger-is-better) criteria for material removal rate and non-beneficial (smaller-is-better) criteria for the surface roughness parameters is obtained by using Equation (3) and (4), as shown in Table 3.

Table 3. Normalized data, WASPAS weighted performance scores and rankings

Exp. no.	Ra	Rz	Rmax	MRR	Qi ⁽¹⁾	Qi ⁽²⁾	Qi	S/N Ratio	Rank
1	0,477	0,527	0,550	0,041	0,268	0,041	0,155	-16,205	16
2	0,508	0,548	0,505	0,338	0,425	0,124	0,274	-11,236	8
3	0,548	0,672	0,650	1,000	0,812	0,234	0,523	-5,6273	1
4	0,513	0,566	0,554	0,081	0,303	0,060	0,181	-14,827	15
5	0,597	0,636	0,685	0,592	0,612	0,182	0,397	-8,025	2
6	0,549	0,619	0,581	0,286	0,426	0,119	0,273	-11,28	9
7	0,273	0,365	0,375	0,101	0,211	0,053	0,132	-17,589	18
8	0,330	0,466	0,477	0,446	0,429	0,127	0,278	-11,128	6
9	1,000	1,000	0,945	0,303	0,632	0,159	0,396	-8,0541	3
10	0,320	0,416	0,423	0,469	0,424	0,125	0,274	-11,23	7
11	0,747	0,756	0,602	0,068	0,376	0,062	0,219	-13,176	12
12	0,711	0,852	0,928	0,433	0,617	0,174	0,395	-8,0599	4
13	0,367	0,438	0,469	0,355	0,385	0,114	0,249	-12,067	11
14	0,388	0,396	0,315	0,223	0,293	0,084	0,189	-14,476	14
15	0,949	0,923	1,000	0,173	0,552	0,118	0,335	-9,5001	5
16	0,265	0,387	0,415	0,268	0,304	0,089	0,196	-14,143	13
17	0,197	0,275	0,260	0,237	0,237	0,070	0,153	-16,291	17
18	0,545	0,653	0,695	0,216	0,411	0,107	0,259	-11,745	10

Subsequently, by using Equations (5) and (6), the weighted normalized sum model and weighted normalized product model was calculated and given in Table 3. Finally, the performance score values of all milling experiments were calculated according to Equation (7) in order to perform the ranking, as shown in Table 3.

The criteria weight values obtained by the entropy method using Equations (9) to (11) are given in Table 4.

Table 4. Entropy criteria weight values

	Ra	Rz	Rmax	MRR
w_j	0,210	0,128	0,144	0,516

In agreement with the results, the highest performance score obtained according to the WASPAS method is 0,523 at experimental run 3. Since it has the highest value among the considered 18 experiments, it can be ranked as the best choice. The levels for the investigated parameters at experimental run 3 can be shortly given as **A1-B1-C3-D3-E3-F3**. Based on the Taguchi concept, the S/N ratios were calculated in order to identify the optimal input values. In this context, the larger-the-better quality characteristic (Equation 8) was used to calculate the S/N ratios, and its values are

shown in Table 3. The average value of the S/N ratio for the performance score according to WASPAS at each level, for each parameter is given in Table 5.

Table 5. S/N ratios for the performance score

Level	A	B	C	D	E	F
1	-11,5	-11,7	-14,3	-13,0	-14,0	-12,5
2	-12,3	-10,9	-12,3	-11,4	-11,4	-11,9
3	/	-13,1	-9,0	-11,3	-10,2	-11,3
Delta	0,746	2,236	5,299	1,695	3,863	1,16
Rank	6	3	1	4	2	5

Based on the results given in Table 5, it is noticeable that the spindle speed has the greatest influence on the overall performance score, followed by the depth of cut and the cooling environment. Thus, they are ranked as the most influential parameters in the milling process.

The main effect plots for the S/N ratio were generated to graphically represent the effect of the milling parameters on the performance score (Fig. 4). It is clearly shown that the overall performance score drastically increases with the increase of spindle speed, feed rate and depth of cut. This is primarily due to the large value of the weight criteria for MRR.

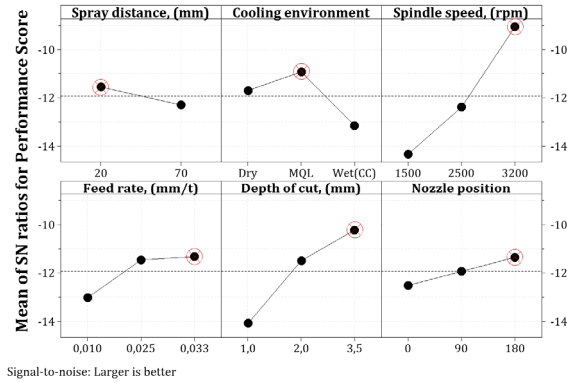


Fig. 4. Main effects plot of S/N ratios for performance score

Fig. 4 also shows the comparison of the performance score under dry, wet and MQL environment. It was found that MQL gives the best results on the performance score. This is mainly because of the lower surface roughness parameters for the MQL cooling environment, probably because of the better penetration ability of oil mist droplets into the chip-tool and tool-workpiece interface. According to [14] the penetration ability of conventional (flood) cooling is limited and it cannot effectively lubricate the interfaces in the cutting zone. On the other hand, oil mist droplets with smaller diameter can directly penetrate into micro-scale fields (capillaries), or they could be vaporized to enter into a capillary [14]. It was found that the spray distance of 20mm, and nozzle position at 180°, found to be the optimal values considering the performance score. Through a comprehensive study of the influence of MQL parameters while milling forged steel using a 20mm end mill, Lutao et. al [15] concluded that the optimal values for the spray distance of 30mm, and the nozzle position relative to the feed direction at 120° give the best results. They conclude that mainly because of this position and spray cone angle the best cooling and lubrication performances are established. Since the results after the S/N analysis are in complete agreement with the previous observation, it can be concluded that the simultaneous optimization of the surface roughness parameters and the MRR in the end-milling operation of AlMgSi1 alloy according to the performance score obtained through the used multi-criteria decision-making method are achieved with the following combination of the investigated parameters: nozzle stand-off

distance of 20 mm; spindle speed of 3200 rpm; feed rate 0,033 mm/tooth; axial depth of cut of 3,5 mm; nozzle position relative to the feed direction of 180° in the MQL cooling environment.

Surface plots for the most dominant parameters were created to further understand the effect of cutting and cooling parameters on the performance score, as shown in Fig. 5, Fig. 6, and Fig. 7.

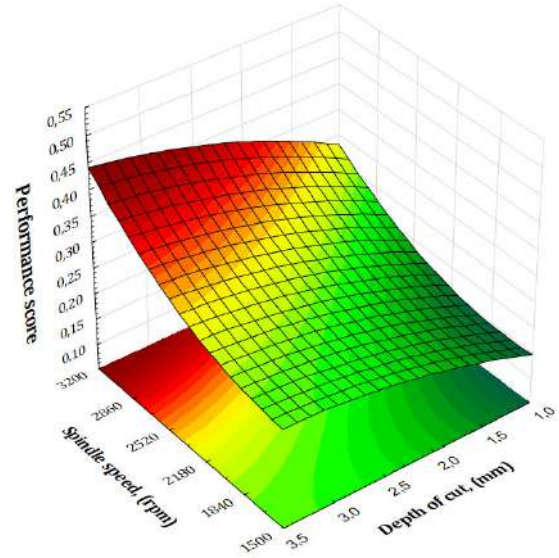


Fig. 5. Surface plot for performance score, depth of cut vs. spindle speed

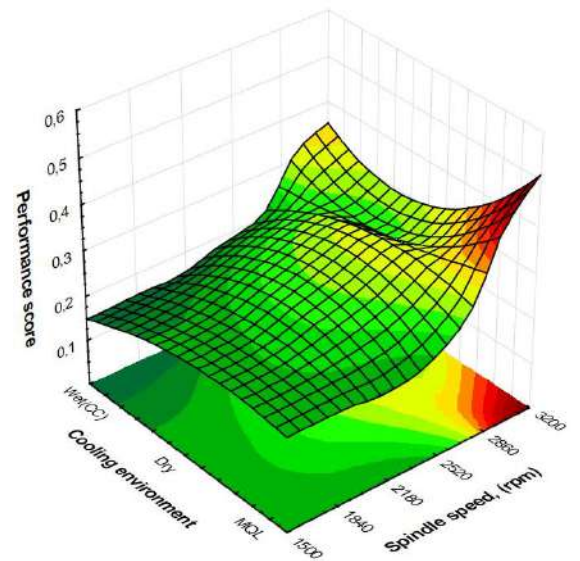


Fig. 6. Surface plot for performance score, cooling environment vs. spindle speed

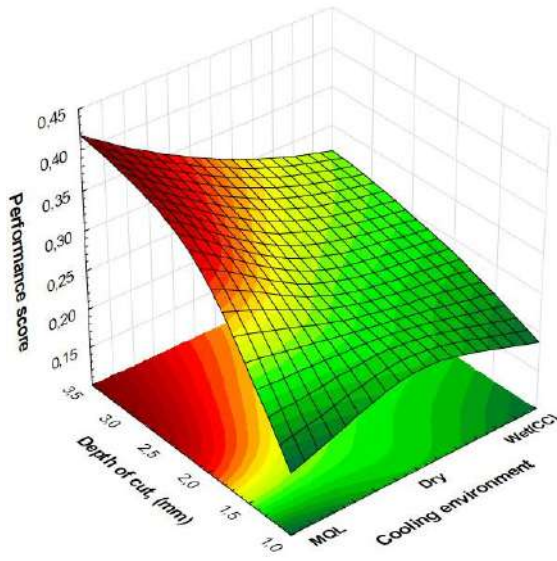


Fig. 7. Surface plot for performance score, cooling environment vs. depth of cut

Table 6. ANOVA for S/N ratio of performance score

Source	DF	Seq SS	Contribution	Adj SS	Adj MS	F-Value	P-Value	Remarks
Spray distance, (mm)	1	2,506	1,36%	2,506	2,506	0,82	0,399	Not significant
Cooling environment, (/)	2	15,471	8,43%	15,471	7,736	2,54	0,159	Not significant
Spindle speed, (rpm)	2	86,17	46,93%	86,17	43,085	14,16	0,005	Significant
Feed rate, (mm/t)	2	10,622	5,79%	10,622	5,311	1,75	0,253	Not significant
Depth of cut, (mm)	2	46,534	25,34%	46,534	23,267	7,65	0,022	Significant
Nozzle position, (deg)	2	4,048	2,20%	4,048	2,024	0,67	0,548	Not significant
Error	6	18,257	9,94%	18,257	3,043			
Total	17	183,607	100,00%					

4.1 Comparative MCDM method analysis

The optimized milling parameters, shortly given as A1-B1-C3-D3-E3-F3 obtained based on the proposed hybrid WASPAS-Taguchi methodology were compared with several other multi-criteria decision-making methods. For this analysis, the methods that according to [16] were the most frequently used in various fields in the last decade were MARCOS (Measurement of Alternatives and Ranking According to Compromise Solution), MABAC (Multi-Attributive Border Approximation Area Comparison) and CoCoSo (Combined Compromise Solution).

Summary of ranking results for selected MCDM methods are shown in Table 7.

Based on the given ranking results for different MCDM methods, it is clear that experimental

The analysis of variance (ANOVA) was performed at 95% confidence level in order to check the statistical significance of the investigated milling parameters on the performance score.

Summary of the ANOVA analysis for S/N ratio of the performance score is given in Table 6.

The results of ANOVA indicate that the highest variation on the performance score comes from the spindle speed and depth of cut, followed by the cooling environment, with percentage contribution of 46,93%, 25,34% and 8,43%, respectively. Lastly, the parameter with the least influence was the spray distance with 1,36% contribution.

Based on the p-value, it can be concluded that only spindle speed and depth of cut have significant effect on the performance score.

run 3 for each tested method is the best option among 18 experiments.

The very last step in the MCDM method analysis is the step of consistency. The main goal of the consistency analysis is to compare the degree of association between ranks using various MCDM methods. In this step the Spearman's rank correlation coefficient was used, which can be determined by using the following equation:

$$R_{sp} = 1 - \frac{6 \cdot \sum_{i=1}^m D_i^2}{m(m^2 - 1)} \quad (12)$$

where m is the number of alternatives and D is the difference between ranks. Spearman's rank correlation coefficient for rankings obtained using WASPAS, MARCOS, MABAC, and CoCoSo method is given in Table 8.

Table 7. Ranking options based on different MCDM methods using entropy weight criteria values

Exp. no.	WASPAS	MARCOS	MABAC	CoCoSo
1	16	16	14	16
2	8	8	7	6
3	1	1	1	1
4	15	14	13	13
5	2	4	2	2
6	9	7	6	7
7	18	18	17	17
8	6	6	9	8
9	3	2	4	4
10	7	9	10	10
11	12	12	12	12
12	4	3	3	3
13	11	11	11	11
14	14	15	15	15
15	5	5	5	5
16	13	13	16	14
17	17	17	18	18
18	10	10	8	9

Table 8. Spearman's rank correlation coefficient

	WASPAS	MARCOS	MABAC
MARCOS	0,983		
MABAC	0,944	0,959	
CoCoSo	0,967	0,977	0,988

According to Table 8, the highest correlation coefficient is 0,988 for MABAC and COCOSO and the lowest is 0,944 for WASPAS and MABAC. The correlations for all other methods are in a very strong correlation.

5. CONCLUSIONS

In the present research, a parametric optimization of the milling parameters was presented by using a hybrid WASPAS-Taguchi technique while machining AlMgSi1 alloy. The entropy method was used to calculate the weight of the selected criteria (surface roughness parameters and the material removal rate). At the same time, six process and cooling/lubrication parameters, including the spindle speed, feed rate, depth of cut, nozzle spray distance, nozzle position relative to the milling direction, and the cooling environment (dry, MQL and conventional) were chosen as the input parameters. For the experimental design,

the Taguchi L18 orthogonal array ($2^1 \times 3^5$) was chosen. From the study results the following conclusions can be drawn:

1. Based on the WASPAS-Taguchi experimental methodology the milling parameters, as well as the cooling/lubrication parameters were simultaneously optimized through a single performance score grade. Experimental run 3 turned out to be the best option among 18 alternatives. In this connection, the optimal parameter levels obtained were: nozzle stand-off distance of 20 mm; spindle speed of 3200 rpm; feed rate 0,033 mm/tooth; axial depth of cut of 3,5mm; nozzle position relative to the milling direction of 180° in the MQL cooling environment.
2. The ranking of the parameters according to the degree of influence on the performance scores can be arranged as: spindle speed, depth of cut, cooling environment, feed rate, nozzle position, and lastly the spray distance.
3. The most dominant parameters on the performance scores were the spindle speed, depth of cut and the cooling environment (MQL technique).
4. ANOVA results showed that the spindle speed and the axial depth of cut were the only statistically significant parameters on the performance score with a contribution of 46,93% and 25,35%, respectively.
5. The comparative analysis with other MCDM methods presented through the Spearman's correlation coefficient showed strong correlation among all used methods.

Acknowledgement

The authors would like to express their gratitude to BOJO-METAL d.o.o Kiseljak, for the possibility of performing the cutting experiments and necessary measurements.

REFERENCES

- [1] Tosun, N., Pihtili, H. (2010). Gray relational analysis of performance characteristics in MQL milling of 7075 Al alloy. *International Journal of Advanced Manufacturing Technology*, vol. 56, p. 509-515. DOI: [10.1007/s00170-009-2118-4](https://doi.org/10.1007/s00170-009-2118-4).
- [2] Dhar, N.R., Kamruzzaman, M., Ahmed, M. (2006). Effect of minimum quantity lubrication (MQL) on tool wear and surface roughness in turning AISI-4340 steel. *Journal of Materials and Processing Technology*, vol. 172, no. 2, p.

- 299-304. DOI: [10.1016/j.jmatprotec.2005.09.022](https://doi.org/10.1016/j.jmatprotec.2005.09.022).
- [3] Wakabayashi, T., Suda, S., Inasaki, I., Terasaka, K., Musha, Y., Toda, Y. (2007). Tribological action and cutting performance of MQL media in machining of aluminum. *CIRP Annals – Manufacturing Technology*, vol. 56, no. 1, p. 97-100. DOI: [10.1016/j.cirp.2007.05.025](https://doi.org/10.1016/j.cirp.2007.05.025).
- [4] Parameshwaran, R., Praveen Kumar, S., Saravanakumar, K. (2015). An integrated fuzzy MCDM based approach for robot selection considering objective and subjective criteria. *Applied Soft Computing*, vol. 26, p. 31-41. DOI: [10.1016/j.asoc.2014.09.025](https://doi.org/10.1016/j.asoc.2014.09.025).
- [5] Gul, M., Guven, B., Guneri, A.F. (2018). A new Fine-Kinney-based risk assessment framework using FAHP-FVIKOR incorporation. *Journal of Loss Prevention Process Industries*, vol. 53, p. 3-16. DOI: [10.1016/j.jlp.2017.08.014](https://doi.org/10.1016/j.jlp.2017.08.014).
- [6] Sennaroglu, B., Varlik Celebi, G. (2018). A military airport location selection by AHP integrated PROMETHEE and VIKOR methods. *Transportation Research Part D: Transport Environment*, vol. 59, p. 160-173. DOI: [10.1016/j.trd.2017.12.022](https://doi.org/10.1016/j.trd.2017.12.022).
- [7] Egle, Š.; Jurgita, A. (2013). Solving the problems of daylighting and tradition continuity in a reconstructed vernacular building. *Journal of Civil Engineering and Management*, vol. 19, no. 6 p. 873-882. DOI: [10.3846/13923730.2013.851113](https://doi.org/10.3846/13923730.2013.851113).
- [8] Sudhagar, S., Sakthivel, M., Mathew, P.J., Daniel, S.A.A (2017). A multi criteria decision making approach for process improvement in friction stir welding of aluminium alloy. *Measurement*, vol. 108, p. 1-8. DOI: [10.1016/j.measurement.2017.05.023](https://doi.org/10.1016/j.measurement.2017.05.023).
- [9] Zavadskas, E.K., Turskis, Z., Antucheviciene, J., Zakarevicius, A. (2012). Optimization of weighted aggregated sum product assessment. *Elektronika Ir Elektrotechnika*, vol. 122, no. 6, p. 3-6. DOI: [10.5755/j01.eee.122.6.1810](https://doi.org/10.5755/j01.eee.122.6.1810).
- [10] Zavadskas, E.K., Antucheviciene, J., Razavi Hajiagha, S.H., Hashemi, S.S. (2014). Extension of weighted aggregated sum product assessment with interval-valued intuitionistic fuzzy numbers (WASPAS-IVIF). *Applied Soft Computing*, vol. 24, no. 6, p. 1013-1021. DOI: [10.1016/j.asoc.2014.08.031](https://doi.org/10.1016/j.asoc.2014.08.031).
- [11] Singh, S., Upadhyay, S.P., Powar, S. (2022). Developing an integrated social, economic, environmental, and technical analysis model for sustainable development using hybrid multi-criteria decision-making methods. *Applied Energy*, vol. 308, 118235. DOI: [10.1016/j.apenergy.2021.118235](https://doi.org/10.1016/j.apenergy.2021.118235).
- [12] Karande, P., Zavadskas, E.K., Chakraborty, S. (2016). A study on the ranking performance of some MCDM methods for industrial robot selection problems. *International Journal of Industrial Engineering Computations*, vol. 7, p. 399-422. DOI: [10.5267/j.ijiec.2016.1.001](https://doi.org/10.5267/j.ijiec.2016.1.001).
- [13] Palanikumar, K. (2011). Experimental Investigation and optimization in drilling of GFRP composites. *Measurement*, vol. 44, no. 10, p. 2138-2148. DOI: [10.1016/j.measurement.2011.07.023](https://doi.org/10.1016/j.measurement.2011.07.023).
- [14] Obikawa, T., Asano, Y., Kamata, Y. (2009). Computer fluid dynamics analysis for efficient spraying of oil mist in finish turning of Inconel 718. *International Journal of Machine Tools and Manufacture*, vol. 49, no. 12-13, p. 971-978. DOI: [10.1016/j.ijmachtools.2009.06.002](https://doi.org/10.1016/j.ijmachtools.2009.06.002).
- [15] Luta, Y., Songmei, Y., Qiang, L. (2012). Influence of Minimum Quantity Lubrication Parameters on Tool Wear and Surface Roughness in Milling Forged Steel. *Chinese Journal of Mechanical Engineering*, vol. 26, no. 3.
- [16] Büşra, A., Seda, A. (2022). Bibliometric Analysis of the MCDM Methods in the Last Decade: WASPAS, MABAC, EDAS, CODAS, COCOSO, and MARCOS. *International Journal of Business & Economic Studies*, vol. 4, no.2, p. 66-85. DOI: [10.54821/uiecd.1183443](https://doi.org/10.54821/uiecd.1183443).



Banja Luka
1–2 Jun 2023.

DEMI 2023

16th International Conference on Accomplishments in Mechanical and Industrial Engineering

www.demi.mf.unibl.org



Programming methods and program verification for 3-axis reconfigurable hybrid kinematics machine

S. Zivanovic^a, G. Vasilic^b, Z. Dimic^c, N. Vorkapic^a, B. Kokotovic^a, N. Slavkovic^a

^aUniversity of Belgrade, Faculty of Mechanical Engineering, Serbia

^bAcademy of technical vocational studies, Belgrade, Serbia

^cLOLA Institute, Belgrade, Serbia

Abstract *This paper presents programming methods and program verification for the 3-axis reconfigurable hybrid kinematics machine MOMA V3, which represents an educational desktop milling machine with a horizontal position of the main spindle. The paper considers the different programming and program verification methods, including parts machining.*

Keywords *programming, CAD/CAM, STEP-NC, STL, verification, virtual machine, reconfigurable, hybrid kinematic machine*

1. INTRODUCTION

This paper considers the 3-axis machine with hybrid kinematics, which was created as a result of upgrading the 2-axis reconfigurable parallel mechanism by adding a serial translatory axis [1].

The concept of the 3-axis reconfigurable machine with hybrid kinematics, presented in this paper, is based on [2]: (i) a 2-axis reconfigurable parallel mechanism developed as a modular system; (ii) a generalized kinematic model of the applied 2-axis reconfigurable parallel mechanism; (iii) open architecture control system based on LinuxCNC (EMC2); (iv) quick and easy reconfiguration of hardware and control system; (v) the possibilities of using different programming methods; (vi) virtual machine configured in object-oriented programming language Python

and implemented in the control system for program verification.

This paper presents part of the research related to the programming methods for considered machine and testing during trial work.

2. RECONFIGURABLE HYBRID KINEMATICS MACHINE MOMA V3

MOMA V3 is established as a modular system on the basis of which the reconfiguration of both the hardware and software parts of the system can be performed.

The parallel mechanism is based on the modular principle, while its reconfigurability is reflected in the fact that the mutual position of modules of the translatory axis can be changed (rotation around the passive rotating axes, for angles α_1 and α_2), and it is also possible to change the lengths of the legs since there is a family of different legs lengths in three nominal sizes ($l_i = 250, 195$ and 180 mm). The configuration of the parallel mechanisms can be easily and quickly changed according to the building program [3].

Corresponding author

Prof. dr Saša Živanović
szivanovic@mas.bg.ac.rs

University of Belgrade, Faculty of Mechanical
Engineering, Belgrade, Serbia

As a basis for building a 3-axis reconfigurable machine with hybrid kinematics, selected types of 2-axis reconfigurable parallel mechanisms with an additional serial translatory axis are used, which is shown in Fig.1.

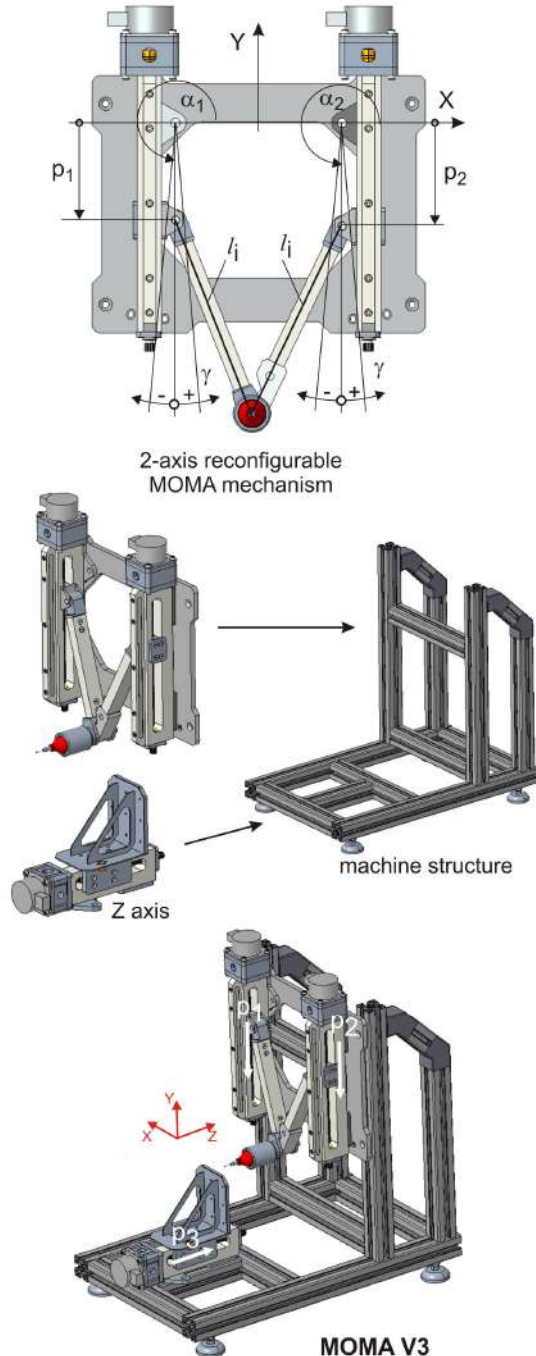


Fig. 1. MOMA V3 – 3 axis reconfigurable hybrid kinematics machine

This machine represents a horizontal milling machine with a main spindle that is driven by a reconfigurable parallel mechanism along the X

and Y axes, while the workpiece is moved along the Z axis (p3).

3. PROGRAMMING METHODS AND PROGRAM VERIFICATION

The paper considers various methods of programming the machine, suitable for education and rapid prototyping by subtractive processes. This approach can be considered a flexible programming method, which depends on the specificity of the machining task. The available standardized CAD/CAM system PTC Creo is used as the usual programming method. A specialized CAM (CUT 3D) is used for programming based on STL, for rapid prototyping. The application of the new programming method, better known as object-oriented programming or programming using the STEP-NC protocol, is also analyzed.

3.1 CAD/CAM

The basic structure of the system for programming using the CAD/CAM system [4] is shown in Fig.3.

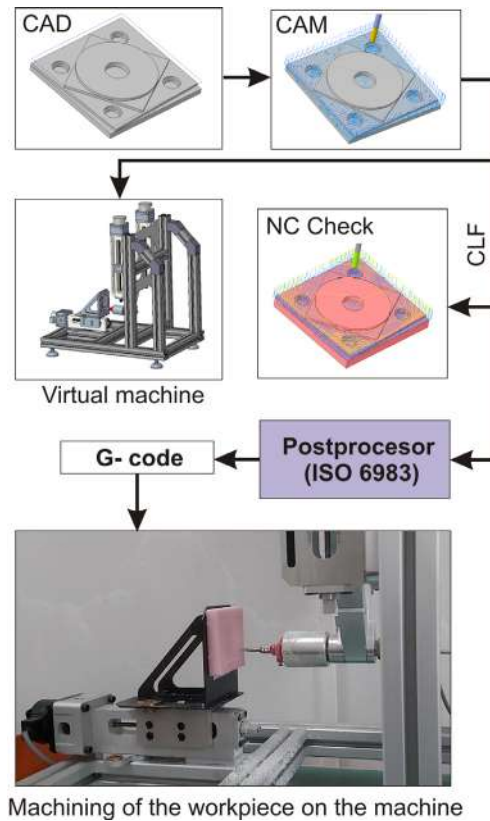


Fig. 2. Programming method based on CAD/CAM system (PTC Creo)

Toolpath verification is possible by simulating moving tools along the tool path, material removal simulating, and simulating the working of virtual machine according to the given program in CLF format. Postprocessing is performed for a 3-axis horizontal milling machine, where G code is obtained according to the ISO6983 standard, which in this case is similar in format to programs for Fanuc CNC systems [4].

The model for the first part planned for machining is a part for testing the accuracy of CNC machine tools according to the ISO 10791-7:1998 standard. This part is scaled to fit the dimensions of the considered machine's workspace. The machining of this part is shown in section 4.

The model of this trial part was used in section 3.2 to prepare the program according to the new programming method based on the STEP-NC protocol.

3.2 Programming based on STL files

The considered machine belongs to the category of desktop milling machines that are used for rapid prototyping. In that case, a subtractive process is used, where part fabrication starts with a single block of solid material larger than the final size of the desired object, and the material is removed layer by layer until the desired shape is reached [5].

A typical programming method based on STL files is shown in Fig. 3. First of all, need to prepare the model and convert it to STL format. An example of programming method used specialized software CUT 3D [6] for programming which is based on an STL file.

Programming includes the following stages: (1) loading of STL file and setting orientation and model size; (2) adjustment of the dimensions of the workpiece and the zero point; (3), (4), (5) planning roughing, finishing and cut out a strategy for milling; (6) preview machining – material removal simulation; (7) save toolpaths in G-code using appropriate postprocessor.

After transferring the program to the machine and preparing the machine for work, the fabrication of the prototype using desktop milling follows.

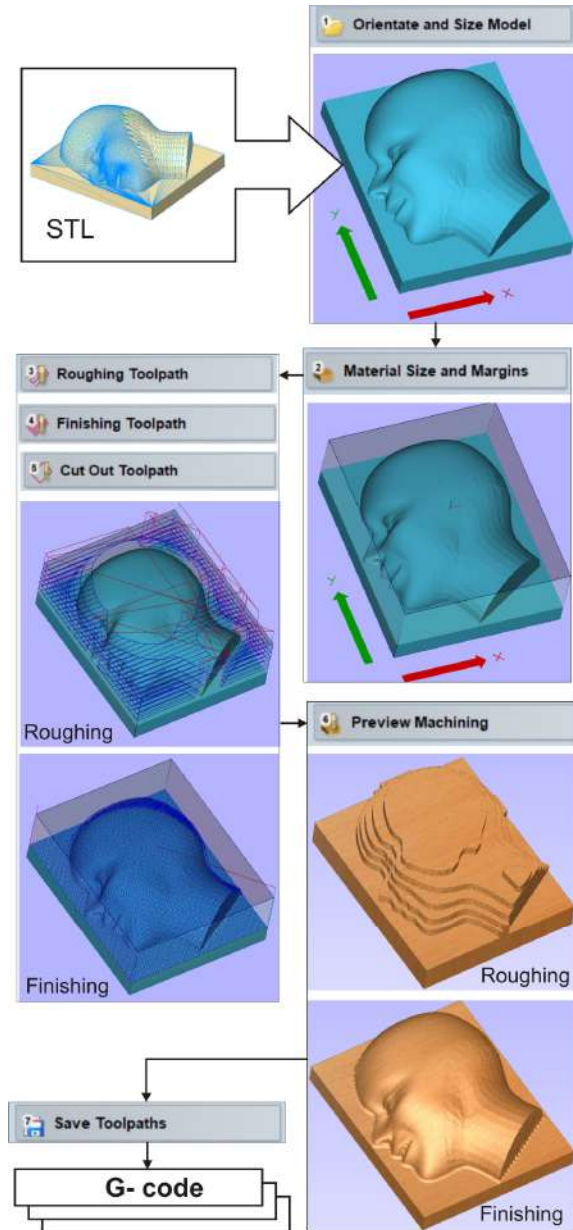


Fig. 3. Programming method based on STL files (Cut3D)

3.2 STEP-NC

This paper also discusses the programming method of the CNC machine tools based on ISO 10303-238 (AP-238) known as STEP-NC (Standard for Product Model Data Exchange for Numerical Control) [7], on the example of a 3-axis reconfigurable hybrid kinematic machine. Today a new standard, STEP-NC, is being used as the basis for the development of the next generation of CNC controllers. The new STEP-compliant NC standard (STEP-NC) is based on the Standard for Exchange of Product data

model (STEP) and has been developed to overcome the shortcomings of G-code [8,9]. The STEP-NC provides object and feature-oriented programming methods and describes the machining operations executed on the workpiece, and not machine-dependent axis motions. It will be running on different machine tools or controllers [10]. If the CNC machine tool can interpret only G-code, corresponding translators or converters will be able to postprocess the STEP-NC program into different NC program types.

At the moment, for most users, this new method of programming based on STEP-NC cannot be completely used with all the benefits provided by STEP-NC, because the resources for its development are not available to everyone [11]. This section shows two possible scenarios (Sc1, Sc2) [8,11] for the indirect programming method based on STEP-NC which is verified on the considered machine, Fig 4.

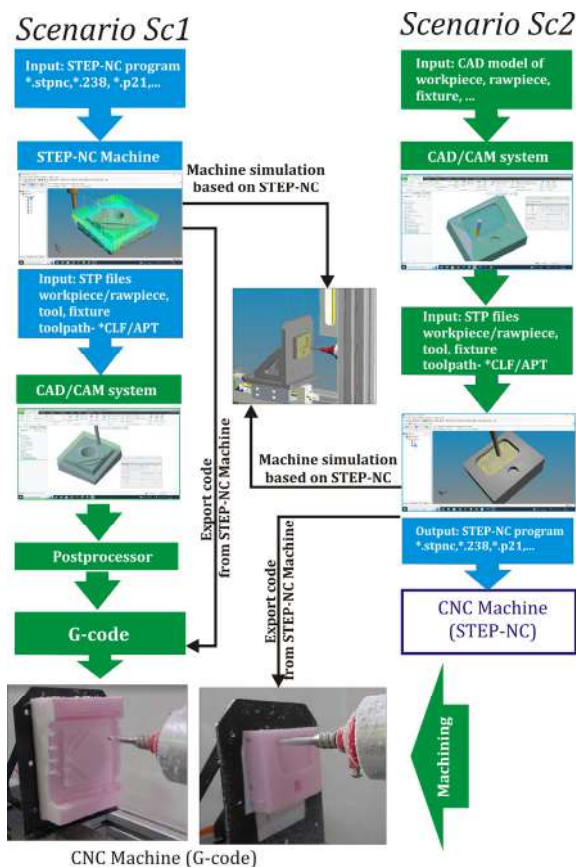


Fig. 4. Scenarios for programming based on STEP-NC

These scenarios are [8]:

Scenario 1 - using the native STEP-NC program, post-processing or converting the STEP-NC program into G-code and executing on the

machine tool which is only able to interpret G-code files.

Scenario 2 - enables the generation of STEP-NC programs based on information from the available CAD/CAM system and licensed software STEP-NC Machine, to exchange technology and machining capabilities on machines that can directly interpret STEP-NC programs, but also on machines that can only execute G code using the first scenario.

Both scenarios [8] were tested on the 3-axis reconfigurable hybrid kinematic machine, by translating the original STEP-NC program to G-code for Fanuc CNC systems, while for scenario 2, an indirect programming method was used to generate the STEP-NC program, which is finally also converted to G code for machining process according to scenario 1.

4. VIRTUAL MACHINE IN CONTROL SYSTEM

The virtual machine has a significant role when developing a control system, primarily for machines that have hybrid kinematics, where it is necessary to integrate solutions of inverse and direct kinematics [1]. In this case, the virtual machine was integrated with the LinuxCNC control system. The basic concept of a configuring virtual machine in the control system is detailed shown in [2].

Configuring a virtual machine is realized under the LinuxCNC software environment and relies on OpenGL and several interface classes written in Python programming language. Python is an interpreted programming language, suitable for scripting tasks, such as the development and configuration of virtual environments [2].

Based on the developed 2-axis reconfigurable virtual machine [2], an upgrade of the virtual machine was realized by adding a serial translatable axis and a new supporting structure of the machine.

New models of machine components were imported in ASCII STL format and are connected according to the kinematic model. The file for kinematics was also corrected by implementing an additional serial translatable axis and adjusting the directions of the coordinate axes according to the standard for machines with a horizontal main spindle.

When the virtual machine is configured and integrated within the control system during the execution of the machining program, the virtual machine components are moving identically as

on a real machine, which was confirmed by machining experiments in section 5.

The illustration of the operation of the virtual machine is shown in Fig. 5, on the example for which the program was prepared by manual programming, and the machining itself on the machine is shown in Fig. 6.

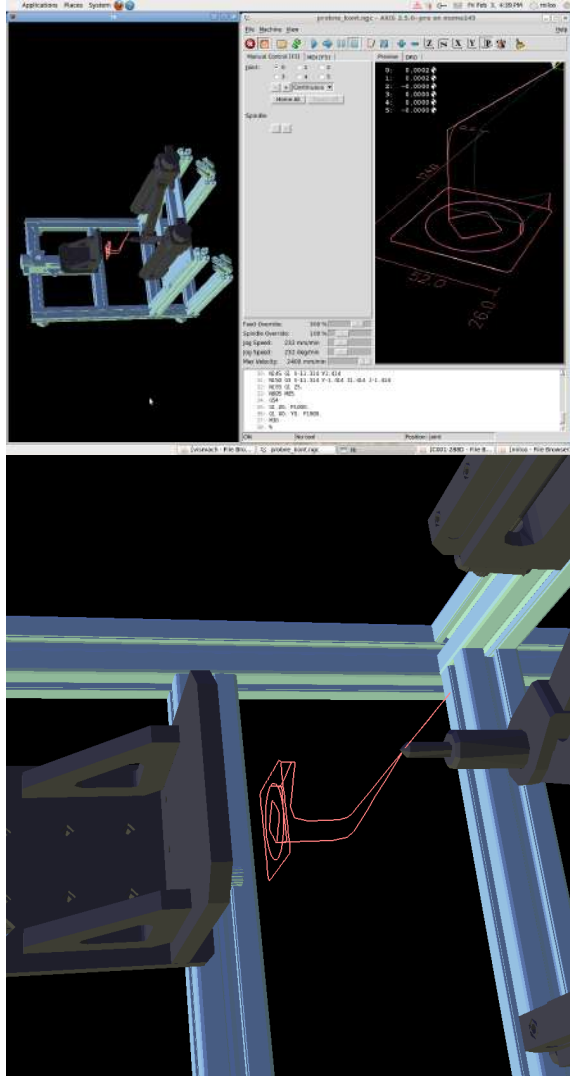


Fig. 5. Virtual machine integrated with control system LinuxCNC

The presented simulation is shown for the initial variant of the machine, which is active after switching on with parameters $\alpha_1 = \alpha_2 = 270^\circ$, and the lengths of the legs are 250 mm.

Virtual machine can easily reconfigure using the G code command because in virtual model implemented additional passive virtual axes for reconfiguration. The first two virtual driven axes are connected to the orientation of driven axes, are labelled as A and B, and take values

of angles γ_i ($\gamma_1 = A$; $\gamma_2 = B$). The third virtual driven axis is labelled as C and is associated with leg length ($l=C$), Fig.6.

The result of such an approach to configuring the control is a reconfigurable virtual machine in Python 3D environment, integrated with graphic interface Axis. Initial configuration, has parameters length of leg $l_1 = l_2 = 250$ mm and driven axes parallel to Y axis, ($A=0$, $B=0$), Fig. 6a. Changing the machine configuration is done using standard G-code functions using - manual data input (MDI). Examples of configurations and adequate G-code commands reconfiguring four configurations are shown in Fig. 6.

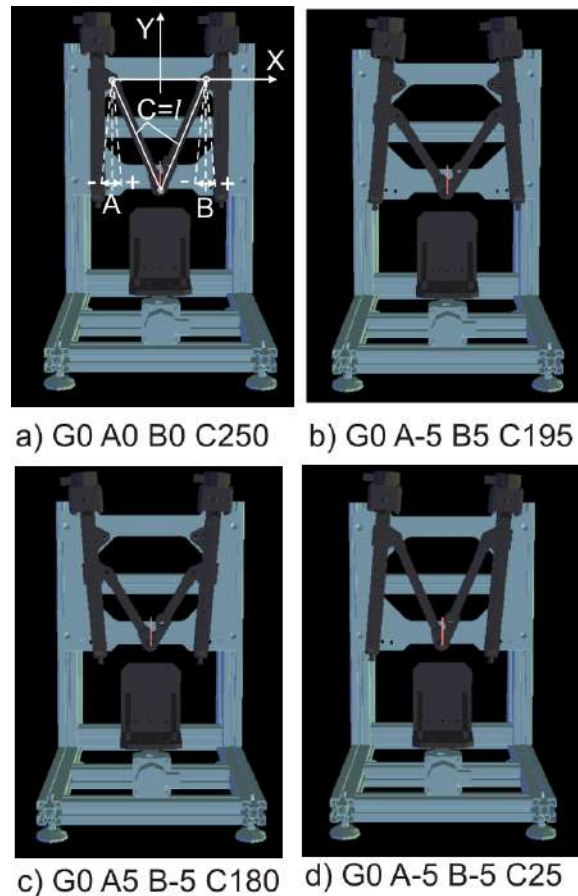


Fig. 6. Reconfigurable virtual machine with additional passive virtual axes

The virtual machine configured runs like a real machine and can be applied for verification of the program, before machining on a real machine. Also, this kind of virtual machine can be used for testing developed control, and analysis of machine operation before to its building.

5. MACHINING TESTS ON MACHINE TOOL MOMA V3

The verification of the prototype of the MOMA V3 machine was achieved during the trial run by testing different programming methods and machining the selected workpieces.

The trial work includes a complete check of the preparation of the machine for work, such as: checking the kinematics file in the control system according to the installed configuration of the machine, compiling the control, moving the machine to the reference position, setup of the workpiece within the boundaries of the workspace, determining the zero point, loading the program (G-code), testing program on the virtual machine (in the control system) and finally processing the part on the machine.

During the trial run, several groups of different parts were machined. Machined parts can be classified into parts of 2D and 2.5D geometry and 3D parts with sculptural surfaces.

In addition to the discussed programming methods, manual programming was also used for machining 2D circular and square contours to quickly check the accuracy and shape of the machined contours, Fig.7. For all samples, the trial machining was carried out in the soft material using the flat endmill tool with a diameter of 4 mm.

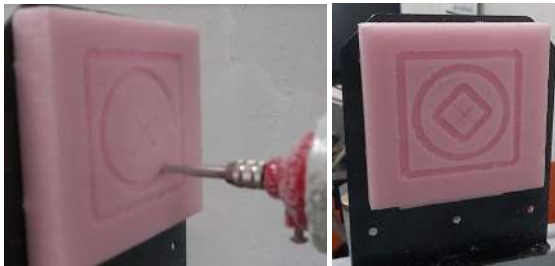


Fig. 7. Machining test 1, Manual programming – 2D test

The following is an example from Fig.8, which refers to a scaled and adapted workpiece for testing the working accuracy of CNC machine tools (according to the ISO 10791-7:1998 standard), which was machined and shown in Fig. 6b.

For the new programming method, both scenarios were tested for the application of the STEP-NC protocol. For scenario 1, the original STEP-NC program for machining the test part NAS979 was machined, Fig.9a. The possibility of translating the STEP-NC program into G-code

and additional scaling due to the adaptation of the dimensions of the test part to the workspace of the machine was used.

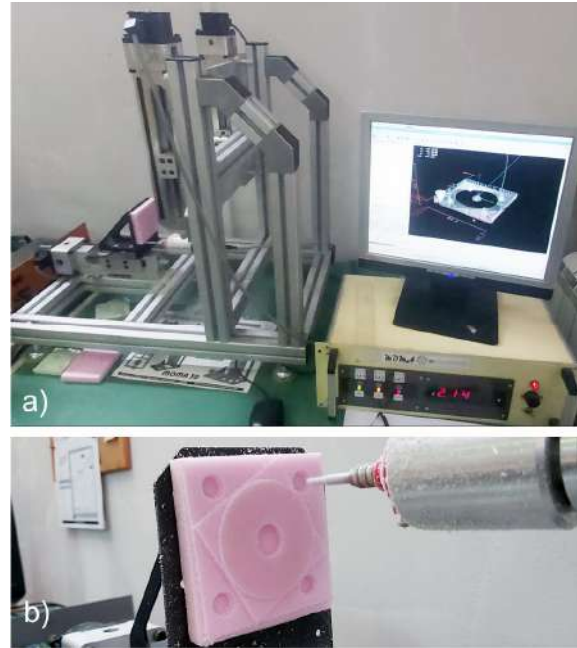


Fig. 8. Machining test 2, CAD/CAM programming method – 2.5D test

An example of scenario 2, where the STEP-NC program was generated for three operations (working steps - WS): WS_1 milling of a flat surface, WS_2 milling of a cylindrical pocket, and WS_3 milling of a rectangular pocket, Fig.9b. Before the generation of the STEP-NC program, the models of the workpiece, rawpiece, and tool in STEP format, as well as the tool path (CLF) in the CAD/CAM system PTC Creo, were previously prepared. These data were integrated into the STEP-NC Machine software, after which the machining simulation was started.

A simulation of machining a part on a MOMA V3 virtual machine loaded from the machine library as a newly added machine, previously configured in the STEP-NC Machine environment [4], is shown in Fig.9b. After the simulation on the virtual machine in the STEP-NC Machine environment, the program was translated to G code using the export option to generate the Fanuc G-code that was loaded into the machine control, after which the machining of the part was realized.

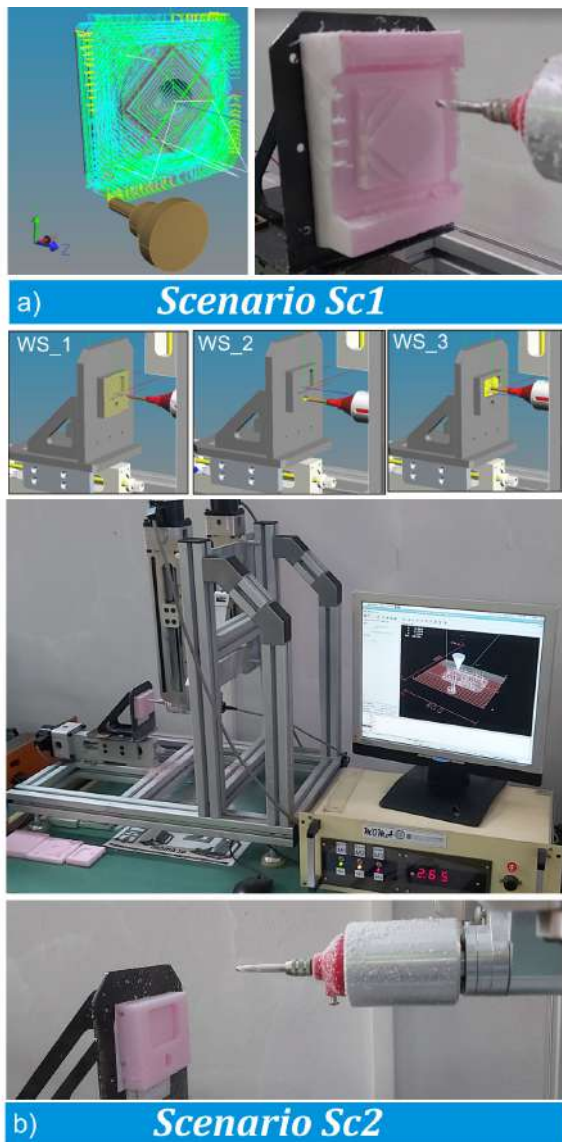


Fig. 9. Machining test 3, STEP-NC

An example of machining parts of sculptural forms, as 3D geometry, is shown in the example of machining the profile of the human head (Fig.3), where the model is in STL format, which corresponds to the programming of machines for rapid prototyping. An example of this machining is shown in Fig.10. In this case, pre-machining is first carried out by removing the material by layers (Fig.10b,c), after which the final machining follows, to remove the characteristic stepped surface and obtain a smooth surface of the workpiece (Fig.10d,e). Based on the milling selected parts carried out during the test operation of the machine, it can be concluded that the configuration of the prototype of the new machine with hybrid

kinematics, as well as the appropriate developed control system for this machine, are correct, i.e., the virtual machine gives a faithful representation of the toolpath as on the real machine. Based on the performed experiments, it can be observed the suitability of the considered machine for: (i) practicing work on reconfigurable machining systems, (ii) verification of the NC program (G-code) on a virtual machine before its execution on the actual machine, (iii) practicing work in reconfiguring the control system when the machine configuration changed, (iv) education for programming with different programming methods.

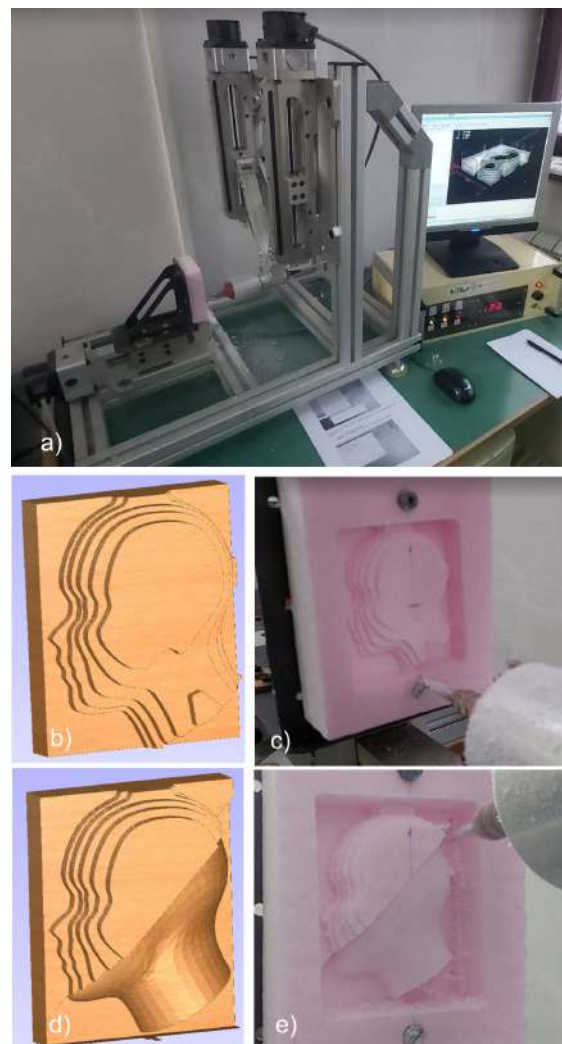


Fig. 10. Machining test 4, 3D tests, programming method based on STL files

6. CONCLUSION

The paper presents programming methods and testing of a horizontal 3-axis reconfigurable machine with hybrid kinematics, which contains a reconfigurable parallel mechanism MOMA that in combination with a serial translational axis, can represent a realistic concept for the construction of industrial machines of this type. The machine presented in this paper is an educational, laboratory-type machine with an open architecture control system (LinuxCNC). The considered 3-axis reconfigurable machine with hybrid kinematics MOMA V3 follows current trends in the development of modern machine tools such as: (i) modernization of the mechanical structure in terms of introducing new concepts of machine tools based on parallel and hybrid kinematics; (ii) adaptation to the specific needs of certain branches of industry, by introducing reconfigurable and adaptable machine tools; (iii) application of the developed machine in education and research; (iv) consideration of new methods in CNC programming, based on the STEP-NC protocol; (v) adoption of digitization and virtualization approaches by the globally adopted strategies for improving industrial production under the Industry 4.0 paradigm.

Acknowledgement

The presented research was supported by the Ministry of Education, Science and Technological Development of the Republic of Serbia through the project "Integrated research in macro, micro, and nano mechanical engineering" (contract no. 451-03-47/2023-01/200105 dated 3 February 2023).

REFERENCES

- [1] Vasilic, G., Zivanovic, S., Kokotovic, B. (2017). Modelling and analysis of 3-axis reconfigurable hybrid kinematics mechanism with translatory actuated joints, Proceedings of 5th International Conference on Advanced Manufacturing Engineering and Technologies, NEWTECH 2017, Editors: Majstorovic, V., Jakovljevic, Z., Lecture Notes in Mechanical Engineering, pp. 429-441, 5th – 9th June 2017, Belgrade, Serbia, Springer International Publishing AG 2017.
- [2] Vasilic, G., Zivanovic, S., Kokotovic, B., Dimic, Z. (2019). Configuring and analysis of a class of generalized reconfigurable 2-axis parallel kinematic machine. *Journal of Mechanical Science and Technology*, vol. 33, no.7, pp.3407-3421.
- [3] Živanović S., Vasilić, G. (2014). Variants of configuring the 2-axis reconfigurable parallel mechanism - MOMA, Proceedings of 2nd International Scientific Conference on Mechanical Engineering Technologies and Applications COMETA 2014, pp.33-40, University of East Sarajevo, Faculty of Mechanical Engineering, Jahorina, RS, B&H.
- [4] Živanović, S., Vasilić, G., Kokotović, B., Vorkapić, N., Dimić, Z., Slavković, N. Configuring and verification of a reconfigurable machine with hybrid kinematics MOMA V3. *Proceedings of the 6th Int. Conference on Mechanical Engineering Technologies and Applications COMETA2022*, November 2022, University of East Sarajevo Faculty of Mechanical Engineering, East Sarajevo-Jahorina, RS, B&H, p.17-19.
- [5] Zivanovic S., Popovic M., Vorkapic N., Pjevic M., Slavkovic N. (2020). An Overview of Rapid Prototyping Technologies using Subtractive, Additive and Formative Processes, *FME Transactions*, vol. 48, no.1, p. 246-253.
- [6] Cut 3D, From: <https://www.vectric.com/products/cut3d>, accessed on: February 1, 2023.
- [7] Step Tools, Inc., From: <http://www.steptools.com/>, accessed on: February 1, 2023.
- [8] Zivanovic, S., Slavkovic, N. (2021). Programming of machine tools and robots for machining using STEP-NC in the era of Industry 4.0, Keynote Lecture, *Proceedings of the 15th International Conference on Accomplishments in Mechanical and Industrial Engineering DEMI 2021*, May, 2021, University of Banjaluka, Faculty of Mechanical Engineering, p. 3-26.
- [9] Bonnard R., Hascoët J.Y., Mognol P. Stroud I. (2018). STEP-NC digital thread for additive manufacturing: data model, implementation and validation. *International Journal of Computer Integrated Manufacturing*, p. 1–20.
- [10] Sääski, J., Salonen, T., Paro, J., Integration of CAD/CAM and NC with STEP-NC, VTT Information Service, Finland. From: <https://publications.vtt.fi/pdf/workingpapers/2005/W28.pdf>, accessed on: February 1, 2023.
- [11] Živanović, S., Glavonjić, M. (2014). Methodology for implementation scenarios for applying protocol STEP-NC. *Journal of Production Engineering*, vol.17, no.1, p. 71-74.



Banja Luka
1–2 Jun 2023.

DEMI 2023
**16th International Conference on
Accomplishments in Mechanical and
Industrial Engineering**
www.demi.mf.unibl.org



Structure and mechanical properties of MIG welded butt-joints of aluminum alloy 2024 T351

D. Milčić^a, M. Milčić^a, D. Klobčar^b, A. Đurić^c, N. Zdravković^a

^aFaculty of Mechanical Engineering, University of Niš, Aleksandra Medvedeva 14, 18000 Niš, Serbia

^bFaculty of Mechanical Engineering, University of Ljubljana, Aškerčeva cesta 6, 1000 Ljubljana, Slovenia

^cUniversity of East Sarajevo, Faculty of Mechanical Engineering, Vuka Karadžića 30, 71123 East Sarajevo, Bosnia and Herzegovina

Abstract This article presents an assessment of the structure and the mechanical properties of butt joint of aluminum alloy 2024 T351 welded with the MIG welding method. The shielding gas used was a mixture of argon and helium. The macro- and microstructures were evaluated by means of a light microscope and a scanning electron microscope using metallographic specimens cut along a plane perpendicular to the welding direction. The mechanical properties of joints have been evaluated on the basis of hardness distribution in the joints and tests of the bending and tensile strength of weld joints.

Keywords Aluminum alloy 2024 T351, TIG welding, Microstructure, Mechanical properties

1. INTRODUCTION

Aluminum structures are often used in transport technology, in the automotive industry, in the industry of rail vehicles, in shipbuilding, in the aviation industry and even in space technologies, because aluminum alloys have a good mechanical properties and low densities [1].

Welded constructions of cars, trains, ships, airplanes, spacecraft, which are made of different aluminum alloys, are most often joined

by classic metal inert gas (MIG) [2,3] and tungsten inert gas (TIG) [4] welding, friction stir (AA5754-AA7075 [5], AA2024-AA7075 [6], AA2219-AA5083 [7] and AA7075-AA6061 [8]), laser and electron beam welding [9].

Fusion welding processes easily join materials that have good weldability. The material is well weldable if it is possible to make a welded joint without defects. The weldability of aluminum alloys is affected by a number of factors such as: oxygen affinity, high thermal expansion and thermal conductivity, high shrinkage during solidification, high solubility of hydrogen in the liquid phase, which decreases drastically during solidification. By welding aluminum alloys, mechanical properties and corrosion resistance in HAZ are reduced, porosity, solidification and liquation cracks appear. Aluminum alloys are welded with additional material with increased content of Si or Mg.

Corresponding author

Prof. dr Dragan Milčić
e-mail dragan.milcic@masfak.ni.ac.rs

Faculty of Mechanical Engineering, University of Niš
Aleksandra Medvedeva 14
Niš, Serbia

If the technology of the welding procedure is not suitable, defects may appear in the area of the weld metal, which reduces the reliability of the welded structure. Weld defects such as porosity, cracks, lack of penetration or lack of fusion may appear [10].

Age-hardenable 2024 aluminum alloy belongs to the 2XXX alloy series where the main alloying element is copper. The mechanical properties of these alloys reach values similar to those of carbon steels. Such a high strength of the alloys is due to the precipitation of CuAl_2 particles during natural or artificial aging. As these alloys do not have good corrosion resistance, they are often coated (plated) with pure aluminum for corrosion protection. They are used for manufacturing parts in the aviation industry due to their high strength, good fatigue properties. With the addition of elements such as Mg and Li, it is possible to reduce the specific density and improve the performance of Al alloys for applications in the manufacture of parts in the aerospace industry [11]. Alloys of the 2XXX series, as a rule, have poor weldability with fusion welding (MIG, TIG), due to high crack sensitivity. Friction stir welding is mainly used for welding these alloys [12, 13]. In this paper, investigations of the structure and mechanical behavior of the welded joint by the MIG welding aluminum alloy 2024 T351 using the filler material S Al 4043A (AlSi5) are given.

2. MATERIALS AND METHODS

The chemical and mechanical properties of the alloys 2024-T351 (according to standards), which are the subject of this research and joined by the MIG process, are given in Tables 1 and 2. The chemical properties of the additional material used during welding are given in Table 3.

Table 1. Chemical properties base material AA 2024 T351, mas %

Mn	Fe	Mg	Si	Cu	Zn	Ti	Al
0.65	0.17	1.56	0.046	4.7	0.11	0.032	Balance

Table 2. Mechanical properties base material AA 2024 T351

Yield strength min R_{eh} (MPa)	Ultimate tensile strength min R_m (MPa)	Elongation at Break min A (%)	Hardness HV
310	425	10	137

The dimensions of the plates used for welding were 300 mm long, 125 mm wide and 8 mm thick. Welding machine was Fronius Transpuls Synergic 4000. Shielding gas was ISO 14175 – I3 – ArHe–30.

Table 3. Chemical composition of the filler material of wire EN ISO 18273 S Al 4043A (AlSi5), mas. %

Mn	Fe	Mg	Si	Cu	Zn	Ti	Be	Al
<0.15	<0.6	<0.2	4.5-5.5	<0.3	<0.1	<0.15	<0.0003	Balance

Welding parameters for MIG process butt welding of aluminum alloy 2024 T351 are given in table 4.

Table 4. Welding parameters for the MIG butt weld welding process

Run	Current I (A)	Voltage U (V)	Wire Feed Speed (m/min)	Welding Speed v (mm/s)	Heat input $H=I \cdot U \cdot \eta / v$ (J/mm)
1	155	21.7	6.3	6.98	385
2	180	23.2	7.5	8.82	379
3	170	22.7	7.3	8.33	371

Figure 1 shows face side of a welded joint. Welded joint made with a backing material (Fig. 2).

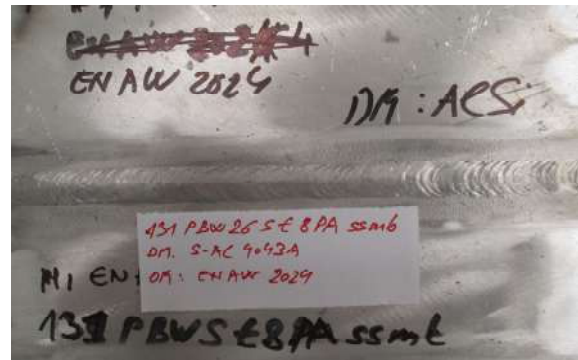


Fig. 1. Face side of the welded joint



Fig. 2. Macrostructure of welded butt joint

Test specimens were cut using an abrasive water jet cutting machine. Test specimens were prepared for testing the macro- and microstructure, for testing hardness, for Charpy impact test, for bend and tensile testing of welded joints.

Vickers hardness was measured on a Willson VH1150 hardness tester. Tensile properties were determined at room temperature using a Shimadzu AG-X 300 kN tensile tester. Test specimens defined by the ASTM E8M standard obtained from welded samples perpendicular to the welded joint were used [7]. Specimens were cut from the welded samples using the water jet cutting process.

The bending tests were carried out on four specimens—in two the tensiled side was the face of the weld and in two the tensiled side was the root of the weld. The test was performed at room temperature using the three-point bending method.

A Leica Q500MC optical microscope (LM) was used to analyze the microstructure of the welded joint. The microstructure was examined on the cross-section of the samples after the usual metallographic preparation and etching in Keller's reagent. The tests were also carried out using the scanning electron microscope JOEL JSM-6610LV (SEM).

3. RESULTS

3.1. Static Tensile Test

Figure 3 shows the specimen after breaking.



Fig. 3. Specimen after a static tensile test

Stress-strain curves is shown in Figure 4, and results are summarized in Table 5. The fracture of specimen was brittle fracture in weld metal (WM).

Table 5. Tensile test results of welded joints

Cross-section area (mm ²)	Yield strength $R_{p0.2}$ (MPa)	Ultimate tensile strength R_m (MPa)	Elongation at break A (%)	Place of fracture
80	209	261	1.2	WM

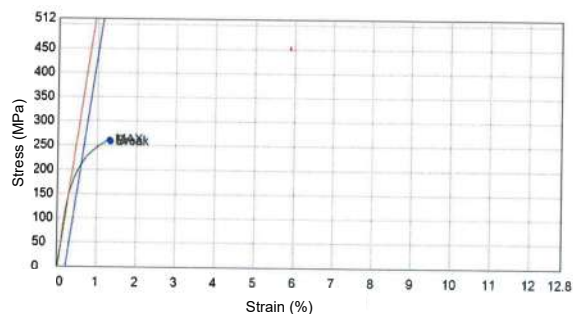


Fig. 4. Stress-strain diagram

3.2. Bending Test

Root bending tests is given in Figure 5.



Fig. 5. Root bend test - moment of brittle cracking

The results shown small bending angle (Fig. 5) until the appearance of a crack crack in both root and face bend test. In Figure 6 is give the appearance of a brittle fracture of bend specimen.



Fig. 6. Brittle fracture

3.3. Hardness distribution

The hardness measurement was made in two lines, i.e., near the face and the root of the weld, three hardness measurements for each of the test zones (weld metal - WM, HAZ and base materials), figure 7. The results of the hardness measurement of the welded joint are presented in Table 6

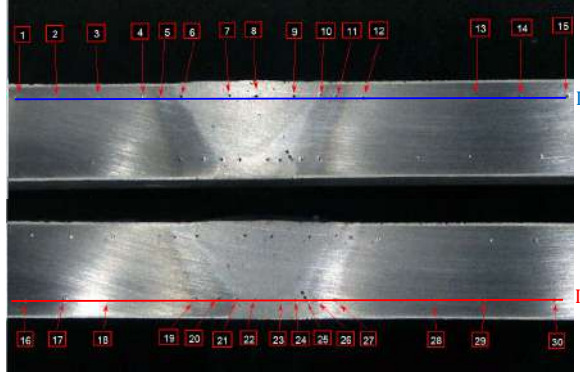


Fig. 7. Hardness measurement of the joint.

Table 6.

Merno mesto I / II	Položaj mesta otiska	Izmerena vrednost (HV)	Merno mesto I / II	Položaj mesta otiska	Izmerena vrednost (HV)
1/16	BM	121.5/145.9	9/24	WM	87.6/93.6
2/17	BM	148.5/150	10/25	HAZ	91.0/115.6
3/18	BM	162.4/142.1	11/26	HAZ	141.9/131.1
4/19	HAZ	125.7/119.7	12/27	HAZ	120.9/121.5
5/20	HAZ	143.7/128.5	13/28	BM	138.4/140.9
6/21	HAZ	122.4/79.3	14/29	BM	145.9/152.4
7/22	WM	93.5/95.9	15/30	BM	161.8/156.2
8/23	WM	82.4/93.0			

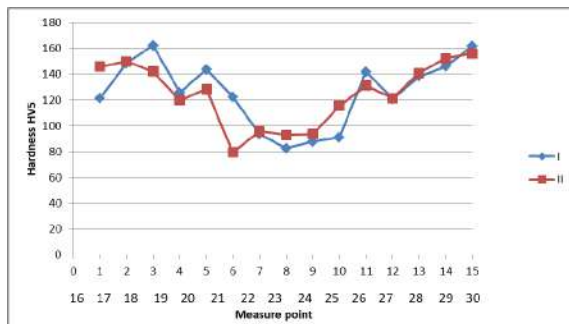


Fig. 8. Hardness distribution of the joint

3.4. Macro- and Microscopic Examinations

Figure 9 presents the macrostructure of the welded joint observed on the cross-section of the weld axis. The joint has a regular symmetrical shape without apparent defects such as cracking, undercutting, and porosity.

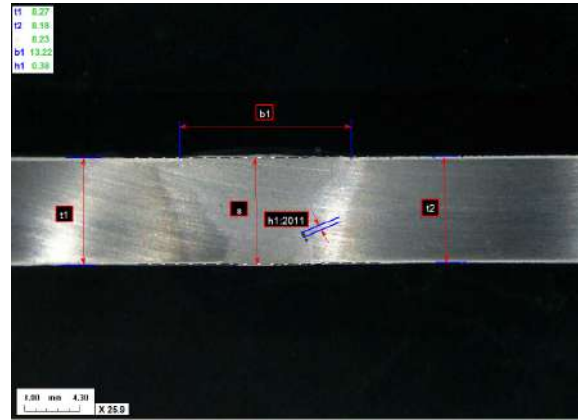


Fig. 9. Macrostructure of a welded joint

The microstructure of samples was examined by optical microscopy. Optical microscopy was performed by a Leica Q500MC microscope. Typical metallographic procedure implies using the Keller's and Barker's reagent to expose morphology.

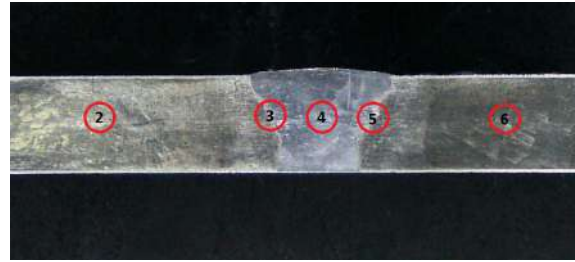


Fig. 10. Appearance of cross-section of the specimen with view microscopic examinations zones
Figure 11 shows the microstructure of the 2024-T351 base metal.

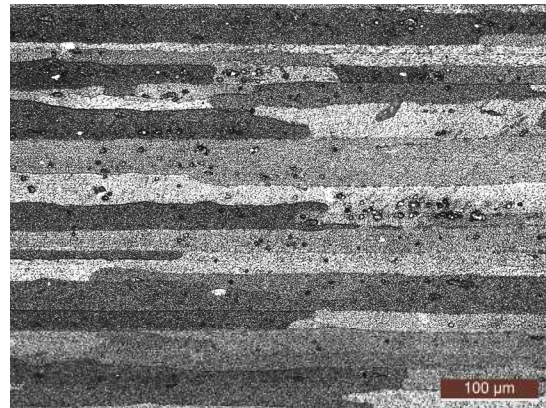


Fig. 11. Microstructure of the base metal (LM)

Figure 12 shows the microstructure of the heat affected zone (HAZ) (zone 3 – fig. 10).

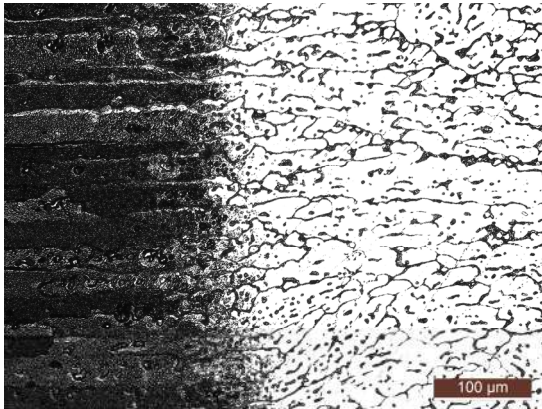


Fig. 12. Microstructure of the heat affected zone (HAZ) (zone 3 – fig. 10) (LM)

Figure 13 shows the microstructure of the weld metal (WM) (zone 4 – fig. 10).

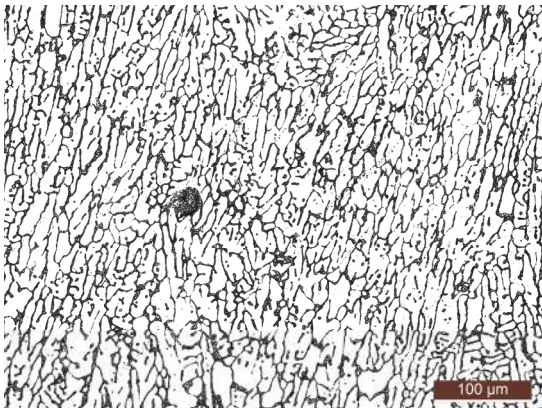


Fig. 13. Microstructure of the weld metal zone (WM) (zone 4 – fig. 10) (LM)

Figure 14 shows the microstructure of the heat affected zone (HAZ) (zone 5 – fig. 10).

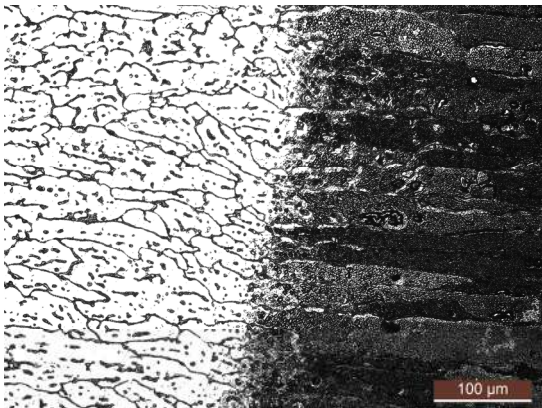


Fig. 14. Microstructure of the heat affected zone (HAZ) (zone 5 – fig. 10) (LM)

4. DISCUSSION

The microstructure of the weld metal obtained by the MIG welding process is significantly different from the microstructure of the base metal.

Accordingly, the mechanical properties of the welded joint are lower than the mechanical properties of the base metal. A low ductility was also observed during the tensile test.

The fracture location of specimen for tensile testing is in weld metal. The appearance of the fracture surface is given in Figure 15. Large pores are observed on the fracture surface.

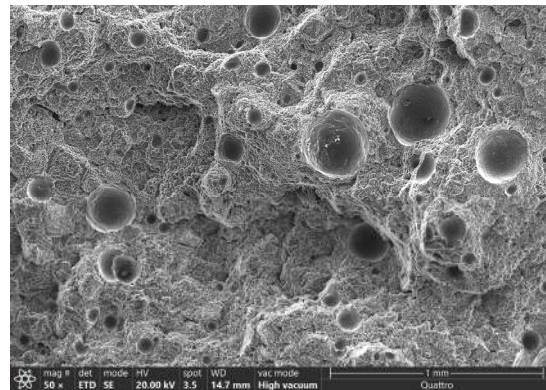


Fig. 15. Fracture surface (SEM)

The results of bending tests indicate poor technological properties of welded joints. A small bending angle until the appearance of a crack indicates that the welded joint are very brittle.

In the structure of the weld metal (fig. 16) are observed intermetallic particles (IMP) Al_2CuFeMn (white phase) on grain boundary and somewhere of the grain with random size. Various grain sizes were present. Grain orientation is dendritic.

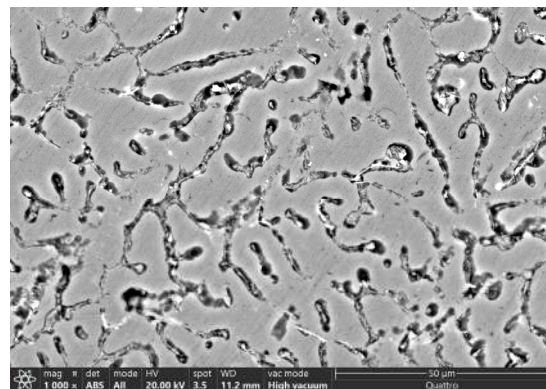


Fig. 16. Microstructure of the weld metal zone (SEM)

In weld metal beside HAZ (fig. 17) are observed IMP precipitated on grain boundary and in the grain to a certain degree with narrow columnar orientation. In HAZ are IMP precipitated on grain boundary and coarse particles were present.

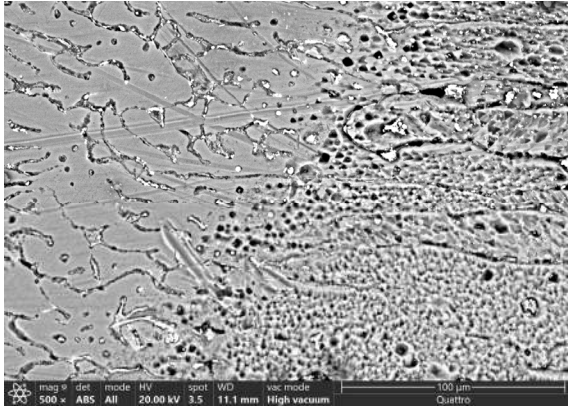


Fig. 17. Microstructure of the heat affected zone (SEM)

The minimum hardness value was recorded in weld metal. The hardness measured near the weld face is was about 85 HV, and measured near the weld root, is about 95 HV. The hardness in the HAZ was about 140 HV, this value was larger than in the weld metal but lower than of the base alloy which is about 160HV.

5. CONCLUSION

Based on the above, it can be concluded:

- The maximum tensile strength of the welded joint is (261 MPa) compared to (424 MPa) of the base alloy 2024-T351 i.e. the reduction in strength is about (40%).
- The fracture of the tensile test specimen was in weld metal with brittle fracture properties.
- Weld metal hardness is 40% lower than base metal hardness AA2024-T351.
- The results of the bending test showed a small bending angle until the appearance of a crack, and the fracture surface of the test specimen indicates a brittle fracture.

Acknowledgement

This research was financially supported by the Ministry of Science, Technological Development

and Innovation of the Republic of Serbia (Contract No. 451-03-47/2023-01/ 200109).

REFERENCES

- [1] Mallick, P.K. (2010). *Materials, Design and Manufacturing for Lightweight Vehicles*. Woodhead Publishing.
- [2] Lean, P.P., Gil, L., Ureña, A. (2003). Dissimilar welds between unreinforced AA6082 and AA6092/SiC/25p composite by pulsed-MIG arc welding using unreinforced filler alloys (Al-5Mg and Al-5Si), *Journal of Materials Processing Technology*, vol. 143-144, p. 846-850. [https://doi.org/10.1016/S0924-0136\(03\)00331-5](https://doi.org/10.1016/S0924-0136(03)00331-5)
- [3] Nawres, J.N. (2016). Mechanical Properties of MIG Joints for Dissimilar Aluminum Alloys (2024-T351 and 6061-T651). *Al-Khwarizmi Engineering Journal*, vol. 12, no. 3, p. 121- 128
- [4] Liamine, K., Mohammed, E.D., Seddik, O., Sami, K. (2022). Dissimilar welding of aluminum alloys 2024 T3 and 7075 T6 by TIG process with double tungsten electrodes. *The International Journal of Advanced Manufacturing Technology*, vol. 118, p. 937-948. <https://doi.org/10.21203/rs.3.rs-408163/v1>
- [5] Kasman, Ş., Yenier, Z. (2014). Analyzing dissimilar friction stir welding of AA5754/AA7075. *The International Journal of Advanced Manufacturing Technology*, vol. 70, no. 1-4, p. 145-156. <https://doi.org/10.1007/s00170-013-5256-7>
- [6] Youbao, S., Xinqi, Y., Lei, C., Xiaopeng, H., Shen, Z., Xu, Y. (2014). Defect features and mechanical properties of friction stir lap welded dissimilar AA2024-AA7075 aluminum alloy sheets. *Materials & Design*, vol. 55, p. 9-18. <https://doi.org/10.1016/j.matdes.2013.09.062>
- [7] Mastanaiah, P., Sharma, A., Reddy, Madhusudhan, G. (2016). Dissimilar friction stir welds in AA2219-AA5083 aluminium alloys: effect of process parameters on material inter-mixing, defect formation, and mechanical properties. *Transactions of the Indian Institute of Metals*, 69(7), 1397-1415. <https://doi.org/10.1007/s12666-015-0694-6>
- [8] Hasan, Mohammed M.; Ishak, Mahadzir; Rejab, Ruzaimi. (2017). Influence of machine variables

- and tool profile on the tensile strength of dissimilar AA7075-AA6061 friction stir welds. *The International Journal of Advanced Manufacturing Technology*, 90(9-12), 2605-2615. <https://doi.org/10.1007/s00170-016-9583-3>
- [9] Himanshu, L., Paranjayee, M. (2021). Cold forming of Al-5251 and Al-6082 tailored welded blanks manufactured by laser and electron beam welding. *Journal of Manufacturing Processes*, vol. 68, Part A, p. 1615-1636. <https://doi.org/10.1016/j.jmapro.2021.06.070>
- [10] Molian, P.A., Srivatsan, T.S. (1990). Weldability of aluminium-lithium alloy 2090 using laser welding. *Journal of Materials Science*, vol. 25, p. 3347-3358. <https://doi.org/10.1007/BF00587697>
- [11] Heinz, A., Haszler, A., Keidel, C., Moldenhauer, S., Benedictus, R. Miller, W. (2000). Recent development in aluminium alloys for aerospace applications, *Materials Science and Engineering A*, vol. 280, no. 1, p.102-107. [https://doi.org/10.1016/S0921-5093\(99\)00674-7](https://doi.org/10.1016/S0921-5093(99)00674-7)
- [12] Milčić, M., Milčić, D., Vuherer, T., Radović, Lj., Radisavljević, I., Đurić, Al. (2021). Influence of Welding Speed on Fracture Toughness of Friction Stir Welded AA2024-T351 Joints. *Materials*, vol. 14, no. 6: 1561. <https://doi.org/10.3390/ma14061561>
- [13] Milčić, M., Vuherer, T., Radisavljević, I., Milčić, D., Kramberger, J. (2019). The influence of process parameters on the mechanical properties of friction stir welded joints of 2024 T351 aluminum alloys, *Materials and technology*, vol. 53, no. 6. p. 771-776. [doi:10.17222/mit.2019.062](https://doi.org/10.17222/mit.2019.062)



Banja Luka
01–02 June 2023.

DEMI 2023

16th International Conference on Accomplishments in Mechanical and Industrial Engineering

www.demi.mf.unibl.org



Towards optimised End-of-Life product disassembly system selection

D. Mlivić^a, Z. Kunica^a, J. Topolnjak^a

^aUniversity of Zagreb, Faculty of Mechanical Engineering and Naval Architecture, Ivana Lučića 5, Zagreb, Croatia

Abstract

With the advancement of technology, human civilization produces more than ever before, with the alarming consequence being the huge amount of waste generated. The disposal of End-of-Life (EoL) products represents one of the biggest problems today. Vast majority of recycling processes would benefit from the inclusion of a disassembly stage, since a large portion of EoL products is an assembly. Disassembly has the potential to significantly improve overall waste reduction by allowing reuse, avoidance of environmental risks and hazards, and finally better sorting of materials. The efficient planning, realization and operation of a disassembly system requires solving of many issues basically related to varieties of EoL products and their various quantities. Thus, a method that would propose an appropriate disassembly system, based on the state of the product in real time is required. By monitoring the state of products, even before they enter their EoL phase, it is possible to have a dynamic solution suggesting the most appropriate type, number and location of disassembly systems. The method for choosing an appropriate disassembly system, preferably automatized, would appear as a new content within product life cycle management, improving the disassembly planning and process, by reducing the planning time, while increasing productivity.

Keywords End-of-Life product, disassembly, planning

1. INTRODUCTION AND STATE OF THE ART

As the technology and life standard in human society rapidly progresses, so does the consumerism culture grow. People buy more than ever before, and the projected lifecycle of a product is shorter than ever [1], so with it the production amounts grow yearly. Life becomes easier, more convenient and longer due to more and more consumer goods. However, the consequence is the fact the world produces more waste than ever before [2], and the question of sustainability becomes extremely important. The manufacturers were only interested in producing as much as possible, without thinking of the problem the waste will inevitably produce. Now a serious investment needs to be done to combat the alarming issue. In order to achieve a

sustainable economy, a complete switch from a linear to a circular economy is needed [1]. Whilst a sustainable circular economy approach is becoming common [3], still more progress needs to be achieved, as the world is showing very high levels of waste generation and dependency on raw materials [4]. Many manufacturers still do not fully recognise the potential of Life Cycle Analysis (LCA) practices for the substantial improvement of their products, especially small to medium sized manufacturers [5]. According to the EU Action Plan on Critical Raw Materials [6], which aims to substantially lessen the human civilization's dependence on raw materials, recycling and re-use are the future of manufacturing. This is in accordance with the standard for ranking waste disposal options based on their environmental impact, the

Lansink ladder [7]. Vast majority of recycling processes would benefit from the inclusion of a disassembly stage, since a large portion of waste is an assembly rather than a single part. Thus disassembly is the basis for achieving this plan, as it improves the overall recycling process itself by allowing reuse, avoidance of environmental risks and hazards, and finally better sorting of materials. The advances in digitalisation are set to be integrated in the form of the European Commission's Recycling 4.0 [8], which is combining Industry 4.0 technologies with circular economy principles to advance the recycling sector. When the potential of waste (in terms of material and energy) is recognised, it is referred to as an End-of-Life product (EoL) – implying it as still a product with potential. Circular economy implies different fields [9], such as the sustainable collection of energy from waste (like biogas, use of compost or construction building material) [10], with disassembly being one of them, and the primary focus of this research.

Before entering the specifics of disassembly, a question may be asked regarding its importance. It can be argued that disassembly is possibly even a nuisance in waste management since disassembly is an additional cost and very time consuming due to a high portion of manual work [11]. If only those arguments were taken into consideration, then it can be argued further that traditional destructive methods such as shredding [12] should be the preferred alternative. While shredding can indeed process EoL products faster and cheaper at first glance, it cannot give saved individual useful component-parts as its output: component-parts get destroyed and subsequently the materials get mixed, which are to be sorted by various processes. In addition, shredding cannot effectively deal with processing components containing hazardous substances [12]. In contrast, disassembly results in integral component-parts which can later be reused or even recycled in a more straightforward way. As such, disassembly is the cleaner solution [6] and preferred by the LCA and circular economy

approach (also in accordance to the Lansink ladder [7]).

Disassembly is done in different ways, ranging from manual disassembly to fully automated disassembly. However, a large part of EoL products is still being treated at traditional manual recycling facilities, either locally or processed abroad in less developed countries [13] [2]. This is due to the products arriving in unpredictable conditions and varying quantities, hence why the flexibility of human workers is preferred to automation. Unfortunately, manual disassembly can't deal with the growing quantities, thus an increase in the share of automation in disassembly is needed in order to successfully deal with the growing quantities of waste.

An ideal solution would be for the manufacturers to handle their product at the end of its lifecycle [14]. Two examples come from a smartphone manufacturer, whose "robots" Liam [15] and Daisy [16] completely automatically disassemble smartphones (a large part of WEEE - Waste Electrical and Electronic Equipment). Whilst positive examples, and indeed the most wanted solutions as attempts to begin addressing automatic disassembly of WEEE, still the vast majority of the company's products get processed in conventional ways [17] [18]. This problem is further emphasized by the fact that their disassembly line can process 1,2 million phones a year [19], while another 200 million phones have been sold in 2020 alone [20].

Manual work is dominant in disassembly [11] and it is always an option for dealing with a large variety of products, but at the same time it cannot cope with the increasing waste quantities and associated health hazards. This presents an issue, as the highest possible level of automation needs to be found for each type of product at a location. Thus, to sum up, the amount of various disassembly system options raises the need for a methodology, to guide the user towards the most appropriate disassembly system.

Corresponding author

mag. ing. mech, Denis Mlivić
denis.mlivic@fsb.hr

*Faculty of Mechanical Engineering and Naval Architecture
Ivana Lučića 5
Zagreb, Croatia*

2. PROPOSED METHOD FOR OPTIMISED EOL PRODUCT DISASSEMBLY SYSTEM SELECTION

The uncertainties and variations found within EoL products lead to uncertainties in the disassembly process [12], which complicates the choice of a disassembly system because disassembly brings specific problems, among them:

- the variety of states an EoL product can end up in
- securing the quantities for automatization
- non-standard components used for maintenance, upgrading/downgrading from the original specification which complicate its automation.

The mentioned reasons, among others, inhibit automation in disassembly [21]. Disassembly is mostly being done manually, which leads to higher costs and lower productivity, and it is questionable if it is, left on its own, able to cope with the growing quantities of waste our civilization produces. Therefore, in order to fulfil the EU Action plan for recycling within sustainability and complete a conversion towards circular economy [2, 3, 6, 9], an increase of the share of automation in disassembly is necessary in order to increase productivity.

The choice of the type of disassembly (manual or automatic), and more specifically the type of system to perform it in, is the first step in disassembly system planning. Thus, the development of a method for choosing the most suitable disassembly system should present the starting point for disassembly system planning. This is exactly the aim of the research: to develop a method for choosing the most suitable disassembly system, solving the specific problem (EoL product in question is to be disassembled, completed with the describing data) with a suitable solution in the form of an appropriate disassembly system, ranging from manual disassembly to fully automated disassembly. Enabled by product traceability, it is deemed possible to have an appropriate disassembly system suggestion, while the product is still in use, even before the EoL phase.

In order to give an appropriate disassembly system suggestion, a clear picture regarding the product (to be disassembled) needs to be given. The product is the basis of any analysis of a

process and the subsequent system, as the product is being processed in a system. Even with successfully obtained large quantities, different products can suggest very different disassembly system options. Thus, the parameters which describe the (current) state of the EoL product to be disassembled present the input for the method, defined by values of those parameters of interest.

3. PARAMETERS OF THE METHOD

The key parameters of interest (and sources of data, where possible) of an EoL product (or disassembly family of EoL products) will be given in the following section. The suggestion will be made based on real-time values of the parameters. Based on these inputs, the method's output will be in the form of the suggested disassembly system. Furthermore, a dynamic characteristic of the suggestion is implied, as it can change if the parameter(s) are sufficiently changed, even while the product is still in use.

The corresponding limit values are extremely product-specific for each type of EoL product, and further research will need to be done for any specific type of product. Along with the parameters, the way each of them effects the suitable suggestion will be given.

3.1 Type of EoL product

The type of EoL product parameter deals with the questions regarding the basic physical characteristics of the product (possibly even representative product [22]). This will define the process functions and later, needed equipment for disassembly. For example, very different equipment is needed to disassemble a household electronic device or a vehicle (in addition to the tools to perform the disassembly, powerful equipment is needed to manipulate them). Some of the questions regarding the material type are:

- What are its size and mass?
- Is the material of the (representative) product toxic in any state, or does it contain any toxic components? Is the material contaminated or radioactive?
- Does it need a special environment to handle the health risks? If a special environment is needed for processing such products, it would guide it towards a highly specialised, low volume automatic

equipment (as manual disassembly should be limited, due to the workers' health risk)

- Are the joining techniques a very specialised technology, for which automated solutions have not yet been developed?

Hazardous types of material would need to be categorised, which require regulated approach for valid reasons (e.g. for the handling of special types of hazardous or toxic material, which require specific handling and/or conform to strict regulations). For example, hazardous waste would preferably be processed without human presence [12].

3.2 Disassemblability

Generally, disassemblability describes the difficulty of the disassembly task. Specifically for this research, the disassemblability parameter describes the difficulty of the disassembly of the EoL product in question, how feasible it is for automated disassembly. A well-designed product with disassembly in mind brings considerable benefits during recycling [23]: especially, applied fastening and joining techniques will dictate in the reversed process of disassembly whether it will be performed with or without damaging the component-parts. Additionally, a product designed with a focus on disassembly will also be more feasible for automation in disassembly, leading towards higher values of the parameter.

3.3 Traceability

Traceability describes how feasible it is to trace a product, in its various life phases. Based on current trends, it is certain that traceability will be even more implemented in a wide range of products, thus it will be one of the key parameters for the selection of an appropriate disassembly system. Traceability is needed in order to gather the information regarding the status of the product among the shareholders, shown in **Error! Reference source not found.**



Fig. 1. Shareholders which need to be involved for successful EoL product tracking

On one hand, some products are very suitable for tracking, which are often of large dimensions and of significant value (meaning it is of interest to track). Such examples are vehicles: automobiles, trucks, motorcycles, farming equipment, etc. They are already widely tracked – the tracking by registration plate is today very well automatized by camera-based systems (e.g. in parking garages and toll booths) and through service centers and insurance. Following, devices which are connected to the network for large amounts of time (mobile phones, personal computers) are also very suitable, as well as products which require special surveillance from the authorities (eg. weapons) or special rules due to their health risks and hazards. Additionally, some products have a very long traceability period. All the mentioned products would gravitate towards higher values of traceability factor.

On the other hand, some products are unsuitable for tracking, products which are either very cheap (limited or no real value which would justify tracking), small or unregulated (no law or regulation specifying their need for control and tracking). Currently some problems might occur. For example, recent regulations aim at banning small plastic straws and cutlery and they present a huge amount of untracked products which must not end up in the environment. **Error! Reference source not found.** shows how the value of the traceability parameter will be assigned.

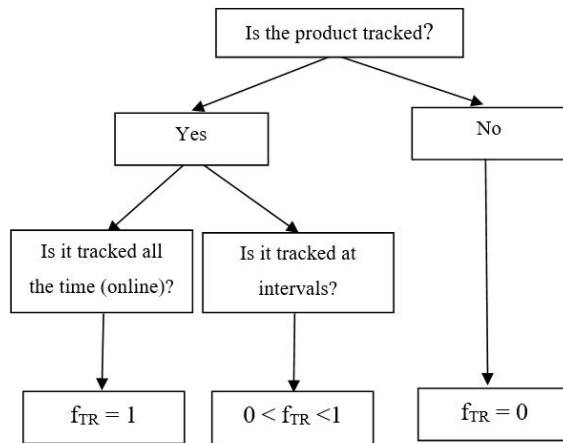


Fig. 2. The logic for assigning the value of the traceability parameter

3.4 Geometrical continuity of the EoL product

The geometrical continuity shows how close the EoL product is to its original specification (which can be closely checked through CAD and/or scanning), needed primarily to determine the possible level of automation of the disassembly system.

EoL products which differ from the original specification (damaged or changed significantly with non-standard components) will be more complicated for automated disassembly, if not impossible. This complicates the disassembly plan, as it will deviate from the disassembly plan for the expected standard EoL products. This can be solved through its digital twin, kept up-to-date with high levels of traceability (however, this depends on the feasibility of traceability of the product, as described in 3.3 Traceability). If the principles of Big Data are implemented, then there is a possibility to determine which amount of EoL products from a batch is changed from the rest, and thus needs to be processed in a different way (leaning towards manual disassembly if sufficiently changed), leading towards higher values of the parameter.

3.5 Quantity

The available quantity of a group of EoL products is one of the key parameters for the choice of disassembly system, as securing the quantities is the key for justifying the cost of automation. Also, it is closely connected with the area covered by

the planned disassembly system, as the product must be relevant for the area.

Research needs to be done on the limit values, which are the key here. For example, what is the annual number of the disassembly family of EoL products of interest sold in the region? This data can lead to defining the lower limits for automatization.

3.6 Cost of collecting

Following the question of quantities, products also vary in their cost of collecting. For some products, the collection is already very well and widely developed, organised and known. For example, the system for gathering and processing plastic and glass bottles is already well-developed and common, thus automation is well-used in those systems. Furthermore, some products are regulated due to their importance or environmental issues, thus also collected in a specific way.

Transport is also included in the cost of collecting, and it again varies wildly between different types of EoL products. Large, bulky, heavy, and/or hazardous EoL products present a larger challenge (therefore also a larger cost) to transport, and is also closely connected to the means of transport chosen for the transport. This can lead to a quantitative-based decision regarding the feasibility of, for example, having two less automatised (thus less productive) systems closer to the areas but with less transport, or a larger one with more transport? Together, the quantity and the cost of collecting are the key inputs for the choice of disassembly system structure and automation level (possibly even examined together).

4. RELATIONSHIP AMONG PARAMETERS

Depending on the values of all the previously described parameters, a unique solution (in the form of the temporary appropriate disassembly system for the EoL product in question) will be given. Still, special cases (closely connected to the type of EoL product, described in 3.1 Type of EoL product) will require a specific solution, regardless of the other factors. For example, hazardous EoL products or EoL products presenting a health-risk for humans will have to be disassembled by automation – regardless of the quantities, traceability etc. Still, here a

criteria of average cost per product can be introduced (similar to the DFA method for choice of assembly system) – implying that the solution may not be optimal. Outside these special cases, the solution will be given depending on the values of the factors for the EoL product of interest.

For example, vehicles are on the higher end of the spectrum, and their disassembly can be more effective as these information could be created and tracked well before the vehicle arrives for disassembly (as this is the case currently, data sharing must be established so the disassembler can gain data).

Low values of the parameters lead to manual disassembly, as either:

- the quantities are not sufficient, or the cost of collecting is expensive,
- the product is too complicated for automated disassembly, or differing too much from the original state,
- the product is not traced enough during its lifetime for a disassembly system suggestion to be ready and prepared, thus leading to manual disassembly as the most adaptable option to handle the product uncertainties.

It is necessary to keep the solution dynamically changeable – if some of the parameters change sufficiently enough to then offer a different solution, it needs to be up to date. This way the user can also experiment with different parameters' values to check how "safe" inside a disassembly solution the parameters currently are. For example, it might be a risk to invest in an automated disassembly system if the solution has barely entered the field of automation, because if it drops below the equipment will not

be suitable anymore and thus not profitable as planned. This way the user can also check the surrounding of the system – what would effect the solution to move towards automation or manual disassembly. With such a dynamically changeable solution he/she can plan for the future.

Regarding the disassembly systems as the method's solution, they will be given as a broad group. As already mentioned before, disassembly is done in different types of disassembly systems. The biggest groups are:

- Manual disassembly system, for the widest variety of EoL products to process, and the lowest quantities.
- Collaborative disassembly system, where a certain part of the disassembly task (either very simple, or difficult for a human to perform, such as manipulating a vehicle [24]) is automatised.
- Flexible automated disassembly, an automated disassembly system for a wider group of EoL products, with a degree of flexibility towards each specific EoL product.
- Single-purpose automated disassembly, for a specific EoL product (or extremely low variation), offering the highest productivity.

The following steps would include, among others, the concept of a disassembly system catered for the EoL product in question.

Error! Reference source not found. shows the relation comparison between the different disassembly system options, and how they are affected by the values of the parameters for the EoL product in question.

Table 1. Comparison table of the systems and parameters

Disassembly system/parameter	<i>Type of EoL product</i>	<i>Disassemblability</i>	<i>Traceability</i>	<i>Geometrical continuity of the EoL product</i>	<i>Available quantity</i>	<i>Cost of collecting</i>
<i>Manual disassembly</i>	Rare, non-standard	Low disassemblability	Not traced	Damaged, non-standard	Low volume	High
<i>Collaborative disassembly</i>	Simple to grasp	High disassemblability	Traced at intervals	Undamaged	Medium to high volume	High
<i>Flexible disassembly</i>	Standard, modular build	High disassemblability	Traced at intervals	Undamaged, unchanged from original specification	Medium to high volume	Low
<i>Automated disassembly</i>	Simplest, also hazardous and dangerous	Very high disassemblability	High traceability	Undamaged, unchanged from original specification	High volume	Low

5. CONCLUSION

Disassembly brings specific issues which hinder its automation, which is why it is done mostly manually, leading to high processing costs and low productivity. The research aims to improve the productivity of disassembly by increasing the share of automation, by means of the choice of an appropriate disassembly system. This leads towards a method for the choice of an appropriate disassembly system for a specific product, deemed possible even during product use (before entering its EoL phase).

The result is a set basis for a programme, in which the user would enter the disassembly scenario and be given an suggestion for an appropriate disassembly system. Depending on the state of the EoL product (or group of EoL products) and its accompanying data (quantity, cost of collecting, achieved level of traceability, among others), a suitable disassembly system will be presented, even while the product is still in use. Furthermore, the user can use the method to check the surrounding of its solution, in order to prepare for any market changes, both positive and negative scenarios (e.g. how much can the quantities drop until automation is no longer feasible, or how much do they need to increase in order to justify automation – these considerations are important when investing in expensive equipment).

This method for the choice the suitable disassembly system would greatly improve the disassembly process, enabling the human civilization to better handle the growing quantities of waste. Such improvements will shorten the preparation time and thus improve their productivity, as the disassemblers will have a ready suggestion (enabled with high-level traceability based on the real-time tracking of the product) before the EoL product even arrives to the facility, also changing the result if a large enough change has been tracked. After the choice of an appropriate disassembly system, the following steps are disassembly process planning and the design of the appropriate disassembly system.

Future research will be aimed towards identifying an example of a product family, to set the key values (as they are extremely unique towards the specific product) for an experiment. Additionally, work needs to be done towards collecting the data (from manufacturers, government agencies, disassemblers) and it's

integration between the shareholders (following the principles of Big Data).

Acknowledgement

This research has been supported by the University of Zagreb.

REFERENCES

- [1] Rocca, R., Rosa P., Sassanelli, C., Fumagalli L., Terzi, S. (2020). Integrating Virtual Reality and Digital Twin in Circular Economy Practices: A Laboratory Application Case. *Sustainability*, vol. 12, no. 6. DOI: [10.3390/su12062286](https://doi.org/10.3390/su12062286)
- [2] Brooks, A. L., Wang, S., Jambrech, J. R. (2018). The Chinese import ban and its impact on global plastic waste trade. *Science Advances*, vol. 4, no. 6. DOI: [10.1126/sciadv.aat0131](https://doi.org/10.1126/sciadv.aat0131)
- [3] Taffuri, A., Sciallo, A., Diemer, A., Nedelciu, C. E. (2021). Integrating Circular Bioeconomy and Urban Dynamics to Define an Innovative Management of Bio-Waste: The Study Case of Turin. *Sustainability*, vol. 13, no. 11. DOI: [10.3390/su13116224](https://doi.org/10.3390/su13116224)
- [4] Aleksandrova, I., Gubernatorov, A. Tools for Implementing the Financing Mechanism for the Waste Processing Industry. 13th International Conference "Management of large-scale system development" (MLSD), Sept. 2020, Moscow. DOI: [10.1109/MLSD49919.2020.9247835](https://doi.org/10.1109/MLSD49919.2020.9247835)
- [5] Glisovic, S., Stojiljkovic, E., Stojiljkovic, P. (2018). The state of play in disseminating LCM practices in the Western Balkan region: the attitude of Serbian SMEs. *International Journal of Life Cycle Assessment*, vol. 23, no. 7, p. 1396-1409. DOI: [10.1007/s11367-015-0894-7](https://doi.org/10.1007/s11367-015-0894-7)
- [6] European Commission. Action Plan on Critical Raw Materials. From: <https://eur-lex.europa.eu/legal-content/EN/TXT/?uri=CELEX:52020DC0474>, accessed on: June 24, 2021.
- [7] Willems, B., Dewulf, W., Duflou, J. R. (2006). Can large-scale disassembly be profitable? A linear programming approach to quantifying the turning point to make disassembly economically viable. *International Journal of Production Research*, vol. 44, no. 6, p. 1125-1146. DOI: [10.1080/00207540500354168](https://doi.org/10.1080/00207540500354168)
- [8] Blömeke, S., Rickert, J., Mennenga, M., Thiede, S., Spengler, T. S., Herrmann, C. (2020). Recycling 4.0 – Mapping smart manufacturing solutions to remanufacturing and recycling operations.

- Procedia CIRP* 90, vol. 90, p. 600-605. DOI: [10.1016/j.procir.2020.02.045](https://doi.org/10.1016/j.procir.2020.02.045)
- [9] McDougall, F. R., White, P. R., Franke, M., Hindle, P. (2001). *Integrated Solid Waste Management: a Life Cycle Inventory*. Blackwell Science.
- [10] Chandrappa, R., Das, D. B. (2012). *Solid Waste Management*. Springer-Verlag, Berlin.
- [11] Das, S. K., Naik, S. (2002). Process planning for product disassembly. *International Journal of Production Research*, vol. 40, no. 6, p. 1335-1355. DOI: [10.1080/00207540110102142](https://doi.org/10.1080/00207540110102142)
- [12] Vongbunyong, S., Chen, W. H. (2015). *Disassembly Automation: Automated Systems with Cognitive Abilities*. Springer.
- [13] Chen, W. H., Foo, G., Kara, S., Pagnucco, M. (2019). Application of a multi-head tool for robotic disassembly. *Procedia CIRP* 90, West Lafayette.
- [14] Apple. Apple's Recycling. From: <https://www.apple.com/me/recycling/>, accessed on: July 12, 2021.
- [15] Mashable. Inside Liam, Apple's super-secret, 29-armed robot that tears down your iPhone. From: <https://mashable.com/2016/03/21/apple-liam-recycling-robot/?europa=true>, accessed on: April 15, 2023.
- [16] Apple. Apple adds Earth Day donations to trade-in and recycling program. From: <https://www.apple.com/newsroom/2018/04/apple-adds-earth-day-donations-to-trade-in-and-recycling-program/>, accessed on April 15, 2023.
- [17] Vox. The model for recycling our old smartphones is actually causing massive pollution. From: <https://www.vox.com/2017/11/8/16621512/where-does-my-smartphone-iphone-8-x-go-recycling-afterlife-toxic-waste-environment>, accessed on April 19, 2023.
- [18] Poschmann, H., Brueggemann, H., Goldmann, D. (2020.) Disassembly 4.0: A Review on Using Robotics in Disassembly Tasks as a Way of Automation. *Chemie Ingenieur Technik*, vol. 92, no. 4, p. 341-359. DOI: [10.1002/cite.201900107](https://doi.org/10.1002/cite.201900107)
- [19] Recycling Today. Commentary: A different perspective on smartphone recycling. From: <https://www.recyclingtoday.com/article/smartphone-recycling-refurbishment-attitudes-changing/>, accessed on: April 19, 2023.
- [20] Forbes. Apple Back On Top: iPhone Is The Bestselling Smartphone Globally In Q4 2020. From: <https://www.forbes.com/sites/dwightsilverman/2021/02/22/apple-back-on-top-iphone-is-the-bestselling-smartphone-globally-in-q4-2020/?sh=4bd3bbe64ca7>, accessed on: April 19, 2023.
- [21] Foo, G., Kara, S., Pagnucco, M. (2022). Challenges of robotic disassembly in practice. *Procedia CIRP* 105, vol. 105, p. 513-518. DOI: [10.1016/j.procir.2022.02.085](https://doi.org/10.1016/j.procir.2022.02.085)
- [22] Kunica, Z. (2016). *Projektiranje proizvodnih sustava*. Sveučilište u Zagrebu, Fakultet strojarstva i brodogradnje.
- [23] Frizziero, L., Liverani, A., Caligiana, G., Donnici, G., Chinaglia, L. (2019). Design for Disassembly (DfD) and Augmented Reality (AR): Case Study Applied to a Gearbox. *Machines*, vol. 7, no. 2. DOI: [10.3390/machines7020029](https://doi.org/10.3390/machines7020029)
- [24] Indra. Indra Auto Recycling. From: <https://www.indra.fr/en/home>, accessed on April 12, 2023.



Banja Luka
1-2 Jun 2023.

DEMI 2023

16th International Conference on Accomplishments in Mechanical and Industrial Engineering

www.demi.mf.unibl.org



Decision support system for material selection

D. Petković^a, M. Madić^a, P. Živković^a

^aFaculty of Mechanical Engineering University of Niš, A. Medvedeva 14, Niš

Abstract *Material selection process is a complex and responsible multi-criteria decision making (MCDM) problem with specific and conflicting objectives. Selection of the most suitable material involves the study of a large number of factors, such as thermal, mechanical, electrical, chemical and physical properties as well as machinability, formability and weldability of available materials. Selection of the most suitable material for a heat exchanger is a multi-criteria decision making (MCDM) problem with diverse objectives. In order to help decision makers in solving this complex task, a decision support system named MCDM Solver is proposed. MCDM Solver is used in decision-making process to rank the materials with respect to several criteria.*

Keywords *Material selection, decision support system, MCDM Solver, heat exchanger*

1. INTRODUCTION

Material selection process is a complex task which needs knowledge of materials engineering, technologies, operational research and design. To select the suitable material for an application necessitates the simultaneous consideration of many conflicting and diverse criteria. Only with a systematic and structured mathematical approach the best alternative for a specific engineering product can be selected. The material selection problems with multiple non-commensurable and conflicting criteria can be efficiently solved by using multi-criteria decision making (MCDM) methods. The MCDM methods have the capabilities to generate decision rules while considering relative significance of considered criteria upon which the complete ranking of alternatives is

determined [1-3].

Decision support system (DSS) is a special class of information system oriented to the decision-making process and aims to support, mainly business decision-making processes. DSS is a symbiosis of information systems, application of functional knowledge and ongoing decision-making process [4]. Its main goal, as well as the goals of other information systems, is to improve the efficiency and effectiveness of an organization.

This paper was aimed at applying developed DSS named MCDM Solver for selecting the most appropriate material for heat exchanger design. MCDM Solver was used to determine the relative significance of considered material properties (performance criteria) and finally perform ranking of competitive material alternatives.

2. MCDM Solver

MCDM Solver is an “on-line” DSS which was developed within the doctoral dissertation of Dušan Petković. The developed DSS is located on the “Virtuode” Company web site [5] and it is

Corresponding author

Dr Dušan Petković, assistant professor
dusan.petkovic@masfak.ni.ac.rs

Faculty of Mechanical Engineering University of Niš
A. Medvedeva 14
Niš, Serbia

available to everyone who registers by creating an account (Fig 1). This DSS offers the possibility of working with maximization, minimization and target criteria [6].

The input data for MCDM Solver:

- Initial matrix of decision-making with target value of criteria (Step 1);
- η - Confidence level of decision maker in significance of the selected criteria (where $\eta=1$ corresponds to 100% confidence level, while $\eta=0$ corresponds to a confidence level of 0);
- Pairwise significance evaluation of the selected criteria.



Fig. 1. MCDM Solver – initial layout

Based on the input data, MCDM Solver can be able to determine the values of the criteria weights (Step 2) and perform ranking of alternatives (Step 3) with the corresponding values by means of the following MCDM methods: Extended TOPSIS [7], Comprehensive VIKOR [8] and Comprehensive WASPAS [6, 9]. Developed DSS architecture is flexible and can be easily upgraded, so the inclusion and analysis of new models that will come in the future is enabled. MCDM Solver has a user-friendly interface, which enables a simple and efficient way of entering the necessary input data [10]. Its application significantly simplifies the solution process of MCDM problems, especially material selection problems and selection problems in machining, since it does not require expert knowledge from the decision making theory by the user (decision maker) and is able to easily handle large decision making matrices [10, 11].

3. HEAT EXCHANGER MATERIAL SELECTION PROCESS

Heat exchanger is device used to transfer heat between two or more fluid streams at different temperatures. Heat exchangers find widespread use in power generation, chemical processing,

electronics cooling, air-conditioning, refrigeration, and automotive applications. The goal of heat exchanger design is to relate the inlet and outlet temperatures, the overall heat transfer coefficient, and the geometry of the heat exchanger, to the rate of heat transfer between the two fluids. A heat exchanger consists of heat exchanging elements such as a core or a matrix containing the heat transfer surface, and fluid distribution elements such as headers, manifolds, tanks, inlet and outlet nozzles or pipes, seals. Usually there are no moving parts in a heat exchanger; however, there are exceptions such as a rotary regenerator, a scraped surface heat exchanger, agitated vessels, and stirred tank reactors [12]. The heat transfer surface is a surface of the exchanger core that is in direct contact with fluids and through which heat is transferred by conduction, Fig. 2.

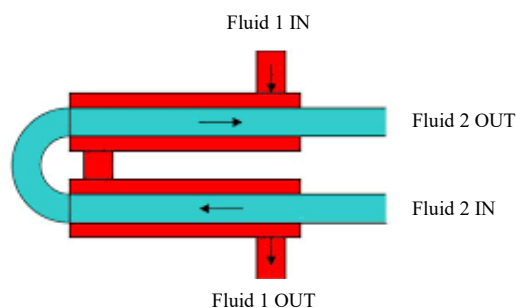


Fig. 2. Schematic view of a heat exchanger

The portion of the surface that also separates the fluids is referred to as the primary or direct surface. The rate of the heat transfer depends both on the heat transfer area and the thermal conductivity of the core material. Therefore heat exchanger material and design determine its efficiency and dimensions.

A material selection process begins by considering the material requirements which are needed for a specific application. Therefore it is necessary to select criteria that can be used to select the most suitable heat exchanger material. Since the general function of a heat exchanger is to transfer heat from one fluid to another (colder), it is primarily that a heat exchanger material must have high coefficient of thermal conductivity. Due to the thermal stresses which occur as a consequence of heat loading it is desirable material having a high strength. In addition, it is essential to choose a material that can withstand corrosion in the

working fluids, which is taken to be water containing chloride ions (seawater). Its maximum service temperature must be adequately above the temperature of the hotter working fluid and the material must have sufficient formability to be drawn into a tube or rolled into a sheet. As higher as possible weldability and solderability/brazability of the material is desirable in order to facilitate joining of the exchanger parts and increase their reliability. Enhanced use of air condition devices in the living area, planes, trains and cars, requires lower their mass. Hence density is also taken as one of the criterion for selection of heat exchanger materials. Additionally, the low cost of the material is preferable [13]. After the selection of the criteria, it is necessary to make a list of potential materials, among

which the best one will be selected according to the criteria. For this application, general list of potential materials is consisted of the metals with both good thermal conductivity and strength, which are resistant to corrosion in saline solutions. Based on the Ashby approach pre-selection process was employed which yield the cooper alloys as the most appropriate materials for this application [14]. Taking carefully into consideration the available cooper alloys with their properties, a list of potential materials for a heat exchanger is created (Table 1) [15-17]. Unfortunately, the cost of the potential materials is not selected as a criterion due to unavailable prices for all considered materials.

Table 1. Potential heat exchanger materials

No.	Material	Thermal conductivity (W/mK)	Yield stress (MPa)	Density (g/cm ³)	Corrosion resistance	Machinability (%)	Formability	Solderability and Brazability	Weldability
M1	UNS C23000	159	125	8.75	good	30	excellent	excellent	good
M2	UNS C26000	120	105	8.53	fair	30	good	excellent	good
M3	UNS C28000	123	160	8.39	fair	40	good	excellent	good
M4	UNS C37000	120	140	8.41	good	70	fair	good	good
M5	UNS C44300	110	152	8.53	excellent	30	good	excellent	good
M6	UNS C46400	116	455	8.41	good	30	good	excellent	good
M7	UNS C60800	79	185	8.17	excellent	20	good	fair	fair
M8	UNS C61300	57	240	7.95	excellent	30	good	fair	good
M9	UNS C65500	36	152	8.53	good	30	excellent	good	excellent
M10	UNS C70600	40	125	8.94	excellent	20	good	excellent	good
M11	UNS C71500	29	170	8.94	excellent	20	excellent	excellent	good
1 – poor; 3 – fair; 5 – good; 7 – excellent									
Target values (T_i)		159	455	7.95	7	70	7	7	7

In this study 4-point scale is used for better understanding and representation of the qualitative attributes and converting linguistic terms into corresponding dimensionless numbers, as shown in Table 1. In order to select

the most suitable material for heat exchanger, MCDM Solver was applied. Before that, it is necessary to create a short list of alternative materials (preselecting) which is given in Table 1. Additionally, determination the most

favourable values in all criteria (Target values - Tj) should to be defined.

4. RESULTS AND DISCUSSION

Based on the input data, i.e. initial decision matrix, confidence level $\eta=1$ and pairwise significance evaluation of the criteria, weights of the criteria are determined (shown in Fig 3).

Figure 3 shows the pairwise significance criteria evaluation interface. The criteria listed are: Thermal conductivity (W/mK), Yield stress (MPa), Density (g/cm3), Corrosion resistance, Machinability (%), Formability, Solderability and Brazability, and Weldability. The weights determined for each criterion are: Thermal conductivity (0.18750), Yield stress (0.10714), Density (0.10714), Corrosion resistance (0.16964), Machinability (0.13393), Formability (0.09821), Solderability and Brazability (0.09821), and Weldability (0.09821).

Fig. 3. Pairwise significance criteria evaluation

MCDM Solver calculation of the subjective weightings (confidence level $\eta=1$) of criteria was carried out based on modified digital logic (MDL) method [18]. This is a pair-wise comparison method, where participants/criteria are presented with a worksheet and asked to compare the importance of two criteria at a time (Fig 3). Thereby thermal conductivity and corrosion resistance are considered as the most influential criteria with weight of 0.1875 and 0.16964 respectively, then machinability (0.13393), yield stress and density (0.10714) and finally as the least influential criteria: formability, solderability and brazability, and weldability (0.09821).

The Step 3 is the ranking of the materials by means of *MCDM Solver*. Ranking orders of materials for heat exchanger design using different MCDM methods (TOPSIS, WASPAS and VIKOR) are shown in Fig. 4. In order to make ranking results clearer and more readable, they are also shown in Table 2. As could be seen, the first three top ranked materials are M6 (UNS C44300), M1 (UNS C23000) and M5 (UNS C46400), respectively.

MCDM Solver

Step 3: Review results

	TOPSIS	WASPAS	VIKOR
M1	3	2	1
M2	10	7	11
M3	6	5	7
M4	4	4	4
M5	2	3	3
M6	1	1	2
M7	7	10	6
M8	5	6	5
M9	11	9	10
M10	9	11	9
M11	8	8	8

Fig. 4. Materials ranking results

The best ranked material is M6 – arsenical admiralty brass which is promoted as the best solution by TOPSIS and WASPAS method. The second ranked material is M1 – red brass which is nominated as the best ranked by VIKOR, while WASPAS and TOPSIS ranked this material as the second and the third one. The third ranked material is M5 – naval brass which is ranked as third one by WASPAS and VIKOR while the second ranked is by TOPSIS method.

Table 2. Ranking results with metrics

Material	TOPSIS	WASPAS	VIKOR
M1	3 0.56462	2 0.73124	1 0.06763
M2	10 0.42359	7 0.60852	11 0.89097
M3	6 0.46305	5 0.6546	7 0.75415
M4	4 0.54036	4 0.69466	4 0.22924
M5	2 0.57067	3 0.70956	3 0.13341
M6	1 0.57115	1 0.75089	2 0.09502
M7	7 0.4604	10 0.57663	6 0.64731
M8	5 0.49311	6 0.61632	5 0.59507
M9	11 0.41173	9 0.58408	10 0.88409
M10	9 0.43424	11 0.57184	9 0.87947
M11	8 0.45231	8 0.58618	8 0.77631

In such cases when there is no stable ranking of the best alternative, the aggregation ranking should be done as well as the analysing performance values (Given in Table 2) of the alternatives (optimality criteria – metrics).

5. CONCLUSION

In this paper, the application of developed DSS named *MCDM Solver* for solving heat exchanger material selection problem is considered. Thanks to *MCDM Solver*, the material selection process is carried out much faster and easier, because it comes down to selection of potential materials and pairwise significance evaluation of the selected criteria. Hence a complex mathematical apparatus is avoided and ranking process became fast, comfortable to work and reliable.

Ranked results showed that UNS C44300 - arsenical admiralty brass alloy and UNS C23000 - red brass alloy are the most preferable materials for the heat exchanger design, respectively.

Acknowledgement

This research was financially supported by the Ministry of Education, Science and Technological Development of the Republic of Serbia.

REFERENCES

- [1] Jahan A., Edwards K. L. (2013). *Multi-criteria Decision Analysis for Supporting the Selection of Engineering Materials in Product Design*, Butterworth-Heinemann.
- [2] Petković, D., Madić, Radenković, G. Knee Prosthesis Biomaterial Selection by Using MCDM Solver. *Proceeding of 15th International Conference on Accomplishments in Mechanical and Industrial Engineering DEMI 2021*, May 2021, Banja Luka, p. 107-112.
- [3] Petković, D., Madić, M. (2022). Selection of non-conventional machining processes using MCDM Solver. *Innovative Mechanical Engineering* vol. 1, no. 2, p. 48-57.
- [4] Čupić M., Tummala R., Suknović M. (2001). *Odlučivanje - formalni pristup*, Fakultet organizacionih nauka, Beograd.
- [5] Virtuode. MCDM Solver. From: <https://virtuodeportalapp.azurewebsites.net/WebTools/MCDMSolver>, accessed on: April 25, 2023
- [6] Petković D., (2017). *Izbor biomaterijala – višekriterijumska analiza i razvoj sistema za podršku odlučivanju*. (In Serbian). PhD thesis. Mašinski fakultet Univerziteta u Nišu.
- [7] Jahan, A., Bahraminasab, M., Edwards, K.L. (2012), A target-based normalization technique for materials selection, *Materials and Design*, Vol. 35, pp. 647-654.
- [8] Jahan A., Mustapha F., Ismail M.Y., Sapuan S.M., Bahraminasab M. (2011) A comprehensive VIKOR method for material selection, *Materials and Design*, Vol. 32, pp. 1215-1221.
- [9] Petković D., Madić M., Radenković G., Ranking of Biomedical Materials by Using Comprehensive WASPAS Method, *Proceedings of the 3rd International Conference Mechanical Engineering in XXI Century - MASING 2015*, September 2015, Niš, p. 339-344.
- [10] Petković D., Madić M., Radenković G. (2021), Knee Prosthesis Biomaterial Selection by Using MCDM Solver, *Advanced Technologies & Materials* Vol. 46 (2), p. 37-41.
- [11] Petković D., Madić M., Radovanović M., Janković P. An example of MCDM solver application for selection problems in machining, *Proceeding of 37th International Conference on Production Engineering*, October 2018, Kragujevac, p. 265 – 268.
- [12] Shah R.K., Sekulić D.R. (2012). *Fundamentals of Heat Exchanger Design*, Wiley India Pvt Ltd; 1st edition
- [13] Petković D., Madić M., Radenković G., Živković P., Tomić M. Heat exchangers materials selection by using MCDM approach. *Proceeding of 12. International Conference on Accomplishments in Electrical and Mechanical Engineering and Information Technology DEMI 2015*, May 2015, Banja Luka, p. 55-60.
- [14] Ashby M.F. (2011). *Materials Selection in Mechanical Design*, Butterworth-Heinemann.
- [15] Martienssen W., Warlimont H. (2005). *Springer Handbook of Condensed Matter and Materials Data*, Springer.
- [16] Cooper Development Association Inc. Cooper, From: <http://www.copper.org/> accessed on: April 25, 2023.
- [17] MatWeb. Material property data. From: <http://www.matweb.com/> accessed on: April 25, 2023.
- [18] Dehghan-Manshadi B., Mahmudi H., Abedian A., Mahmudi R. (2007). A novel method for materials selection in mechanical design: combination of non-linear normalization and a

modified digital logic method. *Materials & Design* vol. 28, p. 8-15.



Banja Luka
1-2 Jun 2023.

DEMI 2023

16th International Conference on Accomplishments in Mechanical and Industrial Engineering

www.demi.mf.unibl.org



Dependence of the Temperature Field on the Number of Simultaneously FDM-Printed PLA Samples

R.-R. Turiac^a, V. Cojocaru^{*a}, N. Bacescu^a, D. Frunzaverde^a, C.-O. Miclosina^a, G. Marginean^b

^aDepartment of Engineering Science, Babeş-Bolyai University, Traian Vuia Square, No. 1-4, 320085 Resita, Romania

^bDepartment of Materials Science and Testing, Westphalian University of Applied Sciences Gelsenkirchen Bocholt Recklinghausen, Neidenburgerstr. 43, 45897 Gelsenkirchen, Germany

Abstract

In the additive manufacturing, the influence of process parameters on the dimensional accuracy, surface quality and mechanical properties of printed parts must be identified. The 3D printing of polymeric and composite materials by fused deposition method (FDM) presents advantages related to the simplicity of equipment and low cost of materials and consumables. Meanwhile, a high number of process parameters are involved in FDM printing. The printing speed, the flow rate and the dimensions of the part (in the XY plane) influence the time between the deposition of two successive layers. In this paper the influence of dimensions of the part (a less studied parameter) is analysed considering three printing layouts: a) the simultaneous printing of five tensile test samples, b) the simultaneous printing of three tensile test samples, c) the individual printing of one tensile test sample. The variation of the temperature measured on the surface of samples is monitored throughout the entire printing process. It is highlighted that the number of specimens printed simultaneously and the position of the specimens on the build plate influence the variation of the temperature of the printed layers.

Keywords

Additive manufacturing, fused filament fabrication (PLA), polylactic acid (PLA), dimensions of the part, number of samples, temperature variation

1. INTRODUCTION

Fused deposition method (FDM) is one of the most widely used additive manufacturing method. It has advantages related to process simplicity and low costs of equipment and materials. The main challenges related to this method are to ensure repeatability in terms of dimensional accuracy and mechanical properties of printed products. The properties of parts made by FDM printing

are influenced by several process parameters as well as by pre-process and post-process factors. The most analysed process parameters are the print head temperature, the build plate temperature, the print speed, the layer thickness, the raster, the infill type and density, the build orientation [1,2].

The adhesion between layers and the adhesion between neighbouring rows from the same layer is determined by the thermal variation of the printed material [3-7].

The thermal variation of the printed material is influenced by [2, 8-12]:

- The type of material;
- The temperature of the print head;
- The temperature of the build plate;
- The printing speed;

Corresponding author

Lect. Dr. Eng. Vasile Cojocaru
vasile.cojocaru@ubbcluj.ro

Department of Engineering Science, Faculty of Engineering,
Babeş-Bolyai University, Traian Vuia Square 1-4, 320085
Reşiţa, Romania

- The layer thickness;
- The dimensions of the printed part;
- The air flows in the printing workspace;
- The type of printer.

For the materials used in FDM printing, the melting and crystallization temperatures are the defining factors for the choice of printhead temperature.

The use of a heated build plate results in slower cooling of the deposited layers, but it should be noted that the influence of the build plate temperature decreases on the upper layers (as the distance between the build plate and the last deposited layer increases).

The use of smaller layer thicknesses results in faster cooling of the printed material, but may also contribute to better diffusion between layers.

The printing speed influences the time interval between the deposition of two successive layers and between the deposition of two neighbouring rows of the same layer. At low printing speeds, the solidification of the previously deposited layer could lead to poor adhesion of the new layer. At very high printing speeds, the dimensional accuracy of the parts may be affected, as the newly deposited layer settles on an unstable substrate.

Several research has investigated the influence of layer thickness, printing speed and printing temperature on the properties of FDM parts. Several papers have analysed the cumulative effect of these parameters, using statistical methods to identify an optimal printing regime [13-14]. What is less studied so far is the influence of part overall dimensions on mechanical properties and dimensional accuracy of the product. Most of the research has been carried out on standardised samples. It is easy to understand that increasing part size, at the same printing speed, the time interval between deposition of two successive layers increases. Therefore, the analysis of the influence of printing speed, layer thickness and printing temperature should be correlated with the product dimensions. Otherwise, extrapolating the results of research carried out on standardised samples to be used on considerably larger parts can produce inaccurate results.

In a broader research, the authors of this paper aimed to investigate the influence of part size on the dimensional accuracy and mechanical behaviour of parts made by the FDM method.

For this purpose, three printing strategies of ISO 527-2 type 1A tensile test samples [15] were used:

- the simultaneous printing of five tensile test samples, placed on the same build plate;
- the simultaneous printing of three tensile test samples, placed on the same build plate;
- the individual printing of a single tensile test sample.

This paper presents the analysis of the temperature variation on the layers surface during printing according to the aforementioned strategies.

2. MATERIALS AND METHODS

The simultaneous printing of five samples on the same build plate is equivalent of printing a part with larger dimensions (compared to the case of printing a single sample or three samples simultaneously).

The following deposition strategy was used for the printing of several samples simultaneously: the first layer was deposited on every sample, then the following layer deposition occurred iteratively, each time starting with sample "5.1" (Fig.1). This strategy was maintained until the last layer was applied.

Figure 1 shows the layout of the build plate for five samples printed simultaneously in the YX orientation according to ISO/ASTM 52921:2013 [16] (the length of the sample is parallel to the Y axis of the printer). An Ultimaker 2+Connect equipment with a build plate size of 223 mm x 220 mm was used for printing.

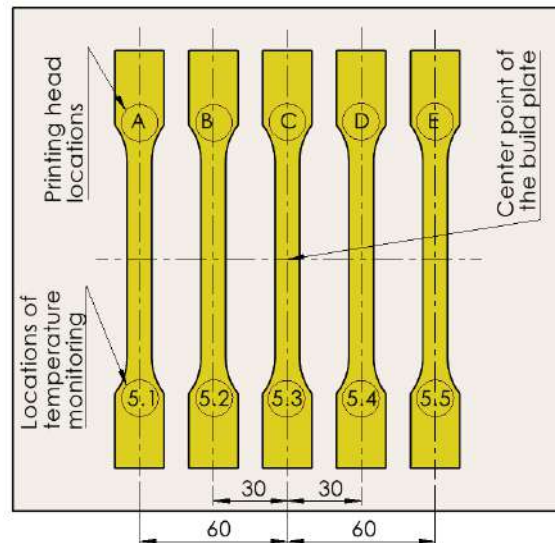


Fig. 1. The layout for 5 tensile samples printed simultaneously.

The five test samples were arranged as follows: the middle test sample (5.3) was placed in the centre of the printing plate (both in relation to the X-axis and the Y-axis). Test sample 5.2 was placed 30 mm to the left (on the X-axis) relative to sample 5.3 and sample 5.1 was placed 30 mm to the left relative to sample 5.2. Symmetrically, samples 5.4 and 5.5 were placed to the right of sample 5.3.

The temperature monitoring on the surface of the layers was carried out for each sample in the areas highlighted in Figure 1. For this purpose, five temperature measurements were taken for the same layer at five distinct moments, defined by the position of the printing head:

- the printhead deposits material in area A of sample 5.1;
- the printhead deposits material in area B of test sample 5.2;
- the printhead deposits material in area C of sample 5.3;
- the printhead deposits material in area D of test sample 5.4;
- the printhead deposits material in area E of sample 5.5.

A layer thickness of 0.2 mm and a total sample thickness of 3 mm was used. This resulted in a total of 15 layers/sample. A total of 75 temperature measurements were made for each test sample built according to this print layout.

The samples were printed from 2.85 mm diameter black filament spool of polylactic acid (PLA). According to the manufacturer's indications the black PLA filament has the melt temperature of 168 °C, the glass transition temperature of 58 °C and the melt flow rate of 8.1 g/10 minutes (for 210 °C and 21.2N).

The temperature was monitored using an Optris Laser Sight infrared thermometer, with a resolution of 0.1 °C. The printer workspace was open at the top (to allow the placement of the thermometer) and closed on the lateral walls.

Figure 3 shows the layout of the three test samples printing simultaneously. The middle sample was kept in the centre of the build plate. The lateral samples were positioned 30 mm from the centre sample. The position of sample 3.1 from Figure 2 is the same as the position of sample 5.2 in Figure 1, and the B areas are in the same position relative to the build plate (also, the positions of samples 5.3 and 3.2, respectively 5.4 and 3.3 coincide).

The temperature measurement of the test samples printed according to the layout shown in Figure 2 was carried out at three moments for each layer:

- the print head deposits material in area B of the sample 3.1;
- the printhead deposits material in area C of sample 3.2;
- the printhead deposits material in area D of test sample 3.3;

A total of 45 temperature measurements were made for each sample built using this print layout.

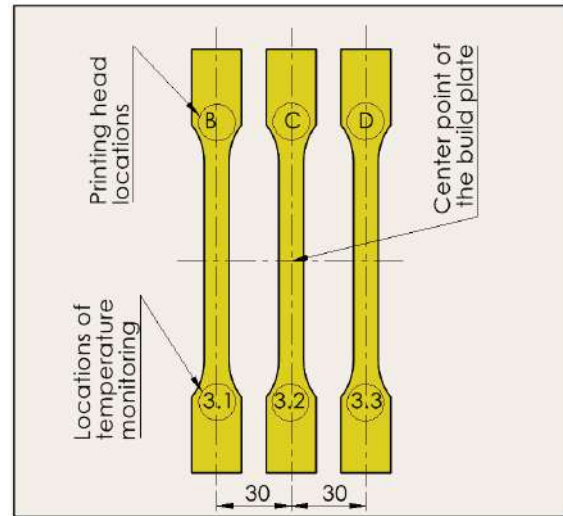


Fig. 2. The layout for 3 tensile samples printed simultaneously.

In the printing of a single sample (Figure 3) its position was set in the centre of the printing plate (the position of sample 1.1 is the same as that of samples 5.3 and 3.2, and areas C in Figures 1, 2 and 3 have the same position relative to the build plate). Only one temperature measurement for each layer was made on this sample, resulting in a total of 15 measurements.

The table 1 summarises the structure of the printed samples and the configuration of the temperature measurements (for example, code 5.1D defines the temperature measurement on sample 5.1 when the print head deposits material in area D of sample 5.4). The strategy of material deposition in the same layer has been kept constant: sample 5.1, sample 5.2, sample 5.3, sample 5.4 and sample 5.5.

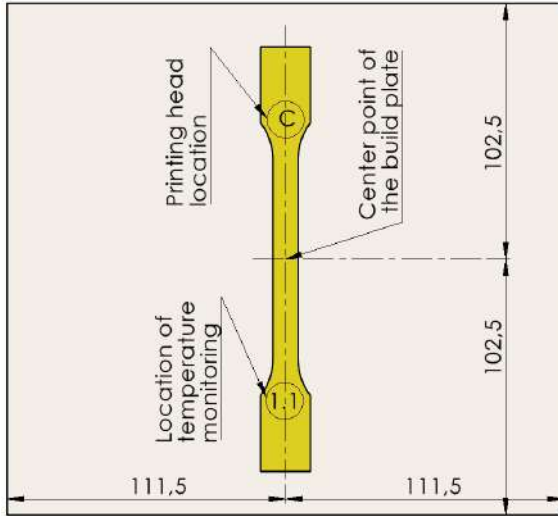


Fig. 3. The layout for one tensile sample printed.

Table 1. The temperature monitoring scheme

Sample Code	Locations of measurements & printing head positions	Number of layers	Total measurements of temperature / sample
5 samples printed simultaneously			
5.1	5.1A, 5.1B, 5.1C, 5.1D, 5.1E	15	5x15=75
5.2	5.2A, 5.2B, 5.2C, 5.2D, 5.2E	15	5x15=75
5.3	5.3A, 5.3B, 5.3C, 5.3D, 5.3E	15	5x15=75
5.4	5.4A, 5.4B, 5.4C, 5.4D, 5.4E	15	5x15=75
5.5	5.5A, 5.5B, 5.5C, 5.5D, 5.5E	15	5x15=75
3 samples printed simultaneously			
3.1	3.1B, 3.1C, 3.1D	15	3x15=45
3.2	3.2B, 3.2C, 3.2D	15	3x15=45
3.3	3.3B, 3.3C, 3.3D	15	3x15=45
1 sample			
1.1	1,1C	15	1x15=15

The print parameters remained constant for all three configurations analysed. The values of the main parameters are shown in Table 2. These values were chosen in correlation with previous research conducted by the authors [17].

Table 2. 3D-printing parameters

Parameters	Values
Layer thickness, t	0.2 mm
Printing head temperature, T_H	210 °C
Build plate temperature, T_B	60 °C
Printing speed, s_p	50 mm/s
Nozzle diameter, d_n	0.40 mm
Filament diameter, d_f	2.85 mm
Build orientation (acc. to [16])	YX
Raster angle, θ	45°/-45°
Infill density	100 %
Number of wall lines, W_L (-)	2
Fan speed	100%

3. RESULTS AND DISCUSSIONS

Figure 4 shows the temperature variation on the sample surface, considering all the measurements obtained during the printing of 5 samples simultaneously (Figure 4). It is shown that the measured temperature has a cyclic variation defined by the number of layers. The cyclic variation shows a higher amplitude for samples 5.1, 5.2 and 5.3 and a lower amplitude for samples 5.4 and 5.5.

Notably, the variations occur in the ranges of the glass transition temperature of PLA (58 °C).

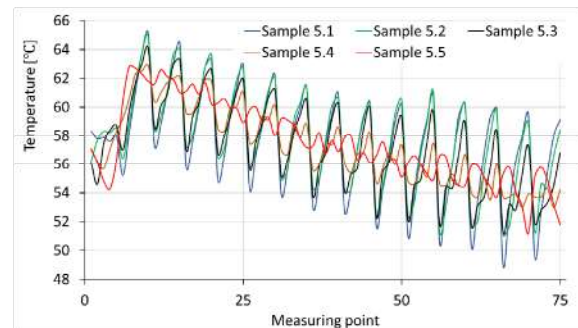


Fig. 4. The variation of the temperature measured on sample surface for 5-samples layout

It can be noticed that the average temperature decreases with increasing the number of layers deposited on the build plate. The decrease of the average temperature for the upper layers is caused by the increase of the distance between the build plate and the current layer (the

influence of the build plate temperature on the current layer decreases).

For a better understanding of the temperature correlation with the measurement points (the positions of the printing head), figure 5 shows the graphical variation for measurements made for two successive layers, 3 and 4. Five measurement points correspond to each layer. The monitoring process corresponding to layer 3 starts at point 11 (deposition of material in area A of sample 5.1) and ends at point 15 (deposition of material in area E of sample 5.5). It is observed that the temperature for sample 5.1 is lower when the printhead deposits material in area A (points 11 and 16) and increases when the printhead moves away from this sample. At the moment of measurement on the layer just deposited, the temperature is lower than the temperature of the printing plate (57.3 °C for layer 3) and after this moment the temperature of the deposited material increases due to the temperature of the printing plate (up to 64.4 °C for layer 3).

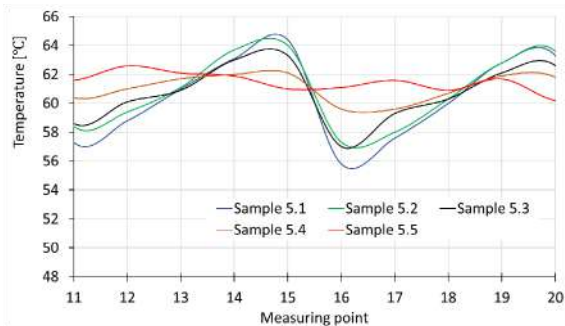


Fig. 5. The variation of the temperature measured on sample surface for five-samples layout (detailed interval corresponding to layer 3 and layer 4)

Figure 6 shows the evolution of temperatures for samples 3.1, 3.2 and 3.3. The cycles of variation associated with the layers can also be seen here. The amplitude of the variations is smaller than the amplitude obtained for the 5 samples printed simultaneously.

Comparing samples 5.2 and 3.1, printed in the same position relative to the centre of the working plate, a variation of about 6°C is observed for sample 5.2 and a variation of about 4 °C for sample 3.1. Also, in the printing of 3 samples simultaneously, larger variations are shown in samples 3.1 and 3.2 (left and centre of the build plate) compared to sample 5.3 (right side of the build plate).

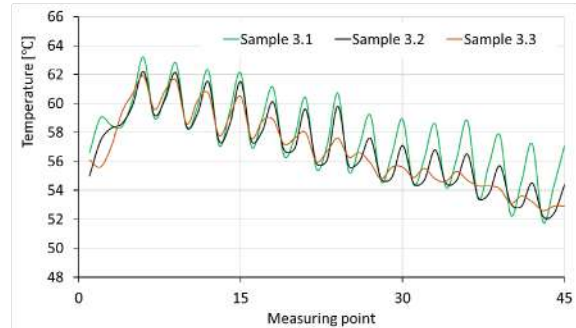


Fig. 6. The variation of the temperature measured on sample surface for three-samples layout

Figure 7 shows the temperature variation on the layer surface for the case of printing a single sample. Here, the time interval between two successive layers is smaller and no cycles of variation associated with the layers are shown.

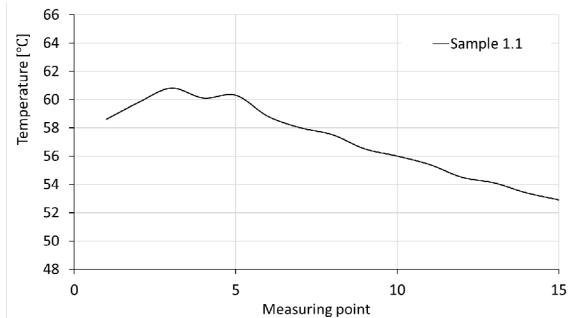


Fig. 7. The variation of the temperature measured on sample surface for one-sample layout

Figures 8 show the curves of the temperature variation measured on sample 5.1, obtained by separating the values according to the position of the print head at the time of measurement:

- The print head in area A of sample 5.1;
- The print head in area B of sample 5.2;
- The print head in area C of sample 5.3;
- The print head in area D of sample 5.4;
- The print head in area E of sample 5.5.

All five curves show a decrease in temperature with increasing the number of the layers deposited. The lowest temperatures correspond to the measurement moment with the printhead on sample 5.1 (area A), while the highest temperatures correspond to the measurement with the printhead on sample 5.5 (area E).

Plotting the same types of curves for samples 5.2 and 5.3 (Figure 9 and figure 10) shows a closeness between the maximum values (print head in area E of sample 5.5) and the minimum values (print head in areas A and B of samples 5.1 and 5.2). This tendency for the curves to

converge to same values is accentuated for samples 5.4 and 5.5 (Figures 11 and 12).

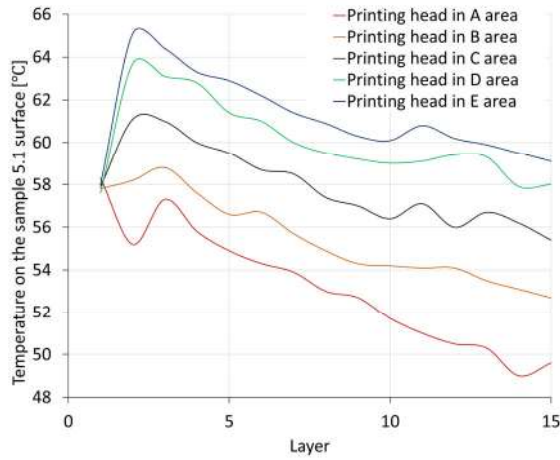


Fig. 8. The variation of the temperature measured on the surface of sample 5.5

Analysing the figures 11 and 12 it can be stated that the moment (print head position) of temperature measurement in the same layer does not have a major influence on the values measured on samples 5.4 and 5.5.

The different temperature variation of the samples positioned on the same build plate may cause a variation of the mechanical properties of the part (for large dimensions parts, the differences in behaviour may occur between different areas of the part – anisotropic behaviour even in the horizontal YX plane). Furthermore, the different temperature variations between the five samples layout, three samples layout and one sample layout indicate that the part sizes should be considered in the analysis of the influence of process parameters on the properties of printed parts.

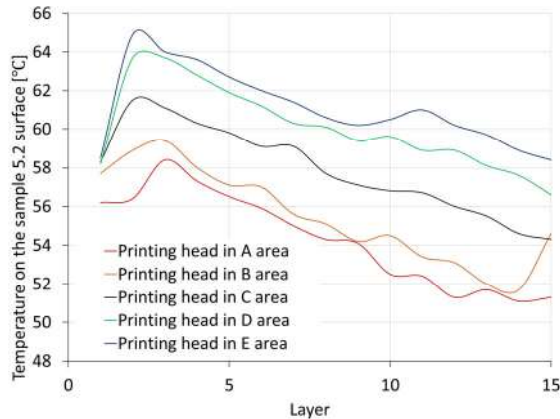


Fig. 9. The variation of the temperature measured on the surface of sample 5.2

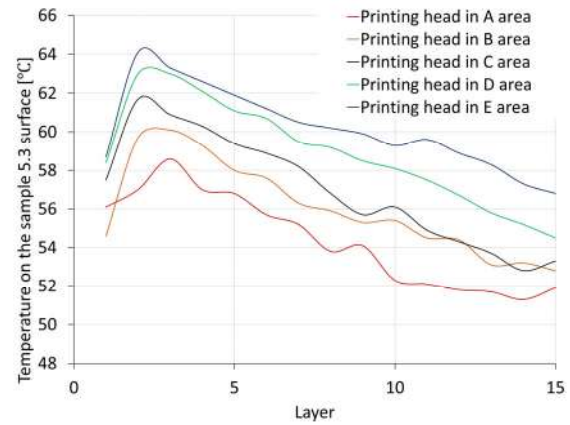


Fig. 10. The variation of the temperature measured on the surface of sample 5.3

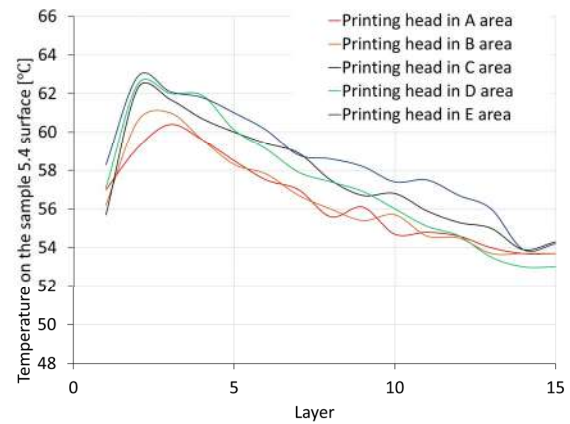


Fig. 11. The variation of the temperature measured on the surface of sample 5.4

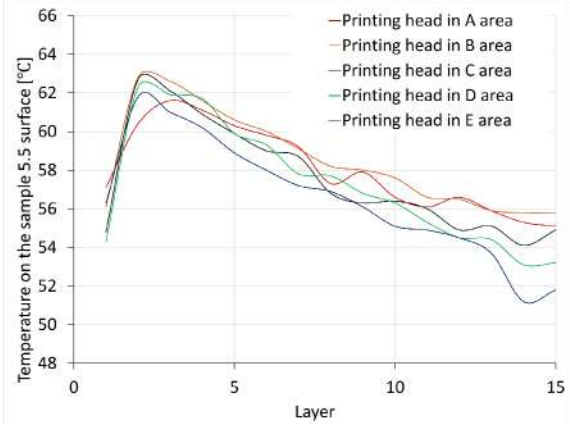


Fig. 12. The variation of the temperature measured on the surface of sample 5.5

The limitations of this analysis are given by the equivalence between samples printed at a certain distance one from each other and a larger part where one layer would have continuity. Also, the deposition strategy and the raster influence the time interval between deposition of two successive layers.

Another limitation is connected to the temperature monitoring procedure (by individual measurements taken at a certain time interval, corresponding to chosen print head positions). In preliminary tests, continuous temperature monitoring was also performed, but the results were difficult to process due to interference in the measurement space of the print head guide columns.

The temperature measurement using a closed-space printer without a cover (in order to position the temperature measuring equipment above the samples) influenced the air flows within the print space and thus the temperature evolution on the surface of the deposited layers. However, this aspect is found in very many FDM printers that have an open or partially open workspace.

4. CONCLUSIONS

In this research paper, the variation of temperature measured on the surface of differently printed samples was analysed.

The results show significant differences between the temperature variations obtained for the simultaneously printed samples on the same build plate. These differences are thought to be caused by the air flows inside the printer and by the design features of the printer (position of fans, position of particle filters, slots in the housing, etc.). The differences in temperature variations depending on the position of the sample on the build plate can generate differences in mechanical properties of the parts, which will be analysed in further research.

The achieved results indicate that part size is an issue to be considered while correlating printing parameters with the mechanical properties of the printed product. The part size influences the time interval between deposition of material on two successive layers of the same part area.

Acknowledgement

The activities of the two master students, Raul Rusalin Turiac and Nicoleta Bacescu, carried out within this research were supported by the Babes-Bolyai University through Special Scholarships for Scientific Activity.

REFERENCES

- [1] Anitha, R., Arunachalam, S., Radhakrishnan, P. (2001). Critical parameters influencing the quality of prototypes in fused deposition modelling. *Journal of Materials Processing Technology*, vol. 118, p. 385-388, DOI: 10.1016/S0924-0136(01)00980-3
- [2] Cojocaru, V., Frunzaverde, D., Miclosina, C.-O., Marginean, G. (2022). The influence of the process parameters on the mechanical properties of PLA specimens produced by fused filament fabrication—A review. *Polymers*, vol.14, no.5, p.886. DOI:10.3390/polym14050886
- [3] Corson, B., Asseko A.C.A. (2019) Effect of the Nozzle Radiation on the Fused Filament Fabrication Process: Three-Dimensional Numerical Simulations and Experimental Investigation, *Journal of Heat Transfer*, vol. 141, p. 082102-1. DOI: 10.1115/1.4043674
- [4] Lepoivre, A., Boyard, N., Levy, A., Sobotka, V., (2020) Heat Transfer and Adhesion Study for the FFF Additive Manufacturing Process, *Procedia Manufacturing*, vol. 47, p. 948-955. DOI: 10.1016/j.promfg.2020.04.291
- [5] Rudolph, N., Chen, J., Dick, T. (2019) Understanding the Temperature Field in Fused Filament Fabrication for Enhanced Mechanical Part Performance. *AIP Conference Proceedings* 2019. DOI: 10.1063/1.5084906
- [6] Schiavone, N., Verney, V., Askanian, H. (2020) Effect of 3D Printing Temperature Profile on Polymer Materials Behavior. *3D Printing and Additive Manufacturing*, vol. 7, no. 6, p. 311-325. DOI: 10.1089/3dp.2020.0175
- [7] Liparoti, S., Sofia, D., Romano, A., Marra, F., Pantani, R. (2021), Fused Filament Deposition of PLA: The Role of Interlayer Adhesion in the Mechanical Performances. *Polymers*, vol. 13, p. 399. DOI: 10.3390/polym13030399
- [8] Spoerk, M., Gonzalez-Gutierrez, J., Sapkota, J., Schuschnigg, S., Holzer, C. (2017) Effect of the Printing Bed Temperature on the Adhesion of Parts Produced by Fused Filament Fabrication. *Plastics, Rubber and Composites*, vol. 47 (1), p. 17-24. DOI: 10.1080/14658011.2017.1399531
- [9] Vanaei, H. R., Shirinbayan, M., Costa, S. F., Duarte, F. M., Covas, J. A., Deligant, M.; Khelladi, S.; Tcharkhtchi, A. (2020) Experimental Study of PLA Thermal Behavior during Fused Filament Fabrication. *Journal of Applied Polymer Science*, vol. 138 (4), p. 49747. DOI: 10.1002/app.49747
- [10] Butt, J., Bhaskar, R. & Mohaghegh, V. (2022). Analysing the effects of layer heights and line widths on FFF-printed thermoplastics. *Int J Adv*

- Manuf Technol*, vol. 121, p. 7383–7411. DOI: 10.1007/s00170-022-09810-z
- [11] Valerga, A.P., Batista, M., Salguero, J., Girot, F. (2018). Influence of PLA Filament Conditions on Characteristics of FDM Parts. *Materials*, vol. 11, no. 8, p. 1322. DOI: 10.3390/ma11081322
- [12] Goh, G.D., Yap, Y.L., Tan, H.K.J., Sing, S.L.; Goh, G.L.; Yeong, W.Y. (2020) Process-Structure-Properties in Polymer Additive Manufacturing via Material Extrusion: A Review. *Crit. Rev. Solid State Mat. Sci.* vol. 45, p. 113–133. DOI: 10.1080/10408436.2018.1549977
- [13] Nyiranzeyimana, G., Mutua, J.M., Mose, B.R., Mbuya, T.O. (2021) Optimization of process parameters in fused deposition modelling of thermoplastics: A review. *Materialwiss. Werkstofftech.*, vol. 52, no.6, p. 682–694. Doi: 10.1002/mawe.202000193
- [14] Cuan-Urquiza, E.; Barocio, E.; Tejada-Ortigoza, V.; Pipes, R.B.; Rodriguez, C.A.; Roman-Flores, A. (2019) Characterization of the Mechanical Properties of FFF Structures and Materials: A Review on the Experimental, Computational and Theoretical Approaches. *Materials*, vol. 12, p. 895. DOI: 10.3390/ma12060895
- [15] International Organization for Standardization. *ISO 527-2:2012, Plastics—Determination of Tensile Properties—Part 2: Test Conditions for Molding and Extrusion Plastics*. International Organization for Standardization: Geneva, Switzerland, 2012.
- [16] International Organization for Standardization. *ISO/ASTM 52921:2013, Standard Terminology for Additive Manufacturing—Coordinate Systems and Test Methodologies*. International Organization for Standardization: Geneva, Switzerland, 2013.
- [17] Frunzaverde, D., Cojocaru, V., Ciubotariu, C.-R., Miclosina, C.-O., Ardeljan, D.D., Ignat, E.F., Marginean, G. The Influence of the Printing Temperature and the Filament Color on the Dimensional Accuracy, Tensile Strength, and Friction Performance of FFF-Printed PLA Specimens. *Polymers*, vol. 14, p. 1978. DOI: 10.3390/polym14101978



Banja Luka
1-2 Jun 2023.

DEMI 2023
**16th International Conference on
Accomplishments in Mechanical and
Industrial Engineering**
www.demi.mf.unibl.org



Determination of the Machinability of Leaded Bronze by Measuring Cutting Forces at Turning with WC - Co Coated Carbide Inserts

N. Šibalić^a, M. Mumović^a, O. Mijanović^a

^aFaculty of Mechanical Engineering, University of Montenegro, Džordža Vasiingtona bb, Podgorica, Montenegro

Abstract As the number of factors that influence cutting forces is large, their determination always presents a significant research challenge during the measurement itself, all with the aim of defining the machinability of the material. Since cutting force is most influenced by the material of the workpiece itself, a material with favorable cutting characteristics was chosen for the workpiece, while other influencing factors will be varied through experimental research. In order to successfully perform measurements, a modern information measuring system was used, as well as other equipment for recording cutting forces during turning processing. The material of the workpiece is leaded bronze CuPb10Sn10 with a diameter of $\varnothing 20$ mm. The machine tool used in the experimental research is a universal lathe with a nominal power of 4 kW, while the tools used are with indexable inserts with a coating of extra fine-grained wolfram cobalt carbide WC - Co. The paper also presents the theoretical foundations of turning technology, as well as the principle of operation. A three-factor orthogonal experimental plan was adopted, where varied parameters are the cutting depth a mm, the feed f mm/rev, and the rotational speed of the main spindle n rpm. The response functions are three force components in three mutually normal directions (F_c – main cutting force, F_r – radial force, and F_t – thrust force). Through the analysis of the measured values, the machinability of the selected material is determined.

Keywords Turning, Cutting forces, Machinability, Leaded bronze, Information measurement system

1. INTRODUCTION

In metal cutting technologies, knowing the intensity of force and torque for individual cutting elements of the tool during turning processing is of exceptional practical importance, the principles of which are defined in the theory of cutting (kinetostatics of the cutting process) through exact equations.

Nikola Šibalić

PhD, Nikola Šibalić
nikola@ucg.ac.me

Faculty of Mechanical Engineering, University of Montenegro
Džordža Vasiingtona bb
Podgorica, Montenegro

Turning is a cutting process that primarily produces radially symmetrical parts such as shafts, bushings, pulleys, as well as many other machine elements. In turning machining, the workpiece performs the main rotary movement, while the tool performs auxiliary linear movement. The cutting tool used in this processing is called a turning tool, which removes material in the shear plane, which leads to the formation of chips. The cutting edge is defined by the intersection of the rake and flank faces, which together form the cutting wedge. The penetration of the cutting wedge of the tool into the material of the object of processing is opposed by cutting forces, so the knowledge of the components of cutting forces has an

extremely important role in determining the processes: machinability of the material, optimization of cutting through the criterion of wear of the cutting tool, development of cutting tools, determination of quality parameters of product manufacturing and control of machines through real-time adaptive feedback systems.

Machinability represents the suitability of the material to be processed by cutting. The term machinability of materials is complex and is considered simultaneously from several aspects and under different processing conditions. Thus, for example, a material with good machinability in turning processing can have low machinability in broaching processing, etc. [1]. Machinability can be determined using several methods such as monitoring tool life, determination of cutting forces, energy consumption, machined surface roughness, and chip shape [2]. Machinability primarily depends on the physical and mechanical properties of the material, the chemical composition, and the structure of the material. Empirical expressions for the main processing factors, which are determined experimentally, are most often used to evaluate the machinability of a material.

Machinability constants express the influence of the primary group of factors (depth of cut and feed) on three mutually perpendicular components of forces during turning F_c , F_r , and F_t , where F_c – the main cutting force that coincides with the direction of the cutting speed, F_r – radial force that is normal to the machined surface and F_t – thrust force that coincides with the direction of the speed of the auxiliary movement, which represents the cutting forces [1], considering other influencing factors through correction coefficients that take into account: the influence of the cutting speed, the material of the workpiece, tool cutting edge angle, the tool cutting edge inclination of the blade, tool geometry, workpiece material condition, tool condition and lubricating properties of coolant. The cutting force components are shown in Fig. 1.

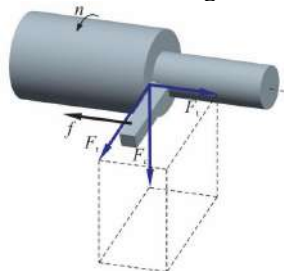


Fig. 1. Cutting forces at longitudinal turning

Considering that in this paper leaded bronze is processed with the adopted cutting tool where the inserts are coated with WC - Co, most of these correction coefficients do not change, it is justified to define the cutting force components with an extended expression, so that in this paper in consideration is also taken of the effect of the rotational speed along with the depth of cut and feed. The values of the cutting forces can be represented mathematically by following functions with sufficient accuracy, so empirical expressions are formed:

$$F_c = C_{f1} a^{x_1} f^{y_1} n^{z_1} \quad (1)$$

$$F_r = C_{f2} a^{x_2} f^{y_2} n^{z_2} \quad (2)$$

$$F_t = C_{f3} a^{x_3} f^{y_3} n^{z_3} \quad (3)$$

where: a – cutting depth, f – feed and n – rotational speed are varied factors, while C_{f1} , C_{f2} and C_{f3} machinability constants, x_1 , y_1 , z_1 , x_2 , y_2 , z_2 , x_3 , y_3 and z_3 machinability parameters.

2. EXPERIMENTAL MATERIAL

The material used in experimental research is leaded bronze, which belongs to copper alloys and has a large industrial application in the oil and petrochemical industry for the production of sliding bearings, fittings, gears, valves, etc. Due to its wide application, the machinability of bronze by the turning process is the subject of numerous studies [2 - 5]. From the rod with a diameter of Ø20 mm, which was manufactured by casting, a workpiece was made that is used in experimental research. Fig. 2 shows a workpiece made of segments on every 15 mm. The segments are separated by 4 mm wide grooves and each of the segments is used for one experimental point. In this way, it is possible for the turning tool to machine an equal length at each experimental point.



Fig. 2. Workpiece from leaded bronze CuPb10Sn10

The chemical composition of the material used is given in Table 1, and the basic mechanical properties in Table 2.

Table 1. Chemical properties of leaded bronze *CuPb10Sn10*

Cu %	Sn %	Pb %
78 ÷ 82	9 ÷ 11	8 ÷ 11

Table 2. Mechanical properties of leaded bronze *CuPb10Sn10*

Yield strength MPa	Tensile strength MPa	Elongation at break %	Brinell hardness HB
110	230	12	70

3. CUTTING TOOL AND THE MACHINE

The cutting tool in this research is a turning tool with indexable inserts. The support used is from the renowned manufacturer *SANDVIK*, and the insert *SNMG 120408E-SM* from the manufacturer *PRAMET* (Fig. 3), which is intended for processing brittle materials such as gray cast iron or in this case leaded bronze.



Fig. 3. Cutting tool with indexable insert

The geometry of the cutting tool directly affects the values of the cutting forces, the energy spent on processing, the working life of the tool, and the quality of the processed surface, so the correct choice of geometry is extremely important. The geometry of the cutting tool used is given in Table 3.

Table 3. Geometrical values of the used turning tool

Parameter	Value
Tool orthogonal clearance	$\alpha_0 = 0^\circ$
Tool orthogonal rake	$\gamma_0 = 5^\circ$
Tool cutting edge inclination	$\lambda_s = -8^\circ$
Tool cutting edge angle	$\chi_r = 45^\circ$
Tool included angle	$\varepsilon_r = 90^\circ$
Nose radius	$r = 0.8 \text{ mm}$

Since the cutting edge angle of the cutting tool used is 45° , in this research it is an oblique cutting. In addition to the geometric parameters of the cutting tool, the material of the cutting tool

and its coating also has an important role. The tool material is tungsten carbide coated with WC-Co coating.

The machine used in the experimental research is the Universal lathe 1A616Π with a power of 4 kW. The machine has 48 gears of main movement in the range from 9 to 1800 rpm and 56 gears of auxiliary movement in the range from 0.034 to 56 mm/rev. The distance between the centers in the working area is 710 mm, and the height of the centers is 165 mm.

4. EXPERIMENTAL RESEARCH

For the implementation of experimental research, the definition of the experiment was made, the experimental plan was adopted, as well as all relevant input parameters. In order to obtain the values of the defined constants and machinability parameters for the given material, the force components were measured in three normal directions and acquired using the information measurement system.

4.1 Information measurement system

The information measurement system includes several components of measuring equipment, that are working together, which ensures reliable results. The information measurement system consists of: a sensor (dynamometer for measuring cutting force components), a charge amplifier, a universal amplifier and an acquisition system. The block diagram of the used information measurement system is shown in Fig. 4.

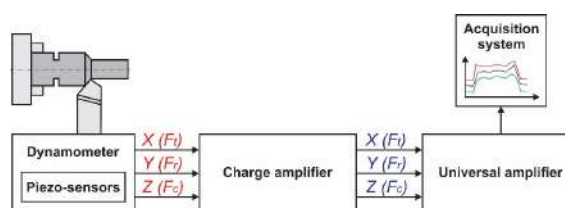


Fig. 4. Information measurement system

The piezo-plate sensor (*Kistler 9257A Dynamometer*) provides a dynamic and quasi-static measurement of three orthogonal force components. The dynamometer has a high stiffness and therefore a high natural frequency. The measuring range is from -5 kN to 5 kN, while at turning process the measuring range for the z-axis ranges from -7.5 kN to 15 kN if the tool tip is

in the proper position. The sensor can be shortly overloaded by 50% compared to the nominal value. The working temperature of the dynamometer is between 0 °C and 70 °C.

A charge amplifier (*Kistler 5806*) also called an integrator converts the electric charge signal into a voltage signal. The charge produced by a piezoelectric sensor is a variable that is difficult to measure due to its nature. For this reason, an electronic device is used that is connected after the sensor. The charge amplifier converts the negative charge produced by the piezoelectric sensor when subjected to a force load into a positive voltage that is proportional to the charge and thus to the applied force. Due to their working principle, force sensors have a negative sensitivity and they produce a negative charge under load.

Universal amplifier (*HBM QuantumX MX840B*) is a universal amplifier with 8 channels. It is a combination of an AD converter and an amplifier, which digitizes and amplifies the electrical voltage signal it receives. Each channel allows acquisition with over 15 different types of sensors. The 15 - pin connector is used as the input connectors. All channels are electrically isolated from each other and from the power inputs.

The data acquisition system consists of a computer on which the *HBM Catman* software package is installed for displaying and processing data obtained from the universal amplifier.

4.2 Experimental plan

For the experimental plan, a three-factor orthogonal plan $k = 3$ was adopted, with varying factors on two levels and repetition in the central point of the plan $n_0 = 4$. The number of experimental points $N = 12$ is determined according to the following equation:

$$N = 2^k + n_0 \quad (4)$$

The limits of the interval of the input factors are adopted according to the condition:

$$X_{0i}^2 = X_{ui} \cdot X_{li}, i = 1, 2, 3 \quad (5)$$

Based on preliminary research and the literature source [6], the values of various parameters of the cutting were adopted: a – cutting depth mm, f – feed mm/rev, and n – rotational speed of the workpiece rpm, which are given in Table 4.

Table 4. Geometrical values of the used turning tool

Input factors:	Upper level (+)	Lower level (-)	Central level (0)
$X_1 = a \text{ mm}$	2.54	1	1.59
$X_2 = f \text{ mm/rev}$	0.18	0.045	0.091
$X_3 = n \text{ rpm}$	1400	900	1120

4.3 Conducting experimental research

As part of the experimental research, the cutting force components were measured according to the adopted experimental plan matrix. Experimental research was done in laboratory conditions. Fig. 5 shows the research site with installed equipment for measuring and acquiring cutting force components.

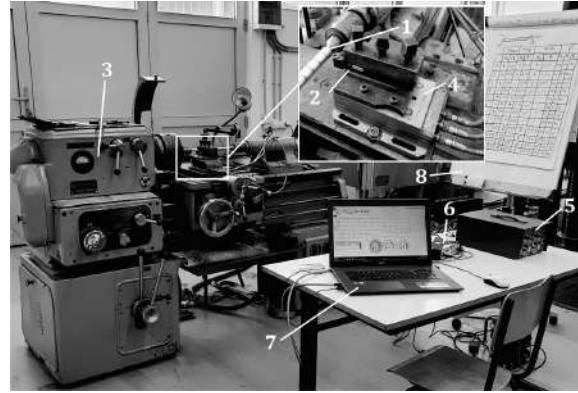


Fig. 5. Research site: 1 – workpiece, 2 – cutting tool, 3 – machine, 4 – dynamometer, 5 – charge amplifier, 6 – universal amplifier, 7 – system for data acquisition, 8 – plan matrix of the experiment

The resulting diagram of the measured components of cutting forces depending on time t is given in Fig. 6.

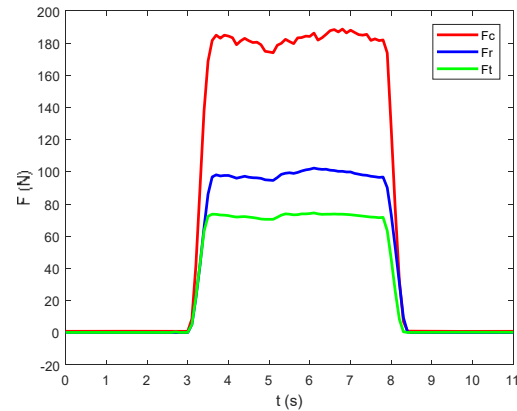


Fig. 6. Cutting forces values at the point of the experimental plan number 6

Table 5 shows the adopted orthogonal plan according to which the experimental research was performed and the output values were obtained.

Table 5. Plan matrix of the experiment

No.	Depth of cut mm	Feed mm/rev	Rotational speed rpm	Main cutting force	Radial force	Thrust force
	$X_1 = a$	$X_2 = f$	$X_3 = n$	Output vectors Y		
X_{ui}	2.54	0.18	1400			
X_{li}	1	0.045	900	F_c N	F_r N	F_t N
X_{0i}	1.59	0.091	1120			
1.	+1	+1	+1	411.4	205.2	172.0
2.	-1	+1	+1	183.6	102.6	73.5
3.	+1	-1	+1	720.0	258.5	231.1
4.	-1	-1	+1	291.9	124.5	86.3
5.	+1	+1	-1	360.9	179.1	154.4
6.	-1	+1	-1	187.9	102.2	74.4
7.	+1	-1	-1	689.1	243.3	208.0
8.	-1	-1	-1	292.3	126.2	85.2
9.	0	0	0	116.2	112.4	93.7
10.	0	0	0	112.2	110.1	92.7
11.	0	0	0	107.4	110.4	90.0
12.	0	0	0	111.8	106.1	91.0

Using the regression analysis of the experimental results, the values of the coefficients and machinability parameters were determined. First, equations (1), (2), and (3) were transformed into logarithmic form, and appropriate substitutions were introduced, so we get equations of the form:

$$y = b_0 x_0 + b_1 x_1 + b_2 x_2 + b_3 x_3 \quad (6)$$

where: b_0 , b_1 , b_2 , and b_3 are linear regression coefficients that are determined according to the plan matrix based on the equations:

$$b_0 = \frac{1}{N} \cdot (y_1 + y_2 + \dots + y_N) \quad (7)$$

$$b_i = \frac{1}{N} \cdot \sum_{j=1}^N x_{ij} y_j, i = 1, 2, 3 \quad (8)$$

Finally, values of coefficient C_{f1} and parameters x_1 , y_1 , and z_1 of machinability are determined for the main cutting force from the equations:

$$x_1 = 2 \cdot \frac{b_1}{\ln(a_{\max}/a_{\min})}; \quad (9)$$

$$y_1 = 2 \cdot \frac{b_2}{\ln(f_{\max}/f_{\min})} \quad (10)$$

$$z_1 = 2 \cdot \frac{b_3}{\ln(n_{\max}/n_{\min})} \quad (11)$$

$$\ln C_{f1} = b_0 + b_1 + b_2 + b_3 - (x_1 \cdot \ln a_{\max} + y_1 \cdot \ln f_{\max} + z_1 \cdot \ln n_{\max}) \quad (12)$$

The resulting values of the machinability parameters can be seen in the decoded version of the empirical equations for the cutting forces in N at the turning process:

$$F_c = 35.1119 \cdot a^{0.8634} f^{-0.3808} n^{0.0849} \quad (13)$$

$$F_r = 31.6999 \cdot a^{0.7084} f^{-0.1697} n^{0.106} \quad (14)$$

$$F_t = 20.9630 \cdot a^{0.9276} f^{-0.1605} n^{0.1212} \quad (15)$$

5. CONCLUSION

Knowing the cutting forces during turning processing allows us to determine the machinability of the material through the influential parameters of the cutting depth and feed. In order to obtain more accurate data, the empirical model for machinability was extended with an influential parameter of the rotational speed. Research in this paper has shown that with the correct choice of tool geometry, using inserts with WC - Co coatings during machining by turning lead bronze, gives a high level of consent between experimental data and the obtained machinability model.

REFERENCES

- [1] Kalpakjian, S., and Schmid, S. (2008). *Manufacturing Processes for Engineering Materials*, Fifth Edit. Pearson Prentice Hall. ISBN-13 978-981-06-7953-8
- [2] Amaral, L., et al. (2018). *Effect of lead on the machinability of brass alloys using polycrystalline diamond cutting tools*, J. Strain Anal. Eng. Des., vol. 53, no. 8, pp. 602-615, doi: 10.1177/0309324718796384.
- [3] Suhail, M., Deepak, A., and Nikam, S. (2014). *Study of Cutting Forces and Surface Roughness in Turning of Bronze Filled Polytetrafluoroethylene*, Int. J. Adv. Mech. Eng., vol. 4, no. 2, pp. 151-160.
- [4] Dobrotă, D., Oleksik, M. and Chicea, A. (2022). *Ecodesign of the Aluminum Bronze Cutting Process*, Materials (Basel), vol. 15, no. 8, doi: 10.3390/ma15082735.
- [5] Amancio, D., et al. (2015). *Morphological analysis of chip generated by the process of turning on bronze aluminium industry used in aeronautics via electronic scanning microscopy*, Mater. Sci. Forum, vol. 805, no. April, pp. 374-379, doi: 10.4028/www.scientific.net/MSF.805.374.
- [6] Klocke, F. et al. (2010). *Recommended machining parameters for copper and copper alloys*, DK1 Monogr. I.18, vol. I.18, pp. 1-64.



Banja Luka
1-2 Jun 2023.

DEMI 2022

16th International Conference on Accomplishments in Mechanical and Industrial Engineering

www.demi.mf.unibl.org



Influence of the layer thickness and the filament color on the surface finish of PLA samples printed by FDM

N. Bacescu¹, D. Frunzaverde^{1*}, R.-R. Turiac¹, V. Cojocaru¹, C.-R. Ciubotariu¹, G. Marginean²

¹Department of Engineering Science, Babes-Bolyai University, Traian Vuia Square, No. 1-4, 320085 Resita, Romania

²Department of Materials Science and Testing, Westphalian University of Applied Sciences Gelsenkirchen Bocholt Recklinghausen, Neidenburgerstr. 43, 45897 Gelsenkirchen, Germany

Abstract Fused deposition modeling (FDM) is one of the most commonly used additive manufacturing technologies due to the relatively low costs of equipment and materials, as well as the simplicity of the process. The quality and properties of FDM printed components are influenced by numerous and interdependent process parameters, as well as the type and color of the filament. The present paper analyzes the extent to which the layer thickness and the color of the filament influence the surface finishing of FDM printed PLA samples.

In order to evaluate the influence of the layer thickness and the PLA color on the surface quality, a number of each two samples were printed using neutral (colorless), black, grey and red PLA and two values of the layer thickness, respectively: 0.05 and 0.20 mm. All other 3D printing parameters were the same for the 8 samples. The surface quality of the samples was evaluated by laser scanning microscopy. The experimental results showed that the surface roughness was influenced both by the layer thickness and the filament color, the latter variable having a significant effect in this respect, as well.

Keywords Additive manufacturing, FDM/FFF, PLA, layer thickness, filament color, surface finish

1. INTRODUCTION

Additive manufacturing (AM) has developed spectacularly in the last decades from rapid prototyping to rapid fabrication. With the help of 3D printing systems, it is possible to create customized or small series products with low production costs and short supply chains, as well as to eliminate waste and to produce only what is needed. Providing the aforementioned advantages and fully digitized processes, AM represents nowadays a revolution in fabrication

technologies.

FDM (Fused Deposition Modelling), known also as Fused Filament Fabrication (FFF) is one of the most commonly used 3D printing technologies [1,2]. The working principle of FDM is to extrude a thermoplastic material through a heated nozzle that melts the polymer and then deposits the filament, layer by layer, onto a build platform. The process is repeated until the part is complete. As a consequence of the layer-by-layer deposition technique, inaccuracy at the level of each layer may occur, as well as improper interlayer adhesion, both phenomena affecting the quality of the print. One of the materials most frequently used for FDM printing is the poly lactic acid (PLA), due to the fact, that it is economically produced from renewable resources [2].

Corresponding author

Univ. Prof. Dr. Eng. Doina Frunzaverde
doina.frunzaverde@ubbcluj.ro

Babes-Bolyai University
CU UBB Resita
Traian Vuia Square, No.1-4
320085 -Resita
Romania

Although FDM provides the opportunity to satisfy the most complex requirements, one has to consider that the printing process is strongly influenced by numerous interdependent parameters, that affect the mechanical properties, surface quality, process repeatability, level of precision and accuracy of the finished products [3]. As revealed by previous research on this topic, the multitude of FDM variables, as well as the lack of standardization makes it very difficult to establish optimal combinations of process parameters, that can assure both good quality and suitable properties of the 3D printed products.

One of the main problems of end user products fabricated by FDM is their usually improper surface finish. A good surface quality contributes to the good functioning of the manufactured parts as well as the reduction of post-processing costs. Therefore, this subject was addressed to by many researchers, trying to define the influence of different parameters on the surface quality and/or to find the proper set of variables that lead to improved surface finish [4-8].

The effect of the layer thickness on the part quality has been studied in various works, most of the authors concluding that it represents a dominant influential factor in this regard [9-13]. About the relation between the layer height and the surface roughness, the researchers manifest a unanimous point of view: a lower layer height improves the surface quality [6, 8-10,13-18]. Altan et al. [10] analyzed the combined effect of three process parameters on the surface roughness and the tensile strength, respectively the layer thickness, the deposition head speed and the nozzle temperature. The authors revealed that the layer thickness was the dominant influential variable for increasing tensile strength and decreasing surface roughness. Anitha et al. selected for comparative ANOVA analysis the layer thickness, the road width and the deposition speed and concluded that the variable most effective in relation to the surface quality is the layer thickness (contribution of 51.57%), compared to the road width (contribution of 15.57%) and respectively speed of deposition (contribution of 15.83%) and that "there is a strong inverse relationship" between layer thickness and surface roughness.

On the contrary, the effect of the PLA filament color on the quality and the properties of FDM printed parts is an often overlooked feature. Only few researchers addressed this topic [19-23]. Pigments, based on their composition, can differently influence both the mechanical properties and the quality of the products obtained by FFF [22]. The concrete composition of the material is known only by the filament manufacturer. Valerga et al [22] concluded that the lack of pigment leads to a smoother and more homogeneous surface. Soares [19] studied the influence of the polylactic acid (PLA) color on the thermal behavior, dimensional accuracy and surface quality using filaments of different colors (natural, green, black). Again, the best results in terms of surface quality were obtained for natural PLA, as "that the parameters used in the study were closer to the ideal parameters to this color of PLA."

The present paper aims to analyze the influence of the layer thickness and the color of the PLA filament on the surface quality of samples obtained by the FDM method. As far as known by the authors, no other experimental investigations were carried out in particular on this topic.

2. MATERIALS AND METHODS

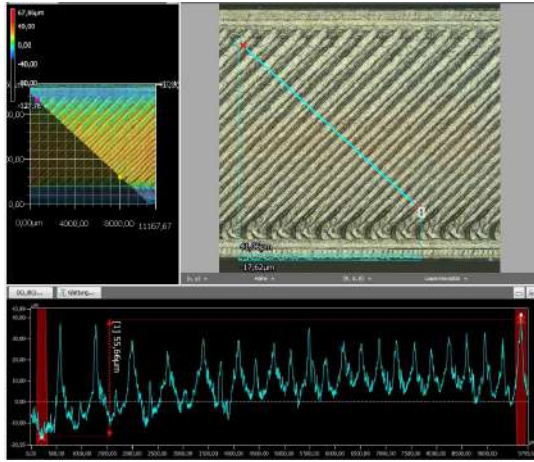
In order to highlight the influence of the layer thickness and the color of the PLA filament on the surface quality, a number of 8 dogbone samples according to ISO 527-2 type 1A [24] were printed using an Ultimaker 2+Connect equipment. The CAD model of the specimens was realized with SolidWorks and the samples thickness was set at 3 mm. The material used was Verbatim PLA with 2.85 mm diameter and the colors of the filaments selected for the experiments were natural, black, gray and red. Two samples were printed for each color and respectively the layer thicknesses of 0.05 mm and 0.20 mm. The other process parameters were the same for all samples, as follows:

- printing temperature: 210°C;
- build plate temperature: 60°C;
- printing speed: 50 mm/s;
- nozzle diameter: 0.40 mm;
- build orientation, according to [25]: YX;
- raster angle: 45°/-45°;
- infill density: 100%;
- number of wall lines: 2.

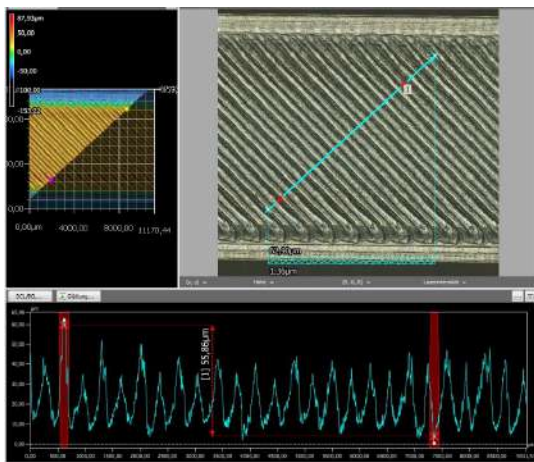
The evaluation of the surface profile was realized using a Keyence VKX-260K confocal laser scanning microscope (CLSM).

3. RESULTS AND DISCUSSIONS

Representative images of the roughness profiles of different colored PLA samples, printed with the two layer heights selected for the experiments are presented in Figures 1-4 and the measured values of the total height of the roughness profile (R_t) are summarized in Table 1. For conformity, one has to consider that the limits for the surface profiles have been set at different values, so that the overall dimensions of the graphs could be kept the same. Therefore, the values in Table 1 have to be taken into account for comparison.

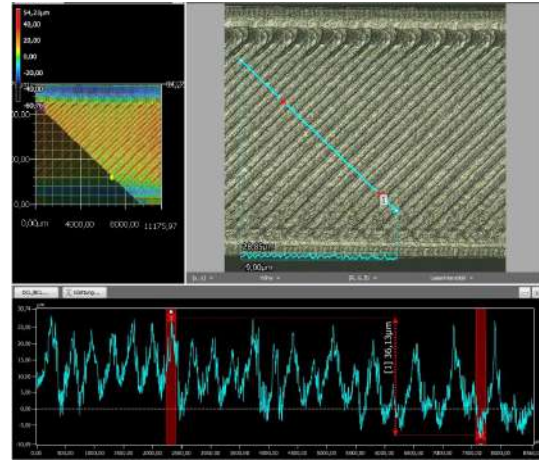


(a)

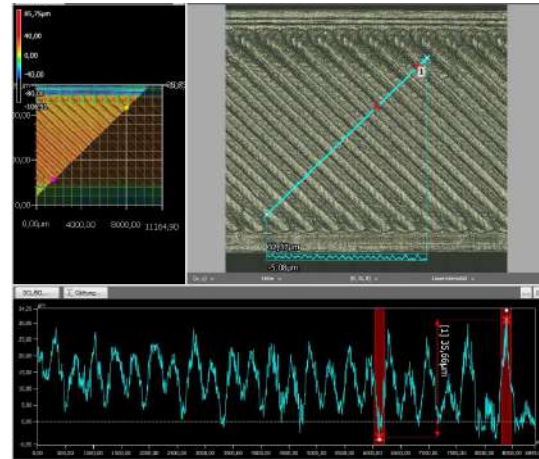


(b)

Fig. 1. Surface profile of the natural PLA sample for the layer thickness equal to: (a) 0.05 mm; (b) 0.20 mm. CLSM capture

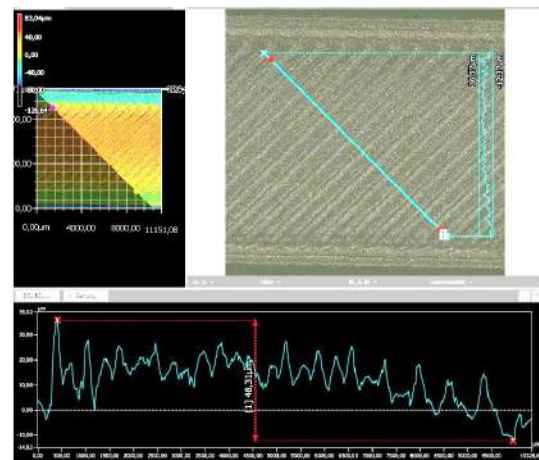


(a)



(b)

Fig. 2. Surface profile of the black PLA sample for the layer thickness equal to: (a) 0.05 mm; (b) 0.20 mm. CLSM capture



(a)

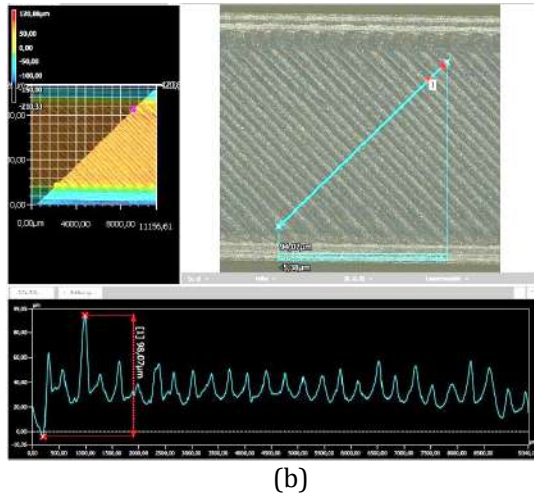


Fig. 3. Surface profile of the grey PLA sample for the layer thickness equal to: (a) 0.05 mm; (b) 0.20 mm. CLSM capture

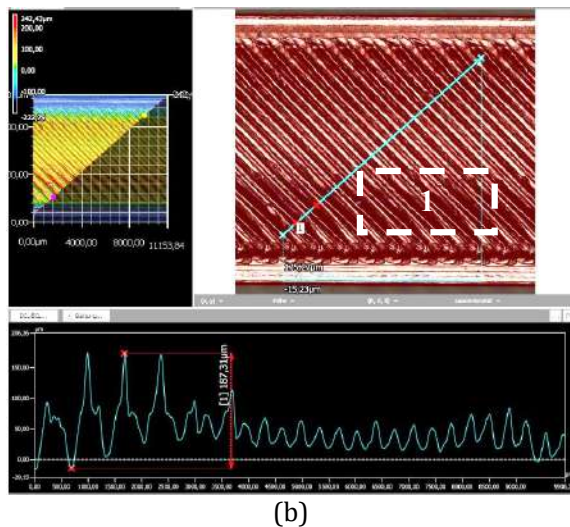
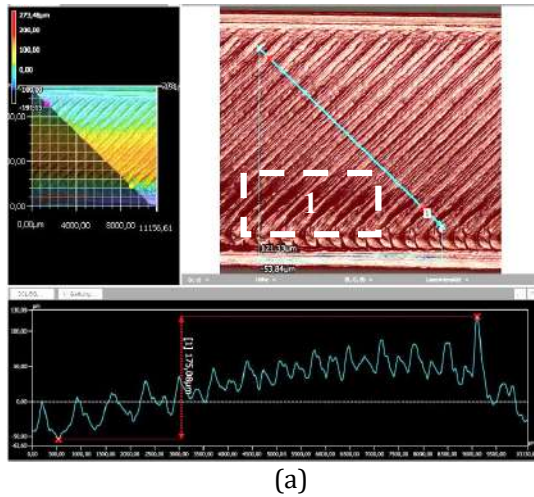


Fig. 4. Surface profile of the red PLA sample for the layer thickness equal to: (a) 0.05 mm; (b) 0.20 mm. CLSM capture

Table 1 Total height of the roughness profile (R_t) for different PLA colours and layer thicknesses

Saple color	Layer thickness [mm]	R_t [μm]	Difference between the two values of R_t [%]
Natural	0.05	55.66	0.36
	0.20	55.86	
Black	0.05	36.13	-1.30
	0.20	35.66	
Grey	0.05	48.31	103.00
	0.20	98.07	
Red	0.05	175.08	6.99
	0.20	187.31	

The images and the values presented above are revealing the fact that the surface roughness of the PLA samples printed by FFF is obviously significant influenced by the filament color. The best surface quality was provided by the black PLA, followed by the natural PLA. In case of the grey PLA samples, whilst the R_t value obtained for the low layer thickness (0.05 mm) was situated between that of the black and the natural PLA, the increased layer height (0.20 mm) led to a doubling of the R_t value. The worst roughness profile resulted in case of the red PLA. For the latter, both surface images show evident aspects of over extrusion (non-uniform filament roads, marked with 1 in Fig.4(a) and (b)). Moreover the profile in Fig. 4.(a) shows significant distortions. This phenomenon can also be noticed in case of the grey PLA sample printed with the 0.05 mm layer height (Fig. 3.(a)).

The findings of the present research are in accordance with the conclusions formulated by other authors [19], who demonstrated that the degradation temperatures and the glass transition temperatures "vary depending on the PLA color" and thereby cause a different thermal behavior of different colored PLA filaments printed under the same conditions. Also influenced by the presence of coloring additives proved to be the thermal conductivity of the PLA filaments. As shown by previous research [26], the distortions that occur during the FFF are a consequence of the successive heating and cooling cycles. In case of the lower layer thickness, the enhanced number of

thermal cycles was generating a higher temperature gradient in case of the PLA colors with less thermal conductivity (the grey PLA and the red PLA).

Contrary to other research [19,22], the natural PLA samples exhibited significant higher roughness than the black PLA specimens. This may be a consequence of the different process parameters that were selected by the authors for the printing of the samples (printing speed, infill density, build plate temperature, nozzle diameter etc.).

Regarding the variation of the total height of the roughness profile with the layer thickness, the experimental results revealed that higher values of the layer thickness lead to decreased surface quality in case of the natural PLA, the grey PLA and the red PLA samples. The differences varied, depending on the PLA filament colour, between 0.36% and 103%.

Conversely, in case of the black PLA, known to have a good thermal conductivity [27,28], the enhanced layer thickness slightly improved the surface quality. Reason therefore might be again the different thermal printing conditions obtained by the selected combination of process parameters in case of this PLA type.

4. CONCLUSIONS

The experimental investigations regarding the influence of the layer thickness and the filament color on the surface finish of PLA samples printed by FDM led to the following conclusions:

- both variables, the layer thickness and the filament color influence the surface quality of the prints obtained by FDM;
- the extent and the sense of the abovementioned influence is strongly affected by the PLA filament color;
- for the selected printing parameters, the best results in terms of surface finishing have been obtained by the black PLA, followed by the natural PLA, the grey PLA and the red PLA;
- when rapid prototyping is developing to rapid fabrication and the surface quality has to be considered, as well as the properties of the print, the filament color is an influential parameter that may not be neglected. Depending on their type, coloring additives can substantially modify the properties and thereby the printing

behavior of the PLA filaments when processed under the same conditions.

Acknowledgement

The activities of the two master students, Nicoleta Bacescu and Raul Rusalin Turiac, carried out within this research were supported by the Babes-Bolyai University through Special Scholarships for Scientific Activity.

REFERENCES

- [1] Balletti, C., Ballarin, M. and Guerra, F. (2017). 3D printing: State of the art and future perspectives. *Journal of Cultural Heritage*, vol. 26, p. 172-182. DOI: 10.1016/j.culher.2017.02.010
- [2] Turner, N.B., Strong, R., Gold, A.S. (2014). A review of melt extrusion additive manufacturing processes: I. Process design and modelling. *Rapid Prototyping Journal*, vol. 20, no. 3, p. 192-204. DOI: 10.1108/RPJ-01-2013-0012
- [3] Cojocaru, V., Frunzaverde, D., Miclosina, C.-O., Marginean, G. (2022). The influence of the process parameters on the mechanical properties of PLA specimens produced by fused filament fabrication—A review. *Polymers*, vol.14, no.5, p.886. DOI:10.3390/polym14050886
- [4] Sukindar, N.A., Ariffin, M.K.A.M., Baharudin, B.T.H.T., Jaafar, C.N.A., Ismail, M.I.S. (2017). Optimization of the parameters for surface quality of the open-source 3D printing. *Journal of Mechanical Engineering*, vol. SI3(1), p. 33-43.
- [5] Kovan, V., Tezel, T., Topal, E.S., Camurlu, H.E. (2018). Printing parameters effect on surface characteristics of 3D printed PLA materials. *Machines. Technologies. Materials*, vol.12, no.7, p. 266-269
- [6] Pérez, M., Medina-Sánchez, G., García-Collado, A., Gupta, M., Carou, D. (2018). Surface quality enhancement of fused deposition modeling (FDM) printed samples based on the selection of critical printing parameters. *Materials*, vol.11, no.8, p.1382. DOI: 10.3390/ma11081382
- [7] Arnold, C., Monsees, D., Hey, J., Schweyen, R. (2019). Surface quality of 3D-printed models as a function of various printing parameters. *Materials*, vol.12, no.12, p.1970. DOI: 10.3390/ma12121970
- [8] Anitha, R., Arunachalam, S., Radhakrishnan, P. (2001). Critical parameters influencing the quality of prototypes in fused deposition modelling. *Journal of Materials Processing*

- Technology, vol. 118, p. 385-388, DOI: 10.1016/S0924-0136(01)00980-3
- [9] Butt, J., Bhaskar, R. & Mohaghegh, V. (2022). Analysing the effects of layer heights and line widths on FFF-printed thermoplastics. *Int J Adv Manuf Technol*, vol. 121, p. 7383-7411. DOI: 10.1007/s00170-022-09810-z
- [10] Altan, M., Eryildiz, M., Gumus, B., Kahraman, Y. 2018. Effects of process parameters on the quality of PLA products fabricated by fused deposition modeling (FDM): Surface roughness and tensile strength. *Mater. Test.*, vol. 60, no. 187-188, p. 471-477, DOI 10.3139/120.111178
- [11] Taşcıoğlu, E., Kitay, Ö., Keskin, A.Ö. et al. (2022). Effect of printing parameters and post-process on surface roughness and dimensional deviation of PLA parts fabricated by extrusion-based 3D printing. *J. Braz. Soc. Mech. Sci. Eng.*, vol. 44, no. 139 DOI: 10.1007/s40430-022-03429-7
- [12] Mendricky, R., Fris, D. (2020). Analysis of the Accuracy and the Surface Roughness of FDM/FFF Technology and Optimisation of Process Parameters, *Tehnički vjesnik*, vol. 27, no. 4, p. 1166-1173. DOI: 10.17559/TV-20190320142210
- [13] Dandgawhal, A., Shukla, A., Ranade, C., Sabnis, S., Tarfe, M. (2022). Experimental Studies on Effect of Layer Thickness on Surface Finish using FDM. *International Research Journal of Engineering and Technology (IRJET)*, vol. 09, no. 06. www.irjet.net
- [14] Nyiranzeyimana, G., Mutua, J.M., Mose, B.R., Mbuya, T.O. (2021) Optimization of process parameters in fused deposition modelling of thermoplastics: A review. *Materialwiss. Werkstofftech.*, vol. 52, no.6, p. 682-694. Doi: 10.1002/mawe.202000193
- [15] Dey, A., Yodo, N. A. (2019). Systematic Survey of FDM Process Parameter Optimization and Their Influence on Part Characteristics. *J. Manuf. Mater. Process.*, vol. 3, no.3, p. 64. DOI: 10.3390/jmmp3030064
- [16] Sai, T., Pathak, V.K. & Srivastava, A. (2020). Modeling and optimization of fused deposition modeling (FDM) process through printing PLA implants using adaptive neuro-fuzzy inference system (ANFIS) model and whale optimization algorithm. *J. Braz. Soc. Mech. Sci. Eng.*, vol. 42, no. 617. DOI: 10.1007/s40430-020-02699-3
- [17] Kandananond, K. (2022). Surface Roughness Reduction in A Fused Filament Fabrication (FFF) Process using Central Composite Design Method. *Production Engineering Archives*, vol. 28, no.2, p.157-163. DOI: 10.30657/pea.2022.28.18
- [18] Buj-Corral, I., Bagheri, A., Sivatte-Adroer, M. (2021). Effect of Printing Parameters on Dimensional Error, Surface Roughness and Porosity of FFF Printed Parts with Grid Structure. *Polymers*, vol. 13, no.8, p. 1213. DOI: 10.3390/polym13081213
- [19] Soares, J. B., Finamor, J., Silva, F. P., Roldo, L., Cândido, L. H. (2018). Analysis of the Influence of Polylactic Acid (PLA) Colour on FDM 3D Printing Temperature and Part Finishing. *Rapid Prototyping Journal*, vol. 24, no. 8, p. 1305-1316. DOI: 10.1108/rpj-09-2017-0177.
- [20] Valerga, A.P., Batista, M., Puyana, R., Sambruno, A., Wendt, C., Marcos, M. (2017). Preliminary study of PLA wire colour effects on geometric characteristics of parts manufactured by FDM, *Procedia Manufacturing*, vol. 13, p. 924-931, DOI: 10.1016/j.promfg.2017.09.161.
- [21] Hanon, M. M., Zsidai, L., Ma, Q. (2021). Accuracy Investigation of 3D Printed PLA with Various Process Parameters and Different Colors. *Materials Today: Proceedings*, vol. 42, p. 3089-3096. DOI: 10.1016/j.matpr.2020.12.1246
- [22] Valerga, A.P., Batista, M., Salguero, J., Girot, F. (2018). Influence of PLA Filament Conditions on Characteristics of FDM Parts. *Materials*, vol. 11, no. 8, p. 1322. DOI: 10.3390/ma11081322
- [23] Frunzaverde, D., Cojocaru, V., Ciubotariu, C.-R., Miclosina, C.-O., Ardeljan, D.D., Ignat, E.F., Marginean, G. The Influence of the Printing Temperature and the Filament Color on the Dimensional Accuracy, Tensile Strength, and Friction Performance of FFF-Printed PLA Specimens. *Polymers*, vol. 14, p. 1978. DOI: 10.3390/polym14101978
- [24] International Organization for Standardization. *ISO 527-2:2012, Plastics—Determination of Tensile Properties—Part 2: Test Conditions for Molding and Extrusion Plastics*. International Organization for Standardization: Geneva, Switzerland, 2012.
- [25] International Organization for Standardization. *ISO/ASTM 52921:2013, Standard Terminology for Additive Manufacturing—Coordinate Systems and Test Methodologies*. International Organization for Standardization: Geneva, Switzerland, 2013.
- [26] Dave, H. K., Prajapati, A. R., Rajpurohit, S. R., Patadiya, N. H., Raval, H. K. (2020). Investigation on Tensile Strength and Failure Modes of FDM Printed Part Using In-House Fabricated PLA Filament. *Advances in Materials and Processing Technologies*, vol. 8, no. 1, p. 576-597. DOI: 10.1080/2374068x.2020.1829951.
- [27] Beniák, J., Šooš, L., Križan, P., Matúš, M., Ruprich, V. (2022). Resistance and strength of conductive PLA processed by FDM additive

manufacturing. *Polymers*, vol. 14, p. 678. DOI: 10.3390/polym14040678.

- [28] Zheng, Y., Huang, X., Chen, J., Wu, K., Wang, J., Zhang, X. (2021). A review of conductive carbon materials for 3D printing: Materials, technologies, properties, and applications. *Materials*, vol. 14, p. 3911. DOI: 10.3390/ma14143911.

Energetics and Thermal Engineering



Banja Luka
1–2 Jun 2023.

DEMI 2023

16th International Conference on Accomplishments in Mechanical and Industrial Engineering

www.demi.mf.unibl.org



Occurrence of cracks due to inadequate turbine shaft construction

Srđan Bulatović^a, Vujadin Aleksić^a, Bojana Zečević^b, Biljana Prochaska^c

^a*Institute for Testing of Materials (IMS Institute), Bulevar vojvode Mišića 43, Belgrade, Serbia*

^b*University of Belgrade, Innovation Centre of Faculty of Technology and Metallurgy, Karnegijeva 4, Belgrade, Serbia*

^c*University of Banja Luka, Faculty of Mechanical Engineering, Bulevar vojvode Stepe Stepanovica 71, Banja Luka, Bosnia and Hercegovina*

Abstract *After several decades of constant exploitation of the horizontal bulb turbine, which is an integral part of the hydroelectric power unit, empirically, the formation of a crack occurs in the turbine shaft due to the influence of corrosion, erosion and cavitation. Through experimental tests and calculations it has been determined that values of bending stresses of the turbine, which occur due to the action of fatigue and corrosion, as well as stress concentration, are bigger than 25 MPa for flanges exposed to water, and in other case bigger than 40 MPa for flanges exposed to 'corrosive water' and can cause the occurrence of surface cracks on the transition radius between the cylindrical part of the shaft and the flange. It has been determined that stress values in the zone under the influence of bending stresses were bigger than allowable values, which led to the occurrence of many cracks due to fatigue corrosion. One of those cracks caused the failure of the shaft and of the whole turbine.*

Keywords *fatigue, crack, turbine shaft, stress concentration*

1. INTRODUCTION

Turbine loads originate during the production of components and equipment assembling (residual stresses), during the process of performing functional requirements in exploitation (stationary and dynamic loads) and during the disturbed process of exploitation (non-stationary dynamic loads). It's clear that component and equipment loads can't be expressed by a simple mathematical function knowing that unpredictable influence of corrosion, erosion and cavitation during exploitation should be taken into account. That's the reason why extensive researches,

tests and inspections of hydropower plant equipment have been undertaken [1 - 7].

Turbine shaft was assembled by welding the cylindrical body of the hollow shaft (outer diameter 1200 mm, internal diameter 600 mm) to the flange, made of 20GSL steel. During welding heat-affected zone has been created, which overlapped the transition diameter. Residual stresses were accumulated at the external surface of the transition area from the shaft to the flange. Anti-corrosive protection in the shaft flange area has been exposed to water. After several hundred thousand hours of use, a huge loss of oil from the regulating system of hydroelectric generating set was noticed. After the exclusion of the hydroelectric generating set from the service and visual inspection of all suspicious locations a crack, 2100 mm long, was detected, through which the turbine oil from the servo motor leaked, on the transition radius

Corresponding author

Phd Srđan Bulatović, Research Associate
srdjan.bulatovic@institutims.rs
Institute for testing of materials-IMS Institute
Bulevar vojvode Mišića 43
Belgrade, Serbia

R80 from the cylindrical part of the shaft toward the runner hub.

2. ASSESSMENT AND ANALYSIS OF STRENGTH AND FRACTURE OF THE TURBINE SHAFT RADIUS

Turbine shaft is subjected to tensile stress due to the effect of the hydraulic force on turbine runner.

Pressure of oil in the servo motor of the runner in the closing stroke and axial hydraulic force load subject the flange to bending. The weight of the runner and of the shaft itself subject the shaft to cyclic bending. Due to the transfer of the force the shaft is subjected to torsion as well.

Combination of cyclic loads and corrosive environment (leakage of water through the seal, poor execution and non-renewal of the corrosion protection) led to the occurrence of the corrosion fatigue on the transition radius (location where value of the stress concentration factor is 3). Corrosion fatigue damages, as far as stress concentration is concerned, act like cracks (stress concentration value is ranging from 3 to 6).

High-cycle fatigue conditions in a corrosive environment the initiation of cracks occurred, and their joining led to the formation of 20-30 mm long cracks, which was confirmed by the existence of corrosion products on the smooth fracture surface. When the load bearing area of the turbine shaft, under low-cycle fatigue conditions, fell under the critical value in the crack growth area the fracture occurred. That segment of the area is embossed and deprived of corrosion products.

Calculation regarding the critical cross-section of the shaft has been carried out through the use of the Theory of Elasticity and data provided by the manufacturer. Taking into account the fact that the fracture is irregularly shaped, it has been adopted that the critical cross-section is positioned at the end of the cylindrical part of the shaft.

Critical cross-section of the turbine shaft is subjected to [7]:

- Axial hydraulic force $F_a=5.5426 \cdot 10^6$ N,
- Moment of torsion $M_t=4.278 \cdot 10^6$ Nm,
- ($P=28000$ kW-turbine power and $n=1.04166$ s⁻¹ - turbine shaft number of revolutions)
- Bending moment $M_o=337768$ Nm (occurs due to the action of the axial hydraulic force and

force that occurs due to the oil pressure in the cylinder of the servo motor of the runner),

- Bending moment $M_o=1964943$ Nm (occurs due to the weight of the runner and weight of the part of the flange as far as the critical cross-section):

- Tensile stress due to the action of the axial hydraulic force:

$$\sigma_z = \alpha_z \frac{F_a}{A_k} = 14,3 \text{ MPa} \quad (1)$$

where: $\alpha_z=2.19$ -stress concentration factor during tension and A_k critical cross-section area.

- Bending stress due to the action of the axial force and force that occurs due to the pressure in the servo motor of the runner

$$\sigma_o = \frac{M_o}{W_o} = \frac{M_o}{h^2/6} = 22,52 \text{ MPa} \quad (2)$$

where: W_o -moment of resistance per length unit of the critical cross-section.

- Torsional stress:

$$\tau = \alpha_t \frac{M_t}{W_t} = \alpha_t \frac{M_t}{\frac{\pi \cdot D^3}{16} \left[1 - \left(\frac{D}{d} \right)^4 \right]} = 20,85 \text{ MPa} \quad (3)$$

where: W_t -polar moment of resistance per length unit of the critical cross-section, $\alpha_t = 1.55$

- stress concentration factor during torsion for

$$\frac{D_p}{D} = \frac{2300}{1200} = 1,916 \quad \frac{R}{D} = \frac{80}{1200} = 0,066 \quad (4)$$

-Equivalent static stress at the critical cross-section:

$$\sigma_m = \sqrt{(\sigma_z + \sigma_o)^2 + 4\tau^2} = \sqrt{(14,3 + 22,52)^2 + 4 \cdot 20,85^2} = 55,6 \text{ MPa} \quad (5)$$

Cyclic stress at the critical cross-section occurs due to the bending moment caused by weights of the runner and of the part of the flange as far as the critical cross-section:

$$\sigma_a = \alpha_s \frac{M_s}{W_s} = \alpha_s \frac{M_s}{\frac{\pi \cdot D^3}{32} \left[1 - \left(\frac{D}{d} \right)^4 \right]} = 24,46 \text{ MPa} \quad (6)$$

where: W_s -moment of resistance per length unit of the critical cross-section, $\alpha_s=1.98$ -stress concentration factor during bending for

$$\frac{D_p}{D} = \frac{2300}{1200} = 1,916 \quad \frac{R}{D} = \frac{80}{1200} = 0,066 \quad (7)$$

2.1 Corrosion fatigue factor of safety

Factor of safety of the turbine shaft, in relation to corrosion fatigue and in conditions of cyclic loading of amplitude $\sigma_a=24.4$ MPa and corrosion is obtained through the use of the following equation:

$$S_\sigma = \frac{\sigma_{-1} - \psi_\sigma \cdot (\sigma_m + \sigma_{MO})}{\sigma_a} \quad (8)$$

where: $\sigma_{-1} = 26.5$ MPa-permanent corrosion fatigue strength of steel 20GSL during the action of the alternating changeable load in the corrosive environment, ψ_σ -coefficient that takes into account the asymmetry of the cycle and is equal to the ratio of the corrosion fatigue strength σ_{-1} and tensile strength R_m .

$$\psi_\sigma = \frac{\sigma_{-1}}{R_m} = \frac{26,5}{480} = 0,0552 \quad (9)$$

σ_m -maximum value of static exploitation stresses at the calculated cross-section, eq. (5).

σ_a -amplitude of cyclic stresses, eq. (6).

σ_{MO} -residual stresses present after casting and heat treatment have not been taken into account ($\sigma_{MO}=0$ MPa) because there were no exact values available.

Permanent corrosion fatigue strength is being determined experimentally by testing the samples in the water and correcting the obtained results through the use of dimensional factors. Factor of safety is less than $S_\sigma=1.5$, the value predicted by the manufacturer's designation.

2.2 Effect of Stress Concentration and Corrosion on Fatigue Strength

At locations of sudden changes of shape of loaded structural components local increase of stress (stress concentration) occurs. Level of stress increase is defined by the ratio of the

maximum local (σ_{\max}) and nominal (σ_{nom}) stress, which is being called the theoretical stress concentration factor [6]:

$$K_t = \frac{\sigma_{\max}}{\sigma_{\text{nom}}} \quad (10)$$

Fatigue strength due to the action of the corrosive environment is defined by the following factor:

$$k_{kor} = \frac{\sigma_{\max(-1)kor}}{\sigma_{\max(-1)}} \quad (11)$$

where: $\sigma_{\max(-1)kor}$, $\sigma_{\max(-1)}$ -fatigue strengths of smooth specimens in the corrosive environment and in the air atmosphere, respectively.

Fatigue strength in the corrosive environment depends on the number of cycles, but also on the length of exposure period of elements to the corrosive environment.

The joint effect of corrosion and stress concentration can be expressed by the following coefficient:

$$K_{fkor} = K_f + \frac{1}{k_{kor}} - 1 \quad (12)$$

where: $K_f=1.98$ -effective stress concentration factor for testing in the air atmosphere, $k_{kor}=0.5$ (for $R_m=480$ MPa) - coefficient of the effect of corrosion for smooth specimens. As far as the turbine shaft is concerned, value of stress concentration coefficient, including the effect of corrosion, is $K_{fkor}=2.98$.

Corrosion fatigue analysis of asymmetric cycle it has been determined that mean tensile stress unfavorably affects, or in other words significantly decreases the dynamic durability amplitude. Mean pressure stresses favorably affect the resistance to corrosion fatigue.

Decrease of fatigue strength of an element with respect to fatigue strength of the smooth specimen is calculated through the use of the overall fatigue strength reduction factor:

$$K_D = \left(\frac{K_f}{k_3} + \frac{1}{k_{kor}} - 1 \right) \frac{1}{k_{po} k_A} \quad (13)$$

$K_f=1.98$ -stress concentration coefficient,

$k_3=0.6$ - cross-section coefficient,

$k_{po}=1$ -coefficient that takes into account technological methods of surface strengthening,

$k_A=1$ -coefficient of anisotropy for steel castings,
 $k_{kor}=0.5$ -corrosion coefficient.

At the end, $K_D=4.28$ for the turbine shaft. Factor K_D can be used in formulas for determination of the factor of safety.

2.3 Analysis of fracture mechanics parameters

To assess material behaviour and structural integrity in the presence of cracks, fracture mechanics parameters are used. Also, fracture mechanics parameters are used for better determine the tendency to crack growth, critical conditions for fracture development, material resistance to rapid crack propagation.

During 1961, Paris, Gomey, and Anderson have first proposed that the crack growth rate, da/dN , might be correlated with the stress intensity factor range, ΔK , when the material is exposed to variable loading of constant amplitude.

Paris-Erdogan equation according to Paris' law [8,9] is the fatigue crack growth rate, which is defined as a function of the stress intensity factor range ΔK :

$$\frac{da}{dN} = C \cdot (\Delta K)^m \quad (14)$$

where C and m are material parameters. These constants are related to the fatigue properties, material microstructure, stress, frequency, cyclic loading, and applied temperature. The constant m is usually between 2 and 4, near 4 for metallic materials. For materials with low static fracture toughness, the value of material parameter m can be as high as 10.

The diagram in Fig. 1 shows three different regimes of crack growth. The fatigue life can be divided into two parts: crack initiation phase (regime A) and propagation phase (regime B). Fatigue crack propagation behaviour is typically described in terms of crack growth rate or crack length extension per cycle of loading (da/dN) plotted against the stress intensity factor range or the change in stress intensity factor from the maximum to the minimum load [10].

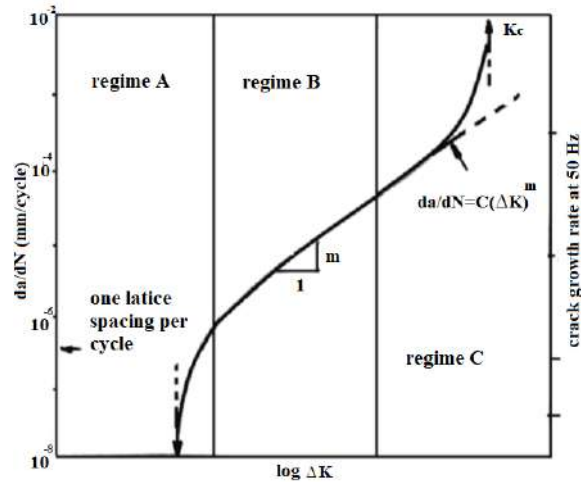


Fig. 1. Different regimes of stable fatigue crack propagation [11]

Using CRACKTRONIC pulsator, in load control conditions [12, 13], the fatigue crack growth rate da/dN and fatigue threshold ΔK_{th} are performed.

Crack growth is monitored by measuring potential drop by strain gauge RUMUL RMF A-5, measuring 5 mm length, located on the specimen face surface, Fig. 2.

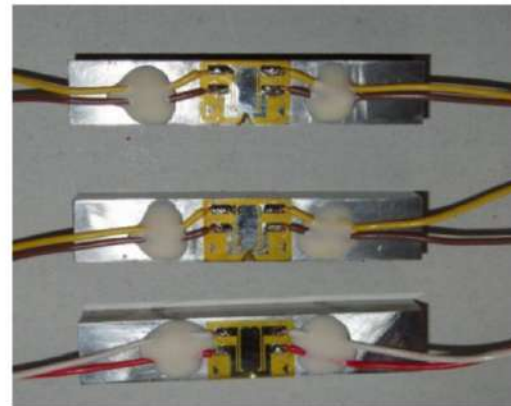


Fig. 2. Strain gauge RUMUL RMF A-5 located on the Charpy specimen (dimensions: 55x10x10 mm) face surface

Strain gauges RUMUL RMF A-5 of 5 mm length are cemented on machined specimens, allowing crack growth monitoring by FRACTOMAT device, based on electrical potential of gauge and connected with instrumentation, Fig. 3. The measuring gauge, a thin resistant measuring foil, is cemented on the specimens in the same way as classical strain gauges. As the crack

grows under the measuring foil causing it to rip, it traces the fatigue crack tip, changing foil electrical resistance linearly with the crack length [14].

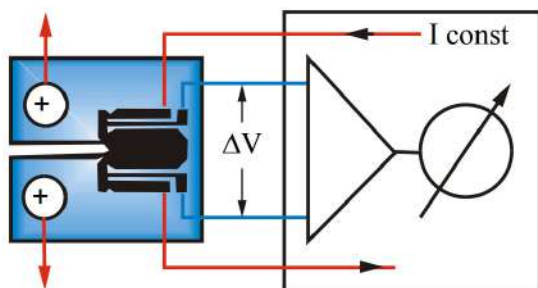


Fig. 3. Scheme of measurement foil and crack growth detection

By reducing the relationship between the fatigue crack growth rate per cycle da/dN and the range of stress intensity factor ΔK is determined the coefficient C and the exponent m . ΔK , which depends on the geometry of the specimen, the length of the crack, and on the range of variable force, ΔP , should be added to the fatigue crack growth rate for current crack length a [12].

Table 1 shows values of the fatigue threshold ΔK_{th} and material parameters-coefficient C and exponent m for fatigue crack growth, according the standard ASTM E647 [15] for determining the stress intensity factor range.

Table 1. Fracture mechanics parameters for specimens taken longitudinally and transversally from the casting

Spec.	Fatigue threshold ΔK_{th} , MPa m ^{1/2}	Coeff. C	Coeff. m	da/dN , m/cycle at $\Delta K=10$ MPa m ^{1/2}
Longitudinal	8,7	$3.0 \cdot 10^{-11}$	2	$5.62 \cdot 10^{-08}$
Transversal	7.4	$3.2 \cdot 10^{-11}$	4	$6.36 \cdot 10^{-08}$

3. CONCLUSION

Calculation of fatigue strength, fracture mechanics parameters and effect of the stress concentration in the corrosive operating environment it can be concluded that cracks and fracture of the turbine shaft before its predicted service lifetime passed occurred due to

the inadequate construction solution regarding the production of the shaft.

More precisely, the mentioned refers to occurrence of initial cracks in corrosive environment and insufficient moment of resistance in the critical cross-section of the transition radius and shaft operation in the corrosive environment, as well as exposure to the leaking water, which caused the bending stress to grow beyond acceptable values.

Acknowledgements

This research is supported by the Ministry of Education, Science and Technological Development of the Republic of Serbia (Contract No. 451-03-47/2023-01/ 200012).

REFERENCES

- [1] Angehrn, R., Eckert, R. Service Life of Horizontal Shafts in Low Head Turbines under Corrosion Fatigue, *IAHR 15th Symposium*, 1990, Belgrade.
- [2] Ohashi, W. (1991). *Vibration and Oscillation of Hydraulic Machinery*, Ashgate, Farnham.
- [3] Vladislavlev. L. A., "Machine Vibration of Hydroelectric Plant", 1972, Moscow.
- [4] Pejovic, S., Maricic, T., Karney B.W. (2009). The Guide to Hydropower Mechanical Design, *ASME "Hydro Power Technical Committee"*, HCI Publications, New edition planned.
- [5] Pejovic S. (1997). Profit Management and Control of Hydropower and Pump Plants, *Proceeding of the International Joint Power Generation Conference*, Denver, Colorado, p. 539–545.
- [6] Peterson R.E. (1974) *Stress concentration factor*, John Wiley&Sons, Inc, New York.
- [7] Hertzberg R. (1995). *Deformation and fracture mechanics of engineering materials*, John Wiley&Sons, Inc, New York.
- [8] Milovic, LJ., Vuherer, T., Radakovic, Z., Petrovski, B., Jankovic, M., Zrilic, M., Danicic, D. (2011). Determination of fatigue crack growth parameters in the welded joint of HSLA steel, *Structural integrity and life*, vol. 11, no. 3, p. 183-187.
- [9] Burzic, M., Manjgo, M., Kozak, D., Prokic-Cvetkovic, R. (2013). The effects of dynamic load on behaviour of welded joint a-387 gr. 11 alloyed steel, *Metalurgija*, vol. 52, no. 1, p. 27-31.
- [10] Alam, M.S. (2005). *Structural integrity and fatigue crack propagation life assessment of welded and weld-repaired structures*. PhD thesis. Louisiana State University and Agricultural and Mechanical College, Baton Rouge.

- [11] Milovic, LJ., Vuherer, T., Radakovic, Z., Petrovski, B., Jankovic, M., Zrilic, M., Danicic, D. (2011). Determination of fatigue crack growth parameters in the welded joint of HSLA steel, *Structural integrity and life*, vol. 11, no.3, p. 183-187.
- [12] Burzic, M., Kutin, M., Puharic, M., Adamovic, Z. (2007). An effect of service conditions to the behavior of welded joint of the alloyed steel 13 Cr Mo 4 4 (Č.7400), *Tehnička dijagnostika*, vol. 6, no. 2, p. 19-25.
- [13] Popovic, O., Prokic-Cvetkovic, R., Sedmak, A., Buyukyildirim, G., Bukvic, A (2011). The influence of buffer layer on the properties of surface welded joint of high-carbon steel, *Materiali in tehnologije /Materials and technology*, vol. 45, no. 6, p. 579- 584, 2011.
- [14] Camagic, I., Burzic Z., Cvetkovic, S. (2008). The usage of the fracture mechanics in determining the growth parameters of the fatigue crack for particular areas of a welded joint, *Welding & Welded structures*, vol. 53, no. 3, p. 97-103.
- [15] ASTM E647. (2002). *Standard Test Method for Measurement of Fatigue Crack Growth Rates*, Annual Book of ASTM Standards, ASTM.



Banja Luka
1-2 Jun 2023.

DEMI 2023

16th International Conference on Accomplishments in Mechanical and Industrial Engineering

www.demi.mf.unibl.org



Experimental research of thermal drying conditions in food dryer

F. Mojsovski^a, V. Mijakovski^b

^aFaculty of Mechanical Engineering, Ss. Cyril and Methodius University, Skopje, Republic of North Macedonia

^bFaculty of Technical Sciences, Kliment Ohridski University, Bitola, Republic of North Macedonia

Abstract

Existing food drying theory cannot offer good enough prediction of the drying process. Therefore, the correct drying conditions were reached by fieldwork activity, conducted on a farm dryer. The dryer was designed with drying room in the form of horizontal one-level support for the dried product. In order to improve the forced convection effect, the dryer was equipped with solar collector, auxiliary heating system, axial ventilators and dumpers. The construction of the drying room is realized in modular concept. Locally grown vegetables and fruits were used in the process of drying, but only research results for tomatoes are here presented. In the drying room, tomatoes shaped into rings with thickness of 4-8 mm, were exposed to a complex process of simultaneous heat and mass transfer. During the drying process, the change of tomato rings moisture content depends on the intensity of air temperature, air humidity and air flow. The tomato rings, with initial moisture content wet basis of 80 to 90 %, were dried to final moisture content wet basis of 6 to 12 %, for three to five days of drying time.

Keywords drying conditions, dryer construction, tomatoes

1. AIMS AND BACKGROUND

The requirement for a more suitable tomato drying process was investigated. An attempt was made to improve the drying conditions with interventions executed on dryer construction. The objective was to create air states and air flows that lead to quality dried tomato slices. Test runs were carried out during the tomato harvest period. Every combination of air state, tomato state and dryer performance that provides quality dried product was used in the next drying process realization. Increase in hot air temperature or velocity, was considered

as primary factor in reaching drying process that enables production of high quality final product.

Despite botanically being a fruit, it's generally eaten and prepared like a vegetable. Tomato is mostly eaten raw, but it is also used as a dried product [1]. The increasing demand for dried food and the long time availability of the dried tomato, favor its use. Sun drying removes only water from the tomato, which concentrates the tomato flavor and nutrition. Fresh tomato consists of 95 % water, 4 % carbohydrates and 1 % fat and protein. Once dried, the tomato is packed in airtight bags or stored in sunflower or olive oil. Sun dried tomatoes are used in salads, pastas and cooked dishes when intensive tomato flavor is needed.

The global consumption of tomatoes is enormous. World production quantity of tomato, in the last three years, was at the level of 180.000.000 tonnes [2]. The United Nations

Corresponding author

Prof. dr Filip Mojsovski
filip.mojsovski@mf.edu.mk

Ss. Cyril and Methodius University
Faculty of Mechanical Engineering
Skopje, Republic of North Macedonia

Economic Commission for Europe (UNECE) in effort to help international trade, encourage high-quality production and protect the consumer interests has issued standard concerning the marketing and commercial quality of dried tomatoes. According to this standard, the final moisture content of dried tomatoes is determined in four levels: high moisture content 25 % - 50 %, regular moisture content 18 % - 25 %, reduced moisture content 12 % - 18 % and low moisture content 6 % - 12 % [3].

Tomato is very popular food in our country. The production quantity of tomato, in the last three years, was at the level of 160.000 tonnes [4]. Only two agricultural products were produced in higher quantities, peppers and potatoes. Local climate and soil are ideal for tomato cultivation. Tomato is a summer season crop. Weather conditions with the maximum temperature between 25 °C and 35 °C are favorable for tomato growth. Minimum temperatures from 4 °C to 8 °C are undesirable, but not critical for some tomato varieties.

Drying of tomato is preservation method, used to prolong its consumption period, to enlarge the list of its popular uses, enhance the product quality and ease the product handling, storage and transport. When the tomato rings have been dried to their optimum moisture content, as any other hygroscopic material, they need to be immediately placed in special bags in order to stop the contact with the surrounding air. Fresh tomatoes can keep satisfactory characteristics, no more than two weeks, while the dried tomatoes up to six months.

There are countless tomato varieties. The influence of the tomato variety on dried product is essential, but its quality depends also on local soil, local climate, maturity, harvesting method, pre-treatment, drying process and post-treatment. The best tomato for drying ought to be fresh, firm, ripe and meaty. When the tomato contains fewer seeds and more pulp, better quality of dried product is provided. The number and shape of liquid caverns in one tomato variety is also important and has great effect on ring thickness selection and also on the intensity of dried product sticking on the support in the drying room.

Various constructions of solar dryers are developed for fruits and vegetables processing, starting from the old-time simple dryer with only one element, horizontal flat support for

dried product, to the nowadays models containing solar collector, auxiliary heating source, heat exchanger, ventilator, elements for control of air temperature and air flow intensity [5].

Forced convection dryer for tomatoes has already wide application in practice.

Location of the dryer ought to be carefully selected. Clean place, remote from any contamination source, possible shadow, usually in the middle of big grass area is considered as an appropriate location. Horizontal terrain, 5 m x 15 m, is sufficient for dryer accommodation. This area is fenced laterally and from the top, by plastic net. Only one door, 1 m x 2 m, is made for communication with the dryer space. Plastic ground cover, 2 m x 2 m, located at the collector entrance is needed to provide clean air inlet.

The air temperature level is crucial for the drying process. Higher temperature means shorter drying time, but the permitted drying temperature in the drying room cannot be surpassed. The maximum permissible temperature is determined by tests. The temperature profile in the drying room is mainly influenced by the collector, the heat transfer between the drying room and the environment and the air flow rate.

In the morning and late in the afternoon, the air temperature at the exit of the collector is close to the surrounding air temperature and for that reason help of auxiliary heating system is needed. At noon the air temperature at the exit of the collector is too high, and therefore atmospheric air is added in the mixing section.

2. EXPERIMENTAL

The research was realized with the use of farm dryer. Functional scheme of convective dryer is shown in Fig.1.

In our research, before drying, tomatoes were washed with water and then cutted at a test thickness of 3 mm, 5 mm and 7 mm. Than the tomatoes can be salted or sulfured. The tomato rings are treated with sulfur dioxide prior to drying. This procedure enables the tomato to keep its bright color, inhibits the microbiological growth and contributes to the unique flavor of the product. The sulfur dioxide, from the sun exposed tomato rings, evaporates slowly and creates barrier to the rodents, birds and insects. In our case, tomato rings were rather treated with salt then with sulfur dioxide.

Tomato is dried from initial moisture content, wet basis, up to 95 % to final moisture content, wet basis, to at least 6 %.

Atmospheric air enters into the solar collector, passes through the heat exchanger and mixing section and dries the tomatoes in the drying room. The air velocity is intensified by axial ventilators. Protective cover is used, at the entrance of atmospheric air in the collector, to stop the elevation of dirt from the ground.

The basic elements of the dryer are: solar collector, heat exchanger, auxiliary heating device, mixing section, drying room, ventilators and dumpers. The solar collector intensifies the

thermal energy flow at the entrance of the drying room. Heat exchanger is used to reheat the inlet air in the drying room. Additional heating is realized with the use of auxiliary heating device which uses liquefied petroleum gas as fuel. In the mixing section, high temperature of the air is lowered by adding atmospheric air. Drying room is covered by plastic foil which can be raised for loading or unloading the dryer.

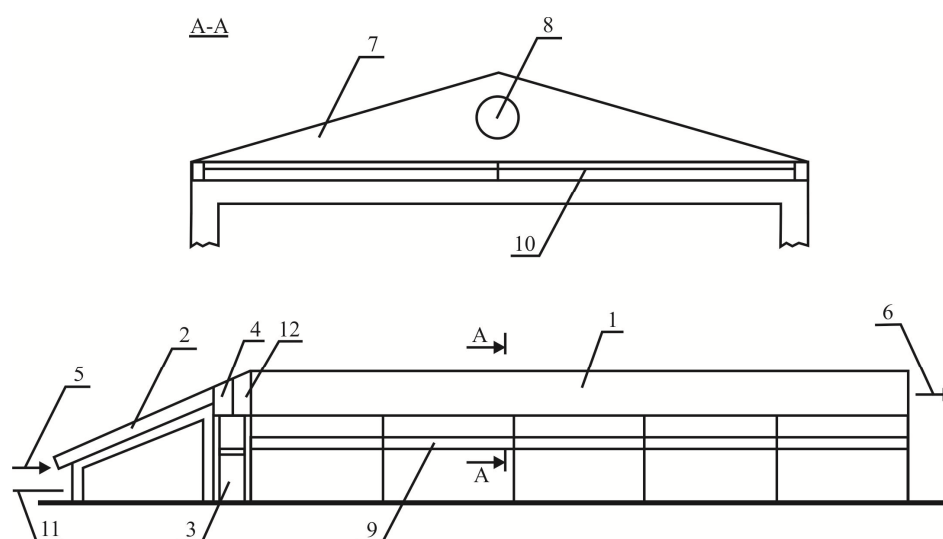


Fig. 1. Functional scheme of convective dryer

1-Drying room, 2-Solar collector, 3-Auxiliary heating source, 4-Heat exchanger, 5-Air inlet, 6-Air outlet, 7-Plastic cover, 8-Axial ventilator, 9-Dryer support, 10-Dried product support, 11-Protective cover, 12- Mixing section

A tent model of dryer was developed, to protect the dried product from direct solar radiation, to reduce the heat losses, to eliminate the influence of wind, dust, rain, birds and insects. The inlet of the solar collector and the air outlet from the drying room are closed by plastic net. The collector entrance and the drying room exit have dumpers to stop the air flow in occasion of bad weather conditions. Dumper is positioned at the drying room entrance in order to regulate the air temperature. Between the solar collector and the drying room, heat exchanger is installed to enable heating of the drying air with the use of auxiliary heating device, and mixing section for regulation of the entrance air temperature. During the period of extreme solar radiation the

air temperature, at the solar collector exit, exceeds 60 °C and ought to be reduced.

To increase the thermal inertia of the drying system, two tests were conducted. Under the supports of the drying room, rocks were placed or metal tanks filled with water. This accumulation of thermal energy, partially reduced the lack of energy during sunless periods.

Five dryers of the same construction were located across the country.

The basic drying room module is the horizontal support, 1.5 m x 1 m. Two trays, with dimensions 0.7 m x 0.9 m, are used. They are made of stainless wire net and covered by plastic net. The hot air has the possibility to flow under the trays.

Two factors are crucial for drying tomatoes successfully: the control of temperature level and air circulation. At temperatures lower than 30 °C, the product will dry slowly, giving bacteria or mold chance to grow. On the other hand, at temperatures higher than 75 °C the tomato cooks or hardens on the outside, while in the inside remains moist. The optimal drying temperature range is between 45 °C and 60 °C.

Properly harvested tomatoes were visually inspected, washed with water and then cutted in rings of 3 mm, 5 mm and 7 mm thickness. The initial moisture content, wet basis of 80 % - 90 %, was reduced in the drying process to final moisture content, wet basis of 6 % - 12 %.

In the next step, the dried product was accepted by vacuum packing device.

For every drying process, tomatoes were arranged at the flat support of the drying room. Those tomato rings that had peel on one side, were placed on the support with the peel-side. In order to retain the tomato juice and seeds in the rings, baking paper is placed under all the tomato rings. The use of this method also reduces the intensive sticking at the flat support.

The moisture content of the samples was controlled by weight measurement at fixed time intervals. Air flow in the drying room was continuously measured, and estimated based on experience and tests conducted in laboratory conditions.

Drying process was inspected by measurements, visual evaluations and tests. The measurements were applied to dried product state, drying medium state and drying room characteristics: 1. initial, modular and final dried material state (moisture content, temperature), 2. initial, modular and final drying medium state (temperature, relative humidity, flow), and 3. dryer (drying time, fuel consumption for additional energy). Digital thermometers, hygrometers and anemometers were applied.

Weather conditions at dryer location (cloudiness, wind intensity and wind direction), were also recorded. Ventilated hygrometers and psychrometric diagram, were used for determining the state of the atmospheric air [6]. The expected weather conditions were planned in accordance to the climatic curve for the dryer location [7].

Three tomato varieties were tested: Hamson, Heinz and Roma.

3. RESULTS AND DISCUSSION

Fresh tomatoes, after washing and cutting, were arranged in one row at the flat support of the drying room.

Tomato rings with thickness of 5 mm were evaluated as the best. This drying product reached 4.5 kg/m² product load.

To keep the drying space in the desired state, needed air flow rate was provided by ventilators. Required supply air flow rate was reached by axial ventilators. Velocities up to 4 m/s were used in accordance to previous gained experience and laboratory conducted tests.

The decrease of moisture content, in the dried tomato rings, was inspected every hour. Selected samples were controlled in the laboratory. When the specified final moisture content was achieved, the drying process was completed. Drying curves were obtained for every drying cycle.

Correct air flows were in the range up to 1 m³/s. Tomato rings were dried until final moisture content, wet basis of 6 % - 12 % was reached. In order to achieve the specified moisture content, tomato rings needed three to five days drying time. Thirty kilograms fresh tomatoes were dried per cycle.

An example of correct operational drying conditions for tomatoes is presented in Table 1.

Table 1. Operational drying conditions for tomatoes

Drying medium	Dried product	Dryer
Period of drying: 1.06 - 30.09	Variety: Hamson	Type: Convective
Air state in atmosphere	Diameter x Height: 7 x 5 cm	Modules: 5
temperature: 20 - 40 °C	Weight : 230 g	Module capacity: 6 kg
relative humidity: 20 - 60 %	Moisture content	Ventilators: 2
Air state in drying room	initial, wet basis, 80-90 %	Orientation: South
temperature: 40 - 60 °C	final, wet basis, 6-12 %	Area: 15 x 5 m
air flow: 0.25 - 1 m ³ /s	Inlet temperature, 25 - 35 °C	Location: Skopje
air velocity: 1 - 4 m/s	Final temperature, 45 - 50 °C	Accumulator: Rocks
	Thickness: 5 mm	Drying time: 3-5 days

4. CONCLUSIONS

Farm dryer for tomato drying is made functionally more advanced with creating conditions for obtaining higher temperatures at the entrance of the drying room and by intensifying the air flow around the dried product.

The proposed dryer construction solution has contributed significantly in the improvement of the drying process for producing quality dried tomatoes. Results from this research showed that the actual drying system has maintained functional stability even in the sunless periods. The stronger heat source and the increased air flow, additionally provide the possibility to dry other vegetables, at higher temperatures and with more intense air flow.

Well rated drying conditions, for locally grown tomato variety, are reached and published.

REFERENCES

- [1] Parnell, T., Suslow, T., Harris, L. (2004). Tomatoes: Safe methods to store, preserve and enjoy. *ANR Publications*, Publication 8116. DOI: [10.3733/ucanr.8116](https://doi.org/10.3733/ucanr.8116)
- [2] FAO (Food and Agriculture Organization of the United Nations). (2020). *FAOSTAT*. Rome, Italy.
- [3] UNECE STANDARD DDP-19. (2007). *Concerning the marketing and commercial quality control of DRIED TOMATOES 2007 Edition*. United Nations. New York, Geneva.
- [4] State Statistical Office: Statistical Yearbook of the Republic of North Macedonia for 2021. (2021). Skopje.
- [5] Mojsovski, F. (2014). Drying conditions for rice and tomato. *International Journal of Mechanical Engineering and Technology*, vol. 5, no. 10, p. 78 - 85.
- [6] (2011). *Handbook HVAC Applications*. ASHRAE (American Society of Heating, Refrigerating and Air-Conditioning Engineers), Atlanta.
- [7] Mojsovski, F. (2010). Prediction of moist air specific enthalpy. *Mechanical Engineering-Scientific Journal*, vol. 29, no. 1, p. 19 - 23.



Banja Luka
1-2 Jun 2023.

DEMI 2023

16th International Conference on Accomplishments in Mechanical and Industrial Engineering

www.demi.mf.unibl.org



Flue Gas Analysis, Necessity or Obligation

Vladimir V. Jovanović^a, Dragoslava D. Stojiljković^a, Nebojša G. Manić^a

^aUniversity of Belgrade, Faculty of Mechanical Engineering, Fuel & Combustion Lab

Abstract *Flue gas analysis is a part of everyday activity of all engineers dealing with combustion and emissions from it. Modern flue gas analyzers are powerful tools for completing various tasks from adjusting the burners/boilers through determining the efficiency to measuring emissions from various sources. One of the crucial questions related to their use in the light of challenges of contemporary requirements for energy efficiency and emission monitoring is: Are they a necessity or obligation? This paper presents key aspects of modern flue gas analyzers and their role in the era of growing concerns about manmade pollution from combustion.*

Keywords *flue gas analysis, combustion efficiency, emission monitoring*

1. INTRODUCTION

From the first fire of prehistoric man to most sophisticated burners of today, combustion is one of the pillars of civilization. Scientists and technicians were gathering knowledge of this process through the centuries of human progress. Basic laws of physics and chemistry provided explanations on the secrets hidden in the flame, but nothing is better than ability to check the theory in practice. Measurement techniques are the key of our investigations of the combustion process. The end of 20th and the beginning of 21st century were fruitful in development of improved and novel methods for analysis of the combustion products.

Flue gas analyzers, been bulky, heavy and sensitive to various impacts during measurements and, overall, very expensive,

have been improved to the level of being small, light and robust in various measurement environments, and what is the best of all, affordable to a wide range of users.

Today, flue gas analyzers are not only used for determination of combustion efficiency, but even more for complex emissions measurement in various industries.

2. FLUE GAS ANALYSIS BASICS

From the aspect of combustion, modern flue gas analyzers are electronic instruments intended for measuring the concentration of certain gaseous substances in the flue gas from boilers or IC engines and determining the efficiency of the combustion process. Primary objective of flue gas analysis is to determine the efficiency of combustion process, therefore to affirm that the combustion is completed to its very end. Dominant fuels in energy production are hydrocarbon based (C_xH_y) so the final combustion products are carbon dioxide (CO_2) and water (H_2O).

Instruments for flue gas analysis are well known as flue gas analyzers and they can be

Corresponding author

dr Vladimir Jovanović
vjovanovic@mas.bg.ac.rs

University of Belgrade, Faculty of Mechanical Engineering,
Fuel & Combustion Lab
Kraljice Marije 16
Belgrade, Serbia

grouped based on following criteria: purpose, method of gas sampling and portability. Based on those criteria there are various types of flue gas analyzers:

1. Purpose: process, security, for the quality control and for emission monitoring
2. Gas sampling: in situ (in the flue gas duct) and extractive
3. Portability: portable and stationary

However, from the point of view of the measurement technique, the criteria of the type of sensors used to measure the concentration of gases is much more important. It should be noted that in analyzer technology the term sensor is sometimes used specifically for very small sensing elements, while larger sensors or sensor systems are described as analyzers. Selected type of sensors should be as follows:

- Electro catalytic,
- Polarographic,
- Optical,
- Calorimetric,
- Photometric,
- Polarography,
- Paramagnetic,
- Chemiluminescence,
- Flame ionization (FID),
- Biological.

Sensors are selected based on gases detected and their properties following the leading criteria for measurement – sensitivity and precision.

Critical measurements, like in legally binding emission monitoring are made using high precision stationary instruments, while regular checks of combustion process are made using portable instruments.

3. WHAT IS ANALYSED?

Every concentration measurement, including flue gas analysis heavily depends on the basis for presenting the results. When it comes to flue gas, this means that the concentration of measured gases could be in wet or dry flue gas.

Wet flue gases containing water vapor, generated from hydrogen combustion or as a result of evaporation of moisture in fuel, are dominant in energy production, as the number of units operating in condensing regime (capable of utilizing latent heat of evaporation) is very limited. However, for the majority of flue

gas analyzers on the market water vapor is absolutely undesirable as it can ruin the sensors or adversely impact the operation of the sensors. Therefore, the condenser/water separator is used in flue gas sampling line before the analyzed gas is lead to the sensors. So, in flue gas analysis the dominant base for presenting the results is dry. Of course, there are the sensors capable for operation with wet flue gas, but they are more expensive and not widely available, except one, the legendary lambda probe that is inevitable and crucial element of every modern IC engine.

First flue gas analyzer, the archaic, but highly accurate Orsat apparatus, was capable of measuring oxygen (O_2), carbon dioxide (CO_2), carbon monoxide (CO), and more including sulfur dioxide (SO_2). This instrument provided vital information on efficiency of combustion process, but lately it was replaced with more versatile, compact analyzers. Modern flue gas analyzers have switched to measuring the concentration of oxygen instead of carbon dioxide due to practical and commercial aspects. Therefore the basic formula for determining the excess air coefficient was

$$\text{changed from } \lambda = \frac{CO_{2\max}}{CO_2} \text{ to: } \lambda = \frac{21}{21 - O_2},$$

where CO_2 and O_2 are measured concentrations of carbon dioxide and oxygen while $CO_{2\max}$ is theoretical, maximum value of concentration of carbon dioxide in wet flue gas for stoichiometric combustion ($\lambda=1$). Having on mind the limitations of modern flue gas analyzers the basis on which the measured values are presented was also changed from wet to dry (flue gas).

Besides this, basic measurement, modern flue gas analyzers are capable of measurement the concentration of carbon monoxide (CO), nitrogen oxide (NO), nitrogen dioxide (NO_2), sulfur dioxide (SO_2), unburnt hydrocarbons (HC), hydrogen sulphide (H_2S), chlorine (Cl_2), hydrogen (H_2), hydrogen halides (HCl, HF), hydrogen fluoride (HF) and solids (dust, soot). Concentration is given in following units of measure:

- Volume – % V/V or ppm (parts per million),
- Mass – mg/m³.

As to provide correct values for comparing results from different measuring conditions, it is necessary to convert the measured values to

standard conditions according to following formula:

$$c_{\text{stand}} = c_{\text{meas}} \cdot \frac{T_{\text{meas}} \cdot p_{\text{stand}}}{T_{\text{stand}} \cdot p_{\text{meas}}},$$

where: c is concentration, T is absolute temperature, p is absolute pressure, index “stand” is for standard conditions ($p=101,3$ kPa, $T=273$ K), and index “meas” is for measurement conditions.

Conversion from volume to mass units of measure is performed according to general formula:

$$X_{\text{mass}} \left(\frac{\text{mg}}{\text{m}^3} \right) = X_{\text{vol}} (\text{ppm}) \cdot \rho_X,$$

where: X is measured component (CO , NO , SO_2 , etc.), and ρ is density of the measured component at standard conditions, index “mass” is for mass concentration, and index “vol” is for volume concentration).

Furthermore, for different plants/processes, reference value of oxygen concentration is defined ($O_{2\text{ref}}$), and accordingly the following formula is used to recalculate the concentration to the reference oxygen concentration:

$$X_{\text{mass}} \left(\frac{\text{mg}}{\text{m}^3} \right) = \left[\frac{21 - O_{2\text{ref}}}{21 - O_2} \right] \cdot X_{\text{vol}} (\text{ppm}) \cdot \rho_X,$$

where: O_2 is measured oxygen concentration.

Finally, there is an option of converting measured values of concentration in energy related units which is made according to following formulas:

$$X_{\text{ener}} \left(\frac{\text{g}}{\text{GJ}} \right) = \left[\frac{21}{21 - O_2} \right] \cdot X_{\text{vol}} (\text{ppm}) \cdot FF \cdot \rho_X,$$

$$X_{\text{ener}} \left(\frac{\text{mg}}{\text{kWh}} \right) = \left[\frac{21}{21 - O_2} \right] \cdot X_{\text{vol}} (\text{ppm}) \cdot FF \cdot 3,6 \cdot \rho_X$$

where: FF is fuel specific factor, and index “ener” is for energy related unit.

Besides direct measurement of emissions, modern portable flue gas analyzers (combustion analyzers), which are widely available on the market, are capable to calculate the efficiency of small combustion units. This is provided based on the direct measurement of O_2 content in dry flue gas (O_2), and simultaneous measurement of flue gas (t_{fg}) and ambient air (t_{aa}) temperature. Those three measured values, combined with fuel specific factors stored in instrument memory for various fuels (A_2 , B) are used for calculation of flue gas heat loss (q_{fg}) according to formula:

$$q_{\text{fg}} = (t_{\text{fg}} - t_{\text{aa}}) \cdot \left[\frac{A_2}{(21 - O_2)} \right] + B \quad [\%].$$

Afterwards, based on this value, and assuming that this is the only (dominant) loss in the boiler/furnace the efficiency (η) is calculated based on formula:

$$\eta = 100 - q_{\text{fg}} \quad [\%]$$

For solid fuels fuel specific factors are zero, so flue gas loss is determined according to the Siegert formula:

$$q_{\text{fg}} = f \cdot \frac{t_{\text{fg}} - t_{\text{aa}}}{CO_2} \quad [\%],$$

where CO_2 is measured carbon dioxide content in dry flue gas (if equipped) or it can be calculated based on $CO_{2\text{max}}$ value stored for predefined fuels in instrument memory and measured O_2 content in dry flue gas according to the following formula:

$$CO_2 = CO_{2\text{max}} \frac{21 - O_2}{21} \quad [\% \text{ } V/V]$$

This is the method for calculation of flue gas heat loss and efficiency of the boiler/furnace according to German methodology. There is also an option to perform the calculations based on British/American methodology which is more complicated and not presented here.

4. NECESSITY, WHY?

In the old days, combustion technicians/burner specialists used their eyes and their experience to check the operation of the burner. They have observed the flame length, color and shape and finally the exhaust gases exiting the chimney. Those were the crucial parameters for determining the effectiveness of the combustion. Yellowish flame indicated air deficiency, while the bluish one indicated stoichiometric flame or excess air. Black smoke exiting the chimney indicated the uncomplete combustion with high concentration of soot and carbon monoxide.

Back in 90's of the 20th century, the author of this paper had a privilege of working together with those men, but equipped with a portable flue gas analyzer, one of the first of its kind. It was a mutual delight when the knowledge and experience met with novel measurement equipment confirming each other results. Since then, long time has passed, and today, situation is completely different. Knowledge and experience are in the backyard while the

modern flue gas analyzers became a standard equipment of every burner specialist providing vital information needed for fine tuning burners, from solid, over liquid to gaseous fuel. From their entering the market, flue gas analyzers were not only the analyzers but a complete tool for determining combustion efficiency. They were equipped with temperature sensors (for ambient air and flue gas) and draught measurement (flue gas positive or negative pressure). Those sensors, as well as fuel specific data stored in their memory provided instant calculation of boiler efficiency.

Today, it is almost impossible to commission the burner, boiler or any energy unit that use combustion for generating the heat, without flue gas analyzer, as it is a versatile tool which can provide all necessary data for evaluation of burner/boiler performance and compliance with legal requirements. Generally, the tasks where gas analyzers are used can be grouped as follows:

1. Adjustment and service measurements (general plant upgrade purposes, localization of process instabilities, checks after repair work or preparation before regulatory measurements).
2. Process measurements for combustion optimization (to improve plant efficiency or to extend the lifetime of the plant).
3. Process measurements for control of a defined gas atmosphere (special furnaces or kilns for processes such as burning, sintering or surface treatment).
4. Process and emission measurements (functional control of flue gas cleaning installations).
5. Emission measurements (at the stack to monitor the emission values of pollutants and to ensure compliance with the official regulations).

Examples of first two applications (burner/boiler and engine emissions) are presented on Figures 1 and 2.

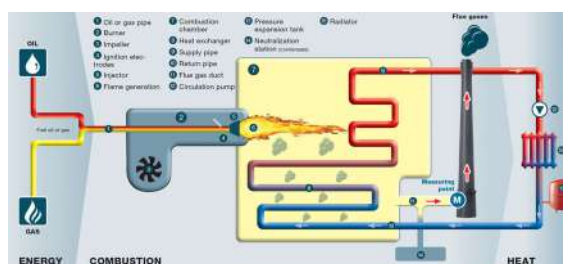


Fig. 1. Burner/boiler emissions measurement (extractive gas sampling) [1]

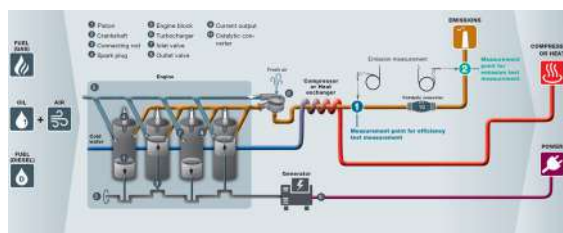


Fig. 2. Engine emissions measurement (extractive gas sampling) [1]

The main objective of fine tuning of the combustion plant (as any other plant) is to operate it in optimum working range. For the burner/boiler this optimum range is found using combustion chart presented on Figure 3 along with all crucial parameters of combustion process. For the IC engines combustion chart is slightly different as they can operate with rich (sub stoichiometric) and lean (supra stoichiometric) air-fuel mixture. This combustion chart is presented on Figure 4. As described previously and presented on Figures 3 and 4, without flue gas analyzers, necessary data wouldn't be available and optimum working range couldn't be reached.

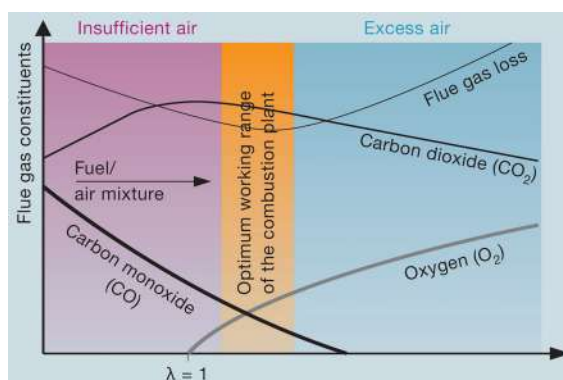


Fig. 3. Combustion chart for burner/boiler [1]

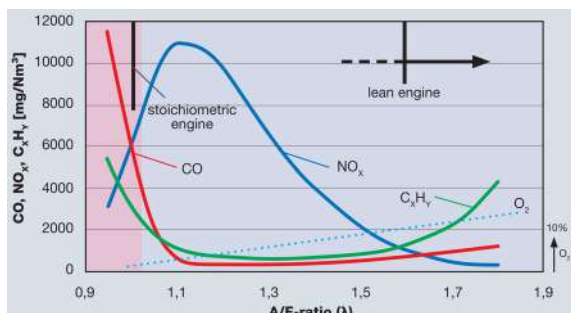


Fig. 4. Combustion chart for IC engine [1]

An example of process control (petrochemical industry) is given on Figure 5. Simplified scheme for complete emission measurements (at the stack to monitor the emission values of pollutants) is given on Figure 6.

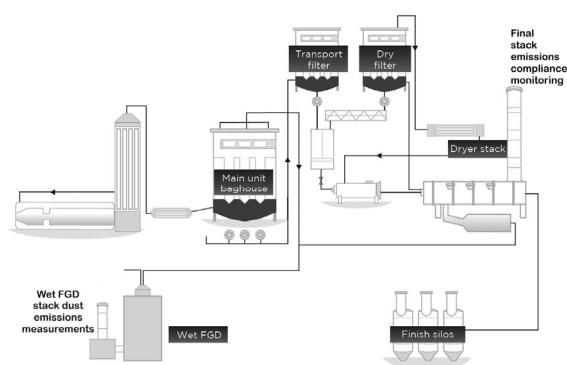


Fig. 5. Process and emission measurements in petrochemical industry [2]

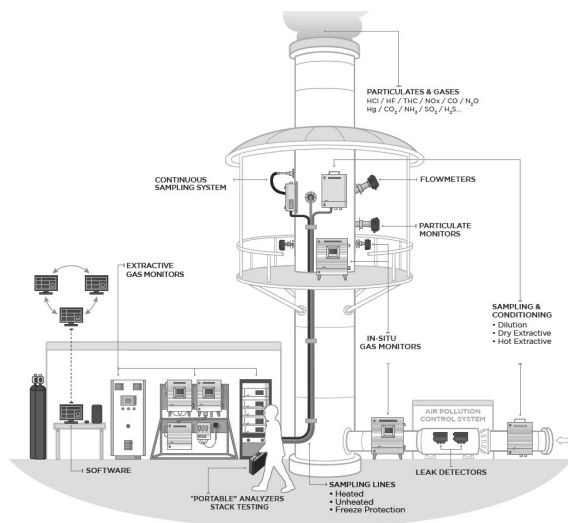


Fig. 6. Complete emission measurements (at the stack to monitor the emission values of pollutants) [2]

Complexity of tasks performed by gas analyzers is even greater and presented applications are just examples.

5. OBLIGATION WHY?

Growing concerns about manmade pollution contributed to development and adoption of directives, laws, and other legal documents imposing the emission limits for various industrial activities, and among them, for combustion. Gas analyzers in general, and flue gas analyzers for combustion specific processes are the cornerstones of effective application of these regulations.

In Europe, as EU and its member countries as parties to the UNFCCC (United Nations Framework Convention on Climate Change), its Kyoto Protocol and the Paris Agreement are required to report to the UN: annually on their greenhouse gas emissions ("greenhouse gas inventories"); and regularly on their climate policies and measures and progress towards the targets ("biennial reports" and "national communications"). Republic of Serbia is also a party to the same.

Fulfillment of the requirements of the specified international obligations isn't possible without application of various gas analyzers.

Furthermore, Emissions Trading System (ETS) has been introduced on the world market and in the core of it are valid data on emissions which wouldn't be available without gas analyzers. Basic elements of ETS design are presented on Figure 7.

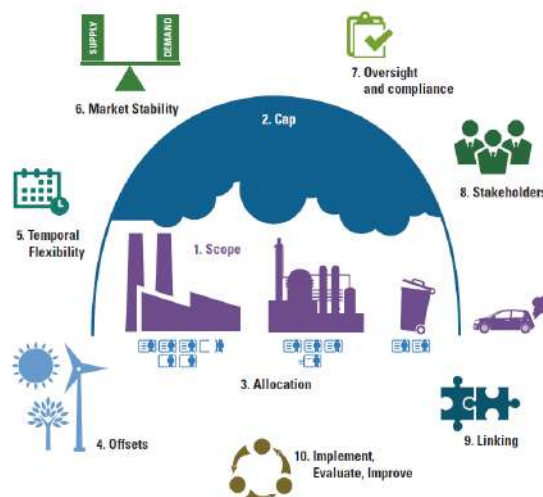


Fig. 7. Basic elements of ETS design [3]

Potential markets for gas analyzers are numerous and they can be addressed from three scopes of emissions as defined in various documents on GHG monitoring. Those scopes are presented on Figure 8.



Fig. 8. Scopes of emissions in GHG monitoring [4]

CONCLUSION

Flue gas analysis and gas analysis in general has reached its maturity. From the tool of a few highly specialized experts it has become an all-purpose tool adjusted for educated technicians and it is present in many aspects of modern industry.

Development of new measurement techniques, novel sensors and versatile software provided state-of-art instruments capable of measuring almost all kind of emissions from various sources of human activity.

Data provided by modern gas analyzers are the basis for regular operation of various devices, plants or systems in many industries plus for the new markets like Emissions Trading System.

REFERENCES

- [1] ***, Technical documentation, White papers and User manuals of different flue gas analyzers
- [2] ENVEA. From: <https://www.envea.global/>, accessed on: April 19, 2023.
- [3] *** (2016). *Emissions trading in practice: A handbook on design and implementation*, International Bank for Reconstruction and Development / The World Bank, Washington, USA.
- [4] 3Degrees. From: <https://3degreesinc.com/resources/scope-1-2-3-emissions/>, accessed on: April 19, 2023.



Banja Luka
1–2 June 2023

DEMI 2023

16th International Conference on Accomplishments in Mechanical and Industrial Engineering

www.demi.mf.unibl.org



Increasing the energy efficiency of educational buildings as a function of adaptation to climate changes

M. Radujković^a, G. Janjić^a

^aUniversity of Banja Luka, Faculty of Mechanical Engineering, Vojvode Stepe Stepanovića 71, 78000 Banja Luka, Bosnia and Herzegovina

Abstract *Changes in microclimate parameters (increase in temperature and the creation of heat islands) require a priority solution to the problems that have arisen on the territory of local self-government units. To predict the future impacts and risks of climate change, local communities use adaptation measures for climate change. One way to combat these consequences is to increase the energy efficiency of buildings. Technical measures in the form of envelope optimization affect primarily the reduction of the need for energy consumption for heating and cooling of buildings, which in the long-term results in a reduction of CO₂ emissions, as well as economic savings. In addition, renewable energy sources, such as solar energy, are increasingly and intensively used to achieve more optimal conditions in the form of energy savings and positive environmental impacts. Of the total amount of thermal energy consumed in public facilities in the City of Banja Luka, the largest share is consumed in educational and cultural facilities, around 70% [1]. Therefore, the direction of action of measures to increase energy efficiency should primarily be directed towards the renovation of these facilities.*

Keywords *energy efficiency, adaptation measures, climate change, active solar systems*

1. INTRODUCTION

In the territory of Bosnia and Herzegovina, according to available data, existing buildings of individual and collective housing consumed the same amount of energy as buildings of similar characteristics in Europe in the 90s of the last century [2]. Buildings, their surroundings, and accompanying facilities produce more CO₂, create more pollution, consume more energy and natural resources than any other business or industry [3].

The subject of this research is energy efficiency measures that can be applied to educational

facilities in the City of Banja Luka to reduce energy consumption for heating. The impacts of the projects implemented so far in this area have been investigated and measures have been proposed that would increase the energy efficiency of these buildings.

The aim of the research is to determine the positive impact of the use of active solar systems and the implementation of thermomechanical measures on educational facilities in the City of Banja Luka. First, it is necessary to determine the energy impact (reduction of energy used for heating and cooling of buildings and achieving a higher degree of energy efficiency). Then determining other positive effects, such as ecological (reduction of carbon dioxide emissions as one of the most harmful greenhouse gases). The tasks that need to be performed in order to achieve the set aim are explaining the basic terms in the field of energy efficiency, technical

Corresponding author

PhD candidate, Milana Radujković
milana.radujkovic@student.mf.unibl.org

University of Banja Luka, Faculty of Mechanical Engineering
Vojvode Stepe Stepanovića 71
78000 Banja Luka, Bosnia and Herzegovina

and other types of measures to increase it. Then it is necessary to analyse the existing documentation for the research area and the effects of the projects implemented so far. After the theoretical part of the work, it is necessary to process adequate data for the buildings in the City in the appropriate software, to obtain information about energy consumption through three different scenarios, and then perform a comparative analysis of the proposed solutions and select the best scenario. The methodology of the work includes the implementation of two phases: the research (theoretical) part of the work, which includes the analysis of previous research in this area, as well as the synthesis of all conclusions reached during the execution of the set tasks, and the practical (experimental) part, which includes the analysis of data on energy consumption in educational buildings and proposal of possible solutions. Part of the data was taken from literature and scientific work, and one part was obtained using software for simulating energy processes and energy consumption called LEAP.

Previous research in this area has shown that there are numerous positive impacts on improving the thermal envelope of buildings and the use of active solar systems. At the same time, it is important to note that positive impacts are visible from many aspects, not only energy. Environmental impacts, in the form of reduction of carbon dioxide emissions and temperature reduction, are of great importance for reducing the negative effects of climate change. Improving energy efficiency and using renewable energy sources are effective ways to reduce the carbon footprint, as well as a very good way to save money [4].

2. MATERIALS AND METHODS

The basic method used in the theoretical part is the method of content analysis, and the studied literature includes books, scientific papers and publications published in the period from 2005 to 2019. In addition, certain quantitative data from professional literature and previous research were considered, which talk about how and to what extent ecological impacts and energy efficiency in buildings are achieved by means of active solar systems and renovation of building envelopes. The practical part includes data analysis and simulations of different scenarios using software tools. The

methodology of the experimental work includes three phases.

The first phase included entering data on energy consumption in educational facilities in the City of Banja Luka into the LEAP (Low Emissions Analysis Platform) software. 2015 was taken as the base year because there are data on energy consumption for that year. The data were taken from the Energy Efficiency Action Plan (EEAP) of the City of Banja Luka for the period from 2016 to 2019, the Sustainable Energy Action Plan of the City of Banja Luka (SEAP), the Development Strategy of the City of Banja Luka for the period from 2018 to 2027, the UNDP publication on the effects of the implementation of the Green Economic Development project (GED) and the statistical publications of the Republic Institute for Statistics of the Republic of Srpska. The following key parameters were taken into account: number of buildings, total area of buildings and total energy consumption on an annual basis.

The second phase included the creation of 3 scenarios. The first scenario refers to the reduction of energy consumption after the renovation of the envelope of a certain number of buildings (preschools and primary schools in a ten-year period, until 2025), the second scenario refers to energy savings after the renovation of the envelope of all buildings (a period of twenty years, until 2035) and the third one refers to the positive effects of the use of active solar systems with the assumption that the envelopes on all investigated buildings have been renewed (a period of thirty years, until the end of the simulation period, in 2045).

The third, final phase included the creation of a simulation of the total energy consumption after the implementation of building envelope renewal measures and the use of active solar systems, as well as an assessment of environmental impacts, with a special focus on carbon dioxide emissions. The following parameters were considered: reduction of energy consumption in buildings (MWh/year) and reduction of carbon dioxide emissions (t/year). The obtained results are presented in tables and figures. The total estimated energy consumption in Banja Luka is 1,479,326.5 MWh/year, and the average energy consumption in public buildings is 353.6 kWh/m²/year [1]. The above values show that the existing facilities are extremely energy

inefficient and that it is necessary to intensify the implementation of measures to increase energy efficiency, as one of the priorities of the future improvement plan in this area. All public buildings in the city area are connected to the city heating plant, that is, a district heating system that uses fuel oil and biomass as fuel. The city heating plant provides the necessary energy only for room heating services, and sanitary water is heated in each facility individually, usually using electric boilers [5]. The specific consumption of thermal energy for room heating according to the types of facilities under the jurisdiction of the City of Banja Luka is given in Table 1 [1]. Primary schools in suburban settlements are not connected to the district heating system, but use wood as an energy source and, to a lesser extent, coal. Most of the educational facilities on the territory of the City were built in the period of the 80s of the last century, when energy-efficient construction measures were not considered enough. So, energy consumption, CO₂ emissions and all the accompanying negative impacts on the environment are also related to this [6].

Table 1. Average energy consumption for heating rooms in buildings under the jurisdiction of the City

Object type	Total (MWh)	Average (kWh/m ² /year)
Local administration buildings	715,0	155,4
Buildings of communal activities and public companies	248,7	155,4
Buildings for education and cultural activities	23.108,0	141,3
Buildings for health and social care	5.768,6	167,5
Other public buildings under the jurisdiction of the City	818,4	113,0
Total	30.658,7	145,0

It is evident from the Table 1 that the highest total consumption of thermal energy for heating rooms (around 75.4%) is in buildings for education and cultural activities. According to the available data, the total consumption of electricity in educational and cultural facilities in the City is 31,098.00 MWh, which is about 70.5% compared to other public facilities. The total area of educational and cultural facilities is 163,536.00 m², so the average electricity consumption is 190.16 kWh/m² [1]. Therefore, there was a priority need to introduce measures

that will affect the reduction of energy consumption in these facilities. According to the available data, electricity is used for lighting, cooling of buildings, preparation of hot water and food and other needs, i.e., for the operation of electrical devices [5].

Banja Luka was one of the local communities that participated in the Green Economic Development (GED) project, which has been implemented by the United Nations Development Program (UNDP) since 2013, and is financed by the Government of Sweden, the Environmental Protection Fund of the Federation of Bosnia and Herzegovina, and the Environmental Protection and Energy Efficiency Fund of the Republic of Srpska, in cooperation with the Ministry of Foreign Trade and Economic Relations of Bosnia and Herzegovina, entity ministries of spatial planning, cantonal ministries and other partners. During that project, in the field of infrastructural measures (implementation of energy efficiency measures), in the City of Banja Luka, measures were implemented on a total of 11 public buildings (primary schools, preschool institutions and the faculty) from 2015 to 2019. Various construction and mechanical works were carried out on them, with the aim of warming the buildings, which contributed to the reduction of energy consumption by about 60%, and therefore CO₂ emissions [7].

An overview of the implemented projects and the effects of each of them is given in Table 2, which shows the most significant economic and environmental effects after the construction of improving the energy efficiency of researched buildings. Based on this, we concluded that the invested funds will pay off and that it is necessary to continue in this direction in the future, on other facilities, both public institutions, as well as residential and commercial buildings in the City of Banja Luka. According to the overall data obtained, the value of all projects is 1,176,631.00 BAM, and the annual savings amount to 206,332.04 BAM, so in less than 6 years, the invested financial resources will pay off. It should be noted that during these projects, 65 new jobs were created, so-called "green jobs", i.e., jobs related to environmental protection, which is also an important aspect of these projects [8].

Table 2. Overview of the impact of implemented projects in the City of Banja Luka within the GED project

Object name and type	Financial value of the project (BAM)	Annual financial savings	CO ₂ emission reduction (t/year)
1	19.100,50	27.846,00	68
2	48.302,76	5.450,00	13
3	129.691,38	6.903,14	18
4	193.154,78	28.895,76	76
5	292.676,65	40.320,90	105
6	71.859,70	31.575,24	83
7	180.298,82	7.308,00	73
8	148.973,86	28.000,00	168
9	92.572,55	30.033,00	172
Total	1 176.631,00	206.332,04	776

1 - Primary School Branko Radičević, 2 - Preschool Ježeva kućica, 3 - Public Institution Center for Preschool Education and Kindergarten Bambi, 4 - Primary School Jovan Cvijić, 5 - Faculty of natural sciences and mathematics, 6 - Primary School Aleksa Šantić, 7 - Music School Vlado Milošević, 8 - Primary School Dositej Obradović, 9 - Primary School Borisav Stanković

3. RESULTS AND DISCUSSION

According to Table 1, the average energy consumption for heating rooms in educational facilities is 141.3 kWh/m²/year. The average consumption of electricity in these facilities is 190.16 kWh/m². The surfaces of the buildings and the total energy consumption according to the categories obtained based on the above average are given in Table 3 and refer to the state before the implementation of the measures listed in Table 2. A total of 11 buildings (7 primary schools, 1 preschool, 1 secondary school, 1 faculty and Centre for Preschool Education and Kindergarten) went through the phase of renovation of the envelope in a period of 5 years.

Table 3. Total energy consumption according to types of educational facilities

Object type	Area (m ²)	Energy consumption for heating MWh/year	Electricity consumption MWh/year
1	6.704,0	947,27	1.274,83
2	62.561,0	8.839,87	11.896,60
3	33.285,63	4.703,25	6.329,59
4	39.974,0	5.648,32	7.601,46
5	4.372,0	617,76	831,38
6	33.087,0	4.675,19	6.291,82
Total	179.983,63	25.431,66	34.225,68

1 - Preschools (22 objects), 2 - Primary schools (urban area - 30 objects), 3 - Primary schools (rural area - 36 objects), 4 - Secondary schools (18 objects), 5 - Other educational facilities (7 objects), 6 - Faculties (16 objects)

Given the lack of precise data on the exact amounts of energy used for heating rooms in educational facilities, an assessment of their percentage representation was made according to the available data for residential buildings in the city area. Buildings in the urban area are connected to a district heating system that uses a combination of fuel oil (42.85%) and biomass (57.15%). Primary schools in rural areas use a combination of wood (75%) and coal (25%) for room heating. The assessment of energy consumption according to the types of energy sources is given in Table 4.

Table 4. Energy consumption according to types of energy sources

Type of energy source	Area (m ²)	Energy consumption MWh/year	Percentage share (%)
Fuel oil	62.860,09	8.882,12	34,93
Biomass	83.837,91	11.846,29	46,58
Wood	24.964,22	3.527,44	13,87
Coal	8.321,41	1.175,81	4,62
Total	179.983,63	25.431,66	100,00

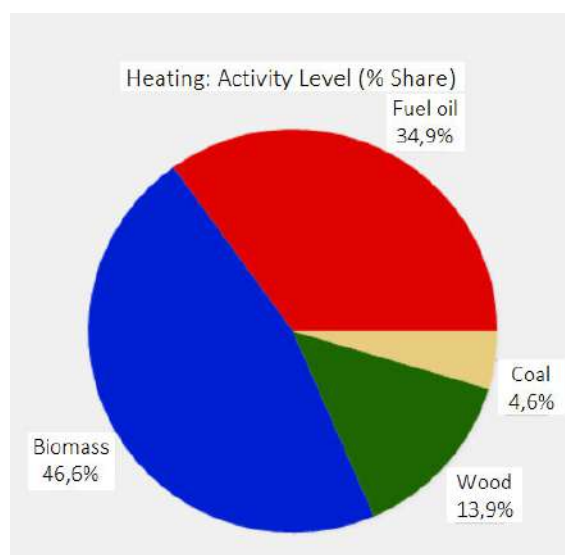


Fig. 1. Percentage representation of types of energy sources

According to scenario 1, it is assumed that all preschool and elementary school facilities in the urban area would be included in the envelope renewal project and a period of 10 years was planned for this phase. Their total area is 69,265.00 m² and, according to the current state, they consume a total of 9,787.14 MWh/year of energy for space heating. The estimate of the reduction of the required energy for space heating after the renewal of the

envelope is 60% (according to the results obtained so far), which would mean that after that 3,914.85 MWh/year of energy will be needed to heat these buildings.

According to scenario 2, the assumption is that the envelopes on all those objects are renewed in a period of 20 years. In that case, the energy consumption for room heating would decrease from a total of 25,431.66 MWh/year to 10,172.66 MWh/year, which also amounts to 60% savings.

Scenario 3 is based on scenario 2, where it is assumed that the buildings are additionally heated using active solar systems, as a renewable energy source. The realization of these measures will require a longer period of time, bearing in mind the capital costs, which are very high. Therefore, it is assumed that the realization of this scenario will take 30 years. A system of solar plate collectors was chosen that uses a liquid working fluid and can be mounted on a flat or sloping roof. According to the manufacturer's specifications, the net area of one panel is 2.35 m², and the yields of this system are about 525 kWh/m².

The assumption is that 20 panels will be installed on each building, which amounts to a total of 6,063 m² of solar collectors. By installing all the panels, around 3,183,075 MWh of additional heat energy can be produced.

The simulation in LEAP for the total period of 30 years showed the impacts of certain scenarios on the total energy consumption and the reduction of CO₂ emissions, which is shown in Table 5 and in Figure 2.

Table 5. Results of energy and environmental effects according to scenarios

Scenario	Energy requirements MWh/year	Reduction of CO _{2eq} emissions t/year
Current state (2015)	59.657,34	12.669,25
Scenario 1 (2025)	53.785,05	9.310,74
Scenario 2 (2035)	44.398,34	5.067,69
Scenario 3 (2045)	41.215,26	3.632,71

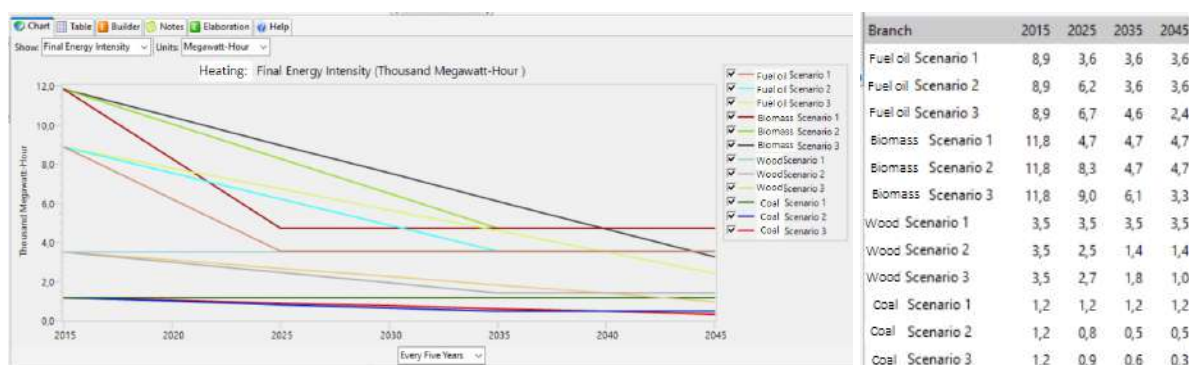


Fig. 2. Energy consumption for heating according to scenarios and types of energy sources

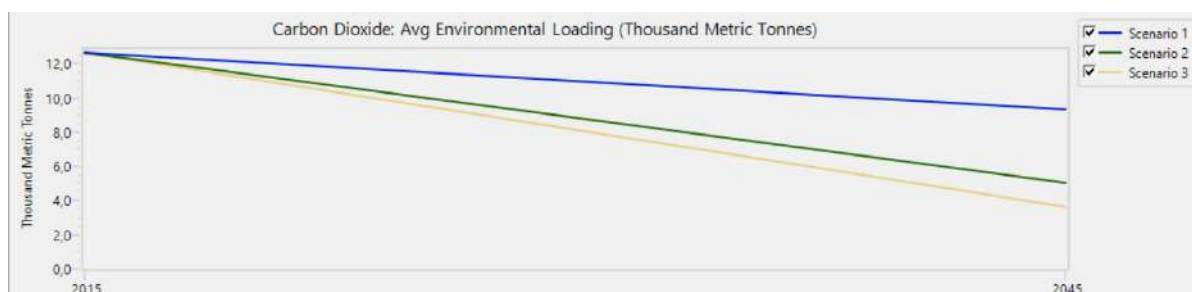


Fig. 3. Reduction of CO₂ emissions according to scenarios

To choose the best scenario, the Super Decisions software was used for multi-criteria decision making. The alternatives represent 3 created scenarios, and the set criteria are as follows: obtained energy effects (total energy savings on an annual basis), economic (capital investment), ecological (reduction of CO₂ emissions) and social effects (creation of new jobs and social acceptability).

Inconsistency	Ecological effects	Energy savings	Capital investment	Social acceptability
Social acceptability	↑ 2	↑ 4	↑ 4	↑ 2
Ecological effects		↑ 3.00000	↑ 3.00000	↑ 3.00000
Energy savings			↑ 4	↓ 3
Capital investment				↓ 4

Fig. 4. Matrix of values for criteria and alternatives

The results showed that scenario number 1 is the best solution, followed by scenario number 2 and in last place is scenario number 3. This order primarily refers to the most important criterion, which is the capital cost for the implementation of the proposed measures to increase the energy efficiency of the buildings.

Table 6. Comparison of alternatives – report

An alternative	Total	Normal	Ideally	Order
Scenario 1	0,76	0,53	1,00	1
Scenario 2	0,42	0,29	0,55	2
Scenario 3	0,23	0,16	0,30	3

4. CONCLUSION

The negative consequences of climate change, of which the creation of heat islands has a major impact on urban areas, should be solved by introducing innovations in the field of construction. Adaptation measures to the changed climatic conditions that were studied in this paper include the renovation of building envelopes using thermomechanical measures and the active solar systems on the roofs of buildings. The effects of the implementation of the mentioned measures were observed with the two most significant effects: energy and environment.

Previous practice in this area and simulation processes carried out using an adequate software solution have shown that by renewing the envelope on educational facilities in the City

of Banja Luka on an annual basis, up to 60% of the energy consumed for heating the facilities can be saved. In addition, active solar systems in the form of plate collectors can also make a significant contribution to the savings of thermal energy obtained by burning fossil fuels. It is also important to mention the ecological aspect of the application of the mentioned measures, which is primarily reflected in the reduction of carbon dioxide emissions, as well as the social aspect (opening of new jobs, so-called green jobs).

Due to all the mentioned positive impacts, the application of thermomechanical measures on buildings should be one of the priority measures when it comes to adaptation to climate changes in urban areas and improvement of the microclimatic features of the space.

REFERENCES

- [1] Action plan for energy efficiency (APEE) of the City of Banja Luka for the period from 2016 to 2019.
- [2] Kulić E. (2019). Energy use in buildings, Proceedings of the International Congress on KGH, pages 135-147 [in Serbian].
- [3] Sozer H. (2010). Improving energy efficiency through the design of the building envelope, Building and Environment 45, pages 2581-2593.
- [4] Zhou D., Park S.H. (2012). Simulation-Assisted Management and Control over Building Energy Efficiency – A Case Study, 2nd International Conference on Advances in Energy Engineering, pages 592 – 600.
- [5] The City of Banja Luka, UNDP (2010). Sustainable energy action plan of the City of Banja Luka (SEAP).
- [6] Development strategy of the City of Banja Luka in the period 2018-2027.
- [7] UNDP, Study of the energy sector in Bosnia and Herzegovina, final report, 2008.
- [8] Green jobs - Analysis of the impact of energy efficiency measures on employment in Bosnia and Herzegovina, Centre for Development and Support, Tuzla, 2016.



Banja Luka
1-2 Jun 2023.

DEMI 2023

16th International Conference on Accomplishments in Mechanical and Industrial Engineering

www.demi.mf.unibl.org



Influence of solar fraction on photovoltaic generated energy at Serbian residential building

Danijela Nikolić^a, Saša Jovanović^a, Vanja Šušteršič^a, Natalija Aleksić^a, Zorica Đorđević^a,

^aFaculty of engineering, University of Kragujevac; Sestre Janjic 6, 34000 Kragujevac, Serbia

Abstract *In buildings, which are large consumers of energy, it is necessary to use technologies of renewable energy sources. One of the best solutions is solar energy, because solar energy is the most promising and reliable energy source, due to its clean and inexhaustible energy source that does not cause pollution. This paper analyzes the energy consumption in a single-family residential building with photovoltaic array. Electricity in the building is used for space heating, lighting, DHW system and electrical appliances. Energy consumption and energy generation data were obtained by simulations performed in the EnergyPlus software, while building was designed in Open Studio plug-in for Google Sketch Up. The analyzed building has located in the city of Kragujevac. This investigation shows the possibility for energy saving in residential Serbian building, with variable solar fraction at photovoltaic array and variable cell efficiency of photovoltaics. Obtained results also shown that concept of Positive net-energy building concept (PNEB) can be achieved, with solar fraction of 0.85, PV cell efficiency of 16 % and proper PV surface area.*

Keywords *building, photovoltaic, solar fraction, generated energy, energy saving*

1. INTRODUCTION

Today, building sector consumes about 40% of total energy consumption in a modern world, while in Serbia this amount is as much as 50% [1]. Buildings energy consumption is related to their exploitation conditions. The largest energy consumer is heating system, then domestic hot water system, electrical appliances and lighting. Concept of energy efficiency building can reduce energy consumption. Energy efficient building means a lower total energy consumption, lower greenhouse gas emission and partially or completely satisfying energy needs with the

energy generated by its own systems of renewable energy sources. These sources do not pollute the environment, which directly contribute to the global warming reduction through lower greenhouse gas emission [2, 3]. Systems of renewable energy generates electrical or thermal energy, and on that way they contribute also to the longer life cycle of the building.

Solar energy is the most promising source of renewable energy and represents the most reliable source of energy because it does not bring pollution, which is disproportionately large in the use of fossil fuels [4]. Photovoltaic (PV) technology represents the direct conversion of solar radiation into electricity. The PV system generates electricity for space heating, lighting, electrical appliances, etc. The rest of the building energy needs are compensated by purchasing electrical energy from the electricity distribution system.

Corresponding author

PhD Danijela Nikolić, Associated Professor
danijela1.nikolic@gmail.com

Faculty of engineering, University of Kragujevac
Sestre Janjić 6
Kragujevac, Serbia

This article reports investigations of the possibilities to decrease energy consumption of Serbian single-family residential buildings with PV array and electric heating systems, through the variation of PV array surface (one or/and two roof surface with PV panels), solar fraction and photovoltaic cell efficiency. The investigated building was located in the city of Kragujevac, Serbia. The building is designed with PV panels on the roof. Electricity generated by the PV array is limited with the size of PV array. Heating system operated from 15 October to 14 April next year. The major objective of this investigation is to determine energy savings in the building when PV array has different cell efficiency and different solar fraction. In this paper, the EnergyPlus software and Open Studio plug-in in Google SketchUp were used.

The analysis show various parameters such as total energy consumption, energy consumption in heating energy consumption, and generated energy by PV array.

2. MODEL OF ANALYZED BUILDING

The modelled single-family residential building is shown in Figures 1 and 2. It is two-store building and it has 10 conditioned zones (2 living rooms with kitchens, 2 halls, 2 bathrooms and 4 bedrooms). The building also has an attic zone.

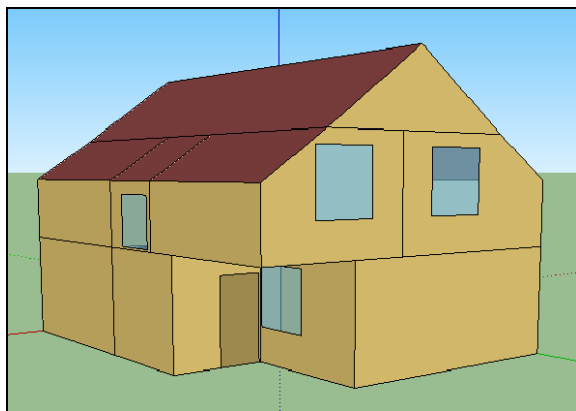


Fig. 1. Modeled building in EnergyPlus

The total floor area of the building is 169 m². First floor has the area of 77 m², while second floor has the area of 92 m². The windows are double glazed with the air gap of 15 mm with the U-value of 2.72 W/(m²K). Inward opening

side-hung windows are implemented in modelled buildings.

The building envelope and roof are thermally insulated by polystyrene (thermal insulation thickness - 0.15 m). The building has the south and north oriented roof with a slope of 37.5°, which is the optimal orientation for slope of solar systems in the region of the Kragujevac [5]. The total roof area (both identical sides) is 114 m². The external wall consists of brick, heavy concrete, insulation, air space and gypsum board, with U value 0.177 W/(m²K). The inner wall consists of two layers of gypsum boards with air space between them. The floor construction consists of lightweight concrete, air layer and acoustic plate, U value 0.517 W/(m²K). The ceiling consists of lightweight concrete, air space and an acoustic plate. Above the ceiling is the non-conditioned attic zone.

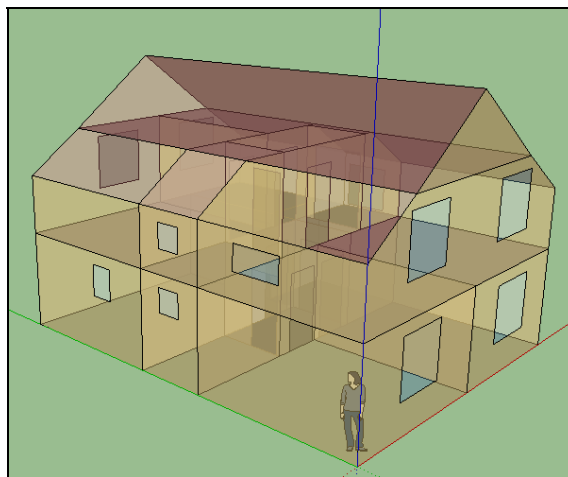


Fig. 2. Modelled building in EnergyPlus - X ray view

The building was simulated through a one year. Heating system (with an electric baseboard heater in every conditioned) operates from October 15 to April 15, which is a common practice in Serbia. Air temperatures in the heated zones are set to 20°C from 07:00-09:00 and from 16:00-21:00, and to 15°C from 09:00-16:00. The simulation time step is 15 min.

3. LOCATION AND CLIMATE

The analyzed building is located in the city of Kragujevac, Serbia. Kragujevac belong to Sumadija region - the central part of the Republic of Serbia. Its average height above sea level is 209 m. Its latitude is 44°10' N and

longitude 20°55 E. The time zone for Kragujevac is GMT+1 h. Kragujevac has a moderate climate, with warm and humid summers, and cold and snowy winters [6].

The EnergyPlus uses weather data from its own database file. This database input file has a large variety of parameters for solar radiation calculating for every day in the year. Daily average solar radiation for Central Serbia, where the analysed house is located, is 1550 kWh/m² [7].

4. MODEL OF PV SYSTEM

The PV system consists of the PV array and an inverter. It is an on-grid system. The operations of the PV array and the electrical heating system are together simulated by using EnergyPlus. Photovoltaic system is installed on the roof of the building (slope angle of 37.5°). Photovoltaic cell efficiency initially set as 12 %. Through the simulations, PV cell efficiency varied, and it was 16 %. Solar fraction at the first moment was 0.5; in the further simulations it was 0.85. The area of considered PV array was 14 m². Through different simulations, PV array is considered on south or north roof side (or both of them).

The main assumption is that when the PV system operates, all generated electricity would be immediately consumed. The PV panel is represented by the mathematical model of Photovoltaic:Simple from EnergyPlus [6], which describes a simple model of PV that may be useful for early phase design analysis. This model allows quick and easy modifications during the simulation routines. The user can set up value for cell efficiency, area and solar fraction [6].

5. RESULTS AND DISCUSSION

5.1 Building energy consumption

The amount of energy consumption in the analysed single-family residential building is obtained by simulations in software package EnergyPlus (Table 1).

The results show the annually energy consumption for heating system, domestic hot water system, electrical equipment and lighting, as well as the total final energy consumption.

The largest part of energy consumption (electricity) is related to the heating system (6610 kWh), then to the domestic hot water

system (3702 kWh). Electrical appliances consume 2357 kWh and lighting consumes 578 kWh annually. Total yearly building energy consumption is 13247 kWh.

Table 1. Energy consumption in building

Energy consumption (kWh)	
Heating	6610
Lighting	578
Electric equipment	2357
DHW system	3702
Total energy consumption	13247

Figure 3 shows the distribution of building energy consumption, in kWh and %. The largest share of energy, 50%, is spent in heating system, then 28% on DHW system. Electrical equipment and lighting spent 8 % and 1 % of total energy consumption, respectively.

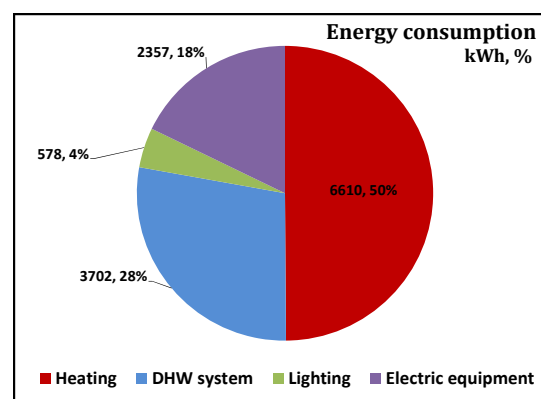


Fig. 3. Distribution of building energy consumption

5.2 Case 1 – 12 % PV cell efficiency, SF 0.5

Case 1 represents the case of 12 % PV cell efficiency. Solar fraction (SF) is 0.5. This value of solar fraction can be explained with shading PV array by other buildings or trees, in combination with presence of dirtiness, or incomplete function of the PV panel due to its damage (hot spot, high temperature, etc.).

Case 1a presents PV array installed at the south roof, Case 1b presents PV array installed at the north roof, and Case 1c presents PV array installed at the complete roof.

Figure 4 shows generated energy by PV array, building energy consumption and building net-

energy consumption. In a Case 1a – with PV array on the south roof, 1731.3 kWh of electricity can be generated, which means that the net-energy consumption in the building is 11515.7 kWh. In a Case 1b – with PV array on the north roof, 1206.7 kWh of electricity can be generated, so net-energy consumption is 12040.3 kWh. When PV array is installed to the both roof sides (Case 1c), generated electricity is 2938 kWh, and net-energy consumption is 10309 kWh. With installing the greater PV array, the amount of generated electricity increases and net-energy consumption decreases, so in the Case 1c, net-energy consumption is lower for 22.2 %, compared to the building without PV array.

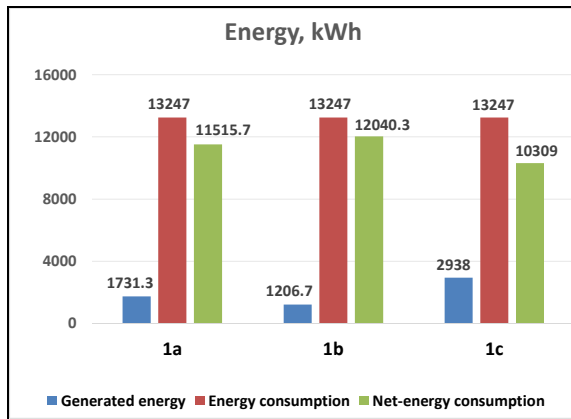


Fig. 4. Case 1 - building energy consumption and generated energy

5.3 Case 2 – 12 % PV cell efficiency, SF 0.85

Case 2 represents the case of 12 % PV cell efficiency and solar fraction of 0.85. Case 2a presents PV array installed at the south roof, Case 2b presents PV array installed at the north roof, and Case 2c presents PV array installed at the complete roof.

The higher value of solar fraction influence to the amount of generated energy. With the solar fraction increasing, generated electricity is increasing too, and building net-energy consumption is decreasing (Figure 5).

In a Case 2a – with SF of 0.85 and PV array on the south roof, the amount of 2943.2 kWh of electricity can be generated, and net-energy consumption in the building is 10303.8 kWh. In a Case 2b – with SF of 0.85 and PV array on the north roof, 2051.4 kWh of electricity can be generated, while net-energy consumption is

11195.6 kWh. When PV array is installed to the both roof sides (Case 2c) and solar fraction is 0.85, generated electricity is 4994.6 kWh, and net-energy consumption is 8252.4 kWh. With higher solar fraction and with installing the PV array of greater surface area, the generated energy increases and net-energy consumption decreases (Figure 5). Compared to the building without PV array, net-energy consumption is lower for 22.2 %, 15.5% and 37.7% for Case 2a, 2b and 2c, respectively.

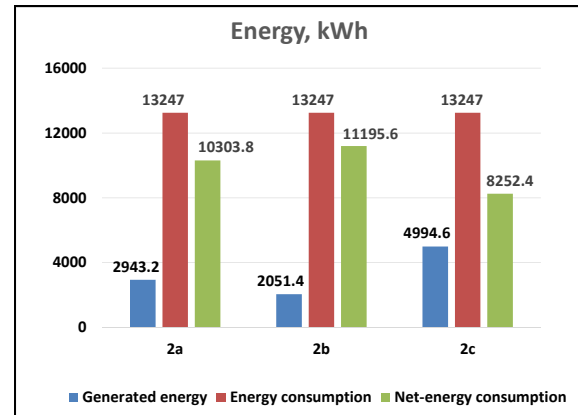


Fig. 5. Case 2 – building energy consumption and generated energy

5.4 Case 3 – 16 % PV cell efficiency, SF 0.85

Case 3 represents the case of 16 % PV cell efficiency and solar fraction of 0.85. As in previous cases, here, Case 3a presents PV array installed at the south roof, Case 3b presents PV array installed at the north roof, and Case 3c presents PV array installed at the complete roof.

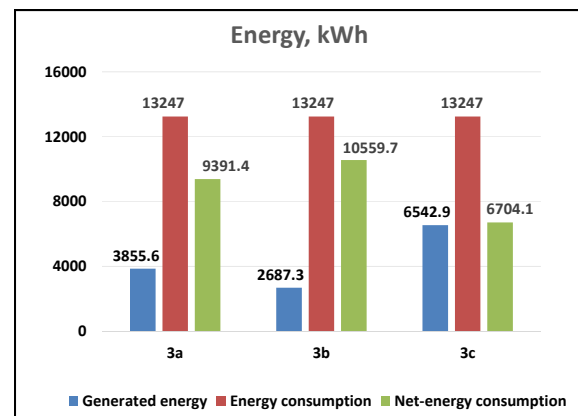


Fig. 6. Case 3 – building energy consumption and generated energy

The higher value of PV cell efficiency directly influence to the amount of generated energy. With the increasing of cell efficiency, generated energy, is increasing too. In that case, net-energy consumption is decreasing (Figure 6).

In a Case 3a – with PV cell efficiency of 16 %, solar fraction of 0.85 and PV array on the south roof, the 3855.6 kWh of electricity can be generated, and net-energy consumption in the building in that case is 9391.4 kWh. In a Case 3b – with PV cell efficiency of 16 %, solar fraction of 0.85 and PV array on the north roof, the amount of generated electricity is 2687.3 kWh, while net-energy consumption is 10559.7 kWh. When PV array with 16 % of cell efficiency is installed to the both roof sides (Case 3c) and solar fraction is 0.85, generated energy has the highest value – 6542.9 kWh, and net-energy consumption is 6704.1 kWh. With higher solar fraction and with installing the PV array with 16 % of cell efficiency to the both roof sides, the generated energy increases and net-energy consumption decreases (Figure 6). Compared to the building without PV array, net-energy consumption is lower for 29.1 %, 20.3% and 49.4% for Case 3a, 3b and 3c, respectively.

5.5 Case 4 – Zero Net-Energy Building

In accordance with previous investigation, it can be concluded that concept of Positive Net-Energy Building (PNEB) can be achieved with the greater surface area of photovoltaic array. In all analysed cases, photovoltaic surface area was 14 m² (in a case of installing at one roof side), i.e. 28 m² (in a case of both roof side).

Table 2. Energy consumption in PNEB building (PV cell efficiency 16 %, PV surface area 57 m², solar fraction 0.85 - Case 4)

Building energy consumption (kWh)	13247
Generated energy (kWh)	13319
Net-energy consumption	-72

Simulation results obtained by EnergyPlus software shown that the concept of PNEB building can be achieved with PV cell efficiency of 16 %, solar fraction of 0.85 and PV surface area of 57 m². In that case (Case 4), generated electricity is 13319 kWh and net-energy consumption is -72 kWh. This means that with PV array of 57 m², surplus of electricity is 72 kWh annually (Table 2).

5.6 Comparison of the obtained results

Figure 7 compared the building energy consumption and generated energy for most favourable analysed cases (Case 1c – PV cell efficiency of 12 %, PV surface area of 28m² and solar fraction of 0.5, Case 2c – PV cell efficiency of 12 %, PV surface area of 28m² and solar fraction of 0.85, Case 3c– PV cell efficiency of 16 %, PV surface area of 28m² and solar fraction of 0.85 and Case 4 – PNEB with PV cell efficiency of 16 %, PV surface area of 57 m² and solar fraction of 0.85).

Based on the obtained simulation results, it can be concluded that installation of PV array can significantly improve building energy efficiency. By comparing Case 1c and 2c, it can be concluded that with increasing of solar fraction from 0.5 to 0.85, there is significant increasing in generated energy (70 %), and also, significant decreasing in net-energy consumption (24.9%). By comparing Case 2c and Case 3c, it can be concluded that with increasing of PV cell efficiency from 12 % to 16 %, there is also significant increasing in generated energy (31%), and also, significant decreasing in building net-energy consumption (18.8 %). By comparing Case 1c and Case 3c, it can be concluded that with increasing of photovoltaic cell efficiency from 12 % to 16 %, and with increasing of solar fraction from 0.5 to 0.85, there is also significant increasing in generated energy (122,7%), and also, significant decreasing in building net-energy consumption (53,8 %).

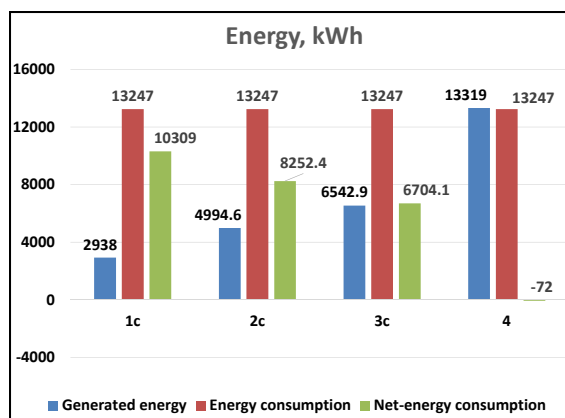


Fig. 7. Comparison of the most favorable cases with Case of PNEB - building energy consumption and generated energy

6. CONCLUSION

The major aim of this investigation was to determine the energy saving in single-family residential building, with different solar fraction on PV array and different photovoltaic cell efficiency. All analysed buildings have had the electric space heating system.

By using PV array with cell efficiency of 16%, it is possible to generate significantly greater amount of electrical energy, compared with PV array of 12% cell efficiency. With the increasing of photovoltaic cell efficiency, there is a significant decrease in the building net-energy consumption.

Solar fraction also influence to energy generation: with increasing the solar fraction, generated electricity is increasing too, while the net-energy consumption is decreasing.

Simulation results shown that it is possible to achieve the concept of positive net-energy building. That is the case with PV cell efficiency of 16 %, solar fraction of 0.85 and PV surface area of 57 m². Then, generated energy is 13319 kWh (which is greater than building energy consumption of 13247 kWh) and net-energy consumption is -72 kWh.

Acknowledgement

This paper presents results obtained within realization of the project TR 33015, funded by Ministry of Education, Science and Technological Development of the Republic of Serbia. The authors would like to thank to the Ministry for their support during these investigations.

REFERENCES

- [1] Bojić M., Nikolić N., Nikolić D., Skerlić J., Miletić I., (2011). A simulation appraisal of performance of different HVAC systems in an office building, *Energy and Buildings*, vol.43, no. 6, p. 2407-2415, <https://doi.org/10.1016/j.enbuild.2010.12.033>
- [2] Nikolić D., Skerlić J., Šušteršič V., Radojević A., Aleksić N., Variances in building energy consumption – influence of domestic hot water system parameters, *Proceeding of 5th International Scientific Conference "Conference on Mechanical Engineering, Technologies and Applications" COMETA 2020*, 2020, Jahorina, Republika Srpska, p. 436-443
- [3] Nikolic D., Lukić N., Radulovic J., Skerlic J., Energy optimization of Serbian buildings using the Hooke-Jeeves algorithm, *Proceeding of 4th International Conference on Renewable Electrical Power Sources ICREPS 2016*, 2016, Belgrade, p. 443-452
- [4] Nikolić D., Skerlić J., Radulović J., Šušteršič V., Radojević A., Terzić I., Possibility for energy saving in Serbian building with photovoltaic-thermal collectors, *Proceedings of 15th International Conference on Accomplishments in Mechanical and Industrial Engineering DEMI 2021*, 2021, Banja Luka, Republika Srpska, p. 173-179
- [5] Bojić M., Nikolić N., Nikolić D., Skerlić J., Miletić I., (2011). Toward a positive-netenergy residential building in Serbian conditions, *Applied Energy*, vol. 88, no. 7, p. 2407-2419, <https://doi.org/10.1016/j.apenergy.2011.01.011>
- [6] Anonymous, *ENERGYPLUS, Input Output Reference - The Encyclopedic Reference to EnergyPlus Input and Output*, University of Illinois & Ernest Orlando Lawrence Berkeley National Laboratory, 2009.
- [7] Lukic N., Babic M. (2008)., *Solarna energija*, Masinski fakultet u Kragujevcu, Centar za RGE, Kragujevac



Banja Luka
1-2 Jun 2023.

DEMI 2023

16th International Conference on Accomplishments in Mechanical and Industrial Engineering

www.demi.mf.unibl.org



Long term simulation of vertical GCHP system for a building with asymmetric cooling and heating loads

M. Đekić^a, E. Tombarević^b

^aING Invest Ltd., 8. Marta, Podgorica, Montenegro

^bFaculty of Mechanical Engineering, University of Montenegro, Džordža Vašingtona bb, Podgorica, Montenegro

Abstract This paper presents the results of numerical simulations of the operation of heating and cooling system of a smaller commercial building in two different climatic zones in Montenegro. The climatic conditions and building physics are such that the cooling load is greater than the heating load. Vertical-borehole ground coupled heat pump uses 16 vertical boreholes in 4-by-4 configuration as the heat sink/source. Numerical simulations performed using EnergyPlus software are conducted to indicate the possibility of optimizing the system in terms of energy savings through increased efficiency or in terms of reduced investment. To this end, two cases are analysed: Case 1 as a baseline case in which only a geothermal exchanger is used for heat rejection and Case 2 as a hybrid system that uses a cooling tower and a plate heat exchanger in the condenser loop as an additional heat rejecter. Simulation results for a 200-year period indicate that the hybrid system with cooling tower should be seriously considered in similar building-climatic conditions cases characterized by such asymmetry between the cooling and heating load.

Keywords Ground-coupled heat pump (GCHP), hybrid systems, borehole heat exchanger, cooling tower, EnergyPlus.

1. INTRODUCTION

At the local, regional and global level, various measures are being implemented to combat climate change. The European Union is leading the way in this, showing a strong determination to reduce greenhouse gas emissions.

The well-known 2020 climate and energy package set by EU leaders in 2007 had three key targets: reducing GHG emissions by 20% compared to the 1990 level, increasing the share of renewables to 20% and reducing

energy consumption by 20% by applying energy efficiency measures. The European Green Deal, approved in 2020 is even more ambitious, setting an overarching aim of making the European Union climate neutral by 2050. As the building sector is responsible for about 40% of EU energy consumption, one of the ways to achieve these goals is the use of more efficient heating and cooling systems, which certainly include geothermal heat pumps. Ground coupled heat pumps systems (GCHP) have not found widespread use in Montenegro so far, but are expected to be an attractive solution for space cooling and heating in the near future. In particular, wide use of the vertical borehole heat exchanger (BHE) configuration is expected, which consists of boreholes (typical diameter DN80-DN125 and depth 100 m) in which one or two U-bended HDPE pipes are placed [1]. Heat

Corresponding author

Marko Đekić, M.Sc. Mech. Eng.
marko.djekic3@gmail.com

ING Invest Ltd.
8. marta
81000 Podgorica, Montenegro

transfer fluid that circulates through the pipes is water or water-glycol solution. Vertical systems have the advantage of requiring smaller land area, less energy consumption for the operation of circulation pumps and higher efficiency due to the fact that the soil temperature does not fluctuate at higher depths during the year. They are suitable for residential and small commercial buildings. In cases where more heat is rejected to the ground in summer (cooling) than it is extracted in winter (heating), the use of hybrid ground coupled heat pump systems (HGCHP) with cooling tower should be considered. With those systems, an additional heat rejecter is added to the condenser loop in a form of a cooling tower which serves to further reject heat to the environment, therefore decreasing the load of BHE in summer and resulting in its balanced load over the year. Using such systems can reduce initial investment of the system by initially reducing the number of required boreholes, while keeping the system efficient with high coefficient of performance. Simulation tools such as EnergyPlus can be used for simulation of GCHP and HGCHP systems. EnergyPlus [2] is whole building energy simulation program for modeling energy and water use in the buildings. In order to perform design and simulation of the system, it is necessary to take into account hourly heating and cooling load profile of the building. For the simulation of heat transfer in the ground, EnergyPlus integrates models using response factors (so called g-functions) developed by Eskilson [3] for long time steps and by Yavuzturk [4] for short time steps.

2. DESCRIPTION OF HVAC SYSTEM

To analyse the benefits of HGCHP in the case of a building with asymmetric cooling and heating load, a small commercial building with a total area of 800 m² is modelled in EnergyPlus. The thermal characteristics of the building envelope (walls, floor, roof, windows) have been adjusted to meet the values proscribed by the rulebook on minimum energy efficiency requirements of buildings in Montenegro. Different climatic conditions were used for the analysis: Podgorica representing the central part and Bar representing the southern part of Montenegro. The corresponding EPW (EnergyPlus weather) files for Podgorica and Bar are set up and integrated in EnergyPlus. The 3D layout of the

building is presented in Fig. 1. The building is divided into five thermal zones. Zone temperatures are set by thermostats at 25°C in summer and 21°C in winter operation mode of the HVAC system.

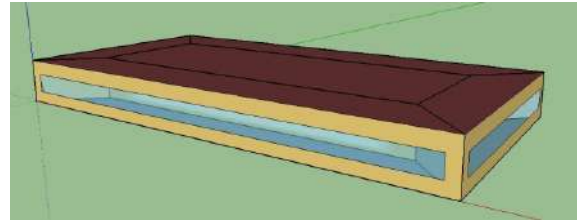


Fig. 1. Layout of the building

Ground-to-water heat pump with vertical borehole heat exchanger is selected for cooling/heating of the building. Fan coil units are selected for space cooling/heating. Temperatures of supply/return water are 7/12°C in cooling mode and 50/45°C in heating mode. Case 1 is the baseline case where heat rejection and absorption is only done via BHE consisting of 16 boreholes in 4-by-4 square configuration. The depth of the boreholes is 76 m and they are set at the distance of 3.66 m. The diameter of the borehole is 12.7 cm and the outer diameter of the pipe is 2.67 cm. The schematic diagram of the system is shown in Fig. 2.

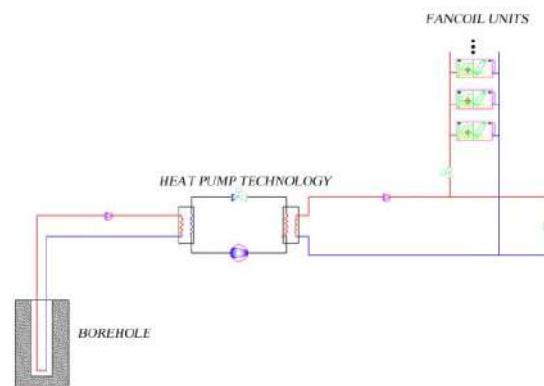


Fig. 2. Schematic diagram of HVAC system - Case 1

Case 2 includes a cooling tower which is added to the condenser loop as an additional heat rejecter. The cooling tower is connected to the condenser circuit via a plate heat exchanger. The cooling tower is controlled with differential control strategy. The temperature of the reference node is compared with the outdoor

wet bulb temperature obtained from weather file. If the temperature difference lies in the specified range, the loop with the cooling tower will be on. The minimum set point temperature is set on 15°C, and maximum set point is set up on 37°C. The schematic diagram of the system is shown in Fig. 3.

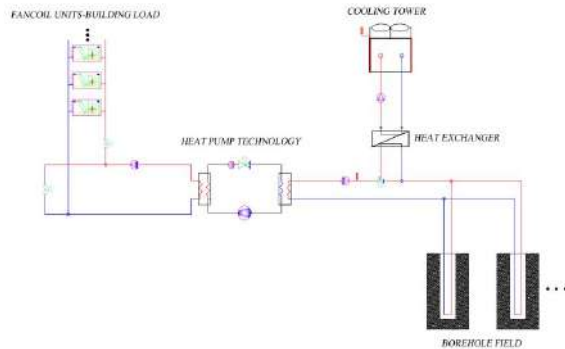


Fig. 3. Schematic diagram of HVAC system - Case 2

3. RESULTS

The hourly heating and cooling loads in the climatic conditions of Podgorica and Bar are shown in Fig. 4 and Fig. 5 respectively. The heating load is presented on the positive, while the cooling load is presented on the negative side of the ordinate. In both cases the cooling load is greater than the heating load (40 kW vs. 26.5 for Podgorica and 40 kW vs. 22 kW for Bar).

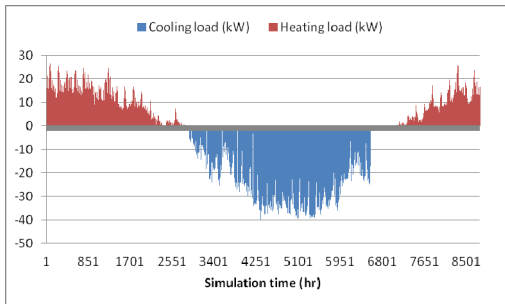


Fig. 4. Annual hourly building load - Podgorica

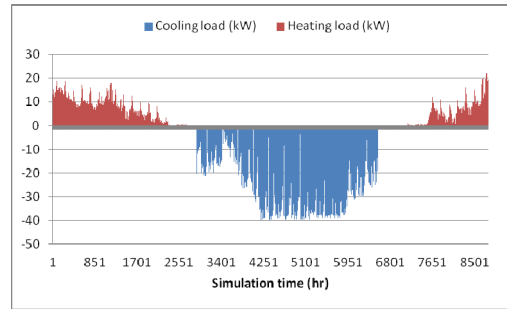


Fig. 5. Annual hourly building load – Bar

The mean daily borehole wall temperature for both cases, in the climate conditions of Podgorica during the simulation period of 20 years is presented in Fig. 6.

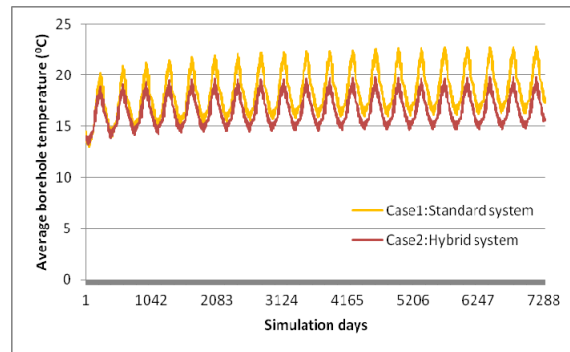


Fig. 6. Borehole wall temperature - Podgorica

It can be seen that in Case 1, the mean borehole wall temperature increases visibly over the years. This is due to the fact that from year to year more heat is rejected to the ground via BHE during the cooling season (summer) than it is absorbed from the ground during the heating season (winter). This imbalance caused by asymmetric heat load results in an increase in the temperature of the borehole wall over the years. During the first year, the mean borehole wall temperature reaches a maximum of 20°C, while at the end of the 20th year of system operation it reaches 23°C. In Case 2 where a cooling tower is added as an additional heat rejecter, the unloading of the BHE is evident. The borehole wall temperature remains fairly constant over the years. Its maximum value during the first year is 19°C and it reaches only 19.8°C in the 20th year of system operation. The high temperatures of the borehole wall cause high heat transfer fluid temperatures at the inlet to the heat pump, as can be seen in Fig. 7.

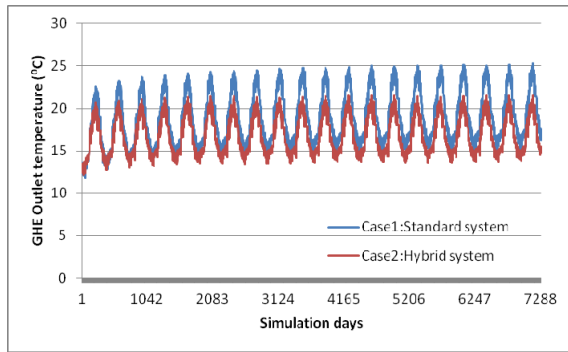


Fig. 7. GHE outlet temperature - Podgorica

In Case 1, the temperature of the fluid during the first year reaches a maximum of 22°C, while its maximum temperature in the last year of the simulation period is 25.5°C. By adding a cooling tower to the condensing circuit, those temperatures are reduced to 20.7°C in the first year, and 21.5°C at the end of the simulation period.

The effect of unequal cooling and heating load on BHE operation is more noticeable in the case of climatic conditions of Bar where the difference between cooling and heating load is larger. The variation of the mean hourly temperature of the borehole wall is presented in Fig. 8.

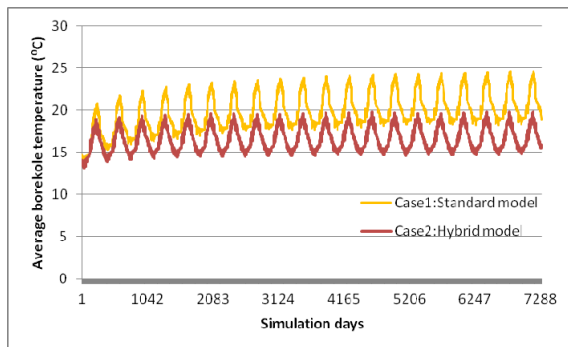


Fig. 8. Borehole wall temperature - Bar

It is clearly visible that in those climate conditions, for the building with a basic GCHP system (Case 1), the increase in the average temperature of the borehole wall over the years is even greater. In the first year, the maximum temperature of the borehole wall reached 20.8°C, while in the last year of the simulation period, the maximum temperature of the borehole wall reached as much as 24.6°C. By

improving the basic system by adding a cooling tower (Case 2), the thermal load of the ground as a source/sink of heat is balanced in the sense that approximately the same amount of heat is extracted from the ground in winter as it is rejected into it in summer. Consequently, the borehole wall temperature has much less growth over the years. The maximum temperature of the borehole wall is 19.6°C in the first year and 20.4°C in the last year of the simulation period.

The hourly variation of the temperature of the heat transfer fluid at the outlet of the geothermal heat exchanger, i.e. at the inlet to the heat pump, is shown in Fig. 9.

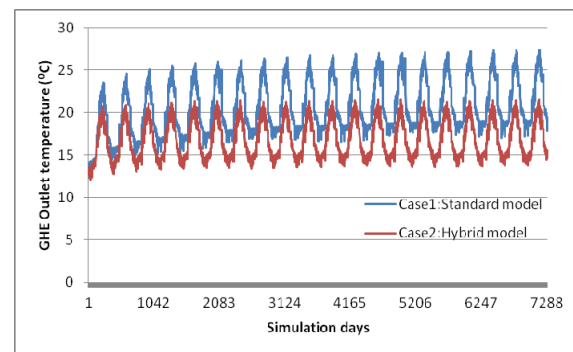


Fig. 9. GHE outlet temperature - Bar

Further evidence of the advantages provided by the hybrid system can be seen by analyzing the graph depicting the water temperature at the geothermal exchanger outlet, which is also the heat pump's inlet. By installing a cooling tower, the temperature of the fluid at the outlet of the geothermal heat exchanger is reduced. In the first year, the temperature reaches a value of 21.6°C, while at the end of the twentieth year it only reaches 22.4°C.

The energy consumption of the heat pump in Podgorica's climatic conditions in case 1 increases over the simulation period in the cooling mode, while it decreases in the heating mode. The total energy consumption for heating and cooling reaches 14,000 kWh at the end of the simulation period. However, in case 2, the total energy consumption for heating and cooling of the heat pump decreases over time, reaching a value of 13,300 kWh in the last year of the simulation. The hybrid system, with a mean COP value of 4.2 in the heating mode and 5.5 in the cooling mode, demonstrates the system's effectiveness.

In Bar's climatic conditions, case 1's energy consumption of the heat pump reaches 12,100 kWh at the end of the simulation period, with energy consumption continually increasing over the years. However, in case 2, the energy consumption decreases and reaches 11,500 kWh. The hybrid system provides a mean COP value of 4.25 in the heating mode and 5.5 in the cooling mode.

4. CONCLUSIONS

Numerical simulations of the operation of HVAC system with GHE have shown that the long-term efficiency depends significantly on the balance of cooling and heating load. In case when cooling load is greater than the heating load, more heat is rejected than is absorbed from the ground. This results in an increase in ground temperature, a decrease in the efficiency of the system in the cooling mode and an increase in the efficiency in the heating mode. The cooling tower as an additional heat rejecter enables long-term reliable operation of the system and high efficiency in both operating modes. Borehole heat exchanger, as the most expensive part of the HVAC system, is critical in terms of investment. The installation of a cooling tower allows for reduction in investment as the BHE can be dimensioned according to the heating load thus reducing the need for expensive drilling of the soil.

REFERENCES

- [1] Chiasson, A.D., (2016). *Geothermal Heat Pump and Heat Engine Systems*. Wiley, Hoboken.
- [2] U.S. Department of Energy (DOE) Building Technologies Office (BTO). EnergyPlus. From: <https://energyplus.net>, accessed on: 16.04.2023.
- [3] Eskilson, P. (1987). *Thermal Analysis of Heat Extraction Boreholes*. PhD thesis. University of Lund.
- [4] Yavuzturk, C. (1999). *Modelling of Vertical Ground Loop Heat Exchangers for Ground Source Heat Pump Systems*. PhD thesis. Oklahoma State University.



Banja Luka
1–2 Jun 2023.

DEMI 2023
**16th International Conference on
Accomplishments in Mechanical and
Industrial Engineering**
www.demi.mf.unibl.org



Performance Analysis of a Biomass-Fired Steam Boiler with FGR Using Agricultural Residue Straw as Fuel

M. Tomić^a, P. Živković^b, J. Škundrić^c, M. Kljajić^a, B. Stepanov^a, Ž. Vlaović^a

^aUniversity of Novi Sad, Faculty of Technical Sciences, Trg Dositeja Obradovića 6, Novi Sad

^bUniversity of Niš, Faculty of Mechanical Engineering, Aleksandra Medvedeva 14, Niš

^cUniversity of Banja Luka, Faculty of Mechanical Engineering, Vojvode Stepe Stepanovića Blvd. Banja Luka, Banja Luka

Abstract This paper presents an analysis of a biomass-fired steam boiler with capacity of 14 MW which produces saturated steam at pressure of 14 barg using agriculture residue straw as fuel. The boiler operates with flue gas recirculation rate of 20%, a common technique to improve the efficiency of the combustion process and reduce emission. Data from the PLS sensors were collected to evaluate the boiler's performance. Thermal calculations were performed to analyze the heat transfer rate, heat loss, and combustion efficiency of the boiler. Three different cases were considered: flue gas recirculation after the bag filters, recirculation after the flue gas channel exit, and without the recirculation. Parallely, the emission of NO_x for all scenarios was discussed. The analysis of the results shows that for both cases flue gas recirculation yields almost the same efficiency. However, the efficiency for lower flue gas recirculation is increased, and without flue gas recirculation was the highest according to both the model and calculations. This suggests that while flue gas recirculation can be an effective way to improve combustion efficiency and reduce emissions, it may not always be the most optimal solution. The findings of this study provide valuable insights into the biomass-fired steam boilers performance and the impact of flue gas recirculation on their efficiency and NO_x emission. These insights can be useful for optimizing the design and operation of similar biomass-fired steam boilers and for promoting the use of renewable energy sources in industrial processes.

Keywords biomass, FGR, NO_x, steam boiler

1. INTRODUCTION

Steam boilers are widely used in various industries for producing steam, which is used for different purposes, such as power generation, heating, and industrial processes. Biomass steam boilers are one of the sustainable alternatives to fossil fuel boilers, and they have gained attention in recent years due to their potential to reduce greenhouse gas emissions and their low-cost fuel source [1]. The combustion of biomass in the boiler generates flue gases, which contain pollutants, including particulate matter (PM), sulphur dioxide (SO₂), nitrogen oxides (NO_x), and carbon monoxide (CO), which have adverse

effects on the environment and human health [2,3]. The reduction of these emissions is of great importance, and the use of flue gas recirculation is a commonly used technique for this purpose.

Flue gas recirculation (FGR) is process where a part of the flue gas is returned to the combustion chamber to lower the combustion temperature. FGR is a possible way to improve combustion and decrease the emissions of carbon monoxide CO, particulate matter PM, and nitrogen oxides NO_x in order to fulfil emission requirements, for NO_x in [3]. The amount of flue gas recirculation depends on the boiler design, fuel characteristics, and emission regulations.

Summarized, the use of flue gas recirculation is commonly used technique to reduce emissions and increase the biomass steam boilers combustion efficiency [3,4].

In this paper, we investigate the performance of a 14 MW steam boiler which produces saturated steam at the pressure of 14 barg, which combusts agriculture residue straw, and operates with flue gas recirculation at a rate of 20%, working on 80% of the maximal power, i.e. 12.57 barg. The aim of this study is to compare the boiler efficiency with flue gas recirculation after the bag filters, flue gas recirculation after the exit from the flue gas channel, and without flue gas recirculation.

Data from PLS sensors, including temperatures at the steam generator furnace exit, after the water heater-economizer 4, and at the last flue gas channel exit, were utilized in this study. The excess air ratio calculation was enabled by measuring oxygen concentration at one point. Additionally, temperature after the bag filter, feed water, and water temperature after the economizer 4 were measured. The efficiency of the boiler was calculated for each case. The results indicated that the highest efficiency, according to both the model and calculations, was achieved without flue gas recirculation.

2. PERFORMANCE EVALUATION OF A BIOMASS-FIRED STEAM BOILER

Biomass is being combusted on a moving grate. The flue gases released transfer their heat to screens placed in the furnace. Downstream, the flue gases leave the furnace through an opening in the rear screen and enter the flue gas duct, which is inclined downward. Screen tubes are placed in the flue gas duct to transfer heat. After leaving the flue gas duct, the flue gases turn 180° and flow upward through a duct in which an evaporator and an economizer - ECO 4 are placed for heat exchange. After passing through ECO 4, the flue gases change direction again, flow downward, and transfer heat to the economizers ECO 3, ECO 2, and ECO 1 before leaving the flue gas duct and entering the cyclone and filter sections. Part of the flue gas is redirected back to the furnace for recirculation.

The steam boiler technical data are:

Boiler thermal power:

- 14 MW (saturated steam)

Water/steam parameters:

- Working pressure - 14 bar •
- Feedwater temperature - 105°C
- Saturated steam temperature - 195°C
- Flue gas temperature at the boiler outlet: 170°C

Fuel type - Corn straw:

- LHV: 16 MJ/kg
- Designed moisture content: 15%
- Ash content on a dry mass: < 8% •
- Designed fuel ash melting point: < 750°C
- Designed fuel nitrogen content: <0.3%
- Designed fuel chlorine content: <0.3%
- Designed fuel sulfur content: <0.1%

Based on the data provided for corn straw, its composition was adopted for the steam boiler thermal design. The calculations were carried out using the procedure described in various books on steam boiler thermal design [5-7].

These books provided the necessary equations and methodologies for determining the convective and radiant heat transfer coefficients in the steam boiler. The convective and radiant heat transfer coefficients are crucial parameters for evaluating the heat transfer process between the hot flue gases and the water/steam in the boiler. In the thermal design of steam boilers, it is important to accurately determine these coefficients to optimize the boiler's efficiency.

The criteria equations for convective heat transfer and radiant heat transfer were also compared in the calculation process. The results showed the difference < 10% between the criteria equations and also radiant heat transfer fluxes [5-8]. This indicates that methods provide accurate results and can be used interchangeably in the thermal design of steam boilers. However, it is important to note that the choice of the appropriate method may depend on the specific characteristics of the steam boiler and the operating conditions. Therefore, it is recommended to consult with experienced professionals in the field to select the most appropriate methodology of the steam boiler thermal design.

The adoption of air excess ratio is a crucial step of the steam boilers calculation. For the

presented case, the excess air ratio was chosen according to the literature recommendations, which dictate a value of 1.2 in the furnace and 1.25 at the exit. The excess air ratio for the first flue gas channel was chosen to be equal to the value at the exit from the furnace, as determined by calculations. However, after the water heater economizer 4, the air excess ratio was found to be 1.345, and thus adopted as such in the calculation.

Similarly, for the two heat exchanger units further calculations were performed to determine the excess air ratio after the evaporator, economizer 3, and economizer 1. Assuming the same rate of growth, the excess air ratio was found to be 1.2975 after the evaporator, 1.3925 after economizer 3, and 1.4875 after economizer 1 at the exit. The excess air ratio was increased for 0.2 after the cyclone and filter to the value of 1.6875, in accordance with literature recommendations.

After thorough analysis and energy balance calculations, the flame adiabatic temperature was determined to be 1324°C. The temperature at the exit of the combustion chamber was found to be 744.6°C, which is consistent with previous findings in the literature. The temperature after economizer 4 was calculated at 366.3°C, and temperature at the exit from the flue gas channel at 181.5°C. These temperatures were calculated for each unit in the steam boiler, ensuring that the heat transfer energy balance between the heat exchanger and flue gases was within +-1%:

- for the flue gases

$$\dot{Q} = \dot{b} \cdot (I'' - I'), \quad (1)$$

- for the heat exchanger

$$\dot{Q} = k \cdot F \cdot \Delta\theta, \quad (2)$$

and in case of water heaters also the comparison with water side was considered:

$$\dot{Q} = \dot{m}_w \cdot c_w \cdot \Delta t_w. \quad (3)$$

The comparison with provided data is presented in the following Fig. 1 and Fig.2.



Fig. 1. Temperature, pressure and mass flow readings

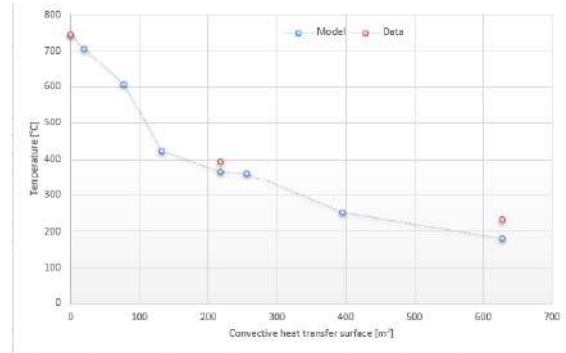


Fig. 2. Comparison of temperature measurements and modelled temperatures

The average RMS between the calculated and the obtained data was found to be 33°C.

The water feed temperature adopted according to the available data was 105.3°C and the temperature at the Economizer 4 outlet was 191.5°C. The calculated water temperature at the economizer outlet (evaporator inlet) was 193.6°C of steam with quality of 0.4%. The difference occurs because in the moment for which the data were presented the water drum was filled to the required level, so the water flow was larger and valued 18.6 t/h. This gives the total heat power of the economizer line 1 to 4 of 1911 kW, compared to the calculated 1990 kW, which gives the total difference of 4%. **THE IMPACT OF FGR ON BOILER PERFORMANCE**

The FGR technique involves the flue gas portion recirculation back to the combustion process. This results in a reduction of the flame temperature and the oxygen concentration, which leads to a decrease of the nitrogen oxides (NO_x) and other pollutants formation. However, this technique can also result in lower combustion efficiency, as the recirculated gas pollutes the combustion air and reduces the oxygen concentration.

According to the methodology presented above, the power and efficiency for the flue gas recirculation (FGR) from the filters and at the boiler outlet were calculated, as well as the case without FGR. In this analysis, the influence of the lower efficiency of the combustion process without FGR was considered. The results of the comparison are presented in the Table 1.

The calculations were performed with the methodology described above, and the results were compared for the cases with and without FGR. Table 1 shows that the power output and the efficiency were slightly lower for the FGR case, as expected. However, the difference in power output was only 1.5%, while the difference in efficiency was over the 4%. Temperatures at the combustion chamber and at the outlet are presented in the Table 2.

As expected, there is no significant difference for the cases where FGR is 20%. However, for reduced FGR, an increase in both efficiency and combustion temperature is observed.

Table 1. Thermal power in [kW] and the efficiency of steam boiler in [%] for different scenarios

Exp no.	FGR- filter (20%)	FGR- exit (20%)	FGR- filter (10%)	Without FGR
Furnace	5670	5816	6421	6946
Exh. manif.	660	661	626	605
Flue gas ch.	968	962	866	755
Evaporator	1625	1613	1363	1146
Ecco 4	442	435	370	323
Turn chmb.	42	39	31	28
Ecco 3	977	950	844	750
Ecco 1-2	572	477	402	289
Net power	10996	10953	10924	10842
Eff.	84.4%	84.5%	86.6%	89.2%

Table 2. Adiabatic temperatures of the flame and flue gas temperature at the exit

Exp no.	FGR- filter (20%)	FGR- exit (20%)	FGR- filter (10%)	Without FGR
Adiabatic temp. of the flame	1324.31	1354.36	1440.50	1698.04
Flue gas temp. at the exit	182.0	185.5	166	170.0

4. NO_x FORMATION ANALYSIS

The concentration of “thermal NO_x” is controlled by the nitrogen and oxygen molar ratios and the combustion temperature. Combustion at temperatures well below 1,300°C forms much smaller ratios of thermal NO_x. For the obtained main species composition (N₂, H₂O, O₂, CO₂) the thermal equilibrium for NO_x is calculated for the adiabatic flame temperature. The concentration was calculated with help of Gasque Chemical Equilibrium Software [9,10]. Gaseq is using the Lagrange Method of Undetermined Multipliers for minimization of the Gibbs free energy of the system to find the equilibrium state/ composition. Several different types of problems can be solved using this software from which the Several different types of problem can be solved, from which the composition at a defined temperature and pressure was investigated.

Table 3. NO_x concentration for different conditions per kg of fuel

Exp no.	FGR- filter (20%)	FGR- exit (20%)	FGR- filter (10%)	Without FGR
Adiabatic temp. of the flame	1324.31	1354.36	1440.50	1698.04
NO _x [kmol/kg]	2.950e-4	3.064e-4	3.705e-4	6.466e-4
Γ _{NO_x}	9.71e-4	9.06e-4	1.24e-3	2.49e-3
Γ _{NO_x} [ppm]	971	906	1240	2490

The results presented in the Tab. 3 are in a good agreement with results of Sartor et al. [11] for small and medium sized combined heat and power biomass plants as they found emissions for wheat straw and whol crop to be in the range 500 to 1030 ppm, while for some biomass fuels it can be significantly over 1300 ppm. As it could be expected the higher temperatures lead to

higher values and concentrations of NO_x in the combustion products.

5. RESULTS AND DISCUSSION

To determine the optimum FGR rate, we need to consider both the boiler efficiency and NO_x emissions. Based on the efficiency the NO_x emissions decrease as the FGR rate increases.

To determine the optimum FGR rate, we need to consider both the boiler efficiency and NO_x emissions, with a weight of X given to NO_x emissions reduction. Based on the information available:

- Efficiency for FGR 0% = 89.2%,
- Efficiency for FGR 10% = 86.6%,
- Efficiency for FGR 20% = 84.4%.

This means that the efficiency decreases as the FGR rate increases.

NO_x emissions for:

- FGR 0% = 6.466e-4 kmol/kg,
- FGR 10% = 3.705e-4 kmol/kg,
- FGR 20% = 2.950e-4 kmol/kg.

This means that the NO_x emissions decrease as the FGR rate increases.

To find the optimum FGR rate, we need to find the point at which the decrease in NO_x emissions balances out with the decrease in efficiency, with the (arbitrary) weight of 5 given to NO_x emission reduction relative to efficiency. We can calculate the weighted efficiency as:

$$\text{Weighted Efficiency} = \text{Efficiency} - (X \cdot \text{NO}_x \text{ Emission Reduction}),$$

where NO_x Emission Reduction is the relative reduction in NO_x emission compared to FGR 0%. For example, for FGR 10%:

$$\text{NO}_x \text{ Emissions Reduction} = (\text{NO}_x \text{ Emissions for FGR 0\%} - \text{NO}_x \text{ Emissions for FGR 10\%}) / \text{NO}_x \text{ Emissions for FGR 0\%}.$$

As we can see from the table, the optimum FGR rate changes to 0% when using a weighted efficiency of 1. This means that if reducing NO_x emissions is equally important as improving efficiency, then FGR should not be used at all. If we increase the weight for NO_x reduction to 5, the highest weighted efficiency is still achieved at 0% FGR rate, but the difference between the

weighted efficiency at 0% and 10% FGR rate has decreased compared to the previous table.

Table 4. Analysis of FGR Rate on NO_x Emissions and Efficiency, with Weighted Reductions 1

FGR Rate	NO _x Emissions [kmol/kg]	Efficiency	NO _x Emissions Reduction	Weighted Efficiency
0%	6.466e-4	89.2%	89.2%	89.2%
10%	3.705e-4	86.6%	81.3%	-4.7%
20%	2.950e-4	84.4%	73.2%	-26.8%

Table 5. Analysis of FGR Rate on NO_x Emissions and Efficiency, with Weighted Reductions 5

FGR Rate	NO _x Emissions [kmol/kg]	Efficiency	NO _x Emissions Reduction	Weighted Efficiency
0%	6.466e-4	89.2%	0%	89.2%
10%	3.705e-4	86.6%	42.6%	81.3%
20%	2.950e-4	84.4%	54.4%	79.3%

6. CONCLUSIONS

Flue gas recirculation (FGR) is an effective and cost-efficient technique for reducing NO_x emissions from burners in certain applications. It is predicted that recirculating up to 20% of the flue gases through the burner can reduce NO_x emissions by as much as 55%. However, this may also reduce the steam boiler's efficiency by almost 5%. To determine the optimum FGR rate, an analysis was performed to find the point at which the decrease in NO_x emissions is balanced with the decrease in efficiency.

The analysis revealed that the FGR rate should be around 10% depending on the weight of emissions compared to efficiency. It is worth noting, though, that this analysis is based on a simplified model, and the actual optimal FGR rate may vary depending on the specific conditions of the boiler and local emission regulations. If energy stability is a priority, then higher efficiency is preferred over NO_x emissions.

NOMENCLATURE

Latin alphabet

\dot{b}	fuel flow, [kg·s ⁻¹]
c_w	water heat capacity, [J·kg ⁻¹ ·K ⁻¹]
F	heat transfer area, [m ²]

I	flue gas enthalpy per kg of fuel, [kJ·kg ⁻¹]
k	overall heat transfer coefficient, [W·m ² ·K ⁻¹]
\dot{m}_w	water mass flow rate, [kg·s ⁻¹]
t _w	water temperature, [°C].

Greek alphabet

$\Delta\theta$	log mean temperature difference, [K].
----------------	---------------------------------------

Acknowledgement

The authors would like to express their sincere gratitude to Mr. Rade Đurić and Mr. Vladan Petrović for their invaluable contribution to this study. Their generous provision of data, including temperature measurements was crucial to the successful completion of this research.

REFERENCES

- [1] Transparency Market Research. From: <https://www.globenewswire.com/news-release/2023/01/09/2584969/0/en/Biomass-Boiler-Market-to-grow-at-a-CAGR-of-18-1-during-the-forecast-period-from-2022-to-2031-TMR-Study.html>, accessed on: April 25, 2023.
- [2] Monks, P. *et al.*, (2017). *The Potential Air Quality Impacts from Biomass Combustion*. Department for Environment, Food and Rural Affairs; Scottish Government; Welsh Government; and Department of the Environment in Northern Ireland, UK.
- [3] Polonini, L.F., Petrocelli, D., Lezzi, A.M. (2023). The Effect of Flue Gas Recirculation on CO, PM and NO_x Emissions in Pellet Stove Combustion. *Energies*, vol. 16, no. 2, p. 954-954. <https://doi.org/10.3390/en16020954>
- [4] Caposciutti, P., *et al.* (2022). An Experimental Investigation on the Effect of Exhaust Gas Recirculation in a Small-Scale Fixed Bed Biomass Boiler, *Chemical Engineering Transactions*, vol. 92, p. 397-402. DOI: 10.3303/CET2292067
- [5] Brkić, Lj., Živković, T. (1987). *Termički proračun parnih kotlova*. Mašinski fakultet Beograd.
- [6] Bogner, M. (2004). *Termotehničar*. AGM, Beograd.
- [7] Đurić, V., Farmakoski V. (1958). *Parni kotlovi - deo I*. Naučna Knjiga, Beograd.
- [8] Radojković N., Ilić, G., Vukić, M., Stojanović, I., Živković P. (2007). *Termodinamika II*. Mašinski fakultet Niš, Niš.
- [9] Morley Chris. Gaseq. From: <http://www.gaseq.co.uk/>, accessed on: April 25, 2023.
- [10] Tomić, M. *et al.*, The pollutant emissions assessment from personal vehicles in the republic of Serbia, *1st International conference on advances in science and technology – COAST 2022*, Herceg Novi, Montenegro, p. 248 – 254.
- [11] Sartor, K. *et al.* (2014). Prediction of SO_x and NO_x emissions from a medium size biomass boiler. *Biomass and Bioenergy*, vol. 65, p. 91 – 100. DOI: <https://doi.org/10.1016/j.biombioe.2014.04.013>



Banja Luka
1–2 Jun 2023.

DEMI 2023

16th International Conference on Accomplishments in Mechanical and Industrial Engineering

www.demi.mf.unibl.org



The concept of estimating the hydropower potential of an ungauged watershed in Montenegro

Milena Ostojic^a, Goran Sekulic^a, David C. Finger^b, Ivana Cipranic^a

^aFaculty of Civil Engineering, University of Montenegro, Podgorica, Montenegro

^bDepartment of engineering, Reykjavik University, Reykjavik, Iceland

Abstract *In recent years, Montenegro, a small Eastern European country, whose primary source of energy production relied on thermal power plants for a long time, has recognized the beneficial role of using renewable energy sources on its path to a green renewable energy transition. Water resources are among the most valuable natural assets in Montenegro, hence harvesting hydropotential represents an opportunity for economic, social and ecological development of paramount importance. However, the lack of continuously measured water runoff in the majority of watersheds in Montenegro makes the planning of hydropower utilization challenging. This concept paper aims to provide insight into the possibilities of determining hydropower potential of an ungauged watershed in Montenegro, through the development of a hydrological model of a larger watershed, under the premise of hydrological analogy. The available measured historical field data is used for building the hydrological model in a chosen software, which is, after calibration and validation, used for predictive purposes. The obtained results facilitate further analysis of the selected ungauged watershed, from the hydropotential perspective. Conclusions regarding the prospects of generalizing and using the procedure for other ungauged catchments in Montenegro can be drawn, as well as potential uncertainties and obstacles that may arise from the suggested method and approximations made.*

Keywords *Hydropower potential, ungauged catchment, hydrological modelling*

1. INTRODUCTION

While global energy mix is still dominated by coal, oil, and gas, the increasing use of renewables is a crucial step towards a more sustainable energy future [1]. In the current shift towards clean energy, hydropower plays a crucial role due to its capacity not only to generate substantial amounts of low-carbon

electricity, but also to offer unparalleled flexibility and storage capabilities [2]. As of 2016, up to 71% of renewable energy worldwide was derived from hydropower, making it the dominant source of renewable energy [3]. Furthermore, global hydropower capacity is expected to increase by 17% between 2021 and 2030 – led by China, India, Turkey and Ethiopia [4].

For Montenegro, a small country in the Western Balkans, water resources represent its greatest natural asset. As much as 95.3% of the waterflows in Montenegro are formed within its territory, i.e. their source and belonging catchment area are located within the country. Montenegro, which has an average runoff of 44

Milena Ostojic

Msc, Milena Ostojic
milenao@ucg.ac.me

Faculty of Civil Engineering
Dzordza Vasingtona bb
Podgorica, Montenegro

l/s/km² (compared to the global average runoff of 6.9 l/s/km²), is among the 4% of territories worldwide with the highest average runoff [5]. Studies [6] show that Montenegro's hydropower potential is significant, with a technical capacity for generating approximately 6000 GWh of electricity annually. This potential estimate is determined by the proposed strategies for directing the natural water flow, identifying favorable sites for constructing large reservoirs, and identifying suitable topographical and geological conditions for implementing the necessary infrastructure. Overall, these factors make hydropower a compelling option for energy production in Montenegro. Only around 17% of the gross hydropower potential in Montenegro is currently harnessed in nine hydroelectric power plants, with a combined annual production of cca 1725 GWh. The largest contribution comes from the two biggest plants: the Perucica hydropower plant located on the Zeta River, which generates 960 GWh per year, and the Piva hydropower plant located on the Piva River, which produces 765 GWh annually. Additionally, seven smaller hydroelectric plants with a total installed capacity of 9 MW balance the annual production with approximately 21 GWh [6]. As the most significant natural resource for electricity production, the main focus is on the potential of river streams such as Tara, Piva, Moraca, Zeta, Lim, Cehotina, Ibar and their tributaries. Since the importance of renewable energy sources is increasingly recognized in Montenegro as well, the official Long term Energy balance of Montenegro, adopted for the period from 2023 to 2025, features the plan to generate around 67% of the total produced electricity from renewable energy sources (of which over 74% will come from hydropower), and the remaining 33% from the Pljevlja Thermal Power Plant [7].

Despite the significant water resources available, Montenegro's water distribution is characterized by a distinct seasonal spatial and temporal pattern, which increases the need for adequate and sustainable water management. The seasonal evolution of water availability is among the most dynamic in Europe, with long periods of low flow which can have significant consequences for the ecological and social environment [8]. On the other hand, the area of about 26,000 hectares of land in Montenegro is threatened by constant or periodic floods [9].

In accordance with this, for accurate assessment of the hydropower potential of a specific site, long-term flow measurements are necessary in order to gain an in-depth understanding of the available water resources and their temporal fluctuations. This information is crucial for predicting the operation of potential hydroelectric power plants. The Institute of Hydrometeorology and Seismology of Montenegro (IHMS) serves as a center for observation, measurement, collection, processing, analysis, and issuance of hydrological data and information. The IHMS can provide hydrological information for the gauging stations, which are mostly located on the main watercourses, as shown on Fig. 1 [5]. However, hydrological data for the majority of tributaries of the aforementioned main rivers (which could be relevant from the hydro-potential aspect) is either not available, due to a relatively poor network of monitoring stations or, even for those that have organized hydrological measurements, the quality of the data may be somewhat lower [10].

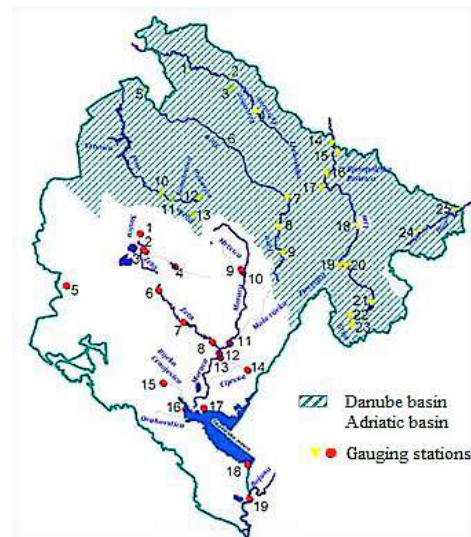


Fig. 1. Locations of measuring stations in Montenegro (Danube and Adriatic basin) [4]

In this regard, numerical modelling can provide a valuable tool in quantifying water availability and identifying suitable locations for hydropower production, thus providing fundamental knowledge for decision makers [11].

2. METHODOLOGY

Hydrologic models are among the most useful techniques to ensure proper and sustainable water management and planning [12]. In regard to hydropower exploitation models may help bridge the gap between limited data availability and the need for accurate predictions of water resource availability in ungauged watersheds. Hydrological models can be classified into three categories: i) black-box models, ii) conceptual models, and iii) physically based models [13]. Considering that black-box models use empirical relationships between inputs and outputs, without representing internal system processes in a conservation of mass, momentum, or energy approach, and that input-output relationships are usually based on statistical methods such as regression equations [14], it is the two latter types of hydrologic models that have been used in most applications [15]. The conceptual hydrological models use simplified mathematical conceptualizations with interconnected storages to represent different components of the hydrological process. They are typically lumped and rely on observed data, with results dependent on data quality. Spatial variability of watershed characteristics is often ignored [16]. Physically based distributed hydrological models divide the terrain of the whole catchment into a number of grid cells at fine resolution and assimilate different terrain data and precipitation to different cells [17]. Even though the development of physically based hydrologic models was initiated to overcome the deficiencies associated with the lumped conceptual models [18], the requirement for more detailed input data on topography, soil properties, land use, and climate variables, makes the feasibility of their application on Montenegrin case studies (with scarce data accessibility) debatable. Hence, for the purposes of this study, a conceptual hydrological model will be used for further analyses, since it represents a good compromise between black-box models, which rely mostly on statistical relations, and physically-based models, which are complex and data-demanding [19].

2.1 Building the model

As a first step, a conceptual hydrological model is developed for a selected case study – a larger gauged watershed of one of the main rivers in

Montenegro. The newest version of HBV-light model, developed at the University of Zurich in 2010 [20], is used to simulate river discharge. The HBV (Hydrologiska Byråns Vattenavdelning) model [21] is a lumped (semi-distributed) bucket-type (conceptual) model that consists of different routines (Fig. 2) and simulates catchment discharge, usually on a daily time step, based on time series of precipitation and air temperature as well as estimates of monthly long-term potential evaporation rates [19].

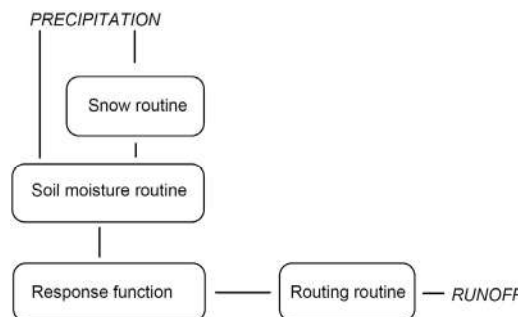


Fig. 2. Schematic structure of the HBV model [22]

When selecting a watershed for modeling purposes, an important consideration was to ensure the availability of a sufficient duration of recorded data from the measurement station. Typically, hydrological data for at least 15 years [23] are required to capture the natural variability of the hydrological cycle and provide more accurate predictions. For the chosen case study, available field measurements from the gauging station, supplied by the IHMS, include the daily values of temperature, precipitation, discharge and snow cover.

The catchment area for the study is delineated by using GIS-based software, through utilizing the latest and complete ASTER global digital elevation models [24] available to the public. These models encompass the Earth's entire land surface, spanning from 83 degrees north to 83 degrees south latitude, with 1 arc-second latitude and longitude postings (~30 m), and an estimated vertical accuracy of 10 m [25]. Even though the catchments of the major watercourses in Montenegro may be regarded as 'medium' in size [26], evident heterogeneity in meteorological variables across the drainage area is accounted for by the functionality of HBV model. HBV allows for a limited representation of catchment characteristics through the specification of different elevation and

vegetation zones. This way, the parameters controlling the different processes can be modified for individual elevation and vegetation zones [27]. For these purposes, Corine Land Cover inventory [28], widely used in land use analysis in the European context, was applied [29]. As the HBV model routines are governed by the parameters which cannot be easily determined due to the lack of parameter measurements from physical systems and limitations of available data, model calibration is applied to adjust parameters within recommended ranges by optimizing observed and simulated discharge data [30]. Normally, between 3 to 10 years of observations are required for calibration, depending on the model complexity and the informational content of the data [31 - 32]. Monte Carlo sampling approach is adopted, and a substantial number of parameter samples is run [33], until a satisfying model efficiency – Nash-Sutcliffe coefficient [34] is reached.

2.2 Modelling the ungauged watershed

There are multiple approaches for parameter estimation in ungauged watersheds that can be applied to continuous simulation models. The typical approach is to look for relationships between optimised parameter values and catchment characteristics [35]. The problem in this regression-based regionalisation of model parameters in Montenegro is the limited number of available catchments with high-quality hydrological data of sufficient spatio-temporal coverage. An alternative approach involves distance-based methods where entire parameter sets are transferred between hydrologically similar catchments using spatial proximity, catchment attributes or any hydrological information available as a similarity metric [36]. According to some studies, when there is a reason to believe that, in the sense of hydrological behaviour, a gauged catchment resembles the ungauged catchment, then it may be worthwhile to adopt the entire set of calibrated parameters from the gauged catchment instead of deriving quantitative relationships between catchment descriptors and model parameters [37]. Since the purpose of this research is to make predictions about ungauged catchments of main tributaries of a selected gauged major watercourse, the modeled gauged watershed is chosen as an

analogue. This selection is based on justified presumption of correspondence of climatic conditions; synchronism of hydrological phenomena; similarity of environmental conditions in terms of relief, geology; hydrogeology and pedology, areal and generic representation of vegetation, exploitation of the catchment areas, etc [38]. Given that watersheds with similar basin characteristics (e.g., soil, topography, land use, precipitation, and temperature) show similar hydrological behavior [39] – the complete set of optimized model parameters will be transposed from the donor (analogue) catchment to the ungauged catchment, similar in terms of its physiographic attributes [40].

3. KEY CHALLENGES

The snow routine of the HBV model simulates the snow pack from observed or forecasted precipitation and temperature [41]. Since the precipitation field data, supplied by the IHMS, refers only to rainfall, whereas the available snow data represents measured height of snow cover [42], it is necessary to transform the observed snow cover into snow water equivalent (SWE), in order to prepare total precipitation amounts for the model. SWE can be calculated from snow depth, d_s , and density, ρ_s , by the expression [43]:

$$SWE = 0.01 \cdot d_s \cdot \rho_s \quad (1)$$

In which SWE is in mm when d_s is in cm and ρ_s is in kg/m^3 . Value of snow density is adopted according to the literature recommendations [44].

For potential evapotranspiration (input data required for the model), longterm monthly average values ("the twelve values") are usually used [20], which are based on direct measurements or, for instance, the Penman-Monteith equation [45 - 46]. However, since evaporation is not directly measured in any of the measuring stations in Montenegro, and the application of Penman-Monteith equation demands an abundance of input variables (soil heat flux, vapor pressure deficit of the air, slope of the saturation vapour pressure temperature relationship, surface and aerodynamic resistances, etc), whose estimation in Montenegrin case study would be challenging due to limited data availability, an alternative approach is used. In such cases, when necessary

meteorological data is missing, the FAO [47] recommends estimating evapotranspiration using the Hargreaves equation [48], which requires a few easily accessible parameters: minimum, maximum and mean temperature, and extraterrestrial radiation (which depends on the latitude and the time of the year) [47].

Mountainous regions, including the catchments of major Montenegrin rivers, are recognized for their vertical variations in environmental parameters, which are linked to changes in elevation above sea level. In the effort to facilitate the calibration of the model parameters, it is essential to constrain the range of parameter values, namely temperature and precipitation gradient, so that they reasonably reflect location-specific climatic and meteorological characteristics of the watershed. For example, even though the actual lapse rate can vary due to various atmospheric factors, such as humidity and atmospheric stability, the average (standard) lapse rate may be adopted for the model, which is about 6.5°C for every 1000m rise in elevation [49]. On the other hand, the amount of precipitation is affected by a number of environmental factors: the direction of the inflow of moist air masses, orography of the land, the phenomenon of precipitation shadow, etc [50]. As a rule, the amount of precipitation increases with the elevation, but this relationship is very often disturbed [50]. In recent years, remotely sensed observations coupled to hydrological models have proven to enhance the estimation of water resources in ungauged basins [11]. So to address this challenge, satellite precipitation products will be considered, since their availability has made them very attractive for hydrological applications in regions that have less-dense and less-consistent ground-based measurements [51]. NASA's Global Precipitation Measurement Mission (GPM), among others, is an international network of satellites providing next-generation global observations of rain and snow [52]. For instance, the precipitation dataset supplies half-hourly and monthly precipitation estimates on a 0.1°x0.1° (roughly 10x10 km) grid over the globe [53]. The results of validation of these datasets in recent studies show generally good agreement between the satellite products and the surface data sets [54]. In addition to the satellite-based method, another alternative approach to obtaining global continuous precipitation estimates is

using numerical weather models and data assimilation techniques to yield model-based reanalysis data [55]. European Centre for Medium Range Weather Forecasts (ECMWF) released the new land component of the fifth generation of European ReAnalysis, the ERA5-Land dataset, which produces a total of 50 variables describing the water and energy cycles over land, globally, hourly, and at a spatial resolution of 9 km [56]. Latest research indicates that ERA5-Land well reproduces the intra-annual variation and spatial-temporal pattern of precipitation [57]. In light of this, both types of datasets, satellite-based and model based precipitation products, will be compared against available field data. Subsequently, the outperforming product will be utilized for further analysis.

4. EXPECTED OUTPUTS

The main output of the study are discharge patterns of the ungauged watershed, which will be used to assess its theoretical hydropower potential - the total energy potential of a given river, considering only the available water in the catchment and its topography [58]. Since the overall efficiency of the power plant will be neglected (the exploitable (realizable) potential will not be analysed), theoretical potential P (in W) will be calculated by using the basic equation:

$$P = \rho * g * Q * H \quad (2)$$

Where: ρ is the density of water (kg/m³), g is the acceleration due to gravity (9.81 m/s²), Q is the discharge (m³/s) and H is the height difference (m).

The expected results of this study will be used to better understand the potential of ungauged basins for hydropower generation, and provide valuable information for decision-makers, investors, and other stakeholders interested in the development of sustainable hydropower projects.

REFERENCES

- [1] Ritchie, H., Roser, M., Rosado, M. (2022). Energy. Published online at OurWorldInData.org. From: <https://ourworldindata.org/energy>, accessed on: April 15, 2023.
- [2] International Energy Agency (IEA). Hydropower has a crucial role in accelerating clean energy transitions to achieve countries' climate ambitions securely - News - IEA. (2021, June 1). From: <https://www.iea.org/news/hydropower-has-a-crucial-role-in-accelerating-clean-energy-transitions-to-achieve-countries-climate-ambitions-securely>, accessed on: April 21, 2023.
- [3] Moran, E. F., Lopez, M. C., Moore, N., Müller, N., & Hyndman, D. W. (2018). Sustainable hydropower in the 21st century. *Proceedings of the National Academy of Sciences*, vol. 115, no. 47, p. 11891–98. DOI: 10.1073/pnas.1809426115
- [4] International Energy Agency (IEA). (2021). *Hydropower Special Market Report—Analysis and Forecast to 2030*. OECD Publishing, Paris, France. DOI: 10.1787/07a7bac8-en
- [5] Zavod za hidrometeorologiju i seizmologiju (ZHMS). Površinske vode – Opšte informacije. (In Montenegrin). From: <http://www.meteo.co.me/page.php?id=136>, accessed on: April 19, 2023.
- [6] Hrvčević, S. (2014). Vodni resursi Crne Gore: Ekonomičnost, raspoloživost, iskorišćenost, prioriteti. (In Montenegrin). *Pogled*, vol. 85. p. 46-61. Inženjerska komora Crne Gore.
- [7] Vlada Crne Gore. (2022). Dugoročni energetske bilans Crne Gore za period od 2023. do 2025. godine. (In Montenegrin). Podgorica.
- [8] Vlada Crne Gore. (2017). Strategija upravljanja vodama Crne Gore. (In Montenegrin). Podgorica.
- [9] Vlada Crne Gore. (2021). Procjena rizika od katastrofa Crne Gore. (In Montenegrin). Nacionalna biblioteka Crne Gore, Cetinje.
- [10] Elektroprivreda Crne Gore A.D. Nikšić. (1999). *Predlog metodologije i smjernica za projektovanje i izgradnju malih hidroelektrana*. (In Montenegrin).
- [11] Finger, D. (2018). The value of satellite retrieved snow cover images to assess water resources and the theoretical hydropower potential in ungauged mountain catchments. *Jökull*, vol. 68, no. 1, pp. 47–66. DOI: 10.33799/jokull2018.68.047
- [12] Dutta, P., & Sarma, A. K. (2020). Hydrological modeling as a tool for water resources management of the data-scarce Brahmaputra basin. *Journal of Water and Climate Change*, vol. 12, no. 1, pp. 152–65. DOI: 10.2166/wcc.2020.186
- [13] Liu, Z., Wang, Y., Xu, Z., & Duan, Q. (2019). Conceptual Hydrological Models. Duan, Q., Pappenberger, F., Wood, A., Cloke, H.L., Schaake, J.C. (editor). *Handbook of Hydrometeorological Ensemble Forecasting*, pp. 389–411., Springer Berlin Heidelberg, DOI: 10.1007/978-3-642-39925-1_22
- [14] Stella, J. M., & Warner, G. S. (2018). Modelling a hydrologic Black-Box. *Tecnología y Ciencias Del Agua*, vol. 09, no. 1, pp. 101–12. DOI: 10.24850/j-tyca-2018-01-07
- [15] Yu, Z. (2003). HYDROLOGY | Modeling and Prediction. Pyle, J., Zhang, F. (editor). *Encyclopedia of Atmospheric Sciences*, Elsevier, pp. 980–987. DOI: 10.1016/b0-12-227090-8/00172-x
- [16] Jaiswal, R. K., Ali, S., & Bharti, B. (2020). Comparative evaluation of conceptual and physical rainfall-runoff models. *Applied Water Science*, vol. 10, no. 1, article number: 48, DOI: 10.1007/s13201-019-1122-6
- [17] Chen, Y., Li, J., & Xu, H. (2016). Improving flood forecasting capability of physically based distributed hydrological models by parameter optimization. *Hydrology and Earth System Sciences*, vol. 20, no. 1, pp. 375–92. DOI: 10.5194/hess-20-375-2016
- [18] Islam, Z. (2011). A review on physically based hydrologic modeling. University of Alberta: Edmonton, AB, Canada. DOI: 10.13140/2.1.4544.5924.
- [19] Seibert, J., & Vis, M. J. P. (2012). Teaching hydrological modeling with a user-friendly catchment-runoff-model software package. *Hydrology and Earth System Sciences*, vol. 16, no. 9, pp. 3315–25. DOI: 10.5194/hess-16-3315-2012
- [20] Seibert, J., & Bergström, S. (2022). A retrospective on hydrological catchment modelling based on half a century with the HBV model. *Hydrology and Earth System Sciences*, vol. 26, no. 5, pp. 1371–88. DOI: 10.5194/hess-26-1371-2022
- [21] Bergström, S. (1992). The HBV model – its structure and applications. SMHI, Sweden, Reports Hydrology, no. 4.
- [22] Seibert, J. (2005). HBV light version 2, user's manual. Department of Earth Sciences, Uppsala University, Uppsala.
- [23] International Finance Corporation. (2015). *Hydroelectric power: A guide for developers*

- and investors. World Bank. Stuttgart. Hydropower Report.
- [24] NASA/METI/AIST/Japan Spacesystems and U.S./Japan ASTER Science Team (2019). ASTER Global Digital Elevation Model V003 [Data set]. NASA EOSDIS Land Processes DAAC. Accessed 2023-04-26 DOI: 10.5067/ASTER/ASTGTM.003
- [25] Abrams, M., Crippen, R., & Fujisada, H. (2020). ASTER Global Digital Elevation Model (GDEM) and ASTER Global Water Body Dataset (ASTWBD). *Remote Sensing*, vol. 12, no. 7, p. 1156. DOI: 10.3390/rs12071156
- [26] Chatterjee, C. Watershed Hydrology: Lesson 15-Types of Watersheds. From: <http://ecoursesonline.iasri.res.in/mod/page/view.php?id=125271>. accessed on: April 10, 2023.
- [27] Girons Lopez, M., Vis, M. J. P., Jenicek, M., Griessinger, N., & Seibert, J. (2020). Complexity and performance of temperature-based snow routines for runoff modelling in mountainous areas in Central Europe. *Hydrol. Earth Syst. Sci. Discuss*, DOI: 10.5194/hess-2020-57
- [28] Cover, Corine Land (2018). European Union, Copernicus Land Monitoring Service. European Environment Agency (EEA)
- [29] Büttner, G. (2014). CORINE Land Cover and Land Cover Change Products. Manakos, I., Braun, M. (editor). *Land Use and Land Cover Mapping in Europe*, Springer Netherlands, pp. 55–74. DOI: 10.1007/978-94-007-7969-3_5
- [30] Wu, H., Chen, B., Ye, X., Guo, H., Meng, X., & Zhang, B. (2021). An improved calibration and uncertainty analysis approach using a multicriteria sequential algorithm for hydrological modeling. *Scientific Reports*, vol. 11, no. 1, DOI: 10.1038/s41598-021-96250-6
- [31] Wagener, T. (2004). Modeling Ungauged Watersheds. Lehr, J. H., Keeley, J. and Lehr, J. (editor), *Water Encyclopedia*, Wiley, pp. 342–45. Portico, DOI: 10.1002/047147844x.sw628
- [32] Yapo, P. O., Gupta, H. V., & Sorooshian, S. (1996). Automatic calibration of conceptual rainfall-runoff models: sensitivity to calibration data. *Journal of Hydrology*, vol. 181, no. 1–4, pp. 23–48. DOI: 10.1016/0022-1694(95)02918-4
- [33] McIntyre, N., Wheeler, H., & Lees, M. (2002). Estimation and propagation of parametric uncertainty in environmental models. *Journal of Hydroinformatics*, vol. 4, no. 3, pp. 177–98. DOI: 10.2166/hydro.2002.0018
- [34] Nash, J. E., & Sutcliffe, J. V. (1970). River flow forecasting through conceptual models part I — A discussion of principles. *Journal of Hydrology*, vol. 10, no. 3, pp. 282–90. DOI: 10.1016/0022-1694(70)90255-6
- [35] Seibert, J. (1999). Regionalisation of parameters for a conceptual rainfall-runoff model. *Agricultural and Forest Meteorology*, vol. 98–99, pp. 279–293. DOI: 10.1016/s0168-1923(99)00105-7
- [36] Pool, S., Vis, M., & Seibert, J. (2021). Regionalization for Ungauged Catchments — Lessons Learned From a Comparative Large-Sample Study. *Water Resources Research*, vol. 57, no. 10. DOI: 10.1029/2021wr030437
- [37] Kokkonen, T. S., Jakeman, A. J., Young, P. C., & Koivusalo, H. J. (2003). Predicting daily flows in ungauged catchments: model regionalization from catchment descriptors at the Coweeta Hydrologic Laboratory, North Carolina. *Hydrological Processes*, vol. 17, no. 11, pp. 2219–2238. DOI: 10.1002/hyp.1329
- [38] Colenbrander, H. J. (1980). Casebook of methods of computation of quantitative changes in the hydrological regime of river basins due to human activities. Unesco. Paris.
- [39] Sisay, E., Halefom, A., Khare, D., Singh, L., & Worku, T. (2017). Hydrological modelling of ungauged urban watershed using SWAT model. *Modeling Earth Systems and Environment*, vol. 3, no. 2, pp. 693–702. DOI: 10.1007/s40808-017-0328-6
- [40] Parajka, J., Merz, R., & Blöschl, G. (2005). A comparison of regionalisation methods for catchment model parameters. *Hydrology and Earth System Sciences*, vol. 9, no. 3, pp. 157–71. DOI: 10.5194/hess-9-157-2005
- [41] Johansson, B., Andreasson, J., & Jansson, J. (2003). Satellite data on snow cover in the HBV model: Method development and evaluation. SMHI. Sweden
- [42] Zavod za hidrometeorologiju i seizmologiju Crne Gore. (2020). Godišnjak meteoroloških i hidroloških podataka. (In Montenegrin). Podgorica
- [43] Pomeroy, J. W., & Gray, D. M. (1995). Snowcover accumulation, relocation and management (No. 7). Saskatoon: National Hydrology Research Institute. Canada.
- [44] MEST EN 1991-1-3:2017 (me) I izdanje (2017). Eurokod 1 - Dejstva na konstrukcije – Dio 1-3: Opšta dejstva - Opterećenja snijegom. Institut za standardizaciju Crne Gore. Podgorica
- [45] Penman, H. L. (1948). Natural evaporation from open water, bare soil and grass. *Proceedings of the Royal Society of London. Series A. Mathematical and Physical Sciences*, vol. 193,

- no. 1032, pp. 120-145. DOI: 10.1098/rspa.1948.0037
- [46] Monteith, J. L. (1965). Evaporation and environment. In *Symposia of the society for experimental biology*, vol. 19, pp. 205-234. Cambridge University Press (CUP) Cambridge.
- [47] Allen, R. G., Pereira, L. S., Raes, D., & Smith, M. (1998). Crop evapotranspiration-Guidelines for computing crop water requirements-FAO Irrigation and drainage paper 56. Fao, Rome, vol. 300, no. 9, pp. D05109
- [48] George H. Hargreaves, & Zohrab A. Samani. (1985). Reference Crop Evapotranspiration from Temperature. *Applied Engineering in Agriculture*, vol. 1, no. 2, pp. 96-99. DOI: 10.13031/2013.26773
- [49] Donald Ahrens, C. (2012). *Meteorology Today: An Introduction to Weather, Climate, and the Environment*, 10th Edition. Cengage Learning Canada Inc.
- [50] Kozak, J., Cebulak, D., Stec, T., & Jaguś, A. (2019). Variation of Precipitation Gradient in Mountain Areas Based on the Example of the Western Beskids in the Polish Carpathians. *Journal of Ecological Engineering*, vol. 20, no. 9, pp. 261-66. DOI: 10.12911/22998993/112502
- [51] Hirpa, F. A., Gebremichael, M., & Hopson, T. (2010). Evaluation of High-Resolution Satellite Precipitation Products over Very Complex Terrain in Ethiopia. *Journal of Applied Meteorology and Climatology*, vol. 49, no. 5, pp. 1044-51. DOI: 10.1175/2009jamc2298.1
- [52] National Aeronautics and Space Administration. The Global Precipitation Measurement Mission (GPM). From: <https://gpm.nasa.gov/missions/GPM>, accessed on: April 25, 2023.
- [53] Huffman, G.J., E.F. Stocker, D.T. Bolvin, E.J. Nelkin, Jackson Tan (2019), GPM IMERG Final Precipitation L3 1 month 0.1 degree x 0.1 degree V06, Greenbelt, MD, Goddard Earth Sciences Data and Information Services Center (GES DISC), Accessed on April 21, 2023, 10.5067/GPM/IMERG/3B-MONTH/06
- [54] Kidd, C., Tan, J., Kirstetter, P., & Petersen, W. A. (2017). Validation of the Version 05 Level 2 precipitation products from the GPM Core Observatory and constellation satellite sensors. *Quarterly Journal of the Royal Meteorological Society*, vol. 144, no. S1, pp. 313-328. DOI: 10.1002/qj.3175
- [55] Xu, J., Ma, Z., Yan, S., & Peng, J. (2022). Do ERA5 and ERA5-land precipitation estimates outperform satellite-based precipitation products? A comprehensive comparison between state-of-the-art model-based and satellite-based precipitation products over mainland China. *Journal of Hydrology*, vol. 605, p. 127353. DOI: 10.1016/j.jhydrol.2021.127353
- [56] Muñoz-Sabater, J., Dutra, E., Agustí-Panareda, A., Albergel, C., Arduini, G., Balsamo, G., Boussetta, S., Choulga, M., Harrigan, S., Hersbach, H., Martens, B., Miralles, D. G., Piles, M., Rodríguez-Fernández, N. J., Zsoter, E., Buontempo, C., & Thépaut, J.-N. (2021). ERA5-Land: a state-of-the-art global reanalysis dataset for land applications. *Earth System Science Data*, vol. 13, no. 9, pp. 4349-83. DOI: 10.5194/essd-13-4349-202
- [57] Wu, X., Su, J., Ren, W., Lü, H., & Yuan, F. (2023). Statistical comparison and hydrological utility evaluation of ERA5-Land and IMERG precipitation products on the Tibetan Plateau. *Journal of Hydrology*, vol. 620, p. 129384. DOI: 10.1016/j.jhydrol.2023.129384
- [58] Tefera, W. M., & Kasiviswanathan, K. S. (2022). A global-scale hydropower potential assessment and feasibility evaluations. *Water Resources and Economics*, vol. 38, p. 100198. DOI: 10.1016/j.wre.2022.100198



Banja Luka
1–2 June 2023.

DEMI 2023

16th International Conference on Accomplishments in Mechanical and Industrial Engineering

www.demi.mf.unibl.org



Air tightness of residential buildings and its impact on energy consumption

E. Tombarević^a, V. Ivanović^a

^aFaculty of Mechanical Engineering, University of Montenegro, Džordža Vašingtona bb, Podgorica, Montenegro

Abstract Awareness of the importance of energy savings in buildings has been increasing in the last two decades. The energy performance of buildings is mainly improved by insulating the envelope and using more efficient heating and cooling system. However, in order to meet increasingly stringent requirements for energy efficiency of buildings it is now necessary to pay more attention to the air tightness of the building envelope. This paper presents the results of the blower door tests before and after the replacement of windows in an apartment in a multi-family residential building in Montenegro. The test results show that with this type of construction, the air tightness can practically be improved to the standard set for passive houses just by replacing the windows. The energy impact of windows replacement is assessed using the national software for calculating the energy performance of buildings based on DIN18599 methodology. Calculations show that the window replacement has significant potential to improve energy efficiency. By increasing air tightness, considerable energy savings for heating have been achieved, especially in relative terms when the building envelope is thermally improved and when it is located in a colder climate zone.

Keywords Air tightness, infiltration, blower door test, energy consumption

1. INTRODUCTION

The issue of global warming has spurred action on various levels, with the European Union (EU) demonstrating a particular commitment to reducing greenhouse gas emissions. The EU has long been at the forefront of the global effort to combat climate change, with the adoption of the EU 20-20-20 directive [1] in 2009 setting a goal of reducing greenhouse gas emissions by 20%, increasing the share of renewable energy to 20%, and improving energy efficiency by 20% by the year 2020. The EU's European Green Deal [2] aims to make the region climate-neutral by 2050, requiring net-zero greenhouse gas emissions. The building sector is a significant factor in achieving environmental goals, as it is the largest energy consumer in Europe with buildings responsible for 40% of EU energy consumption and 36% of energy-related greenhouse gas emissions, the Energy Performance of Buildings

Directive (EPBD) has been amended to prioritize a nearly zero-energy standard for new buildings and long-term renovation strategies for the building sector.

To meet increasingly strict energy efficiency requirements, mere increases in thermal insulation thickness or installation of more efficient heating and cooling equipment are no longer sufficient. It is now crucial to also focus on ventilation systems and the airtightness of building envelopes. Minimum requirements for building envelope airtightness have already been adopted in some countries, which stipulates that the number of air changes per hour must not exceed a certain amount. Enforcing airtightness testing for new and renovated buildings can be an effective way to improve craftsmanship and ensure the buildings meets the prescribed requirements. It is worth noting that it is easier to build an airtight building than to retrofit an existing one.

The energy consumption of a building is significantly affected by its airtightness as air infiltration plays a key role. Several software programs for calculating the energy performance of buildings consider the airtightness of the building envelope. Montenegro recently introduced the MEEC (Montenegrin Energy Efficiency Certification) software [3] for energy performance calculation and certification, which was developed by the Fraunhofer Institute for Building Physics and is based on German standard DIN V 18599 [4]. The software considers infiltration based on the location of the building and the visual condition of the building envelope. However obtaining accurate infiltration values based on the blower door test for every single building is not practical. Statistical data for a large number of buildings categorized by time and type of construction, type of windows, etc., are desirable to achieve the most realistic airtightness values and improve energy calculation accuracy. Unfortunately, no systematic measurements of airtightness has been conducted in Montenegro, leaving energy auditors without adequate data for accurate calculations of energy efficiency measures in both old and new buildings.

In addition, inadequate airtightness can lead to unsatisfactory thermal comfort, the transmission of air pollutants and dust, insufficient sound insulation, and moisture transfer through the envelope resulting in condensation and mold formation. However, well-sealed buildings require careful consideration if appropriate air exchange, either by periodic opening of windows or, preferably, by means of mechanical ventilation. Otherwise, occupants of the building may experience poor indoor air quality, condensation, and mold growth on the walls, highlighting the importance of the adage „build tight, ventilate right“.

Countries with colder climates such as the USA, Canada, and Northern Europe, have paid more attention to airtightness both in research and regulation/professional level. The USA has been researching the airtightness of building envelopes for several decades, leading to the development of comprehensive databases of fan pressurization tests and various infiltration models [5].

Building airtightness is heavily regulated in northern and central Europe. In Ireland, a study conducted on 28 single-family houses from 1944 to 2008, including new and retrofitted homes,

found that newer homes were not necessarily more airtight than older ones [6]. Another study in Finland on 170 detached houses found that those made of concrete and brick were more airtight than those made of timber frame and log [7]. Similarly, a UK study on 287 post-2006 new-build dwellings also found that the type of construction had a significant influence on airtightness [8].

Airtightness is less prioritized in warmer climate countries like Montenegro. This is primarily due to two reasons. Firstly, the winter temperatures are not as low, leading to less heat loss from infiltration. Secondly, opening windows is a conventional method of providing fresh air and cooling during summer months.

Recent studies on airtightness in Mediterranean Europe have shown that the issue is gaining attention. In Greece [9], an analysis of pressurization test results on 20 houses found a correlation between air change rate and frame length factor. A study in southern Italy [10] revealed that older buildings had higher air change rates and that roller shutter boxes were a significant cause of poor airtightness. The air permeability values in Portugal [11] showed a wide variation, even among identical flats in the same building with apparently identical construction characteristics and envelope components. It is likely that this variation is due to factors such as the dimensions of gaps surrounding the roller shutter boxes, as well as possible variable quality of installation craftsmanship. In Spain [12], a comprehensive study of over 400 dwellings found that those in the Mediterranean region were less airtight on average than those in the north.

There are few studies on the impact of windows replacements on airtightness, and a study by D'Ambrosio Alfano et al. [13] found that air-tight certified windows did not consistently improve airtightness after being installed in three Mediterranean residential buildings, with one building improving significantly, another marginally, and the third performing worse due to improper installation.

Leaks in the building envelope contribute significantly to heating and cooling loads, with more studies on the impact of building airtightness in cold than in temperate and warm climate countries. For instance, Jokisalo et al. [7] found that infiltration causes 15-30% of heating energy consumption in typical Finnish houses and 30-50% in poorly sealed ones, while

increasing air change rate from 1 to 10 h⁻¹ raises energy consumption for heating from 4 to 21%. Gillot et al. [14] showed that relatively inexpensive weather proofing measures account for 9% of total energy savings in retrofitted dwellings, with the remainder from thermal insulation and improvement of the heating and ventilation system. A Lithuanian study [15] of mid-sized terraced houses built of different materials concluded that end units are up to 20% less airtight than inside units and exceed heat loss limits prescribed for the building's energy class.

According to Balaras et al. [16], sealing the openings in Greek buildings constructed before 1990 and 10% of those built during the 1990s could lead to a 16 to 21% reduction in space heating energy consumption, while Poza-Casado et al. [17] and Feijó-Muñoz et al. [18] found that infiltration in residential buildings in Spain's Mediterranean provinces caused energy consumption in the range of 8.61-16.44 kWh/m²year for heating and significantly less for cooling.

The study aimed to achieve two objectives: firstly, to determine the extent to which replacement of windows under careful supervision can improve the airtightness of a specific building type through blower door tests, and secondly, to evaluate the effect of increasing building airtightness on energy usage. The paper presented the findings of the airtightness measurements of the same apartment before and after window replacement, along with the results of energy consumption calculations for heating and cooling at varying levels of airtightness.

2. BACKGROUND

It is crucial to distinguish between infiltration and airtightness as they have different meanings. Infiltration refers to the unintended entry of outdoor air into a building through gaps, cracks, or other openings caused by the pressure difference across the building envelope. Infiltration rates are caused by various factors such as building envelope characteristics, geometry, location, wind speed, and temperature. Air tightness, on the other hand, refers to the airflow that infiltrates a building at a specific pressure difference, usually 50 Pa. Unlike infiltration, air tightness is independent of climatic conditions and is an inherent

property of the building envelope. It is important to note that air tightness is the primary envelope property that affects infiltration.

Air leakage in buildings can occur through various pathways, with the most significant contribution often coming from areas such as windows and doors, junctions between walls and flows, and penetrations in the envelope for water and sewer pipes, as well as electrical installations such as sockets and switches. ASHRAE Handbook Fundamentals contains a chapter dedicated to ventilation and infiltration that summarizes two different air leakage distribution among individual building envelope components and systems. However, because many factors can affect air leakage, it can be difficult to assess the air tightness of a building based solely on factors such as its age, materials used, or type of windows and doors.

There are various methods available to assess the air tightness and infiltration rates of buildings. A visual inspection is typically carried out to identify potential leakage points, followed by techniques such as hand inspection, air velocity measurement and the use of smoke or soap bubbles to detect actual leakages. Acoustic measurements and thermal imaging can also be utilized, with higher sound permeability or significant temperature differences across the building envelope indicating higher air infiltration. These methods can be combined with building depressurization and pressurization. Additionally, the tracer gas method can be employed to determine the air change rate under natural meteorological conditions. This method involves introducing a small amount of tracer gas into the building, thoroughly mixing it, and then measuring the rate of change in tracer concentration over time. The fan pressurization method, also known as the blower door test, is the standard procedure used to determine the air tightness of buildings. This method involves extracting air out of the building using a fan, which causes the pressure inside to decrease, thereby drawing in outside air through any unsealed cracks and openings. This procedure is described similarly in various standards [19].

During a blower door test, a fan is mounted on a door to create a pressure difference across the building envelope. The flow of air required to achieve and maintain the given pressure difference is recorded, with greater airflow indicating a leakier building envelope. Airflow

rates are measured at various pressure differences ranging from 10 to 75 Pa, with pressure differences below 10 Pa being avoided due to the influence of wind and temperature differences. The 50 Pa pressure difference is typically used as a reference because it is both achievable with blower door fans and large enough to not be significantly affected by weather conditions. The data collected during the test is fitted to a power law equation:

$$\dot{V} = c_L \Delta p^n. \quad (1)$$

where \dot{V} in m^3/h is the air leakage rate, Δp in Pa is the pressure difference, c_L in $\text{m}^3/\text{h}/\text{Pa}^n$ is the air leakage coefficient, and n is the air flow exponent obtained by fitting the experimental data of $(\Delta p, \dot{V})$ using the least squares method. The air flow exponent has limit values of 0.5 and 1 depending on the size and shape of the leaks. For short and large openings, the exponent is 0.5, while for long and narrow leaks, it is 1.

After obtaining the air leakage coefficient and air flow exponent from the blower door procedure, the air leakage at the reference pressure can be calculated. To compare buildings' air tightness, normalizing the air leakage with building size is desirable. This is done by using the volume of the building, which gives the air change rate at the reference pressure, a commonly used metric. Other metrics include air permeability, specific leakage, and effective leakage area. Table 1 summarizes these air leakage metrics, including their definitions, calculation formulas, and units.

Table 1. Air leakage metrics summary

Metric and definition	Equation	Unit
Air leakage rate at the reference pressure difference of 50 Pa, \dot{V}_{50}	$\dot{V}_{50} = C_L (50 \text{ Pa})^n$	m^3/h
Air change rate at the reference pressure difference of 50 Pa, n_{50} calculated by dividing the air leakage rate at the reference pressure difference of 50 Pa, \dot{V}_{50} , by the internal volume, V .	$n_{50} = \frac{\dot{V}_{50}}{V}$	h^{-1}
Air permeability at the reference pressure difference, q_{50} calculated by dividing the air leakage rate at 50 Pa, \dot{V}_{50} , by the envelope area A_E .	$q_{50} = \frac{\dot{V}_{50}}{A_E}$	$\text{h}^{-1}\text{m}^{-2}$
Specific leakage rate at the reference pressure difference, w_{50} calculated by dividing the air leakage rate at 50 Pa by the net floor area A_F .	$w_{50} = \frac{\dot{V}_{50}}{A_F}$	$\text{h}^{-1}\text{m}^{-2}$
Effective leakage area, ELA the area of a fictitious orifice that allows the same air flow as the building envelope at the pressure difference of 4 Pa.	$ELA = c_L 4^{n-0.5} \sqrt{\frac{\rho}{2}}$	m^2

The infiltration rate induced by the blower door fan at 50 Pa is much higher than the rate occurring with natural pressure differences across the building envelope, which continuously vary with air temperature and wind speed, typically in the range of 1 to 5 Pa. To estimate the infiltration rate as a function of air tightness, relationships have been proposed based on comparing the results of the blower door test and the tracer gas dilution method. An empirical rule of thumb assumes that the mean annual infiltration rate is one-twentieth of the building's air tightness.

3. AIRTIGHTNESS MEASUREMENT

The airtightness measurement was carried out in a three-bedroom apartment located in a multi-family residential building constructed in the mid-1980s. This selection is significant as most of the population of Montenegro lives in buildings of this type constructed between the beginning of the 1970s and the end of the 20th century in the same climate zone, making it relevant for energy consumption analysis. The apartment was chosen for the study as the authors had control over the renovation works, window selection, and installation quality. The apartment is on the first floor and positioned on the northeast-oriented corner. The apartment has a one-bedroom apartment and commercial space below and a three-bedroom apartment above, with two neighbouring apartments, a corridor, and a staircase surrounding it towards the building's interior, as shown in Fig. 1.

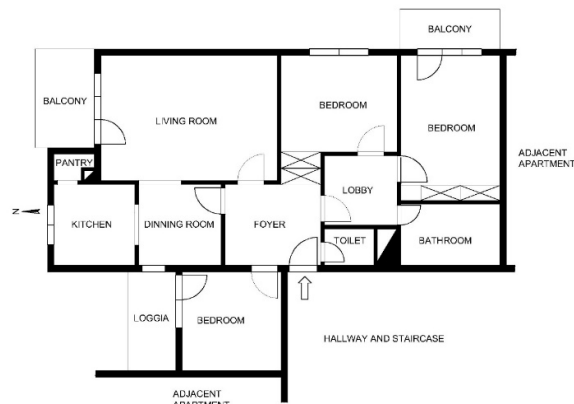


Fig. 1. The arrangement of rooms in the apartment

The building was constructed in a manner typical of the period spanning from the 1970s to the 1990s. The external walls are constructed

from cast-in-place reinforced concrete, with the exception of the walls of the rooms with balconies, which are built of hollow clay bricks. The walls have a thickness of approximately 20 cm and are not thermally insulated, but instead have a layer of foam concrete plaster. Similarly, the horizontal partitions are also made of cast-in-place reinforced concrete.

Former windows and doors of the apartment were wooden, double-glazed, and of the casement type. There were roller shutters on about half of them and no rubber seals. Each pane was in its sash, mounted on its own hinges, and operated independently. Although they were fully functional, they were not regularly maintained.

The biggest factor in increasing the apartment's airtightness during renovation was replacing the old wooden windows and doors with UPVC windows made by a reputable local company. The new windows were Softline 70 AD profiles with 5 chambers, a standard depth of 70mm, and two seals. Additionally, appropriate roller shutters were installed. It's important to follow professional recommendations when installing windows to achieve good airtightness. The gaps between the window frames and the opening on the wall were sealed with polyurethane foam, and the edges were finished by plasterers and tilers. Although the windows weren't installed according to the state-of-the-art RAL guidelines, they were properly sealed.

The apartment airtightness was assessed using the fan pressurization method in accordance with ISO 9972:2015. The apartment envelope was tested and all intentional openings were sealed, as per the standard's procedure. Blower door tests were conducted using BlowerDoor GmbH's Minneapolis Blower Door Model 4.1, which has a flow range from 25 to 7800 m³/h at 50 Pa. The fan was mounted on the apartment's front door, shown in Fig. 2, while the building's front door was left open to keep the hallway pressure close to atmospheric pressure.

Before and after replacing the windows, the apartment underwent a prolonged depressurization period, during which visual, hand, and smoke pen inspections were performed to identify significant leakage areas. Thermal imaging was not feasible as there was no heating or cooling system to create the required temperature difference.

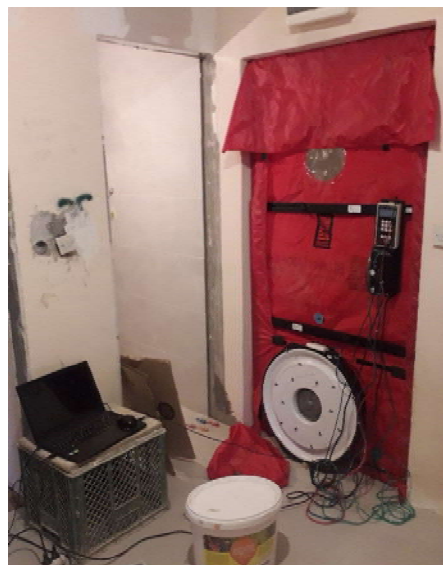


Fig. 2. Blower door fan mounted on the apartment's front door

The ISO 9972:2015 standard requirements were met during both measurements, with wind speed below 6 m/s and the product of building height and indoor-outdoor temperature difference below 250 mK. The calibrated fan was connected to a speed controller, digital pressure gauge DG700, and computer for full automation of the test using TECTITE Express software. The software processed data, fitted regression curves, plotted charts, and calculated airtightness metrics.

Air leakage tests were conducted twice, before and after window replacement. Fig. 3 and Fig 4. display the corresponding air leakage graphs.

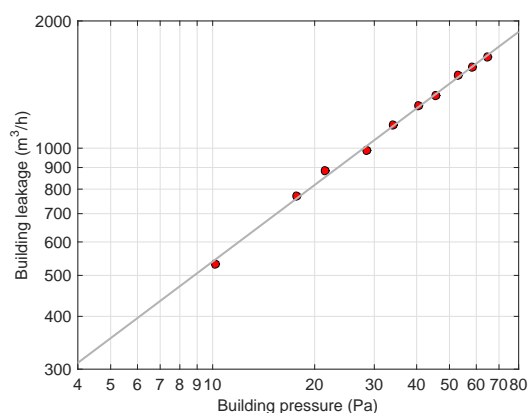


Fig. 3. Air leakage graph before windows replacement

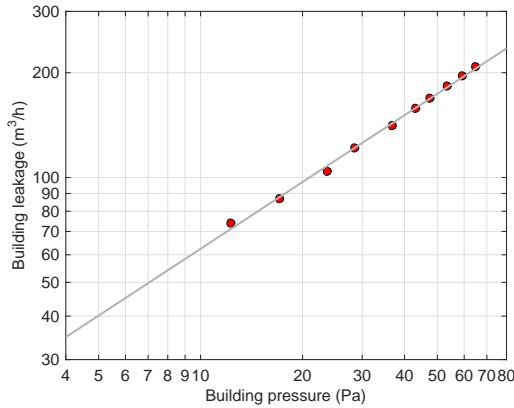


Fig. 4. Air leakage graph after windows replacement

The ordinate values on both graphs indicate a significant improvement in the airtightness of the apartment after window replacement. At a reference pressure difference of 50 Pa, the air leakage rate decreased from 1418 m³/h to 174 m³/h, representing an 88% decrease.

The air change rate at the reference pressure difference of 50 Pa decreased from 6.25 h⁻¹ to 0.77 h⁻¹ after replacing the windows, which is a significant improvement. The old windows had an n_{50} value higher than the Montenegrin rulebook's threshold value of 3 h⁻¹, but the replacement brought it closer to the passive house requirement of 0.6 h⁻¹.

The value of air flow exponent increased from 0.602 to 0.637 after window replacement, indicating a shift from short, large openings to long, narrow leaks.

Table 2 presents a summary of the blower door test results along with the calculated airtightness metrics. The air change rate n_{50} , air permeability q_{50} , and specific leakage rate w_{50} were obtained by dividing the air leakage rate by the internal volume of 227 m³, envelope area of 123 m², and net floor area of 85 m², respectively.

Table 2. Blower door test results before and after replacement of windows

Value	Before	After
Air leakage rate, \dot{V}_{50} (m ³ /h)	1418	174
Air change rate, n_{50} (1/h)	6.25	0.77
Air permeability, q_{50} (m ³ /h/m ²)	11.53	1.41
Specific leakage rate, w_{50} (m ³ /h/m ²)	16.69	2.05
Effective leakage area, ELA (cm ²)	334.5	37.5
Building Leakage Curve		
Air leakage coefficient, c_L (m ³ /h/Pa ⁿ)	134.8	14.4
Air flow exponent, n	0.602	0.637

The almost 90% improvement in airtightness can be attributed almost entirely to the replacement of windows and doors since there were no other significant envelope interventions. The smoke pen test before the renovation detected most of the leaks around the windows, particularly gaps between the sash and frame and around the wooden shutter boxes. The old wooden windows were of poor quality and lacked rubber seals, and poor workmanship during installation and maintenance worsened the problem. Infiltration through walls and horizontal partitions was not significant, as expected due to their cast-in-place reinforced concrete composition.

Replacing windows in this type of construction can significantly improve airtightness to meet the requirements of passive buildings. However, careful supervision during installation is necessary for successful outcomes. This is supported by similar tests conducted in Italy, where one building's airtightness even worsened after installing certified high-performance windows [13].

4. ENERGY IMPACT OF AIRTIGHTNESS

The MEEC software, developed by the Fraunhofer Institute for Building Physics, was used to calculate the energy consumption for heating and cooling. The software follows the German calculation procedure for determining net, final, and primary energy demand for various purposes, including heating, cooling, ventilation, domestic hot water, and lighting, as described in DIN V 18599. Monthly energy balances were calculated for space heating and cooling demands, taking into account all sources of heat and loss, such as internal and solar gains, transmission, and ventilation. The energy impact of infiltration was assessed using a conventional method that considered the volume of air infiltrated and the temperature differences between the indoor and outdoor environments. The daily mean infiltration air change rate is determined based on the building's airtightness at a pressure difference of 50 Pa. When there is no mechanical ventilation, it is determined using the following formula:

$$n_{inf} = n_{50}e \quad (2)$$

where e is the wind shielding coefficient, assumed to be 0.07 by default, which indicates a moderately sheltered building with more than one facade exposed to the wind.

The default user profile settings for residential buildings were used in the analysis. Delivered energy, which depends on technical system losses, was taken into account for the energy impact analysis. A central radiator heating system with biomass boiler and multi-split cooling system commonly used in Montenegro were adopted for the calculations. The analysis aimed to determine the effect of infiltration on delivered energy for heating and cooling, as well as the influence of climate zone and heat transfer coefficient on energy consumption reduction with increased airtightness.

Montenegro has a diverse climate with varying temperature and solar radiation. It is divided into three climate zones for energy calculations, with Climate Zone I being the warmest and covering the coast, and Climate Zone III being the coldest and covering the north.

The current thermal envelope violates the building energy efficiency standards, with about 80% of the external walls made of reinforced concrete with U-value $> 2 \text{ W/m}^2\text{K}$, while the remaining walls made of hollow clay blocks have U-value $> 1 \text{ W/m}^2\text{K}$. The existing double-glazed wooden windows have a U-value of $2.5 \text{ W/m}^2\text{K}$. The standard demands that the U-value of walls not exceed $0.6 \text{ W/m}^2\text{K}$ in Climate zones I and II, and $0.45 \text{ W/m}^2\text{K}$ in Climate zone III. For windows, the maximum allowed U-value is $2 \text{ W/m}^2\text{K}$ across all three climate zones.

Before replacing windows and doors, the existing building envelope in Climate zone I had a delivered energy consumption for heating and cooling of $155.44 \text{ kWh/m}^2\text{year}$, which was reduced to $142.63 \text{ kWh/m}^2\text{year}$, a decrease of 8.2%, after the replacement. Heating energy consumption decreased by 9.5%, while cooling energy consumption only decreased by 0.2%. This is due to the relatively small infiltration heat gains during summer compared to total heat gains from transmission and solar radiation.

To determine the impact of improved airtightness on energy consumption, the calculations were redone for a building with a minimally compliant thermal envelope. With the improved thermal envelope and the same airtightness, energy consumption for heating and cooling decreases by 49.2%. Further energy savings would be achieved by increasing airtightness, reducing delivered energy for heating and cooling by an additional 15.6% when n_{50} is reduced from 6.25 to 0.77. Hence, increasing airtightness has a greater effect on

reducing energy consumption in thermally insulated apartments.

In colder regions like the north of Montenegro (Climate zone III), energy savings are even more attractive due to high energy consumption. If the same building were located in the north of Montenegro, the delivered energy for heating and cooling would be $258.21 \text{ kWh/m}^2\text{year}$. By reducing n_{50} from 6.25 to 0.77, the delivered energy for heating and cooling is reduced to $233.26 \text{ kWh/m}^2\text{year}$, i.e., by $24.95 \text{ kWh/m}^2\text{year}$ or 9.6%.

Table 3 compare the delivered energy for heating and cooling in three climate zones before and after improvements to enhance thermal envelope and airtightness.

Table 3. Delivered energy for heating and cooling

Climate zone	Building envelope	n_{50} (h^{-1})	Delivered energy ($\text{kWh/m}^2\text{year}$)		
			Heating	Cooling	Total
I	Existing	6.25	133.66	21.78	155.44
		0.77	120.90	21.73	142.63
	Improved	6.25	66.28	12.67	78.95
		0.77	53.94	12.67	66.61
II	Existing	6.25	200.86	8.84	209.70
		0.77	181.31	9.06	190.37
	Improved	6.25	101.45	4.85	106.30
		0.77	82.39	5.13	87.52
III	Existing	6.25	254.71	3.50	258.21
		0.77	229.58	3.68	233.26
	Improved	6.25	116.17	1.49	117.66
		0.77	91.36	1.75	93.11

This study also examined the impact of different levels of air tightness on heating and cooling energy consumption. The calculations were performed by gradually increasing the air tightness from 1 to 15. The results showed a linear increase in energy consumption with n_{50} . Colder climates were found to be more affected by infiltration, as indicated by steeper slopes. Increasing the value of n_{50} by one unit led to an increase from $2.3 \text{ kWh/m}^2\text{year}$ in Climate zone I to $4.6 \text{ kWh/m}^2\text{year}$ in climate zone III.

5. CONCLUSIONS

This paper highlights the overlooked issue of building airtightness in Montenegro, where mild climate and cheap energy have led to little attention paid to infiltration. However, with the planned shift towards nearly zero-energy buildings and energy certification, addressing infiltration is crucial. This case study aimed to assess the airtightness of analysed building apartments and quantify the effects of

uncontrolled airflow on energy consumption. Results showed that window replacement significantly reduced the air change rate, making it an effective airtightness measure. Increasing airtightness reduced energy consumption for heating, especially in colder climates, but had little effect on cooling. Energy consumption increased linearly with air leakage rate. For credible results, a larger sample of buildings should be considered for recommendations on airtightness values and future updates of energy efficiency regulation. Using whole-building energy simulation software can also provide insight into time variation of infiltration rates and their impact on indoor air quality.

REFERENCES

- [1] European Parliament and Council. (2009). Directive 2009/28/EC of the European Parliament and of the Council of 23 April 2009 on the promotion of the use of energy from renewable sources and amending and subsequently repealing Directives 2001/77/EC and 2003/30/EC. Official Journal of the European Union L140, 16-62. <https://eur-lex.europa.eu/LexUriServ/LexUriServ.do?uri=OJ:L:2009:140:0016:0062:en:PDF>
- [2] European Commission. (2019). Communication from the commission to the European parliament, European council, the council, the European economic and social committee and the committee of the regions> The European Green Deal. <https://eur-lex.europa.eu/legal-content/EN/TXT/?uri=COM%3A2019%3A640%3AFIN>
- [3] Fraunhofer Institute of Building Physics. (2021). MEEC– Montenegrin Energy Efficiency Certification. From: <https://www.meec.me/index.php/en/>, accessed on: April 27, 2023.
- [4] DIN Standard V 18599-1:2018-09. (2018). *Energy Efficiency of Buildings—Calculation of the Net, Final and Primary Energy Demand for Heating, Cooling, Ventilation, Domestic hot Water and Lighting—Part 1: General Balancing Procedures, Terms and Definitions, Zoning and Evaluation of Energy Sources*. Beuth Verlag GmbH, Berlin.
- [5] Sherman, M.H., Dickerhoff, D. (1998). Airtightness of U.S. dwellings. *ASHRAE Transactions*, vol. 104, p. 1359-1367.
- [6] Sinnott, D., Dyer, M. (2012). Air-tightness field data for dwellings in Ireland. *Building and Environment*, vol. 51, p. 269-275.
- [7] Jokisalo, J., Kurnitski, J., Korpi, M., Kalamees, T., Vinha, J. (2009). Building leakage, infiltration, and energy performance analyses for Finnish detached houses. *Building and Environment*, vol. 44, p. 377-387.
- [8] Pan, W. (2010). Relationships between airtightness and its influencing factors of post-2006 new-build dwellings in the UK. *Building and Environment*, vol. 45, p. 2387-2399.
- [9] Sfakianaki, A., Pavlou, K., Santamouris, M., Livada, I., Assimakopoulos, M.N., Mantas, P., Christakopoulos, A. (2008). Air tightness measurements of residential houses in Athens, Greece. *Building and Environment*, vol. 43, p. 398-405.
- [10] D'Ambrosio Alfano, F.R., Dell'Isola, M., Ficco, G., Tassini, F. (2012). Experimental analysis of air tightness in Mediterranean buildings using the fan pressurization method. *Building and Environment*, vol. 53, p. 16-25.
- [11] Pinto, M., Viegas, J., de Freitas, V.P. (2011). Air permeability measurements of dwellings and building components in Portugal. *Build and Environment*, vol. 46, pp. 2480-2489.
- [12] Feijó-Muñoz, J., Poza-Casado, I., González-Lezcano, R.A., Pardal, C., Echarri, V., Assiego De Larriva, R., Fernández-Agüera, J., Dios-Viéitez, M.J., Del Campo-Díaz, V.J., Montesdeoca Calderín, M., et al. (2018). Methodology for the Study of the Envelope Airtightness of Residential Buildings in Spain: A Case Study. *Energies*, vol. 11, p. 704.
- [13] D'Ambrosio Alfano, F.R., Dell'Isola, M., Ficco, G., Palella, B.I., Riccio, G. (2016). Experimental Air-Tightness Analysis in Mediterranean Buildings after Windows Retrofit. *Sustainability*, vol. 8, p. 991.
- [14] Gillott, M.C., Loveday, D.L., White, J., Wood, C.J., Chmutina, K., Vadodaria, K. (2016). Improving the airtightness in an existing UK dwelling: The challenges, the measures and their effectiveness. *Building and Environment*, vol. 95, p. 227-239.
- [15] Paukštys, V., Cinelis, G., Mockienė, J., Daukšys, M. (2021). Airtightness and Heat Energy Loss of Mid-Size Terraced Houses Built of Different Construction Materials. *Energies*, vol. 14, p. 6367.
- [16] Balaras, C.A., Gaglia, A.G., Georgopoulou, E., Mirasgedis, S., Sarafidis, Y., Lalas, D.P. (2007). European residential buildings and empirical assessment of the Hellenic building stock, energy consumption, emissions and potential energy savings. *Building and Environment*. vol. 42, p. 1298-1314.
- [17] Poza-Casado, I., Meiss, A., Padilla-Marcos, M.Á., Feijó-Muñoz, J. (2021). Airtightness and energy

- impact of air infiltration in residential buildings in Spain. *International Journal of Ventilation*, vol. 20, p. 258-264.
- [18] Feijó-Muñoz, J., Pardal, C., Echarri, V., Fernández-Agüera, J., Assiego de Larriva, R., Montesdeoca Calderín, M., Poza-Casado, I., Padilla-Marcos, M.A., Meiss, A. (2019). Energy impact of the air infiltration in residential buildings in the Mediterranean area of Spain and the Canary Islands. *Energy and Building*, vol. 188-189, p. 226-238.
- [19] ISO 9972:2015. (2015). *Thermal Performance of Buildings-Determination of Air Permeability of Buildings-Fan Pressurization Method*. International Organization for Standardization: Geneva.



Banja Luka
1-2 Jun 2023.

DEMI 2023

16th International Conference on Accomplishments in Mechanical and Industrial Engineering

www.demi.mf.unibl.org



The impact of circulating fluidized bed boilers on the environment - on the example of Stanari TPP

M. Nježić^a, V. Babić^a

^aFaculty of Mechanical Engineering, University of Banja Luka, Vojvode Stepe Stepanovića 71, 78000 Banja Luka, Republic of Srpska, Bosnia and Herzegovina

Abstract *Stanari Thermal Power Plant, with an installed capacity of 300 MW, is a relatively new power plant (commissioned in 2016) with a boiler with a circulating fluidized bed. As it is a new technology of combustion of solid fuel in our country, it is necessary to research the impact of these boilers on the environment. The aim of the research is to determine whether emissions of pollutants are within the limit values prescribed by EU regulations and domestic laws. Emissions of sulphur and nitrogen oxides and solid particles were considered. The emission of nitrous oxide (N₂O) has not been investigated. In addition, it is of interest to investigate if the emissions from this type of power plant could meet possibly stricter requirements. The paper presents methods that are applied in order to reduce mentioned emissions at the concrete thermal power plant in Stanari. The research was carried out by measuring emissions for two months.*

Keywords *thermal power plant, coal combustion, circulating fluidized bed boiler, emissions of pollutants, sulphur oxides, nitrogen oxides, ash*

1. INTRODUCTION

Thanks to the development during the last few decades, large-scale circulating fluidized bed (CFB) boilers are today used for the production of electricity by power companies. They showed high fuel utilization with satisfactory reliability in operation. The development of this technology, along with the ever-increasing reduction of the negative impact on the environment compared to boilers with other combustion technologies, enables their ever-wider use. It is important to highlight that, in addition to fuel, emissions are also affected by

the way these boilers are operated. Stanari TPP is currently the only one in our region with this technology, although more such power plants are expected to be constructed. Hence, it is essential to devote full attention to researching the operation of these boilers, especially their impact on the environment.

2. CFB BOILER OPERATION

The combustion process in CFB boilers occurs under conditions of fast fluidization in the furnace. Fluidization and movement of solid particles (particles of bed (inert material), fuel, sorbent, and ash) are attained by blowing primary air through the fluidizing air distributor at the bottom of the furnace. The velocity of primary air is greater than the transport velocity of particles, i.e. greater than the second critical velocity of fluidization. Fig.1. shows a simplified diagram of a CFB boiler.

Corresponding author

MSc Milana Nježić
njezic.milana@hotmail.com

Faculty of Mechanical Engineering, University of Banja Luka
Vojvode Stepe Stepanovića 71
Banja Luka, Republic of Srpska Bosnia and Herzegovina

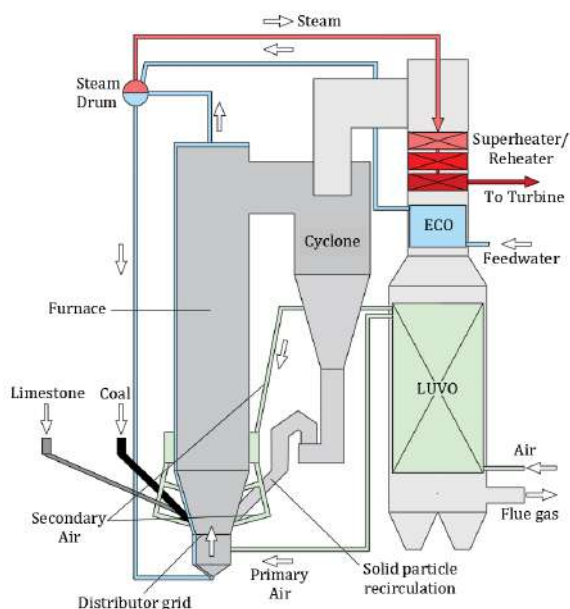


Fig. 1. Diagram of a CFB boiler [2]

Fuel combustion takes place in the furnace, and the generated heat is partly transferred to the evaporator, consisting of tube screens placed on the walls of the furnace, and partly to the heating surfaces in the convective pass (section). The rest of the air (secondary air) required for complete combustion and desulphurisation is brought above the fuel feed ports. The combustion temperature (temperature in the furnace) ranges between 800-900 °C and is lower than the temperature of other combustion technologies. The gas and solid phase (of combustion products) from the furnace pass through cyclones, in which particles of inert material and larger particles of fuel and sorbent are separated. After separation, they are returned to the furnace through specific valves (L-valve or J-valve). The formation of this flow regime depends on the granulation of the inert layer particles because the fuel makes up only about 1-3 % of the total mass of solid particles [1]. The temperature and conditions in the furnace do not change even during load changes, because high concentrations of solid particles and high heat transfer coefficients remain in the furnace (thanks to recirculation). Gaseous combustion products and solid particles, which are not separated in cyclones, go through the convective pass of the boiler, where they transfer the rest of heat to steam, water, and air

in heating surfaces. After leaving the convective pass, the solid particles are separated in one of the flue gas cleaning systems, and flue gas is released into the atmosphere through the stack [2].

Intensive mixing of particles (inert material, unburned fuel, and sorbent) and recirculated gaseous combustion products, ensure more complete combustion, reduced losses due to incomplete combustion (q_3 and q_4), as well as efficient dry desulphurisation. In addition, lower temperatures and a lack of oxygen in the lower section of the furnace slow down the mechanisms of the formation of nitrogen oxides.

3. LITERATURE REVIEW ON EMISSIONS OF POLLUTANTS DURING COAL COMBUSTION IN CFB

3.1. Emission of pollutants and their impact on the environment

The most significant pollutants emitted with gaseous combustion products, depending on the fuel, are carbon dioxide (CO_2), carbon monoxide (CO), volatile organic compounds (VOC), sulphur oxides (SO_x), nitrogen oxides (NO_x), nitrous oxide (N_2O), ammonia (NH_3), heavy metals and solid particles. If fuel contains traces of chlorine, in the combustion products will appear also hydrogen chloride (HCl), dioxins (polychlorinated dibenzodioxins – PCDD), and furans (polychlorinated dibenzofurans – PCDF) [3].

The influence of NO_x should be observed through its global and local impact. Nitrogen monoxide (NO) reacts with ozone in the higher parts of the troposphere/stratosphere and consequently, NO_x affects the reduction of the Ozone layer. The Ozone layer protects the Earth from harmful ultraviolet rays, which contribute to climate change and negatively affect human health. In the stratosphere, half of the total ozone loss occurs as a result of the direct or indirect effects of NO_x [4]. In addition, NO_x produces photochemical smog, which under the influence of sunlight and at high concentrations, reacts and leads to reduced visibility. The atmosphere in urban areas contains hydrocarbons and their free radicals that react with NO_x in the presence of sunlight and create substances that further reduce visibility and harm human health [5]. NO_x also affects the

formation of acid deposition, while N_2O does not affect this phenomenon. Acid depositions are formed by the separation of acidic compounds (nitrates, nitrites, sulphates...) from the atmosphere onto the soil or water. Their appearance has a negative effect on ecosystems, impairs soil quality, damages plants, disturbs the acidity of surface water, and causes corrosion and erosion. Reduction of acid deposits can only be achieved by controlling emissions [6].

SO_x causes irritation and damage to the respiratory organs in humans and acts aggressively on metals, building and construction materials, textile fibres, paper, paints, and varnishes.

SO_x and NO_x are indirect greenhouse gases, while N_2O is a direct greenhouse gas and has a very harmful effect on the environment. SO_x and NO_x dissolve in contact with water and increase the concentration of hydrogen ions, which causes a decrease in the pH value of precipitation ($pH < 5.6$). It is estimated that the contribution of NO_x to the occurrence of acid rain is 30 %, whilst SO_x is about 70 % [4].

Solid particles in the atmosphere reduce the intensity of ultraviolet radiation, scatter light, create haze and reduce visibility. Particles larger than $10\ \mu m$ PM_{10} settle quickly and their impact is limited to the immediate environment of the emission source. Finer $PM_{2.5}$ particles can float in the atmosphere for much longer and settle kilometres away from the source. Fine ($0.1 - 2.5\ \mu m$) and ultrafine ($< 0.1\ \mu m$) particles can enter the alveoli and the bloodstream through the respiratory tract. Furthermore, finer particles contain higher concentrations of heavy metals, strong acids, PAH, and other harmful compounds.

Coal contains about 20 to 30 heavy metals, whereby the most abundant are cadmium (Cd), mercury (Hg), lead (Pb), arsenic (As), chromium (Cr), copper (Cu), nickel (Ni), and selenium (Se). Heavy metals can remain in the ash or transition to the gaseous combustion products, which depends on their characteristics, fuel composition, and operating conditions.

Investigation of coal combustion has shown that most heavy metals first evaporate and then condense into small droplets that are absorbed by the ash particles during the cooling of the combustion products. Heavy metals with a higher boiling point and lower vapour pressure usually remain in the ash at the bottom of the

furnace, while those with a lower boiling point and greater volatility transition to the gaseous products of combustion. Some heavy metals have a carcinogenic effect, and some are toxic. They enter the human body through food because they accumulate in the food chain [3].

CO_2 is a greenhouse gas and directly affects the energy balance in the Earth's atmosphere because it absorbs and re-emits infrared radiation. On the other hand, CO belongs to indirect gases with a greenhouse effect, because it is a precursor of ozone, sulphates, and aerosols and affects climate change [7].

Prediction of SO_x emissions during coal combustion in CFB boilers was simulated using artificial neural networks (Artificial Neural Network - ANN) by researchers Krzywanski J. and Nowak W. [8]. The research was carried out on pilot-scale up to large-scale CFB boilers (up to 261 MW_e). The simulation showed that the ANN can predict SO_x emissions with sufficient accuracy in relation to the operating parameters of the boiler. This approach to process management enables timely detection of a potential increase in emissions, as well as possible changes or malfunctions in the systems for monitoring of harmful emissions into the atmosphere [8].

3.2. Formation of sulphur and nitrogen oxides and solid particles during combustion

Sulphur oxides (SO_x) are formed from combustible sulphur in the coal (organic and pyritic sulphur) during the combustion, i.e. during devolatilization and char combustion. The amount of sulphur that turns into sulphur dioxide (SO_2) depends on the type of sulphur compounds in the fuel, the temperature in the bed, the calcium content in the ash, and the operating conditions [9].

The SO_2 produced in the furnace is divided into three parts - one part is separated during desulphurisation, the other part is transformed into SO_3 , and the rest is emitted into the atmosphere with the flue gasses. It is estimated that SO_3 amounts to 1-3 % of the total amount of generated SO_2 , depending on the residence time of the gas in the furnace, temperature, excess air coefficient, and the presence of catalytic surfaces.

In general, during coal combustion, nitrogen oxides are produced in three ways - thermal,

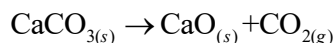
prompt, and fuel NO. The amount of emitted nitrogen oxides depends on the type and characteristics of coal (nitrogen content, age of coal, functional groups in which nitrogen is bound, the content of volatiles, distribution of nitrogen between volatiles and char, structure and reactivity of char, and particle size) [6], and the operating conditions in the furnace (bed temperature, temperature above the bed, concentration of char in the bed and furnace, excess air coefficient, substoichiometric combustion conditions, ratio of primary and secondary air, type of inert material) [10].

One of the conditions for the formation of thermal and prompt NO is a temperature higher than 1500 °C [10], therefore the dominant mechanism of the formation of nitrogen oxides in CFB boilers is fuel NO. Fuel NO is produced by the oxidation of nitrogen from fuel, i.e. nitrogen from volatiles and char. Additionally, the two-stage air supply leads to the formation of a reduction zone (substoichiometric conditions) in the lower part of the furnace, and thus to a reduced amount of oxygen available for the formation of NO_x. However, these conditions in the furnace are at the same time suitable for the formation of N₂O. Increased N₂O emissions are distinctive for this combustion technology.

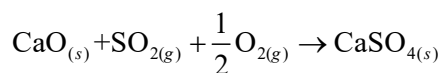
Ash is a solid residue of the combustion process that arises during the transformation of mineral substances out of fuel. Factors that affect the transformation of mineral substances and the formation of ash are combustion temperature, combustion conditions, chemical composition, and physical properties of mineral substances.

3.3. Reduction of sulphur and nitrogen oxides and solid particles emissions during combustion

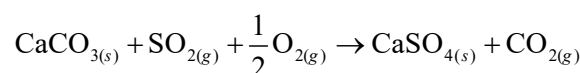
Here we will focus on the mechanisms of reduction of SO_x, NO_x and solid particle emissions applied in Stanari TPP. SO_x emissions are reduced by dry desulphurisation, that is by adding sorbent (in this case limestone) to the furnace during combustion. The partition of SO₂ is carried out by a two-stage mechanism consisting of two basic processes - calcination and sulphation [1, 10, 11]. Calcination of the limestone aims at the formation of calcium oxide (CaO) in reaction [12]:



CaO is porous and can react with SO₂, and create calcium sulphate (CaSO₄) in a process called sulphation [12]:



CaSO₄ is inert, stable, and easy to store. The CO₂ released during calcination expands the pores in the CaO particles, thereby increasing the active surface area on which the sulphation reaction can take place. Also, CO₂ partial pressure can influence the progress of calcination, leading to its interruption and occurrence of direct sulphation [12]:



A diagram of the previously mentioned calcination and sulphation reactions (assuming that the particles are of an ideal spherical shape) is shown on Fig.2.

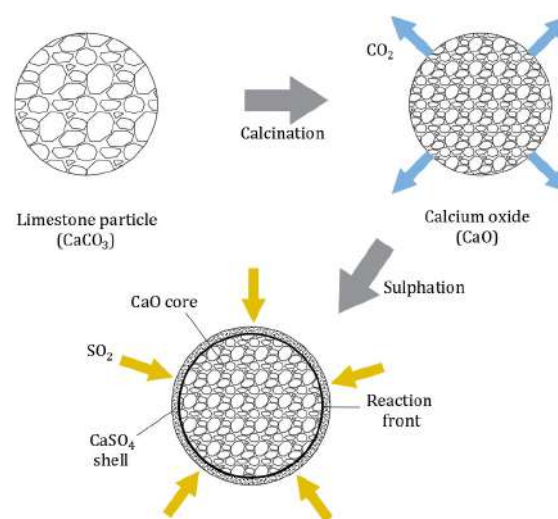


Fig. 2. Calcination and sulphation of limestone particle [2]

It is experimentally proved that the most effective desulphurisation in the CFB boilers at an approximately constant calcium to sulphur molar ratio is in the temperature range of 800-870 °C. If the temperature is higher than 870 °C, small crystals of CaO crystallize, which reduces their active surface area, whilst at temperatures above 1000 °C CaSO₄ decomposes. On the other side, there is almost no desulphurisation at a temperature lower than 750 °C [13].

The choice of suitable operating parameters in the furnace is of crucial importance for the reduction of NO_x emissions. The most significant operating parameters are the temperature in the furnace and the excess air coefficient (the amount of air at the reaction site) [1, 6, 10].

The temperature in the furnace and in the bed directly affect the rate and intensity of the chemical reactions of NO_x formation. As the temperature rises, so does NO_x concentration. Another parameter that noticeably affects NO_x emissions is the excess air coefficient, whose change is achieved and regulated by the multi-stage supply of air into the furnace. Reduction zone, i.e. insufficient amount of O_2 in the lower part of the furnace leads to incomplete combustion and increased content of CO and char, which significantly reduce NO_x . A catalyst for NO reduction reaction with CO is limestone used for desulphurisation [14].

Furthermore, the available amount of O_2 is spent on coal combustion, so the amount available for the formation of oxides is significantly smaller, and thus the formation mechanisms are slowed down. The rest of the air required for complete combustion and efficient retention of SO_2 is added in the form of secondary air, which is brought in above the reduction zone.

However, along with the decrease in temperature and NO_x emissions, there is an increase in unwanted N_2O emissions. The reason for this is the difference in the formation mechanisms, as well as the influence of the conditions in the furnace on the compounds that are released during the devolatilization of coal particles. The reduction of N_2O emissions can be achieved by controlling the coal heating and devolatilization process, and by a higher calcium to sulphur molar ratio (due to the catalytic effect of CaO). Its decomposition can also occur due to the presence of hydrogen radicals (H, OH) in the primary combustion zone at higher temperatures [15].

The reduction of solid particles is carried out by separating them from gaseous combustion products before they are emitted into the atmosphere. Combustion products pass through bag filters, made of natural, synthetic, or mineral materials, whereby solid particles are deposited on the surface of the filter. The mechanisms of particle separation are the initial collision of particles with the filter material,

Brownian diffusion of particles, direct interaction of particles and filter material, electrostatic attraction and gravitational settling, then the effects of sieving and formation of a layer of particles on the filter.

4. DOMESTIC AND EUROPEAN REGULATIONS FOR EMISSIONS OF POLLUTANTS FROM COMBUSTION PLANTS

Emission limit values of pollutants are classified according to the characteristics of the combustion plant itself, that is, according to the type, capacity, age, operating lifetime, and fuel it combusts. Stanari TPP with an installed capacity of 300 MW_e was commissioned in 2016. The fuel is combusted in CFB and the belonging boiler has a thermal power input of 750 MW_{th} . The fuel is lignite from the open pit mine in the possession of TPP.

4.1. Domestic regulations for emissions of pollutants from combustion plants

Permitted emission limit values of pollutants from combustion plants into the atmosphere in the Republic of Srpska are determined by the Rulebook on measures to prevent and reduce air pollution and improve air quality (Official Gazette of the Republic of Srpska, number 3/15, 51/15, 47/16 and 16/19). The Rulebook also defines the classification of combustion plants according to their age, as given below:

Combustion plant type	Date of commissioning
Old large plant	before July 1 st , 1992
Existing large plant	on or after July 1 st , 1992, and before January 1 st , 2018
New large plant	on or after January 1 st , 2018

According to the previously mentioned data, Stanari TPP belongs to the existing large plants. Emission limit values of SO_2 , NO_x , and solid particles for existing large plants that combust coal are shown in Table 1.

Table 1. Emission limit values for Stanari TPP according to domestic regulations in $[\text{mg}/\text{Nm}^3]$, [16]

Thermal power input	SO_2	NO_x	Solid particles
>300 MW_{th}	200	200	20

If a new combustion plant were to be built with a boiler of the same or greater thermal power

input, in which lignite would be combusted in CFB or in a pulverized state, the emission limit values would be lower (stricter regulations) like it is shown in Table 2.

Table 2. Emission limit values for new large plants according to domestic regulations in [mg/Nm³], [16]

Thermal power input of new plant (> 300 MW _{th})	SO ₂	NO _x	Solid particles
Coal combustion in CFB	200	150	10
Pulverized combustion of coal	150	200	10

The aforementioned Rulebook [16] prescribes also limit values for plants with lower thermal power input, which is not of interest in this case.

4.2. European regulations for emissions of pollutants from combustion plants

Permitted emission limit values of pollutants from combustion plants into the atmosphere in the European Union are prescribed by Directive 2010/75/EU of November 24th, 2010 [17] and Decision 2021/2326 on determining the best available techniques (BAT) conclusions for large combustion plants of November 30th, 2021 [18]. According to this Decision [18], existing plants are combustion plants first permitted at the installation or a complete replacement of combustion plant on the existing foundations before the publication of Decision 2021/2326, and new plants are the rest of the plants. Accordingly, Stanari TPP is an existing plant for which apply emission limit values (daily average values or average over the sampling period) shown in Table 3.

Table 3. Emission limit values (daily average values) for Stanari TPP according to EU regulations in [mg/Nm³], [18]

Thermal power input	SO ₂	NO _x	Solid particles
≥300 MW _{th}	220 ¹	165 ²	11

¹ fluidized bed boiler
² FCB boiler combusting coal and/or lignite and lignite-fired PC boiler

Due to the comparison of the emission limit values for existing and new plants according to EU regulations, Table 4 shows the emission limit values for a new plant of the same or

greater thermal power input for the same combustion technologies.

Table 4. Emission limit values for new plants (daily mean values) according to EU regulations in [mg/Nm³], [18]

Thermal power of the new plant (> 300 MW _{th})	SO ₂	NO _x	Solid particles
Coal combustion in CFB	110	125	10
Pulverized combustion of coal	110	125	10

5. MEASUREMENTS OF EMISSIONS OF POLLUTANTS ON STANARI TPP

Emission measuring and monitoring system at the Stanari TPP tracks and displays measured concentrations of SO₂, NO_x, CO, CO₂, O₂, and solid particles. All measuring devices are placed inside the stack. Reference methods and devices used for measuring are shown in Table 5.

Table 5. Equipment for measuring emissions of combustion products

Pollutant	Reference method	Measuring device
CO	Non-dispersive infrared method – NDIR	Extractive gas analyzer GMS 810 (SICK) with sensors that meet the requirements of reference methods. The sensor for measurement of SO ₂ , NO _x , and CO concentrations is UNOR-MULTOR, while for O ₂ concentration is OXOR – both were produced in 2020. The equipment is regularly maintained and calibrated according to the recommendations of reference methods and manufacturers. Note: CO ₂ is not measured continuously, but with a portable analyzer PG-350E (manufactured by Horiba).
SO ₂		
CO ₂		
NO _x	Chemiluminescence method	
O ₂	Paramagnetic method	
Solid particles		The measuring device is SICK Dusthunter SP100 - produced in 2016.

Measurements of emissions of pollutants were carried out during January and April 2022 at the nominal load of the plant, without intentional (planned) changes in production processes or plant outages. It should be emphasized that

during the capital overhaul, which was carried out in February and March of the same year, the filter bags in the plant for solid particle separation were restored. Bags made of polytetrafluoroethylene (PTFE) were replaced with bags made of polyphenyl sulphide (PPS). Bag filters separate ash (which is in Stanari TPP used as inert bed material) and CaSO_4 particles. Ash has a high quartz content (both fly ash and ash from the bottom of the furnace) [19].

Measurements of SO_x , NO_x , and solid particle emissions were performed continuously and obtained values were averaged out into hourly values (values were averaged out by the specified measuring equipment). Precisely, in January were measured 744 values, and in April 720 values.

6. ANALYSIS OF MEASUREMENT RESULTS IN TERMS OF COMPLIANCE WITH DOMESTIC AND EU REGULATIONS

When it comes to domestic regulations, the conditions under which compliance of emissions with permitted limit values is confirmed are defined by the Rulebook [16], according to which continuous measurements of emissions can be evaluated as satisfactory if measurements for operating hours within a calendar year show that [16] :

- no daily average value exceeds the values determined for the plants from Annex I of this Rulebook and
- 95 % of all hourly average values during the year do not exceed double the values permitted in this Rulebook.

Firstly, it is necessary to determine the so-called validated average values. The validated hourly average value is calculated by subtracting the value of the corresponding confidence interval from the measured valid hourly average value. According to the Rulebook, the 95 % confidence interval of a single measured result shall not be higher than the prescribed percentages of emission limit values [16]:

- SO_2 : 20 %;
- NO_x : 20 %;
- Solid particles: 30 %.

The validated daily average values in Table 6 and Table 7 were obtained by subtracting confidence intervals from the measured hourly

values of SO_2 , NO_x and solid particles emissions (intervals for SO_x and NO_x are 20 % each and for solid particles 30 %) and by averaging out those values. Likewise, validated monthly average values for January and April were determined based on validated daily values and they are shown in Table 8. For practicality, only validated daily and monthly average values are shown.

Table 6. Validated daily average values for January 2022 in [mg/Nm^3]

Date of measurement	Validated daily average value		
	SO_2	NO_x	Solid particles
1.1.2022	156,3153	140,6741	6,3712
2.1.2022	158,0517	145,4239	6,6163
3.1.2022	157,8983	144,1326	6,8075
4.1.2022	159,0879	139,0067	7,1302
5.1.2022	162,6247	133,6767	9,5200
6.1.2022	151,2412	139,4266	9,4467
7.1.2022	155,9217	136,5377	8,9627
8.1.2022	153,9244	135,2174	7,4966
9.1.2022	152,8434	133,8780	7,6776
10.1.2022	155,4575	132,9081	7,9996
11.1.2022	158,6832	141,2075	8,7314
12.1.2022	159,1610	152,7716	7,1452
13.1.2022	168,7741	147,7505	7,5082
14.1.2022	174,3300	146,5877	6,6132
15.1.2022	174,3300	146,5877	6,6132
16.1.2022	174,3300	146,5877	6,6132
17.1.2022	166,5217	145,2268	7,7659
18.1.2022	158,6461	146,4586	8,0454
19.1.2022	158,7503	145,5635	8,5408
20.1.2022	157,0769	137,1630	8,7169
21.1.2022	153,2772	139,8789	9,9705
22.1.2022	156,5453	137,3680	9,5005
23.1.2022	148,9441	146,3520	8,7570
24.1.2022	152,8039	144,6203	7,4536
25.1.2022	142,6994	130,8437	9,2129
26.1.2022	143,1712	136,5337	9,4088
27.1.2022	145,0442	140,3273	9,6330
28.1.2022	147,4171	128,7665	10,7624
29.1.2022	154,1337	128,8404	11,4849
30.1.2022	156,2338	124,7319	13,5910
31.1.2022	156,5409	128,4692	12,5082

Table 7. Validated daily average values for April 2022 in [mg/Nm³]

Date of measurement	Validated daily average value		
	SO ₂	NO _x	Solid particles
1.4.2022	159,5078	132,4070	5,2118
2.4.2022	159,6527	134,0152	4,9346
3.4.2022	158,1331	138,3344	5,3561
4.4.2022	157,0431	136,4430	5,0757
5.4.2022	158,0563	135,7442	5,6690
6.4.2022	154,1248	138,8288	4,7855
7.4.2022	158,7750	138,5869	5,0835
8.4.2022	156,5124	133,2472	5,1855
9.4.2022	150,4647	124,8369	5,5254
10.4.2022	158,4224	140,4352	4,9769
11.4.2022	155,4060	148,7913	4,9172
12.4.2022	156,7481	145,6967	4,6775
13.4.2022	158,6093	148,2046	4,5640
14.4.2022	159,7712	147,9620	4,7605
15.4.2022	158,6217	141,3596	5,2624
16.4.2022	158,7585	140,5096	4,4511
17.4.2022	158,4185	146,8818	4,7601
18.4.2022	158,3696	145,9001	4,7009
19.4.2022	158,6102	144,5295	5,4438
20.4.2022	158,1254	142,5686	4,8102
21.4.2022	159,3742	141,2826	5,3463
22.4.2022	158,4735	142,3962	5,1095
23.4.2022	157,7213	139,9421	5,0859
24.4.2022	158,8552	145,4346	4,5343
25.4.2022	158,8139	140,6426	4,8933
26.4.2022	150,3347	138,0811	4,3622
27.4.2022	156,3442	137,1341	5,3554
28.4.2022	150,3067	145,8644	5,5875
29.4.2022	156,5776	153,8448	6,3325
30.4.2022	158,1305	155,0066	5,1591

Table 8. Validated monthly average values for January and April 2022 in [mg/Nm³]

Month	The validated monthly average value		
	SO ₂	NO _x	Solid particles
January 2022	157,1219	139,4683	8,6002
April 2022	157,2354	141,4970	5,0639

After a review of the data from Table 6-8, it can be concluded that no validated average daily value exceeds the prescribed values given in Table 1. However, it is necessary to emphasize that for a completely correct assessment of emissions, it is required to analyse the entire calendar year, which is not the case here.

On the other hand, European regulations define the conditions under which emissions can be assessed as satisfactory within the framework of Directive 2010/75/EU, while the limit values themselves are prescribed in the previously mentioned Decision 2021/2326. Emissions meet the requirements if it is proven that for the operating hours within a calendar year, they fulfil the following conditions [17]:

- no validated monthly average value exceeds the relevant emission limit values set out in the Decision,
- no validated daily average value exceeds 110 % of the relevant emission limit values set out in the Decision and
- 95 % of all the validated hourly average values over the year do not exceed 200 % of the relevant emission limit values set out in the Decision.

The mentioned relevant emission limit values from Decision 2021/2326 [18] for this specific power plant are shown in Table 3.

The process of determining the validated average values is identical for domestic and EU regulations, which is why Tables 6 - 8 are considered applicable in this case, too. By reviewing the data from Tables 6 - 8, it can be concluded that the validated monthly average values for January and April do not exceed the prescribed relevant emission limit values and that no validated average daily value for those two months exceeds 110% of the prescribed emission limit values shown in Table 3.

In addition, it can be seen from Table 8 that the solid particle emissions in April compared to January are reduced by around 40%, which is a consequence of the mentioned filter bag replacement. The emissions of SO₂ and NO_x do not show a significant change. For a completely correct assessment of emissions, an analysis of the entire calendar year is required too.

7. CONCLUSION

At Stanari TPP, dry desulphurisation by adding limestone to the furnace ensures the reduction

of SO₂ emissions to the required extent, so that the emissions are within the prescribed limit values. In the general case, additional wet desulphurisation may be necessary depending on the content of combustible sulphur in the fuel and the operating conditions in the furnace. Managing the primary and secondary air that is blown into the furnace during the combustion of coal in the CFB, ensures that the NO_x emissions are below the limit values, without the application of any additional measures.

During the investigation, emissions of solid particles were lower than the permitted limit values defined by domestic and EU regulations. Emissions of harmful substances from CFB boilers also depend on the operating conditions in the furnace, so it is possible to reduce these emissions by optimizing the combustion process. For this kind of reduction, it is necessary to conduct more research. Today are almost always used computational simulations of processes in furnaces and they are currently in rapid development. The fact is that the EU has already started the process of tightening regulations in the field of environmental protection and that there may be a change (reduction) of prescribed limit values. Future research should be focused on improving the process of coal combustion in CFB and methods for reducing pollution that accompanies such combustion. For instance, one of the ways for reduction could be the application of a regenerative sorbent with a high affinity toward SO₂ at the bed temperature [20].

Within the framework of these investigations, special attention should be paid to N₂O emissions, which are characteristic of combustion in CFB, and have a harmful effect on the environment.

SO₂, NO_x and solid particle emissions from Stanari TPP during January and April 2022 do not exceed the limit values prescribed by domestic legislation and EU regulations and meet all defined requirements regarding environmental protection.

It should be emphasized that the regulations oblige to emissions monitoring throughout the year and that the previous conclusion is valid only for those two months because this research is limited to those two months for objective reasons.

Acknowledgement

On this occasion, we would like to express our special gratitude to the management and personnel of Stanari TPP for the provided data and assistance in this research.

REFERENCES

- [1] Basu, P. (2015). *Circulating Fluidized Bed Boilers: Design, Operation, and Maintenance*. Springer Cham, Heidelberg New York Dordrecht London. DOI: [10.1007/978-3-319-06173-3](https://doi.org/10.1007/978-3-319-06173-3)
- [2] Nježić, M. (2022). *Istraživanje emisija SO_x i NO_x generatora pare sa cirkulacionim fluidizovanim slojem TE Stanari*. (In Serbian). MSc thesis. Mašinski fakultet Univerziteta u Banjoj Luci.
- [3] Gulyurtlu, I., Pinto, F., Abelha, P., Lopes, H., Crujeira, A.T. (2013). Pollutant emissions and their control in fluidized bed combustion and gasification. Scala F. (Editor). *Fluidized bed technologies for near-zero emission combustion and gasification*. Woodhead Publishing. p. 435-480. DOI: [10.1533/9780857098801.2.435](https://doi.org/10.1533/9780857098801.2.435)
- [4] Sloss, L. L. (1991). *NO_x Emissions from Coal Combustion*. IEACR/36, IEA Coal Research, London.
- [5] Wark, K., Warner, C. (1976). *Air Pollution – Its Origin and Control*. Pearson, New York.
- [6] Stojiljković, D. (1999). *Obrazovanje azotnih oksida pri sagorevanju domaćih lignita u spraćenom stanju*. (In Serbian). PhD thesis. Mašinski fakultet Univerziteta u Beogradu.
- [7] Agencija za zaštitu životne sredine Republike Srbije. Vazduh i klimatske promene, NLI 1.8 Emisija gasova sa efektom staklene bašte. From: <http://indicator.sepa.gov.rs/pretraga/indikatori/svefind/1bf6f054ac764d2a97ade52b6ec89f32>, accessed on: October 31, 2022.
- [8] Krzywanski, J., Nowak, W. (2015). Artificial Intelligence Treatment of SO₂ Emissions from CFBC in Air and Oxygen-Enriched Conditions. *Journal of Energy Engineering*, vol. 142, no. 1. DOI: [10.1061/\(ASCE\)JEEY.1943-7897.0000280](https://doi.org/10.1061/(ASCE)JEEY.1943-7897.0000280)

- [9] Nowak, W., Mirek, P. (2013). Circulating fluidized bed combustion (CFBC). Scala F. (Editor). *Fluidized bed technologies for near-zero emission combustion and gasification*. Woodhead Publishing, p. 701-764. DOI: [10.1533/9780857098801.3.701](https://doi.org/10.1533/9780857098801.3.701)
- [10] Oka, S. (2004). *Fluidized bed combustion*. Marcel Dekker, New York.
- [11] Olas, M., Kobylecki, R., Bis, Z. Simultaneous calcination and sulfation of limestone-based sorbents in CFBC - Effect of Mechanical Activation. *Proceedings of the 9th International Conference on Circulating Fluidized Beds in conjunction with the 4th International VGB Workshop "Operating Experience with Fluidized Bed Firing Systems"*, May 2008, Hamburg, p. 931-936.
- [12] Scala, F., Solimene, R., Montagnaro, F. (2013). Conversion of solid fuels and sorbents in fluidized bed combustion and gasification. Scala F. (Editor). *Fluidized bed technologies for near-zero emission combustion and gasification*. Woodhead Publishing; p. 319-387. DOI: [10.1533/9780857098801.2.319](https://doi.org/10.1533/9780857098801.2.319)
- [13] Ma, L., Ning, P., Qing, S., Zhao, W. Effect Element of Circulating Fluidized Bed Boiler Eliminate Sulfur. *International Conference on Power Engineering*, October 2007, Hangzhou, p. 855-858. DOI: [10.1007/978-3-540-76694-0_159](https://doi.org/10.1007/978-3-540-76694-0_159)
- [14] Zijlma, G.J. (2002). *Effect of Air Staging and Limestone addition on Emissions of SO₂ and NO_x in CFB*. (In English). PhD thesis. Technische Universiteit Delft.
- [15] Armesto, L., Boerrichter, H., Bahillo, A., Otero, J. (2003). N₂O emissions from fluidized bed combustion. The effect of fuel characteristics and operating conditions. *Fuel*, vol. 82, p. 1845-1850. DOI: [10.1016/S0016-2361\(03\)00169-8](https://doi.org/10.1016/S0016-2361(03)00169-8)
- [16] *Pravilnik o izmjenama i dopunama Pravilnika o mjerama za prečavanje i smanjenje zagađivanja vazduha i poboljšanje kvaliteta vazduha*, Službeni glasnik Republike Srpske – br. 16. (2019). Ministarstvo za prostorno uređenje, građevinarstvo i ekologiju. Banja Luka.
- [17] *Directive 2010/75/EU of the European Parliament and of the Council of 24 November 2010 on industrial emissions (integrated pollution prevention and control)*, Official Journal of the European Union L 334/17. (2010). The European Parliament and the Council of the European Union.
- [18] *Commission Implementing Decision (EU) 2021/2326 of 30 November 2021 establishing best available techniques (BAT) conclusions, under Directive 2010/75/EU of the European Parliament and of the Council, for large combustion plants (notified under document C (2021) 8580)*, Official Journal of the European Union L 469/1. (2021). The European Commission.
- [19] EFT – Rudnik i Termoelektrana Stanari. (2016). *Fizičko-hemijske karakteristike pepela iz TE Stanari*. Stanari.
- [20] Mathieu, Y., Tzanis, L., Soulard, M., Patarin, J., Vierling, M., Molière, M. (2013). Adsorption of SO_x by oxide materials: A review. *Fuel Processing Technology*, vol. 114, p. 81-100. DOI: [10.1016/j.fuproc.2013.03.019](https://doi.org/10.1016/j.fuproc.2013.03.019)

Thermodynamic analysis of the theoretical cooling system based on measured climate data

Danijela Kardaš Ančić^a, Petar Gvero^a, Mirko Komatina^b

^aUniversity of Banja Luka, Faculty of Mechanical Engineering, Stepe Stepanovića 71, Banja Luka, Bosnia and Herzegovina

^aUniversity of Belgrade, Faculty of Mechanical Engineering, Kraljice Marije 16, Belgrade, Serbia

Abstract The aim of this work is to show how climate data (average monthly outdoor air temperature) affects the COP of the cooling system and the choice of compressor power. This is important for the reason that these systems could be properly planned and designed so they could provide the required cooling effect for which they are used. In this work, the steam compression cooling system is analyzed from the point of view of the change the power of the electric motor for driving the compressor and cooling coefficient of performance of the system depending on the temperature of the outdoor air. The analysis is performed for climate data for the City of Banja Luka in the summer period and the working medium is refrigerant R134a.

Keywords Cooling system, climate data, COP, compressor power

1. INTRODUCTION

During one stroke of the piston in the compressor, which lasts several thousandths of a second, the liquid phase does not have time to evaporate, but remains in the cylinder where it collects and, due to its incompressibility, causes serious compressor failures [1]. In order for the compressor to safely suck dry saturated steam, a liquid separator (separator) is installed in front of it. In it, the speed of the wet steam coming out of the evaporator decreases sharply and its flow direction changes sharply, so that the liquid droplets, due to their greater mass and therefore inertia, are separated and fall towards the bottom of the separator, while the dry steam is sucked in by the compressor. In this work is analyzed refrigerant R134a according to the scheme given in Figure 1. The thermodynamic scheme of the cooling system is adopted with single-stage compression, dry refrigerant suction and damping. Figure

2. represents thermodynamic process in $\log p$ - h and T - s diagrams.

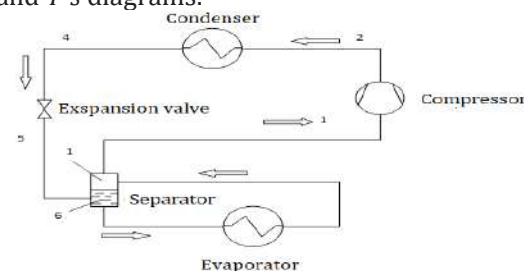


Fig. 1. The thermodynamic scheme of the cooling system

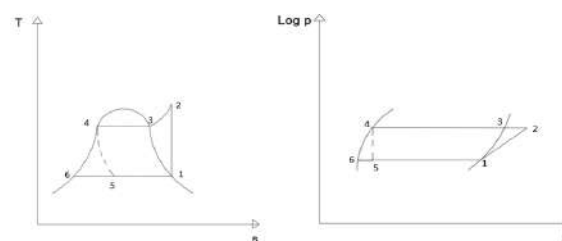


Fig. 2. The thermodynamic process of the ideal theoretical cooling system

The hot liquid of state 4 expands in the expansion valve into the wet vapor of state 5 at a constant enthalpy ($h=const$) of the refrigerant. This process is irreversible, which makes the process thermodynamically weakened. However, compared to the expansion cylinder system, the system is significantly simplified. In the separator, wet vapor of state 5 is separated into hot liquid of state 6 and dry saturated vapor of state 1. From all of the above, the theoretical circular cooling process where it falls into the area of wet steam with a throttle valve and dry suction is practically the most favorable and therefore can be accepted as the basis for further studies of steam compression machines [2]. For this reason, this thermal scheme and theoretical cycle is adopted.

2. THERMODYNAMIC MODEL OF THE REFRIGERATION SYSTEM

2.1. Energy analysis of the system

Evaluation of cooling systems is most often done by the energy transformation coefficient or coefficient of performance (COP). In a cooling device, the useful effect is the heat flow that is brought into the device from the cooled space, and the energy used is the mechanical work used to drive the device. In that case, the heat transformation coefficient is called the cooling coefficient. The main goal of this analysis is to determine the COP of the cooling system for the set initial conditions and the obtained meteorological data. Table 1 presents thermodynamic equations used for energy analysis of cooling system.

Table 1. Equations for energy analysis of the system

Exp no.	Parameter	Equation
1	Specific cooling heat [kJ/kg]	$q_0 = h_1 - h_6$
2	Refrigerant flow [kg/s]	$\dot{m} = \frac{Q}{q_0}$
3	Heat load of the condenser [kW]	$Q_k = \dot{m}(h_2 - h_4)$
4	Volumetric flow of the working fluid through compressor [m ³ /kg]	$V = \dot{m} \cdot v$

5	Theoretical compressor power [kW]	$P = \dot{m}(h_2 - h_1)$
6	COP [-]	$\varepsilon_h = \frac{Q}{P}$

2.2. Model for calculation of the required power of electric motor to drive the reciprocating compressor

Considering the cycle with an ideal-adiabatic compressor, it is assumed that there is no harmful space in the compressor, that the compression occurs according to the isentrope, in which there is no friction and that there are no pressure losses due to the resistance of the steam flow in the valves and channels. It is also assumed that there are no losses of steam flow due to imperfect closing of the suction and discharge valves and imperfect sealing between the piston and the cylinder. In a real compressor, all these phenomena must be taken into account and therefore the cooling capacity, i.e. the actual amount of refrigerant vapor sucked in, will be less than the one that the compressor would suck in if the volume described by the piston during the suction stroke was fully used. Likewise, the actual compression work used will be greater than the theoretically calculated compression work in an ideal compressor. These deviations in the operation of the actual compressor from the ideal are included by the delivery coefficient λ . The delivery coefficient consists of four dimensionless coefficients as their mutual product:

- Volumetric/volume coefficient due to harmful space (volume efficiency) λ_c ;
- Delivery coefficient due to suction dumping λ_{pr} ;
- Delivery coefficient due to heating λ_z ;
- Delivery coefficient due to flow λ_n .

Table 2 present methodology for calculating the delivery coefficient for the analyzed system, as well as determining the required power of the electric motor to drive the reciprocating compressor.

Table 2. Equations for calculation methodology

Exp no.	Parameter	Equation
1	Volumetric/volume coefficient due to harmful space (volume efficiency)	$\lambda_c = 1 - c \left[\left(\frac{p_k}{p_0} \right)^{\frac{1}{m}} - 1 \right]$
2	Delivery coefficient due to suction dumping	$\lambda_{pr} = 1 - \frac{1 + c}{\lambda_c} \left(\frac{\Delta p}{p_0} \right)$
3	Delivery coefficient due to heating	$\lambda_z = 1 - 0,025 \left(\frac{p_k}{p_0} - 1 \right)$
4	Delivery coefficient due to flow	$\lambda = \lambda_c \cdot \lambda_{pr} \cdot \lambda_z \cdot \lambda_n$
5	Real compressor volume [m ³ /s]	$V_s = \frac{V}{\lambda}$
6	Indicated mean effective pressure [MPa]	$p_{it} = \frac{\kappa}{\kappa - 1} p_0 \left[\left(\frac{p_k}{p_0} \right)^{\frac{\kappa - 1}{\kappa}} - 1 \right]$
7	Required theoretical indicator power to drive an idela compressor [kW]	$P_{tk} = V_s \cdot p_{it}$
8	Coefficient of indicator pressure	$\rho = \frac{p_i}{p_{tk}}$
9	Indicated mean effective pressure of real compressor [MPa]	$p_i = \rho \cdot p_{it}$
10	Indicator power [kW]	$P_i = p_i \cdot V_s$
11	Power required to overcome fricton [kW]	$P_{tr} = p_{tr} \cdot V_s$
12	Effective compressor power [kW]	$P_e = P_i + P_{tr}$
13	Mechanical efficiency coefficient	$\eta_m = \frac{P_i}{P_e}$
14	Indicator coefficient of useful effect	$\eta_i = \frac{\lambda}{\rho}$
15	Theoretical compressor power [kW]	$P_T = P_i \cdot \eta_i$
16	The power of electric motor to drive the compressor [kW]	$P_{EM} = (1,15 + 1,2) \cdot P_e$

3. CLIMATOLOGAL DATA AND INITIAL CONDITIONS

Real climate data for Banja Luka are used for the analysis. These data include measurements for the period March - September 2021. The meteorological station was installed in the building of the Faculty of Mechanical Engineering in Banja Luka, and all data can be downloaded in real time or from the archive of measurements on the website <https://www.wunderground.com/dashboard/pws/IBANJA1>. The measurement were performed every 5 minutes, so that several thousand readings are obtained in one day for each measurement parameter. In order to obtain the average value for one month, first the average value per day was determined and then the average value for a certain month. Input data for the average monthly outdoor air temperature for the summer period for the City of Banja Luka are given in Table 3.

Table 3. Average monthly outdoor air temperature

Exp no.	Month	Average outdoor air temperature [°C]
1	March	10.44
2	April	22.02
3	May	19.62
4	June	27.32
5	July	28.32
6	Avqust	31.64
7	September	22.49

The highest average monthly temperature in the summer period is in the August and it's 31.64 °C, and the lowest is in March and it's 10.44 °C.

The following initial conditions are adopted for the analysis:

- Indoor temperature -3°C;
- Cooling capacity 50 kW;
- Reciprocating compressor;
- In order to achive stable operation of the system, the lowest condensation temperature is 25 °C;
- Temperature differences for evaporation is 7 °C and for condensation is 10°C.

Based on the average monthly outdoor air temperatures and adopted temperature differences, the temperature and pressure of evaporation as well as the temperature and pressure of condensation are determined for each month separately. Based on the obtained pressures, the degree of compression in the system is determined. The ratio of condensation and evaporation pressures for all analyzed months is less than 8, which corresponds to one-stage compression. Tables 4, 5 and 6 show the obtained values for each month separately.

Table 4. Evaporation and condensation temperature of the working medium

Exp no.	Month	Average outdoor air temp. [°C]	Evaporation temp. [°C]	Condensation temp. [°C]
1	March	10.44	-10	25
2	April	22.02	-10	32.0
3	May	19.62	-10	29.6
4	June	27.32	-10	37.3
5	July	28.32	-10	38.3
6	August	31.64	-10	41.6
7	September	22.49	-10	32.5

Table 5. Evaporation and condensation pressure of the working medium

Exp no.	Month	Evaporation pressure [bar]	Condensation pressure [bar]	Ratio of condensation and evaporation pressures
1	March	2.006	5.792	2.89
2	April	2.006	8.169	4.07
3	May	2.006	7.618	3.80
4	June	2.006	9.466	4.72
5	July	2.006	9.725	4.85
6	August	2.006	10.625	5.30
7	September	2.006	8.286	4.13

4. RESULTS AND DISCUSSION

Table 5 summarizes the results of the analysis for each month. The values of the COP and the power of the electric motor for driving the compressor are given. Figure 3 gives a graphical representation of the results.

Table 6. The values of the COP and the power of the electric motor for driving the compressor in dependence of temperature of outdoor air

Exp no.	Month	Average outdoor air temperature [°C]	COP	Electric motor power[kW]
1	March	10.44	7.03	12.8
2	April	22.02	6.38	16.1
3	May	19.62	7.031	14.9
4	June	27.32	5.52	19
5	July	28.32	5.11	19.6
6	August	31.64	4.65	21.7
7	September	22.49	5.84	16.3

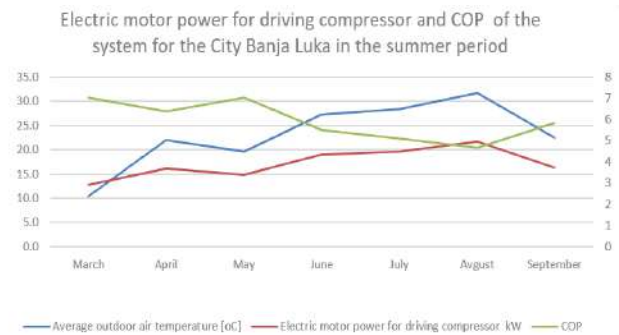


Fig. 3. The values of the COP and the power of the electric motor for driving the compressor in dependence of temperature of outdoor air

The highest COP of the system is 7.03 and corresponds to the lowest outdoor air temperature of 10.4°C and that is for the month of March. On the contrary, for the month of March is the lowest power required to drive the electric motor of the compressor and it's 12.8 kW. The lowest COP of the system is 4.65, which corresponds to the hottest month in the summer period, August, with an outdoor air temperature of 31.6 °C. In this month, the highest power of the electric motor to drive the compressor is required and it is 21.7 kW.

5. CONCLUSION

Looking at the results, it can be concluded that the COP of the system decreases as the temperature of the outside air increases per month, while the required power of the electric motor to drive the compressor increases. The

reason for this is that as the outdoor air temperature increases, the temperature differences that the compressor needs to overcome also increase, and therefore more power is needed to achieve this. As the cooling capacity is a constant value, and as the outdoor air temperature increases, the required power to achieve the same useful effect increases, the COP must decrease. This is important for the reason that these systems could be properly planned and designed so they could provide the required cooling effect for which they are used.

6. LITERATURE

- [1] Đuričković, V. (2000). *Transformatori toplote – termodinamičke osnove*, UNIBL, Beograd – Banja Luka
- [2] Vujić, S. (1983). *Rashladni uređaji*, Faculty of Mechanical Engineering Belgrade, Belgrade
- [3] Markoski, M. (2006). *Rashladni uređaji*, Faculty of Mechanical Engineering Belgrade, Belgrade



Banja Luka
1-2 Jun 2023.

DEMI 2023

16th International Conference on Accomplishments in Mechanical and Industrial Engineering

www.demi.mf.unibl.org



Wastewater as a new source of energy

V. Sustersic^{a*}, N. Aleksic^a, N. Rakic^a, M. Josijevic^a

^aFaculty of Engineering, University of Kragujevac, Sestre Janic 6, 34000 Kragujevac, Serbia

Abstract *Wastewater generated in municipalities and industries contains harmful pollutants which can have a negative impact on the environment. In developed countries, about 70-80% of municipal and industrial wastewater is collected and requires appropriate treatment and disposal. Treating wastewater takes a significant amount of energy – just under 1% of Europe's total energy consumption. However, wastewater contains significant energy potential. From the technical, economic and formal-legal side, they can be used in two ways: by using the thermal energy of wastewater and processing it to the level of technical water and its reuse. Also, sludge from wastewater treatment plant can be used in processes of anaerobic or co-digestion for production of biogas. This paper analyzes the possibility of using heat pumps and heat exchangers for wastewater heat recovery in buildings, as well as the possibility of using sludge in anaerobic digestion or co-digestion processes.*

Keywords *wastewater, co-digestion, heat recovery*

1. INTRODUCTION

The residential sector typically accounts for 30-40% of total energy consumption and carbon dioxide emissions in OECD countries [1]. In its effort to mitigate global warming, the European Union (EU) has set a target to reduce the carbon footprint of its buildings (Energy Performance of Buildings Directive (EPBD) [2]) which requires all new buildings to be nearly zero energy buildings from 2021. At the same time, the increase in the standard of living and the rapid development of the economy led to an increase in the daily production of household waste water.

Environmental protection policy aims to reduce pollution, and appropriate technologies in the field of wastewater heat recovery could contribute to this goal [3]. At the same time, EU Directive 2018/2001 recognized wastewater as a renewable source of heat [4], and the European Green Deal Investment Plan provides additional subsidies to member states for the implementation of waste heat reuse measures [5].

Wastewater from households, industry and the commercial sector contains considerable amounts of thermal energy after discharge into the sewage system [1]. From the technical, economic and formal-legal side, they can be used in two ways: using the thermal energy of wastewater and its reuse using heat pumps and heat exchangers, on the one hand (at the level of consumers, buildings, sewers and facilities), as well as using the sludge created in the wastewater treatment processes in the processes of anaerobic digestion and co-digestion to obtain biogas/energy, on the other hand.

Considering the plans [6] to build a wastewater treatment plants (WWTPs) in all settlements in Serbia, which are larger than 2,000 population equivalent (PE), by the year 2041, it can be adopted that it is profitable and acceptable for cities with over 50,000 PE to have anaerobic digestion and biogas production. In this sense, it can be accepted that in the medium term, these plants will represent a significant potential for the use and production of energy, including through heat pumps [7].

2. WASTEWATER HEAT RECOVERY

The heat energy in the wastewater could be recovered quite easily by using a heat exchanger placed in the wastewater flow and by the subsequent installation of a heat pump. In that scenario, wastewater heat recovery (WWHR) could take place at three different locations in the wastewater: (a) appliance level (usually at the shower), (b) building level (in the building), (c) sewer level (sewer network or a pumping station), and (d) WWTP level (in front of or behind the wastewater treatment plant) (Figure 1).

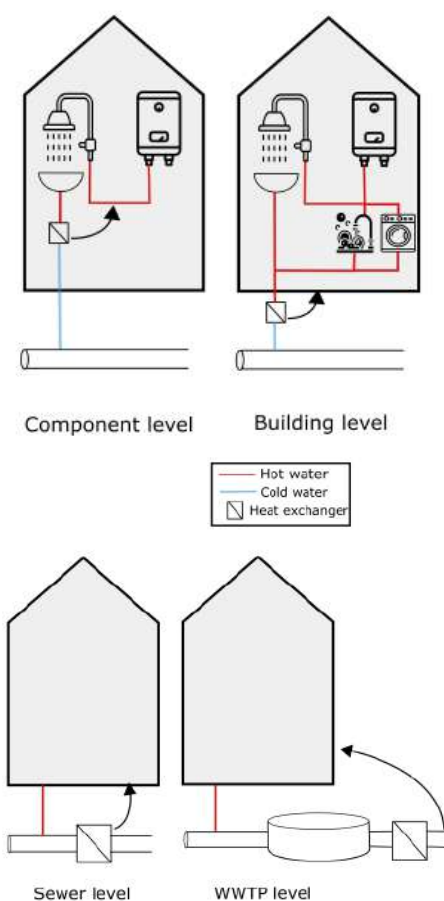


Fig. 1. Possibilities for heat energy recovery from wastewater [1]

The advantage of the last variant is high and continuous flows of (treated) wastewater, but this variant is often associated with unfavorable distances of energy supply, due to the remote location of the WWTP from the settlement. It should also be noted that heat extraction from

wastewater can have an undesirable effect on temperature-sensitive treatment processes in WWTP [8].

In the first two cases, the situation is reversed, i.e. flows of (untreated) wastewater are discontinuous, but usually closer to potential consumers [8].

The implementation of heat pumps in centralized wastewater treatment systems has been known since the 80's of the last century, while more recently the possibilities for heat recovery in buildings have been considered, especially variants of heat recovery at the consumer itself, most often on showers [9].

The average temperature of grey water discharged from household is about 30°C. The installation of horizontal and vertical heat exchangers at the consumer in houses/buildings ensures high efficiency because there is no time delay between the available waste heat and the need for heat energy (Figure 2). In this way, the need for heat storage is eliminated, thus avoiding losses [10].

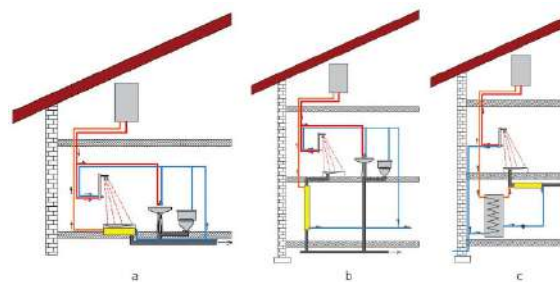


Fig. 2. Different types of drain water heat exchanger in household [11]

There are several places where hot water is used in buildings, including showers, bathtubs, washing machines, sinks, dishwashers, etc. The temperature, flow rate, frequency, and capacity of wastewater flow at a specific location depends on the consumer's water consumption pattern as well as seasonal and daily influence. These waters contain less pollutant and have higher temperature (Table 1).

Table 1. DHW end-use temperature [12, 13]

End-use type	Temperature [°C]
Hand washing	35-60
Washing and shaving	35

Dish washing	55-60
Showering	40-60
Bathing	40

At the level of residential buildings, due to the small volumes of wastewater flow and the high economic costs, heat pumps are not a viable option for heat recovery, but they are suitable for use in non-residential buildings. Facilities such as hotels, dormitories, hospitals are very interesting from the aspect of utilizing the heat of their wastewater using heat exchangers and/or heat pumps. For example, in the hotel facility "Tornik" on Zlatibor, a system for the preparation of sanitary water and central heating with water/water type heat pumps that use the energy of waste sanitary water was installed, and a cooling system was also provided in parallel [14].

Average water temperatures in sewer range from approximately 12°C in the winter, to over 20°C in the summer. But, the temperature of the sewage may drop significantly during cold weather or heavy rainfall, which can temporarily reduce the amount of recoverable heat. When it comes to installing heat exchangers in sewage systems, there are several ways (Figure 3):

- heat exchanger embedded in the sewage pipe,
- heat exchanger integrated in concrete wall of a sewage pipe and
- external heat exchanger placed above the ground [15].

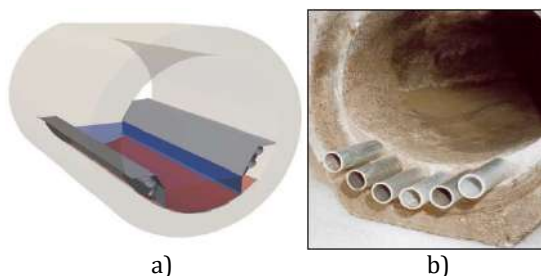


Fig. 3. Different design and types of the heat exchangers [16, 17]

The heat recovery from wastewater can be performed before WWTP from the raw wastewater (locations upstream in sewer network), or after the treatment in the WWTP (Figure 4). Which solution will be chosen depends on specific conditions, but the rule applies that the further we move away from

households, the temperature drops, and the flow increases. On the other hand, the problem of negative impact on the WWTP performance arises as the temperature drops, because the purification efficiency depends on the inlet temperature [18].

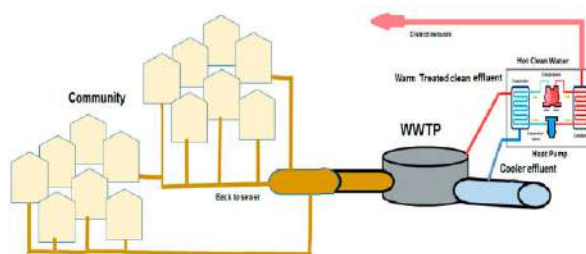


Fig. 4. Possibilities for heat energy recovery from wastewater treatment plant after WWTP [18]

Examples of application of heat pumps for heat recovery from WWTP can be found in Switzerland, Russia, Croatia and Scandinavia. It can be noted that there are significant variations in the coefficient of performance of heat pumps (COP) installed at WWTPs around the world [19]. For example, COP of heat pumps that are installed at WWTPs is 3, unlike those that are installed in buildings which is 7. The difference in temperature results in a difference in the COP of heat pumps on WWTP and buildings [20].

2.1 Legal frameworks

Numerous authors have identified wastewater as a significant source of heat for heating buildings. But, in general, there are no regulatory restrictions for the supply of waste heat into district heating (DH) networks, since virtually all waste heat supply situations are regulated using bi-lateral contracts between the DH network operator/utility and the company "owning" the waste heat [21]. In order to encourage wastewater heat recovery, governments can introduce wastewater heat recovery in their respective building codes and guidelines aimed at improving energy efficiency and reducing energy consumption and emissions. For example, in Germany, the Committee for Industrial Standards was established in 2021 to standardize the different methods used in measurements on wastewater heat recovery devices into a uniform performance and hygiene test procedure. Also,

the EU regulation 812/2013 (Energy labelling of water heaters, hot water storage tanks and packages of water heater and solar device) is getting revised in 2022 to introduce wastewater heat recovery in combination with water heaters to improve their EU energy label [22].

3. BIOGAS RECOVERY BY ANAEROBIC AND CO-DIGESTION

The application of sewage sludge obtained during different wastewater treatments fits into the objectives of the circular economy [21]. Sewage sludge is characterized by a high concentration of organic and nutrient substances, heavy metals and pathogens. Therefore, it is necessary to apply the treatment before energy valorization or final disposal. Wastewater treatment is of vital importance for environmental protection, but it is also an energy-intensive activity. Municipal wastewater treatment accounts for about 3% of global electricity consumption and 5% of global greenhouse gas emissions [23].

On the other hand, waste management, recycling, mitigating climate impacts and reducing GHG emissions represent the main goals of numerous political agendas, due to the increase in the population, increased demand for energy and due to the increase in the amount of waste. Taking into account the negative environmental impacts of landfilling, burning or composting waste, anaerobic digestion represents an economical technology for the production of renewable energy sources, as well as for the treatment of waste and/or sewage sludge containing a high percentage of moisture and energy-rich materials.

During digestion, anaerobic microbes convert different types of biomass and organic waste into biogas (60%-70% methane, 30%-40% carbon dioxide and traces of other gases such as hydrogen and hydrogen sulfide), leaving a nutrient-rich residue, which can be used for tillage use.

Anaerobic co-digestion represents the simultaneous digestion of a homogeneous mixture of two or more substrates of different organic fractions with different origins and physico-chemical compositions, in order to make the most of the complementary characteristics of their composition. It shows better process efficiency than mono-digestion, providing complementary advantages such as

better biogas yield, wider availability of nutrients, lower substrate volume, substrate variability, dilution of toxicity, synergism, etc. [24].

Removing food waste from municipal waste, space can be saved for disposal of inert waste materials with a significantly lower impact on the environment during the operation of the landfill and after its closure. Food waste can come from food preparation, or it can be fruit and vegetable waste. It is mainly characterized as easily degradable, with high moisture content, low pH and highly soluble organic ingredients, which can give a higher energy content per dry mass, i.e. food waste is rich in energy content that can significantly improve biogas yield [25].

Although anaerobic co-digestion is a relatively well-known and widely applied technology in the treatment of wastewater, sewage sludge and manure, the adoption of this technology for food waste management still faces several technical, economic and social challenges, such as the accumulation of volatile fatty acids and process instability, foaming, low buffering capacity, and high cost of transportation and processing.

An ideal co-digestion anaerobic process must include: characterization of food residues and waste production rate, facilities for the collection and separation of biodegradable waste from municipal solid waste, optimal technology for pre-treatment of biodegradable waste before the co-digestion process, regulated control and reactor construction for the desired manipulation of metabolic reaction, improving the quality of biogas in order to reduce the costs of subsequent purification and an efficient plan for using digestate for composting, in order to achieve optimal working conditions and obtain the highest possible yield of biogas (from 10-over 50%) [26].

4. CONCLUSION

Today, about 35% of the EU's buildings are over 50 years old and almost 75% of the building stock is energy inefficient. Wastewater heat recovery is currently not yet officially recognized and therefore its application does not bring constructors any legal improvements in the energy efficiency, despite the obvious energy savings. This paper aims to provide an overview of wastewater heat recovery and the possibility of using sludge in anaerobic

digestion or co-digestion processes. The performance of these systems varies depending on the type of energy users, equipment and system design, as well as their own maintenance.

Instead of the energy consumption that is a common feature of aerobic process, anaerobic digestion is accompanied by the production of biogas that can be used as an energy source. Unlike landfilling, incineration or composting, anaerobic digestion or co-digestion is the only waste treatment method that meets the sustainability requirements by restoring the waste's energy content in the form of the methane and nutrient content. Therefore, co-digestion of municipal organic waste in combination with municipal sludge not only enables the treatment facilities to be energy neutral, but also reduces the costs of municipal organic waste management.

REFERENCES

- [1] Nagpal, H., Spriet, J., Mutali K. M., McNabola, A. (2021) Heat Recovery from Wastewater—A Review of Available Resource, *Water*, 13, 1274. <https://doi.org/10.3390/w13091274>
- [2] Directive (EU) 2018/844 of the European Parliament and of the Council of 30 May 2018 amending Directive 2010/31/EU on the energy performance of buildings and Directive 2012/27/EU on energy efficiency
- [3] Hadengue, B., Morgenroth, E., Larsen A.T. (2022) Screening innovative technologies for energy-efficient domestic hot water systems, *Journal of Environmental Management*, 320 115713, <https://doi.org/10.1016/j.jenvman.2022.115713>
- [4] Directive (EU) 2018/2001 of the European Parliament and of the Council of 11 December 2018 on the promotion of the use of energy from renewable sources. Off. J. Eur. Union 2018, 5, 82–209.7
- [5] Sustainable Europe Investment Plan European Green Deal Investment Plan; Technical Report; European Commission: Brussels, Belgium, (2020). Available online: <https://eurlex.europa.eu/legalcontent/EN/TXT/?uri=CELEX%3A52020DC0021> (accessed on 29 March 2023).
- [6] WATER MANAGEMENT STRATEGY IN THE TERRITORY OF THE REPUBLIC OF SERBIA UNTIL 2034 ("Official Gazette of RS", No. 3/2017) (in Serbian)
- [7] Ivezić, D., Živković, M., Madžarević, A., Pavlović, B. (2022) Possibilities for Utilization of Waste Heat from Wastewater Treatment Plants by Heat Pumps, *Energy, economy, ecology*, XXIII, no 1, p. 162-166
- [8] Huber, F., Neugebauer, G., Ertl, T., Kretschmer, F. (2020) Suitability Pre-Assessment of in-Sewer Heat Recovery Sites Combining Energy and Wastewater Perspectives, *Energies*, 13, 6680. <https://doi.org/10.3390/en13246680>
- [9] Hadengue, B., Joshi, P., Figueroa, A., Larsen, A. T., Blumensaat, F. (2021) In-building heat recovery mitigates adverse temperature effects on biological wastewater treatment: A network-scale analysis of thermal-hydraulics in sewers, *Water Research*, 204, 117552. <https://doi.org/10.1016/j.watres.2021.117552>
- [10] Davila, A.R., Cejudo, M.C.E., Stoughton, K. (2020) *Domestic Hot Water Temperature Maintenance Technology Review*, Technical Report PNNL-SA-156938 United States. <https://doi.org/10.2172/1813897>
- [11] Vaičiūnas, J., Geležūnas, V., Valančius, R., Jurelionis, A., Ždankus, T. (2016) Analysis of Drain Water Heat Exchangers System in Wellness Center, *Journal of Sustainable Architecture and Civil Engineering*, vol. 17, no 4. p. 15-23 <http://dx.doi.org/10.5755/j01.sace.17.4.16294>
- [12] Bertrand, A., Mastruccia, A., Schülerb, N., Aggounec, R., Marécha, F. (2017) Modelling of Domestic Hot Water End-Uses for Integrated Urban Thermal Energy Assessment and Optimisation, *Applied Energy*, vol. 186(P2), p.152-166
- [13] Davila, A.R., Cejudo M.C.E., Stoughton, K. (2021) *Domestic Hot Water Temperature Maintenance Technology Review*, Technical Report PNNL-SA-156938 United States. <https://doi.org/10.2172/1813897>
- [14] Tornikova energana <https://www.inzenjer.net/projekti/tornikova-energana/> (accessed on 29 March 2023).
- [15] Oesterholt, F., Hofman J. (2015) *Feasibility of small scale heat recovery from sewers*, report, BTO 2015.208(s), Water Research Institute
- [16] Podobeková, V., Peráčková, J. (2013) Heat exchangers in sewage pipes, *The Holistic Approach to Environment*, vol. 4, no. 2, p. 91-96
- [17] Niewitecka, K. (2018) Possibilities of heat energy recovery from greywater systems, E3S Web of Conferences 30, *Water, Wastewater and Energy in Smart Cities*, 03003 <https://doi.org/10.1051/e3sconf/2018300303>

- [18] Ali, S.F., Gillich, A. (2021) Opportunities to decarbonize heat in the UK using Urban Wastewater Heat Recovery, *Building Services Engineering Research and Technology*, Vol. 0(0) p.1–18
<https://doi.org/10.1177/01436244211034739>
- [19] Golzar, F., Silveira, S. (2021) Impact of wastewater heat recovery in buildings on the performance of centralized energy recovery – A case study of Stockholm, *Applied Energy*, 297 117141.
<https://doi.org/10.1016/j.apenergy.2021.117141>
- [20] Meggers F, Leibundgut H. (2011) The potential of wastewater heat and exergy: Decentralized high-temperature recovery with a heat pump. *Energy Building*; 43: p. 879–86.
<https://doi.org/10.1016/j.enbuild.2010.12.008>
- [21] Zarei, M. (2020) Wastewater resources management for energy recovery from circular economy perspective, *Water-Energy Nexus*, 3, p. 170–185.
<https://doi.org/10.1016/j.wen.2020.11.001>
- [22] Sevela, P., Frenger, J., Schnieders, J., Pfluger, R. (2022) The potential of Waste Water Heat Recovery Systems in reducing the energy demand for water heating in the EU in a cost-efficient way, CLIMA, the 14th REHVA HVAC World Congress, 22-25 May, Rotterdam, The Netherlands
<https://doi.org/10.34641/clima.2022.439>
- [23] Zhou, X., Yang, F., Yang, F., Feng, D., Pan, T., Liao, H. (2022) Analyzing greenhouse gas emissions from municipal wastewater treatment plants using pollutants parameter normalizing method: case study of Beijing, *Journal of Cleaner Production*, vol 376, 134093
<https://doi.org/10.1016/j.jclepro.2022.134093>
- [24] Mata-Alvarez J, Macé S, Llabrés P (2000) Anaerobic digestion of organic solid wastes. An overview of research achievements and perspectives. *Bioresource Technology* 74:3–16.
[https://doi.org/10.1016/S09608524\(00\)0003-7](https://doi.org/10.1016/S09608524(00)0003-7)
- [25] Bong, C.P.C., Lim, L.Y., Lee, C.T., Klemeš, J.J., Ho, C.S., Ho, W.S. (2018) The characterisation and treatment of food waste for improvement of biogas production during anaerobic digestion – A review, *Journal of Cleaner Production*, vol. 172, p. 1545-1558,
<https://doi.org/10.1016/j.jclepro.2017.10.199>
- [26] Morales-Polo, C., Cledera-Castro, M., Soria, B. Y.M. (2018) Reviewing the Anaerobic Digestion of Food Waste: From Waste Generation and Anaerobic Process to Its Perspectives, *Applied Sciences*, 8, 1804;
<https://doi:10.3390/app8101804>



Banja Luka
1-2 Jun 2023.

DEMI 2023
**16th International Conference on
Accomplishments in Mechanical and
Industrial Engineering**
www.demi.mf.unibl.org



Air Fluidized Bed Thermal Diffusivity Coefficients

J. Janevski^a, P. Živković^a, M. Vukić^a, G. Cvetanović^b, M. Tomić^c

^a Faculty of Mechanical Engineering, University of Niš

^b Faculty of Technology, University of Niš

^c Faculty of Technical Sciences, University of Novi Sad

Abstract The paper presents experimental research of thermal conductivity and thermal diffusivity coefficients of the siliceous sand bed fluidized by gas. It also provides an outline of research on these coefficients conducted so far by various authors. The results were compared according to conditions in the performed experiments. Based on the experimental research, the influence of the process's operational parameters on the obtained values of the bed's thermal conductivity has been analyzed. The results show direct dependence of thermal conductivity on the intensity of mixing, the fluidization rate, and the size of particles. In the axial direction, the coefficients which have been treated have values one order higher than in the radial direction. Comparison of performed experimental research with experimental results of other authors shows good agreement and the same tendency of thermal conductivity change, depending on the particle size and mixing intensity. The research was financially supported by the Ministry of Education, Science and Technological Development of the Republic of Serbia (Contract No. 451- 03-9/2021-14/200109).

Keywords fluidized bed, heat transfer, experiment, thermal diffusivity, thermal conductivity

1. INTRODUCTION

Ever since its emergence, the fluidization phenomenon has attracted the attention of numerous researchers. Its appliance in numerous technological operations stems from its excellent properties, which are reflected in: intensive mixing of solid particles, a high contact-surface between gas and solid particles, an almost constant temperature in the entire bed, as well as simple insertion and removal of the material from the bed. Due to its good characteristics, the fluidized bed has an important application in various industrial processes, such as coal carbonization, drying of small-grained materials, calcination of ores and other materials, cracking distillation of oil derivatives, mixing of powders, freezing of food, gasification of coal, etc. In the past several decades, numerous papers and studies of the process of fluidization and its application have

been published, most of which are based on experimental research. The field of heat conduction has been of high interest to researchers, since the fluidized bed is characterized by high heat conductivity. Yet, despite the variety papers which deal with this problem, their authors' conclusions are highly disparate, sometimes even contradictory. The reasons for this scattering of results lie in different conditions in which these experiments are performed. These facts have motivated experimental research with the main goal of determining thermal diffusivity and thermal conductivity coefficients of the fluidized bed for particles of siliceous sand of different fractions. The influence of the most important parameters on the values of thermal diffusivity and conductivity coefficients of the fluidized bed has been analyzed through obtained experimental results; also, experimental studies of different authors have been considered.

2. THERMAL CONDUCTIVITY OF THE FLUIDIZED BED

Since specific thermal capacity of solid particles is volumetrically higher than specific thermal capacity of a gas by several orders of magnitude, moving particles are basic heat holders in the bed. Transfer of heat by the flow of gas is relatively small and, consequently negligible. In this case, Fourier's equation can be used for describing the process of heat transfer in the fluidized bed, where thermal diffusivity coefficient reflects the intensity of the mixing of material in the bed. Its value can be measured by a modified method of the instantaneous heat source, whose essence is as follows: a strong instantaneous thermal impulse is created in the fluidized bed by quickly pouring a small portion of previously heated particles of that same material, and the moment of achieving maximal temperature τ_{\max} ($\tau_{\max} = r^2/2\alpha$) at certain distance from the heat source is registered. The movement of bubbles enables the mixing of particles in the emulsion phase, both in the direction of the bed's height, and in the radial direction, whereby a certain amount of particles passes through any observed intersection of the bed. Since particles in the non-isothermal bed differ with respect to the value of enthalpy, a resulting flux of warmer particles will appear if their concentration is higher on one side of the observed intersection. Assuming that the concentration of warmer particles per unit of volume changes in the direction of the flow of particles only, their resulting thermal flux per unit of surface can be expressed as:

$$q = -D_s \frac{dH}{dx}. \quad (1)$$

If the following expression of enthalpy is introduced into the expression (1):

$$H = \rho_n \cdot h = \rho_p \cdot (1 - \varepsilon_{mf}) \cdot c_p \cdot t, \quad (2)$$

Corresponding author

Full profesor, Jelena Janevski,
jelena.janevski@masfak.ni.ac.rs

University of Niš
 Faculty of Mechanical engineering
 Niš, Serbia

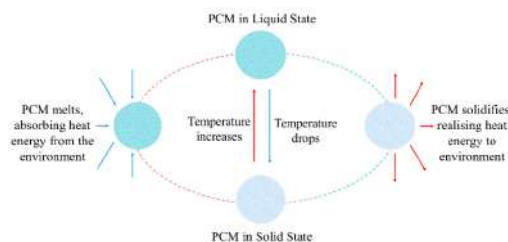


Fig. 1. Phase change processes in phase change materials

Overall, PCMs are a promising solution for energy storage in renewable energy and thermal energy storage systems. The selection of the appropriate PCM depends on various factors such as the required energy storage capacity, melting temperature, thermal conductivity, and stability. Therefore, ongoing research and development of PCM-based energy storage systems are essential to improve the performance and efficiency of renewable energy and TES systems.

However, the volume changes during solid-gas and liquid-gas phase transitions cause practical problems for commercial applications. Solid-liquid PCMs, on the other hand, have been mass-marketed and classified into three groups: organic, inorganic, and eutectics.

Inorganic PCMs are usually salt hydrates or metals. Salt hydrates, which are a mixture of inorganic salts and water, have high thermal energy storage capacity and thermal conductivity. However, their incongruent melting behavior and supercooling phenomenon limit their applications. Metals, on the other hand, have high thermal conductivity and mechanical properties, and are used for high-temperature PCMs. Some metals, such as indium, cesium, gallium, etc., are used for low-temperature PCMs.

Organic PCMs are classified into two major groups: paraffin and non-paraffin. Paraffins, which are the most common type of organic PCM, are stable over numerous phase change cycles and do not exhibit the supercooling phenomenon. Non-paraffin organic PCMs, such as fatty acids, glycols, polyalcohols, and sugar alcohols, have high latent heat capacity, but are flammable and have low thermal conductivity, low combustion temperatures, and transient toxicity. Fatty acids have high stability and do not exhibit supercooling, but are more expensive than technic-grade paraffins, and are of animal or plant origin.

we obtain:

$$q = -D_s \cdot \rho_p \cdot (1 - \varepsilon_{mf}) \cdot c_p \cdot \frac{dt}{dx} = -\lambda \cdot \frac{dt}{dx}, \quad (3)$$

where λ is thermal conductivity coefficient of the fluidized bed, which is defined as:

$$\lambda = D_s \cdot \rho_p \cdot (1 - \varepsilon_{mf}) \cdot c_p = a \cdot \rho_n \cdot (1 - \varepsilon_{mf}) \cdot c_p = a \cdot \rho_n \cdot c_p. \quad (4)$$

3. RESEARCH ON THERMAL DIFFUSIVITY AND THERMAL CONDUCTIVITY OF THE FLUIDIZED BED - A REVIEW

For determining thermal diffusivity coefficient in the axial direction, Borodulja et al. [1] used a glass pipe, length 1m, diameter 80mm. On the upper surface of the bed, an instantaneous surface heat source was created by pouring a small portion (5-7% volumetrically) of particles heated in a furnace up to the temperatures 100-700°C. The time of particle pouring was less than 0.5s. For measuring the temperature of the bed, two thermocouples were used; one of them was placed on the distributor, the other at half the height of the bed. Measurements were performed with several mono-dispersion and poly-dispersion fractions of different types of material for different heights of the stagnant bed. The processing of experimental data has shown that thermal diffusivity coefficient in the axial direction can be described by the following equation:

$$a_a = 0,44(N - 1)^{0,54} Ar^{0,144} (1 - \varepsilon_f)^{-1} \left(\frac{H_{mf}}{D_t} \right)^{1,3} \quad (5)$$

Determination of thermal diffusivity coefficient in the radial direction is performed in a pipe with diameter 175mm. Instantaneous spot heat source was obtained by quickly pouring a small portion of warm sand particles along the axis of the apparatus through a glass pipe 25mm in diameter. For temperature measurement, a thermocouple was placed at the height of the particle pouring from the pipe, at the distance of 60-70mm from the axis.

The research has shown the highly intensive mixing of material in the fluidized bed in the axial direction. Axial thermal diffusivity

coefficient was within $a_a = (10-60) \text{ cm}^2/\text{s}$. Material mixing in the radial direction was relatively small. Radial thermal diffusivity coefficient values were: $a_r = (0.4-1.5) \text{ cm}^2/\text{s}$.

In their published paper [2], Peters, Orlichek, and Schmidt tried to calculate thermal conductivity coefficient by determining the temperature profile of the fluidized bed. The apparatus was in the shape of a parallelepiped, width 65mm, length 450mm, height 480mm, which was not completely filled with sand ($d_{ekv}=0.23\text{mm}$). As a source of heat, they used an electric heater consisting of a wire spiral, which provided heat evenly along the transverse section of the bed. Thermal insulation of the vessel kept heat loss through the wall lower than 7%. Calculated numerical values of thermal conductivity in the axial direction were within (1163-1977) W/mK, while in the radial direction, they were of order (1200-2000) W/mK. Zabrodski [1] states that those values are significantly increased, and that they are practically impossible to obtain in such experimental conditions.

The influence of apparatus geometry can be explained by qualitative conclusions formulated in experimental researches by Lewis, Gilliland, and Girouard. The apparatus they used in their experiment consisted of a vertical column, where the glass sample was located between an electric heater and a section cooled by water. Above the reactor, there was a wide precipitation section and a cyclone, which returned particles into the bed. Thermocouples were placed in a column, additionally connected to a potentiometer, which was used for measurement of temperature and temperature variances within the bed, in the axial and radial directions. The column was insulated by two layers of glass wool, and, since it consisted of several sectors, the distance between the heater and the cooler was changeable. By using various types of material (micro-spheres of catalysts, glass particles, aluminum powder) as particles for fluidization, the values of thermal diffusivity the authors obtained were within (30-600) cm^2/s . These values are matched by values of thermal conductivity which are much higher in comparison with thermal conductivity of e.g. a copper bar. Lewis and associates concluded that thermal conductivity of the fluidized bed is independent of the heater-cooler distance and the height of the stagnant layer, both for the bubble and the piston fluidization system.

Based on the foregoing facts, it can be concluded that research of thermal conductivity of the fluidized bed shows the existence of dispersion of results obtained by various authors, since they show complex dependence of thermal conductivity coefficients on various factors. Therefore, it is very difficult to give any approximation of obtained results by some global empirical dependence. For practical calculations, it is much more reliable to take absolute values of coefficient λ at a given moment, obtained by experimental research in conditions which are similar to calculated.

3. EXPERIMENTAL RESEARCH OF THERMAL CONDUCTIVITY IN THE FLUIDIZED BED

The goal of experimental research of the fluidized bed in this paper is determination of thermal conductivity coefficient and thermal diffusion in axial and radial directions, depending on operational characteristics of the fluidized bed: velocity, fluidization rate, and the size of particles. Experimental research was conducted on a laboratory apparatus made at Mechanical Engineering Faculty of Nis. The apparatus consists of a measuring part, above which is a pipe for the supply of heated sand into the bed, a. air supply device, and a device for measurement, regulation, and registration of the results. Special attention was paid to the construction of the device for the supply of heated sand into the bed. Material, which was previously heated up to 250-350°C, was instantaneously inserted into the fluidized bed by quick surface pouring through the pipe with diameter 45mm onto the bed surface.

A fan from the external environment supplies the air necessary for fluidization. The flow of air is measured by a standard orifice, while a valve enables the desired flow of air. The sections in front and behind the orifice are long enough to stabilize the air flow. A chamber insulated by glass wool enables even distribution of air on the intersection of the operational part of the apparatus. A distributor is placed at the inlet into the operational part of the apparatus, while a tapered extension is placed above, which prevents the removal of minor fractions. Chromel-alumel (K type) thermocouples are used for temperature measurement; one of them is placed just above the distributor, while the other is placed at the bed outlet.

4. PRIOR MEASUREMENTS

In order to start experimental determination of the thermal conductivity coefficient, certain measurements were performed prior to it. Siliceous sand with different fractions was used as material for fluidization. Siliceous sand was selected for its favorable application in numerous processes in fluidized beds (as for carbonization of coal in the fluidized bed). After the sifting in standard sieves, fractions of siliceous sand with average particle diameter 0.3mm, 0.5mm, and 0.9mm, were separated. Within prior measurements, the following characteristics were determined for each fraction:

- actual sand density ρ_p ,
- bulk sand density ρ_n ,
- equivalent particle diameter d_p ,
- porosity at minimal fluidization rate ε_{mf} ,
- minimal fluidization rate U_{mf} .

Bulk particle density of particles was determined by pouring freely a certain mass of sand into a calibrated vessel, while actual density was determined by a picnometer. The value of specific thermal capacity was taken from literature [4].

As mentioned, for determining the thermal diffusivity coefficient in the axial direction, two thermocouples are placed in the axis of the stagnant bed, whereby the first was placed at 43.5mm from the distributor, and the second on the bed surface. After this, the fan is started; by adjusting the air flow, the desired velocity of air at working temperature is obtained. At this working velocity of air, with known minimal fluidization rate, the fluidization rate was determined. In this established state, an already prepared portion of previously heated sand is almost instantaneously, inserted through the fixed pipe. During the movement of inserted hot sand through the fluidized bed, the thermocouples measured the bed temperature, while registration was performed using the acquisition system. For a set fluidization rate, separate bed temperatures were registered at each 0.02s. One can noticed that temperature in the bed increases, due to the movement of hot sand particles. At the same time, the time span between two maximal increases in temperature registered by the thermocouples is read.

For known distance between the thermocouples and read time, the value of thermal diffusivity coefficient is calculated. Since thermal diffusivity is determined in the axial direction, it is assumed that, in the equation ($T_{max} = r^2 / 2\alpha$), the value of $n=1$ [3]. For a certain fluidization rate and the existing conditions, the experiment was repeated several times. The air velocity has been increased and another experiment was performed, for the same sand fraction, in the way described above. After measuring a certain fraction, the operational part of the apparatus was emptied, and another fraction poured; the same experiment is repeated for it.

In the experiment performed, the values of thermal diffusivity coefficient in the radial direction were determined by the same procedure as the values of axial diffusivity. As was described, the difference lay in the positions of thermocouples, which were, in this case, in the same plane, and in the value of constant n , which was now $n=3$.

5. ANALYSIS OF EXPERIMENTAL RESULTS

Based on the experimental results, diagrams of dependence of change in thermal diffusivity coefficient on the fluidization rate were made. The coefficient changed as a parameter within anticipated limits, in both axial and radial directions. A comparative review of the dependence of thermal diffusion coefficient on the fluidization rate for all three sand fractions is given. This dependence is highly complex, so that explanations of the effect of velocity are sometimes contradictory in existing literature. With the increase of the fluidization rate, thermal diffusivity coefficient in the axial direction increases for all three cases of the size of sand particles, whereby different increase rates can be noticed. Naturally, it must be remembered that the main reason for the increase of thermal diffusivity coefficient with the increase of fluidization rate is more intensive mixing of particles. With particles with average equivalent diameter of 0.3mm, thermal diffusivity coefficient continually increases up to the value of the fluidization rate $N=3$, when a sudden increase of its value can be noticed, while the fluidized state becomes similar to one of the 'bad' forms of fluidization.

Uniformity of fluidization is not guaranteed for a certain fluidization rate, so that the character of the bed causes the dispersion of results.

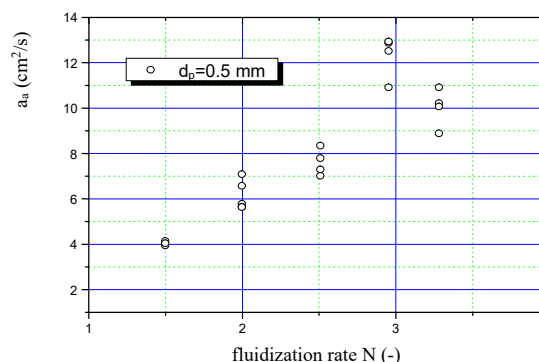


Fig. 1. Dependence $a_a=f(N)$

With particles of average equivalent diameter 0.5mm, a more intense tendency towards the increase of thermal diffusivity coefficient with the increase of the fluidization rate can be noticed (Fig. 1). The maximum of thermal diffusivity coefficient at approximate fluidization rate $N=3$ can be a consequence of increased content of smaller particles in the sand sample. However, it can be confirmed that the main reason for the occurrence of extremes is maximal intensity of mixing of particles, i.e. transition from one form of fluidization to another. In the case of the largest particles, the experiment showed the biggest increase of thermal diffusivity coefficient with the change of the fluidization rate.

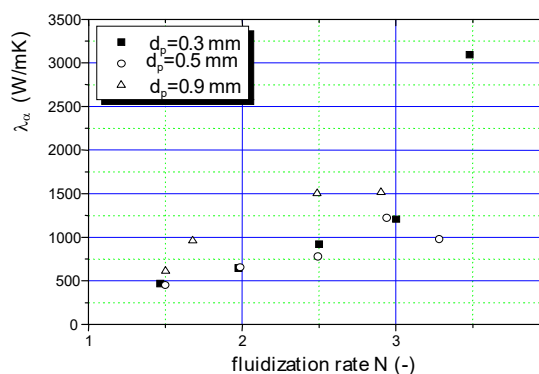


Fig. 2. Dependence $\lambda_a=f(N)$

For assessment of the intensity of mixing in the fluidized bed, coefficient of effective thermal conductivity is authoritative. In view of the interrelationship between thermal conductivity

and thermal diffusivity coefficients, Figure 2 shows the dependence of averaged values of thermal conductivity coefficient on the velocity of the fluidization agent. Since thermal conductivity and thermal diffusivity are connected through specific thermal capacity of particles and the density of the fluidized bed, which directly depends on the porosity of the bed, the way in which thermal conductivity coefficient changes with the fluidization rate is similar to the way in which thermal diffusivity coefficient changes with the fluidization rate. The maximal value of the thermal conductivity, which occurs at fluidization rate of approximately $N=2.5$, once again points to the fact that, at that velocity of the fluidization agent, mixing of particles brings about more intense contacts and collisions of solid particles. The occurrence of the maximum can also be accounted for the decrease in the density of the fluidized bed, and an increase in its porosity with the increase of the gas velocity, which may cause varying of the thermal conductivity coefficient change.

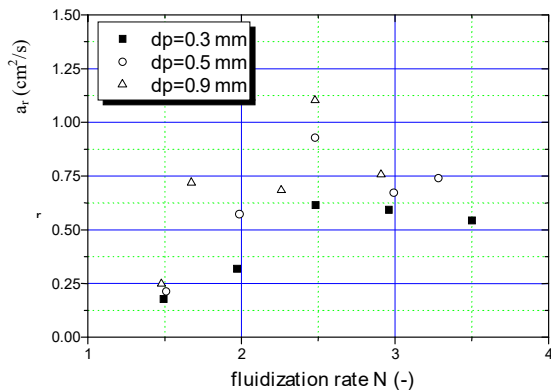


Fig. 3. Dependence $a_r=f(N)$

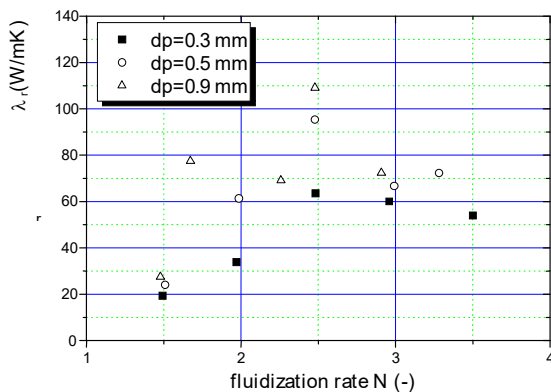


Fig. 4. Dependence $\lambda_r=f(N)$

Generally, the obtained values of thermal diffusivity coefficient in the radial direction are smaller by an entire order (Figures 3 and 4). In contrast to diffusivity coefficient in the axial direction, for this case, what can be observed with all average equivalent diameters is occurrence of the maximum of thermal diffusivity coefficient in the radial direction at fluidization rate $N=2.5$.

According to numerous researchers [1,2], local concentration of particles influences the passage of heat in the sense of its intensification, when the model of annular distribution of particles on the transverse section of the column, with a solid core in the center, a thinned bed around the core, and a dense ring next to the wall, is deteriorated.

At the same time, mixing of particles and the frequency of their mutual collisions increases, which enhances more intensive diffusion of heat. These facts show that within this fluidization rate the most optimal fluidization rate, from the standpoint of the best thermal conductivity, can be found.

Certain fluctuations of the values of thermal diffusivity can be observed in the diagrams of dependence of thermal diffusivity coefficient on the fluidization rate. The cause of these fluctuations may be successive arrival of differently heated particle packages at observed places, and sometimes bubbles which pass through the bed. When bubbles go through the bed, one of the two thermocouples may occur inside a bubble, thus registering the air temperature inside the bubble. Since the air temperature inside a bubble is higher than the temperature of air and of solid particles in the emulsion phase, an increase of temperature will occur at that place at that moment.

By means of their interaction, all treated hydrodynamic parameters influence the global heat transfer in the fluidized bed in a highly complex manner, and, consequently, thermal diffusivity and thermal conductivity coefficients. Domination of some of them occurs only in a limited range. The results obtained through the experiment point to the fact that porosity of the bed, i.e. concentration of particles, although a very important factor of heat transfer in the fluidized bed, is not independent of the particle flux, relative particle and gas velocity, and reverse mixing

6. CONCLUSION

Based on the presented results of experimental and theoretical research of thermal diffusivity and thermal conductivity coefficients in the fluidized bed which have been conducted so far, as well as on the basis of the results of our own experimental research, it has been confirmed that the fluidized bed has very good thermal conductivity, which enables its application in numerous industrial processes of heat exchange.

The results obtained in experimental research have shown that thermal diffusivity and thermal conductivity coefficients depend on the fluidized bed hydrodynamic structure. Although the change in thermal diffusivity and thermal conductivity coefficients differs in axial and radial directions, it generally depends on the fluidization rate and the size of particles.

For all treated fractions of the sand, the values of thermal conductivity coefficient of the fluidized bed in the axial direction were within 450-3100 W/mK, which also represents maximal reached value of all measurements. The obtained values of those same coefficients in the radial direction are within 19-110 W/mK, which provides a satisfactory level of agreement with the results of other authors.

Despite the complexity of the analysis of thermal conductivity through the fluidized bed and existing constraints of the used laboratory apparatuses, the obtained results provide a realistic review of thermal conductivity in the fluidized bed [3], so that they can be used with actual industrial plants, whereby all future theoretical and experimental research of the process of heat conduction in the fluidized bed should be directed towards the creation of a unique physical and mathematical model for thermal conductivity coefficient.

NOMENCLATURE

- a** thermal diffusivity coefficient (m^2/s)
- Ar** Archimedes number
- c_p** specific thermal capacity of solids (J/kgK)
- D_s** solid diffusivity (m^2/s)
- H** enthalpy (kJ/kg)
- N** the fluidization rate
- ϵ_{mf}** porosity of fluidized bed
- ρ_p** solid density (kg/m^3)

REFERENCES

- [1] Peters K., Orlichek A., Schmidt A., Chem. Ing. Tech., Vol.25, No.6, pp. 313-316, 1953
- [2] Jovanovic G. N., Catipovic N. M., Fitzgerald T. J., Levenspiel O., Fluidization (J. R. Grace, J. M. Matsen, eds.), Plenum, New York, pp. 325-332, 1990
- [3] Janevski J., Determination of the thermal conductivity and thermal diffusivity coefficients by gas fluidized beds, MSc. Thesis, Nis, 2000
- [4] Naumann E. B., Chem. Eng. Sci., No.36, pp. 957-966, 1981



Banja Luka
1-2 Jun 2023.

DEMI 2023

16th International Conference on Accomplishments in Mechanical and Industrial Engineering

www.demi.mf.unibl.org



Cascade system for optimal use of deep geothermal energy

S.I. Deaconu^a, M. Topor^a, F. Bu^b, A.M. Blaja^a

^a Politehnica University of Timisora, Victoriei Square No. 2, 300006 Timișoara, Timiș county, Romania

^b Nanjing University of Aeronautics and Astronautics, Nanjing, Jiangsu, China

Abstract *The purpose of this work is focuses on following applications: district heating systems based on geothermal water, greenhouses and fish farming heating, geothermal aqua-parks and renewable power generation by conversion of geothermal energy. Such a project is based on two drilling wells (Doublet) and a primary circuit of geothermal water. The geothermal water is actually a transporter of earth energy. The thermal water is pumped from the production well in a heat exchanger and afterwards, the water is pumped back in the geothermal aquifer, through a reinjection well placed at a specific distance. The energy of the primary circuit is transferred through the heat exchanger to a secondary circuit, being then used for heating purposes, or other cascade applications, as greenhouse heating or aquaculture facilities, electrical power generation, etc. We evaluate the thermal potential of one geothermal project in the western Romania. This value is calculated by considering one Doublet, having a depth of around 4,200m, a flow of 80-85l/s (around 83kg/s), and the thermal water temperature of at least 225°C. By having this potential, we can realize: a project for an extensive greenhouse facility, geothermal district heating system, the warm water supply and a geothermal project with cascade applications.*

Keywords *geothermal water, earth energy, cascade applications, greenhouse heating, electrical power generation.*

1. INTRODUCTION

At the moment, both the European Union and Romania face an increased need in terms of the use of fossil fuels due to the fact that these fuels are polluting and increasingly expensive. For this reason, both in the EU and in Romania there is a notable orientation towards the use of non-conventional and non-polluting fuels. Geothermal energy is included in this category because it is a renewable source and can contribute to significantly reducing carbon emissions and the greenhouse effect. In fig. 1 the map with the distribution of geothermal energy in Romania is presented [1]. Although the production of electricity cannot be totally replaced by the use of non-conventional energy

sources, obtaining energy by using non-conventional and cheap fuels determines the reduction of prices in this field and the substantial reduction of pollution. Promoting technological transfer on the energy market, through the use of non-conventional sources, is a necessity [2].

The Netherlands is the world's second-largest food exporter by value, and the country's 9000 hectares of greenhouses are a big reason why. But keeping those greenhouses the right temperature requires loss of energy, so developing alternative energy sources is a top priority in the country's efforts to meet its ambitious climate targets. The Dutch government has pledged to be free of natural gas by 2030 and reduce CO₂-equivalent

emissions by 49 percent compared to 1990 levels [3]. The greenhouse sector is already taking steps toward using renewable energy, with several geothermal energy plants coming online in recent years. Geothermal heating works by pumping up warm water from deep inside the earth (usually 1,000 to 5,000 meters deep). The warm water can then be used to heat greenhouses, reducing the need for natural gas and other fossil fuels. Heat exchangers play a key role in harnessing the benefits to geothermal energy, ensuring efficient heat transfer between the warm water coming up from the ground and the cooler water that has been used to heat greenhouses or other buildings [5]. The United Nations has adopted 17 Sustainable Development Goals for 2030, known as Global Goals, that world leaders have pledged to achieve. Now it is up to businesses like ours to take us there. Geothermal heating works by extracting the heat from underground water sources. The further underground the water, the hotter it usually is. In the Netherlands, geothermal heat plants pump warm water up from depths of at least 500 meters. After the water has been used, the cooler water is returned to the ground [6].

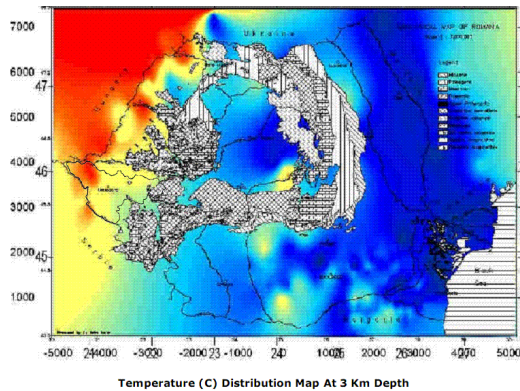


Fig. 1 Geothermal energy map in Romania - EBRD Study.

Such a project is based on two drilling wells (Doublet) and a primary circuit of geothermal water. The geothermal water is actually a transporter of earth energy. The thermal water is pumped from the production well in a heat exchanger and afterwards, the water is pumped back in the geothermal aquifer, through a reinjection well placed at a specific distance [7]. The energy of the primary circuit is transferred through the heat exchanger to a secondary

circuit, being then used for heating purposes, or other cascade applications, as greenhouse heating or aquaculture facilities, electrical power generation, etc (fig. 2). The paper presents the possibility of using geothermal energy for the production of electricity at medium temperatures. In the analyzed area, there is an important geothermal water reservoir of medium temperatures, which can be used for the successful implementation of the solution for obtaining electricity in low-power electro-geothermal stations [8].

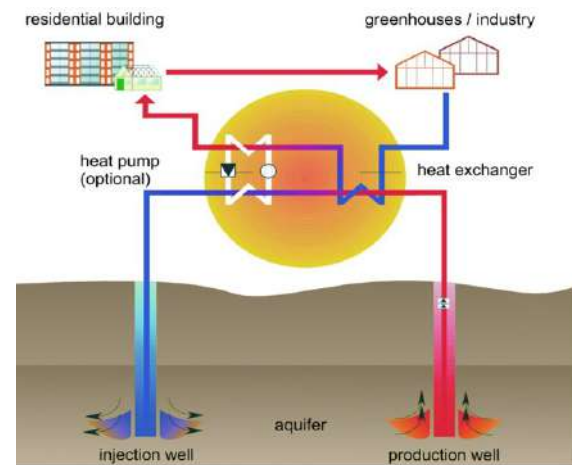


Fig. 2 The primary and secondary circuits of geothermal water for cascade applications.

2. USE OF GEOTHERMAL ENERGY AT MEDIUM TEMPERATURES FOR THE PRODUCTION OF ELECTRICITY

Over time, there have been four different methods used to obtain electricity from geothermal resources: the steam expansion cycle, the organic Rankine cycle (ORC), the Kalina cycle and thermoelectric generators. Analyzing the conversion processes listed above, power plants using thermoelectric generators are eliminated first, as they have an efficiency of only one tenth of the efficiency of the Carnot cycle. The other analyzed processes have an efficiency of approximately half that of the Carnot cycle. The Carnot efficiency is theoretically the highest that can be achieved by converting geothermal energy into mechanical energy. In addition to the low efficiency of the geothermal fluid in a steam expansion system, at low temperatures it is difficult to find suitable turbines that work at low pressure. This is the main reason why processes based on binary cycles were developed. When the

amount of heat is reduced and therefore when the power of the plant is reduced, using fluids other than water, an advantageous situation is reached from an economic point of view. Consequently, in the analyzed case, only the ORC and Kalina cycles are taken into account. In Fig.3, the ORC and Kalina cycles are compared in terms of yield. For the ORC cycle, the working fluid is isopentane [1]. As can be seen from the graph, the Kalina cycle has a better yield than the isopentane ORC cycle. In Fig.4, the ORC and Kalina cycles are compared from the point of view of theoretical net power [2]. Solid lines characterize the Kalina cycle and dashed lines characterize the ORC cycle. Lines marked with (+) define the solution for high power and those marked with (o) are for low cost. As can be seen from the graph, for the same geothermal input temperature, the Kalina cycle theoretically gives a higher net power.

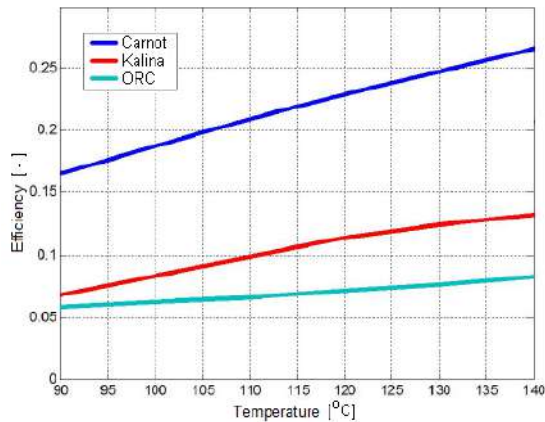


Fig.3 Comparison of Kalina and ORC cycles (isopentane) efficiency.

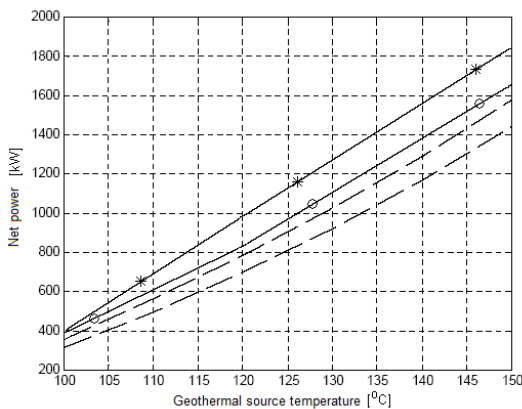


Fig.4 Comparison of net power in the Kalina and ORC (isopentane) cycles.

Geothermal water (Fig.5) with a temperature of 225 degrees C is extracted with a submersible pump.

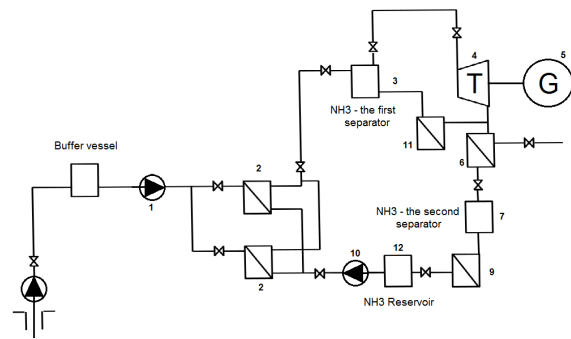


Fig.5 Basic thermal scheme of the electro-geothermal plant.

Geothermal water is circulated through pumps (1) in the heat exchanger of the evaporator (2), which transfers the heat to the working agent (ammonia and water solution). In this way, the temperature of the geothermal water is reduced and then this water is directed to the geothermal plant with the turbine (4) and the generator (5), located nearby. The circulation of the working agent is ensured with the help of the supply pumps (10). After receiving the heat from the geothermal water, the working agent evaporates and its temperature increases. Different separators and tanks also appear in the scheme.

3. CASCADE SYSTEM FOR THE SELECTED GEOTHERMAL PERIMETER

In this geothermal perimeter, at least 2 production wells and 2 reinjection wells could be drilled. Such a project is based on two drilling wells (Doublet) and a primary circuit of geothermal water. The geothermal water is actually a transporter of earth energy. The thermal water is pumped from the production well in a heat exchanger. The energy of the primary circuit is transferred through the heat exchanger to a secondary circuit, being then used for heating purposes, or other cascade applications, as greenhouse heating or aquaculture facilities, electrical power generation, etc.

We evaluate the thermal potential of the geothermal project to over 136MWt. This value is calculated by considering two Doublets, having a depth of around 4,200m, a flow of 80-

85l/s (around 83kg/s), and the thermal water temperature of at least 225°C. The quantity of the produced thermal energy, Q , is calculated according to the formula:

$$Q = m \times C \times (T - T_0) \quad (1)$$

$Q = m$ (the mass of the water in kg) $\times C$ (the specific thermal mass coefficient for water) $\times (T - T_0)$

$$Q = m \times C \times (T - T_0) = 83 \text{ kg/s} \times 4.180 \text{ Ws/kg}^\circ\text{C} \times (225^\circ\text{C} - 30^\circ\text{C}) = 67653300 \text{ Wt} = 68 \text{ MWt}. \quad (2)$$

Therefore, two doublets will generate a thermal energy of $2 \times 68 \text{ MWt} = 136 \text{ MWt}$. By having this potential, we can realize:

Version 1: A project for an extensive greenhouse facility heated with geothermal energy

Taking into consideration that the thermal energy provided by our drilling wells is 136MWt and for a hectare of greenhouse are necessary around 1.5MWt installed thermal capacity, an extensive greenhouse facility with a surface area of 90ha can be established. This greenhouse facility can be built in two stages, 45ha per stage, and each stage being served by a Doublet of geothermal drilling wells. If the greenhouse facility is smaller than 45ha, the rest of the available geothermal energy can be used in cascade also for heating a fish farm (aquaculture). The price of the thermal energy provided by gas heating systems in Romania is around 140 euro for one MWh. However, if somebody would like to build a big greenhouse facility of 90ha heated with gas, he should add to the investment cost also the high cost for the gas connection (if available in the area). As in our project the greenhouse facility will be established in the near vicinity of the doublet, the transport system for the geothermal heat will have moderate costs. The start-up of the first doublet in this geothermal project for a 45ha greenhouse facility, needs a capacity of 68MWt and has approximately following cost values: drilling of two production-reinjection wells (Doublet) 17,000,000 Euro, production pump

450,000 Euro, reinjection pump 220,000 Euro, the infrastructure for the geothermal system (primary circuit) comprises a heat exchanger, recirculating pumps, internal pipes, valves, insulation, transformer station, access roads,

building, etc. 1,700,000 Euro, insulated external pipes (secondary circuit), who connect the greenhouses with the output of the heat exchanger, recirculation pumps, adiabatic insulated buffer reservoir for geothermal water, heating unit for emergency cases, measurement point, etc. 1,100,000 Euro. The subtotal for this investment is 20,020,000 Euro.

The greenhouses must be heated 7 months per year, in the period 1st of October – 1st of May. In our opinion, during the 3 winter months (December, January and February), the greenhouses need an installed capacity of 68MWt, while 42.4MWt are needed in November and March, respectively 12.7MWt in April and October.

The thermal energy needed for the 45ha is calculated as follows:

$$3 \text{ months} \times 30 \text{ days} \times 24 \text{ h} \times 68 \text{ MWt} + 2 \text{ months} \times 30 \text{ days} \times 24 \text{ h} \times 42.4 \text{ MWt} + 2 \text{ months} \times 30 \text{ days} \times 24 \text{ h} \times 12.7 \text{ MWt} = 146,880 + 64,056 + 18,288 = 229,224 \text{ MWh}.$$

We consider that we can attract an investor to build the 45ha of greenhouses if we deliver the thermal energy at a price of approx. 75Euro/MWh during the 7 months in autumn, winter and spring. In this way, the sold thermal energy to the greenhouses during a year will be: $229,224 \text{ MWh} \times 75 \text{ Euro} = 17,191,800 \text{ Euro/year}$ for a geothermal Doublet. For a 2 Doublets project with 90ha of greenhouses, the sold geothermal energy will be double: 34,383,600 Euro/year (at a price of only 53.5% of the price for heating with methane gas). The investment recovery period in this case is 21 months.

Version 2: Geothermal district heating system in the city located near the geothermal perimeter

In this city the centralized heating and the warm water supply are provided by the public heating system, which serves around 65,000 apartments, 4,000 houses, 226 public institutions and 1,937 commercial units. The commercial units (industrial parks, shopping malls, office buildings, commercial stores, private companies, etc.) are paying a price of around 140Euro/MWt (163Euro/Gcal). The inhabitants of Oradea (private citizens) who are heating their apartments and houses through the centralized heating system of the city, pay a price of around 76 Euro/ MWt (88Euro/Gcal). The price difference up to 140Euro/MWt is supported by local subsidies. Having in mind all

the above mentioned, as long as the geothermal project produces thermal energy below the price of 15-20Euro/MWt, through this project could be a competent provider for thermal energy. Furthermore, we have to take into consideration also that the thermal energy from geothermal resources is renewable. The start-up of the first doublet in this geothermal project for an 68MWt thermic capacity has approximately following cost values: drilling of two production-reinjection wells (Doublet) 17,000,000 Euro, production pump 450,000 Euro, reinjection pump 220,000 Euro, the infrastructure for the geothermal system (primary circuit) comprises a heat exchanger, recirculating pumps, internal pipes, valves, insulation, transformer station, access roads, building, etc. 1,700,000 Euro, insulated external pipes (secondary circuit), who connect our secondary circuit with the existing heating system of the city, recirculation pumps, heating unit for emergency cases, measurement point, etc. 10,100,000 Euro. The subtotal for this investment is 29,470,000 Euro. If the project will be extended to 136MWt (2 Doublets), this value will not be added once again, while the rest of the costs will remain the same (49,470,000 Euro). Usually one year comprises 8,760 hours and considering 160 hours are reserved for maintenance, the real time of exploitation for a geothermal system are 8,600 running hours/year. This means that a yearly production (5000 hours equivalents, heating and hot water) of:

$$68\text{MW} \times 5,000\text{hours} \times 75\text{Euro/MWh} = 25.500.000 \text{ Euro/year} \quad (3)$$

The investment recovery period in this case is 23 months.

Version 3: A geothermal project with cascade applications

In recent years in several locations in Europe, which have a particularly high geothermal potential, cascade applications of this energy have been developed. Thus, projects have been built which contain geothermal heated greenhouses, fish farming and geothermal power plants. Using energy conversion systems - Binary Organic Rankine Cycle (e.g. Ormat, Turboden, Cryostar-Linde, Siemens) the geothermal energy is converted into electricity. In this version, the project will produce both electrical energy and thermal energy. The

generated renewable electrical power can be sold in to national electricity network, while the thermal energy can be directed to the city heating system and/or to a greenhouse facility. In the version including also the greenhouses, the electrical power can be used completely for the night illumination of the greenhouses. The price for electrical power for juridical persons in Romania is around 260 Euro for one MWh. Due to the above presented facts, this area is suitable not only for energy generation (12MW through an ORC-system based on the geothermal water temperature), but also for using the cooled geothermal water (the output from the ORC-system) for generating cascades applications thermal capacity of 120MWt (resulting as the difference between the capacity of the two doublets and the power of the power plant with the related losses).

From one year comprises 8,760 hours and considering 160 hours are reserved for maintenance, the real time of exploitation for a geothermal power plant are 8,600 running hours/year. This means that a yearly production of:

$$12\text{MW} \times 8,600\text{hours} \times 75\text{Euro/MWh} = 7,740,000 \text{ Euro/year (at a price of only 29\% of the market price for one MWh)}.$$

The thermal energy needed for the 90ha of greenhouses and for fish farming, is calculated as follows:

$$3 \text{ months} \times 30 \text{ days} \times 24 \text{ h} \times 120\text{MWt} + 2 \text{ months} \times 30 \text{ days} \times 24 \text{ h} \times 74.8\text{MWt} + 2 \text{ months} \times 30 \text{ days} \times 24 \text{ h} \times 22.4\text{MWt} + 5 \text{ months} \times 30 \text{ days} \times 24 \text{ h} \times 22.4\text{MWt (only for fish farming)} = 259,200 + 107,712 + 32,256 + 80640 = 479,808\text{MWh}.$$

The sold thermal energy to the greenhouses and for fish farming, during a year will be: 479,808MWh x 75 Euro = 35,985,600 Euro/year for two geothermal Doublet. Together with the electricity produced we will get 43,725,600 Euro/year. The total cost of investment in power plant, greenhouses and for fish farming, is around 90,000,000 Euro. The investment recovery period in this case is 25 months.

4. CONCLUSIONS

According to the European Directives, starting with 2020, it is mandatory that at least 20% of the thermal energy used in the district heating systems has to be produced from renewable

resources, and only the difference of maximum 80% has to be produced from burning of fossil fuels. By comparing the investment in the geothermal project to the turnover of the total sold energy, it is obvious that the efficiency of the project is good. We strongly believe that the development of this energy project is sustainable both from economical and technical view, but especially from the ecological point of view. It can be seen that the highest investment and the longest investment recovery period is for the cascade application, but also the annual gross profit is the highest in this case.

REFERENCES

- [1] Gavrilesco, O., Maghiar, T. The geothermal system from the University of Oradea - a new strategy simulation for the heat station. International Conference RSEE'98, May 1998, Felix Spa, Romania, pp.6.
- [2] Stecanella, P. A. J., Faria, M. A. A., Domingues, E. G. P., Gomes, H. G., Calixto, W. P. A., Alves, J. Electricity generation using thermoelectric generator - TEG, IEEE 15th International Conference on Environment and Electrical Engineering (EEEIC), 2015, pp. 2104-2108, DOI: 10.1109/EEEIC.2015.7165502.
- [3] Setel, A., Gordan, M., Antal, C., Bococi, D. Use of geothermal energy to produce electricity at average temperatures, 13th International Conference on Engineering of Modern Electric Systems (EMES), 2015, pp.1-4, DOI: 10.1109/EMES.2015.7158398.
- [4] Da Rosa, A. V. Fundamentals of renewable energy processes, 2005, Elsevier Academic Press.
- [5] Erickson, R. W., Maksimovic, D. Fundamentals of Power Electronics, 2001, 2nd Edition, Springer.
- [6] Arifujjaman, Md., Iqbal, M.T., Quaicoe, J.E., 2009, Analysis of Conversion Losses in Grid Connected Small Wind Turbine Systems. The Open Renewable Energy Journal, vol. 2, pp. 59-69.
- [7] Yanbo C., Wen Z., Leijiao G., Jijie Z., 2014, A Two-Stage Wind Grid Inverter with Boost Converter. Journal of Applied Mathematics, pp. 5, Art. ID 816564, DOI: 10.1155/2014/816564.
- [8] Cardoso, V., Eckstein, R.H., Lazzarin, T.B. System based on the Forward converter for connection to the grid of small wind turbines up to 1kW, 2015, IEEE 13th Brazilian Power Electronics Conference and 1st Southern Power Electronics Conference (COBEP/SPEC), pp. 1-6, DOI: 10.1109/COBEP.2015.7420142.



Banja Luka
1-2 Jun 2023.

DEMI 2023

16th International Conference on Accomplishments in Mechanical and Industrial Engineering

www.demi.mf.unibl.org



Comprehensive Study of Rayleigh–Bénard Convection in a Rectangular Tank with Motor Oil

P. Živković^a, M. Tomić^b, J. Janevski^a, G. Cvetanović^c, C. Barz^d

^a Faculty of Mechanical Engineering, University of Niš

^b Faculty of Technical Sciences, University of Novi Sad

^c Faculty of Technology, University of Niš

^d Northern University Center Baia Mare, University of Cluj - Napoca

Abstract Measurements of temperature distribution were performed in a rectangular tank with aspect ratios 4x2x1, using motor oil as a working fluid. The experimental setup was adjusted to be as close to real fuel tanks exposed to solar radiation, as in airplane wings. The measurements were taken at fifteen different positions on the faces of the tank. Probes used are PT100 elements. In order to obtain as uniform temperature as possible, double bottom was used, with water as medium for obtaining the constant surface temperature. The results are compared with those obtained by IR camera. Numerical simulations were performed in order to obtain more detailed information in the form of temperature fields.

The research was financially supported by the Ministry of Education, Science and Technological Development of the Republic of Serbia (Contract No. 451- 03-9/2021-14/200109).

Keywords Rayleigh–Bénard convection, temperature, PT100, motor oil, simulation

1. INTRODUCTION

The Rayleigh–Bénard experiment is a commonly used as a model for the study of turbulence and heat transport in thermal convection. Rayleigh–Bénard convection occurs in a fluid between a lower heated plate with the temperature T_t and an upper cooled plate with the temperature T_h . The temperature difference $\Delta T = T_t - T_h$ between the plates drives the flow. The convection cell is adiabatic at the side walls and has isothermal top and bottom plates. In reality, it is not unknown for the heated and the cooled plate to switch sides, as is common for tanks, which are heated from the Sun.

This kind of convection can be fully described by the Rayleigh number (Ra), the Prandtl number (Pr), the Nusselt number (Nu) and two aspect ratios Γ_x and Γ_y . The Rayleigh and Prandtl numbers are given by:

$$Ra = \frac{\beta g \Delta T h^3}{\nu a}$$

$$Pr = \frac{\nu}{a}$$

the aspect ratios are defined as

$$\Gamma_x = \frac{l}{h} \text{ and } \Gamma_y = \frac{w}{h}$$

and the Nusselt number is defined as

$$Nu = \left. \frac{\partial T}{\partial z} \right|_{z=h} \cdot \frac{h}{\Delta T}$$

where β is the coefficient of thermal expansion, g – gravity acceleration, height between the heating and cooling plate, l – length of the cell, w – width of the cell, ν – kinematic viscosity, a – thermal diffusivity and $\partial T / \partial z|_{z=h}$ – temperature gradient at the heated wall.

The transition to the turbulent regime in air occurs for $Ra \sim 10^6$. In the focus of this investigation, Ra range was $2.58 \times 10^7 < Ra < 5.59 \times 10^7$, so, it can be assumed

that the regime was turbulent for all experiments.

It is important to mention that there were two sets of experiments: with heated plate on the bottom, or classic Rayleigh–Bénard convection – RBC, and with heated plate on the top, for simulation of the insolation and influence of the atmosphere on the fuel tanks, which are being heated mostly from above – RRBC.

2. EXPERIMENTAL SETUP

The tank used for this experiment is shown in figure 1. The dimensions are 500×250×125mm, in x, y and z axis, respectively. The distance between the heated and the cooled plate is represented in z-direction. For obtaining of constant surface temperatures, another tank was added on the heating plate side. This tank volume of about half of the experimental tank, and its dimensions are 500×250×60mm. Electric heater is used for obtaining of the desired temperature as shown in the figure 1, and a mixer is added into the water tank, in order to maintain the constant water temperature. Mixer is placed from the opposite side of the heater, in order to ensure the most uniform water temperature in the tank.



Fig. 1. Front side of the tank, with the heater position

Temperature probes are PT100 elements, with precision of 0.1°C, manufactured by the

Corresponding author

Full profesor, Predrag Živković,
pzivkovic@masfak.ni.ac.rs

University of Niš
 Faculty of Mechanical engineering
 Niš, Serbia

firm Nigos – Niš. Fifteen measuring locations are measuring temperature distribution in the chamber, one is measuring the temperature in the heating water tank and one is measuring the air temperature below the chamber. The cooling plate is air cooled, in order to observe the atmospheric influences on the tank, as is happening in the reality.

For comparing of the results, the lateral sides of the tank are made of plexiglass, as shown in figure 2.

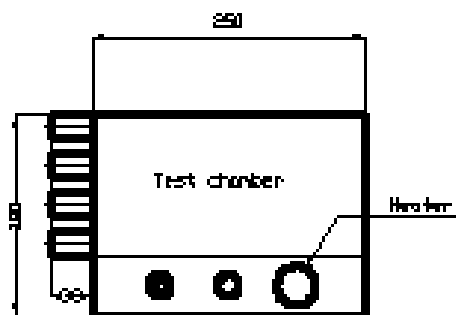


Fig. 2. Disposition of the measuring points on the lateral sides of the tank

As can be seen in figure 2, the measuring positions are ensuring the monitoring of the vertical temperature profile at the left and right sides (eight probes) and in the center (3 probes, on the opposite side) of the largest tank side (x-z plane). Longitudinal temperature distribution in x-axis is measured with 5 probes.

In order to ensure minimal heat loss to the sides of the tank, it was insulated with 2cm sponge (to disable the air flow between the tank and the insulation) and 5cm styrofoam. Water tank was also insulated, in order to minimize heat losses, and improve the system response. Insulation is kept in place with elastic bandages. Insulation is adapted to be removable on either side, in order to make access for the IR camera.

The cooler plate is free to the atmosphere, and was cooled by the air in the test room. The air temperature was measured below the chamber.

In order to enable the free air flow at the cooled plate, the tank was equipped with 50mm feet both from the heated, as from the cooled side, thus allowing for the heated and cooled plates to change positions

3. MEASUREMENT RESULTS

Measurements were performed for about five days each (RBC and RRBC), with different temperature levels. On the figure 3, 5 day continuous measurements and representative stable hourly measurements for RBC are presented. The curve TS01 represents the heating tank temperature, which can be assumed to be the temperature of the heated plate, due to the low thermal resistance of the tank. One can notice that daily temperature change is between 2 and 4°C, with the largest hourly change of 0.2°C, which is at the level of the probes precision. The daily change of the test room temperature is varying between 4 and 7°C (up to 0.2°C per hour, curve TS16), which is at the level of the possibility of commercial control systems to maintain the room temperature per hour.

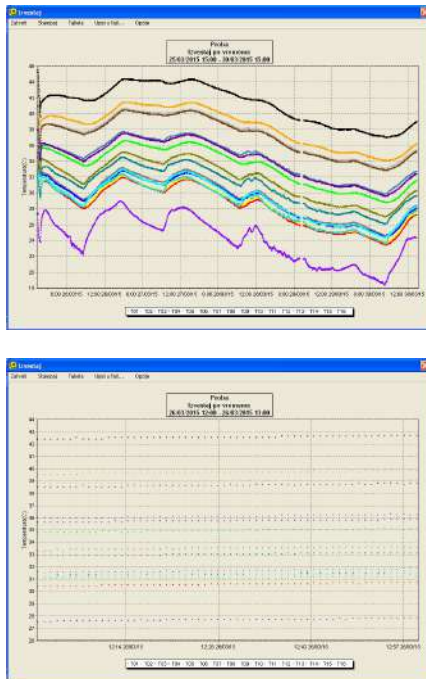


Fig. 3. Long term and selected stable hourly measurements for case of RBC

4. COMPARISON OF THE EXPERIMENTAL AND NUMERICAL RESULTS

The chamber used in the experiment has shown great flexibility. The probes are placed at appropriate locations so that there are 3 or 4 probes that measure temperature in 3 different vertical sections. This arrangement allows measurement with various hydraulic fluids at different temperature regimes and positions of

the warmer and cooler plates. The experiment has shown that the relative stability of the surrounding air has allowed the cooler plate to be directly exposed to external conditions. The measuring system has shown an appropriate response to external conditions, enabling a variety of experiments. Selected Probe TS-05, due to the massive threaded part somewhat increased measurement inertia; yet this has allowed control measurements with the thermal camera. Thermal camera measurements have shown no significant heat loss in the insulated part of the chamber.

Validation of the numerical model is done by comparing the results of numerical and real experiments. Deviations of results that occur in numerical simulation are the result of input errors, model errors, discretization errors, numerical errors, approximations of the actual geometry, etc.

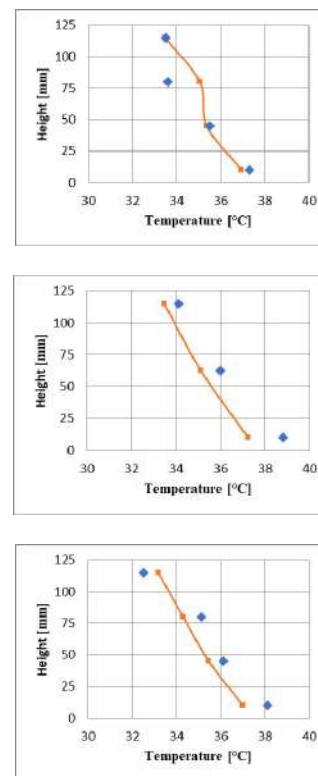


Fig. 4. Comparison of experimental (dots) and numerical results (line) in the left, middle and right vertical cross section of the chamber with oil for temperatures TS01=41.3°C (bottom) and TS16=30.3°C (top)

The deviation of results of numerical simulations of quantity Φ is determined in

relation to the maximum deviation obtained by comparing several points, as:

$$\delta_i = \frac{|\Phi_{i,mer} - \Phi_{i,sim}|}{\Phi_{i,mer}} [\%]$$

where $\Phi_{i,mer}$ is the measured, and $\Phi_{i,sim}$ is the simulated value at the i -th point. The error was in the range 1-8%, which can be regarded as acceptable

5. CONCLUSIONS

The chamber used for this experiment shows high flexibility in the work. The probes are positioned in the adequate locations, and can be used for other fluids, and different temperatures and positions of the heated and the cooled plate. The experiment showed that the influence of the steady environment is allowing for the cooler plate to be directly exposed to the atmosphere. From the other hand, the influence of the air flow over the cooling plate should and will be investigated in much more details, in order to include the influence of the wind to the tank surfaces.

The measuring system is showing appropriate response to the outer disturbances, thus allowing extending of the experiment.

Measurements with the IR camera shows that the heat losses are low enough, but could be further reduced, especially on the probe locations.

The probe sockets are increasing the inertia of the probes, which causes longer time for steadying of the process, but allows the parallel measurement with the IR camera.

Measured results shows the existence of the inert upper zone, for the case when the heated plate is on the upper side. The height of the of the Rayleigh-Benard structures is lower than of ones in the case of the lower heated plate. The fluid mixing is even less intense in this case.

The results obtained by the numerical simulation confirms the experimental results with the error in the range of 1-8%.

REFERENCES

[1] A.Ebert, C.Resagk, A.Thess, Experimental study of temperature distribution and local heat flux for turbulent Rayleigh–Bénard convection of air in a long rectangular enclosure. *International Journal of Heat and Mass Transfer* 51 (2008), pp 4238–4248.

[2] M. Hoelling, H. Herwig, *Asymptotic analysis of heat transfer in turbulent Rayleigh–Bénard convection*, *International Journal of Heat and Mass Transfer* 49 (2006), pp 1129–1136

[3] M. Hoelling, H. Herwig, Asymptotic analysis of the near-wall region of turbulent natural convection flows, *Journal of Fluid Mechanics*, 541 (2005), pp 383–397.

[4] Jovanović M.et. al., Rayleigh–Bénard Convective Instability in the Presence of Thermal Variation at the Lower Wall. *THERMAL SCIENCE*, Year 2012, Vol. 16, Suppl. 2, pp. S331-S343.

[5] A. Maystrenko, C. Resagk, A. Thess, Structure of thermal boundary layer for turbulent Rayleigh–Bénard convection of air in a long rectangular enclosure, *Physics Rev E* 75 (2007), 066303.

[6] R. du Puits, C. Resagk, A. Thess, Structure of thermal boundary layers in turbulent Rayleigh–Bénard convection, *Journal of Fluid Mechanics*, 572 (2007), pp 231–254.

[7] Richter, F.M., Experiments on the stability of convection rolls in fluids whose viscosity depends on temperature, *Journal of Fluid Mechanics*, 89 (1978), pp. 553-560.



Banja Luka
1-2 Jun 2023.

DEMI 2023

16th International Conference on Accomplishments in Mechanical and Industrial Engineering

www.demi.mf.unibl.org



Assessment of the technical justification and profitability of the newly built SHPP-s in Montenegro

V. Vilotijević^a, V. Nikolić^a, U. Karadžić^a, V. Kovijanić^a, I. Božić^b

^aUniversity of Montenegro, Faculty of Mechanical Engineering, Džordža Vašingtona bb, Podgorica 81000, Montenegro

^bUniversity of Belgrade, Faculty of Mechanical Engineering, Belgrade, Kraljice Marije 16, Belgrade 11000, Serbia

Abstract Basic approach to small hydro power plant (SHPP) design implies techno-economic analysis, which determines the SHPP installed parameter more precisely by using the following criteria: the annual electricity production, the annual revenue of the HPP, net present value (NPV), internal rate of return (IRR) and payback period (PB). The SHPP installed parameter represents the ratio of the design flow and the average perennial flow obtained from the flow duration curve at the location of the intended water intake. The main goal of the current research is to compare the 27 newly built SHPPs in Montenegro with the developed methodology, and provide an assessment of their technical justification and profitability. According to the conducted analyses, it can be concluded that 82% of them are designed properly and 18% have serious shortcomings.

Keywords Small hydro power plant, design flow, installed capacity, techno-economic parameters.

1. INTRODUCTION

The construction of small hydropower plants in the Western Balkans in recent years has been followed by many controversies related to environmental, social, hydrological and hydro energetic issues. One of the main problems faced by hydropower engineers was the lack of reliable hydrological data. During 2010 and 2011, flows on 65 small watercourses were measured under the project named the Registry of Small Rivers and Potential Locations of SHPPs at Municipality Level for Central and Northern Montenegro, and relevant flow duration curves (FDCs) have been obtained [1]. This Registry was enhanced during 2018 and 2019 [2]. Location for SHPPs in Montenegro are characterized by relatively low average annual flows and high gross heads. The proper determination of the design flow also proved to be a challenge in terms of technical and economic justification. Due to all of the above

mentioned, a methodology was developed for determining the SHPP installed parameter [3, 4]. The methodology takes into account technical (installed capacity, annual electricity production) and economic parameters (the annual revenue of the HPP, NPV, IRR and PB). The application of techno-economic parameters when determining design flow with different approaches can be found in the literature [5 ÷ 12]. The main goal of the current research is to compare the 27 newly built SHPPs in Montenegro with the developed methodology, and provide an assessment of their technical justification and profitability.

2. METHODOLOGY

This paper investigates 27 (twenty-seven) small watercourses on the territory of Montenegro where small hydropower plants of different capacities have already been built. The SHPP installed parameter is defined as the ratio of the

design flow and averaged perennial flow according to the following equation,

$$K_i = \frac{Q_d}{Q_{av}} \cdot (1) \quad (1)$$

The annual gross income of the small power plant is calculated from the generated energy based on the FDCs and the incentive energy prices (Table 1).

Table 1. Electricity prices depending on the capacity of the power plant [13]

Hydro power plant capacity [MW]	Incentive price [c€/kWh]
$P_{SHPP} < 1$ MW	10.44
$1 \leq P_{SHPP} < 3$ MW	$10.44 - 0.7 \cdot P_{SHPP}$
$3 \leq P_{SHPP} < 5$ MW	$8.87 - 0.24 \cdot P_{SHPP}$
$5 \leq P_{SHPP} < 8$ MW	$8.35 - 0.18 \cdot P_{SHPP}$
$8 \leq P_{SHPP} \leq 10$ MW	6.8

The net present value (NPV) is defined as the value of the net cash flow during exploitation period of SHPP discounted back to its present value, and it is calculated according to the next equation [10,14].

$$NPV = \sum_{t=1}^T \frac{R(t) - C(t)}{(1+d)^t} \quad (2)$$

where are: R – annual net income of the SHPP, C – annual costs of the SHPP (in the first year this implies total investment costs of the project and in all next years the operation and maintenance costs), d – discount rate ($d = 8\%$ for Montenegro), T – the time of cash flow, equal to concession period of 30 years. The internal rate of return (IRR) is the discount rate that reduces the present value of the net project cash flow to zero in a discounted cash flow analysis and can be calculated from eq. (3), as the value of d corresponding to a $NPV = 0$ [10,14].

The payback period (PB) is the period it takes to recover the cost of an investment and it is obtained by dividing total investment costs with net annual income of SHPP.

3. RESULTS AND DISCUSSION

Based on hydrological data (flow duration curves and characteristic flow durations), calculations were made to select the optimal K_i on 27 watercourses on the territory of

Montenegro. These results were compared with the designed values on these constructed plants and the results are shown in Table 2.

Table 2. Values of SHPP installed parameter (K_i – obtained by methodology, K_i^* – constructed)

	SHPP Name	K_i	NPV (kEUR)	IRR (%)	PB (year)	Annual electricity production (GWh)
		K_i^*				
1	Jezerštica	2.2 2.1	1431.92 1402.08	15.69 15.63	6.56 6.59	3.04 3.00
2	Bistrica	1.0 1.2	8810.63 8992.72	22.00 20.96	4.37 4.64	17.44 19.45
3	Orah	1.4 1.4	951.00 951.00	11.38 11.38	9.93 9.93	3.54 3.54
4	Spaljevići	2.2 1.7	422.70 303.96	10.43 9.89	10.98 11.71	2.17 1.96
5	Šekular	1.0 1.7	1146.78 781.74	11.17 9.77	10.21 12.14	4.42 5.51
6	Jelovica 1	1.2 1.7	5149.83 5217.91	22.11 19.93	4.33 4.92	8.82 10.36
7	Jelovica 2	1.1 1.4	-116.56 -175.25	7.32 7.08	17.12 17.91	1.78 1.91
8	Vrelo	1.8 1.3	1630.62 1336.12	16.64 15.82	6.10 6.48	3.22 2.83
9	Piševska	2.5 3.0	523.94 557.97	11.28 11.33	9.92 9.88	2.11 2.21
10	Temnjčka	1.9 1.3	8484.88 7461.46	25.97 27.57	3.57 3.32	15.36 12.53
11	Treskavička	1.9 1.1	4350.62 3894.91	23.59 25.04	3.99 3.71	7.63 6.08
12	Babino poljska	1.5 1.5	5041.42 5041.42	23.43 23.43	4.03 4.03	8.60 8.60
13	Bistrica Majstorovina	1.0 1.6	7086.93 6457.47	21.29 17.52	4.55 5.79	12.52 14.92
14	Bradavac	1.0 0.9	2710.11 2580.22	22.57 22.25	4.19 4.26	4.07 3.92
15	Šeremet	1.7 1.7	2605.95 2605.95	22.45 22.45	4.21 4.21	3.94 3.94
16	Ljevak	1.5 1.0	2290.21 1653.47	18.31 16.86	5.43 6.00	4.04 3.22
17	Kutska 1	1.0 1.2	5044.77 5300.22	23.62 23.06	4.00 4.12	7.95 8.65
18	Kutska 2	1.3 1.2	2083.14 2016.71	17.71 17.63	5.66 5.69	3.81 3.71
19	Mojanska 1	1.1 1.5	2801.65 3006.11	15.80 15.39	6.63 6.83	6.23 7.15
20	Mojanska 2	1.3 1.6	1690.36 1417.61	14.29 12.84	7.44 8.52	2.35 4.35
21	Mojanska 3	1.5 2.0	670.34 723.35	11.86 11.69	9.33 9.53	2.35 2.59
22	Bistrica Lipovska	1.3 1.3	2383.78 2383.78	18.42 18.42	5.39 5.39	4.17 4.17
23	Paljevinška	1.0 1.3	-16.97 -69.33	7.90 7.63	15.56 16.32	1.75 1.93
24	Pecka	2.1	563.35	10.07	11.60	3.17

		2.0	543.97	10.03	11.61	3.16
25	Vrbnica	1.3	10338.05	33.56	2.65	16.23
		2.1	10926.19	29.64	3.06	19.83
26	Štitska	2.2	730.09	11.73	9.49	2.59
		2.0	685.91	11.57	9.65	2.53
27	Mišnica	1.9	365.72	10.71	10.53	1.77
		1.0	124.27	9.12	12.80	1.38

Few typical results are shown in the next figures.

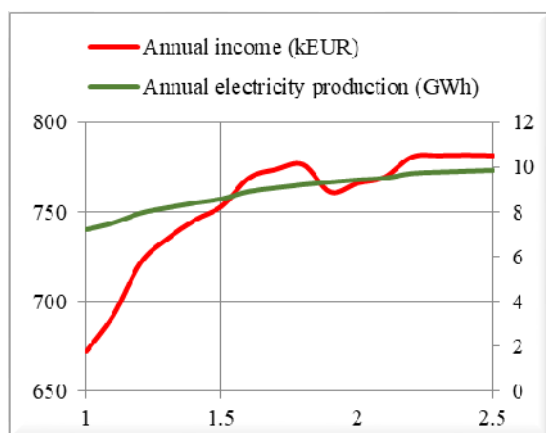


Fig. 1. Annual electricity production and income- SHPP Babinopoljska

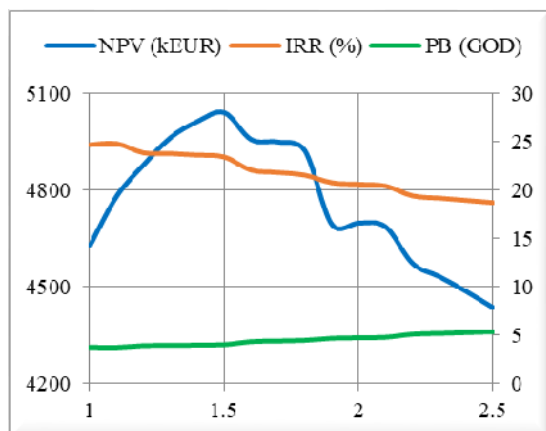


Fig. 2. NPV, IRR and PB- SHPP Babinopoljska

The maximum value of annual production and income for SHPP Babinopoljska is obtained for $K_i = 2.5$ (Fig.1). From Fig.1 it can also be seen that the annual income is constantly increasing up to $K_i = 1.8$, after which due to the increase in installed capacity over 3 MW and the reduction of the incentive price it decreases to $K_i = 1.9$ after which it constantly increases until the end of the range. The maximum values for NPV (5041.42 kEUR) and IRR (24.8%) were obtained

for $K_i = 1.5$ and $K_i = 1.2$. Designed values of K_i on constructed SHPP Babinopoljska is 1.5. For this value annual electricity production is 8.60 GWh, annual income is 753.12 kEUR, NPV is 5041.42 kEUR, IRR is 23.43% and PB is 4.03 years. Comparing the results obtained by applying the developed methodology with the designed parameters it gives the same parameter values. This designed solution seems to be well chosen if the economic aspect is to be observed.

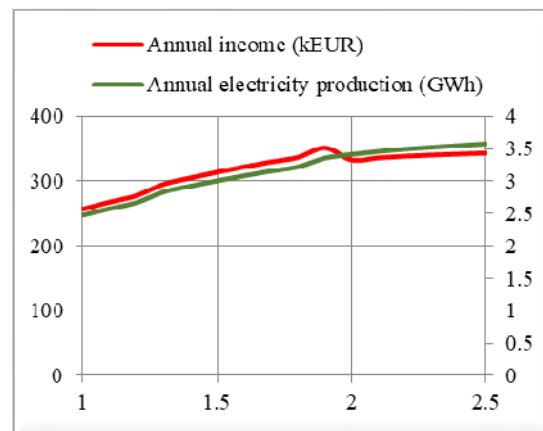


Fig. 3. Annual electricity production and income- SHPP Vrelo

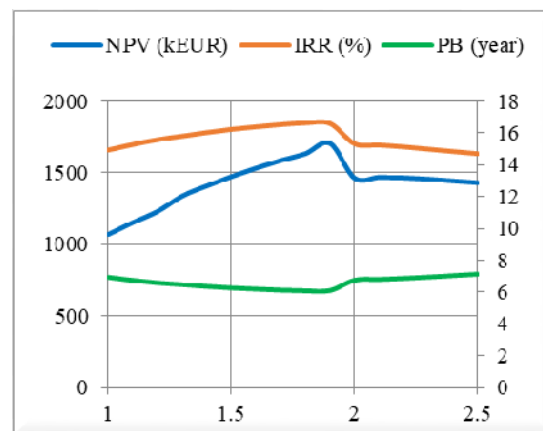


Fig. 4. NPV, IRR and PB- SHPP Vrelo

For SHPP Vrelo the maximum value of annual production 3.58 GWh is obtained for $K_i = 2.5$, while the maximum value of annual income 350.51 kEUR is obtained for $K_i = 1.9$. The maximum values for NPV (1702.64 kEUR) and IRR (16.64%) were obtained for $K_i = 1.9$ and $K_i = 1.8$, (Fig.4). Designed value of K_i on constructed SHPP Vrelo is 1.3. For this value, annual electricity production is 2.83 GWh,

annual income is 295.52 kEUR, NPV is 1336.12 kEUR, IRR is 15.82% and PB is 6.48 years.

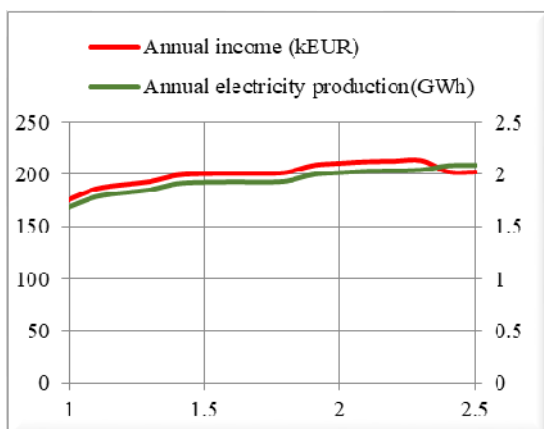


Fig. 5. Annual electricity production and income- SHPP Jelovica 2

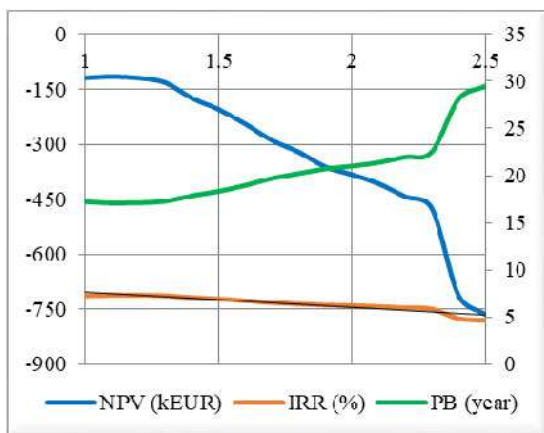


Fig. 6. NPV, IRR and PB- SHPP Jelovica 2

For SHPP Jelovica 2, the maximum value of annual production 2.09 GWh is obtained for $K_i = 2.5$, while the maximum value of annual income 213.05 kEUR is obtained for $K_i = 2.3$. The maximum values for NPV (-116.56 kEUR) and IRR (7.32%) i.e. the corresponding PB (17.12 years) were obtained for $K_i = 1.1$. Designed value of K_i on constructed SHPP Jelovica 2 is 1.4. For this value, annual electricity production is 1.91 GWh, annual income is 199.27 kEUR, NPV is -175.25 kEUR, IRR is 7.08% and PB is 17.91. Based on the obtained results, it can be noted that the NPV has a negative value for the entire K_i range, which indicates that this SHPP was not designed properly or was designed with wrong input data. Also, the maximum IRR value of 7.32% is lower than the adopted discount rate

of 8%, which means that the project is not feasible. The normalized values of NPV and IRR are used for a precise comparison of the results obtained by the methodology and the constructed SHPP solution. Normalized values were obtained by dividing calculated values with optimal ones given with chosen K_i for every plant. With relative values, we are able to check results on the same level and compare different plants. Vertical lines mean constructed K_i and cross points with NPV or IRR lines give constructed NPVs or IRRs. Table 3 shows the criteria for evaluating the validity of the constructed solution.

Table 3. Criteria for evaluating the validity of the constructed solution

Criteria
Optimal solution - (0.85-1.0)
Good solution - (0.6-0.85)
Far from optimal solution - (0.3-0.6)
Bad solution - (0-0.3)

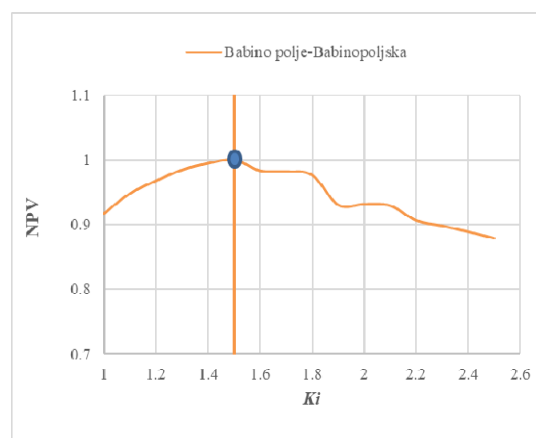


Fig.7. Normalized values of NPV - SHPP Babinopoljska

For SHPP Babinopoljska (Fig.7), the solution obtained by the methodology is the same as the constructed solution. Considering the above, the constructed SHPP installed parameter (NPV=1) is the optimal solution.

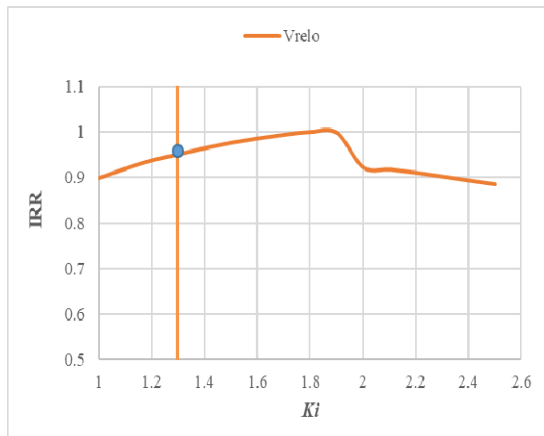


Fig. 8. Normalized values of NPV – SHPP Vrelo

Fig.8 shows normalized values of IRR for SHPP Vrelo. By comparing the constructed SHPP installed parameter and the SHPP installed parameter obtained by the methodology, it can be observed that slightly better results of all considered parameters are provided by the optimal solution. However, the constructed value of the SHPP installed parameter (IRR=0.95) is the optimal solution.

Bearing in mind that for SHPP Jelovica 2, NPV has a negative value and that the maximum IRR value is lower than the adopted discount rate, it can be concluded that this power plant was built as a bad solution.

4. CONSLUSION

The research subject in this paper is 27 small hydropower plants that were built in the period from 2014 to 2023 on the territory of Montenegro. Based on hydrological data (flow duration curves and characteristic flow durations), calculations were made to select the optimal SHHP installed parameter. By comparing the obtained with the constructed results, a conclusion can be drawn as to whether the designed solutions are optimal, good, far from optimal, or bad.

Table 4. Evaluation of the validity of the implemented solutions of SHPPs built in Montenegro

Optimal solution	20 SHPPs
Good solution	3 SHPPs
Far from optimal solution	1 SHPP
Bad solution	3 SHPPs

In all cases, it was found out that choosing the optimal K_i value depending on the annual income and annual electricity production leads to an increase in the annual income, but also to an increase in the price of the investment. From the research it is also concluded that the difference in the investment between the highest income and the maximum NPV and IRR is several times greater than the difference in income. It proves that in all cases NPV and IRR are more influential parameters for choosing the SHPP installed parameter compared to the annual income and annual electricity production. Finally, the developed methodology can serve as a guide for designers and investors of small hydropower plants.

Acknowledgement

REFERENCES

- [1] Vodni zdroje, a.s., Blom, Sweco Hydroprojekt CZ, a.s., Sistem doo, HMZCG. (2011). *Registry of Small Rivers and Potential Locations of SHPPs at Municipality Level for Central and Northern Montenegro*. European Bank for Reconstruction and Development (EBRD) and Ministry of economy, Podgorica, Montenegro.
- [2] Vodni zdroje as, Sweco Hydroprojekt CZ as. (2019). *Enhancement of Registry of Small Rivers for Small Hydropower Projects Potential of up to 10 MW*. European Bank for Reconstruction and Development (EBRD) and Ministry of economy, Podgorica, Montenegro.
- [3] Vilotijević, V., Karadžić, U., Vujadinović, R., Kovijanić, V., Božić, I. (2021). An Improved Techno-Economic Approach to Determination of More Precise Installed Parameter for Small Hydropower Plants, *Water*, vol. 13.
- [4] Vilotijević, V., Karadžić, U., Kovijanić, V., Božić, I., Vujadinović, R. The techno-economic analysis of small hydropower plants installed parameters for three different mountain watercourses. *International Conference Power Plants 2021*, November 2021, Belgrade, Serbia.
- [5] Božić, I. (2022). *Renewable Energy Sources – Small Hydro Power Plants*. University of Belgrade, Faculty of Mechanical Engineering, Belgrade, Serbia. (in Serbian)

- [6] Lopes de Almeida, J.P.P.G., Nenri Lejeune, A.G., Sa Marques, J.A.A., Conceição Cunha. M. (2006). OPAH a model for optimal design of multipurpose small hydropower plants, *Advances in Engineering Software*, vol. 37, p. 236-247.
- [7] Anagnostopoulos, J.S., Papantonis, D.E. (2007). Optimal sizing of a run-of-river small hydropower plant. *Energy Convers. Manag.*, vol. 48, p. 2663-2670.
- [8] Karlis, A., Papadopoulos, D. (2000). A systematic assessment of the technical feasibility and economic viability of small hydroelectric system installations. *Renewable Energy*, vol. 20, p. 253-262.
- [9] Montanari, R. (2003). Criteria for the economic planning of a low power hydroelectric plant. *Renewable Energy*, vol. 28, p. 2129-45.
- [10] Kaldellis, J., Vlachou, D., Korbakis, G. (2005). Techno-economic evaluation of small hydropower plants in Greece: a complete sensitivity analysis. *Energy Policy*, vol. 33, p. 1969-1985.
- [11] Santolin, A., Cavazzini, G., Pavesi, G., Ardizzon, G., Rosetti, A. (2011). Techno-economical method for the capacity sizing of a small hydropower plant. *Water Resources and Management*, vol. 52, p. 2533-2541.
- [12] Mishra, S., Singal, S., Khatod, D. (2012). A review on electromechanical equipment applicable to small hydropower plants. *Int. J. Energy Res*, vol. 36, p. 553-571.
- [13] Government of Montenegro. (2015). *Regulation on the Tariff System for Determining the Feed Cost of Electricity from Renewable Energy Sources and High-Efficiency Cogeneration*. Podgorica, Montenegro.
- [14] Basso, S., Botter, G. (2012). Streamflow variability and optimal capacity of run-of-river hydropower plants. *Water Resources Research*, vol. 48 .



Banja Luka
1-2 Jun 2023.

DEMI 2023

16th International Conference on Accomplishments in Mechanical and Industrial Engineering

www.demi.mf.unibl.org



Paraffin in Latent Heat Storage Systems

P. Živković^a, G. Cvetanović^b, P. Rašković^b, J. Janevski^a, D. Petković^a

^a Faculty of Mechanical Engineering, University of Niš

^b Faculty of Technology, University of Niš

Abstract *The text discusses the growing attention to the optimal use of energy and the development of renewable energy due to numerous problems, including the environmental problem caused by using fossil fuels. Storing energy efficiently is one of the most important parts of using energy efficiently. Among the various methods for energy storage, thermal energy storage, specifically latent heat storage using phase change materials (PCMs), is highlighted as one of the most interesting. Latent heat storage is a method of storing energy in the form of latent heat at constant temperature during the phase transition of materials called phase change materials. These materials release the same stored energy during the crystallization process. The text mentions that solid-liquid PCMs are used in latent heat storage systems (LHSS) that are attracting growing interest in many applications. The text emphasizes the importance of the thermophysical properties of PCM in latent heat thermal energy storage (LHTES) applications. These properties are crucial in determining the effectiveness and efficiency of the energy storage system. Therefore, understanding and optimizing the thermophysical properties of PCMs is essential for developing efficient latent heat thermal energy storage systems. These materials with different properties are widely used in a variety of fields. Paraffin is one of the most used and important PCMs due to its numerous advantages.*

Keywords *paraffin, phase change material, latent heat storage*

1. INTRODUCTION

Phase change materials (PCMs) are substances that store and release thermal energy during phase transitions. The exact origins of PCM discovery are unclear, but it is known that scientists have paid attention to their potential since the early 1900s. In recent times, energy mismanagement and improper use have resulted in environmental and economic problems, making the development of efficient energy demand and renewable energy and storage systems significant. Energy storage is essential in renewable energy, and thermal energy storage (TES) is one of the most important forms of energy storage. TES is achieved by altering the internal energy of a material, such as through sensible heat, latent

heat, or chemical heat. Among these, latent heat storage (LHS) is noteworthy due to its ability to store a large amount of energy at an isothermal process. PCMs perform energy storage through LHS, whereby the material absorbs thermal energy from the surrounding during phase change and releases the stored energy to the surrounding during the reverse process [1].

PCMs can undergo phase transformations such as solid-solid, solid-liquid, solid-gas, and liquid-gas. However, the steep volume changes in solid-gas and liquid-gas phase changes have resulted in many problems for TES systems. On the other hand, solid-liquid PCMs have higher latent heat and sensible volumetric change, making them more economically feasible for TES systems.

2. PHASE CHANGE MATERIALS

Phase change materials (PCMs) are substances that can store and release thermal energy as they undergo phase changes from solid to liquid, or liquid to solid, at a constant temperature, as shown in figure 1.

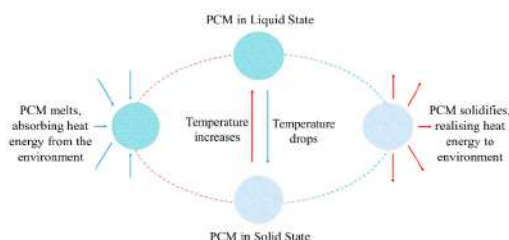


Fig. 1. Phase change processes in phase change materials

Overall, PCMs are a promising solution for energy storage in renewable energy and thermal energy storage systems. The selection of the appropriate PCM depends on various factors such as the required energy storage capacity, melting temperature, thermal conductivity, and stability. Therefore, ongoing research and development of PCM-based energy storage systems are essential to improve the performance and efficiency of renewable energy and TES systems.

However, the volume changes during solid-gas and liquid-gas phase transitions cause practical problems for commercial applications. Solid-liquid PCMs, on the other hand, have been mass-marketed and classified into three groups: organic, inorganic, and eutectics.

Inorganic PCMs are usually salt hydrates or metals. Salt hydrates, which are a mixture of inorganic salts and water, have high thermal energy storage capacity and thermal conductivity. However, their incongruent melting behaviour and supercooling phenomenon limit their applications. Metals, on the other hand, have high thermal conductivity and mechanical properties, and are used for high-temperature PCMs. Some metals, such as

indium, cesium, gallium, etc., are used for low-temperature PCMs.

Organic PCMs are classified into two major groups: paraffin and non-paraffin. Paraffins, which are the most common type of organic PCM, are stable over numerous phase change cycles and do not exhibit the supercooling phenomenon. Non-paraffin organic PCMs, such as fatty acids, glycols, polyalcohols, and sugar alcohols, have high latent heat capacity, but are flammable and have low thermal conductivity, low combustion temperatures, and transient toxicity. Fatty acids have high stability and do not exhibit supercooling, but are more expensive than technic-grade paraffins, and are of animal or plant origin.

Eutectics, which contain at least two types of PCMs, have exceptional properties, such as low-temperature melting and high latent heat storage capacity. However, their complex manufacturing processes make them less practical for commercial applications [2].

Overall, PCMs have great potential for thermal energy storage and management in various applications, such as building materials, textiles, electronics, and transportation. Inorganic PCMs are suitable for high-temperature applications, while organic PCMs are suitable for low-temperature applications. The choice of PCM depends on the specific requirements of each application.

3. APPLICATION OF PARAFFIN IN PCM

Paraffins are a family of saturated hydrocarbons with varying purity and melting points. Technical grade paraffin wax, a by-product of oil refining, is commonly used as a PCM in LHTES applications due to its low cost [3]. Commercial grade paraffin waxes are a combination of different, mainly straight chain, hydrocarbons with more than 15 carbon atoms having melting temperatures ranging from 22 to 68 °C. The various paraffin waxes are easily available, cheap, and can be obtained in a selection of melting point ranges, so a good match can be made between melting range and system operating temperature [4].

Paraffin wax has several advantages over other PCMs. It has a large latent heat, moderate thermal energy storage density, little or no undercooling, low vapour pressure, good

Corresponding author

Full profesor, Predrag Živković,
pzivkovic@masfak.ni.ac.rs

Univerzitet of Niš
 Faculty of Mechanical engineering
 Niš, Serbia

thermal and chemical stability, lack of phase separation, self-nucleating behaviour, varied phase change temperatures, environmental harmlessness, no unpleasant odour, non-toxicity, and is low in price. However, its major drawback is low thermal conductivity, which reduces the rates of heat storage and release during melting and crystallization operations, requiring a large surface area. It is also flammable, and the changes in density in the course of heating/cooling to a melting/solidification temperature, as well as the solid/liquid phase transformation, can cause great volume change.

The thermo physical properties of paraffin waxes presented in available literature represent ranges of values due to incomplete data and scarce studies relating interdependence of thermo physical properties [1, 5].

Table 1. Thermophysical properties of n-paraffins

Materials	Melting point (°C)	Latent heat (kJ kg ⁻¹)	Thermal conductivity (W m ⁻¹ K ⁻¹)
n-Tetradecane (C14)	6	228-230	0.14
n-Pentadecane (C15)	10	205	0.2
n-Hexadecane (C16)	18	237	0.2
n-Heptadecane (C17)	22	213	0.145
n-Octadecane (C18)	28	245	0.148
n-Nonadecane (C19)	32	222	0.22
n-Eicosane (C20)	37	246	
n-Henicosane (C21)	40	200, 213	
n-Docosane (C22)	44.5	249	0.2
n-Tricosane (C23)	47.5	232	
n-Tetracosane (C24)	52	255	

Paraffin-based phase change materials (PCMs) have many potential applications in energy storage and temperature regulation, but they require stabilization in order to be usable. There are two main methods for stabilizing the shapes of paraffinic PCMs: encapsulation and

microencapsulation. Encapsulation involves protecting the PCM with a shell made of polymeric materials with improved mechanical and thermal properties. Macroencapsulation is a simpler and lower cost method than microencapsulation, and typically involves ball, spherical, cylindrical, flat sheet, or tubular shapes. The encapsulation of paraffinic PCMs can be classified into bulk or macroencapsulation, microencapsulation, and nano-encapsulation.

Macroencapsulation is commonly used in transportation, buildings, solar energy storage systems, and heat exchangers. In order to increase the efficiency of heat transfer in these types of capsules, either the size of the capsules should be adequately chosen, or suitable modifiers should be used. For example, aluminium and copper open-cell foams are among the most studied materials, whereas metal oxides, metals, and graphite have also been used as improving agents for heat conductivity. Polyethylene terephthalate pipes and float stone have also been used as shells and enhancers of thermal conductivity.

Microencapsulation involves enclosing the PCM in microcapsules ranging in size from 1 µm to 1 mm. This method performs better than macroencapsulation because of increased contact surface area, shorter discharge and loading times, and improved thermal conductivity. Different materials are used for the shell part of the microcapsules, and there are two major physical and chemical methods for microencapsulation. The most important physical methods are fluidized bed, spray dryer, centrifuge extruder, and similar processes. Chemical methods are often based on polymerization and include in situ suspension and emulsion polymerization, interfacial condensation polymerization, and sol-gel method.

In the suspension or emulsion polymerization method, the insoluble paraffin is first emulsified or suspended in a polar medium, which is predominantly aqueous phase, by means of high-speed stirring. Surfactants are used to stabilize the particles. Lipophilic monomers are then added to the medium, and the conditions are prepared for polymerization. This polymer, which is insoluble in both aqueous and paraffin phases, is formed on the outer surface of paraffin particles and finally, after polymerization,

encapsulates the paraffin as a shell. The size of these capsules depends on the size of emulsion or suspension of paraffin droplets. Sometimes certain additives are added to the medium to improve some of the polymer properties. For instance, in some studies, polyvinyl alcohol (PVA) has been added to the medium with methyl-methacrylate monomer, which is known as one of the most important shell materials. As a result, paraffin has been encapsulated by PVA-modified polymethyl methacrylate (PMMA), forming a smooth surface of the microcapsules [6].

In the interfacial method, the two immiscible liquids, paraffin and monomers, are stirred together, and a thin layer of polymer is formed at the interface. The size of these capsules depends on the stirring rate and the amount of emulsifier. In this method, the paraffin droplets can be polymerized directly into microcapsules with a thin polymer shell.

Overall, the use of paraffin-based PCMs can be improved through encapsulation and microencapsulation methods. The appropriate method to use depends on the specific application and desired properties.

The research on polymeric matrix-based shape-stable phase change materials (PCMs) has gained significant importance in recent years. Among these, paraffin-polymer composite materials are particularly attractive, as they remain solid at paraffin melting point and above, without any softening. These materials have high-energy absorption capacity and can be widely used as stable PCMs with specific properties. However, some common disadvantages such as low thermal stability, low thermal conductivity, and relatively high flammability can restrict their application, particularly in building materials.

Research in this field aims to eliminate these disadvantages and improve the properties of these materials. Suitable additives have been proposed to improve the thermal conductivity, flame retardation, and thermophysical and mechanical properties. The preparation of these composites involves no chemical reaction or chemical bonds between the polymers and paraffin. Therefore, these types of compounds are considered as physical mixtures.

Shape-stable PPCMs have several advantages over other PCMs as they are thermoplastic, allowing them to be melted and crystallized for many cycle numbers. They are also non-toxic

and do not require high-energy consumption during the production process.

Inaba and Tu developed a new type of shape-stable PPCM, which can be used without encapsulation [7]. Feldman et al. prepared plates of shape-stable PCM and determined their high thermal energy storage capacity when used in small chambers. In this type of polymer-based plates, fatty acids are used as PCMs that absorb or release large amounts of heat during melting and solidification, without altering the composition of the shape-stable PCM [8].

Lee and Choi studied the composition of paraffin and high-density polyethylene (HDPE) and introduced it as a shape-stable energy storage material. They also studied the morphology of the high-density polyethylene crystal lattice (HDPE) and its effect on paraffin [9]. Hong and Xin-Shi synthesized polyethylene-paraffin as a shape-stable PCM and recommended a composition consisting of 75% paraffin as a cheap, effective, easy-to-prepare, low-temperature shape-stable PPCM. Xiao et al. prepared a shape-stable PCM based on the composition of paraffin with a thermoplastic elastomer (styrene butadiene rubber) and determined its thermal properties [10].

Despite the benefits, some disadvantages of shape-stable PPCMs are reported. The major problem is the softening and paraffin leakage phenomenon at elevated temperatures. Seiler resolved this problem by adding a different ratio of silica and copolymers to the polyethylene-paraffin composition. Another problem is the low thermal conductivity of the polyethylene-paraffin compound [11]. A lot of research has been conducted to increase this property, including the addition of expanded graphite and metal particles and metal oxides to the paraffin. Alumina nanoparticles have received more attention in recent years to improve this property of PCMs.

Overall, the shape-stable PPCMs have unique controllable structures and are widely used as stable PCMs with specific properties. Researchers are working to overcome their limitations, and further studies are required to eliminate their disadvantages and improve their properties. These materials have great potential for application in building materials, textiles, thermal energy storage, and many other fields.

Researchers have found that addition of the nanoparticles to PCM can decrease or enhance

the latent heat, depending on the type and amount of nanoparticles added.

Adding nanoparticles to paraffin enhances its latent heat and those materials are usually known as nano-PCM. Several research studies have been conducted to investigate the effects of adding nanoparticles to paraffin. Some studies have found that adding nanoparticles can decrease latent heat, while others have succeeded in enhancing latent heat. For example, one study added exfoliated graphite nanoplatelets (xGnPs) particles to fatty acid group PCM, which enhanced nano-PCM latent heat by 0.83% at 10 wt% mass fractions [12]. Another study added Fe_3O_4 to paraffin, which enhanced latent heat by 8.8% at 20 wt% mass fractions [13]. Similarly, adding graphene nanoplatelets to beeswax enhanced its latent heat by 22.32% at 0.3 wt% mass fraction [14]. Adding TiO_2 to PCM salt hydrate enhanced its latent heat by 6.4% at 0.3 wt% mass fraction and adding xGnPs to paraffin enhanced its latent heat by 4% at 1 wt% mass fraction [15].

It is revealed that the increasing amount of latent heat in nano-PCM depends on the number of nano-PCM mass fractions. The authors conducted a study and found that the latent heat of paraffin- Fe_3O_4 nano-PCM increased by 20.67% compared to pure paraffin when Fe_3O_4 was added at 5 wt% mass fractions. Similarly, the latent heat of paraffin-CuO nano-PCM increased by 78.89% at 10 wt% mass fractions, and the latent heat of paraffin- TiO_2 nano-PCM increased by 7.5% at 15 wt% mass fractions. The latent heat of paraffin-ZnO nano-PCM also increased by 20.17% [16].

The increase in latent heat is due to the Brownian motion of the nano-PCM, which increases the probability of agglomeration in the paraffin base fluid. Van der Waals forces between the nanoparticles attract each other and grouping. Lower concentration of nanoparticles enables thermal storage to be more operational per volume unit [17].

4. CONCLUSION

Overall, paraffin wax has the potential to be a highly effective PCM for LHTES applications due to its various advantages. However, its low thermal conductivity must be taken into consideration and addressed in the design and implementation of LHTES systems. Further research is necessary to fully understand the

properties and potential of paraffin wax as a PCM for thermal energy storage.

REFERENCES

- [1] Sharma A, Tyagi V, et al. Review on thermal energy storage with phase change materials and applications. *Renewable and Sustainable Energy Reviews*. 2009;**13**:318-345
- [2] Cvetanovic, G., Stojiljkovic, S., Raskovic, P., Zivkovic, P., (2022), Potentials of clay as a phase change material, *Innovative mechanical engineering*, vol. 1, no. 2, pp.116-129
- [3] Himran, Syukri & Suwono, Aryadi & Mansoori, G Ali. (1994). Characterization of Alkanes and Paraffin Waxes for Application as Phase Change Energy Storage Medium. *Energy Sources*. 16. 117-128. 10.1080/00908319408909065.
- [4] Cui, Yaping & Xie, Jingchao & Liu, Jiaping & Wang, Jianping & Chen, Shuqin. (2017). A review on phase change material application in building. *Advances in Mechanical Engineering*. 9. 168781401770082. 10.1177/1687814017700828.
- [5] Khan Z, Khan Z, Ghafoor A. A review of performance enhancement of PCM based latent heat storage system within the context of materials, thermal stability and compatibility. *Energy Conversion and Management*. 2016;**115**:132-158
- [6] Rahman A, Dickinson ME, Farid MM. Microencapsulation of a PCM through membrane emulsification and nanocompression-based determination of microcapsule strength. *Materials for Renewable and Sustainable Energy*. 2012;**1**(4)
- [7] Inaba H, Tu P. Evaluation of thermo-physical characteristics on shape-stabilized paraffin as a solid- liquid phase change material. *Heat and Mass Transfer*. 1997;**32**:307-312
- [8] Feldman D, Shapiro M, Fazio P. A heat storage module with a polymer structural matrix. *Polymer Engineering & Science*. 1985;**25**(7):406-411
- [9] Lee C, Choi HK. Crystalline morphology in high density polyethylene/paraffin blend for thermal energy storage. *Polymer Composites*. 1998;**19**(6):704-708
- [10] Hong Y, Xin-shi G. Preparation of polyethylene-paraffin compound as a form-stable solid-liquid phase change material. *Solar Energy Materials and Solar Cells*. 2000;**64**:37-44
- [11] Salyer IO. Phase Change Materials Incorporated throughout the Structure of Polymer Fibers. Pat. US 5885475; 1999

- [12] Eanest Jebasingh B 2016 Preparation of organic based ternary eutectic fatty acid mixture as phase change material (PCM), optimizing their thermal properties by enriched solar treated exfoliated graphite for energy storage Materials Today: Proceedings 3 1592-98
- [13] Şahan N, Fois M and Paksoy H 2015 Improving thermal conductivity phase change materials— A study of paraffin nanomagnetite composites Solar Energy Materials and Solar Cells 137 61-67
- [14] Amin M, Putra N, Kosasih E A, Prawiro E, Luanto R A and Mahlia T M I 2017 Thermal properties of beeswax/graphene phase change material as energy storage for building applications Applied Thermal Eng. 112 273-280
- [15] Liu Y and Yang Y 2017 Investigation of specific heat and latent heat enhancement in hydrate salt based TiO₂ nanofluid phase change material Applied Thermal Eng. 124 533-538
- [16] Kim S and Drzal L T 2009 High latent heat storage and high thermal conductive phase change materials using exfoliated graphite nanoplatelets Solar Energy Materials and Solar Cells 93 136-142
- [17] Zabalegui A, Lokapur D and Lee H 2014 Nanofluid PCMs for thermal energy storage: Latent heat reduction mechanisms and a numerical study of effective thermal storage performance Int. J. of Heat and Mass Transfer 78 1145-54

Mechanics and Design



Banja Luka
1–2 Jun 2023.

DEMI 2023

16th International Conference on Accomplishments in Mechanical and Industrial Engineering

www.demi.mf.unibl.org



Analytical functions for graded composite materials modelling

D. Čukanović^a, G. Bogdanović^b, A. Radaković^c, D. Milosavljević^b, N. Velimirović^c

^aUniversity of Priština in Kosovska Mitrovica, Faculty of Technical Sciences, Knjaza Miloša 7, 38220 Kosovska Mitrovica, Serbia

^bUniversity of Kragujevac, Faculty of Engineering, Sestre Janjić 6, 34000 Kragujevac, Serbia

^cState University of Novi Pazar, Vuka Karadžića bb, 36300 Novi Pazar, Serbia

Abstract *The necessity of constant monitoring of the main trends in research and application of materials and technologies is imposed as an obligation in the field of engineering and applied science. The paper presents the fundamental characteristics of functionally graded materials (FGM) and points out their advantages over conventional materials. Considering the variable material characteristics that FGM have in the direction of the plate thickness, special attention was paid to the definition of analytical functions that can adequately describe the mentioned structure. Those functions are the basis for obtaining the FGM mathematical model for stress-strain analysis of plates. A review and systematization of plate theories used in the analysis of conventional composite laminates was performed. The possibilities to adapt and implement previously mentioned plate theories for the analysis of FGM plates are described. Based on the described theoretical foundations, numerical examples were made, appropriate interpretations were given and certain conclusions were reached.*

Keywords *functionally graded materials, analytical functions, plate theory, numerical examples*

1. FUNCTIONALLY GRADED MATERIALS

At the global level, materials appear as one of the most important areas of research through various disciplines. The intensive development of new materials is based on increasing experience and knowledge related the methods for obtaining them (production and shaping), their properties and possibilities of application. Whether they originate as a resource from nature or as a product of artificial substances, all materials have a huge impact on the environment, industry, economy and ultimately

on humans as the end user. The increasing use of new materials in medicine, the airplane industry, the automotive industry, civil engineering enables a more comfortable, reliable and safe living environment [1].

The subject of analysis in this paper are plates made of functionally graded materials (FGM) as modern materials in the family of engineering composites. The basic concept of FGM is to use the properties of available materials in the best possible way by appropriately combining them. This includes reduction of plane stresses, shear stresses through plate thickness and improvement of thermo-mechanical properties. FGM is a composite material composed of two or more constituents with a continuous change of properties in a certain direction. A gradient of thermo-mechanical properties can be along one or more directions. FGM can be designed by controlling the volume fractions of constituents

Corresponding author

PhD, Dragan Čukanović, Associate professor,
dragan.cukanovic@pr.ac.rs

University of Priština, Faculty of Technical Sciences
Knjaza Miloša 7
38220 Kosovska Mitrovica, Serbia

in the desired direction. Therefore, there are different the mathematical functions that describe the obtained gradient of properties in a certain direction. The most commonly used functions for evaluating the effective material properties across the FGM plate thickness are [2]:

- a) power law function,
- b) sigmoidal function,
- c) exponential function,
- d) Mori-Tanaka method.

a) Power law function

This function for describing the change in thermo-mechanical properties of FGM in the direction of plate thickness is one of the most frequently used in the literature. Due to fact that mentioned function is used in this paper for numerical examples it will be described in detail. The change in FGM properties in the direction of plate thickness according to the mentioned function is given as:

$$P(z) = P_b + P_{tb} \left(\frac{1}{2} + \frac{z}{h} \right)^p, \quad P_{tb} = P_t - P_b \quad (1)$$

$$V_f = \left(\frac{1}{2} + \frac{z}{h} \right)^p$$

The presented power law function defines the change in mechanical properties as a function of the volume fraction of FGM constituents in the direction of the plate thickness. $P(z)$ denotes a material characteristic in cross-section “ z ”, h is the total thickness of the plate, P_t is a material property on the top of the plate ($z=h/2$) and P_b a material property on the bottom of the plate ($z=-h/2$). Practically, the index p defines the volume fraction and distribution of constituents in the direction of the plate thickness. A higher value of the index p means a higher proportion of constituent 1 (e.g., metal) and a lower value of the mentioned index means a higher proportion of constituent 2 (e.g., ceramics). FGM adapted for precisely determined and specific purposes in modern constructions can be obtained by varying the index p . Figure 1 shows in detail the change in the volume fraction of the constituents through the plate thickness for different values of the index p . It should be emphasized that at a value of $p=0$ the plate is made of pure ceramic, at values of $p=0.3; 0.5; 1$;

3, the proportion of ceramics decreases, and the proportion of metal increases, so that, theoretically, at values of $p = \infty$, the plate would be made of metal.

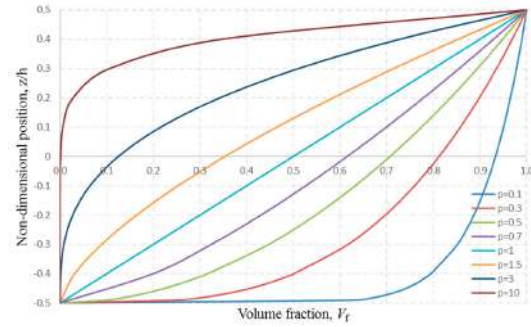


Fig. 1. Variation of the volume fraction of FGM constituents in the direction of plate thickness depending on the index p

b) Sigmoidal function

This function is mostly applied to layered FG plates. For example, plates with ceramic in the center and a gradient change of properties to metal on both extreme edges of the plate (sandwich plate). In such cases, if a single power law function is used, a stress concentration occurs at the interface. Therefore, in order to describe a continuous change of stress it is necessary to use two power law functions, whereby a sigmoidal function is obtained. The change in volume fraction of the constituent from the middle plane towards the upper edge of the plate (V_{f1}) and from the lower edge towards the middle plane (V_{f2}) is given as:

$$V_{f1} = 1 + \left(\frac{z}{h} - \frac{1}{2} \right)^p, \quad 0 \leq z \leq h/2 \quad (2)$$

$$V_{f2} = \left(\frac{z}{h} + \frac{1}{2} \right)^p, \quad -h/2 \leq z \leq 0$$

Then, the effective material characteristics in the direction of the plate thickness are calculated based on the equation (1). Also, the optimal volume fractions of constituents can be achieved by varying the index p .

c) Exponential function

This type function for FGM approximation is most often used in solving and analyzing problems in fracture mechanics. The change of thermo-mechanical properties in the direction

of the plate thickness is given by the following exponential function:

$$P(z) = P_b e^{\left(\frac{z}{h} \ln \left(\frac{P_t}{P_b} \right) \right)} \quad (3)$$

d) Mori-Tanaka method

The Mori-Tanaka method considers the effect of interaction between neighboring constituent particles. Effective material characteristics in the direction of the plate thickness ($K(z)$ -compressibility modulus, $G(z)$ - shear modulus) are calculated as:

$$\frac{K(z) - K_b}{K_t - K(z)} = \frac{V_f^p}{1 + (1 - V_f^p) \left(\frac{K_t - K_b}{K_b + \frac{4}{3} G_b} \right)}$$

$$\frac{G(z) - G_b}{G_t - G(z)} = \frac{V_f^p}{1 + (1 - V_f^p) \left(\frac{G_t - G_b}{G_b + f_b} \right)} \quad (4)$$

where is:

$$f_b = \frac{G_b (9K_b + 8G_b)}{6(K_b + 2G_b)}$$

The effective value of the modulus of elasticity $E(z)$, Poisson's ratio $\nu(z)$ and coefficient of thermal expansion $\alpha(z)$ are calculated based on $K(z)$ and $G(z)$ as

$$E(z) = \frac{9K(z)G(z)}{3K(z) + G(z)}, \quad \nu(z) = \frac{3K(z) - 2G(z)}{2(3K(z) + G(z))}$$

$$\frac{\alpha(z) - \alpha_b}{\alpha_t - \alpha(z)} = \frac{\frac{1}{K(z)} - \frac{1}{K_b}}{\frac{1}{K_t} - \frac{1}{K_b}}, \quad (5)$$

where the volume fraction V_f is given by (1).

2. SHEAR DEFORMATION THEORIES FOR THE ANALYSIS OF FGM PLATES

Composite materials are primarily used in thin-walled constructions. However, with the development of technology and various industrial requirements, there has been a need to use composite materials in both moderately thick and thick structures. Initially, to examine the behavior of moderately thick and thick

plates, the theoretical assumptions for the analysis of thin-walled plates were used. However, theoretical assumptions based on classical plate theory gave good results for thin but not for moderately thick and thick plates. Various plate theories are essential for accurate analysis and prediction of plate behavior under various static and dynamic loading conditions. Depending on the assumed forms of displacement, plate theories can be classified as [3]:

- classical plate theory (CPT),
- first order shear deformation theory (FSDT),
- higher order shear deformation theory (HSDT).

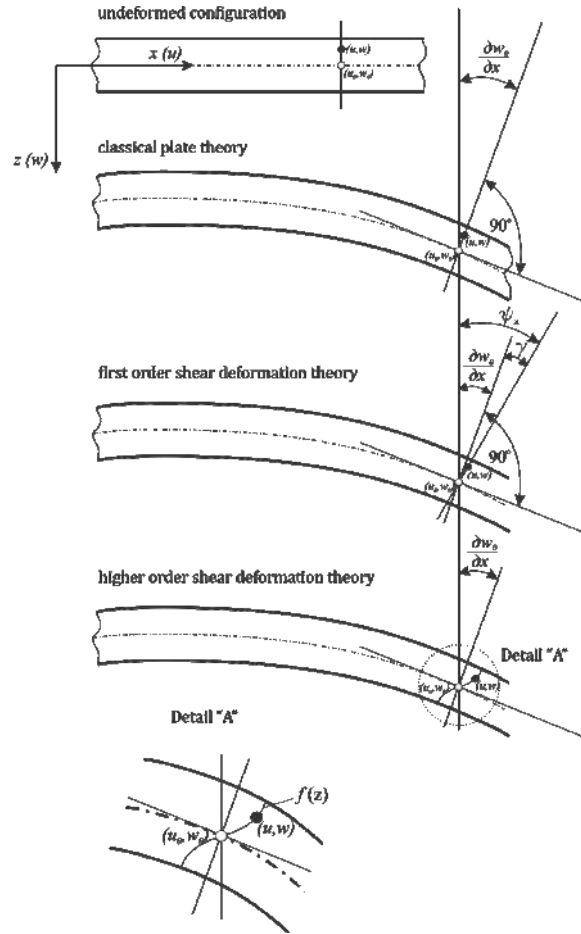


Fig. 2. Different shear deformation theories of plates

The main goal of introducing higher-order theories is to reduce the degree of approximation of real problems described by a mathematical model in order to obtain results as close as possible to experimental results.

HSDT theories should eliminate the disadvantages of applying CPT and FSDT theories to thick and moderately thick plates as well as eliminate the use of correction factors. Figure 2 shows a comparison of different shear deformation theories. It can be clearly seen, in contrast to CPT and FSDT, with higher-order theories incurvation of the cross-section occurs. This practically means that the line normal to the middle plane of the plate does not retain a straight-line shape, but acquires a curvilinear shape (Figure 2 - Detail "A"). The type of this nonlinearity is defined by the function that is used in assumed forms of displacement. At the same time, the main goal is to introduce such an assumed form of displacement to obtain as simple mathematical functions as possible. A simpler mathematical form of the assumed forms of displacement means a shorter calculation time. The different assumed forms of displacement also implies the introduction of a different number of independent variables that define the previously described deformation of line normal to the middle plane. HSDT theories can be based on different shape functions $f(z)$, such as exponential, trigonometric, hyperbolic, etc. The assumed forms of displacement fields in this case are:

$$\begin{aligned} u(x, y, z, t) &= u_0(x, y, t) - z \frac{\partial w_0(x, y, t)}{\partial x} + f(z) \theta_x \\ v(x, y, z, t) &= v_0(x, y, t) - z \frac{\partial w_0(x, y, t)}{\partial y} + f(z) \theta_y \\ w(x, y, z, t) &= w_0(x, y, t) \end{aligned} \quad (6)$$

In addition to HSDT based on shape functions, other forms of these theories based on polynomial functions are used in macro-mechanical analysis.

Based on the he assumed forms of displacement (1) equilibrium equations is obtained by using the relationship between stress and strain in the area of linear elasticity as well as the principle on minimum potential energy [4]. In order to obtain analytical solutions for the equilibrium equations, assumed solution forms and boundary conditions are adopted in accordance with Navier's solution given in [5].

3. NUMERICAL EXAMPLES - COMPARATIVE ANALYSIS BASED ON DIFFERENT THEORIES

Bending and critical buckling temperature of a moderately thick FGM square plate ($a/h=10$, $a/b=1$) was analyzed using different shear deformation theories. The analysis was done for the case of FGM plates of metal (*Al-Aluminum*, $E_m=0.7 \cdot 10^5 [\text{MPa}]$, $\nu=0.3$, $\alpha_m=23 \cdot 10^{-6} [^\circ\text{C}^{-1}]$) and ceramic constituents (*Al₂O₃-Alumina*, $E_c=3.8 \cdot 10^5 [\text{MPa}]$, $\nu=0.3$, $\alpha_c=7.4 \cdot 10^{-6} [^\circ\text{C}^{-1}]$). The effective material characteristics are determined by applying the power law function (1). Figure 3 shows the comparative results of normalized values of vertical displacement of FGM plate using quasi 3D elasticity theory [6], HSDT^R based on Reddy assumed forms of displacement [7] and HSDT (*SF*) based on shape function. Finally, the results for the classical plate theory (CPT) [8] are presented in order to observe certain deficiencies of the mentioned theory. Based on the comparative results, a good match between the results obtained by the HSDT (*SF*) theory with the HSDT^R theory as well as the quasi 3D theory of elasticity can be observed. On the other hand, a large deviation of the results obtained by the CPT theory is clearly visible. This indicates that the mentioned theory does not give satisfactory results in the analysis of moderately thick FGM plates.

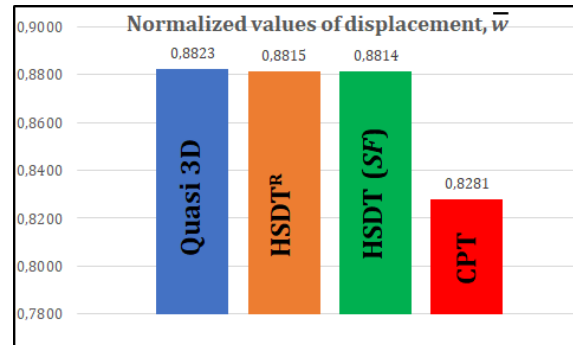


Fig. 3. Comparative results of normalized values of displacement

Figure 4 shows the comparative results of the critical buckling temperature using different theories. Similar to the previous observation the same conclusions are reached. For example, when analyzing a plate $a/h = 10$, the error of the results based on CPT is about 7%.

It can be shown that this error is increasing with further increase in the plate thickness which clearly indicates that with moderately

thick and thick plates CPL does not give satisfactory results for ΔT_{cr} .

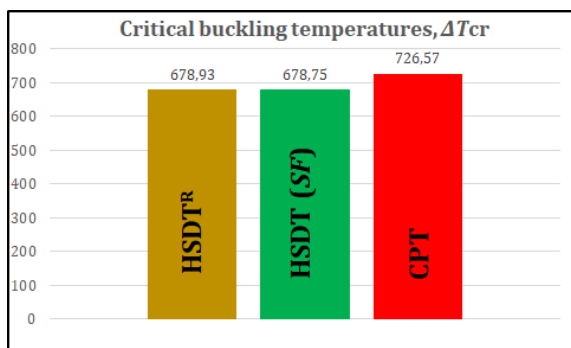


Fig. 4. Comparative results of critical buckling temperatures

4. CONCLUSION

The paper points out the importance and topicality of research into modern composite materials with a special focus on functionally graded materials. Considering the variable thermo-mechanical properties that FGM have in the direction of the plate thickness, special attention has been paid to defining mathematical functions that can adequately describe the mentioned graded structure. An overview of power law, sigmoidal, exponential functions and Mori-Tanaka method for describing variable material characteristics in FGM is given. A comparative review of shear deformation theories for plate analysis is given. A comparative analysis of moderately thick FGM plates consisting of two constituents - metal (Aluminum - Al) and ceramics (Alumina - Al_2O_3) was performed by using different theories. The obtained results of vertical displacement and critical buckling temperature using HSDT (SF) match very well with the results in the literature obtained using HSDT^R and quasi 3D theory. On the other hand, large deviations of the obtained results were observed compared to the results from the literature obtained by the CPT theory.

REFERENCES

[1] Tošić. G., Bogdanović. G., Čukanović. D.,

- Radaković. A. (2022). Functionally graded materials in transport vehicles-overview, fabrication, application, modelling. *IOP Conf. Series: Materials Science and Engineering*, 1271. DOI: [10.1088/1757-899X/1271/1/012014](https://doi.org/10.1088/1757-899X/1271/1/012014)
- [2] Swaminathan, K., Sangeetha, D.M. (2017). Thermal analysis of FGM plates – A critical review of various modeling techniques and solution methods. *Composite Structures*, vol. 160, p. 43-60. DOI: [10.1016/j.compstruct.2016.10.047](https://doi.org/10.1016/j.compstruct.2016.10.047)
- [3] Reddy. J.N., Arciniega. R.A. (2004). Shear deformation plate and shell theories: from Stavsky to present. *Mechanics of Advanced Materials and Structures*, vol. 11, no. 6, p. 535-582. DOI: [10.1080/15376490490452777](https://doi.org/10.1080/15376490490452777)
- [4] Milosavljević. D., Radaković. A., Čukanović. D., Bogdanović. G., Ivanović. L. Comparative bending analysis of composite laminate and functionally graded plates based on the new shape function. *8th International Congress of Serbian Society of Mechanics*, Kragujevac, Serbia, June 28-30, 2021.
- [5] Reddy, J. N., (2004). *Mechanics of Laminated Composite Plates and Shells: Theory and Analysis*. CRC Press LLC, New York, United State of America.
- [6] Wu, C.P., Chiu, K.H., Wang, Y.M. (2011) RMVT-based meshless collocation and element-free Galerkin methods for the quasi-3D analysis of multilayered composite and FGM plates. *Composite Structures*, vol. 93, no. 2, p. 923-943. DOI: [10.1016/j.compstruct.2010.07.001](https://doi.org/10.1016/j.compstruct.2010.07.001)
- [7] Wu, C.P., Li, H.Y. (2010). An RMVT-based third-order shear deformation theory of multilayered functionally graded material plates. *Composite Structures*, vol. 92, no. 10, p. 2591-2605. DOI: [10.1016/j.compstruct.2010.01.022](https://doi.org/10.1016/j.compstruct.2010.01.022)
- [8] Carrera, E., Brischetto, S., Robaldo, A. (2008) Variable kinematic model for the analysis of functionally graded material plates. *AIAA Journal*, vol. 46, no. 1, p. 194-203. DOI: [10.2514/1.32490](https://doi.org/10.2514/1.32490)



Banja Luka
1-2 Jun 2023.

DEMI 2023

16th International Conference on Accomplishments in Mechanical and Industrial Engineering

www.demi.mf.unibl.org



Cold rolled vs. hot rolled steel sections in the design of cantilever racking

R. Vujanac^a, N. Miloradovic^a, S. Vulovic^b, A. Pavlovic^c

^aAssociate professor, Faculty of Engineering University of Kragujevac, Kragujevac, Serbia

^bResearch associate, Institute of Information Technologies, University of Kragujevac, Kragujevac, Serbia

^cJunior assistant professor, Department of Industrial Engineering, University of Bologna, Bologna, Italy

Abstract

Cantilever racks are primarily used for storing goods where one overall dimension is significantly larger than the other two. Thus, they are usually used in warehouses, productions, workshops, but also outdoors, for storing sheets, profiles, pipes or rods in bundles or individually. With adequate implementation of the basic configuration and appropriate additional equipment, pallets, coils, and various unit loads can be stored on the cantilever racks too. They are made stiffened or unstiffened, one - sided or double - sided configuration, depending on whether they have bases and consoles on one or both sides of the column. The connection between the console and the column can be non-adjustable, made by welding or screws, at pre - defined distances, where the console cannot subsequently be moved along the column. An adjustable bracket system made with pins or screws allows the console to be moved along the column by a certain step. They are produced from standard cold rolled and hot rolled steel sections. This paper discusses advantages and disadvantages and provide comparison of usage of these two types of steel sections in the design of cantilever racking system.

Keywords cantilever racking, steel section, design

1. INTRODUCTION

In modern warehouse technics cantilever racks are standard products intended primarily for the storage of long or irregular goods like sheets, profiles, pipes or rods in bundles or individually. But, with adequate implementation of their basic configuration and appropriate accessories, also pallets, coils, and various unit loads can be stored on the cantilever racks too. Depending on the application they are usually

served by powered material handling equipment such as fork lift or side loading trucks, overall cranes or for the lower applications they are hand loaded. They can be used for internal or external storage in the warehouses, productions or workshops. As load bearing structures requirements for their structural design, use and maintenance are given in relevant EN standards, codes or norms. So, when it comes to cantilever racks, FEM code 10.2.09 [1], gives specific guidelines for the design requirements applicable to all types of cantilever rack systems fabricated from steel members in line with more general standards like EN 1990 and EN 1993. On the other hand, standards EN 15629 [2], and EN 15635 [3], provide recommendations regarding the use and maintenance of all rack types.

Corresponding author

PhD, Rodoljub Vujanac
vujanac@kg.ac.rs

Associate professor
Faculty of Engineering University of Kragujevac
Sestre Janjic 6
Kragujevac, Serbia

2. STRUCTURE OF CANTILEVER RACKING

In order to perform the classification of cantilever racks, it is necessary to define elements of the racking structure in the cross - aisle direction (perpendicular to an operating aisle which is defined as space giving access to picking or loading faces of the rack) and down - aisle direction (parallel to an operating aisle) [4].

2.1 Components of cantilever racking

The main components of cantilever racking structure are shown in Fig. 1 and Fig. 2. Column is vertical component (often perforated) on which lie cantilever arms supporting the loads transmitted by them. Base is horizontal member connected to column supported by the floor. Cantilever arm is also horizontal load - carrying member connected at one side to the column in the cross - aisle direction. To ensure cross - aisle stability, the bases usually have minimum the same length as the cantilever arms; in other words, a vertical line running down from the ends of the cantilever arms touches the ends of the base bars.

Cantilever racks with arms and bases on one side of the column form single sided cantilever rack as shown on the Fig. 1. Double sided cantilever rack has arms and bases on two opposite sides of the column, Fig. 2.

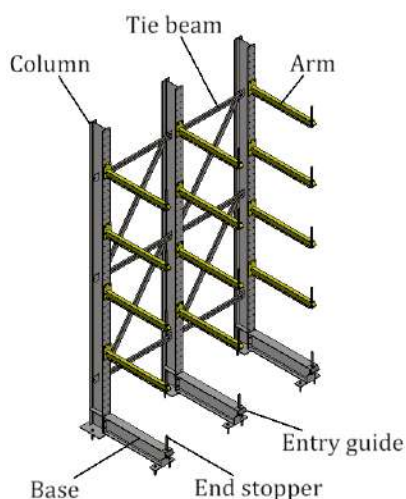


Fig. 1. Un - braced single sided cantilever rack

The down - aisle stability of the rack is provided by the bracing system consisting of horizontal and diagonal bars. They are members that

connecting columns in the down - aisle direction. If adjacent columns in down - aisle direction are connected only with horizontal tie beam cantilever system is considered as un - braced, Fig. 1. The typical configuration of braced cantilever system has down - aisle stability provided by cross - bracing, i. e. bracing with both presence of horizontal and diagonal bars between columns as shown on Fig. 2.

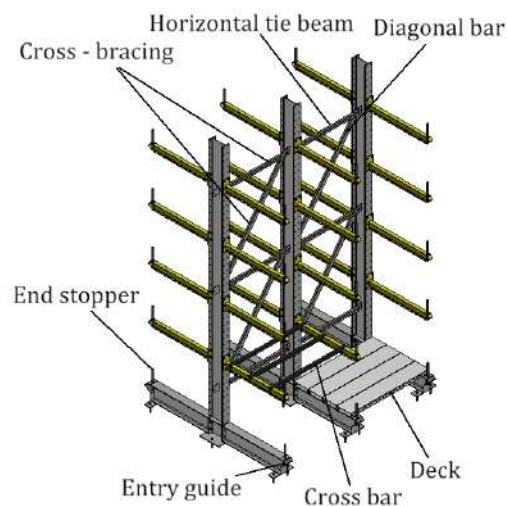


Fig. 2. Braced double sided cantilever rack

Entry guide is the element fixed on the end of the cantilever arm or base which provides sliding of the goods over them during placement. On the same position stands end stopper (fixed or removable) intended to retain unit loads, restricting their sliding or rolling when stored. Deck is derived load carrying surface as steel tile or wire mesh, supported by cantilever arms. Cross bar is a support member connected to arms or bases.

2.2 Types of cantilever racking

Classification of cantilever racks can be done according to several criteria.

Considering the basic components and their layout in the cantilever rack structure, i. e. position of the basis and arms relative to the columns, cantilever racks can be:

- single sided or
- double sided.

Depending of the bracing system in down - aisle direction, cantilever racks can be:

- un - braced cantilever system or
- braced cantilever system.

The criterion that is based on basic material so rack components can be fabricated or pressed, cantilever racks can be made of:

- hot rolled profiles or
- cold rolled steel section.

Based on the type of the connection between the cantilever arm and column, there are several types of cantilever racks, initially classified in two main groups:

- **Non - adjustable arm system** as shown on Fig. 3. In this type of the construction the arm is normally welded, bolted or hooked to the column at a pre - determined spacing and cannot be subsequently adjusted for vertical pitch [1].

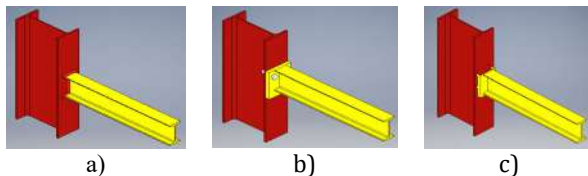


Fig. 3. Non - adjustable arm system: a) welded arm, b) bolted arm, c) hooked arm

- **Adjustable arm system** shown on Fig. 4. The arms in this type of construction are adjustable sometimes according to pre - determined hole or slot pitches in the column as following [1]:
 - *Bolted arm system* which is typical for hot rolled cantilever structures. A type of construction in which the arm is bolted to the column according to pre - determined holes in the column. This design may have multiple holes for adjustment of the vertical pitch.
 - *Hooked arm system*. A type of construction in which the arm is attached to the column by connector hooks. This can be typical solution for both hot rolled and cold rolled cantilever structures.
 - *Pinned arm system*. A type of construction for the cold rolled sections in which the arm is attached to the column by a mechanical fastening other than a bolt or rivet.
 - *Clamped arm system*. A type of adjustable arm system where the arms clamp to the column and are

retained in position by friction. Therefore, they may be located at any vertical position on the column. This is a typical solution for the hot rolled profiles of cantilever structures.

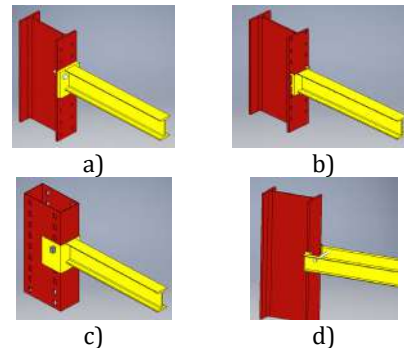


Fig. 4. Adjustable arm system: a) bolted arm, b) hooked arm, c) pinned arm, d) clamped arm

3. COMPARISON OF STEEL PROFILES FOR CANTILEVER RACKING

Hot rolled products represent the category of the most represented products in load - bearing steel structures. Profiles are rolled in two basic shapes, such as *I* and *U* - profiles. Well known European *IPE* profiles with wide parallel foots are the basic structural elements for production of columns and arms of cantilever racks [5]. Cold formed products are obtained by deformation of steel in a cold state in two ways:

- by rolling from a flat strip passing through a series of rollers or,
- by bending a flat strip on a press in a special tool.

Cold formed profiles are made as open or closed sections or profiled sheets for the production of elements of cantilever racks. The advantage of these products is reflected in their light weight, easy transport and handling, and a large selection of shapes.

Figure 5 shows configurations of single side cantilever racks made of cold formed and hot rolled profiles for the same parameters:

- Number of columns $n=3$,
- Column height $H=4000$ mm,
- Base depth $B=1200$ mm,
- Arm depth $C=1200$ mm,
- Number of arms per column $m=5$,
- Load per arm $Q=500$ daN,
- Columns axis distance $A=1500$ mm.

Both configurations were generated using a developed methodology for automatic generation of a 3D model of cantilever racks using connection between CAD software Autodesk Inventor and spreadsheet software Microsoft Excel used for the calculation of all construction parameters of the cantilever rack structure according to EN standards [6].

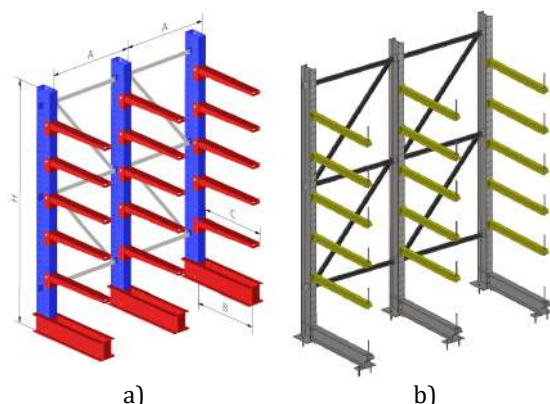


Fig. 5. Single sided cantilever rack made of: a) cold formed profiles, b) hot rolled profiles

Comparison between usage of cold rolled and hot rolled steel section in cantilever racking structure is shown in Table 1.

Table 1. Comparison between cold rolled and hot rolled steel section in cantilever racking structure

Feature	Cold rolled		Hot rolled	
	Adv.	Disadv.	Adv.	Disadv.
Weight of structure	√			√
Production	√			√
Surface protection		√	√	
Transport	√		√	
Installation	√			√
Carrying capacity		√	√	
Elements variety	√			√

In term of total weight of construction as expected cold rolled sections provided lighter construction. Manufacturing efficiency is also on the side of cold formed structure because most of the elements are obtained on modern semi-automatic and/or automatic CNC machines without manual work we have in processing hot rolled profiles (especially drilling and welding). But, the possibility for the better surface protection is on the side of open IPE profiles.

Since the elements of cantilever racks are almost always prefabricated, they are suitable for transport in both cases. Certainly, because they are lighter, cold formed structures are easier for installation process. On the other hand, due to compactness of the section hot rolled profiles are more suitable for the higher load capacity. Less variety of IPE profiles comparing to possible derivation of cold formed sections gives fewer possibilities of combining for different load capacities.

4. CONCLUSION

The previous discussion from several aspects gives the advantages to cold formed profiles in the production of cantilever racks. This was expected primarily from the aspect of the total weight of constructions and therefore the cost price. However, depending on the available tools, machines and processes at the manufacturer, the production of cold-formed structures can still be much more expensive. The production of cantilever racks using hot rolled profiles still can be carried out in a very traditional way.

REFERENCES

- [1] FEM 10.2.09. (2015). *The Design of Cantilever Racking*. European Materials Handling Federation. Hitchin.
- [2] EN 15629:2008. (2008). *Steel Static Storage Systems – Specification of Storage Equipment*. European Committee for Standardization. Brussels.
- [3] EN 15635:2008. (2008). *Steel Static Storage Systems – Application and Maintenance of Storage Equipment*. European Committee for Standardization. Brussels.
- [4] Vujanac, R., Miloradovic, N. (2008). *Basics of Storage and Material Handling Systems*. Faculty of Engineering University of Kragujevac, Kragujevac.
- [5] Budjevac, D., Markovic, Z., Bogavac, D., Tosic, D. (1999). *Metal Constructions, Basics of Calculation and Construction*. Faculty of Civil Engineering University of Belgrade, Belgrade.
- [6] Vujanac, R., Miloradovic, N., Zivkovic, P., Petrovic, L. Automation of Cantilever Racking Designing Process. *Book of Abstracts of 9th International Scientific Conference - Research and Development of Mechanical Elements and Systems IRMES 2019*, September 2019, Kragujevac, p. 154 - 155.



Banja Luka
1-2 Jun 2023.

DEMI 2023

16th International Conference on Accomplishments in Mechanical and Industrial Engineering

www.demi.mf.unibl.org



Control calculation of clearances in high-bay warehouse operated by storage and retrieval machines

N. Miloradović^a, R. Vujanac^a

^a University of Kragujevac, Faculty of Engineering, Sestre Janjic 6, 34000 Kragujevac, Serbia

Abstract *In order to properly design, manufacture, assemble and use rack warehouses operated by storage and retrieval machines (S/R machines), it is important to accurately define the tolerances, deformations and clearances of the system elements, on which both functional safety and economy depend. A high-bay warehouse, including S/R machines is a functional unit with components which are subjects to tolerances resulting from manufacture, erection and operation deformations. S/R machines are designed to safely store unit loads into, and to retrieve them from freely selected locations. Clearances which are too small are risk to operational safety so that handling operations in a warehouse may have to be stopped, but useful storage space is wasted where clearances are too large. The aim of this work is to determine the clearances in order to optimize the factors related to the economic dimensioning, production and assembly required for the safe functioning of the high-bay warehouse based on appropriate FEM regulations. The paper presents a conceptual solution for the arrangement of racks in the warehouse. It also classifies S/R machines according to several criteria. The impacts that have been analysed are quantified as much as possible to provide the basis for determination of the definitive clearances.*

Keywords *Storage and retrieval machines, warehouse, clearances*

1. INTRODUCTION

A special place in storage technology belongs to the so-called narrow aisle racks, which are characterized by the corridor width that is sufficient only for the straight line passage of the storage and retrieval machines carrying the unit load, with very small operational clearances [1].

Manipulation of the unit load in the corridor between the racks is done without the need for the S/R machines to turn directly towards the

rack in order to put down or pick up the unit load. These machines are usually guided along the corridors between the guides (in the case of the forklifts) or on the rails (in the case of the stacker cranes). They can have a fixed or a mobile operator's cabin. The corridors are usually 200 mm to 600 mm wider than the unit load.

The S/R machines are the storage devices with which the load units can be stored, transferred and retrieved. They are operated manually, automatically or combined. The operations of placing and retrieving loads in and out of the rack compartments are performed manually or mechanically, via load handling devices.

The basic characteristic of the stacker cranes (the difference from the rack forklifts) is that they are not freely rotating machines, but are attached to rails on the floor or on the ceiling

Corresponding author

Ph.D. Nenad Miloradović, assoc. prof.
mnenad@kg.ac.rs

University of Kragujevac, Faculty of Engineering
Sestre Janjic 6
Kragujevac, Serbia

and that they move along a straight line in the corridors between the racks, Fig 1 [2].

S/R machines can be moved in longitudinal, vertical and transverse direction [3].

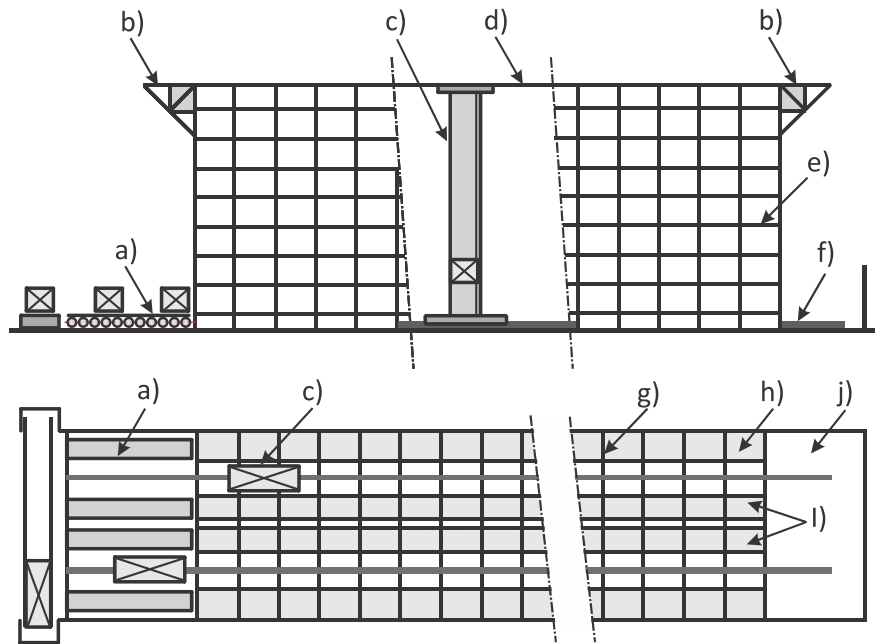


Fig. 1. Narrow aisle racks: a) conveyors, b) S/R machines run-out, c) S/R machines, d) upper guide rail, e) beam, f) bottom rail, g) portal tie beam, h) single entry run, i) double entry run, j) maintenance area

Depending on the previously defined control methods, the classes of the stacker cranes are defined according to FEM regulations [4]:

- Class A
 - manually controlled, where the operator manually controls movements in all directions,
- Class B
 - semi-automatic and automatic machines with positioning by coordinates,
- Class C
 - semi-automatic and automatic machines with positioning by coordinates and additional positioning only in Y direction,
- Class D
 - semi-automatic and automatic machines with positioning by coordinates and additional positioning only in X and Y direction.

2. CLEARANCES

Clearances exist to prevent collisions within the storage systems. Actually, they are required nominal distances between fixed and moving parts, taking into account all individual

tolerances and deformations. The entry clearances are the clearances between the load make-up accessory and the load handling device. The rack compartment clearances exist between the unit load and the rack structure, while the aisle clearances are the clearances between the outer most edge of the S/R machine and the outermost edge of the rack structure or the load, as well as the clearances at the rear of the stored load.

The racking tolerances and deformations influence the operating safety. However, for simplification, only two tolerance categories are defined for the rack design:

- Class 100 (lower tolerance and deformation values), for class B control systems in conjunction with S/R machines, without positioning aids at the toe storage position and for light weight and low to medium height (max. 18 m) storage systems and
- Class 200 (higher tolerance and deformation values), for class A control systems in conjunction with S/R machines with positioning aids at the storage position or manually controlled.

The calculation of clearances takes into account the following influencing factors: floor slab, floor rail, upper guide rail, unit load, S/R machines and rack structure [5].

2.1 Entry clearances

The entry clearances that exist between the load handling device and the load make-up accessory are shown in Fig 2:

- X_1 - on the side of the load handling device which is the furthest from the mast,
- X_2 - on the side of the load handling device which is the closest to the mast,
- Y_1 - between the load handling device and the load supporting beam and
- Y_2 - between the load handling device and the load make-up accessory.

In all cases, the largest respective entry cross-section of the load handling device entering the load make-up accessory will be considered.

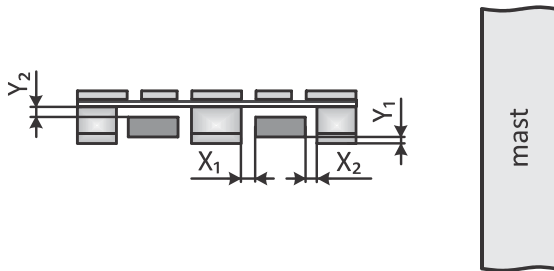


Fig. 2. Fork entry clearances

2.2 Rack compartment clearances

The rack compartment clearances are the minimum distances shown in Fig 3:

- $X_{3.1}$ - between the unit loads and the uprights on the side which is the furthest from the mast,
- $X_{3.2}$ - between the unit loads and the uprights on the side which is the closest to the mast,
- X_4 - between the individual unit loads,
- Y_3 - between the top of the unit load and the rack structure and/or other obstructions,
- Y_4 - between the underside of the raised unit load and the top of the lower support beam,
- Y_5 - between the underside of the higher support beam and the top of the raised unit load.

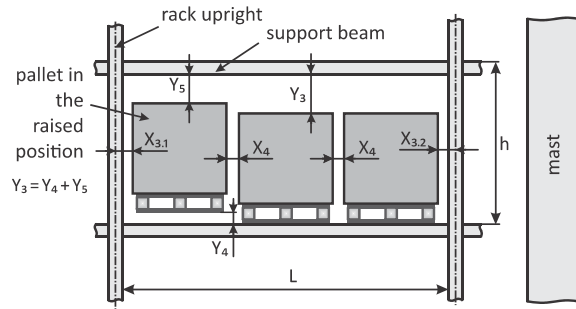


Fig. 3. Aperture clearances

2.3 Aisle clearances

The aisle clearances are the minimum distances shown in Fig 4:

- $Z_{1.1}$ - between the unit load and any obstruction on the building side (e.g. building structure, rainfall pipe),
- $Z_{1.2}$ - between the unit load and the rack structure inner racks,
- $Z_{2.1}$ - between the outermost point of the lifting carriage or the unit load on the lifting carriage and the nominal position of the stored load or the rack structure with a protruding load in the stored position on the outer rack side,
- $Z_{2.2}$ - the same, on the inner rack side,
- $Z_{3.1}$ - between fixed obstructions on the S/R machine (e.g. lifting mechanism or platform) and the stored load or the rack structure. Outer rack side,
- $Z_{3.2}$ - the same, on the inner rack side.

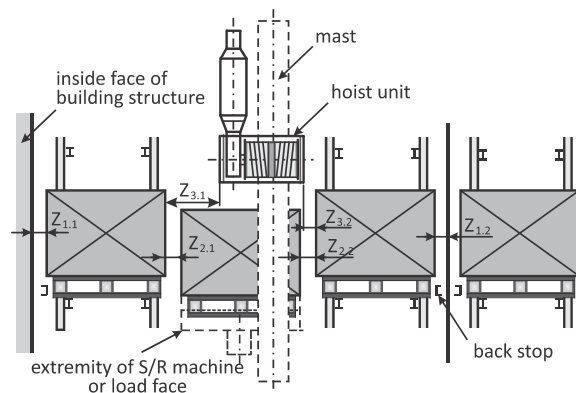


Fig. 4. Aisle clearances

2.4 Special obstructions

Many special conditions should be taken into account in defining the clearances. The

following factors should be considered in the planning phase, particularly when calculating clearances:

- arrangement of fire sprinklers and smoke alarm systems,
- domestic installations (cables, pipes, lighting, ductwork),
- minimum distances (e.g. to the sprinkler nozzles),
- variation of the profile dimensions depending on the rack system,
- protruding components (screw heads, supports, transmitters etc.),
- variations in unstable loads during placement in storage or during the storage period.

3. CONTROL CALCULATION

The assumed technical data of the warehouses for racking class 200, control mode A and C, are:

- silo/rack clad construction with pallet racking,
- building height 20 m, rack length 60 m,
- single-mast S/R machine,
- maximum rated load 1000 kg,
- maximum dimensions of the unit load X, Z, Y = 900 mm x 1300 mm x 1750 mm.

The assumed technical data of the warehouses for racking class 100, control mode B, are:

- free standing racking,
- building height 12 m, rack length 45 m,
- single-mast S/R machine,
- maximum rated load 1000 kg,
- maximum dimensions of the unit load X, Z, Y = 900 mm x 1300 mm x 1100 mm.

The most important influencing factors on the clearances are [6]:

- load and profile check,
- load make-up accessory,
- S/R machine,
- aisle equipment,
- rack structure.

Tables 1, 2, 3 and 4 present the values of the entry clearances. Some values are determined by the machine manufacturer or the person responsible for the design of the system.

Table 1. Entry clearances X₁, mm

Racking class		100	200
Type of control system		B	A C
Load make-up accessory	- centred position	2	- 2
	- pallet tolerance	3	3 3

S/R machine	- positioning accuracy	10	5 10
	- fork parallelity	1	1 1
	- deflection at fork tip due to guide roller clearance	1	1 1
	- torsional and mast oscillation	3	4 4
Rack structure	- verticality	10	4 10
Entry clearances X ₁ :		30	18 31

Table 2. Entry clearances X₂, mm

Racking class		100	200
Type of control system		B	A C
Load make-up accessory	- centred position	2	- 2
	- pallet tolerance	3	3 3
S/R machine	- positioning accuracy	10	5 10
	- fork parallelity	1	1 1
	- guide roller clearance at fork tip	1	1 1
	- mast deformation at the top	4	- 5
	- lifting carriage deformation	1	2 1
Rack structure	- torsional and mast oscillation	3	4 4
	- verticality	10	4 10
Entry clearances X ₂ :		35	20 37

Table 3. Entry clearances Y₁, mm

Racking class		100	200
Type of control system		B	A C
S/R machine	- positioning accuracy	3	6 4
	- tilting of the fork in X - direction	1	1 1
	- tilting of the fork in Z - direction	4	4 4
	- height positioning marker or tolerance of the beam	1	- 1
	- fork sag	5	6 6
	- deflection of the floor rail	1	- -
Aisle equipment	- height tolerance of the floor rail	2	- -
	- supporting beam level	4	- -
Rack structure	- supporting beam height difference	2	2 2
Entry clearances Y ₁ :		23	19 18

Table 4. Entry clearances Y₂, mm

Racking class		100	200
Type of control system		B	A C
Load make-up accessory	- reduced height fork entry	3	3 3
	- deflection of pallet	2	6 6
S/R machine	- positioning accuracy	3	6 4
	- tilting of the fork in X - direction	1	1 1
	- tilting of the fork in Z - direction	-	- -
	- positioning marker	1	- 1
Aisle equipment	- height tolerance of the floor rail	2	- -
Rack	- supporting beam level	4	- -

structure	- deflection of the supporting beams	6	-	-
	- upright compression	1	-	-
	- height difference between supporting beam	2	2	3
Entry clearances Y ₂ : 25 18 18				

Values of the rack aperture clearances are listed in Tables 5 to 9.

Table 5. Rack aperture clearances X_{3.1}, mm

Racking class		100	200
Type of control system		B	A C
Profile	- width	6	6 6
Load make-up accessory	- centring	2	- 2
S/R machine	- positioning accuracy	6	5 6
	- mast manufacture	3	- 3
	- torsion of the lifting carriage	1	2 1
	- load vertically due to sloping of the forks	3	3 3
	- bottom guide roller clearances	1	1 1
Aisle equipment	- mast deformation	15	10 15
	- accuracy of floor rail	1	1 1
	- mast tilting due to height tolerance of the floor rail	3	- 3
	- position markers	2	- 2
Rack structure	- tolerance field of uprights	15	- 15
	- verticality	10	4 10
Rack aperture clearances X _{3.1} : 68 32 67			

Table 6. Rack aperture clearances X_{3.2}, mm

Racking class		100	200
Type of control system		B	A C
Profile	- width	6	6 6
Load make-up accessory	- centring	2	- 2
S/R machine	- offset of the positioning marker at the centring location	4	- 5
	- positioning accuracy	6	5 6
	- mast manufacture	3	- 3
	- twisting of the lifting carriage	2	2 2
	- load vertically due to sloping of the forks	2	3 3
Aisle equipment	- guide roller clearances	1	1 1
	- torsion of lifting carriage	3	4 4
	- accuracy of floor rail	1	1 1
	- mast tilting due to height tolerance of the floor rail	3	- 3
Rack structure	- position markers	2	- 2
	- tolerance field of uprights	15	- 15
structure	- verticality	10	4 10
Rack aperture clearances X _{3.2} : 60 26 63			

Table 7. Rack aperture clearances X₄, mm

Racking class		100	200
Type of control system		B	A C
Profile	- width	10	10 10
Load make-up accessory	- centring	4	- 4
S/R machine	- positioning accuracy	12	10 12
	- mast deformation	-	- -
	- torsion of the lifting carriage	3	4 4
	- guide roller clearances	2	2 2
Aisle equipment	- mast inclination	4	- 4
	- position markers	3	- 3
Rack structure	- verticality	10	6 20
	- load verticality due to deflection of the supporting beams	14	22 22
Rack aperture clearances X ₄ : 62 54 81			

Table 8. Rack aperture clearances Y₃, mm

Racking class		100	200
Type of control system		B	A C
Profile	- height	6	6 6
Load make-up accessory	- reduced height fork entry	4	- 4
S/R machine	- positioning accuracy height	5	12 6
	- height positioning marker or tolerance of the beam	2	- 2
	- fork sag unloaded	4	6 6
	- fork deflection loaded	15	15 15
	- wear of wheels, and floor rail	1	- 1
Aisle equipment	- liftin carriage deformation	4	6 6
	- height of the floor rail	4	- 4
	- deflection of the floor rail	1	1 1
	- supporting beam level	10	20 20
Rack structure	- height difference between supporting beams	2	2 2
	- distance between supporting beams	5	5 5
	- deformation of the supporting beams	10	15 15
	- upright compressor	2	- 4
Rack aperture clearances Y ₃ : 75 88 97			

Table 9. Rack aperture clearances Z_{1.1} and Z_{1.2}, mm

Racking class		100	200
Type of control system		B	A C
Profile	- length of load	5	5 5
Load make-up accessory	- centred position	5	5 5
S/R	- fork extension	4	4 4

machine	- mast manufacture Z - direction	3	3	3
	- torsion of lifting carriage	1	1	1
	- clearance of side guide rollers	1	1	1
	- verticality of the load	26	30	30
	- mast deformation	6	8	8
Aisle equipment	- alignment accuracy of floor rail	2	2	2
	- lateral accuracy of guide rail	4	4	4
	- deflection of guide rail	3	3	3
Rack structure	- tolerance of rear obstruction	15	15	15
	- deformation of inner racks	5	5	5
	- deformation of outer racks	5	15	15
Clearances	inner racks Z _{1.2} :	80	86	86
	outer racks Z _{1.1} :	80	96	96

Tables 10 and 11 show values related to the aisle clearances.

Table 10. Aisle clearances Z_{2.1} and Z_{2.2}, mm

Racking class		100	200
Type of control system		B	A C
Profile	- length of load	10	10 10
Load make-up accessory			
S/R machine	- centred position in Z - direction	10	10 10
	- fork travel	4	4 4
	- side guide roller clearances	1	1 1
Rack structure	- mast oscillation	6	6 6
	- inclination due to height difference between front and rear beams	4	4 4
	- deformation of inner racks	5	5 5
	- deformation of outer racks	5	15 15
Clearances	inner racks Z _{2.2} :	40	40 40
	outer racks Z _{2.1} :	40	50 50

Table 11. Aisle clearances Z_{3.1} and Z_{3.2}, mm

Racking class		100	200
Type of control system		B	A C
Profile	- length of load	5	5 5
Load make-up accessory			
S/R machine	- centred position	5	5 5
	- fork travel	2	2 2
	- side guide roller clearance	1	1 1
Rack structure	- mast oscillation	2	2 2
	- tilted position due to difference in height of front to rear beams	4	4 4
	- deformation of inner racks	4	5 5
	- deformation of outer racks	5	15 15
Clearances	inner racks Z _{3.2} :	23	24 24
	outer racks Z _{3.1} :	24	34 34

4. CONCLUSION

In order to fulfil the investor's basic request to obtain the largest possible storage capacity in the available space, that is, the largest possible amount of stored material, designers must know all the possibilities of the S/R machines, the choice of which will depend on:

- storage unit,
- frequency of the storage units entering into and exiting from the warehouse,
- orientation of the entrance - exit zones,
- the number of the storage units within the high-bay warehouse (storage capacity),
- warehouse connections with external transport.

In this way, the biggest advantage of the warehouses to maximize space utilization and improve operating efficiency will be realized.

REFERENCES

- [1] Vujanac, R., Miloradović, N., Vulović S., Pavlović, A. (2020). A Comprehensive Study into the Boltless Connections of Racking Systems, *Metals*, vol. 10, no. 2, p. 1-17, DOI: 10.3390/met10020276
- [2] FEM 9.101. (1997). *Terminology - Storage and Retrieval Machines - Definitions*, Section IX of FEM, Brussels, Belgium
- [3] FEM 10.3.01. (1997). *Adjustable Beam Pallet Racking (APR) - Tolerances Deformation and Clearances*, Section X of FEM, Brussels, Belgium
- [4] FEM 9.831. (1995). *Calculation Principles of Storage And Retrieval Machines - Tolerances, Deformations and Clearances in the High - bay Warehouse*, Section X of FEM, Brussels, Belgium
- [5] Vujanac, R., Miloradović, N. (2023). *Basics of storage and transport systems* (in Serbian). The Faculty of engineering of the University of Kragujevac, Kragujevac
- [6] Vujanac, R., Miloradovic, N., Zivkovic, P., Petrovic, L. Basis for the design of drive-in and drive-through racking, *Proceeding of X Triennial International Conference Heavy Machinery - HM 2021*, June 2021, Vrnjačka Banja, Serbia, p. 57-63.



Banja Luka
1-2 Jun 2023.

DEMI 2023

16th International Conference on Accomplishments in Mechanical and Industrial Engineering

www.demi.mf.unibl.org



DELAYED ACCELERATION FEEDBACK FRACTIONAL ORDER CONTROL OF CART PENDULUM SYSTEM - SOME STABILITY ISSUES

M. P. Lazarević^a, D. Radojević^a, Lj. Bučanović^b, S. Pišl^a, *PhD student*

^a Faculty of Mechanical Engineering, University of Belgrade, Serbia, st. Kraljice Marije 16, Belgrade

^b Messer Tehnogas AD, Banjički put 62, Belgrade, Serbia

Abstract *This paper deals with the stability problem of an underactuated mechanical system controlled by a fractional order feedback controller. The design problem of a controller PDD2Da type with time delay and acceleration feedback for a cart inverted pendulum is considered in this paper. The delayed signal in the delay feedback can be interpreted as a good-quality prediction of the current position, velocity and acceleration based on their delayed values. A mathematical model of cart inverted pendulum is introduced and a proposed fractional order controller is applied in order to stabilize it. The problem of asymptotic stability of closed-loop neutral time delay fractional order system is solved using the D decomposition approach where stability regions in control parameters space are determined by applying this method. Also, some stability issues of finite time stability for this system are considered and presented in this contribution. Finally, simulation results are carried out to verify the effectiveness proposed method.*

Keywords *acceleration feedback, fractional order control, D decomposition approach*

1. INTRODUCTION

Inverted cart pendulum is one of the most interesting and attractive problems in control theory and its dynamics are representative of many applications. Also, it is an example of underactuated, nonlinear, nonminimum phase and highly unstable system. Because of this, it is very difficult to design a controller for a this kind of system and thus it presents an excellent benchmark for testing different control algorithms. Also, fractional order dynamical systems have drawn much attention from researchers and engineers over the past few decades. Also, fractional control has aroused theoretical and practical interest in the control community because the fractional order controller has tunable integral and differential

orders, creating the possibility to provide better control performance. On the other side, the question of asymptotic stability closed loop of fractional order systems is one of the important issue. First, we suggest using PDD^2D^α fractional type time delay controller in solving problem of angular stabilization of the inverted cart pendulum system. It is proposed using D-decomposition method where it is necessary to determine stability domains in the parameters space of closed loop system. This method enables to obtain analytical forms expressing the boundaries of stability domains in the parameters space. Finally, after stability domains are obtained, one can make a good tuning of fractional order controller parameters.

2. PROBLEM STATEMENT

2.1 Mathematical model of cart pendulum system

Here, it is of interest to study stabilization a underactuated mechanical system – cart pendulum that has two degrees of freedom, (x, θ) , and one control-horizontal force F , Fig.1.

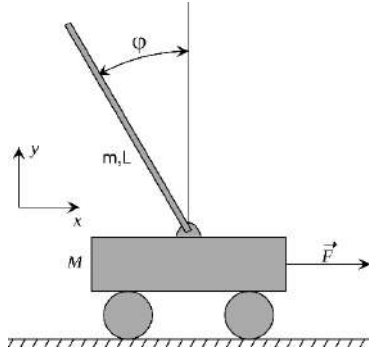


Fig. 1. Cart pendulum system

Applying Lagrange's equations of the second kind in the covariant form [1], one can obtain:

$$(m + M)\ddot{x} - \frac{ml}{2}\ddot{\theta}\cos\theta + \frac{ml}{2}\dot{\theta}^2\sin\theta = F, \quad (1)$$

$$-\frac{ml}{2}\ddot{x}\cos\theta + \frac{ml^2}{3}\ddot{\theta} = \frac{mgl}{2}\sin\theta - k_v\dot{\theta} \quad (2)$$

where are: M - mass of the cart, m - mass of the pendulum, l - total length of the pendulum, k_v - coefficient of viscous friction.

The previous equations can be simplified by applying *inverse dynamic control* [2]. Also, using a conveniently chosen force F , (see [3]), one can get

$$\ddot{x}(t) = u(t), \quad (3)$$

$$\ddot{\theta} = \frac{g}{L}\sin\theta - \frac{k_v}{J}\dot{\theta} + \frac{1}{L}\cos\theta \cdot u \quad (4)$$

where are $g \approx 9.81 [m/s^2]$ and $L = 2l/3$.

3. D-DECOMPOSITION METHOD FOR STABILIZATION OF INVERTED CART PENDULUM

3.1 Stabilizing controller using delayed acceleration feedback fractional order control

In order to design the control system, we must linearize Eq. (4) around the unstable equilibrium position $(\dot{x}, \varphi, \dot{\varphi}) = (0, 0, 0)$ where this control system is also applicable to nonlinear systems if the system motion does not deviate much from the equilibrium position, [2]. In that manner, the linearized system is:

$$\ddot{x} = u \quad (5)$$

$$\ddot{\theta} = -\frac{k_v}{J}\dot{\theta} + \frac{g}{L}\theta + \frac{1}{L} \cdot u \quad (6)$$

Now the goal is to apply adequate control u so as to achieve asymptotic stability for $(\dot{x}, \varphi, \dot{\varphi})$. In order to realize this, it is proposed to introduce the following control, which includes a PDD^2D^α fractional type controller in which a pure time delay also appears:

$$u(t) = -K_p\theta(t-\tau) - K_d\dot{\theta}(t-\tau) - K_a\ddot{\theta}(t-\tau) - K_\alpha\theta^\alpha(t-\tau) - K_x\dot{x}(t) \quad (7)$$

where $K_p, K_d, K_a, K_\alpha, K_x$ denote corresponding proportional and differential gains of the first and second order, a α is fractional order of Caputo derivative, [4]. On the other hand, the delayed signal in the delay feedback can be interpreted as a quality prediction of the current position, velocity and acceleration based on their delayed values, [5]. After substituting (7) into Eqs. (5)-(6), and neglecting $k_v \approx 0$ it yields:

$$\ddot{x}(t) + K_x\dot{x}(t) = -K_p\theta(t-\tau) - K_d\dot{\theta}(t-\tau) \quad (8)$$

$$L\ddot{\theta}(t) - g\theta(t) + K_p\theta(t-\tau) + K_d\dot{\theta}(t-\tau) + K_a\ddot{\theta}(t-\tau) + K_\alpha\theta^\alpha(t-\tau) = -K_x\dot{x}(t) \quad (9)$$

One may notice that in the case $\alpha=1$ we have PDD^2 controller. Formally, we have seven parameters $K_p, K_d, K_a, K_\alpha, K_x, \alpha, \tau$ which can be changed in order to achieve asymptotic stability of closed loop system. Here, we are interested in influence of the K_p, K_d, α, τ on asymptotic stability of the given system. Now, applying the D-decomposition method [6] the stability region in the parameter space (K_p, K_d) can be obtained. So, it is necessary to determine the characteristic polynomial of the system (8),(9) as follows:

$$f(s) = Ls^3 + K_x Ls^2 - gs - K_x g + se^{-\tau s} (K_p + K_d s + K_a s^2 + K_\alpha s^\alpha) \quad (10)$$

One may notice that stability boundaries are curves on which each point corresponds to polynomial (10) having zeroes on the imaginary axes which can be obtained by substituting $s = j\omega$ as well as

$$f(j\omega) = L(j\omega)^3 + K_x L(j\omega)^2 - g(j\omega) - K_x g + (j\omega)e^{-\tau j\omega} (K_p + K_d(j\omega) + K_a(j\omega)^2 + K_\alpha(j\omega)^\alpha) = 0 \quad (11)$$

Real and imaginary part of Eq. (11) is given as:

$$\begin{aligned} \text{Re}(\omega, K_p, K_d, \alpha) &= (\omega \sin(\omega\tau)) K_p - \omega^2 \cos(\omega\tau) K_d \\ &\quad - K_x L \omega^2 - K_x g + \\ &\quad + \omega \sin(\omega\tau) [-K_a \omega^2 + K_\alpha \omega^\alpha \cos(\alpha\pi/2)] \\ &\quad - \omega \cos(\omega\tau) K_\alpha \omega^\alpha \sin(\alpha\pi/2) = 0 \\ &= a_{11} K_p + a_{12} K_d - b_1 = 0 \\ \text{Im}(\omega, K_p, K_d, \alpha) &= (\omega \cos(\omega\tau)) K_p + \omega^2 \sin(\omega\tau) K_d - L \omega^3 - g \omega + \\ &\quad + \sin(\omega\tau) [K_d \omega^2 + K_\alpha \omega^{\alpha+1} \sin(\alpha\pi/2)] + \\ &\quad + \omega \cos(\omega\tau) [-K_a \omega^2 + K_\alpha \omega^2 \cos(\alpha\pi/2)] = 0 \\ &= a_{21} K_p + a_{22} K_d - b_2 = 0 \end{aligned} \quad (12)$$

After solving (12), (13) it follows:

$$K_p = \frac{\Delta_p}{\Delta}, \quad K_d = \frac{\Delta_D}{\Delta} \quad (14)$$

where are

$$\begin{aligned} \Delta &= \begin{vmatrix} a_{11} & a_{12} \\ a_{21} & a_{22} \end{vmatrix} = \begin{vmatrix} \omega \sin(\omega\tau) & -\omega^2 \cos(\omega\tau) \\ \omega \cos(\omega\tau) & \omega^2 \sin(\omega\tau) \end{vmatrix} = \omega^3 \\ \Delta_p &= \begin{vmatrix} b_1 & a_{21} \\ b_2 & a_{22} \end{vmatrix}, \quad \Delta_D = \begin{vmatrix} a_{11} & b_1 \\ a_{12} & b_2 \end{vmatrix} \end{aligned} \quad (15)$$

When changing ω from 0 to ∞ , and $\Delta \neq 0$, equations (14) describe the decomposition curve in the parameter space (K_p, K_d) , at constant values of K_x, K_a , where α, τ, K_α used as parameters.

4. SIMULATION RESULTS

As previously stated, by applying the D-decomposition method, the parameter space (K_p, K_d) , be divided into stable and unstable domains where the stable domain can be determined by checking an arbitrary test point within each domain, and then testing the stability of pseudo-polynomial (10). Particularly, simulations are done for fixed values case $K_a = 1$, $K_\alpha = 1$, $K_x = -1$ and $\tau = 0.1$ where, in particular, was considered the influence of changing parameter of fractional order $\alpha \in (0.5 - 1.2)$, see Fig.2. One may notice that the best result is obtained for $\alpha = 0.5$.

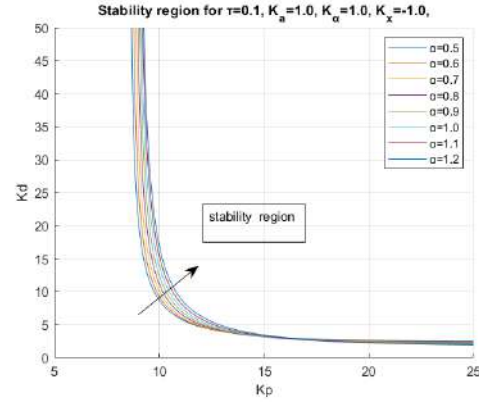


Fig. 2. 2D stability region (K_p, K_d)

The confirmation of the performed stability analysis can be shown by applying the appropriate numerical simulation (impulse response), see Fig.3 where a point is taken in the stable part of the area, i.e. $K_p = 15$, $K_d = 10$, $\alpha = 0.9$, $\tau = 0.1$ sec.

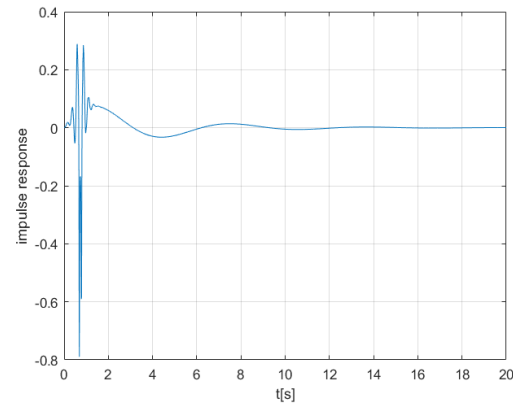


Fig. 3. Impulse response for a point
 $K_p = 15, K_d = 10, \alpha = 0.9, \tau = 0.1 \text{ sec}$

Also, we considered the influence of changing parameter of fractional gain $K_\alpha \in (0.5 - 4.0)$, for fixed parameters $K_a = 1, K_x = -1, \alpha = 0.5, \tau = 0.2$, see Fig.4, where one may conclude that the biggest domain of stability is obtained for $K_\alpha = 4.0$.

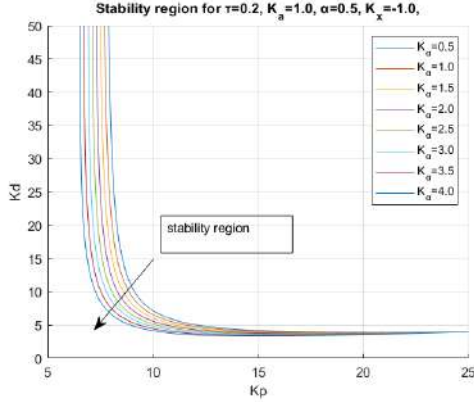


Fig. 4. 2D stability region (K_p, K_d)
 and parameter $K_\alpha \in (0.5 - 4.0)$

Also, we studied influence of time delay τ on the 2D stability domain. On Fig. 5 is presented case for $\tau = 0.1$ and on Fig.6 one may see the case for $\tau = 0.2$.

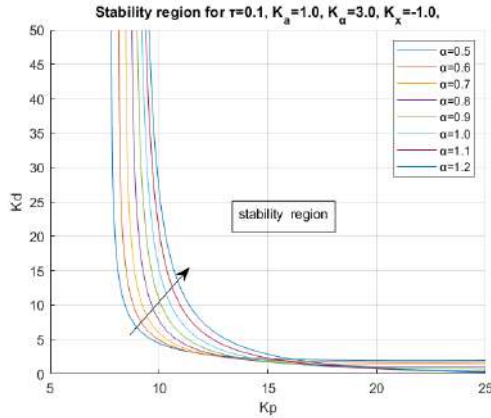


Fig. 5. 2D stability region (K_p, K_d) and $\tau = 0.1$

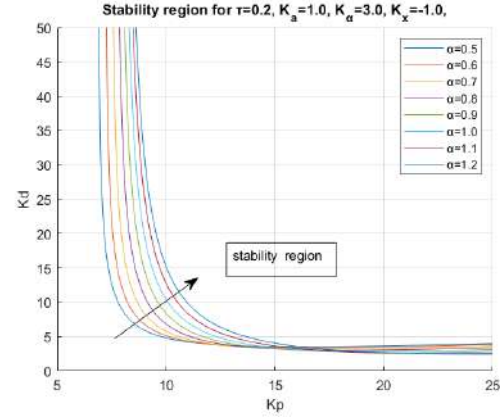


Fig. 6. 2D stability region (K_p, K_d) and $\tau = 0.2$

It is easily concluded that the case $\tau = 0.2$ is better choice than $\tau = 0.1$ because we have the bigger domain of stability where some values of time delay $\tau = (0.01 - 0.25)$ have stabilization effects.

5. CONCLUSION REMARKS

In this article, angular stabilization of inverted cart pendulum system is studied. An attempt has been made to test the effectiveness of delayed acceleration feedback fractional order PDD^2D^α controller for a highly unstable inverted cart pendulum system. Here, D-decomposition method is used for determining stability region in controller parameters space (K_p, K_d) . Advantage of the proposed D-decomposition method is that the stability analysis is done in a visual environment without considering complex analytical solutions where analytical forms expressing the boundaries of stability domains in the parameters space were obtained. Also, an example is given with corresponding test to confirm that considered stability domain is correctly determined.

Acknowledgement

This work is supported by the Ministry of Education, Science and Technological Development of the Republic of Serbia under the Grant No. 451-03-47/2023-01/ 200105 from 03.02.2023.

REFERENCES

- [1] Čović, V., Lazarević, M. P. (2021). *Robot Mechanics*. Faculty of Mechanical Engineering, Belgrade (in Serbian).
- [2] Khalil, H. (2002). *Nonlinear Systems*. Prentice Hall, Upper Saddle River.
- [3] Mandić P., M.P. Lazarević,MP.,M., Šekara, B.,T., (2017). *Stabilization of inverted pendulum by fractional order PD controller with experimental validation: D-decomposition approach*, in: A. Rodić, T. Borangiu (Eds.), *Adv. Intell. Syst. Comput.*, Springer International Publishing, Cham, 2017: pp. 29–37. DOI: 10.1007/978-3-319-49058-8_4
- [4] Kochubei,A., Luchko, Y., (2019). Eds, *Handbook of Fractional Calculus with Applications, Volume 1: Basic Theory*, Walter de Gruyter GmbH, Berlin/Boston, 2019.
- [5] Domoshnitsky,A.,Levi,S. R. H. Kappel,R.H., Litsyn E., Yavich R., (2021). *Stability of neutral delay differential equations with applications in a model of human balancing*, *Math. Model. Nat. Phenom.* 16, 21 DOI: <https://doi.org/10.1051/mmnp/2021008>
- [6] Hamamci, S.E. (2007) *An algorithm for stabilization of fractional-order time delay systems using fractional-order PID controllers*. *IEEE Transactions on Automatic Control*, vol. 52, p. 1964-1969.



Banja Luka
1-2 Jun 2023.

DEMI 2023

16th International Conference on Accomplishments in Mechanical and Industrial Engineering

www.demi.mf.unibl.org



Different approaches to the phases of Industry 4.0 product development

L. Šarović^a, B. Marković^a, A. Đurić^a

^aUniversity of East Sarajevo, Faculty of Mechanical Engineering, Vuka Karadžića 30, 71123 East Sarajevo

Abstract Industry 4.0 is a term used to describe the fourth industrial revolution, characterized by the integration of advanced technologies such as artificial intelligence, the Internet of Things, and cloud computing into manufacturing and industrial processes. This paper provides an overview of Industry 4.0, its components, phases, advantages, challenges, and most importantly, it explains how product creation works in Industry 4.0. There are numerous articles, works and books on this topic, however, the essence remains the same in a number of different approaches. Innovation is what drives the survival of this industry, and the product creation stages are equipped with the best tools of today. This paper presents a product that has changed the lives of many people who will be grateful for the development of Industry 4.0 throughout its lifetime. This is a real example of the positive and humane aspect of the development of Industry 4.0, on the basis of which a conclusion can be drawn as to how the development of that product has progressed.

Keywords Industry 4.0, technologies, product development, smart products

1. INTRODUCTION, INDUSTRY 4.0

Industry 4.0, also known as the Fourth Industrial Revolution, is a term used to describe the current trend of automation and data exchange in manufacturing and other industries.

It represents the integration of advanced technologies such as artificial intelligence, the Internet of Things (IoT), cloud computing and big data analytics to create smart factories and digital supply chains (fig. 1) [1].



Fig. 1. Industry 4.0, advanced technologies

The goal of Industry 4.0 is to improve efficiency, productivity, and profitability by allowing machines and systems to communicate with each other and make real-time decisions based on data analysis. This approach enables manufacturers to respond quickly to changing market demands, customize products at scale, and reduce waste and downtime [2-4]. Industry 4.0 is not just about technology, it also represents a shift in the way companies organize and manage their operations. It

Corresponding author

Lazar Sarović, master student
lsarovic@yahoo.com

University of East Sarajevo, Faculty of Mechanical
Engineering
Vuka Karadžića 30
71123 East Sarajevo
Bosnia and Herzegovina

requires a new approach to workforce development, including reskilling and upskilling employees to work alongside robots and automation systems. It also demands a more collaborative and agile approach to supply chain management and partnerships. The impact of Industry 4.0 is expected to be far-reaching, transforming not just manufacturing, but also healthcare, transportation, energy, and other sectors. While it presents significant opportunities for companies to stay competitive and create value, it also poses challenges in terms of cybersecurity, data privacy, and ethical considerations. With the rise of additive manufacturing (3D printing), it is now possible to create highly customized products on demand, without the need for costly and time-consuming tooling and setup. This enables companies to respond quickly to customer needs and preferences, and to reduce waste and inventory costs. The term "Industry 4.0" was first coined in 2011 by a group of experts from the German government and industry, and it has since gained global recognition. It builds upon the three previous industrial revolutions, which were characterized by the mechanization of production, mass production, and the use of electronics and IT in manufacturing [3].

2. INDUSTRY 4.0 PRODUCT DEVELOPMENT

Industry 4.0 counts numerous smart products. These smart products are usually characterized by a precisely defined manufacturing algorithm that involves going through several precisely defined phases that lead to initialization. Production of Industry 4.0 products is based on artificial intelligence (AI), big data analysis (PDA), and machine learning algorithms (ML) with computer support. What is characteristic for these products is their ability to use very large amounts of data which they use to learn many things about themselves and thus predict future events and potential issues. According to different authors, there are several different steps within this complex algorithm that lead to the development of 4.0 products. According to one of those authors, this scheme involves only 4 phases, each consisting of several sub-phases. Those phases are: monitoring (of environment and usage), management (of connections to other devices and communication with the environment), optimization (of BDA), and autonomy (of ML and decision-making) [4-6].

On the other hand, according to the opinions of other authors, the development of Industry 4.0 products cannot simply pass through these four phases, but through many more phases that make up a slightly different algorithm. These phases are as follows [5] :

1. **Planning and defining customer needs:**

The first phase is planning and defining customer needs. Market research needs to be done, competition analyzed, and the needs and desires of the target audience understood. Based on this knowledge, the manufacturer can create a product specification that reflects market demands.

2. **Conceptualization:** In this phase, a conceptual design of the product is created that will meet the needs of the target audience. This design must be functional and practical while also meeting aesthetic and ergonomic criteria.

3. **Prototype development:** Once the design concept is developed, the manufacturer creates a prototype that can be tested in the real world. The prototype is usually made of cheaper materials and may not be fully functional.

4. **Prototype testing:** Manufacturers test the prototype to see how it behaves in the real world. Testing may include performance, safety, reliability, and functionality testing of the prototype. Based on the results of testing, the manufacturer can improve the product design.

5. **Development of the production process:** When the product design is finalized, manufacturers must develop a production process to be able to produce the product in large quantities. This process involves developing machinery, tools, and manufacturing technologies.

6. **Production:** Once the production process is developed, manufacturers can begin producing large quantities of the product. At this stage, manufacturers must ensure quality control and ensure that the product is produced according to specifications.

7. **Distribution:** When the product is produced, manufacturers must distribute it to the market. This phase involves preparing the product for shipment, storing the product, and delivering the product to customers.

If you look at the phases shown, they are not significantly different from the phases in product development, as scientifically explained. The only difference is that at each phase, techniques and tools belonging to the generation of Industria 4.0 technologies can be used.

These key technologies are: a) Big data and analytics; b) Autonomous robots; c) Simulation; d) Horizontal and vertical system integration; e) The industrial Internet of Things; f) Cybersecurity; g) The cloud; h) Additive manufacturing; i) Augmented reality, [9]. Some may argue on the above list but this list may be adapted according to specific needs.

In addition, each of these phases requires adequate education of the personnel involved, who represent the drivers of the implementation of activities within the technologies of Industry 4.0 (fig. 2).

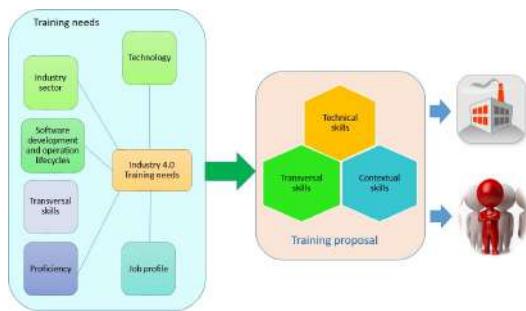


Fig. 2. Industry 4.0, competence framework [9]

Engineering smart products is based on new development achievements that take into account not only the development of products and services, but also their life cycle [6]. These engineering processes include several components, namely: processes, methods, IT tools, information models, and organizational structure. Together, they make up the so-called engineering processes, which have the following sequence: product development, product planning, logistics and distribution planning, maintenance planning, and end-of-life planning.

These are some, so to speak, common steps in creating smart products, which doesn't mean that they shouldn't be deviated from a bit during actual production. Each innovative product is unique in itself and requires different needs and approaches. Nowadays, information systems are quite easy to handle and tailored to human needs, so with

the right personnel possessing the necessary competencies and knowledge, one can quickly and easily achieve the desired solution.

3. CASE STUDY - SMART WHEELCHAIRS

Each industry sector has different training needs since different production processes are employed. These process may be management related (Business Planning and Logistics, Manufacturing Operations and Control, Automation and Machine Control, etc.) or production related (product design, engineering, etc.) [9]. Specific paper [9] defines industry sectors that are directly affected by Industry 4.0 initiatives. (eg. aerospace and defense, automotive, machinery, medical products). For each of those industry sectors an analytical list of core business processes needs to be defined.

Obviously, at the top of the list of applications of Industry 4.0 technologies within the industrial sector are medical products. Thus, on the example of humane-oriented products that are used as medical aids, all stages of product development, adapted to the mentioned use, can be described.



Fig. 2. Smart Wheelchairs [8]

3.1 Why are the smart wheelchairs worth mentioning?

In order to adequately explain the stages in the development of products related to Industry 4.0, the smart wheelchair product is presented here. Smart wheelchairs are useful because they provide many benefits and improve the quality of life for people with disabilities. These wheelchairs usually come with advanced technologies, such as sensors, cameras, and

tracking programs that help users manoeuvre and maintain balance [7]. Additionally, these wheelchairs enable users to have greater independence, allowing them to move around and perform tasks without the need for assistance from others. Furthermore, smart wheelchairs are often equipped with systems for regulating temperature, ventilation, and other features that provide comfort and safety to users.

These wheelchairs can also improve users' health by facilitating easier physical activity and reducing the risk of diseases associated with prolonged sitting. In summary, smart wheelchairs provide many benefits to users, enabling them to lead an independent, self-sufficient, and comfortable life.

This is an outstanding example of using the benefits of product development within Industry 4.0. for the most basic human needs.

3.2 How did the idea for smart wheelchairs come about and who invented it?

The idea for smart wheelchairs emerged from a desire to improve the quality of life for individuals with mobility impairments. As technology advanced, it became possible to integrate sensors, motors, and other electronic components into wheelchairs, creating a more advanced and efficient mode of transportation for people with disabilities. The development of smart wheelchairs has also been driven by a growing demand for personalized mobility solutions that can be customized to meet the unique needs of each user. Overall, the idea for smart wheelchairs was born out of a need to enhance accessibility and independence for individuals with disabilities.

The idea of creating a smart wheelchair is not attributed to one specific person or group. Rather, it is the result of ongoing technological advancements in the fields of robotics, sensors, and assistive technology, as well as the input and collaboration of many researchers, engineers, and individuals with disabilities themselves. The development of smart wheelchairs has been a collective effort involving contributions from many different people and organizations over time.

3.3 How were smart wheelchairs created?

As one of the products of Industry 4.0, smart wheelchairs have emerged using the same technologies as other products in this industry [8]. Although we cannot be certain of the exact process of creating this product, based on conducted research, it can be possible to present an algorithm that is relevant. So, here is a detailed explanation of the process of manufacturing smart wheelchairs step by step:

1. **Product design:** The process begins with the product design phase, which involves developing sketches and plans to ensure that the product incorporates everything necessary to be functional, safe, and comfortable for the user.
2. **Material gathering:** Once the design is approved, the materials needed to manufacture smart wheelchairs are gathered, including the frame, tires, motors, sensors, batteries and electronic components.
3. **Frame fabrication:** The frame, which is the foundation of the wheelchair, is fabricated. The frame is made of metals such as aluminum, steel, or titanium, which are strong and lightweight, and also provide the necessary strength and stability.
4. **Tire assembly:** After the frame is fabricated, the tires are assembled. Tires are important because they provide stability and allow the wheelchair to move on different types of terrain.
5. **Motor addition:** Smart wheelchairs have built-in motors that allow them to move. Motors are added to the frame and connected to the battery.
6. **Sensor addition:** In order for the wheelchair to recognize the environment and navigate towards the desired destination, sensors are added that scan the surroundings. Sensors can also measure the speed and acceleration of the wheelchair, enabling safer driving.
7. **Electronic component connection:** Various electronic components, including sensors, motors, batteries, and wireless networks, must be connected and synchronized to allow the wheelchair to be controlled and communicate with other devices.
8. **Testing and quality:** Once the wheelchairs are manufactured, they are tested to ensure they function properly and are safe for the

user. After passing the tests, the wheelchairs undergo further quality assurance processes to ensure they are produced to the highest standards.

9. Packaging and distribution: Once the wheelchairs are tested and approved for use, they are packaged and distributed to customers. After that, manufacturers and sellers provide customer support through wheelchair service and maintenance.

This example shows how the stages in product development are adapted to a specific example, the development of a smart wheelchair. In each of the mentioned stages in the development of this smart product, it is possible to use some of the technologies implied by Industry 4.0.

4. CONCLUSION

Industry 4.0 overview has been an excellent opportunity to discuss the latest trends and developments in this field and to reflect on the implications of these changes for the manufacturing industry and society as a whole. The innovation within Industry 4.0 is complemented by a holistic approach that takes into account the product life cycle. Product development represents the most important phase, and information technologies are there to facilitate the implementation and presentation of ideas.

Today, in the modern world, there are fully and clearly defined technologies whose use is associated with Industry 4.0, (Big data and analytics, Autonomous robots, Simulation, Horizontal and vertical system integration, The industrial Internet of Things, Cybersecurity, The cloud, Additive manufacturing, Augmented reality. They are applicable in various branches of industry, including the aviation industry and defense, the automotive industry, but also the industry of medical and human-oriented products. Stages in product development, which are defined by different authors outside the context of Industry 4.0. are not significantly different from those experienced within this context. The difference is in the use of technologies that require adequate equipment and devices, and above all educated personnel for their use. The framework for the education of such personnel must be redefined, that is, the educational system adapted to the new needs of society.

In conditions where we are talking about enormously large figures related to the loss of jobs due to the use of Industry 4.0 technologies, especially artificial intelligence, it is important to note that the use of these technologies must be controlled and directed into human-oriented products, such as wheelchairs.

Otherwise, the fear will prevail that the technologies of Industry 4.0., such as IoT, artificial intelligence and others, will dominate the human community and manage people's lives in a negative sense. A realistic basis already exists.

REFERENCES

- [1] Shadravan, A., Parsaei, H. (2023). Proceedings of the International Conference on Industrial Engineering and Operations Management - Impacts of Industry 4.0 on Smart Manufacturing
- [2] Oulovsky, N. (2018). Utjecaj koncepta „Industrija 4.0“ na razvoj distribucijskih sustava. PhD thesis. Sveučilište u Zagrebu. Fakultet prometnih znanosti.
- [3] Ersoy, Y. (2022.). The Journal of International Scientific Researches. The Advantages and Barriers in Implementing of Industry 4.0 and Key Features of Industry 4.0. No: 7(3)
- [4] Majstorović, V., Lazović, T., Mišković, Ž., Mitrović, R. (2022.) Proceedings - 10th International Scientific Conference, Research and Development of Mechanical Elements and Systems. „Smart Products – State of Art“ DOI: 978-86-6060-119-5
- [5] Muminović. A., Pandžić, A., Pervan N., Delić, M. (2022.) Special Edition ASABiH CCII, DTS Vol. 20, pp- 69.80. Product development and design inside Industry 4.0 from rapid prototyping to additive manufacturing. DOI: 10.5644/PI2022.202.21
- [6] Antić, D., Miltenović, V. (2020.) Prvo izdanje. Stepanović, J. (prorektor). Inženjering pametnih proizvoda i usluga. Univerzitet u Nišu. Niš
- [7] Ktistakis, P. (2018.) An Autonomous Intelligent Robotic Wheelchair to Assist People in Need: Standing-up, Turning-around and Sitting-down. (In English). PhD thesis. Wright State University.

- [8] Srna. Velika nada za paraplegičare: Pokretanje invalidskih kolica jezikom. From: <https://www.klix.ba/scitech/nauka/velika-nada-za-paraplegicare-pokretanje-invalidskih-kolica-jezikom/140105078> . Accessed on: April 1st, 2023.
- [9] Fitsilisis, P., Paraskevi, T., Vassilis, G., (2018), International Scientific Journal Industry 4.0, WEB ISSN 2534-997X, PRINT ISSN 2534-8582, „Industry 4.0, required personnel competences“.
- [10] Marković, B., Đurić, A., (2022), Machine and Industrial Design in Mechanical Engineering, Proceedings of KOD 2021, Springer ISBN - 13:978-3030884642, „Education 4.0 for Industry 4.0“, 723-733.



Banja Luka
1-2 Jun 2023.

DEMI 2023

16th International Conference on Accomplishments in Mechanical and Industrial Engineering

www.demi.mf.unibl.org



Methodology review for getting functionally graded lattice structure for simulation and experimental testing

M. Soldo, D. Šaravanja, N. Rašović

*Faculty of Mechanical Engineering, Computing and Electrical Engineering, University of Mostar
Matice hrvatske b.b., 88000 Mostar, Bosnia and Herzegovina*

Abstract *The lattice structure production has rapidly grown in the last decade due to the ease of production through additive manufacturing. The focus occupies functionally graded lattice structure because of mechanical adaptivity properties through varying parameters on unit cells. This paper presents several steps for modelling functionally graded lattice structures for later testing. In the introduction section, general lattice structures divisions are presented. The previous research section gave a few influential research papers last few years. The methodology for modeling functionally graded lattice structure is presented in the third section. Selection test type, unit cell type and unit cell dimensions, multiplication of unit cell, graded cross-section or graded high of testing samples with respecting relative density are some of few essential steps which must be followed to successfully modeled graded samples. Numerical simulation and testing methodology are also presented with several valuable notes. Conclusion gave some future research solutions.*

Keywords *Functionally graded lattice structure, relative density, additive manufacturing*

1. INTRODUCTION

Cellular or lattice structures are constructed from a network of trusses or plates to form porous structures, which hold a high performance-over-weight ratio and can be divided into stochastic and nonstochastic structures [1]. Lattice structures have comparative properties with foam, such as lightweight, high energy absorption and improved strength-to-weight ratio [1]. 3D stochastic (foam) and 3D nonstochastic (periodic) structures can also be divided into two main categories: open-cell and close-cell structures [2]. Cellular shapes can be uniform or non-uniform [3]. This review paper focuses on a three-dimensional non-uniform (graded) open-cell lattice based on struts. Functionally graded lattice structures (Fig. 1.) are defined as a type of lattice structure with various component materials, structural topology or dimensions in

overall volume, which resulting changes in the overall structure mechanical performance [4]. The significant expansion of additive manufacturing enabled the development of various types of functionally graded lattice structures and their application in very complex products. There are currently four strategies to change its gradient: (1) variance on rod diameter of a unit cell, (2) scaling of a unit cell, (3) variance in the type of unit cell and (4) variance in a material component [5]. Variance in rod diameter of unit cells has been most common in research in the last few years because the connectivity of unit cells stays constant. Every change on unit cell morphology leads to problem of ensure the connectivity between unit cells. Variance in material component does not create any problem through designing-structure process, only through production. This paper has several steps which can be useful to follow for getting

usable samples of functionally graded lattice structures for various type of testing.

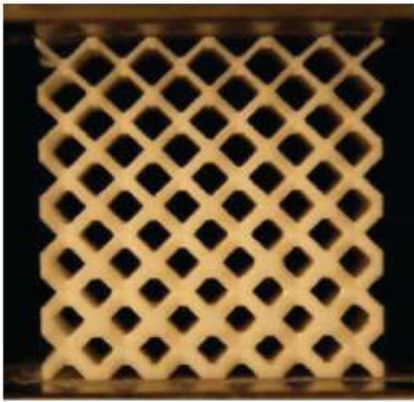


Fig. 1. Example of printed relative density graded BCC lattice structure [6]

2. PREVIOUS RESEARCH

In paper [4], the authors propose bidirectionally graded lattice structures in which the density gradient design is parallel and perpendicular to the loading direction. Different graded size structures with the Body-Center Cubic unit cell were made with respecting same relative density. Results show that manipulation of unit cell size in a conventional BCC structure (to obtain a bidirectionally graded lattice structure) can ensure the compelling connection between unit cells and compressive modulus, yield stress and Plateau stress are significantly higher compared with unidirectionally graded lattice structure with the same relative density. In paper [5], the investigation is based on uniform structure, rod-diameter-variation graded structure and new-size variation graded structure with the same density. Results show that the mechanical properties of graded lattice structures can be accurately predicted by combining the Gibson-Ashby formula. Both mentioned research gave numerical and experimental validation. In paper [7], uniform and bi-directionally graded BCC structures were designed and tested through a uniaxial compression test using finite element modelling. Results show the effect of the relative density of functionally graded lattice structure on energy absorption through different stages of a compression test. Paper [8] also investigates quasi-static compressive responses of BCC-graded lattice structure. Results show that the gradient direction parallel

to the loading direction has better mechanical properties and energy absorption capacity than the uniform structure. Paper [6] investigates the difference between BCC and BCC-z uniform and graded structures. Graded structures were designed with varying relative density through height – from the low-density layers from the top to the high-density layers at their bases. This approach shows benefits in demanding the controlled absorption of impact energy, for example, in personal protection equipment.

3. METHODOLOGY OF MODELING FUNCTIONALLY GRADED LATTICE STRUCTURE

This section proposes crucial steps for modelling samples for later numerical and experimental selected testing.

3.1 Selection test type

Selecting type of the test for samples properties investigation presents first step in this methodology. Each tests settings and minimal number of samples are recommended by standard. Through the detailed study of selected standard, the final dimensions of samples and the number of samples help a lot in subsequent decisions.

3.2 Unit cell type selection

The second step presents creating a wireframe model for unit cell type. The database shows many types of unit cells based on struts (Fig. 2.). There is no general collection of all unit cell types based on struts, and there is no clear division between simple (original) or complex (derived) unit cells. Those divisions, for now, stay on the opinion of every researcher. Here are some of the unit cell types based on struts that can be selected: Cuboctahedron, Simple Cubic, Body Center, Body Center Cubic, Circular, Body Center with Strut, Kelvin (Truncated Octahedron), Face Center, Face Center with vertical Strut, Face Center Cubic, Diamond, Dodecahedron, Hexagonal, Tetrahedron, Tetrakaidecahedron, Triacantahedron, Truncated Cube, Octagonal, Strengthened Octagonal, Octahedron, Rhombidecahedron, Rhombicuboctahedron, Octet-cross, Vector, Icosahedron and so on. By selecting a unit cell type, the designer must be sure that the

multiplication contact between neighbour unit cells must be established. Another guideline for selecting the suitable unit cell will be what is expected for structure results (low stress, high load capacity, stiffness, vibration isolation and similar). Dimensions of the unit cell can be variable. One note is that the unit cell size should be printable. Another note is that the unit cell size should be between 0.1 mm to 10 mm so that the final structure can be considered mesostructure [9].

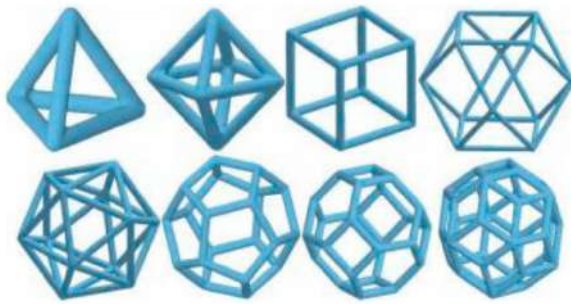


Fig. 2. Some examples of various unit cell types (top row – left to right: tetrahedron, octahedron, simple cubic, vector; bottom row – left to right: icosahedron, dodecahedron, tetrakaidecahedron and triacontahedron [3])

3.3 Unit cells multiplication pattern and gradation through height

The best proof of the variety of unit cell multiplication pattern in three directions (x, y and z) are given in the paper [10], which summarize several investigations on different lattice structure with different dimensions of unit cells and different pattern of multiplication. The suggestion that can be useful in this phase is that multiplication in two directions (x and y) in the horizontal plane should be the same as in the upper plane. The reason is that the different multiplication in the upper planes could bring problems with unit cell connectivity. Good contact between adjacent unit cells (large surface edges of unit cells) means more design freedom through multiplication process. Dimension of the final model will be conditioned through multiplication pattern and the dimension of the unit cell for obtain valid test samples previously mentioned.

A height gradation can be entered here. With respecting multiplication patterns in two

directions (x and y), every height of upper planes can be varied. Varying the height of every new level in samples is possible and unit cells morphology can be also changed (Fig. 3.). In this way, one graded lattice structure level can be larger or smaller than the previous level. This way of varying give different stress results regarding from uniform lattice structure.

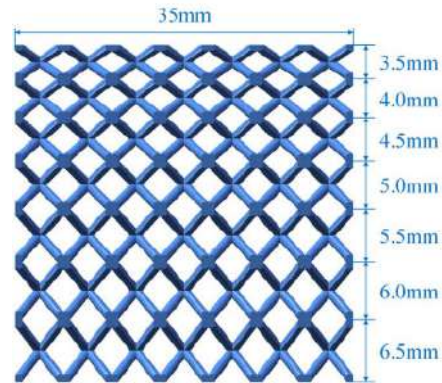


Fig. 3. Size graded BCC lattice structure [5]

3.4 Unit cells cross-section and relative density

Cross sections of a unit cell can be various: triangular, circular, squares, rectangular, hollow and so on. It is up to the designer to choose the shape, but the simplicity of connecting neighbouring unit cells must be ensured. The cross-section is of fourth previously motioned strategies to achieve the gradation. The cross-section size is changed (Fig. 4.) through the sample height – selectively or randomly. Changing in cross-section size leads to porous and relative density change.

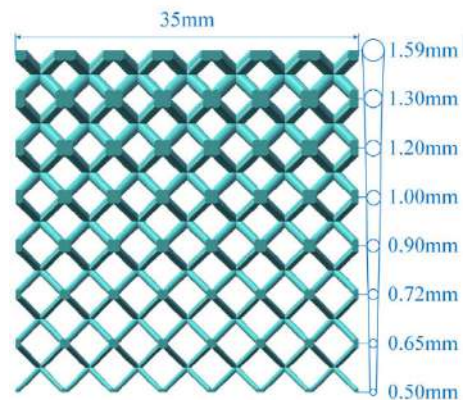


Fig. 4. Rod diameter graded BCC lattice structure [5]

Relative density is the ratio of the lattice structure density to the base material density [10]. It is also equivalent to the volume fraction of the porose structure concerning the solid structure [11]. By the gradation of cross-section size with respecting relative density, samples with the same size and same mass can give different results due to the equal external load. Therein lies the advantage of functionally graded lattice structure over uniform lattice structure.

4. METHODOLOGY FOR SIMULATION AND EXPERIMENTAL TESTING OF FUNCTIONALLY GRADED LATTICE STRUCTURE

4.1 Material characterization and print settings

The first step in this section is printing "dog bone" samples for material characterization samples on tensile machine. Dimensions of examples for this test are prescribed in the standard. After modelling samples, setting up printer settings for making samples is necessary. Those print setup parameters (layer height, wall thickness, temperature, speed) must be used later for lattice structure production. In this way, material characteristics obtained from tensile experiment on "dog bone" should be overwritten on the lattice structure. Also characteristics from tensile testing "dog bone" (the most crucial yield stress/strength and ultimate stress/strength) should be used in numerical simulation properties. On this way, real mechanical properties obtained from tensile test, are used as material properties in numerical simulation. Materials properties of the material are changed during the printing process. One note for printing samples: the test should be conducted two weeks after printing samples to reduce the influence of degradation [4].

4.2 Numerical simulation

There are many software packages for Static Structural numerical simulation, for example CATIA, SolidWorks Simulation, ANSYS Workbench, ABAQUS. Some of the most common steps for setting up simulation are boundary condition, adding material, coefficient

of friction, meshing of samples, test speed and, of course, simulation results. One helpful note is that applying newly detected material properties from the "dog bone" tensile test. Also, meshing the samples can be difficult due to the functionally graded lattice samples complexity. Then symmetry of the sample can be a valuable tool if symmetry in functionally graded lattice structure is detected.

4.3 Printing and testing the samples

Setup printing parameters for graded lattice structure should equal printing parameters (Fig. 5.) of "dog bone". In this way, mistakes for printing should be reduced. Number of functionally graded lattice samples for testing are recommended by standard. As stated earlier, test conducting two weeks after printing samples to reduce the influence of degradation [4].

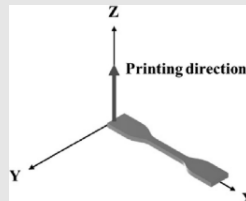
	Parameter	Value
	Layer height (mm)	0.2
	Wall thickness (mm)	0.8
	Nozzle temperature (°C)	230
	Bed temperature (°C)	90
	Infill density (%)	100
	Print speed (mm/s)	40
	Travel speed (mm/s)	130

Fig. 5. The process parameters of the additively manufactured "dog bone" later used as printing parameters for functionally graded lattice samples manufacturing [11]

Standards also prescribe setups for the test. After testing, all necessary results should be collected for the final step – discussing the results.

4.4 Analysis of the results

Analysis of the results is the most crucial step in every investigation. It often happens that the results of the experimental test and results of the numerical simulation are not 100% match, but they should be close to each other. The main reason for inconsistency could be that numerical simulation works in the ideal workspace. The influence of temperature, humidity, irregularity of print, inaccuracy of the printer, and residual stresses can lead to deviation between numerical and experimental

results. Conversely, the researcher must predict the influence of those factors. Even after prediction, if deviation is high and can not be ignored, some previously mentioned steps are not enough respected and modelling and testing repetition is required.

5. CONCLUSION

Functionally graded lattice structures found wide use in engineering applications [12], automotive and biomedicine engineering. Additive manufacturing every day spreads functionally graded lattice applications in other fields. This paper presents critical steps in decision-making for modelling, numerical and experimental testing of functionally graded lattice structures. Future research will be conducted on the application of this methodology on a concrete examples. Application functionally graded lattice structure in final product and testing such a design is a big challenge for designers and the future research can go on that direction. Getting and testing specific products in engineering with functionally graded lattice structure through this methodology can expand and detailed explain some of presented methodology steps.

REFERENCES

- [1] Nguyen C. H. P., Kim Y., Choi Y. (2021). Design for Additive Manufacturing of Functionally Graded Lattice Structures: A Design Method with Process Induced Anisotropy Consideration. *Int. J. Precis. Eng. Manuf. - Green Technol.*, vol. 8, no. 1, pp. 29–45. DOI: [10.1007/s40684-019-00173-7](https://doi.org/10.1007/s40684-019-00173-7)
- [2] Park K. M., Min K. S., Roh Y. S. (2022). Design Optimization of Lattice Structures under Compression: Study of Unit Cell Types and Cell Arrangements. *Materials (Basel)*, vol. 15, no. 1. DOI: [10.3390/ma15010097](https://doi.org/10.3390/ma15010097)
- [3] Pan C., Han Y., Lu J. (2020). Design and optimization of lattice structures: A review. *Appl. Sci.*, vol. 10, no. 18, pp. 1–36. DOI: [10.3390/APP10186374](https://doi.org/10.3390/APP10186374)
- [4] Yang J. (2022). Compressive properties of bidirectionally graded lattice structures. *Mater. Des.*, vol. 218, p. 110683. DOI: [10.1016/j.matdes.2022.110683](https://doi.org/10.1016/j.matdes.2022.110683)
- [5] Bai L. (2020). Mechanical properties and energy absorption capabilities of functionally graded lattice structures: Experiments and simulations. *Int. J. Mech. Sci.*, vol. 182, no. February, p. 105735. DOI: [10.1016/j.ijmecsci.2020.105735](https://doi.org/10.1016/j.ijmecsci.2020.105735)
- [6] Maskery I. (2017). An investigation into reinforced and functionally graded lattice structures. *J. Cell. Plast.*, vol. 53, no. 2, pp. 151–165. DOI: [10.1177/0021955X16639035](https://doi.org/10.1177/0021955X16639035)
- [7] Rodrigo C., Xu S., Durandet Y., Ruan D. (2021). Uniaxial compression of bi-directionally graded lattice structures: Finite element modelling. *IOP Conf. Ser. Mater. Sci. Eng.*, vol. 1067, no. 1, p. 012107. DOI: [10.1088/1757-899x/1067/1/012107](https://doi.org/10.1088/1757-899x/1067/1/012107)
- [8] Bai L. (2021). Quasi-Static compressive responses and fatigue behaviour of Ti-6Al-4 V graded lattice structures fabricated by laser powder bed fusion. *Mater. Des.*, vol. 210, no. September, p. 110110. DOI: [10.1016/j.matdes.2021.110110](https://doi.org/10.1016/j.matdes.2021.110110)
- [9] Nazir A., Abate K. M., Kumar A., Jeng J. Y. (2019). A state-of-the-art review on types, design, optimization, and additive manufacturing of cellular structures. *Int. J. Adv. Manuf. Technol.*, vol. 104, no. 9–12, pp. 3489–3510. DOI: [10.1007/s00170-019-04085-3](https://doi.org/10.1007/s00170-019-04085-3)
- [10] Khiavi S. G., Sadeghi B. M., Divandari M. (2022). Effect of topology on strength and energy absorption of PA12 non-auxetic strut-based lattice structures. *J. Mater. Res. Technol.*, vol. 21, pp. 1595–1613. DOI: [10.1016/j.jmrt.2022.09.116](https://doi.org/10.1016/j.jmrt.2022.09.116)
- [11] Almesmari A., Sheikh-Ahmad J., Jarrar F., Bojanampati S. (2023). Optimizing the specific mechanical properties of lattice structures fabricated by material extrusion additive manufacturing. *J. Mater. Res. Technol.*, vol. 22, pp. 1821–1838. DOI: [10.1016/j.jmrt.2022.12.024](https://doi.org/10.1016/j.jmrt.2022.12.024)
- [12] Rašović N. (2021). Recommended layer thickness to the powder-based additive manufacturing using multi-attribute decision support. *Int. J. Comput. Integr. Manuf.*, vol. 34, no. 5, pp. 455–469. DOI: [10.1080/0951192X.2021.1891574](https://doi.org/10.1080/0951192X.2021.1891574)



Banja Luka
1-2 Jun 2023.

DEMI 2023

16th International Conference on Accomplishments in Mechanical and Industrial Engineering

www.demi.mf.unibl.org



Selection of Zipline Cable

T. Jojić, J. Vladić, R. Đokić

University of Novi Sad, Faculty of Technical Sciences, Trg Dositeja Obradovića 6, 21000 Novi Sad, Serbia

Abstract This paper shows the detailed procedure for the selection of zipline cable i.e. carrying rope. Namely, since there are no standards which define the procedure of choosing a proper zipline rope, the paper gives an overview of some recommendations for choosing a rope. Selection can be made based on the criteria of the deflection of unloaded and loaded state, based on the criteria of breaking force or based on the criteria of ensuring the minimum distance from the ground. Additionally, influences that should be taken into account when choosing ropes are presented to readers. For example loads due to temperature changes, due to freezing (ice buildup on the rope) or loads due to the side wind.

Keywords zipline, cable, wire rope

1. INTRODUCTION

Considering that the zipline has been experiencing its expansion for the last twenty years, there are still no regulations that define the design of this type of device. Therefore, this paper will give an overview of the possibilities for choosing a rope according to the regulations for devices similar to a zipline, such as ropeways and cable cranes, or transmission lines, [1-6].

Given that the rope represents the main element of the mentioned devices, it must be given the greatest attention.

The selection of rope and appropriate calculation will be made for the specific zipline, the construction of which was planned on Fruška Gora in Serbia, [7]. The span of the zipline is 1467 m, while the height difference between the stations is 99 m.

Corresponding author

M.Sc. Tanasije Jojić
tanasijejojic@uns.ac.rs

Faculty of Technical Sciences
Trg Dositeja Obradovića 6
21000 Novi Sad
Serbia

The zipline is designed for the descent of two riders, which means lowering a mass of around 150 kg.

2. CABLE SELECTION

As a condition for the selection of the rope, regulations from the field of cable cars can be used, where it is necessary that the forces in the rope (S), compared to the transverse load (Q), satisfy the condition:

$$\frac{S_{\min}}{Q} \geq 20 \text{ for haul rope}$$

$$\frac{S_{\min}}{Q} \geq 80 \text{ for track rope}$$

According to this, the breaking force of the rope must be:

$$\begin{aligned} S_k &> \frac{20 \cdot Q \cdot g \cdot v_t}{1000} = \\ &= \frac{20 \cdot 150 \cdot 9,81 \cdot 4}{1000} = 117,7 \text{ kN} \end{aligned} \quad \text{for strand rope}$$

$$\begin{aligned} S_k &> \frac{80 \cdot Q \cdot g \cdot v_n}{1000} = \\ &= \frac{80 \cdot 150 \cdot 9,81 \cdot 3,5}{1000} \approx 412 \text{ kN} \end{aligned} \quad \text{for full locked rope}$$

where ν_n and ν_t are the minimum safety factor for the mentioned ropes.

For stranded ropes, this condition is mostly met by ropes with a diameter greater than 12 mm, while for fully locked ropes, this condition is met by ropes with a diameter of about 20 mm.

In the case of ziplines with a relatively small inclination angle, there is an almost linear dependence of the relationship between the breaking force of the rope and its weight per length meter. In those cases the deflections of the rope under the effect of a concentrated load should not exceed a value of 50% higher than the value of the deflection of an unloaded rope, that is:

$$\frac{f_{\text{loaded}}}{f_{\text{unloaded}}} < 1,5$$

where the deflection in the loaded state is:

$$f_{\text{loaded}} = \frac{x \cdot (l - x)}{2 \cdot H} \cdot \left(\frac{q}{\cos \beta} + 2 \cdot \frac{Q}{l} \right)$$

while the deflection in the unloaded state is:

$$f_{\text{unloaded}} = \frac{q \cdot x \cdot (l - x)}{2 \cdot H_0 \cdot \cos \beta}$$

where:

x – current position of the load

l – field span

q – own weight of the rope

Q – weight of a rider

H – horizontal component of the rope force when rope is loaded

H_0 – horizontal component of the rope force when rope isn't loaded

β – inclination angle

Based on the above, it is obtained:

$$\frac{q + \frac{2Q}{l}}{q} \cdot \frac{H_0}{H} < 1,5$$

Knowing that:

$$\frac{H_0}{H} < 1$$

it can be written as:

$$\frac{q + \frac{2Q}{l}}{q} < 1,25$$

that is:

$$q \geq \frac{8Q}{l}$$

For the foreseen mass of two riders, it follows:

$$q \geq \frac{8 \cdot 150}{1467} = 0,82 \frac{\text{kg}}{\text{m}}$$

By looking at the catalogues of certain rope manufacturers [8-10], it can be seen that this condition is mostly met by ropes with a diameter greater than 12 mm.

The third criteria based on which the rope can be selected is the criteria of ensuring the minimum distance from the ground. This must be verified for a fully loaded rope.

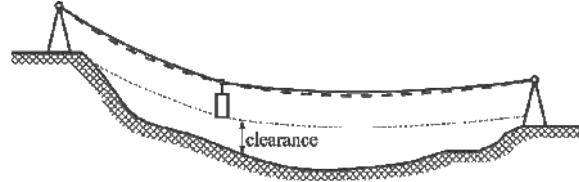


Fig. 1. Ensuring the minimum distance from the ground

The tension, and therefore the rope diameter, depends on the configuration of the terrain. Fig. 2 shows the catenaries for different tensions for one rope.

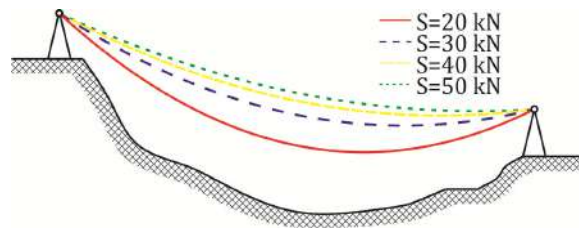


Fig. 2. Catenaries for different tensions of rope

3. ADDITIONAL IMPACTS

Within this point, additional impacts will be analyzed for the case of lowering a mass of 150 kg and a spiral rope with a diameter of 14 mm ($q=0,958 \text{ kg/m}$).

3.1 Impact of passengers descent

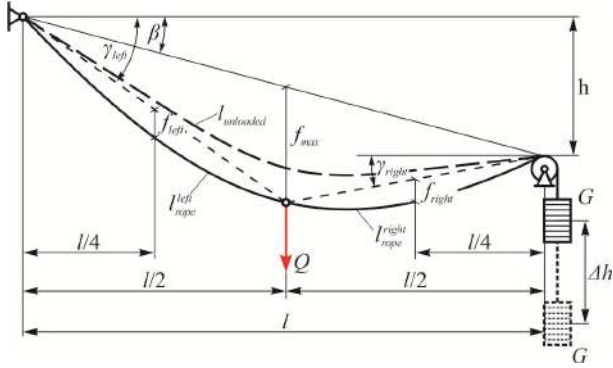


Fig. 3. Determination of the weight displacement

Based on Fig 3, it is possible to determine the weight travel distance during the descent of the passenger down the zipline rope as the difference between the length of the rope in the field when the passenger is in it and the length of the unloaded rope. The maximum value of the length of the rope in the field is obtained when the passenger is in the middle of the span. In that case, based on Fig. 3, it follows that the lengths of the segments on the left (l_{rope}^{left}) and right (l_{rope}^{right}) sides of the load are:

$$l_{rope}^{left} = \frac{l}{2 \cdot \cos \gamma_{left}} + \frac{16}{3} \cdot \frac{f_{left}^2}{l} \cdot \cos^3 \gamma_{left} =$$

$$= \frac{1467}{2 \cdot \cos 8,60^\circ} + \frac{16}{3} \cdot \frac{12,78^2}{1467} \cdot \cos^3 8,60^\circ = 742,42 \text{ m}$$

$$l_{rope}^{right} = \frac{l}{2 \cdot \cos \gamma_{right}} + \frac{16}{3} \cdot \frac{f_{right}^2}{l} \cdot \cos^3 \gamma_{right} =$$

$$= \frac{1467}{2 \cdot \cos 0,93^\circ} + \frac{16}{3} \cdot \frac{12,64^2}{1467} \cdot \cos^3 0,93^\circ = 734,19 \text{ m}$$

where:

$$\gamma_{left} = \arctg \frac{2 \cdot f_{max} + h}{l} = \arctg \frac{2 \cdot 61,47 + 99}{1467} = 8,60^\circ$$

$$\gamma_{right} = \arctg \frac{2 \cdot f_{max} - h}{l} = \arctg \frac{2 \cdot 61,47 - 99}{1467} = 0,93^\circ$$

$$f_{left} = \frac{q \cdot \left(\frac{l}{2}\right)^2}{8 \cdot H \cdot \cos \gamma_{left}} = \frac{0,958 \cdot \left(\frac{1467}{2}\right)^2}{8 \cdot 5097 \cdot \cos 8,60^\circ} = 12,78 \text{ m}$$

$$f_{right} = \frac{q \cdot \left(\frac{l}{2}\right)^2}{8 \cdot H \cdot \cos \gamma_{right}} = \frac{0,958 \cdot \left(\frac{1467}{2}\right)^2}{8 \cdot 5097 \cdot \cos 0,93^\circ} = 12,64 \text{ m}$$

$$f_{max} = \frac{l^2}{8H} \cdot \left(\frac{q}{\cos \beta} + 2 \frac{Q}{l} \right) =$$

$$= \frac{1467^2}{8 \cdot 5097} \cdot \left(\frac{0,958}{\cos 3,86^\circ} + 2 \cdot \frac{150}{1467} \right) = 61,47 \text{ m}$$

while the length of the unloaded rope is:

$$l_{unloaded} = \frac{l}{\cos \beta} + \frac{8}{3} \cdot \frac{f_{unloaded}^2}{l} \cdot \cos^3 \beta =$$

$$= \frac{1467}{\cos 3,86^\circ} + \frac{8}{3} \cdot \frac{50,68^2}{1467} \cdot \cos^3 3,86^\circ = 1474,97 \text{ m}$$

where the maximal deflection of unloaded rope is:

$$f_{unloaded} = \frac{l^2}{8H} \cdot \frac{q}{\cos \beta} = \frac{1467^2}{8 \cdot 5097} \cdot \frac{0,958}{\cos 3,86^\circ} = 50,68 \text{ m}$$

where:

$$\beta = \arctg \frac{h}{l} =$$

– inclination angle

$$= \arctg \frac{99}{1467} = 3,86^\circ$$

$H = 50 \text{ kN} \approx 5097 \text{ kg}$ – horizontal force

The weight displacement when lowering the trolley with a passenger with a total mass of 150 kg is then:

$$\Delta h = l_{rope}^{left} + l_{rope}^{right} - l_{unloaded} =$$

$$= 742,42 + 734,19 - 1474,97 = 1,64 \text{ m}$$

3.2 Ice buildup impact



Fig. 4. Ice buildup on the rope [11]

According to [12] the ice load is calculated based on:

$$q_{ice} = 0,18 \cdot \sqrt{d_{rope} [\text{mm}]} \left[\frac{\text{daN}}{\text{m}} \right]$$

For the rope with a diameter of 14 mm, follows:

$$q_{ice} = 0,18 \cdot \sqrt{14} = 0,67 \frac{\text{daN}}{\text{m}} \approx 0,67 \frac{\text{kg}}{\text{m}}$$

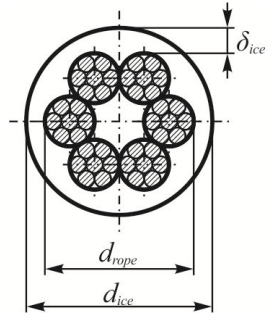


Fig. 5. Frozen rope

Knowing that the density of ice is 920 kg/m^3 , and observing a one-meter section of frozen rope, the diameter of the frozen rope can be determined:

$$q_{ice} = \frac{d_{ice}^2 - d_{rope}^2}{4} \pi \cdot l \cdot \rho_{ice} \Rightarrow d_{ice} = \sqrt{\frac{4 \cdot q_{ice}}{\pi \cdot \rho_{ice}} + d_{rope}^2}$$

or:

$$d_{ice} = \sqrt{\frac{4 \cdot q_{ice}}{\pi \cdot \rho_{ice}} + d_{rope}^2} = \sqrt{\frac{4 \cdot 0,67}{\pi \cdot 920} + 0,014^2} = 0,0335 \text{ m}$$

from there the thickness of the ice is obtained as:

$$d_{ice} = d_{rope} + 2 \cdot \delta_{ice} \Rightarrow \delta_{ice} = \frac{d_{ice} - d_{rope}}{2}$$

or:

$$\delta_{ice} = \frac{d_{ice} - d_{rope}}{2} = \frac{33,5 - 14}{2} = 9,75 \text{ mm}$$

The deflection of frozen rope is then:

$$f_{ice} = \frac{(q + q_{ice}) \cdot l^2}{8 \cdot H \cdot \cos \beta} = \frac{(0,958 + 0,67) \cdot 1467^2}{8 \cdot 5097 \cdot \cos 3,86^\circ} = 86,12 \text{ m}$$

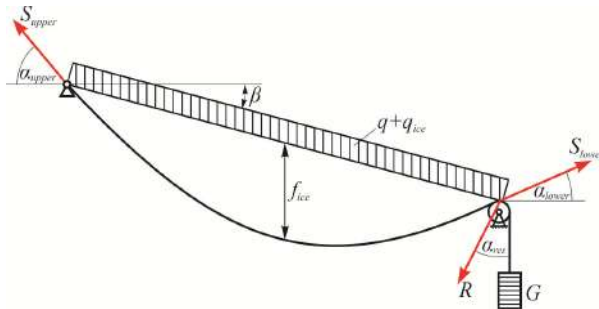


Fig. 6. Rope loaded with ice

The length of the frozen rope is then:

$$l_{frozen} = \frac{l}{\cos \beta} + \frac{8}{3} \cdot \frac{f_{ice}^2}{l} \cdot \cos^3 \beta = \frac{1467}{\cos 3,86^\circ} + \frac{8}{3} \cdot \frac{86,12^2}{1467} \cdot \cos^3 3,86^\circ = 1483,73 \text{ m}$$

3.3 Wind impact

Wind pressure is according to the [12] calculated by the following expression:

$$p_{wind} = \frac{w^2}{16} \left[\frac{\text{daN}}{\text{m}^2} \right]$$

where the w represents the maximal wind velocity at the location where the zipline is built.

According to the Beaufort scale, for gale/fresh gale wind speed amounts between $17,2 \text{ m/s}$ and $20,7 \text{ m/s}$, so it follows:

$$p_{wind} = \frac{w^2}{16} = \frac{18,95^2}{16} = 22,4 \frac{\text{daN}}{\text{m}^2}$$

where:

$$w = \frac{17,2 + 20,7}{2} = 18,95 \frac{\text{m}}{\text{s}}$$

The load of the rope per length unit is then:

$$q_{wind} = p_{wind} \cdot d_{rope} = 22,4 \cdot 0,014 = 0,31 \frac{\text{daN}}{\text{m}} \approx 0,31 \frac{\text{kg}}{\text{m}}$$

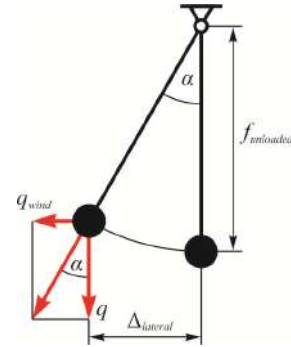


Fig. 7. Lateral deflection of the rope

The angle of rotation of the plane of the rope due to the action of the wind is

$$\alpha = \arctg \left(\frac{q_{wind}}{q} \right) = \arctg \left(\frac{0,31}{0,958} \right) = 17,9^\circ$$

Knowing that the maximal rope deflection amounts to $50,68 \text{ m}$, it follows that the lateral deflection is:

$$\Delta_{lateral} = f_{unloaded} \cdot \sin \alpha = 50,68 \cdot \sin 17,9^\circ = 15,58 \text{ m}$$

3.4 Temperature impact

According to regulations, ropes must be calculated for the following conditions:

- minimal working temperature: -20°C
- maximal working temperature: $+40^{\circ}\text{C}$

If it is assumed that the temperature during installation was 18°C , then the temperature differences for the calculation amounts:

$$\Delta t_1 = 18 - (-20) = 38^{\circ}\text{C}$$

$$\Delta t_2 = 40 - 18 = 22^{\circ}\text{C}$$

According to the previous and assuming that at the temperature of -40°C the rope is completely frozen, the maximal displacement of the tightening weight is:

$$\begin{aligned} \Delta h &= l_{\text{frozen}} - l_{\text{unloaded}} + \alpha_t \cdot \Delta t_1 \cdot l_{\text{frozen}} + \alpha_t \cdot \Delta t_2 \cdot l_{\text{unloaded}} = \\ &= 1483,73 - 1474,97 + \\ &\quad + (38 \cdot 1483,73 + 22 \cdot 1474,97) \cdot 12 \cdot 10^{-6} = 9,83 \text{ m} \end{aligned}$$

where α_t represents linear thermal expansion coefficients for steel:

$$\alpha_t(\text{steel}) = 11 \div 13 \cdot 10^{-6} \left[\frac{1}{^{\circ}\text{C}} \right] \Rightarrow \alpha_t = 12 \cdot 10^{-6} \frac{1}{^{\circ}\text{C}}$$

4. CONCLUSION

The rope is the most essential part of the zipline system and therefore must be given the greatest attention. When choosing a rope for a specific zipline location, designers can be guided by some of the criteria listed in this paper. It would be best if the designers made the choice according to the least favourable criteria for the given situation.

Regardless of the criteria by which the rope was chosen, additional effects such as atmospheric effects, but also the effects of the person's descent down the zipline, must also be checked.

REFERENCES

- [1] Czitary, E. (1962). *Seilschwebbahnen*. Springer-Verlag, Vienna, Austria.
- [2] Samset, I. (1985). *Winch and cable systems*. Norwegian Forest Research Institute, Ås, Norway.
- [3] Günthner, W. A. (1999). *Seilbahntechnik*. Technische Universität München, Germany.
- [4] Sedivy, P. (2012). *Seilbahnbau*. Universität Innsbruck, Austria.
- [5] Dukel'skij, A. I. (1966). *Podvesnye kanatnye dorogi i kabel'nye krany*. Mashinostroenie, Moskva, SSSR.
- [6] Kujbida, G. G. (1989). *Kabel'nye krany*. Mashinostroenie, Moskva, SSSR.
- [7] Vladić, J, Đokić, R, Jojić, T. (2017). *Elaborat – Analiza Sistema ZIP LINE u Vrdniku*. Faculty of Technical Sciences, Novi Sad, Serbia.
- [8] Fatzer Brugg Wire Ropes. From: <https://www.old.fatzer.com/en>, accessed on: 20.03.2023.
- [9] Casar Wire Ropes. From: <https://www.casar.de/de>, accessed on: 20.03.2023.
- [10] Bridon Wire Ropes. From: <https://www.bridon-bekaert.com/>, accessed on: 20.03.2023.
- [11] Douglass, D. et al. (2016). *Sag-Tension Calculation Methods for Overhead Lines*. CIGRE, Paris, France.
- [12] Dragojević, V. et al. (1992). *Pravilnik o tehničkim normativima za izgradnju nadzemnih elektroenergetskih vodova nazivnog napona od 1 kV do 400 kV*, Službeni list SFRJ, Belgrade, Serbia.

Mechatronics and Robotics



Banja Luka
1–2 Jun 2023.

DEMI 2023
**16th International Conference on
Accomplishments in Mechanical and
Industrial Engineering**
www.demi.mf.unibl.org



Assessment of fractional order impact on performance of fractional ILC controller for upper limb exoskeleton

N. Živković^a, M. Lazarević^b, J. Vidaković^a

^aLola institute, Kneza Viseslava 70a, 11030 Belgrade, Serbia

^bFaculty of Mechanical Engineering, The University of Belgrade, Kraljice Marije 16, 11120 Belgrade

Abstract *In this research paper, the application of Iterative Learning Control (ILC), an intelligent control method, is suggested in the form of a fractional-order PD-type controller. The main task of the ILC controller is to reject process model uncertainties, which are often present in complex systems such as various multibody systems, and to sequentially reduce a trajectory tracking error. As a control plant, an exoskeleton support arm with three degrees of freedom is used herein. The control scheme consists of feedback linearization compensating for the known part of the dynamics model and the feedforward ILC controller of the PD α -type. The feedback part of the control system is the classical PD controller. The feedforward control signal is filtered with a lowpass filter to avoid divergent behavior as iterations progress. Finally, simulation results are presented to demonstrate the proposed control system performance applied to the chosen control plant, as well as the achieved error convergence towards the steady-state value for various values of the fractional order.*

Keywords *Iterative learning control, feedback linearization, fractional derivative, trajectory tracking, exoskeleton*

1. INTRODUCTION

Trajectory tracking is one of the main problems in robotics, where the goal is to control a robot's motion to follow a predefined path or trajectory [1]. This problem also arises in various applications, such as industrial automation, autonomous vehicles, surgical and rehabilitation robots [2,3]. Appropriately achieved trajectory tracking enables robots to perform complex tasks accurately and efficiently.

The beginning of Iterative Learning Control (ILC) theory was introduced by Uchiyama and Arimoto in [4] and [5]. ILC can be defined as an

intelligent memory type of control since it uses the information from the past experiences to improve the performance of the system [6]. ILC is particularly well-suited for systems that repeat a task or motion several times, such as robots. Mathematical models of the robot manipulators are idealized version of the real-world dynamics, leaving some degree of uncertainty in the model [7]. The advantage of the ILC algorithms is robustness to uncertainty and repetitive disturbances [8]. Combining model-based control such as feedback linearization and ILC can lead to improved trajectory tracking performance.

After fractional calculus gained popularity over the years, various control algorithms using fractional derivative or integral have been investigated [9]. In this study we investigated how fractional order derivative in ILC controller

Corresponding author

M.Sc. Nikola Živković
nikola.zivkovic@li.rs

Lola institute
Kneza Viseslava 70a
Belgrade, Serbia

influences the error convergence over iterations and overall performance of the system.

In the Section 2, brief theoretical background for ILC and fractional calculus used in this study is laid out. Section 3 consists of controller design description divided into subsection describing feedback linearization and subsection describing fractional order iterative learning controller. Section 4 showcases simulation results of previously presented controller for various values of fractional order derivative in ILC.

2. THEORETICAL BACKGROUND

2.1 Iterative learning control

Iterative learning control algorithms utilize information from previous attempts to refine the control input and improve performance in subsequent iterations. The control system learns from its past errors and adapts the control inputs to achieve the desired output with higher accuracy in each subsequent iteration. The general form of iterative learning control [10, 11] can be given as:

$$\mathbf{u}_{k+1} = \mathbf{Q}(\mathbf{u}_k + \mathbf{L}\mathbf{e}_k), \quad (1)$$

where k is the iteration index, \mathbf{u} is the control signal, \mathbf{e} the error signal and \mathbf{Q} and \mathbf{L} are filter and learning function, respectively. There are many variations of the control law (1) and different approaches to modelling \mathbf{Q} filter and learning function \mathbf{L} [12,13]. In this paper we consider PD-type control algorithm with \mathbf{Q} as lowpass filter:

$$\mathbf{u}_{k+1} = \mathbf{Q}(\mathbf{u}_k + \mathbf{K}_p\mathbf{e}_k + \mathbf{K}_d\dot{\mathbf{e}}_k), \quad (2)$$

where \mathbf{K}_p and \mathbf{K}_d are tuneable gain matrices.

2.2 Fractional calculus

Fractional calculus is a branch of mathematical analysis that extends the concepts of differentiation and integration to non-integer orders. In presented study ILC controller uses fractional order derivative of the error signal. Fractional derivative is calculated using Grunwald-Letnikov definition of fractional derivative [14]:

$$D_R^\alpha y(t) = \lim_{h \rightarrow 0} \frac{1}{h^\alpha} \Delta_h^\alpha y(t), \quad (3)$$

where h is the time step, D_R^α is the fractional derivative operator, $y(t)$ is the function to be differentiated and Δ_h^α is the finite difference notation with detailed explanation in [14].

3. CONTROLLER DESIGN

3.1 Application of feedback linearization control method for robot systems

Feedback linearization is a powerful model-based control technique that allows nonlinear systems to be transformed into fully or partly linear systems, so that they can be controlled using traditional linear control methods [15]. Equations of motion of a robot mechanism (i.e. robot dynamic model) are usually presented in canonical form in the joint-space formulation:

$$\mathbf{M}(\mathbf{q})\ddot{\mathbf{q}} + \mathbf{C}(\mathbf{q}, \dot{\mathbf{q}})\dot{\mathbf{q}} + \mathbf{g}(\mathbf{q}) = \boldsymbol{\tau}, \quad (4)$$

where $\mathbf{M}(\mathbf{q})$ is the inertia matrix, $\mathbf{C}(\mathbf{q}, \dot{\mathbf{q}})$ is the matrix containing centrifugal and Coriolis effects, $\mathbf{g}(\mathbf{q})$ is the vector of gravity forces and $\boldsymbol{\tau}$ is the vector of joint actuation torques. Equations of motion given by (4) can be rewritten in form where the model is split in nominal and uncertain part [7]:

$$(\mathbf{M}_N + \Delta\mathbf{M})\ddot{\mathbf{q}} + (\mathbf{C}_N + \Delta\mathbf{C})\dot{\mathbf{q}} + \mathbf{g}_N + \Delta\mathbf{g} = \boldsymbol{\tau}, \quad (5)$$

where nominal parts of the $\mathbf{M}(\mathbf{q})$, $\mathbf{C}(\mathbf{q}, \dot{\mathbf{q}})$ and $\mathbf{g}(\mathbf{q})$ are denoted with subscript N and uncertain parts are prefixed with symbol Δ . Uncertainty is represented as an additive uncertainty [16]. Applying the feedback linearization method to the system (4) would result in linearized system with following equation:

$$\ddot{\mathbf{q}} = \mathbf{u}, \quad (6)$$

where \mathbf{u} is the new control input. However, uncertainties of the mathematical model are not accounted for in such system, so in order to obtain the system model taking model uncertainties into account, the feedback linearization will be applied to the system represented with Eq. (4). For considered model it is assumed that feedback linearizing control law can only cancel out nominal nonlinearities leaving the uncertain parts. Regarding the previous sentence, linearizing control law is chosen in following form:

$$\tau = \mathbf{M}_N \mathbf{u} + \mathbf{C}_N \dot{\mathbf{q}} + \mathbf{g}_N, \quad (7)$$

where \mathbf{u} is the new control input. Substituting equation Eq. (7) in Eq. (5) with assumption that uncertainties effects on inertia matrix are negligible, meaning that $\mathbf{M}^{-1}\mathbf{M}_N \approx \mathbf{I}$, new system of equations of motion is obtained:

$$\ddot{\mathbf{q}} = \mathbf{u} + \boldsymbol{\eta}, \quad (8)$$

where $\boldsymbol{\eta}$ is vector representing uncertain part of the model and it is equal to:

$$\boldsymbol{\eta} = \mathbf{M}^{-1}(\Delta \mathbf{C} \dot{\mathbf{q}} + \Delta \mathbf{g}). \quad (9)$$

Linearized system (8) can be further subjected to linear control laws which is the topic of the next subsection.

3.2 Iterative learning controller with fractional derivative

Iterative learning controllers have proven to be successful at improving trajectory tracking and uncertainty rejection. Here, we consider PD-type controller in feedback and feedforward PD $^\alpha$ -type control action to improve trajectory tracking and ensure robustness of the system to uncertainties. Linear control law can be divided into feedback and feedforward sections:

$$\mathbf{u}_{k+1} = \mathbf{u}_{k+1}^{\text{ff}} + \mathbf{u}_{k+1}^{\text{fb}}, \quad (7)$$

where feedback $\mathbf{u}_{k+1}^{\text{fb}}$ and feedforward $\mathbf{u}_{k+1}^{\text{ff}}$ terms are defined with following equations respectively:

$$\mathbf{u}_{k+1}^{\text{fb}} = \mathbf{K}_p^{\text{fb}} \mathbf{e}_{k+1} + \mathbf{K}_d^{\text{fb}} \dot{\mathbf{e}}_{k+1}, \quad (8)$$

$$\mathbf{u}_{k+1}^{\text{ff}} = \mathbf{Q}(\mathbf{u}_k + \mathbf{K}_p^{\text{ff}} \mathbf{e}_k + \mathbf{K}_d^{\text{ff}} D^\alpha \mathbf{e}_k), \quad (9)$$

where k is the iteration index, \mathbf{e} is the error vector, $\dot{\mathbf{e}}$ is derivative of error vector, D^α is α -th order fractional derivative operator \mathbf{K}_p^{fb} and \mathbf{K}_d^{fb} are diagonal positive-definite proportional and derivative feedback gain matrices, \mathbf{K}_p^{ff} and \mathbf{K}_d^{ff} are diagonal positive-definite ILC learning gain matrices and \mathbf{Q} is the lowpass filter. Lowpass filter is incorporated to filter out high frequencies which emerge in feedforward signal after apparent error convergence is achieved [17]. Filtering feedforward signal with lowpass filter will cause convergence towards non-zero steady-state value.

4. SIMULATION RESULTS

This section presents the simulation results of the assessment of fractional order impact on error norm convergence and validity of proposed controller. The numerical simulation is carried out in Matlab and Simulink using 3DoF model of exoskeleton for upper limbs. The exoskeleton model is defined in URDF (Unified Robot Description Format) and it consists of two truncated cones representing upper arm link and forearm link and chamfered cube representing shoulder link (Fig 1.). In Fig 1. O_{xyz} is the reference coordinate frame, \mathbf{e}_i are unit vectors representing the joint axes of rotations and C_i are centres of inertia of links both expressed in reference frame.

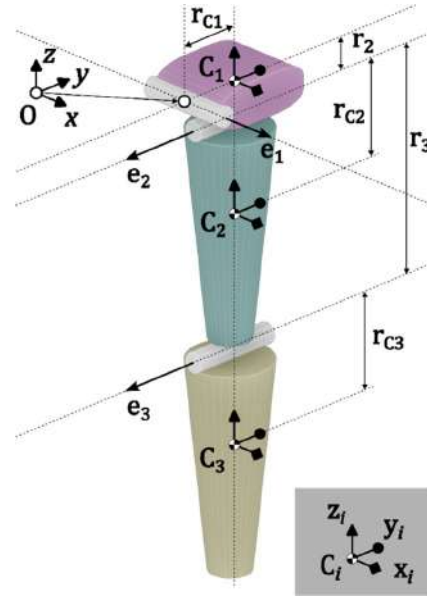


Fig. 1. Structure of the exoskeleton model

Distances between joint axes r_i , distances of centres of inertia from corresponding joint axes r_{Ci} and unit vectors \mathbf{e}_i for exoskeleton model are given in Table 1.

Table 1. Joint parameters of the exoskeleton

Parameter	Joint 1	Joint 2	Joint 3
\mathbf{e}_i	[1,0,0]	[0,-1,0]	[0,-1,0]
r_i [m]	0	0.25	1.1
r_{Ci} [m]	0.25	0.493	0.493

Desired trajectory is defined in joint space coordinates as a fifth order polynomial:

$$q_d = a_0 + a_1 t + a_2 t^2 + a_3 t^3 + a_4 t^4 + a_5 t^5, \quad (10)$$

The exoskeleton system is tasked with reaching certain point in joint space from zero position and returning back to zero for certain time period as shown in Fig 2. Waypoints of the desired trajectory for this simulation are summarized in Table 2.

Table 2. Waypoints of the desired trajectory

Waypoint no.	Joint 1 [rad]	Joint 2 [rad]	Joint 3 [rad]	Time period [s]
1	0	0	0	0
2	1	0.6	0.5	1
3	0	0	0	2

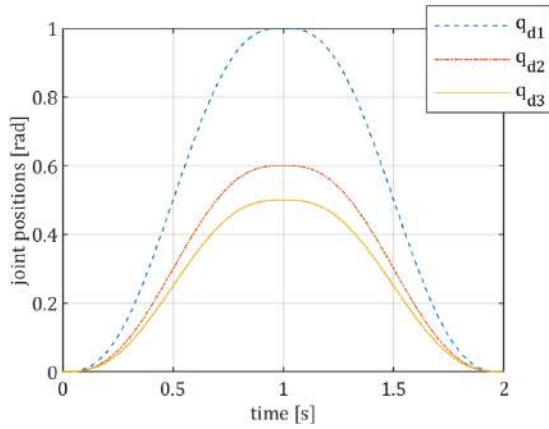


Fig. 2. Desired trajectory in joint space

Feedback gain matrices are chosen by trial and error:

$$\mathbf{K}_p^{\text{fb}} = \text{diag}[20,30,30], \mathbf{K}_d^{\text{fb}} = \text{diag}[10,15,15]$$

Learning gain matrices are chosen as:

$$\mathbf{K}_p^{\text{ff}} = \text{diag}[1,1,1], \mathbf{K}_d^{\text{ff}} = \text{diag}[1,1,1]$$

The cut-off frequency for lowpass filter Q is chosen to be $f_{\text{cut-off}} = 1\text{Hz}$.

The quality of the system response over iterations is evaluated by calculating infinite norm (also known as the max norm) of the error signal $\|\mathbf{e}(t)\|_{\infty}$ for each iteration and plotting it over iteration axis to see if there exists convergence trend towards zero or some non-

zero steady-state value. Results from simulation show that fractional order ranging from zero to 1 in equation Eq. (9) exhibit similar behavior of an error norm over iterations as Fig 3. suggests. The convergence exists, but norms of error signal for different values of fractional order do not vary much between themselves. However, Fig 4. shows that fractional order in interval $\alpha \in [1,2]$ results in significant improvement of an error norm convergence. Increasing fractional order from 1 towards 2 error norm converges faster towards steady-state value. Going beyond fractional order of two, error norm displays divergence, i.e. system becomes unstable, Fig 5.

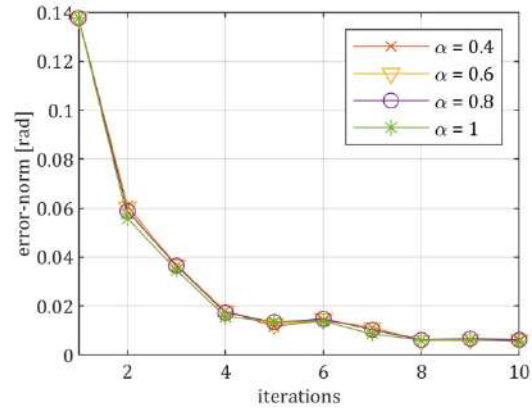


Fig. 3. Error norm for joint 1 for fractional order in interval $\alpha \in [0, 1]$

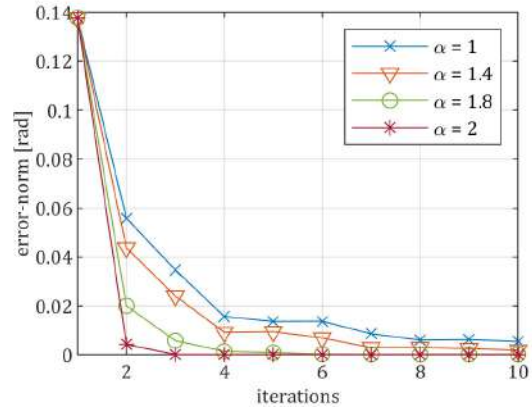


Fig. 4. Error norm for joint 1 for fractional order in interval $\alpha \in [1,2]$

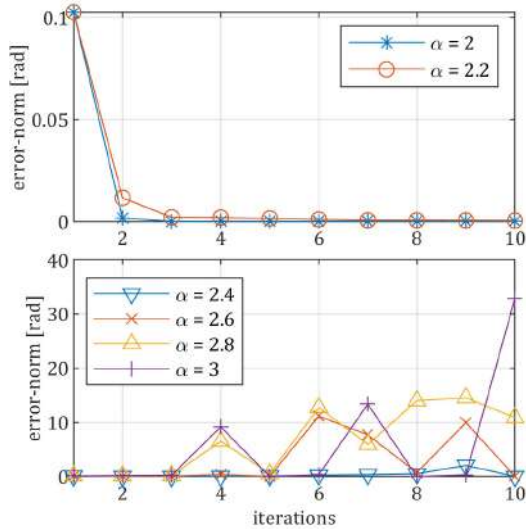


Fig. 5. Error norm for joint 1 for fractional order in interval $\alpha \in [2,3]$

Based on the previous results the best convergence properties, for tested exoskeleton system with uncertainties, achieves controller with fractional order in interval $\alpha \in [1.8, 2.2]$.

5. CONCLUSION

The goal of the presented study was to assess the performance of the proposed fractional iterative learning controller of upper limbs 3DoF exoskeleton system with model uncertainties, taking into account the variation of fractional order values. The control scheme consists of feedback linearization compensating for the determined part of the nonlinear dynamics model and the feedforward ILC controller of the PD^α -type. Numerical simulations of the proposed control method have shown that a fractional order in certain interval between 1.8 and 2.2 gives significantly better control system performance compared to other values. Values of fractional order beyond 2.2 cause system to become unstable. The performance of the fractional order ILC controller in the determined order interval is superior compared to its integer order counterpart.

Acknowledgement

This research has been supported by the research grants of the Serbian Ministry of Science, Technological Development and

Innovations, grant No. 451-03-68/2023-14/200066 and 451-03-47/2023-01/ 200105 from 03.02.2023.

REFERENCES

- [1] Spong, W. M., Hutchinson, S., Vidyasagar, M. (2020). *Robot Modeling and Control*. John Wiley & Sons.
- [2] Siciliano, B., Oussama, K., (2008). *Handbook of Robotics*. Springer, Berlin.
- [3] Freeman, C. T., Rogers, E., Burridge, J. H., Hughes, A., Meadmore, K. L., (2015) *Iterative learning control for electrical stimulation and stroke rehabilitation*. Springer, Berlin.
- [4] Uchiyama, M., (1978) Formulation of high-speed motion pattern of mechanical arm by trial (in Japanese). *Transactions of the Society for Instrumentation and Control Engineers*, vol 14, p. 706-712.
- [5] Arimoto, S., Kawamura, S., Miyazaki, F. (1984) Bettering operation of robots by learning, *Journal of Robot System*, vol 1, p. 123-140.
- [6] Ahn, H. S., Moore, K. L., Chen, Y. (2007) *Iterative Learning Control: Robustness and Monotonic Convergence for Interval Systems*. Springer-Verlag, London.
- [7] Lazarevic, M., Mandic, P., Ostojic, S. Further results on advanced robust iterative learning control and modeling of robotic systems, *Proceedings of the Institution of Mechanical Engineers, Part C: Journal of Mechanical Engineering Science*, 2021, p. 4719 - 4734.
- [8] Ahn, H. S., Chen Y., Moore K. L. (2007) Iterative Learning Control: Brief Survey and Categorization, *IEEE Transactions on Systems, Man, and Cybernetics—PART C: Applications and Reviews*, vol. 37, no. 6, p. 1099 - 1121. DOI: [10.1109/TSMCC.2007.905759](https://doi.org/10.1109/TSMCC.2007.905759)
- [9] Li, Y., Chen, Y. Q., Ahn, H. S., Tian, G. (2013). A survey on fractional-order iterative learning control. *Journal of Optimization Theory and Applications*. vol. 156, no. 1, p. 127 - 140.
- [10] Moore, K. L. (2012) *Iterative learning control for deterministic systems*, Springer.
- [11] Bien, Z., Xu, J. X. (2012). *Iterative learning control: analysis, design, integration and applications*. Springer Science & Business Media.
- [12] Xu, J.-X., Tan, Y. (2003). *Linear and Nonlinear Iterative Learning Control*. Springer, Berlin.
- [13] Owens, D.H., Munde, G.S. Universal adaptive iterative learning control. *Proceedings of the 37th IEEE Conference on Decision and Control*, 1998, p. 181-185.

- [14] Scherer, R., Kalla, S.L., Tang, Y., Huang, J. () The Grunwald-Letnikov method for fractional differential equations. *Computers & Mathematics with Applications*, vol. 62, no. 3, p. 902 - 917. DOI: [10.1016/j.camwa.2011.03.054](https://doi.org/10.1016/j.camwa.2011.03.054)
- [15] Slotine, J., *Applied nonlinear control*, Englewood Cliffs N.J.: Prentice Hall, 1991.
- [16] Astrom, K., Murray R., (2008). *Feedback Systems: An Introduction for Scientists and Engineers*, Princeton University Press, .
- [17] Longman, R.W., Huang, Y-C. (2002). The Phenomenon of Apparent Convergence Followed by Divergence in Learning and Repetitive Control. *Intelligent Automation & Soft Computing*, vol. 8, no. 2, p. 107-128. DOI: [10.1080/10798587.2002.10644210](https://doi.org/10.1080/10798587.2002.10644210)



Banja Luka
1–2 Jun 2023.

DEMI 2023

16th International Conference on Accomplishments in Mechanical and Industrial Engineering

www.demi.mf.unibl.org



Contribution of research on the application of active magnetic bearings in order to reduce the influence of unbalance on the vibrations intensity of a rigid rotor

A. Tomović^a, M. Damjanović^a, R. Tomović^a, J. Jovanović^a

^aFaculty of Mechanical Engineering, University of Montenegro, Džordža Vašingtona bb, 81000 Podgorica, Montenegro;

Abstract Recording and monitoring of vibrations that occur in the bearings in which the rotating elements are supported provide information about the state of the system. The most common cause of vibrations in systems with rotating elements is the unbalance of the rotating elements. Increased mechanical vibrations have a negative impact on the operation of the system, and can often have fatal consequences. With the development of active magnetic bearings, as modern mechatronic systems, the possibility of active control of rotating elements appeared, all in order to maintain the rotor in a balanced position by applying attractive magnetic forces. The development of a mathematical model of the dynamic behavior of a rigid rotor, by means of which it can be confirmed that the use of active magnetic bearings can annul the negative impact of unbalance on the intensity of vibrations of the rotating elements was the aim of this work.

Keywords active magnetic bearings, unbalance, rigid rotor

1. INTRODUCTION

Bearings represent one of the most important components in the construction of a machine, and based on their operation, the working life of the machine can be estimated. By studying the behaviour of the bearing in operation, the operation of the machine itself is also studied, where various patterns such as noise and vibrations can indicate improper operation or failure of the entire system. The problems that occur with conventional bearings led to the discovery of magnetic bearings where there is no physical contact

between the rotor and the stator. The development of technique and technology has created a tendency for modern rotary machines (hydro turbines and wind turbines, generators, electric motors, fans, etc.) to achieve the highest possible rotation speeds during exploitation in order to function more precisely and efficiently. In order for the machine to be able to achieve high rotation speeds, which range up to several thousand revolutions per minute, it is necessary to respond to numerous challenges that appear when working at such high speeds. Magnetic bearings stand out as a realistic and possible solution for meeting the challenges that are imposed in work at high rotational speeds. Unbalance of rotary components is indicated as the main cause for the appearance of vibrations that exceed the permitted prescribed level in rotary machines. Most of the causes from which the unbalance appear can be corrected to a greater or lesser extent with adequate interventions before exploitation. For this

Corresponding author

mr Aleksandar Tomović
aleksandart@ucg.ac.me

Faculty of Mechanical Engineering, University of
Montenegro,
Džordža Vašingtona bb,
81000 Podgorica, Montenegro;

purpose, various static and dynamic rotor balancing procedures are most often used. On the other side, a special circumstance is the occurrence of unbalances during exploitation, which often occur suddenly, as in the case of breakage and tearing of individual parts of the rotary system, e.g. breakage of fan blades or cavitation damage in hydroturbines, etc. [1]. This sudden occurrence of unbalance created the idea of using active magnetic bearings to annul the unbalance that occurs during exploitation.

2. ACTIVE MAGNETIC BEARING FUNCTIONING PROCESS AND THE ATTRACTIVE FORCE CALCULATION

The standard configuration [2] about active magnetic bearings gives the basic principle of operation of a simple system, which consists of a rotor supported in only one direction (Fig. 1):

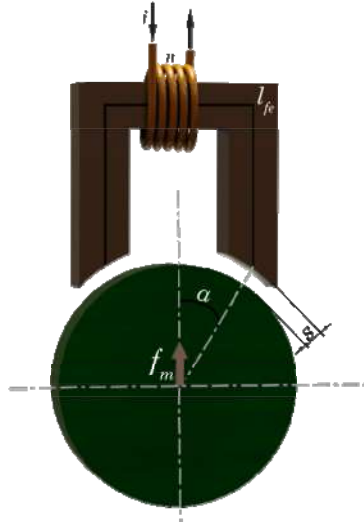


Fig. 1. The schematic representation of the active magnetic bearing simple system.

The sensor measures the rotor deviation from the reference position, and the microprocessor as a controller derives a control signal from the measurement, the amplifier converts this control signal into a control current, and the control current generates a magnetic field in the active magnets, which result in the magnetic forces in such a way that the rotor remains in its floating position. [3]

The equation for calculating the attractive force depending on the current passing through the windings and the air gap is as follows:

$$F = \mu_0 \cdot A_0 \cdot \left(\frac{n \cdot i}{2 \cdot s} \right)^2 = \frac{1}{4} \mu_0 \cdot A_0 \cdot n^2 \cdot \frac{i^2}{s^2} \quad (1)$$

respectively,

$$F = \frac{1}{4} \mu_0 \cdot A_0 \cdot n^2 \cdot \frac{i^2}{s^2} \cdot \cos \alpha = k \cdot \frac{i^2}{s^2} \quad (2)$$

where μ_0 is the magnetic permeability of vacuum, A_0 is the cross-section of the air gap, n is the number of electromagnet windings, magnetic forces act on the rotor with an angle α , i is the current flowing through the windings, s is the air gap between electromagnet and rotor, and $k = \frac{1}{4} \mu_0 \cdot A_0 \cdot n^2 \cdot \cos \alpha$ is a constant that depends on the geometry of the electromagnets used for the AMB system [3].

Since the mentioned case with only one pole of the electromagnet is not used in practice, by combining them and forming a pair of poles, a structural combination of electromagnets is obtained, which enables the control of the ferromagnetic rotor in several axes. The forces exerted by electromagnets on the rotor during operation can be both positive and negative at the same time.

Based on the differential operating mode of the active magnetic bearing system (Fig. 3) and applying the equation for obtaining the attractive force (2), the equation for calculating the attractive force for one pair of electromagnet poles is obtained:

$$F = F_1 + F_2 = k \cdot \left[\frac{(i_0 + i_x)^2}{(s_0 - x)^2} - \frac{(i_0 - i_x)^2}{(s_0 + x)^2} \right] \quad (3)$$

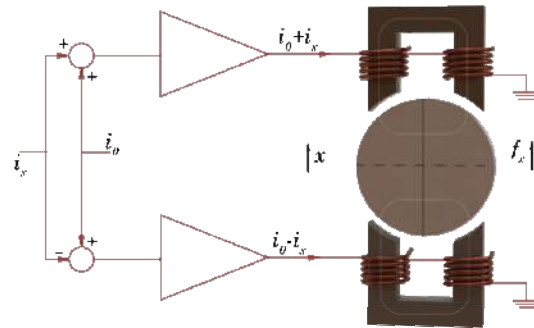


Fig. 2. Differential control of one pair of active magnetic bearing poles

3. THE EQUATIONS OF RIGID ROTOR DYNAMIC MOVEMENT SUPPORTED ON RADIAL ACTIVE MAGNETIC BEARINGS

Assuming that the rotor does not deviate from the reference position and that $x = 0$, i.e. that

the control current is much smaller than the induce current, a linearized equation for the attractive electromagnetic force can be obtained:

$$F_N = \frac{4 \cdot k \cdot f_0}{s_0^2} \cdot \cos \alpha \cdot i_N + \frac{4 \cdot k \cdot f_0^2}{s_0^2} \cdot \cos \alpha \cdot N \quad (4)$$

$$F_Y = \frac{4 \cdot k \cdot f_0}{s_0^2} \cdot \cos \alpha \cdot i_Y + \frac{4 \cdot k \cdot f_0^2}{s_0^2} \cdot \cos \alpha \cdot Y \quad (5)$$

The system analyzed in this paper consists of two radial active magnetic bearings and has five degrees of freedom of movement (two degrees of freedom for translational movement in the radial directions x-y, and two for rotational movement around the x-y axis, and one degree of freedom for rotational movement in the direction of the z axis) and two each displacement sensors that are placed in addition to the radial bearings.

The final equations of the dynamic movement of the rotor supported on radial active magnetic bearings were obtained according to Newton's law of motion (Newton's second law), unbalance equations and the equations for the rigid rotor model with four degrees of freedom of movement in the positions of the magnetic bearings A and B:

$$\begin{aligned} \ddot{x}_A + \frac{J_z \theta_z d_A}{J_x d} (\dot{x}_A - \dot{x}_B) - x_A \left(\frac{2k_x}{m} + \frac{2k_x d_A^2}{J_x} \right) \\ - x_B \left(\frac{2k_x}{m} - \frac{2k_x d_A d_B}{J_x} \right) = t_{xA} \left(\frac{k_l}{m} + \frac{k_l d_A^2}{J_x} \right) \\ + t_{xB} \left(\frac{k_l}{m} - \frac{k_l d_A d_B}{J_x} \right) + s \theta_z^2 \cos \theta_z t \\ + K \cdot \theta_z^2 \cdot \frac{(J_x - J_z) d_A}{J_x} \cdot \sin \theta_z t \end{aligned} \quad (6)$$

$$\begin{aligned} \ddot{x}_B - \frac{J_z \theta_z d_B}{J_x d} (\dot{x}_A - \dot{x}_B) - x_A \left(\frac{2k_x}{m} - \frac{2k_x d_A d_B}{J_x} \right) \\ - x_B \left(\frac{2k_x}{m} + \frac{2k_x d_B^2}{J_x} \right) = t_{xA} \left(\frac{k_l}{m} - \frac{k_l d_A d_B}{J_x} \right) \\ + t_{xB} \left(\frac{k_l}{m} + \frac{k_l d_B^2}{J_x} \right) + s \theta_z^2 \cos \theta_z t \\ + K \cdot \theta_z^2 \cdot \frac{(J_x - J_z) d_B}{J_x} \cdot \sin \theta_z t \end{aligned} \quad (7)$$

$$\begin{aligned} \ddot{y}_A + \frac{J_z \theta_z d_A}{J_y d} (\dot{y}_B - \dot{y}_A) - y_A \left(\frac{2k_y}{m} + \frac{2k_y d_A^2}{J_y} \right) \\ - y_B \left(\frac{2k_y}{m} - \frac{2k_y d_A d_B}{J_y} \right) = t_{yA} \left(\frac{k_l}{m} + \frac{k_l d_A^2}{J_y} \right) \end{aligned} \quad (8)$$

$$\begin{aligned} + t_{yB} \left(\frac{k_l}{m} - \frac{k_l d_A d_B}{J_y} \right) + s \theta_z^2 \sin \theta_z t \\ - K \cdot \theta_z^2 \cdot \frac{(J_x - J_z) d_A}{J_y} \cdot \cos \theta_z t \\ \ddot{y}_B - \frac{J_z \theta_z d_B}{J_y d} (\dot{y}_B - \dot{y}_A) - y_A \left(\frac{2k_y}{m} - \frac{2k_y d_A d_B}{J_y} \right) \\ - y_B \left(\frac{2k_y}{m} + \frac{2k_y d_B^2}{J_y} \right) = t_{yA} \left(\frac{k_l}{m} - \frac{k_l d_A d_B}{J_y} \right) \\ + t_{yB} \left(\frac{k_l}{m} + \frac{k_l d_B^2}{J_y} \right) + s \theta_z^2 \sin \theta_z t \\ - K \cdot \theta_z^2 \cdot \frac{(J_x - J_z) d_B}{J_y} \cdot \cos \theta_z t \end{aligned} \quad (9)$$

In order to obtain a solution for the final equations, an approximation was performed using the Newmark beta method, and then the approximated equations were solved using the Newton-Rapson method.

Based on the derived equations, a case was analyzed that takes into account the situation in which, during the exploitation of a rigid rotor supported on two radial active magnetic bearings, an impetuous and sudden unbalance occurs in the rotor system. This case can occur in exploitation, for example, due to breakage and falling off of parts of the rotor, which will lead to an impetuous change in the mass balance of the rotor system and dislocation of the center of mass in relation to the geometric center of the rotor.

The sudden appearance of an unbalance in the structure of the rotor during exploitation leads to the emergence of a chaotic state in the entire machine system. This chaotic state is manifested by the appearance of mechanical vibrations in the bearings on which the rotor supports. Therefore, the application of active magnetic bearings in such situations stands out as a possible and realistic solution. Active magnetic bearings provide continuous control of a rigid rotor by means of attractive magnetic forces that maintain the rotor in a balanced position.

4. ANALYSIS AND DISCUSSION OF SIMULATION RESULTS

Based on the assumed data, a working simulation in the program environment *Matlab* was carried out in a situation where the rotor exposed to centrifugal force, which occurs e.g. due to the falling off of rotor parts, is not actively controlled, and then due to sudden

situation the active control of the rigid rotor is applied, which leads to the neutralization of the centrifugal force, which is a consequence of the existence of an unbalance.

The initial air gap that exists in the active magnetic bearings A and B is 1 mm. In Fig. 3. the results of the movement of the rigid rotor in active magnetic bearings A and B are presented when active control of the rigid rotor occurs during exploitation. The occurrence of unbalance in the system causes an increase in the amplitude of vibrations in the magnetic bearings A and B.

Analyzing the results, it can be observed that the rigid rotor during exploitation deviates from the reference position due to the presence of centrifugal force. That movement moves within the limits of the air gap that exists between the rigid rotor and the magnetic bearings. Despite the fact that the movement is within the limits

of the air gap, the increase in vibration amplitudes is not good. In order to return the vibration amplitudes to an adequate level, active attractive forces are applied to the rigid rotor in order to return it to its normal state from the aspect of vibrations.

By observing the graphs shown in Fig. 4. it can be observed that in a certain time interval it comes to the active control of the rigid rotor, which results in a visible reduction of the vibration amplitudes. At that moment, the active magnetic bearings position the rotor with attractive control forces and reduce the vibration level to minimum values (Fig. 4). Returning the rotor to a normal state from the aspect of vibrations enables the unobstructed continuation of the exploitation of the rotor until the situation suitable for overhauling the machine.

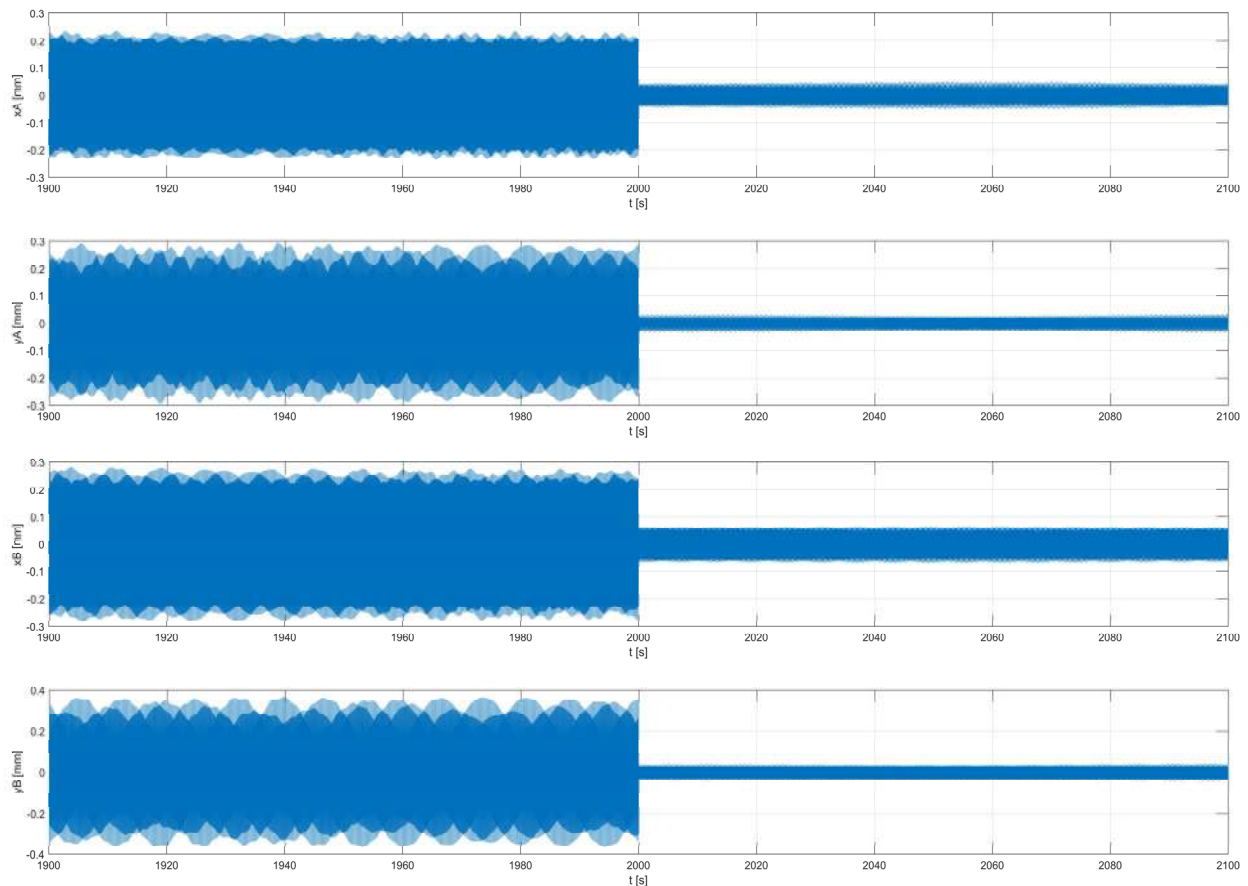


Fig. 3. The rotor movement along the x and y axes for active magnetic bearings A and B with active control of the rigid rotor.

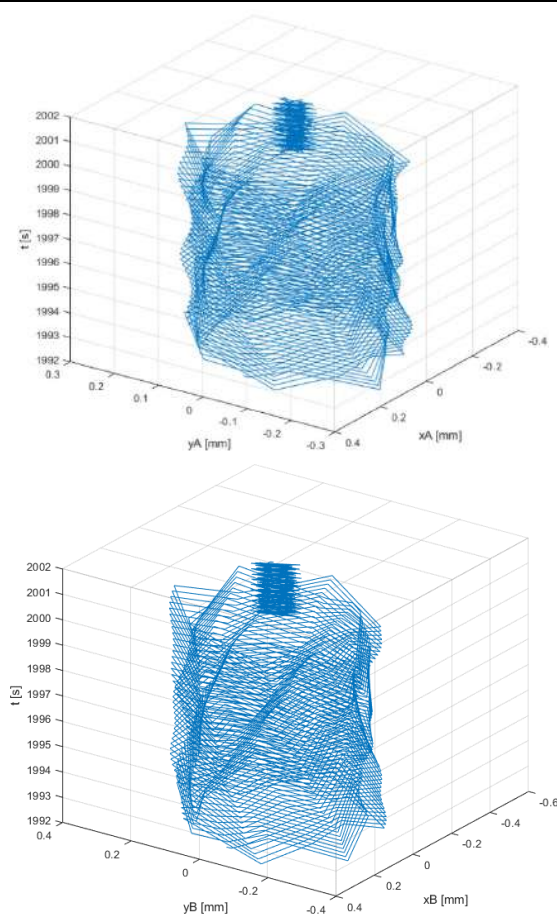


Fig. 4. The graphs of displacement in magnetic bearings A and B over time

The peak vibration amplitude for magnetic bearing A in the case when there is no active control of the rigid rotor in the system is $x_A = 0.2958 \text{ mm}$, while in the situation when the rotor is actively controlled it is $x_A = 0.051 \text{ mm}$. For magnetic bearing B without active rotor control, the vibration amplitude reaches its peak at a value of $x_B = 0.8673 \text{ mm}$, while in the case where there is active control in the system, the amplitude value is $x_B = 0.0638 \text{ mm}$. By comparing these values, it can be determined that there is a reduction of vibrations by approximately 6 times by applying active control using active magnetic bearings.

5. CONCLUSION

Modern technology recognizes a number of effective balancing methods, which can be used to annul or reduce the unbalance that occurred during production to a reasonable level. However, a special problem is a sudden

unbalance during exploitation. In systems where rigid rotors are supported on conventional bearings, the occurrence of unbalance leads to an alarming situation. This alarming situation in most cases means the need for maintenance intervention, stopping the flow of exploitation, which can happen in very unfavorable conditions for production, e.g. in the power plant when the demand for electricity is the highest. As a realistic and possible solution to reduce the amplitude of vibrations caused by the occurrence of unbalance, active magnetic bearings are imposed. This way of supporting the rotating parts of the mechatronic system enables constant monitoring of the vibration level and continuous positioning of the rotor. By continual positioning, the rigid rotor is maintained in an equilibrium position regardless of the disruptive forces that occur in the system during exploitation.

Based on the obtained simulation results, it can be concluded that by using active magnetic bearings, the negative influence of the centrifugal force can be successfully and adequately annulled by means of attractive magnetic forces. In this way, the increased level of vibrations caused by the impetuous and sudden appearance of unbalance is greatly reduced.

REFERENCES

- [1] Tomović, A. (2020). *Istraživanje mogućnosti primjene aktivnih magnetnih ležajeva u cilju smanjenja uticaja debalansa rotora na intenzitet vibracija rotacionih mašina*. (In Serbian). MSc thesis. Univerzitet Crne Gore, Mašinski fakultet Podgorica.
- [2] ISO 14839 – 1: 2018 (E), Mechanical vibration – Vibration of rotating machinery equipped with active magnetic bearings – Part 1: Vocabulary.
- [3] Schweitzer G., Maslen E. H. (2009). *Magnetic Bearings - Theory, Design and Application to Rotating Machinery*, Berlin, Springer-Verlag Berlin Heidelberg
- [4] Naikwad S. (2016). Study of Active Magnetic Bearing, *International Journal of Engineering and Technical Research (IJETR)*, ISSN: 2321-0869, Vol.4 (4).
- [5] Habermann, H., Liard, G. (1980). "An active magnetic bearing system", In Fillon M., Liang H., Liu W.M. (Eds.), *Tribology International*, (pp. 85-90), England, IPC Science and Technology Press Ltd.

- [6] Knospe, C. R., Hope, R. W., Fedigan, S. J., Williams R. D. (1995). Experiments in the control of unbalance response using magnetic bearings, *Mechatronics*, vol. 5, pp. 385–400.
- [7] Chen, Q., Liu, G., Han, B. (2017). Unbalance vibration suppression for AMBs system using adaptive notch filter. *Mech. Syst. Signal Process*, 93, 136–150.
- [8] B. Polajžer (Ed.). (2010). “Magnetic Bearings, Theory and Applications”, Rijeka, Hrvatska, Sciyo.
- [9] A. Chiba, T. Fukao, O. Ichikawa, M. Oshima, M. Takemoto, D. G. Dorrell. (2005). “Magnetic Bearings and Bearingless Drives”, Oxford, Burlington, Great Britain, Elsevier.
- [10] Hutterer, M., Kalteis G., Schrödl, M. (2017). Redundant unbalance compensation of an active magnetic bearing system. *Mechanical Systems and Signal Processing*, 94(), 267–278.



Banja Luka
1–2 June 2023.

DEMI 2023

16th International Conference on
Accomplishments in Mechanical and
Industrial Engineering

www.demi.mf.unibl.org



INTERNAL MODEL CONTROL OF TWO-TANK SYSTEM USING NEURAL NETWORKS

P. Stepanić^a, S. Marinković^a, J. Vidaković^a, N. Dučić^b, N. Živković^a

^a*Lola Institute Ltd., Belgrade, Serbia*

^b*Faculty of Technical Sciences Čačak, University of Kragujevac, Serbia*

Abstract In this paper, the implementation of the controller based on neural networks for controlling two-tank system is presented. A ready-made mathematical model of the Amira DTS200 system, which is a typical example of a slow nonlinear process, is used. Among the most important applications of artificial neural networks is their application in the control of nonlinear processes. The applied controlling structure represents Internal Model Control (IMC). Experimental results of the obtained process response for a given reference input using implemented IMC controller are given.

Keywords *Neural Network, Internal Model Control, Two-Tank System*

INTRODUCTION

Corresponding author

M.Sc, Sandra Marinković
sandra.marinkovic@li.rs

*Lola Institute Ltd.,
Kneza Višeslava 70a
Belgrade, Serbia*

Control of two-tank system is of extreme importance in many industrial processes, such as water control, food and chemical production, and others. Controlling these processes can be challenging due to the non-linear characteristics present in the system dynamics. By knowing the conventional methods of modeling and controlling dynamic processes mathematical models can be formed based on a physical model. Such systems roughly represent the input-output connections of the considered real systems.

In this paper, the application of an artificial neural network in the control of a system of two connected tanks will be investigated. Using a neural network is one way to overcome nonlinearities in the model, which can lead to better control of the system [1]. One of the

characteristics of artificial neural network application in process engineering is that process modeling does not require knowledge of process phenomena, but control is based on learning by extracting existing pattern. Patterns or forms represent the input-output data of the systems themselves, for which control needs to be formed.

In order to achieve optimal control, the nonlinear model of the system will first be considered and how an artificial neural network can be applied to solve control problems. As a control structure, control with an internal model (Internal Model Control – IMC) was used, while the starting point is the finished mathematical model of the AMIRA DTS200 system (sections 1-2).

Then it will be analyzed how the neural network can be used to predict the behavior of the system and optimize the control (section 3).

Finally, the paper will present the results of simulations that demonstrate the effectiveness of the application of artificial neural networks in the control of two tanks (sections 4-5).

This work aims to contribute to the understanding of the application of neural networks in the control of complex systems such as tanks, which may be of importance to various

industries dealing with the control of water and other liquids.

1. MATHEMATICAL MODEL OF TWO-TANK SYSTEM

The mathematical model of the system over which control is performed, consists of two tanks of equal cross-sections (A) [2,3]. The change in the volume of the water in the system depends on the change in the level of the water in the displayed tanks. For the mathematical model that was formed, it was assumed that the pump stops when the voltage is equal to zero, and it works at maximum power when the pump voltage u is equal to the maximum allowed value of 10V. Pump voltage represents the control variable of the system.

The entry of liquid into the system, i.e. the flow in Figure 1 marked with q , depends on the pump voltage.

The liquid from the first tank flows into the second (q_1), while the liquid from the second tank flows out unhindered by the flow q_2 . With the help of valves a_1 and a_2 we can regulate the cross-section of the pipe between the first and second tank and the drain pipe from the second tank, respectively. The water level in the second tank (h_2) represents the regulated output, while valve openings in the system are considered disturbances.

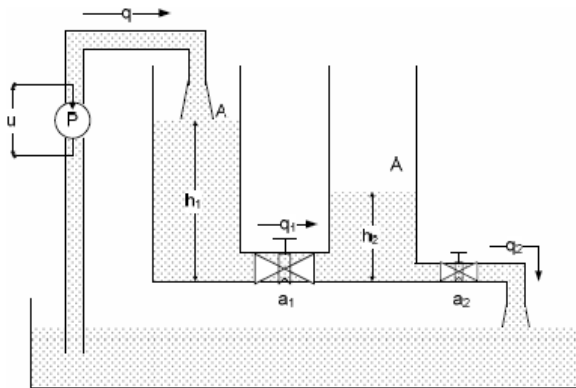


Figure 1. Schematic representation of a two-tank system

For the modeling of the process in this paper, the data obtained by experimental measurements were used, and with the fact that there is a completely non-linear model, which can faithfully reproduce the real system model, the Simulink-realization can be seen in the Figure 2 [4].

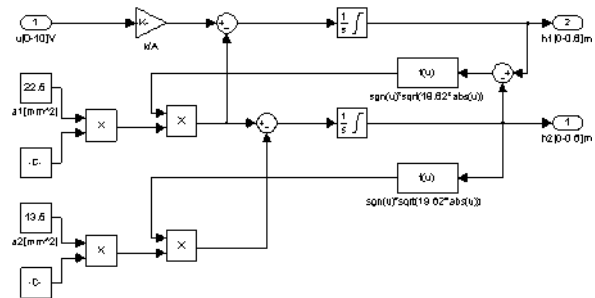


Figure 2. Simulink model of the two-tank system

2. NEURAL NETWORK

The main advantage of neural networks over classical computer algorithms lies in the fact that the network is trained, while for other algorithms it is necessary to know in advance which step should be taken in order to reach a solution. Of course, this advantage can sometimes be a disadvantage because not knowing how to arrive at a solution often makes it impossible to correct mistakes. In order to solve a problem, such as modeling a physical process in a classical way, it is necessary to study the physical process in detail, precisely measuring physical dimensions, taking into account nonlinearities and transport delays. On the other hand, if we use a neural network for modeling, all that is needed is a sufficiently representative set of data for training, and most often these are the inputs and outputs of the given system.

The backpropagation method solves the problem that can arise in multi-layer feedforward networks when we do not know the desired output values of the neurons located in the hidden layers. The basic idea is that the input signal propagates forward, from the input to the output layer, while the error signal propagates backward, from the output to the input layer, changing the weight coefficients of the network in turn.

In this work, the Levenberg-Marquardt backpropagation algorithm was used to train neural networks. This algorithm is a standard method for minimizing the mean square error criterion and is characterized by fast convergence and robustness [5].

For the case of modeling the nonlinear process that is present in the work, the multilayer perceptron can be interpreted as a NARX model

(Nonlinear AutoRegressive with exogenous input) as can be seen in the attached Figure 3 [4].

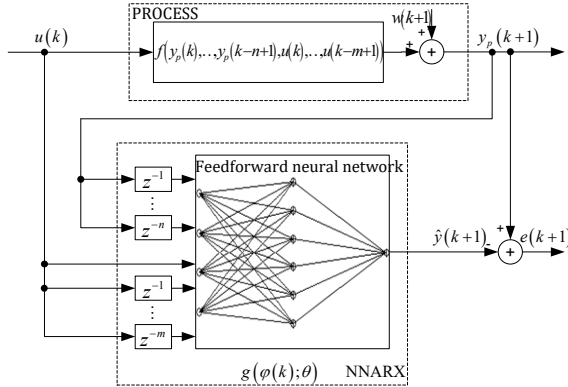


Figure 3. Process modeling using the neural NARX model

3. INTRODUCTION TO CONTROLLER DESIGN USING NEURAL NETWORKS - CONTROL WITH INTERNAL MODEL

In this paper, control with an internal model as a control structure is described and applied. Control with an internal model (IMC) is based on an inverse process model where control takes place in closed-loop. The control structure includes a feedback link based on the difference signal between the process and its model (Figure 4), which as a result compensates for external disturbances. In some cases, it is necessary to apply filtering in front of the inverse controller to smooth out sudden reference changes that can adversely affect the performance of the control structure.

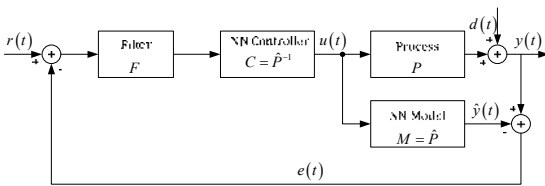


Figure 4. Control with an internal model

Inverse control is based on the application of the inverse process model, which is connected in series with the process, making a system with the instantaneous response of the only gain between the input to the inverse model and the output process. Therefore, the inverse process model, represented by a neural network, acts as a controller [6].

IMC can be applied exclusively to control processes that are stable in the open loop. However, IMC has several features that make it very convenient for industrial process control:

- if the process and the controller are stable and the process model is ideally trained, the closed system is also stable
- if there is an inverse process model, i.e. if it $f_C(\cdot; \theta_C) = f_M^{-1}(\cdot; \theta_M)$, which is used as a controller, the control is ideal and at every moment is $y(t) = r(t)$ regardless of the external disturbance [7]
- the synthesis of the control system is clear and simple

The above properties of IMC are correct under the assumption that the process model and the controller are ideally trained. However, in reality it is impossible to obtain an ideal process model, while an ideal control would require an infinite gain of the controller, so that problems with the stability of the structure would appear. For this reason, a filter is introduced into the control structure, which is designed to reduce the gain of the loop of the closed control circuit, thus increasing the robustness of the control system. A first-order filter is usually used. Figure 5 shows the IMC strategy using the NNARX modeling structure. In order to achieve disturbance compensation without static error, it is necessary for the controller to describe the inverse process model as well as possible. Therefore, training the controller should minimize the deviation between the input signal of the controller $r_F(k)$ and the output signal of the process model $\hat{y}(k)$.

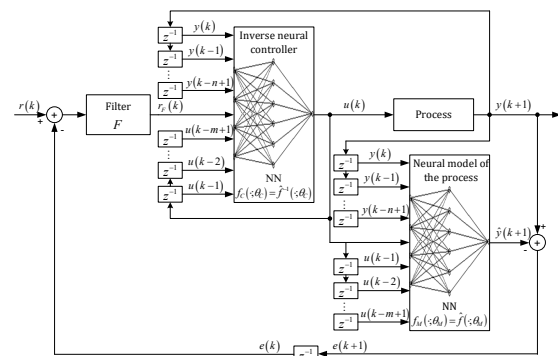


Figure 5. IMC using the NNARX structure

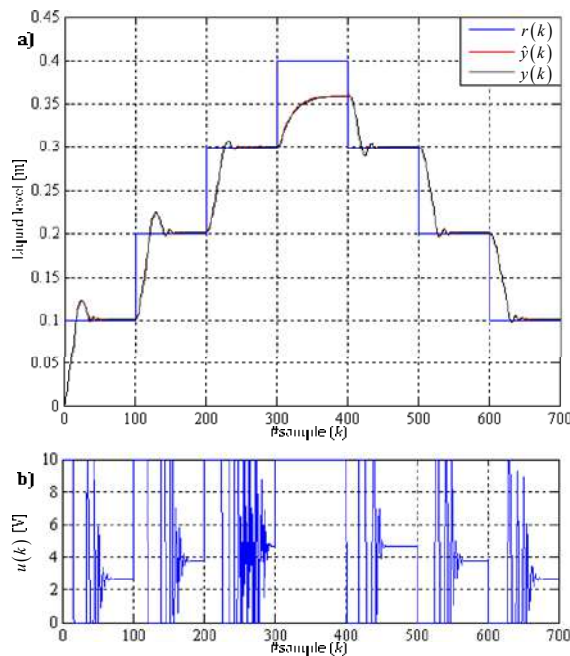


Figure 8. Control with the internal model of the system of two connected tanks when disturbance is included a) process and model response b) control signal

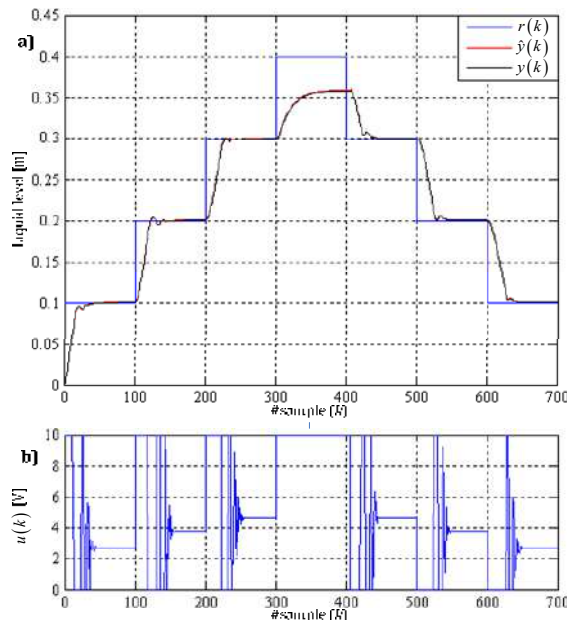


Figure 9. Control with the internal model of the system of two connected tanks with disturbance included and other filter parameters a) process and model response b) control signal

Figure 10 a) shows the behavior of the output signal under the action of disturbances in the control structure with an internal model. In the step $k = 151$, there a disturbance was at the output of the system by opening the valve from

13.5 mm² to 18.5 mm². It can be seen from the picture that the control with the internal model completely succeeds in suppressing the movement. The disturbance lasts until the moment $k = 301$ when the valve opening returns to the previous value.

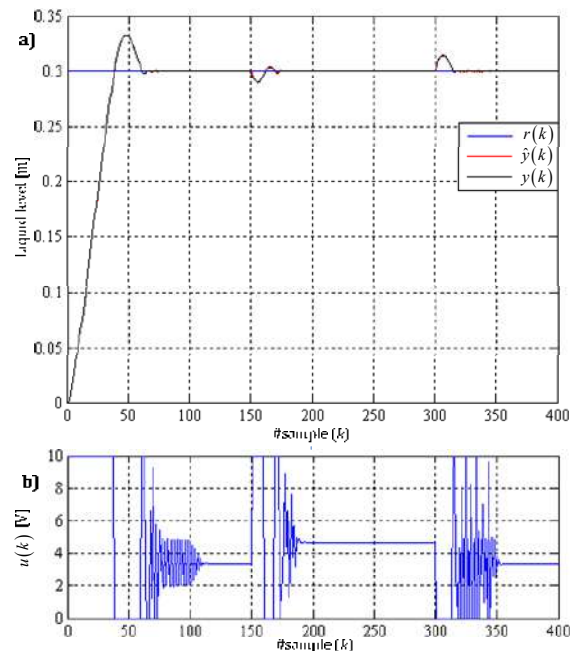


Figure 10. Behavior of the system of two connected tanks with internal model control under disturbance a) output signal of process and model b) control signal

5. CONCLUSION

The development of artificial neural networks has enabled many different structures of neural networks, which can basically be divided into static and dynamic. This paper describes the application of a static neural network in the identification and control of a nonlinear dynamic process. From the standpoint of application in process identification, its most important feature is the ability to approximate arbitrary continuous functions. Regarding the identification of the inverse process and the direct model of the process, the NARX neural network structure was used, which uses the outputs from the process itself as feedback. Therefore, these neural models are structurally stable and the numerical procedures for training network parameters are simpler than for recurrent networks.

A control structure with an internal model is applied within the framework of a real nonlinear mathematical model. By controlling with the

internal model, the disturbance was completely suppressed. By choosing the filter parameters, the gain of the loop of the closed control circuit is reduced, thereby increasing the robustness of the control system and obtaining a quieter control signal.

REFERENCES

- [1] Demuth, H.B., Beale, M.H., De Jess, O., Hagan, M.T., *Neural Network Design*. Martin Hagan, 2014.
- [2] Stepanic, P., Vidakovic, J., Devic, A., Ducic, N., Direct inverse control of two-tank system using neural networks. 38th International Conference on Production Engineering – Serbia, October 2021, Cacak, pp. 131-136.
- [3] Amira DTS200, Laboratory Setup Three-Tank-System, Amira GmbH, Duisburg, 1998.
- [4] MATLAB 2018a, The MathWorks, Inc., Natick, Massachusetts, United States, 2018.
- [5] Hagan, M.T., Menhaj, M., 1994., Training feedforward networks with the Marquardt algorithm, *IEEE Transactions on Neural Networks*, 5(6), pp. 989-993.
- [6] Hagan M.T., Demuth H., *Neural Networks for Control*. Invited Tutorial, American Control Conference. June, 1999, San Diego, pp. 1642-1656, 1999.
- [7] Leontaritis, I. J., Billings, S.A., Input-output parametric models for non-linear systems. Part I: deterministic non-linear systems. Part II: stochastic non-linear systems. *International Journal of Control* 41, pp. 303-344, 1985.



Banja Luka
1-2 Jun 2023.

DEMI 2023

16th International Conference on Accomplishments in Mechanical and Industrial Engineering

www.demi.mf.unibl.org



Synchronization of two non-synchronizable industrial robots

R. Jalić, B. Z. Knežević, D. Erceg

^aFaculty of Mechanical engineering, University of Banja Luka, Bulevar vojvode Stepe Stepanovica 71

Abstract *The main goal of this paper was to connect two controllers of the older generation into one robotic cell, then programmatically realize their synchronized work on servicing and welding certain objects. For this purpose, two controllers manufactured by Yaskawa Motoman were used with the associated manipulators. The hardware solution involved connecting the controllers via General I/O circuit board, where the output of one controller is connected to the input of another and vice versa. The software solution involved parallel programming of two robots for synchronized operation on a common task. During programming, it was necessary to create macro jobs that implemented repetitive actions, such as calling and waiting for robots, grabbing and releasing objects, as well as the actions of starting and stopping the program. For the operator's safety, the robotic cell was externally controlled and a safety light curtain was installed. The conclusion of presented research is that the robotic cell, formed by two robots that are not intended for synchronization, meets the requirements that until now could only be solved with robots of the newer generation. Proposed solution was confirmed by experimental verification.*

Keywords *Industrial robot, Welding robot, Handling robot, Macro Jobs, Safety*

1. INTRODUCTION

The rapid development of the industry and the distinguished demands of customers have led to working conditions in which man cannot meet the required precision and speed. Consequently, there was a need to introduce robots into all branches of industry. According to the ISO 8373:2021 standard, "an industrial robot is an automatically controlled, reprogrammable, multipurpose manipulator, programmable in three or more axes, which can be either fixed in place or fixed to a mobile platform for use in automation applications in an industrial environment" [1]. Such robots have brought many advantages in production processes, some of them are better precision and repeatability, work in dangerous conditions, higher speed, efficiency, etc. [2].

Depending on their function and purpose, industrial robots are divided into several

groups. Two important groups are robots for performing processes such as welding, painting, cutting, among which Welding Robots are of importance for this work, and a group of manipulation robots, i.e. robots for serving, packing and sorting, among which we single out Handling Robots. There are many robot manufacturers, and among the most prominent are Japan's Yaskawa and Fanuc, and Germany's Kuka. Together they make up between 60% and 80% of the total production in the world [3].

Considering that industrial robots are intended for very long-term work, companies still have a large number of robots of the older generation whose age reaches over 15 years. Such robots have significantly modest characteristics compared to robots of newer generations.

In order to use older generation robots in the automation of modern production processes, it is necessary that they work in harmony with other parts of the production system. Exactly

one such synchronization was performed in this work between two robots from the Yaskawa company. On one side is a welding robot consisting of a Motoman NX100 controller with a Motoman HP6 manipulator, while on the other side is a service robot consisting of a Motoman XRC controller with a Motoman UP6 manipulator.

2. EXPERIMENTAL SETUP

As already mentioned, the task is to synchronize the work of two robots of an older generation and thus form a robotic cell in which one robot serves another that welds certain parts. It is a combination of two controllers with manipulators. A Motoman NX100 controller with a Motoman HP 6 manipulator was used as a welding robot, while a Motoman XRC controller with a Motoman UP 6 manipulator was used as a service robot. The robot cell setup is shown in Fig. 1.



Fig. 1. Robotic cell with two robots in synchronization

In order to be able to fully understand the paper, the mentioned robotic cells are described below and their basic specifications are given.

2.1 Handling robot

The service robot consists of a controller, manipulator, Teaching Pendant, an external control and a safety light curtain.

The Motoman XRC controller used a RISC (Reduced Instruction Set Computer) processor, which provided it with much better performance compared to its Pentium-based predecessors. This controller, as well as the

NX100, has the ability to control up to 4 robots. Teaching Pendant with 5.7 inch display is used for programming. Connection is possible via the RS 232 protocol as well as via digital inputs and outputs. The programming language used for programming is Inform II [4].

The characteristics of the Motoman UP6 manipulator are shown in Fig. 2. The manipulator has 6 degrees of freedom and a maximum load of 6 kg. In Fig. 2. the maximum speeds for each of the axes are also shown.

Operation Mode		Vertically Articulated
Degree of Freedom		6
Payload		6kg
Repetitive Positioning Accuracy ²		±0.08mm
Motion Range	S-Axis (turning)	±170°
	L-Axis (lower arm)	+155°, -90°
	U-Axis (upper arm)	+190°, -170°
	R-Axis (wrist roll)	±180°
	B-Axis (wrist pitch/yaw)	+225°, -45°
	T-Axis (wrist twist)	±360°
Maximum Speed	S-Axis	2.44 rad/s, 140°/s
	L-Axis	2.79 rad/s, 160°/s
	U-Axis	2.97 rad/s, 170°/s
	R-Axis	5.85 rad/s, 335°/s
	B-Axis	5.85 rad/s, 335°/s
	T-Axis	8.73 rad/s, 500°/s
Allowable Moment ³	R-Axis	11.8N·m (1.2kgf·m)
	B-Axis	9.8N·m (1.0kgf·m)
	T-Axis	5.9N·m (0.6kgf·m)
Allowable Inertia (GD ² /4)	R-Axis	0.24kg·m ²
	B-Axis	0.17kg·m ²
	T-Axis	0.06kg·m ²
Mass		130kg
Ambient Conditions	Temperature	0° to 45C°
	Humidity	20 to 80% RH (non-condensing)
	Vibration	Less than 0.5G
	Others	<ul style="list-style-type: none"> • Free from corrosive gasses or liquids, or explosive gasses • Clean and dry • Free from excessive electrical noise (plasma)
Power Capacity		1.5kVA

Fig. 2. Basic characteristics of the Motoman UP6 manipulator [5]

More about external control and the safety light curtain will be discussed in the section that describes security.

2.2 Welding robot

The robotic welding cell consists of a Controller NX100, a Motoman HP6 manipulator and a Teaching pendant. In addition, complete welding equipment is necessary, but since it is not the subject of this work, it will not be discussed further.

The NX100 controller with the associated touch-sensitive Teaching pendant represented a real revolution at the time when its production began. The programming language Inform III is used for programming. Fast data processing, a large memory that supports up to 60,000 steps, the ability to control multiple robots (maximum of 4 robots and 36 axes, including robotic and external axes), and high path precision are some of the advantages of this controller. What particularly characterizes this controller is its ability to connect via Ethernet and RS 232 protocol, as well as a large number of digital inputs and outputs [6].

The characteristics of the Motoman HP 6 manipulator are given in Fig. 3. where you can see that it has 6 degrees of freedom of movement, and you can see the maximum range and speed in all 6 axes and other important characteristics. The maximum load that the manipulator can carry is 6 kg.

Operation Mode		Vertically Articulated
Degree of Freedom		6
Payload		6kg
Repetitive Positioning Accuracy ²		±0.08mm
Motion Range	S-Axis (turning)	±170°
	L-Axis (lower arm)	+155°, -90°
	U-Axis (upper arm)	+250°, -175°
	R-Axis (wrist roll)	±180°
	B-Axis (wrist pitch/yaw)	+225°, -45°
	T-Axis (wrist twist)	±360°
Maximum Speed	S-Axis	2.62 rad/s, 150°/s
	L-Axis	2.79 rad/s, 160°/s
	U-Axis	2.97 rad/s, 170°/s
	R-Axis	5.93 rad/s, 340°/s
	B-Axis	5.93 rad/s, 340°/s
	T-Axis	9.08 rad/s, 520°/s
Allowable Moment ³	R-Axis	11.8N·m (1.2kgf·m)
	B-Axis	9.8N·m (1.0kgf·m)
	T-Axis	5.9N·m (0.6kgf·m)
Allowable Inertia (GD ² /4)	R-Axis	0.24kg·m ²
	B-Axis	0.17kg·m ²
	T-Axis	0.06kg·m ²
Mass		130kg
Ambient Conditions	Temperature	0° to 45°C
	Humidity	20 to 80% RH (no-condensing)
	Vibration	Less than 4.9m/s ² (0.5G)
	Others	<ul style="list-style-type: none"> • Free from corrosive gas or liquid, or explosive gas • Free from dust, soot, or water • Free from excessive electrical noise (plasma)
Power Capacity		1.5kVA

Fig. 3. Basic characteristics of the Motoman HP 6 manipulator [7]

3. PROPOSED HARDWER CONFIGURATION FOR SYNCHRONIZATION

The previously described robots need to be connected so that the functions of object manipulation and welding in sync. It is stated that both the XRC controller and the NX100 controller have the ability to control multiple manipulators (maximum 4). At first, this problem seems easily solvable, but the problem is actually much more difficult.

The fact is that many companies in countries in transition have started with partial automation of production facilities in accordance with their possibilities. The consequence of the above is that no consideration was given to the later connection of individual parts of the production plant, and robots were purchased according to the current needs and possibilities. This has led to the situation that companies have several robots that are of different generations and different manufacturers and that are not compatible for connecting to one common controller.

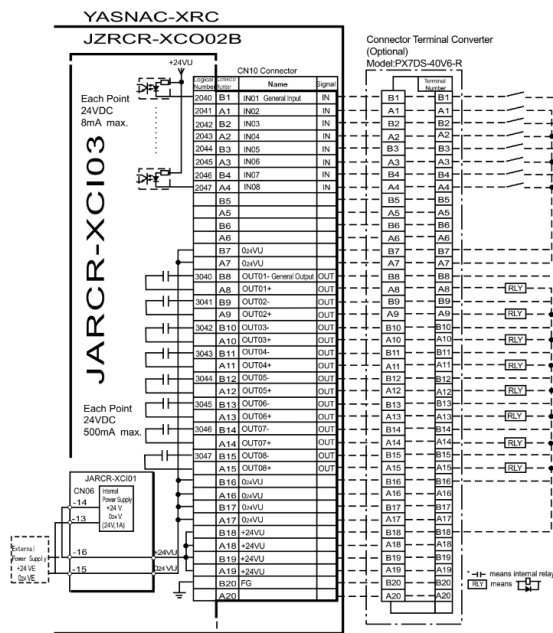
Now that companies want to raise the level of automation, it is necessary to overcome the problem of incompatibility. In order to solve the problem, it is necessary to design a universal way of communication between the controllers. An attempt was made to overcome the problem using Offline programming, but since the XRC as well as newer NX100 controller does not supports this type of programming, it was necessary to find a more universal solution.

Starting from the assumption that robots should communicate like humans, the solution to the problem presented in this paper is that controllers can communicate via digital inputs and outputs according to the Master-slave principle, where one controller will be the master and the other is subordinate to it (slave) - who will execute the received orders [8].

Considering that the Handling robot is the one intended for automation in the company, it was chosen as the Master controller. For communication with the Slave robot (Welding robot), digital inputs and outputs are used. Another type of communication and connection is not possible, for example via communication interfaces, because they are also incompatible.

The XRC and NX100 controllers have many digital inputs and outputs. For this communication, on the XRC controller, the General I/O circuit board - connector CN10 (Fig.

4.) was used. A bus is derived from this connector and components that communicate through digital signals are connected to it. Some of these inputs and outputs have already been used for various functions such as start, stop and light sensor curtain buttons, then for communication with the gripper and safety elements, etc. For communication with the NX100 controller, output A14 (#OT7 in the program) and input A2 (#IN4) were used. Also, in order for the system to function, it is necessary to equalize the reference potentials, and for this purpose connector B7 was used (Fig. 5.).



(Fig. 8). With this, the hardware part of the problem has been solved and we are moving on to the software realization of the problem.

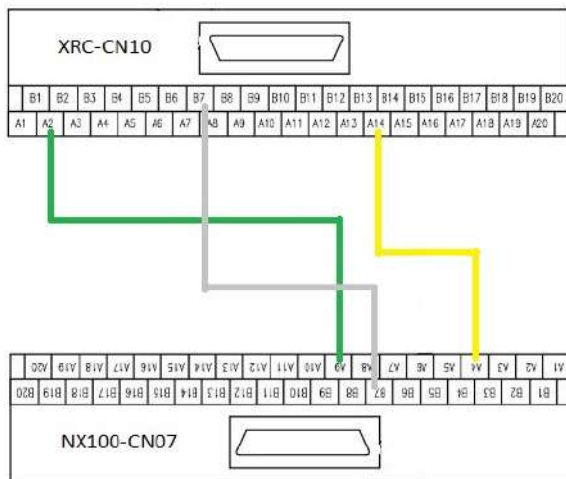


Fig. 8. Controller connection scheme

4. PROPOSED SOFTWARE IMPLEMENTATION

After the hardware connection, it is necessary to program the robots to work on a common task. The Master robot takes the lead and at some moments he calls the Slave robot and instructs him to perform his part of the task. After completing that task, it returns information to the Master robot, which calls it again when necessary. This kind of programming would lead to very complicated programs because, depending on the complexity of the task, these programs would be long, with a large number of repeated instructions. In addition, there are also difficulties such as the increased possibility of errors, difficulties when eliminating them, and more difficult creation and understanding of programs by the operator.

In order to avoid all the listed problems during programming, Macro jobs were created. They bring simplicity of programming, transparency of the program and easier debugging [11]. Programming and editing of Macro jobs is possible only when the controller is in

Management mode. The name of the Macro program can be entered among the instructions in the Inform list, and this is also done in Management mode. This solves the availability of Macro jobs during programming.

In order to solve the problem concerning the topic of this paper, a total of 6 new original Macro jobs were created on the Master robot, and they are: CALL_R2, WAIT_R2, CATCH, RELEASE, START, STOP (Fig. 9).

For easier programming and marking, in the following text, the Master robot will be marked with R1, while the Slave robot will be marked with R2.

The first Macro job, CALL_R2, (Fig. 9. a), represents the initial part of the protocol between robots, where the Master robot calls the Slave robot to perform its part of the task. The proposed initial part of the protocol is defined as a pulse signal with an amplitude of 24 VDC and a duration of 0.1 seconds.

In Fig. 9. b) the Macro job named WAIT_R2 is shown, which realizes the function of waiting for a signal from the Slave robot. Program execution does not continue until the Slave robot sends a signal to the Master.

These two Macro jobs were also created on the Slave robot, only their names are CALL_R1 and WAIT_R1. Depending on the requirements, the program developer can implement three modes of operation:

- The master robot executes part of the program while Macro job WAIT_R1 is activated on the slave robot.
- The slave robot executes part of the program while Macro job WAIT_R2 is activated on the Master robot
- Both robots execute parts of the program, with the robot that finishes its task first, activates Macro job WAIT.

Macro jobs CATCH and RELEASE shown in Fig. 9. c) and d) refer to the operation of the gripper. CATCH Macro job realizes the function of catching an object by sending a impulse

JOB	EDIT	DISPLAY	UTILITY
JOB CONTENT : MASTER	R1		
J: CALL_R2 S:000 R1			TOOL:*
0000 NOP			
0001 PULSE OT#(7) T=0.10			
0002 END			

a)

JOB	EDIT	DISPLAY	UTILITY
JOB CONTENT : MASTER	R1		
J: WAIT_R2 S:000 R1			TOOL:*
0000 NOP			
0001 WAIT IN#(4)=ON			
0002 END			

b)

JOB	EDIT	DISPLAY	UTILITY
JOB CONTENT : MASTER	R1		
J: CATCH S:000 R1			TOOL:*
0000 NOP			
0001 PULSE OT#(5) T=1.61			
0002 TIMER T=1.65			
0003 END			

c)

JOB	EDIT	DISPLAY	UTILITY
JOB CONTENT : MASTER	R1		
J: RELEASE S:000 R1			TOOL:*
0000 NOP			
0001 PULSE OT#(6) T=1.56			
0002 TIMER T=1.65			
0003 END			

d)

JOB	EDIT	DISPLAY	UTILITY
JOB CONTENT : MASTER	R1		
J: START S:000 R1			TOOL:*
0000 NOP			
0001 WAIT IN#(1)=ON			
0002 END			

e)

JOB	EDIT	DISPLAY	UTILITY
JOB CONTENT : MASTER	R1		
J: STOP S:000 R1			TOOL:*
0000 NOP			
0001 WAIT IN#(5)=ON			
0002 END			

f)

Fig. 9. Macro jobs that were created for the proposed solution

signal to the gripper motor. If it is necessary to define the gripping time for the operation of the gripper, it is possible to introduce a timer in the instruction that will ensure that the duration of the signal is within a certain time interval. Also, in this case, it is necessary to introduce an additional timer, which will prevent further execution of the program and thus ensure a safe grip. Macro job RELEASE realizes the function of releasing objects, by sending a reverse polarity signal to the gripper motor, which is realized using a built-in relay.

Macro jobs START and STOP (Fig. 9. e) and f)) are used when starting and stopping the program, and are implemented using the wait function. Since the buttons are placed on the external control, at the beginning of each program it is necessary to use START to start the program execution. When the start button is pressed, the controller receives a signal at input A1, and thus the Macro job START is executed.

An example of calling Macro jobs is shown in Fig. 10. where the initial part of the program, which realizes the function of bringing and welding items, is separated. Calling Macro jobs is very simple, because they can be added among the standard instructions in the Inform List.

JOB	EDIT	DISPLAY	UTILITY
JOB CONTENT : MASTER	R1		
J: PROGRAM S:000 R1			TOOL:*
0000 NOP			
0001 SET B000 0			
0002 #AGAIN			
0003 START			
0004 MOVJ VJ=50.00			
0005 CALL_R2			
0006 WAIT R2			

Fig. 10. An example of calling a Macro job in a program

5. THE CELL SAFETY

When automating the production facility, great attention must be paid to the safety of the participants in the production process. When we say participants, we primarily mean people who are either participants in the production process or just passing by. In addition, manipulators are also considered, so that collisions and damage do not occur, considering that these are very expensive machines.

When it comes to robots, they are specific because their working space exceeds their own dimensions, unlike other machines, and it is necessary to secure a much wider space. In Fig. 11. it can be seen that the robot, in addition to its working space, can also occupy a wider area when returning to the parking position, when switching from one program to another, and

when approaching certain positions. This space is called the manipulation space of the robot [12].

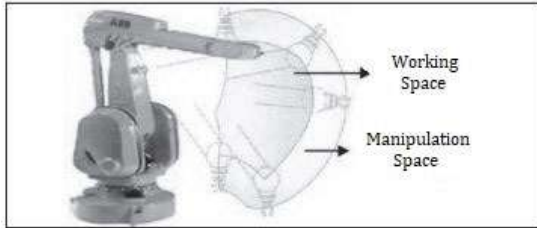


Fig. 11. Working and manipulation area of the robot [12]

In order to protect people in production processes, robots are placed in so-called cages that have one entrance where light sensor curtains are placed (Fig. 12). The program can only be started if the door is closed.

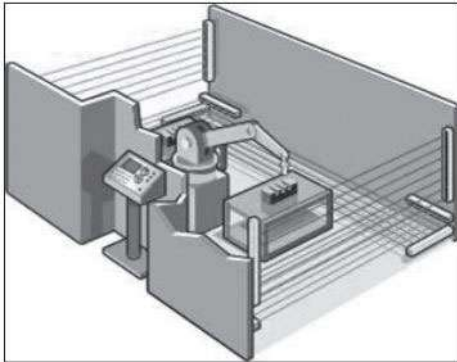


Fig. 12. An example of an enclosed robot workspace [12]

The light sensor curtain represents an important segment for the safety of people when working with robotic cells. It is placed at the entrance to the cage and when detecting an object between the photo sensors, it has the function of a necessary stop button. In addition to the curtain, an important part of safety is the external control, which is located outside the cage and consists of three buttons with light indication (start, stop and light sensor curtain reactivation button). The start button is used to start a programmed work cycle that repeats continuously when everything is ready and when the cage door is closed.

In case of activating the Stop button, the current cycle will end and a new one will not start.

In addition to the mentioned buttons, an emergency stop mushroom button is also implemented for external control. Pressing this

button ensures an immediate stop of both robots, as in the case of activating the safety light curtain.

Fig. 13 shows the external control and safety light curtain, which is functionally connected but not mounted.



Fig. 12. External control and safety light curtain

6. OPERATION AND VALIDATION

To verify the proposed solutions, a program was created by which the Handling robot places the parts on the work table, and the Welding robot welds them. For these needs, the parts that the robots manipulate were modeled and manufactured (Fig. 13.).

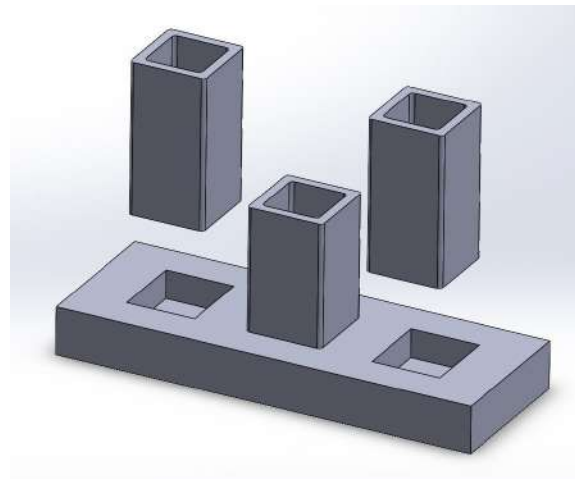


Fig. 13. Models created to validate proposed solutions

During programming, a parallel approach was used where both robots were programmed at the same time. In Fig. 14. a diagram of the

operation of the robot is shown, and based on this diagram, the mode of operation will be explained. Points marked with numbers 1 to 11 represent places where robots communicate with each other.

In point 1, the program starts by pressing the Start button located on the external control, and this is implemented programmatically using the Macro job START.

Then R1 goes to the parking position and after that, using the Macro job CALL_R2 (point 2), it sends a signal to another robot that should also position itself in the parking place. While R1 is being positioned, macro job WAIT_R1 is active on R2 and vice versa.

At point 3, R2 sends a signal to robot R1 that it is ready and then R1 starts working. First, he brings the base item and places it in position on the workstation, and then brings an additional part that is welded to the base part.

At point 4, R1 signals that R2 can start welding by calling the Macro job CALL_R2.

During this time, R1 goes to get the second part and since this operation is shorter than the welding operation, he calls the Macro job WAIT_R2 in a safe position, so that the two manipulators do not collide (point 5).

Point 6 marks the moment when robot R2 finishes welding, and from a safe point sends a signal to robot R1 that it can place the second part as well.

After placing the second part, R1 sends a signal to the robot R2 that it can start welding (Point 7).

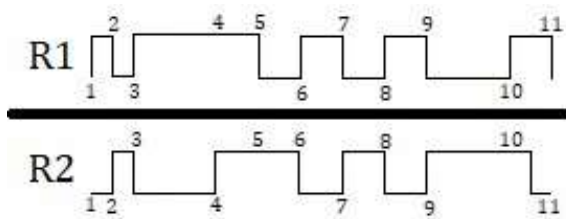


Fig. 14. Comparative diagram of two robots working in synchronization

When he finishes welding the closer sides (point 8), robot R1 rotates the assembly by 180° around the Z-axis, so that R2 can proceed to welding the remaining sides of the objects that were previously inaccessible (point 9).

At point 10, robot R2 has finished welding and sends a signal to robot R1. Then he goes to the

parking position, while robot R1 takes the welded assembly from the workstation.

In point 11, the JUMP function is used, which returns the program to the beginning. The idea is to bring the objects into the grasping position using batch loading so that the Handling robot always picks up one type of object from the same position.

When welding the created assembly, considering that it is a quadrangular model, three sides were welded on each of them, in accordance with the defined welding technology (Fig. 15.).

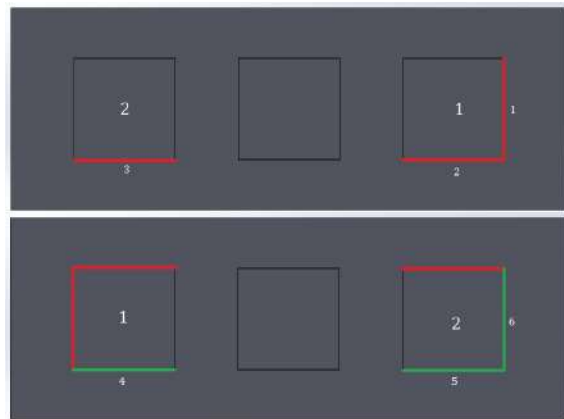


Fig. 15. Welding sequence

In the first position, the sides marked in red are welded in numbered order. Sides 1 and 2 are welded in part 4-6 of the diagram in Fig. 14., while side 3 is welded in part of diagram 7-8. After rotating the assembly along the z-axis, sides 4, 5 and 6 are welded, which is the period between points 9 and 10 on the diagram.

7. CONCLUSION

The solution proposed in the paper realizes the synchronization of two older generation robots that do not have a built-in synchronous operation option. In the research, a joint cell was realized that works in harmony on the manipulation and welding of certain parts. The robots are connected in a Master-Slave relationship. The robot attendant is also the Master robot in the Master-Slave control system, while the welder robot is in the role of Slave.

The connection is made using digital inputs and outputs where the robots communicate with each other using low voltage impulse signals.

For the successful implementation of synchronous programming, it is suggested to use Macro jobs, which define the methods of communication between robots. One Macro job is called when a robot sends a pulse signal to another robot, while another Macro job is used when the robot is waiting for a signal from another robot. In addition to these, Macro jobs were created for the start and stop functions, as well as for gripper management.

Protection of people, participants in the production process, is also one of the topics of this paper. For this purpose, a plan of protection measures was created during the installation of the robot. The conclusion is that the robots must be in a cage with one entrance provided by a safety light curtain, and that the control of the robots during their operation can only be done through external control, which is equipped with buttons for start, stop and reactivation of the safety light curtain, as well as a button for emergency stop.

That this type of system can effectively respond to various tasks was shown on the example of welding an assembly consisting of three parts. Synchronization of the work of several robots is inherent only to controllers of the newer generation, which, with their performance in the form of connecting and managing a large number of manipulators, ensure easy programming and solving complex problems. The robots described in this paper are not compatible with other controllers, they do not have the possibility of offline programming, while the XRC controller does not even have an Ethernet connector. With the proposed solution, problem of using robots of the older generation during company automation has been conceptually and practically solved. By connecting and programming the robot in the manner previously described, it is possible to achieve identical goals as with newer controllers. It is only necessary, depending on the manufacturer and purpose of the robot, to determine free and appropriate digital inputs and outputs, physically connect them, create Macro jobs and program the robots to work on a specific example.

Acknowledgement

The realization of presented research was supported by the company ELAS Metalexpert Banja Luka, and we hereby thank them.

REFERENCES

- [1] ISO 8373:2021. (2021). *Industrial robot – Part 3.6: Automatically controlled, reprogrammable multipurpose manipulator, programmable in three or more axes, which can be either fixed in place or fixed to a mobile platform for use in automation applications in an industrial environment*. International Organization for Standardization. Geneva.
- [2] Al Mamun, A., Buics, L. Automated assistance in hazardous manufacturing processes to improve productivity and reduce workers bodily risks: a literature review. *Proceeding of Int. May Conference on Strategic Management IMCSM 2022*, May 2022, Bor, p. 193 - 209.
- [3] Zhang, Z., Zeng, J. (2022). A Review on Development and Application of Industrial Robot. *Academic Journal of Science and Technology*, vol. 2, no. 2, p. 78-81
- [4] Motoman XRC Controller, From: https://www.motoman.com/getmedia/6e284da6-f2d1-453d-8fc9-2644bd4e101b/xrc_controller.pdf.aspx, accessed on: April 11, 2023.
- [5] Yaskawa Motoman (2001). Motoman UP6 Manipulator Manual, From: <https://www.manualslib.com/manual/2013782/Yaskawa-Motoman-Up6.html#manual>, accessed on: April 10, 2023.
- [6] NX100 Controller, From: https://www.motoman.com/getmedia/a9c00d32-73c1-423d-ad4c-064081b1f39f/NX100_Controller.pdf.aspx, accessed on: April 11, 2023.
- [7] Motoman HP 6, From: <https://www.yaskawa.fr/yaskawa.fr/Robots%20d%27occasion/Brochures/Technical%20Instructions%20HP6.pdf>, accessed on: April 11, 2023.
- [8] Chen, H., Ma, H., Jiang, H., Lv, S., Li, Y., Liu, H. (2022). The Influence of Control Parameters on Precision of Welding Seam Tracking in Manually Control Master-slave Robot Remote Welding System. *Journal of Physics*, Conference series 2218, p. 1-6. DOI:10.1088/1742-6596/2218/1/012045
- [9] Yaskawa Motoman (2001) XRC Instruction Manual, From:

<https://icdn.tradew.com/file/201606/1569362/pdf/7055804.pdf>, accessed on: April 11, 2023.

- [10] NX100 Controller Manual, From: <https://dokumen.tips/documents/nx100-controller-manual.html?page=107>, accessed on: April 12, 2023.
- [11] Hao Tan, A., Pizarro Bejarano, F. Nejat, G. Zhu, Y. Ren, R. (2023) Deep Reinforcement Learning for Decentralized Multi-Robot Exploration with Macro Actions, *IEEE Robotics and Automation Letters*, vol. 8, no. 1, p. 272-279
- [12] Lipnjak, G. (2020). Robotika u funkciji zaštite zdravlja na radu, *Sigurnost*, p. 115-126.



Banja Luka
1-2 Jun 2023.

DEMI 2023
**16th International Conference on
Accomplishments in Mechanical and
Industrial Engineering**
www.demi.mf.unibl.org



Synthesis of the control unit of the desktop robot arm actuated by stepper motors

A. Dević^a, J. Vidaković^a, N. Živković^a, M. Lazarević^b

^aLola institute, Kneza Visaslava 70a, 11030 Belgrade, Serbia

^bFaculty of Mechanical Engineering, The University of Belgrade, Kraljice Marije 16, 11120 Belgrade

Abstract

Small-size (desktop) robot arms are being increasingly used in research and education, where low-cost implementation prevails over the need for high dynamic performance. This paper presents a design of a control unit for a 6DoF desktop robot arm with cylindrical joints actuated with stepper motors. Feedforward control, often chosen as a control strategy for stepper motors due to the simplicity of control algorithms, as well as the cost-effectiveness of the solution, is selected as the control method. The applicative software with GUI developed in Matlab is presented. A trajectory planner based on the solution of the inverse kinematics problem and the user-selected joint velocity profile is implemented. In order to avoid step skipping occurrence, the torque in joints necessary to produce the programmed joints motion have to be achievable by the installed stepper motors. As a part of applicative software, the check on the feasibility of the programmed robot trajectories by numerical simulation of solution of inverse dynamics problem in Simscape Multibody is performed. The microcontroller is used as an interface device that controls the stepper motor drivers. The applicative software communicates with the microcontroller using the TCP protocol.

Keywords Robot arm, control, stepper motors

1. INTRODUCTION

In recent technology trends, robot development has attracted more interest due to the introduction of Industry 4.0 which has highlighted automation and robotics as part of the potential fields for raising the quality of production, automotive and human service industries [1]. Robot arms are used for many industrial applications, such as handling, painting, assembling, welding etc. [2]. Due to mentioned trends in robot development, there is a demand on the market for small-size

(desktop) robots in research and education, etc. where low-cost implementation prevails over the need for high dynamic performance [3-4].

One of the main components in developing a robot arm includes control unit design. In robotics, stepper motors are used as actuators often for low or predictable force/torque requirements, and have proven to be an excellent choice for low-cost and small-size robot manipulators due to the ease of controlling their position without feedback [3]. In this paper, the design of a control unit for a 6DoF desktop robot arm actuated with stepper motors is presented. Feedforward control is selected as a control method as a simple and cost-effective control solution. To achieve successful trajectory tracking by feedforward control, the step skipping occurrence has to be prevented throughout the robot operation. This

Corresponding author

PhD student, Andrija Dević
Andrija.devic@li.rs

Lola institute
Kneza Visaslava 70a
Belgrade, Serbia

implies that the torques in joints necessary to produce the desired joint motion have to be achievable by the installed motors during entire robot operation, i.e. robot must operate under strictly controlled conditions. Herein, this is achieved by verification of given robot trajectories based on the implemented robot dynamic model. The applicative software with GUI developed in Matlab is presented. The application examines the feasibility of the programmed robot trajectories by numerically simulating the solution of the inverse dynamic problem in Simscape Multibody. A microcontroller is used as an interface device and it communicates with the application software via TCP protocol.

This paper is organised as follows. In Section 2, a description of the main features of the 6DoF robot arm is given in short. 3. In Section 3, the control system design for desktop robot actuated by stepper motors is presented, with special emphasis on 1) the designed applicative software with GUI, 2) the implementation of the solution of robot inverse dynamics problem, and 3) microcontroller interface implementation. Concluding remarks are given in Section 4.

2. FEATURES OF 6DOF DESKTOP ROBOT ARM

Development of the robot design starts with a computer-aided design (CAD) model, and simulation of the system motion. The development of the kinematic and dynamic model follows, and is completed by designing a control unit for the robot [5].

At the very beginning of the design of the 6DoF low-cost desktop robot arm with cylindrical joints, it was necessary to adopt the kinematic structure so that the obtained inverse kinematics equations are as simple as possible, as well as to enable construction with relatively simple production of the parts. The design of the 3D model of the mechanical structure is performed in SolidWorks. Stepper motors [6] are selected due to the cost-effectiveness and simplicity of the control unit development. Toothed belts were used herein as a low-cost and simple solution to transmit power from the stepper motor to the joints.

The segments of the robotic arm are made using additive manufacturing which enables relatively simple and cheap production. PET-G plastics

that has an enviable load resistance/price ratio is used to fabricate the robot arm on the 3D printer. The robot mass is 3.9kg, while the maximum payload is 1kg.

In Fig.1, the constructed 6DoF desktop robot arm named AD100 is presented.

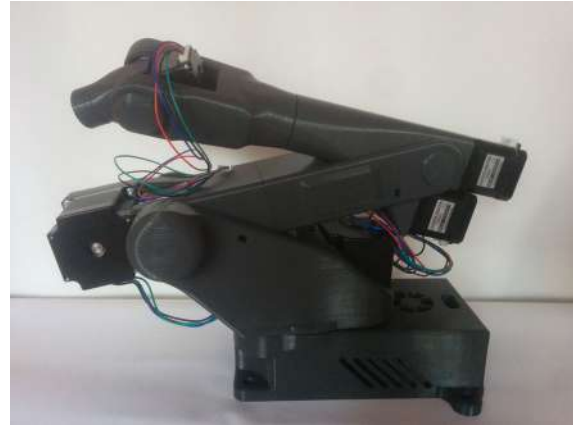


Fig. 1. 6DoF desktop robot arm AD100 [7].

3. CONTROL SYSTEM DESIGN FOR DESKTOP ROBOT ACTUATED BY STEPPER MOTORS

Within the development of the control unit, the basic guidelines were the simplicity of development, reliability of the control unit, and cost-effectiveness. In Fig.2, the block diagram of the control unit of the robot arm with six degrees of freedom and cylindrical joints actuated by stepper motors is shown.

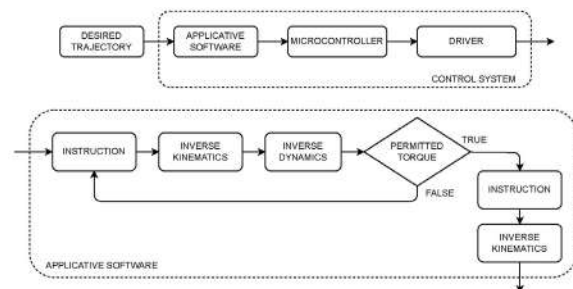


Fig. 2 The block diagram of the control unit of the 6DoF robot arm AD100

The applicative software with GUI is developed in Matlab. Programming of the robot is made possible by setting the desired robot trajectory via the internal and/or external coordinates. Programming of the desktop robotic arm is done in offline mode. 3D visualisation of robot motion for the purpose of verifying the given

programs is implemented. A separate trajectory planner was developed. Torques required to be produced by motors necessary to achieve the desired robot motion are obtained by numerical solution of robot inverse dynamics problem in Simscape Multibody [8]. TCP standard is used for communication between the Matlab GUI application software and the microcontroller that drives the stepper motors.

3.1 Development of Matlab GUI

The applicative software with GUI (Fig. 3) designed in Matlab can be run on Windows, Mac, and Linux operating systems. In this study, the software package RoboDK [9] was used for users to generate robot path programs by offline programming methods, and also to produce the robot path for visualisation purposes.

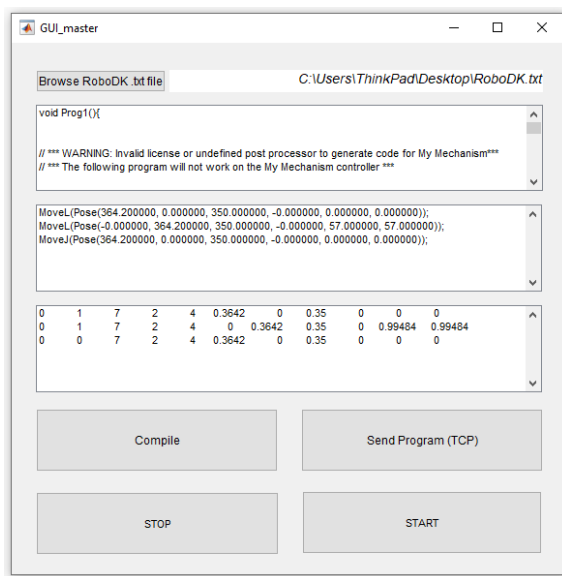


Fig. 3. Matlab GUI

A separate trajectory planner was developed for generating trajectories with an implemented solution of the inverse kinematics problem. Joint robot trajectories (path, velocity, acceleration) are created based on input/output position and/or orientation data, input user choice for generation of the joint velocity profile-linear, trapezoidal, or polynomial, and other parameters. Successive joint positions sent to the microcontroller are obtained by interpolation with an interpolation period of 50 ms. That period of time has been practically

proven to be adequate. Clicking the Compile button starts the part of the application that calculates the desired motors moments for input joint trajectories, which is performed by the simulation diagram in Matlab Simulink. After verifying the feasibility of the programmed trajectory based on the possibilities of installed motors, a Matlab script is executed, which creates packets of information that are prepared to be sent to the microcontroller.

In order to perform the desired movement of the robot, by pressing the Send Program (TCP) button, the application sends previously formed information packets to the microcontroller using the TCP protocol, and finally, by pressing the Start button, the microcontroller actuates the motors and executes the movement of the robot according to the trajectory set by the program.

3.2 Implementation of solution of robot inverse dynamics problem

In order for the stepper motors to be able to achieve the programmed positions and to avoid “skipping steps” (ie. to maintain synchronization) throughout robot operation, it was necessary to examine whether the required motor torques exceed their capabilities for the obtained joints’ motions throughout desired robot operations. A robot dynamic model is time variable, highly non-linear and characterized by coupling effects among the robot joints [10]. The solution of the robot inverse dynamic problem, ie. the calculation of the required robot actuators’ torques/forces from a specification of the robot’s trajectory can be obtained analytically, or by using ready-made modeler/simulator software solutions based on 3D software robot models. The latter avoids solving complicated mathematical expressions [10].

Here, torques required to be produced by motors necessary to achieve the desired robot motion are obtained by numerical solution of robot inverse dynamics problem in Simscape Multibody. The robot model is imported from SolidWorks. In SolidWorks, by selecting the Simscape Multibody Link option from the Tools drop-down menu, a file with the extension .hml is created, which contains all the necessary parameters for creating a dynamic model in Simscape, mass, inertia, center of mass, for each

part of the assembly separately, as well as the type of joints by which they are connected. The simulation model for 6DoF robot AD100 in Simscape Multibody is created and presented in Fig. 4.

The torque/speed curve is obtained from motor manufacturer documentation [6], and is used for comparison of maximum permissible load torque without the motor losing the step.

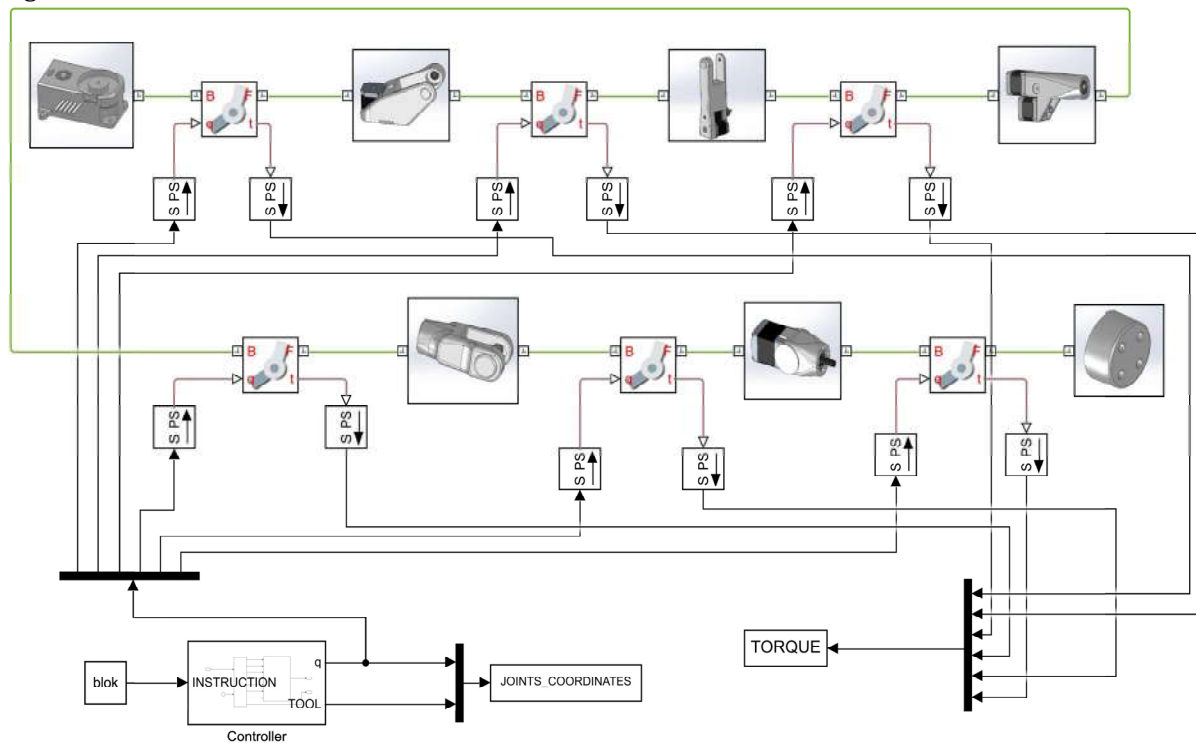


Fig. 4. Simulation diagram for the solution of inverse dynamics problem in Simulink Simscape Multibody

3.3 Microcontroller interface implementation

The application software communicates with the microcontroller using the TCP protocol. The microcontroller program is written in the mikroC compiler. Microchip PIC32MX534F064H, 32-bit microcontroller [11], controls the motors using a driver-type DRV8825 [12]. Via the SPI bus, the microcontroller communicates with the ENC28J60 gateway [13], which enables communication via ethernet with the application software. The electrical schematic contains six more A3144 [14] hall sensors for detecting the end positions of the robot's joints. Initial loading (before moving robot) of all packages into the memory of the microcontroller ensures real-time movement control, i.e. avoids traffic jams in communication. The duration of execution of one package is 50ms. An algorithm has been

implemented that calculates the moments of time according to the data from the package. Those moments of time are the moments in which it is necessary to change the state of the pins on the microcontroller, for all six motors. The core of the algorithm runs in an interrupt routine that allows the robot to move in real time. Based on this algorithm, the distribution of the signal pulses sent to the motor drivers is determined.

4. CONCLUSION

In this paper, the design of a control unit for a 6DoF desktop robot arm with cylindrical joints actuated with stepper motors is presented. Feedforward control is selected as the control method for stepper motors due to the simplicity of control algorithms and cost-effectiveness. The applicative software with GUI developed in Matlab is presented. A trajectory planner based on the solution of the inverse kinematics problem and user-selected joint velocity profile

is implemented. In order to feedforward control to be able to achieve successful trajectory tracking, the check on the torque in joints necessary to produce the desired joints motion is performed by comparison to maximum achievable moments by the installed motors for the desired motor velocity. This check is implemented as a part of applicative software by numerical simulation of solution of inverse dynamics problem in Simscape Multibody based on SolidWorks 3D robot model. A microcontroller is used as a cost-effective interface device, and the application software communicates with the microcontroller using the TCP protocol. It can be concluded that the basic guidelines appointed on the development of the control unit, namely the simplicity of development, reliability of the control unit, and cost-effectiveness have been successfully followed.

Acknowledgement

This research has been supported by the research grants of the Serbian Ministry of Science, Technological Development and Innovations, grant No. 451-03-68/2023-14/200066 and 451-03-47/2023-01/ 200105 from 03.02.2023.

REFERENCES

- [1] Zainudin, W. M. L. W., Shauri, R. L. A., Roslan, M. I., Rosli, M. A., & Ariffin, M. F. M. New Interface using Beaglebone Black for 4-DOF Robot Arm System. *IEEE Symposium on Industrial Electronics & Applications (ISIEA)*, July 2020, pp 1-6. DOI: [10.1109/ISIEA49364.2020.9188079](https://doi.org/10.1109/ISIEA49364.2020.9188079)
- [2] Vidaković, J. Z., Kvrđić, V. M., Lazarević, M. P., Dimić, Z. Z., & Mitrović, S. M. (2017). Procedure for definition of end-effector orientation in planar surfaces robot applications. *Tehnika*. DOI: [10.5937/tehnika1706845V](https://doi.org/10.5937/tehnika1706845V)
- [3] Siciliano, B., Sciacivco, L., Villani, L., & Oriolo, G. (2009). *Robotics: Modelling, Planning and Control*. Springer, pp 191-231
- [4] Sobaszek, Ł., Gola, A., & Varga, J. (2016). Virtual designing of robotic workstations. *Applied Mechanics and Materials*, vol. 844, pp 31-37. DOI: [10.4028/www.scientific.net/AMM.844.31](https://doi.org/10.4028/www.scientific.net/AMM.844.31)
- [5] Dede, M. I. C., & Tosunoglu, S. (2010). Virtual rapid robot prototyping for robot controllers. *International Journal of Design Engineering* 3(3):276-288. DOI: [10.1504/IJDE.2010.039761](https://doi.org/10.1504/IJDE.2010.039761)
- [6] LAM Technologies electronic equipment, NEMA23 Stepper Motor 1.1Nm. From: <https://www.lamtechnologies.com/Product.aspx?lng=EN&idp=M1233032> accessed on: February 25, 2023.
- [7] Devic, A. (2020). *Projektovanje i upravljanje jednog robotskog sistema sa šest stepeni slobode*. (In Serbian). MSc thesis. Faculty of Mechanical Engineering, University of Belgrade.
- [8] MathWorks. Model and simulate multidomain physical systems. From: https://www.mathworks.com/products/simscap_e.html, accessed on: February 9, 2023.
- [9] RoboDK. Simulate Robot Applications. From: <https://robodk.com>, accessed on: February 9, 2022.
- [10] Vidakovic, J., Devic, A., Zivkovic, N., Kvrđić, V., & Stepanic, P. Practical Approaches for Robot Dynamic Model Implementation for Control and Simulation. *Experimental Research and Numerical Simulation in Applied Sciences CNNTech*, 2022, Zlatibor, pp 147-163. DOI: [10.1007/978-3-031-19499-3_8](https://doi.org/10.1007/978-3-031-19499-3_8)
- [11] Microchip. PIC32MX5XX/6XX/7XX Family Data Sheet. From: <http://ww1.microchip.com/downloads/en/devicedoc/61156g.pdf>, accessed on: February 9, 2023.
- [12] TexasInstruments. DRV8825 Stepper Motor Controller IC. From: <https://www.ti.com/lit/ds/symlink/drv8825.pdf>, accessed on: February 9, 2023.
- [13] Microchip. Stand-Alone Ethernet Controller with SPI Interface. From: <http://ww1.microchip.com/downloads/en/DeviceDoc/39662e.pdf>, accessed on: February 9, 2023.
- [14] Allegro MicroSystems. Inc, SENSITIVE HALL-EFFECT SWITCHES FOR HIGH-TEMPERATURE OPERATION. From: <https://www.mpsia.com/download/a3144eul.pdf>, accessed on: February 9, 2023.

*Automotive and
Transportation Engineering*



Banja Luka
1-2 Jun 2023.

DEMI 2023

16th International Conference on Accomplishments in Mechanical and Industrial Engineering

www.demi.mf.unibl.org



Design of experimental research on influencing factors on the particle emission caused by brake wear

S. Vasiljević^a, D. Taranović^b, J. Lukić^b, D. Miloradović^b, J. Glišović^b

^a Academy of Professional Studies Sumadija, Department in Kragujevac, Kosovska 8, 34000, Kragujevac, Serbia

^b University of Kragujevac, Faculty of Engineering, Department for Motor Vehicles and Motors, 6 Sestre Janjić STR., 34000 Kragujevac, Serbia

Abstract *The aim of this paper is to present the design of the experiment to determine the most influential factors on the occurrence of non-exhaust emissions of PM_{2.5} and PM₁₀ particles, namely those caused by vehicle's brake wear. The focus in this case is on the operating parameters of the braking process (vehicle speed, brake pressure and vehicle load), ambient conditions (temperature and air humidity), but also output factors (brake pad temperature at the end of braking, braking torque, braking time, deceleration) and analysis of their connection with the formation of particles. The experimental research was carried out on an inertial brake dynamometer. Classical experiment planning is sometimes too complex and time-consuming, so in the case when the number of factors increases, it is necessary to perform a large number of experimental tests. Experiment planning is a method by which the optimal formula of all influential parameters is found, and as such it represents a very important tool that can be used to respond to a well-defined research goal. The basic idea of a planned experiment is to define a minimal set of experiments in which each factor will be varied in a systematic way.*

Keywords *Brakes, particles, emission, design of experiment, Taguchi method*

1. INTRODUCTION

Experimental measurements represent a complex process of determining different occurrences, phenomena and relationships between different variables. The application of experiments in science is often used to confirm or reject various hypotheses. Often, experiments vary various factors to determine the relationship between those factors.

During experimentation, the factors are varied in a planned manner and in this way,

analysis is enabled, which could lead to correct conclusions. Today, various methods and algorithms have been developed by means of which it is possible to combine various factors in a way that would lead to the correct conclusions during the analysis of the obtained results, as well as the correct connection of the input factors. Design of an experiment is a set of knowledge and techniques that help the experimenter to conduct the experiment in an economical way, to analyse the data, and makes connections between the conclusions from the analysis and the original research objectives. By applying the design of experiments, and in the case of a large number of parameters, combinations of those parameters are obtained so that it is an optimal combination for later analysis. In this way, the number of

Corresponding author

PhD, Jasna Glišović
jaca@kg.ac.rs

Full professor
Sestre Janjić 6 - 34000 Kragujevac,
Kragujevac, Republic of Serbia

measurements that should be performed is reduced.

Designing experiments can be done in different areas, including in the area of performing experiments on vehicles, such as the monitoring the formation of particles due to brake wear.

The airborne particle pollution whose source is the vehicles i.e. traffic is a very serious problem, and it is important from the aspect of the impact on environment and humans. The problems are even bigger if we take into account that it can affect the human immunity, organs, the formation of cancer, but it still has a number of negative effects on other aspects. If we look at the pollution of different European countries in the past 20 years, it can be seen that some of the countries have a high concentration of particles caused by tire and brake wear.

By researching brakes as a source of respirable particles, it is concluded that the formation of particles is the result of the wear process of the elements of the friction pair of the brake, which in the case of disc brakes, as the most applied constructive solution, are the disc (rotor) and brake pads. It is a well-known fact that after a certain number of braking, it is necessary to replace the brake pads due to the wear of the friction linings, but to a lesser extent, the disc wear is also present. All worn brake material is released during vehicle movement, primarily into the air, in the form of particles of various sizes. The harmfulness of particles is reflected not only in their size, but also in their composition, bearing in mind that the composition of particles depends on the material of the source from which they originate, so it is also necessary to analyse the composition of friction pairs that is, the materials used to make them. In some countries, legislation has been introduced that limits the percentage of certain materials in the composition of friction pairs in order to reduce harm. Numerous research projects have been launched in Europe and the world, with the aim of reducing the concentration of emitted particles, and thus reducing their harm, by applying modern production technologies.

The activation of the braking system, as well as its functionality, depends on various parameters. During braking, the friction pairs of the brakes wear out, and thus the formation of particles. Input factors related to braking system activation can also affect wear and particle formation. In order to determine the

relationship of various parameters on the formation of particles and to reach a conclusion about the influence of various factors on the phenomenon, experimental measurements can also be performed.

An example of designing an experimental measurement using the Taguchi method is presented in this paper. The method of designing the experimental measurement based on some input data that were varied during the measurement of PM_{10} and $PM_{2.5}$ particle emissions is explained. Furthermore, an example of analysis using this method based on data obtained by planning an experiment using this method is presented.

2. TAGUCHI DESIGN OF EXPERIMENT AND ANALYSIS METHOD

Applying the Taguchi method is a fairly simple process if the user is sufficiently familiar with the functions offered by the analysis. In this case, the Minitab software package was used for data analysis. The use of parameter arrangement in the Taguchi approach is an engineering method that specializes in determining parameter settings giving optimal levels of quality with minimal variance around target value for a product or technique (Figure 1) [1,2].

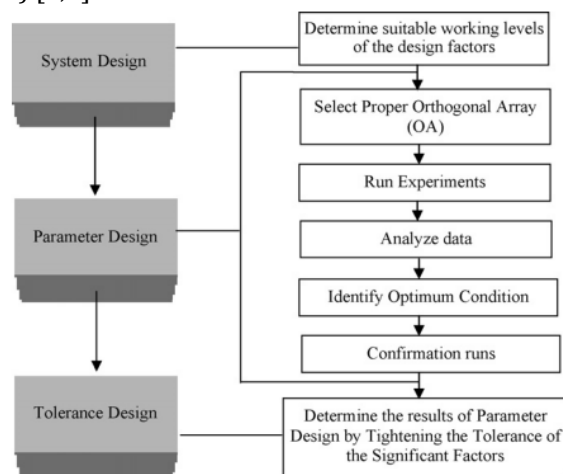


Fig. 1. Taguchi design process [3]

Planning experiments is one of the processes, should to be noted that reducing the combination of factors, and everything is done in several steps [4, 5]. Taguchi configuration is a planned test that allows you to choose an item or cycle that is more reliable in the operating environment. Taguchi's plans note that not all

factors that cause inconsistency can be controlled. These wild factors are called disturbance factors. Taguchi plans attempt to identify control variables (control factors) that limit the influence of a factor on other different variables. During trial and error, signal-to-noise ratios (S/N factor) are controlled to encourage variability of the various factors. An interaction planned with this goal in mind will create a more reliable result. An item designed with this goal in mind will have a more predictable factor performance regardless of the environment in which it is used [6]. Taguchi designs of experiments use symmetric exponents, which measure the effects of elements on the mean and diversity of a reaction.

Taguchi designs use orthogonal arrays, which estimate the effects of factors on the mean and variance of responses. An orthogonal array means that the design is balanced, so the factor levels are equally weighted. Therefore, each factor can be evaluated independently of all other factors, so that the effect of one factor does not affect the evaluation of another factor. This can reduce the time and cost associated with an experiment when fractionated designs are used [6].

The $L(\text{number}) (\text{number}^{\text{exponent}})$ notation informs you of the following:

- $L(\text{number}) = \text{number of runs} (\text{number}^{\text{exponent}})$
- $\text{number} = \text{number of levels for each factor}$
- $\text{exponent} = \text{number of factors}$ [7].

For example, $L27(3^{13})$ means that the design has 27 runs and 13 factors with 3 levels [7]. If the notation is $L (\text{number}^{\text{exponent}} \text{number}^{\text{exponent}})$, then it is a mixed-level design. For example, $L18 (2^1 3^7)$ means that the design has 18 runs, 1 factor with 2 levels and 7 factors with 3 levels [7].

Because of the complexity of the brake pad-disc wear process, a scientific methodology is required to analyse the tribological properties of this friction pair. Design of the experiment (DOE) is one of the most important statistical techniques for studying diverse influencing factors by lowering the number of multiple trials. The Taguchi design technique leads to the removal of unnecessary experiments in the process [8].

In this paper, two different levels were applied to investigate the influence of the design of the

experiment on the obtained research results. Those two levels in this case are mixed levels, namely $L16 (4^2 2^1)$ and $L32 (2^1 4^2)$.

3. PARTICLE MEASUREMENT METHODOLOGY

The examination of the formation of particles that occur during brake wear in this case was carried out in laboratory conditions. The research used an inertial brake dynamometer (Figure 2), which is developed at the Faculty of Engineering at the University of Kragujevac. The application of an inertial brake dynamometer is suitable for simulating and analysing the processes that occur during braking under different test conditions. In the case of measuring particles caused by brake wear on the dynamometer, it is necessary to install additional devices that collect particles or that prevents the collection of particles from the environment.

The device Trotec PC220 was used to measure the emission of particles. This device measures the emission of PM_{10} and $PM_{2.5}$ particles. The device is mounted on the housing inside which there is a disc brake and a brake caliper with brake pads. The display of the installed device on the housing is shown in Figure 3. The reason for using the housing on the inertial brake dynamometer is that there are particles in the atmosphere whose source is not the braking system. The housing enables the extraction of only the particles that are produced during the braking process, which means that the device measures only the particles that are the subject of this research. Before each measurement, the housing is cleaned of particles from the atmosphere and particles from the previous braking process.



Fig. 2. Inertial brake dynamometer Brake Dyno 2020

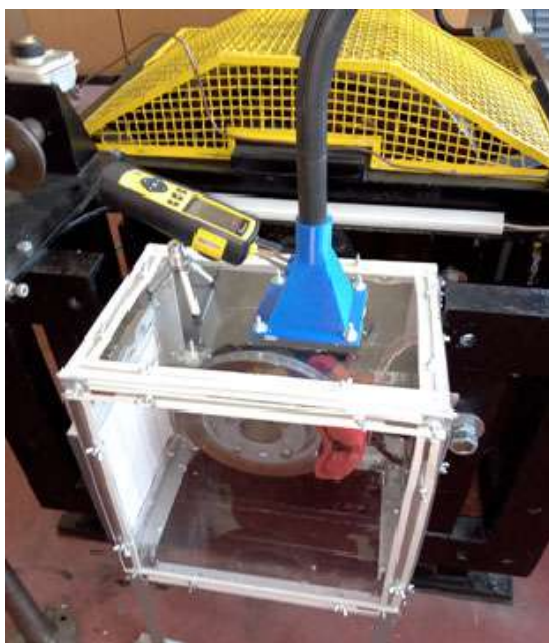


Fig. 3. Housing in which the brake is located on the inertial brake dynamometer

By analysing numerous researches in which different driving tests and cycles were applied [1, 9], the authors obtained data on the most frequently applied parameters that were varied in those tests, as well as their value ranges. Based on those studies, the values of speed, brake pressure and load of one quarter of the vehicle were varied as input braking parameters. The data that were chosen as the parameter values in this case are shown in Table 1. Also, these parameter values were used to design the experiment.

Table 1. Values of parameters that are varied in particle emission measurement

Parameter	Value
Brake pressure in hydraulic system [MPa]	1, 2, 3, 4
Simulated mass of quarter vehicle-load [kg]	150, 250
Simulated initial brake speed [km/h]	20, 40, 60, 80

As a friction pair in this research, a disc and brake pads was used, which are shown in Figure 4. Figure 4a shows the brake pad that was used in this case, it has an eco-friendly formulation, which means that it is applied very a small percentage of metal, i.e. ecologically clean materials were used.

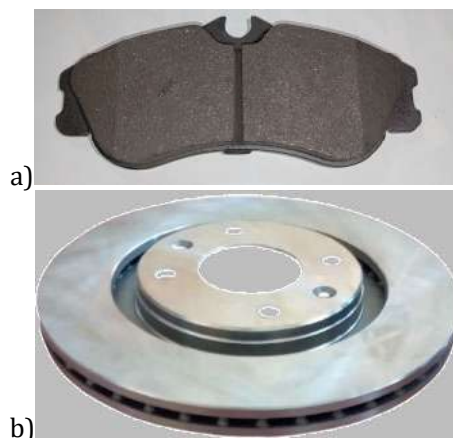


Fig. 4. Applied brake friction pairs, where: a) brake pad, b) brake disc

4. RESULTS ANALYSIS

Using the inertial brake dynamometer in this case, the results related to the formation of PM_{10} and $PM_{2.5}$ particles were obtained. Figure 5 shows the obtained results of particle measurements on an inertial brake dynamometer. These data were used later in the data analysis. In this case, all the data were varied in order to later determine if there is a difference in the obtained data as analysed.

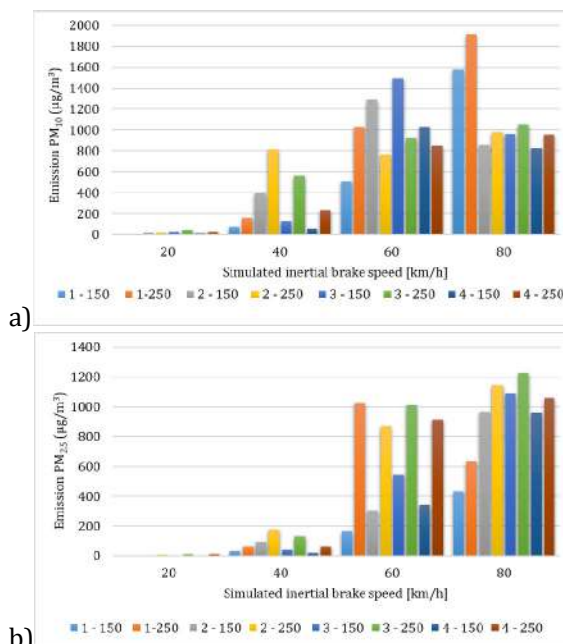


Fig. 5. Obtained results of particles measurements, where: a) PM_{10} , b) $PM_{2.5}$

The obtained measurement data can also be displayed using a 3D diagram, which can be used to display the obtained measurement data

in detail. Figure 6 shows the measurement data based on several analysed parameters. All the data presented refer to the various obtained values of particle emissions.

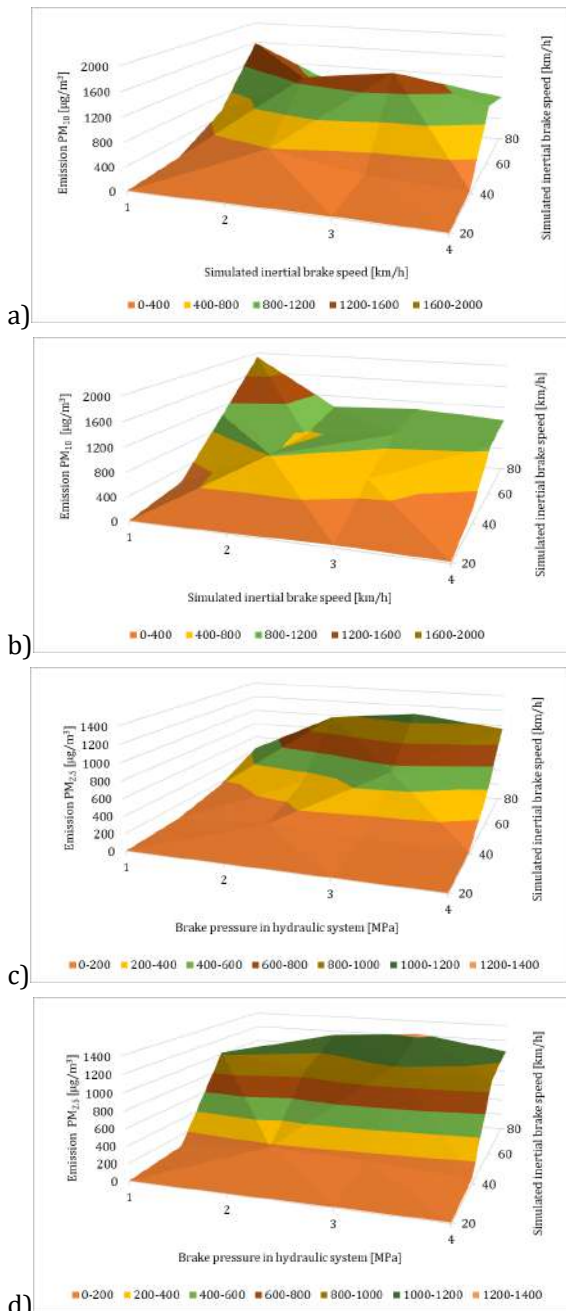


Fig. 6. Obtained results of the particles measurement, where: a) PM₁₀ at a simulated load of 150 kg, b) PM₁₀ at a simulated load of 250 kg c) PM_{2.5} at a simulated load of 150 kg c) PM_{2.5} at a simulated load of 250 kg

By applying the analysis of the interactions of various factors and combining them, the obtained data can also be displayed. Figure 7a

shows the obtained results of varying the parameters for PM₁₀ particles, while Figure 7b shows the data for PM_{2.5} particles. In this case, it is noticeable that some factors have a different effect on the formation of particles, i.e. the intensity of action varies depending on the particles being observed.

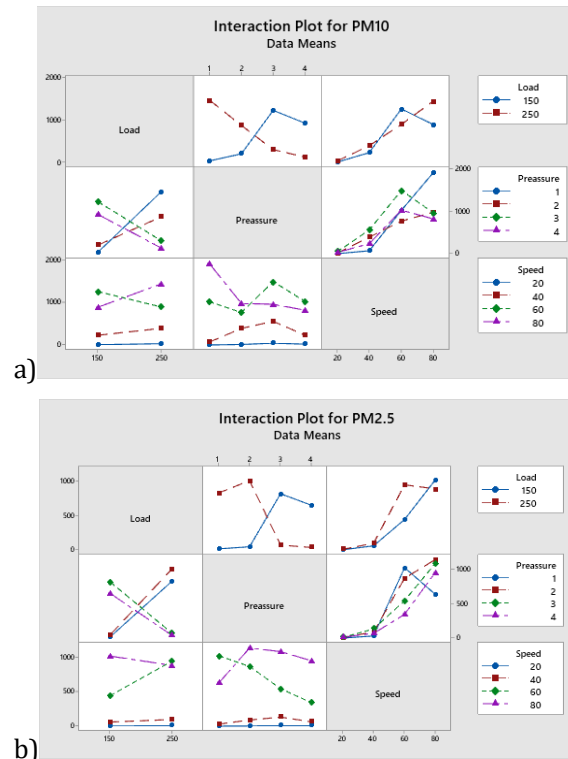


Fig. 7. Obtained results of the analysis of interactions of different parameters: a) PM₁₀, b) PM_{2.5}

Figure 8 and Tables 2 and 3 show data from the analysis of influencing factors on the emission of PM₁₀ particles. Figure 8a and Table 2 show the results of influential factors and S/N ratio in the case of L32. On the other hand, Figure 8b and Table 3 show the results for the analysis case L16. In both cases, looking at the graphic displays, it is noticeable that speed, the load of one quarter of the vehicle, and the pressure in the braking system have the greatest influence on the resulting particle emission. On the other hand, there is a difference in the analysis of tabulated data, where it is noticeable that speed is the most influential factor in both cases. In the case of L32, the most influential factor is the load of one quarter of the vehicle, following by the pressure in the brake system. For the L16 case, the second most influential factor is the

pressure in the brake system, followed by the load.

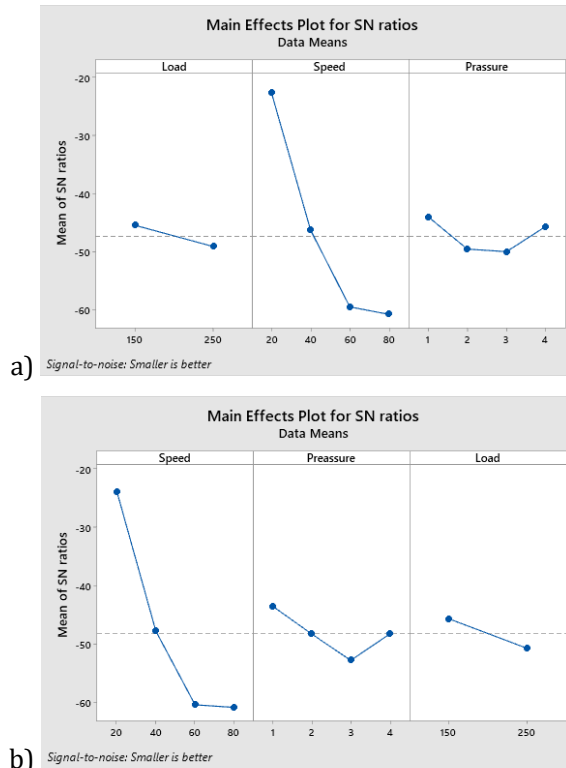


Fig. 8. The obtained results of analysis according to PM₁₀ particles, where: a) L₃₂, b) L₁₆

Table 2. S/N ratio for PM₁₀ – L₃₂

Level	Load	Speed	Pressure
1	-33.89	-10.84	-39.74
2	-41.21	-32.84	-35.81
3		-48.09	-37.06
4		-58.41	-37.58
Delta	7.32	47.57	3.94
Rank	2	1	3

Table 3. S/N ratio for PM₁₀ – L₁₆

Level	Speed	Pressure	Load
1	-23.85	-43.54	-45.71
2	-47.82	-48.30	-50.76
3	-60.41	-52.82	
4	-60.86	-48.28	
Delta	37.02	9.28	5.06
Rank	1	2	3

A graphic presentation of the results of the analysis of the influential factors that affect the emission of PM_{2.5} particles, is given in Figure 9, while the tabular data of the obtained

calculation are shown in Tables 4 and 5. As in the previous case for L₃₂, the most influential factors are the simulated speed, the load of one quarter of the vehicle and pressure in the braking system. In the case of L₁₆, the difference is in the results obtained, where the pressure in the braking system is more influential than the load of one quarter of the vehicle. However, the graphic data show identical diagrams, so it can be concluded that there is an equal effect and influence in both cases.

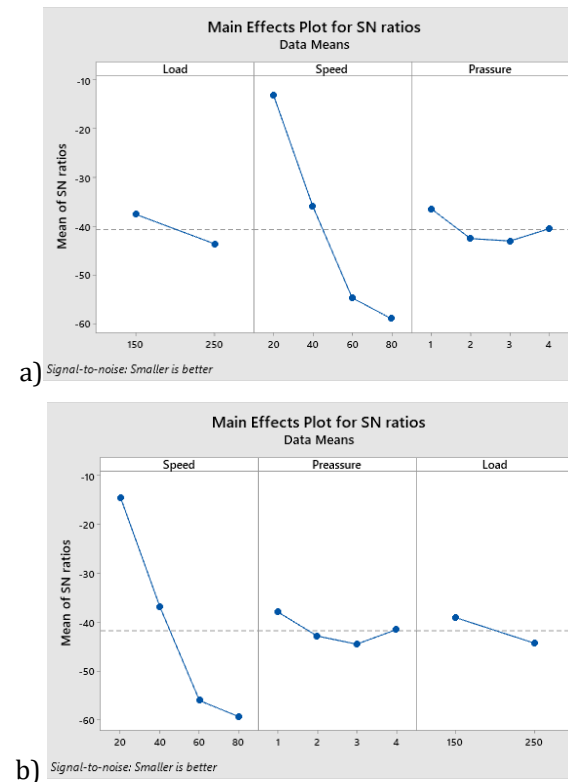


Fig. 9. The obtained results of analysis according to PM_{2.5} particles, where: a) L₃₂, b) L₁₆

Table 4. S/N ratio for PM_{2.5} – L₃₂

Level	Load	Speed	Pressure
1	-37.63	-13.01	-36.45
2	-43.69	-35.88	-42.58
3		-54.72	-43.07
4		-59.03	-40.54
Delta	6.05	46.03	6.62
Rank	3	1	2

Table 5. S/N ratio for PM_{2.5} – L₁₆

Level	Speed	Pressure	Load
1	-14.52	-37.95	-39.12
2	-36.96	-42.89	-44.38
3	-56.11	-44.56	
4	-59.40	-41.59	
Delta	44.88	6.61	5.25
Rank	1	2	3

5. CONCLUSION

The planning of the experiment measuring the emission of particles caused by the wear of friction pairs of brakes is a complex 5, bearing in mind the complex nature of the formation of particles and the effect of various parameters. In this case, the Taguchi method of experiment planning was applied. Two orthogonal arrays, namely L32 and L16, were applied, with the application of three different factors. In both cases, the graphical results led to the same conclusion about the influencing factors. According to the analysis of the calculation data and according to the rank, there was a change in the influencing factors. Thus, in the case of L32, the second most influential factor on particle emission was the load, while in the case of L16, the second most influential factor was the pressure in the braking system. Also, if we consider the third most influential factor in the case of L32 according to the calculation, it was the pressure in the braking system, while in the case of the orthogonal array L16, it turned out that the third most influential factor was the load of one quarter of the vehicle.

Based on the previously concluded, it can be seen that when planning, it is very important to know the specificity of the measurements that are performed. In the case of complex measurements and when there is a smaller number of factors or variations of those factors, it is necessary to determine a proper orthogonal array that would give correct results in the analysis. In this case, the authors concluded that measurements with a larger number of data and variations give, for such cases, better and more accurate results. This conclusion can also be reached by analysing differently presented data, where the correct conclusion and accurate data were reached by applying the orthogonal array L32.

Acknowledgement

The Ministry for education, science and technological development of the Government of the Republic of Serbia supported the research presented in the article (grant number TR35041).

REFERENCES

- [1] Vasiljević, S., Glišović, J., Lukić, J., Stojanović, N., Grujić, I. (2022). Analiza radnih parametara kočenja pri ispitivanju habanja kočnica i nastanka čestica na inercijalnom kočnom dinamometru. *Tehnika-Mašinstvo*, vol. 72, no. 2, p. 195-202. DOI: 10.5937/tehnika2202195V
- [2] Hamzačebi, C. (2021). Taguchi Method as a Robust Design Tool. *Quality Control - Intelligent Manufacturing, Robust Design and Charts*. Li, P., Pereira, P., Navas H. (editors). Quality Control - Intelligent Manufacturing, Robust Design and Charts. IntechOpen, London, DOI: 10.5772/intechopen.94908
- [3] Pang, J. S., Ansari, M. N. M., Zaroog, O. S., Ali, M. H., Sapuan, S. M. (2014). Taguchi design optimization of machining parameters on the CNC end milling process of halloysite nanotube with aluminium reinforced epoxy matrix (HNT/Al/Ep) hybrid composite. *HBRC Journal*, vol. 10, no. 2, p. 138-144. DOI: 10.1016/j.hbrj.2013.09.007
- [4] Zhang, J. Z., Chen, J. C., Kirby, E. D. (2007). Surface roughness optimization in an end-milling operation using the Taguchi design method. *Journal of Materials Processing Technology*, vol. 184, no. 1-3, p. 233-239. DOI: 10.1016/j.jmatprotec.2006.11.029
- [5] Popović, B. (2020). Planiranje, analiziranje i optimizacija eksperimenata. *Journal of Engineering Management and Competitiveness (JEMC)*. vol. 10, no. 1, p. 15-30. DOI: 10.5937/jemc2001015P
- [6] Minitab, Taguchi designs, <https://support.minitab.com/en-us/minitab/21/help-and-how-to/statistical-modeling/doe/supporting-topics/taguchi-designs/taguchi-designs/>, accessed on: april 02, 2023.
- [7] Minitab, Notation for Taguchi designs, <https://support.minitab.com/en-us/minitab/21/help-and-how-to/statistical-modeling/doe/supporting-topics/taguchi-designs/notation-for-taguchi-designs/>, accessed on: april 02, 2023.
- [8] Saurabh, A., Joshi, K., Manoj, A., Verma, P.C. (2022). Process Optimization of Automotive Brake Material in Dry Sliding Using Taguchi and ANOVA Techniques for Wear Control.

Lubricants, vol. 10, no. 161, p. 1-16. DOI: 10.3390/lubricants10070161

- [9] Vasiljević, S., Glišović, J., Stojanović, N., Grujić, I. An overview of non-exhaust brake emission measuring methods. *Proceedings of 15th International Conference on Accomplishments in Mechanical and Industrial Engineering DEMI 2021*, 28-29 May 2021, Banja Luka, Republic of Srpska, p. 339-348.



Banja Luka
1–2 Jun 2023.

DEMI 2023

16th International Conference on
Accomplishments in Mechanical and
Industrial Engineering

www.demi.mf.unibl.org



Impact of non-exhaust particle emissions from motor vehicles on human health

O. Bobičić^a, M. Damjanović^a, D.C. Finger^b, R. Vujadinović^c, B. Matović^c

^aFaculty of mechanical engineering, University of Montenegro, Podgorica, Montenegro

^bDepartment of engineering, Reykjavik University, Reykjavik, Iceland

^cFaculty of mechanical engineering, University of Montenegro, Podgorica, Montenegro

Abstract

According to the World Health Organization (WHO), PM_{2.5} and PM₁₀ are a leading cause of air pollution and have been identified as having detrimental effects on human health even at low concentrations. By reducing exposure to these particles, countries can significantly decrease the incidence of both short- and long-term illnesses, as well as the overall burden of disease. This paper discusses the impact of the size and concentration of particles from braking systems, tires, and road on the respiratory, cardiovascular, and nervous systems of humans. The paper also presents methods for detecting and measuring non-exhaust emissions from motor vehicles, as well as United Nations Economic Commission for Europe (UNECE) regulations for defining standardised laboratory procedures for testing particle emissions resulting from the wear of brakes in light vehicles with a maximum permissible weight of up to 3500 kg. Based on the reviewed literature, possible mitigation measures to reduce fine particulate emissions are presented. In particular, an adaptation of an adequate braking process can significantly mitigate emissions and subsequently reduce harmful effects on human health and the environment.

Keywords non-exhaust emissions, particulate matter (PM), human health

1. INTRODUCTION

Despite all the conducted research, some factors that contribute to the production of non-exhaust emissions have been partially neglected, and their contribution to the overall level of pollutants generated by traffic is decreasing to a much lesser extent compared to exhaust emissions.

Studies have found that the brake system, tire wear, and road surface are the most significant sources of non-exhaust particles (particulate matters), and they can have a substantial impact on human health [1-3]. These PMs are small

enough to penetrate deep into the lungs, where they can cause inflammation [4] and damage to lung tissue. This can lead to a variety of respiratory problems, such as asthma and chronic obstructive pulmonary disease [5]. Moreover, exposure to PM from motor vehicle emissions has also been linked to an increased risk of cardiovascular disease [6,7], and some neurodegenerative phenomena and cognitive disorders [8,9]. Therefore, it is essential to take measures to reduce the emission of particulate matter from motor vehicles and limit our exposure to these harmful pollutants.

This paper provides an overview of previous studies examining non-exhaust emissions and their impact on human health, as well as a review of methods for measuring non-exhaust emissions generated by the brake system (brake discs and pads). A brief overview of the brake testing requirements prescribed by The United Nations Global Technical Regulation (UN GTR) will also be provided.

Corresponding author

Spec. Sci, Ognjen Bobičić
ognjenbobicic@gmail.com

Faculty of mechanical engineering,
University of Montenegro,
Bl Dzordza Vasingtona nn, 81000
Podgorica, Montenegro

2. THE IMPACT OF NON-EXHAUST EMISSIONS ON HUMAN HEALTH

The proliferation of road traffic has resulted in significant repercussions, not limited to direct transportation safety concerns, but also with regards to the visible impact of vehicle emissions on the environment and human health, which has been the focus of research over the past two decades in urban areas worldwide [10], due to the increasing presence of motor vehicles and their emissions as a noteworthy source of particulate matter (PM) in the atmosphere, which can severely affect the respiratory system of humans..

According to the European Environment Agency's reports in 2014 and 2016, between 64% and 92% of the EU urban population is exposed to high concentrations of PM₁₀ and PM_{2.5} particles [11][12], and air pollution is considered the largest environmental risk factor responsible for premature deaths worldwide. The World Health Organization's studies have shown that Europeans' life expectancy can be reduced by an average of about 8.6 months [13][14], or even up to 22 months in the most polluted cities, due to exposure to these particles [14].

Animal studies have demonstrated that exposure to highly polluted ambient air affects lung function and leads to premature death, and the same has been observed in humans, with air pollution contributing to as many as 4.2 million premature deaths globally in 2016 [15][16].

A study conducted in Taipei, Taiwan, investigated the exposure of PM_{2.5} on human health, specifically on the cardiovascular system [17][18]. The study concluded that commuters [18] and cyclists [17] are more exposed to PM on routes with heavy traffic compared to those with less traffic. Moreover, the study revealed that pedestrians [17] walking on sidewalks were more exposed to PM than people travelling in cars for the same purpose.

Particle size plays an important role in determining the impact of particles on human health, depending on how deep they can travel into respiratory structures. The authors from the University of Trento, Italy, have presented a classification overview of particles found in urban environments [19] based on their size and mass characteristics. The particles were divided into three groups: coarse, fine, and ultrafine particles, each with their unique characteristics.

Coarse particles (aerodynamic diameter of 2-20 μ m) [19] are characterised by a larger size and lower numerical representation, but they are considered primary emissions. Fine particles (aerodynamic diameter of 0.1-2 μ m) [19] are more prevalent and have a smaller mass and volumetric range, while ultrafine particles (aerodynamic diameter of 0.01-0.1 μ m) [19] have an even smaller mass and volumetric range and higher numerical representation. Ultrafine particles can be further divided into two groups based on their aerodynamic diameter, smaller than 0.01 μ m (nanoparticles) and those with an aerodynamic diameter between 0.01 and 1 μ m (Aitken mode). Hence, small particles, with a size of 2.5 μ m or less, can penetrate the finest respiratory pathways, while particles of 1 μ m can reach the terminal alveolar structures where oxygen and carbon dioxide exchange occur. Nanoparticles of 0.1 μ m can directly penetrate into the bloodstream [20][21].

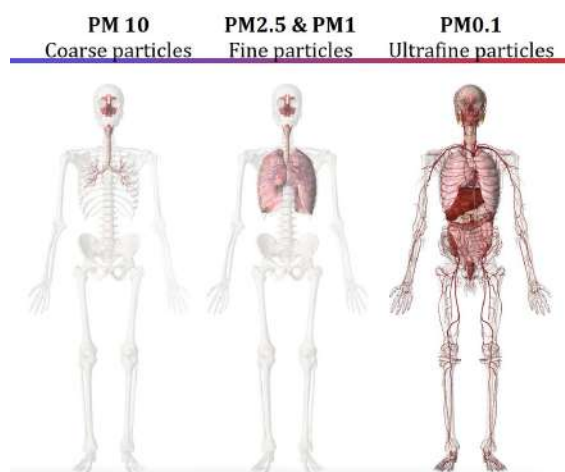


Fig. 1. Representation of particles penetration into the human body depending on the size of their aerodynamic diameter. (Modified from [22])

Given the evident impact of particles on human health, viewed from various aspects, it represents an additional threat for chronically ill individuals and those susceptible to rapid changes in health status. In a study conducted by Gonet and Maher (2019) [23], which examines the impact of particles generated by car operation, it was noted that the concentration and size of particles can be strongly linked not only to respiratory and cardiovascular damage but also to neurodevelopment and cognitive functions. As such, the following sections present research on the impact of particles generated by

road vehicles on the respiratory, cardiovascular, and nervous systems in humans.

2.1 Impact on the respiratory system

The investigation of ambient air pollutants has led to the suspicion that exposure to particles (PM), especially those in the fine (<2.5 mm aerodynamic diameter) and ultrafine range (<0.1 mm;), is considered a key risk factor for many harmful health effects [16][21]. Based on this assumption, it has been concluded that the particular effect of the presence of particles in ambient air is reflected in acute or chronic respiratory problems, which are caused by direct damage to the respiratory organs when inhaling air pollutants. Chronic exposure is associated with cough, sputum production, and reduced lung function [24]. In addition to symptoms, exposure studies in healthy individuals have documented numerous deep inflammatory changes in the respiratory tract, particularly before changes in lung function can be detected [16].

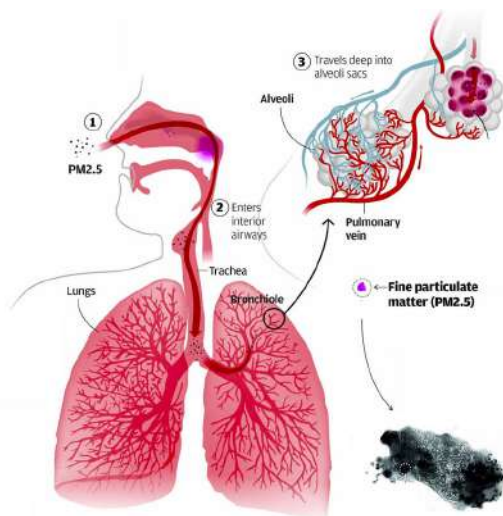


Fig. 2. PM particle (specifically PM_{2.5}) and how it can be synthesised into the bloodstream through the respiratory system. (Modified from [21])

A brief review of the literature by Italian researcher Luigi Vimercati (2011) highlighted that emissions from traffic processes, i.e. braking and tire wear, can play a key role in causing allergic conditions [5]. It was also noted that several pollutants (NO₂, O₃, and PM) are associated with worsening asthma and can

significantly contribute to its pathogenesis. Therefore, based on the collected data, it can be concluded that in most industrialised countries, people living in urban areas tend to be more affected by allergic respiratory diseases than those in rural areas [5].

On another note, one experimental indirect study was conducted to investigate the effect of air pollution on changes in Sprague-Dawley rat lung tissue under whole-body exposure to PM₁ (particles <1 mm in aerodynamic diameter) pollutants at the National Laboratory Animal Center (Taipei, Taiwan) [16]. It was found that the presence of PM₁ particles enhances oxidative stress and inflammatory reactions under subchronic exposure to PM₁, resulting from car work, while suppressing glucose metabolism and actin cytoskeleton signalling. These factors can lead to impaired lung function after chronic exposure to PM₁ associated with traffic [16].

The study made a significant contribution to the investigation of several potential molecular characteristics associated with early lung damage in response to air pollution associated with traffic processes. These results would further contribute significantly to the screening process of individuals who are more significantly exposed to polluted ambient air, primarily supplied with particles resulting from car work and traffic processes.

2.2 Impact on the cardiovascular system

A study by a group of authors from the University of South China [17] examined the impact of PM_{2.5} particles on human health and provided an overview of previous conclusions on this topic. Long-term exposure to PM_{2.5} may not only affect the respiratory system but also cause significant structural changes in the heart muscle, such as myocardial hypertrophy (with increased hypertrophic markers) and harmful ventricular remodelling (changes in the size, shape, structure, and function of the heart muscle) [17, 25, 26].

Previous studies have also discussed how PM_{2.5} can disrupt a significant number of functions in the cardiac autonomic nervous system (ANS) and lead to reduced heart rate variability, which is considered an independent risk factor for cardiovascular morbidity and mortality [6,7,25]. The study also discussed changes in the endocrine system and the

function of the hypothalamus and its hormone secretion, conditioned by changes in the heart muscle, but this association has not been sufficiently investigated.

To the extent of the relevance of the examined data, a connection was found between the increased concentration of PM_{2.5} particles and a range of pathophysiological responses that increase blood pressure and lead to the development of hypertension [17,25,27].

A study conducted in Taiwan examined the effects of PM_{2.5} exposure on the cardiovascular system of healthy travellers using different modes of transportation. The study involved 120 participants who were classified according to their transportation type, including electric subway trains, gasoline-powered buses, cars, scooters, and pedestrians with and without face masks. Measurements of various parameters were taken during six iterations. Results showed that exposure to PM_{2.5} is linked to increased systolic blood pressure and heart rate during walking and riding a gasoline-powered scooter. PM_{2.5} concentration was highest during scooter use and lowest during electric subway train use. The study did not find a significant correlation between PM_{2.5} and the systolic and diastolic blood pressure or heart rate while walking with a face mask. Overall, the study concluded that PM_{2.5} has a visible effect on the cardiovascular system. [17]

2.3 Impact on the nervous system

Previously, we described the relation of particles with changes in the respiratory and cardiovascular systems, while on the other hand, researchers have also investigated the impact of particles on other organs and systems within the human body. The effects of non-exhaust emissions of nanoparticles produced by vehicular processes have also been examined and linked to neurodevelopment and cognitive impairments.

Researchers von Mikecz, A. and Schikowski, T. (2020) from the Leibniz Research Institute for Environmental Medicine studied the effects of nanoparticles in the air on the nervous system through the aggregation of amyloid proteins, neurodegeneration, and neurodegenerative diseases such as Alzheimer's and Parkinson's disease [28]. Also, a study by a group of researchers from the US, Brazil, Germany, and the UK on various forms of cardiovascular and

cerebrovascular diseases indicates their harmful effects on the brain and cognitive processes through vascular and inflammatory mechanisms [28, 29].

Besides age, the environment in which a person lives can also play a role in the development of Alzheimer's and Parkinson's disease. Exposure to certain pollutants in the environment may contribute to an increased risk of developing these diseases. This hypothesis has been confirmed by several studies, which have emphasised that Alzheimer's disease positively correlates with the level of air pollution in urban environments, most significantly with PM [28,30].

Schikowski, T. and Altuğ H.'s (2020) study on the role of air pollution in cognitive decline and impairment [31] confirmed the association between these two components. The collected data is quite heterogeneous, and additional analyses and research are needed to give more importance to this association and explore its relevance in detail [28].

What is also important to emphasise is that the accumulation of amyloid protein within the cells of the central nervous system is a common feature of neuropathology in Alzheimer's and Parkinson's disease and is closely associated with the appearance of amyloid-beta peptides, tau proteins, and alpha-synuclein [28]. In support of this, the study by Gonet and Maher (2019) [23] on urban air and its contribution to the development of dementia and Alzheimer's disease showed typical features of the pathogenesis of Alzheimer's disease, namely aberrant deposition of amyloid-beta peptides and tau proteins in post-mortem brain samples of clinically healthy people and dogs exposed to lifelong air pollution by living in the researched urban areas of Mexico City or Manchester (UK) [30].

Research has shown that nanoparticles generated from traffic processes, specifically from the wear and tear of brakes and tires in automobiles, have the ability to induce amyloid formation in nano-silicon dioxide. Furthermore, a significant amount of these nanoparticles has been detected in postmortem brains of animals and humans with chronic exposure to air pollution in highly urbanised environments. Epidemiological data has also indicated that living near traffic routes is a risk factor for the development of neurodegenerative diseases, such as Alzheimer's disease [8, 23].

Additionally, a study conducted in China [32] to investigate the effects of air pollution on unborn children (during prenatal development) and the development of ADHD in early childhood yielded significant results. It is particularly noteworthy that with an increase in the presence of PM₁₀, PM_{2.5}, and NO₂ during the period considered most sensitive to the development of degenerative behaviours (end of pregnancy and first four months of life), the possibility of hyperactivity in children increases significantly, with a statistically significant association. This conclusion supports the idea that exposure to particles during pregnancy can lead to the development of hyperactive behavior (or ADHD) in early childhood [32].

3. METHODS FOR DETECTING AND MEASURING NON-EXHAUST EMISSIONS FROM BRAKES

It is crucial to bear in mind that particle emissions related to traffic have been proven to have negative health effects. However, despite the scientific community's increasing interest in studying brake emissions, the vast majority of research findings are inconsistent and vary widely. This introduces a significant degree of uncertainty when attempting to assess the contribution of brake wear emissions to ambient PM levels, as brake wear emission factors are dependent on various parameters such as the type of friction material, brake assembly, and driving conditions [33].

One of the primary reasons for the lack of consistency in measuring particulate matter size and number emission factors, so far, is the absence of standardised methodologies for sampling and measuring brake wear particle emissions [34]. As such, researchers have employed different sampling and measurement techniques and devices, leading to variations in reported results. So, brake wear particles can be detected and measured under controlled laboratory conditions or in uncontrolled real-world settings on the road.

In the context of laboratory methods and devices, the most frequently used ones are pin-on-disc tribometers and inertial brake dynamometers [34]. On the other hand, measurements taken on the road [34] are conducted in uncontrolled, real-world conditions, and the methodology used differs significantly from laboratory methods.

3.1 Testing with a brake dynamometer

A brake dynamometer is a testing device or method that is used to simulate the conditions of a vehicle braking system in a laboratory environment. It works by applying a load to the brake system under test and measuring the force generated by the brake during operation. This allows for precise control and evaluation of the brake system's performance under different conditions, such as varying speeds and loads.

To use a brake dynamometer for testing brakes and generating brake PMs, the brake system to be tested is installed onto the dynamometer and connected to its load cell or torque transducer. The brake is then applied under various conditions, such as different speeds and loads, and its performance is evaluated. This evaluation can include measuring the stopping distance, fade resistance, and other characteristics of the brake system.

During testing, brake PMs are generated due to the friction generated between the brake pads and the rotor. These PMs can be collected using appropriate collection methods, such as filters or electrostatic precipitation, and then analysed using techniques such as microscopy or spectroscopy to determine their size, shape, composition, and other properties. [35-38].

3.2 Testing with a pin-on-disc tribometer

One method/device for measuring the wear and friction characteristics of brake pads or other brake components, under different conditions, is through testing with a pin-on-disc tribometer. The device consists of a rotating disc and a stationary pin that is pressed against the disc. The frictional force between the pin and disc is measured using a load cell or torque sensor, while the wear of the materials is measured using a profilometer or other measuring devices.

To use a pin-on-disc tribometer, the disc and pin are installed onto the device and brought into contact with each other. The load is then applied to the system, and the disc is rotated at a specified speed. The pin is pressed against the disc with a specified force, and the frictional force between the two materials is measured using the load cell or torque sensor. The test can be run for a specified duration or until a specified amount of wear has occurred.

These wear debris particles can be in the form of particulate matter (PM), which may contain harmful substances such as metals or other toxins.

To measure the PMs generated during testing, appropriate collection methods can be employed, such as using filters or electrostatic precipitation. These methods allow for the collection of wear debris particles in a controlled manner, which can then be analysed using techniques such as microscopy or spectroscopy. These analyses can provide valuable information on the size, shape, composition, and other properties of the wear debris particles [35][37].

3.3 On-road testing and measurement

In order to measure emissions under real conditions, it is necessary to conduct on-road testing. This method involves driving a vehicle on a designated test route that is designed to represent typical driving conditions. The route includes various driving conditions, including city, suburban, and highway driving, as well as different braking regimes and speeds. During testing, various instruments are used to measure the emissions produced by the vehicle, including sensors and specialised instruments for measuring particulate matter (PM) [39].

On-road testing is also a method used to evaluate brake performance under real driving conditions. It is important to note that on-road testing has some limitations due to the difficulty in controlling all the variables that can affect brake performance, such as road surface, weather conditions, and traffic flows. On-road testing is usually used in combination with other testing methods, as well as with different measuring instruments [35][40].

4. REGULATION AND PROPOSED STANDARDISED MEASUREMENT PROCESSES

Since the 1990s, regulations have limited PM emissions from vehicles by collecting PM from exhaust gases and measuring their concentration. The PN method was introduced in Europe in 2011 to improve testing methodology. While stricter regulations on exhaust emissions have reduced particle emissions, non-exhaust PM, from the wear of brakes and tires, has become a new concern. It accounts for nearly half of all PM generated from road transport

processes [41]. Despite efforts to develop electrification strategies for road transport, even a fully electric vehicles still emit non-exhaust particles in significant quantities [42].

The above-mentioned scenario has required the development of a set of regulations and legal acts that will address this issue over the past decade. In this regard, the United Nations Economic Commission for Europe (UNECE) has developed a proposal for a new United Nations Global Technical Regulation (UN GTR) [43] based on the Worldwide Harmonized Light Vehicle Test Procedures (WLTP), which represents a regulation for defining harmonised laboratory procedures for testing particle emissions resulting from brake wear in light vehicles, with a maximum allowed mass of up to 3500 kg. The aim of the UN GTR is to improve understanding of different brake systems, reduce inconsistencies, and emissions through a harmonised approach to measuring brake particle emissions.

The regulation resulted from the Non-Road Transport PMP Informal Working Group, which was hired by UNECE VP.29 to study non-exhaust particles from road transport, focusing on brakes and tires as the most relevant sources. The group developed new testing cycles to simulate real-world conditions and established guidelines for reporting brake wear particles. UN GTR provides a globally harmonised methodology for measuring brake wear particles in light-duty vehicles in laboratory conditions, but it doesn't cover other vehicle categories (such as off-road vehicles, special purpose vehicles, etc.).

4.1 Test execution

Testing brake emissions consists of three segments, each requiring one or more cycles (trips) under certain conditions. The test itself is performed during the deceleration or stopping process, as this is the way to activate the brake system and, thus the precondition for the formation of particles. The mentioned three segments are:

- **Brake cooling adjustment** [43]– is process used to standardise and uniform the conditions for testing brakes in different locations and under different real conditions involves adjusting the level of airflow and its velocity, taking into account the design and size of the brake housing and the arrangement and

geometry of the air duct system. This process is essential to ensure consistent and comparable results under all testing conditions. This section uses Trip #10 of the WLTP Brake cycle.

- **Brake bedding** [43]- is necessary to pre-test the brake pair under appropriate conditions and stabilise its response before measuring emissions. This procedure should be carried out either with the same brake pairs used during the brake cooling adjustment segment or with completely new brakes, evaluated after cooling adjustment. This procedure must be carried out for all brake pairs on the front and rear. This section uses five repetitions of the WLTP-Brake cycle.
- **Brake emissions measurement** [43]- defines the conditions for measuring particle emissions (PM) during brake testing, which the measuring system must meet. The sampling system determines the amount of PM produced by the brakes during the test itself. PM emissions and testing parameters should be presented as particle mass per distance travelled, for the brake pair being tested. It is necessary to assess emissions for both PM_{10} and $PM_{2.5}$ during testing, using separate sampling systems for each threshold (2.5 μm and 10 μm). This section includes one performance of the WLTP-Brake cycle.

Each of the parameters, requirements of the system, procedures, and trips that further define the aforementioned segments are described in detail in the regulation itself and the WLTP procedure on which the regulation is based.

4.2 Minimum requirements for test equipment and automation

It is important to note the minimum testing system requirements (dynamometer and automation) prescribed by the regulation. The diagram illustrating the principle of the brake dynamometer testing system, as shown below, indicates the interactions with the essential subsystems needed to conduct brake emission tests according to UN GTR.

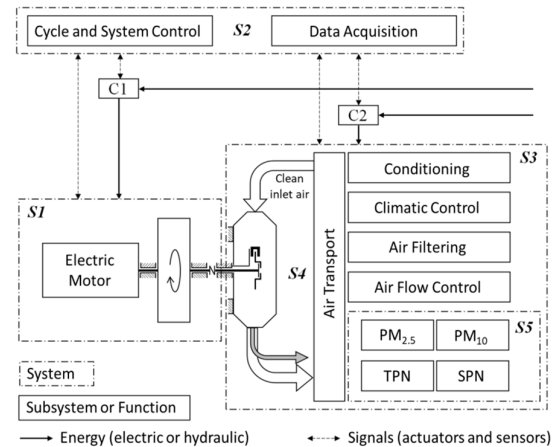


Fig. 3. Layout of the test system with the brake dynamometer, where S1: Brake dynamometer, S2: Automation, control, and data acquisition system, S3: Climatic conditioning unit, S4: Brake enclosure and sampling plane, S5: Emissions measurement system. C1 and C2: Testing facility energy controls and monitoring system. The grey arrow represents the aerosol sample from the brake under testing [43].

The brake dynamometer must comprise the following components at a minimum [43]:

- An electric motor that can vary the rotational speed or maintain it at a constant rate. This motor is also responsible for adjusting the test inertia to simulate actual driving conditions and non-friction braking.
- A servo controller, either hydraulic or electric, that activates the brake being tested.
- A mechanical assembly that facilitates the mounting of the brake being tested, permits the disc or drum to rotate freely, and absorbs the reaction forces produced by braking.
- A robust framework that houses all the mandatory subsystems. The framework must have the capacity to withstand the forces and torque generated by the brake under testing.
- Sensors and devices that gather data and supervise the operation of the testing system.

The automation system performs crucial functions for the brake emissions test. It should accelerate and maintain constant speed during acceleration and cruise events, respectively, while reducing the kinetic energy of rotating masses by modulating the frictional torque during deceleration events. Besides, the system should provide an interface to the operator, stores test data, and manages communication with other testing facility systems. During deceleration events, the automation system uses active torque control to increase or

decrease the total effective test inertia. The electric motor can absorb some kinetic energy equivalent to the road loads and non-friction braking from the vehicle's powertrain. Also, the test system software must have the following functions: automatically execute the driving cycle and closed-loop processes (primarily for brake controls, cooling air handling, and emissions measurements); continuously record data from all relevant sensors to produce specified outputs; and monitor signals, messages, alarms, and emergency stops from the operator and connected systems [43].

5. CONCLUSION

Non-exhaust emissions from motor vehicles, such as those generated by the brake system, tire wear, and road surface, contribute significantly to the overall level of pollutants generated by traffic, and have been found to have a substantial impact on human health. Exposure to PM from motor vehicle emissions has been linked to respiratory problems, cardiovascular disease, neurodegenerative phenomena, and cognitive disorders.

It is clear that the impact of PMs on human health represents an additional threat for chronically ill individuals and those susceptible to rapid changes in health status. The study provides a detailed overview of previous research that examined non-exhaust emissions and their impact on human health, as well as a review of methods for measuring non-exhaust emissions generated by the brake system.

The research concludes that while the scientific community's interest in studying brake emissions is increasing, the vast majority of research findings are inconsistent and vary widely, introducing a significant degree of uncertainty when attempting to assess the contribution of brake emissions to overall particulate matter emissions.

However, with the release of the proposal for a new United Nations Global Technical Regulation (UN GTR) it will now be easier to obtain more reliable data through standardised methods for brake lab testing. This is a significant development as it will lead to more accurate information on the contribution of brake emissions to overall PM emissions and will help policymakers take more effective measures to limit exposure to these harmful pollutants. Precise measurements can inform

the development of new regulations on the amount of particles that brakes can produce, conditional on the use of suitable materials and technologies in the production process. In addition, standardised data on the level of PM can significantly influence the recommendation and development of EURO7 norms [44], which will entail restrictions in the domain of non-exhaust emissions in general.

On another note, by adopting and implementing an effective braking process that is tailored to specific conditions, harmful emissions could significantly be reduced, thus improving human health and the environment, which may require additional research.

It is important to continue to monitor research and develop new methodologies to improve our understanding of the impact of non-exhaust emissions on human health, and to implement measures to reduce these emissions in the future.

REFERENCES

- [1] Zhu, C., Maharajan, K., Liu, K., & Zhang, Y. (2021). Role of atmospheric particulate matter exposure in COVID-19 and other health risks in human: A review. *Environmental Research*, 198, 111281. DOI: [10.1016/j.envres.2021.111281](https://doi.org/10.1016/j.envres.2021.111281)
- [2] Liu, Y., Chen, H., Gao, J., Li, Y., Dave, K., Chen, J., ... & Perricone, G. (2021). Comparative analysis of non-exhaust airborne particles from electric and internal combustion engine vehicles. *Journal of Hazardous Materials*, 420, 126626. DOI: [10.1016/j.jhazmat.2021.126626](https://doi.org/10.1016/j.jhazmat.2021.126626)
- [3] Stafoggia, M., & Faustini, A. (2018). Impact on public health—epidemiological studies: a review of epidemiological studies on non-exhaust particles: identification of gaps and future needs. *Non-exhaust emissions*, 67-88. Department of Epidemiology, Lazio Region Health Service/ASL Roma 1, Rome, Italy. DOI: [10.1016/B978-0-12-811770-5.00003-0](https://doi.org/10.1016/B978-0-12-811770-5.00003-0)
- [4] Grunig, G., Marsh, L. M., Esmaeil, N., Jackson, K., Gordon, T., Reibman, J., ... & Park, S. H. (2014). Perspective: ambient air pollution: inflammatory response and effects on the lung's vasculature. *Pulmonary circulation*, 4(1), 25-35. DOI: [10.1086/674902](https://doi.org/10.1086/674902)
- [5] Vimercati, L. (2011). Traffic related air pollution and respiratory morbidity. *Lung India: official organ of Indian Chest Society*, 28(4), 238. DOI: [10.4103/0970-2113.85682](https://doi.org/10.4103/0970-2113.85682)
- [6] Bourdrel, T., Bind, M. A., Béjot, Y., Morel, O., & Argacha, J. F. (2017). Cardiovascular effects of

- air pollution. *Archives of cardiovascular diseases*, 110(11), 634–642. DOI: [10.1016/j.acvd.2017.05.003](https://doi.org/10.1016/j.acvd.2017.05.003)
- [7] Polichetti, G., Cocco, S., Spinali, A., Trimarco, V., & Nunziata, A. (2009). Effects of particulate matter (PM(10), PM(2.5) and PM(1)) on the cardiovascular system. *Toxicology*, 261(1-2), 1–8. DOI: [10.1016/j.tox.2009.04.035](https://doi.org/10.1016/j.tox.2009.04.035)
- [8] Cristaldi, A., Fiore, M., Oliveri Conti, G., Pulvirenti, E., Favara, C., Grasso, A., Copat, C., & Ferrante, M. (2022). Possible association between PM_{2.5} and neurodegenerative diseases: A systematic review. *Environmental research*, 208, 112581. DOI: [10.1016/j.envres.2021.112581](https://doi.org/10.1016/j.envres.2021.112581)
- [9] Costa, L. G., Cole, T. B., Dao, K., Chang, Y. C., Coburn, J., & Garrick, J. M. (2020). Effects of air pollution on the nervous system and its possible role in neurodevelopmental and neurodegenerative disorders. *Pharmacology & therapeutics*, 210, 107523. DOI: [10.1016/j.pharmthera.2020.107523](https://doi.org/10.1016/j.pharmthera.2020.107523)
- [10] Pant, P., & Harrison, R. M. (2013). Estimation of the contribution of road traffic emissions to particulate matter concentrations from field measurements: A review. *Atmospheric environment*, 77, 78-97. DOI: [10.1016/j.atmosenv.2013.04.028](https://doi.org/10.1016/j.atmosenv.2013.04.028)
- [11] Guerreiro, C., Leeuw, F., Foltescu, V., et al. (2015). *Air quality in Europe - 2014 report*. European Environment Agency, Publications Office Technical Report No 5/2014. DOI: [10.2800/22775](https://doi.org/10.2800/22775)
- [12] Horálek, J., Guerreiro, C., Viana, M., et al. (2016). *Air quality in Europe - 2016 report*. European Environment Agency, Publications Office, Technical Report No 28/2016. DOI: [10.2800/80982](https://doi.org/10.2800/80982)
- [13] Moshhammer, H., Forsberg, B., Künzli, N., & Medina, S. (2009). Improving Knowledge and Communication for Decision Making on Air Pollution and Health in Europe (Aphekom). *Epidemiology*, 20(6), S232-S233. DOI: [10.1097/01.ede.0000362779.45281.f8](https://doi.org/10.1097/01.ede.0000362779.45281.f8)
- [14] Adamiec, E. (2017). Chemical fractionation and mobility of traffic-related elements in road environments. *Environmental Geochemistry and Health*, 39(6), 1457-1468. DOI: [10.1007/s10653-017-9983-9](https://doi.org/10.1007/s10653-017-9983-9)
- [15] GBoDC, N. (2017). Global Burden of Disease Study 2016 (GBD 2016) disability weights. *Seattle, Washington: (IHME) IfHMaE*.
- [16] Jheng, Y. T., Putri, D. U., Chuang, H. C., Lee, K. Y., Chou, H. C., Wang, S. Y., & Han, C. L. (2021). Prolonged exposure to traffic-related particulate matter and gaseous pollutants implicate distinct molecular mechanisms of lung injury in rats. *Particle and fibre toxicology*, 18(1), 1-16. DOI: [10.1186/s12989-021-00417-y](https://doi.org/10.1186/s12989-021-00417-y)
- [17] Chuang, K. J., Lin, L. Y., Ho, K. F., & Su, C. T. (2020). Traffic-related PM_{2.5} exposure and its cardiovascular effects among healthy commuters in Taipei, Taiwan. *Atmospheric Environment: X*, 7, 100084. DOI: [10.1016/j.aeaoa.2020.100084](https://doi.org/10.1016/j.aeaoa.2020.100084)
- [18] Kaur, S., Nieuwenhuijsen, M. J., & Colvile, R. N. (2007). Fine particulate matter and carbon monoxide exposure concentrations in urban street transport microenvironments. *Atmospheric Environment*, 41(23), 4781-4810. DOI: [10.1016/j.atmosenv.2007.02.002](https://doi.org/10.1016/j.atmosenv.2007.02.002)
- [19] Straffelini, G., & Gialanella, S. (2021). Airborne particulate matter from brake systems: An assessment of the relevant tribological formation mechanisms. *Wear*, 478, 203883. DOI: [10.1016/j.wear.2021.203883](https://doi.org/10.1016/j.wear.2021.203883)
- [20] Yang, L., Li, C., and Tang, X. (2020). The impact of PM_{2.5} on the host defense of respiratory system. *Frontiers in cell and developmental biology*, 8, 91. DOI: [10.3389/fcell.2020.00091](https://doi.org/10.3389/fcell.2020.00091)
- [21] Abating Potentially Dangerous Particles 2.5 µm and Smaller. From: <https://www.semiconductor-digest.com/abating-potentially-dangerous-particles-2-5m-and-smaller/>, accessed on: December 21st, 2022.
- [22] Penetration of Particles into the Human Body. From: <https://seetheair.org/2021/03/01/penetration-of-particles-into-the-human-body/>, accessed on: February 11th, 2023.
- [23] Gonet, T., & Maher, B. A. (2019). Airborne, vehicle-derived Fe-bearing nanoparticles in the urban environment: a review. *Environmental Science & Technology*, 53(17), 9970-9991. DOI: [10.1021/acs.est.9b01505](https://doi.org/10.1021/acs.est.9b01505)
- [24] Sydbom, A., Blomberg, A., Parnia, S., Stenfors, N., Sandström, T., & Dahlen, S. E. (2001). Health effects of diesel exhaust emissions. *European Respiratory Journal*, 17(4), 733-746. DOI: [10.1183/09031936.01.17407330](https://doi.org/10.1183/09031936.01.17407330)
- [25] Wang, G., Jiang, R., Zhao, Z., & Song, W. (2013). Effects of ozone and fine particulate matter (PM_{2.5}) on rat system inflammation and cardiac function. *Toxicology letters*, 217(1), 23-33. DOI: [10.1016/j.toxlet.2012.11.009](https://doi.org/10.1016/j.toxlet.2012.11.009)
- [26] Wold, L. E., Ying, Z., Hutchinson, K. R., Velten, M., Gorr, M. W., Velten, C., ... & Rajagopalan, S. (2012). Cardiovascular remodeling in response to long-term exposure to fine particulate matter air pollution. *Circulation: Heart Failure*, 5(4), 452-461. DOI: [10.1161/CIRCHEARTFAILURE.112.966580](https://doi.org/10.1161/CIRCHEARTFAILURE.112.966580)

- [27] Ying, Z., Xu, X., Bai, Y., Zhong, J., Chen, M., Liang, Y., ... & Rajagopalan, S. (2014). Long-term exposure to concentrated ambient PM_{2.5} increases mouse blood pressure through abnormal activation of the sympathetic nervous system: a role for hypothalamic inflammation. *Environmental health perspectives*, 122(1), 79-86. DOI: doi.org/10.1289/ehp.1307151
- [28] von Mikecz, A., & Schikowski, T. (2020). Effects of airborne nanoparticles on the nervous system: Amyloid protein aggregation, neurodegeneration and neurodegenerative diseases. *Nanomaterials*, 10(7), 1349. DOI: [10.3390/nano10071349](https://doi.org/10.3390/nano10071349)
- [29] Thal, D. R., Grinberg, L. T., & Attems, J. (2012). Vascular dementia: different forms of vessel disorders contribute to the development of dementia in the elderly brain. *Experimental gerontology*, 47(11), 816-824. DOI: [10.1016/j.exger.2012.05.023](https://doi.org/10.1016/j.exger.2012.05.023)
- [30] Calderón-Garcidueñas, L., Reynoso-Robles, R., & González-Maciel, A. (2019). Combustion and friction-derived nanoparticles and industrial-sourced nanoparticles: The culprit of Alzheimer and Parkinson's diseases. *Environmental research*, 176, 108574. DOI: [10.1016/j.envres.2019.108574](https://doi.org/10.1016/j.envres.2019.108574)
- [31] Schikowski, T., & Altug, H. (2020). The role of air pollution in cognitive impairment and decline. *Neurochemistry International*, 104708. DOI: [10.1016/j.neuint.2020.104708](https://doi.org/10.1016/j.neuint.2020.104708)
- [32] Liu, B., Fang, X., Strodl, E., He, G., Ruan, Z., Wang, X., ... & Chen, W. (2022). Fetal Exposure to Air Pollution in Late Pregnancy Significantly Increases ADHD-Risk Behavior in Early Childhood. *International Journal of Environmental Research and Public Health*, 19(17), 10482. DOI: [10.3390/ijerph191710482](https://doi.org/10.3390/ijerph191710482)
- [33] Huber, M. P., Fischer, P., Mamakos, A., Steiner, G., & Klug, A. (2022). *Measuring Brake Wear Particles with a Real-Driving Emissions Sampling System on a Brake Dynamometer* (No. 2022-01-1180). SAE Technical Paper. DOI: doi.org/10.4271/2022-01-1180
- [34] Mathissen, M., Grochowicz, J., Schmidt, C., Vogt, R., zum Hagen, F. H. F., Grabiec, T., ... & Grigoratos, T. (2018). A novel real-world braking cycle for studying brake wear particle emissions. *Wear*, 414, 219-226. DOI: [10.1016/j.wear.2018.07.020](https://doi.org/10.1016/j.wear.2018.07.020)
- [35] Vasiljević, J., Glišović, N., Stojanović, I. I., Grujić (2021). An overview of non-exhaust brake emission measuring methods. 15th International Conference on Accomplishments in Mechanical and Industrial Engineering - DEMI. Banja Luka.
- [36] Park, J., Joo, B., Seo, H., Song, W., Lee, J. J., Lee, W. K., & Jang, H. (2021). Analysis of wear induced particle emissions from brake pads during the worldwide harmonized light vehicles test procedure (WLTP). *Wear*, 466, 203539. DOI: [10.1016/j.wear.2020.203539](https://doi.org/10.1016/j.wear.2020.203539)
- [37] Wahlström, J., Leonardi, M., Tu, M., Lyu, Y., Perricone, G., Gialanella, S., & Olofsson, U. (2020). A study of the effect of brake pad scorching on tribology and airborne particle emissions. *Atmosphere*, 11(5), 488. DOI: [10.3390/atmos11050488](https://doi.org/10.3390/atmos11050488)
- [38] Hagino, H., Oyama, M., & Sasaki, S. (2015). Airborne brake wear particle emission due to braking and accelerating. *Wear*, 334, 44-48. DOI: [10.1016/j.wear.2015.04.012](https://doi.org/10.1016/j.wear.2015.04.012)
- [39] zum Hagen, F. H. F., Mathissen, M., Grabiec, T., Hennicke, T., Rettig, M., Grochowicz, J., ... and Benter, T. (2019). On-road vehicle measurements of brake wear particle emissions. *Atmospheric Environment*, 217, 116943. DOI: [10.1016/j.atmosenv.2019.116943](https://doi.org/10.1016/j.atmosenv.2019.116943)
- [40] Oroumiyeh, F., & Zhu, Y. (2021). Brake and tire particles measured from on-road vehicles: Effects of vehicle mass and braking intensity. *Atmospheric Environment: X*, 12, 100121. DOI: [10.1016/j.aeaoa.2021.100121](https://doi.org/10.1016/j.aeaoa.2021.100121)
- [41] Grigoratos, T., Mamakos, A., Arndt, M., Lugovyy, D., Anderson, R., Hafenmayer, C., ... & Giechaskiel, B. (2023). Characterization of Particle Number Setups for Measuring Brake Particle Emissions and Comparison with Exhaust Setups. *Atmosphere*, 14(1), 103. DOI: [10.3390/atmos14010103](https://doi.org/10.3390/atmos14010103)
- [42] Woo, S. H., Jang, H., Lee, S. B., & Lee, S. (2022). Comparison of total PM emissions emitted from electric and internal combustion engine vehicles: An experimental analysis. *Science of The Total Environment*, 842, 156961. DOI: [10.1016/j.scitotenv.2022.156961](https://doi.org/10.1016/j.scitotenv.2022.156961)
- [43] UN GTR(ECE/TRANS/WP.29/AC.3/59). (2023). *Proposal for a new UN GTR on Laboratory Measurement of Brake Emissions for Light-Duty Vehicles*. UNECE (United Nations Economic Commission for Europe), Informal Working Group on Particulate Measurement Programme, Eighty-seventh session, Geneva.
- [44] 2022/0365 (COD). (2022). *Proposal for a Regulation of the European Parliament and of the Council on Type-Approval of Motor Vehicles and Engines and of Systems, Components and Separate Technical Units Intended for Such Vehicles, with Respect to Their Emissions and Battery Durability (Euro 7) and Repealing Regulations (EC) No 715/2007 and (EC) No 595/2009*. European Commission. Brussels.



Banja Luka
1-2 Jun 2023.

DEMI 2023

16th International Conference on Accomplishments in Mechanical and Industrial Engineering

www.demi.mf.unibl.org



Realizing Priorities for Occupational Safety at Agriculture

M. Lutovska^a, V. Mijakovski^b, S. Kjosevski^a

^aFaculty of Technical Sciences, "Mother Teresa" University, Skopje, MK, str. Mirche Acev 4, Skopje

^bFaculty of Technical Sciences, University „St. Kliment Ohridski“, Bitola, MK, str. Makedonska falanga 37, Bitola

Abstract Given the significant under-reporting of accidents in agriculture across Europe, national reporting still places the sector among the leading sectors in terms of risk. According to Eurostat data, over 500 deaths and more than 150000 injuries per year have been registered on average in the last decade.

The main goal of this paper is to examine the causes of accidents and working conditions among this population, as well as to perceive the priorities for safe work in this still labor-intensive branch, where self-employed farmers are exposed to numerous risks that make their work unsafe. The analyzes were done through a survey that included 120 respondents: owners, family members and workers. The largest number of workers, 63.3%, are men, 35.1% belong to the age group of 46-60 years, and 33.8% of the surveyed farmers have only primary education.

Of particular concern is the fact that 43.5% belonged to the category of family members, which gives the answer to why accidents where children are victims occur very often.

Keywords agriculture, occupational safety, farmers

1. INTRODUCTION

The total equivalent agricultural labor force in the EU estimated by Eurostat is 20.5 million EU workers contributing to production in the sector. However, only 9.7 million are full-time workers, while the rest perform part-time activities [1]. So, in 2020, the number of people employed was 874 million people, or 27% of the global workforce, compared to about 1050 million (40%) in 2000 [2]. As a consequence, the EU's agricultural workforce has decreased by 35% over the last decade, and is projected to decrease to 7.9 million in 2030. In addition to the increasing growth of machinery and technology, this downward trend is also

influenced by the decrease in number of smaller family farms, as well as the interconnected drive for economies of scale through larger, more efficient agricultural holdings [1].

On the other hand, agriculture is known as a hazardous industry worldwide, with major challenges in enumerating the size of the workforce and numbers of accidents at work [3]. The wide variation in agricultural accident statistics as well as numerous inconsistencies in recording are mostly due to under-reporting, differences in interpretation criteria, inadequate social insurance schemes for farmers, family labour and undocumented workers. Given the significant under-reporting of the accidents, national reporting still places the sector among the leading sectors in terms of risk across Europe. According to Eurostat data, over 500 deaths and more than 150000 injuries per year have been registered on average in the last decade. Also, there have been 595 deaths caused by tractor overturns, roughly one every

Corresponding author

Prof. Dr Sc Monika Lutovska
monika.lutovska@unt.edu.mk

Faculty of Technical Sciences, "Mother Teresa" University,
str. Mirche Acev 4, Skopje, North Macedonia

week. Moreover, as many as 54% of these deaths involved farmers over 60 years of age [4]. So, most self-employed farmers are not covered by OSH legislation and are rarely inspected, their occupational accidents and diseases are very rarely reported, so they have limited access to OSH resources and training, or often no resources to invest in new, safer machinery and agricultural infrastructure. One of the main problems because accident data for many categories of workers is excluded from official data is that data reporting to Eurostat is not mandatory for the self-employed and family members in agriculture, as they are not considered 'employees' [5].

However, in 2020, Agriculture, forestry and fishing with 11.4% were the only other Statistical classification of economic activities in the European Community (NACE) sections for which double-digit shares of the total number of fatal accidents in EU were recorded [6].

2. TRADITIONAL HAZARDS IN THE SECTOR

Life on a farm as the unique link between home and workplace allows the coexistence of multiple generations, but at the same time it can also pose a risk to the health, well-being and safety of workers. Children and elderly farmers in particular are at high risk of death and injury on the farm. An aging farm workforce and poor access to medical and OSH services further complicates the situation for workers who are already more likely to work alone [2]. On the other hand, every year, a huge number of young people, under the age of 20, are exposed to the safety hazards associated with working in agriculture. As a result, significant numbers of young people are killed, injured or permanently disabled on farms around the world [7].

By Eurostat (2010), work-related health problems most often occur in the "agriculture, hunting and forestry" sector and are the result of physical work and atypical working hours. Therefore, in an EU survey (2012), these workers were ranked higher than all other sectors in reporting that their work affects their health [5].

In Macedonia, the gradual opening in 2021 increased activities in the real sector, but also the number of accidents at work and accidents with fatal outcome. The rate of deaths at work were 3.77, and the activities of the Household sector as employers, which have a total of 11

accidents of which 4 are fatal, largely include things that would be attributed to the activity of agriculture in 2021. The largest number of accidents in this activity occurred with an agricultural machine - a tractor, during agricultural work, transport or when participating in traffic [8].

That is why agriculture continues to be the riskiest occupation with a death rate about eight times higher than the general employed population [9]. The table 1 below describes common agricultural hazards that give a clear picture and can be used to prevent accidents and avoid workplace injuries [7].

Table 1. Occupational hazards in agriculture

Hazard identified	Description
Mechanical hazards	Being struck by falling or moving objects (machinery, bales, tree trunks)
Moving parts of machinery	Injuries due to hands or clothing being caught in rotating parts of the machine
Transportation accidents	Being run over or overturning of vehicles
Tractor over-turns	Turning on tractors without a roll-over protection structure, or without a properly engaged system
Terrain vehicle injuries	Lack of a rollover protection device in farm vehicles and machinery
Falling from a height or depth	Falling from trees, through roofs, mobile stairs, or into dug trenches, wells
Drowning or sinking into mud	Drowning in water tanks, slurry tanks, grain silos, drowning in mud
Electricity (electrocutions)	Lightning strike, electrocution, improper grounding of machinery
Heat/solar UV exposure	Dehydration, skin burns due to exposure to sunlight/UV which can lead to the most severe skin diseases
Use of organic fertilizers	Emissions of toxic and flammable gases (NH ₃ , CO ₂ , CH ₄) due to composting, organic acids/sulfides, hydrogen sulfide
Pesticides exposure	Higher temperatures, and especially heat waves, can affect workers' susceptibility to pesticide absorption.
Dust exposure	Dust from genetically modified products, inorganic (mineral) dust.
Biological agents' exposure	Use of wastewater and organic fertilizers. Exposure to pathogenic organisms and bioaerosols (excessive moisture and mold) especially indoors.
Presence of reptiles, rodents, animals,	Working outdoors also includes hazards due to exposure to ticks,

insects	rodents, reptiles, animal bites and insect stings
Manual work	Labor-intensive activity that involves manual and heavy physical work, night work or work in the early morning
Musculoskeletal disorders	Ergonomic risks associated with awkward posture, repetitive motions and handling loads when harvesting crops manually
Psychosocial risks, stress and monotony	Climate change, uncertainty and unpredictability, financial pressures, increasing demands on food production.
Atypical working hours	Periodic seasonal work, night or early morning work, work involving most of the family members
Self-employed	Family members, children, adults over 60 years old
Labour market conditions	Self-employed, temporary seasonal workers, family and older workers, part-time work. Limited access to OSH services.
Food, energy and environmental demands	Food waste, changing consumption patterns (organic food, non-GMO, reduced meat consumption and production).
Impact of new digital technologies	Improving the health and safety of farmers who will be able to virtually operate and monitor machines and systems
New techniques/genetic improvement of crops	Increased crop yields and quality (reduced use of fertilizers, pesticides, water and energy use and GHG emissions.
Climate Change	Changing rainfall patterns will impact by further increasing irrigation needs.
Extreme weather events, fires	Floods, fires, extreme weather conditions - unsafe working. Risk of toxic gases, explosions, extreme heat, fires.
Rural crime	Theft of property, livestock and machinery, possible violence, insecurity, insurance costs and economic losses.

However, accepting risks as part of everyday life can be a serious problem due to habituation to the dangers and ceasing to actively seek ways to eliminate or reduce them [9].

3. MATERIAL AND METHODS

The main goal of this paper is to examine the causes of accidents and working conditions among this population, as well as to perceive the priorities for safe work in this still labor-intensive branch, where self-employed farmers are exposed to numerous risks that make their work unsafe. The analyses were done through a

survey that included 120 respondents from rural areas in the western part of North Macedonia: owners, family members and workers, and based on the data obtained from questionnaires and interviews.

The largest number of workers, 63.3%, are men, and only 37.7% belonged to the female gender (Figure 1).

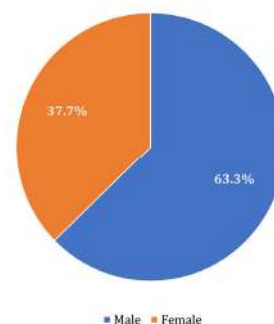


Fig. 1. Gender distribution of surveyed respondents

The age distribution (Figure 2) shows that the labor force in agriculture is relatively middle-aged, and the majority of respondents (35.1%) belong to the age group of 46-60 years.

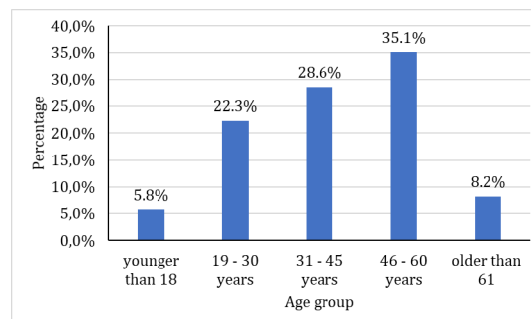


Fig. 2. Age distribution of surveyed respondents

Also, it can be seen that 28.6% belong to the 31-45 years old group, followed by the age group of 19-30 years with 22.3%. The smallest number of agricultural workers, represented by 5.8%, are persons under the age of 18, as well as persons older than 61 with 8.2%.

When it comes to the level of education that agricultural workers have, it is characteristic that more and more farmers with higher education return to the fields and try to realize their ideas by applying modern technologies and digitization of agricultural crop production. According to the survey, their share is 11.4%.

The majority of farmers have high school education (51.5%) participation. Respondents who have not completed any formal education participate with a smaller percentage (3.3%), but the fact that more than 1/3 of this population (33.8%) are farmers with only primary education is particularly worrying (Figure 3).

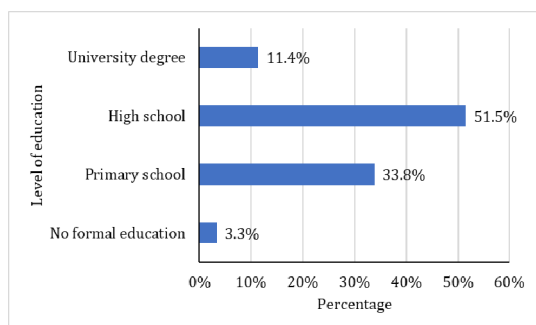


Fig. 3. Level of education of surveyed respondents

Family worker was the most common job position with 50.1%, while the survey results (Figure 4) indicate that 29.6% are farm owners themselves, and 20.3% are seasonal workers.

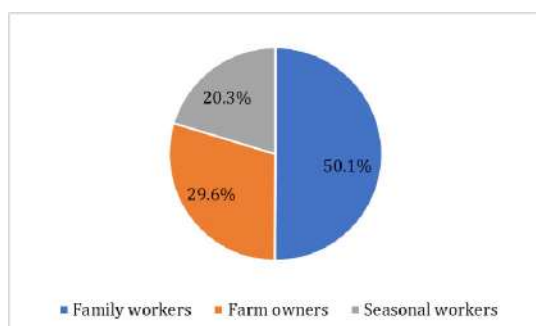


Fig. 4. Job position type of surveyed respondents

Also, of particular concern is the fact that almost half of the workers belonged to the category of family members, which gives the answer to why accidents where children are victims occur very often.

According to the checklist from the survey questionnaire, the most common accidents that happened to the respondents' own farm are listed in the Table 2 below:

Table 2. Types of accidents registered in the survey

Type of accident	Coverage according to the survey questionnaire (%)
Accidents that occurred due to the overturning of a tractor and the crushing of the worker	37.7
Mechanical injuries to the hands or entrapment of fingers during the repair of machines, tractors and other mobile machinery	18.4
Falling from a tree or mobile ladder	17.5
Injuries to the spine while lifting heavy loads or performing manual work	12.2
Leg fractures due to uneven terrain or performing activities at a different height level or falling into a hole	9.1
Traumatized due to stress from accidents that happened on the farm of close family member, where children mostly suffer	2.1
Accidents in which children themselves are the victims	1.9
Lightning strike outdoors	1.1

It is very important to emphasize that among the responses from the survey about injuries experienced or witnessed by the respondents, there is no response that indicates an occupational disease different from a mechanical injury, that requires a longer period of time to be seen the negative effects. Thus, there are no answers about the consequences of exposure to pesticides, organic fertilizers, dust, UV radiation, excessive moisture, mold, atypical working hours (late at night or early in the morning), psychological burdens, stress. This is an indication that people register only the consequences of accidents that are directly visible, but not those that are felt during a longer period of exposure to the hazard.

Herein lie the answers for how low OSH awareness among these workers for the consequences they suffer is, and more worryingly how uneducated this population is, with more than a third of workers having only a primary education. Above all, this is a population marginalized by society, with limited access to rural health services, including OSH health monitoring, as well as OSH advisory support services.

The reasons for such indicators only complement the fact that 60% of agricultural workers are precisely in developing countries,

and only 9% of them are in industrialized countries [10].

4. CONCLUSION

Agriculture is an important sector for the global economy. Between 2000 and 2019, statistics reveal that the global labor value added generated by agriculture, forestry and fisheries combined grew by 73%, reaching \$3.5 trillion in 2019.

Both globally and in Macedonia, increased activities in the real sector in 2021 generate an increase in the number of accidents and deaths, which according to the ILO amounts to 4% of GDP, funds that in poor countries go to compensation for injuries. The losses suffered in this way cost Macedonia more than 400 million euros, which is a staggering number, which in times of health, energy and economic crisis, our fragile economy must not and cannot afford.

In order to reduce the negative impact of agricultural activity on the health of farmers and at the same time to increase social awareness, deeper changes are needed in terms of the way of performing the work, social inclusion, the age structure of the workers, the level of education as well as the application of modern technique and technology in a sustainable and environment friendly way.

Improvements would be aimed at reducing fertilizer use and increasing crop yields and quality, as well as reducing pesticide use by producing crops that are more resistant to pests or diseases. It would also limit the need for water and energy, which would directly affect greenhouse gas emissions. Such measures will ensure a significant improvement in the safety and health of farmers.

On the other hand, the inevitable digitization will have a positive impact on production, but will also result in an increase in the economic gap between small and large farms, a decrease in jobs, a decline in the competitiveness of small family farms, as well as an increase in dependence on large multinational companies.

REFERENCES

[1] EU-OSHA. (2020). *Review on the future of Agriculture and Occupational Safety and Health (OSH)*, Publications Office of the European Union, Luxembourg

[2] FAO. (2021). *Statistical Yearbook 2021 - World Food and Agriculture*, Food and Agriculture Organization of the United Nations, Rome

[3] Merisalu, E., Leppälä, J., Jakob, M., Rautiainen, R.H. (2019). Variation in Eurostat and national statistics of accidents in agriculture. *Agronomy Research*, vol. 17, no. 5, p. 1969-1983. <https://doi.org/10.15159/ar.19.190>

[4] Consejería de economía, hacienda y empleo. (2022). *Análisis de los riesgos emergentes en el empleo verde: una guía práctica*. Instituto Regional de Seguridad y Salud en el Trabajo. Comunidad de Madrid, Madrid

[5] EU-OSHA. (2021). *Agriculture and Forestry: A sector with serious occupational safety and health challenges*, European Agency for Safety and Health at Work

[6] Eurostat. Accidents at work statistics. From: https://ec.europa.eu/eurostat/statistics-explained/index.php?title=Accidents_at_work_statistics#Analysis_by_activity, accessed on: March 11, 2023.

[7] United States Department of Labor. Youth in Agriculture eTool. From: <https://www.osha.gov/etools/youth-agriculture>, accessed on: April 03, 2023.

[8] MZZPR. (2021). *Report on accidents at work. Annual report for 2021*. Macedonian Association for Safety at Work, Skopje

[9] Better Health Channel. Farm safety – risks and hazards. From: <https://www.betterhealth.vic.gov.au/health/healthy-living/farm-safety-risks-and-hazards#bhc-content>, accessed on: April 03, 2023.

[10] ILO. (2000). *Safety and Health in Agriculture. SafeWork, Programme on safety, health and the environment*, Labour Protection Department, Geneva



Banja Luka
1-2 Jun 2023.

DEMI 2023

16th International Conference on Accomplishments in Mechanical and Industrial Engineering

www.demi.mf.unibl.org



Recycling of used engine oil filters in the context of sustainable development

Diana Miruna Armionia^a, Sorin Aurel Rațiu^a, Ioana Ionel^b

^aPolitehnica University of Timișoara, Faculty of Engineering Hunedoara, Revolution Street 5, Hunedoara, 331128, Romania

^bPolitehnica University of Timișoara, Faculty of Mechanical Engineering, Mihai Viteazu Street 1, Timisoara, 300222, Romania

Abstract During the lubrication process of the engine components, a series of contaminants appear that damage the characteristics of the engine oil and reduce the efficiency of the lubrication function. To prevent this, oil filters are used, which separate the particles and purify the lubricant. These filters become hazardous waste once degraded due to the content of engine oil contaminated with dangerous pollutants. In addition to contaminants, they also contain valuable elements that can be recovered. It is therefore recommended to adopt a recycling-based management method. This article briefly shows the process of recovering used oil filters through recycling as a sustainable method of managing this type of hazardous waste.

Keywords oil filters, used engine oil, recycling, hazardous waste, internal combustion engine

1. INTRODUCTION

Due to the constant increase of the demand of vehicles on the global market and of their number, implicitly the quantity of waste generated by the automotive sector also increases. Some of the most common types of such waste are used oil filters.

Car manufacturers, as well as car services, recommend changing the oil filter when changing the oil, at regular intervals, depending on the type of car, the distances traveled between two successive changes or the traffic conditions. The need to regularly change the oil filters is determined by several factors, among which can be mentioned [1]:

- Engine protection: Most current vehicles use "full-flow" filtration systems, in which oil passes directly from the tank to the engine through the filter. This requires increased attention to the quality and condition of the filter, as it is the protective barrier for the engine.

- Reducing the wear of the engine components: a clogged filter leads to the risk of obstruction of the lubrication process. Usually, most filters are designed to avoid such situations, but the passage of oil through the bypass valve, bypassing the filter, also means the passage of contaminants in the engine, which will speed up the wear process for its components.
- Avoiding premature degradation of the new oil: even if only the oil is changed and the used filter is kept, the passage of the new oil through the filter will cause its contamination with the retained impurities and will cause untimely dirt.
- Decreased maintenance costs: the price of an oil change and a new filter will always be lower than the repair costs required for malfunctions caused by the operation of the used oil and filter engine.

For these reasons, oil filters are changed frequently, which means the accumulation of

significant amounts of such waste. The car services are obliged by law to collect separately the hazardous waste (category in which the used oil filters also fall), in order to be subsequently taken over by specialized companies and transported to be recovered. The storage of oil filters in landfills is discouraged, due to the high risk of environmental pollution, as well as the economic value that this waste has.

This paper aims to describe oil filters, offer an overview of the recycling methods for used filters, as well as highlighting the advantages of this process, from both ecological and economic perspectives.

2. GENERAL NOTIONS REGARDING OIL FILTERS

During engine operation, the properties of the oil gradually change, with hard mechanical impurities entering the oil, composed of calamine and metal particles that occur due to wear of the parts, as well as tars and oxidation products. In order to prevent the engine lubrication from being affected by impurities, oil filters (figure 1) must be inserted into the lubrication system.



Fig. 1. General structure and main components of an engine oil filter [2]

The role of oil filters is to purify the oil, maintaining its qualities for a longer period of time and to prevent the penetration of mechanical impurities between the surfaces in contact, in relative motion. They must meet the following requirements [3]:

- constant filtration efficiency, at different engine operating conditions;
- increased operating time;
- low hydrodynamic resistance to oil passage, even if the filter is partially clogged or the oil is cold;
- resistance to high oil pressures, when the oil is cold;
- small size;
- being cheap and easy to maintain.

The process of filtering engine oil is relatively simple (figure 2). The oil enters the filter through the radial holes, is forced to pass through the filter element and then is discharged through the central hole of the filter. To prevent the oil pressure from rising from the filter, if the filter is loaded with impurities, it contains a safety valve that opens and allows the oil to flow directly out of the filter without being filtered [3].

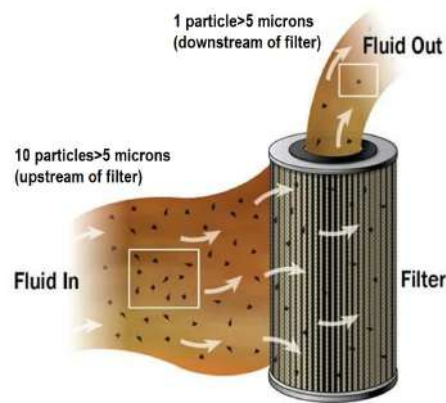


Fig. 2. Scheme of the oil filtration process [4]

Filters are classified according to the following criteria:

- By the size of the impurities retained [5]:
 - coarse filters, which retain particles up to 40 μm . Also called full flow oil filters, this type filters 100% of the engine's oil at full pressure and at a fairly rough level;
 - fine filters, which retain particles up to 1-2 μm . They are known as bypass oil filters and are able to filter a small percentage of the engine's oil at a time, at a lower pressure, and a finer level.
- By the filtration process:
 - static filters;
 - dynamic filters.

3. PROCESSING USED OIL FILTERS FOR RECYCLING

Due to the high content of used engine oil, used oil filters must be processed very carefully. In this sense, a series of current application recycling technologies have been developed by different companies around the world, which allow both the recovery of engine oil extracted from filters and the metal part.

Used oil filters contain three main components: the metal housing, the filter element (made of cellulose or plastic) and the used engine oil. Following the recycling process, these components can be separated and recovered individually.

3.1 Recycling process

In the past, oil filters were not considered a material with recycling potential because of the large volume of residual oil remaining in discarded filters and the small tonnage generated compared to the demand for steel scrap on the market. However, recycling methods for used engine oil have ensured the possibility for its recovery and the current environmental legislation encourages oil-filter recycling, with several countries having banned landfilling of oil filters.

Various processes are available for transforming used oil filters into ferrous scrap. Some of the processes are designed to be performed by the oil filter generator, while others can only be done by a scrap or waste processor. The selection of the process depends upon a number of factors, such as environmental regulations of the respective country or region, capital available for equipment, and the consumer's requirements [6].

The simplest method of recycling used oil filters involves crushing them in order to remove the used oil (by draining), followed by shredding of the crushed filter, to separate the filter element and possible waste oil residues. Finally, the shredded product is sent to companies that use scrap as a raw material, used oil is collected by specialized companies and sent to recycling plants, and the filter element (paper or plastic) is recovered energetically, by incineration. The simplified technological flow of this process is presented in figure 3.

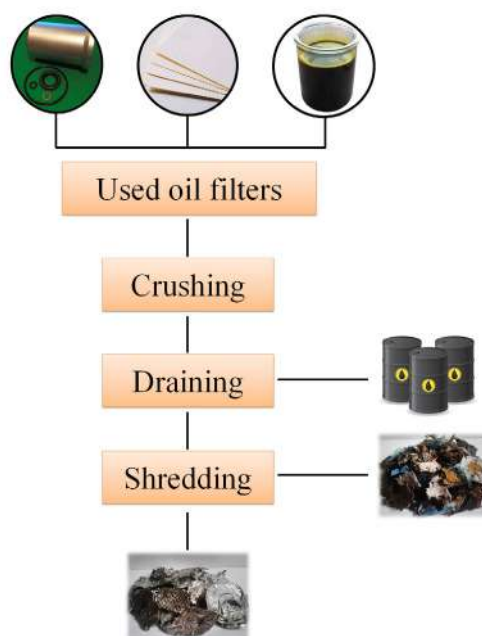


Fig. 3. Simplified technological flow of the oil recycling process

Studies have shown that the recovery rate of this process for used engine oil is 80% and for ferrous waste 100% [6]. Other recycling methods include: gravity draining, punched dome draining, dismantling, crushing, shredding, pyrolysis, direct burning, and various combinations of the above [7].

3.2 Case study: Lucas Lane Inc.

Lucas Lane Inc. is an American company specialized in the recycling of automotive oil filters. The recycling plant recovers approximately 2650 liters of used oil per load of processed filters. During processing, 100 percent of materials are recovered and the entire process is eco-friendly [8].

The process starts where new filters replace the used ones at "generators" sites, such as auto shops, which collect the used filters for Lucas. Once the generators accumulate about 250-300 filters, Lucas Lane employees pick them up and bring them to the recycling plant.

There, the used filters are stored in a concrete bin with specially made drainage pits which collect any dripping oil from the waiting filters. The filters are then placed in a machine which crushes them into eight-inch cubes weighing

roughly 15 kg each. At this stage, 10 percent of their weight is still waste oil (figure 4 a).

After approximately 9000 kg of filters have been crushed, the cubes are loaded into the main chamber of the thermal processing unit, where the filters are slowly heated up to 700° C over 20 hours (figure 4 b). Waste oil is reclaimed during the first nine hours of the heating. During the remaining time, the thermal oven vaporizes the remaining waste oil and carbonizes the rubber gaskets and paper (figure 4 c).



a



b



c

Fig. 4. Aspects from the waste oil recycling process at Lucas Lane Inc. [9]

In the secondary chamber, the oil vapor and smoke are heated to 925° C, burning them up with only heat vapors coming out of the stack. The entire process is 100 percent green. Of the 2650 liters of waste oil Lucas Lane reclaims, about 750 of them are used to fuel the next cycle of thermal processing, and the remaining 1900 is sold to a waste oil recycler for use in the production of asphalt. The premium scrap steel, now entirely separated from the oil, is sold to a steel mill where it is reused [9].

3.3 Advantages of recycling used engine oil filters

The benefits of recycling used oil filters extend both ecologically and economically. Among them, we can mention:

- Avoiding the storage of oil filters in landfills, due to the increased risk of contaminating the environment;
- Recovery of scrap metal and its reintegration into the industrial circuit;
- Ensuring the possibility of recycling the used engine oil that the filters contain, thus avoiding pollution with this type of hazardous waste;
- Energy recovery of the used filter element (filter paper), thus saving other types of fuel and avoiding an additional source of pollution;
- Reducing production costs for recovered metal and recycled engine oil, which can successfully replace new materials, while avoiding pollution associated with the steel and oil industries;
- Respecting the principles of the circular economy, ensuring the development of a sustainable society.

4. CONCLUSIONS

In conclusion, used oil filters represent a waste with high economic value, but also with a high pollutant potential. Environmental legislation prohibits their storage in landfills and encourages finding other management methods. For this reason, it is necessary to recycle them.

In this regard, a number of recycling technologies have been developed, which follow, in general, the stages of collection, crushing, oil drainage, shredding and, possibly, compaction to facilitate transport. The recovered oil is sent to recycling plants to be

treated and transformed into base oil. The filter paper is either incinerated during the heat treatment process of the metal housings of the filters, or extracted and used as fuel. Recycling used oil filters has multiple advantages, both from an economic and ecological perspective and is a process that deserves further exploration and optimization.

REFERENCES

- [1] Champion Auto Parts. How often does your oil filter need to be replaced? From: <https://www.championautoparts.eu/news/how-often-change-oil-filter.html>, accessed on March 6, 2023.
- [2] Comline Auto Parts. Oil Filters. From: <https://www.comline.uk.com/products/oil-filters>, accessed on March 6, 2023.
- [3] Rațiu, S., Alexa, V. (2017). Sisteme auxiliare ale autovehiculelor rutiere. Editura Politehnica, Timișoara.
- [4] Machinery Lubrication. Understanding Filter Efficiency and Beta Ratios. From: <https://www.machinerylubrication.com/Read/1289/oil-filter-efficiency>, accessed on March 6, 2023.
- [5] Filter Supplies. What you need to know about the most common types of filters. From: <https://filtersupplies.com.au/blog/what-you-need-to-know-about-the-most-common-types-of-filters/>, accessed on March 6, 2023.
- [6] Peaslee, K.D. (1994) Recycling Used Automotive Oil Filters. *JOM*, vol. 46, no. 2, p. 44–46. DOI: [10.1007/BF03222557](https://doi.org/10.1007/BF03222557)
- [7] Peaslee, K.D., Roberts, D.E. (1997) Characterization of used automotive oil filters for recycling. *Resources, Conservation and Recycling*, vol. 19, no. 2, p. 81-91. DOI: [10.1016/S0921-3449\(96\)01182-2](https://doi.org/10.1016/S0921-3449(96)01182-2)
- [8] Lucas Lane Inc. Oil filter recycling business helps local man, environment. From: <https://www.howdoyourecycleoilfilters.com/award-press/>, accessed on March 6, 2023.
- [9] Lucas Lane Inc. How Do You Recycle Oil Filters? <https://www.howdoyourecycleoilfilters.com/how-do-you-recycle-oil-filters/>, accessed on March 6, 2023.



Banja Luka
1-2 Jun 2023.

DEMI 2023

16th International Conference on Accomplishments in Mechanical and Industrial Engineering

www.demi.mf.unibl.org



The influence of the crosswind on the lift coefficient, vehicle stability and safety

N. Stojanovic^a, I. Grujic^a, B. Boskovic^b

^aUniversity of Kragujevac Faculty of Engineering, Sestre Janjic 6, 34000 Kragujevac, Serbia

^bAcademy of professional studies Šumadija, Department in Trstenik, Radoja Krstica 19, 37240 Trstenik, Serbia

Abstract *The unadjusted speed of the vehicle, as well as the influence of the lateral wind, are one of causes of traffic accidents. Affected by lateral wind, vehicles have tendency of lateral sliding or drifting, which further affects on the stability during the vehicle control. The aim of this paper is to show, how the lateral wind, as well as the angle of direction of lateral wind, influence on the change of the lift force. Were conducted three virtual experiments, when lateral wind don't exist, and when it acts on the vehicle under angles 45° and 90° with the speed of 25 km/h. The increment of the lift force leads to the disturbance of stable movement of the vehicle in given exploitation conditions. By increment of the wind acting angle, when the wind don't exist and when it acts on the vehicle under angle 90°, the lift force grows approximately 3.6 times, in respect to the case when lateral wind don't exist, that is, when the vehicle is in the peaceful environment without wind.*

Keywords *vehicle, stability, safety, lift force, lateral wind*

1. INTRODUCTION

During the vehicle drive, appears the lift force, which actually represents the vertical component of the air resistance, which tends to reduce the pressure between the contact of the vehicle tyres and road. This causes the reduced steerability on the steering axle, while on the drive axle reduces the drive force. All depending from the distribution of the lift force, on front and rear axle, the lift force will cause the vehicle pitch [1]. Depending from the vehicle tendency of lifting, during the drive with higher speeds, the lift force can influence on the maintaining of straight-line driving [2]. Besides that, it makes

the vehicle more sensitive to the crosswind. The lift force, has the greatest influence, during the drive with higher speeds, what is characteristic for sport cars.

The crosswind can influence on the vehicle safety in the traffic, that is on the appearance of traffic accidents, which influence increases with the increment of the vehicle speed, as well as with the increment of the speed of the crosswind [3, 4]. However, to the greater disturbance of the vehicle stability comes, as well and during the drive with lower speeds, if the acting angle of the crosswind is greater. The crosswind can be present on the viaducts, bridges, or during overtaking large trucks, during driving out of the forested areas, and when the vehicle finds in such situations, can come to it lateral sliding [5], rotation around the vertical axis [6], and even to the roll-over [7], Figure 1. The great number of researches is based on findings, which are the key factors, which can reduce the sensitivity on the

Corresponding author

Ph.D., Ivan Grujic
ivan.grujic@kg.ac.rs

University of Kragujevac Faculty of Engineering
Sestre Janjic 6,
34000 Kragujevac, Serbia

crosswind. By increment of the vehicle mass, wheelbase, the inertial moment of lateral turn of, can be achieve convenient influence on the vehicle stability [8]. Also, and the shape of the rear side of the vehicle influences on the vehicle stability [9]. Besides the shape of the rear side of the vehicle, influence have and the vehicle length during the turning of, because with the increment of the length, comes to the increment of the lift force [10]. Also, and the correct adjustment of the vehicle suspension, can improve the vehicle stability in the driving conditions, where on the vehicle acts crosswind. The position of the aerodynamic centre of pressure (CP), in respect to the centre of gravity (CoG), and neutral steering point (NSP) of steering, are crucial for the projecting of such vehicle, which will be stable in the conditions with crosswind [11, 12], Figure 2. While the reference point is on the middle, between the CoG and NSP, that is, on the middle of the wheelbase.

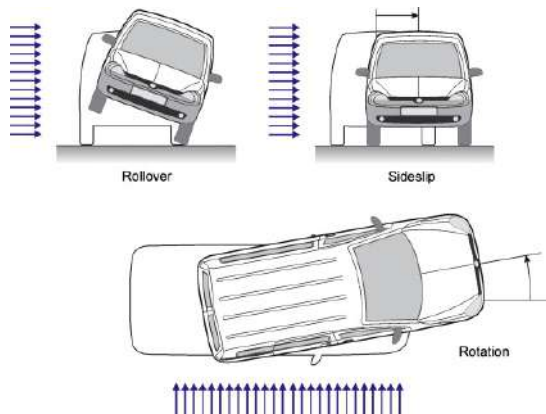


Fig. 1. The influence of the crosswind on the vehicle [6]

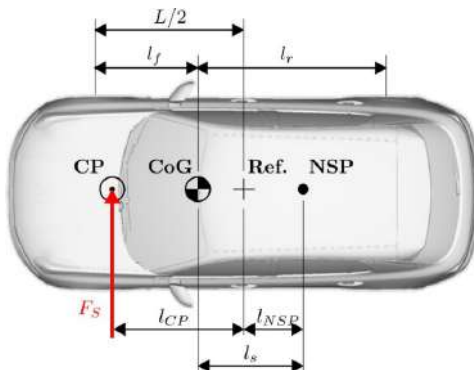


Fig. 2. The position of the pressure centre, gravity centre, reference point and neutral point on the vehicle [8]

The subject of this research is based on the determination of the influence of the crosswind on the vehicle stability, as well as, how the increment of the angle with which crosswind acts on the vehicle, influences on the vehicle lift coefficient, as well as on the lift coefficient of front and rear axle.

2. THREE-DIMENSIONAL MODEL AND BOUNDARY CONDITIONS

The analysis of the vehicle stability for the different conditions of crosswind acting, as well as for the case when the crosswind don't exist, will be performed in Ansys software package, Fluid Flow CFX module. The first necessary step is to create the model of the vehicle. Vehicle was created in its real size, and as such, it was used for the analysis, Figure 3. The next step covers the defining of the space around the vehicle, and after that the definition of the finite elements mesh. The finite element mesh is defined as such, that the smallest elements are along the surface of the vehicle, while the element size rises with increment of the distance from the surface of the vehicle, Figure 4. The next step is the defining of the boundary conditions – input parameters. Input parameters are divided in two groups, and that:

- The characteristics of the environment air, and
- The exploitational characteristics of the vehicle.



Fig. 3. 3D model of the vehicle

Within the air characteristics were defined the ambient pressure ($p=101325$ Pa), ambient temperature ($T=25$ °C) and air density ($\rho=1.225$ kg/m³). While within the vehicle exploitation characteristics were defined vehicle speed, which amounts $v=33.33$ m/s, as well as the speed and direction of crosswind, if exist. In order to simplify the analysis, the

wheels of the vehicle do not rotate. The value of turbulences is not defined, but instead is used Low (Intensity=1%).

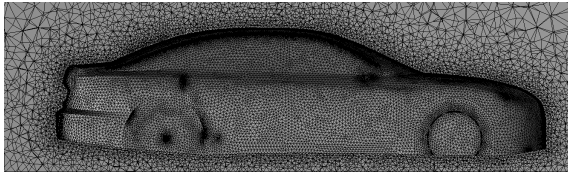


Fig. 4. The mesh

In the paper will be performed three analyses, and that:

1. When the vehicle is driven in the peaceful environment, without the crosswind, and the vehicle speed is 33.33 m/s;
2. The case when the vehicle speed is 33.33 m/s, and on it acts crosswind under angle of 45°, which speed is 6.94 m/s (Figure 5), and
3. The case when the vehicle speed is 33.33 m/s, and on it acts crosswind under angle of 90°, which speed is 6.94 m/s (Figure 5).

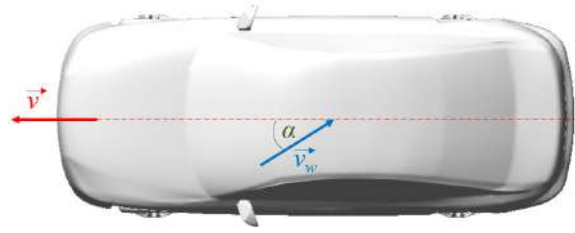


Fig. 5. Defining of the speed and direction for the vehicle and the wind

3. RESULTS AND DISCUSSION

No matter if the vehicle is driven in the peaceful environment, or in the environment where on it acts wind, it comes to the appearance of vortex, behind the rear side of the vehicle, Figure 6. In the case, when on the vehicle acts the wind, it comes to the greater air vortexes, than in case, when the wind doesn't exist. Also, it can conclude, that with the increment of the wind acting angle, increase and vortex behind the vehicle, Figure 6. If observe the vehicle from the top side (Figure 6), it can see, that in the case when the crosswind acts on the vehicle, it comes to the interweaving of vortex streamlines, that is, it comes to the trespass of streamlines from left side to the right, and vice versa. While in the case, when the vehicle is in the environment without wind, the behaviour of vortex streamlines is almost identical, in respect to the middle plane.

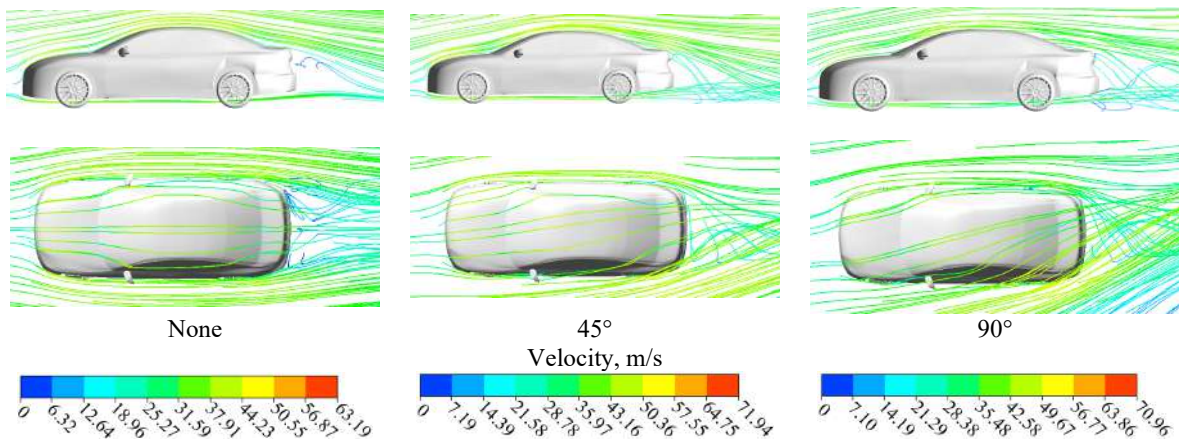


Fig. 6. The path and speed of the air around the vehicle

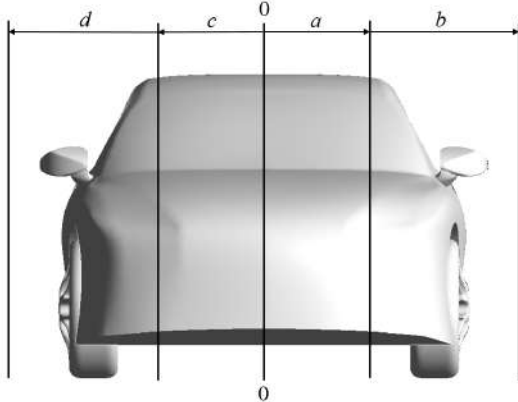
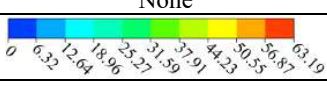
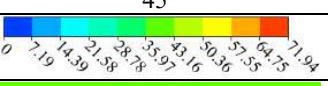
















In Table 1, illustratively is shown the speed of the air around the vehicle in defined planes (see Table 1). The null plane (0-0), represents the middle plane of the vehicle. When on the vehicle

don't acts wind, behind the vehicle, at the height of the vehicle trunk, don't exist air movement, while in the cases when on the vehicle acts crosswind, this phenomena moves down,

beyond the vehicle, which further causes the reduced lift on the rear axle, and increased lift on the front, and by this causes decreased steerability, Table 1. This will be later confirmed and by analysis of lift coefficients for the front and rear axle. By observing the vehicle for the case without crosswind, for planes *a* and *c* (which are at the same distance from middle plane, and that 0.5 m), the behaviour of air flow is almost the same. The same applies and for planes *d* and *b*, which distance from the middle plane is 1.2 m. However, this is not the case, when on the vehicle acts crosswind. For the

case, when the acting angle of the crosswind is 45°, in the plane *a* behind the rear end of the vehicle, comes to the greater drop of the air speed, than in plane *c*. While, above the vehicle, the air speed is greater for the plane *a*, than for the plane *c*. In the plane *b*, at the side where acts the wind, comes to greeter air speeds, and this is not the case for the plane *d*. Which further can cause the vehicle instability, as well as its drift, during some sudden manoeuvre. The same behaviour can be noticed and for the case when the acting angle of the wind is 90°.

Table 1. The air speed in different planes around the vehicle

			
	None	45°	90°
			
0-0			
<i>a</i>			
<i>b</i>			
<i>c</i>			
<i>d</i>			

The highest values of the pressure were recorder for the case without the crosswind, that is when the vehicle is driven in peaceful

environment, and it appears on the frontal surface of the vehicle, which first hits the air. Almost the same behaviour, pressure has and

for the case when the acting angle of the wind is 45° . While when the acting angle of the wind is 90° , the maximal value of the pressure appears on the right side of the frontal surface of the

vehicle. Also, is increasing the pressure on the side where wind acts on the vehicle.

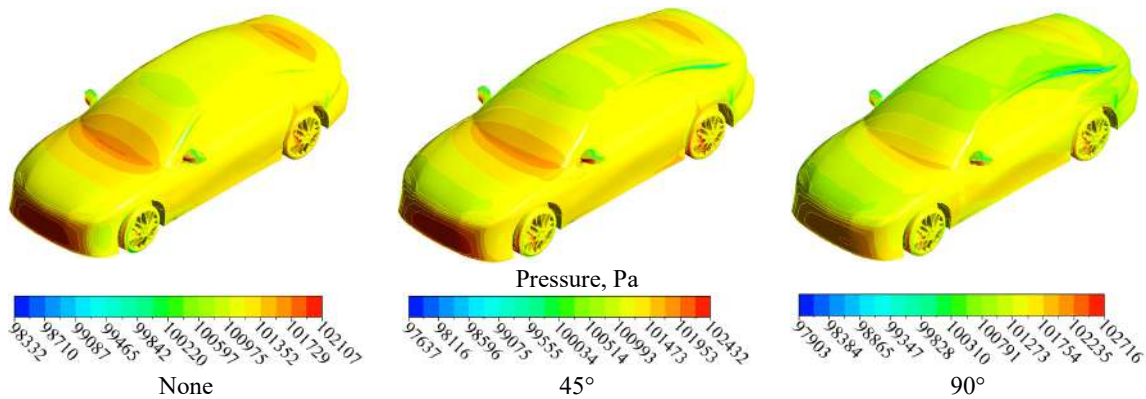


Fig. 7. Pressure distribution on the vehicle surface

The lift coefficient is greater for the case with the crosswind, in respect to the case without crosswind, Figure 8. While with the increment of the acting angle of the crosswind, it rises and the lift coefficient for the front axle. This can cause the reduced steerability, or even worse the loss of contact between the front tyres and road, and the same finding was found when the air speed was observed. This is very inconvenient, especially in the cases of accidental situations, because in the case of some sudden maneuverers can come to the vehicle stability disturbance.

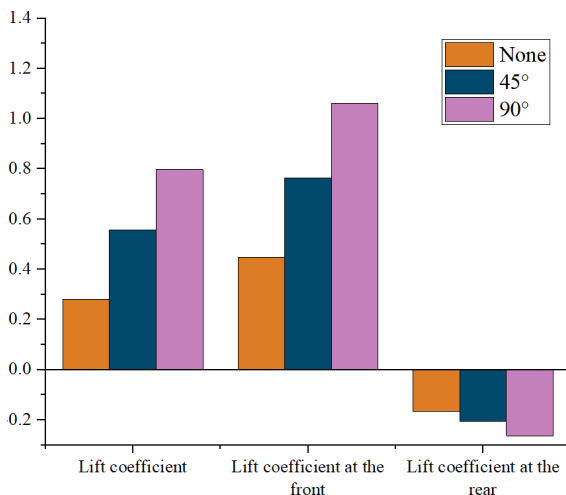


Fig. 8. The vehicle lift coefficient, lift coefficient for the front axle and lift coefficient for the rear axle

Also, in the case, when emergency stopping is necessary, the brake force on the front axle will be decreased. The reduced contact between the front tyres and the road, as well as the value of the force of the crosswind (Figure 9), can cause loss of the vehicle control, in the case of some sudden manoeuvre.

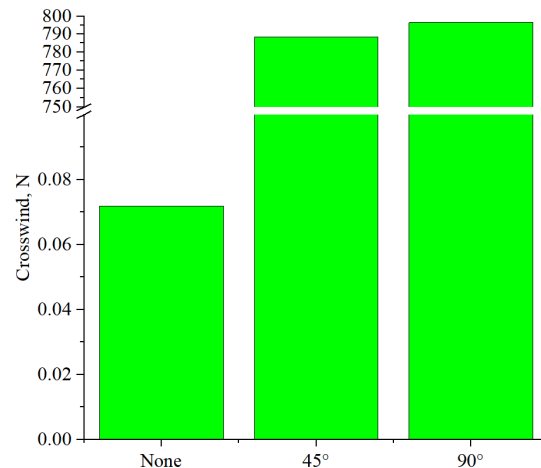


Fig. 9. The crosswind force value

4. CONCLUSION

For safe vehicle driving, that is, for safe participation in the traffic, it is very important, not to come to the vehicle stability disturbance at any moment. By analysis of the influence of crosswind on the lift force value, can conclude that with the increment of the crosswind acting angle, rises the lift force, that is, rises the lift

coefficient. The values of crosswind force, for crosswind acting angles 45° and 90° , are almost the same. So, in the conditions, when the crosswind acts on the vehicle, it is very important, not to do sudden maneuvers, because this will have a negative effect on the vehicle stability, as well as on the safety of the driver and other traffic participants. In future researches, should take into the consideration, the change of the vehicle speed, as well as the speed of the wind, and to investigate how will this affect on vehicle stability, all with the aim to determine the safety of all traffic participants, for the case, when the crosswind acts on the vehicle.

Acknowledgement

This paper was realized within the framework of the project "The research of vehicle safety as part of a cybernetic system: Driver-Vehicle-Environment", ref. no. TR35041, funded by the Ministry of Education, Science and Technological Development of the Republic of Serbia.

REFERENCES

- [1] Janković, A. (2008). *Vehicle Dynamics*. Faculty of Mechanical Engineering, Kragujevac.
- [2] Howell, J., Good, G.L. (1999). The influence of aerodynamic lift on high speed stability. *SAE Technical Paper*, vol. 108, p. 1008-1015.
- [3] Walczak, S. Analysis of vehicle dynamics under sudden cross. *Scientific Conference on Automotive Vehicles and Combustion Engines (KONMOT 2016)*, 22-23 September 2016, Krakow, p. 148. DOI: [10.1088/1757-899X/148/1/012030](https://doi.org/10.1088/1757-899X/148/1/012030).
- [4] Singh, M.G., Nagpurwala, Q., Abdul N., Shankapal, S. (2009). Numerical investigations on crosswind aerodynamics and its effect on the stability of a passenger car. *SAE Technical Paper*, p. 2009-26-0059. DOI: [10.4271/2009-26-0059](https://doi.org/10.4271/2009-26-0059).
- [5] Wang, Y., Zhang, Z., Zhang, Q., Hu, Z., Su, C., (2021). Dynamic coupling analysis of the aerodynamic performance of a sedan passing by the bridge pylon in a crosswind. *Applied Mathematical Modelling*, vol. 89, no. 2, p. 1279-1293. DOI: [10.1016/j.apm.2020.07.003](https://doi.org/10.1016/j.apm.2020.07.003).
- [6] Batista, M., Perković, M. (2014). A simple static analysis of moving road vehicle under crosswind. *Journal of Wind Engineering and Industrial Aerodynamics*, vol. 128, p. 105-113. DOI: [10.1016/j.weia.2014.02.009](https://doi.org/10.1016/j.weia.2014.02.009).
- [7] Kim, S.J., Yoo, C.H., Kim, H.K. (2016). Vulnerability assessment for the hazards of crosswinds when vehicles cross a bridge deck. *Journal of Wind Engineering and Industrial Aerodynamics*, vol. 156, p. 62-71. DOI: [10.1016/j.weia.2016.07.005](https://doi.org/10.1016/j.weia.2016.07.005).
- [8] Brandt, A., Jacobson, B., Sebben, S. (2021). High speed driving stability of road vehicles under crosswinds: an aerodynamic and vehicle dynamic parametric sensitivity analysis. *International Journal of Vehicle Mechanics and Mobility*, vol. 60, iss. 7, p. 2334-2357. DOI: [10.1080/00423114.2021.1903516](https://doi.org/10.1080/00423114.2021.1903516).
- [9] Volpe, R., Ferrand, V., Silva, A.D., Moyne, L.L. (2014). Forces and flow structures evolution on a car body in a sudden crosswind. *Journal of Wind Engineering and Industrial Aerodynamics*, vol. 128, p. 114-125. DOI: [10.1016/j.weia.2014.03.006](https://doi.org/10.1016/j.weia.2014.03.006).
- [10] Howell, J., Windsor, S., Passmore, M. (2021) Some observations on shape factors influencing aerodynamic lift on passenger cars. *Fluids*, vol. 6, no. 1, p. 44. DOI: [10.3390/fluids6010044](https://doi.org/10.3390/fluids6010044).
- [11] Favre, T., Näfver, J.J., Jerrelind, J., Trigell, A.S., Efraimsson, G. (2017). Static coupling between detached-eddy simulations and vehicle dynamic simulations of a generic road vehicle model with different rear configurations in unsteady crosswind. *International Journal of Vehicle Design*, vol. 72, no. 4, p. 332-353. DOI: [10.1504/IJVD.2016.082384](https://doi.org/10.1504/IJVD.2016.082384).
- [12] Buchheim, R., Maretzke, J., Piatek, R. (1985). The control of aerodynamic parameters influencing vehicle dynamics. *SAE Paper*, vol. 94, no. 2, p. 626-639.



Banja Luka
1-2 Jun 2023.

DEMI 2023

16th International Conference on Accomplishments in Mechanical and Industrial Engineering

www.demi.mf.unibl.org



The influence of the hydrogen injection parameters on the combustion process of IC engine

I. Grujic^a, N. Stojanovic^a, M. Petrovic^a

^aUniversity of Kragujevac Faculty of Engineering, Sestre Janjic 6, 34000 Kragujevac, Serbia

Abstract *In order to determine the best injection parameters of hydrogen, an experimental work was performed. The test engine was equipped with the installation for the hydrogen supply, and it was tested how the injection timing and number of injection influence on the combustion process. As the control parameters were taken the engine working stability, as well as the indicating efficiency. It was determined that the injection parameters, significantly influence on the engine working cycle, as well as on the combustion process. The adequate injection timing as well as the adequate number of injections, is crucial, for maintaining the stable work of the IC engine, as well as for indicating efficiency. In order to provide the stable engine work, with the satisfying indicating efficiency, it is necessary provide multiple injections, more accurate two injections, where one serves to provide the adequate amount of fuel for the working cycle, while the second serves to slowdown the combustion process.*

Keywords *IC engine, hydrogen, combustion process, injection parameters*

1. INTRODUCTION

The global concern about the ecology, as well as about the fuel crisis, have forced the engineers to think about the alternatives, which can be used instead the crude oil. In most cases, the electric vehicles are presented as the future of the people mobility. However, the electrification of the entire vehicle park of the world, still has many obstacles, which should overcome. First obstacle is the potential of the production of the electric energy, necessary for the supply and charge of the electric vehicle batteries, as well as necessary infrastructure for this. Second is the recycling of the batterie materials. Then we

have the question, do we have enough materials, necessary for the production of the electric vehicle's components. These obstacles impose the question, how can provide the sustainability of the IC engines. The answer is quite simple, it should give more attention to the alternative fuels, which are more ecologically friendly, and to see the possibility of their usage. Many substances can be successfully used as the substitution for the conventional fuels, and that:

- Natural gas;
- Petroleum gas;
- Alcohols;
- Biofuels;
- Reformulated fuels;
- Hydrogen;

Corresponding author

Ph.D, Nadica Stojanovic
nadica.stojanovic@kg.ac.rs

University of Kragujevac Faculty of Engineering
Sestre Janjic 6
Kragujevac, Serbia

Fuel which in most cases is presented as so-called the fuel of the future is hydrogen. The hydrogen is present in the entire universe, but almost never in free form, as the single chemical

element. The main advantage of the hydrogen is its chemical composition, that is, the hydrogen doesn't have carbon in its chemical composition, how the other fuels have. This theoretically means, that is impossible the appearance of harmful components, such are the carbon-monoxide (CO) and unburnt-hydrocarbons (HC).

Because of the mentioned, many researchers work on the subject of hydrogen use as the fuel for IC engines. In most cases, the main problem of hydrogen use, are the high temperatures caused by the high combustion speed [1], and some of the solutions for this undesirable phenomenon are the Exhaust Gas Recirculation (EGR), water injection, blending biodiesel and ignition delay. It is important to say, that more and more researches are focused on the hydrogen direct injection. The main reason for this are the many limitations of the port fuel injection [2], such are pre-ignition, knocking, backfiring, low volumetric efficiency and compression loss problems. All these limitations cause the limitation of engine achievable load and efficiency. Also, many times, the hydrogen use is considering as the fraction of mixture with different fuels. For example, the addition of the hydrogen as the additive, significantly can be influenced on the engine performances [3]. By increment of the hydrogen volume fraction, the knock resistance is enhanced because of the hydrogen high knock resistance and high octane number. Also, this increase causes and the increment of the peak of the heat release rate and of the cylinder pressure. One of the main reasons, why hydrogen in most cases is considered as the additive, and not as the only fuel, is its influence on the formation of nitric-oxygens (NO_x). The high amount of hydrogen in mixture leads to the increment of the NO_x [4]. This happens due to the high combustion speed, and by this due to the high combustion temperature. So, the main idea is to use mixture, where other fuel will decrease this undesirable phenomenon. By considering many factors such are trend of mitigating climate change worldwide, the contribution of a widespread, reliable and affordable propulsion technology like the IC engine is, it can be said that the future use of IC engines can be very significant, once when the usage of conventional fuels reduces, with the increased use of alternative fuels such is hydrogen. However, it still stays to see how to resolve some of most important

things, and that are the availability and production of hydrogen, as well as its safe storage and use [5].

The aim of this paper was to investigate how the injection parameters influence on the combustion process and by that on the IC engine working cycle of the fueled only by hydrogen.

2. EXPERIMENTAL WORK

In order to see how the injection parameters influence on the IC engine combustion process, the experimental work was conducted. For the investigation, it was modified the experimental test engine. The basic variant of test engine was diesel engine. For the experimental work, engine was equipped with the ignition system. Also, it was equipped with the gas installation, which scheme and main components can be seen on the Figure 1.

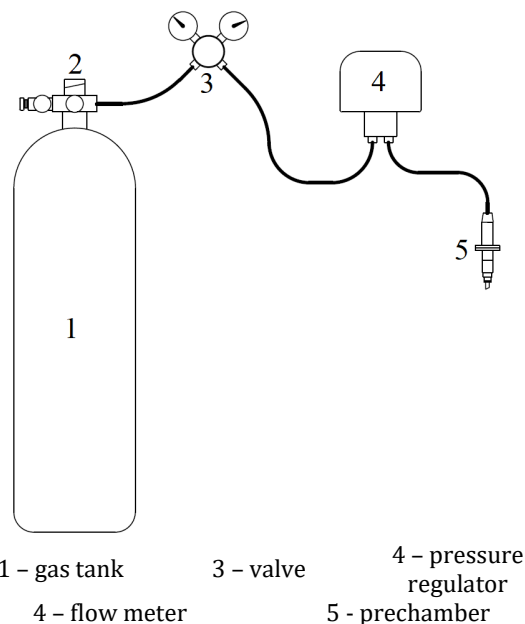


Fig. 1. Gas installation

The main part of the gas installation is the prechamber, which was made to have the same overall dimensions as the diesel injector, so it was mounted instead the diesel injector. In the prechamber were mounted the spark plug, as well as the Gasoline Direct Injection (GDI) injector, which was used for the injection of the hydrogen. The reason for the use of the prechamber, was the idea to stratify the mixture, in order to reduce the combustion

speed of the hydrogen. This was made, because of the fact, that the hydrogen combustion speed is the greatest for the case of the stoichiometric mixture, while lean and rich mixture decrease the hydrogen combustion speed significantly [6]. So, by the use of the prechamber, and injection into it, the mixture in prechamber will be always rich, while the mixture in the cylinder will be always lean. By the addition of the prechamber, it was increased the compression volume, and decreased the compression ratio. The compression ratio was first reduced at 13.3:1, but it was found that this value is too high, and due to this, it was replaced and piston so the compression ratio was reduce to 10.4:1. The scheme of the modified engine is shown on the Figure 2, while the engine specifications before and after modifications are given in Table 1.

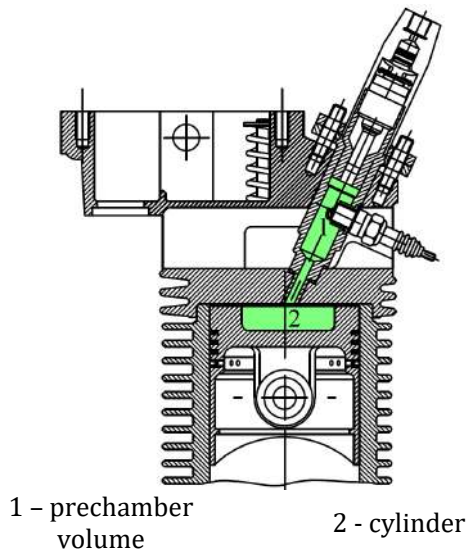


Fig. 2. Modified engine working space

Table 1. Test engine specifications

Name	Value before modification	Value after modification	Unit
Engine bore	85	85	mm
Engine stroke	80	80	mm
Number of cylinders	1	1	-
Displacement	454	454	cm ³
Compression ratio	17.5:1	10.4:1	-

In order to see, how the injection parameters influence on the combustion process, a several injection strategies were tested, and that:

- Injection during the intake stroke;
- Simultaneous injection and combustion;
- Dual-stage injection;

The exact injection parameters are given in Table 2.

Table 2. Injection parameters

Test no.	First injection start, ° BTDC	First injection duration, ms	Second injection start, ° BTDC	Second injection duration, ms
1	344	12	-	-
2	30	12	-	-
3	200	7.2	30	4.8

3. RESULTS AND DISCUSSION

After the conducted experimental work, from the cylinder pressure it was calculated the heat release rate, Figure 3, which also represents and combustion speed.

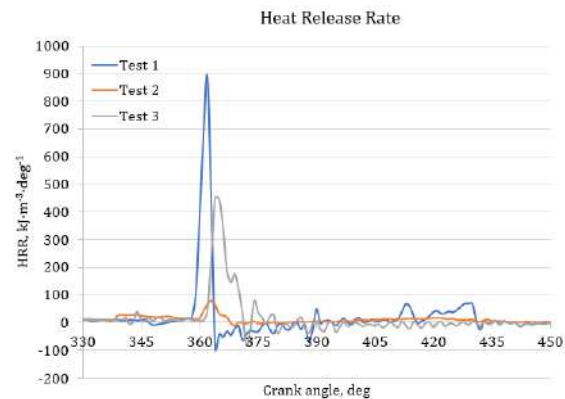


Fig. 3. Heat release rate

It was found that the injection parameters, significantly influence on the combustion process. By observing the Figure 3, it can be said that by earlier injection of hydrogen, rises the combustion speed. The reason for this is the formation of more homogenous mixture. The higher combustion speed is followed with better performances due to the higher maximal pressures in the cylinder. However, also it has its negative sides. First of all, during the Test 1 (injection during the intake stroke), it was very hard to start engine with this approach. The reason for this is a slow engine speed, which allows enough time for the formation of the explosive mixture, which in several case have turned the

engine direction, end caused engine stop. Also, during this test, quite often was present the backfire. The reason for this is because was opened the intake valve, and hydrogen exited into the intake port, after which the HHO gas was formatted, which exploded in intake port. Every explosion was followed with pressure wave, which have disabled the intake of air for next cycle, and this caused the unstable engine work. The Test 2 (simultaneous injection and combustion) have shown as the worst one. During this test, it was impossible to achieve engine load as well as stable regime. Also, the combustion was stretched, what can be seen and from the cumulative heat release, Figure 4.

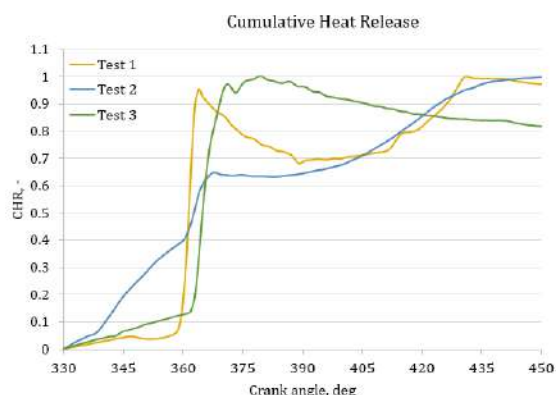


Fig. 4. Cumulative heat release

The stretched combustion is specific by low indicating efficiency which in this case was 22%, while in other two cases was 36% for Test 1, and 34% for Test 3. It can be seen that the center of the combustion (50% of burned mass) is closest to the Top Dead Centre for the Test 1, and due to this, this Test gave the best indicating efficiency.

However, as the best injection parameters, can be ranked the injection parameters used during the Test 3. In this case, the greatest part of the first injection was during the compression stroke, when the intake valve was closed, so in this way, it was avoided the appearance of backfire, and by this was maintained the stable engine work. The role of the second injection was to slow down the combustion, and this was achieved. By slowing down the combustion, are avoided extreme pressure rises ratios, as well as great combustion temperatures. Which means, that this approach is good and from the side of the performances, as well as from the side of the emission, because high temperatures are followed with the rise of NO_x, which is the main pollutant in the case of the hydrogen use.

CONCLUSION

It was conducted the experimental investigation of the combustion process, during the engine work with a hydrogen as only fuel. It was found that the injection parameters significantly influence on the combustion process, and by that on the engine work. The best performances can be achieved by early injection, but this can lead to the unstable work, and great mechanical loads. Simultaneous injection and combustion is not recommendable, because doesn't exist enough time for mixture formation, which leads to the stretched combustion and low efficiency. The best solution is multiple injection, where one injection should be during the compression stroke, in order to avoid the backfire, while the second should be defined around the TDC, in order to enrich the mixture, and to slow down the combustion.

ACKNOWLEDGEMENT

This paper was realized within the framework of the project "The research of vehicle safety as part of a cybernetic system: Driver-Vehicle-Environment", ref. no. TR35041, funded by the Ministry of Education, Science and Technological Development of the Republic of Serbia.

REFERENCES

- [1] Aggarwal, A., Yadav, S., Singh, K., Verma, A.S., Chhabra, S. (2022). Study of utilization of hydrogen as fuel in internal combustion engine. *CIRP Annals - Manufacturing Technology*, vol. 64, no. 3, p. 1211-1216. DOI: [10.1016/j.matpr.2022.03.660](https://doi.org/10.1016/j.matpr.2022.03.660)
- [2] Yip, H.L., Srna, A., Yin Yuen, A.C., Kook, S., Taylor, R.A., Yeoh, G.H., Medwell, P.R., Chan, Q.N. (2019). A review of hydrogen direct injection for internal combustion engines: towards carbon-free combustion. *Applied Sciences*, vol. 9, no. 22, p. 4842. DOI: [10.3390/app9224842X](https://doi.org/10.3390/app9224842X)
- [3] Fu, Z., Li, Y., Chen, H., Du, J., Li, Y., Gao, W. (2022). Effect of hydrogen blending on the combustion performance of a gasoline direct injection engine. *ACS Omega*, vol. 7, no. 15, p. 13022-13030. DOI: [10.1021/acsomega.2c00343](https://doi.org/10.1021/acsomega.2c00343)
- [4] Ali, G., Zhang, T., Wu, W., Yhou, Y. (2020). Effect of hydrogen addition on NO_x formation mechanism and pathways in MILD combustion

- of H₂-rich low calorific value fuels. *International Journal of Hydrogen Energy*, vol. 45, no. 15, p. 9200-9210. DOI: [10.1016/j.ijhydene.2020.01.027](https://doi.org/10.1016/j.ijhydene.2020.01.027)
- [5] Onorati, A., Payri, R., Vaglieco, B.M., Agarwal, A.K., Bae, C., Bruneaux, G., Canakci, M., Gavaises, M., Günthner, M., Hasse, C., Kokjohn, S., Kong, S.C., Moriyoshi, Y., Novella, R., Pesyridis, A., Reitz, R., Ryan, T., Wagner, R., Zhao H. (2022). The role of hydrogen for future internal combustion engines. *International Journal of Engine Research*, vol. 23, no. 4, p. 483-695. DOI: [10.1177/14680874221081947](https://doi.org/10.1177/14680874221081947)
- [6] Gong, C., Jang, M., Bai, X.S., Liang, J.J., Sun, M.B. (2017). Large eddy simulation of hydrogen combustion in supersonic flows using an Eulerian stochastic fields method. *International Journal of Hydrogen Energy*, vol. 42, no. 2, p. 1264-1275. DOI: [10.1016/j.ijhydene.2016.09.017](https://doi.org/10.1016/j.ijhydene.2016.09.017)

Quality and Ecology



Banja Luka
1-2 Jun 2023.

DEMI 2023

16th International Conference on Accomplishments in Mechanical and Industrial Engineering

www.demi.mf.unibl.org



Business Process Re-Engineering for Sustainable Business Processes

M. Rajić^a, B. Šumaković^a, P. Milosavljević^a, Z. Kostić^a

^aUniversity of Niš, Faculty of Mechanical Engineering, Street: Aleksandra Medvedeva 14, Niš, Republic of Serbia

Abstract *Business process reengineering represents an approach for improving the performance of an organization. Having in mind the necessity of optimizing the existing business processes in order to minimize losses and to operate in more sustainable way, it is important to present to small and medium sized enterprises (SME) the fundamental improvements in organizational design. The aim of the study is to analyse the important factors and challenges for BPR in SME application. The comprehensive literature review shows that various factors should be introduced and analysed for BPR application and which factors can affect process performance. Six domains were recognized as limitations for BPR implementation: support of management, technology competence, process design, project planning, change management as well as project management. The survey done in SME in Serbia shows the readiness for innovative approach in organizational performance improvement. The study emphasized the factors that would allow BPR to be implemented with a wider application in different sectors, industries, and regions.*

Keywords *business process reengineering, sustainable processes, implementation of business process reengineering*

1. INTRODUCTION

Business Process Reengineering represents a management approach that aims to improve organizational performance by redesigning business processes. Business Process Reengineering also represents a comprehensive methodology that involves rethinking the entire business process to identify opportunities for improvement. The primary focus of Business Process Reengineering is on the elimination of non-value-added activities and the

simplification of the remaining processes to increase efficiency and effectiveness. Business Process Reengineering aims to break down silos, reduce bureaucracy, and eliminate redundant processes by redesigning business processes from scratch.

Business Process Reengineering was first introduced by Michael Hammer and James Champy [1]. The authors argued that traditional business practices were outdated and inefficient and that radical changes were necessary to compete in the global market. The concept of Business Process Reengineering quickly gained attention, and many organizations began to adopt this approach to improve their operations.

Authors [1] introduced Business Process Reengineering as a radical approach to improving organizational performance by

Corresponding author

PhD, Assistant Professor, Milena Rajić
milena.rajic@masfak.ni.ac.rs

Department of Management in Mechanical Engineering
Faculty of Mechanical Engineering University of Niš
Aleksandra Medvedeva 14, Niš, Republic of Serbia

fundamentally rethinking and redesigning business processes. The authors argued that organizations must move away from traditional ways of doing business and adopt a more innovative and flexible approach to remain competitive in the global market. Since then, numerous research has been conducted on Business Process Reengineering, exploring different aspects of the approach. Some researchers have focused on the benefits of Business Process Reengineering, arguing that it can lead to significant improvements in organizational performance, such as cost reduction, increased efficiency, and improved quality [2,3]. Others have examined the challenges of implementing Business Process Reengineering, highlighting issues such as resistance to change, lack of commitment from senior management, and inadequate resources [4,5]. These challenges can impede the success of Business Process Reengineering initiatives and require careful planning and management to overcome.

Several researchers have also explored the role of information technology (IT) in Business Process Reengineering. IT can enable organizations to automate and streamline processes, reduce errors, and enhance data analysis [6,7]. However, the successful implementation of IT requires careful planning and management to ensure that it aligns with the organization's overall strategy and goals. Recently, researchers have also examined the impact of Business Process Reengineering on organizational culture and employee attitudes. Business Process Reengineering requires a change in mindset and culture, which can be challenging for employees who are accustomed to traditional ways of doing business [8]. However, Business Process Reengineering can also create opportunities for employees to contribute to the redesign process and enhance their job satisfaction and motivation [9]. In addition, other studies have identified the importance of involving employees in the redesign process to ensure buy-in and successful implementation [10].

Moreover, several studies have examined the impact of Business Process Reengineering on organizational performance. For example, a study [11] found that Business Process Reengineering led to significant improvements in operational performance, such as reduced cycle time and improved quality. Another study

[12] found that Business Process Reengineering led to improvements in customer satisfaction and financial performance.

However, there have also been criticisms of Business Process Reengineering. Some scholars have argued that Business Process Reengineering can lead to job losses and decreased employee morale, especially if the redesign process is not managed effectively [13]. Moreover, some studies have found that Business Process Reengineering can be difficult to implement successfully, especially if organizations do not have a clear understanding of their business processes or lack the necessary technological infrastructure [14]. The paper analyses the important factors and challenges for BPR in SME application. The survey done in SMEs in Serbia shows the readiness for innovative approach in organizational performance improvement.

2. APPLICATION OF BUSINESS PROCESS REENGINEERING FOR SUSTAINABLE BUSINESS PROCESSES

Sustainable business processes are crucial for business success in the long run as they provide short-term benefits and long-term positive impacts on the environment, society, and economy. Business Process Reengineering can be used to create sustainable business processes by incorporating environmental and social considerations into the redesign process. Business Process Reengineering can reduce the use of natural resources by identifying the processes that consume the most energy and water and redesigning them to reduce their impact on the environment. For instance, a company that produces plastic bottles can use Business Process Reengineering to redesign its production process to reduce the amount of plastic used, thus reducing the company's carbon footprint [1,5,10, 15].

Business Process Reengineering can also improve social responsibility by creating more equitable and fair business practices. Business Process Reengineering can be used to redesign the supply chain to ensure that suppliers are treated fairly and ethically. Business Process Reengineering can also streamline the hiring process to reduce discrimination and increase diversity in the workplace [1,16].

Another way in which Business Process Reengineering can create sustainable business

processes is by increasing the use of renewable energy. Business Process Reengineering can identify areas where renewable energy can replace non-renewable sources, such as solar panels for electricity and biomass for heating [1, 15-20].

Business Process Reengineering provides several benefits for sustainable business processes. First, Business Process Reengineering can reduce waste and increase efficiency, resulting in cost savings for the business. Second, Business Process Reengineering can improve the company's reputation by demonstrating environmental and social responsibility. Third, Business Process Reengineering can improve employee morale and motivation by creating a workplace that values sustainability and ethical practices [20,21].

3. BUSINESS PROCESS REENGINEERING APPLICATION IN SMEs

The successful implementation of Business Process Reengineering requires careful planning, strategic decision-making, and effective leadership. Small and medium-sized enterprises (SMEs) face unique challenges when implementing Business Process Reengineering due to their limited resources, financial constraints, and lack of expertise [22].

Important Factors for Business Process Reengineering application in SMEs are seen as: (1) Leadership and commitment. Effective leadership and commitment from management are critical factors for successful Business Process Reengineering implementation in SMEs [23]. Management must be willing to support the changes and provide the necessary resources and training to employees.

(2) Process understanding. SMEs need to have a thorough understanding of their business processes to identify areas for improvement and redesign [23]. SMEs can achieve this by conducting process mapping exercises, analysing data, and consulting with employees.

(3) Technology and information systems. The effective use of technology and information systems can improve the efficiency and effectiveness of BPR in SMEs [24]. The use of automation, cloud-based solutions, and other technological tools can simplify business processes and increase productivity.

(4) Communication and training. Effective communication and training are crucial to ensure that employees understand the changes and are willing to adopt new processes [23]. SMEs need to provide training and support to employees to ensure they have the necessary skills and knowledge to implement the changes.

In order to analyse implementation of Business Process Reengineering, especially in SMEs, the challenges should be identified. First of all, limited resources and expertise. SMEs often lack the resources and expertise required to implement Business Process Reengineering successfully [24]. SMEs may not have the financial resources to hire consultants or invest in technology and may not have the necessary expertise in-house. Secondly, resistance to change. Resistance to change is a common challenge in BPR implementations, and SMEs are no exception [25]. Employees may be resistant to change due to fear of job loss, uncertainty, or lack of understanding. Then, time and cost constraints. SMEs face time and cost constraints when implementing BPR due to limited resources and financial constraints [26]. SMEs may not have the luxury of time to test and refine new processes or may not have the financial resources to invest in new technology or hire consultants. And also lack of formal processes. SMEs often lack formal processes or standard operating procedures, which can make it challenging to identify and redesign processes [27]. SMEs may need to invest in process mapping exercises and consulting to develop formal processes.

Even though Business Process Reengineering is a popular management approach that focuses on improving business processes by redesigning them from the ground up, there are some significant limitations that should be identified, especially in SMEs application. Resistance to change is one of the major limitations for BPR implementation [28]. Employees may be resistant to change due to fear of job loss, uncertainty, or lack of understanding. Management must work to overcome resistance to change by providing training, communication, and support to employees. For SMEs is typical that there are limited resources. Business Process Reengineering implementation requires significant resources, including financial resources, time, and expertise [29]. Many organizations may not have the resources to

invest in Business Process Reengineering, which can limit the effectiveness of the approach. Then, one of the most common the lack of leadership and commitment. Business Process Reengineering implementation requires strong leadership and commitment from management [28]. If management is not fully committed to the process, it can be difficult to achieve the desired results. This can result in a lack of motivation and support from employees, which can further limit the effectiveness of Business Process Reengineering.

Lack of integration with technology is certainly present, especially in SMEs. Business Process Reengineering implementation often requires the integration of new technology and information systems [29]. If the organization does not have the necessary technology infrastructure, it can be difficult to implement Business Process Reengineering effectively. This can limit the organization's ability to automate processes and improve efficiency.

Inadequate process understanding is certainly the most important limitation. Inadequate process understanding can limit the effectiveness of Business Process Reengineering implementation [28]. If the organization does not have a thorough understanding of its current processes, it can be difficult to identify areas for improvement and redesign. This can result in ineffective Business Process Reengineering implementation.

And one of the most significant is lack of flexibility. Business Process Reengineering implementation requires flexibility to adapt to changing circumstances [29]. If the organization is not flexible, it may not be able to adjust to changes in the environment, which can limit the effectiveness of Business Process Reengineering.

4. IMPLEMENTATION OF BUSINESS PROCESS REENGINEERING IN SERBIA AND WESTERN BALKAN

Business Process Reengineering has become increasingly important for organizations in Serbia and the Western Balkan region as they seek to improve their competitiveness and adapt to rapidly changing market conditions. While there is limited research on the implementation of Business Process Reengineering specifically in this region, several

studies have examined the broader context of organizational change and improvement.

One of the key challenges for organizations in Serbia and the Western Balkan region is the legacy of socialist-era bureaucratic structures and processes. This has led to a culture of resistance to change, a lack of entrepreneurial spirit, and a focus on process compliance rather than innovation and customer satisfaction. As a result, many organizations in the region have struggled to compete in the global marketplace [30,31].

In recent years, there has been increasing recognition of the need for organizational change and improvement in the region. For example, the Serbian government has launched a series of initiatives aimed at improving the business environment and attracting foreign investment. These initiatives include simplifying administrative procedures, reducing bureaucracy, and improving the efficiency of public services. In addition, several studies have examined the implementation of Business Process Reengineering in specific organizations in Serbia and the Western Balkan region. For example, a study [32] examined the implementation of BPR in a Serbian company in the construction sector. The authors found that the redesign process led to significant improvements in efficiency, productivity, and customer satisfaction. Another study [33] examined the implementation of Business Process Reengineering in a Serbian retail company. The authors found that the redesign process led to improvements in customer satisfaction, employee motivation, and financial performance.

Despite these successes, there are also several challenges to the implementation of Business Process Reengineering in Serbia and the Western Balkan region. These include a lack of awareness and understanding of the Business Process Reengineering approach, a lack of expertise and experience in redesigning business processes, and a lack of support from senior management [34]. To address these challenges, organizations in the region need to invest in education and training for employees and managers, build partnerships with experts and consultants who have experience in Business Process Reengineering, and create a culture of innovation and continuous improvement. In addition, there is a need for government support and incentives to

encourage organizations to adopt Business Process Reengineering and other organizational change initiatives.

5. ASSESSMENT OF READINESS FOR BUSINESS PROCESS REENGINEERING IN SERBIA

In dynamic business conditions, market globalization, increasing standards set by competition on one side and demands from consumers on the other, companies are forced to constantly improve, adapt, or radically redesign their business processes through reengineering. The subject of this master's thesis is an analysis of the extent to which companies in Serbia are ready to apply business process reengineering. This is initiated in companies when the level of existing business processes does not fully satisfy the achievement of the company's mission and vision. The aim of the research is to answer the question of whether there are any limitations to the application of the process of reengineering and what the employees' attitude towards the changes brought by reengineering is. An empirical survey was used for research with thirty-one questions grouped into four areas [35]. The questions and statements from the survey made it possible to determine whether reengineering has been implemented in companies so far, whether there is a need for its application in the future, and what the relationship is between top management and employees regarding the reengineering process. The research results showed that reengineering of business processes is being implemented in companies in Serbia, but in most cases, for less than two years. Top management in companies consider themselves sufficiently professional to carry out and plan the reengineering process. In addition, awareness has been developed that one of the most important conditions for the successful implementation of reengineering is the motivation of employees. One of the key problems is that employees cannot quickly and clearly see the changes brought by reengineering.

The survey questionnaire used to assess readiness consists of 31 questions. Of these, three questions are open-ended, while all others are closed-ended, with the possibility of adding answers for certain questions if they are not covered by the provided options.

The open-ended questions relate to opinions on what led to the success or failure of reengineering, improvements, or certain risks in business. Respondents are allowed to provide their own answers based on their experience, in order to make the results more specific in terms of illustrating real situations in companies.

To measure attitudes and opinions regarding the attitude of managers towards reengineering, other employees, their role, and motivation to participate in changes, the Likert scale was used. A choice of three levels of agreement was offered: agree, partially agree, and disagree, and they were assigned numerical values in order 2, 1, and 0, respectively.

The owners of companies, as well as employees, were contacted by email with a questionnaire explaining why it is necessary to answer the questions in the survey. Data collection lasted for a month and during that time, 35 companies operating in the territory of the Republic of Serbia in Piroć, Niš, Kruševac, Jagodina, Požarevac, Belgrade, Novi Sad, Baćki Jarak, Indija, and Kać were contacted. During that time, the completed questionnaire was sent from 22 companies. Based on those responses, an analysis was performed and presented.

The analysis of the research was conducted on a sample of 22 companies, whose owners, directors, or business unit managers completed a questionnaire. Companies from various industries were included in the research in order to reach a more complete analysis and possibly observe the connection between the application of reengineering in certain business processes and a certain type of activity (Fig.1). More than half of the companies that participated in the survey have been operating on the market for more than 5 years, as many as 73% (Fig.2). As far as the ownership structure is concerned, thirteen companies are domestically owned, eight companies are foreign, while only one of the surveyed companies is under mixed ownership. The Fig. 2 and 3 show the length of business and the company's ownership structure as a percentage.

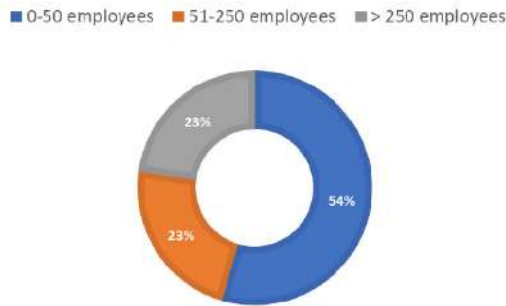


Fig. 1. Business system of the companies that participated in the research

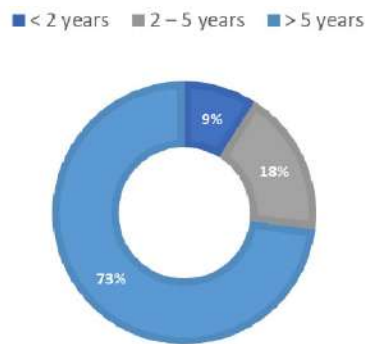


Fig. 2. The length of time a company has been in the market

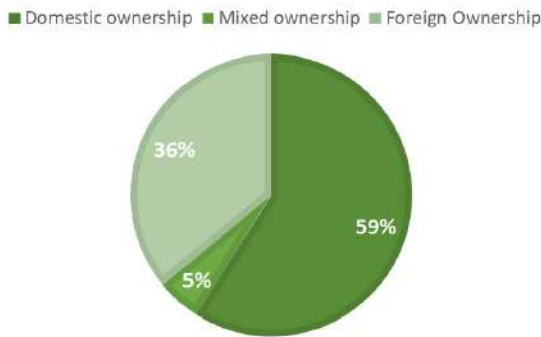


Fig. 3. The ownership structure of the company

Application of ISO (International Organization for Standardization) standards in business greatly increases the competitiveness of companies and products. International standards help harmonize the technical specifications of products and services and reduce barriers to international trade. Standards ensure that consumers feel more confident that the products they use are safe, high-quality, effective and do not harm the environment. Among other things, international standards are strategic tools that represent

guidelines for companies in modern business and the challenges it brings. They enable business to be more efficient, more productive and easier to conquer new markets. In this context, an examination was also carried out to see if the companies apply some of the ISO standards and if the reengineering of business processes was done for the purpose of harmonizing with some of them.

From the Fig.4 shown, it can be seen that companies in Serbia mostly apply ISO 9001, which refers to the implementation of the Quality management system, followed by ISO 14001, ISO 45001, while ISO 50001, which refers to the energy management system, has little application, almost none. . Also, we can see that there are still companies that do not apply international standards in their operations. These companies are both domestically and foreign-owned and belong to the group of small and medium-sized companies. One of the important steps in their further business should be alignment with international standards.

The future reengineering of business processes in all companies would necessarily have to include changes in terms of energy management in view of the upcoming changes in the world market, if companies want to engage in responsible and sustainable business and keep up with the times and competition.

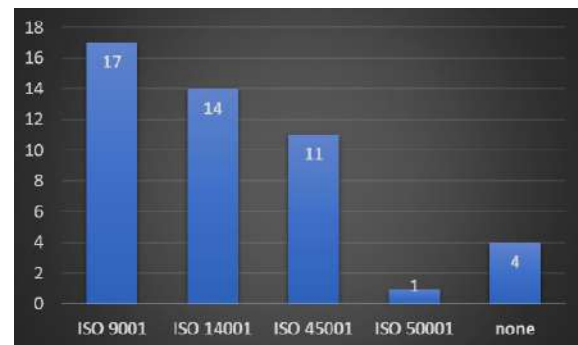


Fig. 4. Application of ISO standards in the surveyed companies

Within the companies that participated in the research, according to the claims of their owners, directors or managers of business units, the process of reengineering has been applied in nineteen companies, while in three it has not been applied.

From the Fig.5, it can be seen that in the majority of examined cases, reengineering is

applied for less than 2 years. It has been applied for more than 5 years in less than one third of the surveyed companies. This data leads to the conclusion that in a relatively small number of companies in Serbia, reengineering is applied over a longer period of time.

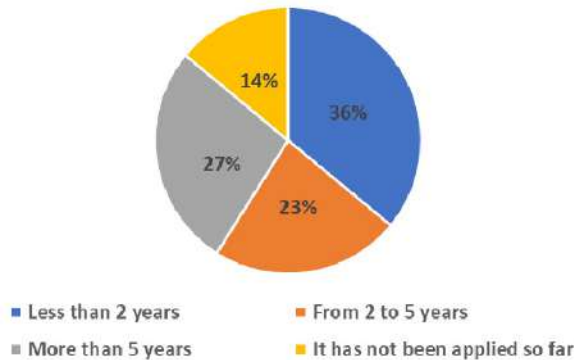


Fig. 5. Period of application of reengineering in the surveyed companies

Table 1. Business processes in which reengineering was done

Business processes in which reengineering was done	Representation of processes in reengineering (%)
Production	50
Technology	41
Maintenance	36
Procurement	32
Quality Control	32
Marketing	23
Logistics	18
Finance	9
No reengineering done so far	14

If the ownership structure of companies is analysed, where reengineering has been applied for more than 5 years, it can be seen that 66% are mostly foreign companies, only one is purely domestically owned. At domestic companies, in approximately 90% of cases, reengineering is carried out in less than 2 years. And if, on the other hand, we take into account the total length of business of the company, this data does not change significantly, because only 12% of them have been operating for less than 2 years. Therefore, in the Serbian market, domestically owned companies are only

recently starting the process of reengineering in order to follow world market trends.

Based on the provided data (Table 1), it can be seen that in companies where reengineering was done, it was mostly present in the area of production and technology. Radical changes were also made in the maintenance, procurement and quality control sector in more than a third of the companies. So far, the least changes have been made in the financial sector. According to the provided data, on the question whether the planned results of reengineering were achieved, 79% of respondents agree that the results were achieved.

As many as 95% of respondents believe that the company's management is professional and motivated enough to develop procedures and set standards for the transformation of business processes. This can be assessed as one of the most important assumptions on which the future outcome of improvements and radical changes that will be made in companies will depend.

One of the most common things that arises in response to the question of what the success of reengineering depended on is the motivation of employees and their engagement and cooperation. This is another proof of how important it is to cultivate a positive business culture in the company in order to achieve the desired changes and for the company to operate successfully.

Also, here we meet with the statement of how important it is that the owner or in general the initiator of the reengineering process has a clear vision and goal of what he wants to achieve with reengineering.

Current situation in companies and possible needs for reengineering are also given:

- 86% of respondents answered that they agree with the fact that the company sees a need for business process redesign - currently or in the near future.
- 79% answered that they agree that the executives believe that the reengineering process should be carried out.
- 67% of respondents believe that consumers influence the initiation of the reengineering process.
- 81% of respondents agree that competition encourages the application of reengineering.

According to the obtained results, it can be concluded that companies feel the need for reengineering and that managers are ready to implement the process. In addition, it can be seen that the competition affects the improvement and monitoring of market trends more than the consumers do.

Table 2. Business processes that need to be improved by reengineering

Business processes in which reengineering was done	Representation of processes in reengineering (%)
Production	64
Quality Control	64
Technology	55
Maintenance	50
Procurement	45
Marketing	32
Logistics	32
Finance	9

If Table 2 is compared with Table 1, where reengineered processes are presented, it can be seen that the production process is still at the top of the table as one of the most important ones that should be constantly improved, as well as technology. Quality control is at the top of the table this time and we conclude that this is the sector in which business process reengineering is being carried out and will be carried out in the coming period. In addition, there is a noticeable difference and the emphasis on maintenance and logistics as segments in which more work is done and in which work will be done on the redesign of business processes. The only sector in which there is no greater expression for changes is the financial sector.

Building on the question of which business process should be improved by reengineering, the question was also raised as to why reengineering of the mentioned business processes should be done.

Analysing the given answers, it can be concluded that the main reason for the reengineering of business processes, cited by as many as 91% of respondents, is the improvement of the quality of existing products and services, followed by the saving of material

resources, which was stated by 73% of respondents, and the rational use of human resources (68%). As two more important reasons for the reengineering process, which were declared by more than half of the respondents, are achieving a competitive advantage and increasing productivity (59%).

Lack of employee motivation and resistance to change, according to respondents, may be the main reasons for not meeting set goals. In addition, respondents believe that vaguely defined goals and results that are not immediately visible can also be an obstacle in achieving the planned results.

The attitude of employees towards business process reengineering is also given:

- 64% of respondents agree that employees are motivated to participate in business process reengineering;
- 52% of respondents agree that employees can quickly and clearly see the results of planned changes;
- 90% of them agree that training and education of employees is required;
- 60% of respondents say that conferences, seminars, trainings are organized for the education and training of employees;
- 86% of respondents agree that employees can express opinions and observations at any time;
- 76% of the respondents say or agree that employees' opinions are taken into account when planning changes in the business system;
- 57% agree that there is resistance to change among employees.

From the attached analysis of the responses, it can be observed that only half of the respondents agree that employees can quickly see the results of the changes, which brings us back to the fact that it is one of the potential problems with the reengineering process that needs to be eliminated. Also, two thirds of respondents think that employees are motivated to participate in the reengineering process. This issue arises during the entire analysis as very important, so this segment should also be given special attention not only during reengineering, but constantly. It can be also observed that it is necessary to improve the education of employees, to include them more in the entire system through various trainings, seminars and conferences.

6. CONCLUSION

The results of the research showed that 86% of the surveyed companies implement the process of business process reengineering. In most foreign-owned companies, reengineering has been implemented for more than 5 years, while the situation is different for domestically owned companies, where the period of implementation is less than 2 years. Only half of the respondents believe that employees can quickly and clearly see the results of planned changes. This is one of the main problems that affects the motivation of employees to accept changes. The results show that more than half of the employees feel resistance to changes.

The study also shows that one of the crucial questions for the success of reengineering is the motivation of employees. Managers are largely aware of this fact, as shown by their responses. When it comes to the correlation between achieved results and employee motivation, it is clear that they are largely dependent on each other.

In conclusion, Business process reengineering can be used as a tool to create sustainable business processes by incorporating environmental and social considerations into the redesign process. Sustainable business processes are essential for the long-term success of businesses, as they not only provide short-term benefits but also have long-term positive impacts on the environment, society, and economy. Therefore, businesses should consider incorporating Business process reengineering into their management strategies to create sustainable business processes.

Incorporating Business process reengineering into management strategies can create sustainable business processes by incorporating environmental and social considerations into the redesign process. Business process reengineering can provide cost savings, improve reputation, and increase employee morale and motivation, making it a valuable tool for sustainable business processes.

Acknowledgement

This research was financially supported by the Ministry of Science, Technological Development and Innovation of the Republic of Serbia (Contract No. 451-03-47/2023-01/ 200109).

REFERENCES

- [1] Hammer, M., Champy, J. (1993) *Business process reengineering. Reengineering the Corporation: A Manifesto for Business Revolution*. New York: HarperCollins Publishers.
- [2] Davenport, T.H., Short, J.E. (1990) The New Industrial Engineering: Information Technology and Business Process Redesign. *Sloan Management Review*, vol. 31, p. 11-27.
- [3] Rummler, G. A., Brache, A. P. (1995). *Improving Performance: How to Manage the White Space on the Organization Chart (2nd ed.)*. San Francisco, CA: Jossey-Bass, Inc.
- [4] Seddon, P.B., Lewis, G.P. (2003) *Strategy and Business Models: What's the Difference. Department of Information Systems*, The University of Melbourne, Victoria.
- [5] Hammer, M. (2001). *The process enterprise: An Executive perspective*. Hammer and Company.
- [6] Chung, S., An, J. B. C., Davalos, S. (2007). Service-oriented software reengineering: SoSR. In *2007 40th Annual Hawaii International Conference on System Sciences (HICSS'07)* IEEE, p. 172c-172c. DOI: 10.1109/HICSS.2007.479
- [7] Terziovski, M., Fitzpatrick, P., O'Neill, P. (2003). Successful predictors of business process reengineering (BPR) in financial services. *International Journal of Production Economics*, vol. 84, no. 1, p. 35-50.
- [8] Klein, H. J., Wesson, M. J., Hollenbeck, J. R., Alge, B. J. (1999). Goal commitment and the goal-setting process: conceptual clarification and empirical synthesis. *Journal of applied psychology*, vol. 84, no. 6, p. 885. DOI: 10.1037/0021-9010.84.6.885
- [9] Fernandes, D., Lynch, J. G., Netemeyer, R. G. (2014). Financial Literacy, Financial Education, and Downstream Financial Behaviors. *Management Science*, vol. 60, no. 8, p. 1861-1883.
- [10] Hammer, M. (2014). *What is business process management?* In *Handbook on business process management 1: Introduction, methods, and information system*. Berlin, Heidelberg: Springer Berlin Heidelberg.
- [11] Venkatraman, N. Henderson, J.C. (1998) Real Strategies for Virtual Organizing. *Sloan Management Review*, vol. 40, p. 33-48.
- [12] Lee, Y.C., He, L.Y., Jiang, J.S., Lian, Q.Y. (2006) The Taiwan customer satisfaction index model in related to sample decision. *Qual Mag*, vol. 42, no. 4, p. 74-77.

- [13] Lacity, M. C., Hirschheim, R. A. (1993). *Information systems outsourcing; myths, metaphors, and realities*. John Wiley & Sons, Inc.
- [14] Al-Mashari, M., Zairi, M. (1999) BPR Implementation Process: An Analysis of Key Success and Failure Factors. *Business Process Management Journal*, vol. 5, p. 87-112. DOI:10.1108/14637159910249108
- [15] Gavrilova, T., Mishra, D. (2019). Sustainability and Business Process Re-engineering. *Procedia Computer Science*, vol. 152, p. 655-663.
- [16] Yadav, J., Ramesh, A. (2018). Injection strategies for reducing smoke and improving the performance of a butanol-diesel common rail dual fuel engine. *Applied energy*, vol. 212, p.1-12.
- [17] Goel, S., Chen, V. (2008). Integrating the global enterprise using Six Sigma: business process reengineering at General Electric Wind Energy. *International Journal of Production Economics*, vol. 113, no. 2, p. 914-927. DOI: 10.1016/j.ijpe.2007.12.002
- [18] Goel, S., Chen, V. (2008). Can business process reengineering lead to security vulnerabilities: Analyzing the reengineered process. *International Journal of Production Economics*, vol. 115, no. 1, p. 104-112. DOI: 10.1016/j.ijpe.2008.05.002
- [19] Lan, Y. C. (2011). Reengineering a green business. *International Journal of Green Computing (IJGC)*, vol. 2, no. 1, p. 1-11. DOI: 10.4018/jgc.2011010101
- [20] Braun, S., Gustafsson, J., Wynstra, J. (2018). Business process reengineering and the design of the value constellation. *International Journal of Operations & Production Management*, vol. 38, no. 5, p. 1145-1167.
- [21] Karakaya, F. (2013). Impact of business process reengineering on sustainable development. *Social Responsibility Journal*, vol. 9, no. 2, p. 251-260.
- [22] Rajic, M., Banic, M., Maksimovic, R., Mancic, M., Milosavljevic, P. (2022). Energy and Utility Management Maturity Model for Sustainable Industry. In *Machine and Industrial Design in Mechanical Engineering: Proceedings of KOD 2021* (pp. 353-361). Cham: Springer International Publishing.
- [23] Johansson, P., Säfsten, K., Winroth, M. (2016). Challenges and success factors for BPR in SMEs: a case study of a Swedish manufacturing company. *Business Process Management Journal*, vol. 22, no. 1, p. 184-204.
- [24] Alonso-Mendo, F., Fitzgerald, G., Frias-Martinez, E. (2009). Understanding web site redesigns in small-and medium-sized enterprises (SMEs): a UK-based study on the applicability of e-commerce Stage Models. *European Journal of Information Systems*, vol. 18, no. 3, p. 264-279.
- [25] Chang, L. J., Powell, P. (1998). Towards a framework for business process re-engineering in small and medium-sized enterprises. *Information Systems Journal*, vol. 8, no. 3, p. 199-215.
- [26] Chang, L. J., Powell, P. (1998). Business process re-engineering in SMEs: current evidence. *Knowledge and Process Management*, vol. 5, no. 4, p. 264-278.
- [27] Aryanezhad, M. B., Khademi, M. (2018). Business process reengineering in SMEs: Benefits, challenges and success factors. *Business Process Management Journal*, vol. 24, no. 3, p. 603-626.
- [28] Al-Mashari, M., Al-Mudimigh, A., Zairi, M. (2016). Business process reengineering: a survey of international experience. *Business Process Management Journal*, vol. 2, no. 3, p. 174-190.
- [29] Davenport, T. H. (1993). *Process innovation: reengineering work through information technology*. Harvard Business Press.
- [30] Rajić, M. N., Maksimović, R. M., Milosavljević, P. (2022). Energy Management Model for Sustainable Development in Hotels within WB6. *Sustainability*, vol. 14, no. 24, p. 16787. DOI:10.3390/su142416787
- [31] Petrović, P., Milačić, V. (2010). National technology platforms of Serbia: A new framework for reengineering of Serbian economy. *Journal of Applied Engineering Science*, vol. 8, no. 3, p. 147-161.
- [32] Jovanović, V., Radanov, P., Panić, B. (2014) Reengineering of business processes in crisis. *Economy and Market Communication Review*, vol. 4, no. 1, p. 71-81. DOI: 10.7251/EMC1401071J
- [33] Taboroši, S., Kovačević, A. (2021). The influence of organizational culture on the reengineering process. *Ekonomski izazovi*, vol. 10, no. 19, p. 58-69.
- [34] Rajić, M. N., Maksimović, R. M., Milosavljević, P. (2023). Emergency Planning and Disaster Recovery Management Model in Hospitality—Plan-Do-Check-Act Cycle Approach. *Sustainability*, vol. 15, no. 7, p. 6303. DOI: 10.3390/su15076303
- [35] Šumaković, B. (2022). *Readiness assessment for business process reengineering in Serbia*. Master Theses, University of Niš Faculty of Mechanical Engineering, Niš, Serbia.



Banja Luka
1–2 Jun 2023.

DEMI 2023

16th International Conference on Accomplishments in Mechanical and Industrial Engineering

www.demi.mf.unibl.org



CALORIFIC VALUE OF WOOD PELLETS

B. Karpe¹, T. Udir², L. Lavrenčič¹, Z. Tanasić³, A. Benčina¹, B. Kosec^{1,4}

¹University of Ljubljana, Faculty of Natural Sciences and Engineering, Aškerčeva cesta 12, 1000 Ljubljana, Slovenia

²LOTRIČ Metrology, d.o.o., Selca 163, 4227 Selca, Slovenia

³University of Banja Luka, Faculty of Mechanical Engineering, S. Stepanovića 71, 78000 Banja Luka, RS, BiH

⁴University of Ljubljana, Faculty of Mechanical Engineering, Aškerčeva cesta 6, 1000 Ljubljana, Slovenia

Abstract

In Slovenia the forest covers almost 60% of the area. In the field of heating of individual residential buildings, the share of wood and wood fuels exceeds 50%.

The use of wood for energy purposes, both in terms of energy independence and ecological acceptability, is therefore certainly welcome, but it is necessary to be aware that wood heating is not environmentally friendly and only efficient use of quality wood fuels provides environmentally friendly heating.

Wood pellets are wood fuels used in modern furnaces and heating systems. They have a relatively high density and low water content, which allows high combustion efficiencies. They are mostly made of spruce and beech wood.

As part of the research, we analyzed air-dried beech or spruce wood and wood pellets from various manufacturers, which are available on the market today.

For each individual type of pellets and air-dried beech or spruce wood, we measured or determined the proportion of moisture, ash, volatile and the most important energy parameter, calorific value, with the C200 IKA calorimeter.

According to the standard ISO 17225 - 2 analyzed wood pellets were classified into quality classes.

Keywords calorific value, wood pellets, energy, ecology

1. INTRODUCTION

Each of us is faced with heating on a daily basis. Energy is needed for heating as well as for other processes in life (for example, transport, food production, car production). We cannot create energy from nothing, nor can we annihilate it, we can only transfer it from one system to another or store it. In Slovenia,

households use more than 80% of total energy, 62% of this energy is used for heating, 19.5% for hot water preparation, and the remaining 20% is used for the operation of electrical appliances, household appliances, lighting and cooking. It should be noted that a lot of energy is also used for transport. Cars consume the most energy, followed by trucks, and a small share of energy is used for public passenger transport. We know several types of renewable energy sources (solar, wind, wood), in addition to these we also know the chemical energy stored in food and beverages, moving energy (sea waves, wind) and finally the energy coming from the heated Earth's interior [1].

Corresponding author

Prof. Borut Kosec
borut.kosec@ntf.uni-lj.si

University of Ljubljana Faculty of Natural Sciences and Eng.
Aškerčeva cesta 12
1000 Ljubljana, Slovenia

There is no shortage of wood biomass in Slovenia, as the country is covered by as much as 60 % of the forest. The availability of wood is limited by the slope of the surface in Slovenia, more than half of the country has a 20 % slope, and a good fifth even over 35 %. In addition to the slope, accessibility is also limited by altitude. The forest boundary ranges from 1600 to 1900 meters above sea level [2].

Burning wood biomass is also a major source of pollution with dust particles in the air. It is important for each individual to be aware of what proper heating looks like and how to recognize poor combustion of wood fuels in a stove boiler. The biggest indicators of proper heating are the color of the flame and smoke. As a rule, the color of the flame should be light in color, and the color of the smoke almost invisible.



Fig 1. Beech wood in different shapes.

2. WOOD AND WOOD PELLETS

Wood biomass or wood fuels are divided into:

- firewood,
- wood chips,
- pellets and
- briquettes.

Pellets are made from dry wood dust and sawdust. Production takes place at high pressure (up to 1000 bar) and the presence of water vapor. As a rule, it should not contain chemicals, only the addition of starch is allowed. The length of the pellets is 5 to 50 mm and the diameter is 6 to 12 mm. Briquettes are larger pieces of various shapes, most often cylindrical in shape. They are similar to firewood in shape, size and method of use. They are used in fireplaces with manual filling. The length of the briquettes is from 60 to 150 mm and the diameter from 50 to 100 mm. They are made by

pressing bark, dry wood dust, shavings and other uncontaminated wood residues. The moisture content should not exceed 10 % and the ash content of combustion should not exceed 0.5 % [2].

Wood pellets are a modern form of wood fuels that are ground into dry wood powder. For better mechanical resistance, they are allowed to add up to 3% starch during the manufacturing process. They have a cylindrical shape with a diameter of 6 to 8 mm and are up to 40 mm long. In 2017, 19 active pellet producers were registered in Slovenia. However, this number has been maintained to this day [2]. Wood pellets are made from all types of wood or other raw materials such as straw, grain and energy grass. Energy grass was developed in Hungary and is used as a stand-alone raw material or as an additive to wood for pelleting. Depending on the choice of wood, the resulting pellets differ in color. In principle, there is no measure of whether lighter pellets are better than darker ones, as has sometimes been claimed. However, it has been proven that pellets are of the highest quality from spruce or fir wood, so these two types are most often used to make pellets. Beech wood pellets can also be found on the market. Such wood contains a predominantly small proportion of ash below 0.5% and is relatively light. However, the types of wood can be mixed with each other as desired, resulting in quality pellets. Some manufacturers also add bark to the wood mixture, which reduces the quality of the pellets due to the higher amount of ash. During the transport of the bark, soil, sand or even small stones accumulate in it, a small percentage of which also enters the pellets, which negatively affects the calorific value of the pellets, causes slag formation during burner operation and increases the amount of ash.

The pellet production process begins with the felling of trees in forests. Various mechanization is used to facilitate work in the forest. The trees they cut down are taken out of the forest and cut to the appropriate length and taken by truck to the central center. This is followed by wood treatment, which can leave up to 30% of sawdust, roundwood and wood dust, which is used to make pellets. Pellet production is divided into five stages. The first stage of pellet preparation is grinding. During the process, different pieces of untreated wood acquire an even structure. The mixture becomes

homogeneous, which is very important in the manufacture of pellets. Grinding is most often carried out with hammer mills and usually takes place in several stages from coarse to final fine grinding. Drying of finely ground material is the second stage of the pellet production process. Fresh wood can contain up to 50% moisture. Drying takes place in electrically operated drum dryers. Drum dryers use hot air and steam. Hot air is used for drying wood and water vapor for controlled humidification as the pellet must not be too dry when it enters the pelleting process. After drying, the humidity is reduced to 8%. The drying phase is crucial, as humidity also affects the calorific value of the pellets - the drier the wood, the higher the calorific value.

The next technological operation is compression or pelleting. The process takes place in special presses called pellets. These contain circular matrices through which pellets are formed. In presses, the raw material is exposed to high pressure and temperature. The compressive force ensures that pellets are obtained from the die which are cut to the prescribed length by knives. The heat released during the process has a positive property as it allows the lignin to be released, which is a binder. Due to this phenomenon, it is not necessary to add additional binder to the pellets, as they will retain their structure even when cooled. The cooling phase follows, as the pellet reaches high temperatures when pressed, up to 95 °C. In the cooling phase, the final shape of the pellets is formed, and they are also stabilized. The last stage is sowing, in which small fractions, dust and debris are removed.

Finally, the cooled and sieved pellets are packed in 15 kg bags, BIG BAG bags, with a capacity of 1000 kg, or left in bulk.

3. QUALITY OF WOOD PELLETS

The quality of pellets is described by a number of factors, the most typical of which are:

- raw material used (origin and origin),
- dimensions (diameter and length),
- water content,
- mechanical resistance,
- bulk density,
- ash content,
- proportion of fine particles,
- calorific value and
- presence of chemical elements.

According to the quality according to the SIST EN ISO 17225 - 2 standard, pellets are classified into three quality classes, namely A1, A2 and B [3]. Individual classes allow different proportions of ash in pellets. They also differ in the value of mechanical resistance. The highest quality pellets include pellets of the highest quality. Class A2 already allows a higher proportion of ash than class A1, while class B allows the highest ash content and slightly lower mechanical stability. Class B allows the use of wood residues and used wood for the production of pellets, which is not suitable for use in the vast majority of domestic stoves. The quality of the pellets is also important for the long-term, economical and reliable operation of the device. Higher quality and proper use extend its lifespan.

4. EXPERIMENTAL

The analysis of pellet quality was performed in the thermotechnical laboratory. We focused on the analysis of ash content, water, calorific value, bulk density, and in addition, we analyzed the ash samples using a scanning electron microscope.

The analysis was performed for five different types of pellets, which are shown in Figure 2.



Fig 2. Testing samples.

The composition of all five analysed samples is as follows:

- Sample 1: Pine
- Sample 2: Fir
- Sample 3: Conifers
- Sample 4: Fir (darker pellets than in sample 2)
- Sample 5: Mixed.

The percentage (content) of ash is small in all five samples (Table 1). This is a positive feature for the user as the intervals between emptying the ash tank are longer.

Tab. 1. Results of ash content

Sample	Ash content (%)
1	0.3570
2	0.4626
3	0.3252
4	0.9055
5	0.9052

The results of the water content are given in Table 2.

Tab. 2. Results of the water content

Sample	Ash content (%)
1	7.2197
2	7.7351
3	6.9814
4	8.0414
5	7.4627

The calorific value of the samples was determined by a calorimeter system IKA C200, which was previously set and calibrated [4]. We chose the isoperibolic program, which is one of the four programs the device offers. The calorific value was measured for air-dried samples as well as dried at 105 °C.

Results of measurements of the calorific values of all five air - dry samples and dried samples at 105 °C are collected in Table 3.

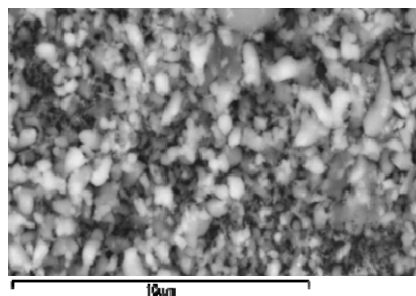
Tab. 3. Calorific values

Sample	Calorific value of air - dry sample (kJ/kg)	Calorific value dried sample at 105 °C (kJ/kg)
1	18536	19958
2	18544	19967
3	18841	20273
4	18364	19887
5	18368	19829

The ash analysis was performed on a field electron microscope on a field emission Thermo Scientific Quattro S. All five ash samples were prepared accordingly. We applied a small amount of ash to the carbon strip, smoothed it and shook off the excess particles. The samples were then placed under a microscope and waited for a vacuum to form. This took about seven minutes. We started to change the resolution, sharpness and magnification in order to get a sharp image. Once we had a sharp image, we performed energy dispersion

spectroscopy (EDS) from this area on the image, which gave us a thorough analysis of the chemical composition of the sample (Figure 3).

We analyzed each sample separately, but found that they changed minimally in composition. All samples contain a lot of carbon and oxygen, on average a good 20 % of carbon, and oxygen just under 40 %. In addition to these two elements, sodium, magnesium, aluminum, silicon, potassium, calcium, manganese and, in small quantities, phosphorus and sulfur are also present in the sample.

**Fig. 3.** The microstructure of sample 1.

5. CONCLUSIONS

Wood pellets are wood fuels used in modern heating stoves. They have a relatively high density and low water content, which allows high combustion efficiencies. They are mostly made of spruce and beech wood.

In our case the analyses of water content and calorific value, all types of pellets achieved classification in the quality class. In other analyzes, however, there were only a few pellets that were classified in quality class A1. The others met standard A2, B, or none at all.

From the results of the presented analyzes, we found that conifers have a higher calorific value than deciduous trees.

REFERENCES

- [1] Obernberger, I., Thek, G., The pellet handbook: the production and thermal utilisation of pellets. London; Washington; Earthscan, 2010.
- [2] Protić, M., Mitić, D., Stefanović, V., Wood pellets production technology. Safety engineering, 1 (2011), pp. 23–26.
- [3] Zielkiewicz, W., Margas, E., Theory of calorimetry. Dordrecht; Boston; London: Kluwer Academic Publishers, 2002.
- [4] Solid biofuels – Method for calorific value determination. SIST EN14918, 2010.



Banja Luka
1–2 Jun 2023.

DEMI 2023

16th International Conference on Accomplishments in Mechanical and Industrial Engineering

www.demi.mf.unibl.org



Effective monitoring and analysis of errors through the application of quality tools

Maja Vuković^a, Goran Janjić^a, Zorana Tanasić^a, Borut Kosec^b, Miroslav Bobrek^a

^aUniversity of Banja Luka, Faculty of Mechanical Engineering, Banja Luka, Republic of Srpska, B&H

^bFaculty of Natural Science and Engineering, University of Ljubljana, Slovenia

Abstract *The quality of the product or service is a key factor in the success of the company as well as the improvement of its competitiveness on the market. In order to achieve this, all employees should participate in achieving quality. The key principle of the quality system is making decisions based on facts, which are reached by collecting, processing, and analyzing data. Various methods are used as an effective tool for a complete overview of the influencing parameters of a process. This paper will show the application of the PARETO diagram, one of the seven basic quality tools, and the 8D report as an aid for resolving and analyzing identified errors with the greatest degree of impact.*

Keywords *quality, control, PARETO diagram, 8D reports*

1. INTRODUCTION

Quality is the strategic goal of every company that wants to survive on the market. Quality management, quality measurement tools, quality standards and many other methods help the company's efforts to operate successfully in all aspects and segments. The success of the organization mostly depends on the quality of products or services. Quality is an important factor in the survival, success and prosperity of a company. Quality management includes the systematic use of various methods, guidelines, techniques and tools in order to meet user requirements and achieve competitive advantage and business success, through the achievement of high-quality products and processes.

Quality management tools are a very important

asset for achieving, monitoring and improving the quality of products and processes in terms of detecting errors and eliminating their causes. They are primarily intended for management, but in their application the participation of all employees is crucial, so that they provide relevant data, which is used as a basis by the management to perform analysis and make decisions.

2. QUALITY MANAGEMENT TOOLS

Quality management tools can be defined as practical techniques, skills, means or as mechanisms that can be applied in solving specific tasks and problems.

The seven basic quality tools (7QC), control sheet, histogram, control charts, pareto diagram, cause-effect diagram, correlation diagram and flow diagram, are used for [1]:

- monitoring the achieved product quality,
- transition from inspection to quality prevention,
- systematic improvement of product/service quality level

Corresponding author

MSc Maja Vuković
maja.vukovic@mf.unibl.org

University of Banja Luka, Faculty of Mechanical Engineering
Vojvode Stepe Stepanovića 75. 78000
Banja Luka, Bosnia and Herzegovina

Seven basic quality tools (7QC) are used effectively as part of various improvement cycles [2]:

- Deming's improvement cycle,
- Kaizen approach,
- DMAIC methodology within Six sigma,
- Lean Six sigma.

This paper will show the application of the Pareto diagram and the 8D report as an aid for solving and analysing identified errors based on received complaints in the XYZ company.

2.1 Pareto diagram

The Pareto diagram is a graphic representation of features (causes, impacts) that are ranked according to the degree of importance, based on established criteria [3].

Pareto's 80-20 rule states: 80% of errors are caused by 20% of factors. This diagram is also known as ABC analysis where the areas with the most significant items are marked with letters A, B and C (Figure 1).

By using the pareto diagram, we separate the important factors (significant minority) from the irrelevant (trivial majority), that is Pareto diagram allows users to focus on key problems that give the most room for improvement [3].

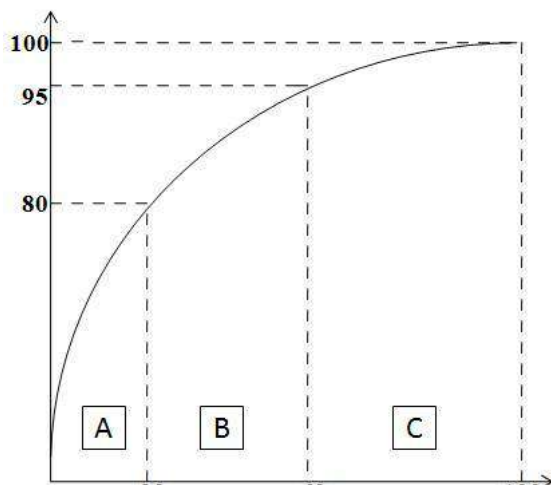


Fig. 1. ABC analysis

Pareto diagram shows, in descending order, the relative importance (participation, influence) of the observed subject in the set of subjects whose analysis is performed. Given this, the relative importance can be based on the number of repetitions, value (profit, costs) and

other measures or indicators as a function of the nature of the analysed subjects [4].

The method is performed in the following steps:

- Selection of problems for analysis,
- Designing the Pareto diagram,
- Determining the degree of significance.

Pareto diagram helps us to make the greatest possible improvements using available resources by showing us where to focus our efforts to get the best results.

2.2 8D report

In 1987, the Ford automobile company developed an 8D problem-solving process and published it in its TOPS (Team Oriented Problem Solving) manual. In the mid-1990s, Ford added another process step, or discipline, which is D0 – Project Planning. This method is now Ford's global standard, and is also called Global 8D. The method was originally intended for manufacturing, engineering and space industries, but it has proven to be extremely useful and relevant and applicable in every industry.

The 8D method is most often applied when errors occur in production or after receiving complaints from customers about the product/service, and the main goal is to find the cause and root of the problem, eliminate the problem and take certain measures to avoid repeating the problem. Using the 8D method will not only efficiently and effectively solve the problem and prevent its recurrence, but it will also significantly improve the reputation with the customer. A positive and quick reaction to any complaint from the customer or to a problem in production is one of the key factors in building business excellence, and in this way the company can stand out from the competition [5]. The 8D method consists of 9 steps/phases starting with step zero and proceeding in the following order [5]:

- D0 – project planning and information gathering
- D1 – forming a team of experts
- D2 – defining the problem
- D3 – taking temporary measures to limit damage
- D4 – analysing and determining the root of the problem
- D5 – selection and verification of corrective measures

- D6 – implementation of corrective measures
- D7 – preventing recurrence of the problem
- D8 – thanking the team for successfully solving the problem.

The biggest advantage of the method is that it allows us a complete and thorough approach to solving current problems, improving processes in the company and preventing their recurrence.

3 CASE STUDY: APPLICATION OF PARETO DIAGRAM AND 8D REPORT

Using a practical example, complaints received in the company XYZ, the application of the Pareto diagram will be shown, i.e. how to use this tool to find key problems and solve them with the help of 8D reports.

3.1 Analysis of complaints received in 2021

The input data for the Pareto diagram is the data obtained from the report on the monitoring if received complaints for a company engaged in the production of precise machine parts. The collected data covers a period of two calendar years, 2021 and 2022.

The analysis was done for each year separately with the aim to show the difference in the frequency of repetition of certain types of errors after the pareto analysis and 8D report.

Following all complaints received in the specified period and analyzing the reasons why they occurred, a group of 17 different types of errors was found (figure 2).

the_type_of_error	error_frequency	number_rec_parts
surface protection	one	29
thread	more than one	20
measure	more than one	10
dimension (outer diameter error)	more than one	10
position tolerances	more than one	7
dimension (internal diameter error)	more than one	7
material defects	one	3
shape tolerances	more than one	2
damage	one	2
packing error	one	2
processing	more than one	1
radius	more than one	1
welding defect	one	1
labelling	one	1
reduction	more than one	1
heat treatment error	one	1
technology error	more than one	1

Fig. 2. Types of errors and their frequency of repetition for the year 2021

For all types of errors, it is determined whether an error can occur at one part once or more than once, as well as the frequency of repetition. After that, a Pareto diagram was created using the SPSS statistical package (figure 3).

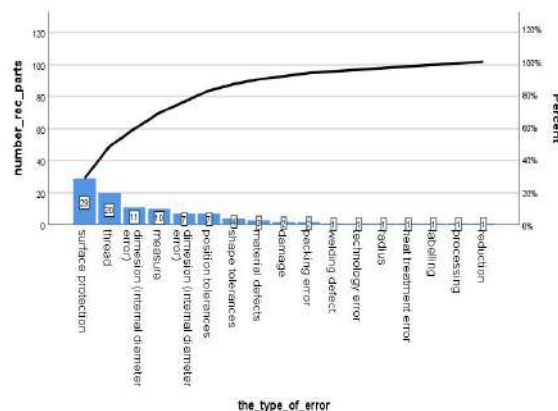


Fig. 3. Pareto diagram for the year 2021

Analysing the Pareto diagram, we came to the conclusion that the highest percentage of errors, due to which complaints occurred, refer to surface protection and thread errors. The mentioned errors were said to be in Area "A" and that they are errors of the highest degree of importance and that it is necessary to find a solution for them in order to prevent their repetition in the future.

A detailed analysis of the mentioned errors was done using the 8D report. Following all the mentioned steps from D0 to D8, we found out that the errors, and therefore complaints, were caused by inadequate training of manual processing workers who were in charge of tapping threads, faulty measuring equipment, poor quality of surface protection from the subcontractor, the rush to meet the delivery deadline to the customers and failure to carry out 100% final control. Based on the established causes that led to these errors, the following corrective measures were defined and implemented:

- worker training
- acquisition of a new machine for threading
- threading on machines whenever possible
- procurement of new thread controllers
- finding new subcontractors for surface protection
- auditing existing subcontractors in order to improve the quality of surface protection
- 100% control of all parts before delivery

- Increasing the number of workers in the final control.

3.1 Analysis of complaints received in 2022

In January and February 2022, all corrective measures defined by the 8D report were implemented and verified (Figure 4).

01 Problem Solving Team
 Date: _____
 Team leader: _____
 Team members: _____

02 Problem Description

No.	Defect type	Description	Defect quantity
1	ESD / Processing failure	Greyscale M15 nut/gangli	1

03 Confirmation of problem
 We talked to our people who made these parts about the need to make to check all positions precisely.
 Responsible: VA _____ Introduced on: _____ Effective from February 2021

04 Cause and Effect Analysis
 Root Cause(s) with evidence: Why could the non-conformity occur?
 The error happened in mass processing. The thread was started on the machine and the front workers were not out to the required depth.
 Responsible: S.T. _____ Completed on: December 2020
 Root Cause(s) with evidence: Why have the non-conformity not been detected?
 Controller did not check the position in detail.
 Responsible: T.V. _____ Completed on: December 2020

05 Preventive measures
 Causative process: _____
 Carelessness of workers and controllers.
 Expected effects: Risk assessment (Probability): _____
 This error does not affect other parts in the production process.
 Production period affected from: _____ to: _____ Responsible: _____ Completed on: _____
 Expected number of further non-conformities: _____

06 Introduction of corrective actions and tracking of effectiveness
 Training of new employees. Measurements are provided for thread measurement.
 Responsible: V.V. _____ Completed on: April 2021

Fig. 4. 8D report

The monitoring of complaints continued for the year 2022 according to the same types of errors that have already been defined. Based on the obtained data, a Pareto diagram was created where it can be seen, that the errors that had the highest frequency in the previous period and for which a detailed analysis was done using the 8D report, now no longer belong to area "A" (figure 5).

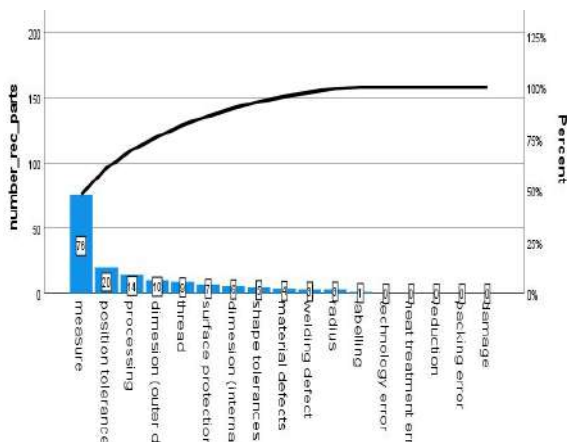


Fig. 5. Pareto diagram for year 2022.

4 CONCLUSION

Managers of modern organizations are required to correctly understand the process of change and apply the adequate knowledge and techniques with the aim of constantly increasing the efficiency and effectiveness of the organization. In order to survive and improve its business, it is necessary to apply modern quality tools and techniques.

In this paper, it is shown that by using the Pareto diagram and 8D report, daily errors in production can be reduced and the quality of delivered products can be increased.

REFERENCES

- [1] Lazić, M. (2006). *Alati, metode i tehnike unapređenja kvaliteta*, Centar za kvalitet, Mašinski fakultet, Kragujevac
- [2] *Quality Management Systems*, translation of DGQ educational material, 10. Issue 2001, SZK, Ljubljana 2002
- [3] Janjić, G., Tanasić, Z., Soković, M. (2021). *Upravljanje kvalitetom*, Univerzitet u Banjoj Luci Mašinski fakultet, Banja Luka
- [4] Vulanović, V. i dr. (1998). *Metode i tehnike unapređenja kvaliteta*, IIS – Istraživački i tehnološki centar, Fakultet tehničkih nauka, Novi Sad
- [5] Begley Schade, M. (2013). *8D Problem Solving Process*. Business Online Learning
- [6] Carter, M. (2012). *The 8-Disciplines Problem Solving Methodology*. Sixsigma.org Inc. Brea California, USA 92821
- [7] Feigenbaum, A.V. (1986). *Total Quality Control*, McGraw Hill. New York
- [8] Buntak K., Martinčević, I., Šebestijan, T. (2017). *Apply of the 8D method to increase the level of quality management within the organization*, 18th Symposium on Quality, Vodice, Croatia, ISBN: 978-953-8067-08-2



Banja Luka
1-2 Jun 2023.

DEMI 2023

16th International Conference on Accomplishments in Mechanical and Industrial Engineering

www.demi.mf.unibl.org



Energy Management Maturity Model for Serbia: Linking ISO 50001 and existing practices

M. Rajić^a, P. Milosavljević^a, R. Maksimović^b

^aUniversity of Niš, Faculty of Mechanical Engineering, Street: Aleksandra Medvedeva 14, Niš, Republic of Serbia

^bUniversity of Novi Sad, Faculty of Technical Sciences, Street: Trg Dositeja Obradovića 6, Novi Sad, Republic of Serbia

Abstract Energy Management Maturity Model represents an advanced and applicable energy management approach for energy management systems, with the aim to provide quantitative metrics as well as guidelines for improvement. In order to be easy to use for different industrial users with optimal applicability, Energy Management Maturity Model should deliver specific and valuable metrics. On this base, five maturity levels were defined and analyzed based on the results conducted in small and medium sized companies in Serbia. It is particularly important to assess and evaluate the energy management of a company, as a vital process for decision support. Periodical energy management assessments are usually performed, to identify opportunities and to provide useful feedback to the companies. The study aims to presents the current state of energy management practices in Serbia linking the domestic practices with energy management ISO 50001 based model. The findings are seen as crucial especially for manufacturing sector as driving sector for economy development and for sustainable production process design.

Keywords energy management, maturity model, ISO 50001

1. INTRODUCTION

Industrial organizations are significant energy consumers, particularly in terms of electricity consumption, and energy costs are a critical factor in managing their operations. To achieve sustainable industry and clean manufacturing, it is necessary to prioritize proper energy management. Many studies have focused on developing models to monitor and manage energy flows, especially in the manufacturing

sector [1-7]. Rational energy use with minimal environmental impact is a growing challenge for organizations. Analysing energy and material flows in manufacturing processes can provide insights into how to design processes that maximize resource savings and minimize negative environmental impact. Manufacturing organizations are the most commonly analysed for the development of energy management models [1-7].

Energy prices and costs are fundamental factors that determine production processes, and over 80% of energy needs in the industry are met using fossil fuels. Energy management systems offer many benefits, including optimizing energy consumption, reducing costs, improving corporate image, and minimizing negative environmental impact. As such, organizations

Corresponding author

PhD, Assistant Professor, Milena Rajić
milena.rajic@masfak.ni.ac.rs

Department of Management in Mechanical Engineering
Faculty of Mechanical Engineering University of Niš
Aleksandra Medvedeva 14, Niš, Republic of Serbia

are increasingly adopting energy management systems to reduce energy losses [8-10].

Energy management is critical, particularly given that energy costs are the largest relative to other costs in the manufacturing cycle. Certified and applied energy management ensures that end-users receive the necessary amount of energy, supplied with minimal costs, while preserving safety and reliability during operations and environmental protection. An Energy Management System (EnMS) requires a systematic and continuous approach and should not be limited to time-limited programs and/or projects. The ISO 50001:2011 standard provides guidelines for designing, implementing, maintaining, and improving an existing energy management system [11].

Effective energy management has become increasingly important, especially given that energy costs are the highest in the manufacturing cycle. Studies, such as those cited in [12,13], demonstrate that certified and applied energy management helps end-users receive the necessary amount of energy with minimal costs while ensuring safety, reliability, and environmental protection. The implementation of an Energy Management System (EnMS) is a systematic and continuous approach that involves defining energy goals, monitoring energy performance, and implementing procedures for continuous improvement, all starting with an energy policy [14]. ISO 50001:2011 provides a management model for developing and implementing an energy policy to achieve objectives and action plans that meet legal requirements and are based on data analysis of energy consumption. However, this standard does not provide specific performance criteria related to energy consumption and efficiency, nor does it provide a clear path to achieving the ultimate goal, leaving organizations to struggle with understanding their position in relation to it [15].

Maturity models have been used in various engineering sectors and fields as a tool for continuous improvement. They are used to assess an organization's current state, rank improvement measures, and manage progress. Maturity levels represent an organizational plan for improvement, with the initial level representing an organization with poor capabilities in a specific domain and the highest level representing a state of total maturity [16-

19]. Maturity models have been applied in a range of sectors, including information technology, healthcare, finance, and production [20-23]. Specific energy maturity models have been developed for different purposes, with an ISO 50001-based energy maturity model being proposed by [17,24,25], and [26] offering a different approach to delivering qualitative metrics in the form of an energy management maturity model.

Maturity models are used in various engineering sectors and fields as a tool for continuous improvement. They can be used to assess the current state of an organization, rank improvement measures, and manage progress. Maturity models have been applied in different studies and industries, including information technology, healthcare, finance, and production. Specific energy maturity models have been developed for different purposes, including the ISO 50001-based energy maturity model. The qualitative metrics in the form of an energy management maturity model were proposed as a different approach to delivering energy management models.

Energy management plays a crucial role in achieving sustainable development goals and reducing the carbon footprint of a country. Serbia, like many other developing countries, faces significant challenges in implementing energy management practices due to various socio-economic factors. However, the adoption of energy management maturity models, such as the ISO 50001 standard, could help Serbia overcome these challenges and achieve its energy efficiency targets. This study will review the Energy Management Maturity Model for Serbia, linking ISO 50001 and existing practices. The Energy Management Maturity Model is a framework for assessing the maturity of energy management practices in organizations. The model is based on a set of maturity levels that range from initial to optimized. The levels are defined based on the level of energy management practices, leadership commitment, and the use of energy performance indicators. The model provides a structured approach for organizations to improve their energy performance and achieve their energy efficiency goals. Energy Management Maturity Model is applicable to all types of organizations, including small and medium-sized enterprises (SMEs), and can be customized to meet specific needs.

2. ENERGY MANAGEMENT MATURITY MODELS

The Energy Management Maturity Model represents a framework for assessing and improving energy management practices in organizations. One of the early works on Energy Management Maturity Model was published by the Lawrence Berkeley National Laboratory [27]. The paper proposed a five-level EMMM framework that provides a roadmap for organizations to achieve energy management excellence. The authors suggested that the Energy Management Maturity Model can help organizations identify their current level of energy management maturity and develop a plan to improve their energy management practices. In [28], researchers evaluated the effectiveness of Energy Management Maturity Model in improving energy management practices in the UK manufacturing sector. The study found that the Energy Management Maturity Model framework can help organizations identify areas for improvement in their energy management practices and develop an action plan to address these areas. However, the study also noted that the effectiveness of Energy Management Maturity Model depends on the commitment and engagement of stakeholders within the organization.

Another study [29] evaluated the application of Energy Management Maturity Model in the Australian mining sector. The study found that the Energy Management Maturity Model framework can help mining companies improve their energy management practices and achieve significant energy savings. However, the study also noted that the implementation of Energy Management Maturity Model requires strong leadership, organizational culture change, and a long-term commitment to energy management. Research done in [30] evaluated the application of Energy Management Maturity Model in the context of ISO 50001 certification in the Portuguese manufacturing sector. The study found that the Energy Management Maturity Model framework can help organizations prepare for ISO 50001 certification and improve their energy management practices. The study also noted that the Energy Management Maturity Model framework can help organizations identify opportunities for cost savings and reduce their carbon footprint.

Study [31] developed an Energy Management Maturity Model based on a review of existing energy management models and frameworks. The model includes five levels of maturity and 20 criteria for assessing energy management practices. The model was tested in six German companies and found to be useful for identifying areas for improvement and tracking progress over time.

Researchers in [32] reviewed and compared several Energy Management Maturity Models, including the ISO 50001 standard, the Energy Management Maturity Model developed by the US Department of Energy, and the Energy Management Capability Maturity Model developed by the University of Cambridge. The study identified common themes and best practices across the models, and highlighted the need for a standardized Energy Management Maturity Model that can be used across different industries and countries. The study [33] developed an Energy Management Maturity Model specifically for small and medium-sized enterprises (SMEs). The model includes five levels of maturity and 17 criteria for assessing energy management practices. The model was tested in six German SMEs and found to be useful for identifying areas for improvement and guiding the development of energy management plans. On the other hand, the study developed an Energy Management Maturity Model specifically for the construction sector [34]. The model includes four levels of maturity and 14 criteria for assessing energy management practices. The model was tested in several Austrian construction companies and found to be useful for identifying areas for improvement and guiding the development of energy management plans.

3. ENERGY MANAGEMENT IN SERBIA

Serbia represents a country heavily dependent on fossil fuels for energy production, with coal accounting for over 70% of electricity generation. This has led to high levels of greenhouse gas emissions and air pollution, which have significant impacts on public health and the environment. In recent years, Serbia has taken steps to improve its energy efficiency and increase the share of renewable energy in its energy mix. In 2013, the country adopted a National Energy Efficiency Action Plan, which set targets for energy savings in various sectors

[35]. In 2019, Serbia also adopted a National Renewable Energy Action Plan, which aims to increase the share of renewable energy in the country's energy mix to 27% by 2020.

In terms of energy management practices, some organizations in Serbia have implemented ISO 50001, the international standard for energy management. However, the adoption of ISO 50001 is not yet widespread, and there is still room for improvement in energy management practices across various sectors [7, 25, 36-38].

To overcome these challenges, Energy Management Maturity Model can be used as a framework to assess the maturity of energy management practices in organizations and provide a roadmap for improvement. Energy Management Maturity Model can help organizations identify gaps in their energy management practices and provide a structured approach for improvement. By linking Energy Management Maturity Model with ISO 50001, organizations can ensure that their energy management practices are aligned with international best practices and standards.

The study [39] evaluated the energy efficiency of public buildings in Serbia and identified the lack of awareness and expertise among building managers, as well as the limited availability of financing, as key barriers to implementation. By using Energy Management Maturity Model and ISO 50001, public buildings in Serbia can develop a structured approach to improve their energy management practices and reduce energy consumption.

Similarly, the implementation of renewable energy sources in Serbia faces significant challenges due to limited financing and supportive policies, as well as the limited awareness and expertise. The analysis [40] suggested that by using Energy Management Maturity Model and ISO 50001, Serbia can develop a structured approach for renewable energy development and ensure that its energy management practices are aligned with international best practices and standards.

4. ENERGY MANAGEMENT MATURITY MODEL FOR SMES IN SERBIA

The proposed model for assessing the maturity level of an EnMS is based on the International Organization for Standardization (ISO) 50001 standard, which follows the PDCA cycle. The model consists of five maturity levels that

reflect the level of compliance with EnMS requirements and the extent to which energy efficiency practices have been implemented within an organization.

Maturity level 1, which represents the minimal level, indicates that the identified processes are not compliant with EnMS, EnMS procedures and policies are not implemented, and energy profile and energy performance indicators are not established.

Maturity level 2, the Planning level, signifies that EnMS requirements are established and known, energy-demanding processes and equipment are monitored, and procedures for monitoring and analysis are established and followed. Moreover, some corrective actions within the EnMS are applied.

At maturity level 3, Implementation, the EnMS requirements and practices are standardized, process indicators and parameters are monitored, documented, and controlled, and employees are continuously involved in communication and documentation within the EnMS.

Maturity level 4, Monitoring, represents that energy-demanding processes and equipment are monitored, measured, and analysed, and the organization conducts internal audits within the EnMS to identify causes of energy efficiency measures' failures.

Finally, at maturity level 5, Improvement, management constantly reviews the established procedures and action plans for continuous improvement within the EnMS. Processes are optimized to be energy-efficient, and the organization operates in accordance with sustainable principles. Action plans are continually reviewed for further enhancement. In the survey, organizations are analysed based on their maturity level, which takes into account not only the organization itself but also the maturity level of processes, equipment, plant, building, and facilities. Each organization is assigned one to five points based on their level of compliance with EnMS requirements and implementation of energy efficiency practices.

5. INDUSTRY VALIDATION: A CASE STUDY

The implementation of the proposed model constituted the subsequent stage in the present study, which spanned over the course of two years, namely 2021 and 2023. The survey participants, consisting of the production and

service organizations, were interviewed through the administration of a questionnaire

that was previously formulated and recommended in [7,36,38].

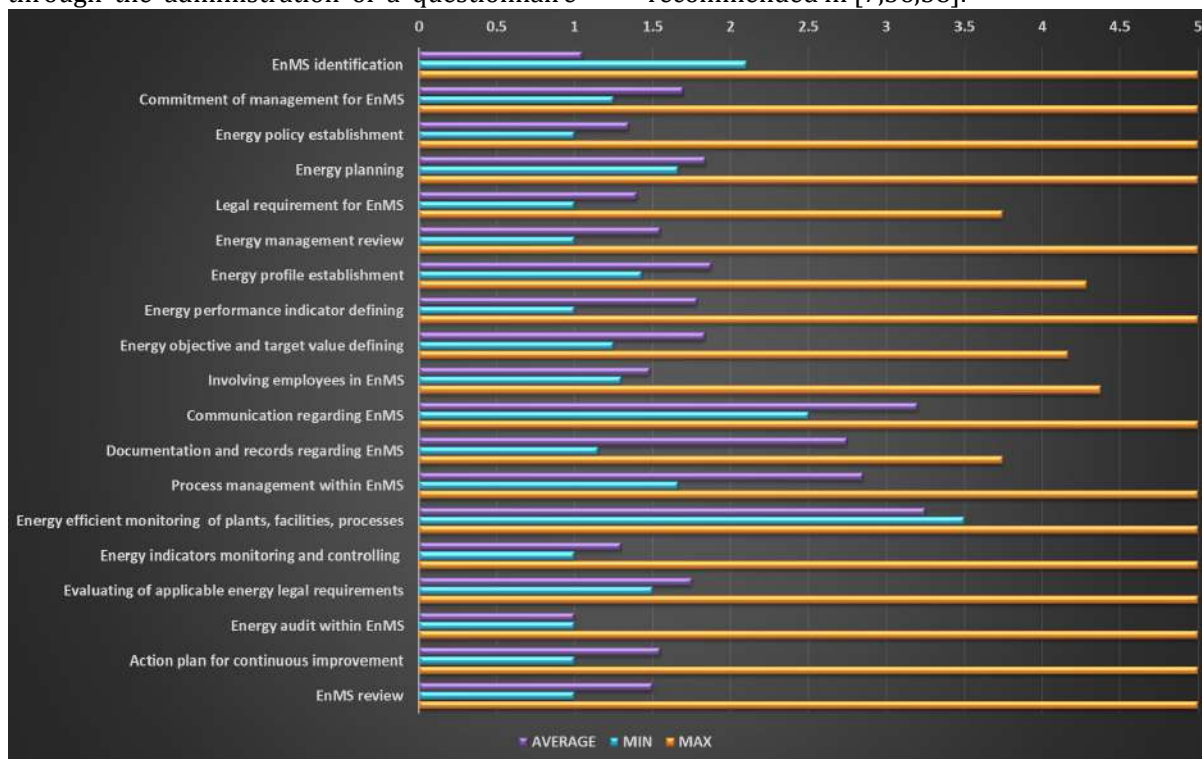


Fig. 1. Average, minimal and maximal maturity levels of analysed organizations



Fig. 2. The PDCA cycle maturity levels of the analysed organizations were averaged for the two-year study period

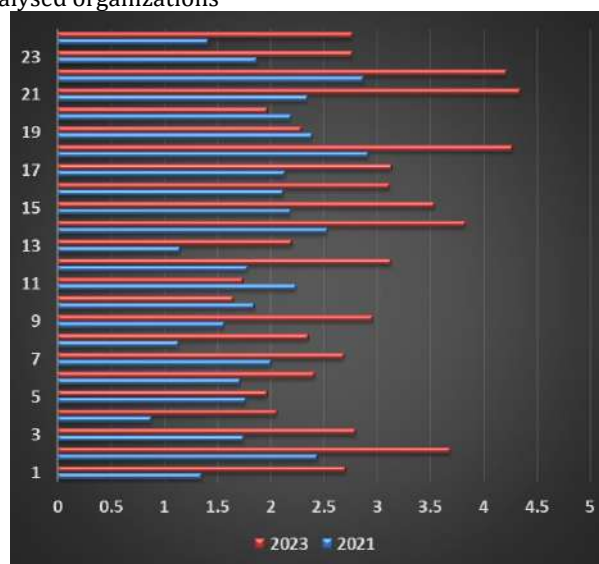


Fig. 3. The maturity levels of 24 organizations analysed over a two-year period were assessed

For each production plant, respondents were required to complete the survey individually, with the results subsequently recorded and preserved for future analyses. The data that were gathered through the surveys conducted on each production plant, facility, and utility

were subjected to a comprehensive analysis with the intent of generating average implementation values, as well as identifying the maximal and minimal values. This analysis was conducted in accordance with the Plan-Do-Check-Act (PDCA) model and the proposed maturity levels. The final results were compared both within the research sample and with data available in relevant literature. The proposed model was tested on a total of 24 organizations that were selected based on the criteria delineated in [7,36]. All of the selected organizations possessed ISO 9001 certification. The findings of the study entailed the computation of various descriptive statistics, namely, the average values, standard deviation, minimum and maximum values, resulting in an average maturity level of 1.84. Attention should be given to certain processes such as "Energy management system identification" (average level of 1.05), "Energy policy establishment", "Legal requirement for Energy management system", "Involving employees in Energy management system" and "Energy indicators monitoring and controlling" (less than 1.5). Of particular note is the finding that "Energy efficient monitoring of plants, facilities, and processes" was observed to have a maturity level of 3.25. Nonetheless, a major limitation of this study is the relatively small research sample. Future work would involve the inclusion of small and medium enterprises (SMEs) in Serbia and a more extensive research sample of production organizations. The results are presented in Fig. 1, which displays the average, minimum, and maximum values for each stage of the model implemented in the analysed organizations. In Fig. 2, the average maturity level of the analysed organizations based on the Plan-Do-Check-Act (PDCA) cycle model was presented for the two analysed years (2021 and 2023), while Fig. 3 summarizes the average results of the analysed organizations for the same period. Both figures demonstrate a notable improvement in the maturity level scores for the PDCA cycle model as well as for each individual organization. Specifically, the "Plan" and "Check" phases of the cycle model experienced more significant improvement.

6. CONCLUSION

In this article, a proposed energy and utility management maturity model was presented.

The model is based on the ISO 50001 process model and organized using the PDCA cycle. The proposed model is specifically adapted and adjusted for production plants, facilities, and processes. The validation of the model was carried out using a questionnaire administered to 24 production organizations in Serbia for two analysed years, 2019 and 2021. The results reveal that all maturity levels are achievable in practice, as evidenced by the minimum and maximum maturity level scores obtained. The model's universality and potential applicability in both production and service organizations are considered to be a significant contribution of this study. The proposed model can be used by both industry and regulatory bodies to monitor energy management maturity levels and progress, for energy regulation revisions, and as the basis for EnMS requirements certification.

Future research will involve a more extensive range of organizations from different sectors in Serbia, including small and medium-sized enterprises. This will result in a more accurate and reliable analysis. Additionally, independent auditors will be involved in model validation, and similar work will be conducted in neighbouring countries to facilitate proper benchmarking of the results.

Energy Management Maturity Model for Serbia, linking ISO 50001 and existing practices, provides a structured approach for organizations to improve their energy performance and achieve their energy efficiency targets. The implementation of Energy Management Maturity Model and ISO 50001 can help Serbia overcome the challenges of limited awareness, expertise, and financing and ensure that its energy management practices are aligned with international best practices and standards. Energy Management Maturity Model and ISO 50001 are essential tools for organizations to achieve sustainable development goals and reduce their carbon footprint.

Acknowledgement

This research was financially supported by the Ministry of Science, Technological Development and Innovation of the Republic of Serbia (Contract No. 451-03-47/2023-01/200109).

REFERENCES

- [1] Thiede, S., Posselt, G., Herrmann, C. (2013). SME appropriate concept for continuously improving the energy and resource efficiency in manufacturing companies. *CIRP Journal of Manufacturing Science and Technology*, vol. 6, no. 3, p. 204-211.
- [2] Ghadimi, P., Li, W., Kara, S., Herrmann, C. (2014). Integrated Material and Energy Flow Analysis towards Energy Efficient Manufacturing. *21st CIRP Conference on Life Cycle Engineering Procedia CIRP*, vol. 15, p. 117 – 122.
- [3] Madloul, N.A., Saidur, R., Rahim, N.A., Kamalisarvestani, M. (2013). An overview of energy savings measures for cement industries. *Renew. Sust. Energy Rev.* vol. 19, p.18-29.
- [4] Rajić, M.N., Milovanović, M.B., Antić, D.S., Maksimović, R.M., Milosavljević, P.M., Pavlović, D.L. (2020). Analyzing energy poverty using intelligent approach. *Energy & Environment*, vol. 31, no. 8, p. 1448-1472.
- [5] Laitner, J.A. (2013). An overview of the energy efficiency potential. *Environ. Innov. Soc. Trans.* vol. 9, p. 38-42.
- [6] Trianni, A., Cagno, E., Bertolotti, M., Thollander, P., Andersson, E. (2019). Energy management: A practice-based assessment model. *Appl. Energy*, vol. 235, p.1614–1636. DOI: 10.1016/j.apenergy.2018.11.032
- [7] Rajic, M., Banic, M., Maksimovic, R., Mancic, M., Milosavljevic, P. (2022). Energy and Utility Management Maturity Model for Sustainable Industry. In *Machine and Industrial Design in Mechanical Engineering: Proceedings of KOD 2021* (pp. 353-361). Cham: Springer International Publishing.
- [8] Yin, R.Y. (2011). *Metallurgical Process Engineering*. New York, USA: Springer Heidelberg.
- [9] Yin, R.Y. (2000). Analysis and Integration of Steel Manufacturing Process. *Acta Metallurgica Sinica*, vol. 36, no. 10, p. 1077-1084.
- [10] Yin, R.Y. (2008). The Essence, Functions, and Future Development Mode of Steel Manufacturing Process. *Scientia Sinica Technologica*, vol. 38, no. 9, p. 1365-1377.
- [11] International Organization for Standardization (ISO). (2018). The 50001:2018 Standard. ISO: Geneva, Switzerland.
- [12] Petrecca, G. (2012). *Industrial Energy Management: Principles and Applications*. Springer Science & Business Media.
- [13] Piper, J.E. (2016). *Operations and maintenance manual for energy management*. Taylor & Francis Group: Routledge
- [14] Introna, V., Cesarotti, V., Benedetti, M., Biagiotti, S., Rotunno, R. (2014). Energy Management Maturity Model: An organizational tool to foster the continuous reduction of energy consumption in companies. *Journal of Cleaner Production*, vol. 83, p. 108–117
- [15] Silva, V.R.G.R.D., Loures, E.D.F.R., Lima, E.P.D., Costa, S.E.G.D. (2019). Energy management in energy-intensive industries: Developing a conceptual map. *Brazilian Archives of Biology and Technology*, vol. 62.SPE
- [16] De Bruin, T., Rosemann, M., Freeze, R., Kaulkarni, U. (2005). Understanding the main phases of developing a maturity assessment model. In *Australasian Conference on Information Systems (ACIS)*, p. 8-19. Australasian Chapter of the Association for Information Systems
- [17] Antunes, P., Carreira, P., da Silva, M. M. (2014). Towards an energy management maturity model. *Energy Policy*, vol. 73, p.803-814.
- [18] Becker, J., Knackstedt, R., Pöppelbuß, D.-W.I.J. (2009). Developing maturity models for IT management. *Bus. Inf. Syst. Eng.* vol. 1, no. 3, p. 213–222
- [19] Becker, J., Niehaves, B., Poeppelbuss, J., Simons, A. (2010). Maturity models in IS research. In: *Proceedings of the 18th European Conference on Information Systems (ECIS 2010)*
- [20] Brooks, P., El-Gayar, O., Sarnikar, S. (2015). A framework for developing a domain specific business intelligence maturity model: application to healthcare. *Int. J. Inf. Manag.* vol. 35, no. 3, p. 337-345.
- [21] Lederman, P.F. (2012). Getting buy-in for your information governance program. *Inf. Manag. J.* vol. 46, no. 4, p. 34-37
- [22] Neff, A.A., Hamel, F., Herz, T.P., Uebernickel, F., Brenner, W., Vom Brocke, J. (2014). Developing a maturity model for service systems in heavy equipment manufacturing enterprises. *Inf. Manag.* vol. 51, no. 7, p. 895-911.
- [23] Backlund, F., Chroneer, D., Sundqvist, E. (2014). Project management maturity models - a critical review: a case study within Swedish engineering and construction organizations. *Procedia Social Behav. Sci.* vol. 119, p. 837-846.
- [24] Jin, Y., Long, Y., Jin, S., Yang, Q., Chen, B., Li, Y., Xu, L. (2021). An energy management maturity model for China: Linking ISO 50001: 2018 and domestic practices. *Journal of Cleaner Production*, vol. 290, p. 125-168 .
- [25] Jovanović, B., Filipović, J. (2016). ISO 50001 standard-based energy management maturity model-proposal and validation in industry.

- Journal of Cleaner Production*, vol. 112, p. 2744-2755
- [26] Finnerty, N., Sterling, R., Coakley, D., Keane, M. M. (2017). An energy management maturity model for multi-site industrial organizations with a global presence. *Journal of Cleaner Production*, vol. 167, p. 1232-1250.
 - [27] McKane, A. (2013). Assessing the costs and benefits of the superior energy performance program.
 - [28] Griffin, P. W., Hammond, G. P., Norman, J. B. (2016). Industrial energy use and carbon emissions reduction: a UK perspective. *Wiley Interdisciplinary Reviews: Energy and Environment*, vol. 5, no. 6, p. 684-714.
 - [29] El-Bidairi, K. S., Nguyen, H. D., Jayasinghe, S. D. G., Mahmoud, T. S., Penesis, I. (2018). A hybrid energy management and battery size optimization for standalone microgrids: A case study for Flinders Island, Australia. *Energy conversion and management*, vol. 175, p. 192-212.
 - [30] Vaquero, P., Dias, M. F., Madaleno, M. Portugal 2020: Improving energy efficiency of public infrastructures and the municipalities' triple bottom line. *Energy Reports*, vol. 6, p. 423-429.
 - [31] Fleiter, T., Schleich, J., Ravivanpong, P. (2012). Adoption of Energy-Efficiency Measures in SMEs-An Empirical Analysis Based on Energy Audit Data from Germany. *Energy Policy*, vol. 51, p. 863-875.
 - [32] Bai, C., Kusi-Sarpong, S., Sarkis, J. (2017). An implementation path for green information technology systems in the Ghanaian mining industry. *Journal of Cleaner Production*, vol. 164, p. 1105-1123.
 - [33] Prashar, A. (2019). Towards sustainable development in industrial small and Medium-sized Enterprises: An energy sustainability approach. *Journal of Cleaner Production*, vol. 235, p. 977-996.
 - [34] Goh, C. S., Rowlinson, S. (2013). Conceptual maturity model for sustainable construction. *Journal of Legal Affairs and Dispute Resolution in Engineering and Construction*, vol. 5, no. 4, p. 191-195.
 - [35] Republic of Serbia Ministry of Mining and Energy. (2013). National Renewable Energy Action Plan of the Republic of Serbia. https://ec.europa.eu/energy/sites/ener/files/documents/serbia_national_renewable_energy_action_plan_nreap_en.pdf
 - [36] Rajić, M. N., Maksimović, R. M., Milosavljević, P., Pavlović, D. (2019). Energy management system application for sustainable development in wood industry enterprises. *Sustainability*, vol. 12, no. 1, p. 76.
 - [37] Rajić, M., Mančić, M., Kostić, Z., Milosavljević, P. (2022). Model of the Circular Economy and its Application in Industry Practice: A Case Study of Serbia. In *New Technologies, Development and Application V* (pp. 1083-1092). Cham: Springer International Publishing.
 - [38] Rajić, M. N., Maksimović, R. M., & Milosavljević, P. (2022). Energy Management Model for Sustainable Development in Hotels within WB6. *Sustainability*, vol. 14, no. 24, p. 16787.
 - [39] Mosurović Ružičić, M., Miletić, M., & Dobrota, M. (2021). Does a National Innovation System Encourage Sustainability? Lessons from the Construction Industry in Serbia. *Sustainability*, vol. 13, no. 7, p. 3591.
 - [40] Golusin, M., Tesic, Z., Ostojic, A. (2010). The analysis of the renewable energy production sector in Serbia. *Renewable and sustainable energy reviews*, vol. 14, no. 5, p. 1477-1483.



Banja Luka
1-2 Jun 2023.

DEMI 2023

16th International Conference on Accomplishments in Mechanical and Industrial Engineering

www.demi.mf.unibl.org



Global electronic waste

B. Dudić^{a,b}, P. Kovač^c, B. Savković^c, E. Beňová^a, D. Ješić^d

^aComenius University, Faculty of Management, Slovakia

^bFaculty of Economics and Engineering Management, Serbia

^cUniversity of Novi Sad, Faculty of Technical Sciences, Serbia

^dInternational Technology and Management Academy – MTMA, Novi Sad, Serbia

Abstract Today, the development of new technologies is constantly progressing, and the demand and consumption of individual types of electrical appliances is increasing, and the share of waste from electrical and electronic equipment is also increasing. Waste from electrical and electronic devices is the source of many components, which with proper evaluation become secondary raw materials, determined before further processing. Electronic waste is currently the fastest growing component of municipal solid waste, because people replace their computers (desktop computers, tablets, notebooks), mobile phones (smartphones), televisions, audio devices and printers more often. Analysed was global electronic waste management market increasing and the volume of electronic waste generated worldwide until 2030 and. The important tasks of waste management include the recovery of electrical waste, which means recycling or energy recovery. The global electronics market size is forecast to increase considerably.

Keywords environment, electronic waste, consumption of energy, waste, waste management

1. INTRODUCTION

After various human activities, waste of different levels is produced. The amount and composition of the waste produced during the mining activity is dependent on the economic and industrial structures of the company. World Bank states in its estimate that the worldwide increase in waste caused mainly by municipal waste by 2025 will increase by up to 70%. As part of the protection of the environment and sustainable development in this area, electrical waste is also a problem. The production of waste has a relatively negative impact on the

environment, as part of the waste does not end up in the waste collection system, but directly reaches the wild, where it pollutes the environment [1,2]. E-waste is often disposed of in landfills. Therefore, it is necessary that all electrical waste, which has already been created, is recycled and energetically reduced [3].

2. GLOBAL ELECTRONIC WASTE MANAGEMENT MARKET

The worldwide consumption of electrical appliances and electronics is responsible for the explosion of e-waste. The amount of discarded electronic products in the world has increased over the past few years, with 20-50 million tons being generated each year. E-waste is currently the fastest growing component of municipal solid waste as people replace their computers (desktops, tablets, laptops), mobile phones

Corresponding author

Dr Branislav Dudić
branislav.dudic@fm.uniba.sk

Comenius University, Faculty of Management
Odbojárov 10, P.O.BOX 95
820 05 BRATISLAVA 25, Slovakia

(smartphones), televisions, audio equipment and printers more often. Computers and mobile phones cause the biggest problem because they are replaced most often these days. E-waste comes from commercial, industrial, institutional, private and other sources.

2.1 Global electronic waste management market size in 2021 and 2029

Electronic waste consists of: metals, copper, iron, tin, nickel, lead, aluminium, zinc, silver, gold, palladium.

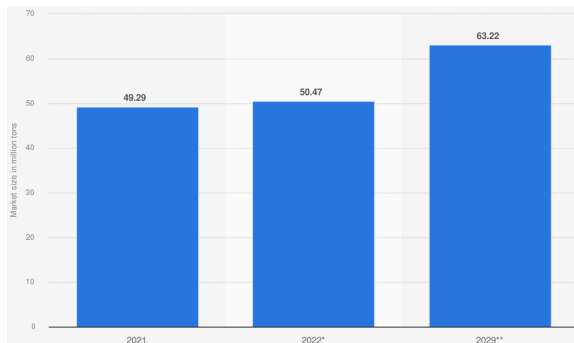


Fig. 1. Global electronic waste management market size in 2021 and 2029 (in million tons) [4]

It is projected that the global e-waste management market size will exhibit a CAGR of 3.3 during the forecast period of 2022 to 2029 to reach a size of more than 60 million tons. There are six main e-waste categories, including screen and monitors, small IT and telecom equipment, and temperature exchange equipment. The category that accounts for the largest share globally is small equipment, which includes products such as electric shavers, microwaves, toasters, and video cameras [4].

2.2 Projected electronic waste generation worldwide

E-waste is very difficult to process and recycle. Our e-waste is increasing every year and is increasing all over the world. And the more electronics, the more e-waste. E-waste processing is an activity in which e-waste is handed over to an e-waste processor for removal of harmful substances, disassembly, scrapping, recovery, environmentally appropriate disposal and other activities leading to environmentally appropriate disposal.

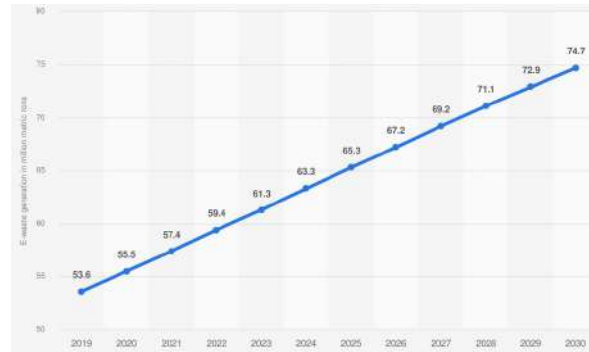


Fig. 2. Projected electronic waste generation worldwide from 2019 to 2030 (in million tons) [5]

The volume of electronic waste generated worldwide in 2019 was roughly 54 million metric tons. Several factors such as increased spending power and the availability of electronics has fuelled e-waste generation in recent decades, making it the fastest growing waste stream worldwide. This trend is expected to continue, with projections showing that by 2030, annual e-waste generation worldwide will have increased by approximately 30 percent.

2.3 Global electronic waste management market

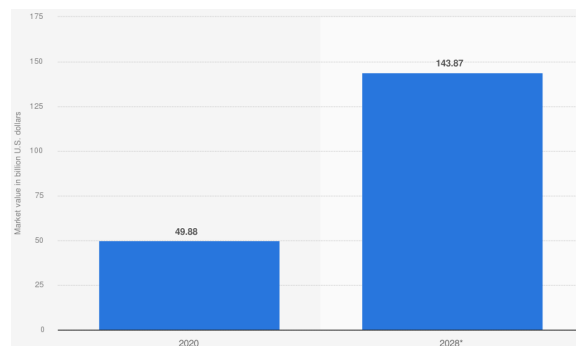


Fig. 3. Important tasks of waste management include the recovery of electrical waste, which means recycling or energy recovery [6]

Recycling of electronic waste

E-waste is very bad for the environment unless it is properly recycled. E-waste recycling is the re-evaluation of materials and substances obtained from e-waste in the production process for the original purpose or to be used as a secondary raw material in another industry [7].

Recycling can be divided into three steps:

- Collection
- Dismantling
- Final processing of metals

In recent years, e-waste has been exponentially increasing due to the high consumption of electronic equipment around the world and the tons of waste produced annually by big tech companies. Manufacturers have therefore started investing more in the electronics recycling market by producing refurbished and recycled electronic devices [8].

Proper recycling of electronic waste helps us preserve precious natural resources. The large number of countries that have decided to recycle e-waste in a safe and sustainable way is growing rapidly every day in the world. At least 70% - 75% of electronic waste should be recycled by 2030.

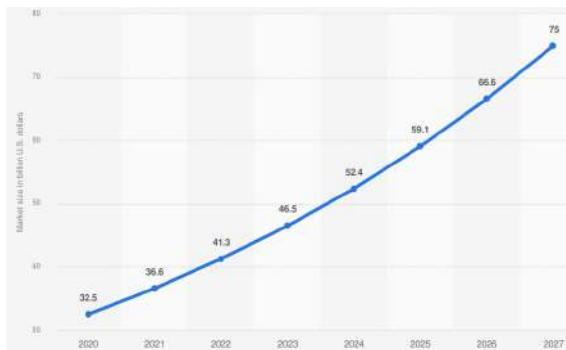


Fig. 4. Size of the global electronics recycling market from 2022 to 2027 (in billion U.S. dollars) [8]

Between 2022 and 2027, the global electronics market size is forecast to increase considerably. Indeed, in 2022, the size of this market amounted to roughly 41 billion U.S. dollars and is forecast to reach a value of 75 billion U.S. dollars by 2027, growing at a compound annual growth rate of 12.7 percent [8].

3. CONCLUSION

Electronic waste is increasing worldwide every year. And the more electronics, the more e-waste. The processing of electronic waste is of great importance to the ecology and economy of the world. Electronic waste contains dangerous substances as well as materials that can be reused. Electronic waste processing removes harmful substances. By recycling e-waste, we

obtain a lot of secondary raw materials about which the general public has no information, health and environmental protection. Precious metals can thus be obtained significantly cheaper than from primary sources. E-waste recycling technologies are economically profitable, but subsidies from the state are also necessary. In 2030, the annual production of e-waste worldwide is expected to increase by approximately 30 percent.

REFERENCES

Reference numbers must be put in brackets [##]. References must be mentioned in the form of [1], [1, 2] or [1 - 3] throughout the paper.

For the list of References use 10 pt Cambria font. Paragraphs in references (every reference) have 3 pt spacing. Please use the following forms for references (journal paper, conference paper, book, book chapter, thesis, report, standard, internet link).

Journal papers:

Surname1, Initials1, Surname 2, Initials2. (Year). Paper title. *Name of journal*, vol. ##, no. #, p. ### - ###. DOI: if it exists

- [1] Elkington, J., & Hailes, J. (1989). *The green consumer guide*. London: Victor Gollancz Ltd.
- [2] Porteous, A. (2008). *Dictionary of environmental science and technology*. John Wiley & Sons.
- [3] O'Callaghan, P. W. (1993). *Energy management*.
- [4] Statista - Fortune Business Insights (September 1, 2022). From: <https://www.statista.com/statistics/1337713/global-e-waste-management-market-size/> accessed on: April 01, 2023
- [5] Statista - World Economic Forum (July 1, 2020). From: <https://www.statista.com/statistics/1067081/generation-electronic-waste-globally-forecast/> accessed on: April 01, 2023
- [6] Statista - Allied Market Research (2023). From: <https://www.statista.com/statistics/1154804/global-e-waste-management-market-value/> accessed on: April 01, 2023
- [7] Avallone, E. A., Baumeister III, T., & Sadegh, A. (2007). *Marks' standard handbook for mechanical engineers*. McGraw-Hill Education.
- [8] Statista - Research and Markets (October 1, 2022). From: <https://www.statista.com/statistics/1309081/global-electronics-recycling-market-size/> accessed on: April 01, 2023

- [9] Factsheet, W. A. R. M. E. R. (1991). Fuel from waste. *The World Resource Foundation, Tonbridge, UK.*



Banja Luka
1–2 June 2023.

DEMI 2023

16th International Conference on Accomplishments in Mechanical and Industrial Engineering

www.demi.mf.unibl.org



INVESTIGATION OF THE INFLUENCE OF CHARACTERISTIC PARAMETERS ON THE ACCURACY OF CT MEASUREMENT

G. Jotić^a, B. Štrbac^b, T. Toth^c, M. Ranisavljev^b, M. Hadžistević^b, M. Dovica^c, B. Runje^d

^aFaculty of Mechanical Engineering Banja Luka, V. Stepe Stepanović 71, 78000 Banja Luka, BiH

^bFaculty of Technical Science Novi sad, Trg Dositeja Obradovića 6, 21102 Novi sad, Serbia

^cFaculty of Mechanical Engineering of the Technical University of Košice, Letná 1/9, Slovak Republic

^dFaculty of Mechanical Engineering and Naval Architecture, Ivana Lučića 5, 10002 Zagreb, Croatia

Abstract Computed tomography (CT) is one of the methods of coordinate measurement which, in the field of dimensional measurement, enables the measurement of the external and internal characteristics of a workpiece by scanning it with X-rays. The X-ray CT is a relatively new technology. It is a non-destructive method that is used for the purpose of dimensional and geometrical analysis of the internal and external characteristics of objects that are not available with other measurement methods. The characteristic of X-ray CT metrology, like other methods of coordinate metrology, is a large number of factors that affect the accuracy of CT measurement results. In this paper an overview of influential factors is provided. The following factors were selected as dominant: the voxel size, number of projections and image averaging methodology. The experiment includes an analysis of the significance of influencing parameters on the accuracy of the CT scanner using Design of Experiment (DOE). The experiment was conducted according to the Taguchi L8 orthogonal array. The obtained results indicate that the selection of appropriate values of influential parameters contributes to the minimization of CT measurement error.

Keywords Coordinate metrology, Computed tomography, accuracy

1. INTRODUCTION

Computed tomography (CT) technology is relatively new and plays an important role in the field of dimensional metrology. The CT measurement systems enable the measurement and analysis of objects made of different types of materials. By applying this technology, it is possible to perform an analysis of the geometry of the internal and external characteristics of the object in order to analyze possible defects and deviations that occurred during the production process. In this way, full

measurement, internal control and comparison with the CAD model of the part or assembly is possible without destroying or disassembling it. The CT scanner uses X-rays for the purpose of computer reconstruction of the cross-sectional tomographic layer based on multiple measurements of X-ray absorption values [1]. However, each of them consists of a radiation source, a rotary table for positioning the object and a sensor that generates a two-dimensional projection image of the object taken at different angles, Figure 1, [2]. Due to the complexity of the implementation of the measurement process by computer tomography, the measurement process is divided into three phases: CT scanning, model reconstructions and analysis of the obtained 3D model [3].

Corresponding author

Senior teaching assistant, Goran Jotić
goran.jotic@mf.unibl.org

Faculty of Mechanical Engineering Banja Luka,
V. Stepe Stepanović 71,
78000 Banjaluka, BiH

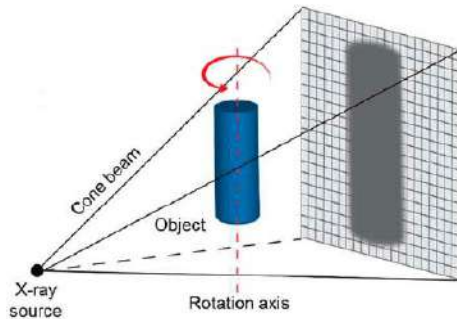


Fig. 1. Basic CT components [2]

The first phase is implemented using a CT device and includes data collection during the rotation of the object through 360 degrees, which is simultaneously exposed to X-ray radiation. In this process, the detector receives attenuated radiation caused by passing through the workpiece, then generates a large number of two-dimensional projection images. Each 2D cross-sectional image corresponds to a view of the object characteristic of one position of rotary table. The scanning phase is followed by the process of 3D model reconstruction based on previously generated 2D images. Each point (pixel) of the 2D images is described by the amount of intensity of the detected radiation. The radiation intensity depends on the total attenuation of the incoming X-ray radiation and the length of the path that the radiation passed through the object [4]. Analysis of 3D models includes dimensional and geometric inspection and CAD to part inspection, Figure 2. The quality of CT measurement results depends on a large number of influential parameters (scanning parameters, type of material, presence of artifacts, etc.).

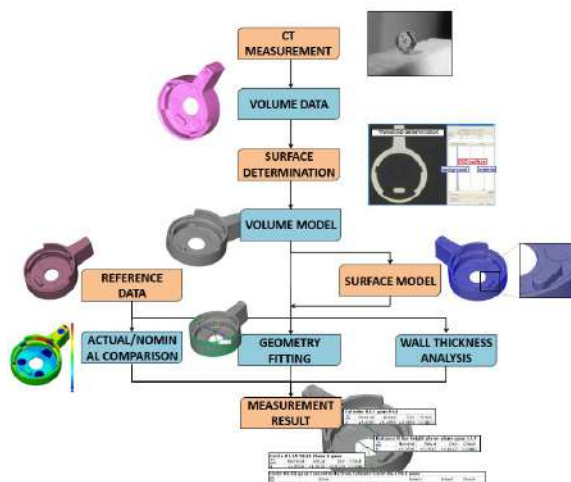


Fig. 2. CT measurement process [5]

It has been proven that the accuracy and measurement uncertainty of dimensional CT measurements are, to a greater or lesser extent, under the influence of these parameters [6]. Even with the latest technological solutions of these systems, CT systems have not yet reached the level of accuracy of coordinate measuring machines (CMM) with contact sensors. One of the main reasons for this is the lack of research in the field of review of influential factors, their interactions and influence on the accuracy of a CT scanner, [7].

Moroni and Petro [8] presented a procedure for testing the performance of CT scanners according to VDI/VDE 2617-13:2005. In this study, which includes a sensor error test (PS and PF), a length measurement error test and a resolution test, two CT scanners were analyzed for which the manufacturers did not define accuracy parameters. An empirical approach to the analysis of measurement uncertainty by X-ray computed tomography is presented in the paper [9]. The research is based on the implementation of the ISO 15 530-3:2013 standard and a review of other empirical methods for estimating CT measurement uncertainty. Villarraga-Gomez et al [10] performed a comparison of dimensional measurements generated on CMM with a contact measuring sensor and an X-ray CT. The internal structures of complex geometry objects were analyzed. Differences in the dimensional analysis of objects using CMM and CT, in the range of dimensions from 0.6 mm to 65 mm, reached a value of up to 5 μm or less for most measurements. In the paper [11], the research of influential factors and their interactions related to the accuracy of CT measurement results was carried out using Design of Experiment (DOE). The influence of geometric magnification, object orientation, number of projections and threshold value on the value of the diameter of cylinders made from different materials was analyzed.

In this paper, the L8 Taguchi orthogonal array was used to design the experiment. The research is based on the dominant input factors analysis and their interaction on the accuracy of the CT scanner. The following factors were analyzed: the voxel size, number of projections and image averaging. The research includes dimensional and geometric analysis of the calibrated test workpiece.

2. MATERIALS AND METHODS

For the purpose of experimental research, a dimensional and geometric inspection of the complex test workpiece was performed. The geometry of the test workpiece was defined with the aim of testing the possibility of realizing different measuring tasks using the X-ray computed tomography, Figure 3. Test workpiece material: AlCu4Mg1 (T351). The accuracy of the CT scanner was analyzed in relation to the calibrated (reference) parallelism tolerance value. The calibrated value was obtained using a CMM with a contact sensor and amounted to 0.0201 mm. Deviations, defined as difference between a measured and calibrated values, were observed output parameters.

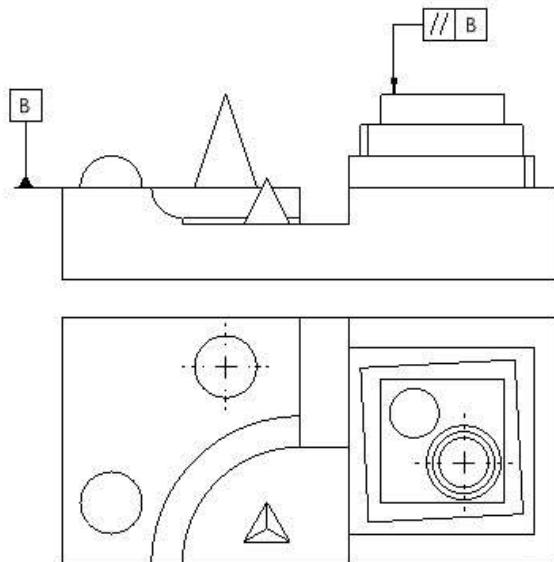


Fig. 3. Test workpiece

CT scanning was conducted on the Phoenix V(tome)xL240 X-ray CT scanner. Table 1 shows the characteristics of the measuring system.

Table 1. CT specifications

Phoenix v tome x L 240	
Max. tube voltage	240 kV
Max. output	320 W
Detail detectability	Up to 1 μm
Min. focus object distance	4.5 mm
Max. voxel resolution	< 2 μm
Geometric magnification (2D)	1.25 times up to 333 times
Geometric magnification (3D)	1.25 times up to 200 times
Max. object size	(600x500) mm

Realization of the object scanning process implies the selection of optimal values of the scanning parameters in order to obtain high-quality of 2D images. Parameter setting included selection of radiation power, filters selection with the aim of noise elimination, positioning of the object, selection of the appropriate orientation of the object, definition of the number of projections and selection of the number of averaged images. After generating the 2D images, a 3D model was reconstructed using the Volume Graphics VGStudio MAX software. The result of the reconstruction of 2D images is a 3D voxel model in different values of the gray scale. The generated STL model is the basis for the implementation of dimensional and geometric inspection. The Zeiss Calypso software was used for the purpose of dimensional and geometric analysis.

The Taguchi design experiment used to suggest parameters that contribute to the generation of optimal CT measurement values. The Taguchi orthogonal array L8 was used to create the experiment. Based on the analysis of influential factors and literature review, a selection of the dominant influencing factors on the accuracy of the results was made. The experiment was performed using three factors at two levels, Table 2.

Table 2. CT parameters and their levels

Parameter	Symbol	Level 1	Level 2
Voxel size (μm)	A	70	140
Number of projections	B	1150	2300
Image averaging	C	yes	no

3. RESULTS AND DATA ANALYSIS

Minitab 20 statistical software was used for statistical data processing and defining the sequence of experiments. Given that the CT measurement process is time-consuming, the Taguchi L8 orthogonal array was selected. Taguchi's experimental design is based on the calculation of the S/N (signal-to-noise) ratio and calculates the S/N ratio for each treatment. The S/N ratio is defined as the ratio between the magnitudes of the input signals and the signals affected by noise [12]. Therefore, the value that maximizes the S/N ratio of each controlled factor becomes robust to noise. In this case, parallelism geometric tolerances were analyzed,

for this reason the S/N ratio "the smaller the better" was used.

$$S/N = -10 \log \left(\frac{1}{n} \sum_{i=1}^n y_i^2 \right) \quad (1)$$

where y_i is the response value of the specific treatment at i repetition, and i is the number of repetitions.

Table 3 shows the Taguchi design and deviation responses for a certain combination of input parameter. Deviations related to parallelism measurement are defined as the difference between measured values and calibration value.

Table 3. Experimental design and calculated results

Exp no.	Parameters			Deviations	
	Image averaging	Number of projections	Voxel size (μm)	Parallelism (mm)	S/N ratio (dB)
1	Yes	1150	70	0.011792	38.5684
2	Yes	1150	140	0.020805	33.6366
3	Yes	2300	70	0.005133	45.7927
4	Yes	2300	140	0.016038	35.8967
5	No	1150	70	0.011873	38.5088
6	No	1150	140	0.020859	33.6141
7	No	2300	70	0.006897	43.2270
8	No	2300	140	0.016409	35.6985

The analysis of the results implies observation of the influence of image averaging, number of projections and voxel size on the parallelism tolerance of the indicated surfaces. Given that the aim is to minimize the parallelism deviation, the "smaller is better" objective function was selected. The S/N ratio values for each iteration are shown in Table 3. The S/N response for each input parameters is shown in Table 4, also mean parallelism tolerance response for all input parameters is shown in Table 5.

Table 4. S/N response table for parallelism tolerance

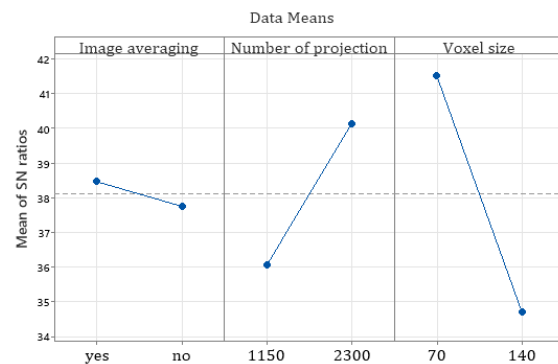
Level	Image averaging	Number of projection	Voxel size
1	38.47	36.08	41.52
2	37.76	40.15	34.71
Delta	0.71	4.07	6.81
Rank	3	2	1

Table 5. Mean response table for parallelism tolerance

Level	Image averaging	Number of projection	Voxel size
1	0.013442	0.016332	0.008924
2	0.014009	0.011119	0.018528
Delta	0.000567	0.005213	0.009604
Rank	3	2	1

Based on the analysis of the S/N ratio, it is possible to determine which of the compared

input factors have the greatest impact on the parallelism tolerance. Based on Table 4 (rank of impact) and Figure 4 (larger graph slope), it can be concluded that the voxel size has the greatest influence on parallelism tolerance, while the image averaging parameter has the least impact.



Signal-to-noise: Smaller is better

Fig. 4. S/N response for parallelism tolerance

As mentioned, the optimal combination of selected factors is for higher values of the S/N ratio. Therefore, the optimal combination of selected factors in accordance with the factor dependence is the voxel size at level 1, then the number of projections at level 2 and the image averaging at level 1, Figure 4.

Analysis of variance (ANOVA) was performed to determine the statistical significance of input parameters on the parallelism tolerance. Thus, the ANOVA test is used to estimate the percentage response magnitude of each factor in an orthogonal experiment, Table 6. The test was conducted with a confidence level of 95 %, i.e., a significance level of 5 %.

Table 6. Results of the ANOVA test

Source	D F	Adj SS	Adj MS	F-Value	P- Value	%
Image averaging	1	0.000001	0.000001	1.50	0.288	0,08
Number of project.	1	0.000054	0.000054	126.68	0.000	22,9
Voxel size	1	0.000184	0.000184	429.99	0.000	76,9
Error	4	0.000002	0.000000			0,08
Total	7	0.000241				100

Based on the F test, it is possible to determine which of the observed factors have a significant impact on the output and by what percentage. The threshold value of F for a confidence level of 95 %, a significance level of 5 %, two levels of variation and 8 experiments is $F_{0.05,1,7}=5,59$. Input parameters with F value less than the threshold value do not have a significant impact on parallelism tolerance. However, the significance of the input parameters can also be determined through the significance level. Given that the level of significance is defined at a value of 5 %, it follows that factors with p value less than 0.05 are significant, and if this value is higher, then they are insignificant.

The results of the ANOVA test indicate that two of the three input factors have a significant impact on parallelism tolerance. The F values for the input parameters voxel size and number of projections are greater than the threshold value, in contrast to the image averaging parameter. We reach the same conclusion by comparing the significance level of p . The p -value for the input parameter image averaging is greater than the threshold value of 0.05, which means that this input parameter is not significant.

4. CONCLUSIONS

Computed tomography (CT) is a relatively new technology. One of the disadvantages is the lack of internationally standardized methods for evaluating the accuracy of CT. In this paper, the influence of image averaging, number of

projections and voxel size on the accuracy of CT measurement results was analyzed. The experiment was carried out according to the Taguchi L8 orthogonal array. The Taguchi technique was used for the purpose of optimizing the measurement process (reducing measurement error). Based on the S/N ratio, it can be concluded that the optimal combination of input parameter levels that result in the smallest measurement error are: voxel size 70 μm , 2400 projections during scanning process, including image averaging during 2D image processing.

As mentioned, the ANOVA test determines the level of influence of measurement parameters on the accuracy of measurement. The test results, Table 6, show that the most influential input parameter on the measurement accuracy is the voxel size with a percentage contribution of 76.9 %, followed by the number of projections with a percentage contribution of 22.9 %. On the other hand, the image averaging parameter has no significant contribution.

Given that the computer tomography is one of the methods of coordinate measurement that enables the realization of measurements of hard-to-reach regions of objects without destruction, this method is interesting for application in a wide range of industrial production processes.

5. ACKNOWLEDGMENTS

This paper is a part of these projects: VEGA 1/0224/18 Research and development of testing and measuring methods in coordinate metrology, KEGA 006STU-4/2018 Modernization of laboratories for measurement of thermal and technical quantities and KEGA 021TUK-4/2022 Implementation of computed tomography in an interdisciplinary technical-natural area.

REFERENCES

- [1] Carmignato, S. (2012). Accuracy of industrial computed tomography measurements. *CIRP Annals*, vol. 61, no. 1, p. 491-494. <https://doi.org/10.1016/j.cirp.2012.03.021>
- [2] Welkenhuyzen, F. (2016). *Investigation of the accuracy of an X-ray CT scanner for dimensional metrology with the aid of simulations and calibrated artifacts*, PhD thesis, KU Leuven, Nederland.

- [3] Müller, P. (2013). *Coordinate metrology by traceable computed tomography*. PhD thesis. Technical University of Denmark.
- [4] Horvatić, N. A., Runje, B. (2017). Capabilities of industrial computed tomography in the field of dimensional measurements. *APEM*, vol. 12, no. 3, p. 245-253. <https://doi.org/10.14743/apem2017.3.255>.
- [5] Müller, P., Hiller, J., Cantatore, A., De Chiffre, L. (2012). A study on evaluation strategies in dimensional X-ray computed tomography by estimation of measurement uncertainties. *International Journal of Metrology and Quality Engineering*, Vol. 3, no. 2, p. 107-115. <https://doi.org/10.1051/ijmqe/2012011>.
- [6] Šokac, M. (2019). Hibridni model za segmentaciju snimaka generisanih primenom kompjuterizovane tomografije. (In Serbian). PhD thesis. Fakultet tehničkih nauka Novi Sad.
- [7] Kruth, J. P., Bartscher, M., Carmignato, S., Schmitt, R., De Chiffre, L., Weckenmann, A. (2011). Computed tomography for dimensional metrology, *CIRP Annals*, vol. 60, no. 2, p. 821–842. <https://doi.org/10.1016/j.cirp.2011.05.006>.
- [8] Moroni, G., Petró, S. (2018). A discussion on performance verification of 3d x-ray computed tomography systems. *Procedia CIRP*, vol. 75, p. 125-130. <https://doi.org/10.1016/j.procir.2018.04.064>.
- [9] Villarraga-Gómez, H., Thousand, J., Smith, S.T. (2020). Empirical approaches to uncertainty analysis of X-ray CT measurements: A review with examples. *Precision Engineering*. Vol. 64, p. 249-268. <https://doi.org/10.1016/j.precisioneng.2020.03.004>
- [10] Villarraga-Gómez, H., Lee, C., Smith, S. T. (2018). Dimensional metrology with X-ray CT: A comparison with CMM measurements on internal features and compliant structures. *Precision Engineering*, Vol. 51, p. 291-307. <https://doi.org/10.1016/j.precisioneng.2017.08.021>.
- [11] Weckenmann, A., Krämer, P. (2010). Predetermination of measurement uncertainty in the application of computed tomography. *Product Lifecycle Management: Geometric Variations*, p. 317-330. doi:10.1002/9781118557921
- [12] Štrbac, B., Ačko, B., Havrišan, S., Matin, I., Savković, B., Hadžistević, M. (2020). Investigation of the effect of temperature and other significant factors on systematic error and measurement uncertainty in CMM measurements by applying design of experiments. *Measurement*, Vol.158. <https://doi.org/10.1016/j.measurement.2020.107692>.



Banja Luka
1–2 Jun 2023.

DEMI 2023
**16th International Conference on
Accomplishments in Mechanical and
Industrial Engineering**
www.demi.mf.unibl.org



Life-cycle comparison of the Hall-Heroult process, inert electrodes, and energy supply in aluminum production

B. Bronkema^a, G. Sævarsdóttir^a, D.C. Finger^a

^aSchool of Engineering, Reykjavik University, Menntavegur 1, 102 Reykjavik, Iceland

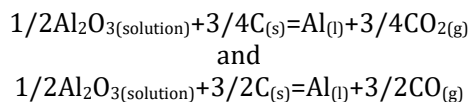
^bFulbright Fellow, 2022-23

Abstract Aluminum (Al) production consumes 14 kWh of electricity per kg Al and produces 1.1 billion tonnes of carbon emissions (CO_{2,eq}) annually. The Hall-Heroult process is currently the only industrial process for Al production, producing two tonnes of CO_{2,eq} per tonne Al by carbon anode electrolysis. Electrodes that do not participate in the electrolysis of alumina can reduce the impact of Al production. Transitioning to inert anodes implies redesign of electrolysis cells to optimize energy requirements. We performed a life-cycle analysis to compare the ecological footprint of Hall-Heroult and inert production using GaBi software and the ecoinvent database, complemented with primary data. Results were calculated for two Hall-Heroult and fifteen inert scenarios, varying power between 13.5 kWh and 17 kWh for six different energy mixes: Icelandic hydropower, global mix, natural gas, coal, nuclear, and geothermal. A final “best-case” scenario uses hydropower data as the power source for alumina refinement (shown in electrolysis). The results reveal that the energy mix dominates the impact on the ecological footprint in the earlier refinement and electrolysis stages. However, using inert electrodes in smelters powered with renewable electricity can lower the carbon footprint of aluminum production by over 80%.

Keywords aluminum production, inert anodes, LCA

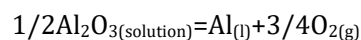
1. INTRODUCTION

Aluminum production alone currently accounts for around 2% of global carbon dioxide emissions. To produce aluminum, bauxite ore is mined and refined to alumina, then processed by electrolysis requiring between 12 and 17 kWh per kg Al [8]. Conventionally, electrolysis requires anodes made of carbon, a feedstock of alumina (aluminum oxide), and electrical energy applied as a DC current in the Hall-Heroult process. The electrolysis produces pure liquid aluminum and carbon dioxide. Carbon monoxide is coevolved, as are smaller amounts of fluorocarbons and sulfur compounds due to impurities in the anodes.



Carbon emissions also occur during the manufacturing of the carbon anodes [6].

Inert metal anodes (IMA), in place of carbon, can eliminate the carbon emissions from alumina electrolysis and limit those produced in anode production, substantially reducing the carbon footprint of the entire smelting process [8]. IMA evolve oxygen rather than carbon dioxide and other hydrocarbons.



Attempts to develop industry-level inert anodes with similar performance to the Hall-Heroult process started in the early 20th century. Anode research mainly focused on three classes of materials: ceramic, metal, and cermet [7]. In the 1990s The Aluminum Company of America – later, Alcoa – patented the process and apparatus for low temperature aluminum electrolysis, recommending the use of inert anodes

composed of 17%wt Cu and 83%wt other oxides, namely NiO and Fe₂O₃. More recently, Padamata et al. confirmed the efficiency of Cu-Ni-Fe anodes in a 2018 review of industry progress. Cu-Ni-Fe anodes form protective oxide layers during electrolysis, slowing down the corrosive effects of the electrolyte [7]. Gunnarsson et al. (2019) revealed the production of Al with 99.22% purity using 20%wt Cu, 42%wt Ni, 38%wt Fe anode and TiB₂ cathode with a 21mm distance between vertical electrodes. This experiment produces low current efficiencies of 71-73%, but low rates of aluminum contamination by electrode material [2].

Directly substituting IMA into existing electrolytic cells would however increase the energy requirement for smelting plants by up to 25% as the reaction products are higher energy molecules [8]. Producing oxygen at the anode instead of carbon dioxide drives up the operating voltage by about one volt, corresponding to over a 3 kWh/kg Al electrical power increase [9]. According to Haupin and Kvande (2000), it is thermodynamically possible to operate inert anode cells at 13.2 kWh/kg Al by reducing the anode-cathode distance and thereby reducing the voltage drop across the electrolyte. Maintaining the power requirement at 13.5 kWh would require the electrolytic cells to be retrofitted [8]. In 1994, Moltech published U.S. Pat. No. 5,362,366 detailing an anode-cathode arrangement for non-consumable anodes and cathodes that maintains the efficiency of conventional electrolysis. These arrangements primarily allow for the new electrodes to be positioned vertically in existing cells, with groups of inert anodes filling the place conventionally filled by a single carbon anode [10].

La Camera et al. (1995) also rely on vertical arrangements to obtain low-temperature electrolysis results in their 1995 patent. Brown (2001) shows that considerable energy savings of up to 30% can be obtained by using vertical electrode cells (VEC) over conventional arrangements while also limiting operating costs due to the reduced rate of anode replacement. However, he also outlines substantial engineering challenges related to the implementation of VEC, namely electrode manufacturing and alumina-feeder technology [1]. In total, alumina electrolysis requires an

anode, cathode, electrolyte, container, method of delivering electricity, alumina feeder, and product extraction system. Out of these elements, it is reasonable to assume that the container, method of delivering electricity, alumina feeder, and product extraction system could remain constant in a retrofit. In addition to the environmental aims of IMA, they also represent a potential for financial and occupational improvement [5]. As IMA theoretically do not participate in the electrolysis reaction, their slow rate of decomposition eliminates many costs associated with frequent replacement of carbon anodes. Anode changing also creates the highest exposure of aluminum workers to particulate matter and toxic gases from the process, so IMA have the potential to improve working conditions in smelters as well [5].

Around 70% of the global carbon dioxide emissions from aluminum smelting currently come from the high electrical energy requirements of the process. The Life Cycle Inventory (LCI) data published by the International Aluminium Institute (IAI) reveals that the geographic location of aluminum smelters and the corresponding energy mix had a significant environmental effect [12]. In a comparative LCA of smelting technologies including pre-baked and inert anodes, Kovács and Kiss (2015) also emphasize the importance of energy mix. However, their LCA does not include emission values related to the retrofit of the smelters required to minimize energy consumption. There is a need to understand how the IMA electrolysis process partnered with the costs of a retrofit compare to the Hall-Heroult process with various energy inputs.

This study aims to focus on the advantages of IMA compared to the Hall-Heroult process and to calculate a full LCA for different energy sources and requirements. In this study, we calculated the LCA for fifteen scenarios, addressing an energy requirement of 13.5 kWh/kg Al, 17 kWh/kg Al (corresponding to roughly a 25% increase), and six different energy mixes.

2. METHODS

To compare the LCA of inert anodes, carbon anodes, and different energy mixes we developed fifteen realistic scenarios (Table 1). For comparative purposes, a GaBi flow was constructed for the Hall-Heroult process to ensure consistent inputs with the modeled IMA process, such as electricity inputs and material flow datasets. The results from this flow are included as Scenarios I and II.

Table 1. Hall-Heroult and IMA scenarios

Scen no.	Process	Power Requirement*	Energy Source
I	HH	14.1**	Hydro
II	HH	14.1**	Global
III	Inert	13.5	Hydro
IV	Inert	17	Hydro
V	Inert	13.5	Global
VI	Inert	17	Global
VII	Inert	13.5	Natural Gas
VIII	Inert	17	Natural Gas
IX	Inert	13.5	Coal
X	Inert	17	Coal
XI	Inert	13.5	Nuclear
XII	Inert	17	Nuclear
XIII	Inert	13.5	Geothermal
XIV	Inert	17	Geothermal
XV	Inert	13.5	Hydro***

* kWh per kg Al

** European average

*** including adjusting the electricity input for the alumina refinement stage

The full LCA was established by the ISO 14044 standards to define a goal and scope of the study. GaBi software by Sphera (Sphera Solutions Inc., 2021) was used to model the LCA process chain, calculate the impact categories, and perform a sensitivity analysis.

2.1 Goal

The goal of this LCA was to fully characterize the effect of a transition to inert electrodes on the aluminum production process. Values obtained from the modeling of inert electrodes were compared to those in the literature relating to carbon anodes in the Hall-Heroult process.

2.2 Scope Definition

Five main unit processes were considered in the model: the electrolytic smelter retrofit process, inert anode manufacturing, inert cathode manufacturing, electrolysis, and inert electrode recycling. These processes occur within the aluminum production chain between the refinement of alumina and the casting of ingots. This LCA represents a gate-to-gate model within the aluminum production process, although it contains a cradle-to-grave model of the inert electrodes themselves. The functional unit for this LCA was defined as 1 tonne Al. This is consistent with other aluminum-related LCAs, such as the one performed by the International Aluminium Industry (*Life Cycle Inventory (LCI) Data and Environmental Metrics*, 2017). In the individual unit processes 1 kilogram Al was used, which was then scaled up in the larger LCA. Electricity inputs to the system were implemented at the highest level of the LCA for ease of comparison. Adjustments to the electricity inputs were critical in comparing Icelandic energy mixes to global energy mixes in the different scenarios considered for the results of this LCA.

2.2 Impact Categories

GaBi Software and ecoinvent environmental quantities were used to assess the environmental impact of the constructed flow. Of the significant number of options available in the software, six impact categories were evaluated: i) global warming potential over 100 years (GWP100), ii) primary energy demand (PED), iii) human toxicity potential (HTP), iv) acidification potential (AP), v) terrestrial ecotoxicity potential (TETP), and vi) freshwater use.

2.3 Sensitivity Analysis

Three main parameters were chosen as the subjects of a sensitivity analysis: the energy source, the method of alumina refinement, and the amount of anode and cathode required per kg of Al. The GWP100 was chosen as the main indicator of environmental impact.

3. RESULTS

The results of the LCA from the fifteen scenarios described by Table 1 were evaluated regarding

the six impact categories: GWP100, PED, HTP, AP, TETP, and freshwater use.

3.1 Global Warming Potential

The GWP100 was calculated and is displayed in Figure 1. The scenario with the highest GWP100 is Scenario X (inert, 17kWh, coal) at 21,881 kg CO_{2,eq} per tonne Al while the scenario with the lowest is Scenario XV (inert, 13.5kWh, hydro) at 820 kg CO_{2,eq} per tonne Al.

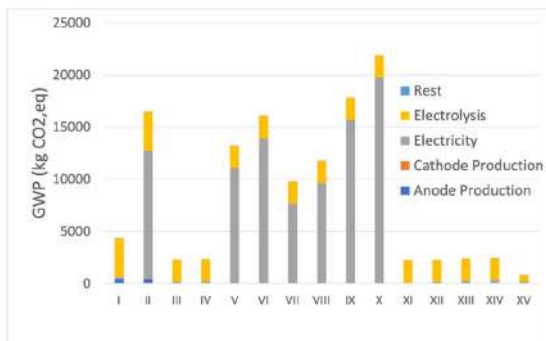


Fig. 1. GWP100 for the fifteen scenarios

3.2 Primary Energy Demand

The PED was calculated for all scenarios. These results are shown in Figure 2. Scenario X (inert, 17, coal) has the highest PED at 319,584 MJ per tonne Al and Scenario III has the lowest PED at 80,052 MJ per tonne Al.

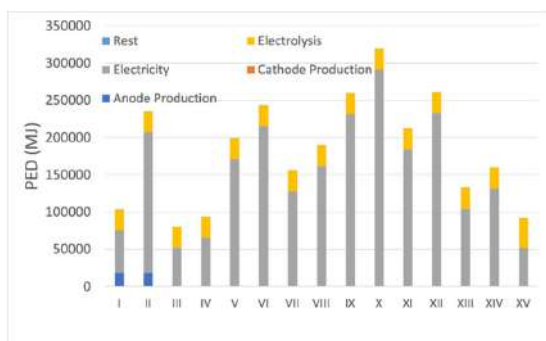


Fig. 2. PED for the fifteen scenarios

3.3 Human Toxicity Potential

In Figure 3, the HTP for the Hall-Heroult and IMA scenarios is displayed. The highest HTP is 17,505 kg DCB_{eq} per tonne Al for Scenario II (HH, 14.1kWh, global) and the lowest HTP is 2,992 kg DCB_{eq} per tonne Al for Scenario XV (inert, 13.5kWh, hydro).

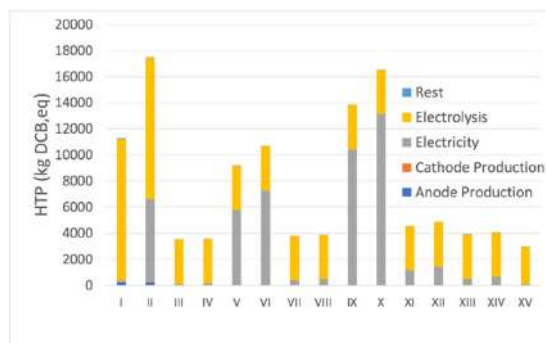


Fig. 3. HTP for the fifteen scenarios

3.4 Acidification Potential

In Figure 4, the AP for the Hall-Heroult and IMA scenarios is displayed. The scenario with the highest AP is Scenario X (inert, 17kWh, coal) at 150 kg SO_{2,eq} per tonne Al while the scenario with the lowest is Scenario XV (inert, 13.5kWh, hydro) at 15 kg SO_{2,eq} per tonne Al.

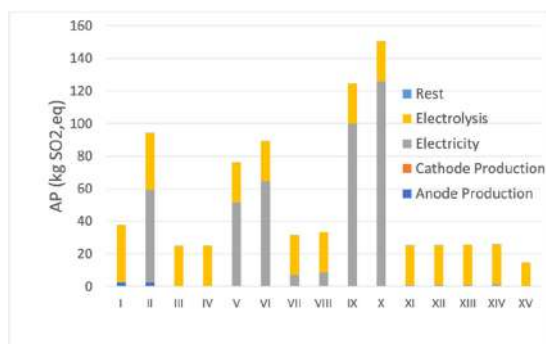


Fig. 4. AP for the fifteen scenarios

3.5 Terrestrial Toxicity Potential

In Figure 5, the TETP for the Hall-Heroult and IMA scenarios is displayed. Scenario X (inert, 17, coal) has the highest TETP at 70 kg DCB_{eq} per tonne Al and Scenario XV has the lowest TETP at 27 kg DCB_{eq} per tonne Al.

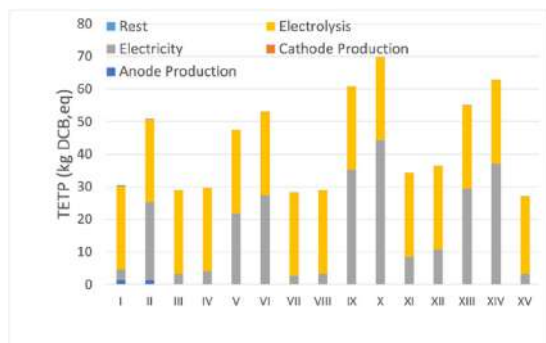


Fig. 5. TETP for the fifteen scenarios

3.6 Freshwater Use

In Figure 6, the freshwater use for the Hall-Heroult process and the IMA scenarios is displayed. The highest freshwater use is 141,460,827 kg H₂O per tonne Al for Scenario IV (inert, 17 kWh, hydro) and the lowest freshwater use is 4,769,210 kg H₂O per tonne Al for Scenario VII (inert, 13.5kWh, gas).

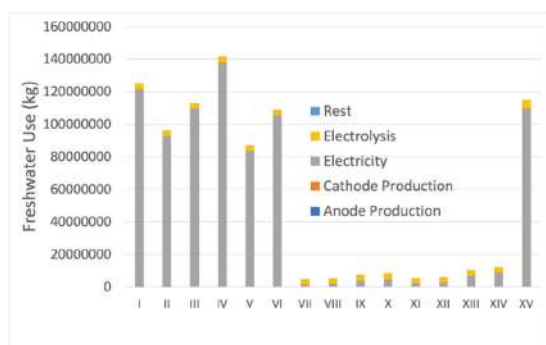


Fig. 6. Freshwater use for the fifteen scenarios

4. DISCUSSION

4.1 Global Warming Potential

As expected, the transition to inert anodes offers significant CO_{2, eq} emissions savings when the appropriate energy mix is used. Powering electrolysis with hydropower, much of the GWP in the HH process comes from anode production, direct emissions from the electrolysis process, and upstream emissions related to alumina production. Although the IMA process maintains these alumina-related emissions, the carbon emissions in the anode production and direct emissions from electrolysis are essentially eliminated. As relates to anode production, although the IMA technology this study is based upon require iron, nickel, and copper (metals not used in comparable quantities in the Hall-Heroult process) and so include in their LCA the corresponding production processes, this effect overall is quite small due to the anodes' long lifetimes and recyclability. The increase in energy requirement modeled in Scenario IV does little to alter these results when the energy source is Icelandic hydropower.

Using global energy mixes – Scenarios V and VI – alters these conclusions significantly. In Scenario V, GWP is still saved with a switch to IMA when the power requirement is 13.5 kWh per kilogram

Al. As in Scenarios III and IV, this is primarily due to the reduction of emissions from the anode production and electrolysis processes. However, with the 17 kWh power requirement of Scenario VI, the GWP of HH and inert production become almost equal, with the HH process at 16,500 kg CO_{2, eq} per tonne Al and the IMA process at 16,100 kg CO_{2, eq}. Scenarios VII to XIV display predictable results with coal-powered electricity producing the highest GWP, followed by natural gas, geothermal, and nuclear. Scenario XV displays the “best case scenario” for aluminum production, specifically for the case of alumina refinement in South America and smelting in Europe. These results were achieved by embedding hydropower data into the alumina refinement process, as well as maintaining the conditions from Scenario III. With a GWP of 820 kg CO_{2, eq}, Scenario XV represents an 81.4% GWP savings from Scenario I and a 64.0% GWP savings from Scenario III.

4.2 Primary Energy Demand

Following a similar trend to GWP, most of the PED savings offered by IMA come from the anode production stage. The fossil-based composition of carbon anodes adds significant chemical energy to the HH LCA and is eliminated in the IMA LCA, resulting in a 23.0% PED savings between Scenarios I and III. This percentage rises to 31.3% when the electrolysis portion of production is isolated by neglecting alumina refinement. For other scenarios, a general trend of PED due to energy source can be seen with coal as the highest, followed by nuclear, then global mix, then geothermal. Hydropower offers the lowest PED per tonne Al.

4.3 Human Toxicity Potential

The carbon anodes in the HH process are the primary cause of the sulfur and perfluorocarbon compounds that affect HTP. Due to this, Scenario III shows a 68.7% reduction in HTP over Scenario I. In this impact category, the electrolysis process appears as the most significant factor as Scenario II tops even Scenario X. However, fluoride present in the electrolyte is the source of hydrofluoric acid emissions and electrolyte composition and interaction for IMA electrolysis is still a point of continued research. Thus, reliable estimates of the HTP reduction requires further study. For

IMA Scenarios VII to XIV, energy source again determines the trend with coal followed by nuclear, then natural gas, then geothermal.

4.4 Acidification Potential

Again due to sulfur compounds present in carbon anodes, IMA are able to offer AP savings over the HH process, with Scenario III having 34.2% less AP than Scenario I. Even with a global mix energy source – Scenarios II and V – IMA offers a 19.3% reduction. Other energy sources cause a decreasing trend with respect to coal, natural gas, geothermal, and nuclear.

4.5 Terrestrial Toxicity Potential

As with other impact categories, the lack of carbon anodes in the IMA process leads to a reduction potential in TETP. Between the hydropower scenarios I and III there is a 5.3% TETP reduction and a 7.0% TETP reduction between the global mix scenarios II and V. Other scenarios are listed in terms of decreasing TETP according to their energy mix: coal, geothermal, nuclear, natural gas.

4.6 Freshwater Use

Common trends for other impact categories are slightly altered for freshwater use, as hydropower uses substantial amounts of freshwater to generate electricity. For this reason, scenarios that include hydropower production – I, II, III, IV, V, VI, and VX – are significantly higher than all other energy mix scenarios.

4.7 Sensitivity Analysis

When focusing on GWP100 as the main environmental indicator, it was found that the source of electricity had the most significant impact on the results. When the global mix energy input was varied by 50% against a default energy source of hydropower, it produced an 18.3% effect on the results. Although the variance of alumina input also had an impact – 5.18% variance of the results with a 50% variation – this can be viewed as a sub-case of power source variation, already identified as the most significant contributor to GWP. Finally, the

electrode input amount had an extremely insignificant effect on the results. This is not surprising, as the longer lifetime and recyclability of the anodes allow their effect to be minimized in the LCA.

4.8 LCA Limitations and Future Research

Although LCA software and databases such as GaBi and ecoinvent attempt to consider all production streams and potential variations, capturing all these perfectly is unlikely, especially in the face of future prediction. Since IMA technology is still not in use at an industrial level, this LCA relies on the validity of current datasets to be accurate in the future, a reasonable assumption for most industrial processes but one that can never be fully verified. Additionally, there is certain knowledge that can be added to this LCA as it becomes available to extend its accuracy. Continued research is needed specifically on possible direct emissions from IMA electrolysis, anode lifetime, and anode recycling processes.

5. CONCLUSION

Although the Hall-Heroult process has been the only industrial option for aluminum production since the 1890s, inert anodes represent the future of this industry. For this reason, it is crucial to fully understand their effect on the environment and climate. When electricity production for aluminum electrolysis comes from renewable sources, such as is the case in Iceland, and power requirements for smelting can be limited to 13.5 kWh per kilogram of pure aluminum, IMA offer over a 90% GWP savings from the Hall-Heroult process, as well as over a 30% reduction in PED. At this power requirement, IMA also offer significant GWP savings using global energy data, although this result is cancelled out if power requirements rise to 17 kWh.

REFERENCES

Journal papers:

- [1] Brown, C. (2001). Next generation vertical electrode cells. *JOM*, vol. 53, no. 5, p. 39-42. DOI: 10.1007/s11837-001-0208-3
- [2] Gunnarsson, G., Óskarsdóttir, G., Frostason, S., & Magnússon, J. (2019). Aluminum Electrolysis

- with Multiple Vertical Non-consumable Electrodes in a Low Temperature Electrolyte. *Light Metals*, p. 803–810. DOI: 10.1007/978-3-030-05864-7_98
- [3] Haupin, W., Kvande, H. (2000). Thermodynamics of Electrochemical Reduction of Alumina. *Light Metals*, vol. 2. DOI: 10.1002/9781118647851
- [4] Kovács, V., Kiss, L. (2015). Comparative Analysis of the Environmental Impacts of Aluminum Smelting Technologies. *Light Metals*, p. 529–534. DOI: 10.1007/978-3-319-48248-4_88
- [5] Kvande, H., Drabløs, P. A. (2014). The Aluminum Smelting Process and Innovative Alternative Technologies. *Journal of Occupational and Environmental Medicine*, vol. 56, no. 5 p. S23–S32. DOI: 10.1097/JOM.0000000000000062
- [6] Padamata, S. K., Singh, K., Haarberg, G. M., & Saevarsdottir, G. (2022). Wettable TiB₂ Cathode for Aluminum Electrolysis: A Review. *Journal of Sustainable Metallurgy*, vol. 8, no. 2, p. 613–624. DOI: 10.1007/s40831-022-00526-8
- [7] Padamata, S. K., Yasinskiy, A., & Polyakov, P. (2018). Progress of Inert Anodes in Aluminium Industry: Review. *Journal of Siberian Federal University. Chemistry*, vol. 11. DOI: 10.17516/1998-2836-0055
- [8] Saevarsdottir, G., Kvande, H., & Welch, B. J. (2020). Aluminum Production in the Times of Climate Change: The Global Challenge to Reduce the Carbon Footprint and Prevent Carbon Leakage. *JOM*, vol. 72, no. 1, p. 296–308. DOI: 10.1007/s11837-019-03918-6

Book chapters:

- [9] Huglen, R., Kvande, H. (2016). How to Minimize the Carbon Footprint from Aluminum Smelters. *Global Considerations of Aluminium Electrolysis on Energy and the Environment* p. 948–955. DOI: 10.1007/978-3-319-48156-2_140

Technical reports:

- [10] de Nora, V., Sekhar, J. A. (1994). *Anode-Cathode Arrangement for Aluminum Production Cells*. Moltech Invent S.A., Luxembourg, Patent, no. 5,362,366.
- [11] La Camera, A. F., Tomaswick, K. M., Ray, S. P., Ziegler, D. P. (1995). *Process and Apparatus for Low Temperature Electrolysis of Oxides*. Aluminum Company of America, Pittsburg, USA, Patent, no. 5,415,742.
- [12] (2017). *Life Cycle Inventory Data and Environmental Metrics for the Primary Aluminium Industry*. International Aluminium Institute. LCA.



Banja Luka
1-2 Jun 2023.

DEMI 2023

16th International Conference on Accomplishments in Mechanical and Industrial Engineering

www.demi.mf.unibl.org



Methodology of evaluation of ecological characteristics of residential buildings in Bosnia and Herzegovina

Dragica Arnautović-Aksić¹

Abstract

Residential buildings are responsible for a large consumption of energy and resources, and their ecological characteristics are therefore of great importance. The paper analyzes several commonly used models for evaluating the ecological characteristics of buildings, with an emphasis on residential buildings. In addition to the models, two software were analyzed, which are used to evaluate the ecological characteristics of buildings, as a whole, as well as their elements. The goal of the research is to examine and find a model that is acceptable for evaluating the ecological characteristics of residential buildings in Bosnia and Herzegovina, although there is no legal obligation to do so yet. The paper aims to point out the importance of evaluating the ecological characteristics of residential buildings because they are the most numerous in the total pool of buildings. For evaluating the ecological characteristics of residential buildings in Bosnia and Herzegovina, taking into account local conditions and available data, the most appropriate software is eco2soft, developed by the Austrian Institute for Buildingsbiology und Ecology (IBO). Using this software, it is possible to evaluate entire buildings during their life cycle, the building envelope or only individual elements of the structure. After evaluating the buildings, we can build buildings with less impact on the environment than we are building them now.

Keywords

Ecological characteristics of buildings, Assessment models and tools, Sustainable architecture

1. INTRODUCTION

~~The work was created as a result of research during the preparation of the doctoral dissertation *Application of wood in residential architecture of Bosnia and Herzegovina from the point of view of environmental safety of buildings* at the Faculty of Architecture of the University of Belgrade.~~

The building sector is responsible for a large part of the consumption of natural resources - raw materials for the production of building materials and energy sources during their entire life cycle. Residential buildings are the dominant type of building, and family houses make up 97,63%¹² of the housing stock. For

this reason, the environmental soundness of family residential buildings is extremely important.

There is no official definition of sustainable architecture, but it is derived from the concept of sustainable development, which was defined in the report entitled „Our Common Future“ issued in 1987 by the World Commission on Environment and Development, the so-called Brundtland Commission: „Sustainable development seeks to meet the needs and wants of today without jeopardizing the ability to meet those of the future“³. The term sustainable

¹ PhD Dragica Arnautović-Aksić, European University Brčko District, Bijeljinska cesta 72-74 (E-mail: dragicagoca@gmail.com)

² Arnautović-Aksić, i drugi (2016). *Tipologija stambenih zgrada Bosne i Hercegovine*, Arhitektonski fakultet u Sarajevu, Sarajevo

³ UN (1992). Report the United Nation Conference on Environment and Development Annex I Rio declaration on environment and

development was developed in the following years in order to develop the concept of sustainable construction from it, and the first international conference on sustainable construction was held in Florida in 1994. Along with the term sustainable construction, the term sustainable architecture is also starting to be used. Numerous authors have dealt with defining the term sustainable architecture. Authors of *A Green Vitruvius. Principles and Practice of Sustainable Architectural Design*⁴ analyzed and listed the terms: environmentally friendly, environmentally conscious, energy conscious, sustainable, greener or, simply, green architecture and concluded that there is no internationally accepted definition for green architecture.

For the purposes of further work, we define sustainable architecture as architecture that provides users with a healthy and comfortable environment during their lifetime of use, while at the same time having minimal harmful effects on the environment, the use of raw materials and the production process of construction materials necessary for its construction, during its construction and use, with maintenance , until its end.

The concept of sustainability can be viewed from three aspects - ecological, economic and social, which also applies to the field of construction. Initially, the research focus was on ecological aspects in the building sector, and numerous models were developed that assessed the environmental impact of buildings, the most famous of which are BREEAM and LEED. Over time, the focus shifted to the other two aspects of sustainability - economic and social.

Given that a large number of different models with different indicators appeared, it was necessary to standardize the area. First, the standards governing the ecological performance of buildings were adopted, followed by those related to the economic and social aspects of sustainable construction. These standards establish a legal framework for assessing all three aspects of sustainability – environmental, **economic and social**⁵. The standards establish a

framework with defining indicators on the basis of which performance is evaluated, as well as the evaluation process itself.

According to the methodology defined by EN standards, the performance evaluation is done for the entire life cycle of the building - from the production of building materials and products, construction, use with maintenance and up to the end of the life of the building, with recycling, reuse or disposal. The ecological performance of buildings is evaluated during the life cycle of buildings using the LCA methodology⁶, while the economic performance is analyzed using the LCCA methodology⁷.

2. OVERVIEW AND ANALYSIS OF EXISTING MODELS AND SOFTWARE FOR ASSESSMENT OF BUILDING SUSTAINABILITY

Models for assessing the sustainability of buildings are developed within state institutions, green building councils or private companies. Some of the models evaluate the entire building, and some only the sustainability of individual elements of the structure. Initially, these were general models for buildings, and later the development of variants for buildings of different types and purposes began, developed for local conditions and regulations, but also for international use, with certain adjustments to local conditions (climatological, legislative, economic, social, etc.)⁸.

In the world exist a very large number of models in the world, the following were selected for analysis in this paper:

1. The code for Sustainable Homes – the model created by the development of BREEAM, the first model for assessing the sustainability of buildings, specially developed for residential buildings;
2. TQB Tool – model developed within the framework of the Austrian Green Building Council;

development from:

<https://un.orgg/documents/ga/conf151/aconf15126-1annex1.thm>, accessed on: March 10, 2013.

⁴ Fitzgerald, E., McNicholl, A., Alcockland, R., Lewis, O., et al. (2008). *A green Vitruvius – Principle and Practice of Sustainable Architecture Design*, Earthscan, Dublin.

⁵ ISO standards and EN standards, most of which were accepted in B&H as BAS standards.

⁶ LCA – Life Cycle Assessment

⁷ LCCA – Life-Cycle Cost Analysis

⁸ The Green Building Council is an association that promotes sustainable construction among experts, but also in the ranks of the economy, as well as in the public sector. The council's activities are numerous and, in addition to promotion, include educational activities, work on improving regulations, as well as technology and knowledge transfer. The council prepared one of the first models for assessing the ecological soundness of LEED buildings.

3. DGNB – a second generation model that includes all aspects of sustainability – ecological, social and economic.

2.1. THE CODE FOR SUSTAINABLE HOMES⁹

The model with the longest tradition is BREEAM¹⁰. It was developed within the framework of the British research institute BRE – Building Research Establishment. BREEAM is applied in 73 countries of the world, in some in its original form, and in some adapted to local regulations, and there are variants for Great Britain, the Middle East and Europe. It was developed for special types of buildings, and the first version for evaluating the ecological characteristics of apartments was Eco Homes. Its transformation and incorporation into the legislation of Great Britain resulted in a new model for apartments, called The Code for Sustainable Homes. The Code for Sustainable Homes has been in force since April 2007, and since April 2008 it has become mandatory for all new homes built in Great Britain.

According to this model, apartments are evaluated in nine categories: energy and CO₂ emissions, water, materials, surface water drainage, waste, pollution, health and well-being, management, ecology, first in the design phase, and after construction they receive a final evaluation. Depending on the importance given to certain categories, some are mandatory, such as energy and water, and must meet the minimum standards for all levels, for some categories it is determined that they must meet the minimum standards as an obligation to enter the further procedure, and for some do not even have minimum standards.

Each category is scored and then additionally weighted, and after that the final number of points is obtained, and by adding the points for each category, the overall rating of the apartment is obtained. Based on the evaluation, apartments can receive a rating from 1 to 6 stars, with the fact that an apartment that receives 6 stars is carbon neutral.

The Code for Sustainable Homes is complementary to the Construction Products Directive. For easier using was created the internet database Green Guide [6], [7]. This

database contains constructive elements of buildings with 13 impact categories and for six types of buildings. Ecological impacts were evaluated: climate change, water consumption, consumption of mineral raw materials, destruction of stratospheric ozone, human toxicity, ecotoxicity of fresh water, nuclear waste, ecotoxicity of land, waste disposal, destruction of fossil fuels, eutrophication, creation of photochemical ozone, acidification. Buildings are typologically divided into: commercial, educational, healthcare, retail, residential and industrial. Building elements that are evaluated are: external walls, internal walls, roofs, floors of the ground floor and first floor, windows, insulation and finishing materials for floors.

In addition to the database, there is also software, which is used via the Internet, the Green Guide Calculator tool, which calculates the ecological characteristics of all elements. Only authorized persons-assessors, who have a license to carry out environmental evaluation of buildings, have access to the software.

2.2. TQB Tool

The model was developed within the framework of the Green Building Council of Austria, and after the version in German language, an English version also appeared. The model was prepared by the Austrian Institute for Ecology¹¹ and the Austrian Institute for Biology and Construction Ecology - IBO¹².

Data on the building can be entered directly on the Council's website, and for registered users it is also possible to download the building calculation's data. In the introductory part, general information about the building is given, and then data is entered for five different categories, each of which can be scored with a maximum of 200 points, and it is possible to achieve a total of 1,000 points. The following categories are especially evaluated¹³:

- A) Location and equipment;
- B) Economy and technical quality;
- C) Energy and supply;
- D) Health and comfort;
- E) Resource efficiency.

⁹ *Code for Sustainable Homes*, Technical Guide, London, 2010, <https://breeam.org>, visited on November 11, 2011.

¹⁰ *BREEAM Communities*, SD5065B, Technical Guidance Manual (2009), London.

¹¹ Das Österreichisches Ökologie – Institut, <http://ecology.at>.

¹² IBO – Österreichisches Institut für Bauen und Ökologie GmbH.

¹³ <http://oegnb.net>.

In the resource efficiency category, materials are classified and scored in detail according to whether their production harms the environment, whether they are regional, the distance of the construction site from the place of production, the use of recycled materials, whether and in which structural elements and in what number or percentage, products are used with an ecological certificate, the eco-efficiency of the entire building with the calculated factor OI3, using the eco2soft software[8].

2.3. DGNB

The DGNB model for assessing the ecological characteristics of buildings was developed by the German Green Building Council and the first version in Germany appeared in 2008 [9].

This model was developed as one of the last, but very quickly, due to its characteristics, it found application in many countries of the world. After the first version, which was general for all types of buildings, special versions were also developed for different types of buildings, as well as for new urban areas with a minimum size of two hectares. The model is applicable in other countries in two ways: by using the international version in English, developed in 2014 according to the valid EN standards, or by adapting it to local legislation and conditions, in cooperation with local partner organizations. A model for 14 key types of buildings has been translated for international use. The model is adapted to EN legislation, standards and technical instructions. The model evaluates buildings throughout their entire life cycle: from the initial planning and development phase of the project through the process of pre-qualification, planning and construction, use and renovation. The model evaluates with over 40 criteria, grouped into six quality groups: ecological, economic, social and functional, technology, production and location. The system is accompanied by software that enables a simpler evaluation process. An additional part is the database with construction products, which is organized in a separate section, called DGNB Navigator. This database helps to use ecologically correct products during the design and construction of buildings, and enables

manufacturers to present their ecological products in one place.

The evaluation of the ecological characteristics of buildings was initially performed only by applying qualitative models, and over time, quantitative models were also developed. In order to facilitate the application of the process of quantitative evaluation, numerous softwares have been developed. Some of them were developed as an aid to some of the already existing models, and some completely independently.

Based on the study of the literature in which models and software are analyzed for assessing the ecological soundness of buildings, as well as their applicability, for the purposes of the research, two software were studied in more detail - Eco2soft and Athena Impact Estimator for buildings.

2.4. ECO2SOFT

The software was developed within the framework of the Austrian Institute for Biology and Construction Ecology IBO – Österreichisches Institut für Baubiologie und Ökologie GmbH, first only as a version in German language, and now also in English [8]. The basis of the software is a detailed database for most building materials used in construction in Austria, but also in neighboring countries, Switzerland and Germany. The basis for evaluating the ecological performance of building elements is the LCA analysis. When calculating the impact on the environment, all elements were taken into account: from the preparation of the raw material, its transport to the place of production, the production of first the material and then the product, until the product leaves the factory (cradle to gate). Impacts due to transport to the construction site, installation and demolition, and disposal at the landfill were not calculated. The ecological performance of individual OI3_{kon} elements is expressed through indicators per unit area: GWP global warming potential (kg CO₂eq./m²), AP acidification potential (kgSO₂eq/m²), PENTR primary energy consumption (MJ/m² or kWh/m²)¹⁵. During the calculation, each layer of material in the structural element is evaluated separately and its evaluation is given in the

¹⁴ DGNB : Deutsche Gesellschaft für Nachhaltiges Bauen.

¹⁵ You can choose one of the options for applying measurement units..

form of the $\Delta OI3$ factor, and thus the influence of the applied materials in complex structural elements, which is the majority, can be seen. In this way, designers are enabled to choose materials with better environmental performance.

For the entire building, the environmental assessment is expressed in total quantities: GWP in kg CO₂eq., AP in kgSO₂eq., PENTR in MJ or kWh/m², and the total ecological quality as OI3. For each element of the structure, the values of heat transfer coefficients are calculated according to EN ISO 6946, and for windows according to EN ISO 10077.

In a special part, called the Components Calculator, ready-made construction elements are given, with calculations of environmental impacts. In this part, the existing structural elements can be changed and completely new ones can be created, in accordance with the wishes of the designers or according to the already created elements for the existing building. After selecting all the necessary elements of the building, from the foundation, facade walls, roof, partition walls and mezzanine structures - the calculation of the ecological performance of the entire building is carried out.

To calculate the building, it is necessary to enter all the required data, from the basic data about the building, the life of the building, to entering the selected constructions with all layers and thicknesses, as well as their surfaces.

The system makes it possible to calculate the ecological performance of the building without data on the heating system and consumption of energy for heating, and it is possible to calculate with the heating system, classic, but also using collectors for hot water heating, as well as photovoltaic panels.

The software is very acceptable because it is possible to analyze the environmental soundness and elements of the building, as well as the entire building.

2.5. Athena Impact Estimator for buildings

Athena Impact Estimator for Buildings is software for assessing the environmental impact of buildings throughout their entire life cycle. Architects can compare different buildings and their impacts on the environment already in the design phase, and choose building

structures with minimum harmful impacts [10], [11].

This is the only software in North America that is based on the international methodology of LCA analysis. Assessment based on LCA is a complex process, but the software is designed for easy use and users of various interests, from scientists-researchers, designers to investors. There are versions for residential and commercial buildings.

Analyzes of the impact of the building are based on the LCA methodology and all phases of the building's life cycle are taken into account.

After entering basic data about the building, place of construction, expected life span, type of building according to users, the amount of final energy by type of fuel is also optionally entered. Based on the choice of materials, it is also possible to determine different life spans of the building. Constructive assemblies can be taken from the database or created by using the material database. The system already contains over 1,200 structural elements, which are used in North America. For materials, a combination of industrial production data from NRMCA¹⁶, databases is used.

After entering all the data about the building, the software calculates the impact on the environment from cradle to grave. The results of the impact assessment can be presented as a total (sum of all indicators), and individual results can also be presented (fossil fuel consumption, acidification potential, global warming potential, human health criterion, ozone depletion potential, smog potential and eutropic potential).

The results can be viewed in the abbreviated form of tables and graphs, for the entire building or for individual parts of the construction. It is possible to compare up to five different buildings at the same time, and make comparative analyzes of different parts of structures or entire buildings. Buildings similar in structure, but with different floor areas, can also be compared, with the results shown per m².

The assessment results are presented in great detail to meet the needs of different users. At the end, the quantities of all used materials are given with their prices for the selected city.

¹⁶ NRMCA – National Ready Mixed Concrete Association:

3. DISCUSSION AND CONCLUSION

After analyzing the selected models and software in terms of their possibilities for evaluating the ecological characteristics of buildings in Bosnia and Herzegovina, the author came to the conclusion that the evaluation process using a software tool is easier to apply than using models. The evaluation process using the model is very complex and requires a lot of data, which at the moment is very difficult or impossible to obtain. The analysis of two software showed that the Austrian software Eco2soft is more applicable for the process of assessing the impact of buildings on the environment.

Research has shown that the application of the Canadian software Athena Impact Estimator for buildings is hardly possible due to too many different parameters applied in it - the size of transport distances and climatic conditions. The distances over which raw materials are transported to production facilities, construction materials and products from the place of production to the place of installation are extremely long, much larger than the distances in Bosnia and Herzegovina. The climate conditions in Canada and Bosnia and Herzegovina also are very different.

When choosing the software, the author chose the Austrian eco2soft, although there are certain differences that can affect the reliability of the results, but they are much smaller than the Canadian one. According to the total area, Austria has an area 1.5 times larger than Bosnia and Herzegovina, and the delivery of raw materials on average is carried out at slightly greater distances than in Bosnia and Herzegovina. On the other hand, rail transport is well developed, and the environmental impacts due to greater distances between raw material extraction sites and processing/production capacities do not have to be significantly different from those in Bosnia and Herzegovina, where raw materials are also transported by rail, but and road traffic. When it comes to technological equipment, it is at a higher level in Austria, so when all the circumstances are taken into account - it can be concluded that the results obtained by applying this software are relatively reliable, but also the only choice in a situation when they do not exist in the country data on the ecological

performance of products that are manufactured or applied in its territory.

Using the eco2wsoft software, it is possible to evaluate all buildings in Bosnia and Herzegovina, even in the design phase, and thus design and build buildings with less harmful impact on the environment.

REFERENCES

- [1] Aranutović-Aksić, i drugi (2016) . *Tipologija stambenih zgrada Bosne i Hercegovine*, Arhitektonski fakultet u Sarajevu, Sarajevo.
- [2] UN (1992). *Report the United Nation Conference on Environment and Development Annex I Rio declaration on environment and development* from: <https://un.orgg/documents/ga/conf151/aconf15126-1annex1.thm>, accessed on: March 10, 2013.
- [3] Fitzgerald, E., McNicholl, A., Alcockland, R., Lewis, O., et al. (2008). *A green Vituvius – Priciple and Practice of Sustainable Architecture Design*, Earthscan, Dublin .
- [4] *Code for Sustainable Homes*, Technical Guide (2010)., London. From: <https://breeam.org>, visited on November 11, 2011.
- [5] *BREEAM Communities*, SD5065B, Technical Guidance Manual (2009), London.
- [6] [https:// greenbooklive.com](https://greenbooklive.com);
- [7] <https://greenguide.org.uk>
- [8] IBO (2011). *OI3-Indicator. IBO Guidelines to calculating the OI3 indicator for buildings* from: <https://ibo.at> visited March 20, 2014.
- [9] DGBN German Sustainable Building Council (2011). *Excellence defined. Sustainable building with a system approach*. DGBN, Stuttgart.
- [10] *Athena EcoCalculator for Assemblies* from [https:// www.athenasmi.org](https://www.athenasmi.org), visited January 10.2016.
- [11] *Athena Impact Estimator for Buildings & LCA Databases* from: <https://athenasmi.org> visited January 10.2016.



Banja Luka
1–2 Jun 2023.

DEMI 2023

16th International Conference on Accomplishments in Mechanical and Industrial Engineering

www.demi.mf.unibl.org



Quality management of the production of plastic injection molding tools

G. Janjić^a, J. Marić^a, Z. Tanasić^a, M. Vuković^a, T. Berlec^b

^aUniversity of Banja Luka, Faculty of Mechanical Engineering, S. Stepanovića 71, 78 000 Banja Luka, BiH

^bUniversity of Ljubljana, Faculty of Mechanical Engineering, Aškerčeva cesta 6, 1000 Ljubljana, Slovenia

Abstract *Quality management is a continuous and dynamic approach to business that seeks to increase the quality, competitiveness and productivity of the organization through the process of continuous improvement of the quality of products, services, processes, people and the environment. The production of plastic injection molding tools is characterized by single production and high product prices. Mistakes in the process of development, design and production of tools most often lead to high costs, non-fulfillment of agreed delivery dates and loss of image with the customer. Because of this, the manufacturer should establish an effective quality management system in its processes, and especially the quality control subsystem. In modern production, product quality control is indispensable and is imposed as a mandatory function of the organization. Controlling and testing of the product during the process of its creation and delivery to the customer is carried out according to pre-defined control points and characteristics for control. These elements are defined in the process of design and technological preparation and are an integral part of the appropriate control documentation. Adequate application of control documentation improves product quality, identifying sources of variation in individual processes and establishing controls for their monitoring. This has the effect of increasing customer satisfaction, reducing waste and improving the financial results of the business. The aim of this paper is to analyze the processes of making plastic injection molding tools and to define and implement the control documentation required for their production.*

Keywords *quality, molding tools, control documentation*

1. INTRODUCTION

The design and introduction of quality systems in industry and other areas of the economy is carried out by implementing a selected standardized model in the conditions of real industrial systems. Standards set requirements in the form of standardized work procedures

that companies should include in the performance of business processes and that as a result have a certain quality of functioning of the company as a whole. The basic direction in the design of quality systems in business systems should be based on a systemic approach with the use of process models and methods and techniques provided by systems theory and information theory.

The business system maintains the development process if its processes of monitoring, measuring, analysing and evaluating performance are carried out successfully. With their help, it is possible to determine the efficiency and effectiveness of the

Corresponding author

Prof. Goran Janjić, PhD
goran.janjic@mf.unibl.org

University of Banja Luka, Faculty of Mechanical Engineering
Vojvode Stepe Stepanovića 71
78 000 Banja Luka, Republic of Srpska, BiH

system and make appropriate management decisions. Depending on the type and structure of the business system and the application of business practices, the documentation of the quality management system can differ significantly. An integral part of the documentation of the quality management system is also the control documentation, which is used for testing and controlling the product during its creation and delivery to the customer.

2. FMEA METHOD

Failure Mode and Effects Analysis - FMEA is one of the risk analysis techniques that provides an analysis of potential errors, identifies the severity of their consequences, determines priorities for the implementation of corrective measures, affects the reduction of waste, processing and production costs, the number of customer failures and warranty costs [1].

In the long term, the FMEA method develops criteria for planning and designing the quality system (provides inputs for the production of control documentation), provides documentation for future reliability analyses in case of system changes, and provides a basis for maintenance planning [2].

3. CONTROL DOCUMENTATION

Controlling and testing of the product during its creation and delivery to the customer is carried out according to pre-defined control points and characteristics for control. Adequate application of control documentation improves product quality, identifying sources of variation in certain processes and establishing controls for their monitoring, which affects the increase of customer satisfaction, reduction of waste and improvement of financial results of operations. Control documentation is focused on processes, operations, and product features that are most important to the customer. To define the control documentation of a specific product, it is necessary to provide appropriate inputs, which are most often: construction drawings, product standards, manufacturing process, deposited samples, production program distribution, production norms, analysis of non-conformities from the previous period, etc. Criteria for control and supervision, as well as suitable methods and techniques, are chosen based on the previously assessed ability of individual

processes, bearing in mind the economic parameters of control operations. The control documentation specifies the intended methods and techniques, sampling and acceptance criteria, and the necessary measuring equipment. The control documentation includes the following documents [3]:

- Quality plans,
- Control plans,
- Technological procedures of the control,
- Checklists,
- Instructions for control and others.

Depending on the type of product, applied production technologies, customer requirements, standard requirements, number of available quality controllers and other conditions, the company creates the necessary control documentation.

3.1 Quality plan

The quality plan is a comprehensive document for the quality management of a specific product or a group of similar products, a service or a project, which includes processes from the customer's request to the monitoring of the customer's satisfaction with the delivered product/service. It shows the implementation processes, responsibilities, procedures and instructions for their implementation, as well as the records that should be created. They may also contain important characteristics that are monitored on the product/service and processes [3].

3.2 Control plan

A control plan is a document that contains detailed procedures that describe how control operations will be carried out and monitored [3]. The control plan is most often created for products that are subject to the traceability procedure, more complex products or at the customer's request. It is often identified with the quality plan, although it is usually one of its outputs. The control plan defines the control operations according to the sequence of execution for certain product realization processes. When selecting control operations and characteristics to be monitored, certain risk analysis methods (FMEA, FTA, ETA, etc.) are usually used. Often, instead of a control plan, organizations create control instructions that

describe the control procedure in detail with all the necessary information.

3.3 Technological procedures of the control

The technological procedures of the control needs to be done with more complex product control operations, when there is a doubt that the control will not be successfully implemented without a detailed presentation of the control operation [3]. In addition to the label and name of the product, the characteristic to be controlled (its labels, required values with tolerance, measured values), control mode and means of control, the technological procedures of the control also contains the following data:

- The necessary sketch or picture of the part with the specified control dimensions (often the same picture also shows the correct position of placing the control means, i.e. the control method),
- A brief description of the activity (phase of control to be carried out and characteristics to be controlled).

3.4 Checklist

A checklist is a document in which the results of product and process control are entered. Its form can be different depending on whether it is intended for recording the value of controlling only one measurement characteristic on products from the sample (e.g. measuring the thickness of the surface protection layer on a sample of products taken from one batch) or for recording all defined measurement characteristics on one product in the course of its production or for the summary display of the number of non-compliant products by type of error within certain series at 100% control, etc. [3]. It can have a form identical to technological procedures of the control.

4. MONITORING THE QUALITY OF THE PRODUCTION OF PLASTIC INJECTION MOLDING TOOLS IN THE COMPANY MANDEKS MOLDING D.O.O.

The company Mandex Molding d.o.o. was founded in 2018 in the municipality of Laktaši BiH, when it started the production of tools. The main activity of the company is the development, design, production and sale of

tools for punching and cutting and plastic injection molding.

4.1 Plastic injection molding tools

Making tools is an extremely complex job that requires a high level of knowledge and great responsibility and commitment from the engineers themselves and all the workers. Plastic injection molding is a cyclic process of primary polymer molding that is performed by injecting a molten polymer of a certain viscosity from an injection unit into a tempered mold. The workpiece hardens in the mold by cooling in the case of thermoplastic materials or by cross-linking in the case of elastomers, elastoplastomers and duromers, followed by ejection from the mold.

The plastic injection molding tool is one of the basic elements of the injection molding system, which directly shapes the workpiece. In addition to the choice of materials, the design of tools and processes significantly affect the properties of injection molded parts. Dimensional accuracy and good microstructure formation and their interaction are particularly important for adequate mechanical and tribological properties, i.e. production of high-quality components [4]. The tool should meet the following requirements:

- Technological: during one work cycle, completely shape one or more products and take the liquid mass, distribute it through the mold, fill the cavities, cool, convert the mass into a solid state and eject the product.
- Structural: it is necessary to take over the forces during injection molding, to ensure the rigidity of the structure, to ensure adequate closing and opening of the tool, to ensure the repeatability of the positioning of the tool, efficient ejection of the product.
- Functional: it is necessary to provide systems for pouring, forming, tempering, ejection, guiding, cantering, receiving, side formers, locking [5]. On the Fig. 1 plastic injection molding tool "DOOR 2x36DIN" is shown.

4.2 FMEA analysis of the plastic injection molding tool manufacturing process

The goal of conducting an FMEA analysis of plastic injection molding tools is to prevent possible failures/mistakes that can potentially cost the company dearly and significantly prolong the tool manufacturing process. The FMEA analysis is the basis for the creation of a control plan, which will be applied in the creation of any plastic injection tool. The process of making plastic injection molding tools consists of several stages: development, design, procurement of materials, production and delivery. A detailed FMEA analysis covers all given processes, and Fig. 2 shows the FMEA segment related to the milling process during the production of movable and immovable form

plates as the two most complex parts where the most errors occur.

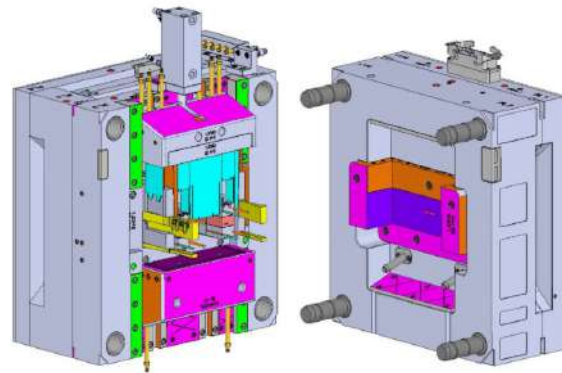


Fig. 1. Plastic injection molding tool "DOOR 2x36DIN"

FMEA analysis																	
Product group/Product: Plastic injection molding tools/ Plate of movable and immovable form											FMEA number: 001.21.42						
Team: Miroslav Lukić, Bojan Vukmirović, Jovan Marić											Date FMEA: (Initially)		03.06.2021.				
Moderator: Jovan Marić											Date FMEA: (Review)		24.06.2021.				
Page: 4/17																	
FMEA process											Action results						
NUMBER	PROCESS OR OPERATION	POTENTIAL FAILURES/ ERRORS	POTENTIAL EFFECTS OF FAILURES/ ERRORS	S	POTENTIAL CAUSES OF FAILURE/ ERRORS	O	FAILURE/ERROR PREVENTION METHODS	FAILURE/ERROR DETECTION METHODS	D	RPN	RECOMMENDED MEASURES	RESPONSIBILITY AND DEADLINE	MEASURES TAKEN	S	O	D	RPN
4.	Milling	Tool calibration error	Length tolerances will not be respected during processing	5	Carelessness of the operator when calibrating the tool	4			4	80	Tool calibration control	Operator from the 03.06.2021]					
5.	Milling	Tool dullness	The specified tolerances will not be respected during processing	6	Lack of tool control, poor tool quality	4			3	72	Greater tool control, operator training	Operator, managem. from 03.06.2021					
6.	Milling	After processing, required measurement, within tolerances	Rework of pieces required, cost increase, delivery delay	3	Operator carelessness, bad tools, G-code entry errors, lack of control	1			3	9	Introduction of control documentation	Operator, managem. 15.06.2021					

Fig. 2. Part of the FMEA analysis of the plastic injection molding tools

4.3 Control documentation for the production of plastic injection tools

After the FMEA analysis, created as a result of the prevention of high-risk errors, the Control Plan for plastic injection molding tools was introduced, shown in Fig. 3.

The control plan for plastic injection molding tools envisages the introduction of a technological control procedure for complex

measurement operations. Fig. 4 shows the technological procedures of the control for the complex contour control operation on the Door 2X36 DIN tool with the entered measurement results of the required characteristics from the tool making process. The tool prepared for delivery to the customer is shown in Fig. 5.

<div>mandeks molding</div> <div>CONTROL PLAN</div>										
Product group/Product: Plastic injection molding tools/ Plate of movable and immovable form							Control plan number: 21-1/10			
Proc./ operation num.	The name of the process/ operation	Machine/ device	Characteristics			Specification of product/process tolerances	Measure- ment technique	Control mode		Corre- ctions
			Nu m.	Product	Process			Sample size	Freq.	
1.	Procurement			Materials, finished parts	Ordering	Perform control: dimension, quantity and order specification, material certificate				Checklist (KL2)
2.	Deep drilling	Cantilever drill		Plate of movable and immovable form	Control of given tolerated dimensions	According to the workshop drawing, perform the control of the tolerated dimensions	Using measuring equipment			Measure- ment Checklist (ML6)
3.	Milling	Milling machine HAAS	1.	Plate of movable and immovable form	Control of given tolerated dimensions	According to the workshop drawing, perform the control of the tolerated dimensions	Measuring with a sliding sc., to reporter, mach. tools			Measure- ment Checklist (ML6)
		Milling machine HAAS	2.	Plate of movable and immovable form	Control of a complex contour	The control shall be carried out using the prescribed technological control procedure	Using a machine tool as a measuring machine			Technol. procedure of the control (TP7)
4.	Electroero- sion (EDM)	Erosimat	3.	Plate of movable and immovable form	Control of given tolerated dimensions	According to the workshop drawing, perform the control of the tolerated dimensions	Measuring with a sliding sc., to reporters and mach. tools			Measure- ment Checklist (ML7)
		Erosimat	4.	Plate of movable and immovable form	Control of a complex contour	The control shall be carried out using the prescribed technological control procedure, perform a preliminary control on the milling machine when making the electrode for EDM	Using the machine when measuring			Technolo- gical procedure of the control (TP8)
5.	Final processing			Tool	Assembly of tools	Check according to the product composition				Checklist (KL2)

Fig. 3. Control Plan for plastic injection molding tools


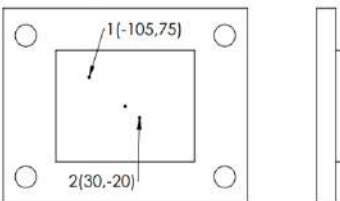
		TECHNOLOGICAL PROCEDURE OF THE CONTROL		Label: 063/21-IMS		
				Date: 7. 6. 2021.		
				Page/Pages: 1/1		
PRODUCT NAME:		DOOR 2X36 DIN TOOL Movable form plate		Product label: P.P.F.001.21		
Material of the product		Standard		Traceability mark		
Tool steel				2019-8-27-PR		
DESCRIPTION OF CONTROL OPERATION:						
Check the profile on the movable form, check it with the machine tool using the measuring tool, in relation to the reference point, locate the assigned values along the X and Y axes, then lower it along the Z axis until it comes into contact with the tool profile. After contact, write down the measured value and compare it with the requested one.						
						
Operation/ characteristic label	A controlled feature	Required value	Measure d value	Feature importance class	Co- ntrol mode	A means of control
2/1	Dimension according to drawing A02.01.01	+0,02 12,62 -0	12,63	A	100%	Machine tool
2/2	Dimension according to drawing A02.01.01	+0,02 13,87 -0	13,89	A	100%	Machine tool

Fig. 4. Technological procedures of the control for the complex contour control operation on the Door 2X36 DIN tool.



Fig. 5. Tool prepared for delivery to the customer

5. CONCLUSION

In today's time of global competition and modern production, quality along with price has become a decisive factor in the market. Quality is also extremely important for companies whose main activity is the development, design, production and sale of tools for injection molding of plastics and tools for punching and cutting. Buyers of these products are very demanding and almost do not tolerate mistakes and deviations from the agreed production deadlines.

In order to achieve the quality of the product required by the customer and to reduce the possibility of errors in the work, the procedure for creating control documentation for the selected group of products, in this case plastic injection tools, is presented. In the first phase, all important processes for the realization of a given group of products were identified, then possible errors in the given processes and their risk levels were identified using the FMEA analysis. In the second phase, control documentation (control plan, technological procedures of the control, control lists, etc.) was created, and part of it is presented in the paper. The created documentation was successfully implemented in the process of making for injection molding tool of cabinet doors DX36 DIN. The demonstration procedure for creating control documentation and its form can, with minor adjustments, be applied to the creation of other products.

REFERENCES

- [1] Stamatis, D.H. (2019). *Risk Management Using Failure Mode and Effect Analysis (FMEA)*, ASQ Quality Press, Milwaukee, Wisconsin
- [2] Tanasić Z., Jotanović S., Janjić G., Vranješ B., Kosec B. Monitoring and improving the performance of production processes, *ETIKUM 2017*, December 2017, Novi Sad, p. 61 - 64
- [3] Janjić, G., Tanasić, Z., Soković, M. (2021). *Quality management*, Faculty of Mechanical Engineering, University of Banja Luka, Banja Luka
- [4] Schubert, D., Wolf, M., Drummer, D. (2023). Interaction of tool and process design on the mechanical and tribological behaviour of an injection-moulded polyamide-steel gear set, *Polymer Testing*, vol. 121, no. 107982, p. 1 - 8. <https://doi.org/10.1016/j.polymertesting.2023.107982>
- [5] Selvaraj, S., Venkataramaiah, P. (2013). Design and Fabrication of an Injection Moulding Tool for Cam Bush with Baffle Cooling Channel and Submarine Gate. *Procedia Engineering*, vol. 64, Pages 1310-1319. <https://doi.org/10.1016/j.proeng.2013.09.212>



Banja Luka
1-2 Jun 2023.

DEMI 2023

16th International Conference on Accomplishments in Mechanical and Industrial Engineering

www.demi.mf.unibl.org



The evaluation of process performance by applying the DEA method for evaluating 3D printers

A. Tomović^a, J. Šaković Jovanović^a, A. Vujović^a

^a Faculty of Mechanical Engineering, University of Montenegro, Džordža Vašingtona bb, 81000 Podgorica, Montenegro;

Abstract *The evaluation of process performance is a very important step in obtaining the information needed to define, improve and manage system processes. Adequate and efficient evaluation of process performance implies the possibility of making quality decisions and solutions for pre-defined problems based on the obtained measurement results. There are a number of models for the evaluation of process performance that have been developed so far. Data Envelopment Analysis (DEA) represents a model based on mathematical programming techniques for evaluation of process performance for various industrial products and technologies, as well as for various physical or virtual production systems, etc. Application of the DEA method makes it possible to determine whether the process is efficient or not based on input and output data. In this paper, the DEA method was applied to evaluate the performance of 3D printers, which are increasingly used for the production of various elements in many spheres of industry and technology. The technical parameters that were used to evaluate the performance of the process using the DEA method refer to 3D printers that are available on the territory of the Balkans.*

Keywords *DEA method, process performance, 3D printers*

1. INTRODUCTION

Efficient performance evaluation provides the opportunity to make adequate decisions on how to react to the situation we are in, based on the measurement results. Management and continuous improvement of business processes cannot be achieved without effective and meaningful evaluation. Process performance measurement represents the language of progress for the organization, and indicates where the organization is and in which direction it is going. It functions as a guide to determine whether the organization is on track

to achieve its goals [1].

The evaluation of the process performance has begun to apply and develop at the beginning of the 20th century. Regardless of the fact that the processes have changed in many ways in relation to the beginning of the application of the practice of evaluating the process performance, this procedure has become more and more important. Engineers and managers get the information needed to define, improve and manage key business and system processes precisely through process performance evaluation.

There is a large number of presented models that consider the problems of process performance evaluation from different aspects. When managers think about a performance measurement system, they generally have in mind a vision of an ideal system that should be based on information availability, reliability and

Corresponding author

mr Aleksandar Tomović
aleksandart@ucg.ac.me

Faculty of Mechanical Engineering, University of
Montenegro,
Džordža Vašingtona bb,
81000 Podgorica, Montenegro;

accountability, and instant access to information [2].

Some of the process performance evaluation models are: Data Envelopment Analysis (DEA), Theory of Constraints (TOC), Balanced Scorecard (BSC), European Foundation for Quality Management (EFQM), Supply-Chain Operations Reference Model (SCOR), Business System Design Decomposition (BSDD), TQM model of the system for performance evaluation, Performance Pyramid, etc.

2. DATA ENVELOPMENT ANALYSIS (DEA) METHOD

Data envelopment analysis (DEA) is a technique that can serve as a useful tool in identifying the best-case scenario for resource use, as well as providing cognition about the maximum gain from efficiency improvements. The DEA method is one of the most popular and widely used mathematical programming techniques for process performance evaluation. Till today, several variations of the technique have been developed: the CCR (Charnes-Cooper-Rhodes) model [3], the BCC (Banker-Charnes-Cooper) model [4], and the context-dependent DEA model [5].

The CCR variant represents the first and oldest type of DEA method variant. It can be represented as a reduction of the multiple-output/multiple-input situation (for each DMU) to the situation of single "virtual" output and "virtual" input. Decision Making Unit (DMU) represents a set or group of characteristics on the basis of which decisions are made. The technical efficiency θ^* of each DMU is evaluated by solving the following minimization problem [6]:

$$\begin{cases} \theta^* = \min \theta \\ \sum_{j=1}^n x_{ij} \lambda_j \leq \theta x_{i0}, i = 1, 2, \dots, m \\ \sum_{j=1}^n y_{rj} \lambda_j \leq \theta y_{r0}, r = 1, 2, \dots, s \\ \lambda_j \geq 0, j = 1, 2, \dots, n \end{cases} \quad (1)$$

where n is the number of DMUs, m is the number of inputs, s is the number of outputs and λ_j are the corresponding input/output coefficients (non-negative scalars) assigned to

each DMU. For the problem shown above implies that the value of θ^* cannot exceed 1. Therefore, all DMUs for which $\theta^* = 1$ are considered efficient, while all other DMUs are considered inefficient. To evaluate this possibility, the slack values for the DMU are usually estimated. The slack values s^- and s^+ of DMU₀ represent the amount by which resource consumption or production needs to be improved for a given unit to reach the efficient frontier, and they are estimated by solving the following maximization problem [7]:

$$\begin{cases} \max \sum_{i=1}^m s_i^- + \sum_{r=1}^s s_r^+ \\ \sum_{j=1}^n x_{ij} \lambda_j + s_i^- = \theta^* x_{i0}, i = 1, 2, \dots, m \\ \sum_{j=1}^n y_{rj} \lambda_j - s_r^+ = \theta^* y_{r0}, r = 1, 2, \dots, s \\ \lambda_j, s_i^-, s_r^+ \geq 0 \forall i, j, r \end{cases} \quad (2)$$

An efficiency factor value of 1 does not guarantee "full efficiency", meaning that some inputs can be reduced or some outputs increased without affecting the need for other inputs or the production of other outputs [8].

3. 3D PRINTERS AND DEA METHOD

The global competition in the field of manufacturing companies has reached a very high level in the 21st century, thanks to the development of technology. Companies of all sizes (micro, small, medium, and large enterprises) try to develop and maintain competitive advantages that will allow them to protect or increase their market share or find new markets. Increasing competition leads to constant pressure to increase production, innovations, development and improvement of products, all with the aim of improving features such as system speed, flexibility, increasing efficiency and product quality.

Today, 3D printing and additive manufacturing technologies are positioned as the number one solution for the design and development of rapid prototyping and visualization, and thanks to the technology, they are increasingly being used for the production of parts and components for various purposes as the primary method of production. Additive manufacturing (AM) technology is a technique

of gradually creating a product by extruding and stacking thin layers of material. With the development of techniques and technologies, the meaning of the term 3D printing has expanded significantly, and it can be said that it is identified with additive manufacturing.

Although more than 30 years have passed since the appearance of 3D printers, it can be said that they still represent a relatively young technology that is still in the phase of improving its characteristics (quality, working material, printing speed, product price, etc.). There are a number of manufacturers on the market who have started to develop their own versions of 3D printers. Some of these systems began and continue to be developed as 'open hardware' projects following the 'open source' software paradigm, while others incorporate proprietary technology [8]. Both variants of systems that perform 3D printing of elements can be found on the market. The use of these printers after their appearance was not at all easy and it was necessary to possess the certain technical knowledge to operate these machines. Whilst the situation is somewhat different today, their use does not require relatively high technical knowledge and is more or less accessible to everyone.

This paper presents the DEA method for evaluating the performance of 3D printers.

In the DEA method, the technical efficiency of a set of decision-making units (DMUs) is assessed by taking into account the number of resources that each DMU (inputs) has used to produce certain products or outcomes (outputs) [9]. The method uses a linear non-parametric programming procedure to identify the most efficient DMUs, which together define the so-called efficient frontier [8]. This method was developed primarily for business companies and organizations, but it is also very useful and is applied to evaluate the technical characteristics of products and systems such as: 3D printers, CNC machines, the automotive industry, mobile phones, various robots, etc.

Currently, there are tons of 3D printers available in the market. According to Internet research, it is estimated that there are more than 150 models and systems from more than 35 suppliers. According to technical specifications and price, 3D printers can be divided into those that fall into the low, medium and high range. Companies deliver 3D printers fully assembled or as kits with the option of self-

assembly on site. In addition to hardware, 3D printers must also have certain software in order to be able to perform work tasks. Along with some printers, companies also offer specially developed software, but it is also possible to use open-source free software that can be found on the Internet, such as Cura, Craftware, Prusaslicer, and/or Repetier.

During operation, it is necessary to adjust the software tools for the specified 3D printer depending on the technical characteristics in order to be able to perform the task (printer workspace dimensions, diameter and the number of nozzles, printing speed, layer thickness, extruder temperature, etc.). In addition to the basic ones, it is possible to set a number of advanced functions such as the grid structure, the definition of the thickness of the layer, etc. These softwares automatically convert drawings into generated G-code based on which printing is done.

4. THE EVALUATION OF 3D PRINTERS

The technical characteristics that were used as parameters in the applied DEA evaluation are: build volume (effective volume of the machine), number of extruder heads, layer thickness, nozzle diameter, nominal power, printing speed, and finally, the market price of the printer. A 3D printer is considered a system whose inputs are related to cost characteristics, while its outputs are related to its technical characteristics and capabilities. Therefore, all the mentioned parameters, except the last one, were evaluated as outputs, while the market price was considered the only input parameter.

The printers analyzed in this paper use standard PLS and ABS plastic filaments and depending on the characteristics and capabilities of the printer, other types of thermoplastic materials can be used.

Table 1. shows fifteen 3D printers that are available in the Balkan market with their specific characteristics listed in the text above. The above data were entered into the Open Source DEA Frontier Excel program [10], after which the evaluation was performed. The evaluation was carried out using the CRS (Constant>Returns-Scale) technique, that is, the CCR technique. The results are shown in Table 2.

From the above table, it can be seen that by evaluating using the DEA method is determined

that according to the input and output parameters, only three out of fifteen mentioned 3D printers are considered efficient.

While the remaining twelve belong to the inefficient category. In Figure 1. the relation

between the price and efficiency of the mentioned 3D printers is shown.

Table 1. Technical characteristics/parameters (outputs) and price (input) for evaluated 3D printers

3D Printer	Build volume (cm ³)	No. of extruders	Layer thickness (mm)	Nozzle diameter (mm)	Nominal power (W)	Printing speed (mm/s)	Weight (kg)	Price (€)
Wanhao Duplicator D12/300	14,520	2	0.4	0.4	350	80	11.8	455
Vivedino Formbot Troodon	80,000	1	0.4	0.4	350	250	38	2,025
Creality Ender 6 Core-XY	25,000	1	0.4	0.4	350	150	30	596
Flashforge Creator PRO	5,039.4	2	0.4	0.4	320	100	14.8	1,224
Felix Robotics Pro XL	144,000	2	0.35	0.5	1600	100	65	16,020
Felix PRO 3 Touch	13,474.9	2	0.25	0.35	350	450	11.5	3,835
Creatbot F430	36,000	2	0.4	0.4	2700	180	48	4,855
Creality CR-6 MAX	64,000	1	0.4	0.4	500	150	16.5	1,065
Zortax M200 Plus	7,200	1	0.09	0.4	320	100	26	2,725
Zortax M300 Plus	27,000	1	0.09	0.4	320	150	18	4,260
Ultimaker S5	23,760	2	0.8	0.8	500	220	20.6	5,990
Ultimaker S3	8,740	1	0.4	0.4	350	170	14.4	4,395
Ultimaker 2+ Connect	10,057.3	1	0.8	0.8	221	150	10.3	2,750
Makerbot Sketch	3,375	1	0.4	0.4	200	120	11.8	1,399
Monoprice MP10 3D Printer	36,000	1	0.4	0.4	250	100	12.5	500

Table 2. Calculation results using the DEA method (DEA Frontier OpenSource)

DMU no.	DMU Name	Efficiency
1	Wanhao Duplicator D12/300	1.00000
2	Vivedino Formbot Troodon	0.60760
3	Creality Ender 6 Core-XY	1.00000
4	Flashforge Creator PRO	0.42647
5	Felix Robotics Pro XL	0.16292
6	Felix PRO 3 Touch	0.46623
7	Creatbot F430	0.72297
8	Creality CR-6 MAX	0.88767
9	Zortax M200 Plus	0.20734
10	Zortax M300 Plus	0.14240
11	Ultimaker S5	0.17210
12	Ultimaker S3	0.15369
13	Ultimaker 2+ Connect	0.33091
14	Makerbot Sketch	0.38282
15	Monoprice MP10 3D Printer	1.00000

DEA evaluation for selected 3D printers was also performed using the Open Source program DEAOS Engine [11].

As with this program, it was possible to take into account only four parameters (one input and three outputs) were selected: price, build volume, nominal power, and printing speed.

Using this software tool, applying only four parameters, instead of the eight used in the DEA Frontier software, the same results were obtained. Of the fifteen listed 3D printers, only three belong to the efficient group:

- Wanhao Duplicator D12/300 dual extruder,
- Creality Ender 6 Core-XY, and
- Monoprice MP10 3D Printer,

while the other twelve 3D Printers were inefficient.

The results obtained using this software are shown in Table 3. and Figure 2.

Table 3. Calculation results using the DEA method (DEAOS Engine OpenSource)

DMU no.	DMU Name	Efficiency (%)
1	Wanhao Duplicator D12/300	100
2	Vivedino Formbot Troodon	59.1
3	Crealty Ender 6 Core-XY	100
4	Flashforge Creator PRO	38.4
5	Felix Robotics Pro XL	16.3
6	Felix PRO 3 Touch	46.6
7	Creatbot F430	72.3
8	Crealty CR-6 MAX	88.8
9	Zortax M200 Plus	17.3
10	Zortax M300 Plus	14.2
11	Ultimaker S5	14.6
12	Ultimaker S3	15.4
13	Ultimaker 2+ Connect	21.7
14	Makerbot Sketch	34.1
15	Monoprice MP10 3D Printer	100

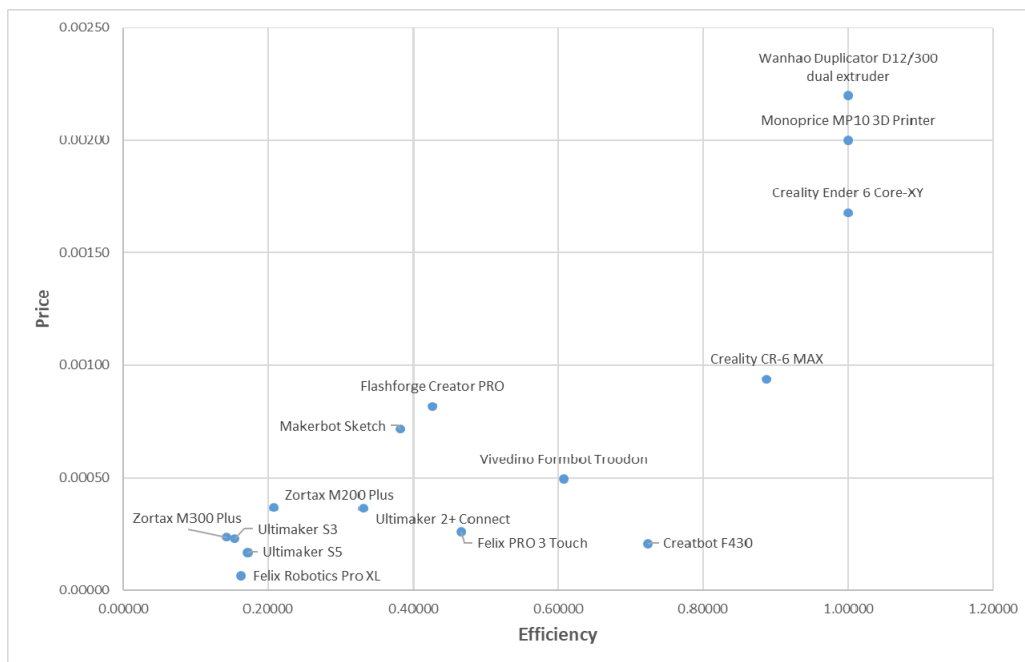
5. CONCLUSIONS

The DEA method is described as a method for evaluating the technical efficiency of 3D printers in this paper. Using the CCR DEA

method, only three of the fifteen evaluated 3D printers achieved maximum efficiency, while for the remaining twelve, only three showed results greater than 50%. Regarding the applicability of the DEA method to the problem at hand, it could be confirmed that the results of the study show that DEA can be a useful approach for preliminary assessment of the technical efficiency of 3D printers, based on readily available data. Considering the relatively large number of 3D printers offered worldwide DEA method can be used to identify and select an adequate and efficient system in a relatively short time.

Using this method, manufacturers can quickly assess the strengths and weaknesses of their products, comparing them with competitors' products, and based on that adjust their strategies for further product development and marketing.

Evaluating process performance is a very important aspect both in business organizations and in business processes. By applying an adequate method, it is possible to evaluate the performance of the process, and thereby contribute to making quality decisions that can be of great importance for the future of the organization, system, and even a specific product.

**Fig. 1.** The relation between the price and efficiency of 3D printers (DEA Frontier Open Source)

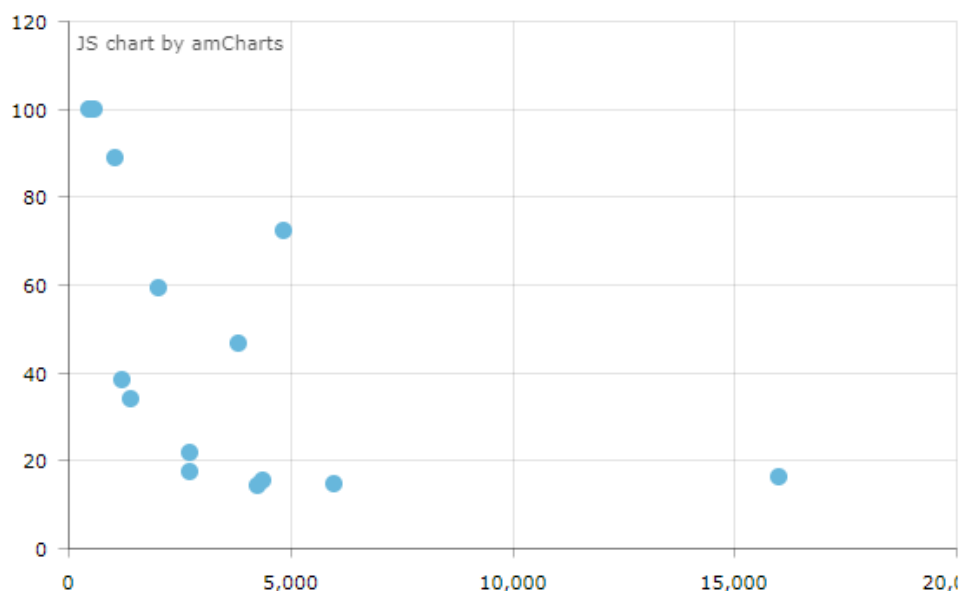


Fig. 2. The relation between the price and efficiency of 3D printers (DEAOS Engine Open Source)

REFERENCES

- [1] Rose, K. H. (1995). A performance measurement model. *Quality Progress*, 28(2), 63-66.
- [2] Spasojević Brkić, V., Milanović, D.D., Knežević, S., Lazić, D., Milanović, T. (2012). Sistem menadžmenta kvalitetom i poslovne performanse. Beograd: Mašinski fakultet.
- [3] Charnes, A., Cooper, W.W., Rhodes, E. (1978). Measuring the efficiency of decision making units. *Eur. J. Oper. Res.* 2, 429-444. [https://doi.org/10.1016/0377-2217\(78\)90138-8](https://doi.org/10.1016/0377-2217(78)90138-8)
- [4] Banker, R.D., Charnes, A., Cooper, W.W. (1984). Some Models for Estimating Technical and Scale Inefficiencies in Data Envelopment Analysis. *Manag. Sci.* 30, 1078-1092. <https://doi.org/10.1287/mnsc.30.9.1078>
- [5] Seiford, L.M., Zhu, J. (2003). Context-dependent data envelopment analysis—Measuring attractiveness and progress. *Omega*, 31, 397-408. [https://doi.org/10.1016/S0305-0483\(03\)00080-X](https://doi.org/10.1016/S0305-0483(03)00080-X)
- [6] Cooper, W. W., Seiford, L., Zhu, J. (2011). Data Envelopment Analysis: History, Models, and Interpretations. https://doi.org/10.1007/978-1-4419-6151-8_1.
- [7] Papatheodorou, T., Giannatsis, J., Dedoussis, V. (2021). Evaluating 3D Printers Using Data Envelopment Analysis. *Applied Sciences*. 11(9):4209. <https://doi.org/10.3390/app11094209>
- [8] Bogetoft, P., Lars, L. (2011). Benchmarking with DEA, SFA and R; Springer: New York, NY, USA. <https://doi.org/10.1007/978-1-4419-7961-2>
- [9] Hwang, S.-N., Chen, C., Chen, Y., Lee, H.-S., Shen, P.-D. (2013). Sustainable design performance evaluation with applications in the automobile industry: Focusing on inefficiency by undesirable factors. *Omega*, 41, 553-558. <https://doi.org/10.1016/j.omega.2012.07.002>
- [10] DEA Frontier™ Free Version [Online]. From: <http://www.deafrontier.net/deafree.html>, accessed on: January 8, 2023.
- [11] DEAOS Engine [Online]. From: <https://engine.deaos.com/welcome.aspx>, accessed on: January 8, 2023.
- [12] Simeunović B. P., (2015). Razvoj modela za mjerenje performansi procesa, doktorska disertacija, Fakultet organizacionih nauka, Univerzitet u Beogradu.



Banja Luka
1-2 Jun 2023.

DEMI 2023

16th International Conference on Accomplishments in Mechanical and Industrial Engineering

www.demi.mf.unibl.org



A survey on Lean methodology implementation in a small and medium enterprises in the Republic of Serbia

D. Pavlović P. Milosavljević S. Mladenović

University of Niš, Faculty of Mechanical Engineering, Aleksandra Medvedeva 14, Niš, Serbia

Abstract Most companies today are going through a phase in which there is a need to respond to the rapidly changing needs of customers. The critical issue facing companies is how to deliver products or service fast, at low cost and with good quality. In order to maintain competitiveness in an expanding global market, many companies have started to use the Lean methodology. Lean methodology has been widely discussed and well-known philosophy, not only in the manufacturing environment, but also in services, public sector and healthcare. Even today, when many are talking about Industry 4.0 Lean methodology represents something that is unavoidable. The aim of the study presented in this paper is to determine the level of application of Lean methods and tools in small and medium production enterprises in the Republic of Serbia. In order to achieve this goal, a survey was conducted in which small and medium enterprises were surveyed. Data were collected using a structured questionnaire consisting of close-ended questions, and were analyzed using various descriptive statistical methods.

Keywords lean methodology, small and medium enterprise, lean tools

1. INTRODUCTION

Rapid changes in the global market caused by different customer demands, technology development, environmental awareness and, recently, socio-economic changes require companies to be flexible, in order to respond to those demands as quickly as possible.

The use of Lean methodology to achieve sustainable competitive advantages has been known in worldwide manufacturing strategy since the early 1980's [1].

There are many definitions of Lean methodology. In [2] Lean is defined as "an

integrated socio-technical system whose main objective is to eliminate waste by concurrently reducing or minimizing supplier, customer, and internal variability". Waste is anything that do not add value to customers and they are not willing to pay for. It is known as a methodology for maximizing customer value while minimizing waste, i.e. create more output with less input, in order to maintain effectiveness, flexibility, and profitability [3-6].

Taiichi Ohno defined 7 Lean wastes within the Toyota Production System as:

- transportation
- inventory
- motion
- waiting
- overproduction
- overprocessing
- defects. [7]

Corresponding author

Dragan Pavlovic
dragan.pavlovic@masfak.ni.ac.rs

Faculty of Mechanical Engineering, University of Nis
Aleksandra Medvedeva 14
Nis, Serbia

According to [8, 9], as a results of implementing Lean, manufacturing companies can expect a reduction of 90% in lead time, 50% increase in productivity, 90% in inventories and 90% in the cost of quality. Based on [10] the productivity can be improved 10-60%, lead time can be reduced from 8-50 %, and quality can be improved to 8-80%.

Lean is not only used in the manufacturing industry, it is a systematic approach for process optimization and waste reduction in the service industry as well.

Lean methodology relies on a set of tools and techniques to identify opportunities for improvement, implement changes, eliminate waste and measure progress. There are over 100 tools, but it's not necessary to know and apply all of them. Some of the most used tools are listed below [11]:

- Single Minute Exchange of Dies (SMED),
- Single Piece Flow,
- Total Productive Maintenance (TPM),
- First-in-first-out (FIFO),
- 5S method,
- Kaizen,
- Just-in-Time (JIT),
- Pull system,
- Kanban;
- Visual management,
- Zero defect,
- SMED;
- Value Stream Mapping (VSM),
- Poka Yoke,
- Cellular manufacturing.

VSM is one of the most used Lean tools [12].

Overall, it can be said that Lean methodology is important in today's global market because it help companies to meet customer expectations, reduce waste, stay competitive, optimize their supply chains, reduce environmental impact, and take advantage of digitalization.

This can be particularly useful for small and medium-sized enterprises (SMEs). Although Lean has been known for many years, many companies, especially small and medium-sized enterprises, still have not heard of or do not use this methodology. Implementation of Lean methodology in SMEs is more challenging than implementation in large companies, and this is one of the reasons why Lean is not applied to a large extent in SMEs [13].

Therefore, the aim of this paper is to show the extent to which SMEs are familiar with the Lean

methodology and whether they using it in their processes. The research focuses on small and medium-sized production enterprises in the Republic of Serbia.

2. METHODOLOGY

A survey with a structured questionnaire was designed to collect data for this study. Collection was facilitated by conducting a survey through Google Forms. To achieve the objectives of research presented in this paper, Serbian production SMEs were selected as the population for the study. The survey was sent to 110 SMEs, and a total of 53 enterprises filled out the questionnaire.

The survey consisted of 20 questions, divided into two parts. The first part, consisted of 10 questions, is mandatory for all companies, and the questions refer to basic information about the company, whether they have applied the ISO 9001 standard, are they familiar with the Lean methodology and whether they apply it in their processes. The second part of the survey is intended only for SMEs that use or have used Lean methodology in their processes. This part of the survey also consists of 10 questions. Some questions in this part of survey were designed on a five-point Likert scale, ranked from 1 to 5, where 1 is lowest and 5 is highest.

3. RESULTS ANALYSIS

This part of the paper presents a detailed presentation of the results obtained by surveying SMEs. The name and main activity of the companies that participated in the survey will not be displayed due to the confidentiality of the data.

The graph in figure 1. represents the number of employees in enterprises participating in the survey. Out of a total of 53 enterprises that filled out the survey, 20 (37.7%) of them have from 51 to 250 employees, while 16 (30.2%) enterprises have between 11 and 50 employees. In total, about 80% of surveyed enterprises have less than 250 employees, which is a common number when it comes to SMEs in the Republic of Serbia.

The largest number of responses, around 68 percent, came from enterprises belonging to the region of southern and eastern Serbia (figure 2).

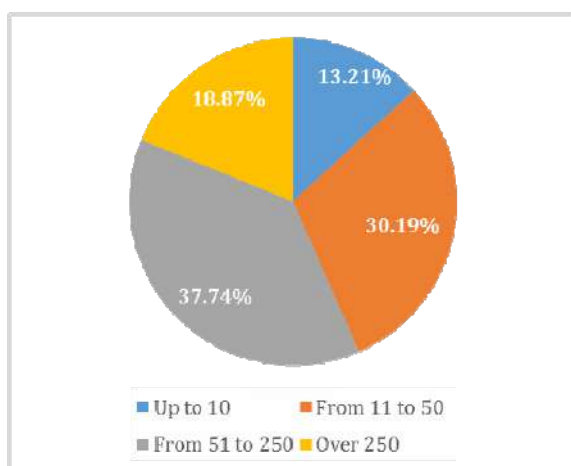


Fig. 1. The number of employees

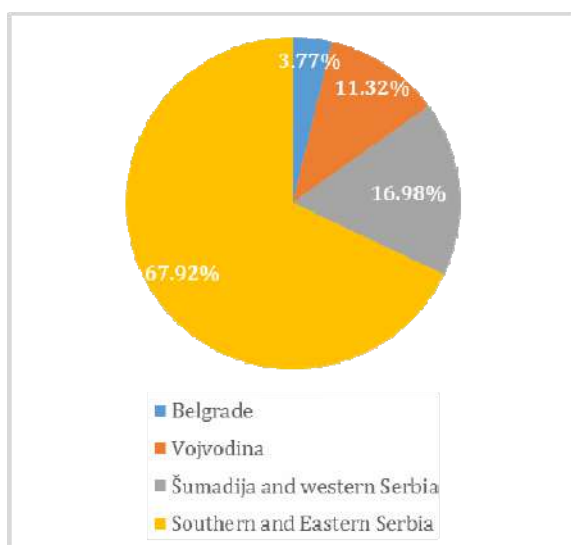


Fig. 2. The region of Serbia where SME is from

When it comes to the production program, 34 enterprises have a high range of products (over 10 types of products), while 19 enterprises have less than 10 types of products, i.e. they have a small range of products. Another characteristic of the production program of the surveyed enterprises is that 24 enterprises have small or medium batch production, and 29 enterprises have high product volumes (figure 3).

A quality management system nowadays is something that every company and SME should have, however, out of a total of 53 surveyed enterprises, 4 of them still do not have the ISO 9001 certificate.

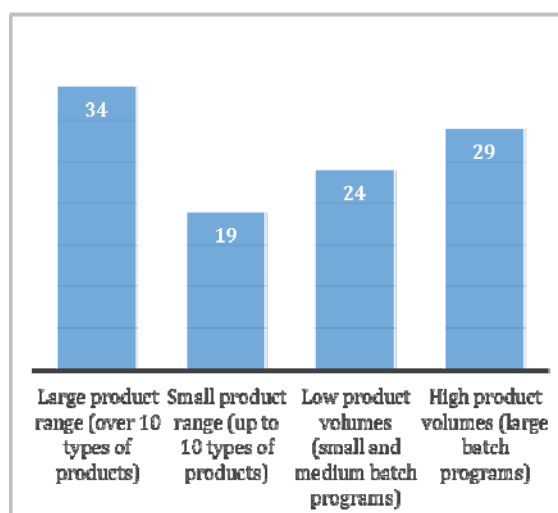


Fig. 3. The production program of enterprise

When it comes to Lean methodology, 28 SMEs are not familiar with this methodology, while even 38 of them do not use Lean in their processes, which is about 72% of surveyed SMEs. Out of 25 SMEs, which are familiar with Lean methodology, 15 of them use it, which is only 28.3% of surveyed SMEs. It is interesting that out of those 15 SMEs, only 3 of them are domestic, while the rest are SMEs with foreign capital and are part of larger international companies.

Only 15 SMEs that use Lean methodology participated in the second part of the survey. 73% of those SMEs have been using the Lean methodology for more than 4 years, while 13% have been using it for 3-4 years, and 14% are in the first two years of using the methodology.

Most SMEs (around 74%) that use Lean methodology have 20 or more employees who have had some kind of training related to Lean. This is a very important factor that affects the success of Lean methodology implementation itself.

There are a large number of Lean tools, but the survey listed only those that are most often used in practice, namely: VSM, 5S method, Pareto, 8 waste, Kanban, Kaizen, Jidoka, Poka-Yoke, Heijunka, Andon, OEE, TPM, SMED, PDCA cycle, KPI, 5 Why, One-piece flow, Tact time, Cellular manufacturing and Standard work. Figure 4 shows the level of application of Lean tools in SMEs.

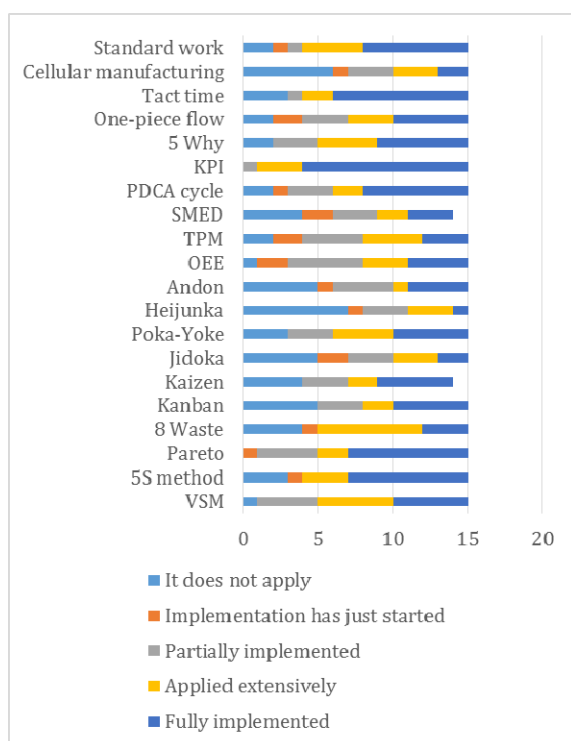


Fig. 4. Application of Lean tools in SMEs

One of the questions in the survey was for SMEs to evaluate the accuracy of some statements that are correlated with certain problems that may arise during the implementation of Lean methodology. The results are shown in figure 5.

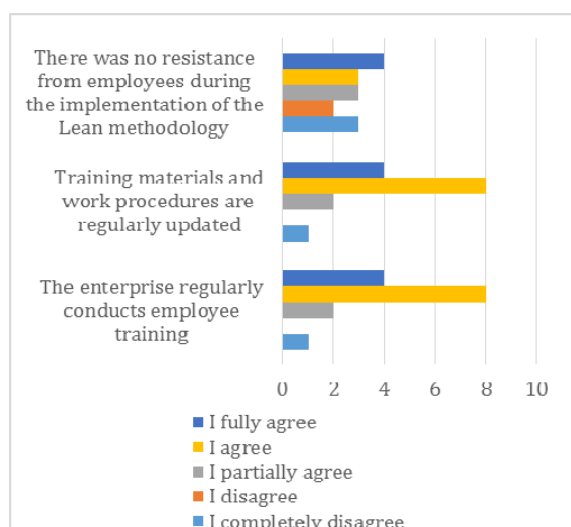


Fig. 5. Statement related to Lean implementation

According to the survey, during the implementation of the Lean methodology, SMEs had no problems with the following: lack of IT

resources, insufficient or incorrect definition of customer value and difficulties in defining KPIs. On the other hand, lack of experts, lack of knowledge about Lean implementation, lack of leadership and employee resistance to change were the problems they faced during the implementation of the Lean methodology.

Almost all SMEs measure KPIs during or after implementing Lean methodology completely or to a great extent, and 11 out of 15 SMEs have fulfilled the Lean methodology implementation plan.

There are many benefits from the implementation of Lean methodology in SMEs [8-10]. Some of them were listed in the survey and SMEs evaluated the benefits of applying the Lean methodology in their enterprises with grades from 1 to 5, where 1 is the lowest and 5 is the highest (figure 6).

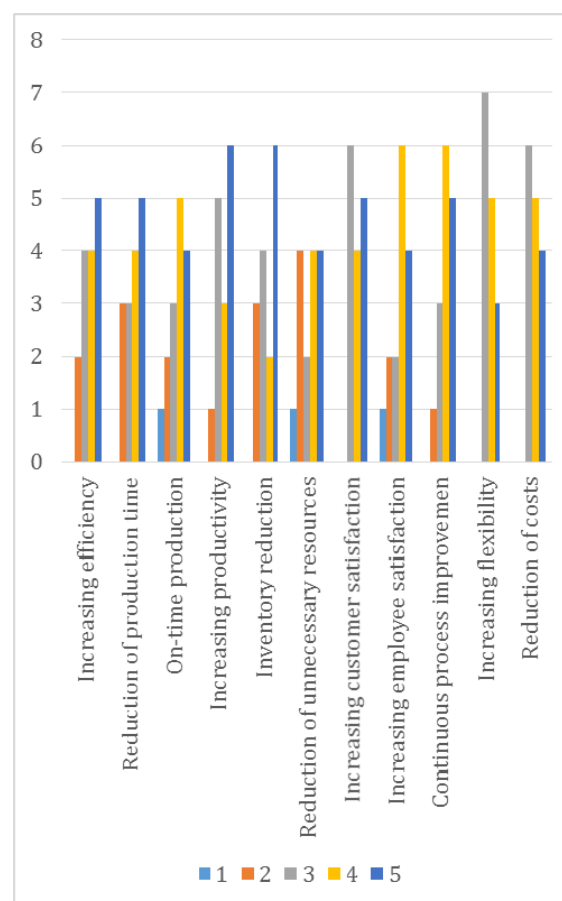


Fig. 6. Benefits of Lean methodology implementation

According to the survey responses, of all the mentioned Lean tools, SMEs had the most difficulty implementing SMED and TPM. And

finally, all SMEs using Lean methodology stated that they will continue to do so.

4. CONCLUSION

Lean methodology is not a tool for improvement or method that can be implemented in the same way and same form in any SME. Each SME is a separate story and methodology of Lean implementation needs to be adapted to the specific situation in that particular enterprise. Which method or tool should be used depends on many factors, such as: the size of the enterprise, the type of the process, volume of production, diversity of products or services etc. The key is that there is no unique path and framework for Lean implementation, and this needs to be tailored for every enterprise separately.

However, there are a number of things that are common to all SMEs that use Lean methodology. They use a similar set of tools, face similar problems and challenges when implementing Lean methodology, have similar results, etc. Those similarities were confirmed based on the results of the survey and are partially presented in this paper.

Acknowledgement

This research was financially supported by the Ministry of Science, Technological Development and Innovation of the Republic of Serbia (Contract No. 451-03-47/2023-01/ 200109).

REFERENCES

- [1] Holweg, M. (2007). The genealogy of Lean production. *Journal of Operations Management*, vol. 25, no. 2, p. 420-437.
- [2] Shah, R., Ward, P.T. (2007). Defining and developing measures of lean production. *Journal of Operations Management*, vol. 25, no. 4, p. 785-805.
- [3] Womack, J., Jones, D., Roos, D. (1990). *The Machine that Changed the World*. Rawson Associates, New York.
- [4] Bhamu, J., Sangwan, K. S. (2014). Lean manufacturing: Literature review and research issues. *International Journal of Operations and Production Management*, vol. 34, no. 7, p. 876-940.
- [5] Chauhan, G., Singh, T. (2012). Measuring parameters of Lean manufacturing realization. *Measuring Business Excellence*, vol. 16, no. 3, p. 57-71.
- [6] James-Moore, S., Gibbons, A. (1997). Is Lean manufacture universally relevant? An investigative methodology. *International Journal of Operations & Production Management*, vol. 17, no. 9, p. 899-911.
- [7] Ohno, T. (1988). *Toyota Production System: Beyond Large Scale Production*. Productivity Press, Portland.
- [8] Rose, A.M.N., Deros, B.Md., Rahman, M.N.Ab., Nordin, N. Lean manufacturing best practices in SMEs. *Proceeding of International Conference on Industrial Engineering and Operations Management*. 2011, Kuala Lumpur, Malaysia, p. 872-877.
- [9] Lathin, D., Mitchell, R. Lean manufacturing: techniques, people and culture. *Proceeding of Annual Quality Congress*. vol. 55, 2001, Milwaukee, Wisconsin, p. 321-325.
- [10] Ferdousi, F., Ahmed, A. (2009). An investigation of manufacturing performance improvement through Lean production: A study on Bangladeshi garment firms. *International Journal of Business and Management*, vol. 4, no. 9, p. 106-114.
- [11] Thakur, A. (2016). A review on Lean Manufacturing implementation techniques: A conceptual model of Lean Manufacturing dimensions. *REST Journal on Emerging trends in Modelling and Manufacturing*, vol. 2, no. 3, p. 62-72.
- [12] Meudt, T., Metternich, J., Abele, E. (2017). Value stream mapping 4.0: Holistic examination of value stream and information logistics in production. *CIRP Annals - Manufacturing Technology*, vol. 66, no. 1, p. 413-416.
- [13] Achanga, P., Shehab, E., Roy, R., Nelder, G. (2006). Critical success factors for Lean implementations within SMEs. *Journal of Manufacturing Technology Management*, vol. 17, no. 4, p. 460-471.

*Maintenance of Engineering Systems
and Occupational Safety Engineering*



Banja Luka
1–2 Jun 2023.

DEMI 2023
**16th International Conference on
Accomplishments in Mechanical and
Industrial Engineering**
www.demi.mf.unibl.org



Importance of examination of collector for impurities after oil purification for human and environmental safety

M. Jaric^a, S. Petronic^b, N. Budimir^a, B. Rajcic^b, Z. Stevic^{c,d}

^aInnovation Centre of the Mechanical Faculty in Belgrade, Kraljice Marije 49a, Belgrade

^bInstitute of General and Physical Chemistry, Studentski trg 3, Belgrade

^cUniversity of Belgrade, Technical Faculty in Bor;

^dUniversity of Belgrade, School of Electrical Engineering in Belgrade

Abstract *The collector for impurities is a temporary tank that collects condensate from the condenser after oil purification process.. Large-scale distillation towers use a reflux system to achieve more complete product separation. The collector, or accumulator, serves as a distribution point for reflux and distillate. This paper deals with a collector that uses water and light hydrocarbons as a working fluid, and is designed to operate under a pressure of 12 bar and a temperature of up to 91° C. Considering the working fluid, and work at elevated pressure, it belongs to the category of pressure vessels of a high level of danger. Its maintenance and regular inspection are a mandatory step in the prevention of failures and/or accident, and thus also in the protection of people and the environment. The paper describes tests of collector for impurities after oil purification and their importance; including a liquid penetrate inspection, ultrasonic measurement and visual inspection. Corrosion rate that occurs during the interaction of the working medium and the material of the collector was estimated such as and appropriate remaining working life. RBI analysis is performed.*

Keywords *Collector, hydrocarbons, nondestructive methods, remaining life, RBI*

1. INTRODUCTION

In engineering practice, the lifetime of a specific plant and individual devices (apparatus, machines, etc.) implies the following stages: development, dimensioning and production technical documentation, production of the device, checking the functionality of the device after production, plant construction, i.e. installation of devices in a suitable complex system, verification functionality after

installation, maintenance, etc. For each of these stages there are developed technical regulations, as well as professional services that supervise them. During the lifetime of use, there are many factors that affect the lifetime of the device, such as working conditions, working medium, etc [1]. For that reason periodical inspection is very important and must follow developed regulations.

Impurities content undesirable components such as carbon-dioxide (CO₂), hydrogen-sulfide (H₂S), nitrogen (N₂), water, etc. can cause health issues, corrosion of process units, and poorer calorific values [2]. Damage and/or failure of the apparatus affect the environment. Damages/failures occurred at oil and gas plants can be catastrophic for the environment.

Corresponding author

PhD, Sanja Petronić
sanjapetronic@yahoo.com
Institute of General and Physical Chemistry
Studentski trg 12/V
Belgrade, Serbia

Chemical and petrochemical facilities generate many dangerous phenomena; these dangerous events must be mitigated by protection layers to reduce the risk to an acceptable level [3]. Some working medium, operating conditions and/or the environment condition can cause corrosion, which results in the loss of material, i.e. a reduction in the thickness of the device's wall. A critical reduction in wall thickness leads to leaks and failure, and corrosion is estimated to account for 19% of the failure factor [4].

In this work, the inspection of the collector for impurities after oil purification is investigated by visual examination (internal and external), liquid penetrate testing and ultrasound measurement. The corrosion rate and remaining life were estimated [5-8]. Suppose the equipment's or components remaining life the engineer can perform the necessary maintenance and be able to plan the replacement of the piece of equipment [9, 10].

In oil&gas and the petrochemical industry, the application of the RBI API methodology, which represents the process of creating an inspection scheme, is of great importance. To effectively integrate risk evaluation and benefit evaluation and facilitate investment decision making, it is firstly needed to analyze risk factors [11-13]. This method is based on the assessment of the probability of failure with the consequences of that failure. In oil&gas and petrochemical plants, a certain percentage of equipment represents a high risk and is given more attention, i.e. more time and money, while less money is allocated for maintenance for equipment that carries a lower risk. In this paper, the RBI inspection of the collector which is in long time service in one upstream oil plant has been calculated and discussed, pointing to the importance of the safety and economy of the plant.

2. TECHNICAL AND EXPERIMENTAL DATA

The collector for impurities after oil purification process is shown in Figure 1.

Technical data are listed in Table 1.

The collector was subjected to external and internal visual inspection, liquid penetrates inspection and ultrasonic measurement. Corrosion rate and remaining life were determined and estimated while RBI analysis was conducted according to the requirements of API 581.

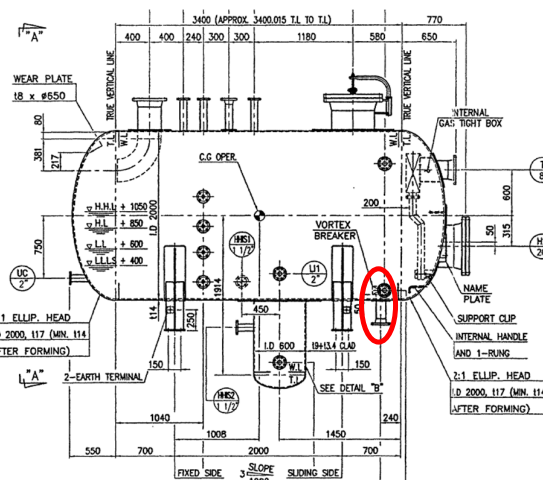


Fig.1. Technical drawing of the collector for impurities after oil purification

Table 1 Technical data

Material	Carbon steel-SA516 Grade70
Working medium	Light carbons and water
Fluid density	0.553 oil/0.986 water kg/dm ³
Design pressure	12.0 bar
Design temperature	91°C
Operating pressure	8.7 bar
Operating temperature	55°C
Joint efficiency	0.85 (spot radiography)
Capacity	13.1 m ³
Year of production	2003

3. RESULTS AND DISCUSSION

3.1. Survey of collector for impurities after oil purification

The collector was shut down for periodical inspection [14, 15]. The inspection covers the conditions of the external metal surfaces, protective coatings and all other external attachments.

Ladders, stairways, platforms, walkways foundations and supports and anchor bolts are in good condition.

The flange on the nozzle F1 (Fig.2) was found to be distorted. This condition of the flange has been spotted also during previous inspection in 2017. The flange is probably distorted during construction period. The flange and nozzle were checked visually and cracks were not spotted. Leaking has not been observed on this location while the vessel was in operation. All other nozzles were found in good condition.



Fig. 2 The flange at the lower nozzle F1 (4") was found distorted, but leaking has not been observed while the vessel was in service

The grounding connections and cables were found to be in good condition. Electrical resistance has been checked by appropriate department and its value is 3.06 Ohms which is in line with the recommendations [15].

All gauge connections, sight glasses and safety valves were found to be in good condition.

External protective coating and external metal surfaces are in good condition.

The internal periodical inspection covers the integrity of internal metal surfaces, main weld joint, nozzle weld attachment and its internal components.

Pitting corrosion can be observed on the lower part of the vessel, Figure 3, especially from 5 to 7 o'clock position). Maximum depth of the pits was found to be 3 mm (only for one pit). Majority of the pits were between 1.0 to 2.0 mm deep. All pits have depth less than corrosion allowance, so according to API 510 Section 7.4.3 this can be ignored. Interior of the elliptical head of the collector has been found corroded in time of examination and also small pits were observed on circular weld joint (shell-head). Additional UT scanning has been performed for needs of estimation of circular weld joint and minimum value thickness in this area from the outside. Minimum measured value of thickness obtained by this scanning was found to be 10.43 mm. Here should be mentioned that this damaging is caused by corrosion and erosion effects.



Fig.3. Pitting corrosion has been observed on the lower part of the shell (from 5 to 7 o'clock position) - majority of the pits are between 1.5 to 2.0 mm deep

The back head of the vessel is corroded (Fig 4). Damaging is caused by corrosion and erosion effect. UT scanning has been performed from the outside. Minimum thickness was found to be 10.43 mm on the left elliptical head.

Penetrant testing results are presented in the Figure 5.

There is no sign of cracks and other irregularities on the inspected locations.



Fig. 4. Left head - close up view on the corroded surface (whole elliptical head has been scanned and minimum thickness was found to be 10.43 mm)



Fig.5. Liquid penetrate inspection performed on weld 1

3.2 Corrosion rates and remaining life

Operating pressure of the collector is 8.7 bar (as per vessel design data), but in reality this pressure is even lower. Maximum pressure is limited to 12 bar by the pressure safety valves. Limiting the pressure to maximum 10 bar will provide additional corrosion allowance of 1.87 mm (actual thickness - required thickness for 10bar = 10.43 mm - 8.56 = 1.87 mm). For this purpose, PSV which protect the collector should be additionally adjusted according to this pressure limit (10 bar).

During one of the first examination of the collector pitting corrosion was observed on the lower part of cylindrical shell and on left elliptical head. This situation was detail analyzed and after that injection of corrosion inhibitor CH1038 was started on 09-Dec-2009.

Here should be mentioned that corrosion inhibitor-CH1038 is belonging to blend of aliphatic amines and aminic derivates in high boiling point aromatic solvent. Result of this activity was manifested in corrosion rate reduction and slow growth of pit depth.

According to previous thickness measuring Corrosion Rate (CR) was calculated according to [16,17] for period 2009 to 2022:

$$CR \text{ (long-term)} = (11.0-10.43)/11.25=0.05067 \text{ mm/year}$$

CR (short-term) could not be certainly determinated because previous and actual thickness readings are almost the same.

Hence, value of Corrosion Rate (long-time) was adopted as a relevant:

$$CR=0.05067 \text{ mm/year.}$$

Remaining Life (RL) of the vessel is:

$$RL = (\text{actual minimum thickness} - \text{required thickness}) / \text{corrosion rate (LT)}$$

$$RL = (10.43 \text{ mm} - 8.56 \text{ mm}) / 0.05067 \text{ mm/year}$$

$$RL = 36.9 \text{ years}$$

4. RBI calculation

RBI analysis is method of estimation of process equipment which including in itself the most probably damage mechanisms which can appear at appropriate process equipment depending on working mediums in the equipment (and their process parameters) and material from which equipment is made. Calculation of risk in API 581 [12] RBI involves the determination of a probability of failure (POF) combined with the consequence of failure (COF) presented by the following equitation:

$$R(t) = P(t) * C(t)$$

The probability of failure is calculated as following [5]:

$$P_f(t) = gff * D_f(t) * F_{MS}$$

The risk for the presented collector for impurities after oil purification is calculated according to [12] and the most important results have been summarized in Table 2. The risk is calculated at the RBI date, the age at the RBI date is 20 years, while a Probability of failure at RBI date is $1.17 \cdot 10^{-3}$.

Table 2 Calculation results summarized for the collector for impurities @ RBI date

Art	0.29361
Inspection Effectiveness	
Category	B
Damage Stage	
Total Damage Factor	72.23
POF with inspection, failures/yr	00.001193
Final Consequence Area	492
The final financial consequence	4760000
Risk, m2/yr	1.3
Risk €/yr	12680

The final consequence area is 946m², and the Total damage factor is 42.66 at RBI date. Table 3 presents numerical values associated with POF and Area-Based COF Categories taken from API 581 standard. In this analysis, these values have been taken as referent values for the iso-risk plot and risk matrix.

Table 3 Numerical values associated with POF and Area-Based COF categories [12]

Cat.	Probability Category (1,2)		Consequence category (3)	
	Probability range	Damage factor	Range cat.	range (m2)
1	$P_f(t) \leq 3.06E-5$	$D_f \leq 1$	A	$CA \leq 9.29$
2	$3.06E-5 < P_f(t) \leq 3.06E-4$	$1 < D_f \leq 10$	B	$9.29 < CA \leq 92.9$
3	$3.06E-4 < P_f(t) \leq 3.06E-3$	$10 < D_f \leq 100$	C	$92.9 < CA \leq 929$
4	$3.06E-3 < P_f(t) \leq 3.06E-2$	$100 < D_f \leq 1000$	D	$929 < CA \leq 9290$
5	$P_f(t) > 3.06E-2$	$D_f > 1000$	E	$CA > 9290$

According to results presented in Table 2 and categories presented in Table 3, the presented collector for impurities after oil purification belongs to category B3 @ RBI date- medium risk. The results have been presented in the Iso-risk plot for the consequence area in Figure 5.

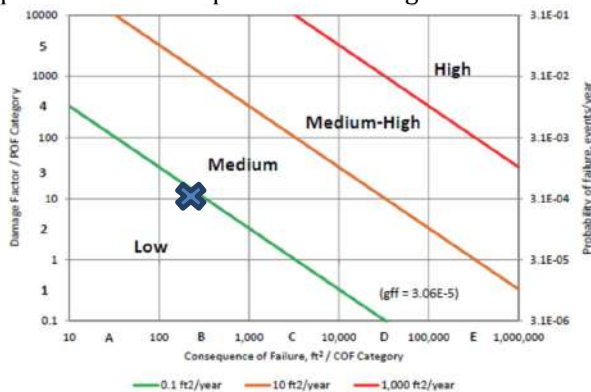


Fig.6 Iso-risk Plot for the Consequence area. The vessel belongs to medium risk

Table 4 presents Numerical Values Associated with POF and Financial-Based COF Categories taken from API 581.

Table 4 Numerical values associated with POF and financial-based COF categories [12]

Cat.	Damage factor	Range cat	Consequence category range (\$)
1	$D_f \leq 1$	A	$FC \leq 10000$
2	$1 < D_f \leq 10$	B	$10000 < FC \leq 100000$
3	$10 < D_f \leq 100$	C	$100000 < FC \leq 1000000$
4	$100 < D_f \leq 1000$	D	$1000000 < FC \leq 10000000$
5	$D_f > 1000$	E	$FC > 10000000$

According to results presented in Table 2 and categories presented in Table 4, the damage factor belongs to Category 3 and Financial Consequence to Range category D.

The risk category of collector for impurities from standpoint of financial consequences is D3 and belongs to medium risk, very close to medium-high risk. That is presented in the Iso-risk plot for financial consequences in Figure7.

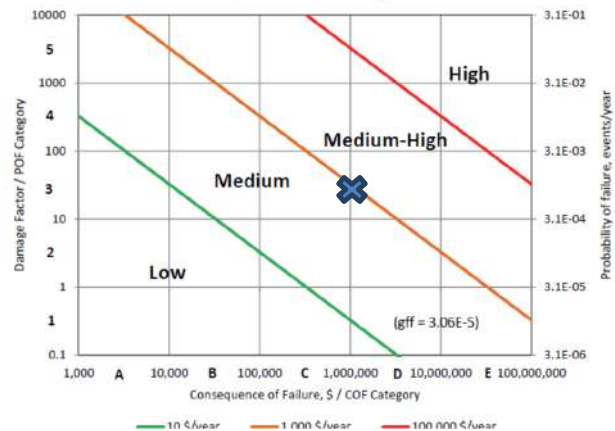


Fig.7 Iso-risk Plot for Financial Consequence. The collector for impurities belongs to medium risk

Figure 8 presents the balanced risk Matrix for Consequence Area and Financial Consequence. After detail analysis of the relevant parameters related to probability of failure (POF) it's combined with the consequence of failure (COF) can be concluded that the collector for impurities belongs to category of medium risk.

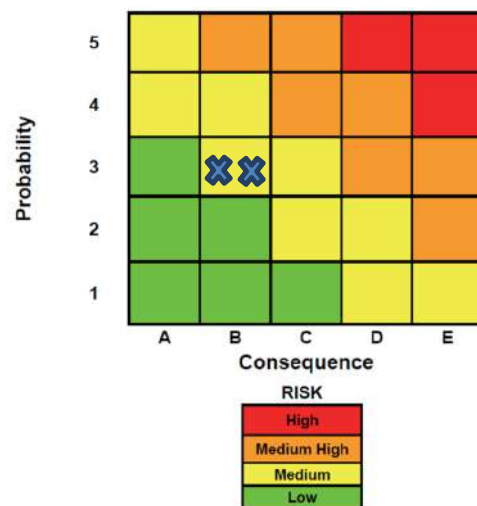


Fig.8 Balanced Risk Matrix for Consequence area and Financial Consequence [5]

5. CONCLUSION

This paper presents the inspection of collector for impurities after oil purification, determination, and analysis of remaining service life, corrosion rate. RBI inspection is applied and calculated in detail. From the presented the next could be concluded:

- All of the essential sections/components of the presented collector for impurities after oil purification satisfy the API 510 and API 572 Code requirements for maintenance inspection/examination hence, presented vessel is safe to operate until the next scheduled inspection.
- Corrosion rate is extremely high affecting the remaining life which is 36.9 years.
- Collector for impurities after oil purification belongs to medium risk, for Consequence Area while for the financial consequence it practically entering in the medium-high risk area.

Acknowledgment. This research was funded by the Ministry of Science, Technological Development and Innovation of the Republic of Serbia through contracts Nos. 451-03-47/2023-01/200051, 451-03-47/2023-01/ 200131, 451-03-47/2023-01/ 200213.

REFERENCES

- [1] Jacimovic, B., Genic, S., Budimir, N., Jaric, M. Acceptance test of induced draft cooling tower with 25 MW nominal heat power, Processing 20, 2007. Belgrade, Serbia.
- [2] Devold, H. (2013). *Oil and Gas Production Handbook – An introduction to oil and gas production, transport, refining and petrochemical industry*, 3rd ed, ABB Industries,
- [3] Zennir, Y., Bouasla, S.E.I., Mechhoud, E. Evaluation of Safety Instrumented System in a petrochemical plant using HAZOP-LOPA-Fault Tree Methodology, Case Study: Naphta Stabilizer-A Reflux Drum (LPG separation) in RA1K, 2020 International Conference on Electrical Engineering (ICEE) September 25-27, 2020, Istanbul, Turkey.
- [4] Wang, X., Duan, Q. (2019). Improved AHP-TOPSIS model for the comprehensive risk evaluation of oil and gas pipelines. *Petroleum Science*, vol. 16, p. 1479–1492, <https://doi.org/10.1007/s12182-019-00365-5>
- [5] Ishizaki, Y., Yonekawa, F., Yumoto, T., Suzuki, T., Hijikawa, S. Remaining life assessment of an external pressure vessel in creep range and inspection findings. *Proceedings of the ASME 2017 Pressure Vessels and Piping Conference*, PVP2017, July 16-20, 2017, Waikoloa, Hawaii, USA
- [6] Dedov, A., Klevtsov, I., Lausmaa, T., Hlebnikov, A., Bojarinova, T. (2016). Corrosion and life assessment of Intrex™ superheater tubes in a CFB oil shale boiler. *Appl. Therm. Eng.* <http://dx.doi.org/doi:10.1016/j.applthermaleng.2015.12.061>.
- [7] ISO 9223. (2012). *Corrosion of metals and alloys. Corrosivity of atmospheres. Classification, determination and estimation*. CEN.
- [8] ISO 9226. (2012). *Corrosion of metals and alloys. Corrosivity of atmospheres. Determination of corrosion rate of standard specimens for the evaluation of corrosivity*. CEN.
- [9] Jayanto, S.T., Chendra, M., Wijayanta, A.T. Estimating corrosion rate and remaining life of a pressure vessel of H₂S absorber. *AIP Conference Proceedings* 2097, 2019. <https://doi.org/10.1063/1.5098182>
- [10] [3] API PR 571. (2020). *Damage Mechanisms Affecting Fixed Equipment in the Refining Industry*, 3rd ed. American Petroleum Institute.
- [11] Li, Z.X., Liu, J.Y., Luo, D.K., Wang, J.J. (2020). Study of evaluation method for the overseas oil and gas investment based on risk compensation. *Petrol. Sci.* vol.17, p.858–871. <https://doi.org/10.1007/s12182-020-00457-7>
- [12] API 581. (2016). *Risk-Based Inspection Methodology*. American Petroleum Institute.
- [13] Pilic, V., Balos, D., Gvozdenac Urosevic, B. (2022). Application of innovative methodology for risk assessment and inspection methods on example of small experimental biomass gasification unit, *Thermal Science* vol. 27, p.151-151. DOI: [10.2298/TSCI220606151P](https://doi.org/10.2298/TSCI220606151P)
- [14] API 510. (2020). *Pressure Vessel Inspector*, American Petroleum Institute.
- [15] API 572. (2020). *Inspection of Pressure Vessels*, American Petroleum Institute.
- [16] ASME SEC VIII, Division 1, 2019 ASME Boiler & Pressure Vessel Code 2019, The American Society of Mechanical Engineers, 2019.
- [17] ASME SEC VIII, Division 2: Alternative Rules, 2017 ASME Boiler & Pressure Vessel Code 2017, The American Society of Mechanical Engineers, 2017.



Banja Luka
1-2 Jun 2023.

DEMI 2023

16th International Conference on Accomplishments in Mechanical and Industrial Engineering

www.demi.mf.unibl.org



Technical diagnostics - the basis of preventive or corrective maintenance?

D. Branković^a, Z. Milovanović^a

^aFaculty of Mechanical Engineering Banja Luka, Stepe Stepanovića 71, 78000 Banja Luka, Bosnia and Herzegovina

Abstract *The sustainability of industrial systems in the increasingly demanding world market depends on the degree of readiness of technical systems to fulfill their designed function within the production processes. Maintenance, as an integral system support for production, can be organized in different ways. For industrial systems with a continuous production process as well as for systems that have high requirements for reliability, concepts of condition based maintenance are applied. The basis of the condition based maintenance is the application of technical diagnostic methods, using modern technical equipment, which can define the current state of elements of technical systems within production processes, as well as predict the system's behavior in the future. This prediction can avoid unwanted failure of equipment and unplanned costs of maintenance, production and therefore business. The paper describes the application of technical diagnostics in a specific industrial plant and a discussion about the nature of plant downtime based on the analysis of diagnostic measurement results and the decision on planned plant shutdown. According to the current development of technical systems used in industrial systems, without adequate equipment for monitoring the condition of the equipment, it will be almost impossible to ensure process control and therefore the realization of planned production and business goals.*

Keywords *technical diagnostics, maintenance, industrial system*

1. INTRODUCTION

Maintenance, as a "combination of all technical administrative and management activities during the life cycle of parts intended to maintain or restore the state of the system in which the required function can be provided" [1], [2], is an integral part of production industrial systems. There are different ways of organizing

maintenance services within industrial systems. The way of organization determines the concept of maintenance. In practice, the following concepts of maintenance can be observed:

- corrective,
- preventive,
- reliability based maintenance (RBM),
- condition based maintenance (CBS),
- logistic,
- totally productive maintenance (TPM),
- self-maintenance,
- maintenance "without maintenance" and others.

Which of the methods will be applied depends on a number of factors that are determined by the characteristics of the industrial systems themselves, such as:

- nature of technological processes,

Corresponding author

PhD Dejan Brankovic, Assistant Professor
University of Banja Luka, Faculty of Mechanical Engineering
Banja Luka
dejan.brankovic@mf.unibl.org

University of Banja Luka, Faculty of Mechanical Engineering
Banja Luka
Stepe Stepanovića 71
Banja Luka, Bosnia and Herzegovina

- dominant requirements in terms of quality, safety or reliability,
- the possibility of organizing within one's own capacities or engaging external support,
- availability of educated maintenance staff,
- the possibility of monitoring certain physical characteristics that can determine working conditions, etc.

2. CONDITION BASED MAINTENANCE. TECHNICAL DIAGNOSTICS

In modern industrial systems, there is a trend of applying the concept of condition based maintenance, which consists of activities of monitoring, analysis and comparison of quantities that describe the working condition of elements or the complete system, and providing a forecast on the behavior of condition parameters in the future period. Condition Based Maintenance (CBM), or as it can also be found in the literature as Predictive Maintenance (PdM), is defined as the result of the behavior of the equipment/s lines before complete failure, while proactive maintenance may require redesign and/or modification of the adopted maintenance procedure, where it is necessary. Condition based maintenance represents a combination of preventive and proactive strategies [3].

The basis of the application of the concept of condition based maintenance is the application of technical diagnostic methods. According to [4], technical diagnostics is the science of recognizing the state of a technical system. By monitoring and analyzing the size of the condition, the occurrence of malfunctions can be predicted. By eliminating the factors of possible system failure, the efficiency and reliability of the system increases.

The basic prerequisite for the implementation of condition based maintenance is the procurement and installation of systems and devices for technical diagnostics, which enable continuous or occasional (according to request) monitoring of the working characteristics of the observed system. Systems and devices for technical diagnostics are usually of high purchase value and require specially trained personnel for their use. The economic justification of investing in technical diagnostic systems has been practically proven in cases of exploitation of industrial facilities with a large capital value, for systems with high requirements for reliability and effectiveness, in the process industry with a

continuous mode of operation and high productivity (e.g. thermal power plants, shipbuilding, aviation industry, nuclear plants etc.).

In order to decide on the method of monitoring and the type of system for technical diagnostics, it is necessary to perform an analysis of the process that needs to be monitored and to see what measurable parameters the process contains, such as vibrations, temperature, noise, pressure, etc. The essence of the technical diagnostic procedures is to observe, measure and compare the obtained values of the monitoring parameters with the limit (allowed) values previously defined. The result of the application of the system of technical diagnostics and the monitoring of quantities that describe the operating state of the system is an indication or alarm on any occurrence of a violation of the operating characteristics of the monitored system. Based on all the mentioned conditions, a decision is made on the choice of maintenance method or strategy for each specific case.

2.1 Application of technical diagnostics in industrial systems

A practical question arises: whether the observed deviation of a monitored operating condition parameter from the normal/optimal value, which the technical diagnostics system defines as a potentially dangerous condition for the further/future operation of the system, and the very activity to eliminate the observed problem by the maintenance department, have a character of preventive or corrective maintenance? As an illustration of the indicated dilemma, a specific example from industrial practice will be cited - technical diagnostics of drive electric motors, **Fig.1.**



Fig. 1. HV electric motor in industrial plant

Within the industrial facility for the production of hygienic paper from Banja Luka, which operates in a continuous production cycle, during regular diagnostic inspections of the state of vibrations of the drive electric motors of the technical system of the paper machine, on 21st March, 2019, an increase in vibration amplitude was observed at the position of bearing L2, the high-voltage (HV) motor for driving fans for drying paper tape, compared to the previous, one-month measurement at the same position, **Fig. 2**, **Fig. 3** and **Fig. 4**.

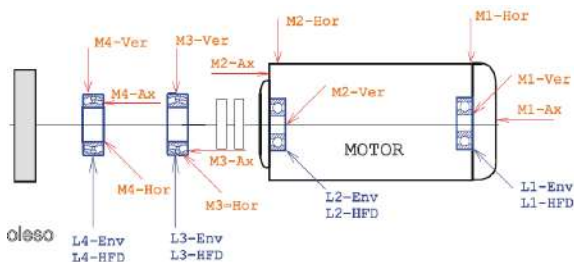


Fig. 2. Diagnostics measuring point on the system motor-coupling-fan

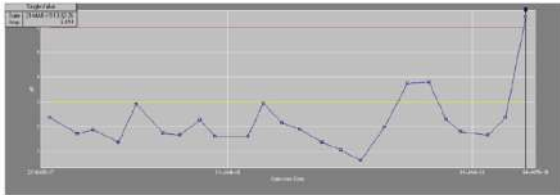


Fig. 3. Data measuring trend on the bearing L2 motor position with Enveloping method

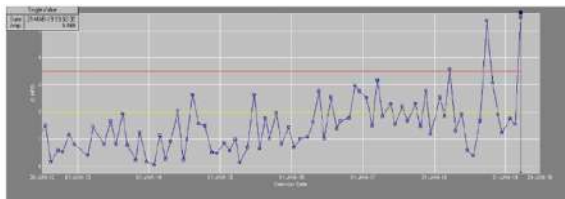


Fig. 4. Data measuring trend on the bearing L2 motor position High-Frequency Detection (HFD method)

A significant increase in the value of the oscillation amplitude above the permissible limits for that type of plant indicated a very soon possible occurrence of catastrophic failure (possibility of breaking the bearing cage, cracking of the ring, etc.). Based on the results of the measurements, a short working meeting of the responsible maintenance and technology

workers was held and a decision was made to stop the plant. The term of the planned stoppage is already defined for the beginning of the first shift of the following day, in order to carry out all organizational and logistical preparations for properly stopping the system and performing maintenance activities.

After preparation, the plant was stopped on March 22nd, 2019 and the engine with the problematic bearing was replaced with a spare engine in the working position. Replacing the engine from the mentioned working position is a complex maintenance activity because it involves hiring a truck crane, partial dismantling of the wall (light partition panel), dismantling of the coupling, careful centering, etc., **Fig.5**.



Fig. 5. Logistics of maintenance activities

In addition to the defined procedures, during the replacement the problem of non-uniformity of the dimensions of the stand and the dimensions of the spare motor appeared because the motors were not from the same manufacturer, which caused an additional modification (cutting the openings on the stand in relation to the openings on the supports of the spare electric motor), **Fig.6**.



Fig. 6. Modification of the placement of the HV motor

All these activities affected the total stoppage of the paper machine plant of 10 hours. As an illustration, the impact of downtime on total production costs can be shown. If the hourly output of the paper machine plant is known to be 4.8t/h, the total production loss (P_L) expressed in tons of paper produced is:

$$P_L = 4,8 \text{ t/h} \cdot 10 \text{ h} = 48 \text{ t} \quad (2.1)$$

Considering the wide production range, if we assume an average gross margin - GM of €340/ton of produced paper, the previously estimated loss of production due to a stoppage of 10 hours converted into monetary cost (M_C) would amount to:

$$M_C = GM \cdot P_L = 340 \frac{\text{€}}{\text{t}} \cdot 48 \text{ t} = 16.320 \text{ €} \quad (2.2)$$

This is only part of the costs related to production, since not all indirect costs are shown (services of external companies, loss of energy for maintaining the paper machine system in "warm" mode, etc.). It is clear that these are significant losses that are especially dominant in continuous production systems.

This loss of working time and loss of production should have been recorded in the production tracking system. The question arose: was the production stoppage the result of preventive or corrective maintenance?

It is evident that monitoring the state and control of the operating parameters of the technical assemblies of the plant in the production system is a form of preventive maintenance with the aim of maintaining a stable continuous production process. But it is also a fact that after noticing a potentially dangerous malfunction or a significant deviation of the monitored parameters from the nominal values for further

work, it was decided and implemented to stop the entire plant. This shutdown, although planned, had the full character of corrective maintenance because the system was stopped due to the transition from the working state to the state of the system in failure, i.e. due to the appearance of a significant malfunction of a part of the production system. Even in the process of deciding on the exact date of the shutdown of the plant, a constructive debate developed regarding the nature of the future shutdown of production. The production sector rightly insisted that the future stoppage is defined as a maintenance stoppage due to a malfunction/failure of a part of the plant, while the maintenance sector explained that the mentioned stoppages are the result of planned monitoring of the condition of the system elements and a planned decision to stop the system preventively, eliminate the malfunction and avoid unplanned stoppages with catastrophic consequences. Both sides have real arguments. Nevertheless, the very nature and scientific definition of the term CBM as "a form of preventive maintenance with subsequent corrective activities that are defined and implemented after monitoring the performance or parameters of the state of the elements of the observed system" [5], give the right to activities that are the result of decisions on the basis of planned monitoring and analysis of system parameters, they are treated as preventive maintenance. Of course, the time (hours) of the resulting stoppage is recorded as time caused by maintenance, but the stoppage is the result of preventive, i.e. proactive maintenance that avoids cancellations with larger and significantly more severe emergency situations (longer downtimes, a greater number of damaged and connected parts, higher costs, possible injury to workers, endangerment of the working and living environment, etc.).

3. CONCLUSION

In contrast to the traditional understanding of maintenance, which understood maintenance activities as carrying out certain repairs in order to return the system from a state of failure to a state of operation, today maintenance is designed to ensure the prevention of unwanted conditions that can impair the ability to work, to ensure an increase in equipment reliability, achieve the maximum effectiveness of the complete production system and ensure the

conditions of a safe and secure working environment for workers and equipment. To that end, an appropriate maintenance strategy is defined as the highest goal of the company's policy and management. The development and application of maintenance concepts according to the state today is conditioned by the accelerated development of technique and technology and the application of electronics in the construction of technical systems. Modern diagnostic equipment gives the possibility of defining the current state of the operating characteristics of the system and a high-quality and reliable prediction (prognosis) of the state of the system in the near or conditionally distant future. Investing in equipment condition monitoring systems represents a significant financial expense, especially in problematic time periods such as, for example. COVID 2019, regional wars, natural disasters, etc. On the other hand, practice shows that failure to invest in maintenance systems is the fastest way to create conditions for failure.

Failure prevention provided by the use of technical diagnostics systems often refers to making decisions about preventive or proactive activities that need to be implemented in order to correct or completely eliminate observed deviations from the designed operating conditions of the equipment. Decisions on corrective actions should be made based on the analysis of connected data and information on system behavior. This is usually the most sensitive part of the maintenance process, because a good diagnosis and decision about what and when something needs to be done can significantly facilitate all subsequent activities and result in the avoidance of significant, unplanned costs. The essence of the decisions that are made based on the data and information obtained using the technical diagnostics system refers to certain corrective maintenance activities to improve some of the monitored quantities that define the state of the system. However, the purpose of carrying out these corrective activities is the implementation of preventive, rather than proactive maintenance, because their implementation prevents the observed system from reaching a far less favorable situation in which, due to a far greater violation of the operating parameters, more serious failure conditions may occur, accompanied by equipment breakdowns, endangering health and the lives of working

personnel, endangering the working and environmental environment, etc. Such undesirable conditions cause high maintenance and production costs. In this sense, technical diagnostics and the concept of condition based maintenance provides the possibility of a safer production process and the achievement of better production results and therefore business, which is a condition for the survival of industrial production systems on the market.

REFERENCES

- [1] Bengtsson M. (2004). Condition based maintenance systems – an investigation of technical constituents and organizational aspects, Malardalen University Licentiate Thesis, No.36.
- [2] Milovanović Z., Branković D. (2021). Maintainability of Industrial Systems, in DQM Monograph Library Quality and Reliability in Practice, Book 11, Prijevor.
- [3] Jeff S. (2006). PDM, Secrets revealed: How to improve your PDM program or start one from scratch, 1st Edition, Allied Reliability, Inc., Tulsa, Oklahoma, pp. 4–35.
- [4] Sebastijanović S. (2002) Machine Constructions Basic Maintenance, JJ Strossmayer University, Mechanical Engineering Faculty in Slavonski Brod.
- [5] EN 13306:2001 Terminologie maintenance, 2001.

Materials and Welding



Banja Luka
1-2 Jun 2023.

DEMI 2023
**16th International Conference on
Accomplishments in Mechanical and
Industrial Engineering**
www.demi.mf.unibl.org



Life assessment using the finite element method of high-strength low-alloy steel samples exposed to low-cycle fatigue

V. Aleksić^a, S. Bulatović^a, B. Zečević^b, A. Maksimović^b, Lj. Milović^c

^aInstitute for testing of materials-IMS Institute, Bulevar vojvode Mišića 43, 11000 Belgrade, Serbia

^bInnovation Centre of the Faculty of Technology and Metallurgy, Karnegijeva 4, 11120 Belgrade, Serbia

^cUniversity of Belgrade, Faculty of Technology and Metallurgy, Karnegijeva 4, 11120 Belgrade, Serbia

Abstract

In the paper, based on the results of experimental research on the behavior of samples in the form of round smooth test specimens (STS) made of high-strength low-alloy steel (HSLA), Nionikral 70 (NN-70), under conditions of low-cycle fatigue (LCF), a computational stress analysis was performed using numerical methods.

Experimental investigations of the behavior of the samples were performed with controlled and fully reversible deformation ($\Delta\epsilon/2 = \text{const}$, $R\epsilon = \epsilon_{\min}/\epsilon_{\max} = -1$), according to the ISO 12106:2003 (E) standard.

For computational analyses, the method of least squares (in the Excel program) and the finite element method (FEM) (in the SolidWorks program) were used. The behavior of HSLA steel during low cycle fatigue (LCF) simulation was analyzed in the Cosmos module of the SolidWorks program.

On the basis of the analysis of the results of the stress-deformation state and the determination of the life span through the isolines of the life span and comparison with the results of experimental tests, a graphic representation is given. Specific load cycles involving the entire round smooth test specimen ligament for a specific load in a wide range of LCF loads were analyzed.

The analyzes showed the justification of the effort to solve the life assessment of steel subjected to low cycle fatigue (LCF) numerically. The results of experimental tests and simulation tests also gave us important data on understanding the LCF behavior of HSLA steel NN-70.

Keywords HSLA, STS, LCF, Experiment, Excel, SolidWorks, FEM

1. UVOD

In the field of engineering structures and constructions, exposed to variable stresses (σ), two types of fatigue are distinguished [1], high cycle fatigue (HCF) (high number of cycles (N))

until failure) which is lower than the limit state σ_T and low cycle fatigue (LCF), with a low number of cycles to failure, but in the domain of plastic stresses.

Low-cycle fatigue of material means low-frequency material fatigue in which the appearance of microcracks and fractures occurs during repeated plastic strain with the number of cycles to failure $N=5 \times 10^4$ changes. Low-cycle fatigue is often referred to as statistical endurance under repeated static loads. The characteristics of the fatigue process during low-cycle fatigue differ from the

Corresponding author

Phd, Vujadin Aleksić, IWE, Research Associate
vujadin.aleksic@institutims.co.yu

Institute for testing of materials-IMS Institute
Bulevar vojvode Mišića 43
Belgrade, Serbia

characteristics of the fatigue process during high-cycle fatigue for the same load levels, so the assessment of the suitability of the material for long-term work must include two types of tests: high-cycle fatigue with high frequency (high frequency value) and low-cycle fatigue at lower frequency values.

Experiences have shown that the time of crack initiation is relatively short, so the life of the structure is usually determined according to the time of crack propagation, or more precisely, according to the time of propagation to the critical crack length.

High strength low alloy steels (HSLA) (Arctic steel [2]) were developed during the 1960s and 1970s to address the welding problems of conventional structural steels and the brittle fracture accidents caused by low temperatures [3]. For these constructions, the most commonly applied shaping procedure is joining by welding. The base material (BM) of high strength low alloy steels, intended for the construction of welded structures in addition to high strength, should have good plasticity, sufficient impact toughness, high resistance to brittle sheet metal, satisfactory machinability, good weldability, and the production process should be economical.

2. PROPERTIES OF HSLA STEEL NN-70

HSLA steel, NN-70 [4] is the Yugoslav version of the American steel HY-100. HSLA steels are generally being used for producing of ship and pressure equipment. The most significant component that influences steel selection is the suitable strength-to-weight proportion of HSLA steels compared with regular low-carbon steels. Ship structures are most commonly being produced by welding. For this reason high strength low-alloy (HSLA) steels, besides high strength as the main properties, should also have exceptional plasticity, adequate toughness and high resistance to brittle damage, as well as adequate workability and good welding performance [5-8].

Due to exposure to complex loading with constant cycles during exploitation, a basic understanding of material behavior and damage mechanisms under fatigue conditions is important. Tables 1 and 2 show the chemical composition and mechanical properties of HSLA steel NN-70 at room temperature [9-33].

Table 1. Chemical composition (%wt) of NN-70 [9-33]

C	Si	Mn	P	S	Cr	Ni	Mo	V	Al	As	Sn
0.106	0.209	0.220	0.005	0.0172	1.2575	2.361	0.305	0.052	0.007	0.017	0.014
Cu	Ti	Nb	Ca	B	Pb	W	Sb	Ta	Co	N	Ceq
0.246	0.002	0.007	0.0003	0	0.0009	0.0109	0.007	0.0009	0.0189	0.0096	0.542

$$C_{eq} = C + Mn/6 + Si/24 + Ni/40 + Cr/5 + Mo/4 + V/14.$$

Table 2. Mechanical properties of NN-70 at room temperature, 20 °C, [9-33]

Microstructure		Tempered martensite + tempered bainite
Ultimate tensile stress, R_m , MPa		854.8
Yield stress, $R_{p0.2}$, MPa		813.4
Modulus of elasticity, E , GPa	static	211.5
	dynamic, LCF	221.4
Percent elongation, A_5 , %		18.4
Impact toughness, J/cm ²		96.83
Crack initiation energy, J/cm ²		39.60
Crack propagation energy, J/cm ²		57.23
Hardness	plate	245-269 HV30
	LCF specimen	252-262 HV10

3. LCF TESTING OF HSLA NN-70 SAMPLES

Tests of steel, NN-70, by low-cycle fatigue with half-amplitude of controlled deformation,

$\Delta\epsilon/2=0.35 - 0.80$, were performed on 10 round smooth test specimens (STS), fig. 1a, made of sticks, 11x11x95 mm from steel plate NN-70, processed according to the drawing from fig. 1b.

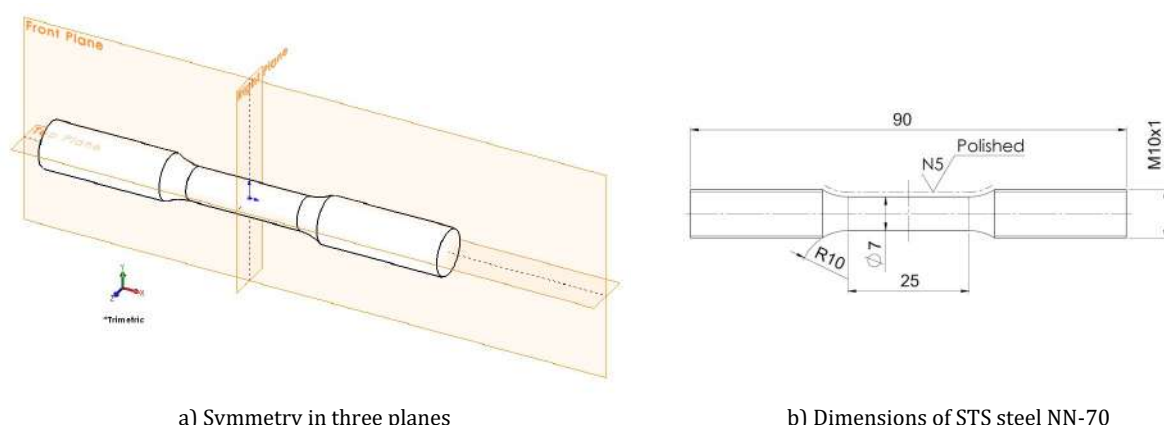


Fig. 1. Specimen for LCF test of steel NN-70 [9–33]

Low cycle fatigue test, in accordance with ISO 12106:2017 (E) [34], was performed on a universal servo-hydraulic MTS machine (rating 500 kN), in the Military Technical Institute in

Žarkovo [13, 21]. The test results of 4 specimens with controlled strain regimes shown in Table 3 were considered.

Table 3. Basic data on controlled strain regimes of LCF test NN-70 [21]

Specimen (Sp)	1	2	3	4	5	6	7
	$\Delta\epsilon/2$ [%]	$\Delta\epsilon/2$ [V]	$\Delta\epsilon/2$ [mm/mm]	Δl [mm]	$\Delta\epsilon$ [%]	T [s]	f [Hz]
	experiment	$\epsilon[V] = \epsilon[V] \cdot 0.2$	1/100	3*25	1*2	experiment	1/6
09	0.35	1.75	0.0035	0.0875	0.70	4.30	0.2326
03	0.50	2.50	0.0050	0.1250	1.00	4.30	0.2326
06	0.60	3.00	0.0060	0.1500	1.20	4.30	0.2326
08	0.80	4.00	0.0080	0.2000	1.60	4.30	0.2326

4. PROCESSING OF TEST RESULTS IN THE EXCEL PROGRAM

Processing of test results was done in the EXCEL program [18, 19, 21, 30]. The results of that processing are shown in Tables 4 and 5 and in Fig. 2, 3 and 4.

Table 4. Characteristic processed test data of LCF steel NN-70 [29, 30]

LCF NN-70, ISO 12106/03 [34]		Stabilization regions		Characteristic cycles of stabilization			
Sp	$\Delta\epsilon/2$, %	y=F, kN; x=N	R ²	N _{bs}	N _{es}	N _f	N _s = N _f /2
09	0.35	F=-0.0002N+24.30	0.95	812	6740	8329	4165
03	0.50	F=-0.0022N+28.57	0.97	256	1271	1402	701
06	0.60	F=-0.0057N+29.66	0.94	127	415	501	251
08	0.80	F=-0.0162N+30.83	0.94	50	165	207	104

N_{bs} – The beginning of stabilization; N_{es} – End of stabilization; N_f – Cycle of failure; N_s – Characteristic stabilization cycle

Table 5. Data of characteristic stabilized hysteresis, N_s, of HSLA steel NN-70 [29, 30]

Sp	y=mx-b; y=F, kN; x= $\Delta\epsilon_p/2$ F=0; $\Delta\epsilon_p/2=b/m$ $\Delta\epsilon_e/2=\Delta\epsilon/2-\Delta\epsilon_p/2$	N _s	$\Delta\epsilon/2$	$\Delta\epsilon_p/2$	$\Delta\epsilon_e/2$	σ_{max} , MPa	σ_{min} , MPa	$\Delta\sigma/2$, MPa
09	$\Delta\epsilon_p/2=(3.04/61.38)/100$	4165	0.0035	0.000495	0.003005	608.14	-689.48	648.81
03	$\Delta\epsilon_p/2=(18.74/109.15)/100$	701	0.0050	0.001717	0.003283	702.84	-707.19	705.01
06	$\Delta\epsilon_p/2=(16.93/76.92)/100$	251	0.0060	0.002201	0.003799	736.15	-698.00	717.07
08	$\Delta\epsilon_p/2=(27.97/65.04)/100$	104	0.0080	0.004301	0.003699	761.87	-709.04	735.46

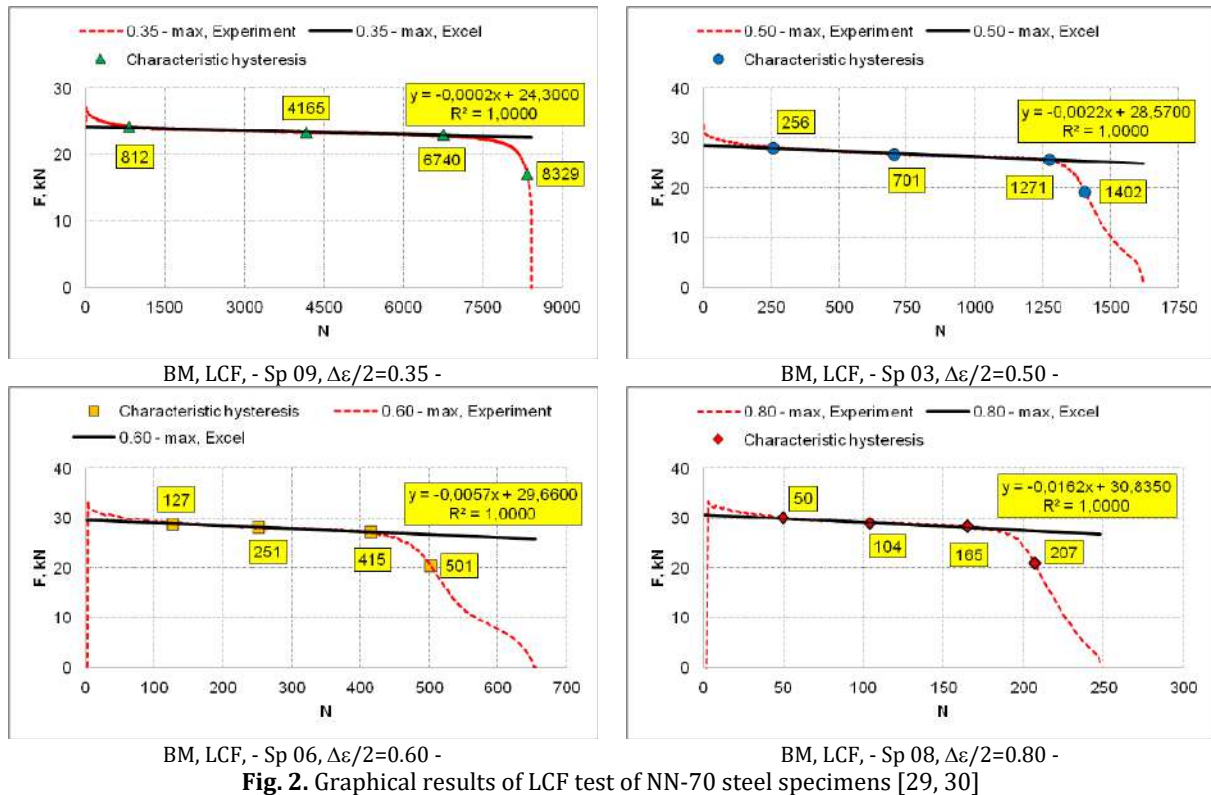


Fig. 2. Graphical results of LCF test of NN-70 steel specimens [29, 30]

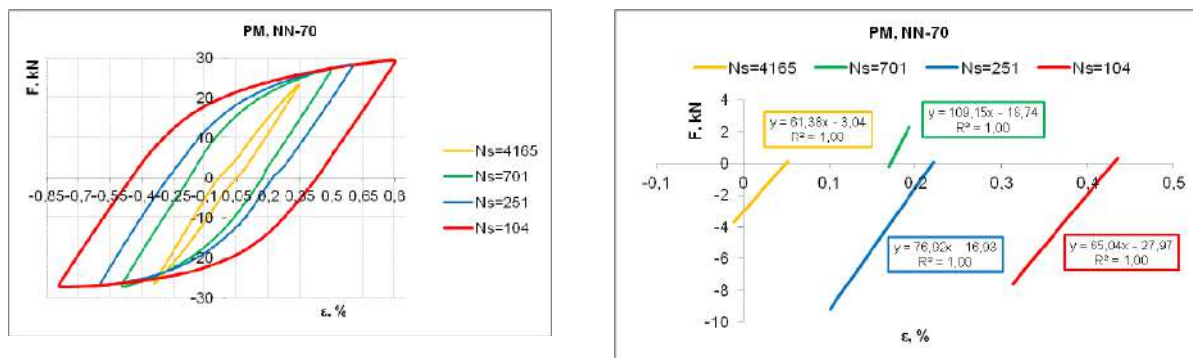


Fig. 3. Graphic view of processed stabilized hysteresis, N_s , LCF testing of HSLA steel NN-70 [29, 30]

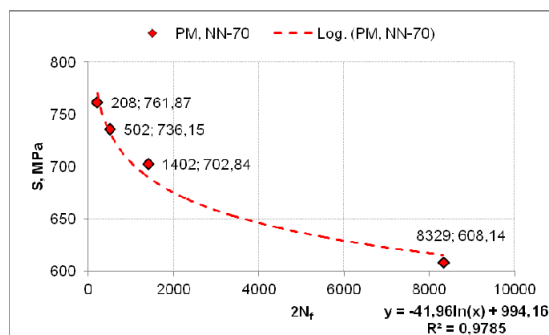


Fig. 4. Dependence $S(\sigma)-2N_f$ obtained in EXCEL by the method of least squares [29, 30]

5. PREPARATION FOR STATIC AND FATIGUE CALCULATION OF FEM IN SOLIDWORKS

Data from Table 2 and data obtained by processing the results of the LCF test into the EXCEL program, Fig. 4, were used for the static and fatigue calculation of the FEM of the BM specimen model in the Cosmos module of the SolidWorks parametric program, and their input is shown in Fig. 5. Initial data on the model, boundary conditions and finite element mesh are shown in Fig. 6.

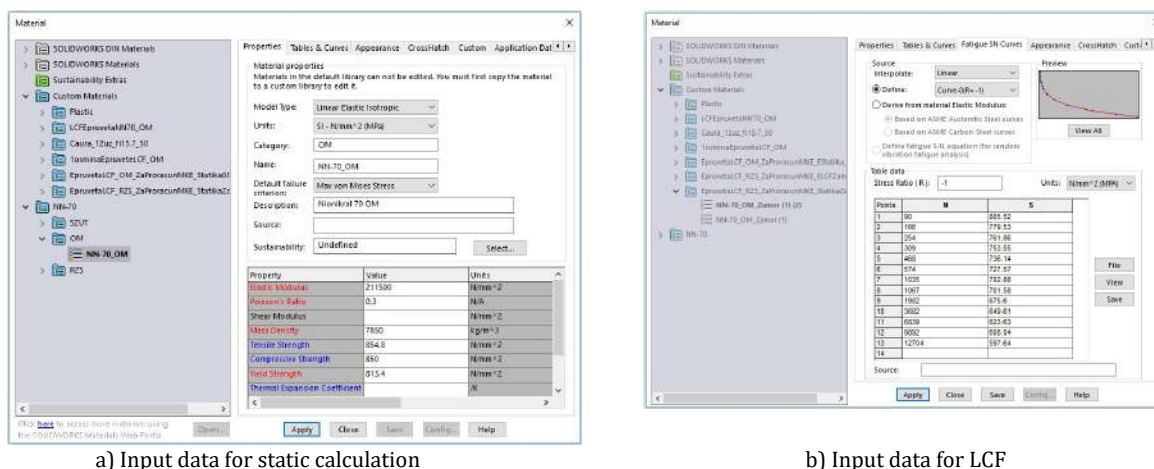
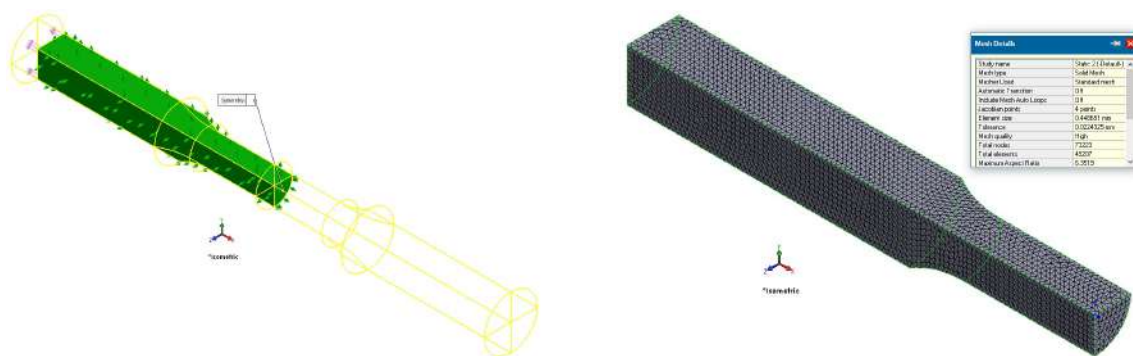


Fig. 5. Data for FEM calculation static and dynamic behaviour of HSLA steel NN-70



Boundary conditions part of BM specimen

Finite element mesh BM specimen

Fig. 6. Initial data on models, boundary conditions and finite element mesh of NN-70 specimen

6. RESULTS OF STATIC AND FATIGUE CALCULATION OF FEM IN SOLIDWORKS

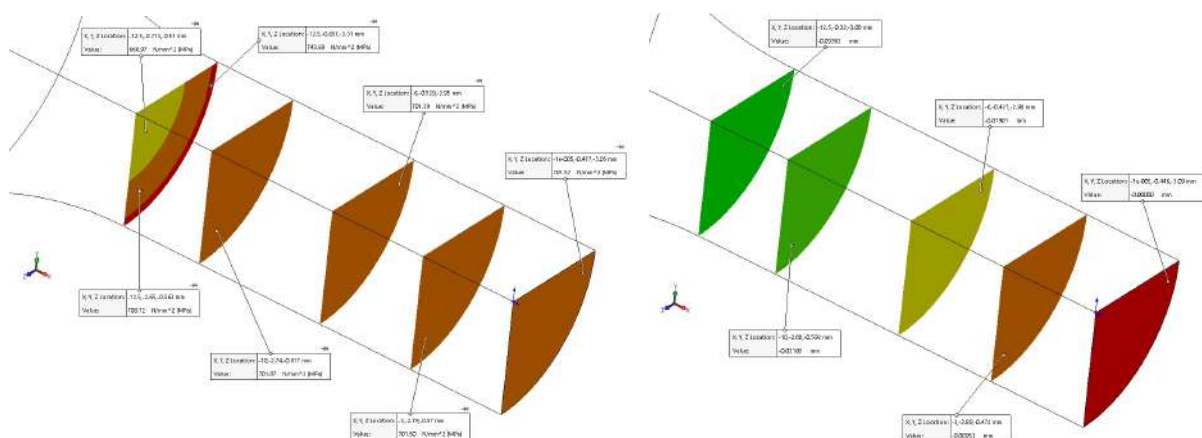
An illustration of the results of the static calculation for a load of 27 kN is shown in Fig. 7 and Table 6.

An illustration of the results of the FEM fatigue test simulation is shown in Fig. 8-10.

Table 6. Results of static calculation and simulation of LCF fatigue FEM in SolidWorks, specimen of steel NN-70

Testing specimen, cross section = 38.5 mm ²						FEM		
	LCF, experiment		Excel	F, kN	S _{Nf} , MPa	N _{fFEM} , fracture in BM	S _{NfFEM} , max, MPa	
	Δε/2	N _f					von Mises	Normal
BM, NN-70			90	31.00	805.52	91	872.08	898.71
			166	30.00	779.53	166	843.94	869.72
	0.80	208	254	29.32	761.87	254	824.81	850.01
			309	29.00	753.55	309	815.81	840.73
	0.60	502	468	28.33	736.15	468	796.96	821.31
			574	28.00	727.57	573	787.68	811.74
	0.50	1402	1035	27.05	702.84	1034	760.96	784.20
			1067	27.00	701.58	1065	759.55	782.75
			1982	26.00	675.60	1979	731.42	753.76
			3682	25.00	649.61	3676	703.29	724.77
			6839	24.00	623.63	6829	675.16	695.78
	0.35	8329	9892	23.40	608.14	9876	658.28	678.38
			12704	23.00	597.64	12681	647.02	666.79

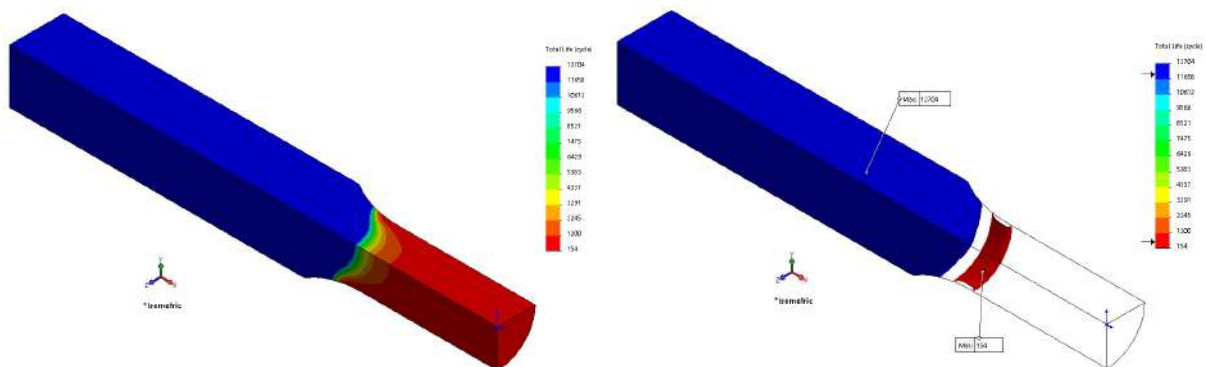
$S_{NF} = -41,96 \ln(N_f) + 994,15$ (from formula in Fig. 4)



Values of normal stresses in sections along the x axis, 0, 3, 6, 10 and 12.5 mm, BM Sp of HSLA steel NN-70

Elongation values in x-axis sections, 0, 3, 6, 10 and 12.5 mm BM Sp of HSLA steel NN-70

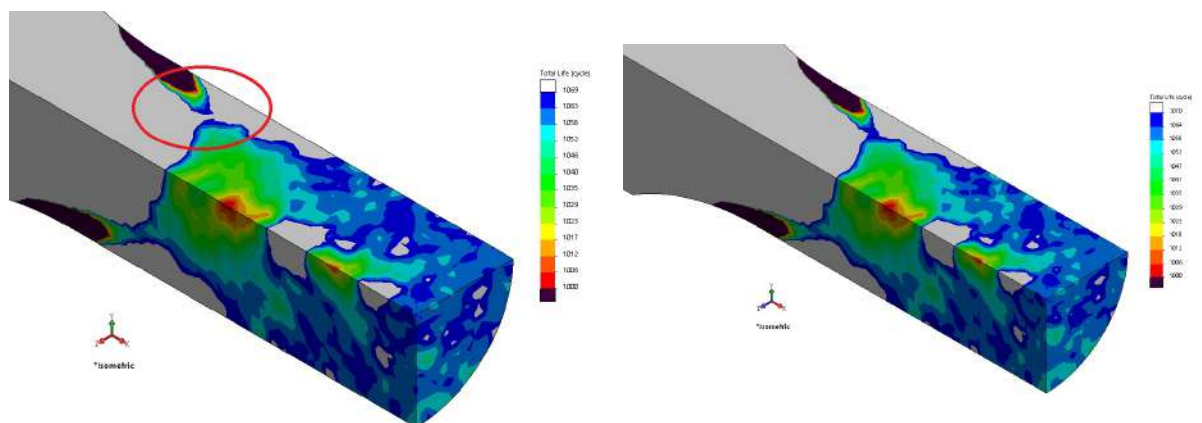
Fig. 7. Results of static calculation of FEM specimen for load 27 kN, HSLA steel of NN-70 (see Table 6)



Isolines of life, BM

Isolines of life, BM, Min i Max

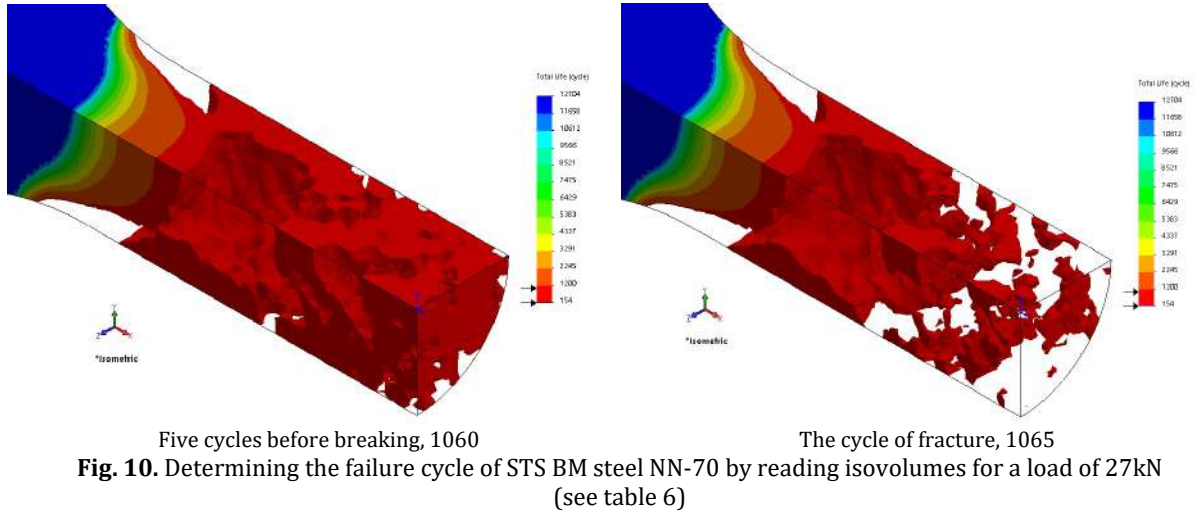
Fig. 8. Isolines of lifetime by section of STS HSLA steel NN-70 for a load of 27 kN



The cycle preceding the breaking cycle, 1069

The cycle of fracture, 1070

Fig. 9. Determination of the failure cycle of STS BM steel NN-70 by reading isosurfaces for a load of 27 kN (see table 6)



In the case of FEM static calculation, the SolidWorks program, in addition to the analysis of the distribution of von Mises stresses, enables the analysis of the results of the calculation of normal stresses (Table 6) as well as the analysis of strains and elongations. The fatigue calculation, in addition to the min and max number of iso-sections of the life cycle, also gives us the percentage of damage to a specific section of the test specimen. The methodology for determining the number of cycles for a round smooth test specimen in which the parts of the test tube separate, i.e. break, for a certain load is shown in Fig. 9 and 10, and the results of the applied methodology are shown in Table 6. Iso-section (surface or volume) of the life cycle that covers the entire

ligament of the test specimen, and it is located between the min and max number of cycles of the life cycle, which is the cycle in which the fracture of the test specimen occurs.

7. DISCUSSION OF RESULTS

By processing the results of the LCF test and calculations in the EXCEL programs, using the least squares method and SolidWorks program using the finite element method, we obtained the necessary data for determining:

1. Cyclic stress-strain curve (1), Table 7 and Fig. 11,
2. Fatigue life curve (2) and transition fatigue life (3), N_{FT} , Table 8 and Fig. 12.

Table 7. Data for Cyclic stress-strain curve (1) of HSLA steel NN-70

$\Delta\epsilon = \frac{\Delta\sigma}{E} + 2\left(\frac{\Delta\sigma}{2K'}\right)^{\frac{1}{n'}}$ (1)	Method	n'	K' , MPa	E , MPa, (determined from cycle $N_{1/4}$)
	Standard [34]	0.047	946.2	221378 (221.4 GPa)

Table 8. Data for fatigue life curve (2) and transition fatigue life (3) of HSLA steel NN-70

$\frac{\Delta\epsilon}{2} = \frac{\sigma_f'}{E} N_f^b + \epsilon_f' N_f^c$ (2) $N_{FT} = \left(\frac{\epsilon_f' \cdot E}{\sigma_f'}\right)^{\frac{1}{b-c}}$ (3)	Method	elastic part			plastic part		N_{FT}
		E , MPa	σ_f' , MPa	b	ϵ_f'	c	
	Standard [34]	221378	1153.8	-0.060	0.1045	-0.594	274

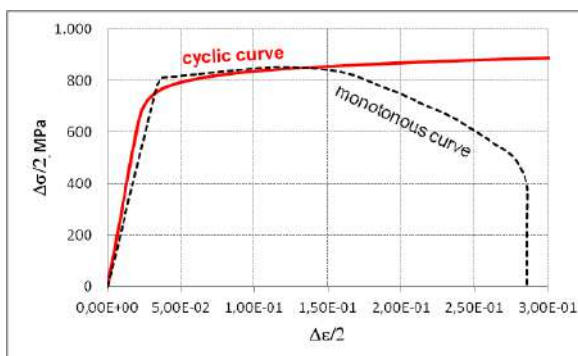


Fig. 11. Cyclic stress-strain curve (1) of HSLA steel NN-70

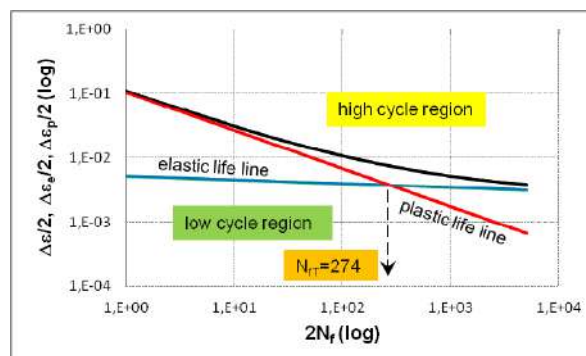


Fig. 12. Fatigue life curve (2) and transition fatigue life (3) of HSLA steel NN-70

8. CONCLUSION

The paper presents the results of the fatigue test (LCF) on a round smooth test specimen, for base metal of HSLA steel NN-70, which was used as input data for the low-cycle fatigue simulation on those test specimens and the FEM calculation in SolidWorks with the aim of obtaining comparative results of the lifetime assessment by testing and FEM calculation.

The methodology for determining the number of cycles during which the parts of the test specimen separate (specimen fracture) applied in this paper enables the calculation, FEM, of the fracture cycle to be determined on other elements made of base metal of HSLA steel NN-70 exposed to low cycle fatigue load (LCF).

As one of the very interesting and promising directions of future research, the application of the presented methodologies is imposed in order to define the size of the fatigue crack, as the main parameter for characterizing the existence of fatigue, under conditions of variable loading, in order to determine the fatigue life, cycle to failure, and assess the resistance of the material to the crack initiation, the development of which can also be followed by NDT methods.

The stabilization area during LCF test of all samples of base metal of HSLA steel NN-70 shows a high degree of agreement with the general equation of the straight line, $y (F \text{ or } \sigma) = m \times (N) + b$, whose coefficients m and b can be determined by linearization and show the weakening of base metal of HSLA steel NN-70.

The obtained results represent a practical contribution to the assessment of the behavior of high strength low-alloy NN-70 under LCF operating conditions.

Acknowledgement

This work was supported by the Ministry of Science, Technological Development and Innovation of the Republic of Serbia (Contracts: No. 451-03-47/2023-02/200012 and No. 451-03-47/2023-01/200287).

REFERENCES

- [1] Aleksić, V., Aleksić, B., Prodanović, A., Milović, Lj. (2020). HSLA Steel-Simulation of fatigue, *New Technologies, Development And Application, Lecture Notes in Networks And Systems, Sarajevo*, vol 128. Springer, p. 314 – 321.
- [2] Barsom, J. M. (1987). Fracture mechanics retrospective: early classic papers 1913-1965, *Edited By Barsom J. M.*, ASTM.
- [3] Almar-Naess, A. (1985). Fatigue Handbook: Offshore Steel Structures, by Tapir, Trondheim, Norway
- [4] Radović, A., Marković, D. (1984). Osvajanje Brodograđevnog Čelika Povišene Čvrstoće-Nionikral-70, VTI, Beograd.
- [5] Arpan, Das., Tamshuk, Chowdhury., Soumitra. Tarafder. (2014). Ductile fracture micro-mechanisms of high strength low alloy steels, *Materials and Design*, vol. 54, p. 1002–1009.
- [6] Tomasz, Ślęzaka., Lucjan, Śnieżeka., (2015). A Comparative LCF Study of S960QL High Strength Steel and S355J2 Mild Steel, *1st International Conference on Structural Integrity, Procedia Engineering*, vol. 114, p. 78– 85.

- [7] Abílio, M. P., De Jesus, A., Ribeiro, S., António, A. Fernandes. (2006). Low And High Cycle Fatigue and Cyclic Elastic-Plastic Behavior Of The P355nl1 Steel, *Journal of Engineering Materials and Technology, Transactions of the ASME*, vol. 128, p. 298-304.
- [8] Alang, N.A., Davies, C.M., Nikbin. K.M. (2016). Low cycle fatigue behaviour of ex-service P92 steel at elevated temperature, *21st European Conference on Fracture, ECF21*, Catania, Italy, *Procedia Structural Integrity*, vol. 2, p. 3177–3184.
- [9] Milović, Lj., Vuherer, T., Radaković, Z., Petrovski, B., Janković, M., Zrilić, M., Daničić, D. (2011). Determination of fatigue crack growth parameters in welded joint of hsla steel, *Structural integrity and life*, vol.11, no.3, p. 183-187.
- [10] Milović, Lj., Bulatović, S., Radaković, Z., Aleksić, V., Sedmak, S., Marković, S., Manjgo, M. (2012). Assessment of the behaviour of fatigue loaded HSLA welded steel joint by applying fracture mechanics parameters, *Structural integrity and life*, vol. 12, no. 3, p. 175–181.
- [11] Bulatović, S., Burzić, Z., Aleksić, V., Sedmak, A., Milović, Lj. (2014). Impact of choice of stabilized hysteresis loop on the end result of investigation of High-strength low-alloy (HSLA) steel on low cycle fatigue, *Metallurgija*, vol. 53, no. 4, p. 477–480.
- [12] Milović, Lj., Bulatović, S., Aleksić, V., Burzić, Z. (2014). Low cycle fatigue of weldments produced of a High strength low alloyed steel, *20th European Conference On Fracture (ECF 20)*, *Procedia Materials Science* 3, p. 1429–1434.
- [13] Bulatović, S. (2014). *Elasto-plastično ponašanje zavarenog spoja od niskolegiranih čelika povišene čvrstoće u uslovima niskocikličnog zamora*, (In Serbian). PhD thesis. Mašinski Fakultet Univerziteta u Beogradu.
- [14] Aleksić, V., Aleksić, B., Milović, Lj. (2016). Methodology for determining the region of stabilisation of low-cycle fatigue, *Book Of Abstracts, 16th International Conference On New Trends In Fatigue And Fracture (NT2F16)*, Dubrovnik, Croatia, p. 189–190.
- [15] Aleksić, V., Milović, Lj., Aleksić, B., Abubkr, M. Hemer. (2016). Indicators of HSLA steel behavior under low cycle fatigue loading, *21st European Conference on Fracture, ECF21*, Catania, Italy, *Procedia Structural Integrity*, vol. 2, p. 3313–3321.
- [16] Aleksić, V., Dojčinović, M., Milović, Lj., Samardžić, I. (2016). Cavitation damages morphology of HSLA Steel, *Metallurgija*, vol. 55, no. 3, p. 423–425.
- [17] Aleksić, V., Milović, Lj., Aleksić, B., Bulatović, S., Burzić, Z., Hemer, A.M. (2017) Behaviour Of Nionikral-70 In Low-Cycle Fatigue, *Structural integrity and life*, vol. 17, no. 1, p. 61–73.
- [18] Aleksić, V., Aleksić, B., Milović, Lj. (2017). Metodologija određivanja pokazatelja ponašanja hsla čelika pri delovanju niskocikličnog zamora, *V Međunarodni Kongres „Inženjerstvo, Ekologija I Materijali U Procesnoj Industriji”*, Jahorina, Bosna I Hercegovina, p. 1123-1135.
- [19] Aleksić, B., Aleksić, V., Hemer, A., Milović, Lj., Grbović, A. (2018). Determination Of The Region Of Stabilization Of Low-Cycle Fatigue HSLA Steel From Test Data. In: *Proceedings Of The 17th International Conference On New Trends In Fatigue And Fracture*, Eds: Ricardo R. Ambriz, David Jaramillo, Gabriel Plascencia And Moussa Nait Abdelaziz, Springer, p. 101–113.
- [20] Aleksić, B., Aleksić, V., Milović, Lj., Hemer, A., Prodanović, A. (2018). Determination of polynomial depending between hardness and cooling time $\Delta t_{8/5}$ of steel Nionikral 70 heat affected zone, *18th International Conference on New Trends in Fatigue and Fracture NT2F18*, Lisbon, Portugal, p. 87–90.
- [21] Aleksić, V. (2019). *Niskociklični Zamor Niskolegiranih Čelika Povišene Čvrstoće*, (In Serbian). PhD thesis. Tehnološko – Metalurški Fakultet Univerziteta U Beogradu.
- [22] Aleksić, V., Milović, Lj., Blačić, I., Vuherer, T., Bulatović, S. (2019). Effect of LCF on behavior and microstructure of microalloyed HSLA steel and its simulated CGHAZ, *Engineering Failure Analysis*, vol. 104, p. 1094–1106.
- [23] Bulatović, S., Aleksić, V., Milović, Lj., Zečević, B. (2021). An analysis of impact testing of high strength low-alloy steels used in ship construction, *Brodogradnja/Shipbuilding/Open Access*, vol. 72, no. 3, p. 1–12.
- [25] Bulatović, S., Aleksić, V., Milović, Lj., Zečević, B. (2021). High strength low alloy steels impact toughness assessment at different test temperatures, *Advanced Technologies & Materials*, vol. 46, no. 2, p. 43–46.
- [26] Bulatović, S., Aleksić, V., Milović, Lj., Zečević, B. (2021). Determination of the coffin-manson equation under low-cycle fatigue conditions, *Structural integrity and life*, vol. 21, no. 3, p. 225–228.
- [27] Aleksić, V., Dojčinović, M., Milović, Lj., Zečević, B., Maksimović, A. (2021). Mehanizmi i morfologije kavitacionog oštećenja čelika Nionikral 70, *Zaštita Materijala*, vol. 62, no. 2, p. 95–105.
- [29] Aleksić, V., Milović, L., Bulatović, S., Zečević, B., Maksimović, A. (2022). Determination of LCF plastic and elastic strain components of steel, *Machine And Industrial Design In Mechanical Engineering. KOD 2021. Mechanisms And Machine Science, Balaton*, vol. 109. Springer, Cham. p. 341–349.
- [30] Aleksić, V., Bulatović, S., Zečević, B., Maksimović, A., Milović, Lj. (2022). Processing of data obtained by the testing of steel under Low cyclic fatigue (part I), *Transactions Of Famena*, vol. XLVI, no. 4, p. 59-72.

- [31] Bulatović, S., Aleksić, V., Milović, Lj., Zečević, B. (2022). Determining of the fatigue crack growth rate of HSLA steel at room temperature, *Advanced Technologies & Materials*, vol. 47, no. 1, p. 1–4.
- [32] Bulatović, S., Aleksić, V., Milović, Lj., Zečević, B. (2022). Application Of Paris' Law Under Variable Loading, *FME Transactions*, vol. 50, no. 1, p. 72–78.
- [33] Bulatović, S., Aleksić, V., Milović, Lj., Zečević, B. (2023). Experimental determination of the critical value of the J-integral that refers to the HSLA steel welded joint, *Tehnički Vjesnik/Technical Gazette*, vol. 30, no. 1, p. 148–152.
- [34] ISO 12106. (2017). *Metallic Materials-Fatigue Testing-Axial-Strain-Controlled Method*, Geneva, Switzerland.



Banja Luka
1–2 Jun 2023.

DEMI 2023

16th International Conference on Accomplishments in Mechanical and Industrial Engineering

www.demi.mf.unibl.org



CHARACTERIZATION AND HEAT TREATMENT OF ARMOUR STEEL OF NEW GENERATION

D. P. Kosec^a, J. Bernetič^b, A. Nagode^c, G. Kosec^d, M. Soković^a, B. Kosec^{c,e}

^aUniversity of Novo mesto, Faculty of Mechanical Engineering, Na Loko 2, 8000 Novo mesto, Slovenia.

^bSAAT d.o.o., Cesta na Lisice 4, 1000 Bled, Slovenia

^cUniversity of Ljubljana, Faculty of Natural Sciences and Engineering, Aškerčeva 12, 1000 Ljubljana, Slovenia

^dSIJ ACRONI d.o.o., c. B. Kidriča 44, 4270 Jesenice, Slovenia

^eUniversity of Ljubljana, Faculty of Mechanical Engineering, Aškerčeva 6, 1000 Ljubljana, Slovenia

Abstract Steel armour plates are intended for ballistic protection of military and civilian vehicles and structures, parts of machines and devices. The work includes heat treatment and characterization of mechanical, microstructural and thermal properties of new steel for ballistic protection with internal code SA600. Steel is the result of the development and knowledge of firm SAAT, d.o.o. in collaboration with scientific institutions and industry partners, produced in an industrial environment. The results of the research carried out as part of the investigation confirmed that the optimal austenitization temperature for SA600 steel is 870 °C and the tempering temperature is 150 °C. Under these conditions, the hardness of the steel is 632 HV10, which means that it is suitably high. The yield strength is 1640 MPa and the tensile strength is 2052 MPa. The $R_{p0.2}/R_m$ ratio is equal to 0.7992 and is correspondingly low. The thermal conductivity increases with temperature and is equal to 28.33 W/m·K at room temperature, and 39.67 W/m·K at 400 °C.

Keywords steel, armour protection, characterization, heat treatment, production, testing, properties

1. INTRODUCTION

Steel armour plates are intended for ballistic protection of military and civilian vehicles and structures, parts of machines and devices. When selecting or developing the appropriate materials for the armour it is necessary to achieve the best possible compromise between the required mechanical properties of materials, its density and the final price of the product [1].

Corresponding author

Prof. Borut Kosec
borut.kosec@ntf.uni-lj.si

University of Ljubljana Faculty of Natural Sciences and Eng.
Aškerčeva cesta 12, 1000 Ljubljana
Ljubljana, Slovenia

With the appropriate production technology, which includes synthesis, hot forming, heat treatment, etc. [2], high strength low alloy steel of good functional properties at affordable prices can be produced. By improving the strength and toughness of the steel, the required thickness and the weight of the armour can be reduced.

New steel for ballistic protection with internal code SA600 belongs to the group of high strength low alloy (HSLA) steels [3]. Steel is the result of the development and knowledge of SAAT, d.o.o. in collaboration with scientific institutions and industry partners, produced in industrial environment of VOEST Alpine GmbH. Table 1 shows the mass percentages of the elements that make up SA600 steel in addition

to iron. The optimal chemical composition enables the achievement of the desired mechanical and physical properties and the planned microstructure.

The relevant mechanical properties are achieved by quenching and tempering [4].

Table 1. Indicative chemical composition of SA600 steel (in m.%)

Element	m. %
C	0.43
Si	0.80
Mn	0.70
Cr	0.80
Ni	0.30
B	0.005
S	0.003
P	0.015
Fe	balance

The optimal chemical composition enables the achievement of the desired mechanical and physical properties and the planned microstructure. The relevant mechanical properties are achieved by quenching and tempering [4].

The first and most important purpose of SA600 steel is resistance to the penetration of projectiles from small arms. The resistance depends mainly on the following mechanical properties: hardness, yield strength, tensile strength, plastic deformation capabilities, impact and fracture toughness, and stretching [5].

With the alloying elements silicon, chromium, molybdenum and boron, the appropriate manufacturing technology and heat treatment, all the desired mechanical properties can be achieved. Table 2 shows the approximate values of the mechanical properties of SA600 sheet steel.

Table 2. Mechanical properties of SA600 steel

Hardness	590 – 640 HB
Yield strength	1600 MPa
Tensile strength	2050 MPa
Elongation	7.5 %
Impact toughness (at - 0°C)	15 J

2. EXPERIMENTAL WORK

The experimental work includes heat treatment and characterization of mechanical, microstructural and thermal properties of new steel for ballistic protection with internal code SA600. In Figure 1 is testing SA600 steel plate from which samples were cut to perform heat treatment, mechanical tests, microstructure analysis and thermal properties description.

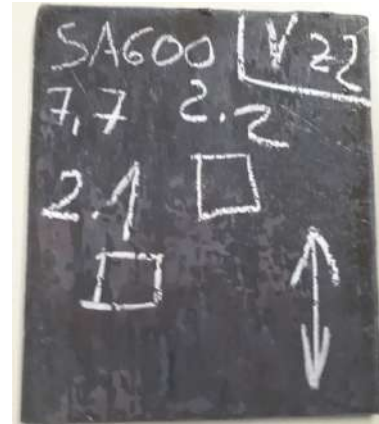


Fig 1. Testing SA600 steel plate

As part of the research (at the Faculty of Mechanical Engineering, University of Ljubljana and in the biggest slovenian steel producer SIJ ACRONI, d.o.o.), we first cut samples from the supplied plates with a water jet for heat treatment and investigations of microstructure and mechanical properties (Figure 2).



Fig. 2. Water jet cutting machine Water Jet NC 2525 D in SIJ ACRONI d.o.o.

We performed heat treatment of SA600 steel in the delivered state, which consisted of hardening and tempering. Based on experience and previous preliminary research, we determined a temperature of 870 °C for the optimal austenitization temperature, i.e. the

Based on the results of hardness measurements, the temperature of 150 °C was chosen as the optimal temperature for the tempering.

The tensile test was performed on a universal tensile / pressure tearing machine INSTRON 1255 in accordance with ISO 6892-1: 2009 [6].

The temperature 150 °C was chosen for the optimal tempering temperature. At this temperature, SA600 steel achieves the most suitable combination of mechanical properties for armour steels.

The hardness in our case is high and amounts to 632 HV (580 - 640 HV is prescribed). The $R_{p0.2}/R_m$ ratio is the lowest at this temperature (0.7992). A low $R_{p0.2}/R_m$ ratio means higher resistance to local steel flow and thus better armour protection. The elongation at this temperature is 7.5% and thus reaches the required elongation value for armour steel.

Measurements and analysis of thermal properties of testing samples from the steel SA600 were performed in accordance with ISO 22007-2 standard [7] In our research, we used one of the most advanced instruments for determining the thermal properties, Hot Disk TPS 2200, a product of Hot Disk AB company, Gothenburg, Sweden [8]. In Figure 7 is instrument Hot Disk TPS 2200 in the Laboratory for Thermotechnical Measurements, Faculty of Natural Sciences and Engineering, University of Ljubljana.



Fig. 7. Instrument Hot Disk TPS

In Figure 8 are presented results of thermal properties measurements at ambient temperature.

In Table 3 are presented thermal properties (thermal conductivity, specific heat and temperature conductivity) of steel SA600 at ambient temperature (approx. 22 °C).

Settings						Numeric Results			
Row	St...	Description	Heating Power	Meas...	Sam...	Sense	Thermal Conductivity	Thermal Diffusivity	Specific Heat
0	C...	jello SA 600_1	500 mW	5s	200 °C	S082	38.45 W/mK	1.748 mm²/s	4.405 MJ/m³K
1	C...	jello SA 600_2	500 mW	5s	200 °C	S082	37.45 W/mK	1.511 mm²/s	4.400 MJ/m³K
2	C...	jello SA 600_3	500 mW	5s	200 °C	S082	37.13 W/mK	1.439 mm²/s	4.400 MJ/m³K
3	C...	jello SA 600_4	700 mW	5s	200 °C	S082	30.56 W/mK	1.330 mm²/s	4.400 MJ/m³K
4	C...	jello SA 600_5	700 mW	5s	200 °C	S082	36.46 W/mK	1.286 mm²/s	4.400 MJ/m³K
5	C...	jello SA 600_6	700 mW	5s	200 °C	S082	36.40 W/mK	1.274 mm²/s	4.400 MJ/m³K
6	C...	jello SA 600_7	500 mW	5s	200 °C	S082	40.42 W/mK	1.421 mm²/s	4.300 MJ/m³K
7	C...	jello SA 600_8	500 mW	5s	300 °C	S082	39.57 W/mK	1.344 mm²/s	4.300 MJ/m³K
8	C...	jello SA 600_9	500 mW	5s	300 °C	S082	38.85 W/mK	1.094 mm²/s	4.300 MJ/m³K
9	C...	jello SA 600_10	700 mW	5s	300 °C	S082	38.74 W/mK	1.037 mm²/s	4.300 MJ/m³K
10	C...	jello SA 600_11	700 mW	5s	300 °C	S082	38.88 W/mK	1.113 mm²/s	4.750 MJ/m³K
11	C...	jello SA 600_12	700 mW	5s	300 °C	S082	40.54 W/mK	1.446 mm²/s	4.300 MJ/m³K

Fig 8. Results of measurements

Table 3. Thermal properties of steel SA600 at ambient temperature

Thermal conductivity	28.33 W/m·K
Specific heat	4.44 MJ/m³K
Temperature conductivity	6.37 mm²/s

The thermal conductivity increases with temperature, and is equal to 28.33 W/m·K at ambient temperature, and 39.67 W/m·K at 400 °C.

3. CONCLUSIONS

The work includes heat treatment and characterization of mechanical, microstructural and thermal properties of new steel for ballistic protection with internal code SA600. Steel is the result of the development and knowledge of firm SAAT, d.o.o. in collaboration with scientific institutions and industry partners, produced in an industrial environment.

The results of the research carried out as part of the investigation confirmed that the optimal austenitization temperature for SA600 steel is 870 °C and the tempering temperature is 150 °C. Under these conditions, the hardness of the steel is 632 HV10, which means that it is suitably high. The yield strength is 1640 MPa and the tensile strength is 2052 MPa. The $R_{p0.2}/R_m$ ratio is equal to 0.7992 and is correspondingly low.

The thermal conductivity increases with temperature and is equal to 28.33 W/m·K at room temperature, and 39.67 W/m·K at 400 °C.

Acknowledgement

The authors want to thank dr. Slavko Ažman⁺ (ACRONI d.o.o.), professor Ladislav Kosec (University of Ljubljana), professor Franc Vodopivec⁺ (Institute of Metals and Technology), dr. Milan Rimac (Metallurgical Institute K. Kapetanovic, Zenica), professor Zijah Burzić (Military Technical Institute, Belgrade) and professor Anton Smolej (University of Ljubljana) for mentorship at study armoured steels.

REFERENCES

- [1] Dobrzanski, L.A., Technical and Economical Issues of Materials Selection, Silesian Technical University, Gliwice, 1997.
- [2] Crouch, I. G., The Science of Armour Material. Amsterdam: Elsevier, 2017.
- [3] Totten, G. E., Steel heat treatment: equipment and process design. Boca Raton: CRC Press, Taylor & Francis Group, 2006.
- [4] Bernetič, J., Development of model for predicting hardenability of high strength low alloy steels: (B. Kosec, A. Smolej), Doctoral Thesis, University of Ljubljana, Ljubljana, 2013.
- [5] Bernetič, J., Kosec, G., Kosec, B., Steel of new generation PROTAC 500, IRT 3000, 8 (2013) 48, 30-31.
- [6] Slovenian standard SIST EN ISO 6892-1:2010: Metal Materials – Tensile Testing Part 1: Testing Methods at Room Temperature (01 – march- 2010).
- [7] International standard ISO 22007 (2009). Plastics – Determination of thermal conductivity and thermal diffusivity – Part 1: General principles. Reference: ISO 22007:2009(E).
- [8] Kosec, B., Karpe, B., Instrument for the thermal properties analysis Hot Disk TPS 2200, IRT3000, 1 (2017), 67.



Banja Luka
1–2 Jun 2023.

DEMI 2023

16th International Conference on Accomplishments in Mechanical and Industrial Engineering

www.demi.mf.unibl.org



Effect of solution annealing parameters on microstructure and mechanical properties of nickel free austenitic steels

J. Halilović^a, D. Sprečić^a, E. Nasić^a, Dž. Kovačević^a

^aUniversity of Tuzla, Faculty of Mechanical Engineering, Urfeta Vejzagića 4, 75000 Tuzla, B&H

Abstract Heat treatment of solution annealing is an important step after hot forging of nickel-free austenitic stainless steels and has significant effects on the microstructure and mechanical properties. The purpose of solution annealing is to remove precipitates and delta ferrite to ensure a fully austenitic microstructure. In this study, the effect of solution annealing parameters on the microstructure of a hot-forged nickel-free austenitic stainless steel Fe-Cr-Mn (Mo)-N was investigated. The results show that the solution annealing temperature and the holding time have a significant effect on the size of the austenitic grain, the content of precipitates and delta ferrite. A series of mechanical tests shows that all solution annealing parameters have a strong influence on tensile strength and elongation. Subsequent heat treatment of solution annealing resulted in higher values of tensile strength and elongation compared to hot forged ingots without heat treatment.

Keywords Nickel free austenitic steel, solution annealing, microstructure, mechanical properties

1. INTRODUCTION

It is impossible to imagine life and production today without iron-based materials, especially steel, as their production and use is far larger than that of other engineering materials. From 1950 until today, stainless steels have seen the greatest increase in consumption [1]. Stainless steels are characterized by corrosion resistance, high strength, high plasticity and high chromium content. The properties of stainless steel are based on chromium, which in the

presence of atmospheric oxygen forms a thin, hard and compact layer of chromium oxide Cr_2O_3 on the metal surface, thus protecting the metal from corrosion [2].

Of all stainless steels, austenitic stainless steels rank first in total production on the world market. They are corrosion resistant in various media and retain their good properties even at very low temperatures [3]. They are alloyed with elements that ensure the formation of an austenitic structure: nickel, nitrogen and copper. The total mass fraction of gammagenic alloying elements is generally above 8% [3].

The need for high tensile strength, non-magnetic behavior and high corrosion resistance led to the development of nickel-free austenitic stainless steel. The nickel in the alloy is completely replaced by manganese to increase nitrogen solubility. Nitrogen (0.5-

Corresponding author

PhD, Jasmin Halilović
jasmin.halilovic@untz.ba

University of Tuzla, Faculty of Mechanical Engineering
Urfeta Vejzagića 4
75000 Tuzla, B&H

0.9%) was added as an alloying element to maintain the austenitic structure [2, 3, 4]. Also, to increase the corrosion resistance of this alloy, 2 to 4% molybdenum was added [3, 4]. Since the alloy is completely nickel-free, it is considered to be comfortable for the human body (does not cause allergic reactions) and is widely used for jewelry, wristwatches, dental covers, coronary stents and in other industries [5, 6].

Due to the numerous advantages made possible by the addition of nitrogen, efforts are being made to develop an economical process that will allow the production of nickel-free austenitic stainless steel with nitrogen in large quantities. Today, there are various manufacturing processes for nickel-free nitrogen-alloyed stainless steels. The difference between the manufacturing processes lies in the way the nitrogen is introduced into the alloy, i.e. the way the alloy is nitrided during its production [7-10]. Each manufacturing process has its own characteristic parameters of alloy nitriding, which have not yet been fully explored.

Nickel-free austenitic stainless steels alloyed with nitrogen are produced in induction furnaces, arc furnaces, AOD furnaces, plasma arc furnaces, by pressure ESR process, pressure arc slag process and by powder metallurgical processes [7-11]. Since not all manufacturing processes provide a ready-to-use product, subsequent heat treatment is also required. Subsequent heat treatment in the form of solution annealing is required to achieve a complete austenitic microstructure with a minimum amount of precipitates and better mechanical properties [2, 7, 11].

In this work, the effects of subsequent heat treatment - solution annealing - on hot-forged austenitic nickel-free Fe-Cr-Mn (Mo)-N steels are investigated, i.e. the influence of solution annealing parameters on the microstructure and mechanical properties of nickel-free austenitic stainless steels is analyzed.

2. EXPERIMENTAL WORK

The test ingots were produced in an open induction furnace with a capacity of 60 kg and a refractory wall (alkaline, 87 % Al₂O₃ + 13 % MgO). They were cast in ingot molds of KV 7 format. The alloy was formed from Armco iron, FeCr, FeMo and FeMn, as well as nitrided FeCr

with minimal carbon content. Nitrided FeCr contained 5.06% N.

All test ingots were hot forged by the primary process from KV7 format to a cross-section thickness of 25 mm. Primary deformation by forging was carried out on a 200 kN hydraulic press in the temperature range from 1120 to 1150 °C. Prior to forging, the head of the ingot was cut off on a band saw and the remainder of the ingot was heated in an induction furnace to a forging temperature of 1150 °C. The 25 mm thick forged form was not suitable for machining by removing the shavings, so its further preparation for taking samples was done by water jet cutting. The cut samples were further prepared according to the standards in suitable test tubes for heat treatment, testing of mechanical properties and for microstructure testing.

According to the experimental plan, the prepared samples were thermally treated (solution annealing) to obtain a complete austenitic structure with a minimum amount of precipitates and delta ferrite. The heat treatment schedule for individual treatments is shown in Table 1. A conventional IPSEN furnace with a maximum operating temperature of 1200 °C was used for solution annealing. The chemical composition of the obtained austenitic stainless steels is given in Table 2. Metallographic analysis of the samples was performed using an optical microscope (Optika XDS-3MET). The mechanical properties were tested on test tubes prepared according to the EN 10002-1 standard - tensile testing (Fig. 1), at room temperature, using a Zwick/Roell tearing machine with a capacity of 30kN.

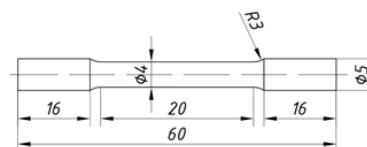


Fig. 1. Tube geometry for the static tension test

Table 1. Heat treatment plan

Exp no.	Parameters of the heat treatment	
	Annealing temperature (°C)	Annealing time (min)
1	920	30
2	1020	30
3	1100	60

Table 2. Composition of austenitic stainless steels (wt%)

Alloy	Cr	Mo	Mn	Si	Ni	N
A1	16,16	2,66	13,54	0,208	≤0,1	0,390
A2	15,83	3,20	13,39	0,218	≤0,1	0,250

3. RESULTS AND DISCUSSION

Under industrial conditions, hardening of austenitic stainless steels is not an equilibrium process, and a two-phase structure of austenite and δ -ferrite is formed [12]. Analyzing the microstructure of the ingots without heat treatment (Table 3.), it can be clearly seen that a two-phase microstructure of austenite and δ -ferrite was formed. In addition to the formation of a two-phase microstructure, it can be seen that chromium nitrides were formed in the form

of precipitates at the grain boundaries or in the form of lamellae in the austenite grain, as well as carbides that precipitate at the grain boundaries. Austenite becomes supersaturated with carbon and chromium at temperatures below A1, which requires an additional increase in the amount of precipitates and δ -ferrite. To obtain a complete austenite microstructure, heat treatment by solution annealing was performed to remove precipitates and the content of δ -ferrite. Water was used as a coolant. Upon heating of the obtained samples, the delta ferrite decomposes into carbides and the sigma phase [2]. The precipitated carbides are usually chromium carbides, since delta ferrite is rich in chromium; depending on the temperature, chromium nitrides can also be precipitated [2, 11].

Table 3. Microstructure of A1 and A2 alloy

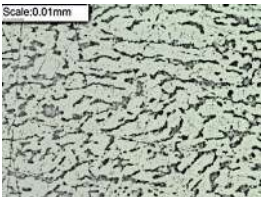
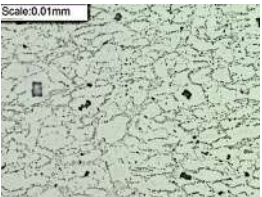
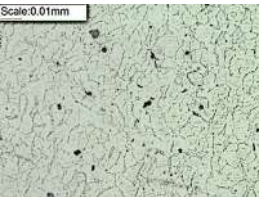
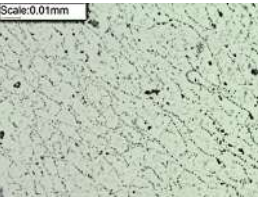
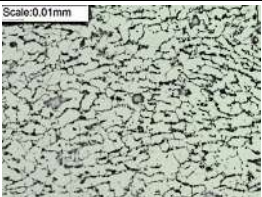
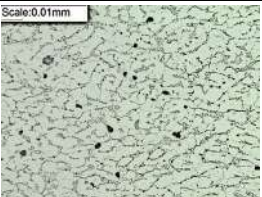
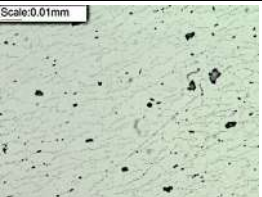
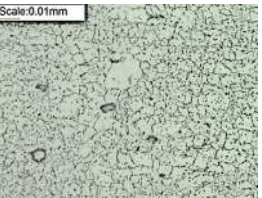
Alloy	Hot forged 950°C	Solution annealed 920°C 30min	Solution annealed 1020°C 30min	Solution annealed 1100°C 60min
A1				
A2				

Table 4. Results of the static tube tensile test

Alloy	A1 Hot forged	A2 Hot forged	A1 Solution annealed 920°C/30min	A2 Solution annealed 920°C/30min	A1 Solution annealed 1020°C/30min	A2 Solution annealed 1020°C/30min	A1 Solution annealed 1100°C/60min	A2 Solution annealed 1100°C/60min
R _m (MPa)	795	817	591	672	654	723	876	789
A (%)	38,4	33	20	23,4	23,2	24	47,8	34,6

The resulting microstructure of the solution-annealed melts is shown in Table 3. From the microstructure analysis, it can be concluded that melts A1 and A2 contain austenite and precipitates in the form of chromium nitride and chromium carbide at a temperature of 920

°C. In addition, the melts have a greater or lesser amount of the sigma phase formed by the dissolution of δ -ferrite. The sigma phase is formed by eutectoid transformation of δ -ferrite, δ -ferrite recrystallizes into the sigma phase and austenite ($\delta \rightarrow \sigma + \gamma$) [2].

The tendency of forming the sigma phase can be predicted by the value of the parameter N_v [13]. If the value for the formation of the sigma phase N_v is greater than 2.52, the formation of the sigma phase occurs [13]. With regard to the chemical composition of the melts, the value for the formation of the sigma phase in melts A1 and A2 is above the threshold value of 2.52, which suggests that the formation of the sigma phase occurred at the annealing temperature of 920 °C.

This suggests that this solution annealing temperature of 920 °C is not sufficient for a complete austenitic microstructure, especially because of the formation of the sigma phase, which is very fragile and degrades the mechanical properties. Annealing the melt at a temperature of 920 °C results in the lowest value for tensile strength due to the appearance of the sigma phase, which deteriorates the tensile strength and the percentage elongation (Table 4, Fig. 2 and Fig. 3).

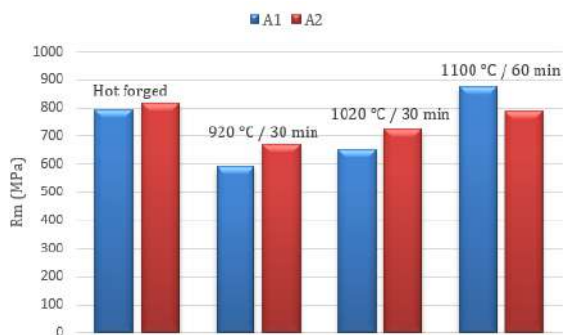


Fig. 2. Dependence of tensile strength on thermal processing

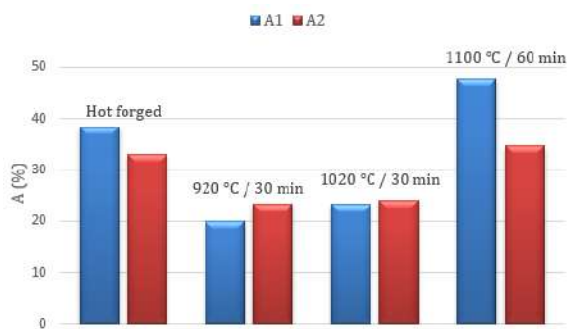


Fig. 3. Dependence of percentage elongation on thermal processing

The second solution annealing plan with an applied temperature of 1020 °C (annealing time

30 minutes) is also not suitable for obtaining a complete austenite microstructure. The application of this temperature resulted in partial melting of the delta ferrite and the formation of distinct grain boundaries between the delta ferrite and austenite phases. In addition to the incomplete dissolution of the delta ferrite, the precipitates were also not completely dissolved. Annealing at a temperature of 1020 °C did not result in the appearance of the sigma phase, which was directly reflected in the improvement of the mechanical properties. However, at the annealing temperature of 1020 °C, incomplete dissolution of the delta ferrite occurred, which affected the tensile strength. The tensile strength is higher due to the occurrence of delta ferrite in larger clusters (larger ferrite grains), which is evident in the microstructure and confirmed by the results of the static tensile test (Table 4, Fig. 2).

To determine at what temperature a complete austenite microstructure can be achieved, an annealing temperature of 1100 °C was also applied for 60 minutes. In melt A1, the applied temperature resulted in the formation of an austenite base with a small amount of precipitates (chromium carbide and chromium nitride) and the lowest amount of delta ferrite. Increasing the molybdenum content in melt A2 resulted in the formation of a larger amount of carbide at the grain boundaries as well as a larger amount of delta ferrite, which can be attributed to the higher nitrogen solubility in the delta ferrite compared to melt A1, which has a lower molybdenum content. Furthermore, it can be seen that abnormal grain growth occurred in melt A2 at a temperature of 1100 °C, which is referred to as secondary recrystallization [2].

Analysis of Figure 2 shows that there is an increase in tensile strength for melts A1 and A2 at an annealing temperature of 1100 °C compared to lower annealing temperatures. The increase in tensile strength is due to the fact that larger chromium nitride clusters do not form. The annealing temperature of 1100 °C resulted in an increase in grain size, which directly affected the increase in percent elongation value. In addition, all analyzed microstructures containing lower amounts of delta ferrite have higher percent elongation (Fig. 3). From the previous analysis, it is evident that the final microstructure is influenced by

several factors, which are the chemical composition, the annealing temperature and the annealing time.

4. CONCLUSIONS

Based on the analysis of the obtained results, the following can be concluded:

- The subsequent heat treatment (solution annealing) provided higher values of tensile strength and percent elongation compared to forged ingots. The annealing temperature of 1100 °C ensures an austenitic structure with a low percentage of precipitates and delta ferrite, and higher values for tensile strength and percent elongation compared to annealing at other temperatures (920 °C and 1020 °C).
- Increasing the annealing temperature increases the elongation, while the tensile strength varies depending on the austenite grain size and delta ferrite content.
- The value of the tensile strength of the material increases with a decrease in austenite grain size and, vice versa, decreases with an increase in austenite grain size.
- The formation of chromium nitride clusters or massive carbides leads to a decrease in tensile strength and percent elongation.
- The value of percent elongation is higher when the precipitate density is lower and the austenite grain size is larger.
- An increase in the delta ferrite content leads to a decrease in the value of the percentage elongation.

REFERENCES

- [1] International Stainless Steel Forum (ISSF). Stainless steel meltshop production. From: <https://www.worldstainless.org/statistics/stainless-steel-meltshop-production/> accessed on: April 18, 2023.
- [2] Halilović, J. (2019). *Uticaj parametara nitiranja i naknadne termičke obrade na mikrostrukturu i mehaničke osobine austenitnih nehrđajućih čelika bez nikla*. (In Bosnian). PhD thesis. Mašinski fakultet Univerziteta u Tuzli.
- [3] Gavriljuk, G.V., Berns, H. (2008). *High Nitrogen Steels - Structure, Properties, Manufacture, Applications*. Springer-Verlag, Berlin.
- [4] Pan, J., Karlén, C., Ulfvin, C. (2000). Electrochemical study of resistance to localized corrosion of stainless steels for biomaterial applications. *Journal of The Electrochemical Society*, 147(3): p. 1021-1025. DOI: [10.1149/1.1393307](https://doi.org/10.1149/1.1393307)
- [5] Buhagiar, J. (2008). *Plasma Surface Engineering and characterisation of Biomedical Stainless Steel*. PhD thesis. University of Birmingham.
- [6] Berns, H. Alloy development and processing, *Proceedings of the 7th International Conference on High Nitrogen Steels HNS 2004*, September 2004. Ostend, Belgium, p. 271 – 282.
- [7] Halilović, J. Butković, S. (2018). Microstructure and mechanical properties of nickel free austenitic stainless steels produced by addition of nitrided ferroalloys during melting in induction furnace. *Journal of Trends in the Development of Machinery and Associated Technology*, vol. 21, no. 1, p. 33 – 36.
- [8] Forch, K., Stein, G., Menzel, J. Technologies of Newly Developed High-Nitrogen Steels, *Proceedings of the 2nd International Conference on High Nitrogen Steels HNS 90*, 1990. Aachen, Germany, p. 258 - 267.
- [9] Li, H.B., Jiang, Z.H., Shen, M.H., You, X.M. (2007). High Nitrogen Austenitic Stainless Steels Manufactured by Nitrogen Gas Alloying and Adding Nitrided Ferroalloys, *Journal of Iron and Steel Research*, vol. 14, no. 3, p. 64-69. DOI: [10.1016/S1006-706X\(07\)60045-4](https://doi.org/10.1016/S1006-706X(07)60045-4)
- [10] Jiang, Z.H., Zhu, H.C., Li, H.B., Li, Y., Liu, F.B. Pressurized metallurgy for high performance special steels and alloys, *IOP Conference Series Materials Science and Engineering*, September 2015, vol. 143, no. 1, Leoben, Austria. DOI: [10.1088/1757-899X/143/1/012038](https://doi.org/10.1088/1757-899X/143/1/012038)
- [11] Halilović, J. Sprečić, D., Nasić, E., Kovačević, Dž. Influence of Delta Ferrite on Mechanical Properties of Nickel Free Austenitic Stainless Steels, *Proceedings of the 8th International Conference New Technologies, Development and Applications*, January 2022. Springer, p. 114 – 121. DOI: [10.1007/978-3-031-05230-9_13](https://doi.org/10.1007/978-3-031-05230-9_13)

- [12] Tehovnik, F., Vodopivec, F., Kosec, L., Godec, M. (2006). Hot ductility of austenite stainless steel with a solidification structure, *Materiali in tehnologije*, vol. 40, no. 4, p. 129 – 137.

- [13] Golanski, G., Zielinski, A., Purzynska, H. (2017). *Precipitation Processes in Creep-Resistant Austenitic Steels*. IntechOpen.
DOI: [10.5772/intechopen.70941](https://doi.org/10.5772/intechopen.70941)



Banja Luka
1-2 Jun 2023.

DEMI 2023

16th International Conference on Accomplishments in Mechanical and Industrial Engineering

www.demi.mf.unibl.org



Finite element calculation of redesigned welded joint at support for frame stage-like structure

Aleksandra Arsić^a, Željko Flajs^b, Vlada Gašić^a, Nenad Zrnić^a

^aUniversity of Belgrade, Faculty of Mechanical Engineering, Serbia

^bInstitute for Materials Testing, Belgrade, Serbia

Abstract

A numerical analysis of welded connection between two steel structures is performed with the usage of the finite element approach. A frame stage-like structure is placed between the main horizontal girders of the structure of the hall. A visual inspection of the frame revealed numerous irregularities of welds which brought demand for redesign and overall check. The emphasis in this paper is comparative calculation of initial and redesigned welded end-joints, without imposing the optimal technical solution. It is used modern and particular finite element software for calculation of welded joints. The values of stresses in the welded joint as well in plates and members are lower than the permitted values for both models. However, the influence on the main structure is reduced with redesigned technical solution. The level of stresses is lower along with reduction of rotational stiffness of the joint. This can be considered as a relief to the main girders of the hall structure and should be a cost and a goal for supporting any additional structure.

Keywords visual inspection, FEA, welded joint, stresses, stiffness

1. INTRODUCTION

As part of the reconstruction and modernization of facilities at the Belgrade Fair, hall number 5 was planned to be equipped to hold various fair events with modern equipment.

Positioning and movement of various equipment that is necessary during the modern manifestations is ensured by the appropriate additional frame stage-like structure made of steel S235JR. It has built-in hooks for hanging steel ropes or chains for carrying equipment which can weigh up to 1 t for all load

combinations. An additional steel structure has been placed in the attic space at the level of the bottom flange of the profile of the main horizontal girders of the steel structure of the hall, Fig. 1.

The structure contains two rows of longitudinal steel girders - UPN 240 with welded cross girders - UPN 180 and diagonal stiffening of box cross-sections with dimensions 60x60x3 mm. Fig. 2 depicts the linkages between the longitudinal and cross profiles of the structure and its connections to the main support of the hall frame.

The primary supporting steel structure of the hall was built in 1971 and made of structural steel which is assumed to correspond to S235JR. The main frame of the hall is a welded I profile 1040 mm high with 20 mm thick flanges and a 10 mm thick rib.

Corresponding author

MSc, Aleksandra Arsić
aarsic@mas.bg.ac.rs

University of Belgrade, Faculty of Mechanical Engineering
Kraljice Marije 16
Belgrade, Serbia



Fig. 1. Roof structure in the attic space

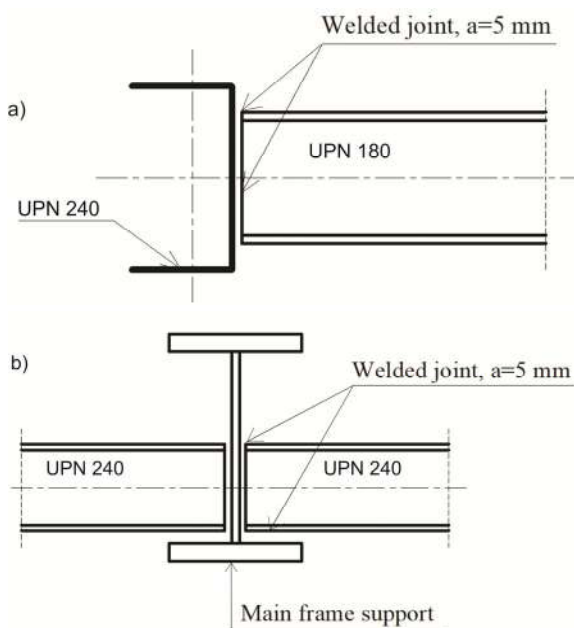


Fig. 2. a) Joints of longitudinal and cross profiles; b) The joint of the longitudinal profiles and main girder

After non-destructive testing (visual inspection) of the welded joints of the additional steel structure, shown in chapter 2, it was determined that the quality of the welded joints does not meet the acceptance criteria prescribed by the standard. Its reconstruction was carried out, whereby the connection of the

additional structure to the main frame of the hall was modified. Due to the new specific design of the joint through the stiffening plates, a numerical analysis of the welded joint was performed and presented in chapter 3. In order to compare the results, a numerical analysis of the initial way of supporting the structure was also carried out.

2. NON-DSTRUCTIVE TESTS OF WELDED JOINTS OF ADDITIONAL STRUCTURE

Properly carried out technical diagnostics of the condition of the elements and profiles of the steel frame, intended for carrying equipment for fair events in hall 5, using non-destructive testing, ensures the strength of the quality of the structure as a whole, provided by the project, without the possibility of immediate damage, safe work for employees, rational techno-economic exploitation, maintenance, and environmental protection.

After 100% visual testing of all available welded joints of the steel structure [1], the following irregularities were found:

- The imperfect shape of the external surfaces of the welds or incorrect geometry of the welded joints on the cross supports and diagonal stiffeners.
- Excess weld metal on the face of butt welds - big bulge on cross members and diagonal stiffeners.
- Linear shearing of parts on longitudinal members.
- Angular shear – the planes of the surfaces are not parallel on the longitudinal members.
- Insufficiently filled groove on the longitudinal members.
- Uneven weld widths on longitudinal members.
- Incompletely welded joints between the longitudinal members and the main frame support.
- Splashing of molten metal on the cross members.

Several mentioned irregularities in the zones of the tested welded joints are shown in Figs. 3-5. Based on the performed tests, it was determined that the quality of the welded joints does not meet the acceptance criteria prescribed by the standard [2]. Stress concentrators, generally, appear at locations

with radiuses inadequately defined during the design process and at welded structures. Various technological, constructional, and exploitation factors influence welded constructions to have a possibility for high level of stress concentration on the fillet and butt

welds with multiple errors. The defects in the welded joints were such that it was necessary to replace the relevant elements and profiles with new ones. Due to that, it was necessary to make changes to the observed construction.



Fig. 3. Irregularity in the butt-welded joint (uneven width of the weld)



Fig. 4. Irregularity in the butt-welded joint (excess weld metal on the face of the weld)



Fig. 5. Irregularity in the welded joint (insufficiently filled grooves)

The main point of support of the additional structure for the roof supports of the hall is completely reconstructed. The emphasis here is only on comparative calculations of joints between the main structure and the additional

structure, without imposing the optimal technical solution. Hence, it is performed strength and stiffness analysis of the initial and redesigned end-joints.

3. NUMERICAL ANALYSIS OF A WELDED JOINT

Numerical analysis was performed for two models of the welded joint between the main girder (welded I section) and longitudinal beam of the additional structure (UPN240).

The first model (M_1) represents the initial way of supporting the additional structure - welded on the bottom flange of the main frame profile (Fig. 2b), while the second joint model is welded joint over steel plates for the rib of the main frame profile (M_2) shown in Fig. 6. Numerical analysis of both models was done in the software package IDEA StatiCa [3].

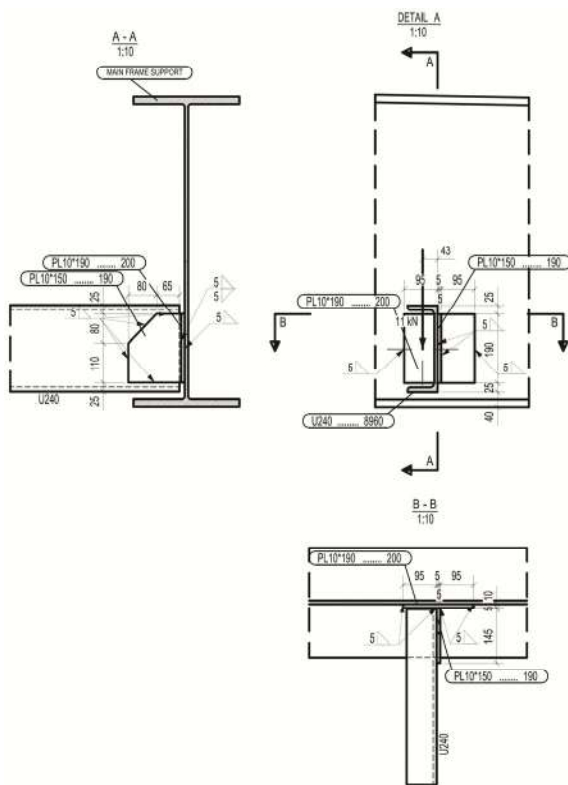


Fig. 6. The details of joint model M_2

IDEA StatiCa combines FEA with the analytical method of joints based on the component method (CM) specified in EN 1993-Part 8 (EC3) [4]. It can be used for structural evaluation or design of a variety of welded and bolted structural steel connections and base plates. This type of custom-made, semi-automated and specialized software are easy-to-use and sufficient for daily engineering practice [5]. Modelling in this software considers an

elastic-plastic material model for all the elements of the joint while the steel members are meshed with 4-node quadrilateral shell elements. The welds are modelled as a special elastic-plastic element on the multi-node constraint (MPC). The software by default use approximation of 8 elements in the critical edge with mesh size between 50 to 10 mm and limit plastic strain of 5%. The joint models are shown in Figs. 7-8.

According to the conceptual design of the additional structure, which is out of scope of this paper, all combinations of loads from modern equipment intended for fair events give a maximum vertical reaction on the main girder with the value of force of 11 kN. The force is applied at the joint node and only conceptually (by the software) depicted to act on the free end of the UNP240 (e.g. on Figs. 9-10).

Global stress states as well as the maximum stress values in welds for joint models M_1 and M_2, respectively, are given in Fig. 9.

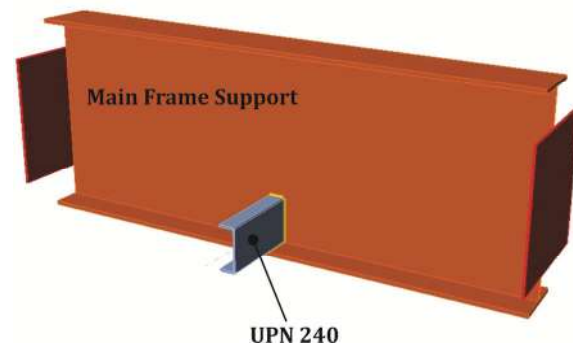


Fig. 7. Joint model M_1

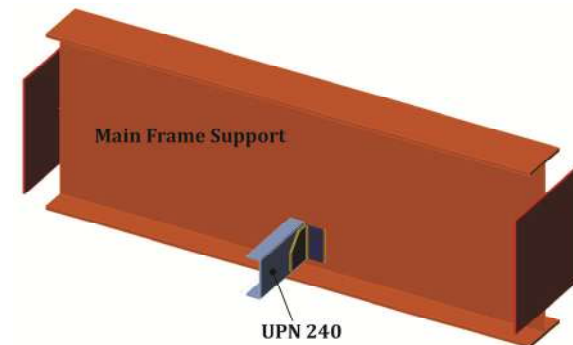


Fig. 8. Joint model M_2

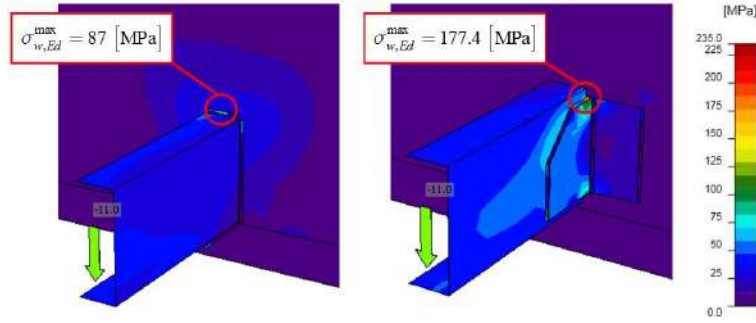


Fig. 9. Maximum equivalent stress of welds: M_1, M_2, respectively

Numerical analysis showed that the values of the equivalent stresses of welds for both models are lower than weld resistance. The permissible stress value for fillet welds is 360 MPa and is determined according to Eq. (1), [4].

$$\sigma_{w,Rd} = \frac{f_u}{\beta_w \cdot \gamma_{M2}} \quad (1)$$

Where $f_u = 360$ MPa is the nominal ultimate tensile strength of the weaker part is joined; $\beta_w = 0.8$ is the appropriate correlation factor; and $\gamma_{M2} = 1.25$ is the partial safety factor, [6].

A comparative analysis of the stress states of models 1 and 2 shows that in M_2 the rib of the main frame support has significantly lower stress values. The highest stress value on the rib of the main support in the first case is 46.7 MPa, while in the second case, the highest value is

13.5 MPa. The elementary structure of hall 5 was relieved by the new method of supporting the additional structure. That is evident from the numerical analysis results, which show that the highest stress values now occur on the additional plates.

The highest equivalent stress in the first model, M_1, occurs on the bottom flange of the UPN profile at the point of contact with the bottom flange of the main support, while in the second model, M_2, the highest equivalent stress is in the upper zone of the connecting plate of the longitudinal element of the additional structure. The exact values and zones for maximum stresses are shown in Fig. 10. Indeed, the values are lower than the yield stress for material S235. According to national regulations, the limit value of stresses can be taken as 157 MPa which is also satisfied.

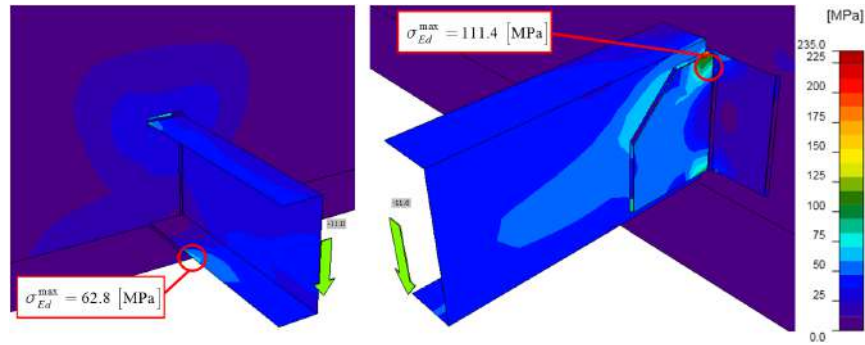


Fig. 10. Maximum equivalent stress in plates: M_1, M_2

Generally, a joint may be classified as rigid, nominally pinned or semi-rigid according its rotational stiffness. The pinned joint (or flexible) permits rotation of connected parts (ϕ), not transmitting bending moments between the elements of the frame [7]; on the

other hand, the rigid connection forbids the relative rotation between the elements and, consequently, transfers bending moments [8]. Semi-rigid joints should be capable of transmitting the internal forces and moments [9]. Therefore, a stiffness analysis was

performed for the given models. The software classified both models as pinned joints, while the moment-rotation behaviour curves are given in Fig. 11.

We can see from the $M - \phi$ diagram that with the new solution of joint between the two structures, the joint is considerably weakened in terms of stiffness (the initial stiffness, $S_{j,ini}$, is double reduced in the second model).

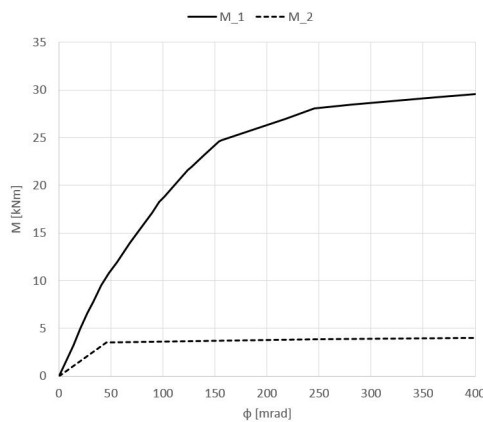


Fig. 11. Stiffness diagram $M - \phi$: M_1 , M_2

This indicates that the main girder of the hall is much relieved because the load is now carried by the so-called pinned joint which does not allow the load to be transferred further to the structure.

4. CONCLUSION

The numerical analysis of joint behaviour between the two structures is carried out. The visual inspection of the initial frame stage-like structure and a way of joining revealed numerous irregularities which brought demand for redesign and overall check.

By the usage of particular finite element analysis, it is performed comparative calculation of initial and redesigned welded end-joints. It is shown for both the models that values of stresses on members and welds do not go beyond permissible values. The level of stresses in the main girder is lower with redesigned joining solution, along with reduction of rotational stiffness. This could be important for the main girders when there is no informations if civil engineer (long time ago) has taken in account additional loads from secondary structures. The results for redesigned joining solution can be considered

as a relief to the main girders of the hall structure. According to the authors, this should be always the goal for supporting any additional structures on the long-lasting civil structures.

Acknowledgement

This work is a result of research supported by the Ministry of Education, Science and Technological Development of the Republic of Serbia by Contract 451-03-47/2023-01/200105, 03.02.2023.

REFERENCES

- [1] Belgrade fair – Hall no. V. (2020). *Vizuelna kontrola zavarenih spojeva*. (In Serbian) Institute for Materials Testing, Belgrade, Serbia, Report, no. VT IMS - 053/19.
- [2] EN ISO 17637:2016. (2016). *Non-destructive testing of welds – Visual testing of fusion-welded joints*. European Committee for Standardization.
- [3] IDEA StatiCa 21.0.0.3277, 2021, <https://www.ideastatica.com/>.
- [4] EN 1993:1–8:2005 (2005). *Design of Steel Structures - Part 8: Design of Joints*. European Committee for Standardization, Brussels.
- [5] Arsić, A., Gašić, V., Zrnić, N. Survey on Design Procedures in Numerical Simulations of End-plate Moment Connections. *Proceeding of XXIV Int. Conference on Material Handling, Constructions and Logistics MHCL 2022*, September 2022, Belgrade, p. 143 - 150.
- [6] EN 1993:1-1:2016 (2016). *Design of steel structures - Part 1-1: General rules and rules for buildings*. European Committee for Standardization, Brussels.
- [7] Banfi, M., Brown, D., Cosgrove, T., Gannon, P. et al. (2014). Joints in steel construction: Simple joints to Eurocode 3. The Steel Construction Institute and The British Constructional Steelwork Association Limited, London.
- [8] Diaz, C., Marti, P., Victoria, P., Querin, O.M. (2011). Review on the modelling of joint behaviour in steel frames. *Journal of Constructional Steel Research*, vol. 67, no. 5, p. 741-758. DOI: <https://doi.org/10.1016/j.jcsr.2010.12.014>
- [9] Faridmahr, I., Tahir, M.Md., Lahmer, T. (2016). Classification System for Semi-Rigid Beam-to-Column Connections. *Latin American Journal of Solids and Structures*, vol. 13, no. 11, p. 2152-2175. DOI: <https://doi.org/10.1590/1679-78252595>



Banja Luka
1-2 Jun 2023.

DEMI 2023

16th International Conference on Accomplishments in Mechanical and Industrial Engineering

www.demi.mf.unibl.org



Influence of injection molding parameters and gate position on the tensile strength of polymer part

Edis Nasić, Denijal Sprečić, Jasmin Halilović, Džemal Kovačević

University of Tuzla, Faculty of Mechanical Engineering, Bosnia and Herzegovina

Abstract *Injection molding technology is commonly used in the production of very complex polymer parts. The different mechanical properties often are an inevitable defect at parts. Namely, in the process of making, zones with reduced mechanical properties often appear, which greatly affects the final quality and behavior of the part in exploitation. It is necessary to produce a part with as favorable and uniform mechanical properties as possible. The above is very difficult to achieve. In this paper, the influence of: holding pressure, injection velocity and gate position on tensile strength – part zone is analyzed. The material used in this research is high-density polyethylene (HDPE). Depending on the gate position, the obtained results showed that the tensile strength of the observed zones on the part differs significantly. Also the results of the research showed that by changing: holding pressure and injection velocity, can be affected on part tensile strength.*

Keywords *Tensile strength, molding parameters, injection molding, gate position, part zone*

1. INTRODUCTION

Parts made of polymer materials are most often made by injection molding. It is a process where the desired shape of the part is obtained by injecting molten material under high pressure into the tool cavity. Precise parts with very complex geometries can be produced. In order to make a quality part, it is necessary to know the tool design specifics, parameters of the process and the material properties. The injection molding process consists of a filling phase, holding pressure and cooling. The polymer material in the stages of injection molding goes through complex transformations such as rapid heating and cooling and phenomena related to shear stresses that occur during the flow of the melt.

Corresponding author

Dr.sci Edis Nasić
edis.nasic@untz.ba

Faculty of Mechanical Engineering Tuzla BiH, Tuzla

Due to very pronounced thermal changes and mechanical shearing of polymer regions during

flow, the crystal morphology of the area is different [1]. In the process, defects such as: deformations, internal stresses, joint lines, differences in strengths, etc., often appear, which reduce the functionality of the part. Process parameters play a significant role in achieving the required mechanical properties. Using different process parameters will lead to a difference in the microstructure of the polymer. Additional melt heating, due to increased viscous friction, which occurs at higher injection velocity, can cause excessive melting of molecules, resulting in their physical damage, distortion of shape, loss of properties and reduction of mechanical properties [2]. Especially in the case of crystalline materials, the mechanical properties are related to the structure and depend on: the degree of crystallization, crystallites size, the molecules concentration and the orientation of linear molecular chains [3].

The geometry of the part and the number of tool cavities affect the choice of the gate position. Gate position further has an impact on the

choice of process parameters, melt flow direction, filling time, cooling, etc. The places where differences in hardness most often occur during the production of parts are: areas in the direction of melt flow, areas perpendicular to the flow direction and areas that are filled faster or later in time. The goal is to achieve uniform mechanical properties in all areas of the part, which is difficult to achieve. This paper presents experimental research and results analysis of holding pressure and injection velocity influence on the tensile strength in two zones of the part in relation to the gate position.

2. EXPERIMENTAL WORK

The parts are produced by injection molding. The material used is HDPE, which belongs to the crystalline polymers group. The basic HDPE characteristics are: linear structural chain, high crystallinity and fair hardness, strength and stiffness. The density is $0,94 - 0,96 \text{ (g/cm}^3\text{)}$, degree of crystallization 70 to 80 (%), crystallization temperature $125 - 140 \text{ (}^\circ\text{C)}\text{}$, [4]. The geometric characteristics and 3D model of the part, sprue, distribution channels and gate are shown in Figure 1.

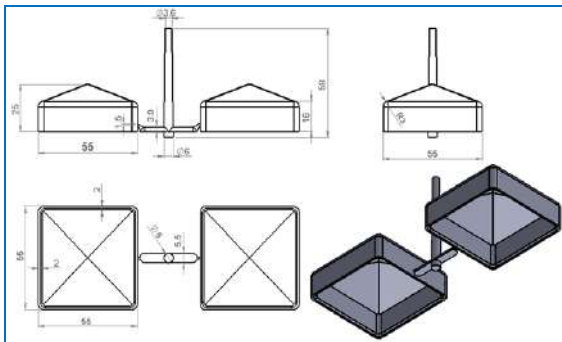


Fig.1. Part geometry and 3D model

To define the parameters and determine the level of holding pressure and injection velocity, test experiments were performed. Chosen values are given in table 1. The experiments were performed at a constant melt temperature of $195 \text{ (}^\circ\text{C)}\text{}$.

Table 1. Parameters of injection molding

Injection Parametar	Unit	Level 1	Level 2
Holding pressure (Phn)	bar	35	55
Injection velocity (Vi)	mm/s	33	36

The holding pressure time is 5,5 (s), constant value as well. Figure 2 shows the profiles of the holding pressure.

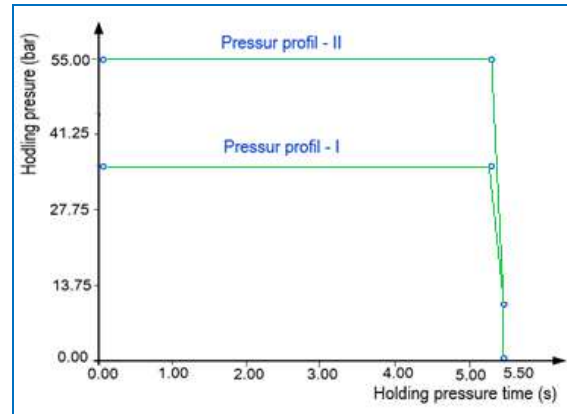


Fig. 2. Holding pressure profiles

The flow of the melt and tool cavity filling direction is shown in Figure 3 a) and b). The part obtained by the injection molding process is shown in Figure 3 c). After injection molding specimens were cut out from the zone 1 and zone 2 as defined on Figure 3 d).

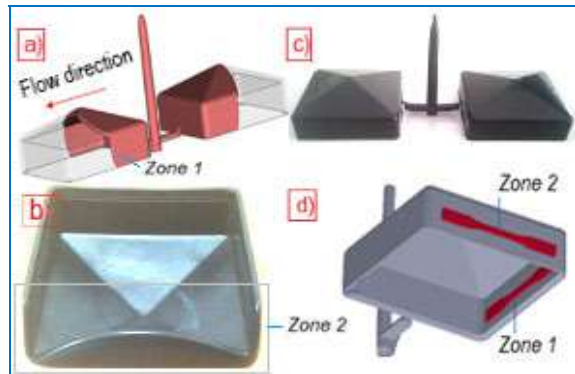


Fig. 3. Flow direction, tool filling and sample cutting zones for tensile tests

Uni-axial tensile tests were performed according to the ISO 527-2 (1 BB) standard on the Zwick/Roell Z030 testing machine.

3. RESULTS AND DISCUSSION

Eight injection molding experiments for each (8) combination of parameters, with three (3) repetitions, are included in this paper. Twenty-four (24) samples were cut from the obtained parts for tensile tests. For the observed zones (defined in relation to the position of the gate), the tensile strength results were obtained by tests performed.

Strength mean values depending on the injection molding process parameters are shown in Figure 4 a) and b).

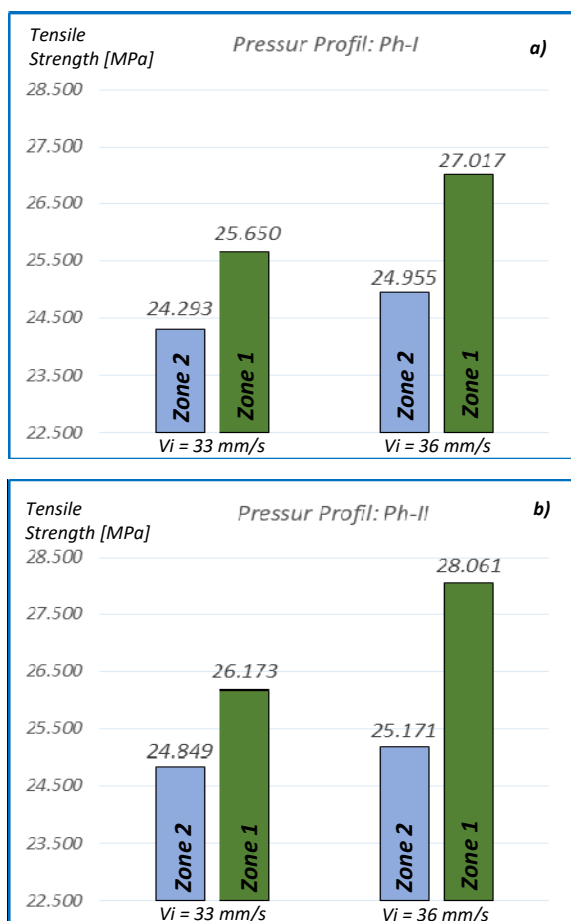


Fig 4. Tensile strengths in zones 1 and 2

Presented results show that the tensile strength is higher in zone 1 (in the flow direction) than in zone 2 (perpendicular to the flow direction). Material HDPE has a linear structure, a high degree of crystallization, which results in better orientation and direction of the polymer molecular chains in the direction of flow. In the direction of flow, the mobility of molecular chains is better, which results in better arrangement and bonding of molecules. Better orientation along the direction of the flow is the primary reason for achieving greater strength in (zone 1). Additionally, the value of the parameters decreases in the tool cavity area that is filled last. Therefore, pressure in the zone 2 is smaller than in the zone 1. Furthermore, specimen orientation in the zone 2 is perpendicular to melt flow. Phenomena described, results in a lower tensile strength achieved, compared to (zone 1). From the presented experimental results, it can be seen, that an increase in holding pressure and injection velocity results in an increase in

tensile strength in the observed zones. Among the parameters, the holding pressure has a greater influence on the strength. The injection pressure and velocity affect the friction between the particles, the shear stresses, and thus the viscous heating.

In the holding phase, a new amount of material is added. It is practically a renewed flow where the melt has a higher temperature and fills the tool cavity, in a certain time, under high pressure. This affects the improved movement of material molecules, further orientation of internal molecular chains, and the reduction of deorientation of molecular chains that were already oriented [1].

Also, higher holding pressure values increase the density of the part [5,6]. Due to the increase in density, the free volume decreases, the degree of crystallinity increases, and the relationship between the molecular chains in the melt is more favorable.

The aforementioned leads to a higher concentration of molecules, better packing, stacking and molecular binding, which ultimately results in an increase in strength with an increase in holding pressure.

At a relatively lower injection velocity, the tool cavity filling time is longer. The melt cools and solidifies faster, especially near the tool wall, and the viscosity increases. When the melt is injected into the tool cavity, higher velocities generate more heat due to viscous heating.

By increasing the injection velocity, the viscosity decreases, the filling time is shorter, an early and excessive hardening is prevented. This leads to improvement of the penetration, orientation, mobility, binding and stacking of linear molecular chains in the structure.

On the other hand, the increase in heat due to increased viscous heating results in the ejection of part of the elevated temperature from the tool. In that case, the cooling is slower, subsequent crystallization of the material occurs [7], which is again favorable for intermolecular assembly and bonding.

The aforementioned are possible reasons for achieving higher strength in the observed zones with an increase in injection velocity.

4. CONCLUSIONS

- The results of experimental research have shown that by choosing the gate position and injection molding parameters, it is possible to influence the mechanical properties of the part.
- The gate position affects the tensile strength of the observed zones of the part. The higher tensile strength is in (zone 1 - in the direction of flow) compared to the area that is filled last (zone 2 - perpendicular to the direction of flow).
- For the observed level of injection molding parameters, an increase in holding pressure and injection velocity results in an increase in part strength in the observed zones.
- The holding pressure has a significantly greater influence, while the injection velocity has a smaller influence especially in (zone 2).
- If the design of the tool is structurally possible, uniform strength in the areas of the part can be achieved with the position of the gate which will ensure that the tool cavity is filled evenly. Uniform strength can also be achieved by optimizing parameters.
- Special attention should be paid when adjusting the parameters of injection molding because those depend on the material used. Especially in the case of amorphous and fiber-reinforced materials.

Guide to Injection Moulding. 2nd Edition First Published.

- [5] Robert A. Malloy (2010). Plastic Part Design for Injection Molding, An Introduction 2nd Edition, Carl Hanser Verlag, Munich.
- [6] Mani Mohammad Reza (2016). Investigating the effect of process parameters on dimensional accuracy and ultimate tensile strength of micro injection moulded micro parts. PhD thesis. University of Nottingham.
- [7] Esben Raahede, Karl Stephan, Stentoft-Christensen, Hans Christian, Islam Aminul, Hans Norgaard (2009). Examining the influence of injection speed and mould temperature on the tensile strength of polypropylene and ABS. Technical University of Denmark.

REFERENCES

- [1] Hongbo Fu, Hong Xu, Ying Liu, Zhaogang Yang, S. Kormakov, Daming Wu and Jingyao Sun (2020). Overview of Injection Molding Technology for Processing Polymers and Their Composites. *ES Mater. Manuf.*, 2020, 8, 3–23.
- [2] Jian Wang, Qianchao Mao, Nannan Jiang and Jinnan Chen (2022). Effects of Injection Molding Parameters on Properties of Insert - Injection Molded Polypropylene Single-Polymer Composites. *Polymers* 2022, 14, 23.
<https://doi.org/10.3390/polym14010023>.
- [3] Subodh Singh Tomar, Ashish Kumar Sinha, Ashish Shrivastava (June 2016). Parametric Study of Injection Moulding Using Polypropylene H200mk Grade, *International Journal of Science*, ISSN: 2455-0108, www.ijoscience.com Volume II Issue III.
- [4] Vannessa Goodship (2017). ARBURG Practical



Banja Luka
1–2 Jun 2023.

DEMI 2023

16th International Conference on Accomplishments in Mechanical and Industrial Engineering

www.demi.mf.unibl.org



Education 4.0: Applying knowledge to practice in a hybrid laboratory for automation and mechatronic: A solution with digital twins and virtual reality

H. Smajic^a, F. Tiryaki^b, D. Janjic^a, T. Duspara^a

^aTH Köln, Faculty of Vehicle Systems and Production, Betzdorfer Str. 2, 50679 Köln, Germany

^bTurkish German University in Istanbul, Department for Mechatronics, Istanbul, Turkey

Abstract *The practical training of students is usually conducted at the university laboratories equipped with systems and components that could be found in the everyday industry. This is done in a way that students get hands-on experience with the systems that they could get in contact with in future. The costs of these components correspond to their quality and are usually high due to their robustness needed for the harsh environment and situations in which they could be found. Keeping that in mind, equipping these laboratories with such components is usually costly. One of the methods of lowering expenses is discussed in this paper. Namely, this method encompasses the implementation of virtual reality technology into education in the field of industrial automation. The goal is to create a virtual machine, which would be connected with either a PLC simulator, or with a real controller and behave as a real system.*

Keywords *Virtual reality, digital twins, Industry 4.0, Internet of things*

1. INTRODUCTION

1.1 Motivation

The inspiration for this topic was born in the automation laboratory at the Technical University in Cologne. Here, students can train their programming skills as well as develop the engineering logic by solving practical problems in the industry production lines. For these purposes, there are 20 workstations available. The workstations contain every crucial element needed for encapsulating the basics of industry automation. The cost of the

components is in a correspondence to their quality and that means that the furnishing such laboratories with high-end industrial equipment usually comes with great costs. Observing the situation at the educational institutions in developing countries, the motivation for this research was born, because of the aspiration to enable as many students as possible to have a decent practical part of the education.

1.2. Industry 4.0 and Internet of things

Although it is often the subject of debate, the name "Industry 4.0" is used everyday and more and more often marks the fourth ongoing industrial revolution. In this, as with any other revolution, there are technologies that characterize it and distinguish it from the standard course of development of the industry. After the arrival of programmable

Corresponding author

M.Sc. Toni Duspara
toni.duspara@th-koeln.de

TH Köln, Faculty of Vehicle Systems and Production
Betzdorfer Str. 2
50679 Köln, Germany

logic controllers on the industrial scene in 1969, just a few decades later, the rapid development of the Internet, i.e. networking devices, began. The term that is increasingly used to describe all networked devices and processes is the "Internet of Things" (IoT) and is the basic term on which Industry 4.0 rests. The main industrial goal of IoT is process automation, analysis and monitoring, reducing workforce needs etc. In terms of business, IoT supports a more strategic way of working, as well as more control over processes. [1]

1.3 Digital Twins

Definition of digital twin. Along with the advancement of new information technologies comes the period of product design based on previously collected data. The design process is becoming more digitized than ever before. Computer aided design, finite element analysis methods (FEA), computer aided engineering (CAE) as well as computer-aided manufacturing (CAM) are some of the tools that helped this digitalization. In order to simulate the structure and behavior of a product and evaluate its performance, products are created in the virtual world in computers. [2] A digital twin is a virtual representation that serves as a digital doppelganger of a physical object or process in real time.

Examples of practical application. The design of the product could be significantly improved by including the feedback received from DT. [3] In addition to design, DT is also used in the manufacturing process in the industry and makes it more confidential, flexible and predictable. First, DT can visualize and update the status in real time, which is useful for monitoring production processes. [3] The digital twin can help construction firms understand how a building works in real time, allowing them to adjust performance to optimize efficiency. Data collected from the digital twin can be used to plan and design future buildings. [4] Manufacturers also use digital twins to predict potential machine downtime so that maintenance activities are minimized. In

addition to the space missions, digital twins have been widely used in the automotive industry to create a virtual model of a connected vehicle. Automotive companies use technology to design the ideal automotive product even before the start of prototype production. They simulate and analyze the production stage and the problems that can arise when the vehicle hits the road. Self-driving cars contain numerous sensors that collect data about the vehicle itself and the environment of the car. Due to the issues of responsibility surrounding autonomous vehicles, creating a digital twin car and testing every aspect of the vehicle helps companies ensure that unexpected damage and injuries are minimized. Some of the applications of digital twins in the automotive industry are road testing and vehicle maintenance. [4]

1.4 Virtual reality

Definition and divisions. An artificial environment experienced through sensory stimuli (such as sights and sounds) provided by a computer and in which one's actions partially determine what happens in an environment can serve as a definition of virtual reality (VR). [5] In everyday use, virtual reality is defined as a computer-generated digital environment that can be experienced and interacted with, as if that environment were real.

Importance of practical education. There are several reasons why theoretical and practical education should not go without each other, especially in the field of natural sciences. When a student prepares for the test, because of the tendency to remember a large amount of material for a very short time, it is often the case that what is remembered is not long-term. Knowledge generally becomes long-lasting when things are learned through observation and practical work. Removing the pressure from students to memorize theory exclusively from books significantly helps in the process of education and relieves stress. [6] The practical work of students also develops a better understanding of matter that is otherwise difficult to imagine solely by reading the theory

from books. The result of the student's work that can be seen in front of him is crucial for understanding the principles of functioning of the theoretically learned. Making mistakes during practical work encourages the student to create a focus on engineering reasoning and finding solutions. This process is mostly very interesting for students, and as a rule, what is interesting falls easily and the learning process itself gives fun and relief from dry theoretical learning. After all, practical work in a specifically specialized field equips the student with the specific skills needed to solve problems that he may encounter in the future in the workplace and thus makes him more complete and ready for industry. Not only is it useful for acquiring practical knowledge, but it allows you to work in groups and thus develop a team spirit. Working in a team is of great importance for every engineer, because working in companies is impossible without a healthy atmosphere, tolerance and understanding.

2. REQUIRED HARDWARE

2.1 PLC System

A programmable logic controller (PLC) is an industrial-scale computer that can be programmed to perform a control function. It is characterized by features such as fast response, easy programming and installation, high speed control, compliance with networking, suitability for testing and high reliability. [7] Unlike a personal computer (PC), the PLC is designed to operate in an industrial environment. One of the main characteristics that make PLC devices suitable for operation is their modular construction. Based on the number of inputs and outputs required, as well as the nature of the signal that needs to be processed, an appropriate number and type of input or output cards can be easily incorporated into the PLC.

Communication protocols – Modbus-TCP.

The Interface of the Modbus-TCP protocol is an Ethernet network, and the data transfer protocol is TCP/IP. The command consists of a part of the Modbus RTU message and a

special header that defines the type and its length. In this paper, there will be only one part of the Modbus-TCP message, and that is the function code.

Table 1. Table of codes for reading and writing Modbus-TCP registers

Function code (hexadec.)	Function code role		Value Type	Access Type
01 (0x01)	Reading digital outputs	Read coil status	BOOL	Read
02 (0x02)	Reading digital inputs	Read digital status	BOOL	Read
03 (0x03)	Reading analog outputs	Read internal registers	16 bit (INT)	Read
04 (0x04)	Reading analog inputs	Read holding registers	16 bit (INT)	Read
05 (0x05)	Write a single digital output	Force one coil	BOOL	Write
06 (0x06)	Write a single analog output	Set up an internal registry	16 bit (INT)	Write
15 (0x0F)	Record multiple digital outputs	Force more windings	BOOL	Write
16 (0x10)	Recording multiple analog outputs	Set up multiple internal registers	16 bit (INT)	Write

In Table 1, function codes with their roles are given and depending on their selection, the type of message to be sent is determined. In this paper, codes 01, 03, 15 and 16 were used in order to read or write down a larger number of BOOL or INT values through Modbus-TCP.

2.2 Visualization

One of the many devices on the market that allow users to enter virtual reality and some of the equipment used for this research are oculus quest VR glasses. [8] For this purpose, Unity Engine was used, which is an extremely popular software for video game development, providing a huge number of advantages over other software available on the market today. Unity offers a visual workflow with drag and drop capabilities. Drag-and-drop development supports Programming with C#. Unity has long supported both 3D and 2D graphics, and tools for both are becoming more sophisticated and easier to use with each subsequent version. [9]

3. THE CONCEPT OF THE PRACTICAL PART OF THE WORK

Given that the aim of the paper is to improve and modernize education by using virtual technologies, it is necessary to create an idea of the type of education in question and the way in which the execution of the practical part of this work was designed. Practical verification of the work of the virtual twin was carried out at workstations in the automation laboratory at the Technical Faculty in Cologne. The automation laboratory consists of 20 workstations for students. Here students have the opportunity to gain their first experience in the practical sense in the field of automation. The objectives of work in the automation laboratory are as follows:

- Functionality (wiring of mechatronic components);
- Working with Software packages from Schneider Electric, Siemens, Festo Didactic etc.

3.1 Workstation layout

Stationary workstations contain all the elements that can be visualized or simulated in most industrial processes. This would mean that practical work on them is a good predisposition to achieve a smooth transition from education to industry.

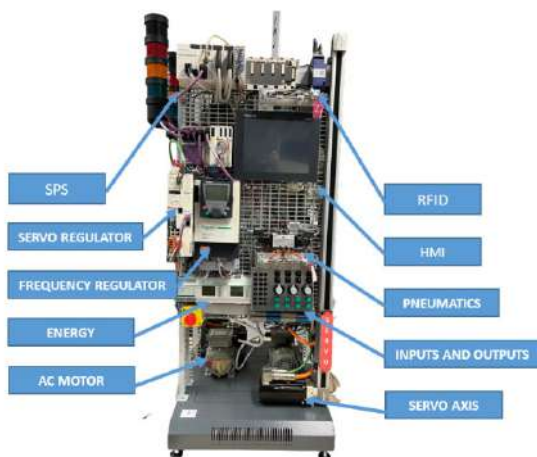


Fig. 1. Graphical representation of a single workstation with tags

3.2 Appearance of the practical part of the work

As already mentioned, the idea of modernized practical education was realized through the student's ability to interactively observe the results of their work in virtual reality. This virtual display is actually a 3D model of the desired machine with assigned functions and features, as well as networking over communication protocols with a real machine. The work is conceived in several steps:

- Modeling of workstations and supporting elements;
- Assign mechanical and lighting functions to created virtual devices;
- Connecting the corresponding variables with each function of objects;
- To communicate with the PLC for the purpose of exchanging information;
- Preparing a script on a PLC to enable two-way communication between a virtual and real machine.

4. CREATING AN ENVIRONMENT IN VIRTUAL REALITY

4.1. Modeling of desired virtual machines

Siemens NX (CAD, CAM, CAE) software was used for modeling assemblies. In order to develop the working environment, it is possible to add elements such as the base, the table on which the working element lies, suitable UI (eng. "User interface") for choosing addresses and connecting to PLC devices, restart programs and individual statistics.



Fig. 2. Arranged virtual environment

4.2. Assigning functions to objects

Functions are assigned to 3D models of objects in unity engine. Each moving element can be assigned a movement corresponding to that in reality. Also, light signaling can be assigned to those elements that need it. It is also possible to assign certain functions to input elements, e.g. pressing a virtual key changes the value of a given BOOL variable from "false" to "true". In a similar way, a change in the value of an INT variable can be simulated using a virtual potentiometer.

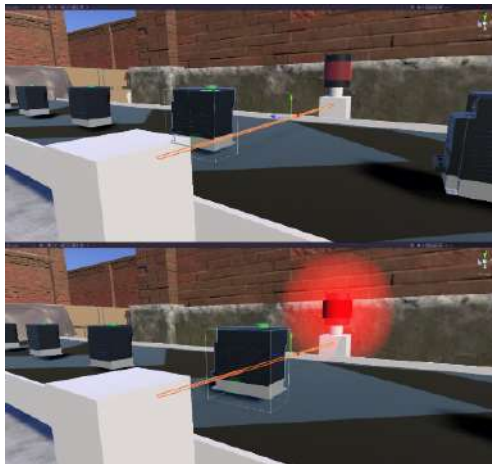


Fig. 2. Example of the application of Collision Body as an air sensor

Using the components and lines of C# code, the movements of the cylinders (two positions, conditioned by the BOOL signal), the movement of the lane on the servo axis (coordinate position using the INT value), as well as the rotation of the AC motor rotor (rotational speed conditioned by the corresponding INT variable) can be assigned.

5. PREPARING A SCRIPT IN UNITY PRO XL TO ADDRESS VARIABLES

5.1. Working memory of a PLC device

The Modicon M340 processing unit uses a memory word type of memory labeled %MW, where each address is 2 bytes or 16 bits in size and stores INT variables. Memory with the start of the address %M is called the "Memory bit" and is only one bit in size, which means that it stores a BOOL type value. In the

Modbus TCP terminology **Error! Reference source not found.** In the case of modicon M340 processors, the number of %M variables it can store is 32634, while this number in %MW variables is 32464.

5.2. Linking physical and virtual variables

In order to achieve successful and coordinated communication between the PLC and the digital twin, a script must be prepared beforehand that will give the corresponding variables the appropriate %MW and %M addresses respectively. **Error! Reference source not found.** represent the input to the PLC are connected to a %M address. In this case, the variable "Taster1_PLC" is the physical input from the buttons on workstation, and the "Key1Mod" input that comes from the virtual world via the Modbus TCP protocol. The combination of these two variables with the function block "OR" is managed by the variable "Key1" which is used when programming in Unity Pro XL as an input variable. The idea is that this variable can be managed either by a physical or virtual key. In a similar way, INT variables of analog inputs were created, the value of which can be determined either by a physical analog input (e.g. potentiometer) or by an analog input potentiometer from the VR world obtained through the Modbus TCP protocol. **Error! Reference source not found.** Similarly, there are INT values that are not analog outputs from the PLC but represent the output of the physical system, such as the speed of rotation of the motor or the position of the servo motor. These values are also important to send to the VR world in order to get the most credible representation of the digital twin. They only need to be saved to the appropriate %MW addresses. However, as the goal in this concept is to work with the simulator, there will be no actual physical output that can be transmitted to VR. Nevertheless, these values can be manually changed in the simulation for the corresponding variable at the corresponding %MW address.

6. ACHIEVING COMMUNICATION

6.1. C# - Library for Modbus TCP Communication

In order not to write certain functions in programming from scratch, stored libraries are used that are imported into the directory of references and whose methods are easily referenced by the user during the writing of the paper. One such library was used in this work to send and receive messages via the Modbus TCP protocol. For the purpose of this work, C# library called EasyModbus was used. [10]

```
this.transactionIdentifier = BitConverter.GetBytes((uint)transactionIdenti
this.protocolIdentifier = BitConverter.GetBytes((int) 0x0000);
this.length = BitConverter.GetBytes((int)0x0006);
this.functionCode = 0x03;
this.startingAddress = BitConverter.GetBytes(startingAddress);
this.quantity = BitConverter.GetBytes(quantity);
Byte[] data = new byte[] { this.transactionIdentifier[1],
    this.transactionIdentifier[0],
    this.protocolIdentifier[1],
    this.protocolIdentifier[0],
    this.length[1],
    this.length[0],
    this.unitIdentifier,
    this.functionCode,
    this.startingAddress[1],
    this.startingAddress[0],
    this.quantity[1],
    this.quantity[0],
    this.crc[0],
    this.crc[1]
};
crc = BitConverter.GetBytes(calculateCRC(data, 6, 6));
data[12] = crc[0];
data[13] = crc[1];
```

Fig. 4. Example library background code for Modbus TCP protocol

EasyModbus offers a wide range of methods that, in addition to the ability to read and write all kinds of values, enables data processing, i.e. conversion of registers into the appropriate type of variable (Double, Float, String, as well as a long version of INT of 4 bytes).

6.2. Using C# to connect variables between VR and PLC

Considering the larger number of BOOL and INT variables that need to be exchanged between PLC and VR world, readcoils (FC01, Table 1) and WriteMultipleCoils (FC15, Table 1) for BOOL and ReadHoldingRegisters (FC04, Table 1) and WriteMultipleRegisters (FC16, Table 1) will be used for INT values. In Figure 5 below, the application of the above methods is shown. When it comes to outputs from the PLC, they only need to be mapped to the digital twin. Values of the position of the servomotor and the speed of turning of the asynchronous motor from the PLC can be used on the corresponding elements on the VR

machine. What also needs to be read is the state of the input into the PLC, both digital and analog. The goal of this is for a person who is in the virtual world to be informed about whether the counter or button is activated or not and in what position the potentiometer is located.

On the Figure 5, the ConvertRegistersToLong method can also be seen. It is a method that combines two registers for reading large INT values (4 bytes). Since virtual reality for PLC, i.e. PLC simulator serves as the environment from which it receives information, from it it is necessary to send all the information relevant to this case. These are the states of virtual buttons, counters, digital and analog sensors, etc.

```
//PLC -> UnityEngine
zylinder1.Zylinder_1_Ausfahren = outputCoils[0];
zylinder1.Zylinder_1_Einfahren = outputCoils[1];
zylinder2.Zylinder_2_Ausfahren = outputCoils[2];
zylinder2.Zylinder_2_Einfahren = outputCoils[3];
ampel_Rot.ampelRot = outputCoils[4];
ampel_Gelb.ampelGelb = outputCoils[5];
ampel_Gruen.ampelGruen = outputCoils[6];

potentiometerSliderPos = plc1.ReadHoldingRegisters(503, 3);
potPos = plc1.ReadHoldingRegisters(506, 3);

readServoPositionMotorSpeed = plc1.ReadHoldingRegisters(600, 4);
servoPosition = ModbusClient.ConvertRegistersToLong(new Int[] { readServoPositionMotorSpeed[0],
motorSpeed = ModbusClient.ConvertRegistersToLong(new Int[] { readServoPositionMotorSpeed[2],
servo.position.y = servoPosition;
motor.motorSpeed = motorSpeed;
allConveyorsSpeed.speedOfAllConveyors = motorSpeed / 1000f;
```

Fig. 5. Example library background code for Modbus TCP protocol

7. Concept testing

The concept of this paper can be tested by running a PLC simulator in Unity Pro XL, which also communicates via Modbus TCP/IP protocol and has its own reserved address "127.0.0.1". After a program has been programmed and uploaded to a PLC simulator, a simulation is done in the virtual world. After successfully connecting to the simulator, it is necessary to put on VR glasses and activate the desired button. In this case, the key that runs a simple program that includes cyclical operation of cylinders and light signals is the number button 1. The image below shows the simulation of the program along with the state of the relevant variables.



Fig. 6. Simulation of the activation of the first key in the VR world (left) and display of the state of variables in Unity Pro XL (right).

The feedback between the virtual reality and the PLC simulator is closed and the registration of virtual inputs into the system, as well as the movement of virtual actors correspond to the behavior of variables in the program. Therefore, it can be said that this case is satisfied. Similarly, it is possible to create a much more complicated virtual facility that would have as many virtual sensors and actuators as the program requires. The program is created in Unity Pro XL and then tested by connecting to a virtual environment.

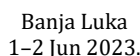
8. SUMMARY AND CONCLUSION

After creating a virtual environment, establishment of communication between the application and the PLC (simulator) using the Modbus TCP communication protocol is described. The knowledge gained by modeling, function assignment, as well as assigning programming scripts to elements in the VR world can be used to create more complex virtual plants, assign variables with appropriate addresses and network with PLC. With good preparation and testing of virtual machines in order to behave as realistically as possible, this concept can be used as a platform for acquiring skills on automation of various plants. When there is programmed VR application, it is mandatory to develop a program in Unity Pro XL software and running the PLC simulator. After starting the program on the simulator, it is only necessary to put on VR glasses and manage the process, that is, give the appropriate inputs, e.g. by

activating the keys. What remains is to observe the process and validate the program.

REFERENCES

- [1] K. Gloss, "3 experts discuss how to navigate the challenges of IoT," 30 September 2019. [Online]. Available: <https://www.techtarget.com/iotagenda/feature/3-experts-discuss-how-to-navigate-the-challenges-of-IoT>
- [2] F. Tao, A. Liu, T. Hu und A. Nee, Digital Twin Driven Smart Design, Elsevier, 2020.
- [3] F. Tao, Z. He, A. Liu und A. Nee, „Digital Twin in Industry: State-of-the-Art,“ IEEE, April 2019.
- [4] C. Dilmegani, „AI Multiple,“ 26 August 2022. [Online]. Available: <https://research.aimultiple.com/digital-twin-applications/>.
- [5] „Merriam-Webster,“ 19 April 2022. [Online]. Available: <https://www.merriam-webster.com/dictionary/virtual%20reality>.
- [6] „Output Education,“ 25 April 2022. [Online]. Available: <https://www.outputeducation.com/10-reasons-why-practical-education-is-more-important-than-theoretical/>.
- [7] F. D. Petruzella, Programmable Logic Controllers, New York: McGraw-Hill Education, 2017.
- [8] C. Hillmann, „Comparing the Gear VR, Oculus Go, and Oculus Quest,“ in Unreal for Mobile and Standalone VR, Singapore, Singapore, Apress, Berkeley, CA, 2019, pp. 141-167.
- [9] J. Halpern, Developing 2D Games with Unity Independent Game Programming with C, New York, NY, USA: Apress, 2019.
- [10] „Stefan Rossman Engineering Solutions,“ 2022. [Online]. Available: <https://sre-solutions.com/>.



16th International Conference on Accomplishments in Mechanical and Industrial Engineering

www.demi.mf.unibl.org

H. Smajic^a, C. Faller^b, F. Tiryaki^c

^c*Turkish German University in Istanbul, Department for Mechatronics, Istanbul, Turkey*

One way to create new systems - manageable for medium-sized companies - is to develop new web-based services, as is another goal of the High-Tech Strategy [4]. With cloud-based software solutions and associated business models that make software more profitable for small companies, combined with consulting services from experts, SMEs (small and medium-sized enterprises) can use the knowledge and experience of experts and continue to focus on their core business. The companies involved in this project see a competitive advantage in being able to optimize their production from a holistic point of view or to support their customers in this effort.

This support can be provided by consulting services from energy suppliers. In times of the energy turnaround, the Energy Services Act obliges energy suppliers to inform their customers about energy efficiency measures [5]. Many energy suppliers see this as an opportunity to transform themselves into partners for energy. The Velbert region is characterized by a relatively high density of small and medium-sized metalworking companies that still maintain personal contacts with their energy suppliers. The municipal energy suppliers of Velbert and Heiligenhaus are showing interest in new business models and would like to remain a long-term partner for medium-sized companies in the region.

The technical core of the development work is a system for energy data collection in combination with production data from the automated plants in order to send it via a CloudEdge controller to the cloud for evaluation. There, the data is available for use by the company, but also by consultants who provide targeted support for SMEs in saving energy, as well as in anonymized form by suppliers who will use it to optimize energy planning in the future. The long-term goal of the project is, on the one hand, to support SMEs in the local region and, on the other hand, to gain knowledge about digital transformation for the suppliers and the university.

Keywords *Energy efficiency, computer applications in energy industry, planning and scheduling, energy system modeling, simulation and analysis, energy management systems*

1. INTRODUCTION

Digitalization is presenting many companies with new challenges:

- What options for digital production optimization are available on the market?
- What makes sense and can be implemented in your own company?
- Which steps have to be taken for the digitalization of production and when?
- What are the costs?

In order to be able to answer these questions competently and provide advice, the first step within the project was to start in-house, i.e. at the Velbert/Heiligenhaus Campus (CVH) of the Bochum University of Applied Sciences. In concrete terms, this involved adding an energy measurement system to the learning factory and bringing the data into the cloud. Resource-saving production begins with acquiring knowledge about the function of the process. Whether this knowledge ends up being used to make production more efficient in terms of product quality, or to build predictive, predictive maintenance that reduces downtime, or to reduce energy costs in production is up to management to decide. However, the often very complex technical processes can only be obtained by observing the process, which is based on measurements and evaluations.

Together with the municipal energy suppliers Velbert and Heiligenhaus, a selection of data was developed that is useful for the respective side (learning factory/municipal energy supplier). The learning factory made the previously locally stored data available selected in the cloud on a server with the background of being able to vary and simulate errors and energy consumption in the learning factory and the goal of gaining knowledge and evaluation criteria for the municipal utilities as energy service providers or directly for the participating SMEs. The main focus in the development of the criteria and the data evaluation is on reusability. This includes the examination of the transferability of the concept to other business sectors and other utilities, as well as the question of the existence of local synergy opportunities related to energy optimization within possibly participating SMEs

(e.g. heat sources/heat demand of locally neighboring SMEs).

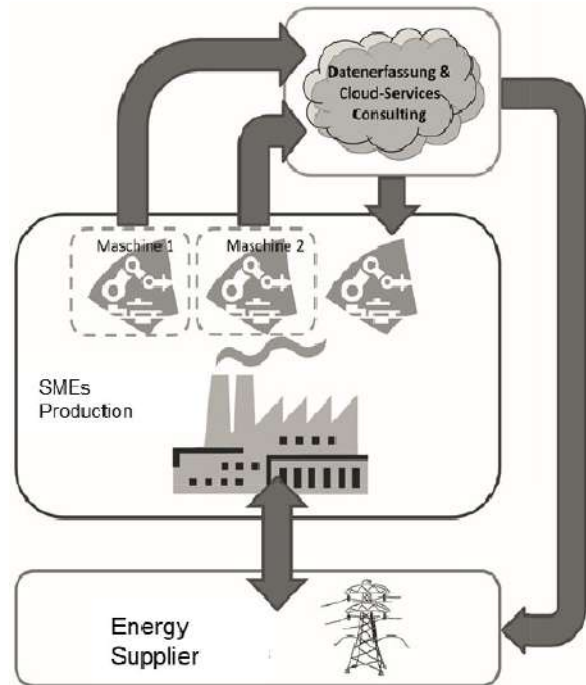


Fig. 1. Networking - energy supplier, SME production operation via cloud

To determine the extent to which companies in the region are interested in resource-efficient production, we conducted a survey of 38 companies in the region in parallel with the development of the cloud. The aim of the survey was to determine whether there is a need or willingness to address the issue of energy efficiency in your own company and what would help you. The results of the survey are briefly presented in chapter 4.

One project partner, the city of Velbert, is the operator of three swimming pools in the region and, together with the Bochum University of Applied Sciences, agreed to initially take measurements in one swimming pool and to test the system on a real application with the aim of jointly gathering experience. If successful, the system could also be installed and adapted for the other two swimming pools. The possibility to work on technically complex, grown systems increases immensely the probability to generate industry-oriented and practical knowledge for all project partners. In the next chapters, the individual steps and results of our approach and implementation will be presented in more detail:

- Learning factory of the Bochum University of Applied Sciences at the Velbert/Heiligenhaus campus into the cloud
- Survey results of small and medium-sized enterprises
- Swimming park of the city Velbert: A reference project for knowledge enhancement o Outlook.

2. ENERGY DATA COLLECTION IN THE CLOUD

In the last years, the automation laboratory of the Bochum University of Applied Sciences built a learning factory for research & teaching at the Velbert/ Heiligenhaus campus according to the latest industry standards with the aim of practically conveying the concepts and strategies of Industry 4.0 to the mainly dual students. The interlinked and automated production system consists of a manufacturing, high-bay warehouse, transfer line, assembly stations, testing stations and shipping station.

This includes the acquisition of machine and operating data (MDE/ BDE), as well as the connection of the Manufacturing Execution System (MES, Hydra from MPDV) to the commercial level (e.g. SAP), also known as "Shop Floor to Top Floor Integration". Since there is still a lack of binding standards for data exchange in production for the implementation of an MES, the learning factory relies on system and manufacturer-independent interfaces such as OPC UA (Unified Architecture) for intelligent networking of the various controllers from different manufacturers (Siemens S7, Schneider Electric, Beckhoff, Mit- subishi Controller). Great attention was paid to the possibility of implementing different production scenarios, allowing students to independently develop and evaluate the optimization criteria for resource- and energy-efficient production and to experience them on the plant. Considering the learning factory as a small medium-sized company, the production costs as well as the energy flows within the company are transparent and can be optimized locally.

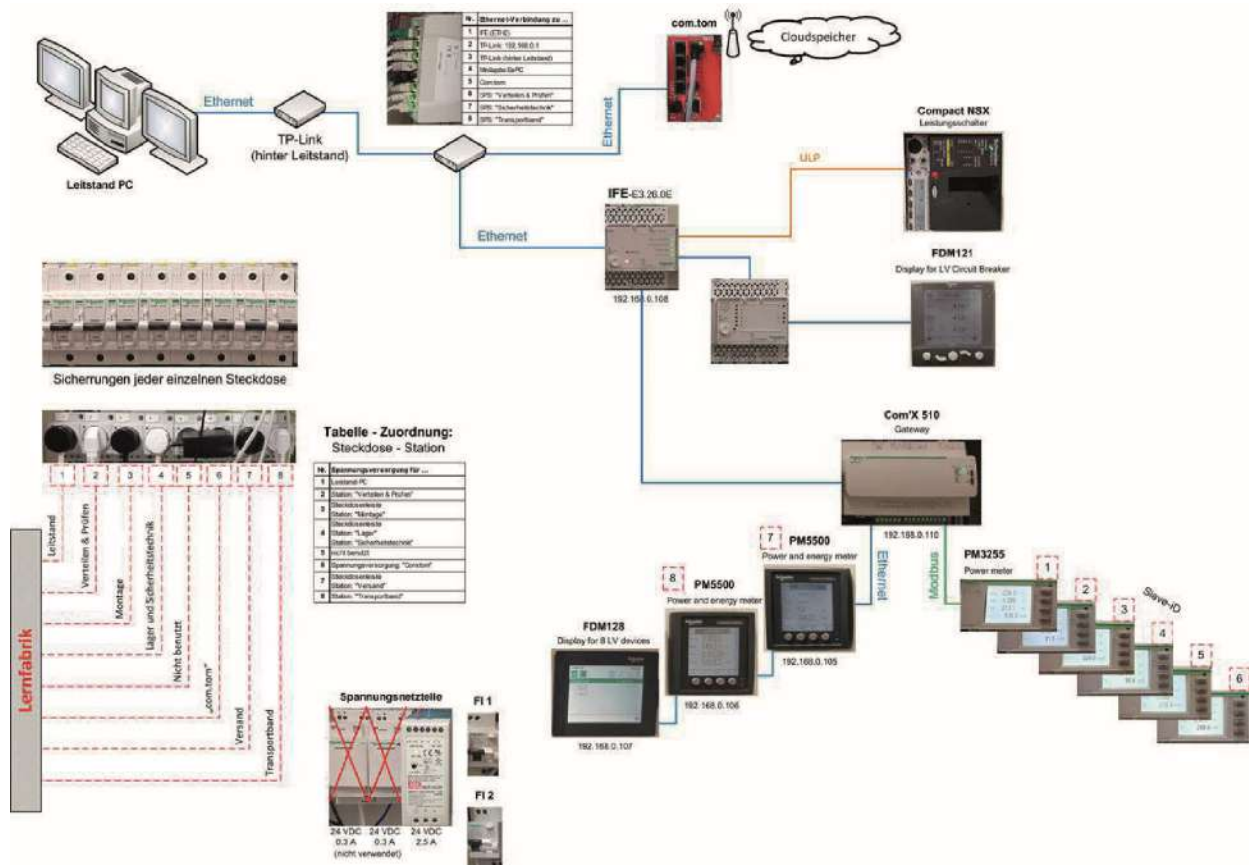


Fig. 2. Test scenario, learning factory networking

The learning factory was expanded within the project to include a central energy data measuring cabinet (Schneider Electric), which records all energy data from the individual stations of the learning factory and stores it on a local server. The existing infrastructure of the laboratory factory is used in the course of the project to run various production processes and perform load simulations. These are intended to gain knowledge regarding optimization possibilities, fault and load scenarios with the aim of determining specific patterns and relevant key figures. The next step was to conduct a market analysis of which cloud solution available on the market is suitable for small and medium-sized businesses. The following criteria were considered important for the comparison:

- Server location in Germany
- Transparent costs
- Secure data transmission (end-to-end encryption, TLS)
- High accessibility of the server
- Allows customer-specific design of user interfaces
- Easy to operate
- Can be extended as required for new project participants
- Easy management of access rights
- Supports as many interfaces as possible (OPC-UA, ModBus TCP/IP, CAN, MBus, etc.)
- Programmable controller on board with analog and digital I/Os for small control applications

All criteria were met by an offer from Beck IPC with the product portfolio: Cloud Edge Controller (differently configurable gateways) plus the online platform Com.Tom Portal for visualization and storage of data on the server in Germany. Fortunately, Beck IPC joined the project as a new project partner and so the learning factory was expanded with the gateway "CTI 100.MBUS.WLAN.W" and the process data was integrated into the cloud platform of the Com.Tom Portal (see Figure 2). Write and read rights were assigned to the platform for the individual project participants (municipal utilities, Beck IPC, Schneider Electric), so that the networking of the individual partners on the platform was successfully achieved. Hereby, exemplary interfaces to all relevant data suppliers (production and energy suppliers) were created

first with regard to the secure data transmission via the Internet, as well as the test and structure of the cloud data collection. Furthermore, the appropriate visualization methodology for different user groups was tested and implemented.

Of course, the MindSphere product from Siemens and Software AG also offers these options. However, primarily as a "Platform as a Service (PaaS)", it offers the creation of a large ecosystem by allowing users to offer powerful industrial applications and digital services as the basis for new business models - precisely in the areas of predictive maintenance, energy data management or resource optimization.

The openness of the IoT operating system, for example through the use of open interfaces (APIs) for the creation of OEM and customer-specific apps as well as open standards for connectivity such as OPC UA, also plays an important role here. The white paper "The Digitalization Productivity Bonus: Sector Insights" [3], published, estimates a cost reduction in production, due to the digitalization of a company, of 6.3 - 9.8 %. The target group for the MindSphere product is large industrial companies. This prospect can be an incentive for the companies to make significant investments with the help of smart financing to digitalize their production. The product is too powerful for our project and the SME target group.

3. SURVEY RESULTS OF MEDIUM-SIZED ENTERPRISES

The transparency of energy flows within a company is still rare, especially in small and medium-sized enterprises, which did not have the need to implement EN 50001 in their company. One of the first steps in the project was to determine the causes of this situation in the small and medium-sized enterprises in the Velbert/Heiligenhaus region. This was achieved by interviewing 38 entrepreneurs from the manufacturing sector in personal conversations (see Figure 3) [1]. In summary, the impression appears that the entrepreneurs are very much interested in resource-efficient production, but they lack the time, the personnel, the urgency and some political framework conditions to dedicate themselves to this topic [2, 5].

Questions	Answers	Reasons
Why can't you go deeper into the topic of energy efficiency	38	busy day-to-day business no staff
Are you ready to invest in energy efficiency	30	Yes
Are you ready to train your employees	35	Yes
Can you give the employee the time to dedicate to the issue?	34	No
Would you create a position for an energy manager	38	No, economically not presentable
Do You Calculate your energy costs for production in common costs	38	Yes

Fig. 3. Survey results

From the point of view of small and medium-sized enterprises, networking with the energy supplier could bring gains if the energy supplier expands its product portfolio with a focus on a service, e.g., through meaningful and lasting energy consulting, maintenance monitoring or specifically adapted tariff offers, in order to be able to obtain energy in a resource-saving and cost-stable manner in the long term.

4. A REFERENCE PROJECT FOR KNOWLEDGE ENHANCEMENT

The more detailed customer consumption and specific production characteristic data, can lead to better forecasting of the energy required (optimization of control power) as well as to better network utilization and network planning in-house. The latter aspects are currently the most cost-intensive items for network operators. In order to become a true energy partner for SMEs, the energy supplier naturally needs access to the detailed energy flows of the companies, as well as technical understanding and, above all, the know-how of the specific process flows in the companies. Only then is he in a position to identify sensible optimization approaches and consequently reduce the customers' energy consumption. To meet this goal, the management of city Velbert decided to gain experience in its own operations and provided access to one of its pools. The implementation of the energy metering systems and the integration of the cloud edge controller at the university was associated with some problems, such as the integration and visibility of the gateway via the centralized Bochum IT network or finding the

ModBus addresses for the relevant data in the different Schneider Electric energy meters, as well as the implementation of the addresses on the Com.Tom server. In summary, it went smoothly, as the system components, Cloud Edge Controller (Beck IPC) and energy measurement systems from (Schneider Electric) communicate with each other without any problems (via Modbus or OPC UA) and both are state of the art. However, the use case becomes interesting and realistic when a technically grown company is faced with the task of implementing energy monitoring. The following goal was developed: To identify energy optimization possibilities for the Park Bad in the WisE-Pro project and to develop sensible measuring points and criteria for monitoring. The targeted network infrastructure for the baths is shown in the following figure:

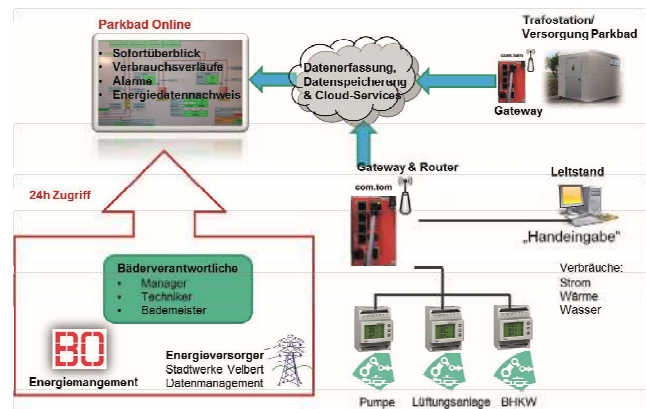


Fig. 4. Network infrastructure for the example facility swimming pool

- In the first step, an energy check was carried out by Bochum University of Applied Sciences in accordance with the guidelines of the Energy Saving Ordinance in order to record the status quo, the infrastructure of existing data, and the operating resources.
- Another benefit could be the acquisition of new customers: Showcase project for energy optimization for small and medium-sized businesses.
- Away from the paper economy: first step: input in lists on PC, possibly tablet Goal: increase automation, reduce errors, enable evaluability.
- Cost savings, maintenance facilitation for employees, operate resources more efficiently, transferability and integration of other baths.

The university uses two Chauvin Arnoux PEL 103 series energy data loggers for the energy measurements, which also have a network analysis function and measurements up to the 50th harmonic. These were used to make long-term measurements at selected locations. The entire operating equipment was recorded and optimization options for saving energy were identified on the topics of CHP operation, power factor correction, soft start of the pumps, asymmetrical network load due to connection of the consumers, illuminants and data maintenance. In the following, we will briefly discuss data maintenance:

Every day, almost 90 data values are read and noted by the pool attendants within the pool, whereby 5 still have to be calculated (CHP operating data, heat quantities, environmental data, water consumption, analysis data of the water, energy meter data). Once a week, 13 more data are noted (chlorine room control, etc.). These are noted by hand in tables, which are then forwarded to the supervising organizational unit on a monthly basis. The data recorded by the EMH electricity meters (active, reactive and apparent power) are retrieved in a 24h cycle by the municipal utilities and stored in another organizational unit. Unfortunately, these meters cannot be read out, as only the licensed proprietary software allows access. Thus, the online data on the platform is then available 24h delayed if no redundant accessible meters are installed. In general, calibrated energy meters that serve as the basis for billing are very difficult to access. Fortunately, there is potential for optimization due to the historically decentralized organizational structure for managing the pools. A way to enter handheld data and store it directly in the cloud could be an improvement for the way everyone works. Using the cloud data, as well as the data measured to date, the following steps are planned:

- Evaluate load curves based on different usage scenarios.
- Develop energy evaluation criteria and methods for selecting relevant cloud data for other companies.

A common problem that is also found in industry is the problem of outsourcing. When measurements have to be performed on equipment or new measuring devices have to be

permanently installed, in most cases the equipment has to be shut down for a short time. In the bathroom, for example, the installation and maintenance of the ventilation system is carried out by an external company. The programming of the ventilation system is handled by another software company. If changes are now made to the ventilation system, e.g. fixed installation of a measuring meter, both companies must be on site for warranty reasons. This of course increases the costs for the installation of a measuring point considerably.

Acknowledgement

In the last year, the park pool is to be integrated into the Com.Tom platform with the relevant measurement data and made accessible to all stakeholders. Furthermore, user-friendly user interfaces will be created according to the needs of the different stakeholders (pool technicians, lifeguards, pool managers). The aim is to provide assistance to the two pool technicians, who are responsible for the supervision and maintenance of three pools, and to send them an alarm in case of emergency. The knowledge and experience gained so far on the basis of individual measurements is to be converted into automated monitoring and evaluation criteria on the platform in a next step. As a desirable add-on, the project developed the idea of making it easier for the pool attendants to take daily meter readings and hand-written documentation by developing an app that photographs the meters and automatically writes the meter readings to the cloud.

REFERENCES

- [1] Podjawerschek, S: Umfrageergebnisse – Energieeffizienz in klein- und mittelständischen Unternehmen im produzierenden Gewerbe in der Region Velbert/Heiligenhaus. Internes Dokument, 2016, 12 Seiten
- [2] Tagesband AALE 2017, 14. Fachkonferenz, 2-3 März 2017, Wildau, S. 45-49
- [3] Whitepaper: The Digitalization Productivity Bonus: Sector Insights, Studie von Siemens Financial Services, November 2017, 35 Seiten
- [4] Bundesministerium für Bildung und Forschung (BMBF): Die neue Hightech-Strategie, Innovationen für Deutschland. 2014, 55 Seiten
- [5] Whitepaper: Energie- & Betriebsdatenmanagement, Siemens 2022.